Faculty of Mathematical, Physical and Natural Sciences

Department of Environmental Biology

PhD Course in Environmental and Evolutionary Biology

XXXIV Cycle

Curriculum: Ecological Sciences

Investigation of the contribution of emission sources to atmospheric particulate matter concentration (PM) and to its redox properties

PhD candidate

Dr. Maria Agostina Frezzini

Maria Agostina Frezzini

Supervisor

Prof. Silvia Canepari

Academic Year 2020/2021

Table of Contents

Description and objectives of the PhD research **5**

1. Introduction **9**

1.1 Particulate Matter: definition and classification 9

1.2 PM chemical composition 11

1.2.1 Inorganic ions *12*

1.2.2 Carbonaceous compounds *12*

1.2.3 Organic fraction *12*

1.2.4 Trace elements *13*

1.3 PM sampling, analysis, and chemical characterization 13

1.3.1 Sampling and measurement methods of PM_{10} and $PM_{2.5}$ *13*

1.3.2 High time resolution PM sampling *15*

1.3.3 PM analysis *18*

2. Effects of PM on environment and human health **20**

2.1 General regulation of PM air pollution 20

2.2 Environmental effects 20

2.3 Effects on human health 21

2.4 Oxidative stress induction 22

3. Traceability of emission sources through elemental chemical analysis and oxidative potential measurements **24**

3.1 PM biomonitoring 25

3.2 Indoor emission sources 26

4. Overview of PM oxidative potential measurement methods **28**

4.1 OP assays 28

4.2 OP in epidemiologic analysis 31

4.3 Critical issue of OP measurement 31

5. (A) Analyses of PM for Localization and Environmental Impact Assessment of PM Released by Specific Emission Sources **35**

5.1 (A1) Identification and spatial mapping of tracers of PM_{10} emission sources using a high spatial resolution distributed network in an urban setting **37**

5.2 (A2) Effects of COVID-19 Lockdown on PM_{10} Composition and Sources in the Rome Area (Italy) by Elements' Chemical Fractionation-based Source Apportionment **66**

5.3 (A3) Spatial Mapping and Size Distribution of Oxidative Potential of Particulate Matter Released by Spatially Disaggregated Sources **118**

5.4 (A4) Urban trees for biomonitoring atmospheric particulate matter: an integrated approach combining plant functional traits, magnetic and chemical properties 147

5.5 (A5) Evaluation of the efficiency of *Arundo donax* L. leaves as biomonitors for atmospheric element concentrations in an urban and industrial area of central Italy 182

5.6 (A6) Lichen transplants for high spatial resolution biomonitoring of Persistent Organic Pollutants (POPs) in a multi-source polluted area of Central Italy 209

6. (B) Chemical analysis and oxidative potential of PM released by indoor and outdoor emission sources 240

6.1 (B1) Seasonal Variations in the Chemical Composition of Indoor and Outdoor PM_{10} in University Classrooms 241

6.2 (B2) Comparison between PM_{10} oxidative potential of indoor and outdoor environments – The INDOMAP project 262

7. (C) Evaluation of PM redox properties and new reports towards standardized OP measurements277

7.1 (C1) Application of DPPH Assay for Assessment of Particulate Matter Reducing Properties 280

7.2 (C2) Effects of Operating Conditions on PM Oxidative Potential Assays..... 304

7.3 (C3) A New Method for the Assessment of the Oxidative Potential of Both Water-soluble and Insoluble PM 334

8. (D) Health effects of atmospheric PM..... 359

8.1 (D1) Toxicological Profile of PM from Different Sources in Bronchial Epithelial Cell Line BEAS-2B 360

8.2 RHAPS project: Redox-activity and Health-effects of Atmospheric Primary and Secondary aerosol 378

8.2.1 (D2) On the redox-activity and health-effects of atmospheric primary and secondary aerosol: phenomenology 403

9. General conclusions and perspectives..... 440

10. Communications at congresses and conferences 443

11. Appendix 445

11.1 (E) Efficiency Evaluation of Food Waste Materials for the Removal of Pollutants from Wastewater..... 445

11.1.1 (E1) Food Waste Materials Appear Efficient and Low-Cost Adsorbents for the Removal of Organic and Inorganic Pollutants from Wastewater 446

11.1.2 (E2) Food Waste Materials as Low-cost Adsorbents for the Removal of Volatile Organic Compounds from Wastewater..... 451

11.2 (F) Analytical chemistry for the characterization of environmental matrices..... 471

11.2.1 (F1) An Analytical Method for the Biomonitoring of Mercury in Bees and Beehive Products by Cold Vapor Atomic Fluorescence Spectrometry 472

11.2.2 (F2) Multi-element characterization and antioxidant activity of Italian extravirgin olive oils . 495

12. References 517

Description and objectives of the PhD research

In the last few years, various epidemiological studies were conducted to estimate the health effects of particulate matter (PM) on human population, placing at the core the association between exposure to PM and several adverse outcomes, especially on cardiovascular and respiratory systems. PM mass concentration is typically used to estimate population exposure. However, this indicator misestimate the overall impact of PM, since it does not consider the multiple toxicological effects of the different pollutants that constitute and determine the intrinsic properties of PM. In fact, the complexity and variability of PM can lead to different responses in biological systems. The hypothesis of the mechanisms of PM-related diseases include oxidative stress, inflammatory responses, and genotoxicity. All of them can be mediated by PM-related reactive oxygen species (ROS) that can be generally grouped into two types: one refers to particle-bound ROS, which are generated in the atmosphere and may be transported into the respiratory system with inhalation; and the other can be generated in cellular environment by PM components both directly and indirectly after inhalation.

To assess the particles' oxidative capacity, several acellular methods, defined as oxidative potential (OP) assays, have been developed and proposed as relevant and valid metric for addressing biological exposure to PM. There is still no agreement regarding the most representative assay to measure the OP of PM, but methods mostly used on the PM filter extracts are the dithiothreitol (OP^{DTT}), the 2′,7′-dichlorofluorescin (OP^{DCFH}), and the ascorbic acid (OP^{AA}) assays. Each assay gives different results and probably simulates just a small part of the many potential mechanisms of oxidative stress induction. Therefore, the synergic application of the three assays on the same PM samples is strongly recommended to have a complete characterization of their redox properties. The study of PM composition and toxicity represents a particularly interesting field of research, aimed to a better understanding of the existing relationships between the chemical composition and sources of PM and its adverse effects on human health and environment, useful to plan the appropriate mitigation measures. It is also worth considering the heterogeneity of emission sources and the role that they play on PM physical and chemical properties. The analysis of PM coming from different sources could allow associating specific chemical composition, which depends on the pollutant origin, with a given biological response. In fact, the role of each chemical component on PM toxicity is still to be fully defined.

One of the goals of this PhD thesis is to improve the knowledge about the existing relationships between PM chemical composition and sources and, therefore, to attempt to estimate PM adverse effects on health and environment through the investigation of PM redox properties.

To this aim, a multidisciplinary study based on the synergic application of traditional and innovative approaches to PM was carried out in this PhD research.

PM field samples were collected at monitoring sites differently impacted by anthropic activities by using different techniques, such as traditional monitoring equipment, cascade impactors, biomonitoring methods and very-low volume samplers allowing spatially-resolved determination of PM chemical components. Furthermore, widespread components of PM produced by specific emission sources and characterized by very different chemical compositions (certified urban dust NIST1648a, brake dust, Saharan dust, coke dust, calcitic

soil dust, incinerator dust, and diesel particulate matter certified material NIST1650b) were used to compare different experimental procedures on PM from defined emission sources.

Chemical characterization of PM samples was obtained by applying advanced and robust analytical procedures for the determination of inorganic ions, water-soluble and insoluble elements, water-soluble organic carbon (WSOC) and levoglucosan (LVG). PM water-soluble and insoluble fraction were separately analyzed through a well-established fractionation procedure to increase the selectivity of elements as source tracers and to estimate the environmental mobility and bio-accessibility of toxic elements.

Much of the PhD experimental research has focused on the investigation of redox properties of PM since in the last few years, the oxidative potential appears to be the central paradigm in the assessment of PM toxicity. However, there are still operative criticisms affecting its relevance as effective realistic metric to quantify the effects of ambient particles on human health, such as the influence of multiple operative conditions on OP obtained results, as well the lack of standardized operative conditions, which make a challenge to representatively compare inter-laboratory data. Therefore, one of the goals of this research was to explore in depth redox equilibria between PM reactive species.

The understanding of redox equilibria in PM primarily regarded the optimization of a method to evaluate the presence of species with reducing/antioxidant behavior in PM. The DPPH radical scavenging assay was adapted and preliminarily applied to PM with the aim of verifying its possible use as an acellular method for estimating the presence of reducing species, thus for expressing PM reducing potential (RP^{DPPH}). The combined application of RP and OP assays to wider sample sets will permit to better understand redox equilibria among PM native species that might occur during sample storage, extraction phase, and/or application of OP assays. Furthermore, the availability of a suitable assay for routinely estimate the amount of reducing species in PM samples could constitute a new and potentially useful tool for acquiring new insight in the field of its redox behavior and health effects.

In order to deepen the critical issues revolving around particles OP, the research was also aimed at investigating the stability of PM redox components by analyzing the variability in OP assays (OP^{DCFH}, OP^{AA}, OP^{DTT}) responses depending on the operating conditions by which tests are performed, by comparing different procedures simultaneously applied on identical samples. In detail, the influence of extraction method, filter-storage, as well as time delay between PM sampling and analysis, on OP measurements, was explored. Furthermore, the influence of supporting membrane, on which PM is collected, on OP measurements was investigated by comparing quartz and PTFE filters performances. Lastly the contribution of water-insoluble PM components to aerosol OP was examined by performing OP assays directly on PM filters, in order to assess their role in particle oxidative activity, as well as to investigate exposure to PM in real-word conditions. In this context, a non-invasive, simple, and efficient method for the detachment of intact particles from PM field filters was applied to PM samples to overcome the uncertainty of results derived from the operatively limits of performing OP assays directly on particles. The procedure consists in the mechanical detachment of PM by using an electrical toothbrush and provided promising results for the assessment of toxicological effects of the

whole PM (water-soluble and insoluble species). In this way, particles can be used entirely for oxidative potential assays and for exposure to human cells or model organisms under real-world conditions.

Another critical issue affecting PM measurements and chemical characterization is the study of the relationship between PM chemical composition and emission sources that sometimes is expensive and requires considerable resources in terms of instrumental equipment.

During the PhD research various monitoring campaigns aimed to improve knowledge about the existing relationships between sources of PM and its related chemical composition were conducted under different conditions and in different geographical areas (i.e. during the national lockdown imposed by Italian government to counter the Covid-19 pandemic). Valuable information for PM source apportionment through a chemical/size fractionation procedure and OP measurements were obtained.

Potential effects of PM composition on biological systems were studied by using an *in vitro* approach based on the cytotoxic, genotoxic, oxidative, and inflammatory response of bronchial epithelial cell line BEAS-2B after the exposure to PM coming from different sources.

In parallel with the described activity, the reliability of PM biomonitoring techniques for the assessment of atmospheric element concentrations was estimated. To this aim, leaf deposition on riparian species (*Arundo donax* (L.)) and lichen transplants (*Evernia prunastri* (L.) Ach.) was used. Furthermore, an integrated approach to assess the effects of PM on functional traits of *Quercus ilex* (L.) in an urban area was carried out comparing results from OP assays when applied on PM deposited on *Q. ilex* leaves, and on filters (traditional monitoring system).

Another line of research was the analysis of PM samples in indoor environments of private dwellings and University classrooms, to study the concentration, the chemical composition, and the OP of indoor and outdoor PM to obtain information about the main indoor and outdoor PM emission sources and exposure of occupants.

Lastly, another important study included in the PhD research was related to the project Redox-activity and Health-effects of Atmospheric Primary and Secondary aerosol (PRIN 2017-RHAPS project), in which our research group participated with OP and elemental analysis of PM samples. RHAPS aims to identify specific properties of PM from anthropogenic sources that are responsible for toxicological effects and can be used as new metrics for health-related outdoor pollution studies. The main goal of RHAPS project was to provide a new assessment of the sources and nature of PM components responsible for adverse health effects in real-world conditions. The experimental field monitoring campaign have been recently completed and data elaboration is still ongoing. The contributions of PM chemical components directly emitted in the atmosphere ("primary" aerosols) or formed *in situ* by chemical reactions ("secondary" aerosols) to OP of PM will be assessed. In turn, the effect of OP and other physical-chemical properties of PM (size-dependent composition, water solubility, particle mass/number/surface, etc.) on toxicological endpoints will be investigated. Field campaigns were carried out in the southern part of the Po Valley and involved the best available technologies for PM characterization of several research institutes. Furthermore, laboratory experiments in an atmospheric simulation chamber are included in the activities and are focused on the link between the OP carried by atmospheric secondary organic aerosol (SOA) and PM toxicity.

Supplementary research activities were focused on the evaluation of the capability of food waste materials as low-cost adsorbents for the removal of Volatile Organic Compounds (VOC) from wastewater, and on the analytical characterization of biological matrices (i.e. bees and beehive products, olive oil) to evaluate their potential of accumulating toxic elements, allowing the monitoring of this kind of pollutants concentrations in the environment for integrated measurements. In this context, rapid analytical methods for routinely analyzing a significant number of biological samples were developed and validated.

1. Introduction

1.1 Particulate Matter: definition and classification

Particulate Matter (PM) consists in a heterogeneous and complex mixture of solid particles and liquid droplets suspended in the atmosphere, with an aerodynamic diameter ranging between 0.01 and 100 μm (i.e. soot, dust, differently originated salts, fly ashes, trace metals, viruses, bacteria, fungi, spores, and pollen; Ramli et al., 2020; Ali et al., 2019; EPA, 1997). PM can be classified by different criteria: the type of emission sources that release it, its formation process, and its aerodynamic properties. The varieties of emission sources responsible for PM origination can be divided in two main groups:

- **Natural emission sources**: sea salt and spray, soil erosion, volcanic eruptions, wildfires, biogenic sources (i.e. pollen, plant residues, spores), disintegration of rocks (Viana et al., 2014; Yatkin and Bayram, 2008)
- **Anthropogenic emission sources:** industries, vehicles, cooking activities, domestic heating, agricultural processes, incinerators and power plants, tobacco smoke (Pulong et al., 2017; Pant & Harrison, 2013).

According to the mechanisms of formation, PM can be classified as **primary** or **secondary**:

- **Primary particles**: emitted directly from the emission sources into the atmosphere in particulate form.
- **Secondary particles**: generated in the atmosphere, formed by the conversion mode gas-particle due to the condensation of natural and anthropogenic vapors, or generated by the evolution of a primary particle.

Lastly, the atmospheric particles can be classified referring to the aerodynamic diameter (a.d.), that is the size of a unit-density sphere (1 g/cm3) with the same aerodynamic characteristics (same settling velocity in air) as the given particle (John, 2001; Hinds, 1999). In this case, airborne PM can be divided into three sub-classifications related to dimensional properties: **modal classification**, based on the mechanisms of particle formation and consequently on their number, surface area and mass distribution (Whitby 1978); **dimensional (size) cut-off**, based on the efficiency of the sampling head device during the PM collection, and **dosimetric classification**, based on the particles' ability to enter and penetrate the respiratory tracts.

The **modal classification** (Figure 1) includes the nucleation mode, with the "ultra-fine" fraction (ultra-fine particles, UFP), with an aerodynamic diameter less than 0.1 μm, the accumulation mode, with fine fraction including particles having an aerodynamic diameter between 0.1 and 1-2 μm, and the coarse mode, meaning particles with an aerodynamic diameter between 1-2 and 100 μm. UFP are generated by combustion activities and atmospheric transformations of various precursors (i.e. NOx, SO_2, NH_3; Westerdahl et al., 2005). The fine particles are introduced by combustion activities such as fossil fuels (vehicles, power plants and other industries), biomass burning and tobacco smoke and, more generally, by coagulation and condensation of ultrafine particles. Finally, the coarse particles mostly originate from events such as construction activities, farming, mining, windstorms, and resuspension of dusts by wind and traffic (Baron et al., 2001).

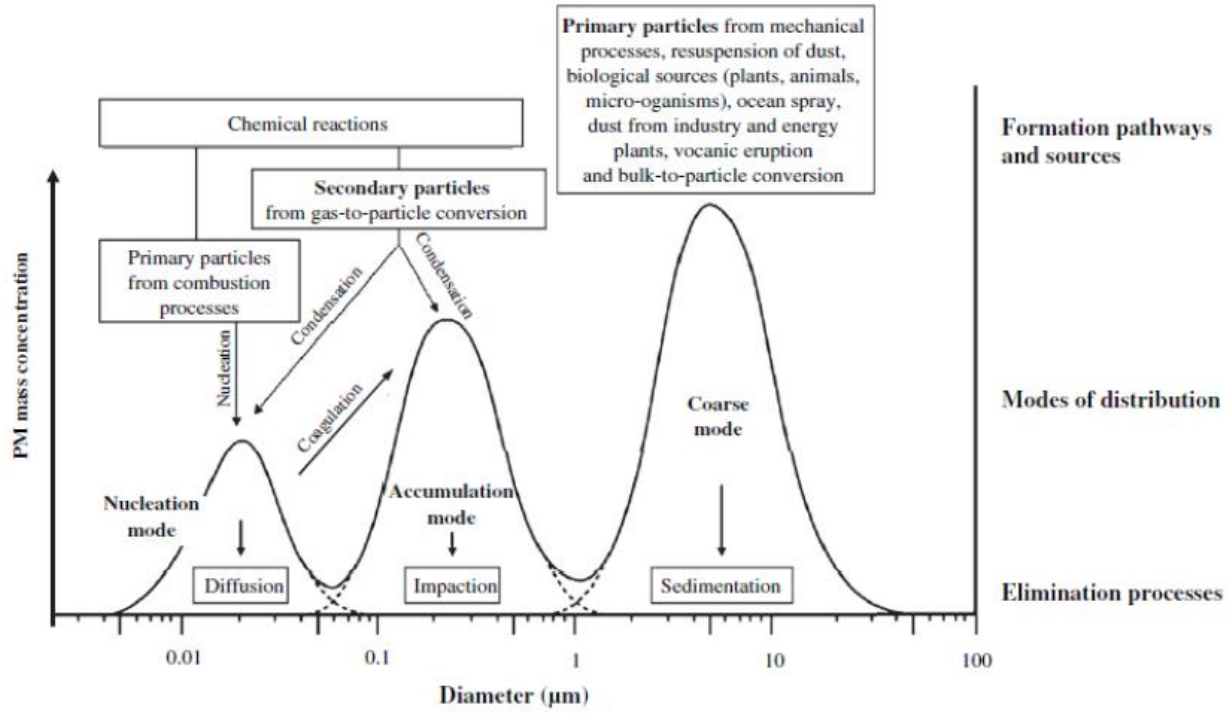

Figure 1. Idealized size distribution of particle in ambient air (Araujo and Nel, 2009).

The **dimensional (size) cut-off classification** refers to the collection of particles above or below a specific aerodynamic size range. The abbreviation PMx (particulate matter with an aerodynamic diameter below x μm) indicates the fraction of PM that has been collected by a selective inlet impactor with a 50% efficiency cut-off at X μm aerodynamic diameter (Directive 2008/50/EC; EC 1997). The PM collecting instruments usually used in the air sampling collect particles that fall within a size range rather than one single size. The reason why size selective sampling has gained a lot of attention is due to the need of measuring particle size fractions that have a special importance, such as for health studies, visibility, source apportionment, to measure mass size distributions, or to collect segregated particles for chemical analysis. The most commonly available sampling heads for commercial samplers collect mainly PM_{10} and $PM_{2.5}$ fractions, being the most interesting for both health effects and investigations on the life cycle of airborne particles. The fine fraction will be intended for $PM_{2.5}$, while the coarse term is used for particles with aerodynamic diameter between 2.5 and 10 μm, defined as PM_{10} (EPA 1999). Conventional PM_{10} and $PM_{2.5}$ samplers show a 50% efficiency in collecting particles with 10 ± 0.5 μm or 2.5 ± 0.5 μm aerodynamic diameter.

The **dosimetric classification** groups particles as inhalable, thoracic, and respirable, according to their upper size cuts and on the capability of airborne particles to enter, infiltrate, deposit and react with the different zones of the respiratory system. The inhalable particles only enter the respiratory tract, beginning with the nose and mouth; the thoracic ones pass through the larynx, reaching the lung airways and gas-exchange regions of the lung; the respirable particles are more inclined to reach the gas-exchange region of the lung. The last-mentioned fraction includes the respirable "high risk" particles that exerts harmful effects on children and people suffering from cardio-pulmonary diseases (Mark, 1999). The deposition of particles in the respiratory system is shown in Figure 2.

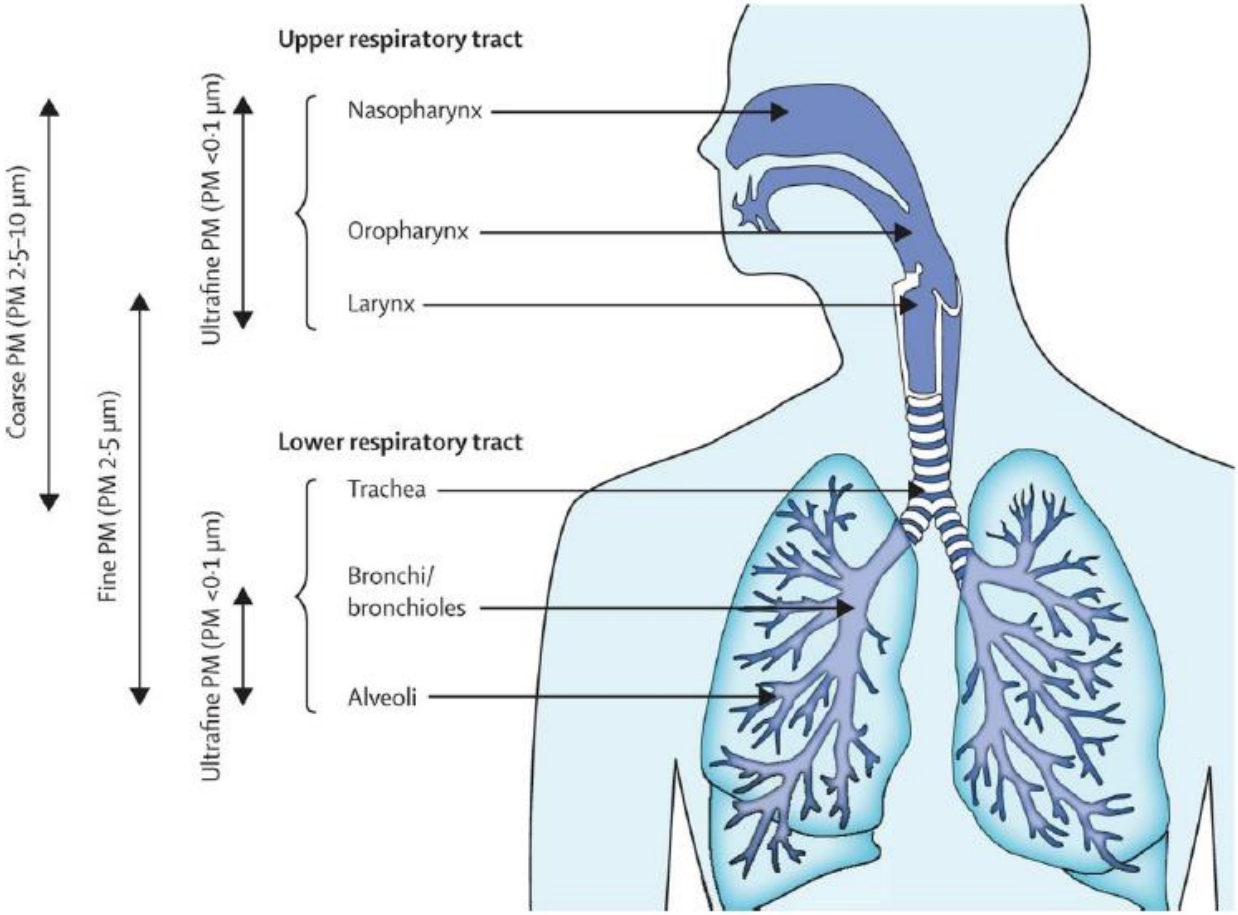

Figure 2. Respiratory collection of particles (Task, 1966).

1.2 PM chemical composition

The composition of PM is extremely heterogeneous and depends on source origin and emission, physical-chemical changes in the atmosphere and size fractions. Chemical species can be grouped in:

- **Macro-components:** inorganic ions (i.e. F^-, Cl^-, NO^{3-}, SO_4^{2-}, PO_4^{3-}, and NH_4^+), elements (i.e. Al, Ca, Fe, K, Mg and Na) and the carbonaceous fraction that exceed more than 1% of the PM mass (Perrino et al., 2010);
- **Micro-components:** elements and organic compounds present in trace amount (< 1% of PM mass; Canepari et al., 2014).

Sulphate, ammonium, hydrogen ions, elemental carbon (EC), primary and secondary organic compounds, as well as certain transition metals are predominantly found in the PM fine fraction, while crustal materials such as Ca, Al, Si, Mg and Fe, are mostly discovered in *coarse* particles. Nitrate and potassium can occur in both the fine and the coarse fractions.

Lastly, the coarse fraction can contain bioaerosol particles such as allergens, pollen, spores, plants, and fragments of insects (Marcovecchio and Perrino, 2021; Perrino and Marcovecchio, 2016; Huffman et al., 2010), which recently attracted the attention of the scientific community due to their multiple health impacts, including asthma and related respiratory allergies (Rosianu et al., 2021).

1.2.1 Inorganic ions

The ions, anions (i.e. Cl^-, NO^{3-}, SO_4^{2-} CO_3^{2-}, SiO_4^{4-}), and cations (i.e. Na^+, NH_4^+, K^+, Mg^{2+}, Ca^{2+}), are included in the inorganic macro-components and can be divided into two groups depending on their primary or secondary nature. The **primary ions** include chlorides, that originate mainly from marine aerosol, even in locations far from the coast, but they are also emitted from waste incinerators and power stations; sodium and magnesium coming from marine aerosol and partly from soil resuspension; calcium, coming from soil, mineral dust disposal, wildfires and industrial activities; potassium, coming from soil, biomass combustion, mineral incinerators, and agricultural fertilization; sulphates, present as secondary species and predominantly derived from the atmospheric oxidation of anthropogenic sulphur-containing compounds (Mamane et al., 2008); silicates and carbonates, coming from soil since they are mainly present in the Earth's crust.

The **secondary inorganic compounds** originate from different gaseous precursors such as sulphide oxides, nitrogen oxides, as products of oxidation of the nitrogen (air or fuel) with oxygen, under conditions of elevated temperature, and mainly emitted during combustion phenomena (Wang et al., 2007), and ammonia, coming from the microbiological activity of the soil and sea and originated by stock farms and vehicular exhausts.

1.2.2 Carbonaceous compounds

The carbonaceous fraction of PM consists of major components, black carbon (BC), organic aerosol (OA) or organic carbon (OC), and brown carbon (BrC) and elemental carbon (EC) (Costabile et al., 2017). Elemental carbon (EC) is emitted directly into the atmosphere, predominantly from combustion processes as either single particles or clusters with variable shape and size (Barone et al., 2006); organic carbon (OC) is represented as multiple compounds with other precursor gases, such as furans, carboxylic acids, polycarboxylic aromatic acids, aliphatic acids, and polycyclic aromatic hydrocarbons (PAHs). OC can be directly emitted into the atmosphere from primary sources such as biomass burning, combustion processes transport (diesel vehicles) and industries; in addition, it and can be introduced by secondary organic aerosol formation via atmospheric oxidation reactions of Volatile Organic Compounds (VOCs), forming products that have low enough volatility to form aerosol via either nucleation or gas-to-particle partitioning to pre-existing particles (Jaoui and Kamens, 2001).

1.2.3 Organic fraction

The organic fraction generally include the VOCs, that are emitted as gases from certain solids or liquids from anthropogenic and biogenic sources, such as the combustion of fuels and evaporation of solvents and can be adsorbed on PM surface (Seinfeld and Pandis, 2012); the PAHs, released from both natural (forest fires and volcanic eruption) and anthropogenic sources, particularly from incomplete combustion of organic fuels (Di Vaio et al., 2016; Lee, 2010). In the atmosphere, the PAHs can undergo degradation by photochemical reactions, and they can deposit on the ground, both by dry and/or wet deposition. Most PAHs are persistent organic pollutants (POPs) in the environment, a relevant group of air pollutants including polychlorinated dibenzodioxins (PCDDs), polychlorinated dibenzofurans (PCDFs) and polychlorinated biphenyls (PCBs). The relevance of these organic compounds as air pollutants is due to their toxicity and ability to persist in the

environment for a long time and to biomagnify through the food chain, determining adverse effects on wildlife and humans (Thakur and Pathania, 2020; Lohmann et al., 2001; Ueno et al., 2005).

1.2.4 Trace elements

Trace metal components, such as Ag, As, Ba, Cd, Ce, Co, Cr, Cu, La, Mn, Nb, Ni, P, Pb, Rb, Sb, Sc, Se, Sn, Sr, Te, Ti, V and Zn, originated from anthropogenic and natural sources. The release of trace elements into the atmosphere by anthropogenic activities is much more significant and is attributable to fossil fuel combustion, industrial processes, cremation, flight emissions, and metal processing at high temperatures (Ramli et al., 2020; Morakinyo et al., 2016; Dubey et al., 2012). Furthermore, traffic emissions release high levels of Cr, Ni and Mo (Das et al., 2015). Other sources of trace elements can be identified with the waste incineration, mainly emitting elements in the fine fraction (i.e. Cu, Zn, Cd, Sb, Pb, Ca, Cr, Mn, and Ni) (Ramli et al., 2020; Abbas et al., 2001), and with soil resuspension from paved roads, releasing elements mainly contained in the coarse fraction (i.e. Ti and Fe). Natural sources responsible for trace element emission are soil dust formation, sea spray, which leads to an enrichment in Cd, Cu, Ni, Pb and Zn, and forest fires, originating metals such as Cu, Pb and Zn (Sharma and Agrawal, 2005).

1.3 PM sampling, analysis, and chemical characterization

1.3.1 Sampling and measurement methods of PM_{10} and $PM_{2.5}$

An ambient air sampling system must be able to collect a sample that is representative of the atmosphere at a particular site. The sampling of PM can be sampled by different types of equipment that separates out the size fraction of concern. The measure of airborne particulate matter is effectively defined by the European Committee for Standardization (CEN). For PM_{10}, the European Reference Method is described in the CEN standard EN 12341, adopted by CEN in November 1998 (CEN 1998) while for $PM_{2.5}$ the standard are set in the EN 14907 adopted in 2005 (CEN 2005). These systems allow sampling PM according to the particle aerodynamic size. The conventional samplers are active system of PM collection, with a pump generating the pressure gradient necessary to draw the airflow through a collecting material: a filtration membrane able to retain the selected particles. A sampling head cut and select the particles of a certain size depending on their aerodynamic diameter. In addition, other major components of most sampling systems are the inlet manifold, that transports material from the ambient atmosphere to the collection medium (i.e. filter surface), and a flow measurement device that measures the volume of air associated with the sampling system (Vallero, 2008).

Active conventional samplers can be divided in two groups: the high-volume samplers (HVS) that permit to collect high amounts of dust on large filters (diameter 150 mm) and the low volume samplers (LVS) that allow to collect small amounts of dust on filter membranes of 47 or 37 mm diameter. A constant flow rate of 68 m^3 h^{-1} (1133 L min^{-1}) is required for a high-volume sampler, and 2.3 m^3 h^{-1} (38 L min^{-1}) for a low volume sampler to maintain the required PM cut point.

Among the low-volume samplers, low-cost and small devices for sampling PM were frequently applied in recent studies (Smart Sampler or High Spatial Resolution Samplers, HSRS, Fai Instruments, Fonte Nuova, Roma, Italy) (Massimi et al., 2020a, 2020b; Catrambone et al., 2019; Massimi et al., 2017).

Smart samplers are cheap, small, light, automatic, self-powered (with a power supply system constituted by a rechargeable battery and a small solar panel) and characterized by a flow of 0.5 L/min (with a very low consumption of 0.2 W for the intake system). These devices can be set on the territory in a high number of units at affordable cost. In fact, they can be set up on different sampling stands, such as railings, streetlights, and balconies. Consequently, they can be used to realize an extensive monitoring network with a huge spatial resolution. Furthermore, with the smart samplers it is possible to have a good representativeness of analytical data of the PM composition (Massimi et al., 2020a, 2020b; Catrambone et al., 2019; Massimi et al., 2017).

Particles can be also fractionating in restricted ranges of different aerodynamic diameters through multistage impactors, or cascade impactors, each stage (two or more) of which removes particles of progressively smaller diameter. Each impactor stage consists of a specific aerodynamic diameter range and successive stages are aimed to collect smaller particles (Hering et al., 1978). PM sampling in multiple stages permits the determination of the chemical composition as a function of the particle size, for a detailed chemical size evaluation. The air stream containing the various size airborne particles are accelerated to a uniform velocity by a pump and flows through the first large jet nozzle and impacts on a collection plate oriented perpendicular to the axis of the nozzle. Particles pass through every plate and are exhausted through a back-up filter. Larger particles are collected on the first plate, while the smaller particles follow the air stream into the following nozzles, with smaller jet and a higher velocity, permitting the smaller particles to be collected on the successive collection plates (Vallero, 2008).

Different filtering membranes can be used to collect PM, such as glass and quartz fiber, polytetrafluoroethylene (PTFE), and polycarbonate filters. The choice depends on the chemical analysis to perform after PM collection. Table 1 reported some advantages and disadvantages of the most used filters used for PM collection.

Table 1. Commonly used filter media for PM sampling (Vallero, 2008).

Filters	Advantages	Disadvantages
Polycarbonate filters	- Low blank levels - Low hygroscopicity - Low blank weight	- Inappropriate for carbon analysis
Cellulose fiber filters	- Low ash content	- Can easily ignite - Absorb water - Enhance the artifact formation of sulphate and nitrate
Glass fiber filters	- High retention capacity - Ability to withstand high temperatures - Non-hygroscopic	- Release of material due to the fibrous structure - Fragile, must be handled with care
Quartz filters	- Resistance to high temperatures - Available to analyze carbonaceous compounds by means of thermal methods	- Tendency to adsorb volatile organic compounds.
PTFE filters	- No release of material due to the continue structure - Low blank value, suitable to analyze trace elements - Low hygroscopicity - Negligible tendency to absorb or react with gases	- Fast clogging with high PM concentrations. - High blank weight - Typically very brittle, require careful handling

1.3.2 High time resolution PM sampling

In the last few years, the development of time-resolved techniques for the chemical characterization of atmospheric particles has gathered growing consensus between researchers, as these techniques are essential for the comprehension of the complex physical-chemical behavior of atmospheric pollutants. Furthermore, the optimization and the employment of high time resolved instruments for collecting aerosol particles permit to identify and investigate a series of phenomena difficult to trace with samplings with daily resolution. Among these, sporadic events, such as long-range transport from neighboring countries or local occasional emissions (i.e. biomass burning; Saarnio et al., 2013), affect PM composition and knowledge about the timing and intensity of these specific episodes may be important to assess human exposure and to establish right risk mitigating strategies. Therefore, the use of instruments for obtaining high-time-resolution data is useful to

acquire information about the behavior of individual PM sources, thus permitting to increase the information relative to the discrimination of contribution due to different local emission sources and to identify and characterize episodes of long- range transport. Lastly, these techniques do not involve sampling on membrane filters, therefore are not subjected to sampling artifacts.

The high time resolution PM sampling techniques are divided into physical methods, such as optical particle counters, and chemical methods. In this PhD research, the attention will be focused on a system belonging to the second category: the Particle Into Liquid Sampler (PILS).

The PILS was developed by Weber et al. (2001) and allows obtaining PM_X samples of particulate in aqueous solutions, with high temporal resolution.

The system consists of three main components:

1. particle growth zone;
2. particle impact and collection of the solution section;
3. the section of direct connection to the instrument used for the analysis, such as IC, ICP-MS, UV-Vis (Simonetti et al., 2018a; Oakes et al., 2010; Timonen et al., 2010).

The principle on which the operation of PILS is based provides a growth of particles in supersaturated water vapor thus creating droplet sufficiently large to be collected by inertial impaction and chemically analyzed online or offline. In detail, the system (Figure 3) consists of vapor generator placed perpendicularly at the inlet of the sampled air flow, a central cylinder which acts as a growth chamber, and finally an impact structure where the particles are successively collected. The water vapor, which is obtained by heating deionized water through a system of electrical resistances, meets the flow of sampled air (inlet by a vacuum pump at about 15 L/min) at the beginning of the conical structure. This happens for two reasons: to avoid the high temperature of the vapor that can change the structure and composition of the particulate, and to ensure that it works in supersaturation conditions. Furthermore, in order to maintain the supersaturated environment constant, the heating temperature must be constant and, therefore, the temperature value is constantly checked by a thermocouples' system.

The sampled particulate move along the growth chamber up to the impact surface by an inertial push. The impact plate is made of quartz, which is continually "washed" by the collection solution. To make homogeneous the whole impact surface, a steel grid is applied around the quartz plate.

Since ambient gases are also present in the aerosol sample, and they influence the particle measurement, it is necessary to place denuders inline, upstream of the PILS to remove gas phase species (Orsini et al., 2003). Lastly, the system is equipped with a PM_X head.

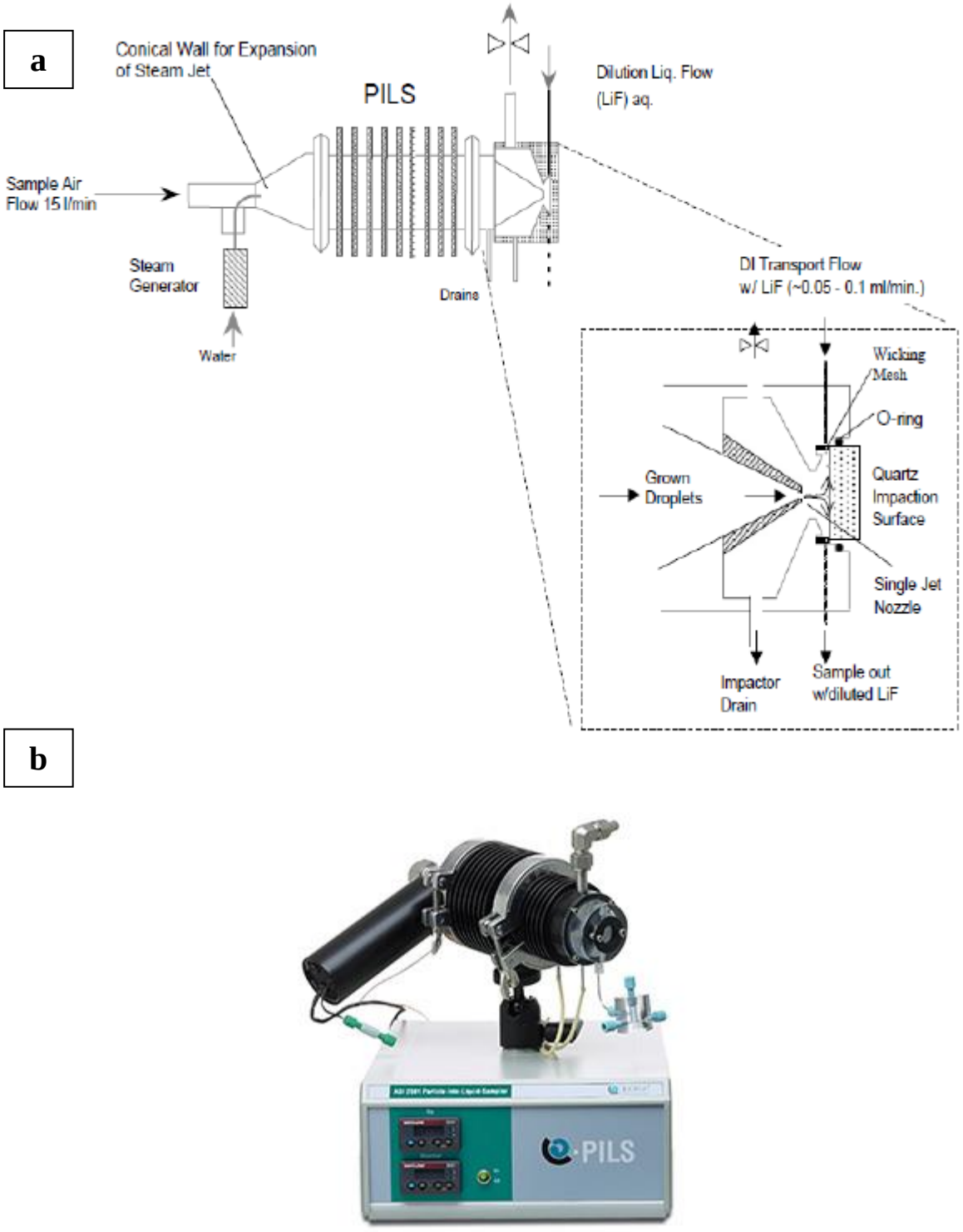

Figure 3. Schematic representation of Particle Into Liquid Sampler (panel a; PILS; Orsini et al., 2003), and picture of the instrument (panel b).

1.3.3 PM analysis

After sampling, PM filters are subjected to weight determination and chemical analysis. The mass of PM deposited on filters is gravimetrically determined weighting filters before and after sampling, after conditioning at 50% relative humidity (R.H.) and 20 °C for 48 hours, using a microbalance, as required by the UNI EN 12341 (2014).

Mass concentration units for ambient measurements are mass (μg) per volume of sampled air (m^3).

The chemical composition of particulate pollutants is determined in two forms: specific elements, or ions, or specific compounds. The determination of chemical composition is useful in identifying the sources of airborne particles and in understanding the fate of particles in the atmosphere.

Elemental analysis is used to describe the individual elements present in a sample, but not the chemical form in which it is present. Macro-elements Al, Fe, K, Mg, Ca, Ti, S and Si are analyzed by energy-dispersive X-Ray fluorescence (XRF), a non-destructive technique used for direct elemental analysis. Inner shell electrons are excited to higher energy levels. When excited electrons return to their original state, energy with wavelengths characteristic of each element present in the sample is emitted. These high-energy photons are detected and analyzed. Therefore, the type and quantity of the elements present in the sample are determined (Perrino et al., 2020; Barnaba et al., 2017; Dzubay, 1977). Subsequently, PM are water-extracted from the filters (in most cases), then acid-digested in a microwave oven to obtain the PM mineralized residue fraction. Trace metals are determined in both the water-soluble and residue fractions by inductively coupled plasma with optical (ICP-OES) and mass spectrometer detection (ICP-MS).

In detail, in this research work PTFE filters were subjected to a chemical fractioning procedure, previously optimized, and validated (Canepari et al., 2006a, 2006b, 2010), for the determination of the water-soluble and insoluble fraction of the elements in PM samples. After the PM water-extraction, the solution is divided in two aliquots. One aliquot is analyzed for anions (Cl^-, NO_3^- , SO_4^{2-}) and cations (Na^+, NH_4^+, Mg^{2+}, Ca^{2+}) by Ion Chromatography (DX 100, DIONEX Co., CA-USA),

The other aliquot is filtered through cellulose nitrate filter (NC; pore size 0.45 μm) and analyzed for a wide range of elements (Al, As, Ba, Be, Bi, Cd, Ce, Co, Cr, Cs, Cu, Fe, Ga, K, La, Li, Mg, Mn, Mo, Na, Nb, Ni, P, Pb, Rb, Sb, Se, Sn, Sr, Te, Ti, Tl, U, V, W, Zn, Zr) by ICP-OES and/or ICP-MS. The residual filter and the NC filter are acid-digested in a mix of HNO_3 and H_2O_2 (2:1) using a microwave oven and the obtained residue fraction is then analyzed by ICP-OES (Vista MPX CCD Simultaneous, Varian, Victoria, Mulgrave, Australia) and/or ICP-MS (Bruker 820-MS, Billerica, MA, USA, equipped with a glass nebulizer, 0.4 mL min^{-1}; Analytik Jena AG, Jena, Germany) for the same elements of the soluble fraction.

Overall, this procedure allows the determination of macro-elements (including Al and Si, which show a low recovery after the acid digestion), soluble inorganic ions and the extracted and residual fractions of micro and trace elements on a single PM filter. Furthermore, the determination of the same element with different analytical techniques (i.e. Fe, Mg, S) makes it possible to check the quality control of the determinations by means of inter-techniques comparison (Canepari et al. 2009). For each detected element, external standard calibration curve is performed, and internal standards are used to assure the control of the elemental analysis.

The **inorganic ionic fraction** is analyzed through different analytical procedures. Analysis of anions is possible by colorimetric techniques and ion chromatography. Sulfate, sulfite, nitrate, chloride, and fluoride are determined by ion chromatography, the most used analytical method for ionic determination.

A variety of methods is available for the measurement of the **carbonaceous compounds** of the aerosols collected on filters. The recommended method to determine EC is based on the volatilization and oxidation of the sample, followed by the determination of the evolved CO_2, either directly or after conversion to CH_4 by a flame ionization detector (FID). In addition, elemental carbon (EC) and organic carbon (OC) can be analyzed through thermo-optical analysis (TOA) using the NIOSH-QUARTZ temperature protocol.

2. Effects of PM on environment and human health

2.1 General regulation of PM air pollution

PM pollution has become a global concern and requires targeted control measures and emission reduction regulations to assure a sustainable development for the next generations. Ambient PM is regulated in terms of mass concentration (in $\mu g\ m^{-3}$).

The European Union (EU) has developed an extensive body of legislation which establishes standards and objectives for several pollutants in air. The EU's air quality Directive 2008/50/EC Directive on Ambient Air Quality merged into a single directive the existing legislation, and established PM concentrations thresholds that shall not be exceeded in a given period of time. The Directive promoted further studies in the air quality field and recognized, for the first time, the limits of the only PM mass concentration determination. It introduced the measurement of the $PM_{2.5}$ mass concentration, considered potentially more dangerous to human health, while the limit values for PM_{10} have remained unaltered.

In Italy, the key environmental legislation is Legislative Decree n. 152/2006, named "*Norme in materia ambientale*", "*Codice dell'Ambiente*" or Environmental Consolidated Act.

The Legislative Decree 13rd August 2010 (amendments and additions were made to this by Legislative Decree n. 250 of 24th December 2012), n. 155 implements the Directive 2008/50/EC and 2004/107/EC (concerning arsenic, cadmium, nickel, mercury, and PAHs in ambient air). The Decree reorganized and repealed some previous regulations that governed the matter in a fragmented way and established a single regulatory framework for the assessment and management of ambient air quality. According to the Decree, to comply with the limit values is necessary to mitigate, prevent and reduce harmful consequences for human health and the environment overall.

Selected air quality guideline values are summarized in the Table 2.

Table 2. Values recommended by Legislative Decree n. 155/2010 for atmospheric particles concentration ($\mu g/m^3$).

Particles	Exposure time	Guideline values ($\mu g/m^3$)
PM_{10}	24-hour mean	50 (35 days of exceedance)
	Annual mean	40
$PM_{2.5}$	Annual mean	25

2.2 Environmental effects

It is well known that PM pollution can have serious effects on the environment, such as climate change, tropospheric ozone formation, visibility impairment and hydrology disruption, and, of course, on living organisms.

Particles become available to the **vegetation** directly via the two deposition pathways, wet and dry deposition, and indirectly by changing soil chemistry or the amount of radiation reaching the Earth's surface. Indirect effects through the soil are usually the most relevant because they can alter nutrient cycling and inhibit plant

nutrient uptake (Grantz et al., 2003). Measurable direct responses of the vegetation to both coarse and fine PM include reduction in photosynthesis, changes in soil salinity, and foliar effects that result from nitrate and sulfate and their associations in the form of acidic and acidifying deposition and trace elements and heavy metals (Grantz et al., 2003).

The major effect of fine particles on vegetation is dominated by occult and wet deposition of dissolved ions containing hydrogen, sulphates, and nitrates. This process is called **acid rain**: gaseous components (SO_2, SO_3, NO_x and CO_2) coming from combustion and industrial activities can be transformed in acid (H_2SO_4, HNO_3, HNO_2) by means of reactions with H_2O or OH radical, giving rise to acid precipitations. These phenomena can cause serious alterations of the chemical composition of the vegetation resulting in a rapid decline of some forests.

Finally, the uptake of heavy metals could result in metabolic effects in plant tissues above ground by limiting the uptake of essential nutrients. However, in many cases, the impacts of specific chemical constituents of PM are not well understood due to the heterogeneous nature of PM composition (Grantz et al., 2003).

PM plays a determinant role in **global warming** through its radiative effects (Chubarova et al., 2019), which depends on the particle size and chemical composition and can lead to a cooling or a warming effect: on one hand, particles reflect sunlight, leading to a cooling of the earth surface, on the other, they have a role in the absorption of terrestrial infrared radiations, contributing positively to the global warming.

The light absorption is directly related to the chemical composition of the particles; carbonaceous substances strongly absorb the solar radiation: EC, which is often referred to as BC, has been reported as the most effective light absorbing carbonaceous component, along with brown carbon (BrC), but some OC species can also absorb radiation (Park and Son, 2017; Laskin et al., 2015; Barry and Chorley, 1992).

Lastly, the abundance of PM in the environment is very crucial for the acceleration of the **atmospheric corrosion phenomena** (Gil et al., 2017). In fact, particles can corrode materials such as calcareous stones through acid rain, playing a pivotal role in the deterioration of materials used in buildings and cultural monuments, causing therefore an inestimable damage (De Marco et al., 2017).

2.3 Effects on human health

Several studies have generally demonstrated the detrimental effects of PM on human health. Particulate matter with the aerodynamic diameter of less than 10 μm (PM_{10}) can deeply penetrate the human respiratory tract and cause a variety of chronic and acute health effects depending on the exposure time to the pollutant.

Short-term exposure to PM can determine several forms of **cardiovascular and respiratory diseases**, such as bronchitis, asthma, changes in heart rate variability (Miri et al., 2017). Long-term exposure can lead to congenital heart defects and deleterious effects on the cardiovascular system (Hamanaka and Mutlu, 2018; Agay-Shay et al., 2013), such as myocardial infarction, arteriosclerosis, and ischemic heart disease (Zhang et al. 2014); **pre-term birth risk and adverse birth outcomes** (Schifano et al., 2013; van den Hooven et al., 2012), lung cancer, negative effects on natural development and cognitive capacities leading to **Alzheimer's disease, and dementia** (Losacco and Perillo, 2018). PM exposure may be also linked to **obesity** and new-onset **type 2 diabetes** in adults (Losacco and Perillo, 2018; Janghorbani et al., 2014).

Several studies indicates that the chemical composition, surface area and other characteristics of PM are potentially more closely linked to the induction of toxic responses. The BC, OC, nitrates, and sulphates are frequently associated with respiratory and cardiovascular illness in a short time lag (Janssen et al., 2012; Kim et al., 2012). Metals as As, Co, Cr, Ni, Pb, e Hg can enter the body threatening human health, especially that of children (Maas et al., 2010). Chronic exposure to these metals can cause various diseases, such as brain pathologies (Fang et al., 2013) and neurological and developmental disorders (Chen et al., 2019). Furthermore, some metals may also act as cofactors in the onset of other diseases (Fang and Zheng, 2014).

In recent times it has been widely hypothesized the direct role of PM as a carrier for Severe Acute Respiratory Syndrome Coronavirus 2 (**SARS-CoV-2**), or Coronavirus disease 2019 (**Covid-19**) (Tung et al., 2021; Setti et al., 2020), as well as the indirect role via upregulation of angiotensin-converting enzyme 2 (ACE2) that represents the main entrance for SARS-CoV-2 infection due to the higher affinity of the spike glycoprotein of SARS-CoV-2 for ACE2, whose receptors provide an adhesion site for SARS-CoV-2 to invade cells (Vankadari and Wilce, 2020; Wrapp et al., 2020; Hoffmann et al., 2020). The possibility that exposure to air pollutants may contribute to increasing the vulnerability of a population to COVID-19 is plausible (Contini and Costabile, 2020). However, the role of PM in SARS-CoV-2 transmission remains unclear and the interpretation of data is still uncertain and will continue to be a focus of additional research in future years (Tung et al., 2021; Contini and Costabile, 2020).

Most epidemiological studies have used the total mass of PM as a principal metric to correlate the exposure levels with adverse health outcomes (Cohen et al., 2017). However, in the last recent years, has become increasingly aware that PM mass as exposure metric does not reveal the intrinsic PM chemical characteristics or toxic potential, which is crucial for identifying and investigating adverse health effects and, thus, the involved emission sources (Dey et al., 2021; Costabile et al., 2019; Yang et al., 2016).

2.4 Oxidative stress induction

An actual common thesis claims that one of the major biological pathophysiological mechanisms involved in developing damaging health effects and promoting chronic diseases is the PM ability to induce oxidative stress. Oxidative stress occurs when natural antioxidant defenses cannot counterbalance the excess of reactive species or radical species (reactive oxygen/nitrogen species; ROS and RNS, respectively) resulting in a redox state change in cells that can initiate inflammation in respiratory and cardiovascular systems, alter DNA, protein, lipids and, in general, cells and tissues (Feng et al., 2016).

ROS are any oxygen-containing molecules that have one or more unpaired electrons, making them highly reactive, such as hydrogen peroxide (H_2O_2) singlet oxygen, hydroperoxy radical (HO_2), alkoxy radicals (RO), alkylperoxy (ROO), ozone (O_3), hydroxyl radical (•OH) and superoxide anion ($O_2^{\bullet-}$) (Thompson, 2018; Cross et al., 1994). These species can enter the body via PM inhalation with ROS directly bound to the particles, defined as particle-bound ROS, and/or can be intracellularly generated by catalytic generation of ROS in vivo via cellular redox reactions stimulated by specific inhaled PM components (Dellinger et al., 2001; Obrien, 1991). These different species varies considerably in reactivity and longevity and may elicit different effects in cells and tissues (Øvrevik, 2019). Furthermore, they can react with metals, oxygen, or other substances to

form catalytic cycles that increase oxidative stress and regenerate mediators of the reactions (Thompson, 2018).

The respiratory tract lining fluid (RTLF) is the interface between the respiratory tract epithelial cells and the inhaled PM. As the first line of defense, it contains a variety of antioxidants, including low molecular mass antioxidants, such as ascorbic acid (AA), reduced glutathione (GSH) and metal-binding proteins, enzymatic antioxidants, such as superoxide dismutase (SOD), that catalyzes the dismutation of O_2^- to H_2O_2 and O_2, catalase (CAT), that decomposes H_2O_2 to H_2O, and glutathione peroxidases (GPXs), that reduces H_2O_2 by oxidizing GSH (Cross et al., 1994; Kelly et al., 2003). These antioxidants defend against oxidative damage of intracellular ROS and maintain a balanced oxidative status in living organisms. If cellular antioxidant defense systems are overwhelmed, the oxidative stress occurs and trigger a cascade of adverse events associated with necrotic and/or apoptotic cellular processes. Therefore, the right balance between oxidizing and antioxidant substances is essential to maintain unaltered physiological functions.

Several studies indicates that the chemical composition, surface area and other characteristics of PM are potentially closely linked to the induction of toxic responses (Moreno-Rios et al., 2022; Visentin et al., 2016; Kelly et al., 2012). Although there is still debate about which particle components are responsible for ROS generation, there is accumulating evidence that pro-oxidative organic chemical compounds and transition metals play a pivotal role in ROS production (Xia et al., 2006).

For example, transition metals such as iron (Fe), copper (Cu) are considered important in PM induced formation of ROS through the Fenton reaction:

$$Fe^{2+} + H_2O_2 \rightarrow Fe^{3+} + OH\cdot + OH^-$$

$$Fe^{2+} + O_2 \longrightarrow Fe^{3+} + O_2^-$$

$$Fe^{2+} + O_2^- + 2H^+ \longrightarrow Fe^{3+} + H_2O_2$$

Furthermore, the organic fraction of PM, including compounds such as PAHs and quinones, can catalyze production of ROS by undergoing redox recycling and reducing oxygen to produce superoxide radicals (Cho et al., 2005).

The inflammatory response after deposition depends also on particles surface area in addition to their composition. Indeed, fine particles and their larger surface area are more prone to induce adverse effects than coarse ones (Sager et al., 2008; Duffin et al., 2007). Ultrafine particles can reach the alveoli and diffuse into the cardiovascular system by crossing the air-blood barrier (Nozza et al., 2021; Upadhyay et al., 2014).

Therefore, to investigate the possible harmful effects caused by exposure to PM and its contribution to the onset and spread of adverse events, it is important to focus on two aspects: the study of the chemical composition of particles and the measurement of the oxidative potential (OP).

3. Traceability of emission sources through elemental chemical analysis and oxidative potential measurements

As already mentioned, PM exhibits a very complex and variable composition and toxicology. Information about concentration, size, and form of the various chemical species in PM and the relative relevance of single source contributions to PM mass concentration and composition, can be of great help in providing valuable information for the source apportionment, the study of particle ageing processes and the identification of health and climate effects (Bernardoni et al., 2017; Gao et al., 2016; Liu et al., 2015; Cassee et al., 2013; Canepari et al., 2008). Furthermore, knowledge of key chemical constituents of PM is essential to properly plan PM control strategies and mitigation measures to protect citizens health, as well as to verify the effectiveness of PM emission regulation and control.

Although most of the studies reported the determination and the investigation of total element concentration, in the last years different procedures have been developed to study the solubility of elements, their mobility and their bioaccessibility (Canepari et al., 2009a, 2009b). The technique that will be discussed in this work is the **chemical fractionation procedure** for the determination of water-soluble and insoluble fraction of elements consisting in the independent measurement of elemental fractions characterized by different solubility (Canepari et al., 2009a, 2009b). Chemical fractionation procedure improve the selectivity of elements as source tracers since it allows assessing the chemical form in which each element is released in PM, and for many elements, the water-soluble and insoluble fractions are released by different typical emission sources (Massimi et al., 2020b). Therefore, the procedure ensures a better accuracy in the use of tracers for the identification of PM sources, and it constitutes a precious key tool for evaluating the strength of PM emission sources.

Source apportionment is a technique to identify and quantify the emission contribution from different sources at receptor site, which is the base of air pollution control and an increasing importantly component in air quality planning and management (Hopke 2016). Several receptor models are commonly applied to the chemical data in PM source apportionment, including Chemical Mass Balance (CMB), and multivariate models, such as the Positive Matrix Factorization (PMF) (Pio et al., 2020; Querol et al., 2007; Reff et al., 2007; Paatero and Tapper, 1994).

Over recent years, it has become increasingly relevant to link the chemical species and compounds, and emission sources of PM with its oxidative potential, which could provide useful information about sources that release PM with greater potential toxicity, thus evaluating human exposure (Cesari et al., 2019; Taghvaee et al., 2019; Yu et al., 2019).

Results from studies on the correlation between PM chemical composition and its OP revealed the components having a strong redox activity, such as metals (i.e. Fe, Cu, Mn, and V), WSOC, EC, OC, and PAHS (Chirizzi et al., 2017; Samara et al., 2017; Charrier and Anastasio, 2012; Akhtar et al., 2010; Kleinman et al., 2007).

One of the most frequently adopted approaches in estimating source contributions to OP are: linear or multi-linear regression between OP and chemical species concentrations to identify known tracers of specific sources (Pietrogrande et al., 2018b; Verma et al., 2009), the quantitative analysis performed applying multi-linear

regression to the outputs of receptor models (i.e. Principal Component Analysis, PCA; Chemical Mass Balance, CMB; Positive Matrix Factorization, PMF) regressing contributions of PM sources against measured OP values (Park et al., 2018; Simonetti et al., 2018b). Lastly, another approach is the inclusion of the OP results to the input in the PMF receptor model coupled with data from other different measurement techniques (Cesari et al., 2019; Costabile et al., 2017; Verma et al., 2014). However, the number of these studies is still limited, and they do not always consider relevant variables, such as seasonal cycles (Weber et al., 2021). Therefore, this research field is innovative and promising, although it requires long monitoring campaigns to obtain extensive dataset to process, and the involvement of different measurement techniques.

Integrated knowledge of PM chemical composition, oxidative potential, emission sources, geographical area peculiarities, and meteorological data will permit to incorporate PM chemical properties in epidemiological modeling studies for health risk assessment and risk mitigation strategies development, to properly mitigate the adverse health effects of PM pollution.

3.1 PM biomonitoring

Increasing concerns about atmospheric pollution caused by PM highlight the requirement to establish strategy controls, mitigations plans and control actions.

Effective air pollution investigation involves the identification of the emission sources of PM, the evaluation of their relative contributions and related risk assessment, as well as the development of appropriate analytical methods (Kousehlar and Widom, 2020). However, long-term sampling and measurements of PM require a large number of monitoring sites to obtain a high spatial monitoring network, and appropriate equipment that sometimes requires considerable resources.

The **biomonitors** are organisms mainly used for the quantitative determination of contaminants and can be classified as being sensitive or accumulative (Conti and Cecchetti, 2001).In the last years, different types of biomonitors were proposed as atmospheric pollutant passive samplers, such as trees, lichens, and mosses, with an improved monitoring spatial resolution (Massimi et al., 2021a; Castellani et al., 2020; Ristorini et al., 2019; Gratani et al., 2008).

Airborne PM has shown a higher potential to be captured by trees (Chiam et al., 2019). The main advantage of plants as PM biomonitors is their wide distribution that provides a high density of sampling points (Moreno et al., 2013). Plants can be used as biomonitors through ecological investigation thanks to their simple identification and sampling, their innate characteristics, their ubiquity, and their large amount of biomass (Giordano et al., 2021; Nowak et al., 2006). Moreover, the use of plants for biomonitoring can provide information also about their adverse effects on living systems, considering that plants that are the primary receptors for air pollutants (Stevens et al., 2020; Solgi et al., 2020).

It has already been proven that trees and shrubs efficiently remove PM from ambient air and recent studies highlighted that data regarding collected PM on leaves are comparable to those obtained by air quality monitoring stations near sampled trees (Muhammad et al., 2020; Baldacchini et al., 2017; Popek et al., 2013; Sæbø et al., 2012). Other researchers suggested that properly designed and maintained urban meadows should

serve as a valuable supplement to other elements of nature-based solutions, such as shrubs and trees, for air pollution monitoring and mitigation in cities (Przybysz et al., 2021).

Several studies demonstrated that lichens and mosses have a great capacity to retain pollutants due to their ability to accumulate them. For these reasons, this kind of biomonitors can serve as a tool for high spatial resolution analysis emerging as a valid alternative to traditional air quality monitoring networks (Massimi et al., 2021a; Castellani et al., 2020). For example, De Agostini et al. (2020) used moss transplants (*Hypnum cupressiforme* Hedw. moss bags) to assess the air quality around an oil refinery in Sardinia Island (Italy) and, after a monitoring period of 16 years, the authors confirmed the capacity of *H. cupressiforme* moss bags to provide relatively stable measurements. Massimi et al. (2019) demonstrated the reliability of lichens (*Evernia prunastri* (L.) Ach.) as biomonitors, due to their capacity of bioaccumulation of the elements that was found to be well correlated with the PM_{10} element concentrations obtained through the traditional monitoring tools.

The use of biomonitors as passive samplers can integrate information during in-field measurements being an efficient supplement to be used in synergy with the traditional monitoring systems. Furthermore, this approach is easy and inexpensive and permits to perform long-term and large-scale measurements thus obtaining robust and reliable dataset.

3.2 Indoor emission sources

Air pollution and its impact on human health are one of the most critical issues regarding the environmental implications related with atmospheric PM (Duarte et al., 2021). Air pollution exposure occurs both outdoors and indoors environments, in which people usually spend long time and receive most of the exposure to both outdoor and indoor-generated PM pollution (Bekö et al., 2020). In fact, PM can readily infiltrate into various indoor environments and adversely impact the indoor air quality.

Human activities, such as cooking, cleaning, and indoor sports activities, are likely to increase indoor PM, and exposure studies showed that indoor PM contributes substantially to personal exposure, and the indoor PM concentration levels may exceed those outdoors (Zhang et al., 2021; Kim et al., 2015; Lai et al., 2004). Furthermore, epidemiologic studies highlighted the relationship between indoor PM concentration and health disorders, such as lung malfunctioning, cardiovascular disease, respiratory symptoms, asthma, and premature births (Zhang et al., 2021, and references therein; Yamamoto et al., 2014).

Several studies have investigated the impact of PM on indoor air quality, but the chemical characterization of indoor PM and the apportionment of its emission sources is still object of intense research. In fact, chemical composition of indoor PM varies over time as a consequence of the activities carried out by people, due to the existance of primary and secondary indoor sources, such as cigarette smoke, cooking, and domestic heating (Tofful et al., 2021). Furthermore, indoor concentrations of primary biological aerosol due to the direct shedding of particles from bodies and clothing (skin flakes, hair, and other organic emissions), or to the presence of plants and pets (Marcovecchio and Perrino, 2021) should be considered.

In detail, recent studies highlighted that the indoor activities are able to increase the indoor particle number concentrations (He et al., 2004). For example, concentration of organic species was always higher indoors than outdoors, and was associated to the presence of people inside the house, to housekeeping activities and to the

use of the fireplace for cooking and/or domestic heating (Tofful et al., 2021). Furthermore, Cu concentration was higher due to the use of electric appliances equipped with brush motors, and the presence of a customary smoker was clearly traced by observing the concentration of soluble Cd (Tofful et al., 2021). Other research demonstrated that ndoor biomass burning a predominant source of indoor PM by increasing concentration of $PM_{2.5}$, EC and OC (Luo et al., 2021).

Overall, the identification and the characterization of indoor PM emission sources appears to be crucial because the focused estimation of the health effects due to the total exposure to indoor contaminants is essential to address the effect of indoor air quality to health outcomes, and represents one of the most challenging effords for the public health institutions

4. Overview of PM oxidative potential measurement methods

Oxidative potential (OP) of PM is considered one of the most relevant predictive factors for the assessment of PM toxicity (Delfino et al., 2011; Gupta et al., 2019), since it is intrinsically influenced by different physiochemical properties governing PM ability to cause oxidation of target molecules, including size, surface area, chemical composition and bioavailability of chemical species, synergistic interactions between chemical species and emission source impacts (Andrade et al., 2020). Therefore, OP predicts the PM intrinsic capacity to elicit damaging oxidative reactions and inflammations and is frequently proposed as a more biologically appropriate metric for addressing human exposure than bulk PM mass concentration. In fact, it recently emerged as a promising and integrative method for assessing health impacts induced by PM in a wide variety of environments (Yang et al., 2016; Bates et al., 2019; Nishita-Hara et al., 2019). Indeed, it is increasingly recognized that this PM property is more closely associated with adverse health impacts than ordinarily used PM mass concentrations.

4.1 OP assays

Reactive species can exist on PM or can be generated *in vivo* by specific compounds of inhaled particles, which chemically interacts with fluids and cells in the body. Multiple acellular tests are developed for quantifying these two phenomena and the related particles oxidative potential (Bates et al., 2019), leading to a rapid rise in OP measurements worldwide. One group of cell-free methods measure the capacity of PM to oxidize certain naturally occurring antioxidants in the human lung lining fluid over time, such as ascorbic acid and glutathione (OP^{AA} and OP^{GSH} assays, respectively), or a cellular reductant surrogate, such as dithiothreitol (OP^{DTT} assay), using units of time rate-of-change of volume-based concentration (nmol depletion per min per m^3 of sampled air), while particle-bound ROS techniques typically record radical species levels in units of concentration (i.e. 2',7'-dichlorofluorescein, OP^{DCFH}, assay).

The OP measurements used and discussed in this research work are the OP^{AA}, OP^{DTT} and OP^{DCFH} assays.

The **ascorbic acid (AA)** is an important dietary water-soluble antioxidant in the human respiratory lung tract fluid (RTFL), with a concentration of around 100-200 μM (Cross et al., 1994). AA can both act as an antioxidant by scavenging radicals and preventing oxidation of lipids and proteins, or as a pro-oxidant by reducing redox-active metals which can react with H_2O_2 to form the destructive • OH (Buettner and Jurkiewicz, 1996; Mahoney and Graf, 1986). The OP^{AA} consists in the measurement of the AA depletion that can be monitored via UV-Vis detection over a given time (Fang et al., 2016). The decrease in concentration of the ascorbic acid corresponds to the capacity of the PM reactive species to catalyze the transfer of electrons from AA to oxygen, determining oxidative potential.

The 1,4-**dithiothreitol** (termed as dithiothreitol**)** acts as a chemical surrogate of cellular reducing agents, such as nicotinamide adenine dinucleotide (NADH) and nicotinamide adenine dinucleotide phosphate (NADPH) (Kumagai et al., 1997, 2002). The assay is based on the measurement of the DTT depletion rate over time, due to PM components able to transfer electrons to DTT, whose concentration is proportional to the concentration of redox-active species (Figure 3). The concentrations of DTT over a given time points are determined via UV-Vis detection, thanks to the production of a yellow chromophore (Cho et al., 2005).

The OP^{AA} and OP^{DTT} assays mimic the crucial initial step of *in vivo* production of ROS or other radical species (Kumagai et al., 2002; Gupta et al., 2019). Therefore, these assays have considerable physiological relevance in the assessment of particle toxicity.

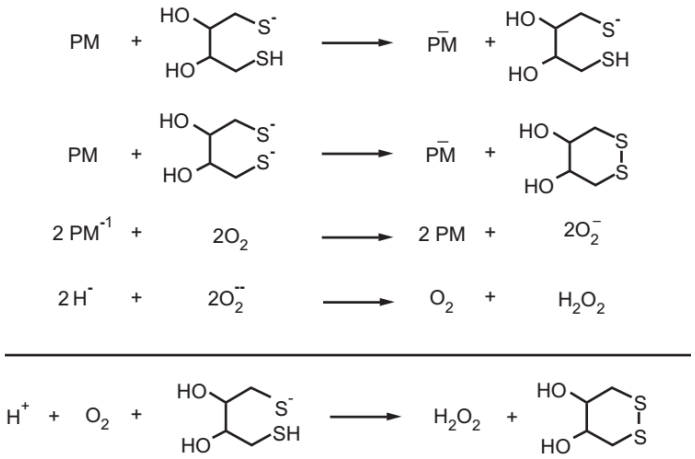

Figure 4. Basic mechanism of DTT oxidation by O_2 with PM as a catalyst (Cho et al., 2005).

The 2',7'-**dichlorofluorescein** (OP^{DCFH}) assay is commonly used in biological field as an indicator of oxidative stress in quantifying intracellular ROS generation, through a fluorescent-based probe on alveolar macrophage cell cultures derived from rat lung tissue (Venkatachari et al., 2005, 2007; Fuller et al., 2014). However, the test has been adapted to be performed on PM samples for determining total particle-bound ROS (Hung and Wang, 2001; Zhou et al., 2018) and is conventionally included in OP assays in several works in this research field (Simonetti et al., 2017; Crobeddu et al., 2017; Bates et al., 2019; Daellenbach et al., 2020; Zhang et al., 2021). DCFH is a non-fluorescent reagent that becomes fluorescent (DCF) when oxidized in the presence of ROS and horseradish peroxidase (HRP), a redox enzyme that primarily reacts with hydrogen peroxide and organic hydroperoxides. Figure 4 shows the reaction between DCFH /HRP with peroxides. Fluorogenic intensity of DCF is measured and converted to hydrogen peroxide equivalents, which is used as an indicator of the ROS reactivity, after calibration of the instrument with H_2O_2 standard.

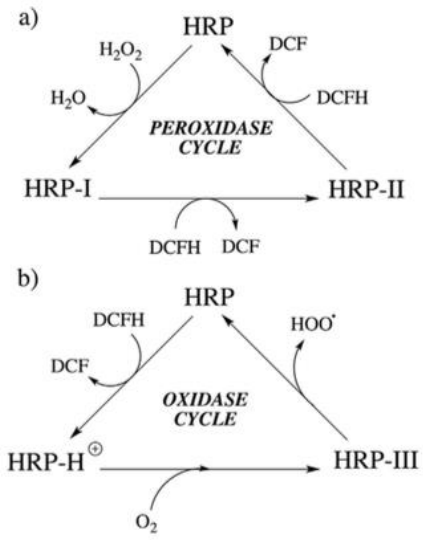

Figure 5. Reaction between DCFH /HRP with peroxides (Berglund et al., 2002). In the cycle a) it is shown the initial reaction of H_2O_2 with the HRP enzyme, followed by the DCFH reaction that leads to the formation of DCF fluorescence product. In cycle b) is reported the reaction of HRP with O_2 generating DCF.

All these acellular assays have their own sensitivities to different pathways of reactive species formation, depending on the nature of individual chemical compounds constituting PM samples and, thus, also on emission sources. Therefore, the combined application of different acellular methods on the same PM sample is strongly suggested and often considered advantageous in providing insightful assessment of particles OP (Ayres et al., 2008; Lin and Yu, 2020; Manigrasso et al., 2020).

Numerous studies have shown that OP^{AA} is mainly related to the redox activity of transition metals, but recent applications show further affinity for organic compounds, especially for quinones (Mudway et al., 2004). OP^{DTT} well correlates with both organics (i.e. WSOC, EC, OC, BC, quinones and hydroxyquinones) and transition metals (i.e. Cu and Mn) (Charrier and Anastasio, 2012; Visentin et al., 2016). Lastly, OP^{DCFH} is particularly sensitive to transition metals (i.e. Fe, Ni) and organics (See et al., 2007; Wang et al., 2010).

The particle size also play a crucial role in OP assays sensitivity. OP^{AA} is particularly sensitive to particles in the coarse mode, especially to those generated by vehicular traffic, such as brake abrasion and re-suspended road dust (Simonetti et al., 2018b). OP^{DTT} and OP^{DCFH} assays appear more sensitive to particles belonging to the fine mode, such as those generated by combustion processes, even if the DCFH assay shows higher sensitivity than DTT to particles in the larger size range (Simonetti et al., 2018b). Table 3 shows a short comparison of the discussed OP assays in terms of different sensitivity to chemical species, size, and emission sources.

Table 3. Short overview of OP acellular assays (Pietrogrande et al., 2018a; Simonetti et al., 2018b; Bates et al., 2019; Rao et al., 2020).

OP assay	Species	Size	Emission sources
OP^{AA}	Inorganic ions (Ca^{2+}, Mg^{2+}) Metals (Cu, Fe, Mn, Pb, Zn) Organics (OC)	Coarse mode	Non-exhaust traffic emissions. Resuspended soil from vehicular traffic. Long-range transport of Sahara dust.
OP^{DTT}	Inorganic ions (K^{+}) Metals (Cu, Fe, Mn) Organics (OC, EC, PAHs)	Fine mode	Biomass burning. Brake/tire wear. Fossil fuel combustion. Photochemical aging.
OP^{DCFH}	Inorganic ions Metals (Cr, Fe, La, Ni, Si, Zr) Organics	(Predominantly) Fine mode	Combustion. Biomass burning. Secondary aerosol.

4.2 OP in epidemiologic analysis

Toxicological, clinical, and epidemiologic analyses using acellular assays highlight that to a high OP correspond more serious health endpoints (Bates et al., 2019; Abrams et al., 2017; Yang et al., 2016). For example, OP^{DTT} has been shown to be most associated biological endpoints in several toxicological clinical, and epidemiological studies and has been appeared to be linked with various acute cardiorespiratory endpoints (Lionetto et al., 2019; Yang et al., 2016; Delfino et al., 2013; Steenhof et al., 2011). Furthermore, the positive association between OP measured by the DDT assay and asthma/wheeze in epidemiological and clinical studies was frequently highlighted. (Øvrevik, 2019)

On the other hand, OP^{AA} has been found to have no association with other adverse health endpoints in multiple studies, suggesting that this assay may be of limited utility in future epidemiologic studies of PM toxicity and effects (Bates et al., 2019; Øvrevik, 2019)

The relationship between PM exposure and the onset of adverse effects, including the toxicological mechanisms of action, are still not completely elucidated. One of the key issues with most OP assays is that they are not precise enough and do not sufficiently discriminate between different reactive species, and different assays detect different species and with varying efficiency (Øvrevik, 2019). Moreover, the lack of consistent association between OP and other PM-induced effects could be also related to study designs. Anyway, understanding the current state of knowledge on OP assays could guide future research investigating the epidemiologic relevance of various OP assays and deepen the relationship between PM and health endpoints.

4.3 Critical issue of OP measurement

In recent years, OP appeared to be the central paradigm in the assessment of PM toxicity and emerged as a useful multipollutant, multisource health indicator providing knowledge on the relationship between PM and

health endpoints. However, there are still several criticisms regarding the effectiveness of this metric to quantify the effects of ambient particles on human health. The key issue is represented by the lack of standardized operative conditions by which OP assays are performed. To date, no real consensus has emerged towards standardized protocols, adding variation in experimental design among laboratories that may contribute to dissimilarities between OP results, meaning that results are not directly comparable across studies (Guo et al., 2019; Lin and Yu, 2019). As a result, the ability of OP predict PM oxidant generating capacity has still to be extensively verified.

The most common approach in OP measurement is the collection of PM onto filters, followed by extraction into a liquid medium for performing OP assays. The choice of both the PM filters extraction methods and medium seems to alter OP quantification. In fact, although ultrasonic bath is the most common approach, some researchers studied the impact of sonication-derived free radicals on OP results, highlighting both the increase of free radicals in the systems, and the degradation of some compounds (Mutzel et al. 2013; Khurshid et al., 2014; Miljevic et al., 2014). This evidence has provided motivation for conducting further investigations to identify an alternative **extraction method**, such as vortexing, magnetic stirrer or orbital shaking, to avoid ultrasound-induced radicals (Perrone et al., 2016; Khurshid et al., 2014).

Other recent studies analyzed the effect derived by the choices of **extraction solvent** (i.e. methanol, water, phosphate buffer) and highlighted that the different filter extraction procedures generate differences in the measured OP of particles. For example, in a study comparing OP^{AA} and OP^{DTT} performed on different filter types and extraction solvents, Yang et al. (2014) found that the choice between methanol or water extraction had a significant effect on OP^{DTT}, but not on OP^{AA}. Pietrogrande et al. (2021) tested phosphate buffer, Gamble's solution, and methanol as extraction solvents on $PM_{2.5}$ filters and established that the phosphate buffer resulted the solvent that provided the most sensible measure of OP^{DTT}. The Milli-Q water remains the most used extraction solvent, especially when a detailed PM chemical characterization, mostly performed on the soluble fraction of PM, is required (Massimi et al., 2020; Simonetti et al., 2018b; Conte et al., 2017; Fang et al., 2015). Verma et al. (2012) revealed that an extraction with both Milli-Q water and methanol, performed in parallel on the same sample, is useful to extract both the hydrophobic and hydrophilic fractions of PM that equally contribute to OP. To continue, Calas et al. (2017) performed OP^{DTT} using extraction solutions that mimic lung fluid composition, the Gamble's solution, the artificial lysosomal fluid (ALF)'s solution and Gamble's solution added with dipalmitoylphosphatidylcholine (DPPC) (the major phospholipid of lung surfactant) in comparison with Milli-Q water. They found significant differences in OP^{DTT} obtained results depending on the selected extraction solutions. However, every extraction medium has its pros and cons and differs in various properties, such as pH, ionic strength, from physiological fluids encountered by PM in lung (Calas et al., 2017; Wiseman, 2015).

In the literature, most of the OP assays have been applied to polytetrafluoroethylene (PTFE) filters, despite other PM **sampling membrane** are often used, including quartz filters. Yang et al. (2014) found that OP measured using quartz filters was significantly lower than that obtained using PTFE membrane filters.

However, there is still a lack of information regarding the effect of the type of filter used for the OP measurement.

There are a broad range of **analytical techniques** applied for the analysis of PM OP. In fact, some researchers adapted or optimized reaction mixture composition. For example, in executing OP^{DTT} most researchers followed the experimental protocol developed by Cho et al. (2005). Other (Kramer et al., 2016; Lin and Yu, 2011; Rattanavaraha et al., 2011) adopted the method from Li et al. (2009), that is a simplified version. Lin and Yu (2019) reported that to a higher initial DTT concentration correspond to a higher DTT consumption rate for both organics and metals and, obviously, this may cause problems in the representativeness of the DTT assay. Certainly, the use of different methods adds difficulties to the inter-comparison of the obtained OP results.

Another potential factor altering OP measurements is the **time delay** between filter sampling and OP analyses, that seems to play a crucial role in misestimating particles OP, due to the possible decomposition and/or chemical transformation of the highly reactive components, prior to analysis (Fuller et al., 2014; Campbell et al., 2019). Indeed, it has already been suggested that the aging of the particles on membrane filter surfaces can cause an underestimation of collected reactive species (Hedayat et al., 2015). Online measurement technologies and semi-automated systems for measuring OP have been developed to overcome these phenomena and could constitute a valid alternative to avoid the loss of reactive species before analyses (King and Weber, 2013; Fuller et al., 2014; Wragg et al., 2016; Campbell et al., 2019). However, ROS are still mainly quantified by offline assays in extracts of aerosol particles collected on filters (Fuller et al., 2014).

In this context, an additional important point is related to the stability of the species. In fact, it is possible that within the conditions that influence OP results, there is also the reaction and/or competition between oxidant and **reducing species** naturally occurring in PM. In fact, some studies proved the presence of species with likely antioxidant and reducing characteristics such as phenols from wood burning, phenolic compounds from different sources, pollen, airborne bioaerosols that are biological in origin, and biological and vegetable components (Marcovecchio and Perrino, 2021; Buiarelli et al., 2019; Simoneit et al., 2007).

Lastly, another additional challenge in optimizing OP acellular measurements is assessing the contribution of **insoluble species** to PM oxidative capacity. As mentioned, OP assays are usually performed on water-soluble fraction of PM samples. Therefore, only water-soluble species are considered by OP assays. However, different studies suggested that water-insoluble components of PM play a determinant role in OP measurements and called into question of whether these components would be bioavailable *in vivo* (Daher et al., 2011; McWhinney et al., 2013; Conte et al., 2017). There is a growing consensus in wanting to explore the toxicological potential of insoluble particles. In fact, water-soluble and water-insoluble fractions of particulate matter exhibit different mechanisms of action in the body, and the insoluble fraction of PM often emerged as capable of generating oxidative damage, such as the disruption of the cell membrane (Knaapen et al., 2002; Daher et al., 2011; Zou et al., 2016; Conte et al., 2017; Gao et al., 2017; Piacentini et al., 2019).

To conclude, OP measurements are strongly influenced by synergic actions of multiple operative conditions altogether and no standardized experimental design is available to date, leading to variations in operative

conditions across laboratories. This may generate dissimilarities between OP results, thus reducing the reliability of OP assays to provide an accurate overview of the PM capability of inducing oxidative stress in living organisms. The application of standardized methods could permit to pool results from different laboratories facilitating the building of a large-scale OP database, thus, to perform population-level epidemiology studies and to identify the real role of OP to predict health outcomes.

5. (A) Analyses of PM for Localization and Environmental Impact Assessment of PM Released by Specific Emission Sources

Over the years, various epidemiological studies have spotlighted strong correlations between the exposure to particulate matter (PM) and the onset of disparate diseases. One of the most efficient tools for the formulation of better control strategies of the atmospheric pollutant is the PM source apportionment, which is relevant to identify the role of different particulate matter emission sources. In fact, the study of the spatial distribution of PM and its chemical compounds is essential for a reliable identification of emission sources, the evaluation of particle dispersion over the territory, the assessment of personal exposure and the development of focused pollution management strategies.

One of the main difficulties in PM monitoring is attributable to the complex nature of emission sources and to the differences in spatial and temporal scales over which the various components of PM operate, especially in urban environments (Zwack et al., 2011; Sportisse, 2009). In fact, urban areas are massively affected by different local emission sources, as well as sources producing dust typically dispersed over long distances. The development of extensive monitoring networks is crucial to provide data of PM mass concentrations and chemical compounds. However, the monitoring stations often can not cover a large area and PM-related data close to monitoring sites can be different to other distanced environments. Typically, in air quality control, the dispersion of air pollutants released from different emission sources is estimated through atmospheric dispersion mathematical models, without using wide and expensive monitoring networks. The modeling approach offers a series of advantages, such as the reduction of time and costs and the possibility of covering very large areas. However, these models also present some limitations, such as reducible error results due to the large number of different sources and the complexity of PM transport and transformation processes that the models scarcely consider, or due to inadequate air quality data input (Massimi et al., 2017; Almeida et al., 2006). Therefore, in the last few years, self-powered, automatic and very-low volume device for PM sampling on membrane filters has been developed with the purpose of allowing spatially-resolved determination of PM chemical components. This innovative sampler (High Spatial Resolution Sampler, HSRS; FAI Instruments, Fonte Nuova, Rome, Italy) assures long-term (1-2 months) collection of PM working autonomously for long periods of time and have already and successfully been employed for the construction of wide and dense air quality monitoring networks across urban and industrial areas (Massimi et al., 2017). In fact, the HSRS can be placed at short distance between each other, by covering a large area, and they are very quiet and very small. The employment of this innovative samplers permit to obtain a good representativeness of data and a substantial reduction of maintenance costs of the monitoring network (Massimi et al., 2020b; Catrambone et al., 2019; Massimi et al., 2017).

The approach described below can be also applied to estimate the exposure to PM and relative health risk for the individuation of the spatial relationships between OP data and PM sources and for identifying the relative relevance of single source contributions in building up OP values.

During the PhD research, the HSRS were employed in a wide and dense network across Terni, an urban and industrial hot spot of Central Italy (23 sampling sites, about 1 km between each other), for 15 consecutive

months, during which the spatial distribution of PM_{10} mass and elements was evaluated and mapped, as well as OP values. The HSRS were also placed in the city of Amersfoort (Netherlands) at 17 sites in a 5-month monitoring period (from September 2018 to February 2019), to assess the monthly spatial distribution of PM_{10} mass, and PM_{10} chemical compounds.

Always with a view to assess health and environmental impact due to PM emission and exposure, during the lockdown period adopted by Italy during 2020 to contrast the spread of the Coronavirus disease 2019 (Covid-19), PM monitoring campaign was carried out at three sampling sites in the Rome area (Montelibretti, Sapienza and Saredo), in which 24-h PM_{10} samples were collected and chemically characterized for organic and elemental carbon, levoglucosan, ions and macro- and trace-elements. The contribution to PM_{10} mass concentration and composition of emission sources during pre-lockdown, lockdown and post-lockdown periods, was assessed by applying the Positive Matrix Factorization (PMF) to the obtained chemical data (Paatero and Tapper, 1994; Querol et al., 2007). The lockdown condition of forced abatement of anthropic sources offered unique and relevant opportunities to quantify the reduction of the impact of anthropogenic sources of PM.

In recent years, biomonitoring appears as a low-cost and complementary method to standardized measurements of air pollutants by making up for the shortcomings of the traditional monitoring network, and to analyze air quality, thus obtaining information related to the population's exposure to air pollutants, aimed to wider spatio-temporal coverage, and to larger and more detailed database of air pollutants. At the same time, increasing attention has been given to the amelioration of air quality exerted by Green Infrastructures (GI), which can play a relevant role as Nature Based Solutions capable of adsorbing atmospheric pollutants like particulate matter (PM). However, PM can affect the functionality of vegetation through direct and indirect damages and, accordingly, its capacity to provide Ecosystem Services, including the biomonitoring activity PM accumulation capacity (Rai, 2016; Bussotti and Pollastrini, 2015; Sæbø et al., 2012). Indeed, a multidisciplinary biomonitoring activity comprehensive of a large number of sites and species should be promoted to detect emission sources and distribution patterns of airborne persistent pollutants when it is impossible, to apply a high-density instrumental monitoring of PM.

To verify the reliability of the biomonitoring techniques urban trees (*Quercus ilex* (L.)), lichen transplants (*Evernia prunastri* (L.) Ach.), and leaf deposition on riparian species (*Arundo donax* (L.)) were used along with other traditional monitoring techniques for the assessment of atmospheric element concentrations and for the evaluation of the impact of PM anthropogenic emission sources.

5.1 (A1) Identification and spatial mapping of tracers of PM_{10} emission sources using a high spatial resolution distributed network in an urban setting

Atmospheric Research (2021), 262, 105771-105784, doi: 10.1016/j.atmosres.2021.105771

Lorenzo Massimi[1,*], Joost Wesseling[2], Sjoerd van Ratingen[2], Iqra Javed[3], Maria Agostina Frezzini[1], Maria Luisa Astolfi[4], Silvia Canepari[1], Roel Vermeulen[5]

[1] Department of Environmental Biology, Sapienza University of Rome, P. le Aldo Moro, 5, Rome 00185, Italy;
[2] National Institute for Public Health and the Environment (RIVM), Antonie van Leeuwenhoeklaan 9, 3721 MA Bilthoven, Netherlands;
[3] School of Chemistry and Pharmaceutical Sciences, TUD – Technological University Dublin, City Campus;
[4] Department of Chemistry, Sapienza University of Rome, P. le Aldo Moro, 5, Rome 00185, Italy;
[5] Institute of Risk Assessment Sciences (IRAS), Utrecht University, Yalelaan 1, 3584 CL Utrecht, Netherlands.

*Corresponding author

Keywords: PM_{10} composition; chemical fractionation; source tracer; spatial distribution; seasonal variation; firework.

Abstract

We employed an experimental approach for high spatial resolution sampling and analysis of PM_{10}, allowing identification and spatial mapping of tracers of PM_{10} emission sources. Very-low-volume samplers were used at 17 sites in Amersfoort and at one regulatory reference site in Utrecht, The Netherlands, in a 5-month monitoring period (from September 2018 to February 2019), to assess the monthly spatial distribution of PM_{10} mass and PM_{10} chemical compounds. By performing principal component analysis on the obtained spatially-resolved data, selective and reliable source tracers were identified for soil dust (Ca^+, Cl^-, insoluble Al, Ce, Li, U and V), brake dust (insoluble Fe, Mn, Mo, Nb, Sb, Sn, W and Zr, water-soluble Fe, Mn, Mo and Sb), industrial and/or agricultural emissions (NH_4^+, water-soluble As, Co, Fe, Mn, Mo, Pb, Sb, Se, Sn and Ti), secondary organic and inorganic aerosols (water-soluble organic carbon, NO_3^- and SO_4^{2-}), biomass domestic heating (water-soluble organic carbon, levoglucosan, water-soluble Cs, Li, Rb and Tl) and New Year's Eve fireworks (K^+, Mg^{2+}, Na^+, water-soluble Al, Ba, Bi, Cr, Cu and Sr). The autumn and winter spatial mapping of the identified source tracers allowed us to effectively assess and localize the impact of the different PM_{10} sources and to evaluate the diffusion of the PM_{10} particles. This approach proved to be very effective to trace low-intensity PM_{10} sources and to map their seasonal spatial distribution. The obtained spatially-resolved chemical data can be used in further studies to evaluate spatial relationships between the concentration of PM_{10} air pollutants and adverse outcomes for human health. This approach promises to be a powerful tool for obtaining seasonal and spatially-resolved information about PM composition and sources in several study areas. The obtained information can be integrated with data from existing networks for a more reliable geo-referenced assessment of population exposure to PM, having high impact on the air quality management.

1. Introduction

Over the years, various epidemiological studies have spotlighted strong correlations between the exposure to particulate matter (PM) mass concentration and the onset of asthma, lung cancer, diabetes, and cardiovascular diseases (Pope and Dockery, 2006; Øvrevik et al., 2019; Schmitz et al., 2019). However, chemical characterization of PM is essential for the assessment of toxicological effects of the various PM components and for the evaluation of their impact on human health (Strak et al., 2012). Moreover, chemical analysis of PM allows identifying source tracers useful for the delineation of the impact of different emission sources.

Temporal and spatial distribution of PM compounds is highly variable, since it depends on different meteorological conditions and on the location and seasonal strength of the sources (Perrino et al., 2010; Canepari et al., 2014; Korhonen et al., 2019). However, conventional devices generally used for the collection of PM on membrane filters for subsequent analyses enable obtaining good temporal resolution, but do not allow assessing the spatial distribution of PM components with high resolution. In fact, their high cost and large size make it possible for them to be used only on a few points in large areas. The information obtained at these points is generally extended to wider areas by using mathematical models, which may not be able to correctly describe the complexity of transport and transformation processes of the PM compounds (Setton et al., 2010; Kloog et al., 2013; Minguillón et al., 2014).

In this study, an experimental approach for high spatial resolution sampling and analysis of PM_{10}, which allows the spatial mapping of the concentrations of PM_{10} mass and PM_{10} chemical components, was employed in the city of Amersfoort, The Netherlands. Recently developed, small-sized and very-low volume samplers (High spatial resolution sampler, HSRS; FAI Instruments, Fonte Nuova, Rome, Italy; Massimi et al., 2017; Catrambone et al., 2019) were used at 17 sites (approximately 1 km of distance between each other) in Amersfoort and at one regulatory reference site in Utrecht, during a 5-month monitoring period (from September 2018 to February 2019), to assess the monthly spatial distribution of PM_{10} compounds (water-soluble organic carbon, levoglucosan, ions, water-soluble and insoluble elements). This approach, previously described in Massimi et al. (2020b), has proven to be very effective for the impact assessment of spatially disaggregated and intensive emission sources of PM in a heavily contaminated area of Central Italy. However, it has never been used in less polluted areas with weaker emissions of PM, such as Amersfoort, The Netherlands (population ~156,000, non-industrialised).

This study is aimed to evaluate the efficiency of this experimental approach for the localization and impact assessment of PM_{10} sources, through the spatial mapping of chemical tracers of PM emissions, in an area with low anthropogenic impact. This approach may allow to identify local and/or temporal isolated events of air pollution, such as the burning of New Year's Eve fireworks (Greven et al., 2019). Moreover, it provides spatially-resolved chemical data on PM_{10} air pollution that can be used in further studies to relate spatial distribution of PM compounds with health effects and mortality (Knaapen et al., 2002; Toro et al., 2019; Chen and Hoek 2020; Fischer et al., 2020).

2. Materials and Methods

2.1 Study Area

Amersfoort (52°9′N 5°23′E) is a medium-sized city of 63.86 km^2 located in the center of the Netherlands, in the province of Utrecht. Amersfoort has one of the largest Dutch railway junctions with its three stations (Amersfoort Centraal, Schothorst and Vathorst), it is crossed by two highways (A1 and A28), and residential biomass combustion occurs during the cold season, especially in the south of the city (Fig 1).

In Amersfoort, throughout the year, the temperature typically ranges from 0 °C to 23 °C; the warmer season lasts about three months, from June to early September, while the colder months are December, January and February.

The average wind speed undergoes significant seasonal variations during the year. The windiest period is autumn and winter, with an average wind speed of over 18 km/h. In general, the predominant wind comes from the south-west. In the autumn-winter months, the predominant wind comes mainly from the south and sometimes from the west (Gelaro et al., 2017). Wind direction and wind speed roses for the 5-month monitoring period, compared to those of the period 2011–2020 (source of the data: https://www.knmi.nl/nederland-nu/klimatologie/uurgegevens), are reported in supplementary material S1.

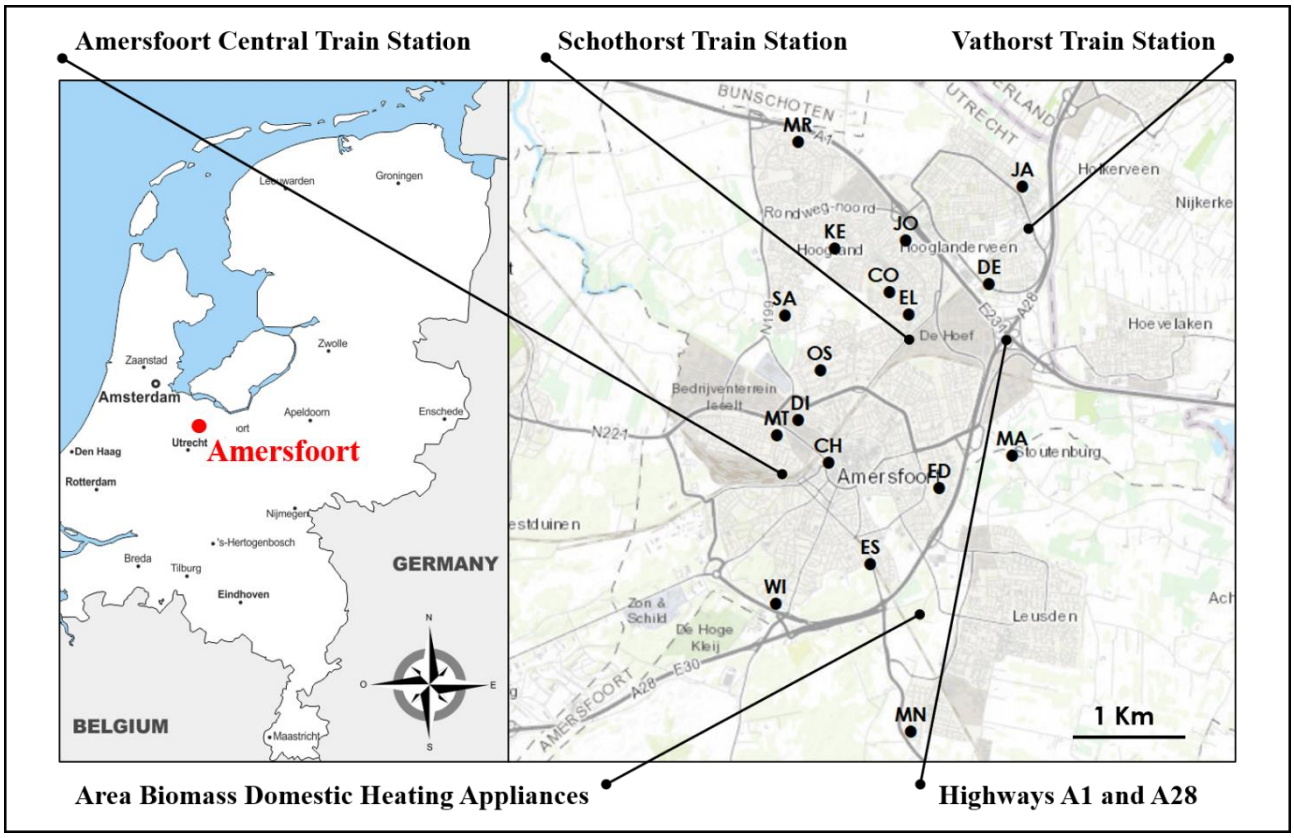

Fig. 1. Map of the 17 sampling sites in Amersfoort ~~the study area (Amersfoort,~~ (Netherlands) with the location of the main local emission sources of PM (ArcMap 10.3.1, ArcGis Desktop; ESRI, Redlands, CA, USA).

2.2 Sampling Sites

The sampling sites were chosen with the support of the Amersfoort city hall and the National Institute for Public Health and the Environment (RIVM, Bilthoven, Netherlands). Amersfoort city hall and RIVM recommended the best locations for the deployment of the HSRS, according to the presence of local emission sources and to their previous PM monitoring. The HSRS were installed and employed at 17 sites (MR, JA, KE, JO, CO, EL, DE, SA, OS, DI, MT, CH, ED, MA, ES, WI, MN) in Amersfoort, covering the study area with a spatial resolution of approximately 1 km (Fig. 1) and at one regulatory reference site (RS) in Utrecht, to identify reliable vehicular traffic tracers and to check PM_{10} variations not due to local emissions. At site JO, two samplers were employed to monitor sampling and analysis repeatability. All devices were installed within 6 m above ground level to ensure homogeneous sampling conditions. The geographical coordinates of the 17 sampling sites in Amersfoort and of the regulatory reference site (RS) in Utrecht are reported in Table 1. The possible local emission sources of PM in proximity of each site are detailed in Table 2, where the approximate distances (calculated using the software ArcMap 10.3.1; ArcGis Desktop; ESRI, Redlands, CA, USA) from each sampling site to potential sources are reported.

The 5-month monitoring campaign was carried out from September 8th 2018 to February 17th 2019.

Table 1. Geographical coordinates (decimal degrees) of the 17 sampling sites in Amersfoort and of the regulatory reference site (RS) in Utrecht.

Geographical Coordinates of the 17 Sampling Sites in Amersfoort		
	Latitude	**Longitude**
MR	52.204549°	5.376669°
JA	52.197903°	5.431991°
KE	52.188428°	5.385851°
JO	52.189775°	5.403229°
CO	52.181914°	5.399245°
EL	52.178557°	5.404134°
DE	52.18313°	5.423743°
SA	52.178312°	5.37347°
OS	52.170157°	5.382377°
DI	52.162568°	5.376833°
MT	52.160291°	5.371474°
CH	52.156056°	5.384303°
ED	52.152208°	5.411654°
MA	52.157256°	5.42963°
ES	52.140702°	5.394428°
WI	52.134736°	5.371209°

MN	**52.115462°**	**5.404635°**

Geographical Coordinates of the Regulatory Reference Site in Utrecht		
	Latitude	**Longitude**
RS	**52.105862°**	**5.124655°**

Table 2. Approximate distances (m) from each of the 17 sampling site in Amersfoort to potential local emission sources of PM; the shorter distances of the sources from each site are indicated in bold.

Sapling Site	Closest Commercial Area	Closest Trafficked Street	Highway A1	Highway A28	Closest Bus Stop	Closest Traffic Light (T) and/or Roundabout (R)	Closest Railway Track	Closest Train Station	Closest Farmland	Landfill
JA	2000	**110**	1800	**500**	220	250 (R)	520	**600**	400	2200
MR	1200	800	**200**	4900	**70**	830 (T)	3600	3800	**300**	**1000**
JO	400	150	**280**	2400	200	190 (T)	1200	1700	1700	**1300**
KE	800	300	1300	3200	240	720 (T) 560 (R)	1900	2000	1400	**1600**
CO	400	600	1000	2000	280	700 (T)	800	850	2400	2100
DE	**150**	**25**	**340**	750	180	560 (T) **70 (R)**	**260**	1200	900	2700
EL	350	270	1000	1700	**90**	330 (T)	290	**400**	2300	2500
SA	1200	270	2700	3600	190	440 (T) 380 (R)	1900	2100	350	3000
OS	700	240	2800	2700	100	470 (T) 220 (R)	870	1500	600	3600
MA	400	600	1500	750	500	800 (T)	1300	2300	**0**	5300
ED	500	770	2700	**280**	220	250 (T)	1600	2600	400	5500
DI	**0**	220	3600	3000	160	350 (T) 500 (R)	620	1000	1300	4600
MT	**270**	170	4100	3100	150	260 (T)	700	**700**	1500	4800
CH	450	140	3800	2200	**40**	**50 (T)**	**200**	800	2200	5000
ES	1300	**30**	4500	650	160	**100 (T)**	**60**	2000	700	6700
WI	2800	170	6000	**500**	200	280 (T)	1800	2100	2300	7600
MN	900	140	6500	2100	220	170 (T)	800	1000	**240**	9600

2.3 Sampling Equipment

The High spatial resolution sampler (HSRS; FAI Instruments, Fonte Nuova, Rome, Italy) is an automatic, small-sized and silent device (20x20x20 cm) that operates with a low flow rate: 0.5 L min^{-1}. It was equipped with 37 mm PTFE membrane filters (2 μm pore size, PALL Corporation, Port Washington, NY, USA) and worked in parallel at all sites for five 1-month sampling periods: September/October 2018, October/November 2018, November/December 2018, December/January 2019, and January/February 2019. The start and stop dates of each sampling period are reported in Table 3.

In the December/January monitoring period, one of the two samplers used at JO was stopped from 30/12/2018 to 3/1/2019 in order not to sample PM_{10} released by the burning of New Year's Eve fireworks, while the other one was left operating during the entire period.

Table 3. Start and stop dates of the five sampling periods.

Start and Stop Dates of the Five Sampling Periods				
Season	**Sampling**	**Period**	**Start Date**	**Stop Date**
Autumn	**1°**	**September/October**	8/9/2019	7/10/2018
	2°	**October/November**	13/10/2018	11/11/2018
	3°	**November/December**	17/11/2018	12/12/2018
Winter	**4°**	**December/January**	18/12/2018	13/1/2019
	5°	**January/February**	19/1/2019	17/2/2019

2.4 Analytical Procedure

PTFE membrane filters were weighed before and after sampling to gravimetrically determine PM_{10} mass concentrations. Each membrane filter was subjected to a chemical fractionation procedure, which consists out of ~~and~~ extraction in water of the PM filter and in the digestion of the residue; elemental analysis was performed in both fractions (Canepari et al., 2006a, 2006b). This chemical fractionation procedure allows increasing the selectivity of the elements as source tracers (Astolfi et al., 2006; Canepari et al., 2009; Perrino et al., 2010; Astolfi et al., 2017), since, for many elements, the water-soluble and insoluble fractions are released by different PM emission sources (Massimi et al., 2020b).

In short, the polymethylpentene support ring was removed from each PM filter, which underwent ultrasound assisted extraction for 30 minutes in 10 mL of deionized water (Arioso UP 900 Integrate Water Purification System, Cole-Parmer Co Ltd., Saint Neots, England, UK). The water-extracted solution was then filtered through a cellulose nitrate filter (pore size 0.45 μm, Merck Millipore Ltd., Billerica, MA, USA). The PM filter containing the insoluble residue and the cellulose nitrate filter used for the filtration were then subjected to a microwave assisted acid digestion (Ethos Touch Control with Q20 rotor, Milestone, Bergamo, Italy) using 2

mL of ultrapure HNO_3 (67%; Promochem, LGC Standards GmbH, Wesel, Germany) and 1 mL of H_2O_2 (30%; Promochem, LGC Standards GmbH, Wesel, Germany). The digested solution was then diluted to 50 mL with deionized water and filtered using syringe filters (cellulose nitrate; diameter 25 mm, pore size 0.45 µm, GVS Filter Technology, Morecambe, England, UK).

Elements in the water-soluble (Al_s, As_s, Ba_s, Bi_s, Co_s, Cr_s, Cs_s, Cu_s, Fe_s, Li_s, Mn_s, Mo_s, Pb_s, Rb_s, Sb_s, Se_s, Sn_s, Sr_s, Ti_s, Tl_s) and insoluble (Al_i, Ce_i, Fe_i, Li_i, Mn_i, Mo_i, Nb_i, Sb_i, Sn_i, U_i, V_i, W_i, Zr_i) fractions were analyzed by a quadrupole inductively coupled plasma mass spectrometer (ICP-MS; model 820-MS; Bruker, Bremen, Germany) equipped with a glass nebulizer (0.4 mL min^{-1}; Analytik Jena AG, Jena, Germany). For each element, the external standard calibration curve was performed in the range 1-500 µg L^{-1} by serially diluting stock standard solutions (1000 ± 2 mg L^{-1}; Exaxol Italia Chemical Manufacturers Srl, Genoa, Italy; Ultra Scientific, North Kingstown, RI, USA; Merck Millipore Ltd., Billerica, MA, USA). To control nebulizer efficiency, Y (1000 ± 2 mg L^{-1}; Panreac Química, Barcelona, Spain) was set at 5 µg L^{-1} as internal standard for all measurements. The instrumental conditions and performance of the method are detailed in Astolfi et al. (2020) and Canepari et al. (2009) respectively.

In addition to the elements, the soluble fraction of PM was analyzed for water-soluble organic carbon (WSOC), ions and levoglucosan (LVG).

WSOC was analyzed by TOC-VCSH (Shimadzu Corporation, Kyoto, Japan), using the NPOC (non-purgeable organic carbon) procedure (Saarikoski et al., 2007). An aliquot of 0.5 mL of the water-extracted solution of PM, diluted 1:10 with deionized water and 100 µL of HCl 10 M (Promochem, LGC Standards GmbH, Wesel, Germany) was used for the WSOC analysis.

Ions (Ca^{2+}, Cl^-, K^+, Mg^{2+}, Na^+, NH_4^+, NO_3^-, SO_4^{2-}) were analyzed by ion chromatography (IC) (ICS1000, Dionex Co., CA, USA) using a total of 1 mL of the water-extracted solution.

Finally, an aliquot of 0.5 mL of the extracted solution, diluted 1:2 with deionized water, was analyzed for LVG by High-Performance Anion-Exchange Chromatography with Pulsed Amperometric Detection (HPAEC-PAD). A Dionex DX-500 series ion chromatograph equipped with a DC ICS-3000 oven, a GP40 Gradient Pump, and a CarboPac™ PA10 analytical and guard column was used for LVG analysis; a Dionex ED50/ED50A Electrochemical Cell equipped with disposable gold electrodes was employed as electrochemical detector (Perrino et al. 2019).

2.5 Data Analysis

The detection limit (LOD) of each analyte was set at 3 times the standard deviation (SD) of 10 replicate blank determinations.

Duplicate concentration data obtained for each monitoring period (except for December/January period) at site JO for PM_{10} and for the analyzed PM_{10} compounds were used to calculate the relative standard deviations (RSDs) in order to assess the sampling and analysis repeatability. The RSDs obtained in the December/January monitoring period are not indicative of the sampling and analysis repeatability, since one of the two samplers used at JO was stopped from 30/12/2018 to 3/1/2019 to assess the release of PM_{10} chemical components due to the burning of New Year's Eve fireworks. In the December/January period the chemical compounds with

RSDs > 50% were considered to be related to PM_{10} by the use of fireworks. LODs and RDSs of all the analyzed variables are reported in supplementary material S1.

Concentration data determined at each site in the September/October, October/November and November/December monitoring periods were averaged to obtain autumn mean concentrations, while data obtained for December/January and January/February periods were averaged to obtain winter mean concentrations.

2.6 Principal Component Analysis

Emission tracers of the main PM_{10} sources were identified and clustered by performing principal component analysis (PCA) on the concentration data of PM_{10} and ~~for~~ of all the analyzed PM_{10} components.

The matrix of the data (3960 data points) used for the PCA is composed of 90 samples: 18 samples (one sample per site) for each of the 5 sampling periods, and of 44 variables: PM_{10} mass and WSOC, LVG, Ca^{2+}, Cl^{-}, K^{+}, Mg^{2+}, Na^{+}, NH_4^{+}, NO_3^{-}, SO_4^{2-}, Al_s, As_s, Ba_s, Bi_s, Co_s, Cr_s, Cs_s, Cu_s, Fe_s, Li_s, Mn_s, Mo_s, Pb_s, Rb_s, Sb_s, Se_s, Sn_s, Sr_s, Ti_s, Tl_s, Al_i, Ce_i, Fe_i, Li_i, Mn_i, Mo_i, Nb_i, Sb_i, Sn_i, U_i, V_i, W_i and Zr_i concentration (ng m^{-3}). The matrix of the data was transformed by column mean centering and row and column autoscaling before performing the PCA (Conti et al., 2007; Massimi et al., 2017). PCA was carried out using the statistical software CAT (Chemometric Agile Tool;) based on the R-project for statistical computing, Ver. 3.0, 32-bit.

2.7 Data Interpolation and Spatial Mapping

Spatially-resolved data of the autumn and winter monitoring periods were interpolated by using the ordinary kriging (OK) method (Johnston et al., 2001) to create a continuous surface from the 17 measured sample points in Amersfoort and predict the values at unmeasured points (Kumar et al., 2007). Ordinary kriging is a geostatistical interpolation method in which the distance and the degree of variation between known data points are considered to estimate values in unknown locations by using as estimator a linear combination of the observed values with weights, which are derived from a semivariogram function (Xie et al., 2011, Paramasivam and Venkatramanan, 2019). The spherical semivariogram model was used to interpolate the high spatial resolution data and the experimental semivariances were fitted by weighted least-squares approximation (Jian et al., 1996).

The autumn and winter spatial distribution of PM_{10} and PM_{10} chemical components was mapped using the software ArcMap 10.3.1 (ArcGis Desktop; ESRI, Redlands, CA, USA).

3. Results and Discussion

3.1 Concentrations of PM_{10} Mass and PM_{10} Chemical Compounds

From Fig. 2, we can observe an increase in PM_{10} mass concentration at all the sampling sites in winter, especially in the January/February monitoring period. This increase can be explained by the greater intensity of typical winter sources such as biomass domestic heating and by a less efficient mixing of the lower

atmosphere in the colder period, which leads to frequent temperature inversions and to stronger atmospheric stability (Hendriks et al., 2013).

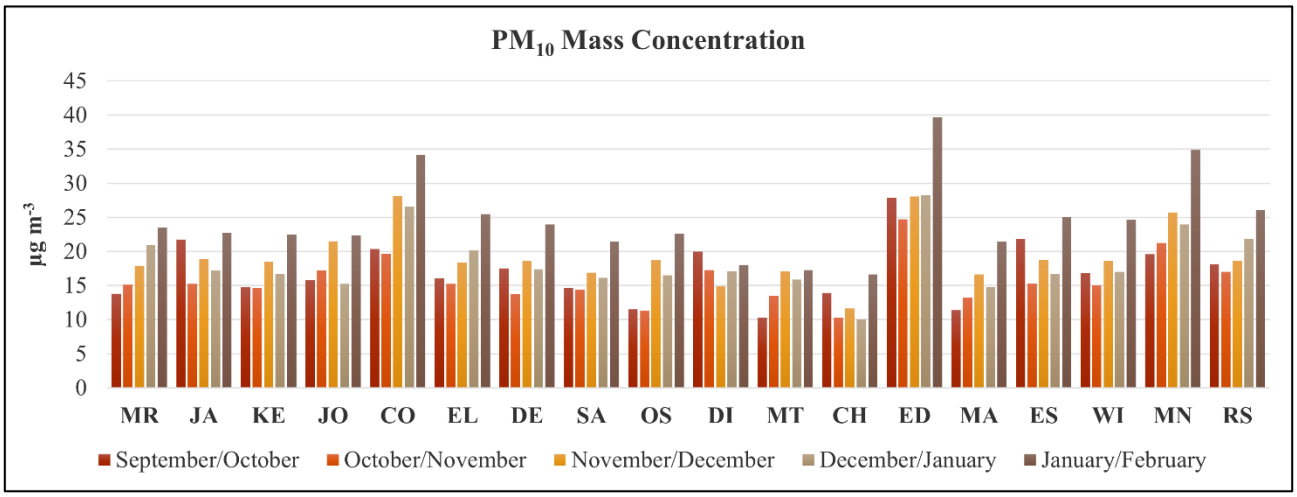

Fig. 2. PM_{10} mass concentrations (µg m^{-3}) obtained at the ~~18~~ 17 sampling sites in Amersfoort and at the regulatory reference site (RS) in Utrecht in the 5-month monitoring period.

Mean PM_{10} mass concentration at all the sites was very low: 17 µg m^{-3} in autumn and 22 µg m^{-3} in winter. As it can be seen from Tables 4 and 5, in which autumn and winter concentrations of PM_{10} mass and PM_{10} components are reported, the highest PM_{10} mass concentration (34 µg m^{-3}) was found in winter at ED, which is the closest site to the highway A28 (Table 2), located in an area where biomass domestic heating appliances were used (Fig. 1). Relatively high winter PM_{10} mass concentration was recorded also at CO (30 µg m^{-3}) and at MN (29 µg m^{-3}), which are sites located, respectively, near the highway A1 and in the area where domestic biomass combustion occurred in the colder period. The lowest PM_{10} mass concentration was found in autumn at CH (12 µg m^{-3}), located in the city center, while the highest autumn PM_{10} mass concentrations were recorded at ED, CO and MN (27, 23 and 22 µg m^{-3}, respectively).

From Tables 4 and 5, we can observe that the concentrations of WSOC, LVG, K^+, Mg^{2+}, Na^+, NH_4^+, NO_3^-, SO_4^{2-} and of all the elements in the water-soluble fraction of PM_{10} were higher in winter, while the concentrations of Ca^+, Cl^- and insoluble elements were higher in autumn. This different behaviour can be reasonably explained by the different emission sources that release these PM_{10} components. In fact, WSOC, LVG, K^+, Mg^{2+}, Na^+, NH_4^+, NO_3^-, SO_4^{2-} and water-soluble elements are generally in the fine fraction of PM (Canepari et al., 2019), originated by the accumulation of ultrafine particles released by combustion sources, such as biomass domestic heating, which is a winter emission source, and the burning of New Year's Eve fireworks. On the contrary, Ca^+, Cl^- and insoluble elements are usually in the coarse fraction of PM, associated to soil (Ca^+, Cl^-, Al_i, Ce_i, Li_i, U_i and V_i; Canepari et al., 2008; Pant and Harrison, 2013) or brake abrasion dust (Fe_i, Mn_i, Mo_i, Nb_i, Sb_i, Sn_i, W_i and Zr_i; Querol et al., 2012; Namgung et al., 2016), whose resuspension is greater in autumn (Massimi et al., 2020b). Concentrations of PM_{10} mass and PM_{10} chemical compounds obtained at all sampling sites in each monitoring period are reported in supplementary material S2.

Table 4. Concentrations of PM_{10} mass (µg m^{-3}) and PM_{10} chemical compounds (ng m^{-3}) obtained at the 17 sampling sites in Amersfoort and at the regulatory reference site (RS) in Utrecht in the autumn monitoring period.

	MR	JA	KE	JO	CO	EL	DE	SA	OS	DI	MT	CH	ED	MA	ES	WI	MN	RS
PM_{10}	16	19	16	18	23	17	17	15	14	17	14	12	27	14	19	17	22	18
WSOC	3243	4185	4260	3615	5955	3675	2340	2370	2870	2910	2820	1531	6256	2804	2831	3270	6015	4175
LVG	644	639	698	678	1119	618	658	518	565	556	771	546	829	583	599	851	919	613
Ca^{2+}	207	360	217	308	324	226	256	230	333	344	257	210	388	242	307	204	294	281
Cl^-	3056	2506	2307	3084	4220	2677	2722	2408	2200	2414	2241	1266	3413	2086	2573	2048	3624	3385
K^+	105	114	118	148	155	106	206	114	156	147	119	71	244	164	180	95	215	200
Mg^{2+}	66	67	66	79	101	69	70	63	60	75	52	39	95	58	62	53	88	78
Na^+	520	493	580	768	767	502	602	463	434	666	413	366	817	482	579	400	699	591
NH_4^+	794	709	683	938	1280	738	774	707	610	451	667	358	1062	576	723	631	1117	771
NO_3^-	1338	1244	1285	1647	2041	1337	1299	1185	1320	991	1144	602	1751	1032	1215	1093	1804	1437
SO_4^{2-}	553	491	566	714	857	557	552	497	496	377	470	316	763	439	506	482	792	607
Al_s	4.2	5.7	7.0	9.6	13	6.5	7.9	8.2	13	8.0	5.6	4.4	9.4	5.6	6.5	8.1	13	5.8
As_s	0.41	0.43	0.53	0.50	0.84	0.49	0.37	0.42	0.42	0.38	0.45	0.30	0.71	0.36	0.37	0.46	0.62	0.35
Ba_s	2.9	3.2	2.9	3.4	3.5	4.4	3.9	3.8	2.6	2.3	2.9	1.7	3.8	1.8	2.7	2.8	3.4	6.7
Bi_s	0.019	0.019	0.022	0.027	0.034	0.021	0.025	0.025	0.019	0.013	0.019	0.014	0.034	0.020	0.021	0.022	0.033	0.019
Co_s	0.024	0.033	0.033	0.034	0.049	0.034	0.032	0.032	0.037	0.032	0.028	0.019	0.058	0.026	0.047	0.039	0.045	0.037
Cr_s	0.17	0.22	0.20	0.23	0.31	0.21	0.19	0.18	0.21	0.19	0.20	0.14	0.30	0.17	0.20	0.21	0.28	0.22
Cs_s	0.018	0.020	0.022	0.023	0.031	0.021	0.019	0.018	0.019	0.019	0.018	0.012	0.030	0.018	0.017	0.020	0.031	0.022
Cu_s	4.2	4.8	4.0	5.8	7.3	6.1	6.8	4.3	3.9	7.5	3.8	2.5	6.9	3.4	5.8	5.1	5.2	13
Fe_s	10	15	14	16	22	13	14	11	13	12	14	6.4	24	11	16	14	21	17
Li_s	0.028	0.051	0.047	0.049	0.069	0.043	0.040	0.040	0.042	0.050	0.041	0.023	0.073	0.037	0.039	0.044	0.070	0.053
Mn_s	2.4	2.7	2.6	2.9	3.9	2.8	2.8	2.5	2.4	2.7	2.3	1.4	4.0	2.2	2.6	2.7	3.6	3.5
Mo_s	0.29	0.34	0.30	0.36	0.50	0.40	0.32	0.30	0.32	0.38	0.33	0.23	0.43	0.26	0.30	0.32	0.42	0.37
Pb_s	0.91	1.1	1.3	1.4	2.0	1.1	1.1	1.2	1.2	0.8	1.1	0.57	2.0	1.1	1.0	1.4	2.0	0.8
Rb_s	0.21	0.23	0.27	0.27	0.36	0.29	0.26	0.22	0.25	0.35	0.22	0.16	0.38	0.24	0.27	0.29	0.37	0.22
Sb_s	0.41	0.47	0.45	0.54	0.67	0.51	0.55	0.41	0.41	0.44	0.39	0.27	0.75	0.39	0.47	0.49	0.63	0.66
Se_s	0.31	0.32	0.38	0.41	0.51	0.47	0.31	0.39	0.34	0.38	0.32	0.27	0.51	0.35	0.33	0.38	0.59	0.42
Sn_s	0.14	0.16	0.15	0.19	0.23	0.16	0.16	0.14	0.15	0.11	0.13	0.076	0.23	0.13	0.16	0.16	0.21	0.18
Sr_s	1.1	1.5	1.2	1.3	1.6	1.3	1.2	1.3	1.1	1.5	1.0	0.7	1.6	1.0	1.1	1.1	1.7	1.4
Ti_s	0.078	0.090	0.090	0.12	0.17	0.10	0.090	0.082	0.11	0.076	0.10	0.053	0.18	0.081	0.11	0.093	0.15	0.11
Tl_s	0.019	0.022	0.023	0.025	0.034	0.023	0.021	0.020	0.020	0.019	0.019	0.015	0.035	0.019	0.020	0.024	0.034	0.023
Al_i	69	151	134	126	87	128	164	86	124	153	123	67	129	64	54	104	104	76
Ce_i	0.19	0.18	0.14	0.16	0.20	0.13	0.18	0.13	0.16	0.19	0.11	0.10	0.19	0.11	0.14	0.14	0.19	0.17
Fe_i	242	270	214	301	266	250	394	226	219	323	192	154	350	165	306	232	285	649
Li_i	0.061	0.056	0.054	0.054	0.068	0.053	0.072	0.054	0.065	0.075	0.059	0.033	0.078	0.050	0.051	0.061	0.066	0.048
Mn_i	3.0	4.0	3.2	3.7	3.7	3.2	4.3	3.0	3.0	4.2	2.9	2.4	4.4	2.4	3.3	3.0	3.8	5.6
Mo_i	0.27	0.36	0.28	0.37	0.37	0.33	0.45	0.25	0.31	0.49	0.28	0.22	0.48	0.20	0.39	0.31	0.40	0.71
Nb_i	0.028	0.031	0.027	0.035	0.035	0.028	0.040	0.030	0.028	0.045	0.024	0.023	0.048	0.021	0.033	0.033	0.032	0.080
Sb_i	0.81	1.2	0.85	1.0	1.1	0.65	1.2	0.90	0.85	1.1	0.78	0.87	1.5	0.79	0.88	1.1	1.0	1.8
Sn_i	1.7	2.1	1.9	2.5	2.5	1.8	2.9	1.9	1.7	2.5	1.4	1.4	3.2	1.5	2.4	2.3	2.4	5.1
U_i	0.0030	0.0045	0.0034	0.0036	0.0054	0.0034	0.0048	0.0035	0.0048	0.0047	0.0040	0.0027	0.0045	0.0038	0.0039	0.0035	0.0048	0.0046
V_i	0.22	0.16	0.22	0.22	0.28	0.18	0.25	0.16	0.14	0.30	0.17	0.15	0.25	0.18	0.25	0.19	0.34	0.28
W_i	0.022	0.043	0.042	0.037	0.068	0.030	0.034	0.037	0.036	0.055	0.035	0.029	0.062	0.029	0.058	0.046	0.056	0.041
Zr_i	0.45	0.50	0.36	0.54	0.50	0.44	0.76	0.44	0.40	0.63	0.36	0.30	0.64	0.28	0.53	0.42	0.48	1.2

Table 5. Concentrations of PM_{10} mass (µg m^{-3}) and PM_{10} chemical compounds (ng m^{-3}) obtained at the 17 sampling sites in Amersfoort and at the regulatory reference site (RS) in Utrecht in the winter monitoring period.

	MR	JA	KE	JO	CO	EL	DE	SA	OS	DI	MT	CH	ED	MA	ES	WI	MN	RS
PM_{10}	22	20	20	19	30	23	21	19	20	18	17	13	34	18	21	21	29	24
WSOC	5011	4755	5175	5430	6510	5525	5070	4875	5220	1977	4057	2422	6960	3990	5550	4170	6780	5040
LVG	1772	1212	1270	1803	2451	1590	1165	1374	1657	763	1383	863	2764	1424	1465	1404	2291	1344
Ca^{2+}	127	99	126	95	133	176	154	103	203	180	133	77	141	106	94	82	257	173
Cl^-	1376	1239	1224	688	1609	1725	1141	1072	1120	1375	1447	680	1821	996	1101	966	1659	1577
K^+	648	384	364	279	519	430	265	342	488	304	297	159	460	209	222	230	374	380
Mg^{2+}	142	117	104	71	143	118	104	102	129	89	96	62	160	90	93	92	143	140
Na^+	821	715	784	532	956	947	709	675	1076	695	662	452	1083	635	677	657	1078	980
NH_4^+	1346	1093	1186	1363	1395	1453	1244	1161	1172	592	836	669	1786	1120	1398	1107	1350	1424
NO_3^-	3763	3482	3406	3867	5637	4278	3500	3168	3391	2337	2272	2005	5751	3240	3832	3235	5708	4054
SO_4^{2-}	1528	1292	1256	1212	1981	1754	1158	1243	1204	701	939	762	1927	1075	1309	1089	1837	1445
Al_s	22	19	13	19	23	15	16	14	17	13	11	9.6	22	8.4	14	11	18	16
As_s	0.39	0.34	0.62	0.51	0.65	0.50	0.31	0.43	0.51	0.26	0.47	0.30	0.91	0.42	0.33	0.32	0.70	0.34
Ba_s	35	25	15	14	22	14	15	19	30	20	15	7.6	25	11	13	13	19	22
Bi_s	0.48	0.62	0.34	0.37	0.61	0.33	0.35	0.34	0.37	0.35	0.31	0.13	0.59	0.24	0.28	0.26	0.45	0.40
Co_s	0.029	0.039	0.033	0.030	0.041	0.034	0.029	0.034	0.023	0.024	0.025	0.020	0.060	0.026	0.055	0.034	0.050	0.037
Cr_s	0.67	0.54	0.43	0.47	0.77	0.47	0.43	0.44	0.44	0.41	0.41	0.29	0.78	0.35	0.43	0.41	0.62	0.54
Cs_s	0.028	0.026	0.029	0.033	0.040	0.030	0.028	0.026	0.029	0.013	0.026	0.020	0.047	0.025	0.030	0.026	0.042	0.029
Cu_s	18	14	9.1	8.4	16	12	13	10	8.7	13	8.7	5.5	17	6.8	10	8.3	14	20
Fe_s	14	17	20	16	31	21	18	17	13	11	12	12	37	14	24	20	27	21
Li_s	0.059	0.066	0.054	0.041	0.080	0.064	0.061	0.054	0.058	0.046	0.053	0.033	0.096	0.048	0.058	0.051	0.084	0.064
Mn_s	2.8	2.7	2.8	2.4	4.0	3.2	2.8	2.6	2.4	2.1	2.1	1.7	4.4	2.3	3.0	2.4	3.7	3.7
Mo_s	0.32	0.33	0.33	0.38	0.50	0.41	0.33	0.26	0.33	0.28	0.30	0.25	0.51	0.29	0.37	0.30	0.51	0.37
Pb_s	1.4	1.4	1.7	1.8	2.5	1.7	1.3	1.3	1.6	1.1	1.2	1.2	3.8	1.4	1.7	1.5	2.5	1.1
Rb_s	0.43	0.37	0.36	0.40	0.51	0.38	0.35	0.31	0.32	0.31	0.33	0.30	0.56	0.38	0.29	0.26	0.41	0.32
Sb_s	0.48	0.46	0.52	0.54	0.72	0.58	0.50	0.45	0.45	0.37	0.40	0.34	0.86	0.46	0.62	0.48	0.74	0.67
Se_s	0.50	0.43	0.45	0.57	0.75	0.54	0.41	0.36	0.44	0.31	0.38	0.32	0.74	0.39	0.54	0.43	0.70	0.46
Sn_s	0.21	0.20	0.24	0.29	0.32	0.24	0.21	0.19	0.23	0.15	0.16	0.11	0.31	0.20	0.33	0.22	0.42	0.24
Sr_s	14	8.4	4.7	4.5	8.9	5.6	6.7	5.3	11	9.1	5.4	2.6	9.3	4.1	4.1	4.3	6.8	8.3
Ti_s	0.16	0.14	0.15	0.17	0.27	0.17	0.14	0.17	0.14	0.11	0.11	0.089	0.25	0.13	0.17	0.14	0.26	0.18
Tl_s	0.025	0.023	0.029	0.033	0.038	0.030	0.024	0.022	0.024	0.015	0.023	0.018	0.044	0.023	0.026	0.023	0.037	0.026
Al_i	115	120	132	58	63	79	93	102	108	95	81	31	72	105	32	83	71	119
Ce_i	0.29	0.18	0.12	0.10	0.16	0.15	0.16	0.17	0.13	0.17	0.13	0.093	0.19	0.10	0.13	0.16	0.16	0.21
Fe_i	248	178	180	150	253	267	324	210	187	211	153	132	250	174	224	246	217	508
Li_i	0.052	0.041	0.034	0.026	0.044	0.047	0.059	0.022	0.022	0.035	0.027	0.019	0.028	0.021	0.020	0.038	0.049	0.045
Mn_i	3.3	2.7	2.8	2.2	3.2	3.2	3.5	2.7	2.5	3.2	2.3	1.9	3.1	2.4	2.5	3.2	2.8	4.8
Mo_i	0.28	0.29	0.26	0.19	0.37	0.37	0.45	0.27	0.23	0.30	0.22	0.20	0.39	0.25	0.31	0.33	0.26	0.59
Nb_i	0.033	0.031	0.023	0.019	0.029	0.034	0.050	0.025	0.020	0.026	0.021	0.024	0.047	0.029	0.037	0.032	0.029	0.081
Sb_i	0.95	0.85	0.76	0.63	1.0	1.0	1.3	0.64	0.77	0.73	0.64	0.85	1.4	1.0	0.94	1.0	0.97	1.8
Sn_i	2.4	2.1	2.0	1.9	2.8	2.6	3.2	2.0	1.7	1.9	1.6	1.5	3.0	1.9	2.5	2.5	2.6	4.6
U_i	0.0025	0.0047	0.0039	0.0017	0.0033	0.0033	0.0040	0.0051	0.0036	0.0030	0.0025	0.0026	0.0030	0.0033	0.0022	0.0046	0.0036	0.0045
V_i	0.31	0.11	0.22	0.16	0.23	0.23	0.31	0.17	0.11	0.21	0.22	0.20	0.23	0.11	0.20	0.20	0.22	0.51
W_i	0.038	0.034	0.037	0.025	0.044	0.041	0.047	0.025	0.028	0.042	0.027	0.026	0.053	0.035	0.059	0.041	0.036	0.041
Zr_i	0.43	0.36	0.32	0.27	0.44	0.48	0.62	0.40	0.28	0.43	0.30	0.28	0.43	0.32	0.39	0.40	0.35	0.84

3.2 Identification of PM_{10} Source Tracers

To identify emission tracers of the main PM_{10} sources acting in Amersfoort during the 5-month monitoring period and to cluster the samples depending on their spatial and temporal distribution, explorative PCA was performed.

Three significant components accounting for 73.3% of the total variance were obtained (the scores and loadings are shown in supplementary material S3); the variance explained by each component is: 32.9%, 22.9% and 17.5%. First component (PC1) clusters the samples (scores) depending on the monthly concentration variability of PM_{10} chemical compounds (loadings). Therefore, samples collected in autumn (in the September/October, October/November and November/December monitoring periods), in which higher concentrations of Ca^+, Cl^- and insoluble elements were obtained (Tables 4 and 5), are almost all plotted on the left part of the score plot. On the contrary, winter samples (of the December/January and January/February periods), containing higher concentrations of WSOC, LVG, K^+, Mg^{2+}, Na^+, NH_4^+, NO_3^-, SO_4^{2-} and water-soluble elements, are mostly plotted on the right part of the score plot.

From Fig. 3, we can observe that for each monitoring period, samples collected at DI, MT, CH and MA, where higher concentrations of crustal components of PM_{10} (Ca^+, Cl^-, Al_i, Ce_i, Li_i, U_i and V_i) were found, are separated along PC1 from samples collected at CO, ED and MN, containing higher concentrations of WSOC, LVG, NH_4^+, NO_3^-, SO_4^{2-} and water-soluble elements (Tables 4 and 5). Indeed, Ca^+, Cl^-, Al_i, Ce_i, Li_i, U_i and V_i are all clustered as soil dust tracers in the group A of the loading plot (panel b), while WSOC, LVG, NH_4^+, NO_3^-, SO_4^{2-}, As_s, Co_s, Cs_s, Fe_s, Li_s, Mn_s, Mo_s, Pb_s, Rb_s, Sb_s, Se_s, Sn_s, Ti_s and Tl_s are clustered in the groups C, D and E.

Group C contains the water-soluble fraction of elements (Fe_s, Mn_s, Mo_s and Sb_s) presumably released by industrial emissions (Kim and Jo, 2006; Mooibroek et al., 2011; Mbengue et al., 2014) and partly emitted by brake abrasion (Garg et al., 2000; Thorpe and Harrison, 2008), along with their insoluble fraction (group B), which is more strongly associated to brake dust (Abbasi et al., 2012; Kam et al., 2013, Massimi et al., 2020b).

On the other hand, group D is composed of water-soluble elements (As_s, Co_s, Pb_s, Se_s, Sn_s and Ti_s) and NH_4^+ , whose release can be more reliably attributed to industrial (Mooibroek et al., 2011; Fernández-Camacho et al., 2012; Park et al., 2014) and/or agricultural sources (Battye et al., 2003; Shen et al., 2011). In fact, NH_4^+ is formed in the atmosphere by the protonation of NH_3, which is mainly released by the decomposition of organic matter from animal farming and by the use of nitrogen fertilizers in agriculture (Pozzer et al., 2017).

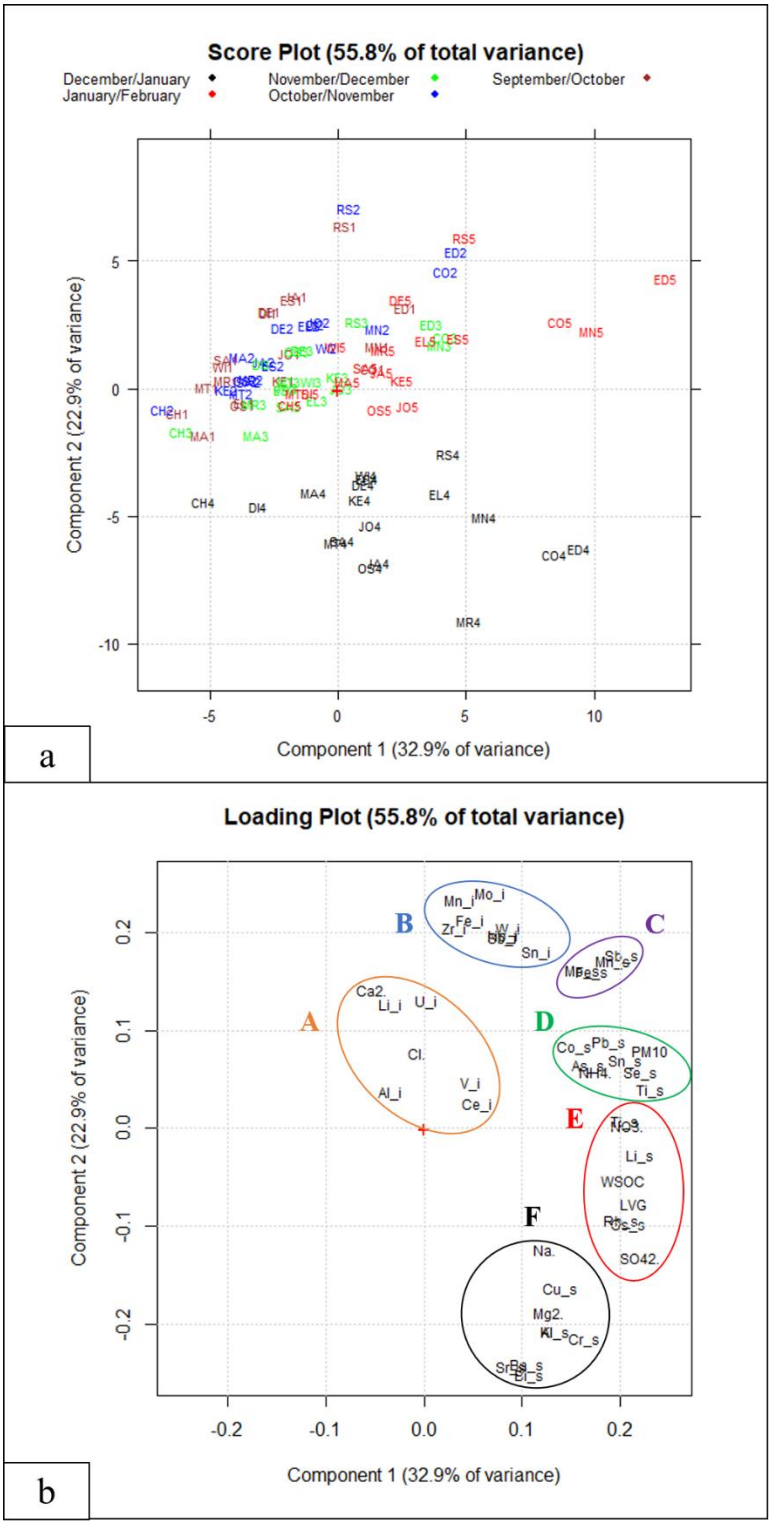

Fig. 3. Score (panel a) and loading (panel b) plot of the PCA (PC1/PC2) performed on the concentration data (ng m^{-3}) of PM_{10} mass and PM_{10} chemical compounds obtained at the 17 sampling sites in Amersfoort and at the regulatory reference site (RS) in Utrecht in the 5-month monitoring period.

Finally, group E contains secondary inorganic ions (NO_3^-, SO_4^{2-}) and biomass burning tracers (WSOC, LVG, Cs_s, Li_s, Rb_s and Tl_s), which were most likely emitted by biomass domestic heating sources (Cheng et al., 2014; Frasca et al., 2018; Simonetti et al., 2018b; Massimi et al., 2020a), especially in winter at CO, ED

and MN (Tables 4 and 5). In fact, LVG is a highly selective biomass burning tracer (Simoneit et al., 2004; Engling et al., 2006; Sullivan et al., 2008), since it is a dominant organic component emitted in fine wood smoke (Simoneit et al., 1999; Schauer et al., 2001). Water-soluble Cs, Li, Rb and Tl are also known to be produced by wood burning and they can be used as effective biomass domestic heating tracers (Canepari et al., 2014; Frasca et al., 2018; Massimi et al., 2020b). Water-soluble organic carbon is a less selective tracer, since it is also derived from biogenic materials, soil dust and fuel combustion (Urban et al., 2012); despite this, a considerable fraction of WSOC is generally produced by the combustion of biomass for residential heating (Graham et al., 2002; Massimi et al., 2020a). Moreover, WSOC is an indicator of water-soluble secondary organic particles (Weber et al., 2007, Ervens et al., 2011) that can be formed during the aging process of biomass burning smoke (Lee et al., 2008, Adler et al., 2011). On the other hand, NO_3^- and SO_4^{2-}, which are clustered in the same group, are tracers of secondary inorganic aerosols (secondary sulfates and/or nitrates), whose production strongly depends on several chemical and micro-meteorological factors (Pathak et al., 2009) and can be enhanced by wood burning and fireworks episodes (Cheng et al., 2014). Therefore, in group E the chemical components that trace the secondary fraction of PM_{10} (both inorganic and organic) and PM_{10} particles released by biomass burning are clustered. Potassium ion is also usually deemed to be a reliable wood burning tracer, since it is produced by the combustion of biomass (Chow et al., 2007). However, it is plotted in group F instead of group E, because its concentration in PM_{10} was affected by the burning of New Year's Eve fireworks.

Second component (PC2) separates all the samples collected in the December/January monitoring period from the others, since they showed higher concentrations of K^+, Mg^{2+}, Na^+,Al_s, Ba_s, Bi_s, Cr_s, Cu_s and Sr_s (clustered in the group F), which are tracers of the burning of fireworks (Wang et al., 2007; Moreno et al., 2010; Tanda et al., 2019). As a confirmation of this, all these chemical compounds, in the December/January period, showed RSD > 50% (supplementary material S1) at site JO, where one of the two samplers used was stopped from 30/12/2018 to 3/1/2019 to assess the release of PM_{10} components due to the New Year's Eve fireworks. From Fig. 4, we can observe the different contribution in concentration of these compounds at JO due to the burning of fireworks during the five days in which one of the two samplers was stopped. These chemical components are contained in salts used to give white (K^+, Mg^{2+} and Al_s), silver (Mg^{2+}, Al_s, Cu_s and Cr_s), yellow (Na^+), green (Ba_s), blue (Cu_s) and red (Sr_s) colors to the fireworks; K^+, Cu_s and Cr_s are used to provide glitter effects, K^+ is also used as rocket propellant, while Mg^{2+}, Al_s and Bi_s are useful common metallic fuels to produce sparks, glitter and crackling stars (Russel, 2009; Nakatsubo et al., 2014; Tian et al., 2014).

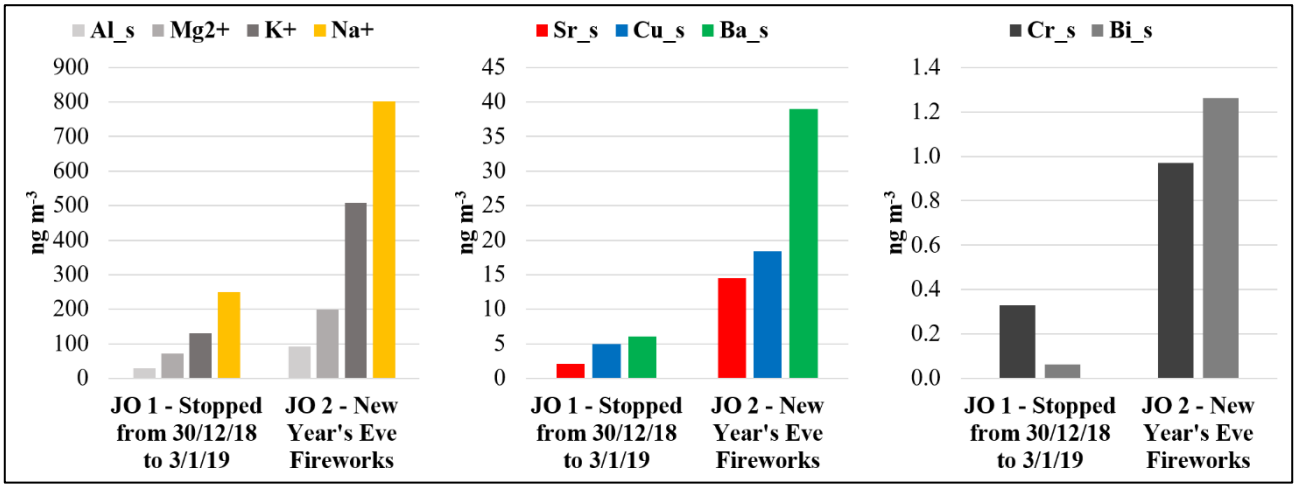

Fig. 4. Concentrations of K^+, Mg^{2+}, Na^+,Al_s, Ba_s, Bi_s, Cr_s, Cu_s and Sr_s released by the burning of New Year's Eve fireworks at JO.

It is worth noting that chromium is present on the vast majority of the water-soluble species as Cr(VI) (Brown et al., 2014), which has been classified as 'Group A carcinogen' by the U.S. Environmental Protection Agency (EPA; U.S. Environmental Protection Agency, 1984). Therefore, water-soluble Cr released by the burning of fireworks might be toxic. Moreover, PC2 clusters the samples collected at sites DE, ED and RS, containing higher concentrations of Fe_i, Mn_i, Mo_i, Nb_i, Sb_i, Sn_i, W_i and Zr_i (clustered in the group B), which were very likely released from non-exhaust vehicular traffic sources by abrasion and resuspension of vehicle/train brake disks and pads lining (Abbasi et al., 2012; Querol et al., 2012; Kam et al., 2013; Namgung et al., 2016; Massimi et al., 2020b). In fact, RS is a traffic regulatory reference site in Utrecht, while DE and ED are sites very close to the Amersfoort highways A1 and A28, respectively (Fig. 1; Table 2).

3.2 Spatial Mapping of PM_{10} Source Tracers

The spatial distribution of the identified PM_{10} source tracers was mapped to delineate and localize the impact of the different emission sources acting in Amersfoort. Maps of the autumn and winter spatial distribution of PM_{10} mass concentration and of one representative tracer for each identified PM_{10} source (panel b; Fig. 3) are shown below.

From Fig. 5, we can observe that PM_{10} mass concentration increased at all the sampling sites in winter (panel b), due to more frequent episodes of atmospheric stability (Hendriks et al., 2013) and to the greater use of biomass domestic heating during the colder period, as previously discussed. Moreover, the transport of PM_{10} particles across the study area seems to have been driven by the predominant wind coming from the south (Gelaro et al., 2017), since the highest PM_{10} mass concentrations were recorded at ED, CO, EL and MN (Table 5), which are located along the south-north direction, in proximity of the two highways and of townhouses heated by biomass burning appliances (Fig.1; Table 2), while the lowest concentrations were recorded at OS, MT, CH and MA (Table 4).

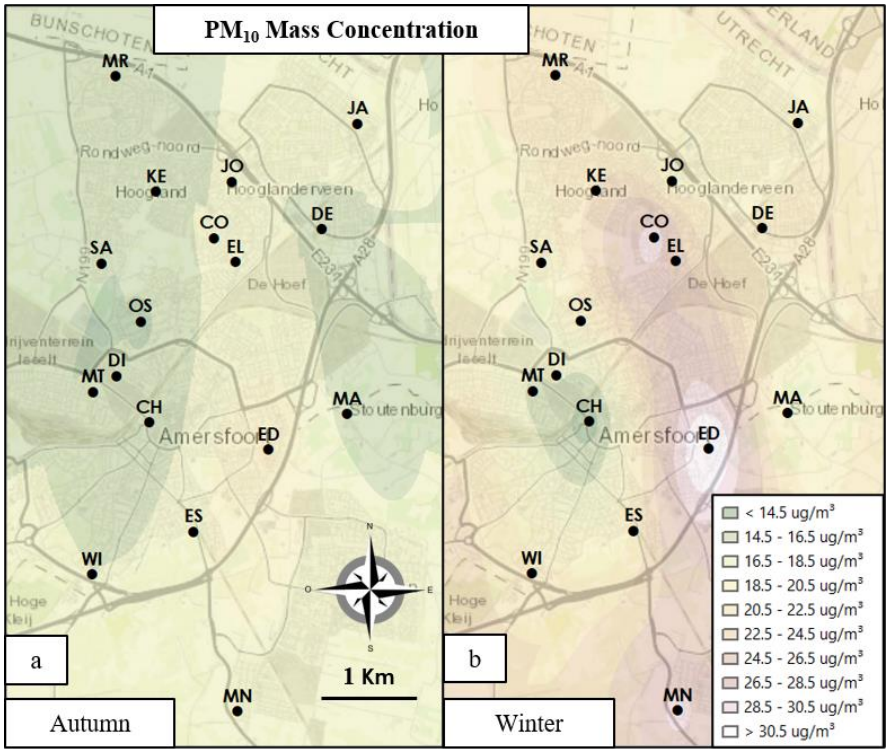

Fig. 5. Map of the autumn (panel a) and winter (panel b) spatial distribution of PM_{10} mass concentration.

The elements analyzed in both the water-soluble and insoluble fraction (Al, Fe, Li, Mn, Mo, Sb and Sn) showed very different spatial distributions. As an example, the spatial maps of water-soluble and insoluble Li and Sn are reported in Fig. 6 (panels a-d) and Fig. 7 (panels a-d), respectively.

From Fig. 6, it can be seen that Li_s concentrations were clearly higher during the winter period (panel b) in the area where residential biomass combustion occurred (Fig. 1). The highest values were recorded, here too, at ED, CO, EL and MN (Table 5). The spatial distribution of Li_s (panels a, b) was almost identical to those of all the identified tracers of biomass burning (WSOC, LVG, Cs_s, Li_s, Rb_s and Tl_s) and secondary inorganic ions (NO_3^-, SO_4^{2-}), thus confirming the prevailing transport of the particles released from south to north. Spatial maps of all the analyzed chemical compounds are reported in supplementary material S4. On the contrary, the insoluble fraction of Li (panels c, d), a soil resuspension tracer (Canepari et al., 2008; Pant and Harrison, 2013; Massimi et al., 2020b), showed a completely different seasonal variability and spatial distribution. In fact, its concentration was higher in autumn. Low spatial variability was observed for Li_i concentrations, revealing a homogeneous distribution of the soil dust, due to the lack of intensive soil local sources. A very similar behaviour was observed also for all the other crustal components of PM_{10} (Ca^+, Cl^-, Al_i, Ce_i, Li_i, U_i and V_i).

From Fig. 7, we can observe that the concentrations of Sn_s, a tracer of industrial emissions (Fernández-Camacho et al., 2012; Canepari et al., 2014), were higher at KE, JO, ED, CO, EL, ES and MN, especially in winter (panel b) due to the stronger atmospheric stability. A practically identical spatial distribution was noted for all the other identified tracers of industrial and/or agricultural sources (NH_4^+, As_s, Co_s, Pb_s, Se_s, Sn_s and Ti_s). Peak concentrations were found at ES and MN (Table 5), which are sites in the southernmost area;

it is thus conceivable that industrial and/or agricultural sources located further south or at the southern end of Amersfoort released particles that were transported to the study area by the predominant south wind. On the other hand, in autumn (panel c) as well as in winter (panel d), insoluble Sn concentrations were found to be higher at sites in proximity of trafficked streets, traffic lights, roundabouts, railway tracks, train stations and the highways A1 and A28 (Table 2), confirming vehicle/train brake abrasion as the main emission source of Sn_i. Indeed, the highest Sn_i concentrations were recorded in autumn at JO, DE, ED and ES (Table 4) and in winter at CO, EL, DE and ED (Table 5), which are all traffic sites. Concentrations of Sn_i did not considerably increased in winter, since brake abrasion is a mechanical process less sensitive to seasonal variations of atmospheric conditions (Canepari et al., 2019). A very similar spatial pattern was observed also for all the other brake dust tracers (Fe_i, Mn_i, Mo_i, Nb_i, Sb_i, W_i and Zr_i). Figures 5 and 6 also show that water-soluble and insoluble species of Li and Sn were released into the atmosphere by different sources. This confirms the effectiveness of the chemical fractionation procedure in increasing the selectivity of the elements as source tracers (Perrino et al., 2010; Massimi et al., 2020b).

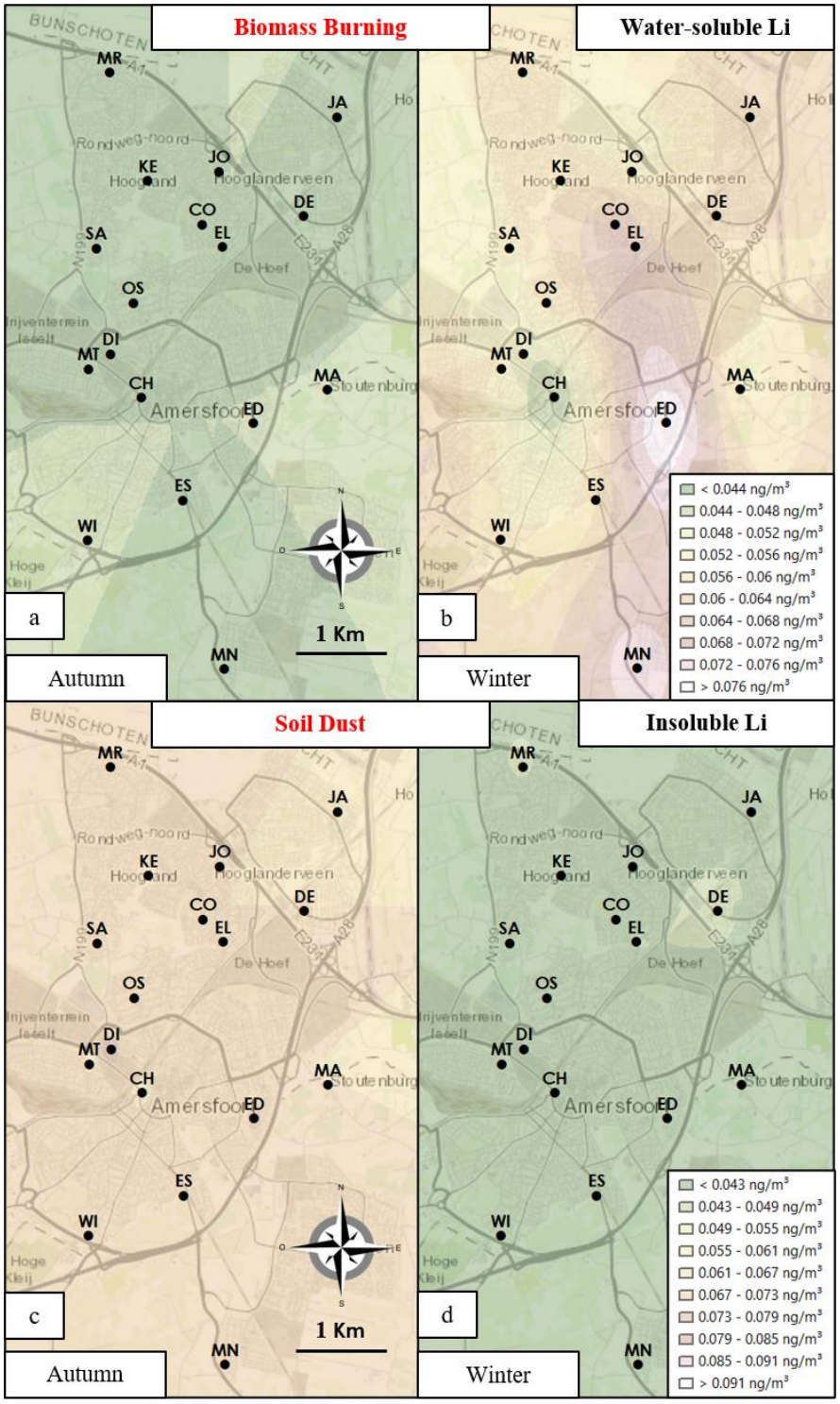

Fig. 6. Map of the autumn and winter spatial distribution of water-soluble Li (panels a,b) and insoluble Li (panels c,d).

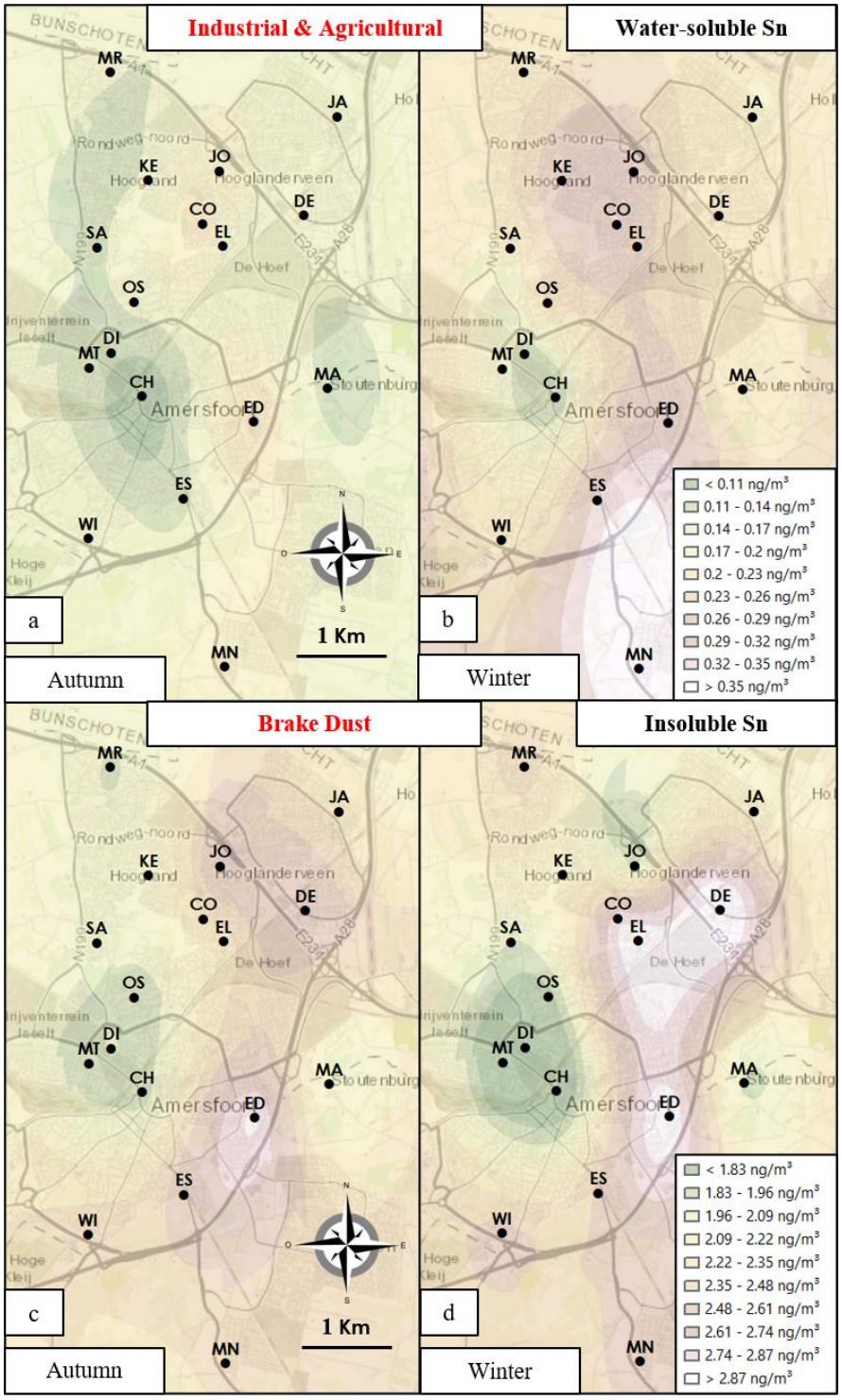

Fig. 7. Map of the autumn and winter spatial distribution of water-soluble Sn (panels a,b) and insoluble Sn (panels c,d).

Finally, in Fig. 8, autumn and winter spatial maps of water-soluble Sb (panels a,b) and Bi (panels c,d) are reported. Water-soluble Sb, as well as Fe_s, Mn_s and Mo_s, showed a similar spatial distribution to that of the brake dust tracers in autumn (panel a) and to that of the tracers of industrial and/or agricultural emissions

in winter (panel b). This because Sb_s was probably released by both industrial (Kim and Jo, 2006; Mbengue et al., 2014) and non-exhaust vehicular traffic emissions (Garg et al., 2000; Thorpe and Harrison, 2008).

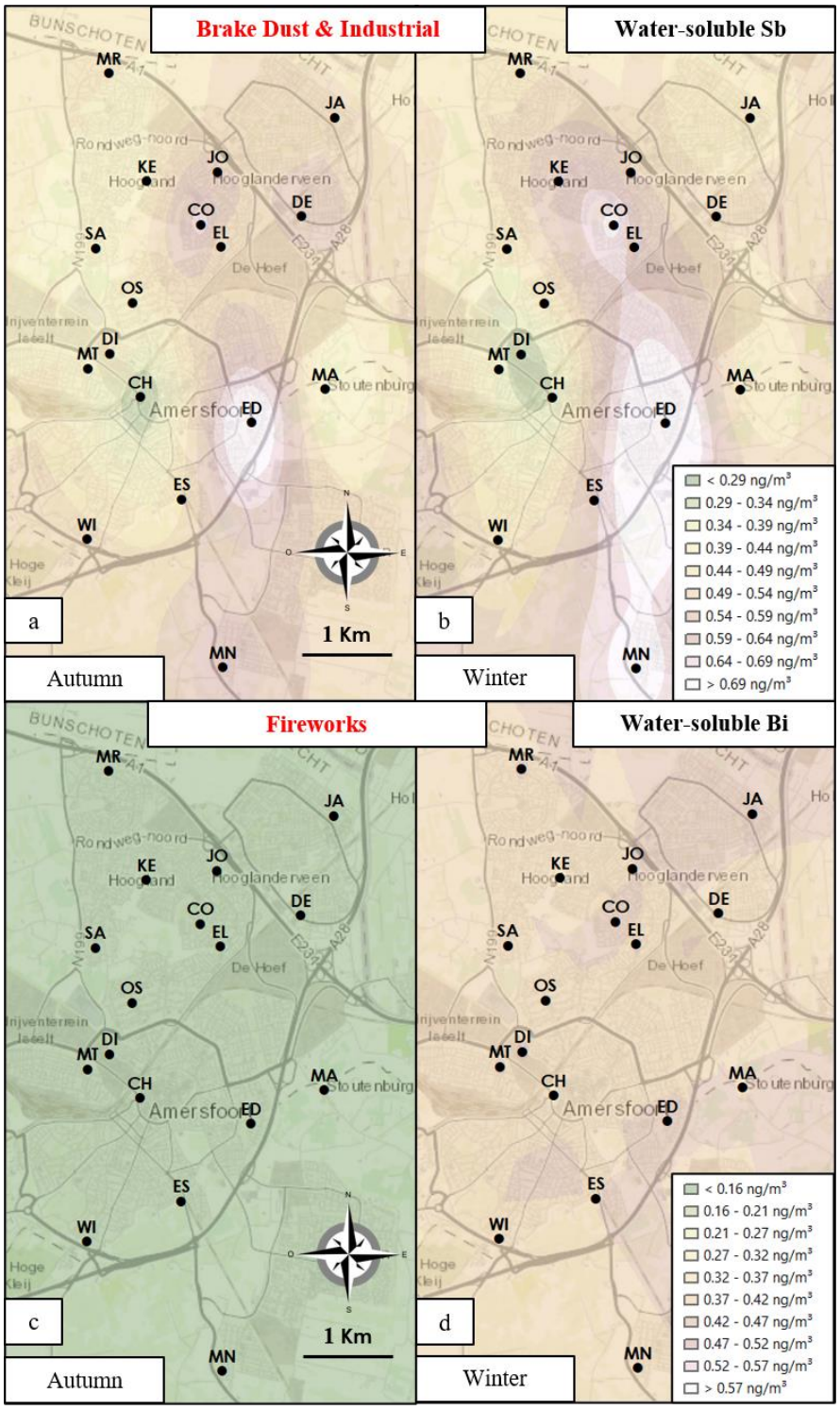

Fig. 8. Map of the autumn and winter spatial distribution of water-soluble Sb (panels a,b) and water-soluble Bi (panels c,d).

Water-soluble Bi concentrations were found to be very low in autumn (panel c) and remarkably higher in winter (panel c) at all the sampling sites, since it was released by the burning of fireworks during the New

Year's Eve, in the December/January monitoring period. In fact, as previously discussed, Bi_s is used in fireworks as metallic fuel to produce sparks, glitter and crackling stars. Its homogeneous spatial distribution reveals the widespread use of fireworks across the study area. The same behavior was observed also for all the other elements released by the burning of fireworks (K^+, Mg^{2+}, Na^+,Al_s, Ba_s, Cr_s, Cu_s and Sr_s).

4. Conclusions

The study of the autumn and winter spatial distribution of PM_{10} mass and PM_{10} chemical components in Amersfoort allowed us to identify, through the spatial mapping of chemical tracers of PM emissions, the main PM_{10} sources acting in the study area, and to evaluate the diffusion of the PM_{10} particles.

By applying the principal component analysis on the obtained spatially-resolved data, samples collected in each monitoring period at the different sites were clustered depending on the concentration variability of the PM_{10} chemical compounds. Selective and reliable source tracers were identified for soil dust (Ca^+, Cl^-, Al_i, Ce_i, Li_i, U_i and V_i), brake dust (Fe_i, Fe_s, Mn_i, Mn_s, Mo_i, Mo_s Nb_i, Sb_i, Sb_s, Sn_i, W_i and Zr_i), industrial and/or agricultural emissions (NH_4^+, As_s, Co_s, Fe_s, Mn_s, Mo_s, Pb_s, Sb_s, Se_s, Sn_s and Ti_s), secondary organic and inorganic aerosols (WSOC, NO_3^- and SO_4^{2-}), biomass domestic heating (WSOC, LVG, Cs_s, Li_s, Rb_s and Tl_s) and the burning of New Year's Eve fireworks (K^+, Mg^{2+}, Na^+,Al_s, Ba_s, Bi_s, Cr_s, Cu_s and Sr_s).

A marked increase in PM_{10} mass concentration occurred at all the sites in winter, due to the stronger atmospheric stability and to the greater use of biomass domestic heating during the colder period. The transport of PM_{10} particles across the study area seems to have been driven by the predominant wind coming from the south.

Each identified source showed characteristic autumn and winter spatial distributions, depending on the sources strength and on the seasonal variation of atmospheric conditions. Soil dust emissions were found to be higher in autumn and widespread across the study area, brake dust appeared to be emitted in higher concentrations at the traffic sites in autumn as well as in winter, as expected. On the contrary, the chemical compounds contained in PM_{10} particles released by industrial and/or agricultural emissions were found to be more concentrated at the southern end of Amersfoort, especially in winter. A similar behavior was observed for the secondary organic and inorganic aerosols and for the biomass burning particles, which were found in higher concentration in winter, in the southern area, where biomass domestic heating systems were employed, especially in the colder period. Finally, PM_{10} particles released in winter by the burning of New Year's Eve fireworks showed a homogeneous distribution across the study area.

This experimental approach proved to be very effective to trace PM_{10} sources and to map their seasonal and spatial distribution in areas with weak emissions of PM, such as Amersfoort. Furthermore, it allowed us to overcome the limits connected to the study of PM diffusion through the use of mathematical models, and the limits associated to the high cost of a traditional air quality monitoring network. Moreover, the acquired geo-referenced and spatially-resolved chemical data can be used in further studies to evaluate spatial relationships between the concentration of PM_{10} air pollutants and adverse outcomes for human health. Further

investigations are necessary to achieve a full impact assessment of the PM_{10} sources in the study area and to plan the mitigation measures that are needed to protect citizens health.
This approach promises to be a powerful tool for obtaining seasonal and spatially-resolved information about PM composition and sources in several study areas. The obtained information can be integrated with data from existing monitoring networks for a more reliable geo-referenced assessment of population exposure to PM, having high impact on the air quality management.

Author Contributions: L. Massimi conceived and planned the monitoring and the experiments; L. Massimi, J. Wesseling and S. van Ratingen performed the samplings; L. Massimi, I. Javed, M.A. Frezzini and M. L. Astolfi performed the chemical analyses; L. Massimi elaborated the data and wrote the manuscript; L. Massimi, S. Canepari and R. Vermeulen coordinated the group and supervised the manuscript.

References

Abbasi, S., Olander, L., Larsson, C., Olofsson, U., Jansson, A., Sellgren, U. 2012. A field test study of airborne wear particles from a running regional train. Proceedings of the Institution of Mechanical Engineers, Part F: Journal of Rail and Rapid Transit, 226(1), 95-109.

Adler, G., Flores, J. M., Riziq, A. A., Borrmann, S., Rudich, Y. 2011. Chemical, physical, and optical evolution of biomass burning aerosols: a case study. Atmospheric Chemistry and Physics, 11(4), 1491.

Astolfi, M. L., Canepari, S., Catrambone, M., Perrino, C., Pietrodangelo, A. 2006. Improved characterisation of inorganic components in airborne particulate matter. Environmental Chemistry Letters, 3, 186-191.

Astolfi, M. L., Di Filippo, P., Gentili, A., Canepari, S. 2017. Semiautomatic sequential extraction of polycyclic aromatic hydrocarbons and elemental bio-accessible fraction by accelerated solvent extraction on a single particulate matter sample. Talanta, 174, 838-844.

Astolfi, M. L., Protano, C., Marconi, E., Massimi, L., Brunori, M., Piamonti, D., Migliara, G., Vitali, M., Canepari, S. 2020. A new treatment of human hair for elemental determination by inductively coupled mass spectrometry, Analytical Methods, 12, 1906–1918.

Battye, W., Aneja, V. P., Roelle, P. A. 2003. Evaluation and improvement of ammonia emissions inventories. Atmospheric Environment, 37(27), 3873-3883.

Belis, C. A., Karagulian, F., Amato, F., Almeida, M., Artaxo, P., Beddows, D. C. S., ... & Hopke, P. K. 2015. A new methodology to assess the performance and uncertainty of source apportionment models II: The results of two European intercomparison exercises. Atmospheric Environment, 123, 240-250.

Brown, R. J., Van Aswegen, S., Webb, W. R., Goddard, S. L. 2014. UK concentrations of chromium and chromium (VI), measured as water soluble chromium, in PM10. Atmospheric Environment, 99, 385-391.

Canepari, S., Cardarelli, Giuliano, A., E., Pietrodangelo, A. 2006a. Determination of metals, metalloids and non-volatile ions in airborne particulate matter by a new two-step sequential leaching procedure Part A: Experimental design and optimization. Talanta, 69(3), 581-587.

Canepari, S., Cardarelli, E., Pietrodangelo, A., Strincone, M. 2006b. Determination of metals, metalloids and non-volatile ions in airborne particulate matter by a new two-step sequential leaching procedure: Part B: Validation on equivalent real samples. Talanta, 69(3), 588-595.

Canepari, S., Perrino, C., Olivieri, F., Astolfi, M.L. 2008. Characterisation of the traffic sources of PM through size-segregated sampling, sequential leaching and ICP analysis. Atmospheric Environment, 42(35), 8161-8175.

Canepari, S., Pietrodangelo, A., Perrino, C., Astolfi, M. L., Marzo, M. L. 2009. Enhancement of source traceability of atmospheric PM by elemental chemical fractionation. Atmospheric Environment, 43(31), 4754-4765.

Canepari, S., Astolfi, M. L., Farao, C., Maretto, M., Frasca, D., Marcoccia, M., Perrino, C. 2014. Seasonal variations in the chemical composition of particulate matter: a case study in the Po Valley. Part II: concentration and solubility of micro-and trace-elements. Environmental Science and Pollution Research, 21(6), 4010-4022.

Canepari, S., Astolfi, M. L., Catrambone, M., Frasca, D., Marcoccia, M., Marcovecchio, F., Massimi, L., Rantica, E., Perrino, C. 2019. A combined chemical/size fractionation approach to study winter/summer variations, ageing and source strength of atmospheric particles. Environmental Pollution, 253, 19-28.

Catrambone, M., Canepari, S., Cerasa, M., Sargolini, T., Perrino, C. 2019. Performance evaluation of a very-low-volume sampler for atmospheric particulate matter. Aerosol Air Quality Research.

Chen, J., Hoek, G. 2020. Long-term exposure to PM and all-cause and cause-specific mortality: A systematic review and meta-analysis. Environment international, 105974.

Cheng, Y., Engling, G., He, K. B., Duan, F. K., Du, Z. Y., Ma, Y. L., Liang, L., Lu, Z., Liu, J., Zheng, M., Weber, R. J. 2014. The characteristics of Beijing aerosol during two distinct episodes: Impacts of biomass burning and fireworks. Environmental Pollution, 185, 149-157.

Conti, M. E., Iacobucci, M., Cucina, D., Mecozzi, M. 2007. Multivariate statistical methods applied to biomonitoring studies. International Journal of Environment and Pollution, 29(1-3), 333-343.

Engling, G., Herckes, P., Kreidenweis, S. M., Malm, W. C., Collett Jr, J. L. 2006. Composition of the fine organic aerosol in Yosemite National Park during the 2002 Yosemite Aerosol Characterization Study. Atmospheric Environment, 40(16), 2959-2972.

Ervens, B. T. B. W. R., Turpin, B. J., & Weber, R. J. 2011. Secondary organic aerosol formation in cloud droplets and aqueous particles (aqSOA): a review of laboratory, field and model studies. Atmospheric Chemistry & Physics Discussions, 11(8).

Fernández-Camacho, R., Rodríguez, S., De la Rosa, J., de la Campa, A. S., Alastuey, A., Querol, X., González-Castanedo, Y., Garcia-Orellana, I., Nava, S. 2012. Ultrafine particle and fine trace metal (As, Cd, Cu, Pb and Zn) pollution episodes induced by industrial emissions in Huelva, SW Spain. Atmospheric Environment, 61, 507-517.

Frasca, D., Marcoccia, M., Tofful, L., Simonetti, G., Perrino, C., Canepari, S. 2018. Influence of advanced wood-fired appliances for residential heating on indoor air quality. Chemosphere, 211, 62-71.

Fischer, P. H., Marra, M., Ameling, C. B., Velders, G. J., Hoogerbrugge, R., de Vries, W., Wesseling, J., Janssen, N. A. H., Houthuijs, D. 2020. Particulate air pollution from different sources and mortality in 7.5 million adults - The Dutch Environmental Longitudinal Study (DUELS). Science of The Total Environment, 705, 135778.

Garg, B. D., Cadle, S. H., Mulawa, P. A., Groblicki, P. J., Laroo, C., Parr, G. A. 2000. Brake wear particulate matter emissions. Environmental Science & Technology, 34(21), 4463-4469.

Gelaro, R., McCarty, W., Suárez, M. J., Todling, R., Molod, A., Takacs, L., Randles, C. A., Darmenov, A., Bosilovich, M. G., Reichle, R., Wargan, K., Coy, L., Cullather, R., Draper, C., Akella, S., Buchard, V., Conaty, A., da Silva, A. M., Gu, W., Kim, G., Koster, R., Lucchesi, R., Merkova, D., Nielsen, J. E., Partyka, G., Pawson, S., Putman, W., Rienecker, M., Schubert, S. D., Sienkiewicz, M., Zhao, B. 2017. The modern-era retrospective analysis for research and applications, version 2 (MERRA-2). Journal of Climate, 30(14), 5419-5454.

Graham, B., Mayol-Bracero, O. L., Guyon, P., Roberts, G. C., Decesari, S., Facchini, M. C., Fuzzi, S., Andreae, M. O. 2002. Water-soluble organic compounds in biomass burning aerosols over Amazonia 1. Characterization by NMR and GC-MS. Journal of Geophysical Research: Atmospheres, 107(D20), LBA-14.

Greven, F. E., Vonk, J. M., Fischer, P., Duijm, F., Vink, N. M., Brunekreef, B. 2019. Air pollution during New Year's fireworks and daily mortality in the Netherlands. Scientific reports, 9(1), 1-8.

Hendriks, C., Kranenburg, R., Kuenen, J., van Gijlswijk, R., Kruit, R. W., Segers, A., van der Gon, H. D., Schaap, M. 2013. The origin of ambient particulate matter concentrations in the Netherlands. Atmospheric Environment, 69, 289-303.

Jian, X., Olea, R. A., & Yu, Y. S. 1996. Semivariogram modeling by weighted least squares. Computers & Geosciences, 22(4), 387-397.

Johnston, K., Ver Hoef, J. M., Krivoruchko, K., Lucas, N. 2001. Using ArcGIS geostatistical analyst. Vol. 380. Esri.

Kam, W., Delfino, R. J., Schauer, J. J., Sioutas, C. 2013. A comparative assessment of $PM_{2.5}$ exposures in light-rail, subway, freeway, and surface street environments in Los Angeles and estimated lung cancer risk. Environmental Science: Processes & Impacts, 15(1), 234-243.

Kim, M. K., Jo, W. K. 2006. Elemental composition and source characterization of airborne PM 10 at residences with relative proximities to metal-industrial complex. International archives of occupational and environmental health, 80(1), 40-50.

Kloog, I., Ridgway, B., Koutrakis, P., Coull, B.A., Schwartz, J.D. 2013. Long- and short term exposure to $PM_{2.5}$ and mortality using novel exposure models. Epidemiology 24, 555-561.

Knaapen, A. M., Shi, T., Borm, P. J., Schins, R. P. 2002. Soluble metals as well as the insoluble particle fraction are involved in cellular DNA damage induced by particulate matter. In Oxygen/Nitrogen Radicals: Cell Injury and Disease (pp. 317-326). Springer, Boston, MA.

Korhonen, A., Lehtomäki, H., Rumrich, I., Karvosenoja, N., Paunu, V. V., Kupiainen, K., Sofiev, M., Palamarchuk, Y., Kukkonen, L., Kangas, L., Karppinen, A., Hänninen, O. 2019. Influence of spatial resolution on population PM 2.5 exposure and health impacts. Air Quality, Atmosphere & Health, 12(6), 705-718.

Kumar, A., Maroju, S., Bhat, A. 2007. Application of ArcGIS geostatistical analyst for interpolating environmental data from observations. Environmental Progress, 26(3), 220-225.

Leardi, R., Melzi, C., Polotti, G. CAT (Chemometric Agile Tool). Available online: http://gruppochemiometria. it/index.php/software (accessed on 1 February 2020).

Lee, S., Kim, H. K., Yan, B., Cobb, C. E., Hennigan, C., Nichols, S., Chamber, M., Edgerton, E.S., Jansen, J.J., Hu, Y.T., Zheng, M., Weber, R.J., Russell, A.G. 2008. Diagnosis of aged prescribed burning plumes impacting an urban area. Environmental science & technology, 42(5), 1438-1444.

Massimi, L., Ristorini, M., Eusebio, M., Florendo, D., Adeyemo, A., Brugnoli, D., Canepari, S. 2017. Monitoring and evaluation of Terni (Central Italy) air quality through spatially resolved analyses. Atmosphere, 8(10), 200.

Massimi, L., Simonetti, G., Buiarelli, F., Di Filippo, P., Pomata, D., Riccardi, C., Ristorini, M., Astolfi, M. L., Canepari, S. 2020a. Spatial distribution of levoglucosan and alternative biomass burning tracers in atmospheric aerosols, in an urban and industrial hot-spot of Central Italy. Atmospheric Research, 104904.

Massimi, L., Ristorini, M., Astolfi, M. L., Perrino, C., Canepari, S. 2020b. High resolution spatial mapping of element concentrations in PM10: A powerful tool for localization of emission sources. Atmospheric Research, 105060.

Mbengue, S., Alleman, L. Y., Flament, P. 2014. Size-distributed metallic elements in submicronic and ultrafine atmospheric particles from urban and industrial areas in northern France. Atmospheric Research, 135, 35-47.

Mooibroek, D., Schaap, M., Weijers, E. P., Hoogerbrugge, R. 2011. Source apportionment and spatial variability of PM2. 5 using measurements at five sites in the Netherlands. Atmospheric Environment, 45(25), 4180-4191.

Moreno, T., Querol, X., Alastuey, A., Amato, F., Pey, J., Pandolfi, M., Kuenzli, N., Bouso, L., Rivera, M., Gibbons, W. 2010. Effect of fireworks events on urban background trace metal aerosol concentrations: is the cocktail worth the show? Journal of Hazardous Materials, 183(1-3), 945-949.

Minguillón, M. C., Cirach, M., Hoek, G., Brunekreef, B., Tsai, M., de Hoogh, K., Jedynskag, A., Kooterg, I. M., Nieuwenhuijsen, M., Querol, X. 2014. Spatial variability of trace elements and sources for improved exposure assessment in Barcelona. Atmospheric Environment, 89, 268-281.

Nakatsubo, R., Tsunetomo, D., Horie, Y., Hiraki, T., Saitoh, K., Yoda, Y., Shima, M. 2014. Estimate of Regional and Broad-based Sources for PM 2.5 Collected in an Industrial Area of Japan. Asian Journal of Atmospheric Environment (AJAE), 8(3).

Namgung, H. G., Kim, J. B., Woo, S. H., Park, S., Kim, M., Kim, M. S., Bae, G. N., Park, D., Kwon, S. B. 2016. Generation of nanoparticles from friction between railway brake disks and pads. Environmental Science and Technology, 50(7), 3453-3461.

Øvrevik, J. 2019. Oxidative potential versus biological effects: A review on the relevance of cell-free/abiotic assays as predictors of toxicity from airborne particulate matter. International Journal of Molecular Sciences, 20, 4772.

Paramasivam, C.R., Venkatramanan, S. 2019. An Introduction to Various Spatial Analysis Techniques. GIS and Geostatistical Techniques for Groundwater Science, 3, 23-30.

Pant, P., Harrison, R.M. 2013. Estimation of the contribution of road traffic emissions to particulate matter concentrations from field measurements: a review. Atmospheric Environment 77, 78-97.

Park, S. S., Cho, S. Y., Jo, M. R., Gong, B. J., Park, J. S., Lee, S. J. 2014. Field evaluation of a near–real time elemental monitor and identification of element sources observed at an air monitoring supersite in Korea. Atmospheric Pollution Research, 5(1), 119-128.

Perrino, C., Canepari, S., Pappalardo, S., Marconi, E. 2010. Time-resolved measurements of water-soluble ions and elements in atmospheric particulate matter for the characterization of local and long-range transport events. Chemosphere, 80(11), 1291-1300.

Perrino, C., Tofful, L., Dalla Torre, S., Sargolini, T., Canepari, S. 2019. Biomass burning contribution to PM10 concentration in Rome (Italy): Seasonal, daily and two-hourly variations. Chemosphere, 222, 839-848.

Pope III, C. A., Dockery, D. W. 2006. Health effects of fine particulate air pollution: Lines that connect. Journal of the Air & Waste Management Association, 56, 709–742.

Pozzer, A., Tsimpidi, A. P., Karydis, V. A., De Meij, A., Lelieveld, J. 2017. Impact of agricultural emission reductions on fine-particulate matter and public health. Atmospheric Chemistry and Physics, 17(20), 12813.

Querol, X., Moreno, T., Karanasiou, A., Reche, C., Alastuey, A., Viana, M., Font, O., Gil, J., de Miguel, E., Capdevila, M. 2012. Variability of levels and composition of PM_{10} and $PM_{2.5}$ in the Barcelona metro system. Atmospheric Chemistry and Physics, 12(11), 5055-5076.

Russell, M. S. 2009. The chemistry of fireworks. Royal Society of Chemistry.

Schmitz, O., Beelen, R., Strak, M., Hoek, G., Soenario, I., Brunekreef, B., Vaartjes, I., Dijst, M. J., Grobbee, D. E., Karssenberg, D. 2019. High resolution annual average air pollution concentration maps for the Netherlands. Scientific data, 6, 190035.

Setton, E., Marshall, J.D., Brauer, M., Lundquist, K.R., Hystad, P., Keller, P., Cloutier Fisher, D. 2010. The impact of daily mobility on exposure to traffic-related air pollution and health effect estimates. Journal of Exposure Science and Environmental Epidemiology 21, 42-48.

Schauer, J. J., Kleeman, M. J., Cass, G. R., Simoneit, B. R. 2001. Measurement of emissions from air pollution sources. 3. C1− C29 organic compounds from fireplace combustion of wood. Environmental Science and Technology, 35(9), 1716-1728.

Shen, J., Liu, X., Zhang, Y., Fangmeier, A., Goulding, K., Zhang, F. 2011. Atmospheric ammonia and particulate ammonium from agricultural sources in the North China Plain. Atmospheric Environment, 45(28), 5033-5041.

Simoneit, B. R., Schauer, J. J., Nolte, C. G., Oros, D. R., Elias, V. O., Fraser, M. P., Rogge, W.F., Cass, G. R. 1999. Levoglucosan, a tracer for cellulose in biomass burning and atmospheric particles. Atmospheric Environment, 33(2), 173-182.

Simoneit, B. R., Elias, V. O., Kobayashi, M., Kawamura, K., Rushdi, A. I., Medeiros, P. M., Rogge, W. F., Didyk, B. M. 2004. Sugars dominant water-soluble organic compounds in soils and characterization as tracers in atmospheric particulate matter. Environmental Science and Technology, 38(22), 5939-5949.

Simonetti, G., Frasca, D., Marcoccia, M., Farao, C., Canepari, S. 2018. Multi-elemental analysis of particulate matter samples collected by a particle-into-liquid sampler. Atmospheric Pollution Research, 9(4) 747-754.

Squizzato, S., Masiol, M., Brunelli, A., Pistollato, S., Tarabotti, E., Rampazzo, G., & Pavoni, B. 2013. Factors determining the formation of secondary inorganic aerosol: a case study in the Po Valley (Italy). Atmospheric chemistry and physics, 13(4), 1927-1939.

Strak, M., Janssen, N. A., Godri, K. J., Gosens, I., Mudway, I. S., Cassee, F. R., Lebret, E., Kelly, F.G., Harrison, M.R., Brunekreef, B., Steenhof, M., Hoek, G. 2012. Respiratory health effects of airborne particulate matter: the role of particle size, composition, and oxidative potential - the RAPTES project. Environmental Health Perspectives, 120(8), 1183-1189.

Sullivan, A. P., Holden, A. S., Patterson, L. A., McMeeking, G. R., Kreidenweis, S. M., Malm, W. C., Hao, W. M., Wold, C. E., Collett Jr, J. L. 2008. A method for smoke marker measurements and its potential application for determining the contribution of biomass burning from wildfires and prescribed fires to ambient PM2.5 organic carbon. Journal of Geophysical Research: Atmospheres, 113(D22).

Tanda, S., Ličbinský, R., Hegrová, J., & Goessler, W. 2019. Impact of New Year's Eve fireworks on the size resolved element distributions in airborne particles. Environment international, 128, 371-378.

Thorpe, A., Harrison, R. M. 2008. Sources and properties of non-exhaust particulate matter from road traffic: a review. Science of the total environment, 400(1-3), 270-282.

Tian, Y. Z., Wang, J., Peng, X., Shi, G. L., Feng, Y. C. 2014. Estimation of the direct and indirect impacts of fireworks on the physicochemical characteristics of atmospheric PM10 and PM2. 5. Atmospheric Chemistry and Physics, 9469.

Toro, R., Downward, G. S., van der Mark, M., Brouwer, M., Huss, A., Peters, S., Hoek, G., Nijssen, P., Wim M., M., Sas, A., Laar, T., Kromhout, H., Vermeulen, R. 2019. Parkinson's disease and long-term exposure to outdoor air pollution: a matched case-control study in the Netherlands. Environment international, 129, 28-34.

Urban, R. C., Lima-Souza, M., Caetano-Silva, L., Queiroz, M. E. C., Nogueira, R. F., Allen, A. G., Cardoso, A.A, Held, G., Campos, M. L. A. 2012. Use of levoglucosan, potassium, and water-soluble organic carbon to characterize the origins of biomass-burning aerosols. Atmospheric Environment, 61, 562-569.

U.S. Environmental Protection Agency, 1984. U.S. Environmental Protection Agency. Health Effects Assessment for Hexavalent Chromium, EPA 540/1-86-019, U.S. EPA, Washington DC (1984).

Wang, Y., Zhuang, G., Xu, C., An, Z. 2007. The air pollution caused by the burning of fireworks during the lantern festival in Beijing. Atmospheric Environment, 41(2), 417-431.

Weber, R. J., Sullivan, A. P., Peltier, R. E., Russell, A., Yan, B., Zheng, M., de Gouw, J., Warneke, C., Brock, C., Holloway, J.S., Atlas, E.L., Edgerton, E. 2007. A study of secondary organic aerosol formation in the anthropogenic-influenced southeastern United States. Journal of Geophysical Research: Atmospheres, 112(D13).

Xie, Y., Chen, T. B., Lei, M., Yang, J., Guo, Q. J., Song, B., & Zhou, X. Y. 2011. Spatial distribution of soil heavy metal pollution estimated by different interpolation methods: Accuracy and uncertainty analysis. Chemosphere, 82(3), 468-476.

Supplementary Materials

Available at https://www.sciencedirect.com/science/article/pii/S0169809521003276

5.2 (A2) Effects of COVID-19 Lockdown on PM_{10} Composition and Sources in the Rome Area (Italy) by Elements' Chemical Fractionation-based Source Apportionment

Atmospheric Research (2022), 266, 105970-105986, doi: 10.1016/j.atmosres.2021.105970

Lorenzo Massimi[1], Adriana Pietrodangelo[2*], Maria Agostina Frezzini[1], Martina Ristorini[3], Nayma De Francesco[4], Tiziana Sargolini[2], Antonio Amoroso[5], Alessandro Di Giosa[5], Silvia Canepari[1], Cinzia Perrino[2]

[1] Department of Environmental Biology, Sapienza University of Rome, P. le Aldo Moro, 5, Rome, 00185, Italy;

[2] C.N.R. Institute of Atmospheric Pollution Research, Via Salaria, Km 29,300, Monterotondo St., Rome, 00015, Italy;

[3] Department of Bioscience and Territory, University of Molise, Pesche (IS), 86090, Italy;

[4] Department of Chemistry, Sapienza University of Rome, P. le Aldo Moro, 5, Rome, 00185, Italy;

[5] ARPA Lazio, Regional Environmental Protection Agency, Via Boncompagni 101, Rome, 00187, Italy.

*Corresponding author

Keywords: particulate matter; elements; chemical fractionation; source tracer; receptor modelling; PMF.

Abstract

During the national lockdown imposed by Italian government (from March 9th to May 18th 2020) to counter the Covid-19 pandemic, 24-h PM_{10} samples were collected at three sites in the Rome area (Central Italy), two urban (Sapienza and Via Saredo, highly impacted by vehicular traffic) and one peri-urban (Montelibretti, more impacted by biomass domestic heating). Further, at Sapienza and Montelibretti PM_{10} daily sampling had been carried out in the period immediately before lockdown, and at Via Saredo samples were additionally collected also after the end of lockdown. PM_{10} was chemically speciated for main components (major elements, inorganic ions, EC, OC, levoglucosan), and trace elements. The latter were chemically fractionated and considered for their water-soluble and insoluble fractions, which proved to be more source-selective than total element. Three datasets were thus built and analyzed by Positive Matrix Factorization (PMF), with the aim of identifying and apportioning mass contributions of sources acting in the periods before, during and after lockdown, in the Rome area. Identified emission sources were mostly from long-range advection (two different contributions of mineral dust, fresh sea spray, heavy oil combustion), while local sources (vehicular traffic and biomass burning) were strongly abated during lockdown, with respect to previous sampling period, and inorganic secondary aerosol showed a progressive increment of sulfates, driven by seasonal evolution from winter to spring. Since the lockdown interrupted all non-essential productive and work activities, thus reducing the chemical fingerprinting of local sources, this occurrence allowed to clearly describe both profiles and source contribution estimates of long-range transported PM_{10} components. Moreover, it allowed assessing the reduction of the impact of anthropogenic sources (such as vehicular traffic) and the efficiency of mitigation measures generally taken to control PM_{10} mass concentration. Acidic sulfates (bisulfate and letovicite) resulted

associated to mineral dust transport events, and the role of chemically fractionated elements as source-specific tracers was further confirmed.

1. Introduction

During 2020, Coronavirus disease 2019 (Covid-19) has rapidly spread from Wuhan City of China to the rest of the world, representing the new public health threat worldwide (Coccia, 2020; Singhal, 2020; Wang et al., 2020). As a result, several lockdown-based policies have been adopted by different countries to prevent the spread of the virus, including lessening of many human activities (i.e. industries, manufacturing, transport and vehicular traffic, construction works, etc.) As a consequence, considerable decrease in anthropogenic emissions of air pollutants and outstanding changes in ambient air quality and atmospheric composition were widely observed. Therefore, over the last year, numerous studies on the air quality impacts of Covid-19 control measures have been conducted (Collivignarelli et al., 2020; Kumar et al., 2020; Guevara et al., 2021; Arregocés et al., 2021; Manchanda et al., 2021; Shen et al., 2021; Querol et al., 2021). These studies regarded several pollutants, including airborne particulate matter (PM), which is considered as one of the air pollutants exerting most harmful effects on human health (EPA, 1997; World Health Organization, WHO, 2016; Ali et al., 2019; Ramli et al., 2020; Briz-Redón et al., 2021).

Particulate matter has a very complex and variable composition and toxicology, mostly depending on local emitting sources, advected contributions and chemistry of the lower troposphere (i.e. ageing and secondary aerosol formation). Therefore, information about concentration and form of the various chemical species in PM is essential to evaluate the relative relevance of single source contributions and properly plan PM control strategies and mitigation measures to protect citizens health. In Italy, European daily limit value for PM_{10} mass concentration (50 $\mu g/m^3$ for no more than 35 days per year; EU, 2008, Directive 2008/50/EC) is often exceeded in urban areas, especially during the winter season (Tomassetti et al., 2020). As a result, in urban areas such as Rome (Central Italy), policies of traffic reduction, such as traffic stop or green zone design, are frequently taken to control and reduce the mass concentrations of PM in conditions of continue exceedance of the legal limit for several days (Cesaroni et al., 2012). Like for many urban contexts, where PM pollution mainly derives from traffic, commercial and industrial activities, biomass domestic heating and residential energy use (Borck and Pflüger, 2019; Grondys, 2019; Fan et al., 2020), the Rome area is affected by a multi-source pollution. Furthermore, contributions from natural sources, including sea-salt and mineral dust, and secondary aerosol formation significantly affect PM mass concentration in Rome (Perrino et al., 2009 and 2010). This makes a challenge to accurately assess the weight of each source contribution to PM, to the goal of properly addressing PM control strategies and mitigation measures.

To counter the Covid-19 pandemic, the Italian government imposed a national lockdown from March 9th to May 18th 2020, restricting the movement of the population except for necessity or health circumstances, interrupting all non-essential productive and work activities and closing schools and universities (DPCM 11/03/20; DPCM 26/04/20; Guzzetta et al., 2021). The 2-months stop of proactive activities and vehicle circulation offered unique and relevant opportunities to quantify the reduction of the impact of anthropogenic sources of PM due to lockdown, and to assess thus the efficiency of the mitigation measures generally adopted

in Rome. Moreover, the lockdown condition of forced abatement of anthropic sources, allowed evaluating unambiguously the fingerprint of natural emissions on PM concentration and composition.

In this framework, a monitoring campaign was carried out in the urban and peri-urban area of Rome, at three sampling sites, in which PM_{10} samples were collected and chemically characterized for organic and elemental carbon, levoglucosan, ions and macro- and trace-elements. Trace elements were chemically fractionated to increase their selectivity as source tracers (Canepari et al., 2006a, 2006b). The contribution to PM_{10} mass concentration and composition of emission sources during pre-lockdown, lockdown and post-lockdown periods, was assessed by applying the Positive Matrix Factorization (PMF) to the obtained chemical data (Paatero and Tapper, 1994; Querol et al., 2007).

2. Materials and Methods

2.1 Sampling Sites

Rome (41°54'39"24 N, 12°28'54"48 E) is the largest (1300 km^2) and most populated (2.8 million of inhabitants) urban area of Italy (Perrino et al., 2019; Roma Capitale, 2019). With the absence of heavy industrial activities within its territory, vehicular traffic can be considered as the main local emission source of this area (Battista et al. 2016; Roma Capitale, 2015). In addition, seasonal influence of domestic heating, together with more frequent atmospheric stability episodes during winter, can be also considered responsible for higher PM_{10} mass concentration (Perrino et al., 2008). Due to its proximity to the Tyrrhenian coast (about 30 km), PM_{10} is also affected by the influence of marine aerosol, with natural breezes that are expected to be more frequent and intense in the daytime and during summer season (Di Bernardino et al., 2021). Previous studies have also underlined natural advection episodes of desert dust, in some cases even stronger than anthropogenic emissions (Gobbi et al., 2019).

In this urban context, daily PM_{10} samples were collected at three sampling sites, two urban sites: “Sapienza” and “Via Saredo”, and one peri-urban site: “Montelibretti” (Fig. 1). The site Sapienza is located within the Experimental Botanical Garden of Sapienza – University of Rome, in the close proximity of busy roads, bus Terminus and tram stops (at about 300 meters) and can thus be considered as a traffic site. Via Saredo is located within the facility of Environmental Protection Agency of Lazio Region (ARPA Lazio), on the building rooftop. This site is in a residential area crossed by urban arteries impacted by severe traffic conditions. Finally, Montelibretti is situated at about 30 km North-East from Rome, within the Institute of Atmospheric Pollution Research of National Research Council of Italy (CNR-IIA). This site is less affected by vehicular traffic but is located in an area where biomass domestic heating appliances are frequently used during winter.

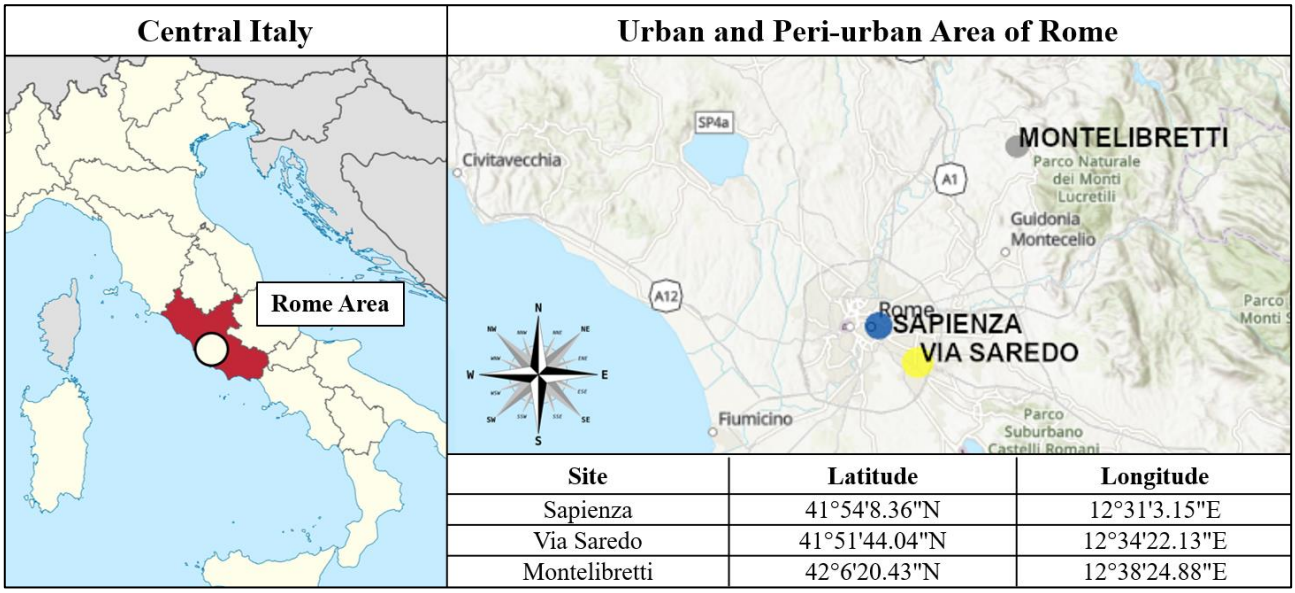

Site	Latitude	Longitude
Sapienza	41°54'8.36"N	12°31'3.15"E
Via Saredo	41°51'44.04"N	12°34'22.13"E
Montelibretti	42°6'20.43"N	12°38'24.88"E

Fig. 1. Map of the three sampling sites in the study area (Rome, Central Italy).

2.2 Sampling Periods

Daily PM_{10} filters were collected during different sampling periods at the three sites as reported in Table 1. At Sapienza, PM_{10} samples were collected from February 2nd (about one month earlier than the beginning of the national lockdown) to May 14th 2020. At Via Saredo, PM_{10} filters were collected from March 31st to June 14th 2020 (about one month later than the end of the lockdown). Finally, at Montelibretti, PM_{10} samples were collected in two separate periods, the first one from January 9th to February 7th 2020 (before lockdown), and the second one from March 14th to May 17th 2020 (during lockdown).

Table 1. PM_{10} sampling periods at the three sites during pre-lockdown, lockdown and post-lockdown.

	Pre-lockdown (before March 9th 2020)	**Lockdown (March 9th - May 18th 2020)**	**Post-Lockdown (after May 18th 2020)**
Sapienza	February 2nd - March 8th 2020	March 9th - May 14th 2020	
Via Saredo		March 31st - May 18th 2020	May 19th - June 14th 2020
Montelibretti	January 9th - February 7th 2020	March 14th - May 17th 2020	

2.2 Sampling Equipment

Sequential samplers working at the flow rate of 2.3 $m^3 h^{-1}$ were employed at the three sampling sites for the collection of 24-h (from midnight to midnight) PM_{10} filters. A DADOLAB Gemini dual channel sampler (Dado lab srl, Cinisello B., MI, Italy), two DIGITEL DPA14 low volume aerosol samplers (Digitel Elektronik AG, Volketswil, Zurich, Switzerland), and a FAI SWAM 5a dual channel (beta attenuation automatic) monitor (Fai Instruments, Fonte Nuova, Rome, RM, Italy) were used at Sapienza, Via Saredo and Montelibretti, respectively. All the samplers were equipped with sampling head systems for PM_{10} certified UNI EN 12341 (2014).

One of the two sampling lines at each site was equipped with Quartz membrane filters (Tissuquartz 2500QAT, 47 mm diameter, pore size 2µm, Pall Life Sciences, NY, United States), while the second line was equipped with Polytetrafluoroethylene (PTFE) membrane filters (47 mm diameter, pore size 2µm, Whatman, Maidstone, United Kingdom).

Moreover, 10 Quartz and 10 PTFE blank filters were left in the unloader of each sampler to be subsequently used for field blanks' analysis and minimum detection limits (MDL) determination.

2.3 Analytical Procedure

Daily PM_{10} filters were chemically analyzed for PM_{10} macro- and micro-components.

Quartz membrane filters were analyzed for elemental carbon (EC) and organic carbon (OC) by thermo-optical analysis (Carbon Aerosol Analyzer, Sunset Laboratory, OR, United Stated), through the application of the NIOSH-quartz temperature protocol (Perrino et al., 2014).

PTFE membrane filters were firstly used for the gravimetric assessment of PM_{10} mass concentration by using an automated microbalance with a sensitivity of 1 µg (mod. ME5, Sartorius AG, Gottingen, Germany) after conditioning the membrane filters at 20 °C and 50% of relative humidity for 48 hours. Subsequently, X-ray fluorescence (X-Lab2000, SPECTRO Analytical Instruments) was employed for the determination of sulfur (S), chloride (Cl), sodium (Na), potassium (K), magnesium (Mg), calcium (Ca), silicon (Si) and aluminum (Al).

PTFE membrane filters were then subjected to the chemical fractionation procedure, consisting in the water-extraction of PM_{10} and in the acid digestion of the residue, followed by elemental analysis of both the soluble and insoluble fractions. This procedure was already optimized (Canepari et al., 2006a, 2006b) and widely used (Astolfi et al., 2018; Massimi et al., 2020b) for increasing the selectivity of the elements as source tracers (Astolfi et al., 2006; Canepari et al., 2009; Perrino et al., 2010), since for many elements the soluble and insoluble fractions are released by different emission sources (Massimi et al., 2020b). Materials and methods of the chemical fractionation are reported in Canepari et al. (2006a and b), and widely detailed in Massimi et al. (2020b). Both the water-extracted and acid-digested solutions were analyzed for 40 elements (Al, As, B, Ba, Be, Bi, Ca, Cd, Ce, Co, Cr, Cs, Cu, Fe, Ga, Ge, K, Li, Mg, Mn, Mo, Na, Nb, Ni, P, Pb, Rb, Sb, Se, Sn, Sr, Te, Ti, Tl, U, V, W, Zn, Zr) by using a quadrupole inductively coupled plasma mass spectrometer (ICP-MS; model 820-MS; Bruker, Bremen, Germany) equipped with a glass nebulizer (0.4 mL min^{-1}; Analytik Jena AG,

Jena, Germany). For each element, external standard calibration curve was performed in the range 1-500 µg L^{-1} by serially diluting stock standard solutions (1000 ± 2 mg L^{-1}; Exaxol Italia Chemical Manufacturers Srl, Genoa, Italy; Ultra Scientific, North Kingstown, RI, USA; Merck Millipore Ltd., Billerica, MA, USA). To control nebulizer efficiency, Y and Rh (1000 ± 2 mg L^{-1}; Panreac Química, Barcelona, Spain) were used as internal standards for all measurements and set at 5 µg L^{-1} and 20 µg L^{-1}, respectively. The instrumental conditions are detailed in Astolfi et al. (2020).

In addition to the elements, the soluble fraction of PM_{10} was analyzed for anionic and cationic components and for levoglucosan (LVG). Ions (Ca^{2+}, Cl^-, K^+, Mg^{2+}, Na^+, NH_4^+, NO_3^-, SO_4^{2}) were analyzed by ion chromatography (IC; ICS1000, Dionex Co., Sunnyvale, CA, USA), while levoglucosan was analyzed by High-Performance Anion-Exchange Chromatography with Pulsed Amperometric Detection (HPAEC-PAD). Additional information about the instrument setup and analytical conditions are largely described by Perrino et al. (2019).

2.4 Positive Matrix Factorization

A receptor modelling approach (RM) based on positive matrix factorization (PMF) was employed to identify sources acting during sample collection, and apportion PM_{10} sample mass to source contributions. Source apportionment by RM is based on the requirement that the mass balance equation:

$$x_{ij} = \sum_{k=1}^{p} g_{ik} f_{kj} + e_{ij} \quad (1)$$

is obeyed, where x_{ij} is the measured mass fraction of species j in sample i, g_{ik} is the mass contribution of the source k to sample i, f_{kj} is the fractional abundance of the species j in source k, and e_{ij} is the residual between the measured and modelled mass fraction of species. The PMF (Paatero and Tapper, 1994) is a factor analysis technique consisting in a weighted least square fit, where non-negativity constraints are imposed in the factor computational process, to reduce rotational freedom of the input data matrix. A more detailed description of PMF technique is found elsewhere (Paatero, 1999; Hopke, 2000).

The U.S. EPA-PMF v5.0 software (Norris et al., 2014) was used in this work, that is accomplished by the Multilinear Engine (ME-2) platform (Paatero, 1999).

To obtain an input data matrix suitable for PMF analyses, the number of chemical variables required to be reduced with respect to the available PM_{10} samples. The percentage of selected variables for PM_{10} source apportionment respect to the total number of PM_{10} chemical components analyzed is of 29%. The number of analyzed variables not used for PMF analysis is of 69, most of them are elements less selective in tracing different emission sources respect to those used in this study. The following variables were selected to be used for the PMF: EC, OC, levoglucosan, SO_4^-, Cl^-, Na^+, K^+, Mg^{2+}, NH_4^+, NO_3 ions, total Al, Si and Ca, soluble fraction of Cs, Ni, Rb, Tl and V, insoluble fraction of Cs, Cu, Fe, Li, Mo, Rb, Sb, Sn, Ti and V, and PM_{10} mass concentration. The variables were chosen depending on their ability to selectively trace PM_{10} emission sources, which is widely documented in previous studies (Perrino et al., 2009, Masiol et al., 2010; Tian et al., 2013; Sharma et al., 2016). To the goals of input variable selection, species determined by more than one technique

(namely: ICP-MS (soluble fraction) and IC, or ICP-MS (total element) and XRF) were checked for internal consistency by linear regression. Na, K, Mg were included in PMF as ion species, while Ca, Si and Al were included as total element determined by XRF. Major species (EC, OC, levoglucosan, nitrate, sulfate and ammonium ions (NSA) were all included, while trace elements were selected for their soluble or insoluble fraction, based on previous knowledge of the role of element fraction as source tracer (Canepari et al., 2014 and 2019; Massimi et al., 2020b).

PMF analysis was performed separately at each site, to the aim of evidencing possible site-related differences of sources impact. The same chemical variables were employed for each PMF to make PMF outputs comparable among different computations on different sites. Preliminary PMF analyses of separated pre- and post-lockdown periods produced unstable solutions due to limited temporal coverage. Therefore, for each site, all samples collected in the different periods were combined in the same PMF runs. For Via Saredo, missing data were automatically replaced by median value. For Sapienza and Montelibretti, median values were calculated separately for the pre-lockdown and lockdown periods and used to replace missing data in the combined analysis. Minimum detection limit of each variable was set as mean plus 3 times the standard deviation (SD) of 10 replicate blank determinations, data below MDL were replaced with MDL/2. Percentages of data above MDL range 80-100 for all selected variables. Uncertainties calculations were based on the approach by Polissar et al. (1998) for data below MDL, and by the equation-based method described by Norris et al. (2014) for data greater than MDL. For median-replaced data, uncertainties were calculated as four times the species median.

The final input matrices for PMF at the three sites include 29 chemical variables and 94 (Sapienza and Montelibretti) or 75 (Via Saredo) PM_{10} daily samples. MDL and descriptive statistics of the variables used for the PMF are reported in Tables 2, 3 and 4.

At all sites, the signal-to-noise (S/N) criterion (Paatero and Hopke, 2003) was ≥ 2 for all selected variables, indicating that they retain far larger signal than noise. All variables were thus categorized in the PMF model as *strong*, with the exception of PM_{10} (total variable).

PMF solutions were investigated in Q robust mode. During preliminary analysis, 5 to 9 factors were extracted at each site by initial steps of 50 consecutive runs and approaching to local minima was monitored by the Q robust/Q expected ratio (Q_{rob}/Q_{exp}). The final number of factors was determined as best compromise between the Q_{rob}/Q_{exp} trend and the physical soundness of extracted factor profiles. Diagnostic species ratios of factor profiles were assessed to this goal. Factors describing long-range transport contributions were checked by backtrajectory analysis (HYSPLIT Trajectory Model). Final solution was obtained by 100 runs.

Error estimation of PMF factor analytic solutions was performed by classical bootstrap (BS), displacement of factor elements (DISP), and bootstrap enhanced by displacement (BS-DISP), available with the PMF v5.0 package.

3. Results and discussion

3.1 PM_{10} Mass Concentration

PM_{10} mass concentration was monitored to evaluate its variability in the study area among pre-lockdown, lockdown and post-lockdown (Tables 2, 3 and 4).

During pre-lockdown and lockdown, mean concentration at Sapienza was 29±11 µg/m³ and 20±11 µg/m³, respectively, while at Montelibretti, it was 32±15 µg/m³ and 21±10 µg/m³, respectively. The decrease in PM_{10} mass concentration (of about 10 µg/m^3) in the lockdown period can be due to different factors acting simultaneously, such as a more efficient mixing of the lower atmosphere, which is typical of the warmer period (Perrino et al., 2008), the decrease in the strength of typical winter sources like biomass domestic heating (Massimi et al., 2020a), and the decreased impact of all non-essential productive and work activities reduced during the lockdown. However, the latter factor would have been expected to lead to a larger decrease in PM_{10} mass concentration than observed. Reasons for this lower-than-expected decrease will be discussed in the following paragraphs. On the other hand, at Via Saredo, mean PM_{10} mass concentration during lockdown and post-lockdown was 19±7 µg/m³ and 20±11 µg/m³, respectively, indicating that the resumption of productive and work activities during post-lockdown leaded to a very-weak increase in PM_{10} mass concentration.

Table 2. MDL and descriptive statistics of PM_{10} mass and PM_{10} chemical compounds concentrations determined at Sapienza.

			Sapienza							
			Pre-lockdown				Lockdown			
	UoM	MDL	Mean	Std. Dev.	Median	Range (min-max)	Mean	Std. Dev.	Median	Range (min-max)
PM_{10}	µg/m³	-	29	11	30	7.2 - 48	20	11	17	8.1 - 65
OC	µg/m³	0.4	7.2	3.5	6.5	1.2 - 15	4.9	2.5	3.9	2.1 - 12
EC	µg/m³	0.12	1.8	0.88	1.6	0.31 - 3.8	0.47	0.29	0.41	0.11 - 1.4
LVG	µg/m³	0.051	0.45	0.35	0.36	0.0042 - 0.13	0.21	0.21	0.14	0.015 - 0.84
SO_4^-	µg/m³	0.011	1.1	0.6	1.1	0.11 - 2.6	1.9	1.7	1.6	0.47 - 11
Cl^-	µg/m³	0.0021	2.5	3.2	12	0.11 - 12	5.7	1.1	1.8	0.017 - 49
Na^+	µg/m³	0.0022	16	15	12	0.13 - 6.2	0.66	0.79	0.34	0.027 - 3.4
K^+	µg/m³	0.0051	0.31	0.15	0.28	0.053 - 0.65	0.19	0.15	0.15	0.057 - 0.59
Mg^{2+}	µg/m³	0.0051	0.21	0.19	0.15	0.025 - 0.77	0.11	0.11	0.064	0.016 - 0.49
NH_4^+	µg/m³	0.0021	0.42	0.53	0.21	0.016 - 2.6	0.51	0.31	0.39	0.12 - 1.3
NO_3^-	µg/m³	0.0051	3.6	2.7	3.1	0.6- 12	1.4	0.9	1.1	0.23 - 4.6
Al	µg/m³	0.012	0.057	0.028	0.056	0.001 -0.10	0.14	0.14	0.11	0.016 - 0.73
Si	µg/m³	0.011	0.18	0.089	0.18	0.0038 - 0.33	0.66	0.68	0.46	0.073 - 3.5
Ca	µg/m³	0.013	0.76	0.22	0.76	0.17 - 1.3	0.84	1.11	0.61	0.085 - 6.2
Soluble Cs	ng/m³	0.00093	0.039	0.042	0.026	0.00046 - 0.18	0.022	0.042	0.014	0.0038 - 0.11
Soluble Ni	ng/m³	0.081	0.25	0.34	0.096	0.041 - 1.5	0.28	0.21	0.21	0.041 - 0.98
Soluble Rb	ng/m³	0.021	1.2	1.1	0.96	0.011 - 4.1	0.83	0.93	0.44	0.14 - 3.3
Soluble Tl	ng/m³	0.00051	0.065	0.11	0.037	0.00025 - 0.56	0.039	0.051	0.024	0.0052 - 0.25
Soluble V	ng/m³	0.074	0.33	0.23	0.29	0.037 - 0.77	0.52	0.42	0.41	0.081 - 1.8
Soluble Cs	ng/m³	0.0016	0.049	0.022	0.051	0.014 - 0.11	0.042	0.029	0.035	0.0079 - 0.15
Insoluble Cu	ng/m³	0.86	18	10	17	4.5 - 49	3.4	1.8	2.9	0.94 - 11
Insoluble Fe	ng/m³	32	631	348	614	132 - 1792	250	156	201	50 - 818
Insoluble Li	ng/m³	0.012	0.084	0.053	0.083	0.0059 - 0.25	0.15	0.17	0.089	0.024 - 0.88
Insoluble Mo	ng/m³	0.039	1.2	0.7	1.1	0.24 - 3.7	0.37	0.21	0.31	0.061 - 0.98
Insoluble Rb	ng/m³	0.052	0.53	0.26	0.51	0.14 - 1.3	0.46	0.33	0.36	0.11 - 1.8
Insoluble Sb	ng/m³	0.23	2.1	1.9	1.7	0.31 - 11	0.59	0.49	0.42	0.12 - 1.9
Insoluble Sn	ng/m³	0.18	4.1	2.5	4.1	0.58 - 12	0.91	0.51	0.78	0.089 - 2.7
Insoluble Ti	ng/m³	0.61	5.5	2.6	5.2	1.1 - 10	6.5	5.5	5.1	1.5 - 30
Insoluble V	ng/m³	0.068	0.51	0.32	0.47	0.033 - 1.7	0.54	0.49	0.36	0.033 - 2.5

Table 3. MDL and descriptive statistics of PM_{10} mass and PM_{10} chemical compounds concentrations determined at Via Saredo.

			Via Saredo							
			Lockdown				Post-lockdown			
	UoM	MDL	Mean	Std. Dev.	Median	Range (min-max)	Mean	Std. Dev.	Median	Range (min-max)
PM_{10}	µg/m³	-	19	7	18	10.0 - 34	20	11	18	10.0 - 34
OC	µg/m³	0.4	4.6	2.2	3.8	1.6 - 9.2	3.4	0.9	3.3	1.9 - 5.6
EC	µg/m³	0.12	0.49	0.24	0.43	0.19 - 1.1	0.55	0.21	0.48	0.31 - 1.1
LVG	µg/m³	0.051	0.21	0.11	0.18	0.053 - 0.47	0.11	0.029	0.11	0.037 - 0.17
SO_4^-	µg/m³	0.011	1.9	0.9	1.6	0.47 - 3.8	1.1	0.4	1.1	0.44 - 2.5
Cl^-	µg/m³	0.0021	0.55	0.98	0.099	0.015 - 3.9	0.88	1.2	0.25	0.016 - 4.5
Na^+	µg/m³	0.0022	0.56	0.66	0.25	0.026 - 2.6	0.86	0.88	0.49	0.035 - 3.3
K^+	µg/m³	0.0051	0.18	0.091	0.15	0.071 - 0.36	0.11	0.047	0.098	0.036 - 0.22
Mg^{2+}	µg/m³	0.0051	0.085	0.076	0.054	0.016 - 0.32	0.12	0.11	0.075	0.016 - 0.41
NH_4^+	µg/m³	0.0021	0.54	0.37	0.46	0.097 - 1.3	0.24	0.11	0.23	0.065 - 0.58
NO_3^-	µg/m³	0.0051	1.3	0.6	1.3	0.25 - 2.7	1.1	0.6	0.96	0.19 - 2.9
Al	µg/m³	0.012	0.14	0.11	0.096	0.039 - 0.47	0.23	0.25	0.14	0.026 - 1.1
Si	µg/m³	0.011	0.59	0.44	0.42	0.16 - 2.1	0.96	1.11	0.58	0.11 - 4.6
Ca	µg/m³	0.013	0.67	0.36	0.62	0.18 - 1.8	0.92	0.67	0.75	0.25 - 3.5
Soluble Cs	ng/m³	0.00093	0.017	0.012	0.013	0.0031 - 0.042	0.0058	0.0035	0.0055	0.0012 - 0.017
Soluble Ni	ng/m³	0.081	0.29	0.24	0.22	0.041 - 0.85	0.13	0.14	0.11	0.041 - 0.88
Soluble Rb	ng/m³	0.021	0.62	0.39	0.48	0.19 - 1.5	0.25	0.15	0.23	0.039 - 0.75
Soluble Tl	ng/m³	0.00051	0.026	0.017	0.021	0.0036 - 0.068	0.013	0.014	0.0079	0.0013- 0.069
Soluble V	ng/m³	0.074	0.52	0.46	0.34	0.058 - 1.5	0.25	0.17	0.19	0.043 - 0.71
Soluble Cs	ng/m³	0.0016	0.044	0.019	0.041	0.018 - 0.089	0.071	0.049	0.061	0.0092 - 0.21
Insoluble Cu	ng/m³	0.86	2.8	1.1	2.6	1.3 - 5.7	4.9	2.6	3.9	1.5 - 13
Insoluble Fe	ng/m³	32	237	83	209	113 - 449	357	224	286	73 - 1151
Insoluble Li	ng/m³	0.012	0.069	0.079	0.036	0.0059 - 0.28	0.18	0.24	0.11	0.0059 - 0.98
Insoluble Mo	ng/m³	0.039	0.33	0.14	0.29	0.14 - 0.65	0.41	0.21	0.36	0.13 - 0.99
Insoluble Rb	ng/m³	0.052	0.46	0.19	0.41	0.18 - 0.79	0.71	0.52	0.58	0.079 - 2.2
Insoluble Sb	ng/m³	0.23	0.59	0.32	0.59	0.12 - 1.2	0.77	0.64	0.52	0.12 - 3.1
Insoluble Sn	ng/m³	0.18	0.95	0.39	0.93	0.41 - 2.1	1.2	0.6	1.1	0.37 - 3.1
Insoluble Ti	ng/m³	0.61	6.8	3.2	5.6	2.7 - 14	10	9	8	1.5 - 46
Insoluble V	ng/m³	0.068	0.58	0.28	0.53	0.18 - 1.4	0.82	0.62	0.65	0.21 - 3.1

Table 4. MDL and descriptive statistics of PM_{10} mass and PM_{10} chemical compounds concentrations determined at Montelibretti.

			Montelibretti							
			Pre-lockdown				Lockdown			
	UoM	MDL	Mean	Std. Dev.	Median	Range (min-max)	Mean	Std. Dev.	Median	Range (min-max)
PM_{10}	µg/m³	-	32	15	34	3.5 - 59	21	10	18	5.2 - 49
OC	µg/m³	0.4	11	5	11	1.9 - 20	4.7	2.7	3.8	1.7 - 12
EC	µg/m³	0.12	1.1	0.5	1.2	0.083 - 1.9	0.36	0.26	0.29	0.066 - 1.2
LVG	µg/m³	0.051	1.2	0.6	1.3	0.056 - 2.1	0.26	0.27	0.13	0.022 - 0.97
SO_4^-	µg/m³	0.011	0.46	0.23	0.44	0.035 - 0.92	1.8	1.2	1.6	0.41 - 7.8
Cl^-	µg/m³	0.0021	0.53	0.71	0.23	0.042 - 3.1	0.41	0.79	0.12	0.011 - 4.1
Na^+	µg/m³	0.0022	0.46	0.52	0.21	0.067 - 2.1	0.51	0.61	0.26	0.033 - 3.1
K^+	µg/m³	0.0051	0.67	0.31	0.73	0.048 - 1.1	0.24	0.17	0.19	0.048 - 0.72
Mg^{2+}	µg/m³	0.0051	0.067	0.062	0.036	0.017 - 0.25	0.082	0.078	0.054	0.013 - 0.39
NH_4^+	µg/m³	0.0021	0.79	0.51	0.77	0.031 - 2.1	0.49	0.34	0.35	0.11 - 1.6
NO_3^-	µg/m³	0.0051	3.2	1.6	3.2	0.18 - 5.9	1.2	0.8	1.1	0.065 - 4.1
Al	µg/m³	0.012	0.089	0.078	0.071	0.0091 - 0.31	0.14	0.16	0.08	0.0072 - 1.1
Si	µg/m³	0.011	0.38	0.35	0.28	0.033 - 1.3	0.61	0.69	0.36	0.038 - 4.3
Ca	µg/m³	0.013	0.61	0.29	0.62	0.072 - 1.2	0.71	0.67	0.54	0.069 - 3.4
Soluble Cs	ng/m³	0.00093	0.15	0.09	0.15	0.0073 - 0.31	0.052	0.052	0.029	0.0035 - 0.28
Soluble Ni	ng/m³	0.081	0.25	0.011	0.23	0.041 - 0.59	0.32	0.19	0.28	0.039 - 1.2
Soluble Rb	ng/m³	0.021	2.9	1.6	3.1	0.16 - 5.4	1.1	0.9	0.78	0.19 - 4.2
Soluble Tl	ng/m³	0.00051	0.092	0.046	0.11	0.0071 - 0.16	0.033	0.038	0.021	0.0041 - 0.22
Soluble V	ng/m³	0.074	0.12	0.085	0.088	0.022 - 0.34	0.39	0.29	0.31	0.049 - 1.2
Soluble Cs	ng/m³	0.0016	0.081	0.066	0.065	0.011 - 0.32	0.058	0.037	0.051	0.0093 - 0.16
Insoluble Cu	ng/m³	0.86	5.4	2.6	5.6	1.1 - 11	1.8	0.9	1.6	0.43 - 4.6
Insoluble Fe	ng/m³	32	226	103	215	44 - 494	169	137	125	16 - 736
Insoluble Li	ng/m³	0.012	0.091	0.068	0.069	0.014 - 0.31	0.14	0.16	0.081	0.017 - 0.88
Insoluble Mo	ng/m³	0.039	1.1	1.1	0.6	0.059 - 4.7	0.12	0.11	0.093	0.019 - 0.64
Insoluble Rb	ng/m³	0.052	0.41	0.21	0.38	0.091 - 0.97	0.45	0.31	0.37	0.063 - 1.5
Insoluble Sb	ng/m³	0.23	1.1	1.1	0.92	0.12 - 5.5	0.49	0.46	0.35	0.12 - 2.5
Insoluble Sn	ng/m³	0.18	1.4	0.6	1.4	0.19 - 2.6	0.48	0.29	0.42	0.089 - 1.4
Insoluble Ti	ng/m³	0.61	5.4	3.6	4.7	0.76 - 16	5.3	5.5	3.5	0.31 - 27
Insoluble V	ng/m³	0.068	0.46	0.25	0.43	0.11 - 1.2	0.45	0.43	0.34	0.033 - 2.3

3.2 Chemically Fractionated Trace Elements for Source Apportionment

Trace elements in PM are still scarcely considered as selective source markers, although their recently highlighted relevant role in identifying PM sources (Massimi et al., 2020b; Perrino et al., 2020; Zhou et al., 2020). This may be due to the difficulty in discriminating tracer species that can be associated to more than one source (Querol et al., 2007). However, the chemical fractionation procedure (Canepari et al., 2006a, 2006b, 2010) allows assessing the chemical form (soluble and insoluble) in which each element is released in PM, which may be typical of its emission source (Massimi et al., 2020b), thus being very efficient for the identification of several sources (Yadav and Rajamani, 2006; Feng et al., 2009; Canepari et al., 2010; Betha et al., 2014; Li et al., 2015).

In this study, before employing chemically fractionated elements for PM_{10} source apportionment, linear correlation coefficients (R^2) were checked between reliable and commonly used source markers and trace elements in the soluble and insoluble fractions.

In Fig. 2, comparisons between the daily variability in concentration of soluble Rb and LVG (panel a), of insoluble Rb and Si (panel b), of soluble V and soluble Ni (panel c), and of insoluble V and Si (panel d), at Sapienza during lockdown (from March 14th to May 13th) are shown. LVG, Si and Ni are widely recognized as highly selective tracers of biomass burning (Chowdhury et al., 2007; Sharma et al., 2016; Massimi et al., 2020a), crustal dust (Pant and Harrison, 2012; Tian et al., 2013; Perrino et al., 2020) and heavy oil combustion (Reddy et al., 2005; Okuda et al., 2007; Moreno et al., 2010), respectively.

The temporal trend of soluble Rb (panel a) was practically identical to that of LVG (R^2 = 0.95), both showing a marked decrease from the colder to the warmer period. The same behavior was observed for soluble Cs (R^2 = 0.92; supplementary material S1), confirming the possible use of the soluble fraction of Rb and Cs as robust tracers for biomass burning sources. On the contrary, the insoluble fraction of Rb (panel b) showed a completely different trend, closely matching that of Si (R^2 = 0.81); similar behaviour is also shown by the insoluble fraction of Cs, Li and Ti (R^2 = 0.75, 0.92 and 0.88, respectively; supplementary material S1) which are contained in soil (Canepari et al., 2019; Massimi et al., 2020b), and of V (panel d). Maximum values of Si and of insoluble Rb, Cs, Li, Ti and V were observed during March 29th-30th, April 8th-10th, 18th-20th, and May 13th-14th. These days were characterized by events of mineral dust advection from desert regions (see section 3.5), thus confirming the reliability of these species as tracers of crustal dust. Moreover, since advection days occurred within the lockdown period, this presumably contributed to the lower-than-expected decrease of PM_{10} mass concentration during lockdown with respect to other periods (see section 3.1).

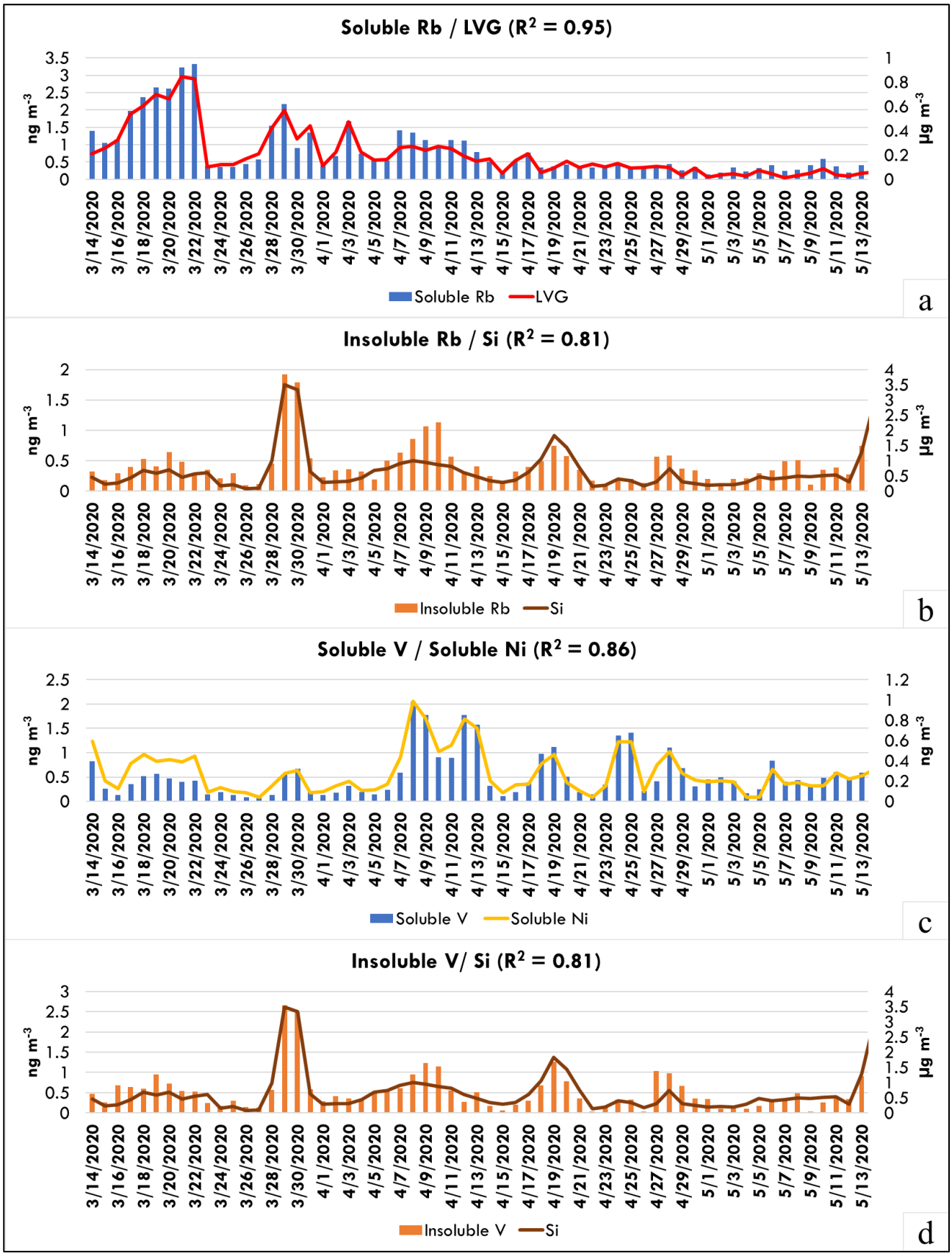
Soluble Rb / LVG (R^2 = 0.95)
ng m-3
µg m-3
Soluble Rb
LVG
a
Insoluble Rb / Si (R^2 = 0.81)
ng m-3
µg m-3
Insoluble Rb
Si
b
Soluble V / Soluble Ni (R^2 = 0.86)
ng m-3
ng m-3
Soluble V
Soluble Ni
c
Insoluble V/ Si (R^2 = 0.81)
ng m-3
µg m-3
Insoluble V
Si
d

Fig. 2. Comparison between concentrations of soluble Rb and LVG (panel a), insoluble Rb and Si (panel b), soluble V and soluble Ni (panel c), and insoluble V and Si (panel d), obtained at Sapienza from March 14th to May 13th (lockdown period).

On the other hand, from panel c, we can observe a high correlation (R^2 = 0.86) between concentrations of soluble V and soluble Ni. Both V and Ni are commonly employed in the form of total element, for their source selectivity with heavy oil combustion (Allouis et al., 2003; Moreno et al., 2010). The chemical fractionation put on evidence, in addition, that the soluble V and Ni are more involved than their insoluble fraction in describing the fingerprint of this source. Peaks of soluble V and Ni observed on the first week of April and, minor, on April 24th-28th (Fig.2, panel c) correspond to advections of heavy oil burning dust (Campanelli et al., 2021), as it will be discussed in section 3.5; however, these peaks are not observed for the insoluble V (panel d) and Ni (not reported).

For Cs, Rb and V, the solubility percentage is of 65%, 88% and 20% respectively.

Finally, Cu, Fe, Mo, Sn, Sb in their insoluble fraction, are known to be emitted by mechanical abrasion of vehicles components, since they are commonly used as components of tires, brake pads and linings (Amato et al., 2011; Tofful et al., 2020; Massimi et al., 2021). The high inter-correlation between temporal variability of insoluble Sb and Sn (supplementary material S1) confirmed their efficiency to trace brake dust (Querol et al., 2012; Kam et al., 2013; Namgung et al., 2016; Canepari et al., 2019; Massimi et al., 2020b). Moreover, the ability of chemically fractionated elements to trace different sources is supported by documented existence of very substantial differences in the size distribution of the two fractions of the considered elements (Canepari et al., 2019; Massimi et al., 2020b). These considerations encourage the use of chemically fractionated trace elements for the identification of emission sources in PM_{10} source apportionment studies (Canepari et al., 2009; Perrino et al., 2010; Massimi et al., 2021).

3.3 Source Apportionment

The most stable PMF solution extracts 7 factors at both urban traffic sites Sapienza and Via Saredo, and 8 factors at Montelibretti. Scaled residuals are within ± 3 SD for most species, with symmetrical distribution; exceptions concern, at all sites, Ca, the soluble fraction of Ni and Tl, and the insoluble fraction of Cs, Mo and Sb.

The rotation by F-peak did not improve the interpretability of factor profiles, therefore the base case with F-peak = 0 was considered as best fit (Belis et al., 2019). G-space plots were examined to exclude the presence of oblique edges between factors, and the Q_{robust}/Q_{exp} indicator was monitored. The best solution at each site showed Q_{robust}/Q_{exp} ranging 1.2-1.3.

The effect of measurement errors and of rotational ambiguity on solutions were investigated by classical bootstrap (BS), displacement of factor elements (DISP), and bootstrap enhanced by displacement (BS-DISP) tools available by EPA PMF v5.0. Regardless of data perturbation approaches, source tracers of each factor

contribution show tight variability intervals, as shown in supplementary material S2, indicating that the factors extracted in the final solution are generally neither affected by uncertainties of data measurement, nor by rotational ambiguity during PMF runs. Higher uncertainties are instead associated to species not representing source tracers, by factor, as indicated by larger intervals of variability estimated by DISP and BS-DISP analyses.

Factors identified at all sites are vehicular traffic, biomass burning, sea spray, heavy oil combustion, two different mineral dust profiles, and ammonium sulfate and organics. In addition, ammonium nitrate is extracted at Montelibretti. From Fig. 3, we can observe the chemical profiles of the factors identified by PMF at Sapienza during the entire monitoring period, while chemical profiles of the factors identified at Via Saredo and Montelibretti are reported in supplementary material S3. The related average percent source contributions to PM_{10} mass concentration for pre-lockdown, lockdown and post-lockdown are shown in Fig. 6.

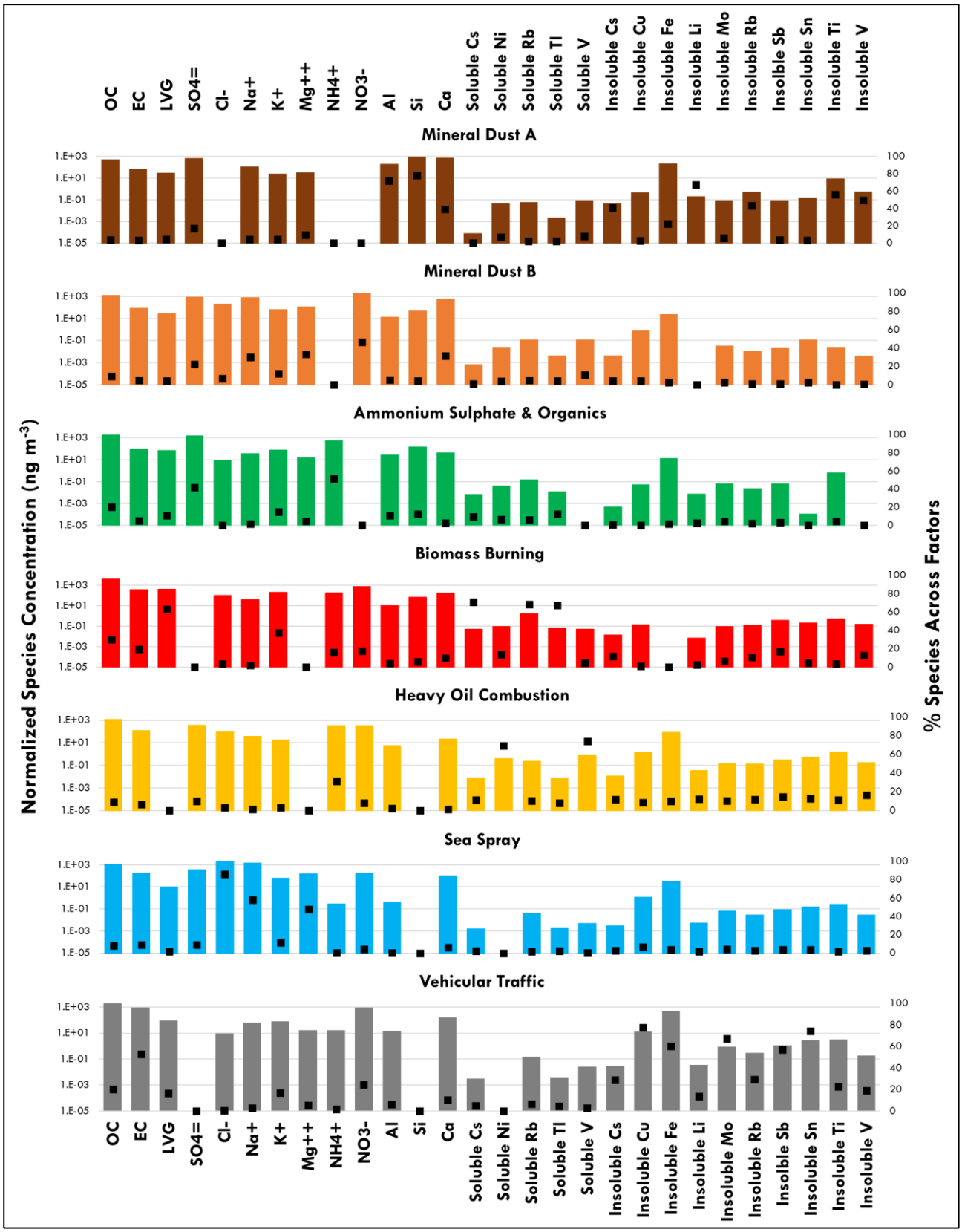

Fig. 3. Chemical profiles of the factors identified by PMF at Sapienza during the entire monitoring period.

3.3.1 Vehicular traffic

Most abundant species describing this factor are organic and elemental carbon, and to minor extent Ca and insoluble Fe. EC/OC ratios are 0.4, 0.2 and 0.1 at Sapienza, Via Saredo and Montelibretti, respectively, comparable to the variability range of traffic profiles determined at Italian cities in recent years. In particular, traffic profiles no. 147, 265, 270, 280 and 290 (related to Milan, Genoa, Bari and Civitavecchia) of the SPECIEUROPE repository (Pernigotti et al., 2016) show EC/OC ratio ranging 0.3 – 0.8. At Montelibretti, the OC abundance in the profile is far larger than at the two urban sites, while the EC abundance is lower. Most probable explanation for this difference is the perturbation due to biomass burning, that during the first sampling period was considerably active at Montelibretti. Furthermore, it has to be noted that the non-exhaust component is also included in this factor. The PMF model was not able to disaggregate it from the exhaust part due to unavailability of selective tracers for the exhausts, whereas non-exhaust tracers were largely used. The non-exhaust is described by the presence of Ca, that is commonly related to asphalt abrasion, and of the insoluble fraction of Fe, Cu, Mo, Sb and Sn. The variability of the Ca/insoluble Fe ratio at the three sites (0.3, 0.9. and 1.1 at Sapienza, Montelibretti and Via Saredo, respectively) depends on the almost doubled abundance of Ca at Via Saredo with respect to the other sites, likely due to the presence of gravel in the public park in the nearby of sampling site, and to the lower abundance of insoluble Fe at Montelibretti. A large variability in the Ca/Fe ratio is anyway observed in traffic profiles, i.e. ranging 0.1 – 0.8 for the above cited ones. The variance of insoluble fraction of Fe, Cu, Mo, Sb and Sn is mostly explained by the vehicular traffic factor, with percent of total species ranging 60-80 %.

3.3.2 Biomass burning

This factor is mainly described by OC, EC, LVG and K^+, representing respectively the 35-50%, 4-5%, 3-5% and 2.8% of the PM_{10} mass contribution apportioned to this source. Both LVG and K^+ are widely acknowledged as selective tracers of biomass combustion (Pant and Harrison, 2012; Nguyen et al., 2013; Liu et al., 2017; Chowdhury et al., 2007; Sharma et al., 2016).

Inter-site differences of profile are very limited, which is explained by the fact that all sites are in the same area, where comparable biomass types are expected to be burned. The EC/OC, LVG/OC, K+/LVG and Cs/Rb (soluble fractions) ratios observed in the biomass burning profile of the three sites are reported in Table S3.1, with the respective variability range calculated on a number of biomass burning profiles available in SPECIEUROPE. Values of the ratios fall within the range of the available profiles.

At Via Saredo, however, either EC/OC and K+/LVG are out of the respective range, because of the lower percent abundance of EC and LVG in the biomass burning profile with respect to the other sites. This can be partly due to the almost negligible strength of this source during late spring, when samples were collected at Via Saredo. Nevertheless, at this site the LVG explained by biomass burning is 44% of total species, comparably with the 47% explained at Montelibretti (and 60% at Sapienza). It has to be noted that Cs/Rb has been rarely considered as diagnostic ratio of biomass burning. As shown in Table S3.1, with respect to other

diagnostic ratios, the Cs/Rb shows narrow variability within SPECIEUROPE biomass burning profiles, ranging 0.04-0.06. At the three sites of this study, Cs/Rb values calculated on the total element (available in the extended dataset not used for PMF) fall within the above range, namely: 0.07 ± 0.01 (median 0.07; min-max: 0.05-0.1) at Montelibretti and Via Saredo, and 0.05 ± 0.01 (median 0.05; min-max: 0.03-0.08) at Sapienza. Nevertheless, using in the PMF the soluble fraction of Cs and Rb, instead of total, resulted in highly efficient tracing of biomass burning. This indicates that soluble Cs, Rb and Tl (not shown) are far more selective tracers of biomass burning than the total element content. Indeed, by using the total element, source tracing can be perturbed by the influence of other sources, that are better marked by the insoluble fraction of same elements, as previously discussed (paragraph 3.2). Values of soluble Cs/Rb in the biomass burning profile of this study range 0.01-0.03.

3.3.3 Sea spray

Sea spray is identified by dominant abundances in the profile of Cl^-, Na^+, $SO_4^=$, Mg^{2+}, Ca and K^+, listed by decreasing order of species percent in the PM_{10} mass apportioned to factor, for the three sites. Abundances of these species strictly resemble those of fresh sea salt (Seinfeld and Pandis, 2006); this is shown in supplementary material S3, where the sea spray profiles of this study are compared with the reference profile of fresh sea salt. Diagnostic ratios between each of the above species and Na^+ are almost equal to those of the reference profile, confirming that the PMF model provided accurate estimation of the chemical fingerprint. The only exception concerns NO_3^-, the abundance of which is atypically higher than expected for this profile. Likely, this is a collinearity problem, since a significant fraction of total NO_3^- is contributed by mineral dust, in this study, and transport events observed during last part of the sampling period often include both sea spray and mineral dust contributions.

3.3.4 Heavy oil combustion

This factor is mainly described by the soluble fraction of V and Ni, and by $SO_4^=$, NH_4^+, OC, EC and the insoluble fraction of Fe. The variance of soluble Ni and V is explained by 70-80 % of total species, depending on the site, while $SO_4^=$, NH_4^+, OC, EC and insoluble Fe are explained by about 20-30%, 30-40% and 5-10% (OC, EC and insoluble Fe), respectively. The source-selective role of V and Ni as tracers of the combustion of crude oils is well acknowledged, particularly concerning exhausts from diesel engines of marine vessels (Pey et al., 2013; Corbin et al., 2018; Zhao et al., 2021). Besides V and Ni, Fe is the most abundant transition metal in exhausts of heavy oil combustion. V, Ni and Fe are indeed observed in metal-carbon inclusions (in soot, char and other carbon particles emitted by marine engines), forming crystals or microcrystals with S and Ca, and acting as nuclei for the condensation of aromatic compounds during combustion (Popovicheva et al., 2009). The V/Ni ratio associated to shipping emissions ranges 2–5, as observed in profiles available by the SPECIEUROPE repository (Pernigotti et al., 2016), and by different authors (Viana et al., 2009; Corbin et al.,

2018; Zhao et al., 2021). Since in this study the soluble fraction of V and Ni was used in PMF, slightly different values of V/Ni, ranging 1.9-2.1, are observed in the heavy oil combustion profiles.

Factor identity of this profile was thus checked against literature source profiles, by using ratio-ratio scatter plots (Robinson et al., 2006) of the V/Ni and Fe/EC diagnostic ratios. In this type of plot, different source categories are expected to cluster separately from each other with respect to same source tracers, depending on the values of diagnostic ratios. The V-Ni rich profiles of this work were thus compared by ratio-ratio plot with all SPECIEUROPE source profiles (including non-shipping ones) where V, Ni, Fe and EC are available (Figures S3.5, S3.6 and S3.7).

Daily PM_{10} samples collected at each site were also included in the plots, to assess which days cluster close to literature profiles. The ratio-ratio plots confirm that the V-Ni rich factors of this study fall within the cluster of heavy oil combustion profiles. Concerning individual PM_{10} samples, those distributing closest to heavy oil combustion profiles correspond to those more contributed by the V-Ni rich PMF factor, by site.

3.3.5 Mineral Dusts

Two different mineral dust profiles have been identified, Mineral Dust A and Mineral Dust B, which will be referred to as MD-A and MD-B for the rest of this paragraph.

The MD-A is described by significantly higher abundances of Si, Ca, Al and the insoluble fractions of Fe, Ti, V, Li and Rb with respect to MD-B, while the latter is far more enriched in Na, K and Mg ions, and NO_3^-. Si, Ca, Al and insoluble Fe represent on average 10% (Si), 8% (Ca) and 2% (Al and insoluble Fe) of PM_{10} mass apportioned to MD-A, and less than half percent values, respectively, of PM_{10} apportioned to MD-B. Conversely, NO_3^- and Na, K and Mg ions are contributed by the MD-B by about one order of magnitude higher percentages than by the MD-A. It is worth mentioning that the MD-A profile is strictly comparable among the sites, and the MD-B profile is comparable at Via Saredo and Montelibretti, while at Sapienza this profile is affected by larger PMF modelling error, making it poorly reliable. This is also shown in Figure S3.3, where both profiles are compared at the three sites for the only species affected by small-size error, after applying the BS, DISP and BS-DISP methods. Since Montelibretti is located far from the two urban sites, this likely indicates that mineral dusts observed in this study were transported from other areas. The average percent contributions to PM_{10} mass by MD-A and MD-B are similar, both inter-site and within-site, with values of 14%, 22% and 24 % (MD-A) and 13%, 13% and 21 % (MD-B) at Montelibretti, Via Saredo and Sapienza, respectively. However, the two profiles indicate that crustal materials of MD-A and MD-B largely differ in their chemical nature, indicating different source origins. From the MD-A profile, a composition rich in silicates, Ca-rich minerals and metal oxides can be hypothesized, while the MD-B profile suggests a composition rich in nitrates and other salts. Nevertheless, most mineral dust advection episodes occurred during the same days for both MD-A and MD-B, suggesting that both contributions followed common transport pathways to receptors. In particular, the MD-A factor profile seems to be attributable to dust advection events from African deserts, given its enrichment in Ti and V (insoluble fraction), which are

commonly reported in literature as source tracers of dust intrusions from Sahara and Sahel regions (Perez et al., 2008; Linares et al., 2021). However, interferences of local crustal materials on the MD-A and MD-B profiles cannot be excluded. Indeed, most dust outbreaks occurred during lockdown, when local traffic was almost turned off, and the PMF was not able, thus, to resolve the individual contributions neither of local dust re-suspension by vehicles riding, nor of short-range transport from Rome outskirts. This aspect was thus further investigated by comparison with literature profiles. A large number of Sahara and Sahel dust profiles had been previously observed to separate efficiently both from profiles of local geological areas of Rome outskirts and from road dust profiles, by ratio-ratio plot of crustal-specific diagnostic ratios (Pietrodangelo et al., 2013). Following the same approach, in this work, the Al/Ca versus Ti/V plot has been thus employed to assess the distribution of MD-A and MD-B profiles with respect to local geological and Sahara/Sahel dust profiles previously analyzed. From Fig. 4 it is evident that both MD-A and MD-B are separated from re-suspended desert topsoil, road dust, and local geological airborne dust profiles. The MD-A falls close to main group of profiles of African dust outbreaks, thus supporting the hypothesis of a transport from African deserts. Differently, the MD-B separates from all profile groups, suggesting a non-local origin other than Sahara or Sahel regions.

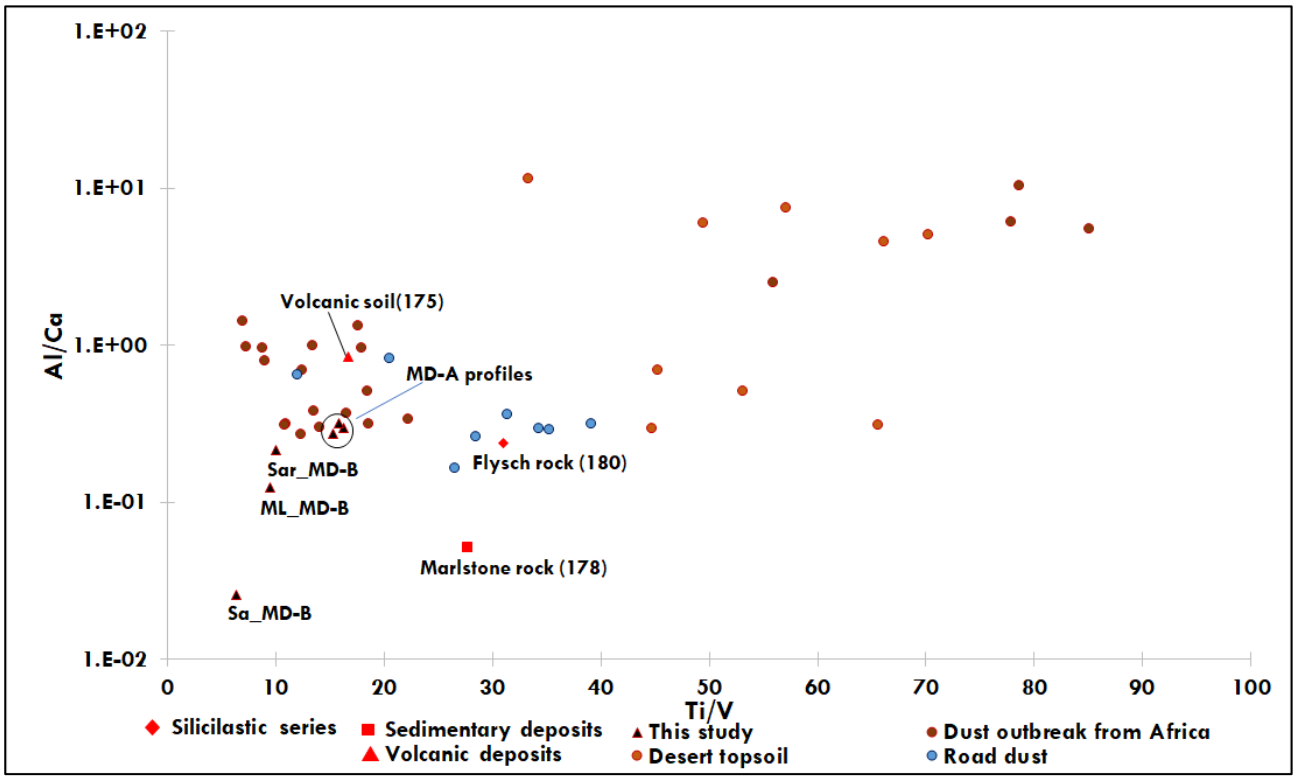

Fig. 4. Al/Ca and Ti/V ratio-ratio plot comparing different African mineral dust, urban road dust and local (Latium) geological dust chemical fingerprints in the PM_{10} fraction, with the MD-A and MD-B factor profiles of this study. The following abbreviations are adopted: ***Sa*** for Sapienza, ***Sar*** for Via Saredo, and ***ML*** for Montelibretti sites. Local dust profiles are indicated by the SPECIEUROPE name and ID number.

3.3.6 Secondary Ammonium Nitrate and Sulfates

These two contributions were only identified at Montelibretti, while at Sapienza and Via Saredo stable PMF solutions extract only secondary sulfates combined to organics.

Ammonium nitrate formation is fostered by emissions of gaseous precursors from large vehicle traffic fluxes, intensive use of wood and other biomass combustion, and intensive agriculture and farming activities emitting ammonia (Amato et al., 2016). At Montelibretti, located in a country area, the latter two factors are dominant while road traffic plays a minor role. On the other side, at Sapienza and Via Saredo, which are mainly impacted by traffic emissions, these were strongly limited during most sample collection, due to lockdown. Therefore, biomass burning is expected to be the only source of ammonium nitrate precursors, in this study, and it is expected to affect Montelibretti during the first sampling period. As a matter of fact, in addition to NH_4^+ and NO_3^- , represented by this factor for the 47% and 38% respectively of total species, the ammonium nitrate profile (Fig. S3.2) is characterized by levoglucosan, EC and K^+, indicating a partial source mixing with biomass burning, and by OC, representing particulate and condensed semi-volatile organics emitted during combustion (Stefenelli et al., 2019).

The profile of secondary sulfates combined to organics is characterized by $SO_4^=$, NH_4^+ and OC, representing 15-20%, 5-7% and 25-35%, respectively, of the average PM_{10} mass apportioned to this factor. Similar source strength is observed regardless of site (Fig. 6), with increasing intensity from pre-lockdown (5% and 6% average of total PM_{10} mass, at Sapienza and Montelibretti) to lockdown (average 15% of total PM_{10} mass at Sapienza and Via Saredo, and 25% at Montelibretti), coherently with the regional nature of this contribution and with the season-related enhanced photochemical activity. It is worth considering that the increase from the pre-lockdown to lockdown periods has to be evaluated with respect to either inorganic and organic species, since the PMF attributes 20-30% of OC variance to this profile, at all sites.

Organics in secondary sulfates profiles are frequently observed (Bernardoni et al., 2011; Amato et al., 2016; Silvern et al., 2017; Dai et al., 2020), with OC profile abundances that can reach sulfate ones. Factors giving rise to significant OC percentages in ammonium sulfates profiles are commonly ascribed to the source mixing that establishes between the ammonia- nitric acid- sulfuric acid regimes forming ammonium sulfates and nitrate (Seinfeld and Pandis, 2006) and the combustion sources emitting organics. To evaluate differences in sulfates and organic matter between lockdown and pre- or post- lockdown periods, in Fig.5 the ammonium sulfate apportioned to main forming species and the total organic matter (OM) are reported.

The total ammonium sulfate was apportioned to individual sulfates estimated by chemical equivalent ratios, considering an airborne aerosol where S-rich species are dominant (in the warm season) and form, in turn, ammonium bisulfate, letovicite and sulfate (Seinfeld and Pandis, 2006; Lehmann et al., 2007). Total OM was estimated as total OC multiplied by a factor α, accounting for non-C atoms in organic compounds; the α value was set to 1.8, as in previous studies in the Rome area (Perrino et al., 2019). From pre-lockdown to lockdown a significant decrease of the OM is observed at Sapienza and Montelibretti (47% and 59%, respectively), suggesting that shutting down anthropic and business activities during lockdown also let to a sharp decrease

of local emissions of organics and, consequently, of their influence on secondary aerosol formation. Concerning the apportioned sulfate species, their temporal evolution and relationship with transport events are discussed in section 3.4.

As a complement of ammonium sulfate apportionment, ammonium nitrate was obtained, by NH_4^+ exceeding the neutralization of sulfates, at the three sites (Fig. 5). As expected from seasonal evolution, highest contributions are observed at Montelibretti during pre-lockdown, accounting for 9% of total PM_{10} mass, and to minor extent at Sapienza (4% of total PM_{10}), while starting from lockdown period to the end of sampling a flat contribution of about 1% is observed at all sites. The apportionment by chemical equivalent ratios allowed to assess that the PMF model overestimated the mass contribution of secondary nitrate at Montelibretti, probably due to the source mixing between secondary nitrate and biomass burning. Therefore, in Fig. 6 and Fig. 7 mass contributions of secondary nitrate are those calculated by chemical equivalents. Conversely, minor or negligible differences are observed between the ammonium sulfate PMF profile and the resulting sum of secondary sulfates calculated by chemical equivalentswith the OM source contribution estimate ascribed by PMF to ammonium sulfate profile. InFig. S3.8 the daily trends of these contributions and of the measured $SO_4^=$ are shown at the three sites. The daily difference between contributions of ammonium sulfate calculated by PMF and secondary sulfates calculated by chemical equivalents ratio (the latter strictly overlapping to measured $SO_4^=$) is proportional to the OM apportioned to PMF ammonium sulfate, calculated as percent of total species in the profile. This is particularly evident at Sapienza and Via Saredo in the lockdown period.

Finally, the non-ammonium nitrate part of total NO_3^- (which will be referred to as 'non-ammonium nitrate NO_3^-' for the remaining part of the work) , determined by difference,

shows similar contributions irrespective of the period and site, representing on average 7-10%, 4-6% and 6-7% of total PM_{10}, at Sapienza, Montelibretti, and Via Saredo respectively. The areal and temporal homogeneity suggests a non-local origin of the non-ammonium nitrate NO_3^-. To assess this aspect, the NO_3^- fraction apportioned to MD-B by PMF was calculated, as percent of total species in the MD-B profile. In Fig. S3.9 it is evident that both the time trend and daily mass of non-ammonium nitrate NO_3^- are clearly similar to those of the NO_3^- fraction apportioned to MD-B. Since these two contributions are estimated by different apportionment methods, their similarity supports the hypothesis that both methods describe the same contribution, and that it originates from sources other than atmospheric formation of secondary aerosol. This is also coherent with the nitrate-rich composition of the MD-B profile, as it will be further discussed in paragraph 3.5. Other forms of secondary nitrate, like those related to potassium, are not observed in this study, as confirmed by the poor linear regression of non-ammonium nitrate NO_3^- with potassium ion shown in Fig. S3.9.

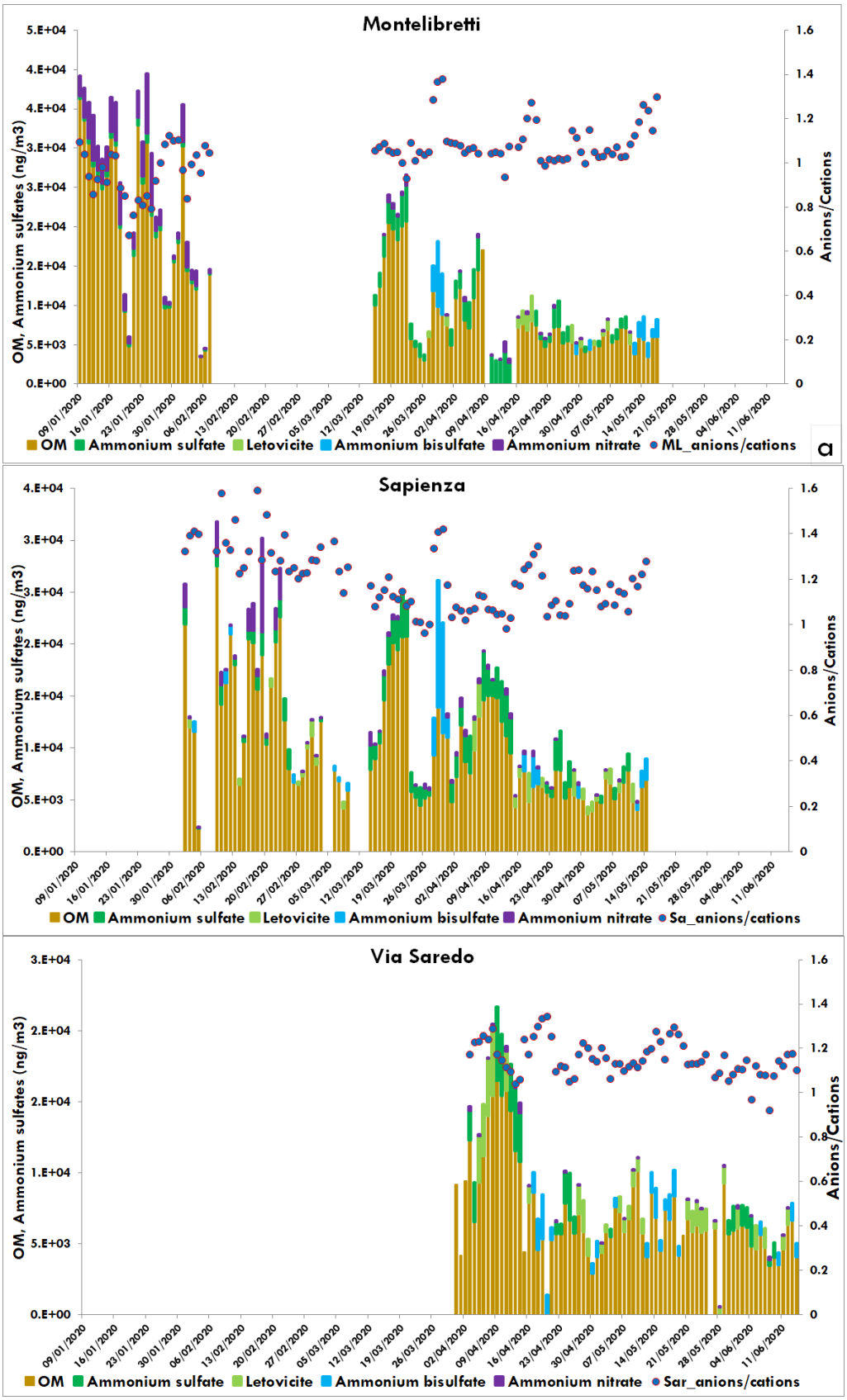

Fig. 5. Daily mass contribution of secondary nitrate, secondary sulfates and total organic matter(OM) at the three sites of this study. The anions/cations ratio is also reported on the secondary y-axis.

3.4 Ion Balance Analysis

The sum of chemical equivalents of anions and cations has been considered to evaluate the charge neutrality of samples and investigate reasons of eventual deviations from ion balance. Anions vs cations linear regression at the three sites show R^2 coefficient and slope ranging 0.91-0.98 and 1.1-1.3, respectively, indicating that acidic species were generally neutralized during the sampling periods. However, daily trends of the anions/cations ratio indicate that, during specific days, PM_{10} samples were particularly acidic, with ratio values ranging 1.4-1.6. In Fig. 5, the anions/cations ratio is compared to secondary sulfates and nitrate species apportioned by ammonia- nitric acid- sulfuric acid regimes (see paragraph 3.3.6). Highest anions/cations values clearly correspond to days where sulfates formation equilibria are dominated by ammonium bisulfate or, in minor cases, by letovicite, thus indicating that collected aerosol was significantly acidic in these days (Seinfeld and Pandis, 2006). Interestingly, these findings were similarly observed at all sites. Days affected by ammonium bisulfate-rich aerosol, namely March 28^{th}-30^{th}, April 17^{th}-20^{th} and May 12^{th}-20^{th}, correspond to mineral dust advection events, as discussed in paragraph 3.5, suggesting that air masses conveying mineral dusts likely run into acidic aerosols during their transport path.

3.5 Relative Relevance and Time Trend of Source Contributions to PM_{10} Mass Concentration

Relative relevance and time trend of single source contributions to PM_{10} mass concentration during pre-lockdown, lockdown and post-lockdown are shown in Fig. 6 and Fig. 7, respectively.

From Fig. 6, we can observe that the contribution to PM_{10} from vehicular traffic was considerably reduced from pre-lockdown to lockdown, as expected, due to the reduction of movement of the population during lockdown. The decrease was from 25% (panel a) to 6% (panel b) at Sapienza, and from 13% (panel e) to 6% (panel f) at Montelibretti, where the reduction was less evident due to the lower impact of this source during pre-lockdown. On the other hand, the resumption of non-essential productive and work activities after lockdown led to an increase of traffic contribution, as it can be observed at Via Saredo, where percent of PM_{10} mass concentration from vehicular traffic increased from 10% (panel c) to 19% (panel d) during post-lockdown. From Fig. 7, we can observe the time trend of the contribution from traffic in the pre- and post-lockdown periods, ranging from 0.5 to 15 $\mu g\ m^{-3}$, with minimum values in correspondence of the weekend days, while values were continuously very-low at all sites during lockdown.

Regarding biomass burning, the contribution to PM_{10} was reduced from pre-lockdown to lockdown at Sapienza (from 13% to 10%), as well as at Montelibretti (from 38% to 15%), where the decrease was more considerable, this site being more influenced by biomass domestic heating sources during pre-lockdown. However, in this case, the decrease in contribution during lockdown was not due to the Covid-19 quarantine but to the reduced strength of biomass heating emissions in the warmer period. In fact, from panels a and c of Fig. 7, we can observe that biomass burning contribution to PM_{10} declined a month after the lockdown restrictions began, in late March, when temperatures rose and the use of domestic heating systems was greatly reduced. Therefore,

the contribution from biomass burning was reduced even more at Via Saredo (from 11% to 3%), during post-lockdown warmer months.

Transport events of sea spray mainly occurred during pre-lockdown and where more consistent during the second half of February (panel a of Fig. 7) at Sapienza, which is closer to the Tyrrhenian Sea (about 30 km) and where marine aerosols contributed for 18% to the PM_{10} mass concentration. On the contrary, in the lockdown period, sea spray advections were less frequent and intense and occurred mainly during late April and middle May (in connection with dust events; Fig. 7), thus in this period marine aerosols contributed only for 3-8 % to total PM_{10} at all monitored sites (Fig. 6). During post-lockdown, events of sea spray occurred at the beginning of June (panel b of Fig. 7) and contributed to 11% to PM_{10} mass concentration recorded at Via Saredo (panel d of Fig. 6).

The contribution from heavy oil combustion was instead greater during lockdown at all sites, ranging from 10 to 11% to total PM_{10} (Fig. 6) and was presumably associated to events of long-distance transport of dust from coal industries and coal burning for domestic use in North African regions, and from wildfire smoke in Balkan and Eastern Europe crossing the Adriatic Sea towards central and southern Italy, in agreement with recent reporting by Kirchner et al. (2020) and Campanelli et al. (2021), respectively. Transport events occurred during the first week of April and, to minor extent, during April 24th-28th. (Fig. 7). No transport of dust from heavy fuels combustion was instead recorded during pre-lockdown and post-lockdown, when this contribution was very low (ranging from 1 to 6% of total PM_{10}) at all sites.

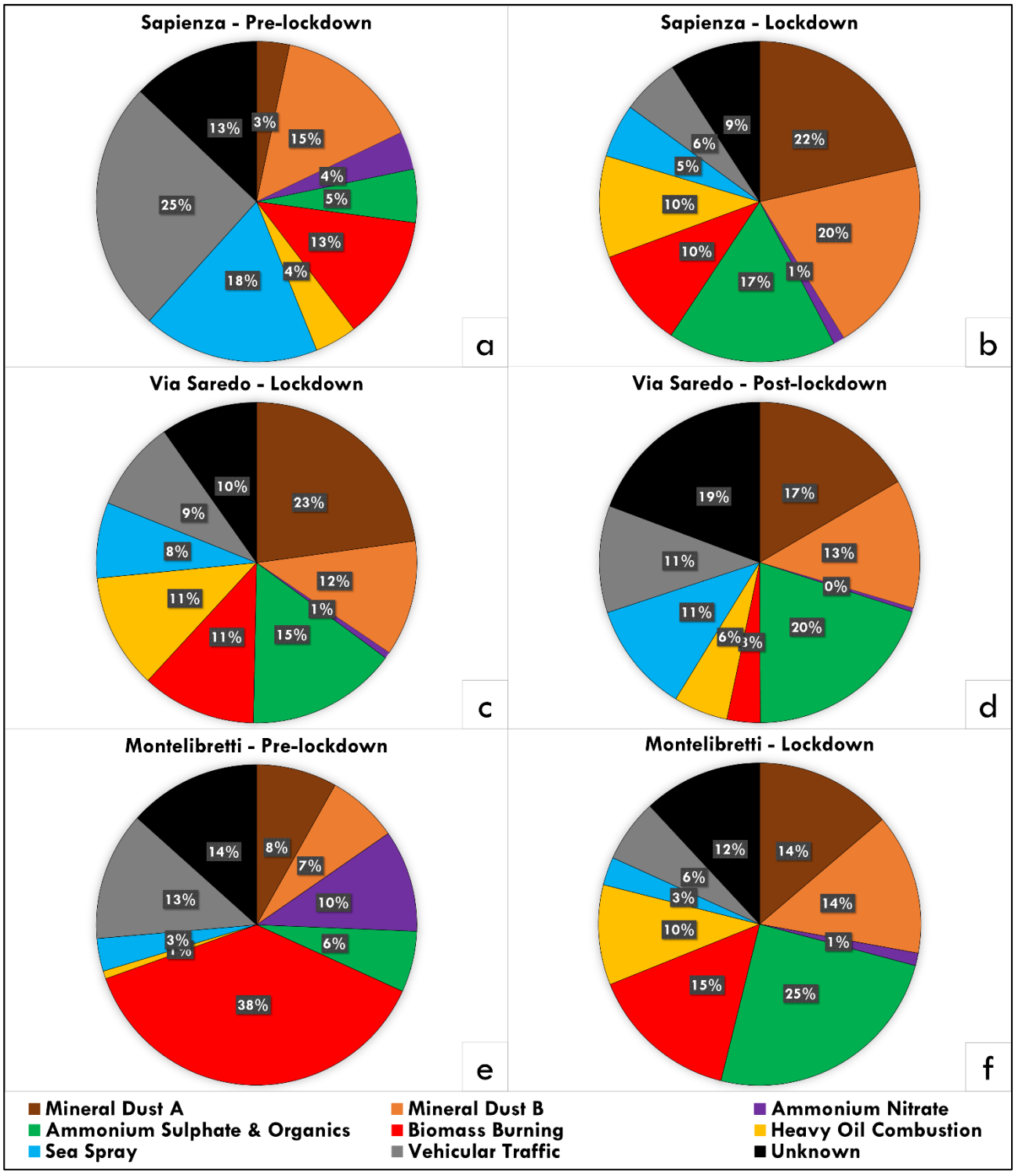

Fig. 6. Source apportionment of PM_{10} during pre-lockdown (Sapienza (panel a) and Montelibretti (panel e)), lockdown (Sapienza (panel b), Via Saredo (panel c) and Montelibretti (panel f)), and post-lockdown (Via Saredo (panel d)). Values are reported as average percent of the total measured PM_{10} mass concentration.

Regarding mineral dusts, major advection episodes of desert dust from remote regions occurred during lockdown and interested all sites, contributing together from 28 to 42% of total PM_{10} mass concentration. From

Fig. 7 we can observe that MD-A and MD-B incursion events occurred during the same days, indicating common transport pathways. Moreover, this areal and temporal homogeneity is coherent with a non-local origin. The main peaks in the time trend of these factors were observed on March 28th-30th, when mass contribution from MD-B was much greater, reaching about 40 µg m^{-3} to total PM_{10} at Sapienza, and on April 17th-20th and May 12th-20th, when instead the main contribution was from MD-A. As previously discussed, MD-A is attributable to dust advection events from African deserts, such as Sahara and Sahel, while MD-B contribution probably derived from incursion of dust from the eastern desert regions of Kazakhstan (Campanelli et al., 2021) (long-range transport contributions were checked by backtrajectory analysis; HYSPLIT Trajectory Model).

Finally, high increase of ammonium sulfates due to the warm season was observed during lockdown at all sites (from 5-6 to 15-25 % of total PM_{10}), contributing, as well as mineral dust advections, to the lesser than expected decrease in PM_{10} mass concentration from pre-lockdown to lockdown. Highest contributions from ammonium nitrate were found at Montelibretti (9% of PM_{10} mass concentration) and to minor extent at Sapienza (4% of total PM_{10}) during pre-lockdown, as expected from seasonal evolution. On the contrary, from the lockdown period to the end of sampling, a flat contribution of about 1% was observed at all sites, as previously discussed. In particular, the time trend of non-secondary nitrate matches specifically with MD-B mineral dust contribution, while acidic sulfates (bisulfate and letovicite), differently from the regional distribution of ammonium sulfate, resulted associated to mineral dust transport events, likely due to collinear transport of different air masses.

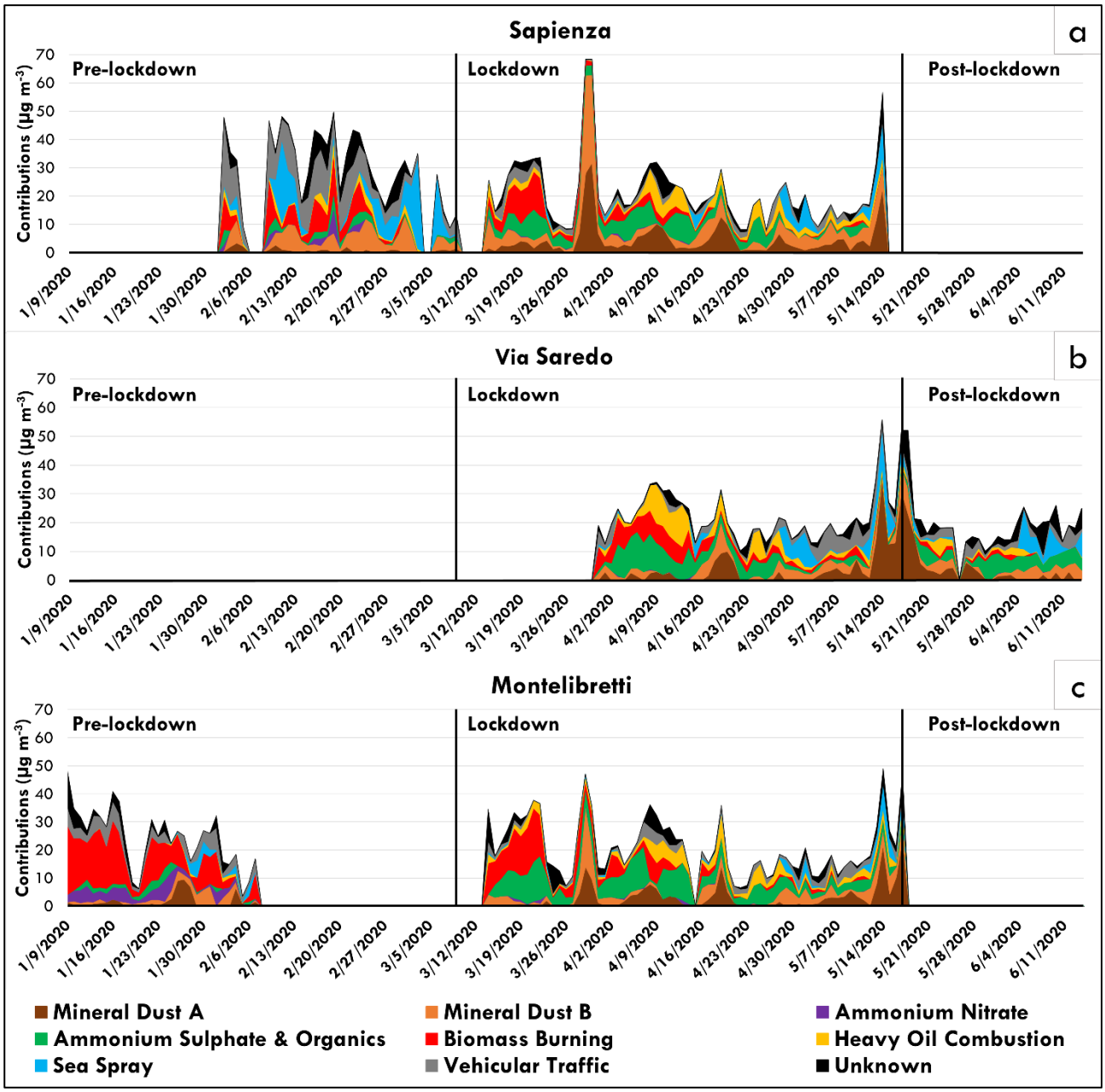

Fig. 7. Time trend of source contributions to PM_{10} mass concentration (µg m^{-3}) at Sapienza (panel a), Via Saredo (panel b) and Montelibretti (panel c) during pre-lockdown, lockdown and post-lockdown.

4. Conclusions

The impact of the lockdown-based policy adopted by Italy during 2020 to contrast the spread of the Coronavirus disease 2019 (Covid-19) was evaluated in this work for the Rome area (Italy), concerning the relative strength and time evolution of local and non-local acting sources. To this aim, daily PM_{10} samples chemically speciated, collected during pre-lockdown, lockdown and post-lockdown periods at the urban sites of Sapienza and Via Saredo, and at the peri-urban site of Montelibretti, were analyzed by PMF. Chemically fractionated elements, considered for soluble and insoluble fractions instead of total concentration, were used

in the PMF input dataset, in addition to conventional analytical speciation. From pre-lockdown to lockdown, a significant abatement of local sources (vehicular traffic and biomass burning) was observed at all sites. Concerning biomass burning this is explained by the seasonal evolution from cold to warmer seasons that overall coincides with the transition from the pre-lockdown period to the establishment of the lockdown measures (from March 9th to May 18th 2020). However, the strong reduction of vehicular traffic observed during lockdown has to be only attributed to circulation restrictions adopted by the lockdown policy, providing an experimental trial of the efficiency of PM control strategies and mitigation measures addressing vehicular traffic in the Rome area. As additional consequence of forcing the reduction of local anthropogenic activities and their source strength, the non-local source contributions (two different mineral dust - MD-A and MD-B - advected from desert regions, sea spray, and heavy oil combustion) that mainly occurred during lockdown, were poorly influenced by the chemical fingerprint of local sources. This allowed to describe their profile and estimate mass contributions more accurately than obtainable from PMF input datasets of PM collected during routine periods. The MD-A is described by significantly higher abundances of Si, Ca, Al and the insoluble fractions of Fe, Ti, V, Li and Rb with respect to MD-B, while the latter is far more enriched in Na, K and Mg ions, and non-secondary NO_3, thus indicating a composition richer in nitrates and other salts.

High overlapping of insoluble Rb, Ti, V, Cs and Li, which were previously observed to selectively trace desert dust, with Si and Al, indicate that mineral dust contributions of this study are more probably long-range transported than local. This is further supported by ratio-ratio plot comparison with profiles of African dust outbreaks, local mineral dust and road dust of the Rome area, showing that both MD-A and MD-B profiles are not assignable to local dusts and that MD-A is clearly assigned to African desert outbreaks. The sea spray profiles of this study were compared with a reference profile of fresh sea salt; diagnostic ratios showed to be almost equal to those of the reference profile. Heavy oil combustion profiles match those reported in literature for significant diagnostic ratios (V/Ni, Fe/EC). Since in this study the soluble fraction of V and Ni were used for PMF, instead of total element, the observed profile matching confirms the high selectivity of soluble V and Ni for heavy oil combustion tracing. Finally, the poor influence of local sources allowed to separate and apportion the sulfates and nitrate contributions due to secondary processes from contributions of other sources (e.g. non-secondary nitrate from MD-B dust, and non-secondary sulfates from long-range collinear transport paths).

Overall, the contribution from vehicular traffic was considerably reduced by Covid-19 lockdown; however, a more considerable decrease in PM_{10} mass concentration would have been expected during lockdown. This was not the case due to the greater strength of long-range transport events of mineral dust from desert regions during lockdown and to the increase in contribution of secondary aerosols due to seasonal evolution. Nevertheless, the forced abatement of traffic emissions (combined to season-related quenching of domestic heating) led to considerable compositional changes of PM, with strong reductions of components of health concern (EC, organics). The accurate characterization of PM obtained by combining conventional chemical speciation to non-conventional approaches (chemical fractionation by water-solubility of trace elements,

apportionment of secondary inorganic species by chemical equivalent ratios) allowed to obtain enhanced information about the relative relevance of single source contributions to PM mass concentration, which is of critical importance to improve understanding of air pollution and reduce uncertainties in future air quality scenarios.

Author Contributions: A. Amoroso, A. Di Giosa, S. Canepari and C. Perrino conceived and planned the monitoring and the experiments; M. A. Frezzini, N. De Francesco, T. Sargolini and A. Amoroso performed the samplings; M.A. Frezzini, M. Ristorini, N. De Francesco and T. Sargolini performed part of the chemical analyses; L. Massimi and A. Pietrodangelo elaborated the data and wrote the manuscript; L. Massimi, A. Pietrodangelo, S. Canepari and C. Perrino coordinated the group and supervised the manuscript.

References

Ali, M. U., Liu, G., Yousaf, B., Ullah, H., Abbas, Q., Munir, M. A. M. (2019). A systematic review on global pollution status of particulate matter-associated potential toxic elements and health perspectives in urban environment. Environmental geochemistry and health, 41(3), 1131-1162.

Allouis, C., Beretta, F., D'Alessio, A. (2003). Structure of inorganic and carbonaceous particles emitted from heavy oil combustion. Chemosphere, 51(10), 1091-1096. https://doi.org/10.1016/S0045-6535(02)00714-2

Amato, F., Alastuey, A., Karanasiou, A., Lucarelli, F., Nava, S., Calzolai, G., Querol, X. (2016). AIRUSE-LIFE+: a harmonized PM speciation and source apportionment in five southern European cities. Atmospheric Chemistry and Physics, 16(5), 3289-3309.

Amato, F., Viana, M., Richard, A., Furger, M., Prévôt, A. S. H., Nava, S., Querol, X. (2011). Size and time-resolved roadside enrichment of atmospheric particulate pollutants. Atmospheric Chemistry and Physics, 11(6), 2917-2931.

Arregocés, H. A., Rojano, R., Restrepo, G. (2021). Impact of lockdown on particulate matter concentrations in Colombia during the COVID-19 pandemic. Science of the Total Environment, 764, 142874. https://doi.org/10.1016/j.scitotenv.2020.142874

Astolfi, M. L., Marconi, E., Protano, C., Vitali, M., Schiavi, E., Mastromarino, P., Canepari, S. (2018). Optimization and validation of a fast digestion method for the determination of major and trace elements in breast milk by ICP-MS. Analytica Chimica Acta, 1040, 49-62.

Astolfi, M.L., Canepari, S., Cardarelli, E., Ghighi, S. and Marzo, M.L. (2006), Chemical Fractionation of Elements in Airborne Particulate Matter: Primary Results on PM10 and PM2.5 Samples in the Lazio Region (Central Italy). Annali di Chimica, 96: 183-194. https://doi.org/10.1002/adic.200690018

Astolfi, M. L., Marconi, E., Protano, C., Canepari, S. (2020). Comparative elemental analysis of dairy milk and plant-based milk alternatives. Food Control, 116, 107327.

Battista, G., Pagliaroli, T., Mauri, L., Basilicata, C., De Lieto Vollaro, R. (2016). Assessment of the air pollution level in the city of Rome (Italy). Sustainability, 8(9), 838.

Belis, C., Favez, O., Mircea, M., Diapouli, E., Manousakas, M., Vratolis, S., Gilardoni, S., Paglione, M., Decesari, S., Mocnik, G., Mooibroek, D., Salvador, P., Takahama, S., Vecchi, R. and Paatero, P. (2019). European guide on air pollution source apportionment with receptor models, EUR 29816 EN, Publications Office of the European Union. ISBN 978-92-76-09001-4. https://doi.org/10.2760/439106, JRC117306

Bernardoni, V., Vecchi, R., Valli, G., Piazzalunga, A., Fermo, P. (2011). PM10 source apportionment in Milan (Italy) using time-resolved data. Science of the Total Environment, 409(22), 4788-4795. https://doi.org/10.1016/j.scitotenv.2011.07.048

Betha, R., Behera, S. N., Balasubramanian, R. (2014). 2013 Southeast Asian smoke haze: fractionation of particulate-bound elements and associated health risk. Environmental Science and Technology, 48(8), 4327-4335. https://doi.org/10.1021/es405533d

Borck, R., Pflüger, M. (2019). Green cities? Urbanization, trade, and the environment. Journal of Regional Science, 59(4), 743-766. https://doi.org/10.1111/jors.12423

Briz-Redón, Á., Belenguer-Sapiña, C., Serrano-Aroca, Á. (2021). Changes in air pollution during COVID-19 lockdown in Spain: a multi-city study. Journal of Environmental Sciences, 101, 16-26. https://doi.org/10.1016/j.jes.2020.07.029

Campanelli, M., Iannarelli, A. M., Mevi, G., Casadio, S., Diémoz, H., Finardi, S., Dinoi, A., Castelli, E., di Sarra, A., Di Bernardino, A., Casasanta, G., Bassani, C., Siani, A. M., Cacciani, M., Barnaba, F., Di Liberto, L., Argentini, S. (2021). A wide-ranging investigation of the COVID-19 lockdown effects on the atmospheric composition in various Italian urban sites (AER–LOCUS). Urban Climate, 39, 100954. https://doi.org/10.1016/j.uclim.2021.100954

Canepari, S., Cardarelli, E., Giuliano, A., Pietrodangelo, A. (2006a). Determination of metals, metalloids and non-volatile ions in airborne particulate matter by a new two-step sequential leaching procedure part A: Experimental design and optimization. Talanta, 69(3), 581–587. https://doi.org/10.1016/j.talanta.2005.10.023

Canepari, S., Cardarelli, E., Pietrodangelo, A., Strincone, M. (2006b). Determination of metals, metalloids and non-volatile ions in airborne particulate matter by a new two-step sequential leaching procedure: Part B: Validation on equivalent real samples. Talanta, 69(3), 588-595. https://doi.org/10.1016/j.talanta.2005.10.024

Canepari, S., Perrino, C., Olivieri, F., Astolfi, M. L. (2008). Characterisation of the traffic sources of PM through size-segregated sampling, sequential leaching and ICP analysis. Atmospheric Environment, 42(35), 8161-8175.

Canepari, S., Pietrodangelo, A., Perrino, C., Astolfi, M. L., Marzo, M. L. (2009). Enhancement of source traceability of atmospheric PM by elemental chemical fractionation. Atmospheric Environment, 43(31), 4754-4765.

Canepari, S., Astolfi, M. L., Moretti, S., Curini, R. (2010). Comparison of extracting solutions for elemental fractionation in airborne particulate matter. Talanta, 82(2), 834-844. https://doi.org/10.1016/j.talanta.2010.05.068

Canepari, S., Astolfi, M. L., Farao, C., Maretto, M., Frasca, D., Marcoccia, M., Perrino, C. (2014). Seasonal variations in the chemical composition of particulate matter: a case study in the Po Valley. Part II: concentration and solubility of micro-and trace-elements. Environmental Science and Pollution Research, 21(6), 4010-4022.

Canepari, S., Astolfi, M. L., Catrambone, M., Frasca, D., Marcoccia, M., Marcovecchio, F., Perrino, C. (2019). A combined chemical/size fractionation approach to study winter/summer variations, ageing and source strength of atmospheric particles. Environmental Pollution, 253, 19-28.

Cesaroni, G., Boogaard, H., Jonkers, S., Porta, D., Badaloni, C., Cattani, G., Forastiere, F., Hoek, G. (2012). Health benefits of traffic-related air pollution reduction in different socioeconomic groups: the effect of low-emission zoning in Rome. Occupational and Environmental Medicine, 69(2), 133-139. https://doi.org/10.1136/oem.2010.063750

Chowdhury Z, Zheng M, Schauer JJ, Sheesley RJ, Salmon LG, Cass GR, Russell AG (2007) Speciation of ambient fine organic carbon particles and source apportionment of PM2.5 in Indian cities. Journal of Geophysical Research 112:D15303

Coccia, M. (2020). Two mechanisms for accelerated diffusion of COVID-19 outbreaks in regions with high intensity of population and polluting industrialization: the air pollution-to-human and human-to-human transmission dynamics. MedRxiv. https://doi.org/10.1101/2020.04.06.20055657.

Collivignarelli, M. C., Abbà, A., Bertanza, G., Pedrazzani, R., Ricciardi, P., Miino, M. C. (2020). Lockdown for CoViD-2019 in Milan: What are the effects on air quality?. Science of the Total Environment, 732, 139280. https://doi.org/10.1016/j.scitotenv.2020.139280

Corbin, J. C., Mensah, A. A., Pieber, S. M., Orasche, J., Michalke, B., Zanatta, M., Czech, H., Massabò, D., Buatier de Mongeot, F., Mennucci, C., El Haddad, I., Kumar, N.K., Stengel, B., Huang, Y., Zimmermann, R.,

Prevot, S.H., Gysel, M. (2018). Trace metals in soot and PM2. 5 from heavy-fuel-oil combustion in a marine engine. Environmental Science and Technology, 52(11), 6714-6722. https://doi.org/10.1021/acs.est.8b01764

Dai, Q., Liu, B., Bi, X., Wu, J., Liang, D., Zhang, Y., Feng, Y., Hopke, P. K. (2020). Dispersion normalized PMF provides insights into the significant changes in source contributions to PM2. 5 after the COVID-19 outbreak. Environmental Science and Technology, 54(16), 9917-9927. https://doi.org/10.1021/acs.est.0c02776

Di Bernardino, A., Iannarelli, A. M., Casadio, S., Perrino, C., Barnaba, F., Tofful, L., Cacciani, M. (2021). Impact of synoptic meteorological conditions on air quality in three different case studies in Rome, Italy. Atmospheric Pollution Research, 12(4), 76-88.

EPA, (1997). Reference Method for the Determination of Particulate Matter as PM10 in the Atmosphere. Federal Registrer, 62, No 138, Appendix M to part 50.

EU, 2008. Directive 2008/50/EC of the European Parliament and of the Council of 21 May 2008 on ambient air quality and cleaner air for Europe. Official Journal of the European Union L152 (11/06/2008), 1–44.

Fan, H., Zhao, C., Yang, Y. (2020). A comprehensive analysis of the spatio-temporal variation of urban air pollution in China during 2014–2018. Atmospheric Environment, 220, 117066.

Feng, X. D., Dang, Z., Huang, W. L., Yang, C. (2009). Chemical speciation of fine particle bound trace metals. International Journal of Environmental Science & Technology, 6(3), 337-346.

Government of Italy. Decree of the president of the Council of Ministers 11 March 2020. March 11, 2020. https://www.gazzettaufficiale.it/eli/id/2020/03/11/20A01605/sg

Government of Italy. Decree of the president of the Council of Ministers 26 April 2020. April 26, 2020. https://www.gazzettaufficiale.it/eli/id/2020/04/27/20A02352/sg

Gobbi, G. P., Barnaba, F., Di Liberto, L., Bolignano, A., Lucarelli, F., Nava, S., Wille, H. (2019). An inclusive view of Saharan dust advections to Italy and the Central Mediterranean. Atmospheric environment, 201, 242-256.

Grondys, K. (2019). The impact of freight transport operations on the level of pollution in cities. Transportation Research Procedia, 39, 84-91. https://doi.org/10.1016/j.trpro.2019.06.010

Guevara, M., Jorba Casellas, O., Soret, A., Petetin, H., Bowdalo, D., Serradell Maronda, K., Tena, C., van der Gon, H.D., Kuenen, J., Peuch, V., Pérez García-Pando, C. (2021). Time-resolved emission reductions for atmospheric chemistry modelling in Europe during the COVID-19 lockdowns. Atmospheric Chemistry and Physics, 21, 773-779. https://doi.org/10.5194/acp-21-773-2021

Guzzetta, G., Riccardo, F., Marziano, V., Poletti, P., Trentini, F., Bella, A., Andrianou, X., Del Manso, M., Fabiani, M., Bellino, S., Boros, S., Urdiales, A.M., Vescio, M.F., Piccioli, A., COVID-19 Working Group, Brusaferro, S., Rezza, G., Pezzotti, P., Ajelli, M., Merler, S. (2021). Impact of a nationwide lockdown on Sars-cov-2 transmissibility, Italy. Emerging infectious diseases, 27(1), 267. https://dx.doi.org/ 10.3201/eid2701.202114

Hopke, P. K. (2000). A guide to positive matrix factorization, in workshop on UNMIX and PMF as applied to PM2. 5. Edited by Willis, RD, RTP, NC. EPA 600/A-00/048.

Kam, W., Delfino, R. J., Schauer, J. J., Sioutas, C. (2013). A comparative assessment of $PM_{2.5}$ exposures in light-rail, subway, freeway, and surface street environments in Los Angeles and estimated lung cancer risk. Environmental Science: Processes & Impacts, 15(1), 234-243.

Kirchner, M., Freier, K.P., Denner, P., Ratz, G., Jakobi, G., Körner, W., Ludewig, E., Schaub, M., Schramm, K.-W., Weiss, P., Moche, W. (2020). Air concentrations and deposition of chlorinated dioxins and furans (PCDD/F) at three high alpine monitoring stations: Trends and dependence on air masses. Atmospheric Environment, 223, 117199. https://doi.org/10.1016/j.atmosenv.2019.117199

Kumar, P., Hama, S., Omidvarborna, H., Sharma, A., Sahani, J., Abhijith, K. V., Debele, S.E., Zavala-Reyes, J.C., Barwise, Y., Tiwari, A. (2020). Temporary reduction in fine particulate matter due to 'anthropogenic emissions switch-off'during COVID-19 lockdown in Indian cities. Sustainable cities and society, 62, 102382. https://doi.org/10.1016/j.scs.2020.102382

Legislative Decree, 2010. Decreto Legislativo 13 agosto 2010, n. 155. Attuazione della direttiva 2008/50/CE relativa alla qualità dell'aria ambiente e per un'aria più pulita in Europa (GU n.216 del 15-9-2010 - Suppl. Ordinario n. 217).

Lehmann, C. M., Bowersox, V. C., Larson, R. S., Larson, S. M. (2007). Monitoring long-term trends in sulfate and ammonium in US precipitation: Results from the National Atmospheric Deposition Program/National Trends Network. In: Brimblecombe P., Hara H., Houle D., Novak M. (eds) Acid Rain - Deposition to Recovery. Springer, Dordrecht. https://doi.org/10.1007/978-1-4020-5885-1_7

Li, H., Wang, J., Wang, Q. G., Qian, X., Qian, Y., Yang, M., Fengying, L., Lu, H., Wang, C. (2015). Chemical fractionation of arsenic and heavy metals in fine particle matter and its implications for risk assessment: a case study in Nanjing, China. Atmospheric Environment, 103, 339-346. https://doi.org/10.1016/j.atmosenv.2014.12.065

Linares, C., Culqui, D., Belda, F., López-Bueno, J. A., Luna, Y., Sánchez-Martínez, G., Hervella, B., Diaz, J. (2021). Do Saharan Dust Intrusions Affect the Incidence and Severity of COVID-19 in Spain?. Environmental Science and Pollution Research. Preprint under consideration. https://doi.org/10.21203/rs.3.rs-180563/v1

Liu, B., Wu, J., Zhang, J., Wang, L., Yang, J., Liang, D., Dai, Q., Bi, X., Feng, Y., Zhang, Q. (2017). Characterization and source apportionment of PM2. 5 based on error estimation from EPA PMF 5.0 model at a medium city in China. Environmental Pollution, 222, 10-22.

Manchanda, C., Kumar, M., Singh, V., Faisal, M., Hazarika, N., Shukla, A., Lalchandani, V., Goel, V., Thamban, N., Ganguly, D., Tripathi, S. N. (2021). Variation in chemical composition and sources of PM2. 5 during the COVID-19 lockdown in Delhi. Environment international, 153, 106541. https://doi.org/10.1016/j.envint.2021.106541

Masiol, M., Rampazzo, G., Ceccato, D., Squizzato, S., Pavoni, B. (2010). Characterization of PM10 sources in a coastal area near Venice (Italy): an application of factor-cluster analysis. Chemosphere, 80(7), 771-778.

Massimi, L., Simonetti, G., Buiarelli, F., Di Filippo, P., Pomata, D., Riccardi, C., Ristorini, M., Astolfi, M. L., Canepari, S. (2020a). Spatial distribution of levoglucosan and alternative biomass burning tracers in atmospheric aerosols, in an urban and industrial hot-spot of Central Italy. Atmospheric Research, 239, 104904. https://doi.org/10.1016/j.atmosres.2020.104904

Massimi, L., Ristorini, M., Astolfi, M. L., Perrino, C., Canepari, S. (2020b). High resolution spatial mapping of element concentrations in PM10: A powerful tool for localization of emission sources. Atmospheric Research, 244, 105060. https://doi.org/10.1016/j.atmosres.2020.105060.

Massimi, L., Wesseling, J., van Ratingen, S., Javed, I., Frezzini, M. A., Astolfi, M. L., Canepari, S.,Vermeulen, R. (2021). Identification and spatial mapping of tracers of PM10 emission sources using a high spatial resolution distributed network in an urban setting. Atmospheric Research, 262, 105771.

Moreno, T., Querol, X., Alastuey, A., de la Rosa, J., de la Campa, A. M. S., Minguillón, M., Pandolfi, M., González-Castanedo, Y., Monfort, E., Gibbons, W. (2010). Variations in vanadium, nickel and lanthanoid element concentrations in urban air. Science of the Total Environment, 408(20), 4569-4579.

Namgung, H. G., Kim, J. B., Woo, S. H., Park, S., Kim, M., Kim, M. S., Bae, G. N., Park, D., Kwon, S. B. (2016). Generation of nanoparticles from friction between railway brake disks and pads. Environmental Science and Technology, 50(7), 3453-3461.

Nguyen, Q. T., Skov, H., Sørensen, L. L., Jensen, B. J., Grube, A. G., Massling, A., Glasius, M., and Nøjgaard, J. K. (2013). Source apportionment of particles at Station Nord, North East Greenland during 2008–2010 using COPREM and PMF analysis. Atmospheric Chemistry and Physics, 13(1), 35-49.

Norris, G., Brown, S., (2014). EPA Positive Matrix Factorization (PMF) 5.0 Fundamentals and User Guide. EPA PMF 5.0 Manual.

Okuda, T., Nakao, S., Katsuno, M., Tanaka, S. (2007). Source identification of nickel in TSP and PM2. 5 in Tokyo, Japan. Atmospheric Environment, 41(35), 7642-7648.

Paatero, P. (1999). The multilinear engine—a table-driven, least squares program for solving multilinear problems, including the n-way parallel factor analysis model. Journal of Computational and Graphical Statistics, 8(4), 854-888.

Paatero, P., Hopke, P. K. (2003). Discarding or downweighting high-noise variables in factor analytic models. Analytica Chimica Acta, 490(1-2), 277-289.

Paatero, P. and Tapper, U. (1994), Positive matrix factorization: A non-negative factor model with optimal utilization of error estimates of data values. Environmetrics, 5, 111-126. https://doi.org/10.1002/env.3170050203

Pant, P., Harrison, R. M. (2012). Critical review of receptor modelling for particulate matter: a case study of India. Atmospheric Environment, 49, 1-12.

Perez, L., Tobias, A., Querol, X., Künzli, N., Pey, J., Alastuey, A., Viana, M., Valero, N., Gonzalez-Cabrè, M., Sunyer, J. (2008). Coarse Particles From Saharan Dust and Daily Mortality. Epidemiology, 19(6), 800-807.

Pernigotti, D., Belis, C. A., Spano, L. (2016). SPECIEUROPE: The European data base for PM source profiles. Atmospheric Pollution Research, 7(2), 307-314. http://source-apportionment.jrc.ec.europa.eu/specieurope/index.aspx

Perrino, C., Catrambone, M., Dalla Torre, S., Rantica, E., Sargolini, T., Canepari, S. (2014). Seasonal variations in the chemical composition of particulate matter: a case study in the Po Valley. Part I: macro-components and mass closure. Environmental Science and Pollution Research, 21(6), 3999-4009.

Perrino, C., Canepari, S., Catrambone, M., Dalla Torre, S., Rantica, E., Sargolini, T. (2009). Influence of natural events on the concentration and composition of atmospheric particulate matter. Atmospheric Environment, 43(31), 4766-4779. https://doi.org/10.1016/j.atmosenv.2008.06.035

Perrino, C., Catrambone, M., Canepari, S. (2020). Chemical composition of PM10 in 16 urban, industrial and background sites in Italy. Atmosphere, 11(5), 479.

Perrino, C., Catrambone, M., Pietrodangelo, A. (2008). Influence of atmospheric stability on the mass concentration and chemical composition of atmospheric particles: a case study in Rome, Italy. Environment international, 34(5), 621-628.

Perrino, C., Canepari, S., Pappalardo, S., Marconi, E. (2010). Time-resolved measurements of soluble ions and elements in atmospheric particulate matter for the characterization of local and long-range transport events. Chemosphere, 80(11), 1291-1300. https://doi.org/10.1007/s11356-014-4019-9

Perrino, C., Tofful, L., Dalla Torre, S., Sargolini, T., Canepari, S. (2019). Biomass burning contribution to PM10 concentration in Rome (Italy): Seasonal, daily and two-hourly variations. Chemosphere, 222, 839-848.

Pey, J., Pérez, N., Cortés, J., Alastuey, A., Querol, X. (2013). Chemical fingerprint and impact of shipping emissions over a western Mediterranean metropolis: Primary and aged contributions. Science of the total environment, 463, 497-507. https://doi.org/10.1016/j.scitotenv.2013.06.061

Pietrodangelo, A., Salzano, R., Rantica, E., Perrino, C. (2013). Characterisation of the local topsoil contribution to airborne particulate matter in the area of Rome (Italy). Source profiles. Atmospheric Environment, 69, 1-14. https://doi.org/10.1016/j.atmosenv.2012.11.059

Polissar, A. V., Hopke, P. K., Paatero, P., Malm, W. C., Sisler, J. F. (1998). Atmospheric aerosol over Alaska: 2. Elemental composition and sources. Journal of Geophysical Research: Atmospheres, 103(D15), 19045-19057.

Popovicheva, O., Kireeva, E., Shonija, N., Zubareva, N., Persiantseva, N., Tishkova, V., Demirdjian, B., Moldanovà, J., Mogilnikov, V. (2009). Ship particulate pollutants: Characterization in terms of environmental implication. Journal of Environmental Monitoring, 11(11), 2077-2086. https://doi.org/10.1039/B908180A

Querol, X., Viana, M., Alastuey, A., Amato, F., Moreno, T., Castillo, S., Pey, J., de la Rosa, J., Sanchez de la Campa, A., Artinano, B., Salvador, P., Garcia Dos Santos, S., Fernandez-Patier, R., Moreno-Grau, S., Negral, L., Minguillon, M.C., Gil, J.I., Inza, A., Ortega, L.A., Santamaria, J.M., Reff, A., Eberly, S. I., Bhave, P. V. (2007). Receptor modeling of ambient particulate matter data using positive matrix factorization: review of existing methods. Journal of the Air & Waste Management Association, 57(2), 146-154. https://doi.org/10.1080/10473289.2007.10465319

Querol, X., Moreno, T., Karanasiou, A., Reche, C., Alastuey, A., Viana, M., Font, O., Gil, J., de Miguel, E., Capdevila, M. (2012). Variability of levels and composition of PM_{10} and $PM_{2.5}$ in the Barcelona metro system. Atmospheric Chemistry and Physics, 12(11), 5055-5076.

Querol, X., Massagué, J., Alastuey, A., Moreno, T., Gangoiti, G., Mantilla, E., Duéguez, J.J., Escudero, M., Monfort, E., Pérez García-Pando, C., Petetin, H., Jorba, O., Vasquez, V., de la Rosa, J., Campos, A., Muñóz, M., Monge, S., Hervás, M., Javato, R., Cornide, M. J. (2021). Lessons from the COVID-19 air pollution decrease in Spain: Now what?. Science of The Total Environment, 779, 146380. https://doi.org/10.1016/j.scitotenv.2021.146380

Ramli, N. A., Yusof, N. F. F. M., Shith, S., Suroto, A. (2020). Chemical and biological compositions associated with ambient respirable particulate matter: a review. Water, Air, & Soil Pollution, 231(3), 1-14.

Reddy, M. S., Basha, S., Joshi, H. V., Jha, B. (2005). Evaluation of the emission characteristics of trace metals from coal and fuel oil fired power plants and their fate during combustion. Journal of Hazardous Materials, 123(1-3), 242-249.

Robinson, A. L., Subramanian, R., Donahue, N. M., Bernardo-Bricke, A., Rogge, W. F. (2006). Source apportionment of molecular markers and organic aerosol 1. Polycyclic aromatic hydrocarbons and methodology for data visualization. Environmental science & technology, 40(24), 7803-7810. https://doi.org/10.1021/es0510414

Roma Capitale, LA POPOLAZIONE DI ROMA. STRUTTURA E DINAMICA DEMOGRAFICA Anno 2019, (in English: Rome Population. Demographic Structure and Dinamic) Available online: https://www.comune.roma.it/web-resources/cms/documents/La_popolazione_a_Ro ma2019.pdf (accessed on 2nd June 2021)

Roma Capitale, Piano Generale del Traffico Urbano (in English: City Urban Traffic General Plan). April 2015. Available online: https://www.comune.roma.it/pcr/it/dip_mob_delibere.page (accessed on 2nd June 2021).

Seinfeld, J.H. and Pandis, S.N. (2006) Atmospheric Chemistry and Physics: From Air Pollution to Climate Change. 2nd Edition, John Wiley & Sons, New York.

Sharma, S. K., Mandal, T. K., Jain, S., Sharma, A., Saxena, M. (2016). Source apportionment of PM 2.5 in Delhi, India using PMF model. Bulletin of environmental contamination and toxicology, 97(2), 286-293.

Shen, J., Bigi, A., Marinoni, A., Lampilahti, J., Kontkanen, J., Ciarelli, G., Bianchi, F. (2021). Emerging Investigator Series: COVID-19 lockdown effects on aerosol particle size distributions in northern Italy. Environmental Science: Atmospheres, 1, 214-227. https://doi.org/10.1039/D1EA00016K

Silvern, R. F., Jacob, D. J., Kim, P. S., Marais, E. A., Turner, J. R., Campuzano-Jost, P., Jimenez, J. L. (2017). Inconsistency of ammonium–sulfate aerosol ratios with thermodynamic models in the eastern US: a possible role of organic aerosol. Atmospheric Chemistry and Physics, 17(8), 5107-5118. https://doi.org/10.5194/acp-17-5107-2017

Singhal, T. (2020). A review of coronavirus disease-2019 (COVID-19). The indian journal of pediatrics, 87(4), 281-286. https://doi.org/10.1007/s12098-020-03263-6

Stefenelli, G., Jiang, J., Bertrand, A., Bruns, E. A., Pieber, S. M., Baltensperger, U., Marchand, N., Aksoyoglu, S., Prévôt A.S.H., Slowik, J.G., Haddad, I. E. (2019). Secondary organic aerosol formation from smoldering and flaming combustion of biomass: a box model parametrization based on volatility basis set. Atmospheric Chemistry and Physics, 19(17), 11461-11484. https://doi.org/10.5194/acp-19-11461-2019

Tian, Y., Wu, J., Shi, G., Wu, J., Zhang, Y., Zhou, L., Zhang, P., Feng, Y. (2013) Long-term variation of the levels, compositions and sources of size-resolved particulate matter in a megacity in China. Science of The Total Environment, 463, 462-468, https://doi.org/10.1016/j.scitotenv.2013.06.055.

Tofful, L., Perrino, C., Canepari, S. (2020). Comparison study between indoor and outdoor chemical composition of PM2. 5 in two Italian areas. Atmosphere, 11(4), 368.

Tomassetti, L., Torre, M., Tratzi, P., Paolini, V., Rizza, V., Segreto, M., Petracchini, F. (2020). Evaluation of air quality and mobility policies in 14 large Italian cities from 2006 to 2016. Journal of Environmental Science and Health, Part A, 55(7), 886-902. https://doi.org/10.1080/10934529.2020.1752070

UNI, E., 2014. 12341: (2014). Air Quality–Determination of the PM10 fraction of suspended particulate matter. Reference method and field test procedure to demonstrate reference equivalence of measurements methods.

Viana, M., Amato, F., Alastuey, A., Querol, X., Moreno, T., Garcia Dos Santos, S., Herce, M.D., Fernández-Patier, R. (2009). Chemical tracers of particulate emissions from commercial shipping. Environmental science & technology, 43(19), 7472-7477. https://doi.org/10.1021/es901558t

Wang, C., Horby, P. W., Hayden, F. G., Gao, G. F. (2020). A novel coronavirus outbreak of global health concern. The lancet, 395(10223), 470-473. https://doi.org/10.1016/S0140-6736(20)30185-9.

World Health Organization. (2016). Ambient air pollution: A global assessment of exposure and burden of disease.

Yadav, S., Rajamani, V. (2006). Air quality and trace metal chemistry of different size fractions of aerosols in N–NW India—implications for source diversity. Atmospheric Environment, 40(4), 698-712. https://doi.org/10.1016/j.atmosenv.2005.10.005

Zhao, J., Zhang, Y., Xu, H., Tao, S., Wang, R., Yu, Q., Chen, Y., Zou, Z., Ma, W. (2021). Trace Elements From Ocean-Going Vessels in East Asia: Vanadium and Nickel Emissions and Their Impacts on Air Quality. Journal of Geophysical Research: Atmospheres, 126(8), e2020JD033984. https://doi.org/10.1029/2020JD033984

Zhou, X., Strezov, V., Jiang, Y., Yang, X., Kan, T., Evans, T. (2020). Contamination identification, source apportionment and health risk assessment of trace elements at different fractions of atmospheric particles at iron and steelmaking areas in China. PloS one, 15(4), e0230983. https://doi.org/10.1371/journal.pone.0230983

Supplementary Materials

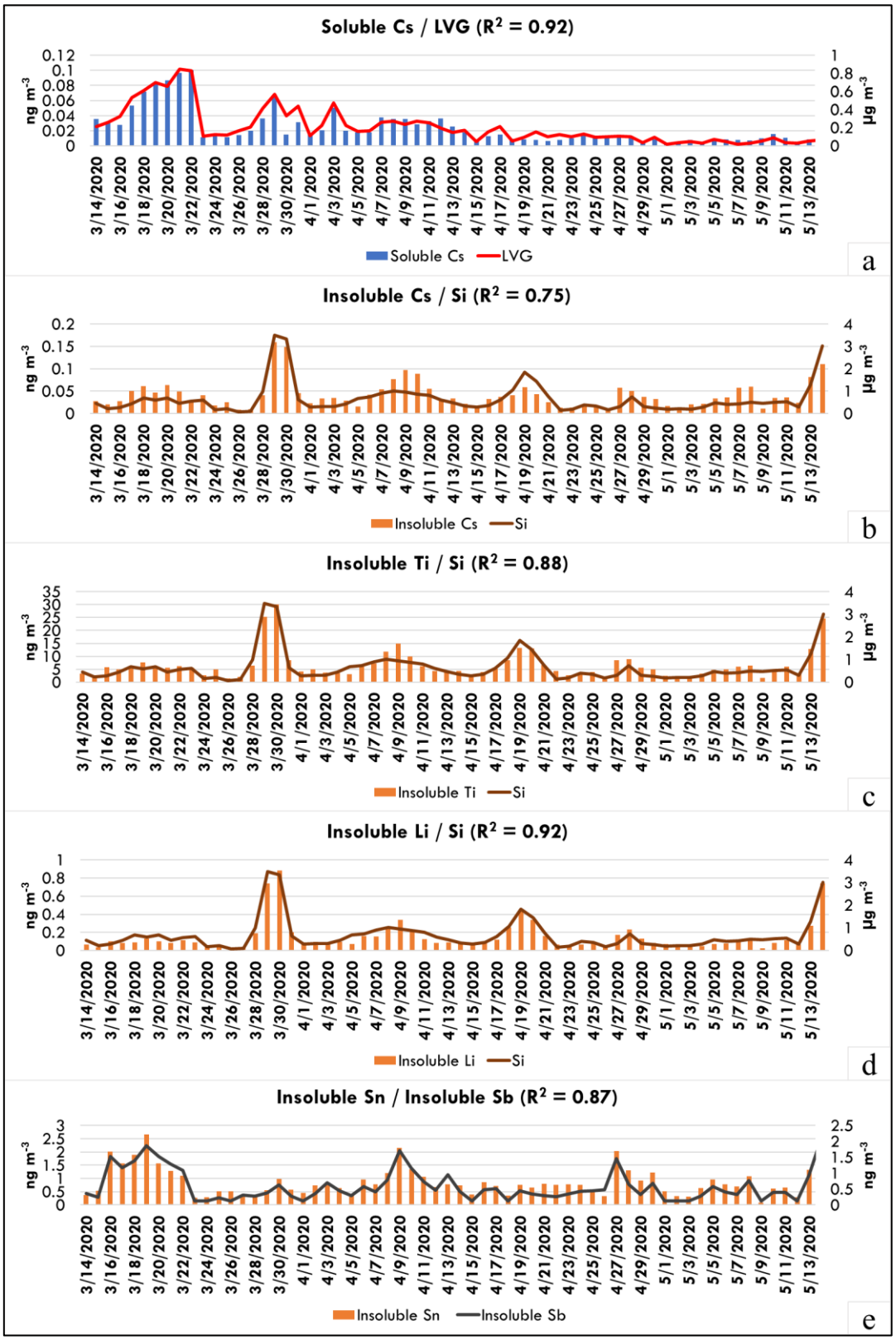

Fig. S1.1. Comparison between concentrations of soluble Cs and LVG (panel a), insoluble Cs and Si (panel b), insoluble Ti and Si (panel c), insoluble Li and Si (panel d), and insoluble Sn and insoluble Sb (panel e), obtained at Sapienza from March 14th to May 13th (lockdown period).

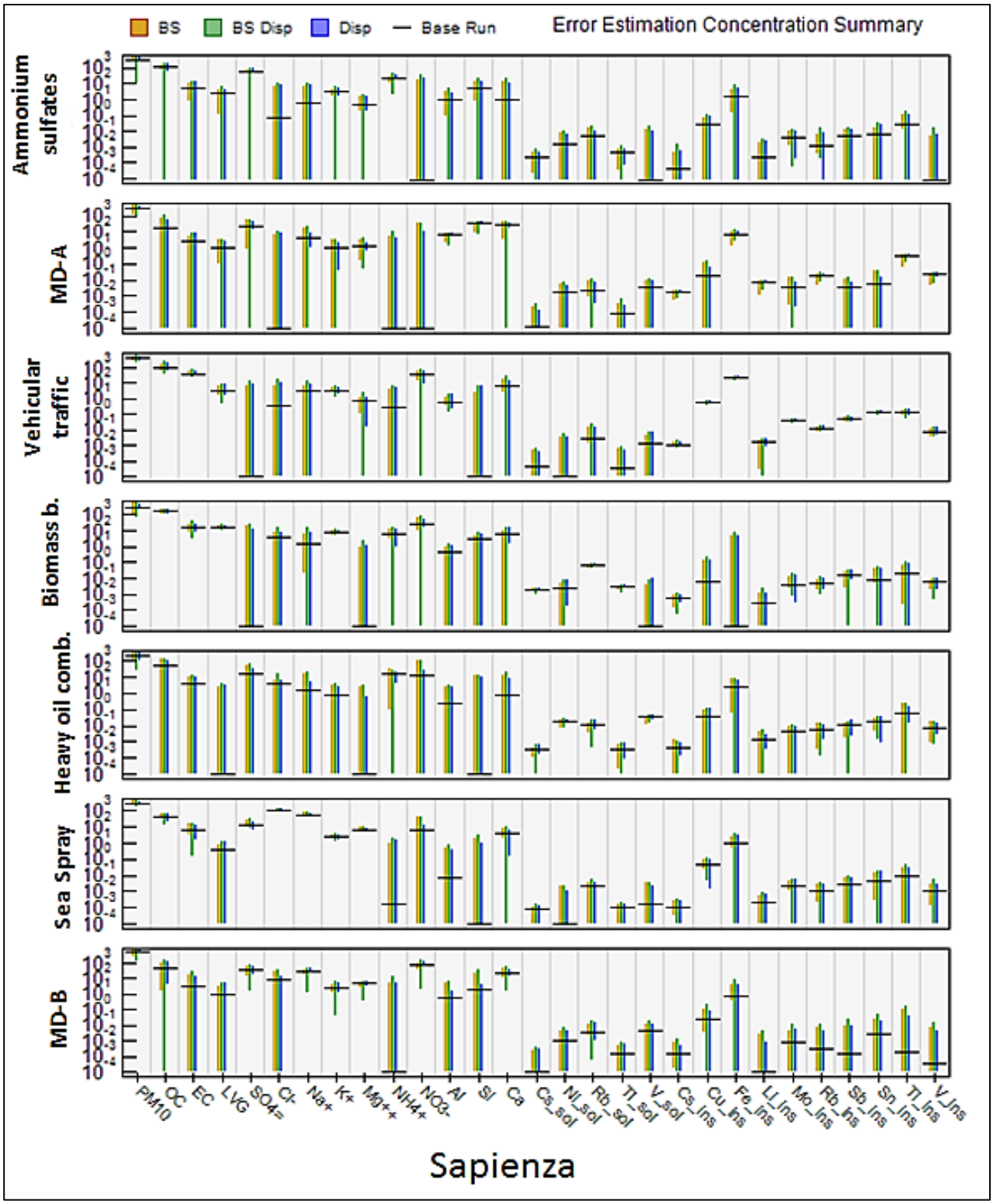

Fig. S2.1. Summary of BS, DISP and BS-DISP error estimation results at Sapienza. MD-A: Mineral dust A; MD-B: Mineral dust B; Biomass b.: biomass burning. The soluble and insoluble fraction of elements are indicated with *sol* and *ins*, respectively, to improve visualization. Concentration unit is ng m^{-3}.

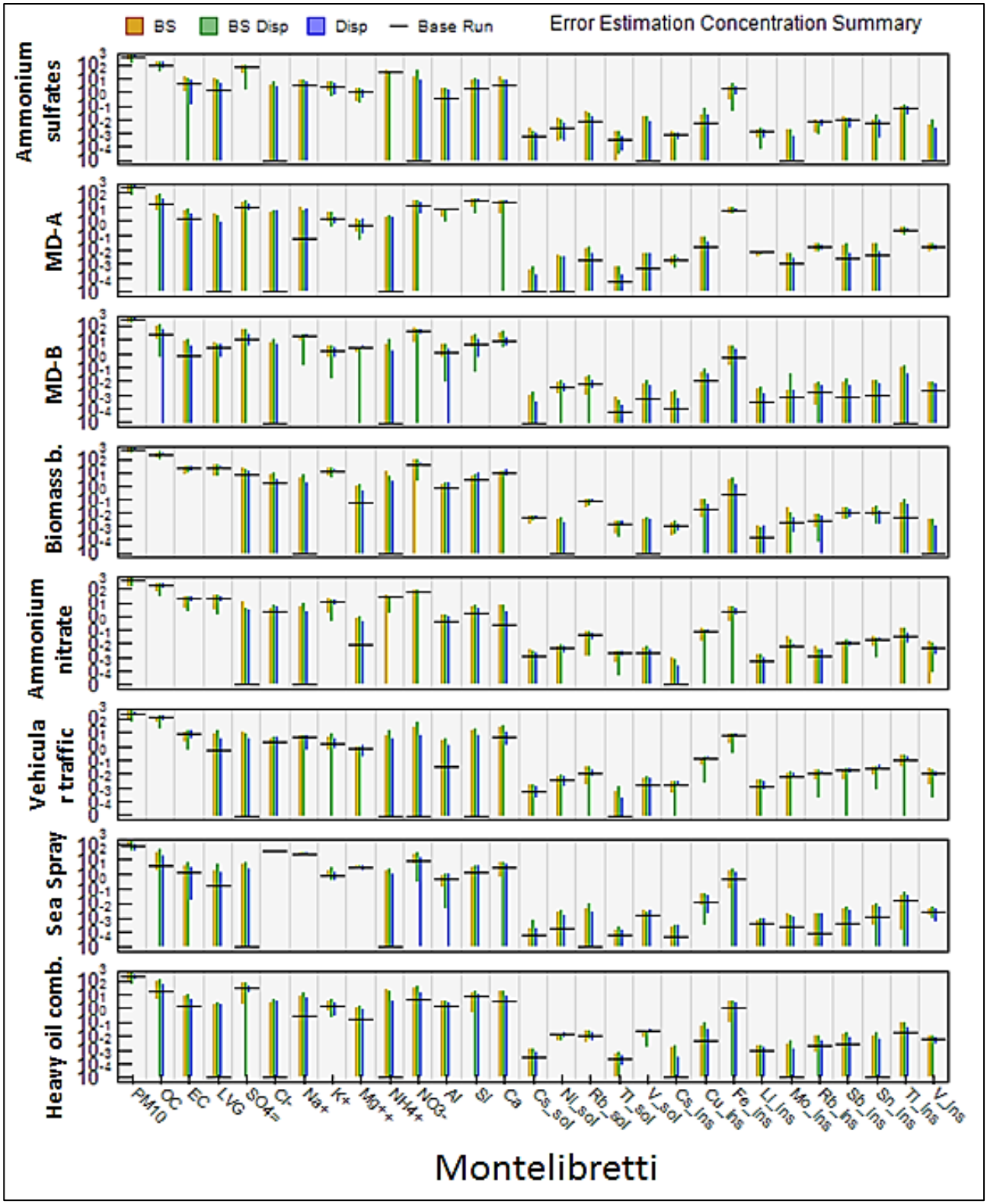

Fig. S2.2. Summary of BS, DISP and BS-DISP error estimation results at Montelibretti. MD-A: Mineral dust A; MD-B: Mineral dust B; Biomass b.: biomass burning. The soluble and insoluble fraction of elements are indicated with *sol* and *ins*, respectively, to improve visualization. Concentration unit is ng m^{-3}.

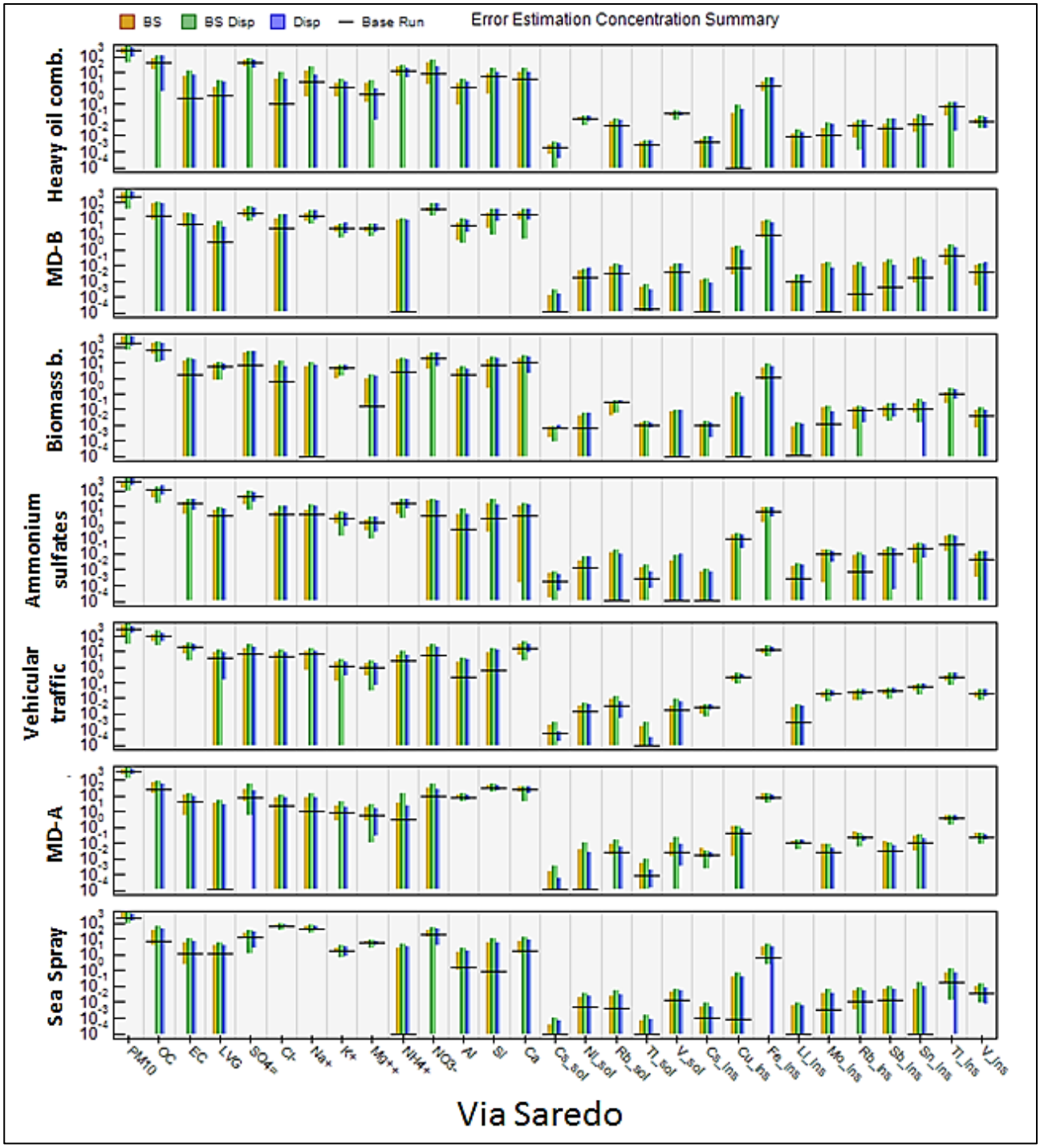

Fig. S2.3. Summary of BS, DISP and BS-DISP error estimation results at Via Saredo. MD-A: Mineral dust A; MD-B: Mineral dust B; Biomass b.: biomass burning. The soluble and insoluble fraction of elements are indicated with *sol* and *ins*, respectively, to improve visualization. Concentration unit is ng m^{-3}.

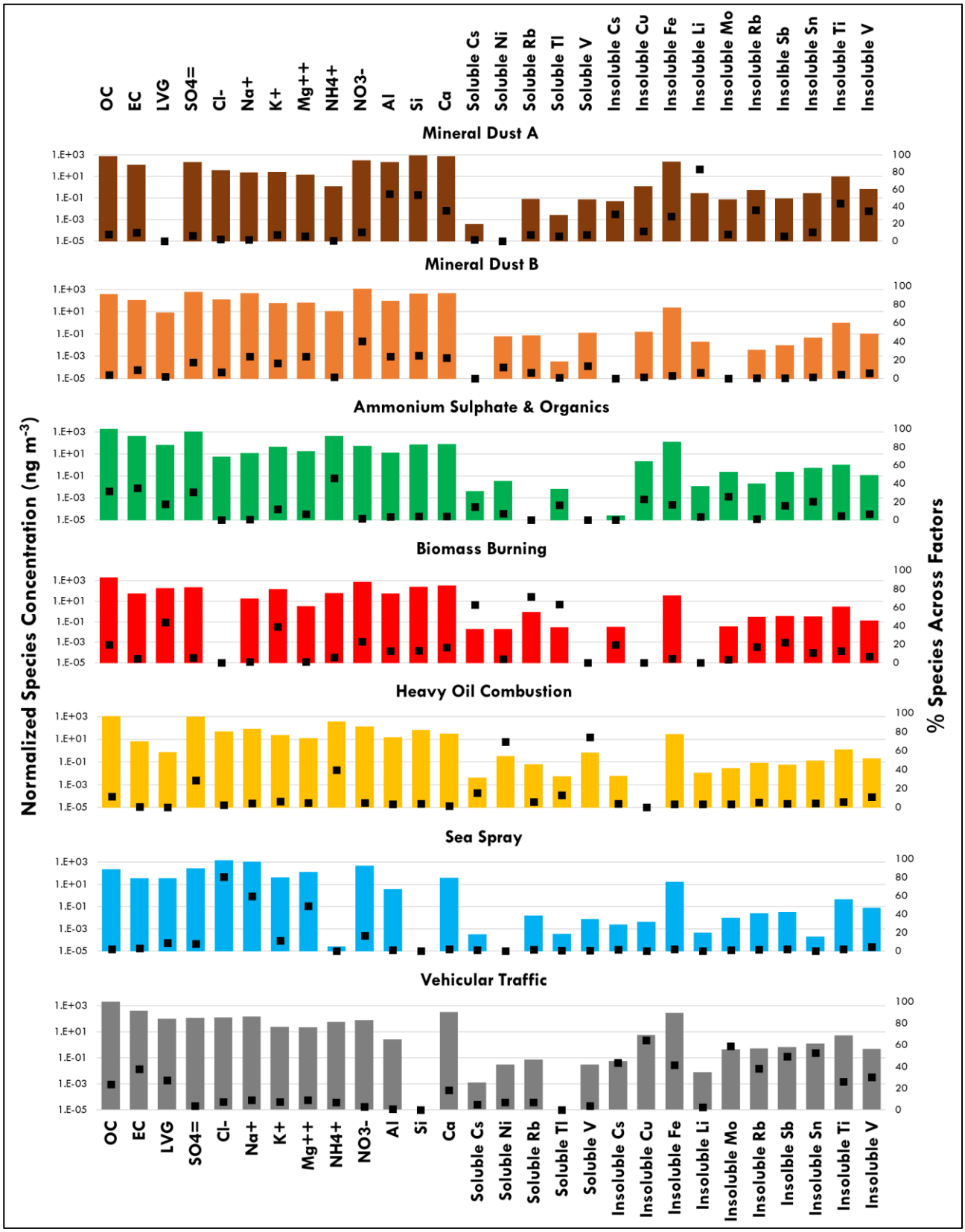

Fig. S3.1. Chemical profiles of the factors identified by PMF at Via Saredo during the entire monitoring period.

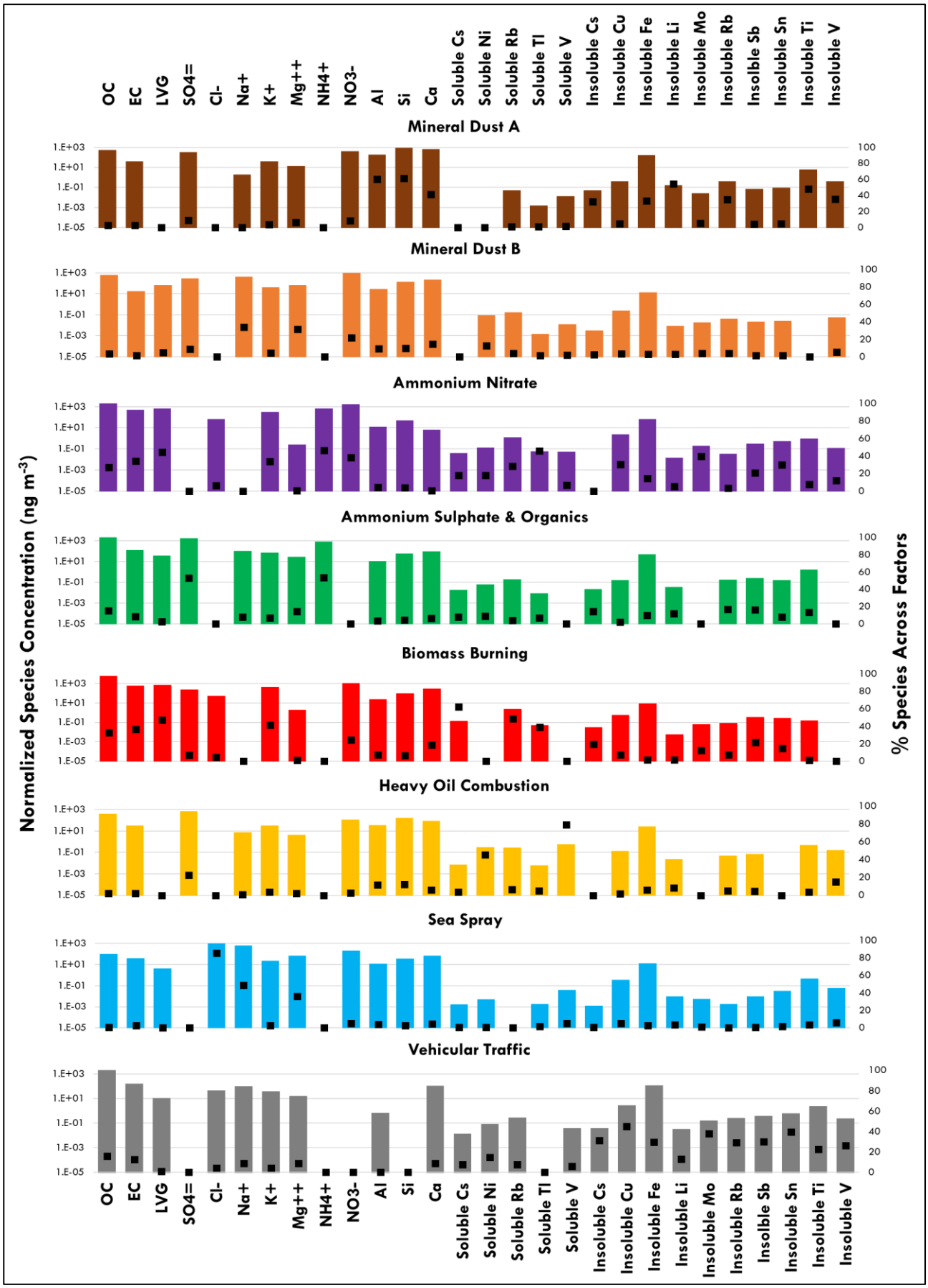
OC
EC
LVG
SO4=
Cl-
Na+
K+
Mg++
NH4+
NO3-
Al
Si
Ca
Soluble Cs
Soluble Ni
Soluble Rb
Soluble Tl
Soluble V
Insoluble Cs
Insoluble Cu
Insoluble Fe
Insoluble Li
Insoluble Mo
Insoluble Rb
Insolble Sb
Insoluble Sn
Insoluble Ti
Insoluble V
Mineral Dust A
Mineral Dust B
Ammonium Nitrate
Ammonium Sulphate & Organics
Biomass Burning
Heavy Oil Combustion
Sea Spray
Vehicular Traffic
1.E+03
1.E+01
1.E-01
1.E-03
1.E-05
100
80
60
40
20
0
Normalized Species Concentration (ng m-3)
% Species Across Factors

Fig. S3.2. Chemical profiles of the factors identified by PMF at Montelibretti during the entire monitoring period.

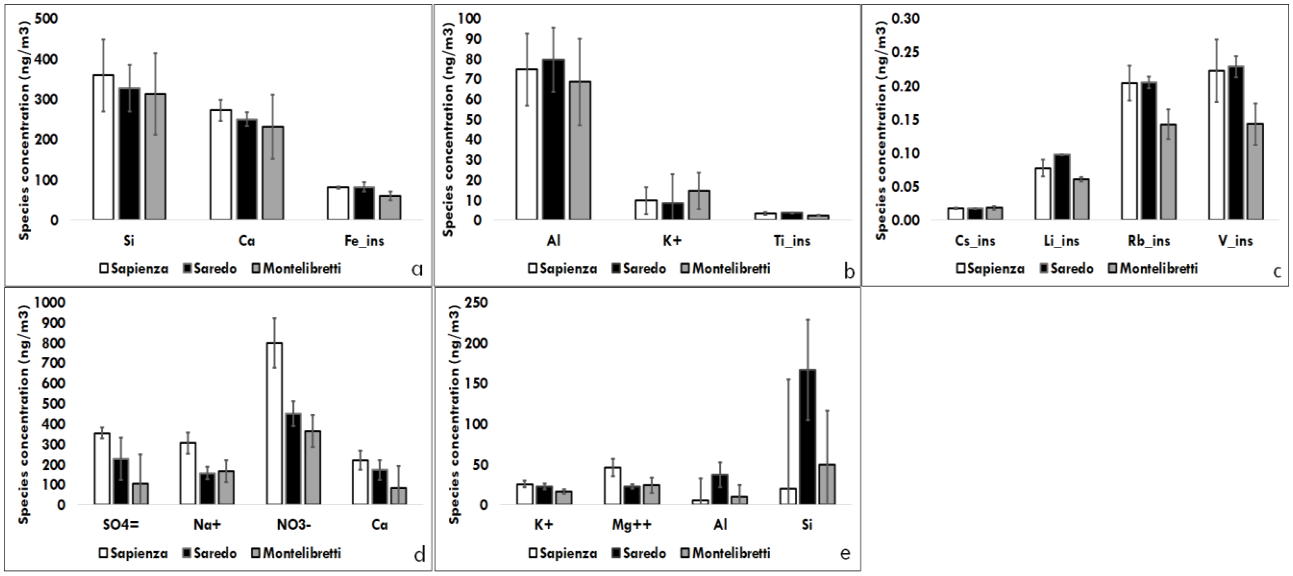

Fig. S3.3. MD-A (a, b, c) and MD-B (d, e) profiles determined at the three sites of this study. Only species for which a small-size error is estimated by at least two out of three error estimation methods (BS, DISP and BS-DISP) are reported, by each profile, for inter-site comparison.

a, b, c: major, minor and trace species, respectively, of MD-A profile; d, e: major and minor species, respectively, of MD-B profile. Error bars are species uncertainties in the profile.

Table S3.1. Diagnostic ratios of the biomass burning profiles determined at the three sites by PMF are compared with the variability range of same ratios for biomass profiles available in the SPECIEUROPE repository (Pernigotti et al., 2016). All profiles used here (namely, profiles no.: 5 to 8, 67, 150, 184, 187 to 192, 224 to 226, 248 to 252) refer to PM_{10} size fraction.

	Range (min – max)	**Sapienza**	**Via Saredo**	**Montelibretti**
EC/OC	0.1 – 1	0.1	0.03	0.1
LVG/OC	0.01 – 0.3	0.1	0.1	0.1
K+/LVG	0.02 – 0.5	0.5	0.8	0.6
Cs/Rb [1]	0.04 – 0.06	0.03	0.02	0.01

[1] Calculated on the soluble fraction of Cs and Rb for the profiles determined in this study, and on the total element for the SPECIEUROPE biomass burning profiles.

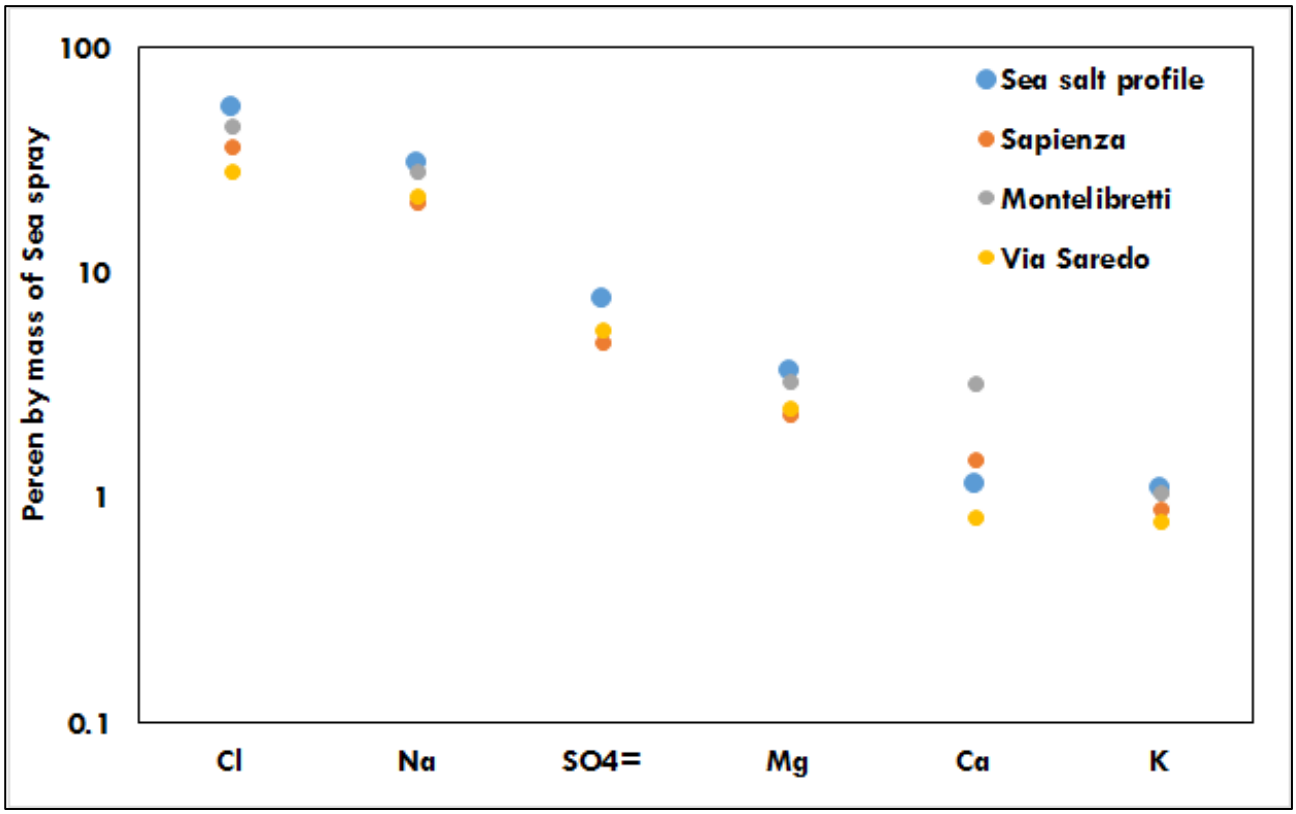

Fig. S3.4. Chemical profile of reference fresh sea salt (Seinfeld and Pandis, 2006) and of sea spray factor profiles estimated by PMF in this study. In the latter, the ion fraction of Cl, Na, Mg and K have been used. Only major species are reported.

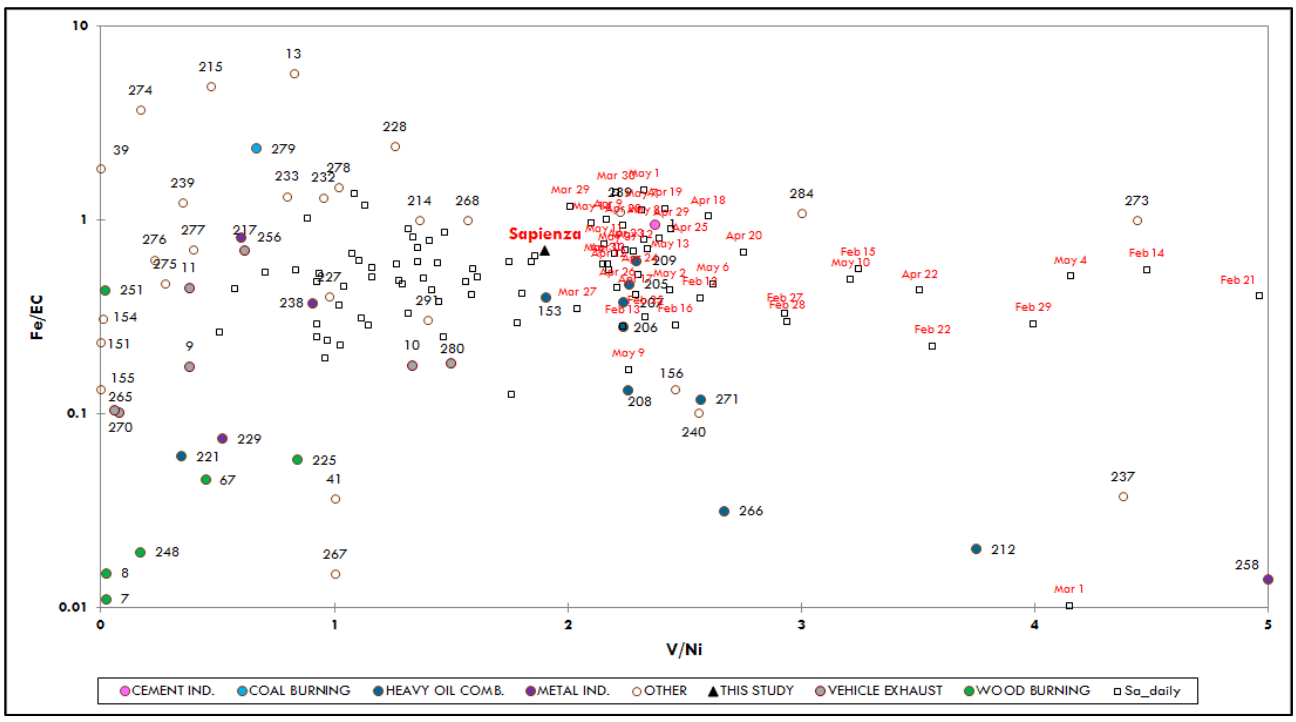

Fig. S3.5. Ratio-ratio scatter plot of selected SPECIEUROPE source profiles (identified by ID number), heavy oil combustion profile estimated by PMF at Sapienza (Sa), and daily PM_{10} samples collected at same site. The

variability range of axes has been limited to the area of the plot of main interest for this work, to the aim of improving visualization of data. To same goal, dates are reported only for daily samples affected by heavy oil combustion.

Fig. S3.6. Ratio-ratio scatter plot of selected SPECIEUROPE source profiles (identified by ID number), heavy oil combustion profile estimated by PMF at Via Saredo (Sar), and daily PM_{10} samples collected at same site. The variability range of axes has been limited to the area of the plot of main interest for this work, to the aim of improving visualization of data. To same goal, dates are reported only for daily samples affected by heavy oil combustion.

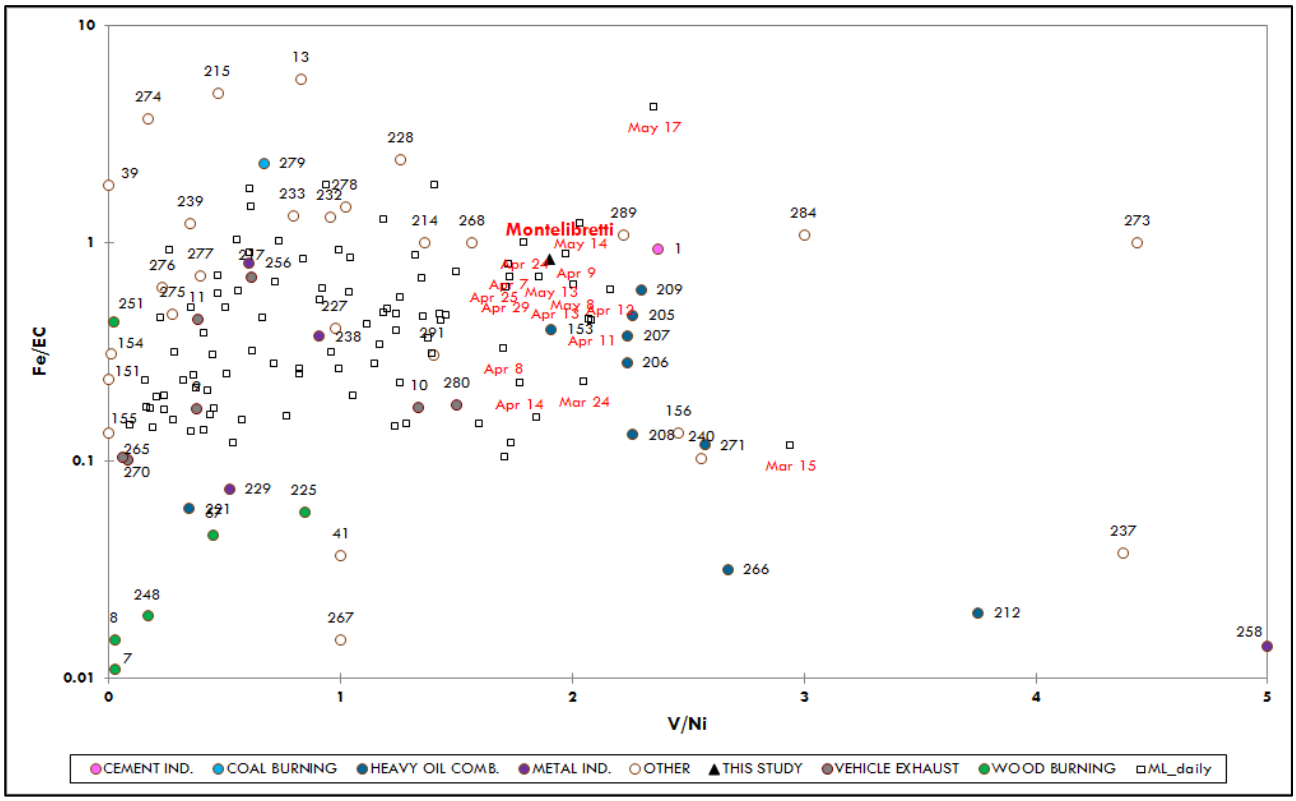

Fig. S3.7. Ratio-ratio scatter plot of selected SPECIEUROPE source profiles (identified by ID number), heavy oil combustion profile estimated by PMF at Montelibretti (ML), and daily PM_{10} samples collected at same site. The variability range of axes has been limited to the area of the plot of main interest for this work, to the aim of improving visualization of data. To same goal, dates are reported only for daily samples affected by heavy oil combustion.

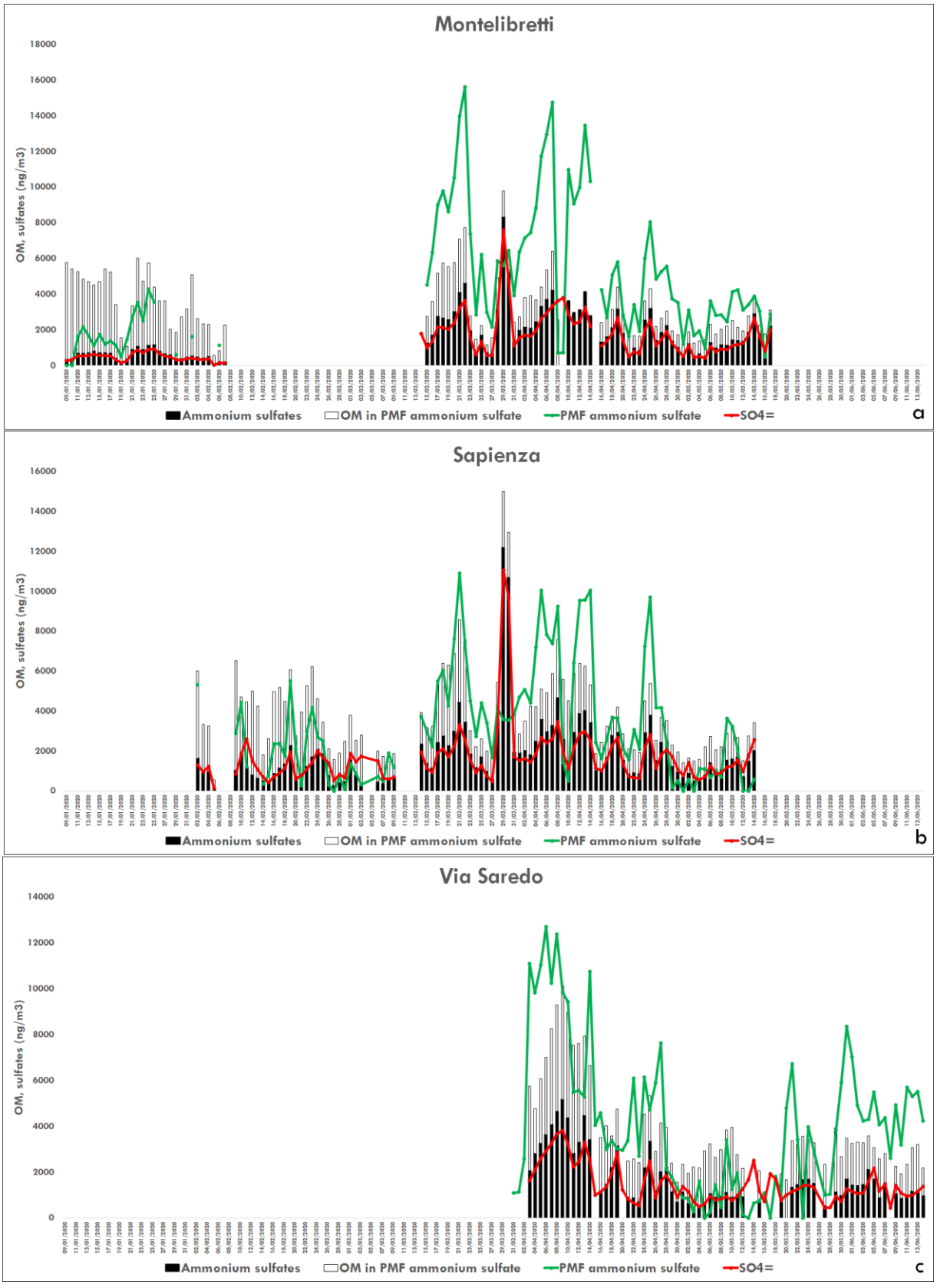

Fig. S3.8. Daily mass contribution of secondary sulfates estimated by chemical equivalent ratios and by PMF, organic matter apportioned to secondary sulfates and measured $SO_4^=$, at the three sites of this study.

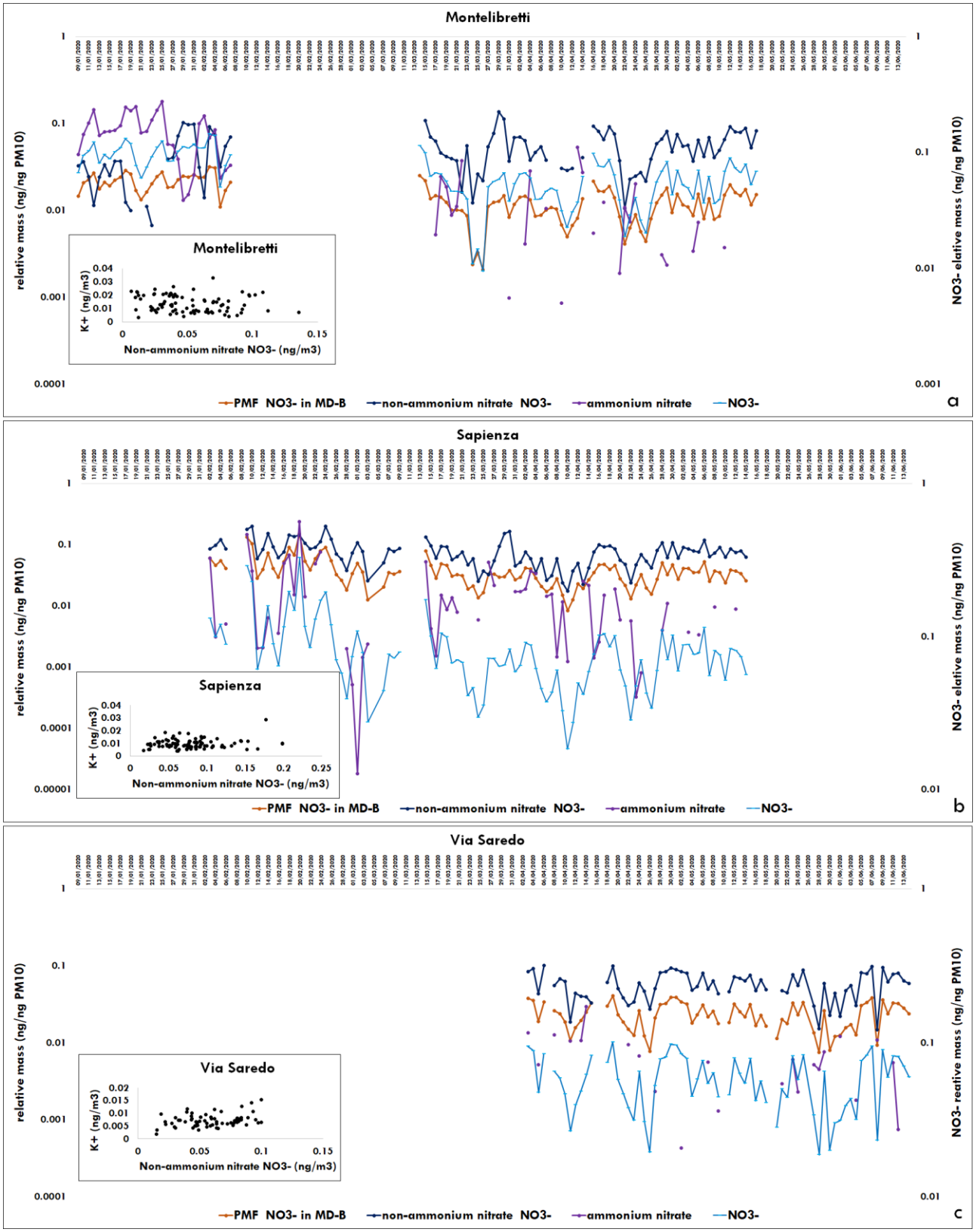

Fig. S3.9. Daily concentrations (relative mass in PM_{10}) of NO_3^- contributions estimated by chemical equivalent ratios, and of NO_3^- fraction apportioned to MD-B profile by PMF, at the three sites. Total measured NO_3^- is

reported on the secondary axis, for comparison. Regression between potassium ion and non-ammonium nitrate NO_3^- is also reported at each site.

References

Pernigotti, D., Belis, C. A., Spano, L. (2016). SPECIEUROPE: The European data base for PM source profiles. Atmospheric Pollution Research, 7(2), 307-314. http://source-apportionment.jrc.ec.europa.eu/specieurope/index.aspx

Seinfeld, J.H. and Pandis, S.N. (2006) Atmospheric Chemistry and Physics: From Air Pollution to Climate Change. 2nd Edition, John Wiley & Sons, New York.

5.3 (A3) Spatial Mapping and Size Distribution of Oxidative Potential of Particulate Matter Released by Spatially Disaggregated Sources

Environmental Pollution (2020), 266, 115271, doi: 10.1016/j.envpol.2020.115271

Lorenzo Massimi[1,*], Martina Ristorini[2], Giulia Simonetti[1], Maria Agostina Frezzini[1], Maria Luisa Astolfi[1], Silvia Canepari[1]

[1] Department of Chemistry, Sapienza University of Rome, P. le Aldo Moro, 5, Rome 00185, Italy;

[2] Department of Bioscience and Territory, University of Molise, Pesche (IS), 86090, Italy.

*Corresponding author

Keywords: Spatial variability; Size distribution; PM source; Ascorbic acid (OP^{AA}) assay; 1,4-dithiothreitol (OP^{DTT}) assay; 2',7'-dichlorodihydrofluorescein (OP^{DCFH}) assay

Abstract

The ability of particulate matter (PM) to induce oxidative stress is frequently estimated by acellular oxidative potential (OP) assays, such as ascorbic acid (AA) and 1,4-dithiothreitol (DTT), used as proxy of reactive oxygen species (ROS) generation in biological systems, and particle-bound ROS measurement, such as 2',7'-dichlorodihydrofluorescein (DCFH) assay. In this study, we evaluated the spatial and size distribution of OP results obtained by three OP assays (OP^{AA}, OP^{DCFH} and OP^{DTT}), to qualitative identify the relative relevance of single source contributions in building up OP values and to map the PM potential to induce oxidative stress in living organisms. To this aim, AA, DCFH and DTT assays were applied to size-segregated PM samples, collected by low-pressure cascade impactors, and to PM_{10} samples collected at 23 different sampling sites (about 1 km between each other) in Terni, an urban and industrial hot-spot of Central Italy, by using recently developed high spatial resolution samplers of PM, which worked in parallel during three monitoring periods (February, April and December 2017). The sampling sites were chosen for representing the main spatially disaggregated sources of PM (vehicular traffic, rail network, domestic heating, power plant for waste treatment, steel plant) present in the study area. The obtained results clearly showed a very different sensitivity of the three assays toward each local PM source. OP^{AA} was particularly sensitive toward coarse particles released from the railway, OP^{DCFH} was sensible to fine particles released from the steel plant and domestic biomass heating, and OP^{DTT} was quite selectively sensitive toward the fine fraction of PM released by industrial and biomass burning sources.

1. Introduction

Particulate matter (PM) air pollution is one of the major risk factors for human health worldwide (Anderson et al., 2012; Lubczyńska et al., 2017). Various epidemiological studies have spotlighted strong correlations

between exposure to PM and the onset of cardiovascular and respiratory diseases (Pope and Dockery, 2006). Indeed, over the years, it has been associated to a great number of adverse outcomes for human health, such as respiratory and cardiovascular diseases, cancer, diabetes, metabolic disorders, atherosclerosis and neurodegenerative diseases (Strak et al., 2012; Gupta et al., 2019; Øvrevik et al., 2019). Several epidemiological studies have spotlighted strong correlations between PM exposure and the onset of cardiopulmonary diseases (Brunekreef et al, 2002; Pope et al, 2006). However, most of the studies use PM mass concentration as exposure indicator, which misestimates the overall impact of PM, since it does not take into account the multiple toxicological effects of the different pollutants that make up particulate matter. This limitation can be overcome by identifying possible relationships between PM toxicity and its specific physic-chemical properties. In fact, during the last few decades, the complex and variable composition of PM has been widely investigated and many studies have revealed that several PM properties, such as chemical composition and particle dimension, influence its health and environmental effects (Ricci and Cirillo, 1985; Hlavay et al., 2001; Kelly et al., 2012). Nevertheless, not enough evidence that associates each property to specific outcomes has been yet identified (WHO, 2013).

Nowadays, there is a growing scientific consensus in affirming that generation of reactive oxygen species (ROS) is one of the major mechanisms by which PM exerts its adverse biological effects (Li et al., 2015), leading to oxidative stress responses and thus to different chronic and acute systemic inflammations (Li et al., 2003; Esposito et al., 2014; Pirrino et al., 2017). Indeed, PM ability to generate oxidative stress in biological systems has been demonstrated to contribute to genotoxicity and cytotoxic mechanisms responsible for cell damages (Marcoccia et al., 2017; Piacentini et al., 2019). PM capacity to trigger damaging oxidative reactions and inflammations is defined as oxidative potential (OP), which is a measure of PM ability to oxidise target molecules, by generating ROS in acellular environments. Over the last years, OP has been proposed as a biologically relevant metric for addressing PM exposure (Yang et al., 2016; Simonetti et al., 2018a, 2018b; Gao et al., 2020), since it appeared to be more reliable than PM mass concentration (Delfino et al., 2011; Gupta et al., 2019). However, the variability in chemical composition of PM and in the contributions of different sources, reduces the correlation with health outcomes and may thus limit the potential of OP as a global toxicological indicator.

To date, various acellular assays for the measurement of OP, such ascorbic acid (AA), 1,4-dithiothreitol (DTT) and 2',7'-dichlorodihydrofluorescein (DCFH), have been used to estimate the toxicity of PM released by different emission sources (Bates et al., 2019). Ascorbic acid and 1,4-dithiothreitol ($HSCH_2CH(OH)CH(OH)CH_2SH$) are strong reducing agents; DTT and AA assays involve the controlled incubation of the anti-oxidant (DTT or AA) in PM aqueous extracts under controlled conditions and the measurement of its depletion over time (Cho et al., 2005; Stoeger et al., 2008; Fang et al., 2016; Campbell et al., 2019). The antioxidant loss rate represents the capacity of PM reactive species to catalyze the transfer of electrons from AA or DTT to oxygen, providing an estimation of the OP. On the other hand, 2',7'-dichlorodihydrofluorescein assay, formerly developed for the in-vitro determination of ROS in biological cells

(Lebel et al., 1992; Wang and Joseph, 1999; Halliwell and Whiteman, 2004), is today one of the most used methods for particle-bound ROS measurement in PM (Venkatachari et al., 2005, 2007). It is based on the oxidation of DCFH, a non-fluorescent reagent, to DCF, a fluorescent compound, in the presence of ROS and horseradish peroxidase (HRP), a redox enzyme that primarily reacts with hydrogen peroxide and organic hydroperoxides. The measured fluorescence intensity is converted into hydrogen peroxide equivalents, which is used as an indicator of the ROS reactivity (Hung and Wang, 2001; Perrone et al., 2016). However, each of these methods has been deemed sensible toward PM coming from different emission sources and characterized by very different physic-chemical properties (Ayres et al., 2008; Simonetti et al., 2018b; Frezzini et al., 2019; Piacentini et al., 2019). Therefore, none of the OP assays can be a-priori considered as representative of ROS generation pathways in biological organisms (Fang et al., 2015).

The knowledge of the relative relevance of the single source contributions in building up OP values can be of great help for the identification of the emission sources mainly responsible for ROS generation. Source apportionment of OP results from field campaigns have been attempted in some studies, but conflicting results were found (Fang et al., 2016; Perrone et al., 2016; Chirizzi et al., 2017; Calas et al., 2018). Therefore, this study was aimed to improve the knowledge about the existing relationships between OP values and sources of PM, useful to properly address PM mitigation measures to protect citizens health. In this study, we describe an innovative experimental approach, transferable to other monitoring campaigns, for the spatial mapping of OP^{AA}, OP^{DCFH} and OP^{DTT}, which represents a powerful tool for geo-referenced assessment of PM potential to induce oxidative stress and harmful effects on human health. This innovative approach, allows to qualitatively evaluate possible associations between OP values and different sources of PM, overcoming the use of receptor models, often used to investigate the contribution of sources to measured OP with different assays (Cesari et al., 2019). To this aim, we applied the AA, DCFH and DTT assays to the aqueous extracts of PM_{10} sampled by a recently developed very-low volume device (Massimi et al., 2017, 2019; Ristorini et al., 2020), in a wide and dense monitoring network (23 sampling sites, about 1 km between each other) across Terni (Central Italy). The study area includes various spatially disaggregated intensive local PM sources (vehicular traffic, rail network, domestic heating, power plant for waste treatment, steel plant) (Capelli et al., 2011; Guerrini, 2012; Massimi et al., 2020a, 2020b) and is characterized by peculiar meteorological conditions that reduce air pollutants transport, thus favoring their accumulation (Ferrero et al., 2012). These factors have been associated with an increase of morbidity and mortality due to the onset of cardiovascular and respiratory environment-related diseases, which made this area of national interest for environmental remediation (SENTIERI-ReNaM, 2016) and particularly suitable for the spatial mapping of the OP of PM released by different sources. To our knowledge, the comparison of the three OP assays applied to PM_{10} spatially-resolved samples has never been undertaken so far.

To obtain a more reliable identification of the sources responsible for OP, the evaluation of the spatial variability was supported by the study of the size distribution of OP, able to provide information on the relative relevance of combustive and abrasive-mechanical sources in building up OP values (Simonetti et al., 2018a;

Manigrasso et al., 2020). Furthermore, size distribution analysis of OP of PM provides information on the penetration capacity of particles responsible for OP in the respiratory system, thus resulting considerably valuable for the evaluation of exposure to PM and relative health risk.

2. Materials and Methods

2.1 Study Area

The study area is the city of Terni, of 211.90 km^2 and of about 112,000 inhabitants (Sgrigna et al., 2015), located in a basin of the Region Umbria (42° 34'N; 12°39' E), in Central Italy. The peculiar geomorphology of the Terni basin, limits air mixing and air pollutants transport, especially during the frequent winter episodes of atmospheric stability (Morini et al., 2016; Curci et al., 2015; Ferrero et al., 2012).

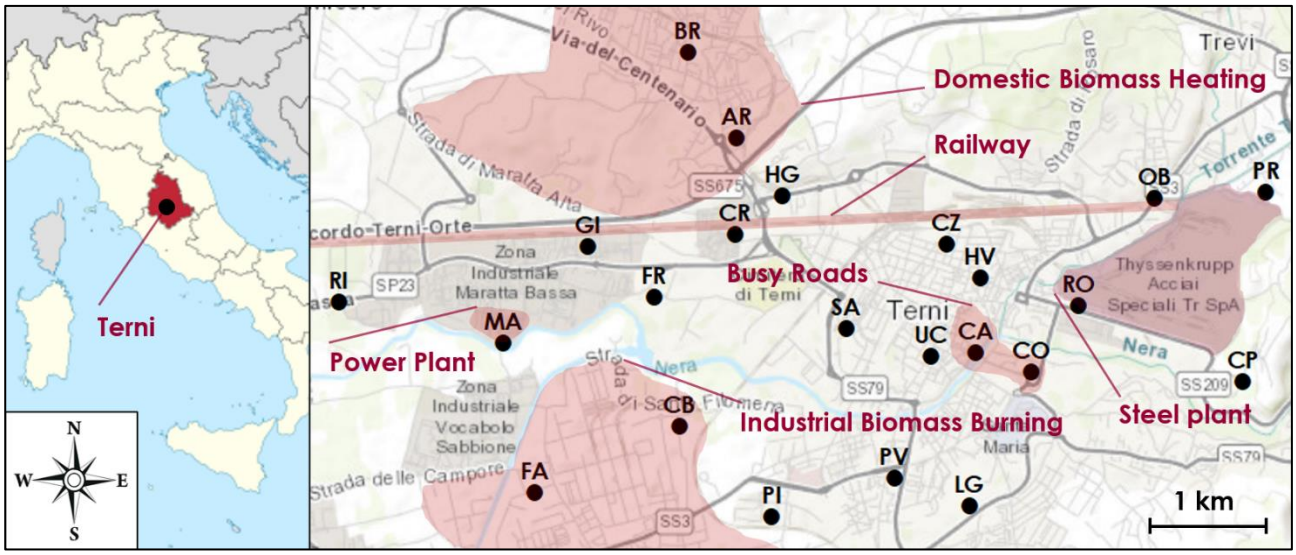

Fig. 1. Map of the 23 sampling sites in the study area (Terni, Central Italy; latitude: 42.5681, longitude: 12.6508, decimal degrees) with the location of the main local PM_{10} emission sources (ArcMap 10.3.1, ArcGis Desktop; ESRI, Redlands, CA, USA).

In Fig. 1 are shown the 23 sampling sites that were selected to cover the whole area with around 1 km spatial resolution and to study the contributions of the main local PM_{10} emission sources. In detail: RI and MA sites are located in the West of the city, near the power plant for waste treatment; GI, CR and HG are situated in the close proximity to the railway, in the North-West of the city; CZ, HV, SA, UC, CA and CO are located in the city center, between the rail network and busy roads; FA and CB, in the South-West of the city, are close to a carpentry and a craftsmanship lab and, along with PI, PV and LG, are affected by industrial biomass burning, such as the burning of carpentry waste products; FR, BR and AR, in the North of the city, are situated near townhouses frequently heated by biomass burning appliances; finally, RO, OB, PR, CP are located around the steel plant in the East of the city.

The 23 sampling sites (RI, MA, FA, GI, FR, CB, PI, BR, AR, CR, HG, SA, PV, LG, CZ, HV, UC, CA, CO, RO, OB, PR, CP) have already been studied (Massimi et al., 2017, 2019) and spatial variability of element concentrations in PM_{10} has been widely evaluated (Massimi et al., 2017, 2020a, 2020b). Spatial maps of elements tracing the main local PM_{10} sources in Terni have been obtained (Massimi et al., 2020b); therefore, localization and spatial distribution of the emission sources in the study area is well known.

2.2 Sampling Equipment

2.2.1 High Spatial Resolution Sampler

The High spatial resolution sampler (HSRS; FAI Instruments, Fonte Nuova, Rome, Italy) operates with a very-low flow rate (0.5 L min^{-1}), it is self-powered (with a rechargeable battery and a solar panel), assures long-term (1-2 months) collection of PM_{10} and has very good sampling efficiency and high repeatability for stable and fine PM_{10} chemical compounds (Catrambone et al., 2019).

23 HSRS, equipped with 37 mm Polytetrafluoroethylene (PTFE) membrane filters (2 μm pore size, PALL Corporation, Port Washington, NY, USA), were used to collect PM_{10} samples and worked in parallel at the 23 sites for three monitoring periods: February (January 21st - February 20th, 2017; 30-day sampling), April (April 1st - May 1st, 2017; 31-day sampling) and December (November 25th, 2017 - January 15th, 2018; 51-day sampling) 2017, allowing the collection of 23 PM_{10} samples per monitoring period.

2.2.2 Micro-Orifice Uniform Deposition Impactor

The Micro-orifice uniform deposition impactor (MOUDI; model 110-NR; MSP Corporation, Shoreview, MN, USA) is a low-pressure cascade impactor (flow rate of 30 L min^{-1}) for the collection of size-segregated PM samples through 10 impaction stages, with cut-size aerodynamic diameters of 0.18, 0.32, 0.56, 1.0, 1.8, 3.2, 5.6, 10 and 18 μm.

Three MOUDI, equipped with 47 mm PTFE membranes (2 μm pore size, PALL Corporation, Port Washington, NY, USA), were used to collect PM samples with different size fractions and worked in parallel in the center (CA), West (MA) and East (PR) of the city for 20 days (February 15th - March 6th, 2018).

Sampling efficiency and repeatability of MOUDI were assessed in Canepari et al., 2019 and in Simonetti et al., 2018a. The relative repeatability for all the considered variables was found to be below 10%.

It is worth noting that long-duration samplings carried out by MOUDI may lead to bouncing-off phenomena that can be responsible for a modification of the original size distribution of atmospheric particles (Canepari et al., 2019). However, to our knowledge, there are no solid and recognized methods to correct the data for this artefact; furthermore, PTFE membrane filters are generally considered as a suitable sampling material able to minimize the bouncing-off (Giorio et al., 2013).

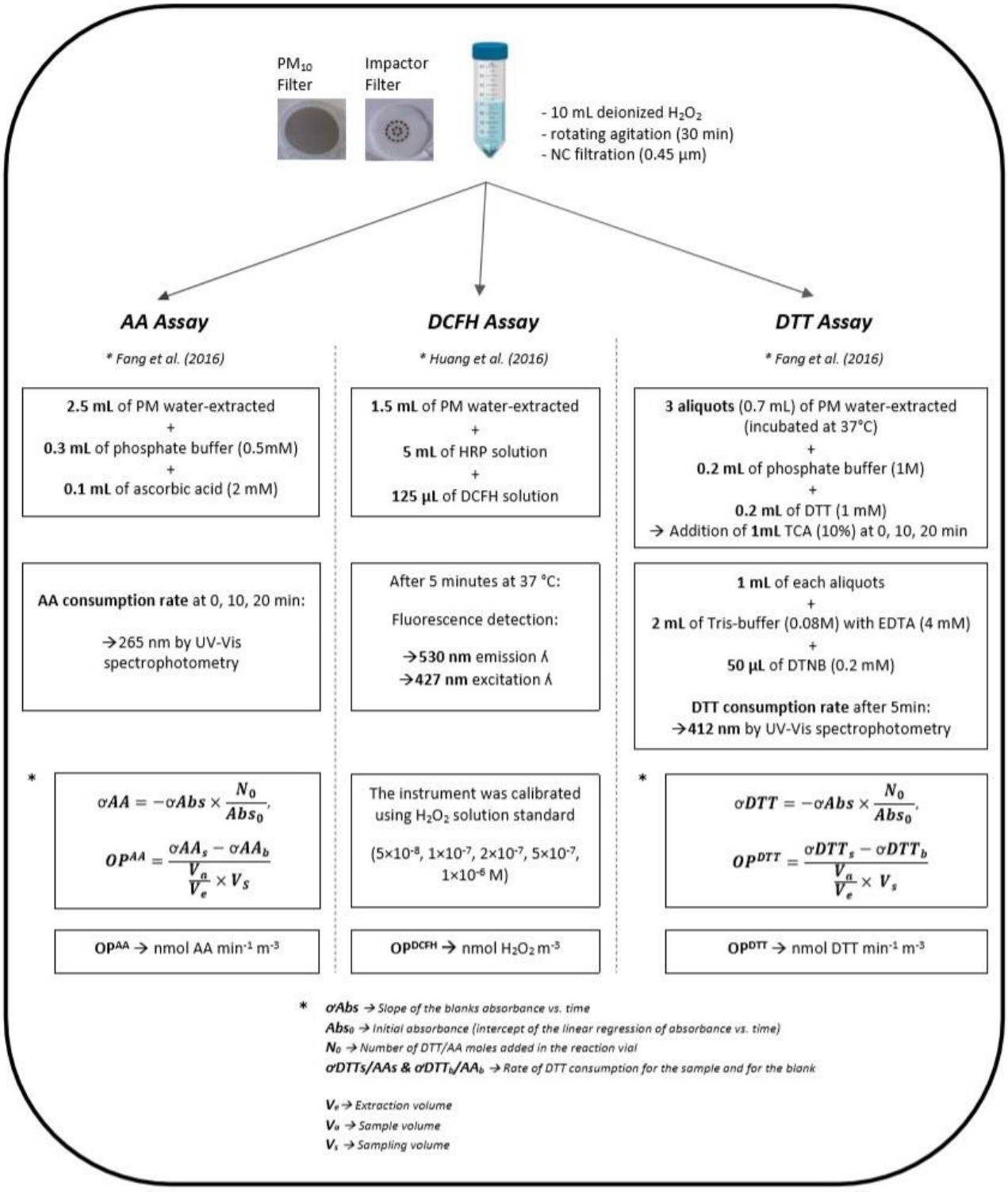

Fig. 2. Block diagram of the conducted samples preparation and OP analytical procedures for the AA, DCFH and DTT assays applied to the PM aqueous extracts.

2.3 Analytical Procedures

PTFE membrane filters were weighed before and after sampling, in order to determine PM mass concentrations. Mass concentration was determined gravimetrically by using an automated microbalance (1

mg sensitivity, mod. ME5, Sartorius AG, Goettingen, Germany). Membrane filters were equilibrated for 2 days at 20 °C and 50% RH before and after sampling. Subsequently, PM field samples were treated by following the procedure detailed in Massimi et al. (2017, 2020a, 2020b). Briefly, after the removal of the supporting polymethylpentene ring from the PTFE membrane filter, each field filter was extracted in 10 mL of deionized water (produced by Arioso UP 900 Integrate Water Purification System, USA) by rotating agitation (60 rpm; Rotator; Glas-Col, USA) for 30 minutes, to avoid ROS generation upon ultrasonic irradiation, commonly used to efficiently extract the PM from the filters. In fact, ultrasonic waves triggers the formation and collapse of cavitation bubbles in the solution, inside which high temperatures and pressures can be reached. These conditions may lead to pyrolysis of the molecules present inside the cavitation bubbles, which results in the production of free radicals (Mutzel et al., 2013; Khurshid et al., 2014; Miljevic et al., 2014). After the extraction by rotating agitation, the obtained solution was filtered through a nitrocellulose filter (NC; pore size 0.45 μm; Merck Millipore Ltd., Billerica, MA, USA). The water-extracted solution was then split in proper aliquots for the different OP analytical procedures. Conducted samples preparation and OP analytical procedures for the AA, DCFH and DTT assays applied to the PM aqueous extracts are summarized in the block diagram of Fig. 2. Further details on the followed AA, DCFH and DTT analytical procedures and used reagents are reported in supplementary material S1. For the quality control and assurance in AA, DCFH and DTT measurements (evaluated in Simonetti et al., 2018a, 2018b and in Piacentini et al., 2019), different tests to assess the repeatability and efficiency of the three OP assays were performed in our lab on a large amount of PM field filters not stored, stored for 15 days in the fridge, in the freezer (-20°C) and at constant ambient temperature, and then extracted by ultrasonic irradiation, rotating agitation (60 rpm) and by using the vortex (2000 rpm). The obtained results showed high repeatability (10-15 %) of the OP values obtained by applying the three OP assays to the PM field samples extracted by rotating agitation.

2.4 Spatial Mapping

Spatial mapping of OP^{AA}, OP^{DCFH} and OP^{DTT} was performed by the software ArcMap 10.3.1 (ArcGis Desktop; ESRI, Redlands, CA, USA). The OP^{AA}, OP^{DCFH} and OP^{DTT} values obtained at the 23 sampling sites for each monitoring period were interpolated by using the spherical semivariogram model (Jian et al., 1996) of the ordinary kriging (OK) method (Johnston et al., 2001), in order to create a continuous surface from the 23 measured sample points and to predict the values at unmeasured locations (Kumar et al., 2007). OK is one of the most used kriging techniques for describing data spatial continuity (Gia Pham et al., 2019). The used OK estimator is given by a linear combination of the observed values with weights, which are derived from the kriging equations, using experimental semivariances fitted by a spherical function (Xie et al., 2011).

3. Results and Discussion

3.1 PM_{10} Mass Concentration

Spatially-resolved data obtained by sampling in parallel at the 23 sites during the three monitoring periods allowed us to evaluate the spatial variability of PM_{10} mass concentration in Terni. PM_{10} mass concentrations determined in February, April and December 2017 are reported in Table 1.

From Table 1, we can observe that the concentration increased at all the sampling sites in the winter monitoring periods (February and December). Mean PM_{10} mass concentration was: 41 ± 7 μg m^{-3} in February, 19 ± 5 μg m^{-3} in April and 33 ± 7 μg m^{-3} in December. This behavior is mostly due to frequent temperature inversions during the colder season, which lead to severe episodes of atmospheric stability (Moroni et al., 2013; Curci et al., 2015), and to the major strength of typical winter sources, such as domestic biomass heating. In fact, in both February and December, high PM_{10} mass concentration was recorded at sites located near townhouses heated by biomass burning appliances (FR, BR and AR).

Table 1. PM_{10} mass concentration determined at the 23 sampling sites in the three monitoring periods (February, April and December 2017).

Site	PM_{10} Mass Concentration (μg m^{-3})		
	February	**April**	**December**
RI	52	21	44
MA	38	22	32
FA	33	21	38
GI	39	15	23
FR	46	12	32
CB	31	23	24
PI	40	18	34
BR	51	24	48
AR	34	14	36
CR	38	21	32
HG	53	10	35
SA	29	15	22
PV	47	21	34
LG	47	28	36
CZ	48	15	39
HV	45	16	35
UC	33	20	24
CA	46	20	36
CO	44	20	35
RO	40	16	29
OB	41	21	30
PR	32	30	26
CP	32	20	24
Mean	**41**	**19**	**33**
SD	**7**	**5**	**7**

3.2 Spatial Mapping of OP

Spatial variability of OP^{AA}, OP^{DCFH} and OP^{DTT} was evaluated, the OP values obtained at the 23 sites in the three monitoring periods are reported in supplementary material S2. Spatial mapping of OP^{AA}, OP^{DCFH} and OP^{DTT} allowed us to assess spatial relationships between the three OP assays and local emission sources of PM.

From Fig. 3, we can observe that high OP^{AA} values were recorded at sites close to the railway. In particular, the highest OP^{AA} values were found at the sites located near the rail station (GI, CR and HG), where trains brake entering the residential area of the city, releasing the highest amount of dust by abrasion of rolling stock (Massimi et al., 2020b). Therefore, AA assay seems to be particularly sensitive toward particles released from the rail network by mechanical abrasion of train brakes. This source releases particles rich in some transition metals, such as Cu, Fe and Mn (Abbasi et al., 2012; Querol et al., 2012; Kam et al., 2013; Namgung et al., 2016). In various studies, OP^{AA} was found to be sensitive to transition metals (Vidrio et al., 2008; Charrier and Anastasio, 2011; Simonetti et al., 2018b; Piacentini et al., 2019) and has been strongly positively correlated with the main elements tracing non-exhaust traffic emission, such as Cu, Fe and Mn (Shiraiwa et al., 2017; Pietrogrande et al., 2018a, 2018b; Bates et al., 2019). However, these elements, generally considered as robust tracers of vehicular traffic, in Terni were found to be released at much higher concentration from the railway (Massimi et al., 2020b). Moreover, these results confirmed the high OP^{AA} activity shown at underground station in Gupta et al. (2019). It is worth nothing that relative high OP^{AA} values were recorded at the sites influenced by the rail network emission in all the monitoring periods, in accordance with the non-seasonal character of this source. In April (panel b), the OP^{AA} response to particles released from the railway, turned out to be higher and more localized at GI, CR and HG, presumably because of the more efficient mixing of the lower atmosphere during the warmer season, which led to a less horizontal diffusion of the released particles.

On the other hand, in Fig. 4 we can note that high OP^{DCFH} values were recorded at sites close to the steel plant (RO, OB, PR and CO) in all the monitoring periods and at sites near townhouses frequently heated by biomass burning appliances (BR, AR and CR) in winter (panels a and c). In this case, the high OP^{DCFH} values recorded at BR, AR and CR in February (panel a) and December (panel c), confirmed the relationships between OP^{DCFH} and PM released by domestic biomass heating. In fact, in previous studies, the same sites were identified as the most impacted by biomass burning contributions (Massimi et al., 2020a; 2020b). Relative high OP^{DCFH} values were also recorded at RO, OB, PR and CO in all the monitoring periods. These sites are close to the steel plant and have proven to be the most affected by particles released from the steel plant by abrasive machining of steel from the rolling plants and/or by combustive processes from the furnaces for the annealing of the cold rolled product (Massimi et al., 2020b). The relevance of steel plant related emissions on OP^{DCFH} values is particularly evident in April (panel b), when the strength of biomass burning emissions is weaker.

Hence, DCFH assay seems to be particularly sensitive toward particles released from the steel plant and partly from domestic biomass heating. It is worth mentioning that in February, increased OP^{DCFH} values were also measured at sites near the railway (GI, CR and HG); this indicates a contribution to OP^{DCFH} also from particles released by abrasion of rolling stock. These results are in agreement with the findings of See et al. (2007) and Wang et al. (2010), which have shown a positive correlation between ROS and both transition metals (including Fe) and organic concentrations.

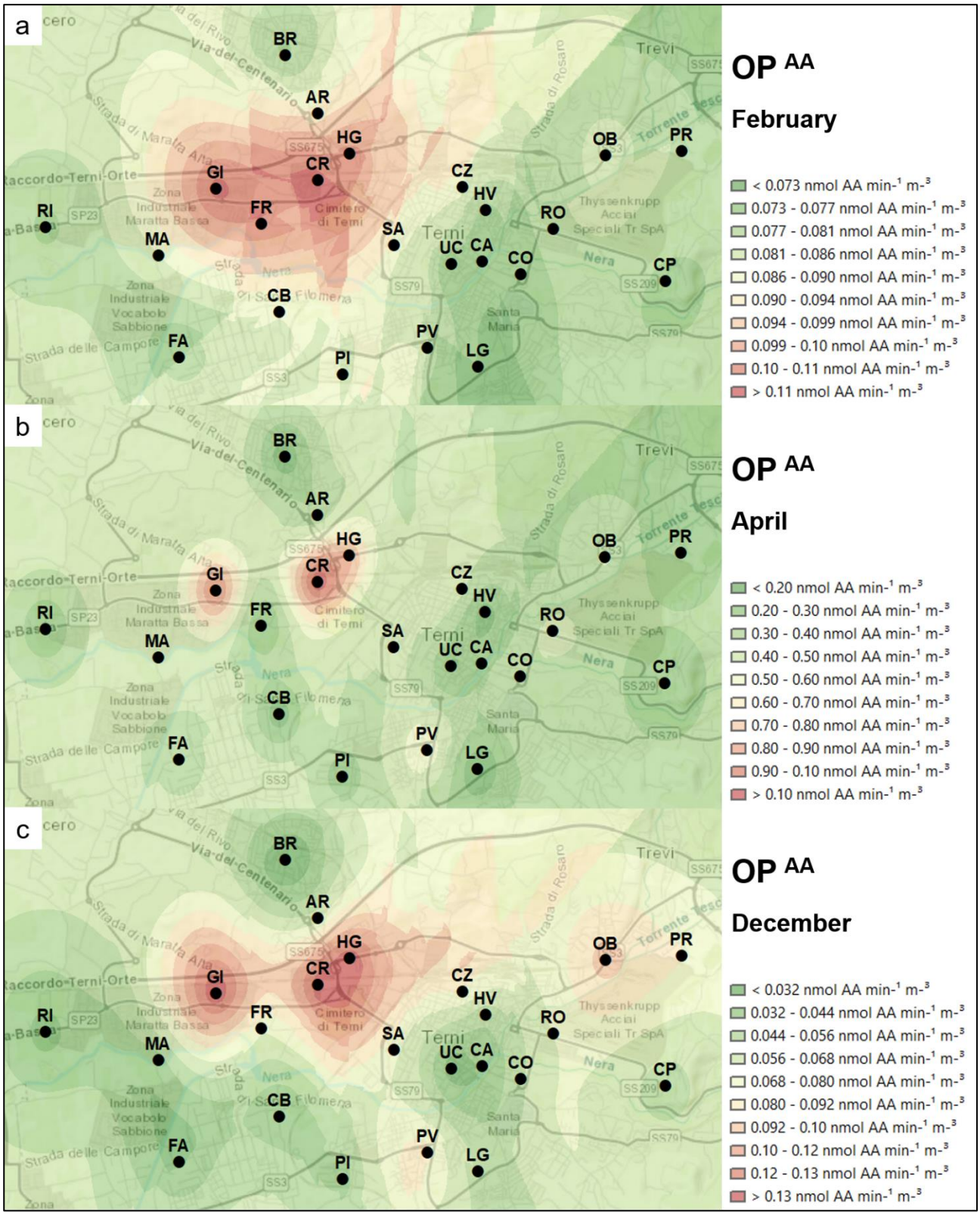

Fig. 3. Spatial mapping of OP^{AA} in February (panela a), April (panel b) and December (panel c) 2017.

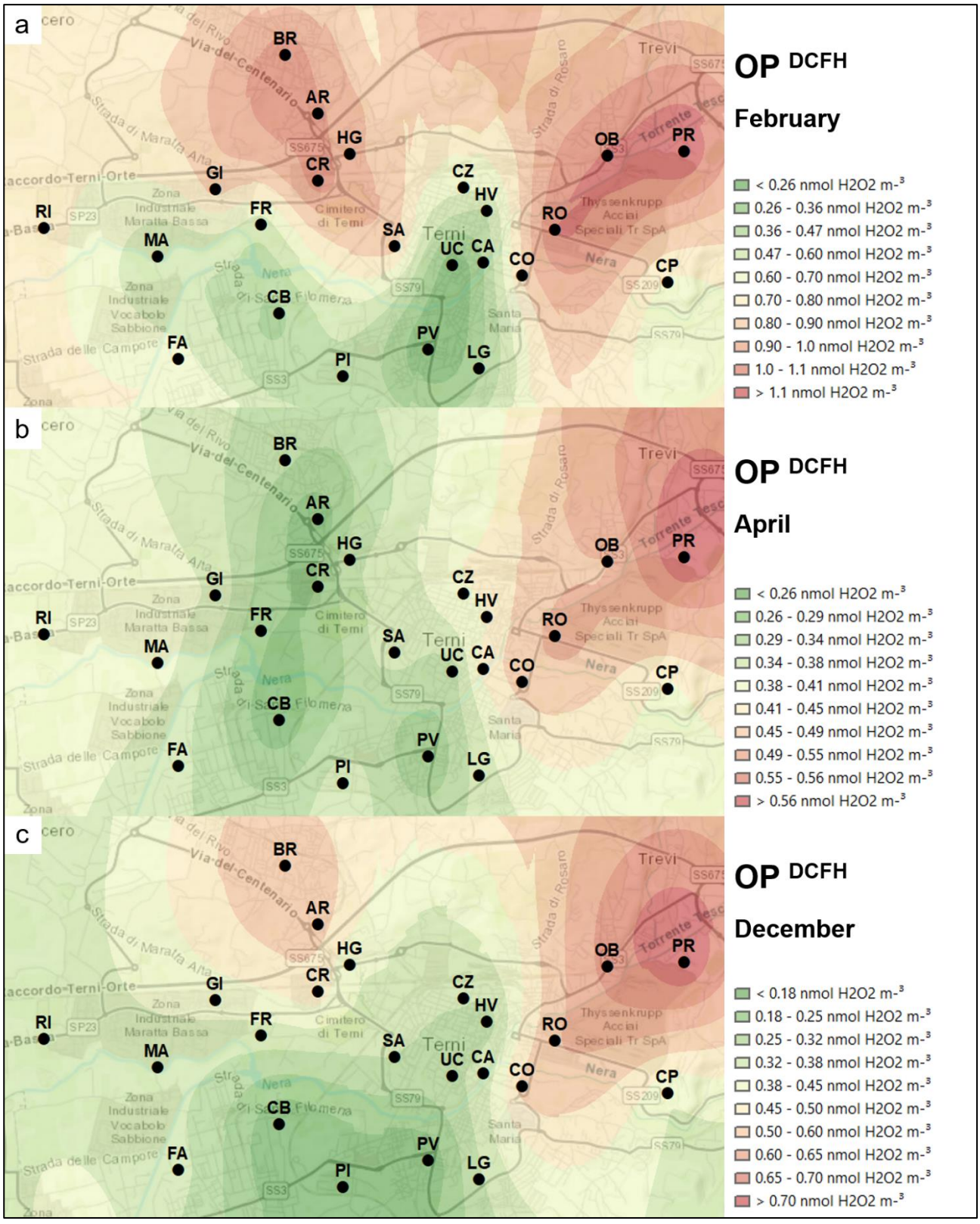

Fig. 4. Spatial mapping of OP^{DCFH} in February (panela a), April (panel b) and December (panel c) 2017.

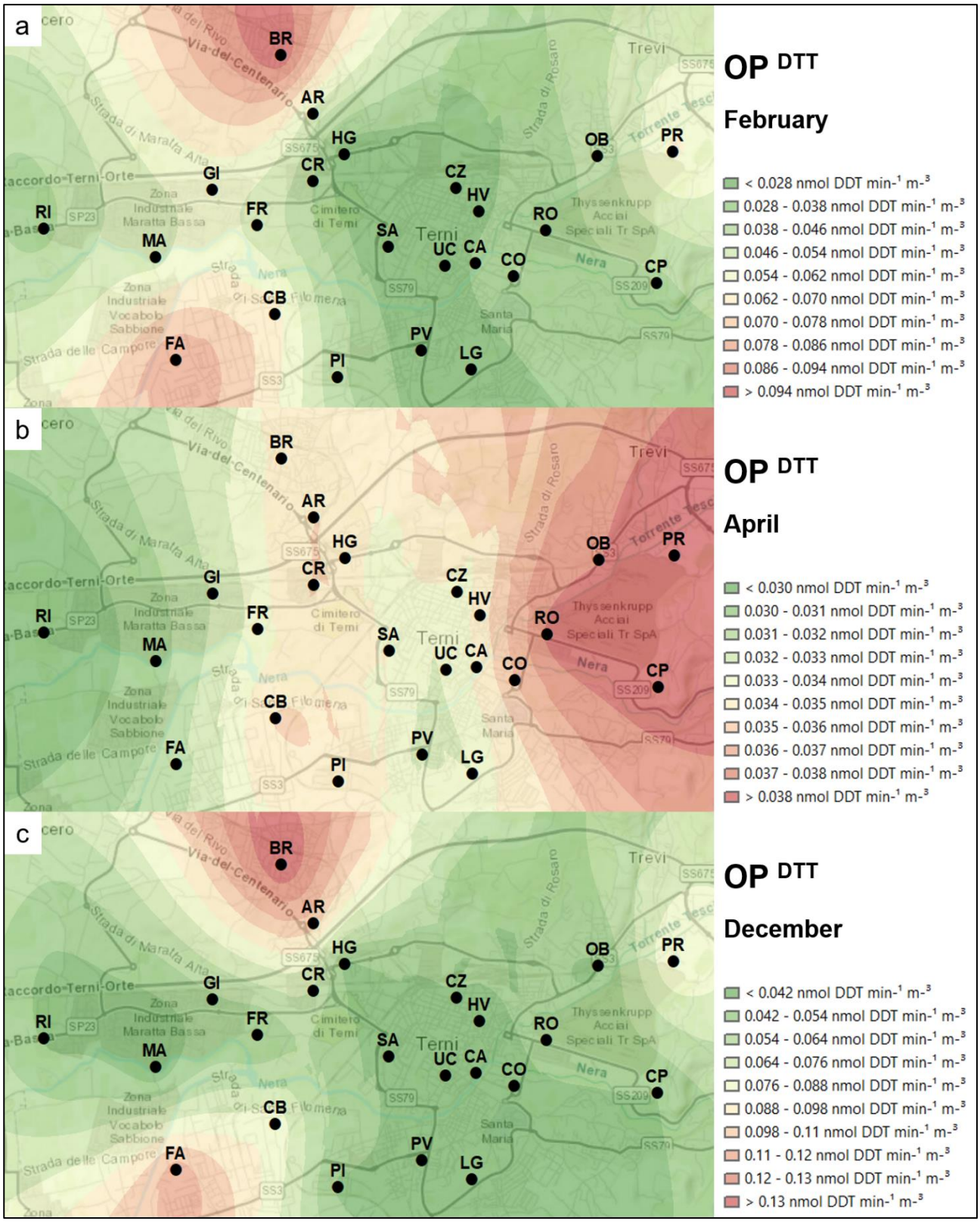

Fig. 5. Spatial mapping of OP^{DTT} in February (panela a), April (panel b) and December (panel c) 2017.

Finally, from Fig. 5, we can observe that in February (panel a) and December (panel c), the highest OP^{DTT} values were recorded at sites close to townhouses where domestic biomass heating systems are prevalent (BR and AR) and at FA and CB. Previous studies demonstrated that these sites were affected by the emissions from burning of carpentry waste products (Massimi et al., 2020a; 2020b). Moreover, relative high OP^{DTT} values (supplementary material S2) occurred in all the monitoring periods at PR, which is the site most impacted by a source related to combustive processes associated to the steel production, such as casting, annealing and hot rolling of steel. This source releases particles rich of water-soluble Cr, Ga, Li, Mn and Zn (Massimi et al., 2020b). In April (panel b), when biomass burning appliances are not used, OP^{DTT} values turned out to be lower in all the Terni basin, except for the area affected by the steel plant (RO, OB, PR, CO and CP), where the highest OP^{DTT} values were recorded. Therefore, in general, DTT assay appears to be sensitive to combustion sources, in particular toward particles released by both industrial (panel b) and biomass burning (panel a and c) emissions. However, since biomass burning has a seasonal trend, a strong variability of the OP^{DTT} values at the sites influenced by this source is observed in the three monitoring periods, due to the stronger biomass burning contribution in the colder season. In fact, biomass burning and secondary organic aerosols are deemed to be the largest contributors to the OP^{DTT} (Verma et al., 2018). To corroborate this, despite various chemical components in atmospheric aerosols have been demonstrated to be well-correlated with OP^{DTT}, including water-soluble transition metal ions, water-soluble organic compounds and quinones (Wong et al., 2019), numerous studies have shown strong correlations of OP^{DTT} with K, a robust biomass burning tracer, and organic compounds, such as levoglucosan, associated to wood combustion sources (Pietrogrande et al., 2018a; Bates et al., 2019; Wang et al., 2019; Hakimzadeh et al., 2020).

3.3 Size *Distribution of OP*

Size distribution of OP^{AA}, OP^{DCFH} and OP^{DTT} was evaluated by analyzing size-segregated PM samples collected at CA, MA and PR. The OP^{AA}, OP^{DCFH} and OP^{DTT} values recorded in each size fraction at CA, MA and PR are reported in supplementary material S3.

Fig. 6 shows the mean concentration of the PM mass and the mean size distribution of the OP in Terni. Size distribution of PM mass concentration showed a bimodal profile, while OP^{AA}, OP^{DCFH} and OP^{DTT} size profiles were substantially unimodal, since AA, DCFH and DTT assays responded selectively to fine or coarse particles. In fact, from Fig. 6, we can observe that AA assay was found to be mainly sensitive to coarse particles (1.8-10 μm), showing a broad maximum in the size range 3.2-5.6 μm, while DCFH and DTT assays turned out to be more sensitive toward the fine fraction of PM (0.18-1.8 μm), with the highest OP values in the size fractions 0.56-1 μm and 0.32-0.56 μm, respectively. These findings are in line with previous publications, which have demonstrated higher OP^{AA} sensitivity toward redox active components in coarse aerosols (Godri et al., 2011; Manigrasso et al., 2020) and higher OP^{DCFH} and OP^{DTT} values in the fine fraction of PM (De Vizcaya-Ruiz et al., 2006; Ntziachristos et al., 2007; Steenhof et al., 2011; Janssen et al., 2014). Moreover, these results confirmed the findings of paragraph 3.2. In fact, particles released by re-suspension of dust and

mechanical processes, such as brake abrasion, to whom OP^{AA} was found to be more sensitive, are typically present in the coarse fraction of PM. On the contrary, combustion processes (such as biomass burning and hot works from the furnaces of the steel plant), to whom OP^{DCFH} and OP^{DTT} appeared to be more sensitive, mainly produce particles belonging to the fine fraction of PM (Shiraiwa et al., 2017; Canepari et al., 2019), which contain water-soluble metals and organics, generally associated with higher intrinsic redox activity.

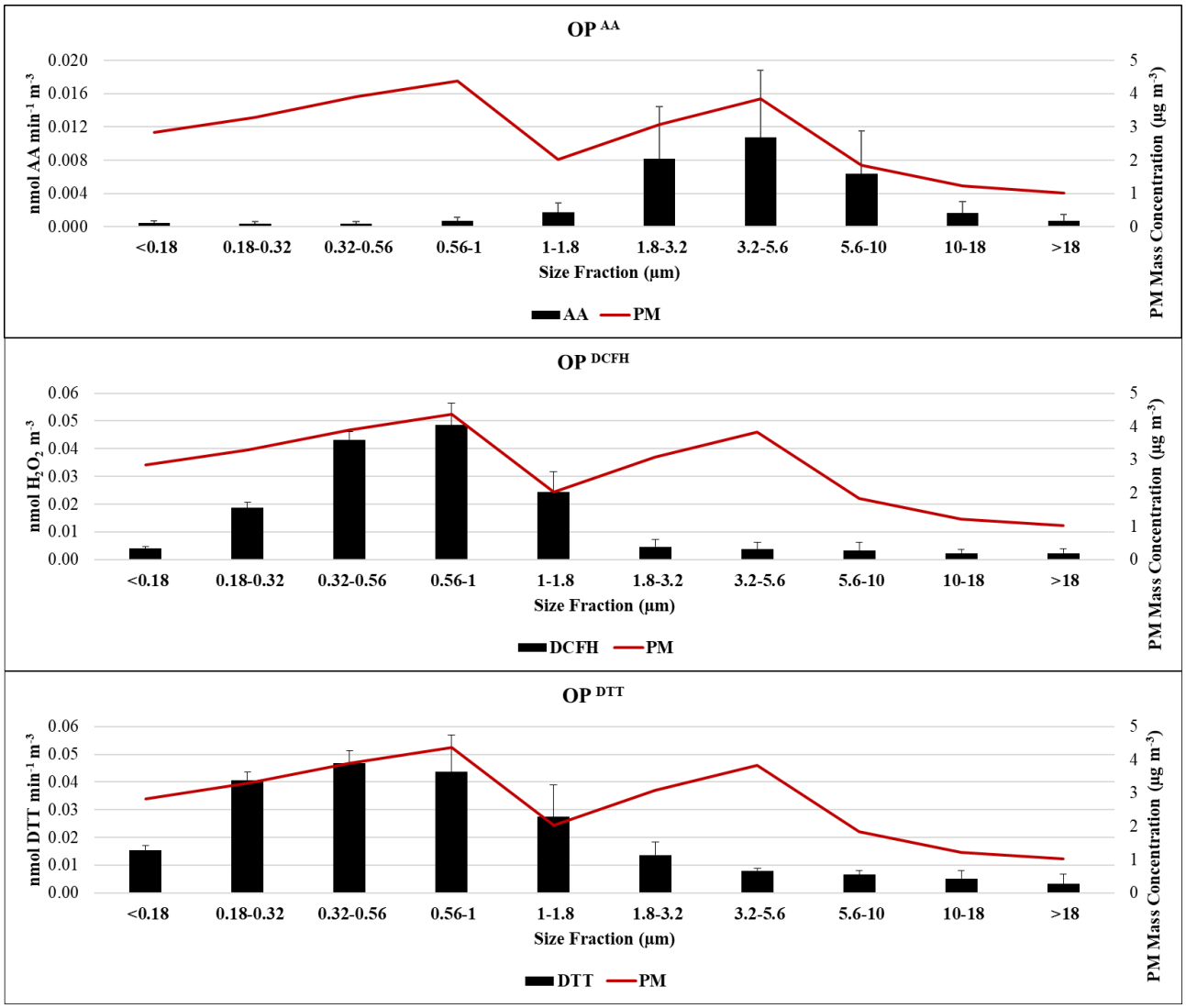

Fig. 6. Mean concentration of the PM mass and mean OP^{AA}, OP^{DCFH} and OP^{DTT} values of size-segregated PM samples collected at CA, MA and PR.

4. Conclusions

In this study, an innovative experimental approach, based on the spatial mapping of OP^{AA}, OP^{DCFH} and OP^{DTT}, for geo-referenced assessment of PM potential to induce oxidative stress, was described. This approach allowed us to map the spatial variability of OP^{AA}, OP^{DCFH} and OP^{DTT}, proving to be a powerful tool, transferable to other monitoring campaigns, for the individuation of spatial relationships between oxidative potential of

PM and its chemical composition and sources. The obtained results showed that OP^{AA} was particularly sensitive toward coarse particles (1.8-10 μm) released from the rail network (GI, CR and HG) by abrasion of train brakes. On the contrary, OP^{DCFH} appeared to be particularly sensitive to fine particles (0.18-1.8 μm) released from the steel plant (RO, OB, PR and CO) and domestic biomass heating (BR, AR and CR), while OP^{DTT} was found to be specifically sensitive toward the fine fraction of PM (0.18-1.8 μm) released by both industrial and biomass burning sources, such as domestic biomass heating (BR and AR) and the burning of carpentry waste products (FA and CB). Overall, these results showed that biomass burning may play a key role in PM potential to generate ROS.

The described approach promises to be very effective for the identification and localization of the emission sources mainly responsible for ROS generation and provides a reliable tool for spatially-resolved evaluation of exposure to PM and relative health risk.

Author Contributions: L. Massimi and S. Canepari conceived and planned the monitoring and the experiments; L. Massimi and M. Ristorini performed the samplings; L. Massimi, M. Ristorini and G. Simonetti performed the OP analyses; L. Massimi and G. Simonetti elaborated the data; L. Massimi wrote the manuscript; M. A. Frezzini and M. L. Astolfi reviewed a previous version of the manuscript; L. Massimi and S. Canepari coordinated the group and supervised the manuscript.

Supplementary Materials

Details on the followed OP analytical procedures for the AA, DCFH and DTT assays applied to the PM aqueous extracts and used reagents.

S1.1 AA Procedure

AA procedure is described by Fang et al. (2016). First, 0.3 mL of 0.5 mM phosphate buffer and 0.1 mL of 2 mM ascorbic acid were added to 2.5 mL of water-extracted solution from each sample. The absorbance of the solutions was analyzed by using UV-Vis absorption spectrometry (UV-Vis, Varian Cary 50 UV-Vis Spectrometer) at 265 nm wavelength and at different reaction times (0, 10, and 20 minutes) to acquire the depletion rate of AA. OP^{AA} was calculated as the depletion rate per volume unit (nmol AA min^{-1} m^{-3}) using the following equations:

$$\sigma AA = -\sigma Abs \times \frac{N_0}{Abs_0}, \qquad OP^{AA} = \frac{\sigma AA_s - \sigma AA_b}{\frac{V_a}{V_e} \times V_S}$$

where σAbs is the slope of the absorbance of blanks vs. time (min^{-1}), Abs_0 is the initial absorbance calculated from the intercept of the linear regression of absorbance vs. time, N_0 is the number of AA moles added in the reaction vial (200 nmol), σAA_s and σAA_b are the rate of AA consumption for the sample and for the blank, respectively (nmol min^{-1}), V_e and V_a are the extraction volume (10 mL) and sample volume added to the reaction vial (2.5 mL) respectively, and V_s is the sampling volume (m^3) for each PM sample.

S1.2 DCFH Procedure

The DCFH assay applied on PM field samples was adapted from Huang et al. (2016). Firstly, operating in the dark, 4.873 mg of 2',7'-dichlorodihydrofluorescein diacetate (DCFH-DA, Sigma-Aldrich, USA) was dissolved in 5 mL of ethanol and mixed with 20 mL of 0.01 M NaOH, in order to promote the de-acetalization. Then the solution was kept for 30 minutes in a dark room. The HRP solution was prepared dissolving 3.15 mg of HRP (Type VI, essentially salt-free, lyophilized powder, ≥ 250 units/mg solid) in 1 L of phosphate buffer 25 mM at pH 7.4. Aliquots of 1.5 mL of the water-extracted solution from each PM sample was mixed with 5 mL of HRP solution and with 125 µL of DCFH solution and then kept for 5 minutes at 37 °C. The mixture was then analyzed with a fluorescence detector (Jasco FP-920) at 530 nm wavelength (427 nm excitation wavelength). The instrument was calibrated using standard H_2O_2 solution (30%; Promochem, LGC Standards GmbH, Wesel, Germany; 5×10^{-8}, 1×10^{-7}, 2×10^{-7}, 5×10^{-7} and 1×10^{-6} M). The calibration curve was used to convert the obtained fluorescence intensity of the samples into H_2O_2 equivalents and to acquire OP^{DCFH} values (nmol H_2O_2 m^{-3}) for each of them.

S1.3 DTT procedure

According to the method reported in Fang et al. (2016), 0.2 mL of 1M phosphate buffer and 0.1 mL of 1 mM DTT were mixed with three aliquots (0.7 mL) of the water-extracted solution from each PM sample, then incubated at 37 °C in a thermostatic bath (HAAKE DC3, Fisons). At regular intervals (0, 10 and 20 minutes), 1 mL of trichloroacetic acid 10% was added to one of the aliquots to stop the reaction. Then, 1 mL of each solution was taken and mixed with 2 mL of Tris-buffer (0.08M, containing EDTA 4 mM) and with 50 µL of 5,50-dithiobis-2-nitrobenzoic acid (DTNB) 0.2 mM. After 5 minutes, the absorbance of the solutions was measured at 412 nm by UV-Vis spectrophotometry. An operative blank was always measured in parallel. OP^{DTT} was calculated as DTT consumption rate per volume unit (nmol DTT min^{-1} m^{-3}) using the following equations:

$$\sigma DTT = -\sigma Abs \times \frac{N_0}{Abs_0}, \qquad OP^{DTT} = \frac{\sigma DTT_s - \sigma DTT_b}{\frac{V_a}{V_e} \times V_s}$$

where σAbs is the slope of the absorbance of blanks vs. time (min^{-1}), Abs_0 is the initial absorbance calculated from the intercept of the linear regression of absorbance vs. time, N_0 is the number of DTT moles added in the reaction vial (100 nmol), σDTT_s and σDTT_b are the rate of DTT consumption for the sample and for the blank, respectively (nmol min^{-1}), V_e and V_a are the extraction volume (10 mL) and sample volume added to the reaction vial (0.7 mL) respectively, and V_s is the sampling volume (m^3) for each PM sample.

Table S2.1. OP^{AA}, OP^{DCFH} and OP^{DTT} values determined at the 23 sampling sites in the three monitoring periods (February, April and December 2017).

Site	OP^{AA} (nmol AA min^{-1} m^{-3})			OP^{DCFH} (nmol H_2O_2 m^{-3})			OP^{DTT} (nmol DTT min^{-1} m^{-3})		
	February	**April**	**December**	**February**	**April**	**December**	**February**	**April**	**December**
RI	0.048	0.17	0.012	0.73	0.38	0.35	0.034	0.027	0.041
MA	0.078	0.49	0.025	0.46	0.40	0.34	0.050	0.029	0.030
FA	0.040	0.29	0.014	0.61	0.36	0.37	0.087	0.030	0.12
GI	0.18	0.97	0.19	0.82	0.39	0.42	0.056	0.031	0.051
FR	0.12	0.16	0.052	0.50	0.28	0.34	0.050	0.029	0.041
CB	0.060	0.11	0.025	0.34	0.22	0.040	0.066	0.041	0.084
PI	0.075	0.23	0.026	0.44	0.40	0.13	0.039	0.039	0.040
BR	0.031	0.10	0.0032	1.1	0.54	0.61	0.10	0.035	0.14
AR	0.078	0.33	0.043	1.0	0.47	0.58	0.050	0.038	0.10
CR	0.15	1.1	0.17	1.1	0.42	0.55	0.037	0.041	0.064
HG	0.13	0.85	0.16	0.90	0.50	0.33	0.024	0.030	0.039
SA	0.081	0.43	0.073	0.83	0.38	0.33	0.021	0.034	0.038
PV	0.11	0.61	0.10	0.15	0.25	0.051	0.025	0.028	0.041
LG	0.036	0.10	0.042	0.35	0.36	0.31	0.021	0.029	0.034
CZ	0.13	0.43	0.10	0.61	0.41	0.36	0.023	0.028	0.042
HV	0.024	0.14	0.032	0.46	0.40	0.16	0.026	0.038	0.040
UC	0.050	0.18	0.0032	0.17	0.30	0.33	0.025	0.032	0.034
CA	0.079	0.24	0.029	0.36	0.45	0.31	0.030	0.033	0.036
CO	0.079	0.39	0.058	0.80	0.47	0.62	0.038	0.038	0.037
RO	0.082	0.44	0.070	1.1	0.50	0.60	0.035	0.042	0.045
OB	0.11	0.42	0.11	1.1	0.47	0.69	0.040	0.036	0.040
PR	0.082	0.19	0.085	1.2	0.61	0.87	0.063	0.041	0.087
CP	0.066	0.20	0.042	0.65	0.38	0.32	0.034	0.039	0.042
Mean	**0.083**	**0.37**	**0.064**	**0.69**	**0.41**	**0.39**	**0.043**	**0.034**	**0.055**

Table S3.1. Mean concentration of the PM mass and OP^{AA}, OP^{DCFH} and OP^{DTT} values of size-segregated PM samples collected at CA, MA and PR.

Size Fraction (µm)	PM Mass Concentration (µg m^{-3})	OP^{AA} (nmol AA min^{-1} m^{-3})					OP^{DCFH} (nmol H_2O_2 m^{-3})					OP^{DTT} (nmol DTT min^{-1} m^{-3})				
		CA	**MA**	**PR**	**Mean**	***SD***	**CA**	**MA**	**PR**	**Mean**	***SD***	**CA**	**MA**	**PR**	**Mean**	***SD***
<0.18	2.8	0.00046	0.00067	0.00015	**0.00042**	*0.00026*	0.0032	0.0039	0.0047	**0.0039**	*0.0007*	0.014	0.015	0.017	**0.015**	*0.001*
0.18-0.32	3.3	0.00068	0.00023	0.00016	**0.00035**	*0.00028*	0.017	0.019	0.021	**0.019**	*0.002*	0.038	0.041	0.043	**0.041**	*0.003*
0.32-0.56	3.9	0.00063	0.00040	0.00018	**0.00041**	*0.00023*	0.041	0.046	0.043	**0.043**	*0.003*	0.043	0.052	0.045	**0.047**	*0.005*
0.56-1	4.4	0.0010	0.00088	0.00022	**0.00071**	*0.00043*	0.046	0.058	0.042	**0.048**	*0.008*	0.046	0.056	0.029	**0.044**	*0.013*
1-1.8	2.0	0.0021	0.0026	0.00043	**0.0017**	*0.0012*	0.023	0.032	0.018	**0.024**	*0.007*	0.031	0.037	0.015	**0.027**	*0.011*
1.8-3.2	3.1	0.013	0.011	0.0010	**0.0082**	*0.0063*	0.0019	0.0049	0.0071	**0.0046**	*0.0026*	0.014	0.018	0.0088	**0.014**	*0.005*
3.2-5.6	3.8	0.016	0.014	0.0015	**0.011**	*0.008*	0.0017	0.0032	0.0065	**0.0038**	*0.0024*	0.0071	0.0080	0.0089	**0.0080**	*0.0009*
5.6-10	1.8	0.0092	0.0095	0.00053	**0.0064**	*0.0051*	0.0016	0.0013	0.0068	**0.0032**	*0.0031*	0.0052	0.0062	0.0083	**0.0066**	*0.0016*
10-18	1.2	0.0022	0.0026	0.000077	**0.0016**	*0.0014*	0.0016	0.0013	0.0038	**0.0022**	*0.0014*	0.0045	0.0026	0.0082	**0.0051**	*0.0028*
>18	1.0	0.00056	0.0015	0.000047	**0.00071**	*0.00074*	0.0011	0.0014	0.0043	**0.0023**	*0.0018*	0.0012	0.0012	0.0073	**0.0032**	*0.0035*

References

Abbasi, S., Olander, L., Larsson, C., Olofsson, U., Jansson, A., Sellgren, U. 2012. A field test study of airborne wear particles from a running regional train. Proceedings of the Institution of Mechanical Engineers, Part F: Journal of Rail and Rapid Transit, 226(1), 95-109.

Anderson, J. O., Thundiyil, J. G., Stolbach, A. 2012. Clearing the air: a review of the effects of particulate matter air pollution on human health. Journal of Medical Toxicology, 8(2), 166-175.

Ayres, J. G., Borm, P., Cassee, F. R., Castranova, V., Donaldson, K., Ghio, A., Harrison, R.M., Hider, R., Kelly, F., Kooter, I.M., Marano, F., Maynard, R.L., Mudway, I., Nel, A., Sioutas, C., Smith, S., Baeza-Squiban, A., Cho, A., Duggan, S., Froines, J. 2008. Evaluating the toxicity of airborne particulate matter and nanoparticles by measuring oxidative stress potential - a workshop report and consensus statement. Inhalation Toxicology, 20(1), 75-99.

Bates, J. T., Fang, T., Verma, V., Zeng, L., Weber, R. J., Tolbert, P. E., Abrams, J. Y., Sarnat, S. E., Klein, M., Mulholland, J. A., Russell, A. G. 2019. Review of acellular assays of ambient particulate matter oxidative potential: Methods and relationships with composition, sources, and health effects. Environmental Science & Technology, 53(8), 4003-4019.

Brunekreef, B., Holgate, S. T. 2002. Air Pollution and Health. Lancet 360, 1233–1242.

Calas, A., Uzu, G., Kelly, F., Houdier, S., Martins, J., Thomas, F., Molton, F., Charron, A., Dunster, C., Oliete, A., Jacob, V., Besombes, J., Chevrier, F., Jaffrezo, J. 2018. Comparison between five acellular oxidative potential measurement assays performed with detailed chemistry on PM10 samples from the city of Chamonix (France). Atmospheric Chemistry and Physics, 18, 7863–7875.

Campbell, S. J., Utinger, B., Lienhard, D. M., Paulson, S. E., Shen, J., Griffiths, P. T., Stell, A.C., Kalberer, M. 2019. Development of a physiologically relevant online chemical assay to quantify aerosol oxidative potential. Analytical Chemistry, 91(20), 13088-13095.

Canepari, S., Astolfi, M. L., Catrambone, M., Frasca, D., Marcoccia, M., Marcovecchio, F., Massimi, L., Rantica, E., Perrino, C. 2019. A combined chemical/size fractionation approach to study winter/summer variations, ageing and source strength of atmospheric particles. Environmental Pollution, 253, 19-28.

Capelli, L., Sironi, S., Del Rosso, R., Céntola, P., Rossi, A., Austeri, C. 2011. Olfactometric approach for the evaluation of citizens' exposure to industrial emissions in the city of Terni, Italy. Science of the Total Environment, 409(3), 595-603.

Catrambone, M., Canepari, S., Cerasa, M., Sargolini, T., Perrino, C. 2019. Performance evaluation of a very-low-volume sampler for atmospheric particulate matter. Aerosol Air Quality Research, 19, 2160-2172.

Cesari, D., Merico, E., Grasso, F. M., Decesari, S., Belosi, F., Manarini, F., De Nuntiis, P., Rinaldi, M., Volpi, F., Gambaro, A., Morabito, E., Contini, D. 2019. Source apportionment of PM2.5 and of its oxidative potential in an industrial suburban site in south Italy. Atmosphere, 10(12), 758.

Charrier, J. G., Anastasio, C. 2011. Impacts of antioxidants on hydroxyl radical production from individual and mixed transition metals in a surrogate lung fluid. Atmospheric Environment, 45 (40), 7555− 7562.

Chirizzi, D., Cesari, D., Guascito, M. R., Dinoi, A., Giotta, L., Donateo, A., Contini, D. 2017. Influence of Saharan dust outbreaks and carbon content on oxidative potential of water-soluble fractions of PM2.5 and PM10. Atmospheric Environment, 163, 1–8.

Cho, A. K., Sioutas, C., Miguel, A. H., Kumagai, Y., Schmitz, D. A., Singh, M., Fernandez, F.A., Froines, J. R. 2005. Redox activity of airborne particulate matter at different sites in the Los Angeles Basin. Environmental Research, 99(1), 40-47.

Curci, G., Ferrero, L., Tuccella, P., Barnaba, F., Angelini, F., Bolzacchini, E., Carbone, C., Denier van der Gon, H. A. C., Facchini, M. C., Gobbi, G. P., Kuenen, J. P. P., Landi, T. C., Perrino, C., Perrone, M. G., Sangiorgi, G., Stocchi, P. 2015. How much is particulate matter near the ground influenced by upper-level processes within and above the PBL? A summertime case study in Milan (Italy) evidences the distinctive role of nitrate. Atmospheric Chemistry and Physics, 15(5), 2629-2649.

Delfino, R. J., Staimer, N., Vaziri, N. D. 2011. Air pollution and circulating biomarkers of oxidative stress. Air Quality, Atmosphere & Health, 4(1), 37-52.

De Vizcaya-Ruiz, A., Gutiérrez-Castillo, M. E., Uribe-Ramirez, M., Cebrián, M. E., Mugica-Alvarez, V., Sepúlveda, J., Rosas, I., Salinas, E., Garcia-Cue´llar, C., Martinez, F., Alfaro-Moreno, E., Torres-Flores, V., Osornio-Vargas, A., Sioutas, C., Fine, P.M., Singh, M., Geller, M.D., Kuhn, T., Miguel, A.H., Eiguren-Fernandez, A., Schiesti, R.H., Reliene, R., Froines, J. 2006. Characterization and in vitro biological effects of concentrated particulate matter from Mexico City. Atmospheric Environment, 40, 583-592.

Fang, T., Verma, V., Bates, J. T., Abrams, J., Klein, M., Strickland, M. J., Sarnat, S. E., Chang, H. H., Mulholland, J. A., Tolbert, P. E., Russell, A. G. 2015. Oxidative potential of ambient water-soluble PM 2.5 measured by Dithiothreitol (DTT) and Ascorbic Acid (AA) assays in the southeastern United States: contrasts in sources and health associations. Atmospheric Chemistry & Physics Discussions, 15(21) 30609-30644.

Fang, T., Verma, V., Bates, J. T., Abrams, J., Klein, M., Strickland, M. J., Stefanie E., Sarnat, S. E., Chang, H. H., Mulholland, J. A., Tolbert, P. E., Russell, A. G., Weber, R. J. 2016. Oxidative Potential of Ambient Water-Soluble PM2.5 in the Southeastern United States: Contrasts in Sources and Health Associations between Ascorbic Acid (AA) and Dithiothreitol (DTT) Assays. Atmospheric Chemistry, 16, 3865–3879.

Ferrero, L., Cappelletti, D., Moroni, B., Sangiorgi, G., Perrone, M. G., Crocchianti, S., Bolzacchini, E. 2012. Wintertime aerosol dynamics and chemical composition across the mixing layer over basin valleys. Atmospheric Environment, 56, 143-153.

Frezzini, M. A., Castellani, F., De Francesco, N., Ristorini, M., Canepari, S. 2019. Application of DPPH Assay for Assessment of Particulate Matter Reducing Properties. Atmosphere, 10(12), 816.

Gao, D., Mulholland, J. A., Russell, A. G., Weber, R. J. 2020. Characterization of water-insoluble oxidative potential of PM2.5 using the dithiothreitol assay. Atmospheric Environment, 224, 117327.

Gia Pham, T., Kappas, M., Van Huynh, C., Hoang Khanh Nguyen, L. 2019. Application of ordinary kriging and regression kriging method for soil properties mapping in hilly region of Central Vietnam. ISPRS International Journal of Geo-Information, 8(3), 147.

Giorio, C., Tapparo, A., Scapellato, M.L., Carrieri, M., Apostoli, P., Bartolucci, G.B. 2013. Field comparison of a personal cascade impactor sampler, an optical particle counter and CEN-EU standard methods for PM10, PM2.5 and PM1 measurement in urban environment. Journal of Aerosol Science, 65, 111-120.

Godri, K. J., Harrison, R. M., Evans, T., Baker, T., Dunster, C., Mudway, I. S., Kelly, F. J. 2011. Increased oxidative burden associated with traffic component of ambient particulate matter at roadside and urban background schools sites in London. PloS one, 6(7).

Guerrini, R. 2012. Qualità dell'aria nella provincia di Terni tra il 2002 e il 2011. Quad ARPA Umbria, 81-87.

Gupta, T., Singh, S. P., Rajput, P., Agarwal, A. K. 2019. Measurement, Analysis and Remediation of Environmental Pollutants. Springer.

Hakimzadeh, M., Soleimanian, E., Mousavi, A., Borgini, A., De Marco, C., Ruprecht, A. A., Sioutas, C. 2020. The impact of biomass burning on the oxidative potential of PM2. 5 in the metropolitan area of Milan. Atmospheric Environment, 224, 117328.

Halliwell, B., Whiteman, M. 2004. Measuring reactive species and oxidative damage *in vivo* and in cell culture: How should you do it and what do the results mean? British Journal of Pharmacology, 142, 231–255.

Hlavay, J., Polyak, K., Weisz, M. 2001. Monitoring of the natural environment by chemical speciation of elements in aerosol and sediment samples. Presented at the Whistler 2000 Speciation Symposium, Whistler Resort, BC, Canada, June 25–July 1, 2000. Journal of Environmental Monitoring, 3(1), 74-80.

Huang, W., Zhang, Y., Zhang, Y., Fang, D., Schauer, J. J., 2016. Optimization of the Measurement of Particle-Bound Reactive Oxygen Species with 2',7'-dichlorofluorescin (DCFH), Water Air Soil Pollution, 227, 164.

Hung, H. F., Wang, C. S. 2001. Experimental determination of reactive oxygen species in Taipei aerosols. Journal of Aerosol Science, 32, 1201–1211.

Janssen, N. A., Yang, A., Strak, M., Steenhof, M., Hellack, B., Gerlofs-Nijland, M. E., Kuhlbusch T., Kelly, F., Harrison R., Brunekreef, B., Cassee, F., Hoek, G. 2014. Oxidative potential of particulate matter collected at sites with different source characteristics. Science of the Total Environment, 472, 572-581.

Jian, X., Olea, R. A., Yu, Y. S. 1996. Semivariogram modeling by weighted least squares. Computers & Geosciences, 22(4), 387-397.

Johnston, K., Ver Hoef, J. M., Krivoruchko, K., Lucas, N. 2001. Using ArcGIS geostatistical analyst (Vol. 380). Redlands: Esri.

Kam, W., Delfino, R. J., Schauer, J. J., Sioutas, C. 2013. A comparative assessment of PM2.5 exposures in light-rail, subway, freeway, and surface street environments in Los Angeles and estimated lung cancer risk. Environmental Science: Processes & Impacts, 15(1), 234-243.

Kelly, F. J., Fuller, G. W., Walton, H. A., Fussell, J. C. 2012. Monitoring air pollution: Use of early warning systems for public health. Respirology, 17(1), 7-19.

Khurshid, S. S., Siegel, J. A., Kinney, K. A. 2014. Indoor particulate reactive oxygen species concentrations. Environmental research, 132, 46-53.

Kumar, A., Maroju, S., Bhat, A. 2007. Application of ArcGIS geostatistical analyst for interpolating environmental data from observations. Environmental Progress, 26(3), 220-225.

Lebel, C. P., Ischiropoulos, H., Bondy, S. C. 1992. Evaluation of the probe 2',7'-dichlorofluorescin as an indicator of reactive oxygen species formation and oxidative stress. Chemical Research in Toxicology, 5, 227–231.

Li, R., Kou, X., Geng, H., Xie, J., Yang, Z., Zhang, Y., Cai, Z., Dong, C. 2015. Effect of ambient PM 2.5 on lung mitochondrial damage and fusion/fission gene expression in rats. Chemical Research in Toxicology, 28, 408-418.

Lubczyńska, M. J., Sunyer, J., Tiemeier, H., Porta, D., Kasper-Sonnenberg, M., Jaddoe, V. W., Xavier Basagaña, X., Dalmau-Bueno, A., Forastiere, F., Wittsiepe, J., Hoffmann, B., Nieuwenhuijsen, M., Hoek, G., de Hoogh, K., Brunekreef, B., Guxens, M. 2017. Exposure to elemental composition of outdoor PM2.5 at birth and cognitive and psychomotor function in childhood in four European birth cohorts. Environment international, 109, 170-180.

Manigrasso, M., Simonetti, G., Astolfi, M. L., Perrino, C., Canepari, S., Protano, C., Antonucci, A., Avino, P., Vitali, M. 2020. Oxidative Potential Associated with Urban Aerosol Deposited into the Respiratory System and Relevant Elemental and Ionic Fraction Contributions. Atmosphere, 11(1), 6.

Marcoccia, M., Ronci, L., De Matthaeis, E., Setini, A., Perrino, C., Canepari, S. 2017. In-vivo assesment of the genotoxic and oxidative stress effects of particulate matter on *Echinogammarus veneris*. Chemosphere, 173, 124–134.

Massimi, L., Ristorini, M., Eusebio, M., Florendo, D., Adeyemo, A., Brugnoli, D., Canepari, S. 2017. Monitoring and evaluation of Terni (Central Italy) air quality through spatially resolved analyses. Atmosphere, 8(10), 200.

Massimi, L., Conti, M. E., Mele, G., Ristorini, M., Astolfi, M. L., Canepari, S. 2019. Lichen transplants as indicators of atmospheric element concentrations: a high spatial resolution comparison with PM_{10} samples in a polluted area (Central Italy). Ecological Indicators, 101, 759-769.

Massimi, L., Simonetti, G., Buiarelli, F., Di Filippo, P., Pomata, D., Riccardi, C., Ristorini, M., Astolfi, M.L., Canepari, S. 2020a. Spatial distribution of levoglucosan and alternative biomass burning tracers in atmospheric aerosols, in an urban and industrial hot-spot of Central Italy. Atmospheric Research, 104904.

Massimi, L., Ristorini, M., Astolfi, M.L., Perrino, C., Canepari, S. 2020b. High Resolution Spatial Mapping of Element Concentrations in PM_{10}: a Powerful Tool for Localization of Emission Sources. Atmospheric Research, 105060.

Miljevic, B., Hedayat, F., Stevanovic, S., Fairfull-Smith, K. E., Bottle, S. E., Ristovski, Z. D. 2014. To sonicate or not to sonicate PM filters: Reactive oxygen species generation upon ultrasonic irradiation. Aerosol science and technology, 48(12), 1276-1284.

Morini, E., Touchaei, A. G., Castellani, B., Rossi, F., Cotana, F. 2016. The impact of albedo increase to mitigate the urban heat island in Terni (Italy) using the WRF model. Sustainability, 8(10), 999.

Mutzel, A., Rodigast, M., Iinuma, Y., Böge, O., Herrmann, H. 2013. An improved method for the quantification of SOA bound peroxides. Atmospheric Environment, 67, 365-369.

Namgung, H. G., Kim, J. B., Woo, S. H., Park, S., Kim, M., Kim, M. S., Bae, G. N., Park, D., Kwon, S. B. 2016. Generation of nanoparticles from friction between railway brake disks and pads. Environmental Science and Technology, 50(7), 3453-3461.

Ntziachristos, L., Froines, J. R., Cho, A. K., Sioutas, C. 2007. Relationship between redox activity and chemical speciation of size-fractionated particulate matter. Particle and Fibre Toxicology, 4(1), 5.

Øvrevik, J. 2019. Oxidative potential versus biological effects: A review on the relevance of cell-free/abiotic assays as predictors of toxicity from airborne particulate matter. International Journal of Molecular Sciences, 20, 4772.

Perrone, M. G., Zhou, J., Malandrino, M., Sangiorgi, G., Rizzi, C., Ferrero, L., Dommen, J., Bolzacchini, E. 2016. PM chemical composition and oxidative potential of the soluble fraction of particles at two sites in the urban area of Milan, Northern Italy. Atmospheric Environment, 128, 104-113.

Pietrogrande, M. C., Perrone, M. R., Manarini, F., Romano, S., Udisti, R., Becagli, S. 2018a. PM10 oxidative potential at a Central Mediterranean Site: Association with chemical composition and meteorological parameters. Atmospheric Environment, 188, 97-111.

Pietrogrande, M. C., Dalpiaz, C., Dell'Anna, R., Lazzeri, P., Manarini, F., Visentin, M., Tonidandel, G. 2018b. Chemical composition and oxidative potential of atmospheric coarse particles at an industrial and urban background site in the alpine region of northern Italy. Atmospheric Environment, 191, 340-350.

Piacentini, A., Falasca, G., Canepari, S., Massimi, L. 2019. Potential of PM-selected components to induce oxidative stress and root system alteration in a plant model organism. Environment International, 132, 105094.

Pope III, C. A., Dockery, D. W. 2006. Health effects of fine particulate air pollution: Lines that connect. Journal of the Air & Waste Management Association, 56, 709–742.

Querol, X., Moreno, T., Karanasiou, A., Reche, C., Alastuey, A., Viana, M., Font, O., Gil, J., de Miguel, E., Capdevila, M. 2012. Variability of levels and composition of PM10 and PM2.5 in the Barcelona metro system. Atmospheric Chemistry and Physics, 12(11), 5055-5076.

Ricci, P. F., Cirillo, M. C. 1985. Uncertainty in health risk analysis. Journal of Hazardous Materials, 10(2-3), 433-447.

Ristorini, M., Astolfi, M.L., Frezzini, M.A., Canepari, S., Massimi, L. 2020. Evaluation of the efficiency of Arundo donax L. leaves as biomonitors for atmospheric element concentrations in an urban and industrial area of Central Italy. Atmosphere, 11(3), 226.

See, S. W., Wang, Y. H., Balasubramanian, R. 2007. Contrasting reactive oxygen species and transition metal concentrations in combustion aerosols. Environmental Research, 103(3), 317-324.

SENTIERI-ReNaM, GdL, Binazzi, A., Mangone, L. 2016. SENTIERI - Epidemiological study of residents in national priority contaminated sites: incidence of mesothelioma. Epidemiologia e Prevenzione, 40 (5 Suppl1), 1-116.

Sgrigna, G., Sæbø, A., Gawronski, S., Popek, R., Calfapietra, C. 2015. Particulate Matter deposition on Quercus ilex leaves in an industrial city of central Italy. Environmental Pollution, 197, 187-194.

Shiraiwa, M., Ueda, K., Pozzer, A., Lammel, G., Kampf, C. J., Fushimi, A., Enami, S., Arangio, A.M., Fröhlich-Nowoisky, J., Fujitani,, Y., Furuyama, A., Lakey, P.S.J., Lelieveld, J., Lucas, K., Morino, Y., Pöschl, U., Takahama, S., Takami, A., Tong, H., Weber, B., Yoshino, A., Sato, K. 2017. Aerosol health effects from molecular to global scales. Environmental Science & Technology, 51(23), 13545-13567.

Simonetti, G., Conte, E., Perrino, C., Canepari, S. 2018a. Oxidative potential of size-segregated PM in a urban and an industrial area of Italy. Atmospheric Environment, 187, 292–300.

Simonetti, G., Conte, E., Massimi, L., Frasca, D., Perrino, C., Canepari, S. 2018b. Oxidative potential of particulate matter components generated by specific emission sources. Journal of Aerosol Sciences, 126, 99-109.

Steenhof, M., Gosens, I., Strak, M., Godri, K. J., Hoek, G., Cassee, F. R., Mudway, I.S., Kelly, F.J., Harrison, R.M., Lebret, E., Brunekreef, B., Janssen, N.A., Pieters, R.H. 2011. In vitro toxicity of particulate matter (PM) collected at different sites in the Netherlands is associated with PM composition, size fraction and oxidative potential-the RAPTES project. Particle and fibre toxicology, 8(1), 26.

Stoeger, T., Takenaka, S., Frankenberger, B., Ritter, B., Karg, E., Maier, K., Shulz, H., Schmid, O. 2009. Deducing in vivo toxicity of combustion-derived nanoparticles from a cell-free oxidative potency assay and metabolic activation of organic compounds. Environmental Health Perspectives, 117(1), 54-60.

Strak, M., Janssen, N. A., Godri, K. J., Gosens, I., Mudway, I. S., Cassee, F. R., Lebret, E., Kelly, F.G., Harrison, M.R., Brunekreef, B., Steenhof, M., Hoek, G. 2012. Respiratory health effects of airborne particulate matter: the role of particle size, composition, and oxidative potential - the RAPTES project. Environmental Health Perspectives, 120(8), 1183-1189.

Venkatachari, P., Hopke, P. K., Grover, B. D., Eatough, D. J. 2005. Measurement of particle-bound reactive oxygen species in rubidoux aerosols. Journal of Atmospheric Chemistry, 50, 49–58.

Venkatachari, P., Hopke, P. K., Brune, W. H., Ren, X., Lesher, R., Mao, J., Mitchell, M. 2007. Characterization of wintertime reactive oxygen species concentrations in Flushing, New York. Aerosol Science and Technology, 41, 97–111.

Verma, V., Sioutas, C., Weber, R. J. 2018. Oxidative Properties of Ambient Particulate Matter - An Assessment of the Relative Contributions from Various Aerosol Components and Their Emission Sources. Multiphase Environmental Chemistry in the Atmosphere, 389–416.

Vidrio, E., Jung, H., Anastasio, C. 2008. Generation of hydroxyl radicals from dissolved transition metals in surrogate lung fluid solutions. Atmospheric Environment, 42 (18), 4369−4379.

Wang, H., Joseph, J. A. 1999. Quantifying cellular oxidative stress by dichlorofluorescein assay using microplate reader. Free Radical Biology & Medicine, 27, 612–616.

Wang, Y., Arellanes, C., Curtis, D. B., Paulson, S. E. 2010. Probing the source of hydrogen peroxide associated with coarse mode aerosol particles in Southern California. Environmental Science & Technology, 44(11), 4070-4075.

Wang, M., Beelen, R., Eeftens, M., Meliefste, K., Hoek, G., Brunekreef, B. 2012. Systematic evaluation of land use regression models for NO_2. Environmental Science & Technology, 46(8), 4481-4489.

Wang, J., Lin, X., Lu, L., Wu, Y., Zhang, H., Lv, Q., Liu, W., Zhang Y., Zhuang, S. 2019. Temporal variation of oxidative potential of water soluble components of ambient PM2. 5 measured by dithiothreitol (DTT) assay. Science of The Total Environment, 649, 969-978.

WHO 2013. Review of evidence on health aspects of air pollution – REVIHAAP. First Results. WHO's Regional Office for Europe, Copenhagen, 28 pp., http://www.euro.who.int/ data/ assets/pdf file/0020/182432/e96762-final.pdf, 2013.

Wong, J. P., Tsagkaraki, M., Tsiodra, I., Mihalopoulos, N., Violaki, K., Kanakidou, M., Sciare, J., Nenes, A., Weber, R. J. 2019. Effects of atmospheric processing on the oxidative potential of biomass burning organic aerosols. Environmental Science & Technology, *53*(12), 6747-6756.

Xie, Y., Chen, T. B., Lei, M., Yang, J., Guo, Q. J., Song, B., Zhou, X. Y. 2011. Spatial distribution of soil heavy metal pollution estimated by different interpolation methods: Accuracy and uncertainty analysis. Chemosphere, 82(3), 468-476.

Yang, A., Janssen, N. A., Brunekreef, B., Cassee, F. R., Hoek, G., Gehring, U. 2016. Children's respiratory health and oxidative potential of PM2.5: the PIAMA birth cohort study. Journal of Occupational and Environmental Medicine, 73(3), 154-160.

5.4 (A4) Urban trees for biomonitoring atmospheric particulate matter: an integrated approach combining plant functional traits, magnetic and chemical properties

Ecological Indicators (2021), 126, 107707, doi: 10.1016/j.ecolind.2021.107707

Lina Fusaro[*1, 2], Elisabetta Salvatori [3], Aldo Winkler[4], Maria Agostina Frezzini[2], Elena De Santis[2], Leonardo Sagnotti[4], Silvia Canepari[2], Fausto Manes[2]

[1] National Research Council, Institute of BioEconomy, Via dei Taurini 19, 00185 Rome, Italy

[2] Department of Environmental Biology, Sapienza University of Rome, p.le Aldo Moro 5, 00185, Rome, Italy

[3] ENEA, Italian National Agency for New Technologies, Energy and Sustainable Economic Development, SSPT - STS, R.C. Casaccia, Via Anguillarese, 301 - 00123 S.Maria di Galeria, Rome, Italy

[4]Istituto Nazionale di Geofisica e Vulcanologia, Via di Vigna Murata 605, 00143 Rome, Italy

*Corresponding author

Keywords: PM injury; biomonitoring; urban green; functional traits; magnetic properties, oxidative potential.

Abstract

Increased attention has been given to particulate matter (PM) that, as well as worsening air quality, is responsible for chronic and acute respiratory or cardiovascular diseases. Currently, most of the studies are focused on the capacity of plants and other biological media to adsorb PM, whereas few works explore the functional damage due to PM on urban vegetation. The present study, considering *Quercus ilex* L. as target species for its wide distribution in the Mediterranean urban and natural areas, pointed out that PM accumulation, inferred from magnetic and chemical properties, has almost no effects on structural morpho-functional traits as Relative Water Content or Specific Leaf Area but can impair processes related to the first photochemical reactions suggesting shading effect on leaves. PSI functionality and thus, carbon assimilation related processes, are impaired to a lesser extent by the oxidative potential of PM. Our results showed that, although several oxidative stressors can simultaneously affect morpho-functional traits, the interdisciplinary approach tested here can be a key tool to enlarge the spatial scale of biomonitoring activities as much as possible, and highlight a functional indicator of PM injury. This is needed to enhance the knowledge about the complex processes that are implied in the dynamic relationship between air quality, vegetation functionality and ecosystem services provisioning in urban areas.

1. Introduction

Nowadays, air pollution is a major concern especially in the urban environment, where most of the global population lives. Emission of atmospheric pollutants is strictly connected with human activities, industries and, above all, combustion processes, which produce a large number of pollutants, whose chemical composition is extremely heterogeneous (WHO, 2004). Among them, particulate matter (PM), a complex

mixture of solid particles and liquid droplets of different diameters and chemical nature, is one of the most dangerous and harmful pollutants for human health (Costabile et al., 2020).

Indeed, it is well known that PM pollution causes stroke, chronic and acute respiratory or cardiovascular diseases (Orioli et al., 2018), and it is linked to premature mortality. It was estimated that in 2016 indoor and outdoor air pollution caused 7 million deaths worldwide, that are mainly due to the exposure to fine and ultrafine PM of 2.5 μm or less in diameter ($PM_{2.5}$) (WHO, 2019). Furthermore, recent studies have hypothesized a positive association between the concentration of airborne $PM_{10-2.5}$ and the spread of the novel Coronavirus (SARS-CoV-2), (Comunian et al., 2020; Setti et al., 2020; Yao et al., 2020; Zoran et al., 2020). In particular, it has been suggested that high PM pollution can either trigger lung inflammation and enhance the population sensitivity to the virus (Conticini et al., 2020; Fattorini and Regoli, 2020), or act as a direct virus "carrier", thus increasing the risk of its airborne diffusion (Sanità di Toppi et al., 2020; Tung et al., 2021).

In urban areas, trees and shrubs play an important role in removing air pollutants, especially particulate ones, through dry deposition on the leaf surface (Blanusa et al., 2015). Plants improve air quality providing an important ecosystem service to the population serving as a natural sink for pollutants (Fusaro et al., 2017a; Manes et al., 2016; Mukherjee and Agrawal, 2018). Since the greater the tree cover, the greater the pollution removal, urban vegetation can be used for phytoremediation, but also air monitoring: plants can be used as biomonitors through ecological investigation thanks to their simple identification and sampling, their ubiquity and their large amount of biomass (Nowak et al., 2006). On the other side, PM can damage plants that are the primary receptors for air pollutants (Stevens et al., 2020).

In this context, leaf functional traits (FT), i.e. morphological, physiological and phenological characteristics that influence plant performance and its function in the ecosystem (Violle et al., 2007), can play a pivotal role in both phytoremediation and biomonitoring. FT influence the ecological efficiency of plant species in removing PM, since it depends on leaf shape and morphological features (Grote et al., 2016; Sæbø et al., 2012), and are useful for screening plant health, used as indicators of air pollution and other environmental stress injuries (Bussotti and Pollastrini, 2015).

Rai (2016) made an exhaustive overview of the reached results on the physiological, biochemical and morphological alterations caused by PM, showing that PM deposition on leaves negatively affects photosynthetic activity and protein synthesis, also increasing plant susceptibility to pathogens.

PM can have remarkable magnetic properties arising from magnetite-like ferrimagnetic particles (Flanders, 1994; Hunt et al., 1984), often associated with heavy metals such as Cd, Cr, Zn (Georgeaud et al., 1997; Hunt et al., 1984). The magnetic properties of PM may arise from combustion processes related to industry, domestic heating, or vehicles, as well as from abrasion products from street surfaces and brake systems (e.g. Hoffmann et al., 1999; Jordanova et al., 2004). Especially in urban areas, vehicular traffic represents the main source of PM associated with magnetite-like minerals (Gonet and Maher, 2019; Sagnotti et al., 2009), mostly emitted by the abrasion of disk brakes (Chaparro et al., 2020; Gonet et al., 2021; Winkler et al., 2020). In urban contexts,

the magnetic susceptibility of leaves decreases with increasing distance from the roadside, confirming the relationship between vehicular traffic and the emission of magnetic iron (Szönyi et al., 2007).

Rock magnetism methods have been widely used to biomonitoring air pollution using tree leaves, barks, mosses and lichens, being efficient PM receptors (for a review, Hofman et al., 2017). Magnetic properties detected on tree leaves mostly depend on the concentration and the grain size of magnetite-like minerals accumulated on the samples, with the magnetic susceptibility being the fastest, most used and practical parameter (Kapper et al., 2020).

To better understand the biological responses to PM of living organisms, the oxidative potential (OP) of particles can be assessed. OP provides a proxy of the oxidative capacity of PM and the oxidative stress processes, hypothesizing that PM components cause the formation of reactive oxygen species (ROS), that can lead to the membrane and cell damages (Ficociello et al., 2020; Piacentini et al., 2019; Simonetti et al., 2018). Among existing OP acellular assays, the ascorbic acid (OP^{AA}), which is expressed as the consumption rate of AA by particles over time, has been widely assessed as an indicator of particles OP (Campbell et al., 2019; Pietrogrande et al., 2019). OP^{AA} measurement seems to be particularly influenced by inorganic components and, in detail, different studies support that non-exhaust traffic emissions affect OP^{AA} results (Bates et al., 2019; Massimi et al., 2020). Indeed, ascorbic acid is a physiological, non-enzymatic antioxidant located in the apoplast and used as a defense against ROS; it increases under high pollution conditions, being one of the most sensitive leaf functional traits to air pollutants (Mukherjee and Agrawal, 2018).

Ecophysiological, magnetic and chemical methods are all useful tools to determine PM harmful effects on urban vegetation as well as the composition of particulate matter and the grain size, assuming a significant role in biomonitoring air pollution. Although the importance of such methods is widely known, still very few works have focused on the correlation between these three scientific fields, showing a lack of interdisciplinary studies related to PM. In this context, an integrated approach is crucial to achieving a better comprehension of the effects of PM and the biological response it induces on urban vegetation. In this paper, we measured leaf functional traits, like the specific leaf area (SLA), the relative content of chlorophyll and the chlorophyll *a* fluorescence, correlating them with both magnetic properties and oxidative potential of PM deposited on leaves, determining also the elemental composition of the bioaccumulated particles. *Quercus ilex* L. has been chosen as target species for its widespread use in urban contexts in the Mediterranean urban areas and for its efficiency in accumulating magnetic PM (Moreno et al., 2003). The hypothesis to be tested is that the photosynthetic performance of *Q. ilex* decreases with increasing values of magnetic susceptibility, which is considered a proxy of the accumulation of traffic-related magnetic dust.

The experimental field campaign tests if the applied integrative approach can be used as an effective tool to biomonitoring air quality and the vegetation stress condition related to PM exposure and accumulation. Since PM can affect photosynthesis through several physiological mechanisms from impairing photosystems functionality, slowing down the processes related to the first photochemical reactions, to affecting the

reduction of end acceptors on PSI side, or damaging the pigments, it could be highly valuable to finalize the analysis of strengths and weakness of biomonitoring to highlight the most suitable functional indicators.

2. Material and Methods

2.1 Sites selection and characterization

The sampling was conducted within the city of Rome, Italy, in sites where *Q. ilex* trees were present, having comparable age and morphological characteristics (diameter at breast height between 0.80 and 1.20 m, crown radius ranging from 1 to 2 m) and for which the outer part of the crown was accessible.

Fig. 1 Spatial distribution of experimental sites. The green markers represent the control sites of Castelporziano Estate (CP) and Villa Ada urban park (VA) (see text for further details).

In particular, eight sites were selected (Fig. 1): Castelporziano Estate (CP), Villa Ada urban park (VA), Porta Pinciana (PP), Via Salaria (VS), Viale Mazzini (MZ), Quirino Majorana (QM), Re di Roma (RdR), Vigna Murata (VM). The sites selection was based on the following criteria i) the characteristics of the green infrastructure element (Bolund and Hunhammar, 1999): peri-urban forest, CP; urban forest, VA; street tree lines, PP, VS, MZ, QM; trees in an open square, RdR; grouped trees in large lawn, VM; ii) the site's location in respect to the city center, and in different urban settlements; iii) the annual average PM_{10} concentrations (μg m^{-3}) derived, for each experimental site, from integrated modelling system (Sebastiani et al., 2021) (Table 1).

Experimental site	PM_{10} annual mean
CP	12
VA	22

MZ	23
PP	25
VM	25
RdR	26
VS	26
QM	27

Table 1 PM_{10} annual mean concentration ($\mu g\ m^{-3}$) for each experimental site was retrieved from the integrated modeling system elaborated by Regional Environmental Protection Agency monitoring network, ARPA Lazio, 2018 (Sebastiani et al., 2021).

Furthermore, seasonal PM_{10} concentration (recorded from Regional Environmental Protection Agency, ARPA Lazio, monitoring network) of the urban settlements considered in the present study, was also taken into account, for an indication of the mean state of the air quality, considering only those monitoring stations located nearby the experimental sites (Appendix A and B).

Specifically, CP is a natural peri-urban forest within a protected area of about 6000 ha, located 25 km from Rome city center and close to the Tyrrhenian coast (3 km) (Fig. 1). Annual PM_{10} concentration in this site is the lowest (12 $\mu g\ m^{-3}$, Table 1). VA site is instead a fairly well preserved natural forest (Fusaro et al., 2019) located inside the urban forest of a historical Villa that, with an extension of 160 ha, is one of the largest urban parks in the Rome city center (Fig. 1). VA has a higher annual concentration of PM_{10} than CP (22 $\mu g\ m^{-3}$), but lower than the other sites (Table 1), comparable to the urban background level (Canepari et al., 2009, Appendix A). Based on the green infrastructure characteristics (natural forests) as well as on the PM annual values, not directly affected by traffic-related emissions, CP and VA were considered as control sites. In PP site, the sampled trees are street trees close to a traffic light, located at the borders of the large urban park of Villa Borghese, in the historical city center. PM_{10} average annual concentration in this site is 25 $\mu g\ m^{-3}$ (Table 1). VS, MZ and QM are all street trees with similar green infrastructure characteristics (linear elements, surrounded by impervious surfaces) but are located in different urban contexts.

In particular, VS site is in the city center, close to VA (Fig. 1), and borders an intense traffic road, traveled by more than 2000 vehicles per hour (Rome Municipality, 2020; Alessio et al., 2002), is therefore characterized by high annual PM_{10} levels (26 $\mu g\ m^{-3}$, Table 1). MZ is placed in a residential neighborhood in the city center, with better air quality (PM_{10} = 23 $\mu g\ m^{-3}$, Table 1), while QM is located in a densely urbanized neighborhood in the South-Western part of the city, close to via Portuense avenue, with a high traffic rate (2050 vehicles/h, Rome Municipality, 2020) and the highest PM_{10} annual values (27 $\mu g\ m^{-3}$, Table 1).

RdR site is in a large circular open square lined by *Q. ilex* trees, located in the commercial area in the central-southern part of the city (Fig. 1), characterized by intense car traffic (2200 vehicles/h, Rome Municipality, 2020) and, accordingly, fairly high PM concentration (annual mean 26 $\mu g\ m^{-3}$, Table 1). Finally, in VM site, the sampled trees are grouped in a lawn along an expressway in a suburban area of the south-western quadrant

of the city, characterized by a lower urbanization density and by the presence of large agricultural and semi-natural spaces (Fig. 1). VM has an average annual PM_{10} concentration of 23 μg m^{-3} (Table 1) and is close to via Laurentina, an avenue travelled by around 1500 vehicles/h (Municipality of Rome, 2020).

2.2 Experimental design

The field campaign was carried out on 6 and 7 March 2019 during two consecutive days with stable meteorological conditions, more than 15 days from the last rain event, to avoid the influence of rainfall on the PM leaf deposition (Xu et al., 2017). Indeed, the last rain event registered by the Servizio Integrato Agrometeorologico della Regione Lazio in the Rome city center (Lanciani Station, 41° 92' N, 12°52' E) was registered on February 11th. In March the minimum temperature was 8.10 ± 1.77, maximum was around 18.13 ± 2.52 and the mean was 12.81 ± 1.40, with four rainy days after the 12 of March.

For each experimental site, four to five representative adult trees were sampled, and sun-exposed, fully developed leaves, were collected at 1.50 m height from the outer part of the crown next to the road. For each tree, twigs were detached, stored in sealed plastic bags to avoid dehydration, and brought to the laboratories where morpho-functional traits, magnetic properties and chemical analysis were carried out. In particular, for each tree, twigs were collected in three different portions of the crown to represent the natural variability of light and PM exposure in the crown of the urban street trees (Janhäll, 2015; Sgrigna et al., 2015). In each crown portion, 3 twigs were sampled: one was used for morpho-functional traits measurements, one for magnetic and one for chemical analysis. Morpho-functional traits were measured on one leaf for each twig and data were aggregated for each sampled tree (n = 4 - 5). For magnetic and chemical analysis, leaves collected from the twigs were pulled together and measurements were performed on three subsamples for each site (n = 3).

2.3 Magnetic characterization

Magnetic measurements were performed at the paleomagnetic laboratory of INGV. Dried leaves were pressed inside 8 cm^3 plastic cubes for measuring the mass-specific magnetic susceptibility (χ), which was determined on AGICO KLY5 Kappabridge dividing the bulk susceptibility values, after subtraction of the empty holder, for the net weight of the samples.

Leaves fragments, irregularly dimensioned and shaped, were pushed inside pharmaceutical gel caps #4, around 0.15 mL capacity, for the hysteresis characterization with the Princeton Measurement Corporation Micromag 3900 Vibrating Sample Magnetometer (VSM).

The coercive force (B_C), the saturation remanent magnetization (M_{RS}, or SIRM) and the saturation magnetization (M_S) were measured in magnetic fields up to 1.0 T and their values were calculated after subtracting the high field linear paramagnetic trend, achieved after saturation of the ferromagnetic component. Mass-specific magnetization values for the concentration-dependent magnetic parameters were calculated dividing the magnetic moments by the net weight of the samples. The coercivity of remanence (B_{CR}) was extrapolated from backfield remagnetization curves up to −1 T, following forward magnetization in a +1 T

field. The magnetic measurements were performed on dried leaves since the content of water influences the mass and the susceptibility of the samples (Szönyi et al., 2008).

Moreover, the domain state and magnetic grain-size of the magnetic particles of the samples were compared to theoretical magnetite according to the hysteresis ratios M_{RS} /M_S vs. B_{CR} /B_C in the "Day plot" (Day et al., 1977; Dunlop, 2002a, 2002b).

2.4 Morpho-functional traits measurements

Leaf- Relative Water Content (RWC, %) was calculated as follows:

$$RWC = \frac{FW-DW}{TW-DW} \times 100$$

where FM is leaf fresh mass, DW is leaf dry mass, and TW is leaf turgor mass, water-saturated leaf weight measured after 10–12 h in water saturating conditions (petiole in water). Then leaves were dried in the oven at 80°C until the stable dry weight was reached. Specific Leaf Area ($cm^2\ gr^{-1}$) was measured on the same leaves collected for RWC, calculated as the ratio between leaf area and dry weight.

The relative chlorophyll content, $Chl_{SPAD,}$ was estimated in vivo using a portable chlorophyll meter (SPAD-502DL Plus,160 Minolta; Spectrum Technologies Ltd., Plainfield, IL, USA). This instrument provides an estimation of the relative amount of leaf chlorophyll content based on the transmitted radiation in the red and near-infrared wavelengths and the resulting values are reported in arbitrary units.

Chlorophyll *a* fluorescence, ChlF, measurements were performed after 1 h of sample dark adaptation, necessary to reduce the effects of transient photoinhibition (Desotgiu et al., 2012).

After dark adaptation, the primary acceptors reach a complete oxidation state and then are exposed to a saturating red actinic light pulse of 3000 μmol photons $m^{-2}\ s^{-1}$ of 1 s duration and the kinetics of the polyphasic prompt fluorescence transient (FT) rise is recorded by a direct fluorometer, Handy PEA (Hansatech Instruments, Norfolk, UK). The FT plotted on a logarithmic time-scale, exhibits a series of steps labeled as O (F_0, when all the reaction centres of the PSII are open) J (2 ms), I (30 ms) and maximum P level (Fm, when all the PSII reaction centres are fully reduced). The first part of the FT (O–J) expresses the photochemical events, giving information about the accumulation of reduced QA (primary electron acceptor quinone of PSII). The J–I–P region of the FT reflects the velocity of ferredoxin reduction beyond the PSI. The FT was elaborated using the JIP-test, a tool that translates this polyphasic fluorescence transient into a constellation of biophysical parameters, which quantify the single steps of the photochemical pathway through both photosystem II (PSII) and photosystem I (PSI) (Strasser et al., 2010). In this study the following JIP-test parameters were considered: RC/ABS, a pool of active reaction center (RC) per PSII antenna complex; DI_0/RC, effective dissipation in an active RC; TR_0/RC, reducing QA energy flow for each RC; ET_0/RC, the electron transport beyond QA^- per RC; ΔV_{IP}, the efficiency of electron transport to reduce the end acceptors beyond the PSI; PI_{TOT}, Total Performance Index (potential) for energy conservation from photons absorbed by PSII to the reduction of PSI end acceptors.

2.5 Chemical characterization

For each sites, three replicates of 10 leaves randomly chosen as subsample, were put in the Falcon tubes with 50 mL of deionized water (produced by Arioso UP 900 Integrate Water Purification System, USA) and, then, stirred for 30 min with a rotary shaker (60 rpm; Rotator; Glas-Col, USA) to extract the water-soluble fraction of PM deposited on leaves. After the extraction, the solutions were filtered through a cellulose nitrate filter (0.45 µm pore size, Merck Millipore Ltd., Billerica, MA, USA). Consequently, the solutions were split into proper aliquots to perform AA assay and chemical analyses through the utilization of inductively coupled plasma mass spectrometry (ICP-MS, Bruker 820-MS, Billerica, MA, USA).

AA assay was performed on water-soluble fraction of samples, following previously detailed and widely used procedures (Frezzini et al., 2019; Massimi et al., 2020). Briefly, 2.5 mL of the filtered aqueous extracts were mixed with 300 µL of phosphate buffer (0.5 mM at pH 7.4) and 100 µL of ascorbic acid solution (2 mM). Then, the depletion of AA was monitored for 20 minutes by recording the decrease in absorbance by UV-Vis spectroscopy at 265 nm (Varian Cary 50 Bio UV-Vis; Varian Inc., Palo Alto, CA, USA). OP^{AA} was calculated as the depletion rate per unit of mass of sampled leaves (nmol AA min^{-1} g^{-1}) using the following equations:

$$\sigma AA = -\sigma Abs \times \frac{N_0}{Abs_0}, \qquad OP^{AA} = \frac{\sigma AA_s - \sigma AA_b}{\frac{V_a}{V_e} \times V_S}$$

where σAbs is the slope of the absorbance of blanks vs. time (min-1), Abs_0 is the initial absorbance calculated from the intercept of the linear regression between absorbance and. time, N_0 is the number of AA moles added for the reaction (200 nmol), σAAs and σAAb are the rate of AA consumption for the sample and the blank, respectively (nmol min^{-1}), V_e and V_a are the extraction volume (50 mL) and sample volume added to the reaction vial (2.5 mL) respectively, and m is the leaves dry weights of each leaves sample (g).

The concentrations (ng g^{-1}) of 29 inorganic elements (Al, As, B, Ba, Be, Cd, Ce, Co, Cr, Cs, Cu, Fe, K, La, Mn, Mo, Ni, Pb, Rb, Sb, Se, Sn, Sr, Ti, Tl, V, W, Zn and Zr) were determined in water-extracted fractions by adapting an analytical procedure allowing the determination of PM micro-components and trace elements (Canepari et al., 2006).

2.6 Statistical Analysis

All data i.e. seasonal PM air concentration, magnetic measurements, morpho-functional traits, chemical analysis were compared using one-way ANOVA with the site as a fixed factor, and the means significantly different at $p < 0.05$ were identified using post hoc Student–Neuman–Keuls test. A multivariate statistical technique, the Principal Component Analysis (PCA), was used to investigate the structures of variability within the different experimental sites. The selection of the principal factors was based on those with eigenvalues greater than 1.

Pearson correlation analysis was performed to assess the applicability of morpho-functional traits as indicators of PM damage, testing the relationship between traits (RWC, SLA, Chl_{SPAD}, JIP-test parameters) magnetic measurements and chemical analysis. Data were aggregated at the site level. All analyses were performed using Statistica software, version 7.0 (StatSoft, Tulsa OK, USA).

3. Results

3.1 Magnetic properties

Mass specific magnetic susceptibility values, at the site level, ranged from 0.9 to 44.6 × 10^{-8} m^3 kg^{-1} (Fig. 2), and the lowest values were measured in the CP samples. Low values were measured also in VA (the urban forest inside a large green park) and MZ (street trees in a residential neighborhood). PP, VM had an intermediate susceptibility whereas RdR, VS and QM showed the highest susceptibility.

The hysteresis loops measured on all samples were similar in shape: narrow, saturated well before 1T (Appendix C), with a modest variability of both coercivities (5.9 mT < B_C < 7.7 mT; 34.0 mT < B_{CR} < 41.6 mT, at site level). All the samples from site CP and one sample from VA, whose magnetization was too low to produce hysteresis loops satisfactory defined, were neglected.

The concentration-dependent magnetic parameters obtained from hysteresis loops varied, at the site level, from 1.6 to 32.7 mAm^2kg^{-1} and from 0.1 to 2.3 mAm^2kg^{-1} for M_S and M_{RS}, respectively, and SIRM/ χ values, at the site level, ranged from 3.38 to 6.21 kA/m.

It was not possible to estimate the Curie temperature using magnetothermic cycles, due to the low susceptibility values and the disturbance caused by the burning of organic matter during heating.

The M_{RS}/M_S vs. B_{CR}/B_C ratios (Fig. 3) show that the values from all sites are located in a cluster in the middle-right side of the Day plot, between the theoretical curves calculated for mixtures of a single domain (SD) and multidomain (MD) magnetite grains and for a mixture of SD and superparamagnetic (SP) magnetite grains (Dunlop, 2002a, 2002b).

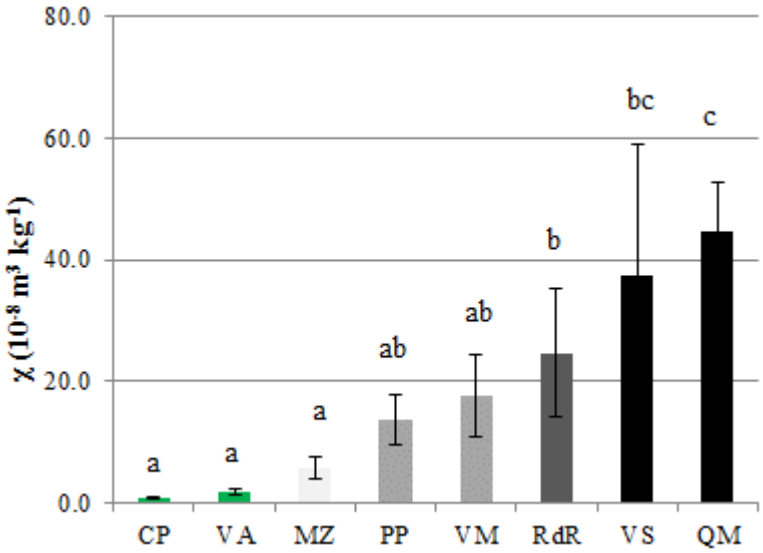

Fig. 2 Magnetic susceptibility of *Q. ilex* leaves in the different experimental sites. Bars denote mean ± standard deviation, and those not accompanied by the same letters are significantly different at $p<0.05$.

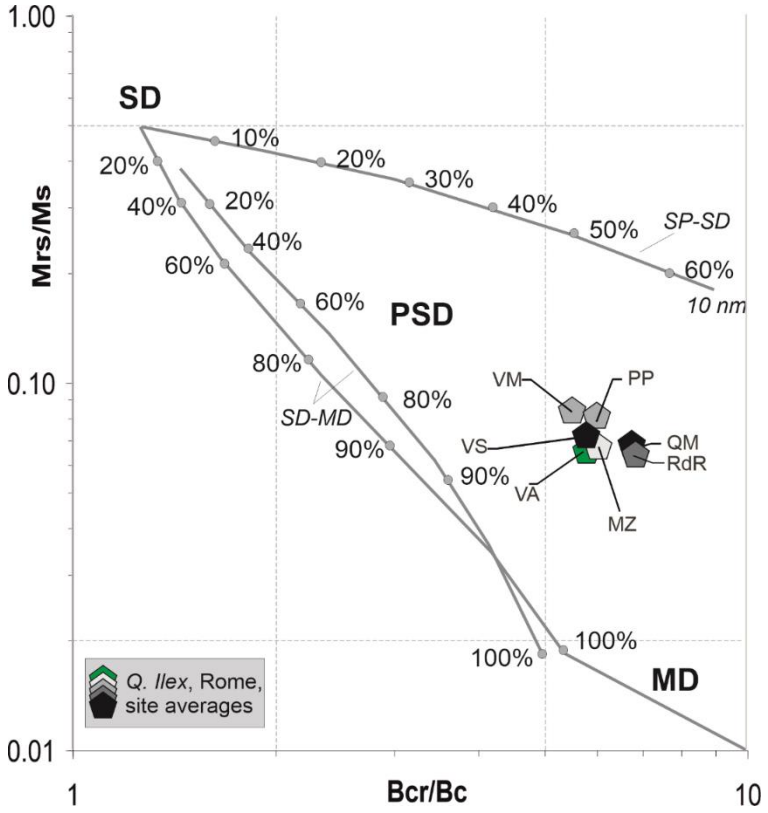

Fig. 3 Bilogarithmic Day plot of the hysteresis ratios M_{RS}/M_S vs. B_{CR}/B_C. Data are shown as site averaged; pentagons' colors according to the site classification. SD: single domain; PSD: pseudo single domain; MD: multi domain; SP: superparamagnetic.

3.2 Morpho-functional traits

All sites presented close values of RWC, except for PP that showed the minimum value and MZ the maximum. SLA was slightly but significantly lower in control sites CP and VA, as well as in VM, meaning higher sclerophyll degree. MZ presented high SLA, i.e. the lowest sclerophyll degree, together with the sites with high PM accumulation (RdR, VS, QM). The lowest Chl_{SPAD} values were measured in CP and VS, the highest in VA. No substantial differences were detected among the other experimental sites (Table 2).

Site	**RWC**	**SLA**	**Chl_{SPAD}**	**n**
CP	81.90 ± 4.44ab	64.16 ± 10.38a	47.37 ± 1.72a	4
VA	80.45 ± 8.82ab	61.82 ± 1.24a	54.04 ± 2.84b	5
MZ	90.88 ± 7.35b	85.11 ± 11.8b	51.66 ± 2.53ab	4
PP	67.15 ± 16.6a	75.82 ± 4.12ab	52.13 ± 4.65ab	4
VM	81.22± 4.6ab	64.07 ± 6.5a	51.52 ± 3.35ab	5
RdR	79.95 ± 10.7ab	82.20 ± 12.3b	49.7 ± 1.85ab	5
VS	81.73 ± 3.22ab	86.09 ± 7.8b	48.70 ± 4.48ab	5
QM	77.16 ± 10.08ab	77.52 ± 7.9ab	50.75 ± 2.51ab	5

Table 2 Relative Water Content (%), Specific Leaf Area ($cm^2\ gr^{-1}$) and Chlorophyll relative content, Chl_{SPAD} (SPAD units) measured in the experimental sites. Values express mean ± standard deviation and those not accompanied by the same letters are significantly different at $p<0.05$. n, indicates the number of replicates for each site (sampled trees).

The values of JIP-test parameters are shown in Fig. 4 in the different sites. RC/ABS had lower values in the sites characterized by the higher susceptibility (RdR, VS, QM), increasing in intermediate and control sites (Fig. 4 a). The dissipation per active reaction centre (DI_0/RC, Fig. 4 b) followed an opposite pattern: the lowest values were measured in the VA, MZ, CP and VM sites. DI_0/RC slightly increased going towards the sites with higher magnetic susceptibility values (RdR, and VS) with the exceptions of QM that presented DI_0/RC comparable to the control sites CP, and with those presented an intermediate accumulation as PP.
The functional parameters which expressed the specific energy fluxes (per QA reducing PSII RC), as TR_0/RC and ET_0/RC, increased in the sites where PM accumulated on leaves was higher, like RdR, VS and QM (Fig 4 c, d). VA showed the lower value of both parameters whereas CP control site presented an intermediate value of TR_0/RC and the lowest value of ET_0/RC, together with VA. Finally, ΔV_{IP} and PI_{TOT} (Fig. 4 e, f) highlighted a pattern similar to RC/ABS among sites: VA, VM presented higher functionality of the IP phase and total photosynthetic performance, but in general, ΔV_{IP} presented slight differences among sites, with VA showed the maximum and QM the minimum. Following what was displayed by other parameters, CP did not present the trend of sites with lower magnetic susceptibility.

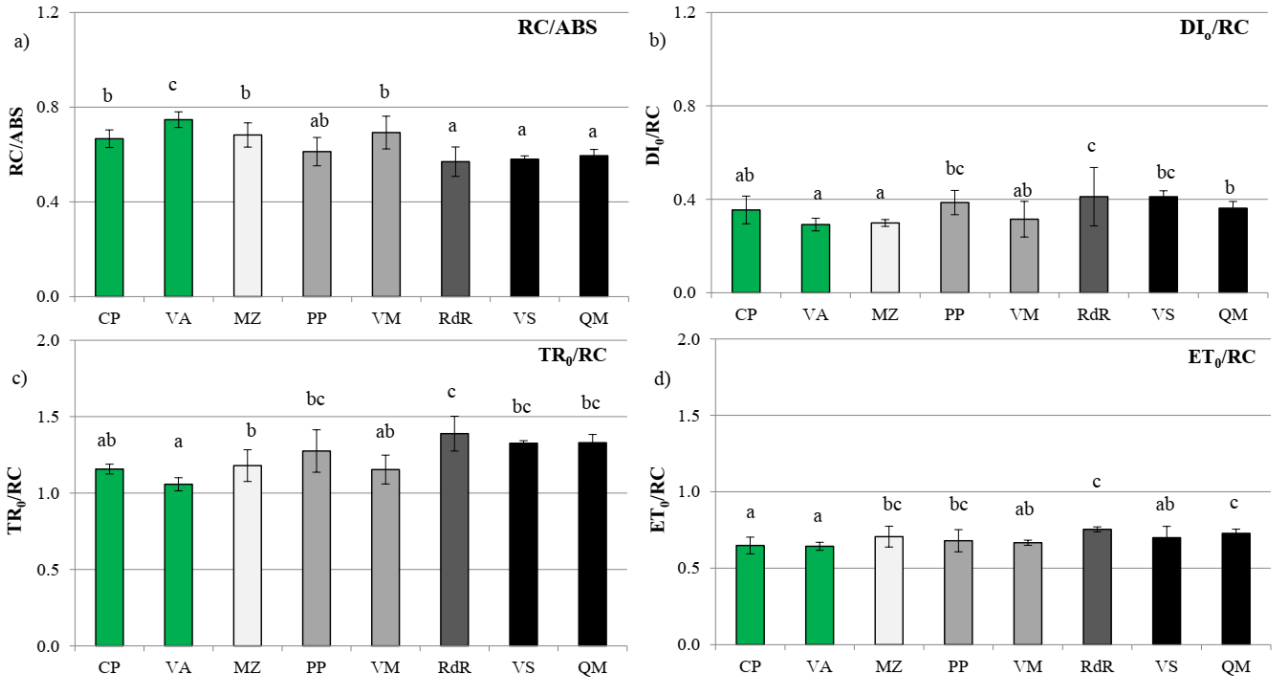

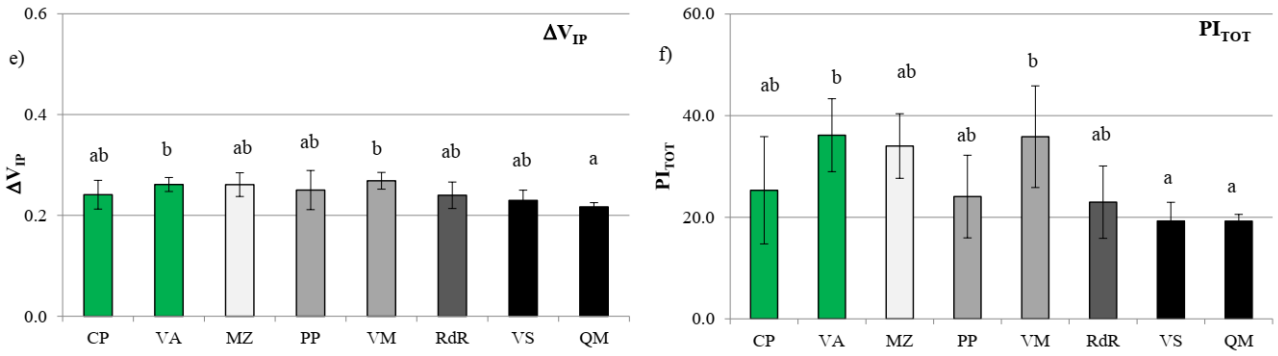

Fig. 4 JIP-test parameters in the experimental sites. The green bars indicated the two control sites: CP, Castelporziano and VA, Villa Ada urban park. Light, dark grey and black bars indicated sites with low, intermediate or higher magnetic susceptibility levels (see Figure 2), respectively. A detailed sites description is reported in Material and Methods. Bars denote mean ± standard deviation (n = 4 - 5) and those not accompanied by the same letters are significantly different at $p<0.05$.

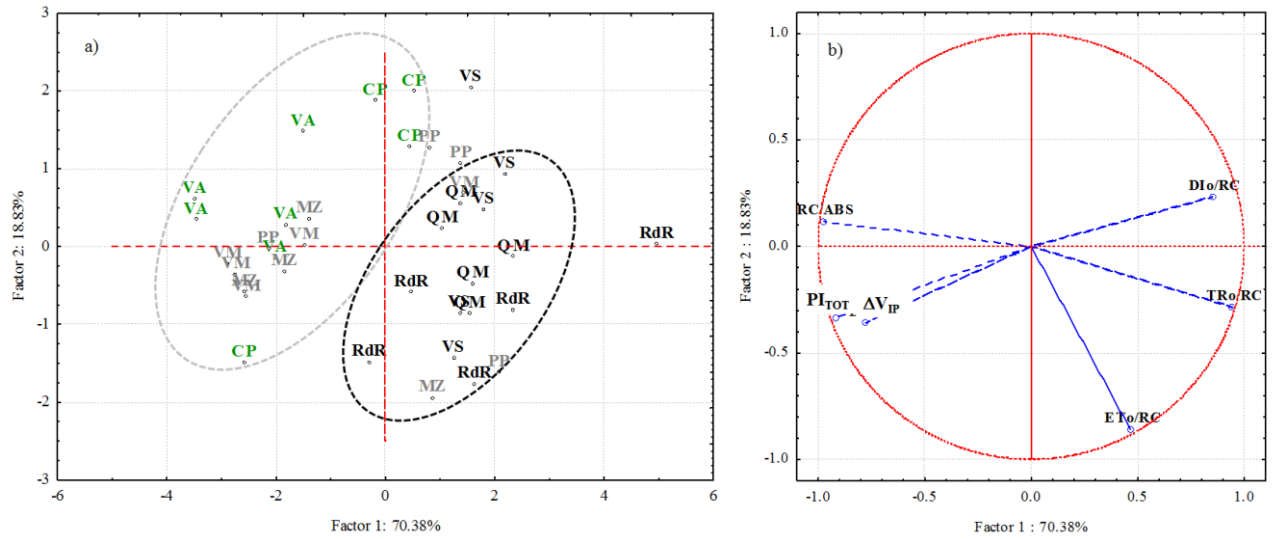

Fig. 5 Principal Component Analysis of the studied sites based on JIP-test parameters (RC/ABS, DI_0/RC, TR_0/RC, ET_0/RC, ΔV_{IP}, PI_{TOT}) (a) and factors' loadings (b). For each site, the replicates (numbers of trees) are reported.

For a better understanding of the capacity of ChlF to discriminate the *Q. ilex* functionality in the different sites, PCA was applied. The sites with the high PM accumulation, grouped on the dark circle, are separated from the control sites, grey circle, whereas the sites with intermediate PM accumulation (MZ, PP, VM) have greater dispersion. RC/ABS, PI_{TOT} and ΔV_{IP} are negatively related to Factor 1 (the factors' loading are -0.975, -0.915 and -0.777 respectively). Most of the records belonged to RdR, VS and QM are positively related to Factor 1, where TR_0/RC and DI_0/RC reached the higher loading (0.944 and 0.851 respectively) and records of those sites are negatively related to ET_0/RC (- 0.859 on Factor 2).

3.3 Chemical characterization

Sites	Cu	Fe	Mo	Sb	Sn	Pb	K	La	Ce	OP^{AA}
CP	44 ± 10a	1028 ± 218a	2.1 ± 0.15a	1.8 ± 0.39a	1.1 ± 0.45a	0.45 ± 0.03a	53400 ± 6299a	0.58 ± 0.51a	1.3 ± 0.62a	9.3 ± 2.97a
VA	106 ± 8.1a	1249 ± 100a	2.6 ± 0.11a	3.8 ± 0.82a	0.69 ± 0.49a	0.77 ± 0.68a	63482 ± 4487bc	0.53 ± 0.16a	1.1 ± 0.11a	12 ± 2.7a
MZ	397 ± 75a	2682 ± 84a	8.1 ± 2.8a	8.6 ± 2.3a	5.7 ± 1.7a	7.9 ± 5.6bc	86126 ± 22835c	1.2 ± 0.14a	2.8 ± 0.92a	38 ± 9.8b
PP	496 ± 104a	2406 ± 548a	7.9 ± 2.1a	9.8 ± 2.5a	6.2 ± 1.2a	5.6 ± 0.77b	88057 ± 22835c	1.4 ± 0.27a	2.5 ± 0.42a	49 ± 7.4b
VM	409 ± 195a	3255 ± 1818ab	7.5 ± 1.9a	7.9 ± 3.8a	6.1 ± 2.9a	3.8 ± 0.99b	57929 ± 10881ab	1.7 ± 0.44ab	3.7 ± 1.3ab	54 ± 12b
RdR	1458 ± 274b	5330 ± 626bc	21 ± 5.2b	19 ± 4.7b	16 ± 2.5b	16 ± 0.84e	197979 ± 41003d	2.1 ± 0.39bc	4.4 ± 0.55bc	153 ± 11c
VS	1453 ± 568b	6579 ± 2563c	21 ± 6.9b	26 ± 9.1b	23 ± 10b	10 ± 0.23cd	139412 ± 57119cd	2.6 ± 0.92c	5.7 ± 1.9c	166 ± 37c
QM	1456 ± 218b	6382 ± 328c	20 ± 0.55b	25 ± 1.6b	17 ± 1.4b	14 ± 3.2de	137061 ± 22899cd	3.7 ± 0.73d	7.5 ± 0.73d	204 ± 17d

Table 3 Chemical composition of the dust deposited on leaves: concentrations of some detected elements (ng g^{-1}) and the oxidative potential measured through the ascorbic acid assay (OP^{AA}; nmol AA min^{-1} g^{-1}) assay. Values express mean ± standard deviation and those not accompanied by the same letters are significantly different at $p<0.05$.

For each experimental site, Table 3 shows the concentrations of some of the more indicative analyzed elements in the soluble fraction of dust deposited on the leaves surface, and the results of OP measured through the AA assay. Concentrations of other analysed elements are reported in Appendix D. The differences among sites in terms of chemical elements' concentration followed a similar pattern for Cu, Fe, Mo, Sb and Sn, that are well-known tracers of non-emissive traffic contribution, such as brake and tire wear (Zhang et al., 2020). For these elements, in agreement with the magnetic measurements, the concentration at the traffic sites was higher than the one at the sites considered as control (CP, VA). The higher values were detected in RdR, VS and QM sites. The lowest values of K, La and Ce were measured only in CP and VA control sites, whereas MZ presented intermediate values together to PP, VM. The highest concentrations were detected in RdR, VS and QM. Pb showed the following trend: CP and VA< PP and VM < MZ < VS < RdR and QM, which differed from what was detected for the other chemical species. Lastly, the OP^{AA} measurements of control sites (CP and VA) had the lower recorded values, while MZ, PP and VM showed intermediate values,

in accordance with magnetic measures. RdR, VS and QM showed higher OP^{AA} in the order RdR < VS< QM , following the findings of the susceptibility and chemical analysis.

	RC/ABS	**DI_0/RC**	**TR_0/RC**	**ET_0/RC**	**ΔV_{IP}**	**PI_{TOT}**	**Cu**	**Fe**	**Mo**	**Sb**	**Sn**	**Pb**	**K**	**La**	**Ce**	**OP^{AA}**	**χ**
RC/ABS	1	**-0.930**	**-0.984**	-0.770	0.762	**0.906**	**-0.860**	-0.787	**-0.857**	-0.826	-0.838	-0.816	-0.828	-0.713	-0.704	-0.815	-0.755
DIo/RC		1	**0.876**	0.547	-0.686	**-0.888**	0.722	0.624	0.709	0.677	0.723	0.615	0.730	0.485	0.482	0.652	0.595
TR_0/RC			1	**0.863**	-0.717	**-0.841**	**0.904**	0.828	**0.905**	**0.858**	**0.859**	**0.900**	**0.895**	0.754	0.747	**0.855**	0.779
ET_0/RC				1	-0.523	-0.541	**0.851**	0.781	**0.869**	0.783	0.759	**0.984**	**0.914**	0.718	0.725	0.801	0.668
ΔV_{IP}					1	**0.928**	-0.741	-0.699	-0.705	-0.755	-0.715	-0.608	-0.617	-0.729	-0.719	-0.798	-0.751
PI_{TOT}						1	-0.744	-0.676	-0.717	-0.744	-0.737	-0.617	-0.660	-0.655	-0.638	-0.750	-0.709
Cu							1	**0.974**	**0.997**	**0.982**	**0.972**	**0.929**	**0.915**	**0.882**	**0.899**	**0.980**	**0.921**
Fe								1	**0.976**	**0.986**	**0.980**	**0.868**	0.811	**0.928**	**0.954**	**0.977**	**0.962**
Mo									1	**0.979**	**0.976**	**0.939**	**0.916**	**0.874**	**0.896**	**0.970**	**0.909**
Sb										1	**0.985**	**0.874**	**0.837**	**0.914**	**0.930**	**0.979**	**0.953**
Sn											1	**0.849**	**0.838**	**0.855**	**0.886**	**0.948**	**0.919**
Pb												1	**0.949**	0.795	0.804	**0.887**	0.773
K													1	0.659	0.676	**0.841**	0.695
La														1	**0.993**	**0.946**	**0.974**
Ce															1	**0.956**	**0.977**
OP^{AA}																1	**0.966**
χ																	1

Table 4 Pearson correlation analysis between JIP-test parameters, magnetic susceptibility and chemical species. The r-values underlined and highlighted in bold are significantly correlated at $p < 0.05$ and $p < 0.01$ respectively.

The Pearson correlation analysis between JIP-test parameters, magnetic susceptibility and chemical species is shown in Tab. 4. When the correlation was significant, the selected JIP-test parameters are negatively correlated to the considered chemical elements and OP^{AA} as well as to susceptibility except for TR_0/RC and ET_0/RC that showed a positive correlation. DI_0/RC did not show any correlation with the chemical and magnetic parameters, whereas RC/ABS, ΔV_{IP}, PI_{TOT} showed a negative correlation with Cu, Fe, Mo, Sb, Sn, Pb, La, K, Ce, OP^{AA} and χ. All the chemical elements increased with χ, showing a direct correlation with a high r score between 0.977 to 0.686.

4. Discussion

PM is a major concern to human health and lately the attention on this pollutant increased, since it could be a co-factor that enhances the morbidity of infections such as the COVID-19 (Zoran et al., 2020). In Italy, vehicular traffic is responsible for about 40 % of PM_{10} emission (ISPRA, 2016), and its effects should be carefully monitored in cities like Rome, where the proportion between vehicles (including private cars and two-wheelers) and inhabitants is one of the highest in Europe, with roughly 75 vehicles x 100 inhabitants (Municipality of Rome, 2020).

The conventional PM monitoring methods employ high-cost instrumental stations that can frame the general PM concentration in different city context (Appendix A), but are not available for extensive sampling across the city (Norouzi et al., 2015), making important to develop an effective alternative monitoring activity of PM within urban areas with different traffic intensity. Monitoring approaches based on plants as biological indicators of air pollution can be a successful solution, as leaves have a high capability to intercept and accumulate PM (Przybysz et al., 2019). Most of the studies are focused on the capacity of plants to adsorb PM on leaves, whereas few works considered the functional damage that PM deposition may cause to urban vegetation (Han et al., 2020).

In the current study, *Q. ilex*, a native species also widespread in urban areas in Mediterranean Basin, has been used for biomonitoring of PM in different areas inside the Municipality of Rome. Several studies agree that *Q. ilex* is a good biomonitor for pollutants like ozone, polycyclic aromatic hydrocarbons (PAHs) (Alfani et al., 2001), but *Q. ilex* leaves can be effective in the absorption of particles as well through trichomes and leaf longevity that allow long-term loading of PM (Sgrigna et al., 2015). It has been well documented that the accumulation of particles on leaves depends on leaf characteristics such as hair density and wax content, leaf shape and morphology (Muhammad et al., 2020). Indeed an experiment on 96 plant species with contrasting morphological and anatomical leaf characteristics (Muhammad et al., 2019), showed that the highest leaf remanent magnetization by mass was observed on leaves of *Q. ilex* that was in the most effective group of net particle accumulators together with *Pseudotsuga menziesii*, *Thuja plicata*, *Juniperus communis*, *Picea pungens glauca* and *Rhododendron*.

Magnetic studies performed on leaves allow to discriminate the experimental sites providing useful information for a biomonitoring campaign from different points of view: PM accumulated on the leaf, emission sources and particle size (Sagnotti et al., 2009). The PM accumulated on leaves detected by magnetic

susceptibility follows the PM air concentration gradient highlighted by mean annual values (Table 1), showing also the similarity between VA and MZ, in accordance to urban background air monitoring stations (Villa Ada and Cipro) that are close to these experimental sites (Appendix A and B).

Furthermore, magnetic measurements pointed out that sites with higher PM annual mean air concentration, such as VS or QM, show the highest magnetic susceptibility. In the other experimental sites (i.e. PP, VM, RdR), the magnetic susceptibility is lower and, accordingly, the amount of PM accumulated to the leaves too. Two concurrent issues can be used as an explanatory factor. On one side, the emissions related to vehicular traffic might be less intense (i.e. VM), on the other side, green infrastructures typologies, local urban settlement and road structure can strongly influence the dynamics of PM deposition on leaves (Łowicki, 2019; Qin et al., 2020). Indeed, in RdR, even close to Magna Grecia monitoring station, that shows the highest PM concentration along with Fermi in winter (Appendix A), dispersion could be favored relative to deposition and accumulation since in RdR the trees sampled are part of a circular line in a large open square, thus air circulation and dispersion of pollutants can be higher than in narrower street as VS or QM (Mei et al., 2018) .

The hysteresis loops, that provide indications about the concentration, composition and grainsize of the magnetic particles, are all very similar between the sampled sites and differ mainly for the concentration-dependent magnetic parameters, thus suggesting that the variations of the magnetic properties are due to different concentration of magnetic minerals, which are similar for composition and grain size. The significant correlation between χ, M_S ($R^2 = 0.87$) and M_{RS} ($R^2 = 0.81$), points out that all the concentration-dependent magnetic parameters are indicative of the same ferrimagnetic fraction, and that χ, the easiest magnetic parameter to be measured, is suitable as an indicator of the concentration-dependent magnetic properties (Table 4). Indeed, the range of coercivity values, and other magnetic parameters such as the low values of the saturation field and the SIRM/χ values, all suggest that magnetite-like minerals are the main magnetic carriers, in agreement with former studies focused on the characterization of magnetic airborne particulate matter in Rome (Sagnotti et al., 2009).

In the Day plot, the magnetic particles of *Q. ilex* leaves fall in a region of the plot in-between the theoretical trends for SD-MD and SD-SP pure magnetites, near "brake" samples and far from "diesel" and "gasoline" exhausts, which instead follow the theoretical trends for mixtures of a single domain (SD) and multidomain (MD) magnetites (Sagnotti and Winkler, 2012, Appendix E). The Day plot highlights the possible coexistence of SP and SD/MD particles that might result from two processes in which the friction between a brake pad and the cast-iron brake disc produce Fe-bearing particles.

At brake pad temperatures below 200 °C, abrasive processes dominate, and wear particles >1 μm are mostly generated. At higher operational temperatures (>200 °C), the concentration of nanoparticles (<100 nm) increases due to evaporation, condensation and aggregation processes, increasing by four to six orders of magnitude the emission rate of particles, thus constituting >90% of total brake dust and constituting a major source of airborne magnetic nanoparticles (Gonet and Maher, 2019).

However, the obtained results tend to corroborate the first emissive process: none of the magnetic properties diagnostic of the relevant presence of ultrafine SP particles, e.g. the enhancement of magnetic susceptibility,

and low SIRM/χ values, supported the presence of ultrafine magnetic particles. Moreover, in traffic-related PM, a SP behavior may occur as coating of MD particles and is originated by localized stress in the oxidized outer shell surrounding the unoxidized core of magnetite-like grains; thus it cannot be considered as a direct proxy for the overall content of ultrafine <30 nm particles (Sagnotti and Winkler, 2012).

This result can explain why morpho-functional traits as chlorophyll concentration (Chl_{SPAD}) or relative water content (RWC), which are mostly damaged by ultrafine particles able to penetrate inside the leaves through stomata, were not affected in our case (Rai et al., 2016). RWC was inside the range of good hydration for *Quercus* species (Salvatori et al., 2016) indicating that, in the conditions experienced in this study, PM deposited and accumulated on leaves is not a determinant factor in plant water status. Overall, it is not possible to exclude the presence of ultrafine SP particles, since they are more difficult to be recognized with standard room temperature magnetic measurements, for their intrinsically unstable magnetic properties.

The results of the current study reinforce the evidence that leaves are suitable indicators of the non-combustible fraction of PM, following what has been found by former studies (Winkler et al., 2020). Indeed, the hysteresis ratio values of the sampled leaves fall in the same cluster defined in other experimental activities carried out on lichens transplanted in Milan, *Q. ilex* leaves sampled in Rome, Italy, as well as in previous experimental campaigns, or PM filters and dust arising from fuel exhausts and brakes' emissions (Appendix E). To confirm this interpretation, we notice that the SIRM/χ values (5.3±1.0 kA/m) are compatible with those typical of the brake emissions (6.7±2.5 kA/m) and distinct from those typical for gasoline and diesel exhaust emissions (13.8±6.3 kA/m and 14.5±12.1 kA/m, respectively) as reviewed in Gonet and Maher, 2019.

On the other hand, vehicle brake wear was by far the most dominant source of airborne magnetite in the roadside environment of two sites in UK, being responsible for between ~68 and 85% of the total airborne magnetite content (Gonet et al., 2021), thus confirming that non-exhaust sources of vehicular traffic, notably brake abrasion, are the main driver of PM air pollution in urban contexts. In conformity to hysteresis properties and results from other studies, magnetic susceptibility is positively correlated with non-exhaustive traffic source tracers as Cu, Fe, Mo, Sb, Sn, Pb (Hofman et al., 2017). The mixed nature of PM metals detected on leaves underlined the role of vehicular traffic as one of the main sources of PM pollution in large cities (Amato et al., 2013). La, K, and Ce that are usually more related to road dust, constituted also by soil dust (Simonetti et al., 2018), increased from control to more polluted sites, suggesting that passing traffic facilitates resuspension of soil particles that had been deposited on roads (Hasheminassab et al., 2020).

PM impact on vegetation is often underestimated but can play a pivotal role in plant physiology through direct and indirect damages (Rai, 2016). Among morpho-functional traits, SLA did not show variations attributable to PM. However, control sites have higher sclerophyll degree (lower SLA values) due to inherent ecological conditions as solar radiation, supporting plants in counteracting the oxidative stress since lower SLA means higher responsiveness and high photosynthesis capacity per surface unit supporting efficient detoxification processes (Bussotti, 2008). On the other side this morpho-functional trait influence directly the biomonitoring activity of PM inasmuch as lower leaf area means less PM accumulation capacity (Sæbø et al., 2012). In our experiment, Chl_{SPAD} remained almost constant through the different sites, even in those with high PM

accumulation. Despite this result, photosystems functionality was affected by PM exposure decreasing as PM on leaves increased. We hypothesize that PM alters the optical properties of leaves reducing the incident photosynthetically active radiation (PAR) on the leaf surface, because of changes in the reflectance in the visible and short wave infrared radiation (Popek et al., 2018; Rai, 2016). RC/ABS that provides information about the first photochemical reactions in the antenna and on PSII acceptor side, highlights a decreasing amount of electrons flow. RC/ABS decreases because of several processes as photoinhibition, downregulation, or shading adaptation (Pavlík et al., 2012). When the light energy is not appropriately transferred to electron transport, the photosynthetic apparatus suffers an overexcitation and thus RC/ABS decreases. However, this down-regulation mechanism entails an increase of the energy dissipation as heat, DI_0/RC (Pollastrini et al., 2020; Salvatori et al., 2013), that we do not observe in our case study. Analyzing the changes within the constellation of parameters obtained from the JIP-test, shading adaptation seems the prevalent mechanism. PM accumulated on the adaxial surface absorbs and scatter light, and shading condition results in a physiological acclimation with an increase of the antenna size that can cause a decrease of RC/ABS via increasing of Chl to RC (Valladares and Niinemets, 2008). It is worth notice that TR_0/RC and ET_0/RC are directly correlated with χ, i.e. increased with the PM accumulation, meaning that as a compensatory mechanism, the decrease of the incoming electron flow implies an increase of trapping and electron transport flow beyond the QA^- per active RC. The trend of PI_{TOT}, that decrease in RdR, VS and QM sites, was connected to its component RC/ABS, but also to the decreased capacity to reduce the final electron acceptors beyond PSI (ΔV_{IP}) that is lower in the sites most exposed to PM. RC/ABS, PI_{TOT} and ΔV_{IP} are effective in discriminating sites in line with their low (CP, VA) or high (RdR, VS and QM) PM accumulation as showed by PCA (Fig. 5), whereas, the higher dispersion of MZ, VM and PP data, might be related to site-specific conditions that can affect photosystems functionality increasing the variability of physiological response (Medrano et al., 2009). In general, this data could be explained by a general increase of oxidative potential with PM accumulation on leaves. PM can generate oxidative stress depending on its chemical nature, since the heavy metals present in road-side PM can affect leaf pH, antioxidant activity or pigments content and the related functional processes (Rai, 2016 and references therein). The chemical elements present in PM, can induce the cellular generation of reactive oxygen species (Gao et al., 2020) and this PM capability can be evaluated through ascorbic acid assay, an effective approach to estimating the ecotoxicology of particles. As already demonstrated through PM sampled on filters, OP^{AA} values were strongly correlated with tracers of brake dust abrasion, confirming the high sensitivity of this assay towards non-emissive traffic contribution, even in the case of PM deposited on leaves (Moufarrej et al., 2020). Indeed, between OP^{AA} and χ there is a tight correlation confirming that also in leaves soluble Fe is strongly associated with ROS activity as found by Cheung et al., 2010 on filters.

Quercus ilex has been proven a tolerant species to moderate oxidative stress, able to respond to ROS production enhancing the antioxidant defense through different mechanisms (Fusaro et al., 2017b; Hasanuzzaman et al., 2020). The first enzymatic defense involves the activation of Super Oxide Dismutase (SOD) that consumes the redox potential used for reducing end acceptors of PSI and accordingly producing a ΔV_{IP} decrease even if the trapping capacity and electron transport rate increase per active reaction center. It is interesting to notice

that the elements that can have higher oxidative stress potential on vegetation, such as Cu, Fe, Mo, Pb (Bernardini et al., 2016) have not shown substantial differences in concentration between RdR, VS and QM, that anyway present different amount of total PM accumulated (χ = RdR < VS < QM). Thus, the variation of functional indicators relative to PSI seems to respond to the chemical species concentration, as for Al and Zn are double of what was measured in the other sites (Appendix D), and ΔV_{IP} and PI_{TOT} showed a higher correlation with OP^{AA} then χ. Beyond this general framework, established under the obtained results, the low performance of CP registered although the small PM accumulation, can depend on natural stress as sea spry and soil salinity that inherently insist on this control site in the winter period, as has been found in previous studies in that area (Fusaro et al., 2019; Mereu et al., 2009). Indeed, ChlF parameters in CP site highlight a general low performance of photosystems in processing energy incoming rather than a specific action of stress on PSII or PSI, highlighting chronic stress on photosystems functionality in that natural site.

5. Conclusions

In the present study, several morpho-functional traits were measured to find out the most effective indicators of PM impairment on plant functionality. Among the analysed morpho-functional traits, photosystem functionality, measured by prompt fluorescence of chlorophyll, is the most suitable to detect the PM effects. In our case study, PM does not produce an alteration of plant water status or structural damage to pigments, whereas ChlF highlights two mechanisms of action. On the PSII side, the shading effect is prevalent on *Q. ilex*, and RC/ABS can be used as a good indicator of PM accumulated on the leaf surface. On PSI side, the concentration of chemical species might drive a slight impact on PSI functionality and thus on carbon assimilation, since the decrease in the relative contribution of electron flow to the PSI end acceptors (ΔV_{IP}) is present. This result can be linked to oxidative stress imposed by PM and detected by an ascorbic acid trial (OP). Correlation between indicators obtained from different approaches pointed out that PI_{TOT} and DI_0/RC can respond also to other oxidative stressors than PM since they are less or not correlated at all to the magnetic susceptibility and elemental content concentration as well.

The magnetic susceptibility measured on *Q. ilex* leaves is confirmed to be a robust proxy for the bioaccumulation of trace metals, since its tight positive correlation with chemical species detected on leaves. Magnetic and chemical analyses, in conformity with previous studies in the urban area, highlighted that non-exhaust traffic emission (i.e.brake abrasion) are the main sources of the magnetic and metallic fraction of PM bioaccumulated on leaves in the proximity of roads. Leaves provide useful information about PM accumulation that can be uncoupled to PM air concentration because the deposition process on leaves surface can be influenced by green infrastructures typologies and street aerodynamic features. Leaves frame a long-term exposure to PM, the more appropriate dimension to evaluate its effects on urban vegetation functionality and the negative feedback on the provisioning of ecosystem services.

Experimental activities should be promoted on species that are more sensitive than *Q. ilex* that shows an adaptive response to PM stress for low to intermediate accumulation, having functional damage only for high PM on leaves. If this species is highly suggested to stakeholders as a key element of green infrastructure

finalized to PM removal due to its high bioaccumulation potential and functional tolerance, it is not suitable for monitoring variation of functionality linked to the effects of low air quality in our city.
A multidisciplinary biomonitoring activity comprehensive of a large number of urban sites should be promoted to detect emission sources and distribution patterns of airborne persistent pollutants when it is impossible to apply a high-density instrumental monitoring of PM.

Author contributions: Lina Fusaro: Conceptualization, Methodology, Investigation, Formal analysis, Data curation, Visualization, Writing - original draft, Writing - review & editing. Elisabetta Salvatori: Conceptualization, Methodology, Investigation, Visualization, Writing - original draft, Writing - review & editing. Aldo Winkler: Methodology, Investigation, Writing - original draft, Writing - review & editing. Maria Agostina Frezzini: Investigation, Resources, Writing - review & editing. Elena De Santis: Investigation, Resources. Leonardo Sagnotti: Methodology, Writing - review & editing, Supervision, Funding acquisition. Silvia Canepari: Writing - review & editing, Supervision, Funding acquisition. Fausto Manes: Conceptualization, Methodology, Writing - review & editing, Supervision, Funding acquisition.

Supplementary Material

Experimental site	Reference air quality monitoring station	Station Type	Season	PM_{10} Mean ± st. dev	PM_{10} Max - Min	n
CP	Castel di Guido	Rural	Spring	20 ± 7.7a	37 - 6	89
VA	Villa Ada	Urban Background		23 ± 7.6b	52 - 11	88
MZ	Cipro	Urban Background		23 ± 8.2b	56 - 9	91
RdR	Magna Grecia	Urban Traffic		27 ± 9.1c	66 - 13	91
QM	Fermi	Urban Traffic		29 ± 10c	65 - 14	85
CP	Castel di Guido	Rural	Summer	20 ± 5.9a	48 - 8	95
VA	Villa Ada	Urban Background		20 ± 5.4a	34 - 9	49
MZ	Cipro	Urban Background		20 ± 5.6a	37 - 8	95
RdR	Magna Grecia	Urban Traffic		21 ± 5.1a	33 - 11	95

QM	Fermi	Urban Traffic		26 ± 7.1b	48 - 11	87
CP	Castel di Guido	Rural		17 ± 6.1a	39 - 9	88
VA	Villa Ada	Urban Background		n.a	n.a.	n.a.
MZ	Cipro	Urban Background	Autumn	25 ± 9.7b	62 - 4	89
RdR	Magna Grecia	Urban Traffic		24 ± 9.9b	48 - 8	89
QM	Fermi	Urban Traffic		35 ± 13c	72 -12	89
CP	Castel di Guido	Rural		17 ± 8.2a	31 - 9	72
VA	Villa Ada	Urban Background		27 ± 11b	59 - 8	63
MZ	Cipro	Urban Background	Winter	29 ± 13b	63 - 9	74
RdR	Magna Grecia	Urban Traffic		32 ± 12c	78 - 10	73
QM	Fermi	Urban Traffic		31 ± 9.9c	51 -9	74

Appendix A. Seasonal PM_{10} concentration (µg m^{-3}) at the air quality monitoring stations (ARPA Lazio) within the metropolitan city of Rome. The monitoring stations were selected in different urban context: rural, Castel di Guido, that it is not close to any of our experimental sites, but can give indications of the PM concentration in the peri-urban context (i.e. Castelporziano site); urban background, Villa Ada, inside the historical Villa nearby VA experimental sites, and Cipro, located in a residential neighborhood nearby MZ experimental site; urban traffic, Magna Grecia and Fermi nearby RdR and QM experimental sites, respectively. The study sites close to the monitoring stations were reported in the table (experimental site), and their spatial collocation is showed in Appendix B. Daily values were grouped seasonally and mean, maximum and minimum values are reported. Values express mean ± standard deviation and those not accompanied by the same letters are significantly different at $p<0.05$. n, indicates the number of measurements used to calculate seasonal mean and st. dev.

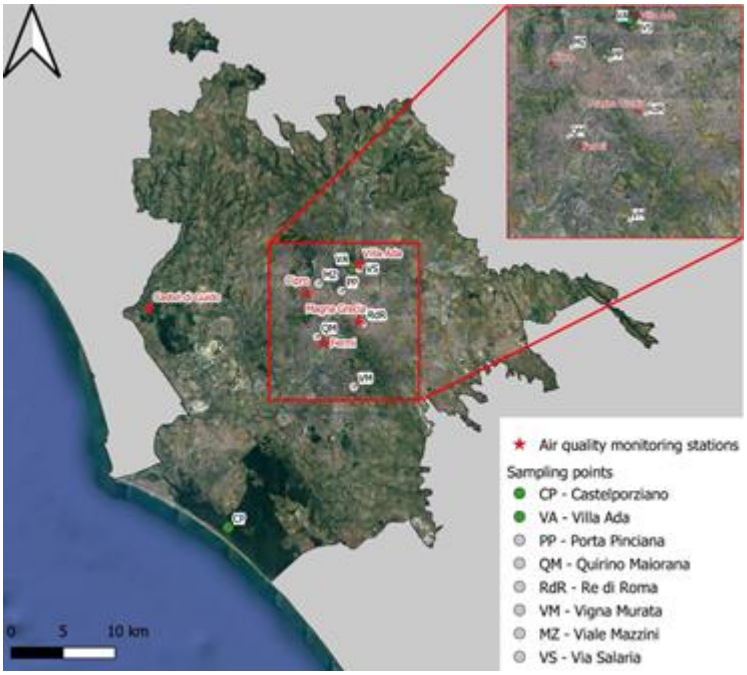

Appendix B. Spatial distribution of the air quality monitoring stations of Regional Environmental Protection Agency monitoring stations (ARPA Lazio) and experimental sites considered in the study.

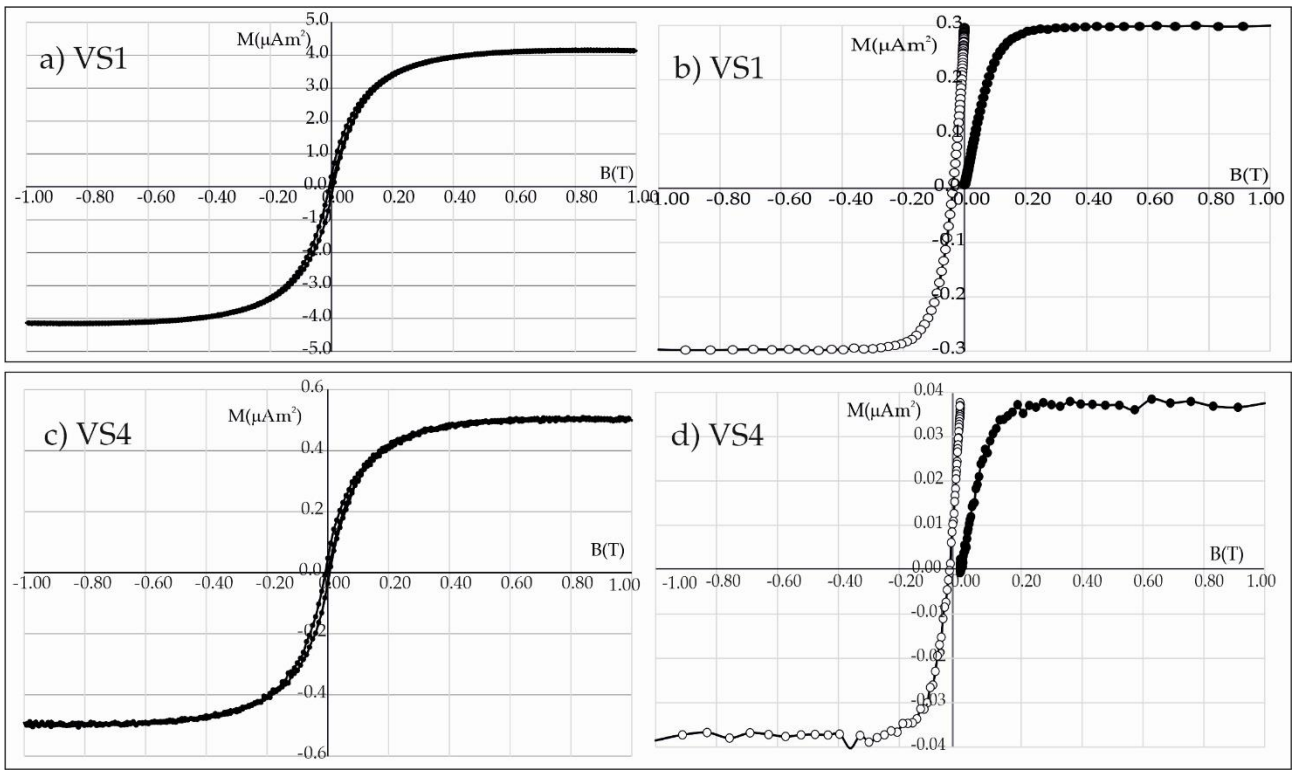

Appendix C. Hysteresis loops, corrected for high-field linear trend (a, c), isothermal remanent magnetization and backfield application (b, d) for samples VS1 and VS4, the most and the least intense of the site, respectively. Original data, not divided by mass.

	UoM	CP	VA	MZ	PP	VM	RdR	VS	QM
		Mean ± SD	Mean ± SD	Mean ± SD	Mean ± SD	Mean ± SD	Mean ± SD	Mean ± SD	Mean ± SD
Al	ng/g	638 ± 104	497 ± 78	923 ± 236	713 ± 158	1119 ± 605	2262 ± 431	2971 ± 1792	1825 ± 240
As	ng/g	< LOD	< LOD	< LOD	< LOD	< LOD	< LOD	< LOD	< LOD
B	ng/g	< LOD	388 ± 154	513 ± 400	385 ± 220	204 ± 108	1689 ± 857	914 ± 354	1997 ± 91
Ba	ng/g	< LOD	252 ± 91	212 ± 77	257 ± 108	543 ± 342	731 ± 134	670 ± 284	686 ± 63
Be	ng/g	< LOD	0.15 ± 0.11	0.22 ± 0.095	0.27 ± 0.11	0.42 ± 0.17	0.81 ± 0.32	1.1 ± 0.77	0.79 ± 0.15
Cd	ng/g	< LOD	< LOD	< LOD	< LOD	< LOD	< LOD	< LOD	< LOD
Co	ng/g	2.5 ± 0.87	2.3 ± 0.28	3.3 ± 1.2	3.6 ± 0.38	3.9 ± 2.1	6.6 ± 1.9	7.9 ± 3.7	8.6 ± 0.53
Cr	ng/g	< LOD	< LOD	< LOD	< LOD	< LOD	43 ± 5.8	< LOD	< LOD
Cs	ng/g	0.69 ± 0.12	3.4 ± 0.83	0.69 ± 0.27	0.97 ± 0.24	0.62 ± 0.26	1.4 ± 0.37	1.5 ± 0.59	1.3 ± 0.21
Mn	ng/g	3274 ± 714	3706 ± 1004	429 ± 124	763 ± 188	1063 ± 511	1026 ± 236	1748 ± 793	1099 ± 66
Ni	ng/g	< LOD	< LOD	< LOD	< LOD	< LOD	< LOD	< LOD	< LOD
Rb	ng/g	386 ± 88	1032 ± 162	246 ± 82	516 ± 151	400 ± 155	830 ± 170	693 ± 346	398 ± 73
Se	ng/g	< LOD	< LOD	< LOD	< LOD	< LOD	< LOD	< LOD	< LOD
Sr	ng/g	180 ± 37	260 ± 21	406 ± 94	383 ± 93	635 ± 319	649 ± 120	997 ± 390	1100 ± 114
Ti	ng/g	9.4 ± 4.3	13 ± 2.3	25 ± 11	21 ± 6.5	26 ± 15	57 ± 35	77 ± 46	47 ± 10
Tl	ng/g	0.74 ± 0.25	0.97 ± 0.32	0.46 ± 0.16	1.8 ± 0.56	0.56 ± 0.12	0.69 ± 0.21	2.2 ± 0.45	3.3 ± 0.83
V	ng/g	7.7 ± 1.9	7.7 ± 1.1	12 ± 4.2	9.9 ± 0.18	14 ± 7	23 ± 4	22 ± 6	26 ± 1.6
W	ng/g	< LOD	< LOD	1.5 ± 0.41	1.3 ± 0.091	1.7 ± 0.041	2.9 ± 0.24	3.2 ± 0.99	2.8 ± 0.13
Zn	ng/g	< LOD	< LOD	597 ± 38	1024 ± 321	713 ± 416	1599 ± 305	1667 ± 703	1671 ± 117
Zr	ng/g	2.4 ± 0.47	2.4 ± 0.23	5.9 ± 1.2	5.2 ± 1.3	10 ± 2.5	13 ± 2.3	19 ± 9	14 ± 1.6

Appendix D. Element concentrations (ng/g) detected in the water-soluble fraction of PM deposited on *Quercus ilex* L. leaves at the 8 experimental sites. Further details about limits of detection (LODs) are reported below.

	UoM	LODs
Al	ng/g	53
As	ng/g	34
B	ng/g	38
Ba	ng/g	296
Be	ng/g	0.049
Cd	ng/g	5.5
Ce	ng/g	0.39
Co	ng/g	0.69
Cr	ng/g	32
Cs	ng/g	0.17
Cu	ng/g	2.5
Fe	ng/g	273
K	ng/g	1269
La	ng/g	0.15
Mn	ng/g	4.6
Mo	ng/g	1.3
Ni	ng/g	74
Pb	ng/g	0.81
Rb	ng/g	13
Sb	ng/g	0.41
Se	ng/g	25
Sn	ng/g	0.52
Sr	ng/g	0.68
Ti	ng/g	8.5
Tl	ng/g	0.099
V	ng/g	1.8
W	ng/g	0.78
Zn	ng/g	464
Zr	ng/g	0.037

Limits of detection (LODs) of the concentrations of elements detected in the water-soluble fraction of PM deposited on *Quercus ilex* L. leaves, set at 3 times the standard deviation of 10 replicate blank determinations.

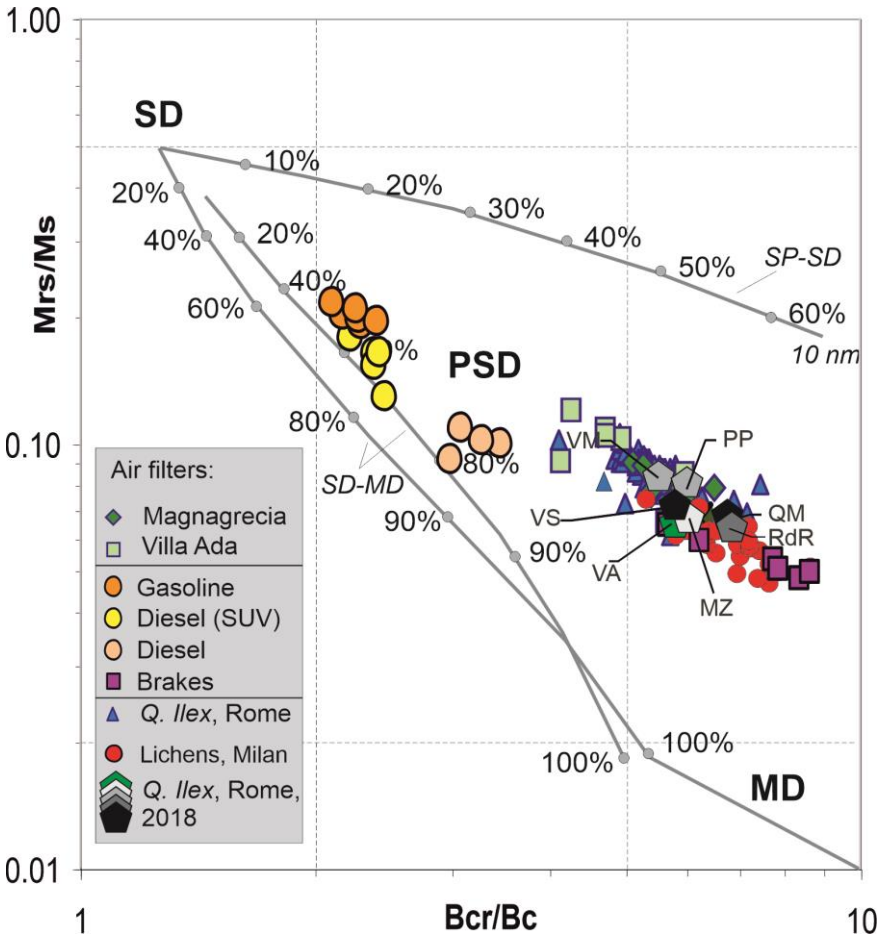

Appendix E. Bilogarithmic Day plot of the hysteresis ratios Mrs/Ms vs. Bcr/Bc for the *Quercus ilex* L. (pentagons) compared with data presented in literature. In particular: lichens transplanted in Milan (Winkler et al., 2020), *Quercus ilex* L. from high traffic areas of Rome (green triangles) (Szönyi et al., 2007), air filters from monitoring stations in Rome (green diamonds and squares) (Sagnotti et al., 2006), different kinds of fuel exhausts (orange, yellow and pink dots) and brake dusts (purple squares) (Sagnotti et al., 2009). The SD (single domain), PSD (pseudo-single domain) and MD (multidomain) fields and the theorethical mixing trends for SD-MD and SP-SD pure magnetite particles (SP, superparamagnetic) are taken from Dunlop 2002a, b. Modified after Winkler et al., 2020.

References

Alessio, M., Anselmi, S., Conforto, L., Improta, S., Manes, F., Manfra, L., 2002. Radiocarbon as a biomarker of urban pollution in leaves of evergreen species sampled in Rome and in rural areas (Lazio—Central Italy). Atmospheric Environment 36, 5405–5416. https://doi.org/10.1016/S1352-2310(02)00409-0

Alfani, A., Maisto, G., Vittoria Prati, M., Baldantoni, D., 2001. Leaves of Quercus ilex L. as biomonitors of PAHs in the air of Naples (Italy). Atmospheric Environment 35, 3553–3559. https://doi.org/10.1016/S1352-2310(01)00087-5

Amato, F., Schaap, M., Reche, C., Querol, X., 2013. Road Traffic: A Major Source of Particulate Matter in Europe, in: Viana, M. (Ed.), Urban Air Quality in Europe, The Handbook of Environmental Chemistry. Springer, Berlin, Heidelberg, pp. 165–193. https://doi.org/10.1007/698_2012_211

Bates, J.T., Fang, T., Verma, V., Zeng, L., Weber, R.J., Tolbert, P.E., Abrams, J.Y., Sarnat, S.E., Klein, M., Mulholland, J.A., Russell, A.G., 2019. Review of Acellular Assays of Ambient Particulate Matter Oxidative Potential: Methods and Relationships with Composition, Sources, and Health Effects. Environ. Sci. Technol. 53, 4003–4019. https://doi.org/10.1021/acs.est.8b03430

Bernardini, A., Salvatori, E., Guerrini, V., Fusaro, L., Canepari, S., Manes, F., 2016. Effects of high Zn and Pb concentrations on Phragmites australis (Cav.) Trin. Ex. Steudel: Photosynthetic performance and metal accumulation capacity under controlled conditions. International Journal of Phytoremediation 18, 16–24. https://doi.org/10.1080/15226514.2015.1058327

Blanusa, T., Fantozzi, F., Monaci, F., Bargagli, R., 2015. Leaf trapping and retention of particles by holm oak and other common tree species in Mediterranean urban environments. Urban Forestry & Urban Greening 14, 1095–1101. https://doi.org/10.1016/j.ufug.2015.10.004

Bolund, P., Hunhammar, S., 1999. Ecosystem services in urban areas. Ecological Economics 29, 293–301. https://doi.org/10.1016/S0921-8009(99)00013-0

Bussotti, F., 2008. Functional leaf traits, plant communities and acclimation processes in relation to oxidative stress in trees: a critical overview. Global Change Biology 14, 2727–2739. https://doi.org/10.1111/j.1365-2486.2008.01677.x

Bussotti, F., Pollastrini, M., 2015. Evaluation of leaf features in forest trees: Methods, techniques, obtainable information and limits. Ecological Indicators 52, 219–230. https://doi.org/10.1016/j.ecolind.2014.12.010

Campbell, S.J., Utinger, B., Lienhard, D.M., Paulson, S.E., Shen, J., Griffiths, P.T., Stell, A.C., Kalberer, M., 2019. Development of a Physiologically Relevant Online Chemical Assay To Quantify Aerosol Oxidative Potential. Anal. Chem. 91, 13088–13095. https://doi.org/10.1021/acs.analchem.9b03282

Canepari, S., Cardarelli, E., Perrino, C., Catrambone, M., Pietrodangelo, A., Strincone, M., 2006. Two-stage chemical fractionation method for the analysis of elements and non-volatile inorganic ions in PM10 samples: Application to ambient samples collected in Rome (Italy). Atmospheric Environment 40, 7908–7923. https://doi.org/10.1016/j.atmosenv.2006.07.005

Chaparro, Marcos A. E., Chaparro, Mauro A. E., Castañeda-Miranda, A.G., Marié, D.C., Gargiulo, J.D., Lavornia, J.M., Natal, M., Böhnel, H.N., 2020. Fine air pollution particles trapped by street tree barks: In situ magnetic biomonitoring. Environmental Pollution 266, 115229. https://doi.org/10.1016/j.envpol.2020.115229

Cheung, K.L., Ntziachristos, L., Tzamkiozis, T., Schauer, J.J., Samaras, Z., Moore, K.F., Sioutas, C., 2010. Emissions of Particulate Trace Elements, Metals and Organic Species from Gasoline, Diesel, and Biodiesel Passenger Vehicles and Their Relation to Oxidative Potential. Aerosol Science and Technology 44, 500–513. https://doi.org/10.1080/02786821003758294

Comunian, S., Dongo, D., Milani, C., Palestini, P., 2020. Air Pollution and COVID-19: The Role of Particulate Matter in the Spread and Increase of COVID-19's Morbidity and Mortality. International Journal of Environmental Research and Public Health 17, 4487. https://doi.org/10.3390/ijerph17124487

Conticini, E., Frediani, B., Caro, D., 2020. Can atmospheric pollution be considered a co-factor in extremely high level of SARS-CoV-2 lethality in Northern Italy? Environmental Pollution 261, 114465. https://doi.org/10.1016/j.envpol.2020.114465

Costabile, F., Gualtieri, M., Ancona, C., Canepari, S., Decesari, S., 2020. Ultrafine Particle Features Associated with Pro-Inflammatory and Oxidative Responses: Implications for Health Studies. Atmosphere 11, 414. https://doi.org/10.3390/atmos11040414

Day, R., Fuller, M., Schmidt, V.A., 1977. Hysteresis properties of titanomagnetites: Grain-size and compositional dependence. Physics of the Earth and Planetary Interiors 13, 260–267. https://doi.org/10.1016/0031-9201(77)90108-X

Desotgiu, R., Cascio, C., Pollastrini, M., Gerosa, G., Marzuoli, R., Bussotti, F., 2012. Short and long term photosynthetic adjustments in sun and shade leaves of Fagus sylvatica L., investigated by fluorescence transient (FT) analysis. Plant Biosystems - An International Journal Dealing with all Aspects of Plant Biology 146, 206–216. https://doi.org/10.1080/11263504.2012.705350

Dunlop, D.J., 2002a. Theory and application of the Day plot (Mrs /Ms versus Hcr /Hc) 1. Theoretical curves and tests using titanomagnetite data. Journal of Geophysical Research 107, 2056. https://doi.org/10.1029/2001JB000486

Dunlop, D.J., 2002b. Theory and application of the Day plot (Mrs/Ms versus Hcr/Hc) 2. Application to data for rocks, sediments, and soils. Journal of Geophysical Research (Solid Earth) 107, 2057. https://doi.org/10.1029/2001JB000487

Fattorini, D., Regoli, F., 2020. Role of the chronic air pollution levels in the Covid-19 outbreak risk in Italy. Environmental Pollution 264, 114732. https://doi.org/10.1016/j.envpol.2020.114732

Ficociello, G., Inverni, A., Massimi, L., Buccini, G., Canepari, S., Uccelletti, D., 2020. Assessment of the effects of atmospheric pollutants using the animal model Caenorhabditis elegans. Environmental Research 191, 110209. https://doi.org/10.1016/j.envres.2020.110209

Flanders, P.J., 1994. Collection, measurement, and analysis of airborne magnetic particulates from pollution in the environment (invited). Journal of Applied Physics 75, 5931–5936. https://doi.org/10.1063/1.355518

Frezzini, M.A., Castellani, F., De Francesco, N., Ristorini, M., Canepari, S., 2019. Application of DPPH Assay for Assessment of Particulate Matter Reducing Properties. Atmosphere 10, 816. https://doi.org/10.3390/atmos10120816

Fusaro, L., Marando, F., Sebastiani, A., Capotorti, G., Blasi, C., Copiz, R., Congedo, L., Munafò, M., Ciancarella, L., Manes, F., 2017a. Mapping and Assessment of PM10 and O3 Removal by Woody Vegetation at Urban and Regional Level. Remote Sensing 9, 791. https://doi.org/10.3390/rs9080791

Fusaro, L., Mereu, S., Salvatori, E., Spano, D., Manes, F., 2019. DROUGHT STRESS AFFECTS TEMPERATURE RESPONSE OF LEAF DARK RESPIRATION IN MEDITERRANEAN COASTAL MAQUIS SPECIES. Annali di Botanica 9, 39–52. https://doi.org/10.13133/2239-3129/14621

Fusaro, L., Palma, A., Salvatori, E., Basile, A., Maresca, V., Karam, E.A., Manes, F., 2017b. Functional indicators of response mechanisms to nitrogen deposition, ozone, and their interaction in two Mediterranean tree species. PLOS ONE 12, e0185836. https://doi.org/10.1371/journal.pone.0185836

Fusaro, Lina, Salvatori, E., Mereu, S., Manes, F., 2019. Photosynthetic traits as indicators for phenotyping urban and peri-urban forests: A case study in the metropolitan city of Rome. Ecological Indicators 103, 301–311. https://doi.org/10.1016/j.ecolind.2019.04.033

Georgeaud, V.M., Rochette, P., Ambrosi, J.P., Vandamme, D., Williamson, D., 1997. Relationship between heavy metals and magnetic properties in a large polluted catchment: The Etang de Berre (south of France). Physics and Chemistry of the Earth 22, 211–214. https://doi.org/10.1016/S0079-1946(97)00105-5

Gonet, T., Maher, B.A., 2019. Airborne, Vehicle-Derived Fe-Bearing Nanoparticles in the Urban Environment: A Review. Environ. Sci. Technol. 53, 9970–9991. https://doi.org/10.1021/acs.est.9b01505

Gonet, T., Maher, B.A., Kukutschová, J., 2021. Source apportionment of magnetite particles in roadside airborne particulate matter. Science of The Total Environment 752, 141828. https://doi.org/10.1016/j.scitotenv.2020.141828

Grote, R., Samson, R., Alonso, R., Amorim, J.H., Cariñanos, P., Churkina, G., Fares, S., Thiec, D.L., Niinemets, Ü., Mikkelsen, T.N., Paoletti, E., Tiwary, A., Calfapietra, C., 2016. Functional traits of urban trees: air pollution mitigation potential. Frontiers in Ecology and the Environment 14, 543–550. https://doi.org/10.1002/fee.1426

Han, D., Shen, H., Duan, W., Chen, L., 2020. A review on particulate matter removal capacity by urban forests at different scales. Urban Forestry & Urban Greening 48, 126565. https://doi.org/10.1016/j.ufug.2019.126565

Hasanuzzaman, M., Bhuyan, M.H.M.B., Zulfiqar, F., Raza, A., Mohsin, S.M., Mahmud, J.A., Fujita, M., Fotopoulos, V., 2020. Reactive Oxygen Species and Antioxidant Defense in Plants under Abiotic Stress: Revisiting the Crucial Role of a Universal Defense Regulator. Antioxidants 9, 681. https://doi.org/10.3390/antiox9080681

Hasheminassab, S., Sowlat, M.H., Pakbin, P., Katzenstein, A., Low, J., Polidori, A., 2020. High time-resolution and time-integrated measurements of particulate metals and elements in an environmental justice community within the Los Angeles Basin: Spatio-temporal trends and source apportionment. Atmospheric Environment: X 7, 100089. https://doi.org/10.1016/j.aeaoa.2020.100089

Hoffmann, V., Knab, M., Appel, E., 1999. Magnetic susceptibility mapping of roadside pollution. Journal of Geochemical Exploration 66, 313–326. https://doi.org/10.1016/S0375-6742(99)00014-X

Hofman, J., Maher, B.A., Muxworthy, A.R., Wuyts, K., Castanheiro, A., Samson, R., 2017. Biomagnetic Monitoring of Atmospheric Pollution: A Review of Magnetic Signatures from Biological Sensors. Environ. Sci. Technol. 51, 6648–6664. https://doi.org/10.1021/acs.est.7b00832

Hunt, A., Jones, J., Oldfield, F., 1984. Magnetic measurements and heavy metals in atmospheric particulates of anthropogenic origin. Science of The Total Environment, Highway Pollution 33, 129–139. https://doi.org/10.1016/0048-9697(84)90387-5

Janhäll, S., 2015. Review on urban vegetation and particle air pollution – Deposition and dispersion. Atmospheric Environment 105, 130–137. https://doi.org/10.1016/j.atmosenv.2015.01.052

Jordanova, D., Hoffmann, V., Fehr, K.T., 2004. Mineral magnetic characterization of anthropogenic magnetic phases in the Danube river sediments (Bulgarian part). Earth and Planetary Science Letters 221, 71–89. https://doi.org/10.1016/S0012-821X(04)00074-3

Kapper, K.L., Bautista, F., Goguitchaishvili, A., Bógalo, M.F., Cejudo-Ruíz, R., Cervantes Solano, M., 2020. The use and misuse of magnetic methods to monitor environmental pollution in urban areas - Uso y abuso de métodos magnéticos en el monitoreo de contaminación ambiental en áreas urbanas. Boletín de la Sociedad Geológica Mexicana 72, 1–44.

Łowicki, D., 2019. Landscape pattern as an indicator of urban air pollution of particulate matter in Poland. Ecological Indicators 97, 17–24. https://doi.org/10.1016/j.ecolind.2018.09.050

Manes, F., Marando, F., Capotorti, G., Blasi, C., Salvatori, E., Fusaro, L., Ciancarella, L., Mircea, M., Marchetti, M., Chirici, G., Munafò, M., 2016. Regulating Ecosystem Services of forests in ten Italian Metropolitan Cities: Air quality improvement by PM10 and O3 removal. Ecological Indicators 67, 425–440. https://doi.org/10.1016/j.ecolind.2016.03.009

Massimi, L., Ristorini, M., Astolfi, M.L., Perrino, C., Canepari, S., 2020. High resolution spatial mapping of element concentrations in PM10: A powerful tool for localization of emission sources. Atmospheric Research 244, 105060. https://doi.org/10.1016/j.atmosres.2020.105060

Medrano, H., Flexas, J., Galmés, J., 2009. Variability in water use efficiency at the leaf level among Mediterranean plants with different growth forms. Plant Soil 317, 17–29. https://doi.org/10.1007/s11104-008-9785-z

Mei, D., Wen, M., Xu, X., Zhu, Y., Xing, F., 2018. The influence of wind speed on airflow and fine particle transport within different building layouts of an industrial city. Journal of the Air & Waste Management Association 68, 1038–1050. https://doi.org/10.1080/10962247.2018.1465487

Mereu, S., Salvatori, E., Fusaro, L., Gerosa, G., Muys, B., Manes, F., 2009. A whole plant approach to evaluate the water use of mediterranean maquis species in a coastal dune ecosystem. Biogeosciences Discuss. 6, 1713–1746. https://doi.org/10.5194/bgd-6-1713-2009

Moreno, E., Sagnotti, L., Dinarès-Turell, J., Winkler, A., Cascella, A., 2003. Biomonitoring of traffic air pollution in Rome using magnetic properties of tree leaves. Atmospheric Environment 37, 2967–2977. https://doi.org/10.1016/S1352-2310(03)00244-9

Moufarrej, L., Courcot, D., Ledoux, F., 2020. Assessment of the PM2.5 oxidative potential in a coastal industrial city in Northern France: Relationships with chemical composition, local emissions and long range sources. Science of The Total Environment 748, 141448. https://doi.org/10.1016/j.scitotenv.2020.141448

Muhammad, S., Wuyts, K., Samson, R., 2020. Immobilized atmospheric particulate matter on leaves of 96 urban plant species. Environ Sci Pollut Res 27, 36920–36938. https://doi.org/10.1007/s11356-020-09246-6

Muhammad, S., Wuyts, K., Samson, R., 2019. Atmospheric net particle accumulation on 96 plant species with contrasting morphological and anatomical leaf characteristics in a common garden experiment. Atmospheric Environment 202, 328–344. https://doi.org/10.1016/j.atmosenv.2019.01.015

Mukherjee, A., Agrawal, M., 2018. Use of GLM approach to assess the responses of tropical trees to urban air pollution in relation to leaf functional traits and tree characteristics. Ecotoxicology and Environmental Safety 152, 42–54. https://doi.org/10.1016/j.ecoenv.2018.01.038

Norouzi, S., Khademi, H., Faz Cano, A., Acosta, J.A., 2015. Using plane tree leaves for biomonitoring of dust borne heavy metals: A case study from Isfahan, Central Iran. Ecological Indicators 57, 64–73. https://doi.org/10.1016/j.ecolind.2015.04.011

Nowak, D.J., Crane, D.E., Stevens, J.C., 2006. Air pollution removal by urban trees and shrubs in the United States. Urban Forestry & Urban Greening 4, 115–123. https://doi.org/10.1016/j.ufug.2006.01.007

Orioli Riccardo, Antonucci Chiara, Scortichini Matteo, Cerza Francesco, Marando Federica, Ancona Carla, Manes Fausto, Davoli Marina, Michelozzi Paola, Forastiere Francesco, Cesaroni Giulia, n.d. Exposure to Residential Greenness as a Predictor of Cause-Specific Mortality and Stroke Incidence in the Rome Longitudinal Study. Environmental Health Perspectives 127, 027002. https://doi.org/10.1289/EHP2854

Pavlík, M., Pavlíková, D., Zemanová, V., Hnilička, F., Urbanová, V., Száková, J., 2012. Trace elements present in airborne particulate matter—Stressors of plant metabolism. Ecotoxicology and Environmental Safety 79, 101–107. https://doi.org/10.1016/j.ecoenv.2011.12.009

Piacentini, D., Falasca, G., Canepari, S., Massimi, L., 2019. Potential of PM-selected components to induce oxidative stress and root system alteration in a plant model organism. Environment International 132, 105094. https://doi.org/10.1016/j.envint.2019.105094

Pietrogrande, M.C., Russo, M., Zagatti, E., 2019. Review of PM Oxidative Potential Measured with Acellular Assays in Urban and Rural Sites across Italy. Atmosphere 10, 626. https://doi.org/10.3390/atmos10100626

Pollastrini, M., Salvatori, E., Fusaro, L., Manes, F., Marzuoli, R., Gerosa, G., Brüggemann, W., Strasser, R.J., Bussotti, F., 2020. Selection of tree species for forests under climate change: is PSI functioning a better

predictor for net photosynthesis and growth than PSII? Tree Physiology 40, 1561–1571. https://doi.org/10.1093/treephys/tpaa084

Popek, R., Przybysz, A., Gawrońska, H., Klamkowski, K., Gawroński, S.W., 2018. Impact of particulate matter accumulation on the photosynthetic apparatus of roadside woody plants growing in the urban conditions. Ecotoxicology and Environmental Safety 163, 56–62. https://doi.org/10.1016/j.ecoenv.2018.07.051

Przybysz, A., Nersisyan, G., Gawroński, S.W., 2019. Removal of particulate matter and trace elements from ambient air by urban greenery in the winter season. Environmental Science and Pollution Research 26, 473–482.

Qin, H., Hong, B., Huang, B., Cui, X., Zhang, T., 2020. How dynamic growth of avenue trees affects particulate matter dispersion: CFD simulations in street canyons. Sustainable Cities and Society 61.

Rai, P.K., 2016. Impacts of particulate matter pollution on plants: Implications for environmental biomonitoring. Ecotoxicology and Environmental Safety 129, 120–136. https://doi.org/10.1016/j.ecoenv.2016.03.012

Sæbø, A., Popek, R., Nawrot, B., Hanslin, H.M., Gawronska, H., Gawronski, S.W., 2012. Plant species differences in particulate matter accumulation on leaf surfaces. Science of The Total Environment 427–428, 347–354. https://doi.org/10.1016/j.scitotenv.2012.03.084

Sagnotti, L., Taddeucci, J., Winkler, A., Cavallo, A., 2009. Compositional, morphological, and hysteresis characterization of magnetic airborne particulate matter in Rome, Italy. Geochemistry, Geophysics, Geosystems 10. https://doi.org/10.1029/2009GC002563

Sagnotti, L., Winkler, A., 2012. On the magnetic characterization and quantification of the superparamagnetic fraction of traffic-related urban airborne PM in Rome, Italy. Atmospheric Environment 59, 131–140. https://doi.org/10.1016/j.atmosenv.2012.04.058

Salvatori, E., Fusaro, L., Manes, F., 2016. CHLOROPHYLL FLUORESCENCE FOR PHENOTYPING DROUGHT-STRESSED TREES IN A MIXED DECIDUOUS FOREST. Annali di Botanica 6, 39–49. https://doi.org/10.4462/annbotrm-13263

Salvatori, E., Fusaro, L., Mereu, S., Bernardini, A., Puppi, G., Manes, F., 2013. Different O3 response of sensitive and resistant snap bean genotypes (Phaseolus vulgaris L.): The key role of growth stage, stomatal conductance, and PSI activity. Environmental and Experimental Botany 87, 79–91. https://doi.org/10.1016/j.envexpbot.2012.09.008

Sanità di Toppi, Luigi, Sanità di Toppi, Lorenzo, Bellini, E., 2020. Novel Coronavirus: How Atmospheric Particulate Affects Our Environment and Health. Challenges 11, 6. https://doi.org/10.3390/challe11010006

Sebastiani, A., Marando, F., Manes, F., 2021. Mismatch of regulating ecosystem services for sustainable urban planning: PM10 removal and urban heat island effect mitigation in the municipality of Rome (Italy). Urban Forestry & Urban Greening 57, 126938. https://doi.org/10.1016/j.ufug.2020.126938

Setti, L., Passarini, F., De Gennaro, G., Barbieri, P., Perrone, M.G., Borelli, M., Palmisani, J., Di Gilio, A., Torboli, V., Fontana, F., Clemente, L., Pallavicini, A., Ruscio, M., Piscitelli, P., Miani, A., 2020. SARS-Cov-2RNA found on particulate matter of Bergamo in Northern Italy: First evidence. Environmental Research 188, 109754. https://doi.org/10.1016/j.envres.2020.109754

Sgrigna, G., Sæbø, A., Gawronski, S., Popek, R., Calfapietra, C., 2015. Particulate Matter deposition on Quercus ilex leaves in an industrial city of central Italy. Environmental Pollution 197, 187–194. https://doi.org/10.1016/j.envpol.2014.11.030

Simonetti, G., Conte, E., Perrino, C., Canepari, S., 2018. Oxidative potential of size-segregated PM in an urban and an industrial area of Italy. Atmospheric Environment 187, 292–300. https://doi.org/10.1016/j.atmosenv.2018.05.051

Stevens, C.J., Bell, J.N.B., Brimblecombe, P., Clark, C.M., Dise, N.B., Fowler, D., Lovett, G.M., Wolseley, P.A., 2020. The impact of air pollution on terrestrial managed and natural vegetation. Philosophical Transactions of the Royal Society A: Mathematical, Physical and Engineering Sciences 378, 20190317. https://doi.org/10.1098/rsta.2019.0317

Strasser, R.J., Tsimilli-Michael, M., Qiang, S., Goltsev, V., 2010. Simultaneous in vivo recording of prompt and delayed fluorescence and 820-nm reflection changes during drying and after rehydration of the resurrection plant Haberlea rhodopensis. Biochimica et Biophysica Acta (BBA) - Bioenergetics, 16th European Bioenergetics Conference 2010 1797, 1313–1326. https://doi.org/10.1016/j.bbabio.2010.03.008

Szönyi, M., Sagnotti, L., Hirt, A.M., 2008. A refined biomonitoring study of airborne particulate matter pollution in Rome, with magnetic measurements on Quercus Ilex tree leaves. Geophysical Journal International 173, 127–141. https://doi.org/10.1111/j.1365-246X.2008.03715.x

Szönyi, M., Sagnotti, L., Hirt, A.M., 2007. On leaf magnetic homogeneity in particulate matter biomonitoring studies. Geophysical Research Letters 34. https://doi.org/10.1029/2006GL029076

Tung, N.T., Cheng, P.-C., Chi, K.-H., Hsiao, T.-C., Jones, T., BéruBé, K., Ho, K.-F., Chuang, H.-C., 2021. Particulate matter and SARS-CoV-2: A possible model of COVID-19 transmission. Science of The Total Environment 750, 141532. https://doi.org/10.1016/j.scitotenv.2020.141532

Valladares, F., Niinemets, Ü., 2008. Shade Tolerance, a Key Plant Feature of Complex Nature and Consequences. Annual Review of Ecology, Evolution, and Systematics 39, 237–257. https://doi.org/10.1146/annurev.ecolsys.39.110707.173506

Violle, C., Navas, M.-L., Vile, D., Kazakou, E., Fortunel, C., Hummel, I., Garnier, E., 2007. Let the concept of trait be functional! Oikos 116, 882–892. https://doi.org/10.1111/j.0030-1299.2007.15559.x

Winkler, A., Contardo, T., Vannini, A., Sorbo, S., Basile, A., Loppi, S., 2020. Magnetic Emissions from Brake Wear are the Major Source of Airborne Particulate Matter Bioaccumulated by Lichens Exposed in Milan (Italy). Applied Sciences 10, 2073. https://doi.org/10.3390/app10062073

Xu, X., Zhang, Z., Bao, L., Mo, L., Yu, X., Fan, D., Lun, X., 2017. Influence of rainfall duration and intensity on particulate matter removal from plant leaves. Science of The Total Environment 609, 11–16. https://doi.org/10.1016/j.scitotenv.2017.07.141

Yao, Y., Pan, J., Wang, Weidong, Liu, Z., Kan, H., Qiu, Y., Meng, X., Wang, Weibing, 2020. Association of particulate matter pollution and case fatality rate of COVID-19 in 49 Chinese cities. Science of The Total Environment 741, 140396. https://doi.org/10.1016/j.scitotenv.2020.140396

Zoran, M.A., Savastru, R.S., Savastru, D.M., Tautan, M.N., 2020. Assessing the relationship between surface levels of PM2.5 and PM10 particulate matter impact on COVID-19 in Milan, Italy. Science of The Total Environment 738, 139825. https://doi.org/10.1016/j.scitotenv.2020.13982.

5.5 (A5) Evaluation of the efficiency of *Arundo donax* L. leaves as biomonitors for atmospheric element concentrations in an urban and industrial area of central Italy

Atmosphere (2019), 11 (3), 226, doi: 10.3390/atmos11030226

Martina Ristorini[1,2], Maria Luisa Astolfi[3], Maria Agostina Frezzini[3], Silvia Canepari[3], Lorenzo Massimi[3*]

[1] Department of Bioscience and Territory, Università del Molise, Pesche (IS), 86090, Italy

[2] Institute of Terrestrial Ecosystem research – Council of National research (IRET-CNR) Via G. Marconi 2, 05010 Porano (TR), Italy

[3] Department of Chemistry, Sapienza University of Rome (Rome), 00185, Italy

*Corresponding author

Keywords: air quality; biomonitoring; particulate matter; leaf deposition; source tracer.

Abstract: Washed and unwashed *A. donax* leaves were analyzed for elements and results were compared with the element concentrations detected in river water and PM_{10} samples. Samples were collected along the river Nera in Terni, an urban and industrial hot-spot of Central Italy, where element concentrations show relevant spatial gradients both in air and river water. Elemental contents of washed and unwashed leaves were compared to differentiate between the superficial deposition on leaves of atmospheric elements and the uptake into leaf tissues. These results were compared with the water-soluble and insoluble element concentrations detected in PM_{10} samples collected on membrane filters by using innovative high spatial resolution samplers. The comparison among leaf and atmospheric concentrations of PM_{10} elements showed a similar trend for Ni, Mo, Cr, Ti and Fe, which are reliable tracers of the PM_{10} contribution by steel plant and vehicular traffic. Soluble species appeared to be mainly bounded into leaf tissues, while insoluble species were deposited on their surface. On the other hand, the element concentrations detected in washed *A. donax* leaves were poorly correlated with those measured in river water samples. The obtained results proved that *A. donax* leaves are reliable biomonitors for the evaluation of the atmospheric concentrations of PM elemental components.

1. Introduction

Arundo donax L., commonly known as giant reed, is a tall perennial grass of the family Poaceae, typical of riparian areas and characterized by a great productivity, growing up to 10 cm per day in optimal conditions [1-2]. Numerous studies had underlined the potential of this species for the phytoremediation of heavy-metals contaminated waters and soils, due to its tolerance to high concentrations of heavy metals, such as Cd, Cr, Ni [3-4] and its ability to absorb and bioaccumulate contaminants in its tissues [5]. These characteristics make this species suitable for being used as bioindicator of heavy-metals contamination of waters and soils, providing an alternative to the traditional sampling and analytical procedures applied to this task [6].

On the other hand, numerous studies have underlined the potential of biomonitoring to assess particulate matter (PM) atmospheric pollution [7-9]. In this context, urban trees and shrubs leaves are often proposed as efficient

and low-cost passive biomonitors for PM [10-12], thanks to the ability of vegetation to affect airborne particles dispersion and deposition [13]. Specifically, the evaluation of chemical and physical characteristics of leaf deposited particles can be used to achieve information about the role and the impact of anthropogenic PM emission sources [14-15], these characteristics being influenced directly by the type of emission process and source [16-17]. PM is an extremely heterogenous mixture of airborne solid particles and liquid droplets, varying in size, shape, chemical composition, solubility, toxicity and origin [18] and is considered one of the most relevant air pollutants in terms of human health effects [19-21]. Dry deposition of PM on leaves is a complex and dynamic process, being influenced both by species-specific characteristics of the vegetation and chemical-physical characteristics of airborne particles themselves [22-23]. To date, due both to the high complexity of dry deposition processes and the heterogeneity of PM, the achievement of a complete characterization of leaf deposited particles is difficult to obtain. Numerous analytical procedures have been applied for the achievement of this task, but it is still uncertain which procedure is the most efficient. One of the main sources of uncertainty is connected to the leaf washing procedure, being still unsure whether this step should be carried out or not. In fact, the efficiency of the leaf washing, in combination with the chemical and physical characteristics of the particles, such as their dimension and solubility, able to influence their encapsulation in leaf structures (waxes layer or stomata pores) [24-25], could affect the efficiency of any analytical procedures applied in the characterization of leaf deposited particles.

This study was aimed to evaluate the influence on element concentrations in *A. donax* leaves of two types of environmental contaminations to which plants are exposed: atmospheric PM pollution and river water contamination. To this aim, *A. donax* leaves, PM_{10} sampled filters and water samples were collected in parallel at sites impacted by different pollution sources and element concentrations in the three matrices were compared. Washed and unwashed leaves were analyzed in order to differentiate between PM superficial deposition and the uptake into leaf tissues. The study was carried out in Terni city, an urban and industrial hot-spot of Central Italy. The choice of Terni as study area was mainly driven by the presence in this territory of various strong anthropogenic local emission sources, including typical urban ones such as vehicular traffic and domestic heating, but also a wide steel industry pole and a power plant for waste treatment. The impact of these sources determines very relevant spatial variations of the element concentrations in both PM and river water, making this area particularly suitable for studying correlations among biomonitors and environmental condition.

2. Materials and methods

2.1 Study area and sampling sites

Terni is a city of Central Italy characterized by the presence of numerous PM anthropogenic emission sources such as an extensive steel plant, occupying about 158 ha in the East of the city, a power plant for waste treatment in the West and typical urban emission sources, like vehicular traffic and biomass domestic heating. Terni is located within an intramountain depression, whose peculiar meteorological conditions negatively

affect the dispersion of airborne particles and increase their accumulation. Different studies have already underlined the impact of these anthropogenic sources for what regards the atmospheric concentrations of PM and some of its elemental components [26-28]. Six sampling sites (TE1, TE2, TE3, TE4, TE5, TE6) were individuated along the river Nera and chosen for the collection of *A. donax* leaves and river water samples. TE1 is located near the power plant, in the western part of the city, TE2 and TE3 near the main trafficked streets of the city center, and TE4, TE5 and TE6 are sited around the steel plant, in the eastern part of the city (Figure 1, Table 1). In particular, TE6 is located upstream from the wastewater systems for the treatment of the steel plant effluents.

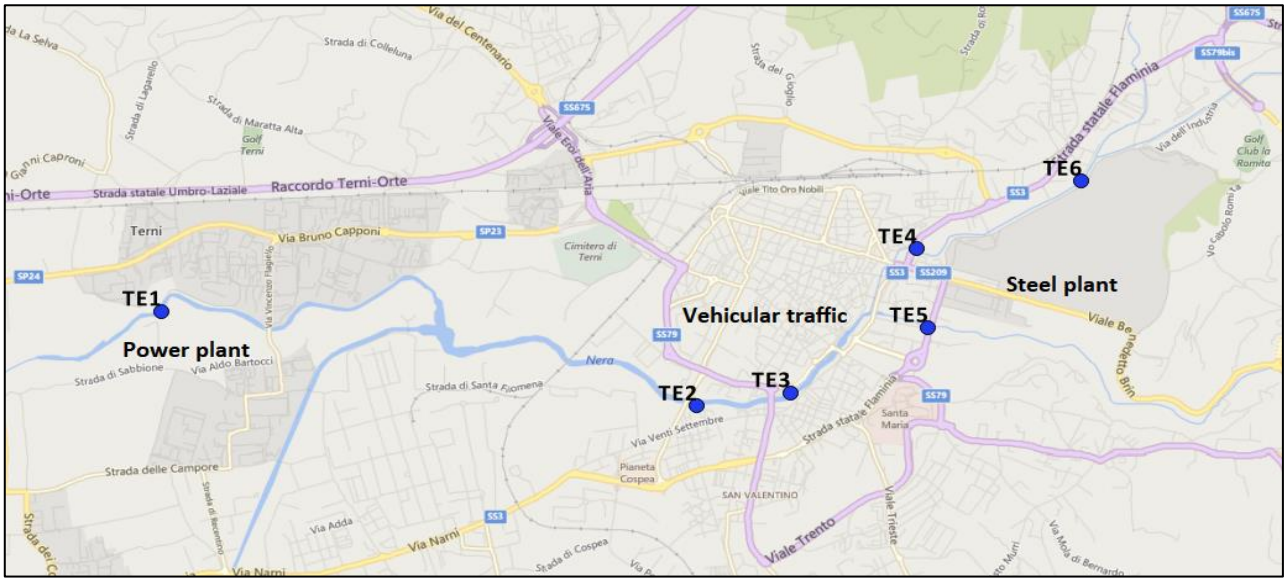

Figure 1. Sampling sites of *A. donax* leaves and river water samples along the river Nera in Terni (Central Italy). Highlighted the main PM anthropogenic emission source present in the study area.

Table 1. Latitude and longitude of the six sampling sites in Terni.

SAMPLING SITES	LATITUDE	LONGITUDE
TE1	42°33'43.84"N	12°35'47.18"E
TE2	42°33'22.27"N	12°38'21.02"E
TE3	42°33'25.29"N	12°38'47.81"E
TE4	42°33'58.02"N	12°39'24.08"E
TE5	42°33'40.12"N	12°39'27.33"E
TE6	42°34'13.53"N	12°40'11.41"E

2.2 *Arundo donax* leaves and river water samples collection and preparation

A. donax leaves and river water samples were monthly collected at the six sampling sites (Figure 1) from March to July 2017, for a total of 5 samples per site (one per month). For each site, 3 plants were selected and 6 leaves were collected from each plant for a total of 18 leaves per sampling site and 108 leaves (18 leaves per 6 sites) per collection period. Leaves were detached from the same internode (second-last from the top of the

stems) and stored at -18 °C in paper bags, to avoid external contamination. *A. donax* leaves collected at North-East of the Terni basin (42°38'25.95"N, 12°48'34.98"E), far from the direct impact of anthropogenic emission sources, were used as background samples. In addition, in each sampling period, about 50 mL of river water samples were collected for each sampling site, for a total of 30 water samples (6 samples of 50 mL per sampling). River water samples were taken from 10 to 15 cm below the water surface, according to APHA, 1998 [30]. Half of the collected leaves were washed thoroughly three times with deionized water (produced by Arioso UP 900 Integrate Water Purification System). The dry weight calculation (30 replicates) was carried out by oven drying 1 g of fresh leaves at 60 ± 2 °C until constant weight. Washed and unwashed leaves were then pulverized by grinding in a mill with Teflon balls and the obtained powders were homogenized and weighed (analytical balance Gibertini Europe 60; Gibertini Elettronica Srl, Milan, Italy). Subsequently, about 30 mg of each sample was subjected to a microwave assisted acid digestion (Ethos Touch Control with Q20 rotor, Milestone, Bergamo, Italy) for 30 min at 180°C by using a HNO_3/H_2O_2 mixture (2:1, v/v; 2 mL of ultrapure concentrated HNO_3 67%, Promochem, LGC Standards GmbH, Wesel, Germany; 1 mL of H_2O_2 30%, Promochem, LGC Standards GmbH, Wesel, Germany). The digested solutions were then diluted to 100 mL of deionized water.

2.3 PM_{10} samples collection and preparation

PM_{10} was monthly sampled on Teflon membrane filters (PTFE membranes, 37 mm diameter, 2 μm pore size, PALL Corporation, Port Washington, New York, NY, USA) from March to July 2017 at 23 monitoring sites spread over the Terni basin by using innovative and very-low volume (0.5 l min^{-1}) PM_{10} samplers (High spatial resolution sampler - HSRS, Fai Instruments, Fonte Nuova, Italy). The localization and the geographical coordinates of the 23 PM_{10} sampling sites as well as the characteristics of the used HSRS are deeply described in Massimi et al. 2017 and Massimi et al. 2019 [9, 27]. The monthly collected PM_{10} membrane filters were subjected to a chemical fractionation procedure, previously optimized and validated [31-32], useful to separate the water-soluble and insoluble fraction of each PM_{10} elemental component, thus increasing its selectivity as source tracer [9, 33-34]. Firstly, after removing the supporting polymethylpentene ring from each membrane filter, PM_{10} filters were extracted in 10 mL of deionized water for 30 min at 25 °C by using an ultrasonic bath (Proclean 10.0 ultrasonic cleaner, Ulsonix, Germany) and then filtered on cellulose nitrate filters (0.45 μm pore size, Merck Millipore Ltd., Billerica, MA, USA). Secondly, both the membrane and cellulose nitrate filters were acid-digested for 30 min at 180°C in the microwave oven by using the HNO_3/H_2O_2 mixture (2:1, v/v) previously described. The digested solutions were then diluted to 50 mL with deionized water.

2.4 ICP-MS analysis

The collected river water samples and all the acid-digested solutions were filtered with syringe filters (25 mm diameter, 0.45 μm pore size, GVS Filter Technology, Morecambe, England, UK) before instrumental analysis. The concentrations of 16 elements (Ba, Cd, Cr, Cs, Cu, Fe, Li, Mn, Mo, Ni, Pb, Rb, Sb, Sn, Sr, Ti) were determined in all the samples (river water samples, water-extracted and acid-digested PM_{10}, washed and

unwashed *A. donax* leaves) by a quadrupole inductively coupled plasma mass spectrometer (ICP-MS, model 820-MS; Bruker, Bremen, Germany) equipped with a glass nebulizer (0.4 mL min^{-1} ; Analytik Jena AG, Jena, Germany). External matrix-matched standard calibration curves were performed for all the analyzed elements in the 1-500 µg L^{-1} range by serially diluting standard stock solutions (1000 ± 2 mg L^{-1}; Exaxol Italia Chemical Manufacturers Srl, Genoa, Italy). To control the nebulizer efficiency, yttrium and rhodium were set at 5 µg L^{-1} as internal standards for all measurements and were prepared from standard stock solutions (1000 ± 2 mg L^{-1}; Panreac Química, Barcelona, Spain; Ultra Scientific, North Kingstown, RI, USA; Merck Millipore Ltd., Billerica, MA, USA). The values of blanks, subjected to similar sample preparation and analytical procedures, were deducted from all measurements and the limits of detection (LODs; supplementary material S1; Table S1.1, S1.2, S1.3) were set at 3 times the standard deviation (Std Dev) of 10 replicate blank determinations. Standard deviations of the replicates were all below 20%. The used instrumental conditions and the performance of the method are detailed in Astolfi et al. 2018 [35].

2.5 Data elaboration

Elemental (n=16) concentrations were determined in *A. donax* leaves collected at each site (Figure 1, Table 1) for each of the 5 collection months. The concentrations determined in the washed and unwashed *A. donax* leaves were divided by the dry weight of each sample (ng mg^{-1}). Then, monthly element concentrations were averaged for each monitoring site (supplementary material S2; Table S2.1, Table S2.2). Element concentrations (µg L^{-1}) were determined in river water samples collected at each site (Figure 1, Table 1) for each of the 5 collection months. Monthly element concentrations were averaged for each monitoring site and are reported in supplementary material S2 (Table S2.3). The element concentrations of the water-soluble and insoluble PM_{10} were divided by the air volume sampled on each PM_{10} membrane filter (ng m^{-3}). Total concentrations were calculated as the sum of the two solubility fractions. Since the *A. donax* leaves were collected at different sites with respect to the PM_{10} samples, ordinary kriging (OK, spherical semivariogram model) interpolation [36-37] was applied to the PM_{10} soluble, insoluble and total element concentrations determined at the 23 PM_{10} sampling sites in order to estimate their concentrations (supplementary material S2; Table S2.4, S2.5) at the leaves collection sites (TE1, TE2, TE3, TE4, TE5, TE6) and to properly compare the obtained results.

2.6 SEM analysis of PM_{10} samples

PM_{10} sampling on polycarbonate membranes (PCTE membranes, 37 mm diameter, 0.8 µm pore size, Sterlitech Corporation, Kent, Washington, USA) was carried out for three days, from the 2nd to the 4th of March, by using two HSRS working in parallel at the air quality station "Prisciano", located in the East of the city (42°34'20.30"N 12°40'44.23"E), in the proximity of the steel plant, and controlled by the regional agency for environmental protection (ARPA Umbria). Small portions of each polycarbonate membrane were cut, fixed to aluminum stubs by self-adhesive carbon disks (TAAB, 12mm diam.) and coated with an ultra-thin carbon layer

in a vacuum evaporator (108 Carbon A; Scientific Instruments Ltd., Cressington, England, UK). Micrographs of each sample were acquired by a high-resolution field emission scanning electron microscopy (HR-FESEM; model AURIGA; Carl Zeiss Microscopy GmbH, Jena, Germany) equipped with an energy dispersive spectrometer for X-ray microanalysis (XEDS; model QUANTAX; Bruker Italia S.r.l., MI, Italy). Micrographs were acquired through the use of backscatter electron detector (BSD) at magnification ranging from 25,000x to 600,000x and at working distance (WD) ranging from 9.6 mm to 12.4 mm.

3. Results and discussion

3.1 Element concentrations in *Arundo donax* leaves

Figure 2 reports the concentrations of elements associated to the steel plant emission (Cr, Fe, Mo, Ni and Ti) in unwashed and washed leaves. All these elements showed a marked concentration gradient in both washed and unwashed leaves, indicating that the measured concentrations are sensitive to environmental concentrations. A similar trend was found for all the considered elements, with higher concentrations at sites surrounding the steel plant.

Chromium, Ni and Ti showed higher concentrations (ng mg-1) in leaves collected at TE5 and TE6 (Figure 2a, d and e), which are the sites closest to the steel plant. Furthermore, for these elements, concentrations in unwashed leaves are significantly higher than those in washed leaves. This means that a major part of the measured concentrations in unwashed leaves is probably due to superficial deposition of atmospheric particles. PM_{10} particles containing these elements are known to be emitted at high concentrations by the steel plant [27]. Chromium is usually used to increase the steel resistance to chemical oxidation and nickel is used to increase the steel strength, ductility and toughness [38]. The variation of the leaf deposition of these elements among the selected sites underlined the impact of the steel industry pole and proved the efficiency and reliability of the *A. donax* leaf deposition for the individuation of the steel plant tracers and for obtaining information on their variability along the river Nera.

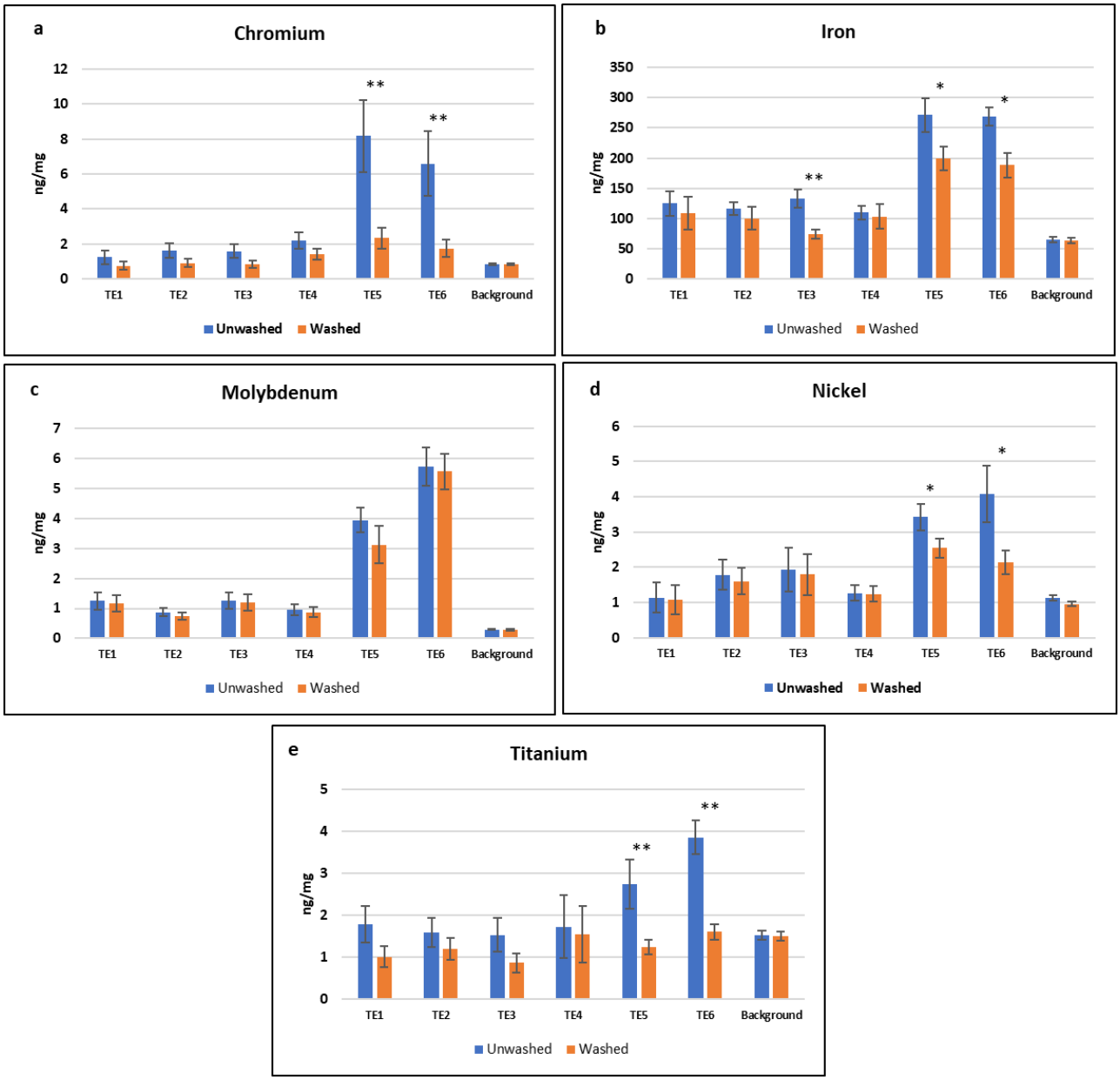

Figure 2. Concentrations (ng mg^{-1}) of Cr, Fe, Mo, Ni and Ti, detected in unwashed and washed leaves at the six sites along the river Nera in Terni (panel a, b, c, d and e). P values evaluated by applying paired sample t-test (* $p<0.05$; ** $p<0.001$).

In panel b of Figure 2, we can observe that Fe concentrations (ng mg^{-1}) detected in unwashed leaves were higher at the sampling sites TE3, TE5 and TE6. Also in this case concentrations are significantly higher in unwashed leaves than in washed ones. Iron is the main component of stainless steel and higher deposition values in *A. donax* leaves collected at TE5 and TE6, which are the closest sites to the steel plant, confirmed its attribution to emissions from the steel industry pole. However, Fe is also a well-known tracer for vehicular traffic, being related to the mechanical abrasion of brakes and vehicle components [27, 39-40]. The increase of Fe concentration at TE3, located near the city center is mainly related to its emission from the close busy

roads. Therefore, the trend of the Fe deposition underlined the impact of two different emission sources: steel plant (at TE5 and TE6) and vehicular traffic (at TE3).

In the specific case of molybdenum, higher concentrations were found at the same collection sites (TE5 and TE6) as Cr, Ni and Ti, also in this case highlighting the impact of the steel plant. In fact, also Mo is typically used as secondary component to improve the resistance of stainless steel [38]. However, Mo concentrations in washed and unwashed leaves are very similar, indicating that this element is deeply bound to the leaves (Figure 2c). This difference may be due to a different uptake process (i.e. root absorption from water or soil) or by the different chemical and/or physical characteristics of atmospheric particles deposited on leaves. Further details on these issues can be obtained by comparing the element concentration in leaves with those found in atmospheric PM_{10} and river water samples.

3.2 Comparison between leaf deposition and PM_{10} element concentrations

To evaluate the potential of this biological approach for the assessment of the impact of the anthropogenic PM emission sources, we compared the elemental amount superficially deposited on leaves (superficial deposition, SD; calculated as difference between the element concentration measured in unwashed and washed leaves) with the spatially-resolved atmospheric concentrations detected in the PM_{10} sampled through HSRS (supplementary material S2; Table S2.4, Table S2.5).

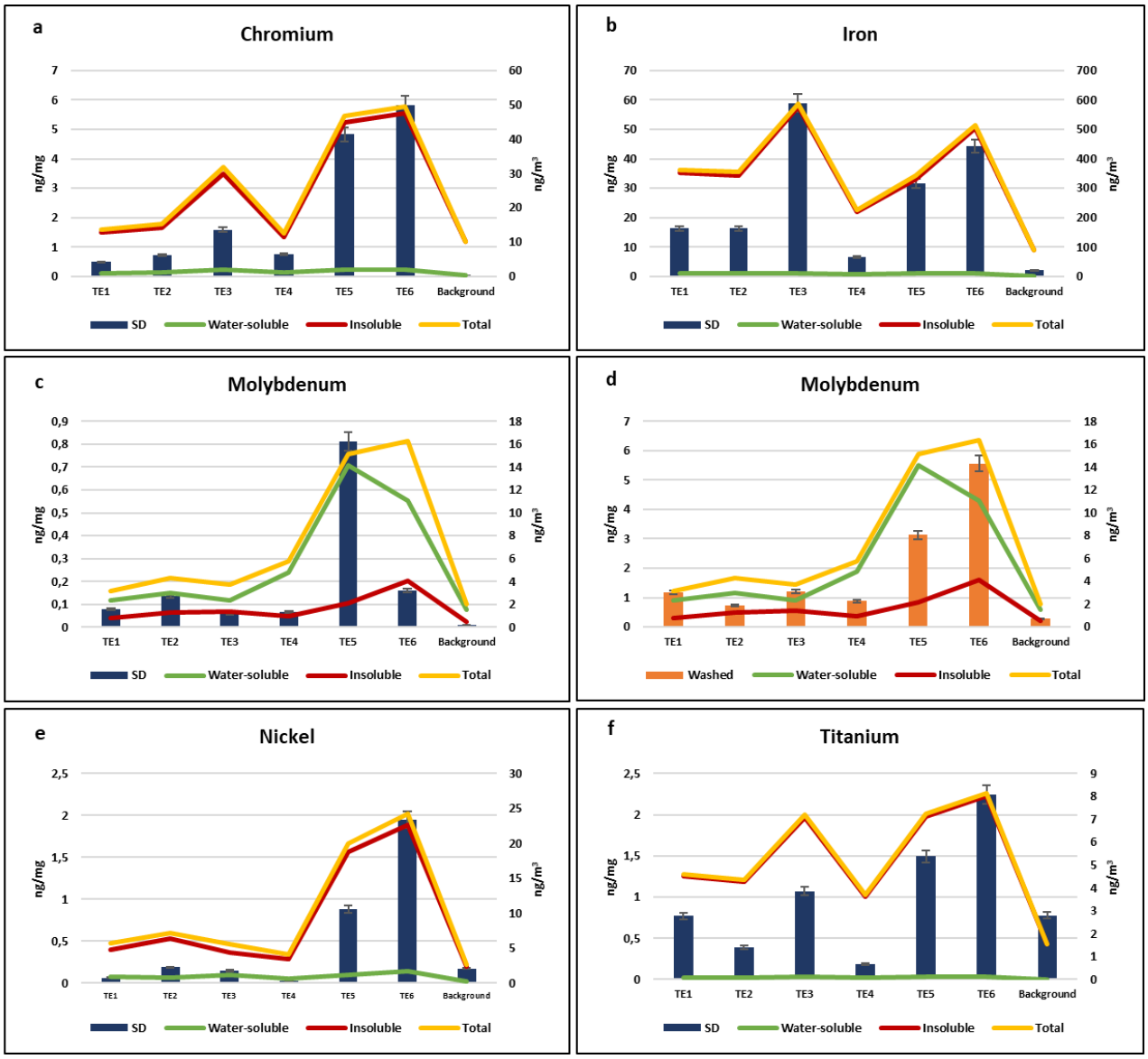

Figure 3. Comparison between SD of Cr, Fe, Mo, Ni and Ti (ng mg^{-1}) and their concentrations in the water-soluble, insoluble and total fraction of PM_{10} (ng m^{-3}) (panels a, b, c, e and f). Comparison between Mo concentrations in washed leaves (ng mg^{-1}) and in the water-soluble, insoluble and total fraction of PM_{10} (ng m^{-3}) (panel d).

From Figure 3, we can observe that, for most of the identified steel plant tracers (Cr, Fe, Ni and Ti), the SD showed a similar trend to total concentrations in PM_{10} (Figure 3a, b, e and f). For these elements, the difference between unwashed and washed concentration in *A. donax* leaves seems then to be reliably representative of their atmospheric concentrations. In the case of Mo, much poorer correlations between concentrations in superficially deposited dust and PM_{10} concentration were found (Figure 3c); for this element, we reported also the comparison between concentrations in PM_{10} and in washed leaves (Figure 3d), which showed a much higher correlation. In order to investigate the reasons of the different behavior of Mo respect to the other steel

plant tracers, we considered the solubility and the morphological characteristics of particles emitted by the steel plant.

Among all parameters, dimensions and morphological characteristics of airborne particles have proven to be able to influence the deposition of particulate matter on leaves and their interaction with leaf tissues [23, 41-42]. For this reason, we carried out SEM analyses on PM_{10} sampled on polycarbonate membranes through HSRS working near the steel plant (Figure 4).

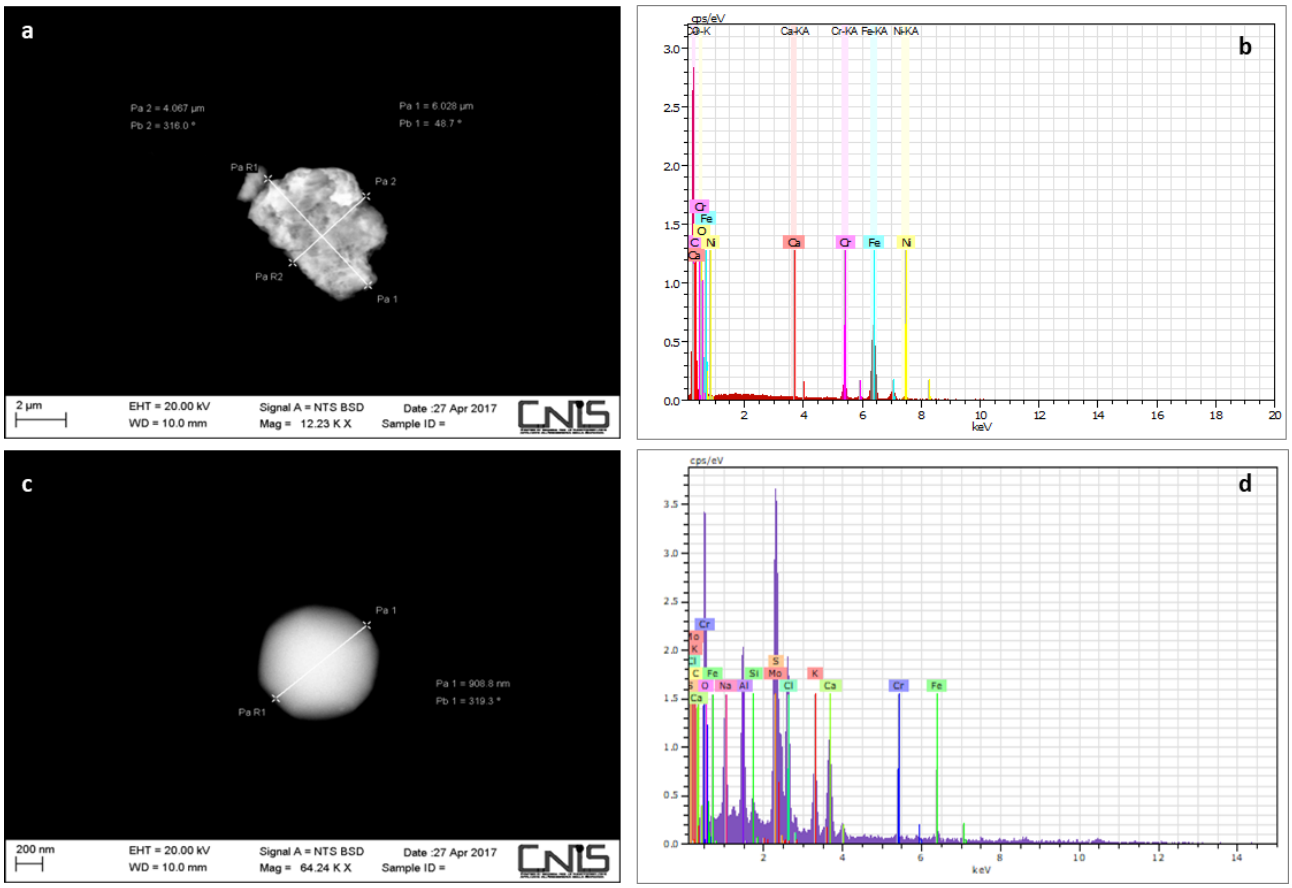

Figure 4. SEM micrograph (a) and respective EDX spectrum (b) of a steel particle (Cr, Fe and Ni) sampled near the steel plant. SEM micrograph (c) and respective EDX spectrum (d) of a Mo particle sampled near the steel plant.

From Figure 4, we can observe the micrograph (panel a) with the respective EDX spectrum (panel b) of a particle containing the basic stainless steel components: Cr, Ni and Fe. This steel particle is coarse (up to 5 µm of diameter) and is characterized by an irregular, angular and sharp morphology. The peculiar dimension and morphology of this and other analyzed coarse particles with the same chemical composition, seems to be related to mechanical-abrasive emission processes. Differently, in the panel c, we can observe a fine particle (with diameter smaller than 1 µm) containing Mo and spherical in shape, which is the typical morphology of airborne particles formed by high temperature processes [43-44]. Even though these two types of particles were emitted by the same emission source (steel plant), they appeared to be characterized by different

dimension and morphology, revealing the presence of two different emission processes (high temperature and mechanical-abrasive processes). The different physical characteristics of these two types of particles may be considered responsible for the different behavior observed in Figure 2 and 3. In particular, coarse particles containing Cr, Fe, and Ni seem to have been deposited on the leaf surfaces, making it easy to wash them off and to detect significant differences between washed and unwashed leaves. The fine particles containing Mo could be instead more likely encapsulated into the waxes layer or stomata pores situated on the leaf surface, making more difficult to wash them out from the leaves [24-25]. This can result in the lowest difference between unwashed and washed leaves, detected for molybdenum concentrations. In Figure 3 we also reported water-soluble and insoluble fractions of each element in PM_{10}. As it can be noted, Cr, Fe, Ni and Ti are almost exclusively present as insoluble species, while Mo is mainly present in the water soluble fraction. Besides the small dimensions of particles containing Mo and their consequent easier encapsulation within the leaf structure, the different behavior of Mo respect to the other considered elements may be due also to the higher solubility of species containing Mo that might be then directly absorbed by the leaf surface. Table 2 reports Pearson's correlation coefficients (ρ) calculated between elements superficially deposited on leaves or bounded to leaf tissues (washed leaves) and their concentrations in the water-soluble and insoluble fractions of PM_{10}. In general, the highest positive correlations were found between concentrations in insoluble fraction of PM_{10} and SD of Cr, Fe, Ni, Mn, Ti and Zn. Most of these elements (Cr, Ni, Fe, Ti) are tracers of the steel plant; as already showed, particles containing these elements are mainly characterized by coarse dimensions. Mn is also well correlated to SD; this element is often used as tracer of non-combustive emissions from vehicular traffic [16, 45]. This source produces particles scarcely soluble and belonging to the coarse dimensional fraction of PM as well [46]. It is then reasonably hypothesizing that coarse and insoluble particles are deposited on leaf surface and easily washed out during the leaf washing step. For this kind of PM contribution the determination of SD may constitute a reliable biomonitoring procedure. In the case of Mo, as already

pointed out, a good correlation was found between washed leaves and soluble fraction of PM_{10}. Mo is present in PM_{10} mainly as soluble species belonging to the fine fraction; these characteristics promote a stronger interaction with leaf structure and washing procedure is not able to detach Mo-containing particles. A positive correlation was found also between washed leaves and insoluble Ni. In this regard, it is worth noting that fine particles containing Ni were also individuated through SEM analysis (supplementary material S3; Figure S3.1). These particles are probably released by the same high temperature process but contain Ni as insoluble species. The correlation between washed leaves and Ni might indicate that the uptake into leaf tissues is mainly driven by physical interaction of small particles with waxes layer and stomata pores. Correlations between SD results and PM_{10} element concentrations were much lower for all the other analyzed elements, tracers of other PM sources, whose strength was lower than the steel plant. For example, correlations were poor for water-soluble Cd, Cs, Rb and Tl, which have been identified as reliable tracers for biomass burning in the Terni basin (47-48) and weak for insoluble Cu and Sn, which are well-known as rail network and vehicular traffic tracers (9, 27, 49-50). Superficial deposition of atmospheric elements can be then considered reliable only for the evaluation of the impact of strong PM sources.

3.3 Comparison between river water samples and *A. donax* leaves elemental content

To evaluate the potential influence of river water pollutants on the elemental content of the leaves, where heavy metals adsorbed by roots can be stored and transferred [51-52], we analyzed the element concentrations of water samples collected from the river Nera at the same collection sites of the *A. donax* leaves (Figure 1). Since metals adsorbed by roots are expected to be included in leaf tissues, element concentrations in river water were compared with the element concentrations in washed leaves (Figure 5).

The steel plant tracers (Cr, Fe, Mo, Ni and Ti), previously individuated for PM, showed their maximum concentrations in the river water samples collected at TE5 (Figure 5). On the contrary, high concentrations were not found at TE6, where high concentrations in A. donax washed leaves where instead found. Since wastewater systems for the treatment of the effluents from cold and hot rolling sections of the steel plant are located in the southern part of the steel industry pole, at the close proximity to TE5 [53], we can reasonably hypothesize that the higher concentrations of Cr, Fe, Mo, Ni and Ti at TE5 water samples are related to local disposal of steel plant waste water in the Nera river. Due to the heavy metal bioaccumulation ability described for this riparian species [54-55], high concentrations of these steel plant tracers in washed leaves, might be then due to the influence of river water contamination. The very relevant differences at TE6 (located upstream from the steel plant wastewater systems but is strongly affected by the atmospheric emissions of this industrial pole) underlined the lower reliability of leaves for the evaluation of the river heavy-metals contamination.

We also calculated Pearson's correlation coefficients between element concentrations detected in river water samples and washed leaves (Table 3). Correlations were in general much lower than those related to PM_{10} concentrations. The highest correlation between these two datasets was found for Cd; this result could be explained by considering the iper-accumulation ability of *A. donax* toward Cd. However, in this set of

measurements, Cd showed a low variability in both river water and washed leaves (supplementary material S2; Table S2.2, S2.3) and this is reasonably the main reason of the good correlation found. The use of this riparian species seems then to have a low reliability for the evaluation of the concentration in the river water.

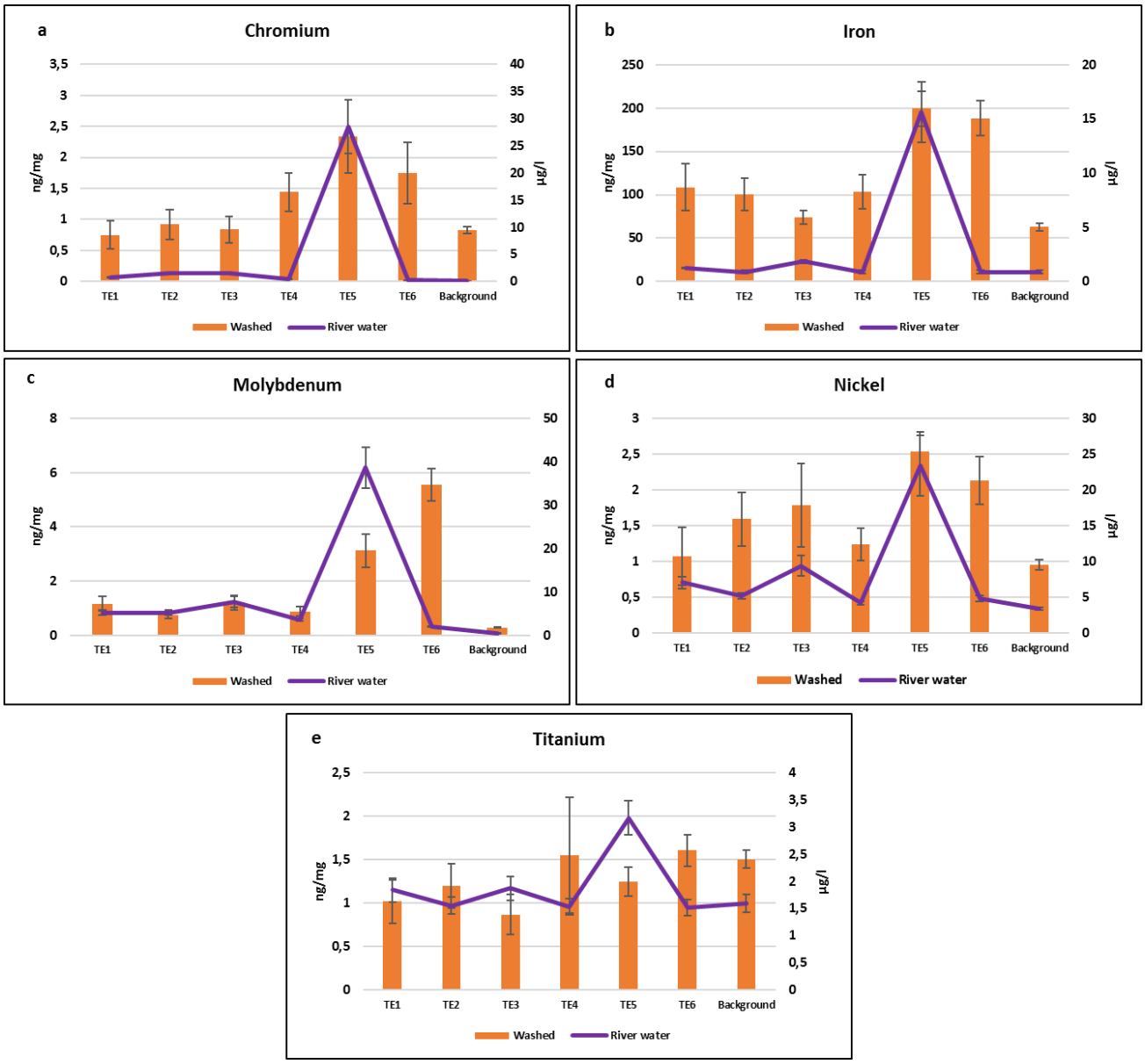

Figure 5. Comparison of Cr, Mo, Ni and Ti concentrations between river water samples (µg L^{-1}) and *A. donax* leaves (ng mg^{-1}).

Table 2. Pearson's correlation coefficients calculated between SD and leaf-bound atmospheric elements (washed leaves) and their concentrations in the water-soluble and insoluble fractions of PM_{10}. Mean monthly concentrations at each site were included in the elaboration (N=30). Positive linear correlations (Pearson's coefficient > 0.8) between the two variables are reported in red.

Pearson's	Ba	Cd	Cr	Cs	Cu	Fe	Li	Mn	Mo	Ni	Pb	Rb	Sb	Sn	Sr	Ti
SD/Water soluble PM10	-0,06	0,31	0,74	0,31	-0,39	0,49	0,62	0,77	0,78	0,77	0,21	0,00	-0,65	0,34	-0,56	0,79
SD/Insoluble PM10	-0,12	0,22	0,87	0,38	-0,08	0,93	0,25	0,92	0,16	0,95	-0,79	0,12	-0,74	0,53	-0,62	0,93
Washed leaves/Water soluble	0,01	0,18	0,49	0,10	0,08	0,31	0,67	0,73	0,90	0,63	0,02	0,51	0,45	-0,43	0,19	0,17
Washed leaves/Insoluble	-0,59	0,24	0,59	-0,14	0,18	0,02	-0,03	0,75	0,35	0,82	0,55	-0,08	0,43	-0,66	0,21	0,01

Table 3. Pearson's correlation coefficients calculated between element concentrations in river water samples and their concentration in washed leaves. Mean monthly concentrations at each site were included in the elaboration (N=30). Positive linear correlations (Pearson's coefficient > 0.8) between the two variables are reported in red.

Pearson's	Ba	Cd	Cr	Cs	Cu	Fe	Li	Mn	Mo	Ni	Pb	Rb	Sb	Sn	Sr	Ti
Washed leaves/ River Water	0,38	0,81	0,76	0,18	0,34	0,53	-0,20	-0,79	0,17	0,71	-0,10	-0,35	0,06	-0,20	-0,44	-0,23

4. Conclusion

For the first time in this study, we were able to compare the different influence of PM atmospheric pollution and river contamination, acting in parallel in the study area of Terni, on the elemental content of *A. donax* leaves.

Superficial deposition results of Cr, Fe, Ni and Ti, showed higher values at the closest sites to the steel industry pole (TE5, TE6), highlighting the impact of the steel plant emission. At these same sites, molybdenum was found at highest concentrations in both washed and unwashed leaves. SEM/EDX micrographs of PM_{10}, sampled near the steel plant, revealed dimensional and morphological differences between particles containing Mo and particles containing Ni, Cr and Ti. Furthermore, Mo species contained in PM_{10} are much more soluble than those containing the other steel plant tracers (Ni, Cr and Ti). These chemical and morphological differences seemed to affect the kind of interaction of particles containing Mo with the leaf structures. Superficial deposition results of Fe, showed higher values also at the site close to heavily trafficked streets (TE3), highlighting the impact of the vehicular traffic emission acting in the city center.

The good correlations between the elemental amount superficially deposited and atmospheric concentrations of Cr, Fe, Ni, Mn, Zn and Ti, confirmed the reliability of these results for the evaluation of the impact related to strong emission sources, such as the steel plant and vehicular traffic emissions in the study area of Terni.

Elemental analysis of river water samples showed concentration peaks for the steel plant tracers at a site close to the steel industry pole (TE5), revealing the presence of a relevant local emission source (wastewaters systems for the treatment of the effluents of the steel plant). Nevertheless, element concentrations in washed leaves and river water samples were poorly correlated, underlying a lower efficiency of this biological approach for the evaluation of the river contamination.

These preliminary results encourage further investigations on the utilization of this riparian species, largely distributed in urban areas of Italy, for future studies on PM leaf deposition and its application as a low-cost alternative for the monitoring of atmospheric PM and its elemental components.

Author Contributions: S. Canepari and L. Massimi conceived and planned the monitoring and the experiments; M. Ristorini and L. Massimi performed the samplings; M. L. Astolfi and L. Massimi performed the chemical analyses; M. Ristorini and L. Massimi elaborated the data; M. Ristorini wrote the manuscript; S. Canepari and L. Massimi coordinated the group and supervised the manuscript.

Supplementary Materials

Table S1.1. Limits of detection (LODs) of the concentrations (µg/L) detected in river water samples of the analyzed elements, set at 3 times the standard deviation (SD) of 10 replicate blank determinations.

	UoM	**LODs**
Ba	µg/L	1.6
Cd	µg/L	0.0088

Cr	µg/L	0.24
Cs	µg/L	0.0095
Cu	µg/L	0.15
Fe	µg/L	1.8
Li	µg/L	0.011
Mn	µg/L	0.11
Mo	µg/L	0.99
Ni	µg/L	0.14
Pb	µg/L	0.02
Rb	µg/L	0.026
Sb	µg/L	0.0094
Sn	µg/L	0.043
Sr	µg/L	0.7
Ti	µg/L	0.079

Table S1.2. Limits of detection (LODs) of the concentrations (µg/L) detected in PM_{10} samples, of the water-soluble and insoluble fraction of the analyzed elements, set at 3 times the standard deviation (SD) of 10 replicate blank determinations.

	UoM	**LODs Water-soluble Fraction**	**LODs Insoluble Fraction**
Ba	µg/L	3.7	0.44
Cd	µg/L	0.0038	0.0031
Cr	µg/L	0.081	0.86
Cs	µg/L	0.0033	0.0017
Cu	µg/L	0.2	0.24
Fe	µg/L	3	9.6
Li	µg/L	0.0063	0.004
Mn	µg/L	0.17	0.17
Mo	µg/L	0.049	0.012
Ni	µg/L	0.35	0.17

Pb	µg/L	0.1	0.15
Rb	µg/L	0.031	0.023
Sb	µg/L	0.0094	0.0094
Sn	µg/L	0.013	0.027
Sr	µg/L	0.2	0.57
Ti	µg/L	0.15	0.4

Table S1.3. Limits of detection (LODs) of the concentrations (µg/L) detected in washed and unwashed *A. donax* leaves of the analyzed elements, set at 3 times the standard deviation (SD) of 10 replicate blank determinations.

	UoM	**LODs *A. donax* leaves**
Ba	µg/L	6.7
Cd	µg/L	0.33
Cr	µg/L	0.22
Cs	µg/L	0.0021
Cu	µg/L	0.12
Fe	µg/L	30
Li	µg/L	0.014
Mn	µg/L	1.1
Mo	µg/L	0.13
Ni	µg/L	0.18
Pb	µg/L	0.059
Rb	µg/L	0.028
Sb	µg/L	0.011
Sn	µg/L	0.019
Sr	µg/L	0.63
Ti	µg/L	0.47

Table S2.1. Mean values and standard deviations calculated between monthly values of element concentrations detected in unwashed *A. donax* leaves at the six monitoring sites.

***A. donax* unwashed leaves element concentrations**													
		TE1		**TE2**		**TE3**		**TE4**		**TE5**		**TE6**	
	UoM	**Mean**	**Std Dev**	**Mean**	**Std Dev**	**Mean**	**Std Dev**	**Mean**	**Std Dev**	**Mean**	**Std Dev**	**Mean**	**Std Dev**
Ba	ng/mg	13	3.3	5	1.9	16	4.2	16	4.3	32	8.6	47	15
Cd	ng/mg	0.26	0.1	1.6	0.53	3.4	0.94	1.6	0.47	3.9	1.4	0.26	0.069
Cr	ng/mg	1.2	0.38	1.6	0.42	1.6	0.4	2.2	0.47	6.2	2.1	6.6	1.8
Cs	ng/mg	0.18	0.061	0.23	0.074	0.2	0.063	0.078	0.028	0.071	0.023	0.031	0.011
Cu	ng/mg	5.7	1.3	6.6	1.4	5.2	1.2	5.1	1.3	8.9	2.2	11	2.5
Fe	ng/mg	125	20	117	11	133	15	110	11	271	28	269	15
Li	ng/mg	0.037	0.011	0.047	0.018	0.053	0.018	0.036	0.0084	0.055	0.014	0.086	0.02
Mn	ng/mg	36	10	26	6.0	15	5.6	51	16	31	11	128	43
Mo	ng/mg	1.2	0.29	0.87	0.14	1.3	0.28	0.94	0.18	3.9	0.41	5.7	0.64
Ni	ng/mg	1.1	0.43	1.8	0.42	1.9	0.63	1.3	0.23	3.4	0.37	4.1	0.81
Pb	ng/mg	0.2	0.063	0.15	0.048	0.18	0.052	0.35	0.12	0.3	0.072	0.33	0.14
Rb	ng/mg	30	8.6	36	11	33	9.2	31	8.8	25	7.2	26	9.5
Sb	ng/mg	0.021	0.0069	0.009	0.003	0.039	0.017	0.01	0.0025	0.009	0.0023	0.024	0.009
Sn	ng/mg	0.053	0.015	0.055	0.018	0.051	0.015	0.06	0.019	0.055	0.015	0.058	0.021
Sr	ng/mg	17	3.5	22	5.0	23	5.0	32	7.4	28	6.7	53	13
Ti	ng/mg	1.8	0.44	1.6	0.34	1.5	0.4	1.7	0.75	2.7	0.58	3.8	0.4

Table S2.2. Mean values and standard deviations calculated between monthly values of element concentrations detected in washed *A. donax* leaves at the 6 monitoring sites.

***A. donax* washed leaves element concentrations**													
		TE1		**TE2**		**TE3**		**TE4**		**TE5**		**TE6**	
	UoM	**Mean**	**Std Dev**	**Mean**	**Std Dev**	**Mean**	**Std Dev**	**Mean**	**Std Dev**	**Mean**	**Std Dev**	**Mean**	**Std Dev**
Ba	ng/mg	5.3	1.4	5.4	1.8	5.3	1.4	16	4.2	31	8.3	46	15
Cd	ng/mg	0.26	0.1	1.1	0.39	3.3	0.92	1.6	0.46	3.8	1.4	0.26	0.068
Cr	ng/mg	0.75	0.23	0.92	0.24	0.84	0.21	1.4	0.31	2.3	0.59	1.7	0.49
Cs	ng/mg	0.16	0.055	0.21	0.069	0.16	0.051	0.078	0.027	0.069	0.023	0.022	0.0075
Cu	ng/mg	5.2	1.2	6.5	1.4	5.1	1.2	4.5	1.2	7.4	1.8	8.7	1.9

Fe	ng/mg	109	27	100	18	74	8	103	20	199	20	188	20
Li	ng/mg	0.026	0.0079	0.029	0.011	0.03	0.01	0.033	0.0077	0.045	0.012	0.062	0.014
Mn	ng/mg	35	10	24	5.6	14	5	48	15	27	9.1	121	40
Mo	ng/mg	1.2	0.27	0.74	0.12	1.2	0.27	0.88	0.17	3.1	0.67	5.6	0.59
Ni	ng/mg	1.1	0.4	1.6	0.38	1.8	0.58	1.2	0.22	2.5	0.27	2.1	0.33
Pb	ng/mg	0.14	0.043	0.047	0.015	0.18	0.051	0.13	0.048	0.29	0.071	0.25	0.1
Rb	ng/mg	29	8.4	36	11	34	9	30	8.6	25	7.1	25	9.3
Sb	ng/mg	0.02	0.0067	0.009	0.003	0.0089	0.0039	0.0093	0.0024	0.0092	0.0023	0.0089	0.0034
Sn	ng/mg	0.016	0.0043	0.015	0.0048	0.017	0.0044	0.048	0.015	0.017	0.0043	0.016	0.0055
Sr	ng/mg	16	3.2	18	4.2	15	3.3	31	7.2	27	6.5	52	13
Ti	ng/mg	1	0.25	1.2	0.26	0.87	0.23	1.5	0.67	1.2	0.17	1.6	0.18

Table S2.3. Mean values and standard deviations calculated between monthly values of element concentrations detected in river water samples at the six monitoring sites.

River water element concentrations													
		TE1		**TE2**		**TE3**		**TE4**		**TE5**		**TE6**	
	UoM	**Mean**	**Std Dev**	**Mean**	**Std Dev**	**Mean**	**Std Dev**	**Mean**	**Std Dev**	**Mean**	**Std Dev**	**Mean**	**Std Dev**
Ba	µg/l	96	11,2	66	5,3	71	6,0	60	4,3	95	11	86	9,0
Cd	µg/l	0,012	0,00057	0,013	0,00065	0,019	0,0014	0,033	0,0042	0,036	0,0050	0,034	0,0044
Cr	µg/l	0,84	0,022	1,56	0,077	1,61	0,082	0,53	0,0089	28	5,4	0,30	0,0028
Cs	µg/l	0,15	0,016	0,14	0,014	0,20	0,028	0,10	0,0068	0,24	0,038	0,11	0,0077
Cu	µg/l	1,4	0,19	0,84	0,065	1,4	0,18	0,93	0,079	2,15	0,42	1,28	0,15
Fe	µg/l	1,2	0,068	1,9	0,16	1,9	0,16	1,9	0,17	16	2,8	1,9	0,17
Li	µg/l	6,3	1,1	4,9	0,65	7,2	1,4	5,4	0,79	7,9	0,87	4,7	0,6
Mn	µg/l	0,12	0,014	0,13	0,014	0,13	0,014	0,14	0,0028	0,06	0,016	0,06	0,013
Mo	µg/l	5,2	0,59	5,2	0,59	7,8	1,3	3,6	0,28	39	4,6	2,0	0,087
Ni	µg/l	7,1	0,83	5,2	0,45	9,4	1,5	4,2	0,29	23	4,2	4,9	0,39
Pb	µg/l	0,14	0,017	0,035	0,0029	0,053	0,0066	0,037	0,0032	0,029	0,0019	0,037	0,0032
Rb	µg/l	3,3	0,56	1,7	0,15	2,3	0,27	1,8	0,16	2,6	0,35	2,0	0,20
Sb	µg/l	0,094	0,016	0,055	0,0054	0,091	0,015	0,051	0,0047	0,19	0,026	0,055	0,0055

Sn	µg/l	0,20	0,028	0,23	0,030	0,0094	0,0002	0,012	0,00035	0,024	0,0013	0,053	0,0064
Sr	µg/l	978	172	859	133	1084	211	904	147	986	175	900	146
Ti	µg/l	1,8	0,22	1,6	0,15	1,9	0,22	1,5	0,15	3,2	0,32	1,5	0,15

Table S2.4. Mean values and standard deviations calculated between monthly values of interpolated concentrations of water-soluble fraction of PM_{10} elements at the six monitoring sites.

Water-soluble interpolated PM_{10} element concentrations													
		TE1		**TE2**		**TE3**		**TE4**		**TE5**		**TE6**	
	UoM	**Mean**	**Std Dev**	**Mean**	**Std Dev**	**Mean**	**Std Dev**	**Mean**	**Std Dev**	**Mean**	**Std Dev**	**Mean**	**Std Dev**
Ba	ng/m^3	6.1	0.33	4.7	0.45	4.1	0.29	4.7	0.26	5.3	0.16	4.8	0.28
Cd	ng/m^3	0.03	0.0044	0.047	0.006	0.052	0.0041	0.032	0.003	0.039	0.0048	0.05	0.0052
Cr	ng/m^3	0.88	0.12	1.3	0.073	2.0	0.12	1.1	0.25	1.9	0.3	1.9	0.28
Cs	ng/m^3	0.012	0.00069	0.017	0.0015	0.017	0.00022	0.015	0.00035	0.015	0.00091	0.016	0.0015
Cu	ng/m^3	2.5	0.2	2.6	0.21	2.7	0.15	1.5	0.22	2.5	0.26	1.9	0.2
Fe	ng/m^3	9.8	1.1	11	0.72	10	0.8	7.5	1.7	9.9	1.2	12	1.6
Li	ng/m^3	0.059	0.0065	0.088	0.0042	0.12	0.0067	0.085	0.019	0.11	0.011	0.12	0.016
Mn	ng/m^3	4.2	0.28	4.3	0.19	2.6	0.27	3.8	0.59	4.8	0.61	5.6	0.65
Mo	ng/m^3	2.3	0.15	3.0	0.12	2.4	0.24	4.8	0.92	14	1.0	11	1.1
Ni	ng/m^3	0.92	0.15	0.81	0.075	1.2	0.08	0.68	0.2	1.1	0.26	1.7	0.54
Pb	ng/m^3	0.32	0.031	0.41	0.039	0.42	0.072	0.4	0.031	0.29	0.031	0.36	0.1
Rb	ng/m^3	0.34	0.026	0.43	0.042	0.4	0.007	0.3	0.033	0.36	0.026	0.37	0.017
Sb	ng/m^3	0.45	0.048	0.35	0.019	0.26	0.031	0.51	0.074	0.31	0.034	0.29	0.039
Sn	ng/m^3	0.25	0.026	0.16	0.008	0.18	0.017	0.15	0.016	0.16	0.019	0.17	0.02
Sr	ng/m^3	1.7	0.14	2.1	0.14	1.4	0.12	1.7	0.17	1.9	0.17	1.8	0.18
Ti	ng/m^3	0.08	0.01	0.091	0.008	0.12	0.016	0.089	0.028	0.1	0.018	0.13	0.013

Table S2.5. Mean values and standard deviations calculated between monthly values of interpolated concentrations of insoluble fraction of PM_{10} elements at the six monitoring sites.

Insoluble interpolated PM_{10} element concentrations													
		TE1		**TE2**		**TE3**		**TE4**		**TE5**		**TE6**	
	UoM	**Mean**	**Std Dev**	**Mean**	**Std Dev**	**Mean**	**Std Dev**	**Mean**	**Std Dev**	**Mean**	**Std Dev**	**Mean**	**Std Dev**
Ba	ng/m^3	7.3	1.1	6.9	1.1	4.9	1.3	6.2	1.1	6.5	0.92	4.0	1.1

Cd	ng/m^3	0.006	0.00067	0.022	0.0049	0.016	0.0051	0.021	0.0037	0.025	0.006	0.026	0.0054
Cr	ng/m^3	13	0.48	14	1.2	30	0.92	12	1.9	45	6.9	48	4.1
Cs	ng/m^3	0.021	0.007	0.03	0.01	0.035	0.0093	0.025	0.12	0.031	0.008	0.032	0.011
Cu	ng/m^3	8.9	0.99	7.3	0.11	9.3	0.36	4.7	0.45	11	0.75	6.6	0.52
Fe	ng/m^3	351	15	344	23	577	16	218	30	332	48	504	68
Li	ng/m^3	0.12	0.0062	0.1	0.0081	0.15	0.0076	0.087	0.01	0.15	0.026	0.1	0.022
Mn	ng/m^3	6.3	0.23	7.1	0.56	3.5	0.34	5.3	0.53	11	0.88	14	0.85
Mo	ng/m^3	0.8	0.023	1.3	0.21	1.4	0.14	0.96	0.18	2.1	0.48	4.1	0.21
Ni	ng/m^3	4.8	0.49	6.3	0.63	4.3	0.46	3.4	1.0	19	1.1	23	2.9
Pb	ng/m^3	3.0	0.15	3.3	0.12	4.6	0.21	3.0	0.38	4.5	0.25	3.4	0.51
Rb	ng/m^3	0.45	0.066	0.32	0.049	0.43	0.041	0.16	0.055	0.44	0.045	0.3	0.059
Sb	ng/m^3	0.66	0.014	0.4	0.0053	0.3	0.032	0.64	0.044	0.73	0.031	0.25	0.038
Sn	ng/m^3	2.0	0.1	1.7	0.13	2.1	0.14	0.85	0.08	2.3	0.078	1.0	0.13
Sr	ng/m^3	1.2	0.17	1.4	0.14	1.0	0.16	2.4	0.47	2.3	0.67	1.3	0.21
Ti	ng/m^3	4.5	0.12	4.3	0.49	7.1	0.48	3.6	0.58	7.1	0.41	8.0	1.0

Table S2.6. Mean values and standard deviations calculated between monthly values of interpolated concentrations of the total fraction of PM_{10} elements at the six monitoring sites.

Total interpolated PM_{10} element concentrations													
		TE1		**TE2**		**TE3**		**TE4**		**TE5**		**TE6**	
	UoM	**Mean**	**Std Dev**	**Mean**	**Std Dev**	**Mean**	**Std Dev**	**Mean**	**Std Dev**	**Mean**	**Std Dev**	**Mean**	**Std Dev**
Ba	ng/m^3	13	0.87	12	1.2	9.0	1.3	11	0.90	12	0.82	8.8	1.1
Cd	ng/m^3	0.036	0.0029	0.069	0.0073	0.068	0.0041	0.054	0.0021	0.063	0.0055	0.076	0.0065
Cr	ng/m^3	14	0.45	15	1.1	32	0.98	13	2.1	47	4.0	49	4.4
Cs	ng/m^3	0.033	0.0065	0.047	0.010	0.052	0.0090	0.041	0.011	0.046	0.0093	0.048	0.011
Cu	ng/m^3	11	0.74	9.9	0.18	12	0.093002	6.1	0.25	13	0.39	8.5	0.41
Fe	ng/m^3	361	14	355	24	588	19	226	31	343	47	514	62
Li	ng/m^3	0.18	0.0099	0.19	0.022	0.27	0.015001	0.17	0.036	0.26	0.034	0.23	0.047
Mn	ng/m^3	11	0.25	11	0.63	6.1	0.076	9.1	1.0	16	1.3	20	1.1
Mo	ng/m^3	3.1	0.11	4.3	0.14	3.8	0.34	5.8	1.2	15	1.5	16	1.1
Ni	ng/m^3	5.7	0.45	7.1	0.57	5.5	0.24	4.1	1.3	20	1.2	24	2.5

Pb	ng/m^3	3.3	0.16	3.7	0.12	5.1	0.093	3.4	0.37	4.8	0.27	3.9	0.59
Rb	ng/m^3	0.79	0.074	0.76	0.082	0.83	0.045	0.46	0.070	0.80	0.056	0.67	0.084
Sb	ng/m^3	1.1	0.014	0.75	0.0042	0.57	0.0057	1.2	0.070	1.0	0.044	0.54	0.062
Sn	ng/m^3	2.3	0.082	1.8	0.14	2.3	0.14	1.0	0.085	2.4	0.094	1.2	0.12
Sr	ng/m^3	2.9	0.28	3.5	0.47	2.4	0.19	4.1	0.44	4.2	0.51	3.1	0.44
Ti	ng/m^3	4.6	0.12	4.4	0.48	7.2	0.44	3.7	0.41	7.2	0.41	8.1	0.72

Fig. S3.1 SEM micrograph (a) and respective EDX spectrum (b) of a steel particle (Fe, Ni and Cu) sampled near the steel plant.

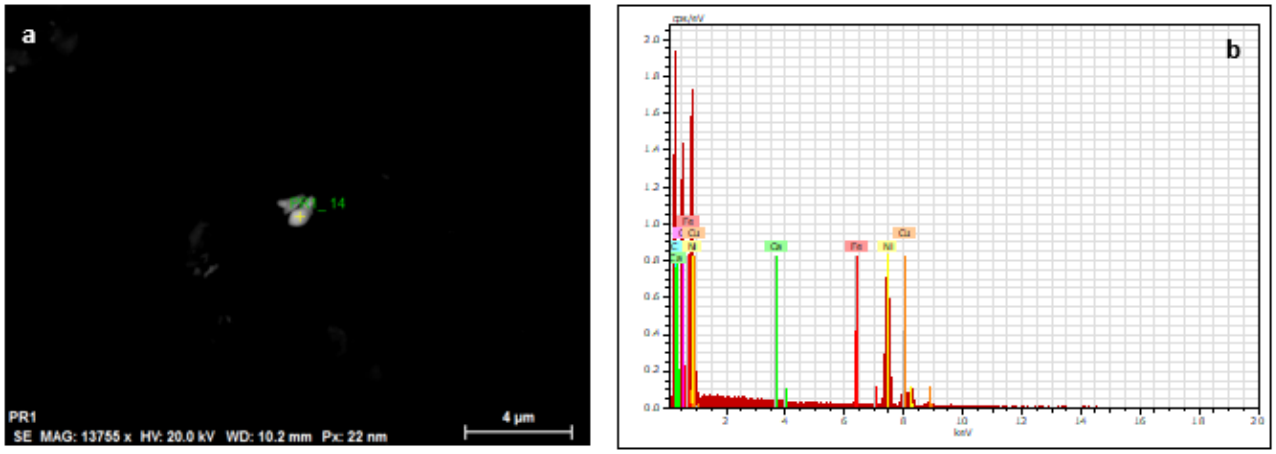

Table S4.1 Certified values for the SRM 1515 (apple leaves) used and accuracy obtained by SRM (ng mg^{-1}).

Apple leaves SRM 1515					
		Certified value		**Accuracy obtained**	
	UoM	**Mean**	**Std Dev**	**Mean**	**Std Dev**
Ba	ng/mg	49	2	41	0.98
Cd	ng/mg	0.013	0.002	0.014	0.001
Cr	ng/mg	0.3*	-	0.36	0.07
Cu	ng/mg	5.6	0.24	5.8	0.25
Fe	ng/mg	83	5	99	0.4
Mn	ng/mg	54	3	57	0.83
Mo	ng/mg	0.095*	-	0.11	0.03
Ni	ng/mg	0.91	0.12	1.2	0.3
Pb	ng/mg	0.47	0.024	0.51	0.08

Rb	ng/mg	10	0.82	9.3	0.21
Sb	ng/mg	0.013*	-	0.016	0.003
Sn	ng/mg	0.2*	-	0.32	0.04
Sr	ng/mg	25	3	28.7	0.2

* = values of these elements have to be considered as informative concentrations.

References

1. Perdue, R. E. Arundo donax—Source of musical reeds and industrial cellulose 1958, Econ Bot, 12: 368. https://doi.org/10.1007/BF02860024
2. Bell, G. P. Ecology and management of Arundo donax, and approaches to riparian habitat restoration in Southern California 1997, Plant Invasions: studies from North America and Europe, pp. 103-113.
3. Nsanganwimana, F.; Marchand, L.; Douay, F.; Mench, M. Arundo donax L., a candidate for phytomanaging water and soils contaminated by trace elements and producing plant-based feedstock. A review 2014, Int J Phytoremediation 16, 982–1017. DOI: 10.1080/15226514.2013.810580
4. Papazoglou, E. G.; Karantounias, G. A.; Vemmos S. N.; Bouranis, D. L. Photosynthesis and growth responses of giant reed (Arundo donax L.) to the heavy metals Cd and Ni 2005, Environ. Int. 31(2), 243-249. https://doi.org/10.1016/j.envint.2004.09.022
5. Bonanno, G. Comparative performance of trace element bioaccumulation and biomonitoring in the plant species Typha domingensis, Phragmites australis and Arundo donax 2013, Ecotoxicol. Environ. Saf. 97, 124-130. https://doi.org/10.1016/j.ecoenv.2013.07.017
6. Bonanno, G. Arundo donax as a potential biomonitor of trace element contamination in water and sediment 2012, Ecotoxicol. Environ. Saf. 80, 20–27. doi:10.1016/j.ecoenv.2012.02.005
7. Szczepaniak, K.; Biziuk, M. Review: Ecotoxicology, Aspects of the biomonitoring studies using mosses and lichens as indicators of metal pollution 2003, Environ. Res 93, 221–230. doi:10.1016/S0013-9351(03)00141-5
8. Abril, G. A.; Wannaz, E. D.; Mateos, A. C.; Pignata, M. L. Biomonitoring of airborne particulate matter emitted from a cement plant and comparison with dispersion modelling results 2014 Atmos. Environ. 8, 154-163, https://doi.org/10.1016/j.atmosenv.2013.10.020
9. Massimi, L.; Conti, M. E.; Mele, G.; Ristorini, M.; Astolfi, M. L.; Canepari, S. Lichen Transplants as Indicators of Atmospheric Element Concentrations: a High Spatial Resolution Comparison with PM10 Samples in a Polluted Area (Central Italy) 2019, Ecol. Indic. 101, 759-769. DOI: 10.1016/j.ecolind.2018.12.051

10. Urbat, M.; Lehndorff, E.; Schwark, L., Biomonitoring of air quality in the Cologne conurbation using pine needles as a passive sampler—Part I: magnetic properties 2004, Atmos. Environ. 38 (23), 3781-3792 https://doi.org/10.1016/j.atmosenv.2004.03.061
11. Lin, V. S. Research highlights: natural passive samplers – plants as biomonitors 2015. Environ. Sci.: Processes Impacts 17, 1137-1140. DOI: 10.1039/C5EM90016F
12. Sgrigna, G.; Baldacchini, C.; Esposito, R.; Calandrelli, R.; Tiwary, A.; Calfapietra, C. Characterization of leaf-level particulate matter for an industrial city using electron microscopy and X-ray microanalysis 2016, Sci Total Environ 548–549, 91–99. http://dx.doi.org/10.1016/j.scitotenv.2016.01.057
13. Janhall, S. Review on urban vegetation and particle air pollution e Deposition and dispersion 2015, Atmos. Environ. 105, 130-137. http://dx.doi.org/10.1016/j.atmosenv.2015.01.052
14. Gratani, L.; Crescente, M. F.; Varone L. Long-term monitoring of metal pollution by urban trees 2008, Atmos. Environ. 42, 8273–8277, doi:10.1016/j.atmosenv.2008.07.032.
15. Baldacchini, C.; Sgrigna, G.; Clarke, W.; Tallis, M.; Calfapietra, C. An ultra-spatially resolved method to quali-quantitative monitor particulate matter in urban environment 2019, Environ Sci Pollut Res Int. 26 (18), 18719-18729. doi: 10.1007/s11356-019-05160-8.
16. Thorpe, A.; Harrison, R. M., Sources and properties of non-exhaust particulate matter from road traffic: A review 2008, Sci. Total Environ. 400 270-282. doi:10.1016/j.scitotenv.2008.06.007
17. Slezakova, K.; Pires, J. C. M.; Pereira, M. C.; Martins, F. G.; Alvim-Ferraz, M. C. Influence of traffic emissions on the composition of atmospheric particles of different sizes—Part 2: SEM–EDS characterization 2008, J. Atmos. Chem. 60 (3), 221–236. https://doi.org/10.1007/s10874-008-9117-y
18. Pope III, C. A.; Burnett, R. T.; Thun, M. J.; Calle, E. E.; Krewski, D.; Ito, K.; Thurston, G. D. Lung cancer, cardiopulmonary mortality, and long-term exposure to fine particulate air pollution 2002, Jama, 287(9), 1132-1141.
19. Ebelt, S.T.; Petkau, A.J.; Vedal, S.; Fisher, T.V.; Brauer, M. Exposure of chronic obstructive pulmonary disease patients to particulate matter: relationships between personal and ambient air concentrations 2000, Journal of the Air and Waste Management Association 50 (7), 1081–1094.
20. Chen, L. C.; Lippmann, M. Effects of Metals within Ambient Air Particulate Matter (PM) on Human Health 2009, Inhal. Toxicol. 21(1), 1-31, DOI: 10.1080/08958370802105405
21. Anderson, J. O.; Thundiyil, J. G.; Stolbach, A. Clearing the Air: A Review of the Effects of Particulate Matter Air Pollution on Human Health 2012, J. Med. Toxicol. 8, 166–175 DOI 10.1007/s13181-011-0203-1
22. Sæbø, A.; Popek, R.; Nawrot, B.; Hanslin, H.M.; Gawronska, H.; Gawronski, S.W.; Plant species differences in particulate matter accumulation on leaf surfaces 2012, Sci Total Environ 427–428, 347–354. doi:10.1016/j.scitotenv.2012.03.084

23. Petroff, A.; Mailliat, A.; Amielh, M.; Anselmet, F.; Aerosol dry deposition on vegetative canopies. Part I: Review of present knowledge 2008, Atmos. Environ. 42, 3625–3653. doi:10.1016/j.atmosenv.2007.09.043
24. Terzaghi, E.; Wild, E.; Zacchello, G.; Cerabolini, B. E. L.; Jones, K. C.; Di Guardo, A. Forest Filter Effect: Role of leaves in capturing/releasing air particulate matter and its associated PAHs 2013, Atmos. Environ. 74, 378-384. https://doi.org/10.1016/j.atmosenv.2013.04.013
25. Hofman, J.; Wuyts, K.; Van Wittenberghe, S.; Brackx, M.; Samson, R. On the link between biomagnetic monitoring and leaf-deposited dust load of urban trees: Relationships and spatial variability of different particle size fractions 2014, Environ. Poll. 189, 63-72. https://doi.org/10.1016/j.envpol.2014.02.020
26. Sgrigna, G.; Sæbø, A.; Gawronski, S.; Popek, R.; Calfapietra, C. Particulate matter deposition on Quercus ilex leaves in an industrial city of central Italy 2015, Environ. Pollut. 197, 187–194. http://dx.doi.org/10.1016/j.envpol.2014.11.030
27. Massimi, L.; Ristorini, M.; Eusebio, M.; Florendo, D.; Adeyemo, A.; Brugnoli, D.; Canepari, S. Monitoring and evaluation of Terni (Central Italy) air quality through spatially resolved analyses 2017, Atmosphere 8(10), 200. doi:10.3390/atmos8100200
28. Moroni, B.; Ferrero, L.; Crocchianti, S.; Perrone, M. G.; Sangiorgi, G.; Bolzacchini, E.; Cappelletti, D. Aerosol dynamics upon Terni basin (Central Italy): results of integrated vertical profile measurements and electron microscopy analyses 2013, Rendiconti Lincei 24 (4) 319–328. doi: 10.1007/s12210-013-0230-8
29. Manigrasso, M.; Protano, C.; Astolfi, M. L.; Massimi, L.; Avino, P.; Vitali, M.; Canepari, S. Evidences of copper nanoparticle exposure in indoor environments: Long-term assessment, high-resolution field emission scanning electron microscopy evaluation, in silico respiratory dosimetry study and possible health implications 2017, Sci Total Environ 653, 1192-1203. https://doi.org/10.1016/j.scitotenv.2018.11.044
30. APHA, (1998) Standard methods for examination of water and waste water (20th. Ed.). Washington DC: American Public Health Association
31. Canepari, S.; Cardarelli, E.; Giuliano, A.; Pietrodangelo, A. Determination of metals, metalloids and non-volatile ions in airborne particulate matter by a new two-step sequential leaching procedure Part A: Experimental design and optimization 2006, Talanta 69, 581–587. doi:10.1016/j.talanta.2005.10.023
32. Canepari, S.; Cardarelli, E.; Pietrodangelo, A.; Strincone, M. Determination of metals, metalloids and non-volatile ions in airborne particulate matter by a new two-step sequential leaching procedure Part B: Validation on equivalent real samples 2006, Talanta 69, 588–595. doi:10.1016/j.talanta.2005.10.024

33. Canepari, S.; Pietrodangelo, A.; Perrino, C.; Astolfi, M. L.; Marzo, M. L. Enhancement of source traceability of atmospheric PM by elemental chemical fractionation 2009, Atmos. Environ. 43 (31), 4754-4765. https://doi.org/10.1016/j.atmosenv.2008.09.059
34. Piacentini, D.; Falasca, G.; Canepari, S.; Massimi, L. Potential of PM-selected components to induce oxidative stress and root system alteration in a plant model organism 2019, Environ. Int. 132, 105094. https://doi.org/10.1016/j.envint.2019.105094
35. Astolfi, M. L.; Marconi, E.; Protano, C.; Vitali, M.; Schiavi, E.; Mastromarino, P.; Canepari, S. Optimization and validation of a fast digestion method for the determination of major and trace elements in breast milk by ICP-MS 2018, Anal. Chim. Acta 1040, 49-62. https://doi.org/10.1016/j.aca.2018.07.037
36. Cressie, N. Spatial Prediction and Ordinary Kriging 1988, Math. Geol. 20 (4), 405–421. https://doi.org/10.1007/BF00892986
37. Cressie, N. The origins of kriging 1990, Math. Geol. 22 (3),239–252. https://doi.org/10.1007/BF00889887
38. Blair, M.; Stevens, T.L. Steel Castings Handbook, 6th ed.; Steel Founders' Society and ASM International: Novelty, OH, USA, 1995; pp. 2–34.
39. Adachi, K.; Tainosho, Y. Characterization of heavy metal particles embedded in tire dust 2004, Environ. Int. 30 (8), 1009-1017. https://doi.org/10.1016/j.envint.2004.04.004
40. Birmili, W.; Allen, A. G.; Bary, F.; Harrison, R. M. Trace Metal Concentrations and Water Solubility in Size-Fractionated Atmospheric Particles and Influence of Road Traffic 2006, Environ. Sci. Technol. 40, 1144-1153. DOI: 10.1021/es0486925
41. Litschke, T.; Kuttler, W. On the reduction of urban particle concentration by vegetation – a review 2008, Meteorol. Z. 17, (3), 229-240. DOI: 10.1127/0941-2948/2008/0284
42. Morakinyo, T. E.; Lam, Y. F. Simulation study of dispersion and removal of particulate matter from traffic by road-side vegetation barrier 2016, Environ Sci Pollut Res 23, 6709–6722. DOI 10.1007/s11356-015-5839-y.
43. Umbrìa, A.; Galan, M.; Munoz, M.J.; Martìn, R. Characterization of atmospheric particles: analysis of particles in the Campo de Gibraltar 2004, Atmosfera 17 (4), 191-206. ISSN 0187-6236.
44. Bouhsina, S.; Cazier, F.; Noual, H.; Dewaele, D.; Delbende A.; Courcot, D.; Aboukais, A. Characteristics of suspended particulate matter emitted from an iron and steel company – A multi technique approach for search of tracers 2008, Chem. Eng. Trans. 16:79.
45. Song, F.; Gao, Y. Size distributions of trace elements associated with ambient particular matter in the affinity of a major highway in the New Jersey–New York metropolitan area 2011, Atmospheric Environ. 45 (37), 6714-6723. https://doi.org/10.1016/j.atmosenv.2011.08.031
46. Canepari, S.; Perrino, C.; Olivieri, F.; Astolfi, M. L. Characterisation of the traffic sources of PM through size-segregated sampling, sequential leaching and ICP analysis 2008, Atmospheric Environ. 42(35), 8161-8175. https://doi.org/10.1016/j.atmosenv.2008.07.052

47. Simonetti, G.; Buiarelli, F.; Di Filippo, P.; Pomata, D.; Riccardi, C.; Ristorini, M.; Astolfi, M. L.; Canepari, S. Spatial Distribution of Levoglucosan and Alternative Biomass Burning Tracers in an Urban and Industrial Hot-spot of Central Italy, ATMOSRES- paper under review
48. Minguillón, M. C.; Querol, X.; Baltensperger, U.; Prévôt, A. S. H. Fine and coarse PM composition and sources in rural and urban sites in Switzerland: Local or regional pollution? 2012, Sci Total Environ 427–428, 191-202. https://doi.org/10.1016/j.scitotenv.2012.04.030
49. Gietl, J. K.; Lawrence, L.; Thorpe, A., J.; Harrison, R. M. Identification of brake wear particles and derivation of a quantitative tracer for brake dust at a major road 2010, Atmos. Environ. 44 (2), 141-146. https://doi.org/10.1016/j.atmosenv.2009.10.016
50. Dongarrà, G.; Manno, E.; Varrica, D. Possible markers of traffic-related emissions 2008, Environ. Monit. Assess. 154:117. https://doi.org/10.1007/s10661-008-0382-7
51. Mirza, N.; Pervez, A.; Mahmood, Q.; Shah, M. M.; Shafqat, M. N. Ecological restoration of arsenic contaminated soil by Arundo donax L 2011, Ecol. Eng. 37, 1949– 1956. doi:10.1016/j.ecoleng.2011.07.006
52. Barbosa, B.; Boléo, S.; Sidella, S.; Costa, J.; Duarte, M.; Mendes, B.; Cosentino, S. L.; Fernando A. L. Phytoremediation of Heavy Metal-Contaminated Soils Using the Perennial Energy Crops Miscanthus spp. and Arundo donax L. 2015, Bioenerg. Res. 8, 1500–1511. DOI 10.1007/s12155-015-9688-9
53. Capelli, L.; Sironi, S.; Del Rosso, R.; Céntola, P.; Rossi, A.; Austeri, C. Olfactometric approach for the evaluation of citizens' exposure to industrial emissions in the city of Terni, Italy 2011, Sci. Total Environ. 409 (3), 595-603. https://doi.org/10.1016/j.scitotenv.2010.10.054
54. Sabeen, M.; Mahmood, Q.; Irshad, M.; Fareed, I.; Khan, A.; Ullah, F.; Hussain, J.; Hayat, Y.; Tabassum S. Cadmium Phytoremediation by Arundo donax L. from Contaminated Soil and Water 2013, BioMed Research International, 9 pages http://dx.doi.org/10.1155/2013/324830
55. Atma, W.; Larouci, M.; Meddah, B.; Benabdeli, K.; Sonnet, P. Evaluation of the phytoremediation potential of Arundo donax L. for nickel-contaminated soil 2017, Int J Phytoremediat 19 (4), 377-386, DOI:10.1080/15226514.2016.1225291

5.6 (A6) Lichen transplants for high spatial resolution biomonitoring of Persistent Organic Pollutants (POPs) in a multi-source polluted area of Central Italy

Ecological Indicators (2021), 120, 106921, doi: 10.1016/j.ecolind.2020.106921

Lorenzo Massimi[1], Federica Castellani[2,3], Carmela Protano[2*], Marcelo Enrique Conti[4], Arianna Antonucci[2], Maria Agostina Frezzini[1], Mara Galletti[5], Giustino Mele[4], Andrea Pileri[5], Martina Ristorini[6], Matteo Vitali[2], Silvia Canepari[1]

[1] Department of Chemistry, University of Rome La Sapienza, P.le Aldo Moro, 5, 00185 Rome, Italy;

[2] Department of Public Health and Infectious Diseases, University of Rome La Sapienza, P.le Aldo Moro, 5, 00185 Rome, Italy;

[3] Department of Ecological and Biological Sciences, Tuscia University, Largo dell'Università snc, 01100 Viterbo, Italy

[4] Department of Management, University of Rome La Sapienza, Viale del Castro Laurenziano 9, 00161 Rome, Italy;

[5] ARPA Umbria, Via Carlo Alberto dalla Chiesa, 23, 05100, Terni, Italy

[6] Department of Bioscience and Territory, University of Molise, Pesche (IS), 86090, Italy;

*Corresponding author

Keywords: Biomonitor; *Evernia prunastri*; Polychlorinated dibenzodioxins; Polychlorinated dibenzofurans; Polychlorinated biphenyl

Abstract

The ability of lichen transplant *Evernia prunastri* (L.) Ach. to reflect air concentration and spatial distribution of 7 polychlorinated dibenzodioxins (PCDDs), 10 polychlorinated dibenzofurans (PCDFs), and 23 polychlorinated biphenyls (PCBs) was evaluated through the construction of a wide and dense biomonitoring network. For this purpose, 23 lichen transplants were placed in a highly polluted area in Central Italy, characterized by the presence of different local emission sources such as a power plant, a steel plant, vehicular traffic, and domestic heating. The high spatial resolution data obtained from lichens were used to map the spatial distribution of the studied compounds, useful to identify the location and strength of target compounds sources over the territory. The maps showed that the highest concentrations of the pollutants were detected, as expected, in the sites close to the power plant and to the steel plant, confirming their important role as persistent pollutants emission sources. The statistical analysis performed on the spatially resolved data allowed us to identify the steel plant as the main source of PCDD/Fs, while PCBs were emitted by both the steel plant and the power plant. Finally, the efficiency of lichen transplants to reflect PCDD/Fs and PCBs atmospheric concentrations was assessed by comparing lichen data with POPs deposition measured by bulk deposition samplers at sites impacted by intensive emission sources; good results were achieved from the comparison (R^2 > 0.79). Lichen transplants have demonstrated to be suitable biomonitors of POPs, allowing to obtain a high

spatial monitoring network. The low-cost biomonitoring and experimental approach described in this study can be applied to other monitoring campaigns for identifying localizing emission sources of POPs in areas contaminated by several disaggregated sources.

1. Introduction

The International Agency for the Research on Cancer (IARC) classified outdoor air pollution as Group 1 carcinogen (i.e., carcinogenic to humans) (IARC, 2016), confirming the great concern for public health due to air quality issue. Air pollutants are a complex mixture of inorganic and organic compounds, and many of them are of toxicological interest. A relevant group of air pollutants is the so-called Persistent Organic Pollutants (POPs), including polychlorinated dibenzodioxins (PCDDs), polychlorinated dibenzofurans (PCDFs) and polychlorinated biphenyls (PCBs) (Avino and Russo, 2018). These compounds are released into the environment from different combustion sources, such as domestic heating, vehicle and industrial emissions (e.g., waste-to-energy plants), but also from processes of metal forming and machining that involve elemental chlorine (Alcock et al., 2001 Yu et al., 2006; Eckhardt et al., 2007; Li et al., 2010; Thacker et al., 2010; Protano et al., 2015). When PCDD/Fs and PCBs are released in the atmosphere, they are distributed between gas and particulate phases depending on concentration, chemical-physical properties, meteorological parameters (e.g., temperature, wind speed, humidity), and air particulate matter (PM) levels (Hoff et al., 1996; Mi et al., 2012; Barbas et al., 2018).

The relevance of PCDD/Fs and PCBs as air pollutants is due to their toxicity and ability to persist in the environment for a long time and to biomagnify through the food chain (Thakur and Pathania, 2020). Therefore, the study of the spatial distribution of POPs over the territory is essential to assess environment-related human health risks (Vitali et al., 2019). However, to date, some limitations reduce the possibility to perform appropriate environmental monitoring campaigns for these pollutants. The main restriction is related to sampling duration and volume flow rate (24h and 2.3 $m^3 h^{-1}$, usually), that do not permit to detect low air levels of target pollutants (Augusto et al., 2013). Besides, conventional air samplers and/or bulk deposition samplers cannot be placed in numerous sites due to their expensiveness and logistic problems (Gao et al. 2015; Kardel et al. 2018). Consequently, POPs dispersion over the territory is typically estimated through mathematical models, often revealing limitations due to the complexity of the represented system (Irwin, 2014; Vitali et al., 2016; Kim et al., 2017). The development of "smart" and low-cost air monitoring systems that allow overcoming the described limitations could be useful for refining dispersion model predictions. For this reason, over the last decades, the development of methods using plants, algae, lichens, and mosses as biomonitors generated increasing interest due to their easy in operation, rapidity, and inexpensiveness (Conti and Cecchetti, 2001; Protano et al., 2015; Massimi et al., 2019; Ndlovu et al., 2019). Lichens are considered effective tools for a long-term sampling of air pollutants because of their ability to accumulate many different contaminants and their suitability for different scenarios (Sett et al., 2016). Accumulation of detectable amounts of air pollutants in lichens depends on several factors, such as chemical-physical properties of the compound (e.g., solubility in water and vapor pressure), its air concentration, atmospheric conditions over the sampling period (e.g., temperature, rainfall) and the lichen species. Biomonitoring campaign may be carried out by using native

(i.e., lichens already present in the area) or transplanted lichens (i.e., species collected from unpolluted sites and transplanted into the study area; Bergamaschi et al., 2007; Augusto et al., 2013; Van der Wat and Forbes, 2014). However, lichen transplants are more suitable to achieve an extended monitoring network that allows studying the spatial distribution of atmospheric pollutants (Protano et al., 2014; Conti et al., 2016; Lucadamo et al., 2016; Vannini et al., 2017).

Bulk deposition sampler, a passive monitoring method that allows collecting both wet and dry atmospheric depositions, is another monitoring tool frequently used to assess outdoor air quality(Jones and Duarte-Davidson, 1997; Fang et al., 2011; Argiriadis et al., 2014; Qu et al., 2019) Although it could be reductive to consider lichens just passive collectors, due to the complexity of the processes governing the bioaccumulation, numerous studies suggest that lichen thalli might reflect the air pollutants deposition from the atmosphere (Tyler, 1989; Sloof, 1995; Reis et al., 1999; Bari et al., 2001; Godinho et al., 2008). Therefore, in this study, POPs accumulation in transplanted lichens was compared with POPs deposition measured by bulk deposition samplers at sites impacted by the most intensive emission sources of the study area. The aim of this study is to use the low-cost lichen transplants for obtaining high spatial resolution data of POPs and mapping their spatial distribution, in order to evaluate the efficiency of lichen transplants to reflect PCDD/Fs and PCBs atmospheric concentrations and to assess PCDD/Fs and PCBs spatial variability according to the different strength of the sources present over the territory. To this aim, we built a wide and dense biomonitoring network (i.e. 23 biomonitoring sites, about 1 km between each other) across Terni, a very polluted area in Central Italy, characterized by the presence of numerous and diversified emission sources of air pollutants, and we performed a long-term air monitoring campaign by using transplanted lichens.

2. Materials and methods

2.1 Study area

Lichen transplants (*E. prunastri*) were placed at 23 monitoring sites in Terni, one of the most polluted areas of Central Italy (Moroni et al., 2013). Terni is a small city (212 km^2) characterized by the presence of several urban and industrial emission sources (vehicular traffic, domestic heating, a power plant for waste treatment and a steel plant) (Guerrini, 2012) and by peculiar meteorological conditions, which limit air mixing and air pollutants transport (Ferrero et al., 2012). The biomonitoring campaign was carried out for 13 months, from December 17th, 2016 to January 15th, 2018.

2.2. Sampling sites

The individuation of the most appropriate monitoring sites, as described in Massimi et al. (2017, 2020a, 2020b), was challenging and time-consuming. Indeed, the 23 monitoring sites were selected with the aim to represent the contribution of the emission sources present over the territory. The sampling sites were chosen with the support and help of ARPA Umbria (regional agency for environmental protection), which provided us a PM_{10} dispersion grid that was used as a reference system and recommended us the best locations for the deployment of the lichen transplants, according to their previous PM and POPs monitoring and analyses. The lichen transplants were deployed in order to cover the whole basin with a spatial resolution of about 1 km and

to be as close as possible to potential local POPs sources. For each selected monitoring site, geographical coordinates, type of site, and main local emission sources are reported in Table 1. In each of the 23 sites, a lichen transplant was deployed. At 4 of the 23 monitoring sites (Ind-MA, Ind-PR, Urb-LG, Res-BR), selected on a geographical approach (respectively, one for each north, south, east and west direction) and on the basis of different levels of air pollution previously measured by ARPA Umbria, data of bulk deposition samplers for monitoring POPs concentrations were used and compared with lichen data to assess their efficiency (Figure 1).

Table 1. Name, type of site, main local emission sources, and geographical coordinates of the 23 monitoring sites in Terni city.

Site	Type of site and main emission source	Geographical Coordinates	
		Latitude	Longitude
Ind-RI	Industrial, power plant	42° 33′ 52.02" N	12° 35′ 21.94" E
Ind-MA	Industrial, power plant	42° 33′ 41.42" N	12° 36′ 19.05" E
Ind-FA	Industrial, power plant	42° 33′ 03.19" N	12° 36′ 29.76" E
Ind-GI	Industrial, power plant	42◦ 34′ 06.28" N	12° 36′ 48.27" E
Ind-FR	Industrial, power plant	42° 33′ 53.22" N	12° 37′ 11.44" E
Ind-CB	Industrial, power plant	42° 33′ 20.30" N	12° 37′ 20.45" E
Res-PI	Residential, domestic heating	42° 32′ 56.96" N	12° 37′ 52.26" E
Res-BR	Residential, domestic heating	42° 34′ 56.19" N	12° 37′ 23.30" E
Res-AR	Residential, domestic heating	42° 34′ 34.23" N	12° 37′ 39.88" E
Ind-CR	Industrial, power plant	42° 34′ 09.49" N	12° 37′ 39.81" E
Urb-HG	Urban, vehicular traffic	42° 34′ 19.32" N	12° 37′ 56.02" E
Urb-SA	Urban, vehicular traffic	42° 33′ 45.16" N	12° 38′ 18.45" E
Urb-PV	Urban, vehicular traffic	42° 33′ 06.96" N	12° 38′ 35.20" E
Urb-LG	Urban, vehicular traffic	42° 32′ 59.75" N	12° 39′ 01.16" E
Urb-CZ	Urban, vehicular traffic	42° 34′ 06.90" N	12° 38′ 52.97" E
Urb-HV	Urban, vehicular traffic	42° 33′ 58.33" N	12° 39′ 04.74" E
Urb-UC	Urban, vehicular traffic	42° 33′ 38.09" N	12° 38′ 47.62" E
Urb-CA	Urban, vehicular traffic	42° 33′ 39.01" N	12° 39′ 03.11" E

Ind-CO	Industrial, steel plant	42° 33′ 34.23" N	12° 39′ 22.62" E
Ind-RO	Industrial, steel plant	42° 33′ 51.16" N	12° 39′ 39.15" E
Ind-OB	Industrial, steel plant	42° 34′ 18.64" N	12° 40′ 05.57" E
Ind-PR	Industrial, steel plant	42° 34′ 20.30" N	12° 40′ 44.23" E
Ind-CP	Industrial, steel plant	42° 33′ 31.65" N	12° 40′ 36.04" E

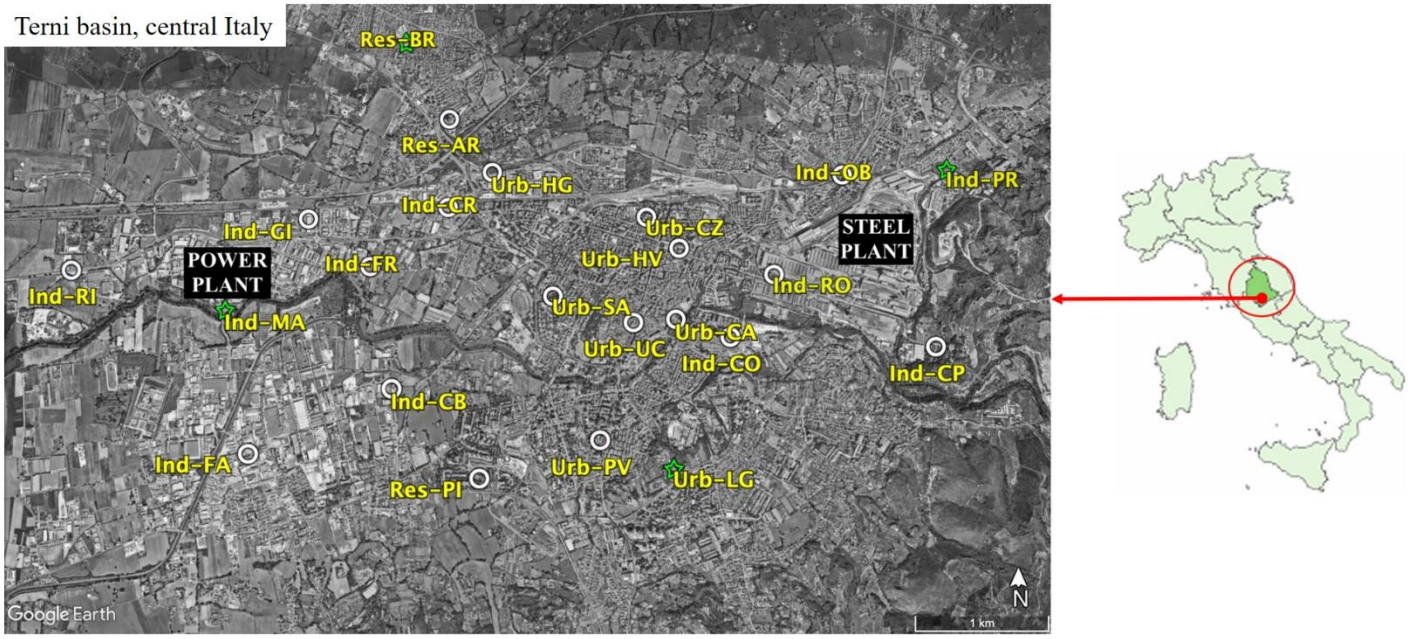

Figure 1. Map of the 23 monitoring sites (Ind-RI, Ind-MA, Ind-FA, Ind-GI, Ind-FR, Ind-CB, Res-PI, Res-BR, Res-AR, Ind-CR, Urb-HG, Urb-SA, Urb-PV, Urb-LG, Urb-CZ, Urb-HV, Urb-UC, CA, Ind-CO, Ind-RO, Ind-OB, Ind-PR, Ind-CP) in Terni. The sites where deposition samplers and lichen transplants are both present are marked with a green star (Ind-PR, Res-BR, Urb-LG, Ind-MA; Google Earth).

2.3 Lichen collection and transplant

The suitability of *E. prunastri* to subsist in diverse environments over time was previously tested (Conti et al., 2004). However, as recommended by VDI (Verein Deutscher Ingenieure; the Association of German Engineers) a pre-conditioning study was conducted to minimize the effects of additional factors than air pollution (Castellani et al., 2020; VDI, 1991, 1995). Thalli were previously transplanted for three months at the same collection sites (i.e., two or three trees in which we installed lichen transplants) of the National Park of Abruzzo (Boudreault et al., 2013). At the end of this control study, lichens looked healthy, and the sample loss was negligible (< 5% of samples).

Lichen collection was extensively described in Massimi et al. (2019). Briefly, in November 2016, *E. prunastri* thalli were collected at National Park of Abruzzo (Central Italy; 41°48′30.2″N; 13°47′11.3″E), an unpolluted area sited 120 km away from Terni. All thalli were gathered from trees stumps with inclination < 10%, at the height of 1–2 m above the terrain. Then, 10 g of thalli was split into two parts of 5 g, fixed on a support composed of two plastic nets and transplanted at the 23 selected monitoring sites (Figure 1). Standard deviations of distributions of the POPs analyzed in the two subsamples were all below 20% and results confirmed data homogeneity for subsamples. Thus, we merged data of the analyzed subsamples. To ensure homogeneous and representative sampling conditions, all biomonitors were located 2 m above the ground with the same southern exposition. After the exposure period (13 months), the transplanted lichens were collected, stored in a cooler, and transported to the laboratory. In the laboratory, as described in Conti et al. (2004), unwashed lichen samples were sorted to remove as much extraneous material (i.e., soil, mosses, other lichen species, etc.) and stored in the dark at < -10 °C in closed containers. Once taken out of the freezer, thermal equilibrium with the external temperature was established and then the samples were dried for 48 h at 35°C until constant weight and extracted following the EPA 1613: 1994 method. The samples were then pulverized by using a ball mill.

2.4 Deposition samples

Atmospheric depositions of organic pollutants were assessed by using bulk collectors, that allow the sampling of both wet and dry depositions. Each collector, consisting of a funnel connected to a polytetrafluoroethylene bottle, was exposed to the atmosphere for one month. Considering the whole duration of the monitoring campaign (13 months), 13 deposition samples were collected at each of the 4 monitoring sites (Ind-PR, Res-BR, Urb-LG, Ind-MA; Figure 1).

2.5 Analytical determinations

2.5.1 Analytical determination for lichen samples

Lichen samples were analyzed immediately after the collection from the unpolluted site, in order to obtain PCDD/Fs and PCBs initial concentration (blank), and after 13 months of exposure.

The set of analyses was carried out by the laboratory of the Terni district of the Environmental Protection Agency of Umbria (Italy), accredited in accordance with ISO/IEC 17025 standards. The determination of target analytes was performed by using a gas chromatograph coupled to high resolution magnetic sector mass spectrometry (DFS Magnetic Sector GC-HRMS) (Thermo Scientific, Bremen, Germany). All the lichen samples were extracted by accelerated solvent extraction (ASE; Thermo Scientific Dionex ASE 350 Accelerated Solvent Extractor). Briefly, 3 g of grinded thalli were added with 50 μL of $^{13}C_{12}$-labelled polychlorinated biphenyls surrogates standard solutions at 10 ng mL^{-1} in isoctane (PCB-28, PCB-31, PCB-44, PCB-52, PCB-77, PCB-95, PCB-99, PCB-101, PCB-105, PCB-110, PCB-118, PCB-123, PCB-128, PCB-138,

PCB-146, PCB-149, PCB-151, PCB-153, PCB-157, PCB-167, PCB-170, PCB-180, PCB-187) and 50 μL of $^{13}C_{12}$-labelled dioxins/furans surrogates standard solutions at 4-8 ng mL^{-1} in isoctane (2,3,7,8-TCDD, 1,2,3,7,8-PeCDD, 1,2,3,4,7-HxCDD, 1,2,3,6,7,8-HxCDD, 1,2,3,7,8,9-HxCDD, 1,2,3,4,6,7,8-HpCDD, OCDD, 2,3,7,8-TCDF, 2,3,4,7,8-PeCDF, 1,2,3,7,8-PeCDF, 1,2,3,4,7,8-HxCDF, 1,2,3,6,7,8-HxCDF, 1,2,3,7,8,9-HxCDF, 2,3,4,6,7,8-HxCDF, 1,2,3,4,6,7,8-HpCDF, 1,2,3,4,7,8,9-HpCDF, OCDF). After isotopic enrichment, samples were extracted with two consecutive ASE cycles at 150°C and 1500 psi by a mixture hexane/acetone (50:50). Extracts (about 20 mL each) were then purified to minimize interferences by a multilayer column (Na_2SO_4, silica, $NaHCO_3$ - Na_2SO_4 mixture, 12 mL H_2SO_4 96% - 20 g celite mixture, Na_2SO_4). The column was eluted with 70 mL hexane, the eluate was concentrated by rotary evaporator to about 2 mL, quantitatively transferred to the top of a second column packed with basic alumina. This second column was washed with 10 mL hexane (not collected) and eluted with 40 mL of n-hexane-dichloromethane mixture (50:1) to collect PCBs and then with 60 mL of n-hexane-dichloromethane mixture (50:50) to collect PCDD/Fs. Both eluates were evaporated to dryness under a gently nitrogen flux and, finally, recovered with 50 μL of 2,2,4-trimethylpentane. The quantification of all the analytes and $^{13}C_{12}$-surrogate/internal standards was performed by isotopic dilution technique applied on the two most abundant product ions for native and ^{13}C-labelled standard, respectively.

Despite the complexity of the applied analytical determination, the recoveries for all the analyzed compounds were between 60% and 120%, in accordance with EPA method 1613:1994.

2.5.2 Analytical determination for deposition samples

The 13 deposition samples collected in each of the four selected sites were analyzed for their content in PCDD/Fs and PCBs. Briefly, all samples were spiked with 50 μL of $^{13}C_{12}$-labelled PCBs and 50 μL of $^{13}C_{12}$-labelled PCDD/Fs surrogate standard solutions, the same used for lichen samples. After the isotopic enrichment, samples were filtered by glass fiber filters, the filtrate was added with dichloromethane (DCM; 20:1 v/v; 50 mL of DCM each liter of filtrate), and the organic phase was collected. The glass fiber filters were then extracted by ASE, applying the same conditions used for lichens. The two final extracts (the organic phase and the ASE extract of each deposition sample) were then gathered together, treated, and analyzed, as previously indicated for lichen extracts.

2.6 Meteorological Records

Meteorological data were recorded in Terni by a WatchDog 2000 Series weather Station (model 2700; Spectrum Technologies Ltd., Bridgend, Wales, UK) located on the top of a building at Urb-AR sampling site, 30 m above ground level, in order to avoid street canyon interference effects on the wind speed and direction. Wind speed (m/s), wind direction (degrees) and wind gust (m/s) were recorded during all the monitoring campaign, from December 17th, 2016 to January 15th, 2018. The wind rose for the entire monitoring period was created using the software WRPLOT View 7.0 – Freeware (Lakes Environmental Consultants Inc., Waterloo, ON, Canada).

2.7 Data elaboration and statistical analysis

2.7.1 Spatial mapping of POPs

Concentrations of PCDD/Fs and PCBs found in lichen samples after 13 months of exposure in the 23 sampling sites were mapped by using the ArcMap 10.3.1 software (ArcGis Desktop; ESRI, Redlands, CA, USA). Ordinary kriging (OK) was used to estimate pollutant concentrations in the unmeasured locations in order to obtain a continuous surface (Johnston et al., 2001; Kumar et al., 2007). Kriging is a geostatistical interpolation technique that considers both the distance and the degree of variation between known data points to estimate values in unknown areas (Paramasivam and Venkatramanan, 2019). In the OK, data derives from a stochastic process, which is divided into a constant but unknown trend component and an error component (Beelen et al., 2009). The OK estimator is given by a linear combination of the observed values with weights, which are derived from the kriging equations using a semivariogram function (Xie et al., 2011). The experimental semivariances were fitted by a spherical function, by weighted least-squares approximation (Jian et al., 1996). This function was then used for the kriging.

2.7.2 Multivariate statistical analysis

Multivariate statistical analysis was carried out by using the statistical software R (R-project for statistical computing, Ver. 3.0, 32-bit). Principal component analysis (PCA) was performed on the spatially resolved concentrations of PCDD/Fs and PCBs to cluster the tracers of the main emission sources over the territory. Before performing the PCA, the matrix of the data was transformed by column mean centering and row and column autoscaling in order to correct for different variable scaling and units.

3. Results and discussion

3.1 Accumulation of POPs in lichen transplants

Tables 2 (PCBs) and 3 (PCDD/Fs) report the concentrations (ng kg^{-1} dw) of the monitored compounds found in the blank sample and in the 23 exposed lichens, the limits of detection (LOD), calculated at the concentration at which signal to noise ratio (S/N) of each compound is > 3, and the sum of concentrations of the compounds recorded at each site.

Table 2. Limits of detection (LOD), concentrations of single congeners (ng kg^{-1} dw), and the sum of concentrations (ng kg^{-1} dw) of PCBs determined in the blank sample and the 23 exposed lichens in Terni.

ng kg^{-1}	LOD	Blank	Ind-RI	Ind-MA	Ind-FA	Ind-GI	Ind-FR	Ind-CB	Res-PI	Res-BR	Res-AR	Ind-CR	Urb-HG	Urb-SA	Urb-PV	Urb-LG	Urb-CZ	Urb-HV	Urb-UC	Urb-CA	Ind-CO	Ind-RO	Ind-OB	Ind-PR	Ind-CP
PCB-28	0.61	19	67	134	90	124	68	92	73	112	144	130	51	104	69	96	151	63	85	173	57	108	92	182	42
PCB-31	0.61	137	<LOD	<LOD	<LOD	<LOD	<LOD	<LOD	<LOD	<LOD	<LOD	<LOD	<LOD	<LOD	<LOD	<LOD	3.8	<LOD	<LOD	2.6	<LOD	<LOD	<LOD	9.5	<LOD
PCB-44	0.61	2.1	34	93	46	48	26	41	21	37	36	51	16	40	18	28	119	19	31	48	31	60	41	64	20
PCB-52	0.61	30	20	131	36	48	10	32	11	24	26	49	<LOD	32	0,97	23	165	16	18	40	18	62	42	68	6.1
PCB-77	0.15	25	<LOD	3.1	<LOD	19	3.4	<LOD	<LOD	<LOD	<LOD	<LOD	<LOD	<LOD	<LOD	1.2	<LOD	1.2	<LOD	5.1	<LOD	26	2.2	27	<LOD
PCB-95	0.61	46	<LOD	96	8.6	29	<LOD	<LOD	<LOD	<LOD	<LOD	23	<LOD	<LOD	<LOD	2.2	77	<LOD	<LOD	15	<LOD	62	33	55	<LOD
PCB-99	0.61	17	12	73	16	34	13	18	3.6	6.1	2.8	24	<LOD	3.6	<LOD	13	30	6.1	16	24	8.9	47	32	54	5.5
PCB-101	0.61	88	<LOD	136	<LOD	45	<LOD	<LOD	<LOD	<LOD	<LOD	26	<LOD	<LOD	<LOD	0.51	35	3.5	<LOD	13	<LOD	95	50	100	<LOD
PCB-105	0.15	15	131	314	124	137	188	114	103	151	137	140	90	121	16	101	82	123	181	246	135	1076	229	406	93
PCB-110	0.61	<LOD	134	334	132	209	131	152	43	93	72	173	76	86	42	97	131	96	134	174	102	326	224	332	88
PCB-118	0.15	74	93	342	78	290	182	131	77	57	47	150	30	44	<LOD	79	62	94	113	175	59	512	198	376	31
PCB-123	0.15	<LOD	5.3	12	4.6	17	9.3	7.4	7.4	5.5	5.2	8.8	2.9	5.7	0.61	5.5	5.5	8.1	6.8	11	5.9	37	10	14	3.6
PCB-128	0.61	<LOD	20	77	38	7.3	42	23	<LOD	<LOD	3.3	16	20	6.7	4.8	15	12	0.34	28	21	1.8	80	15	72	29
PCB-138	0.61	8.6	128	358	129	282	154	162	107	100	83	196	88	94	33	85	78	117	141	197	106	427	250	403	98
PCB-146	0.61	41	<LOD	<LOD	<LOD	<LOD	<LOD	<LOD	<LOD	<LOD	<LOD	<LOD	<LOD	<LOD	<LOD	<LOD	<LOD	<LOD	<LOD	<LOD	<LOD	5.3	<LOD	8.1	<LOD
PCB-149	0.61	13	64	177	89	140	71	66	43	50	41	101	37	48	17	44	58	60	85	101	55	201	148	187	53
PCB-151	0.61	7.2	11	37	20	28	12	12	6.2	9.9	5.8	21	5.1	7.4	<LOD	7.7	13	7.2	17	20	9.7	44	34	40	9.8

PCB-153	0.61	62	59	236	80	186	77	87	36	42	23	122	25	25	<LOD	44	34	14	87	127	48	291	182	291	38
PCB-157	0.15	1.4	8.9	34	10	40	17	19	13	9.4	10	24	8.6	9.1	1.1	6.5	2.9	9,1	14	20	11	107	20	40	7.3
PCB-167	0.15	2.3	9.1	31	8.6	26	14	13	9.8	8.6	7.1	16	6.4	7.3	0.79	5.9	4.1	5.3	9.7	16	7.5	54	19	34	5.2
PCB-170	0.61	1.7	92	177	95	198	114	129	93	86	61	139	85	71	32	60	68	64	110	133	95	342	189	306	100
PCB-180	0.61	33	75	193	94	202	110	129	83	90	65	142	66	58	10	55	112	15	119	152	93	356	193	301	100
PCB-187	0.61	10	35	102	58	86	55	47	41	55	34	70	28	33	12	32	54	67	69	77	46	138	90	132	49
ΣPCBs	-	634	1000	3092	1157	2197	1298	1275	772	937	802	1621	636	794	258	802	1295	791	1263	1791	890	4456	2092	3503	776

Table 3. Limits of detection (LOD), concentrations of single congeners (ng kg^{-1} dw), and the sum of concentrations (ng kg^{-1} dw) of PCDFs and PCDDs determined in the blank sample and the 23 exposed lichens in Terni.

ng kg^{-1}	**LOD**	**Blank**	**Ind-RI**	**Ind-MA**	**Ind-FA**	**Ind-GI**	**Ind-FR**	**Ind-CB**	**Res-PI**	**Res-BR**	**Res-AR**	**Ind-CR**	**Urb-HG**	**Urb-SA**	**Urb-PV**	**Urb-LG**	**Urb-CZ**	**Urb-HV**	**Urb-UC**	**Urb-CA**	**Ind-CO**	**Ind-RO**	**Ind-OB**	**Ind-PR**	**Ind-CP**
2,3,7,8-TCDF	0.061	0.33	0.23	0.078	0.29	0.49	0.27	0.49	0.38	0.39	0.21	0.24	0.15	0.11	<LOD	0.41	<LOD	0.52	0.38	0.61	0.17	0.52	0.44	1.6	<LOD
1,2,3,7,8-PCDF	0.061	<LOD	0.41	0.21	0.35	0.48	0.44	0.58	0.55	0.47	0.37	0.48	0.37	0.33	0.089	0.31	0.24	0.58	0.66	0.56	0.35	0.61	0.53	1.4	0.21
2,3,4,7,8-PCDF	0.031	0.041	0.43	0.29	0.35	0.84	0.46	0.62	0.58	0.47	0.42	0.63	0.39	0.31	0.098	0.47	0.23	0.61	0.58	0.71	0.35	0.67	0.71	1.8	0.24
1,2,3,4,7,8-HxCDF	0.061	0.13	0.28	0.17	0.22	0.73	0.31	0.41	0.45	0.29	0.26	0.34	0.27	0.22	<LOD	0.29	0.12	0.41	0.35	0.51	0.27	0.49	0.39	1.1	0.097
1,2,3,6,7,8-HxCDF	0.061	0.11	0.29	0.19	0.47	0.58	0.29	0.36	0.41	0.28	0.26	0.37	0.27	0.23	<LOD	0.29	0.13	0.35	0.36	0.46	0.27	0.48	0.46	1.1	0.084
2,3,4,6,7,8-HxCDF	0.061	0.21	0.18	0.084	0.14	0.64	0.19	0.33	0.29	0.25	0.18	0.34	0.16	0.11	<LOD	0.19	<LOD	0.27	0.29	0.31	0.22	0.37	0.27	0.84	<LOD

1,2,3,7,8,9-HxCDF	0.061	<LOD	0.066	<LOD	<LOD	0.17	0.076	0.12	0.11	0.068	0.11	0.15	0.086	<LOD	<LOD	0.061	<LOD	0.12	0.13	0.22	0.061	0.15	0.14	0.29	<LOD
1,2,3,4,6,7,8-HpCDF	0.061	0.34	0.65	0.53	0.77	1.3	0.69	1.1	1.3	0.81	0.82	1.1	0.82	0.49	<LOD	0.57	0.24	1.1	0.95	1.1	0.95	1.2	1.2	2.2	0.33
1,2,3,4,7,8,9-HpCDF	0.061	0.071	0.086	<LOD	0.21	0.24	0.093	0.29	0.35	0.57	0.086	0.12	0.29	<LOD	<LOD	0.17	<LOD	0.16	0.084	0.085	0.15	0.12	0.11	0.29	0.19
OCDF	0.061	<LOD	0.26	0.51	0.38	0.48	0.57	0.41	0.35	0.29	0.33	0.44	0.38	0.24	0.19	0.22	0.16	0.39	0.44	0.52	0.47	0.42	1.1	0.69	0.21
ΣPCDFs	-	1.2	2.9	2.1	3.2	6.1	3.4	4.8	4.7	3.9	3.1	4.2	3.2	2.1	0.38	3.1	1.1	4.6	4.2	5.1	3.3	5.1	5.3	11	1.4
2,3,7,8-TCDD	0.031	0.031	<LOD	<LOD	0.037	0.13	<LOD	<LOD	<LOD	0.039	<LOD	<LOD	<LOD	<LOD	<LOD	<LOD	<LOD	0.038	0.11	0.053	0.042	<LOD	<LOD	0.073	<LOD
1,2,3,7,8-PCDD	0.031	<LOD	0.076	0.034	0.081	0.075	0.12	0.089	0.12	0.095	0.089	0.087	0.11	0.068	<LOD	0.11	0.049	0.099	0.14	0.086	0.076	0.12	0.068	0.24	<LOD
1,2,3,4,7,8-HxCDD	0.091	<LOD	<LOD	<LOD	<LOD	0.23	<LOD	<LOD	<LOD	0.092	<LOD	<LOD	<LOD	<LOD	<LOD	<LOD	<LOD	<LOD	<LOD	<LOD	<LOD	<LOD	<LOD	0.11	<LOD
1,2,3,6,7,8-HxCDD	0.091	<LOD	0.15	<LOD	<LOD	0.19	0.11	0.14	0.12	0.095	<LOD	0.11	<LOD	<LOD	<LOD	<LOD	<LOD	0.11	0.11	0.14	<LOD	0.17	0.14	0.31	<LOD
1,2,3,7,8,9-HxCDD	0.091	<LOD	<LOD	<LOD	<LOD	<LOD	<LOD	0.12	0.093	<LOD	0.11	0.14	<LOD	<LOD	<LOD	<LOD	<LOD	0.11	0.13	0.11	<LOD	0.12	0.16	0.22	<LOD
1,2,3,4,6,7,8-HpCDD	0.061	0.15	0.59	0.51	0.77	1.3	0.91	1.1	1.1	0.79	0.64	0.93	0.73	0.45	0.34	0.49	0.31	1.1	1.1	1.1	0.79	1.1	0.97	1.2	0.32
OCDD	0.061	0.17	1.3	1.2	2.7	6.6	6.3	2.6	2.7	1.7	1.5	2.2	1.8	1.4	2.1	1.3	0.92	2.8	3.5	2.7	1.8	2.8	4.2	2.3	0.74
ΣPCDDs	-	0.35	2.1	1.8	3.6	8.5	7.5	4.1	4.1	2.8	2.3	3.5	2.7	1.9	2.4	1.9	1.3	4.3	5.2	4.2	2.7	4.2	5.6	4.4	1.1

The most abundant PCB congeners detected in the study area were PCB-105, PCB-118, and PCB-138 (Table 2). These compounds were quite widespread in the territory, but the highest concentrations were recorded at the industrial sites (Ind-MA, Ind-RO, Ind-PR), confirming the power plant and the steel plant as relevant sources of these compounds (Choi et al., 2008; Liu et al., 2013). Regarding PCDDs and PCDFs (Table 3), the most abundant congeners were 1,2,3,4,6,7,8-HpCDD, OCDD, and 1,2,3,4,6,7,8-HpCDF. This profile is in good agreement with that found by Aristizabal et al. (2011) in an urban environment, and the small discrepancy could be attributed to the different sources of emission present over the two territories.

Table 4 shows the comparison between concentrations (ng kg^{-1} dw) of ΣPCDD/Fs and ΣPCBs measured in Terni and those previously reported for other urban and industrial sites of different geographical areas (Augusto et al., 2009; Protano et al., 2015; Augusto et al., 2016; Vitali et al., 2019).

Table 4. Lowest and highest concentrations (ng kg-1 dw) of ΣPCDD/Fs and ΣPCBs in lichens in Terni (present study) and other urban and industrial sites of different geographical areas.

				ΣPCDD/Fs		**ΣPCBs**	
References	**Study Area**	**Lichen Species**	**Exposition Time**	**min**	**max**	**min**	**max**
Augusto et al., 2004	Portugal	Native *Xantoria parietina*	-	73	1913		
Augusto et al., 2007	Portugal	Native *Ramalina canariensis*	-	198	1219		
Augusto et al., 2009	Portugal	Native *Xantoria parietina*	-	171	345	-	-
		Native *Ramalina canariensis*	-	392	1059	-	-
Suutari et al., 2010	Finland	Native *Cladonia* sp.	-	3.3	8.3		
		Native *Bryoria fuscescens*	-	6.5	7.1		
		Native *Usnea* sp.	-	19			
Augusto et al., 2015	Portugal	Native *Xantoria parietina*	-	19	75		
		Native *Ramalina canariensis*	-	12	86		
Protano et al., 2015	Italy	Transplanted *Pseudevernia furfuracea*	3 months for PCBS, 6 months for PCDDs/Fs	60	109	3298	4631
Augusto et al., 2016	Portugal	Transplanted *Ramalina canariensis*	7 months	35	64	-	-
Vitali et al., 2019	Italy	Native *Xantoria parietina*	-	14	114	868	7685
This work	Italy	Tranplanted *Evernia prunastri*	13 months	2.4	16	285	4456

As we can observe from Table 4, the sum of PCDD/Fs (ng kg^{-1} dw) accumulated in lichens in this work is much lower than the levels recorded in the previous studies. Also, PCBs show lower concentrations, despite the fact that the differences are less pronounced and clear, because of the lack of literature data. This difference between concentrations may be attributed to different sampling conditions, such as the use of different lichen

species, the use of native or transplanted biomonitor, and to the different exposure time (Augusto et al., 2013). Moreover, these lower concentrations can also be attributed to the introduction of severe emission limits for European waste incinerator and for industrial plants (Directive 2000/76/EG, 2000) which seem to have been efficiently reduced industrial emission of PCDD/Fs (Bruckmann et al., 2013; Augusto et al., 2015). Although this Directive also deals with PCBs, their decrease in the environment is less pronounced and mostly affects less chlorinated congeners, probably because of their higher gas-phase reactivity (Bruckmann et al., 2013). However, it should be noted that the effects of the Directive on the reduction of the POPs emissions could be successfully evaluated over a very long time, given the persistence of this class of compounds.

3.3 Spatial mapping by using lichen transplants

Concentration data obtained at the 23 monitoring sites (as reported in Tables 3 and 4) were used to map the spatial distribution of the target analytes. The spatial maps represent a simple and efficient method to identify the location and strength of the sources of the studied compounds over the territory (Massimi et al., 2020a; 2020b). Moreover, they provide reliable information about horizontal diffusion of the studied POPs, allowing the assessment of their distribution over the territory.

Figure 3 shows the spatial maps of the sum of Σ_7PCDDs (panel a), Σ_{10}PCDFs (panel b) and Σ_{23}PCBs (panel c).

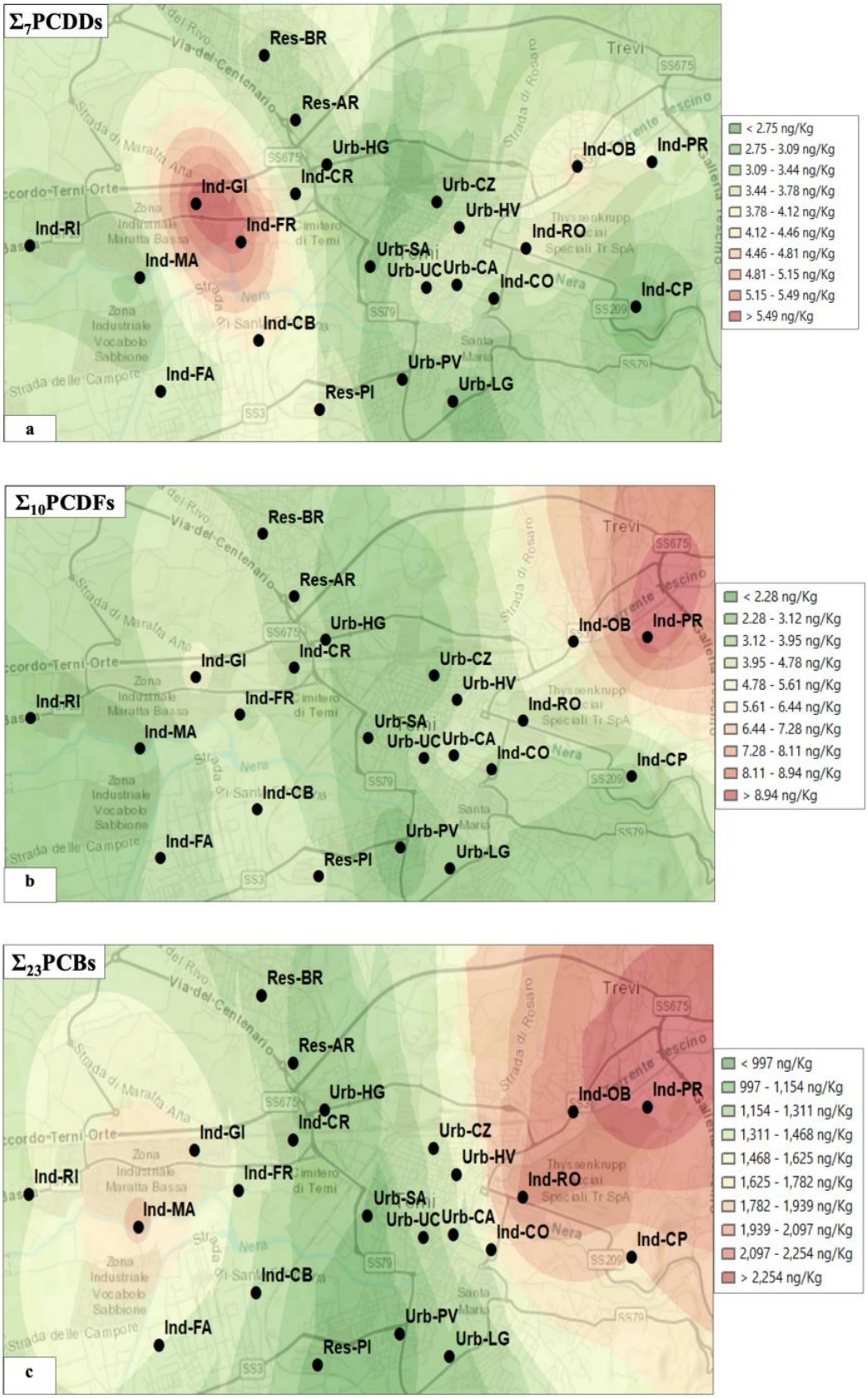

Figure 3. Maps of the spatial distribution of PCDDs (panel a), PCDFs (panel b), and PCBs (panel c) accumulated in lichen transplants after 13 months of exposure.

As shown in Figure 3, the highest concentrations of PCDFs (panel b) (11 ng kg^{-1}, Table 3) were recorded at Ind-PR, located in the proximity to the steel plant (Figure 1). Indeed, steel plants are well known as emission sources of these pollutants, due to several metallurgical processes such as sintering and blast furnace iron making (Choi et al., 2008). High concentrations of PCDD/Fs (8.5 and 6.1 ng $kg^{-1,}$ respectively; Table 3) were also recorded at Ind-GI, sited about 1 km north-east from the power plant. The higher levels found at Ind-GI respect to those recorded at Ind-MA (8.5 vs. 1.8 ng kg^{-1} for PCDDs and 6.1 vs. 2.1 ng kg^{-1} for PCDFs; Table 3), which is the closest site to the power plant, may be attributed to wind-transport. In fact, the Ind-GI area is affected by air currents that can transport the pollutants from Ind-MA (South-West) to Ind-GI (North-East), according to the wind rose obtained by using the acquired meteorological data (Figure 4).

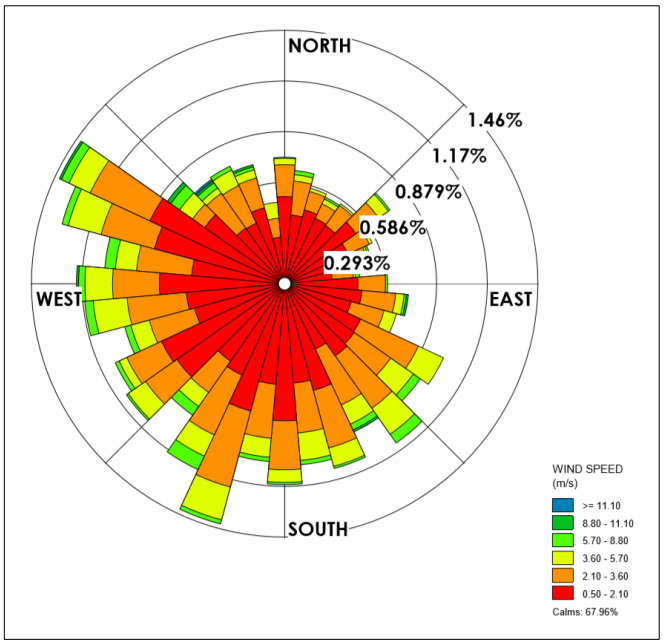

Figure 4. The wind rose of the 13-month monitoring period (WRPLOT View 7.0 – Freeware; Lakes Environmental Consultants Inc., Waterloo, ON, Canada)

The meteorological data confirmed that the weather of Terni is characterized by very-low winds (wind speed lower than 11.10 m/s), whose predominant directions are from South-West to North-East (more intense) and from North-West to South-East. The local circulation is often weak, and this leads to reduced atmospheric layers mixing, which is generally responsible of higher concentrations of air pollutants. This would also explain the elevated concentrations of PCDDs recorded at Ind-FR (7.5 ng kg^{-1}; Table 3). However, except for the two industrial areas, the concentrations of PCDDs and PCDFs were homogeneous in all the city.

Regarding PCBs, high concentrations were recorded at Ind-RO (4456 ng kg^{-1}; Table 2) and Ind-PR (3503 ng kg^{-1}; Table 2), the two prevailing impact sites of the steel plant (Massimi et al., 2019, 2020b). Also, for this class of compounds, the steel plant was confirmed to be a relevant source of organic pollutants, deriving from various thermal processes in the iron and steel industry (Aries et al., 2004). Elevated concentrations of PCBs were also recorded at Ind-MA, underlining the influence of waste incineration as a relevant emission source.

It worth be noting that PCBs are mainly present in the atmospheric gas phase and have a lower residence time in the atmosphere, thus being less horizontally diffused. Differently, PCDD/Fs are mostly coated on PM particles and more easily affected by wind transport (Barbas et al., 2018).

3.4. Principal component analysis on concentrations measured in lichens

PCA was applied to cluster the POPs (loadings) tracing the main emission sources in Terni, according to their different spatial distribution among the 23 sampling sites (scores) during the 13-month monitoring period. The PCA was performed for source identification based on the spatial variability of POPs concentrations; since we had many variables from many different locations, PCA was used to reduce the dimensionality of this data, making much simpler identifying the important spatial patterns and to confirm the results obtained by the spatial mapping of POPs concentrations.

Five significant components accounting for 89.3% were obtained; the variance explained by each component is 59.61%, 15.57%, 6.14%, 5.08% and 2.87% (Table 7). The first and the second PCs (PC1 and PC2) explain the 75.2% of the total variance, were considered. PCA results are summarized in the biplot of Fig. 5, while loadings and scores are shown in Tables 6 and 7, respectively. The biplot well separates 4 clusters of monitoring sites, each characterized by its emission profile. The first cluster, in the central part of the biplot (Figure 5), consists of samples of several monitoring sites (Ind-RI, Ind-FA, Ind-GI, Ind-FR, Ind-CB, Res-PI, Res-BR, Res-AR, Ind-CR, Urb-HG, Urb-SA, Urb-PV, Urb-LG, Urb-CZ, Urb-HV, Urb-UC, CA, Ind-CO, Ind-OB, Ind-CP) and is characterized by the presence of different organic pollutants (PCB-28, PCB-31, PCB-77, PCB-146, 1,2,3,7,8,9-HxCDF, 1,2,3,4,7,8,9-HpCDF, OCDF, 2,3,7,8-TCDD, 1,2,3,4,7,8-HxCDD, 1,2,3,6,7,8-HxCDD, OCDD), which do not show high variance among the samples. This is probably due to the high diffusion in the study area of the POPs characterizing this cluster, mainly released by widespread sources such as vehicular traffic and/or domestic heating and thus showing low concentration variability across the sites. On the contrary, the second and the third cluster are characterized by the presence of the two major impact sites of the steel plant, Ind-RO (on the lower right of the biplot) and Ind-PR (at the top right of the biplot). The monitored geographical area is characterized by the presence of two different organic pollutants emission sources related to the steel plant: Ind-RO, characterized by the prevailing emission of PCBs, and Ind-PR, characterized by the predominant emissions of PCDD/Fs. This emissions trend could be attributed to different steel processes, that probably occur at different temperatures, promoting the formation of one class of compounds rather than another one (Xu et al., 2018). The fourth cluster identified by the biplot is characterized by the presence of the power plant site (Ind-MA) and was dominated by the prevailing emission of PCBs.

Overall, the PCA confirmed the identification, localization and impact assessment of local POPs emission sources, which were individuated in the paragraph 3.3. These results encourage the use of the biomonitoring and experimental approach described in this study in other monitoring campaigns for the individuation and localization of POPs emission sources in areas contaminated by several disaggregated sources.

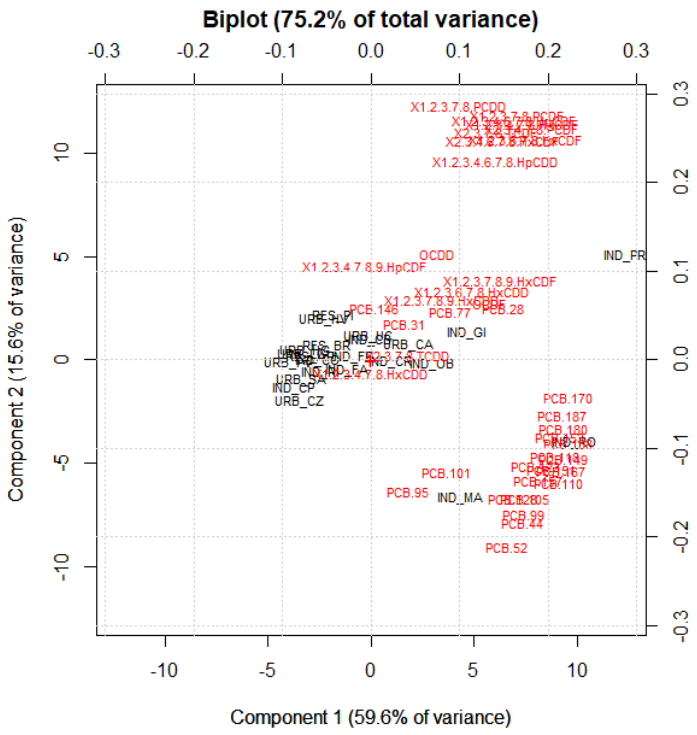

Figure 5. Biplot of the PCA (PC1 and PC2) performed on the concentration data yielded at each monitoring site after 13 months of exposure.

Table 6. Loadings of the five components obtained by the PCA performed on the concentration data yielded at each monitoring site after 13 months of exposure.

	PC1	PC2	PC3	PC4	PC5
2,3,7,8-TCDF	0.14	0.26	0.14	0.087	0.048
1,2,3,7,8-PeCDF	0.16	0.28	0.057	0.072	0.046
2,3,4,7,8-PeCDF	0.18	0.26	0.078	-0.02	0.0033
1,2,3,4,7,8-HxCDF	0.17	0.27	0.0058	0.00089	-0.087
1,2,3,6,7,8-HxCDF	0.17	0.25	0.053	-0.04	-0.022
2,3,4,6,7,8-HxCDF	0.15	0.25	-0.0093	0.018	-0.053
1,2,3,7,8,9-HxCDF	0.15	0.089	0.13	-0.12	-0.14
1,2,3,4,6,7,8-HpCDF	0.16	0.27	-0.027	-0.04	-0.11
1,2,3,4,7,8,9-HpCDF	-0.0064	0.11	0.13	0.26	-0.15
OCDF	0.13	0.064	-0.12	-0.47	0.29
2,3,7,8-TCDD	0.041	0.0047	-0.12	-0.05	0.069

1,2,3,7,8-PeCDD	0.11	0.29	0.052	0.26	0.19
1,2,3,4,7,8-HxCDD	0.00077	-0.014	-0.11	-0.07	-0.016
1,2,3,6,7,8-HxCDD	0.11	0.077	0.18	0.031	0.13
1,2,3,7,8,9-HxCDD	0.081	0.068	0.16	-0.051	0.27
1,2,3,4,6,7,8-HpCDD	0.14	0.22	-0.31	-0.15	-0.22
OCDD	0.075	0.12	-0.48	-0.34	0.11
PCB-28	0.15	0.058	0.25	-0.18	-0.57
PCB-52	0.15	-0.21	0.25	-0.21	-0.19
PCB-101	0.086	-0.13	0.14	0.047	0.14
PCB-153	0.21	-0.087	0.015	-0.067	0.049
PCB-138	0.22	-0.094	-0.01	-0.047	0.0011
PCB-180	0.22	-0.078	-0.07	0.066	0.045
PCB-77	0.091	0.054	-0.022	0.21	-0.021
PCB-123	0.19	-0.12	-0.31	0.18	-0.18
PCB-118	0.21	-0.11	-0.10	0.023	-0.016
PCB-105	0.17	-0.16	-0.19	0.31	-0.071
PCB-167	0.21	-0.12	-0.11	0.087	-0.082
PCB-157	0.19	-0.14	-0.25	0.23	-0.15
PCB-31	0.039	0.041	0.049	0.049	0.091
PCB-44	0.17	-0.18	0.23	-0.19	-0.27
PCB-95	0.042	-0.15	0.13	0.096	0.18
PCB-99	0.17	-0.17	0.17	-0.13	0.11
PCB-110	0.21	-0.14	0.078	-0.098	0.079
PCB-151	0.21	-0.12	0.015	-0.11	0.096
PCB-149	0.22	-0.11	-0.02	-0.12	0.055
PCB-146	0.0042	0.059	0.064	-0.025	0.015
PCB-187	0.22	-0.063	-0.04	-0.023	0.033
PCB-128	0.16	-0.16	0.12	0.17	0.21
PCB-170	0.22	-0.042	-0.09	0.084	0.065

Table 7. Variance % and scores of the five components obtained by the PCA performed on the concentration data yielded at each monitoring site after 13 months of exposure.

	PC1	PC2	PC3	PC4	PC5
Variance %	59.61	15.57	6.14	5.08	2.87
Ind-RI	-2.5	-0.62	0.22	0.33	0.38
Ind-MA	4.4	-6.7	2.4	-1.7	0.11
Ind-FA	-1.1	-0.44	0.34	-0.58	-0.14
Ind-GI	4.6	1.4	-2.1	-1.6	-0.94
Ind-FR	-0.83	0.16	-2.1	-0.85	1.2
Ind-CB	-0.054	0.96	-0.081	0.0011	-0.53
Res-PI	-1.8	2.2	-0.94	0.82	-0.71
Res-BR	-2.1	0.71	0.68	1.2	-1.1
Res-AR	-2.9	0.18	0.48	-0.22	-1.3
Ind-CR	0.94	-0.081	0.081	-1.1	-1.1
Urb-HG	-3.2	0.48	-0.23	0.67	0.58
Urb-SA	-3.4	-0.92	0.57	0.21	-0.83
Urb-PV	-3.9	-0.11	0.25	0.43	0.28
Urb-LG	-3.2	0.32	0.44	0.48	-0.38
Urb-CZ	-3.4	-2.1	0.50	0.69	0.85
Urb-HV	-2.1	2.1	-1.1	-0.32	-0.36
Urb-UC	-0.11	1.1	-0.92	-0.27	0.71
Urb-CA	1.8	0.77	0.024	-1.5	-2.1
Ind-CO	-2.6	-0.0054	-0.61	-0.18	0.21
Ind-RO	10	-4.1	-2.9	3.1	-0.39
Ind-OB	3.1	-0.21	-1.2	-3.1	1.5
Ind-PR	12	5.1	3.3	1.1	1.2
Ind-CP	-3.7	-1.3	0.15	1.2	1.1

3.2 Comparison between concentrations measured in lichens and deposition samples

POPs accumulation in transplanted lichens was compared with POPs deposition data obtained by using four

deposition samplers at sites impacted by the most intensive emission sources of the study area (Ind-MA, Ind-PR, Urb-LG, Res-BG).

The concentrations found in lichens after 13 months of exposure were compared with the concentrations recorded by using 1-month-exposed bulk deposition samplers. To this aim, the levels obtained by the analysis of deposition samples were averaged to obtain 13-months concentrations. The mean concentrations and the standard deviations obtained from the analysis of the deposition samples are reported in Table 5.

Table 5. Limits of detection (LOD), average concentrations, standard deviations (Std.dev.), and the sum of concentrations of PCBs (ng m^{-2} d), PCDDs (pg m^{-2} d), and PCDFs (pg m^{-2} d), determined in deposition samples in 4 sampling sites.

Deposition samples (ng m^{-2} d)

PCB	LOD	Ind-PR	Ind-MA	Res-BR	Urb-LG
-28	0.091	0.27	0.14	0.11	<LOD
-31	0.045	0.32	0.17	0.12	0.096
-44	0.045	0.27	0.17	0.091	0.076
-52	0.031	0.45	0.29	0.15	0.14
-77	0.0021	0.078	0.029	0.017	0.014
-95	0.045	0.55	0.41	0.15	0.15
-99	0.018	0.31	0.21	0.063	0.059
-101	0.045	0.89	0.59	0.21	0.19
-105	0.0091	0.53	0.32	0.072	0.068
-110	0.045	1.1	0.78	0.23	0.22
-118	0.018	1.1	0.67	0.17	0.16
-123	0.0021	0.038	0.0091	0.0021	0.0031
-128	0.0051	0.27	0.19	0.048	0.036
-138	0.031	1.3	0.82	0.23	0.21
-146	0.0091	0.17	0.11	0.033	0.025
-149	0.023	0.84	0.48	0.17	0.16
-151	0.0091	0.19	0.11	0.043	0.042
-153	0.045	1.3	0.74	0.25	0.21
-157	0.0031	0.049	0.028	0.0071	0.0061

-167	0.0031	0.081	0.047	0.015	0.011
-170	0.0091	0.51	0.26	0.099	0.082
-180	0.018	1.1	0.55	0.21	0.16
-187	0.018	0.43	0.21	0.094	0.071
ΣPCBs	-	12	7.3	2.6	2.2
Std.dev.	-	0.42	0.26	0.078	0.073

Deposition samples (pg m^{-2} d)

	LOD	**Ind-PR**	**Ind-MA**	**Res-BR**	**Urb-LG**
2,3,7,8-TCDF	0,091	2.3	1.9	1.5	1.4
1,2,3,7,8-PeCDF	0.091	0.97	0.56	0.56	0.43
2,3,4,7,8-PeCDF	0.061	1.9	0.91	0.78	0.83
1,2,3,4,7,8-HxCDF	0.091	1.4	0.79	0.81	0.78
1,2,3,6,7,8-HxCDF	0.091	1.4	0.82	0.82	0.77
2,3,4,6,7,8-HxCDF	0.091	1.9	1.1	1.1	0.91
1,2,3,7,8,9HxCDF	0.091	0.98	0.73	0.71	0.67
1,2,3,4,6,7,8-HpCDF	0.15	4.3	2.2	2.2	1.8
1,2,3,4,7,8,9-HpCDF	0.15	1.3	0.81	0.77	0.75
OCDF	0.15	3.2	2.7	2.1	1.7
ΣPCDFs	-	26	16	19	14
2,3,7,8-TCDD	0.061	0.14	0.12	0.12	0.12
1,2,3,7,8-PeCDD	0.061	0.29	0.17	0.14	0.21
1,2,3,4,7,8-HxCDD	0.091	0.76	0.61	0.61	0.61
1,2,3,6,7,8-HxCDD	0.091	1.2	0.71	0.69	0.68
1,2,3,7,8,9-HxCDD	0.091	1.1	0.66	0.67	0.65
1,2,3,4,6,7,8-HPCDD	0.15	6.9	2.9	4.3	2.5
OCDD	0.15	16	11	12	9.1
ΣPCDDs	-	20	12	11	10
Std.dev.	-	1.1	0.74	0.61	0.48

The highest concentrations of POPs were detected at Ind-PR, both for transplanted lichen (3503 ng kg^{-1} for

PCBs, 4.4 ng kg^{-1} for PCDDs, 11 ng kg^{-1} for PCDFs; Table 2 and 3) and deposition samples (12 ng m^{-2} d for PCBs, 26 pg m^{-2} d for PCDDs, 20 pg m^{-2} d for PCDFs; Table 5).

Figure 2 shows the sum of the concentrations of Σ_7PCDDs (Figure 2, panel a), Σ_{10}PCDFs (Figure 2, panel b) and Σ_{23}PCBs (Figure 2, panel c) respectively found in lichens (ng kg^{-1}, black line) and deposition samples (pg m^{-2} d or ng m^{-2} d, white histograms) at the four monitoring sites (Ind-PR, Ind-Ma, Res-BR, and Urb-LG). Regarding Σ_7PCDDs and Σ_{10}PCDFs, lichen samples showed the lowest levels at Ind-MA (1.8 and 2.1 ng kg^{-1}, respectively; Table 3); on the contrary, the lowest concentrations in deposition samples were detected at Urb-LG. This may be explained by considering that PCDD/Fs are mainly present in atmosphere coated on PM particles (Barbas et al., 2018) and, due to a slower diffusion rate through lichen thalli, they tend to settle on lichen surface making them more susceptible to mechanical wash off phenomena, which would contribute to decrease their concentrations (Augusto et al., 2013). Moreover, lichens are probably not able to quantitatively collect PCDD/Fs when concentrations are too low, as demonstrated by the lowest concentrations found in lichen transplants at Ind-MA, Res-BR, and Urb-LG compared to those recorded in deposition samples (Figure 2a and 2b).

Regarding PCBs, concentrations found in lichens were in good agreement with those recorded in deposition samples, except for Ind-MA, where PCBs concentration was found to be considerably higher in the lichen sample than in the correspondent deposition sample. This may be explained by considering that PCBs are mainly present in the atmospheric gas phase (Barbas et al., 2018), making bioaccumulation more efficient.

Overall, despite the described differences, the efficiency of lichen transplants to reflect PCDD/Fs and PCBs atmospheric concentrations was confirmed, as reported in Figure 2.

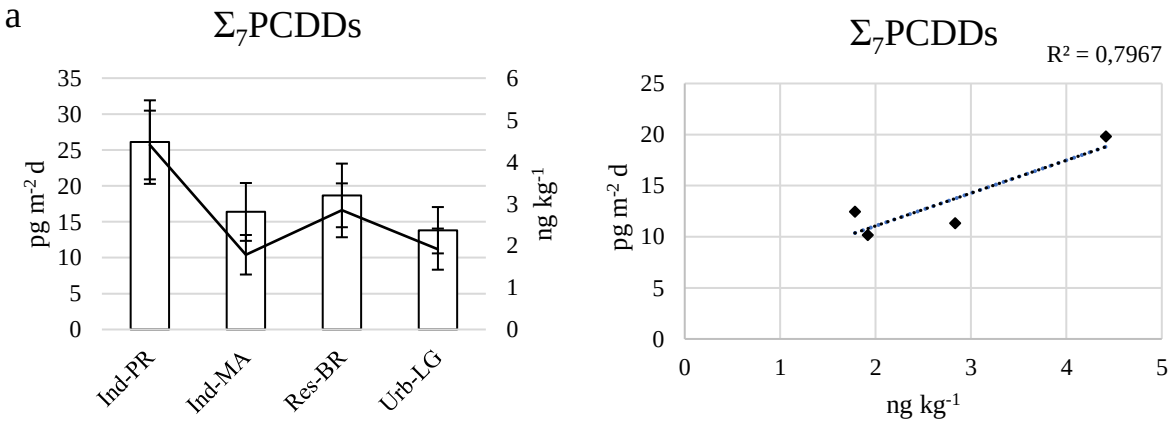

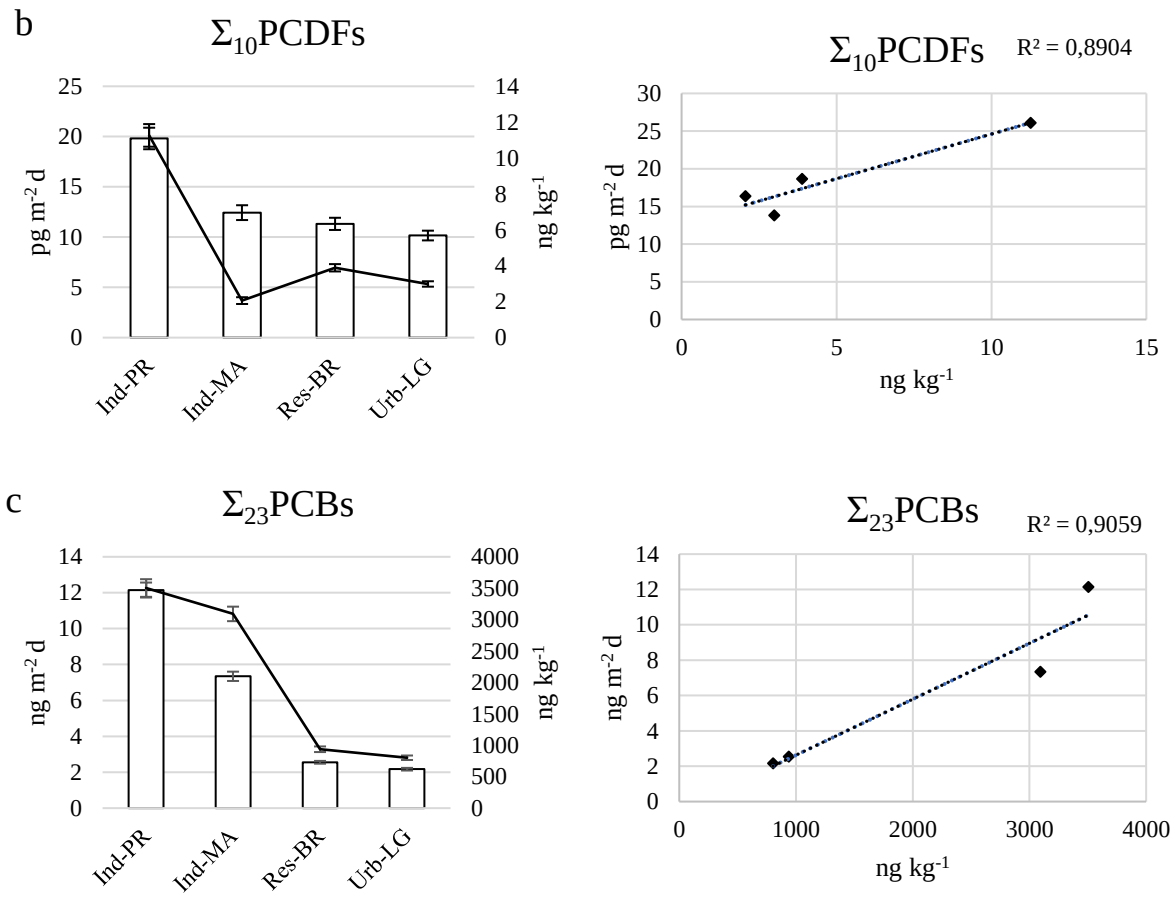

Figure 2. Comparison between the sum of the concentrations of Σ_7PCDDs (panel a), Σ_{10}PCDFs (panel b) and Σ_{23}PCBs (panel c) accumulated in lichens (ng kg^{-1}, black line) and collected with bulk deposition samplers (pg m^{-2} d or ng m^{-2} d, white histograms) at four monitoring sites (Ind-PR, Ind-Ma, Res-BR, and Urb-LG). The linearity response (as R^2) between POPs bioaccumulated in lichens and collected with deposition samplers is also reported.

4. Conclusions

This study demonstrates the ability of transplanted lichen *E. prunastri* to reflect the air concentration and spatial variability of PCDDs, PCDFs, and PCBs, and encourage their use as low-cost biomonitors for obtaining high spatial resolution data of POPs and mapping their spatial distribution. Power plant predominantly emitted PCBs, while steel plant was characterized by the presence of two different emission points, one characterized by the emission of PCBs and the other characterized by the emission of PCDD/Fs. This trend could be attributed to different steel processes that probably occur at different temperatures.

Lichen thalli transplants have demonstrated to be a suitable and cost-effective biomonitor of PCDDs, PCDFs, and PCBs. This approach can effectively complement the traditional air monitoring methods in order to achieve more complete monitoring networks for assessing the spatial variability of PCDDs, PCDFs, and PCBs. Moreover, we believe that the experimental approach described in this study can be applied to other monitoring

campaigns for identifying and localizing POPs emission sources in areas contaminated by several disaggregated sources.

References

Alcock, R.E., Sweetman, A.J., Jones, K.C., 2001. A congener-specific PCDD/F emissions inventory for the UK: do current estimates account for the measured atmospheric burden? Chemosphere 43, 183-194. https://doi.org/10.1016/S0045-6535(00)00173-9

Argiriadis, E., Rada, E.C., Vecchiato, M., Zambon, S., Ionescu, G., Schiavon, M., Ragazzi, M., Gambaro, A., 2014. Assessing the influence of local sources on POPs in atmospheric depositions and sediments near Trento (Italy). Atmos. Environ. 98, 32-40. https://doi.org/10.1016/j.atmosenv.2014.08.035

Aries, E., Anderson, D.R., Ordsmith, N., Hall, K., Fisher, R., 2004. Development and validation of a method for analysis of ' 'dioxin-like" PCBs in environmental samples from the steel industry. Chemosphere. 54, 23–31. https://doi.org/10.1016/S0045-6535(03)00762-8

Aristizábal, B.H., Gonzalez, C.M., Morales, L., Abalos, M., Abad, E., 2011. Polychlorinated dibenzo-p-dioxin and dibenzofuran in urban air of an Andean city. Chemosphere. 85, 170–178. https://doi.org/10.1016/j.chemosphere.2011.06.035

Augusto, S., Pinho, P., Branquinho, C., Pereira, M. J., Soares, A., Catarino, F., 2004. Atmospheric dioxin and furan deposition in relation to land-use and other pollutants: a survey with lichens. J. Atmos. Chem. 49, 53-65.

Augusto, S., Máguas, C., Catarino, F., Branquinho, C., 2007. Interpreting the dioxin and furan profiles in the lichen Ramalina canariensis Steiner for monitoring air pollution. Sci. Total Environ. 377, 114-123. https://doi.org/10.1016/j.scitotenv.2007.01.089

Augusto, S, Máguas, C, Branquinho, C., 2009. Understanding the performance of different lichen species as biomonitors of atmospheric dioxins and furans: potential for intercalibration. Ecotoxicology. 18(8), 1036–42. https://doi.org/10.1007/s10646-009-0360-z

Augusto, S, Máguas, C, Branquinho, C., 2013. Guidelines for biomonitoring persistent organic pollutants (POPs), using lichens and aquatic mosses - a review. Environ. Pollut. 180, 330–8. https://doi.org/10.1016/j.envpol.2013.05.019

Augusto, S., Pinho P., Santos, A., Botelho, M.J., Palma-Oliveira, J., Branquinho, C., 2015. Declining trends of PCDD/Fs in lichens over a decade in a Mediterranean area with multiple pollution sources. Sci. Total Environ. 508, 95–100. http://dx.doi.org/10.1016/j.scitotenv.2014.11.065

Augusto, S., Pinho, P., Santos, A., Botelho, M.J., Palma-Oliveira, J., Branquinho, C., 2016. Tracking the Spatial Fate of PCDD/F Emissions from a Cement Plant by Using Lichens as Environmental Biomonitors. Environ. Sci. Technol. 50, 2434−2441. http://dx.doi.org/10.1021/acs.est.5b04873

Avino, P. and Russo, M.V., 2018. A Comprehensive Review of Analytical Methods for Determining Persistent Organic Pollutants in Air, Soil, Water and Waste. Curr. Org. Chem. 22, (10), 939-953. https://doi.org/10.2174/1385272822666180404144834

Barbas, B., de la Torre, A., Sanz, P., Navarro, I., Artíñano, B., Martínez, M.A., 2018. Gas/particle partitioning and particle size distribution of PCDD/Fs and PCBs in urban ambient air. Sci. Total Environ. 624, 170–179. https://doi.org/10.1016/j.scitotenv.2017.12.114

Bari, A., Rosso, A., Minciardi, M.R., Troiani, F., Piervittori, R., 2001. Analysis of heavy metals in atmospheric particulates in relation to their accumulation in explanted Pseudoevernia furfuracea thalli. Environ. Monit. Assess. 69, 2005-2220. https://doi.org/10.1023/A:1010757924363

Beelen, R., Hoek, G., Pebesma, E., Vienneau, D., de Hoogh, K., Briggs, D.J., 2009. Mapping of background air pollution at a fine spatial scale across the European Union. Sci. Total Environ. 407(6), 1852-1867. https://doi.org/10.1016/j.scitotenv.2008.11.048

Bergamaschi, L., Rizzio, E., Giaveri, G., Loppi, S., Gallorini, M., 2007. Comparison between the accumulation capacity of four lichen species transplanted to an urban site. Environ. Pollut. 148, 468-476. https://doi.org/10.1016/ j.envpol.2006.12.003.

Bruckmann, P, Hiester, E, Klees, M, Zetzsch, C., 2013. Trends of PCDD/F and PCB concentrations and depositions in ambient air in Northwestern Germany. Chemosphere. 93, 1471–8. https://doi.org/10.1016/j.chemosphere.2013.07.029

Boudreault, C., Coxson, D., Bergeron, Y., Stevenson, S., Bouchard, M., 2013. Do forests treated by partial cutting provide growth conditions similar to old-growth forests for epiphytic lichens? Biol. Conserv. 159, 458–467. https://doi.org/10.1016/j.biocon.2012.12.019

Castellani, F., Massimi, L., Vitali, M., Canepari, S., Guidotti, M., Conti, M. E., Protano, C., 2020. High spatial resolution analysis of polybrominated diphenyl ethers (PBDEs) using transplanted lichen Evernia prunastri: A case study in central Italy. Sci. Total Environ. 140590. https://doi.org/10.1016/j.scitotenv.2020.140590

Choi, S.D., Baek, S.Y., Chang, Y.S., 2008. Atmospheric levels and distribution of dioxin-like polychlorinated biphenyls (PCBs) and polybrominated diphenyl ethers (PBDEs) in the vicinity of an iron and steel making plant. Atmos. Environ. 42, 2479–2488. doi:10.1016/j.atmosenv.2007.12.032

Conti, M.E., Cecchetti, G., 2001. Biological monitoring: lichens as bioindicators of air pollution assessment—a review. Environ. Pollut. 114, 471-492. https://doi.org/10.1016/S0269-7491(00)00224-4

Conti, M.E., Tudino, M., Stripeikis, J., Cecchetti, G., 2004. Heavy metal accumulation in the lichen Evernia prunastri transplanted at urban, rural and industrial sites in Central Italy. J. Atmos. Chem., 49, 83-94. https://doi.org/10.1007/s10874-004-1216-9

Conti, M.E., Jasan, R., Finoia, M.G., Iavicoli, I., Plá, R., 2016. Trace elements deposition in the Tierra del Fuego region (south Patagonia) by using lichen transplants after the Puyehue-Cordón Caulle (north Patagonia) volcanic eruption in 2011. Environ. Sci. Pollut. Res., 23, 6574-6583. https://doi.org/10.1007/s11356-015-5858-8

Conti, M.E., Plà, R., Simone, C., Jasan, R., Finoia, M.G., 2020 Implementing the monitoring breakdown structure: native lichens as biomonitors of element deposition in the southern Patagonian forest connected with the Puyehue volcano event in 2011—a 6-year survey (2006–2012). Environ. Sci. Pollut. Res.. https://doi.org/10.1007/s11356-020-10001-0

Directive 2000/76/EG. Directive 2000/76/EC of the European Parliament and of the Council of December 4th 2000 on the Incineration of Waste; 2000

Eckhardt, S., Breivik, K., Manø, S., Stohl, A., 2007. Record high peaks in PCB concentrations in the Arctic atmosphere due to long-range transport of biomass burning emissions. Atmos. Chem. Phys., 7, 4527–4536, www.atmos-chem-phys.net/7/4527/2007/

Fang, M., Choi, S.D., Baek, S.Y., Park, H., Chang, Y.S., 2011. Atmospheric bulk deposition of polychlorinated dibenzo-p-dioxins and dibenzofurans (PCDD/Fs) in the vicinity of an iron and steel making plant. Chemosphere. 84(7), 894-899. https://doi.org/10.1016/j.chemosphere.2011.06.016

Ferrero, L., Cappelletti, D., Moroni, B., Sangiorgi, G., Perrone, M.G., Crocchianti, S., Bolzacchini, E., 2012. Wintertime aerosol dynamics and chemical composition across the mixing layer over basin valleys. Atmos. Environ. 56, 143–153. https://doi.org/10.1016/j.atmosenv.2012.03.071

Gao, M., Cao, J., Seto, E., 2015. A distributed network of low-cost continuous reading sensors to measure spatiotemporal variations of PM2. 5 in Xi'an, China. Environ. pollut. 199, 56-65. https://doi.org/10.1016/j.envpol.2015.01.013

Godinho, R.M., Wolterbeek, H.T., Verburg, T., Freitas, M.C., 2008. Bioaccumulation behaviour of transplants of the lichen Flavoparmelia caperata in relation to total deposition at a polluted location in Portugal. Enviro Pollut 151, 318-325. https://doi.org/10.1016/j.envpol.2007.06.034

Guerrini, R., 2012. Qualità dell'aria nella provincia di Terni tra il 2002 e il 2011. Quad ARPA Umbria 81–87

Hoff, R.M., Strachan, W.M.J., Sweet, C.W., Chan, C.H., Shackleton, M., Bidleman, T.F., Brice, K.A., Burniston, D.A., Cussion, S., Gatz, D.F., Harlin, K., Schroeder, W.H., 1996. Atmospheric Deposition of Toxic Chemicals to the Great Lakes: A Review of Data through 1994. Atmos. Environ. 30, 3505–3527. https://doi.org/10.1016/1352-2310(96)00046-5

International Agency for the research on Cancer (IARC), 2016. Outdoor Air Pollution Volume 109. Monographs on the Evaluation of Carcinogenic Risks to Humans. IARC Working Group on the Evaluation of Carcinogenic Risk to Humans. International Agency for Research on Cancer, Lyon (FR).

Irwin, J.S., 2014. A suggested method for dispersion model evaluation. J. Air Waste Manage. Assoc. 64 (3), 255–264. https://doi.org/10.1080/10962247.2013.833147

Johnston, K., Ver Hoef, J. M., Krivoruchko, K., Lucas, N., 2001. Using ArcGIS geostatistical analyst. Vol. 380. Esri.

Jones, K. C. and Duarte-Davidson, R., 1997. Transfers of Airborne PCDD/Fs to Bulk Deposition Collectors and Herbage. Environ. Sci. Technol. 1997, 31, 10, 2937-2943. https://doi.org/10.1021/es970133t

Kardel, F., Wuyts, K., De Wael, K., Samson, R., 2018. Biomonitoring of atmospheric particulate pollution via chemical composition and magnetic properties of roadside tree leaves. Environ. Sci. Pollut. R. 25(26), 25994-26004. https://doi.org/10.1007/s11356-018-2592-z

Kim, B.U., Bae, C., Kim, H.C., Kim, E., Kim, S., 2017. Spatially and chemically resolved source apportionment analysis: Case study of high particulate matter event. Atmos. Environ. 162, 55–70. https://doi.org/10.1016/j.atmosenv.2017.05.006

Kumar, A., Maroju, S., Bhat, A., 2007. Application of ArcGIS geostatistical analyst for interpolating environmental data from observations. Environmental Progress, 26(3), 220-225. https://doi.org/10.1002/ep.10223

Li, Y., Wang, P., Ding, L., Li, X., Wang, T., Zhang, Q., Yang, H., Jiang, G., Wei, F., 2010. Atmospheric distribution of polychlorinated dibenzo-p-dioxins, dibenzofurans and dioxin-like polychlorinated biphenyls around a steel plant Area, Northeast China. Chemosphere. 79 (3), 253-258. https://doi.org/10.1016/j.chemosphere.2010.01.061

Liu, G., Zheng, M., Cai, M., Nie, Z., Zhang, B., Liu, W., Du, B., Dong, S., Hu, J., Xiao, K., 2013. Atmospheric emission of polychlorinated biphenyls from multiple industrial thermal processes. Chemosphere. 90, 2453–2460. http://dx.doi.org/10.1016/j.chemosphere.2012.11.008

Lucadamo, L., Corapi, A., Loppi, S., De Rosa, R., Barca, D., Vespasiano, G., Gallo, L., 2016. Spatial Variation in the Accumulation of Elements in Thalli of the Lichen Pseudevernia furfuracea (L.) Zopf Transplanted Around a Biomass Power Plant in Italy. Arch. Environ. Con. Tox. 70, 506–521. https://doi.org/10.1007/s00244-015-0238-4

Massimi, L., Ristorini, M., Eusebio, M., Florendo, D., Adeyemo, A., Brugnoli, D., Canepari, S., 2017. Monitoring and Evaluation of Terni (Central Italy) Air Quality through Spatially Resolved Analyses. Atmosphere, 8, 200; https://doi.org/10.3390/atmos8100200

Massimi, L., Conti, M.E., Mele, G., Ristorini, M., Astolfi, M.L., Canepari, S., 2019. Lichen transplants as indicators of atmospheric element concentrations: a high spatial resolution comparison with PM10 samples in a polluted area (Central Italy). Ecol. Indic. 101, 759–769. https://doi.org/10.1016/j.ecolind.2018.12.051

Massimi, L., Simonetti, G., Buiarelli, F., Di Filippo, P., Pomata, D., Riccardi, C., Ristorini, M., Astolfi, M.L., Canepari, S. 2020a. Spatial distribution of levoglucosan and alternative biomass burning tracers in atmospheric aerosols, in an urban and industrial hot-spot of Central Italy. Atmos. Res. 104904. https://doi.org/10.1016/j.atmosres.2020.104904

Massimi, L., Ristorini, M., Astolfi, M.L., Perrino, C., Canepari, S. 2020b. Spatial Mapping of Element Concentrations in PM10: a Powerful Tool for Localization and Impact Assessment of Emission Sources. Atmos. Res. Under Review.

Mi, H.H., Wu, Z.S., Lin, L.F., Lai, Y.C., Lee, Y.Y., Wang, L.C., Chang-Chien, G.P., 2012. Atmospheric Dry Deposition of Polychlorinated Dibenzo-p-Dioxins/Dibenzofurans (PCDD/Fs) and Polychlorinated Biphenyls (PCBs) in Southern Taiwan. Aerosol Air Qual. Res. 12, 1016–1029. https://doi.org/10.4209/aaqr.2012.07.0172

Moroni, B., Ferrero, L., Crocchianti, S., Cappelletti, D., 2013. Aerosol dynamics upon Terni basin (Central Italy): Results of integrated vertical profile measurements and electron microscopy analysis. Rend. Lincei Sci. Fis. Nat. 24, 319–328. https://doi.org/10.1007/s12210-013-0230-8

Ndlovu, N.B., Frontasyeva, M.V., Newman, R.T. and Maleka, P.P., 2019. Moss and Lichen Biomonitoring of Atmospheric Pollution in the Western Cape Province (South Africa). AJAC. 10, 86-102. https://doi.org/10.4236/ajac.2019.103008

Paramasivam, C.R., Venkatramanan, S., 2019. An Introduction to Various Spatial Analysis Techniques. GIS and Geostatistical Techniques for Groundwater Science, 3, 23-30. https://doi.org/10.1016/B978-0-12-815413-7.00003-1

Protano, C., Guidotti, M., Owczarek M., Fantozzi, L., Blasi, G., Vitali, M., 2014. Polycyclic Aromatic Hydrocarbons and Metals in Transplanted Lichen (Pseudovernia furfuracea) at Sites Adjacent to a Solid-waste Landfill in Central Italy. Arch. Environ. Contam. Toxicol. 66, 471–481 https://doi.org/10.1007/s00244-013-9965-6

Protano, C., Owczarek M., Fantozzi, L., Guidotti, M., Vitali, M., 2015. Transplanted Lichen Pseudovernia furfuracea as a Multi-Tracer Monitoring Tool Near a Solid Waste Incinerator in Italy: Assessment of Airborne Incinerator-Related Pollutants. Bull. Environ. Contam. Toxicol. 95,644–653 https://doi.org/10.1007/s00128-015-1614-5

Qu, C., Albanese, S., Lima, A., Hope, D., Pond, P., Fortelli, A., Romano, N., Cerino, P., Pizzolante, A., De Vivo, B., 2019. The occurrence of OCPs, PCBs, and PAHs in the soil, air, and bulk deposition of the Naples

metropolitan area, southern Italy: Implications for sources and environmental processes. Environ. Int. 124, 89-97. https://doi.org/10.1016/j.envint.2018.12.031

Reis, M.A., Alves, L.C., Freitas, M.C., Van, O., Wolterbeek, H.T., 1999. Lichens (Parmelia sulcata) time response model to environmental availability. Sci. Total Environ. 232, 105-115. https://doi.org/10.1016/S0048-9697(99)00113-8

Sett, R. and Kundu, M., 2016. Epiphytic Lichens: Their Usefulness as Bio-indicators of Air Pollution. Donnish Journal of Research in Environmental Studies Vol 3(3), 017-024. ISSN: 2984-858X

Sloof, J.E., 1995. Lichens as quantitative biomonitors for atmospheric trace-element deposition using transplants. Atmos. Environ. 29, 11-20. https://doi.org/10.1016/1352-2310(94)00221-6

Suutari, A., Ruokojärvi, P., Kiviranta, H., Verta, M., Korhonen, M., Nieminen, M., Hallikainen, A., Laaksonen, S., 2010. Airborne organic pollutants in Finnish reindeer food chain. In: E. Pongrácz, M. Hyvärinen, S. Pitkäaho, R.L. Keiski (Ed.), Clean air research at the University of Oulu (pp. 25-27). Proceeding of the SkyPro conference, June 3rd, 2010, University of Oulu, Finland. Kalevaprint, Oulu, ISBN 978-951-42-6199-2.

Tyler, G., 1989. Uptake, retention and toxicity of heavy metals in lichens. A brief review. Water Air and Soil Pollut. 47, 321-333. https://doi.org/10.1007/BF00279330

Thacker, N., Kashyap, S., Sheikh, J., Trivedi, J., Thokchom, B., Agnihotri, A., 2010. Dioxin Releases in Waste Incinerations and Thermal Processes. Bull. Environ. Contam. Toxicol. 85, 624–627. https://doi.org/10.1007/s00128-010-0137-3

Thakur, M., Pathania, D., 2020. Environmental fate of organic pollutants and effect on human health. Abatement of Environmental Pollutants. Trends and Strategies 12, 245-262. https://doi.org/10.1016/B978-0-12-818095-2.00012-6

Van der Wat, L., Forbe, P.B.C., 2015. Lichens as biomonitors for organic air pollutants. TRAC - Trends in Anal. Chem. 64, 165-172. https://doi.org/10.1016/j.trac.2014.09.006

Vannini, A., Paoli, L., Nicolardi, V., Di Lella, L.A., Loppi, S., 2017. Seasonal variations in intracellular trace element content and physiological parameters in the lichen Evernia prunastri transplanted to an urban environment. Acta Botanica Croatica 76 (2), 171–176.

VDI, 1991. VDI 3799 Blatt 2 - Zurückgezogen Messung von Immissions-Wirkungen; Ermittlung und Beurteilung phytotoxischer Wirkungen von Immissionen mit Flechten; Verfahren der standardisierten Flechtenexposition. Berlin.

VDI, 1995. VDI 3799 Blatt 1 - Zurückgezogen Messen von Immissionswirkungen - Ermittlung und Beurteilung phytotoxischer Wirkungen von Immissionen mit Flechten - Flechtenkartierung zur Ermittlung des Luftgütewertes (LGW), Berlin.

Vitali, M., Antonucci, A., Owczarek, M., Guidotti, M., Astolfi, M.L., Manigrasso, M., Avino, P., Bhattacharya, B., Protano, C., 2019. Air quality assessment in different environmental scenarios by the determination of typical heavy metals and Persistent Organic Pollutants in native lichen Xanthoria parietina. Environ. Pollut. 254, 113013. https://doi.org/10.1016/j.envpol.2019.113013

Vitali, L., Morabito, A., Adani, M., Assennato, G., Ciancarella, L., Cremona, G., Giua, R., Pastore, T., Piersanti, A., Righini, G., Russo, F., Spagnolo, S., Tanzarella, A., Tinarelli, G., Zanini, G., 2016. A Lagrangian modelling approach to assess the representativeness area of an industrial air quality monitoring station. Atmos. Pollut. Res. 7 (6), 990–1003. https://doi.org/10.1016/j.apr.2016.06.002

Xu, S., Chen, T., Li, X., Yan, J., Cen, K., 2018. Behavior of PCDD/Fs, PCBs, CBzs and PAHs during Thermal Treatment of Various Fly Ash from Steel Industry. Aerosol Air Qual. Res. 18, 1008–1018. https://doi.org/10.4209/aaqr.2017.11.0514

Yu, B.W., Jin, G.Z., Moon, Y.H., Kim M.K., Kyoung J.D., Chang Y.S., 2006. Emission of PCDD/Fs and dioxin-like PCBs from metallurgy industries in S. Korea. Chemosphere. 62, 494–501. https://doi.org/10.1016/j.chemosphere.2005.04.031

6. (B) Chemical analysis and oxidative potential of PM released by indoor and outdoor emission sources

Many scientific studies have linked PM exposure to a series of significant health problems, including cardiopulmonary and respiratory diseases.

As people spend most of their time indoors, PM impact on human health is even greater in indoor environments, especially for older adults, children, and pregnant women, who constantly stay indoors, and those with existing respiratory problems. Indoor air pollution is due to the presence of pollutants found in indoor environments. The common sources of indoor air pollutants are from natural and biological sources, from combustion sources (e.g. heating, cooking, lighting), from man-made sources (e.g. vacuuming, dusting, and sweeping), as well as from buildings material (Tofful et al., 2021; Slezakova and Morais, 2012). In addition, the resuspension of deposited particles onto indoor surfaces represent a consistent PM source (Tofful et al., 2021). Furthermore, a substantial part of indoor pollution is dominated by the infiltration from outdoor particles, such as from vehicular traffic or industrial emissions.

People often divided their time between home and work; therefore, it is important to examine air quality in both residences and workplaces (Henninger, 2013). For this reason, in the VIEPI project (Integrated evaluation of the exposure to indoor particulate matter) framework, the concentration, chemical composition, and redox properties of particulate matter (PM_{10} and $PM_{2.5}$) in a 5-story building in the Sapienza University of Rome (Italy) was conducted, in six classrooms by placing indoor and outdoor PM samplers for 1 year, to investigate the PM composition and sources in indoor academic environments, the occupants' role and their exposure to pollutants.

Another study was conducted within the INDOMAP project and involved different domestic environments for 12 months in Rome (Italy). In detail, simultaneous outdoor and indoor samplings of PM_{10} were conducted in independent houses in order to provide a detailed chemical characterization of PM collected outdoor and inside a domestic environment, to study the indoor and outdoor source contributions to indoor PM_{10}, underlining the role of indoor activities and outdoor sources on the indoor air quality, and, finally, also to assess OP of indoor particles in relation to both the indoor and the outdoor environmental conditions, for investigating the health impact of particles present in indoor sources. To date, only a few studies have focused on examining the differences and the relationships between indoor and outdoor OP of PM, and very limited studies had examined the influence of domestic activities in determining indoor OP.

6.1 (B1) Seasonal Variations in the Chemical Composition of Indoor and Outdoor PM_{10} in University Classrooms

Sustainability (2021), 13(4), 2263, doi: 10.3390/su13042263

Luca Tofful [1], Maria Catrambone [1], Marco Giusto [1], Salvatore Pareti [1], Elena Rantica [1], Tiziana Sargolini [1], Silvia Canepari [1,2], Maria Agostina Frezzini [2], Lorenzo Massimi [2], Martina Ristorini [2], Armando Pelliccioni [3] and Cinzia Perrino [1,*]

[1] C.N.R., Institute of Atmospheric Pollution Research, Monterotondo St. (Rome), 00015, Italy

[2] Sapienza University, Chemistry Department, Rome, 00185, Italy

[3] INAIL, Department of Occupational and Environmental Medicine, Epidemiology and Hygiene, Monte Porzio Catone (Rome), 00078, Italy

[*] Corresponding author

Keywords: air quality; PM sources; infiltration; air-conditioning; mass closure

Abstract: In the VIEPI project (Integrated evaluation of the exposure to indoor particulate matter) framework, we carried out a 1-year study of the concentration and chemical composition of particulate matter (PM) in a 5 story building in the Sapienza University of Rome (Italy). Each sampling had a duration of 1 month and was carried out indoors and outdoors in six classrooms. The chemical analyses were grouped to obtain information about the main PM sources. Micro-elements in their soluble and insoluble fractions were used to trace additional sources. Indoor PM composition was dominated by soil components and, to a lesser extent, by the organics, which substantially increased when people crowded the sites. The penetration of PM components was regulated by their chemical nature and by the dimensions of the particles in which they were contained. For the first time in crowded indoor environments, three different chemical assays aimed to determine PM redox properties complemented chemical composition measurements. These preliminary tests showed that substantially different redox properties characterized atmospheric particles in indoor and outdoor sites. The innovative characteristics of this study (time duration, number of considered environments) were essential to obtain relevant information about PM composition and sources in indoor academic environments and the occupants' role.

1. Introduction

Atmospheric pollution in indoor environments poses a significant threat to human health because we spend much more time inside homes, schools, offices, and vehicles than in the open air [1,2]. For this reason, the exposure, (i.e., the product of pollutant concentration and time over which a person is in contact with that

pollutant) is much higher indoors than outdoors for most of the people, particularly in urban areas. This is especially true for children, older people, and other vulnerable groups [3–6].

In indoor sites, air quality is generally a more complicated issue than in outdoor environments, as pollutants produced inside add to those that penetrate from outdoor by infiltrating through the doors, windows and cracks of the building. Accordingly, the concentration of indoor pollutants is determined not only by the parameters that regulate their indoor production but also from those determining their concentration outdoors (meteorology, source intensity, formation, transformation, and deposition mechanisms) and by the way they penetrate through the building shell [7]. Concerning particulate matter (PM), these difficulties are further complicated by the variety of chemical species that constitute this group of pollutants, each with its sources, and by the wide range of its size distribution. The size of atmospheric particles, which vary from a few nanometers to tens of micrometers, significantly influences how they penetrate from the external environment. An extensive scientific literature has addressed the link between particle size and infiltration factor, i.e., the equilibrium fraction of ambient particles that penetrate indoors and remains suspended [8–10]. The conclusions reached are not unequivocal, as the infiltration factors measured by different researchers vary in the range of 0.3–0.82 for $PM_{2.5}$ and 0.17–0.52 for PM_{10} [9]. In general, the infiltration factor of $PM_{2.5}$ is higher than that of PM_{10} because the gravitational setting is stronger for larger particles. For all the above reasons, there are few scientific studies fully describing the chemical composition of indoor particulate matter and comprehensively studying its different sources (penetration from outside and inside production [5,11–15]. Among the practical difficulties related to the design of a complete chemical characterisation study, there is the need to carry out many side-by-side simultaneous samplings. This necessity contrasts with the annoyance caused by the presence of several sampling instruments, generally cumbersome and noisy. Consequently, most of the studies focused on particle number concentration [16–18], or mass concentration [19,20], or specific PM components [21–23]. University classrooms provide a particularly suitable environment for the study of indoor pollution. Here, many of the sources that characterize domestic environments and, mainly, those related to combustion processes, are absent (e.g., cooking activities, cigarette smoke, wood heating, candle burning, but also use of household appliances and personal hygiene products). These features simplify the problem of apportioning PM sources, as it has been shown that in residential environments the primary sources contributing to indoor air concentrations are related to combustion processes [24–29]. Moreover, crowded environments, such as university classrooms, offer the opportunity to study the effects of people's presence on PM concentration and composition [30]. In this study, carried out within the VIEPI project (Integrated evaluation of the expo- sure to indoor particulate matter) [31], some university environments of different size were studied for a whole year. Indoor and outdoor samplings were carried out in parallel, placing a first series of samplers inside environments ranging from a small research laboratory to a vast lecture hall, and a second series of samplers immediately outside them. It has been chosen to carry out long-duration samplings (one month each) and to use very quiet instrumentation of very small size, operating at the flow rate of 0.5 l min^{-1}.

This work aimed to determine the main chemical components of PM in different university environments, quantify the weight of the main sources, evaluate their seasonal variations, and study the infiltration dynamics

and their link with the particle size. On some samples, we also determined, for the first time in crowded indoor environments, the oxidative potential, that is the capability of ambient particles to generate in-vivo reactive oxygen species, a possible metric for estimating PM effects on health [32,33]. We also measured reducing species, with the aim to provides new, additional information about PM components that might be able to counteract the oxidative properties of the aerosol. In addition to the high number of measured parameters and the long duration of the measurement period, which make the results more robust and reliable, the novelty of the study is in the choice of university classrooms (much more crowded than school classrooms) during the regular activity of the students, which allows a better comprehension of occupants' role.

2. Materials and Methods

2.1 Sampling Procedure

The study was carried out at the Physics Department of the Sapienza University of Rome, Italy (Google coordinates: 41°54'06" N; 12°30'57" E). Six indoor sampling sites located in the same five-story building were considered: a Lecture Hall (LH, at the ground floor, 1150 m^3), a computer room (CR, at the 2nd floor, 450 m^3), three identical classrooms (A3 and A4 at the 2nd floor, A7 at the 4th floor, 570 m^3) and a physics laboratory (SL, at the 4th floor, about 300 m^3). The building is located inside the University campus, in Rome's central area, at about 50 m from a high-traffic road. A limited number of cars are allowed to enter the campus area. A detailed description of the sampling site is reported in Pelliccioni et al. (2020) [31]. Each indoor site was equipped with very-low-volume samplers operating at the flow rate of 0.5 L min^{-1} (Smart Sampler, Fai Instruments, Fonte Nuova, Rome, I). These devices were specifically designed to perform long-time samplings (1–2 months) aimed to study the long-term variations and spatial variability of the concentration of PM and its components. Their performance, evaluated by Catrambone et al. [34], is satisfactory: the repeatability of the measurements is 2.0–5.5% for inorganic ions, 10–17% for polycyclic aromatic hydrocarbons (PAH), 5.2% for levoglucosan, 5.6–16% for elements, 8.2% for PM mass concentration.

In each indoor sampling site, we arranged three PM_{10} samplers, equipped with Teflon (PTFE membrane filters with ring, 37 mm, 2.0 µm pore size, Whatman, Maidstone, UnitedKingdom), Quartz (QM-A quartz filters, 37 mm, Whatman) and polycarbonate filters (Isopore membrane filters, Millipore, Burlington, MA, USA), respectively. With the only exception of A3, each sampling site was also equipped with identical samplers located outdoor, immediately out of the window, about 30 cm from the wall. Outdoor samplers were also set on the building terrace (T1) and another building's terrace at the same heightfrom the ground (T2), at about 200 m from T1. Additional very-low-volume samplers equipped with $PM_{2.5}$ impactors, and Teflon filters were set at all outdoor sites and atA3 and A4.

We also ran 24-h measurements of PM_{10} concentration at the ground floor using a beta attenuation monitor (SWAM 5aDual Channel Monitor, FAI Instruments, Fonte Nuova, Rome, Italy). To obtain information about the mixing properties of the lower atmosphere,we ran natural radioactivity measurements on a 1-h basis, using an automated monitor determining the total beta activity of the short-lived Radon progeny (PBL Mixing

Monitor,FAI Instruments, Fonte Nuova, Rome, Italy). Natural radioactivity due to Radon progenyincreases when atmospheric stability increases and decreases during advection or when the atmospheric mixing is efficient. It can be successfully used for describing changes in the mixing properties of the boundary layer [35–38]. All samplings were carried out from 1 November 2017, to 3 October 3 2018.

2.2 Analytical Procedure

Samples collected on Teflon filters were weighted using a microbalance (ME5, Sartorius AG, Goettingen, Germany), after conditioning at 50% R.H. and 20 ˚C for 48 h. Then they were analysed for their elemental content (Si, Al, Fe, Na, K, Mg, Ca and minor elements) by energy-dispersion X-ray fluorescence (XRF) (XEPOS, Spectro Analytical Instruments, Kleve, Germany). After XRF analysis, which is non-destructive, the samples were extracted for 20 + 20 min under sonication in deionized water and filtered using cellulose nitrate filters (0.45 pore size). The solutions were analysed for their ionic content (chloride, nitrate, sulfate, sodium, potassium, ammonium, magnesium, calcium) by ion chromatography (IC) (ICS1000, Dionex Co., Sunnyvale, CA, USA). Then they were analysed for the solublefraction of elements (As, Ba, Cd, Ce, Co, Cr, Cs, Cu, Fe, Li, Mn, Mo, Ni, Pb, Rb, Sb, Sn,Sr, Ti, U, Tl, V, Zn) by Inductively Coupled Plasma Optical Emission Spectrometry with mass detection (ICP-MS) (Brucker 820-MS, Billerica, MA, USA). The residual (insoluble) fraction on both the sampling membrane and the filtration membrane was subjected to microwave-assisted acid digestion using HNO_3:H_2O_2 (2:1), filtered again at 0.45 µm, and analysed by ICP-MS (same elements as for the extracted fraction). Chemical fractionation based on elemental solubility provides insight into the chemical form in which the element is released; thus, it adds useful information for the identification of PM sources and the estimation of the elemental bio-accessibility. The overall procedure, which allows a complete characterisation of the inorganic fraction of PM on a single collection filter, is described in Canepari et al. [39] and Perrino et al. [40,41]. The overall procedure allows a complete sample-by-sample quality control of the results by inter-technique comparison,as described in Canepari et al. [42]. The error associated with the measurements carried out with his method is below 20% (10% for most of the components). An overall discussion of the error sources is also reported in Canepari et al. [42].

Quartz filters were analysed for elemental carbon (EC) and organic carbon (OC) by thermo-optical analysis (TOA) (OCEC Carbon Aerosol Analyzer, Sunset Laboratory, Tigard, OR, USA) using the NIOSH-QUARTZ temperature protocol.

Polycarbonate filters were used to determine bioaerosol (not discussed in this paper) and the redox properties of PM, using three different acellular methods. Two methods determine proxies of the oxidative potential (OP) and are based on ascorbic acid (AA) [43] and 2′,7′-dichlorofluorescin (DCFH) [44]. The analytical procedures are extensively de- scribed elsewhere [45,46]. Briefly, to detect oxidative potential by ascorbic acid (OP^{AA}), PM samples were extracted in water and added with phosphate buffer and ascorbic acid solution. The antioxidant depletion rate (nmol AA min^{-1} m^{-3}) was acquired by UV-Vis absorption spectrophotometry (Varian Cary 50 UV-Vis Spectrometer) at 265 nm. To detect OPDCFH, the water-extracted solutions were added with horseradish peroxidase enzyme solution and 2′,7′-dichlorodihydrofluorescein diacetate solution, kept for 5 minutes at 37 ◦C, and analyzed for DCFH using a fluorescence detector (Jasco FP-920) at 530 nm

wavelength (427 nm excitation wavelength).

A third test, based on 2,2-diphenyl-l-picrylhydrazyl (DPPH) measures reducing species [47], was recently adapted to atmospheric PM by Frezzini et al. [48]. The water- extracts were added with DPPH solution in ethanol, kept at room temperature in the dark, and analysed by UV-Vis absorption spectrophotometry at 517 nm to determine DPPH radical scavenging.

3. Results and Discussion

3.1 Mass concentration of PM_{10}

3.1.1 Outdoor PM_{10}

PM_{10} concentration during the twelve months of the study at the three outdoor sites located at a different height from the ground, and the two sites located on the terraces are reported in Figure 1 (1-month sampling time). In the same graph, we also show PM_{10} values obtained by averaging, for each month, the daily concentrations measured at the university campus, close to the building (at the ground floor) and at the site "Arenula", belonging to the urban network of the Regional Environmental Protection Agency of the Lazio region (ARPA Lazio), located about 4.4 km from the university campus.

The data reported in Figure 1 show that the temporal patterns of the 1-month measurements generally follow those resulting from 24-h measurements at the Campus and incentral Rome; values about 20% higher were recorded during the first two months. The results of the outdoor measurements carried out at different heights of the building werein very good agreement, and it was not possible to detect any vertical gradient.

PM_{10} concentration was in the range 13–40 $\mu g/m^3$, with a seasonal pattern showinghigher values during the cold months (December–January) and minimum concentrations during the summer. This is a typical pattern for urban areas in central Italy: the increase in concentration during the winter is mainly due to both the emission from domestic heating and the more frequent occurrence of atmospheric stability periods. The time pattern of natural radioactivity (Supplementary material, Figure S1) shows, for the first three months of the study, the succession of stability periods, characterized by high valuesof natural radioactivity during the night but also during the middle hours of the day,and advection periods, characterized by low values during the whole day. Atmospheric stability events became less frequent during the late winter. Then, from the beginning of the spring, natural radioactivity took the pattern that is characteristic of the warm season: a regular succession of high values during the night (stability) and low values during theday (convective mixing). At the beginning of the fall, the pattern began to take on again the typical characteristics of the cold season.

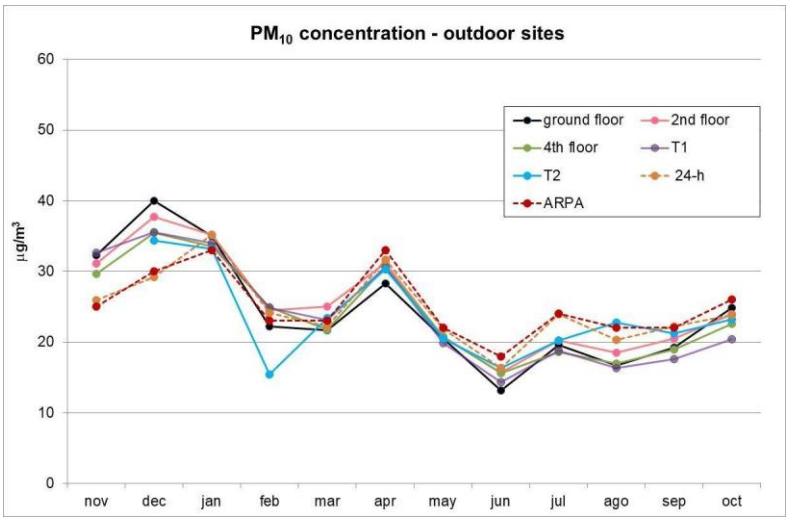

Figure 1. Particulate matter (PM_{10}) concentration at the five outdoor sites (1-month sampling time) and mean monthly concentration at the ground floor of the University campus and at the Regional Environmental Protection Agency (ARPA) site "Arenula" (1-day sampling time).

The increase in concentration recorded on April (Figure 1) was not due to variations in the mixing properties of the lower atmosphere, but it was most likely due to the many desert dust intrusions from the arid regions of North Africa towards Central and South Italy that took place on April 3–4, 11–20, and 24–30. Figure 2 (left side graph) shows the daily concentration of PM_{10} during April 2018, as measured at the University Campus and at the ARPA station "Arenula", and of the coarse fraction of PM, calculated by the difference between PM_{10} and $PM_{2.5}$ concentration at the same ARPA site. The data shows that most of the increase in PM_{10} concentration was due to the increase in the coarse fraction, as expected for desert dust intrusions. The right side panel of Figure 2 shows the dust surface concentration on Europe and North Africa on April 16th, when the desert dust transport reached its maximum intensity, as forecast by the Dust REgional Atmospheric Model (BSC-DREAM8b), operated by the Barcelona Supercomputing Center [49].

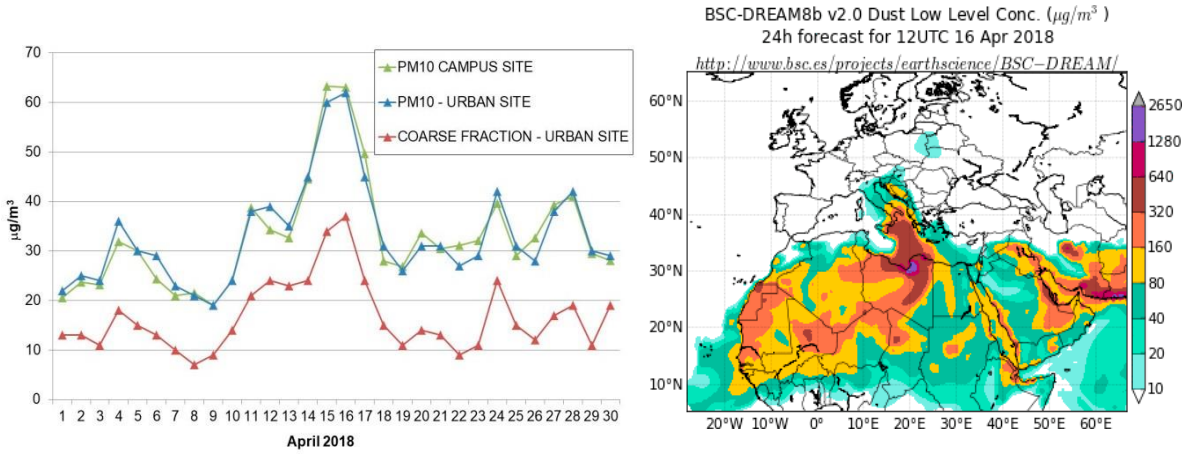

Figure 2. Concentration of PM_{10} at the university campus and concentration of PM_{10} and the coarse PM fraction at the urban ARPA site "Arenula" during April 2018 (left side panel); dust transport from North-

Africa on April 16th, as modelled by the Dust REgional Atmospheric Model (DREAM) (right side panel).

3.1.2 Indoor PM_{10}

Indoor PM10 concentration recorded at the six sites is shown in Figure 3. The time patterns were in good agreement, with the only exception of the concentration recorded at SL in March, when some renovation works took place inside the laboratory. We can differentiate two groups of sites: the three identical classrooms (A3, A4, A7), where we recorded higher concentration, and the other three indoor sites. The difference between the two groups was high during classes months (November, December considering Christmas holidays, January, April, May, June, October), it decreased when the classrooms were used for individual studying or exams (February, March, July, September), and it became negligible during August, when the Department was closed. The three classrooms belonging to the first group were characterized by a high occupancy rate (ratio between the number of people and the volume of the environment), as these classes were often full. Instead, the Lecture Hall (LH) has twice the volume of A3, A4, and A7, but only a fraction of the 300 available seats were generally occupied. The Computer Room (CR) and the laboratory (SL) are smaller and were much less crowded than the classrooms. Moreover, during the cold period (May-October), air conditioners were switched on at SL (all day long) and, less frequently, at CR (only during classes). These observations are a further confirmation of the fundamental role played by the presence of people in determining PM concentration in indoor environments.

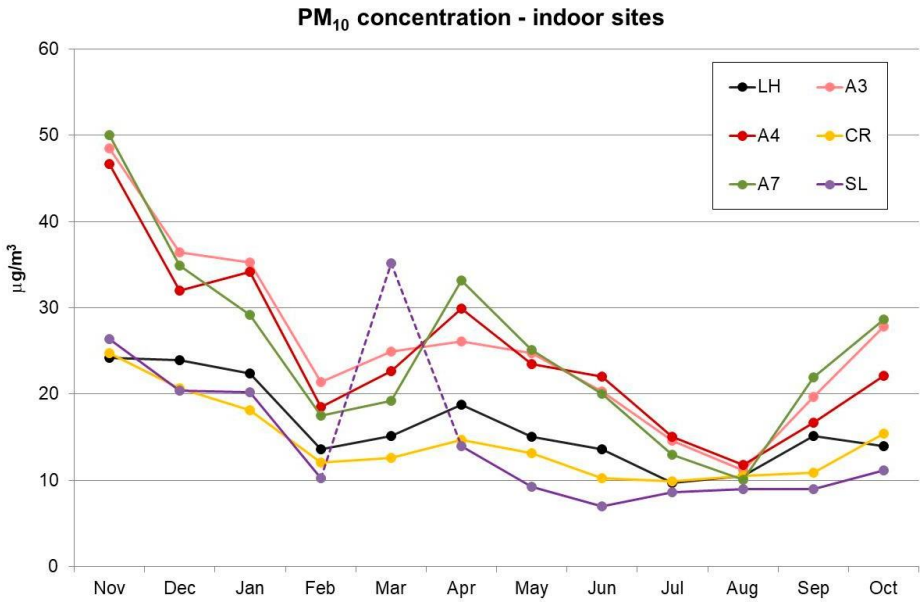

Figure 3. PM_{10} concentration at the six indoor sites (1-month sampling time). On March there were renovation works at SL (dotted line).

3.2 Chemical Composition of PM_{10}

The comparison between the gravimetric determination of PM_{10} and the mass re- constructed by adding the main PM_{10} chemical components is shown in Figure 4. To compute the reconstructed mass we considered

elements as oxides [50,51], calculated carbonate as the sum of calcium ion multiplied by 1.5 and magnesium ion multiplied by 2.5 (stoichiometric ratios in $CaCO_3$ and $MgCO_3$), and multiplied organic carbon (OC) by a conversion factor to take into account non-C atoms in organic molecules (mainly H and O) to obtain organic matter [26,52]. The conversion factor was set as 1.8 and 1.3 for the outdoor and the indoor sites, respectively. The choice of these values is a critical issue, given the current poor knowledge of the speciation of organics in PM, particularly in indoor environments [53].

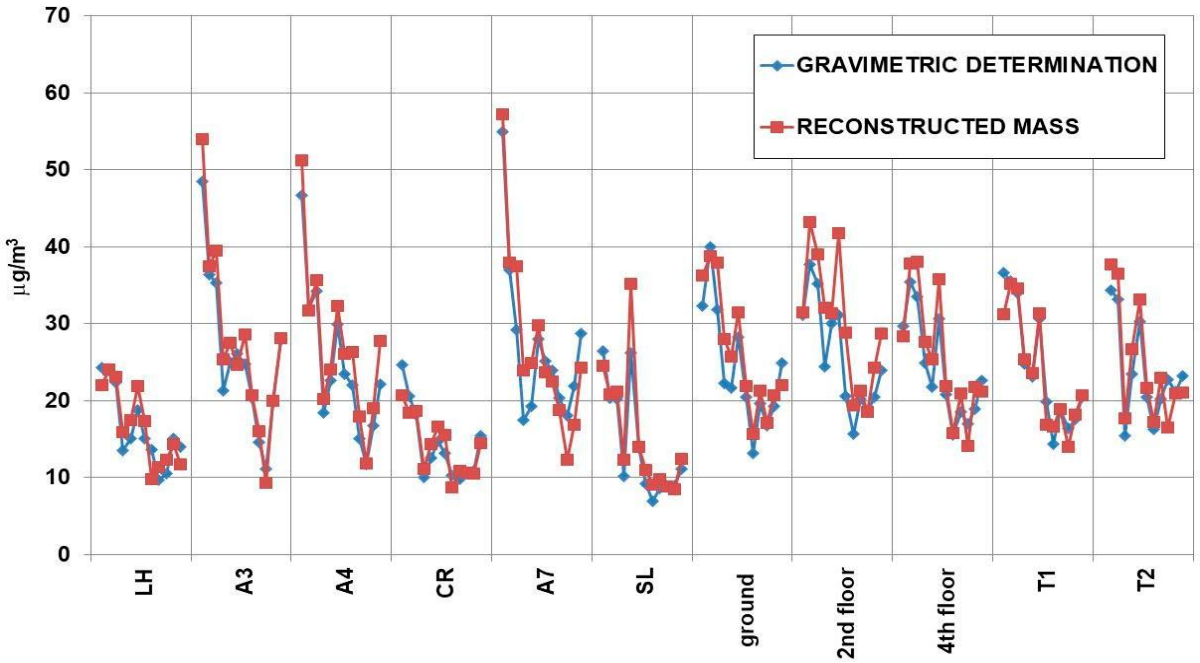

Figure 4. Comparison between the gravimetric determination of PM_{10} and the mass reconstructed from the chemical analyses.

A satisfactory mass closure was obtained, with the reconstructed mass accounting for 105.5 14.0% of the gravimetric mass in indoor sites and 107.1 12.5% in outdoor sites. Pearson's coefficients of the regressions between the two data sets were 0.934 and 0.854 forindoor and outdoor sites, respectively. These good results constitute a confirmation of thereliable analytical quality of the data.

The good results obtained at the mass closure allowed us to group the concentrationof the main components to get a picture of the primary sources of PM: soil, sea, secondaryproduction of inorganic species, traffic, and biosphere (organics). Details about the algorithms are reported in Farao et al. [54] and Perrino et al. [41]. Briefly, the contribution of soil was calculated by adding the concentration of elements (as metal oxides) that are generally associated with mineral dust: Al, Si, Fe, the insoluble fractions of K, Mg, and Ca (calculated as the difference between XRF and IC determinations), calcium and magnesium carbonate; sea-salt was estimated from the sum of Na^+ and Cl^-, multiplied by 1.176 to take into account minor sea-water components; secondary inorganics were calculated as the sum of non-sea-salt sulfate, nitrate and ammonium; the contribution of road traffic was estimatedby adding elemental carbon to an equivalent amount of organic carbon; the remaining organic carbon, multiplied by 1.8 (outdoor) or 1.3 (indoor), constituted the organics.

Figure 5 reports the time pattern of the five primary PM sources at the indoor and outdoor sites during the study year. In general, the time patterns at the outdoor sites showa good agreement, while the indoor data need further discussion.

An excellent agreement among the six indoor sites was observed only for the sea-salt,but the concentrations were much lower than those recorded outdoors. The particles released by this source, in fact, have no indoor contributions and have large dimensions and consequent low infiltration rate.

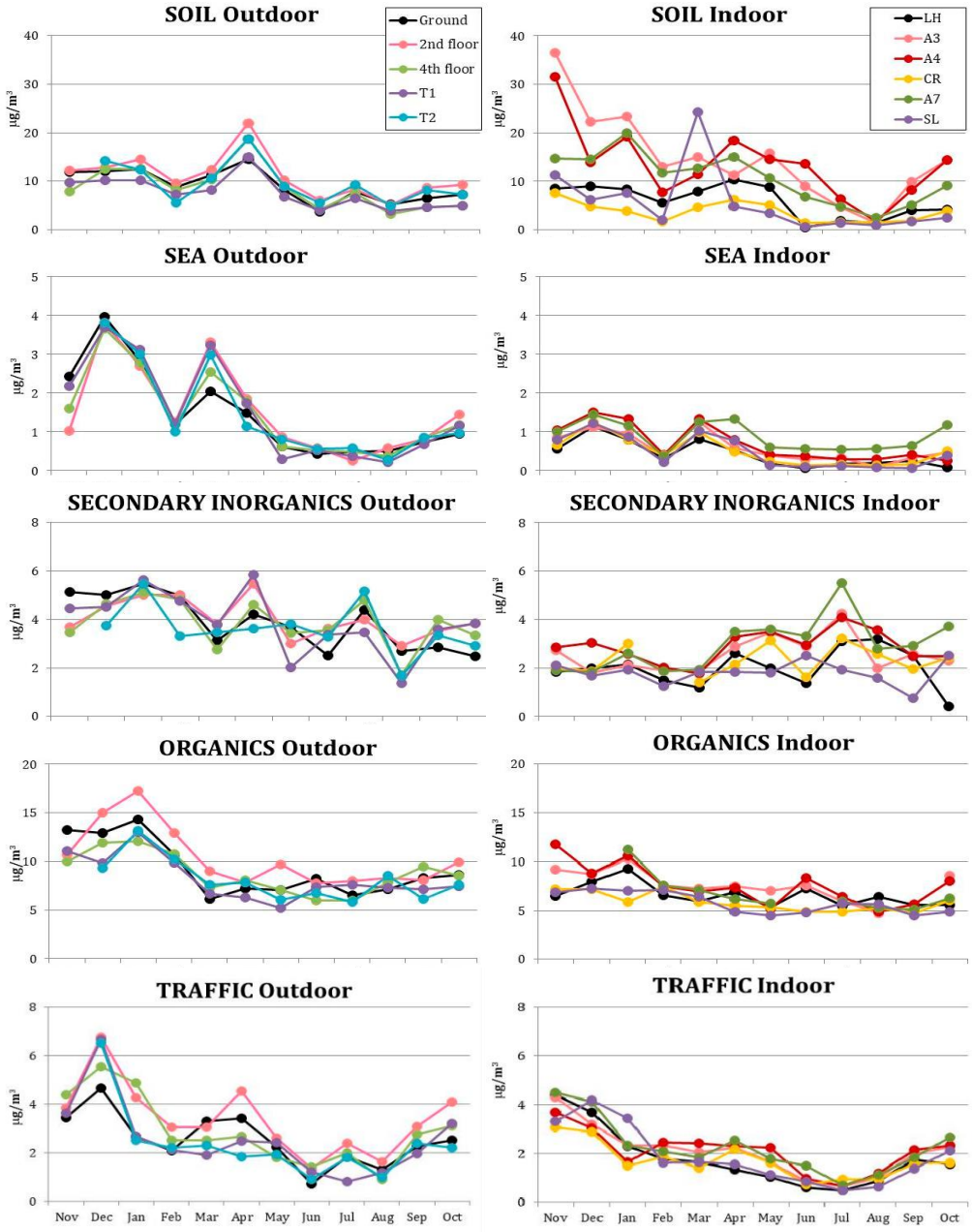

Figure 5. Outdoor and indoor time patterns of the main sources of PM_{10}.

Soil, the other natural PM source, shows a significant increase in the indoor concentration at the three classrooms (A3, A4, A7), particularly during lesson months (November, December, January, April, May, June, October). At the other three indoor sites, soil components' concentrations were generally lower than

outdoors, particularly during the summer, when air conditioning was on (at CR and SL). For these PM components, indoor production due to the students' presence and movements counterbalanced the low infiltration rate due to the large dimensions of these particles. As a result, indoor concentration was lower than outdoor when the rooms were empty. For the same reason, the high outdoor concentration recorded in April, due to desert dust intrusions, did not cause a significant increase in indoor PM. In August, when the building was closed, the concentration of soil components was lower than outdoors at all the indoor sites. These observations indicate that soil components were the main responsible for the pattern of PM_{10} concentration shown in Figure 3. It is worth noting that the increase in concentration recorded in April at SL, due to renovation works, was well explained by the increase in soil components.

Secondary inorganic species, which include ammonium nitrate and ammonium sulphate, showed a marked decrease in the transition from outdoor to indoor air during the winter months, a reduction that was not observed during the rest of the year. During the cold period, in fact, ammonium nitrate prevails over ammonium sulphate. When entering into heated indoor environments, this species' equilibrium shifts towards its gaseous precursors (nitric acid and ammonia), which are subsequently lost by deposition and adsorption on indoor surfaces [8,55]. As a consequence, its concentration in the particle phase decreases dramatically. Instead, during the summer months, most of the secondary inorganics were constituted by ammonium sulphate, a species of photochemical formation, thermostable, and contained in small particles (good infiltration capacity). For these rea- sons, during the warm period, outdoor and indoor concentrations of secondary inorganics were very close.

The indoor concentration of organics shows a flat pattern. Small differences betweenthe three classrooms and the other three sites can be detected, having the same shape discussed for soil components. These differences can be interpreted as the contribution of bioaerosol (skin flakes) released by the students. More investigations are needed to understand why low indoor-to-outdoor ratio was observed for the organics during the cold months.

The particles emitted by vehicle exhausts are characterized by small dimensions. Forthis reason, they easily infiltrate, and their indoor time pattern and concentration were similar to those recorded outdoors.

Table 1 reports, for each month and each PM_{10} macro-source, the average concentration, standard deviation, and indoor/outdoor ratio (I/O) at the six indoor and five outdoor sites. For each indoor site, I/O was calculated considering the outdoor site located on thesame floor.

In the case of soil, I/O were variable: the highest values (0.9–1.8) were recorded during the winter when the occupancy rate was at its maximum, and the lowest one in August when the building was empty (0.3). Instead, for sea-salt, very low I/O (0.3–0.4) were recorded throughout the winter when the natural ventilation was scarce, and highervalues occurred during the spring and summer (0.5–0.6) when windows and doors were frequently opened.

I/O for secondary inorganics was 0.4–0.5 during the cold months because of the indoor shift in the ammonium nitrate equilibrium towards the gas phase, while it approached one during the summer period when indoor concentrations were mainly due to ammonium sulphate infiltration. I/O of the organics was in the range of

0.6–0.9. These values depend on many factors, including the variation in the occupancy of the indoor sites, the seasonality and changes in the intensity of the outdoor sources, and the different chemico-physical nature of the particles emitted by each primary and/or secondary source. In the case of traffic emission, a homogeneous source of fine, combustion particles, I/O did not show adefined seasonal pattern and was in the range of 0.6–0.9.

3.3 Composition of $PM_{2.5}$

Additional measurements of $PM_{2.5}$ allowed us to obtain more information about theinfiltration of smaller particles. Figure 6 shows the concentration of potassium (K) and ammonium (NH_4^+) in PM_{10} at the outdoor sites (left side of each graph) and the indoor sites (right side of each graph) during December and June (blue bars). Where available, concentrations in $PM_{2.5}$ are also reported (red bars).

	SOIL			SEA			SEC. INORGANICS			ORGANICS			TRAFFIC		
	INDOOR □g/m^3	OUTDOOR □g/m^3	I/O	INDOOR □g/m^3	OUTDOOR □g/m^3	I/O	INDOOR □g/m^3	OUTDOOR □g/m^3	I/O	INDOOR □g/m^3	OUTDOOR □g/m^3	I/O	INDOOR □g/m^3	OUTDOOR □g/m^3	I/O
Nov	18.3 ± 12.5	10.4 ± 2.0	1.8	0.8 ± 0.2	1.8 ± 0.6	0.5	2.2 ± 0.4	4.2 ± 0.8	0.5	8.3 ± 2.2	11.2 ± 1.4	0.7	3.9 ± 0.6	3.8 ± 0.4	1.0
Dec	11.7 ± 6.5	12.4 ± 1.4	0.9	1.3 ± 0. 2	3.8 ± 0.1	0.3	2.0 ± 0.5	4.5 ± 0.5	0.5	8.0 ± 0.8	11.8 ± 2.4	0.7	3.5 ± 0.6	5.9 ± 1.0	0.6
Jan	13.7 ± 8.0	12.4 ± 1.5	1.1	1.0 ± 0.2	2.9 ± 0.2	0.3	2.4 ± 0.4	5.3 ± 0.3	0.4	9.1 ± 2.2	14.0 ± 2.0	0.6	2.3 ± 0.7	3.5 ± 1.3	0.6
Feb	7.0 ± 4.8	7.9 ± 1.6	0.9	0.3 ± 0.1	1.2 ± 0.1	0.3	1.7 ± 0.3	4.6 ± 0.7	0.4	7.3 ± 0.4	10.9 ± 1.2	0.7	2.0 ± 0.3	2.4 ± 0.4	0.8
Mar	12.6 ± 6.8	10.5 ± 1.5	1.2	1.1 ± 0.2	2.8 ± 0.5	0.4	1.7 ± 0.3	3.4 ± 0.4	0.5	6.6 ± 0.6	7.3 ± 1.1	0.9	1.8 ± 0.5	2.6 ± 0.6	0.7
Apr	11.0 ± 5.1	17.8 ± 3.1	0.6	0.8 ± 0.3	1.6 ± 0.3	0.5	2.7 ± 0.6	4.8 ± 0.9	0.6	6.4 ± 1.1	7.4 ± 0.7	0.9	2.0 ± 0.5	3.0 ± 1.0	0.7
May	9.7 ± 5 0	8.6 ± 1.2	1.1	0.3 ± 0.2	0.6 ± 0.2	0.5	2.9 ± 0.8	3.2 ± 0.7	0.9	5.5 ± 0.9	7.0 ± 1.7	0.8	1.6 ± 0.4	2.2 ± 0.3	0.7
Jun	5.3 ± 5.4	4.7 ± 1.0	1.1	0.3 ± 0.2	0.5 ± 0.1	0.5	2.4 ± 0.8	3.3 ± 0.5	0.7	6.6 ± 1.6	7.2 ± 0.9	0.9	0.9 ± 0.3	1.1 ± 0.3	0.8
Jul	3.4 ± 2.1	7.9 ± 1.0	0.4	0.3 ± 0.2	0.4 ± 0.1	0.6	3.7 ± 1.2	4.4 ± 0.7	0.8	5.7 ± 0.5	6.8 ± 1.0	0.8	1.0 ± 0.2	1.8 ± 0.6	0.6
Aug	1.6 ± 0.5	4.5 ± 0.9	0.3	0.2 ± 0.2	0.4 ± 0.1	0.6	2.6 ± 0.7	2.1 ± 0.7	1.3	5.4 ± 0.6	7.8 ± 0.6	0.7	1.0 ± 0.2	1.2 ± 0.3	0.8
Sep	5.1 ± 3.3	6.5 ± 1.9	0.8	0.3 ± 0.2	0.8 ± 0.1	0.4	2.2 ± 0.8	3.5 ± 0.4	0.6	5.1 ± 0.5	7.8 ± 1.2	0.7	1.8 ± 0.3	2.5 ± 0.4	0.7
Oct	8.0 ± 5.4	6.7 ± 1.8	1.2	0.5 ± 0.4	1.1 ± 0.2	0.4	2.3 ± 1.1	3.3 ± 0.6	0.7	6.6 ± 1.4	8.4 ± 1.0	0.8	2.1 ± 0.4	3.0 ± 0.7	0.7

Table 1. Indoor and outdoor concentration (mean ± standard deviation) and I/O ratio of PM_{10} macro-sources. Number of data is N=6 and N=5 for indoor and outdoor sites, respectively.

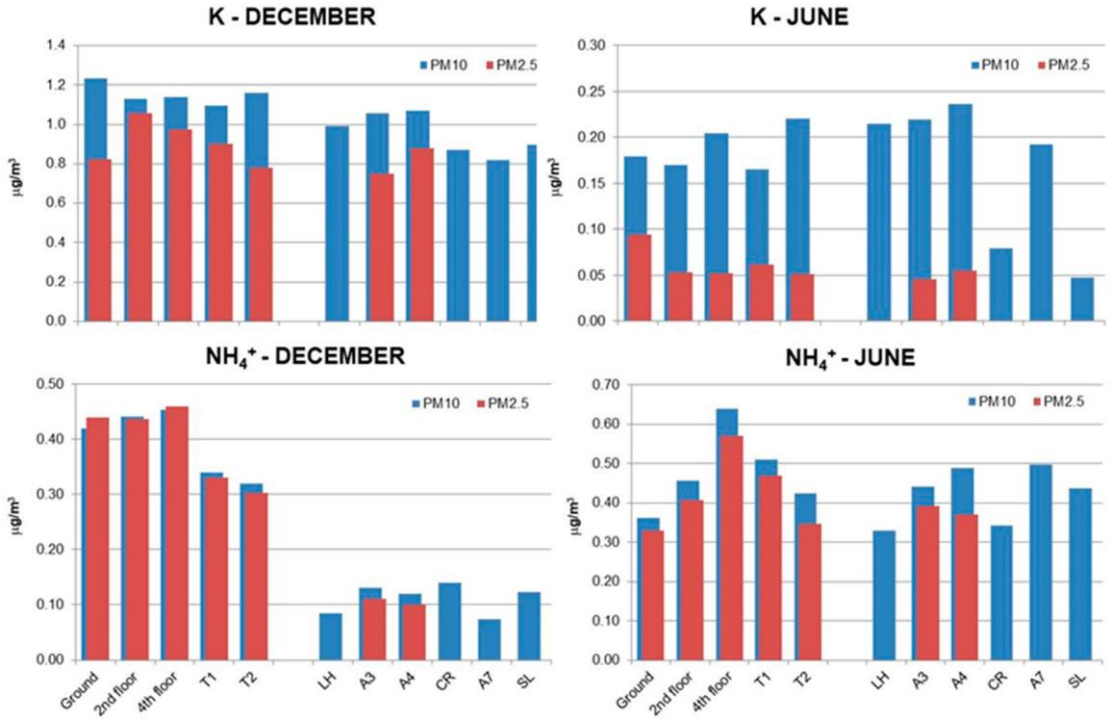

Figure 6. Potassium and ammonium concentration in PM10 and PM2.5 during December and June.

In the case of potassium, the differences between December and June, and, within thesame month, between PM_{10} and $PM_{2.5}$ depended on the dominant emission source. K is released into the atmosphere by wood combustion for domestic heating and soil abrasion and re-suspension. The first source is active only during the cold season and emits particles in the fine size range; the second source prevails during the summer and releases particles in the coarse range. Accordingly, in December, the indoor concentration values of K were always close to those recorded outdoors (I/O > 0.8), and values in $PM_{2.5}$ were a substantialfraction of those in PM_{10}. In June, instead, the coarse fraction prevailed (K in $PM_{2.5}$ << K inPM_{10}) and indoor concentrations were generally higher than outdoor (natural ventilationby windows and doors, plus the effects due to the presence of the students), except for CRand SL, where air conditioning was switched on.

Instead, ammonium was only in the fine PM fraction, and its concentrations in $PM_{2.5}$and PM_{10} were very similar at all sites and during both periods. During December its indoor concentration dropped down because it was mainly in the form of ammonium nitrate. During June, due to the prevalence of ammonium sulphate, I/O was about 0.9. It is worth noting that the air conditioning had low efficiency in removing fine particles, and ammonium concentration at CR and SL were comparable to those determined at the other sites.

3.4 Micro-Elements

The insoluble fractions of Cr and Zn are not reported due to the low reliability of theanalytical results (Cr is not efficiently recovered during the acid digestion, and Zn showsvery high blank concentrations in membrane

filters).

Table 2 details the yearly mean concentration of micro- and trace-elements in indoor and outdoor PM_{10}; element concentrations in $PM_{2.5}$ are reported in Supplementary Material (Table S1). In this study, the soluble and insoluble fractions of each element were considered independently, to increase the selectivity of elements as source tracers. It is well known, in fact, that each PM source is responsible for the emission of particular chemical species,each one having its solubility [39,56,57].

Table 2. Indoor and outdoor concentration (yearly mean ± standard deviation) and I/O ratio of micro- and trace-elements in the soluble and insoluble fraction of PM_{10}. The limits of detection (LOD) and the number of data > LOD (N) are reported for each element.

	SOLUBLE FRACTION						INSOLUBLE FRACTION					
	LOD	INDOOR		OUTDOOR		I/O	LOD	INDOOR		OUTDOOR		I/O
	ng/m^3	N	ng/m^3	N	ng/m^3		ng/m^3	N	ng/m^3	N	ng/m^3	
As	0.2	61	0.40±0.25	50	0.41±0.18	1.0	0.3	-	<LOD	-	<LOD	-
Cd	0.07	49	0.10±0.05	47	0.15±0.05	0.7	0.1	-	<LOD	-	<LOD	-
Ce	0.01	25	0.02±0.01	28	0.03±0.02	0.6	0.2	64	0.9±0.6	47	0.6±0.2	1.3
Co	0.05	30	0.07±0.05	27	0.05±0.03	1.1	0.05	52	0.15±0.12	42	0.13±0.05	1.3
Cr	0.1	59	0.2±0.1	54	0.3±0.1	1.0	-	-	-		-	-
Cs	0.01	53	0.02±0.01	43	0.03±0.02	0.8	0.01	70	0.03±0.02	58	0.05±0.01	0.6
Cu	0.5	71	4.2±1.4	59	8.1±4	0.5	1	70	8±5	59	13±5	0.6
Fe	5	66	13±7	58	17±6	0.8	100	67	360±237	59	574±227	0.6
Li	0.02	52	0.05±0.02	44	0.05±0.02	0.8	0.05	66	0.13±0.08	58	0.18±0.10	0.8
Mn	0.5	72	3.0±1.7	59	3.4±1.6	0.8	0.5	55	3.6±1.7	59	6.1±3.0	0.5
Mo	0.05	68	0.33±0.15	58	0.37±0.12	0.9	0.1	64	0.4±0.2	60	1.0±0.5	0.5
Ni	0.2	41	0.7±0.4	46	0.7±0.4	0.9	0.5	67	1.4±0.7	56	1.7±1.0	0.9
Pb	0.1	72	0.4±0.2	59	0.5±0.3	0.9	0.5	69	3.7±1.8	59	4.0±1.4	0.9
Rb	0.1	71	0.6±0.5	58	0.8±0.6	0.8	0.1	45	0.4±0.2	40	0.6±0.3	0.6
Sb	0.1	72	0.8±0.3	58	1.0±0.3	0.8	0.2	71	1.2±0.5	59	1.5±0.6	0.8
Sn	0.02	69	0.17±0.10	53	0.15±0.06	1.1	0.1	70	1.7±0.5	60	2.8±1.2	0.6
Sr	0.5	67	2.8±1.9	58	2.7±1.7	1.0	0.5	50	2.6±1.9	40	2.6±1.3	1.1
Ti	0.1	32	0.2±0.2	35	0.2±0.1	1.2	0.5	72	8.2±6.1	60	8.9±4.0	1.0
Tl	0.01	61	0.04±0.02	51	0.06±0.03	0.8	0.01	-	<LOD		<LOD	-
U	0.001	-	<LOD	-	<LOD	-	0.001	48	0.011±0.007	43	0.014±0.008	0.7
V	0.2	71	1.2±0.9	58	1.1±0.8	1.0	0.2	71	0.8±0.4	60	1.1±0.6	0.7

Zn	2	61	14±12	58	16±8	0.9	-	-	-	-	-	-

The data show that indoor and outdoor concentration levels were comparable for allthe considered elements, with I/O ratio in the range of 0.5–1.3; values higher than one were generally found for crustal elements and were due to the re-suspension of depositedparticles. As academic environments are characterized by the absence of combustion sources, these results suggest that the concentration of elements of anthropic origin in indoor environments was dominated by the infiltration from outdoors. Furthermore, I/Oratios of the soluble fractions were generally closer to unity than those of the insoluble fractions, indicating that soluble species infiltrate more efficiently.

This behavior may be better understood considering the combination of the dimensional and chemical fractionation. As well known, the size of the particles released by each emission source reflects the emission process: combustion produces fine particles, while coarse particles are mainly released by abrasive-mechanical processes [58]. Figure 7 reports the dimensional and chemical fractionation of each element in this study's indoor and outdoor environments, calculated from the two elemental fractions in PM_{10} and $PM_{2.5}$, as described in Canepari et al. [39]. The results show that the soluble fraction of almost all the considered elements was contained in the fine fraction of PM, while scarcely soluble species dominated the coarse fraction. These findings agree with previous studies, which indicate combustion sources as the main responsible for the presence of soluble (and then bio-accessible) species containing elements that affect human health [39,59]. These smaller— and soluble—particles are more able to infiltrate in indoor environments. Furthermore,it can be observed that both the chemical and the size distribution were very similar in indoor and outdoor environments, confirming that the infiltration from outdoors was theprimary process responsible for the indoor build-up of elements.

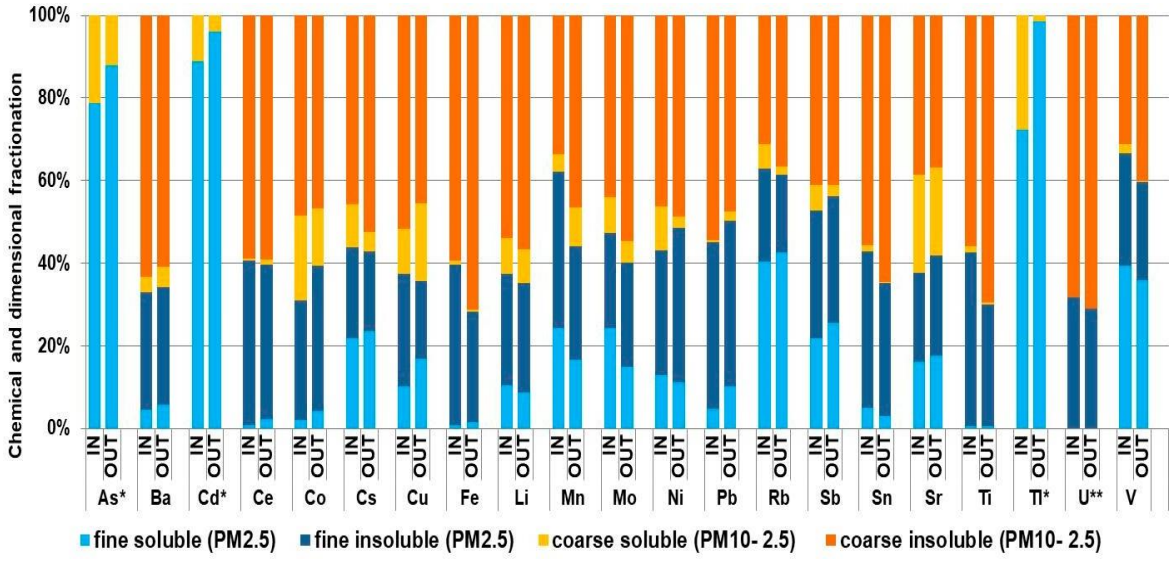

Figure 7. Chemical and dimensional fractionation of micro- and trace-elements in outdoor and indoor samples (yearlymean values). * not detectable in the residual fraction; ** not detectable in the soluble fraction.

The behavior of the particles released by specific sources may be characterized moreaccurately by considering

some selective source tracers. Among the considered elements, the soluble fractions of Cs, Rb, Li, and Tl have been identified as reliable tracers of biomass burning, Cu, Sb, Mo, Ba, and Sn in their insoluble fraction have been used as tracers of brake abrasion coming from non-exhaust traffic contribution, Ni and V (soluble fraction) are known to be mainly released by coke and heavy oil combustion, Sr, Ce, U, and the insoluble fraction of Rb, Cs, Li have a crustal origin and may be used to trace the contribution of soil [57–62]. As the concentrations of all the elements associated with each source show the same time and space variability, these groups of elements are expected to be highly correlated. The high Pearson coefficients obtained by these groups of elements in the correlation matrices related to the whole database of this study ($R2 > 0.7$) confirm their reliability as source tracers (Supplementary Material, Tables S2 and S3 for the soluble and insoluble fractions, respectively).

In Figure 8, we report the yearly pattern of a selected tracer of the first three sources: the soluble fraction of Rb for biomass burning, the insoluble fraction of Cu for brake abrasion and the soluble fraction of V for heavy oil combustion. For each tracer, as already observed for PM_{10} and its macro-sources, the results obtained at different heights from the ground were in good agreement, and no vertical gradients were detected.

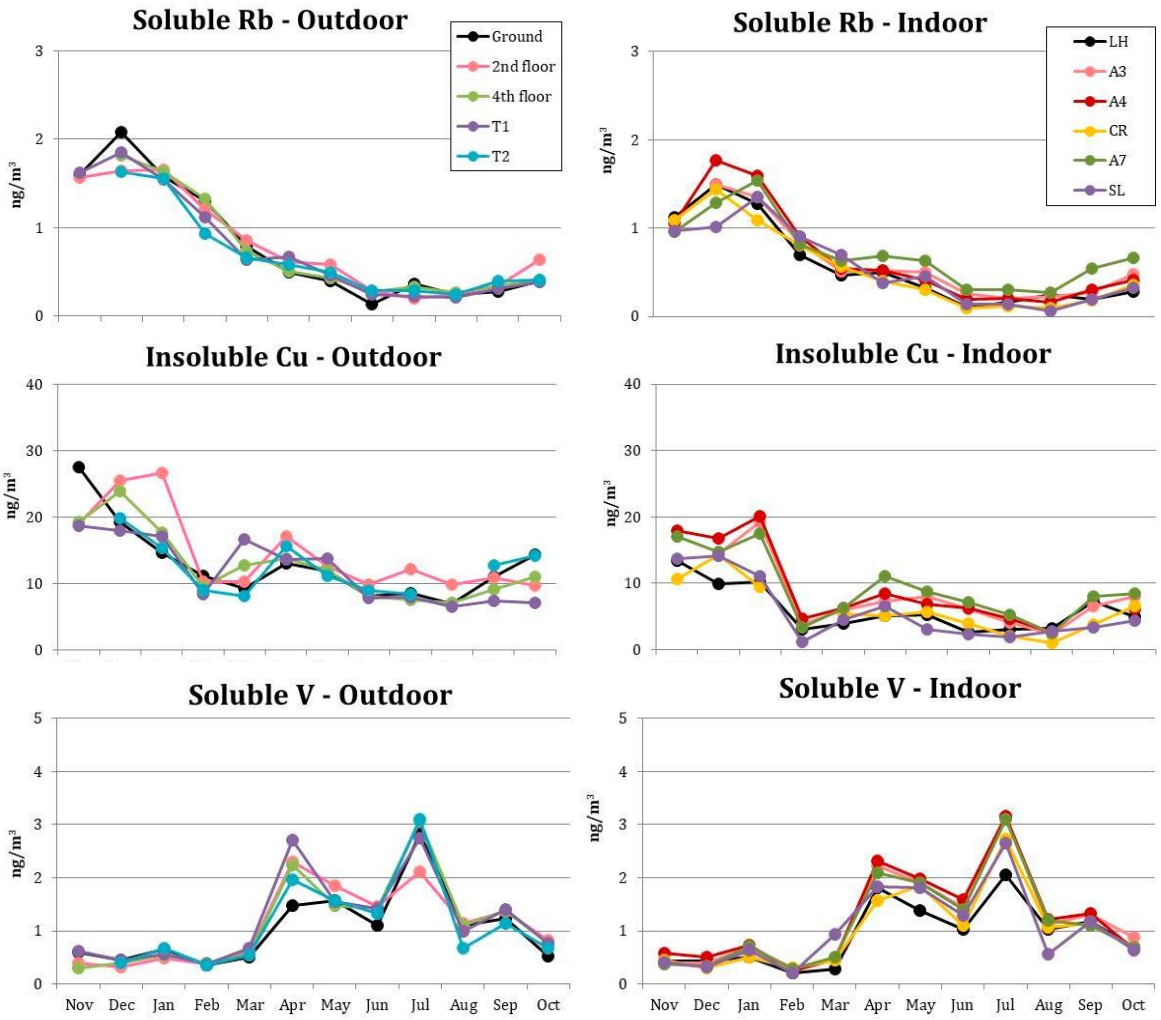

Figure 8. Outdoor and indoor time patterns of the soluble fraction of Rb, the insoluble fraction of Cu and the soluble fraction of V.

The tracer of biomass burning showed, as expected, a marked seasonal trend, with higher values during the cold months. A very similar pattern was detected indoors. Indoor and outdoor concentrations were not so much different (I/O = 0.8) because combustion particles, in the fine size range, have a good ability to infiltrate inside the building.

In the case of brake abrasion, outdoor results were more variable, but without significant differences among the sampling sites. The time pattern of this tracer recalls that of the traffic source (Figure 5). Indoors, we detected a similar time pattern but lower concentrations, in agreement with the larger size of these particles (I/O = 0.6). As in the case of soil (Figure 5), the tracer concentration at A3, A4, and A7 was slightly higher than at the other sites, indicating that for particles from brake abrasion a small contribute due to the presence of the students may add to the infiltration from outdoors. Particles from heavy oil combustion are typically in the finest size range of PM. In this case, indoor and outdoor time patterns were superimposable, and I/O was close to one, confirming, once again, that the infiltration inside the building depends on the particle dimensions. The seasonal trend shows higher values between April and July, probably due to a summer increase in ship traffic.

3.5 Redox Properties

To have a first insight about the redox properties of PM, which are a fundamental step in the comprehension of the mechanisms behind PM toxicity, some of the indoor and outdoor samples were analysed for their oxidative potential by ascorbic acid (OP^{AA}) and 2′,7′-dichlorofluorescin (OP^{DCFH}), two assays widely used as a proxy of the ability of PM to induce oxidative stress in the target organisms. Moreover, we also applied a test based on 2,2-diphenyl-l-picrylhydrazyl (RP^{DPPH}), able to measure reducing species.

Figure 9 shows the results obtained by applying the three methods to the samples collected on polycarbonate filters at sites A7 and LH during November and April. In all cases, the pairs of measurements carried out at the two sites during the same periods gave similar results, in agreement with the small differences detected for most chemical components of PM among all outdoor sites and among all indoor sites (Figure 5).

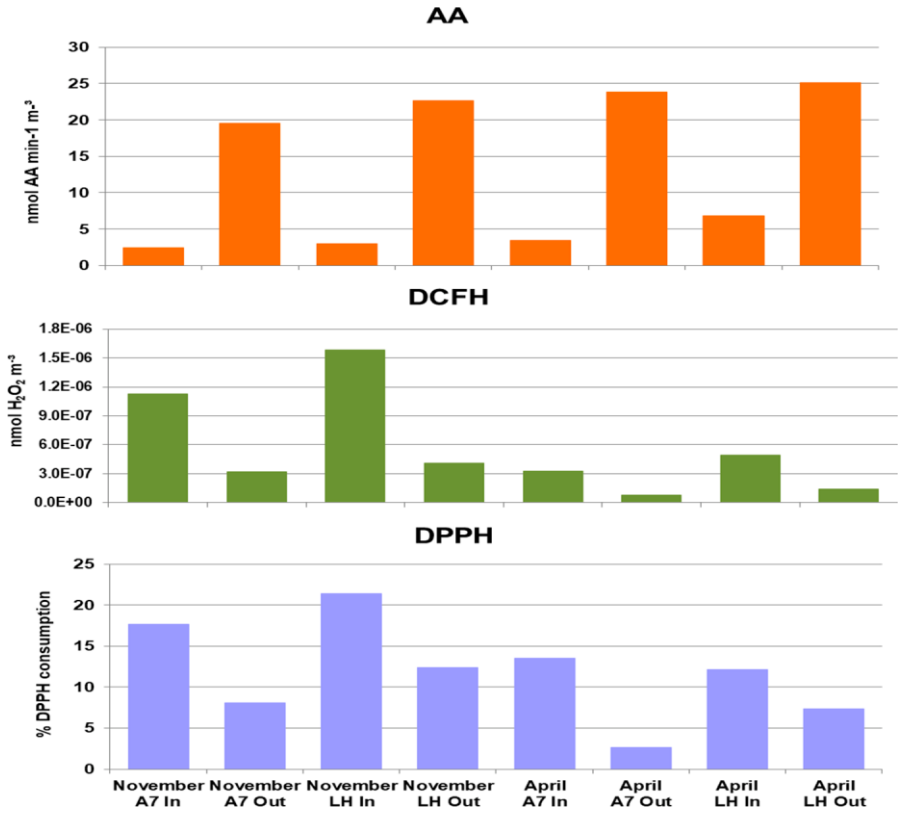

Figure 9. Redox properties of PM_{10} determined by ascorbic acid (AA), 2′,7′-dichlorofluorescin (DCFH), and 2,2-diphenyl-l-picrylhydrazyl (DPPH) assays at A7 and Lecture Hall (LH) during November and April.

OP^{AA} showed much higher values outdoors, with no significant differences betweenthe two periods. In the literature, the results obtained by this assay are generally attributed to non-exhaust traffic emission, in particular to brake abrasion [32,45]. However, in thesepreliminary results, I/O ratios of OP^{AA} appear lower than expected based on this only attribution. The same discrepancy was already reported by Szigeti et al. [63], although to alesser extent. OP^{DCFH} showed the opposite pattern, with higher values recorded indoors and during the cold period. This assay determines reactive oxygen species (ROS) that were originally present on the particles; the results are generally related to combustion sources (in urban areas, road traffic and biomass burning for domestic heating). The higher values obtained for the outdoor samples collected during the cold period agree with this interpretation. However, given the absence of combustion sources inside the classrooms, the much higher OP^{DCFH} values in indoor environments need additional explanation. It has been hypothesized that the atmospheric bioaerosol can be responsible for ROS generation and subsequent inflammation in the target body [64]. As indoor environments where many people groupare characterized by high bioaerosol concentration [65], it is plausible that indoor OP^{DCFH} increases as a consequence of the presence of people.

RP^{DPPH} shows a similar pattern, with higher values indoors and during the cold period. Up to now, there is no information about the chemical species related to the outcomes of this assay. Our results, however, suggest

that the presence of people can be responsible for the emission of some reducing species. The same species might also be responsible for the low values obtained in indoor environments at the OP^{AA} test. It is worth noting, in fact, that the results of the RP^{DPPH} assay can also be expressed in terms ofequivalents of ascorbic acid (a natural antioxidant), highlighting a direct link between thetwo tests.

It should be underlined that the studies about the oxidative potential and, most of all,the reducing potential of PM are still in their development phase and that there is a gap of knowledge in identifying the chemical species responsible for the redox properties of the atmospheric aerosol. In addition, the ability of chemical proxies to simulate biologicaloxidation mechanisms are still a matter of debate [66]. Our preliminary results suggest a strong need to deepen the studies about PM's redox properties in indoor environments where many people gather.

4. Conclusions

Long-duration samplings allowed us to obtain a representative and reliable picture of the concentration trend of PM and its chemical components both indoors and outdoors in the various sites of a University building during students' regular activity.

We could evaluate the seasonal trend of the main PM sources, the infiltration capacity of the particles produced by each source and the relevance of additional indoor PM production. Indoors, most of PM increase was due to soil and organic species, with an essential role of the presence of people. Particles of different sizes showed a different infiltration degree: coarse particles infiltrated to a smaller extent, while finer particles showed higher infiltration capacity. In the first group, we find particles of natural origin, such as sea-salt components (I/O in the range 0.3–0.6), but also anthropic particles, such as those released by brake abrasion (I/O ratios about 0.6). In the case of soil particles, despitethe low infiltration rate (I/O = 0.3 on August, when the building was empty), I/O valueswere up to 1.8 because of the re-suspension of deposited particles and the introductionof particles from outdoors on students' boots. Fine particles produced by traffic, biomass burning, and heavy oil combustion showed I/O in the range 0.6–1.0.

Although preliminary, chemical assays of oxidative potential indicated that indoor particles show different redox characteristics from outdoors, suggesting an important rolerelated to the presence of people. Since the exposure to atmospheric particles occurs mainly indoors, this aspect deserves further investigation in the future.

Although the air quality in the considered indoor environments would benefit from a better airtightness of the building, the contribution to PM of the organic species due to people's presence would be not influenced by this measure. Instead, using air conditioners, convector heaters, and heat pumps, which are able to reduce particles concentration, mainly the coarse fraction, might be of great benefit to the occupants.

Author Contributions: Conceptualisation, S.C., C.P.; formal analysis: L.T., M.A.F., L.M., C.P.; funding acquisition: A.P., C.P.; investigation: L.T., M.C., M.G., S.P., E.R., T.S., M.A.F., L.M., M.R.; methodology: S.C., C.P.; project administration: A.P., C.P.; resources: L.T., M.C., E.R., T.S.; supervision: C.P.; validation:

L.T., M.C.; visualization: S.C., C.P.; writing - original draft: S.C., C.P.; writing—review and editing: S.C., C.P. All authors have read and agreed to the published version of the manuscript.

Supplementary Materials

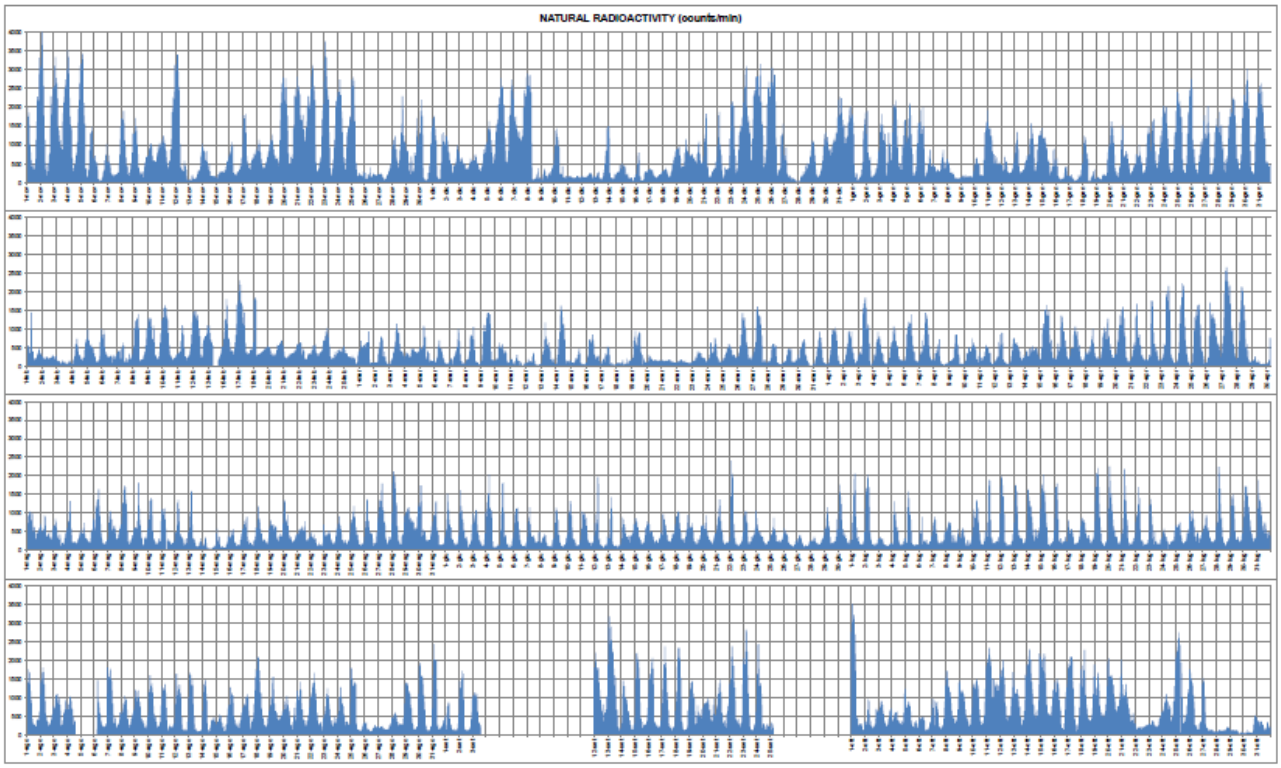

Figure S1. Time pattern of natural radioactivity during the study period.

Table S1. Indoor and outdoor concentration (yearly mean ± standard deviation) and I/O ratio of micro- and trace-elements in the soluble and insoluble fraction of $PM_{2.5}$. Limits of detection (LOD) and number of data > LOD (N) are reported for each element.

	SOLUBLE FRACTION						INSOLUBLE FRACTION					
	LOD	INDOOR		OUTDOOR		I/O	LOD	INDOOR		OUTDOOR		I/O
	ng/m³	N	ng/m³	N	ng/m³		ng/m³	N	ng/m³	N	ng/m³	
As	0.2	20	0.39±0.21	47	0.42±0.18	0.9	0.3	-	<LOD	-	<LOD	-
Cd	0.07	18	0.07±0.04	47	0.16±0.09	0.7	0.1	-	<LOD	-	<LOD	-
Ce	0.01	8	0.01±0.01	25	0.04±0.03	0.9	0.2	18	0.4±0.2	44	0.3±0.2	0.9
Co	0.05	10	0.06±0.05	29	0.05±0.03	0.7	0.05	16	0.10±0.06	44	0.09±0.04	1.0
Cr	0.1	16	0.2±0.1	55	0.3±0.1	0.8	-	-	-	-	-	-
Cs	0.01	18	0.02±0.01	46	0.03±0.02	0.8	0.01	18	0.02±0.02	45	0.02±0.01	0.9
Cu	0.5	20	1.7±0.7	59	4.8±4.0	0.5	1	24	4±3	61	5±3	0.8
Fe	5	16	7±3	54	14±9	0.8	100	22	166±87	51	230±197	0.7
Li	0.02	18	0.03±0.02	46	0.03±0.02	1.0	0.05	22	0.06±0.03	57	0.09±0.05	0.9
Mn	0.5	24	2.5±1.8	61	2.4±1.6	1.2	0.5	24	1.9±0.9	61	3.2±2.0	0.6

Mo	0.05	22	0.25±0.13	53	0.29±0.12	0.9	0.1	18	0.3±0.1	52	0.5±0.4	0.5
Ni	0.2	22	0.4±0.2	43	0.7±0.5	0.8	0.5	22	1.0±0.5	57	1.4±0.8	0.7
Pb	0.1	24	0.3±0.2	57	0.5±0.3	0.5	0.5	24	2.7±1.4	61	3.4±1.6	0.8
Rb	0.1	24	0.5±0.5	56	0.7±0.6	0.9	0.1	14	0.3±0.1	37	0.3±0.2	1.0
Sb	0.1	24	0.6±0.2	59	0.9±0.4	0.8	0.2	24	0.9±0.3	61	1.1±0.6	0.9
Sn	0.02	24	0.15±0.07	47	0.15±0.11	0.9	0.1	24	1.1±0.9	61	1.4±1.1	0.7
Sr	0.5	22	1.2±0.6	55	1.3±1.2	0.8	0.5	18	1.4±0.7	42	1.6±1.2	0.8
Ti	0.1	10	0.2±0.2	29	0.2±0.1	0.7	0.5	24	4.2±3.1	61	3.7±2.3	0.7
Tl	0.01	18	0.03±0.01	51	0.06±0.03	0.7	0.01	-	<LOD	-	<LOD	-
U	0.001	-	<LOD	-	<LOD		0.001	16	0.006±0.004	32	0.006±0.004	1.0
V	0.2	24	1.0±0.8	60	1.1±0.9	0.8	0.2	22	0.7±0.4	57	0.7±0.4	1.0
Zn	2	22	9±7	51	12±6	0.9	-	-	-	-	-	-

Table S2. Correlation matrix of elemental concentration in indoor and outdoor samples: soluble fraction.

	As	*Cd*	*Cr*	*Cs*	*Cu*	*Fe*	*Li*	*Mn*	*Mo*	*Ni*	*Pb*	*Rb*	*Sb*	*Sn*	*Sr*	*Ti*	*Tl*	*V*	*Zn*
As	1.0																		
Cd	0.3	1.0																	
Cr	0.5	0.3	1.0																
Cs	0.6	0.3	0.5	1.0															
Cu	0.2	0.4	0.4	0.4	1.0														
Fe	0.3	0.3	0.5	0.2	0.5	1.0													
Li	0.4	0.3	0.4	0.4	0.4	0.6	1.0												
Mn	0.6	0.2	0.5	0.5	0.3	0.5	0.5	1.0											
Mo	0.5	0.3	0.5	0.6	0.5	0.3	0.4	0.6	1.0										
Ni	-0.2	0.4	0.0	-0.3	-0.2	0.2	0.1	0.0	-0.1	1.0									
Pb	0.1	0.4	0.1	0.5	0.6	0.1	0.1	0.0	0.4	-0.2	1.0								
Rb	0.7	0.2	0.4	1.0	0.5	0.3	0.5	0.5	0.6	-0.4	0.3	1.0							
Sb	0.3	0.3	0.3	0.5	0.6	0.5	0.6	0.4	0.5	0.1	0.4	0.5	1.0						
Sn	0.2	0.1	0.2	-0.1	-0.1	0.3	0.3	0.3	0.4	0.4	0.0	-0.2	0.1	1.0					
Sr	0.3	0.0	0.5	0.5	0.3	0.4	0.5	0.3	0.5	-0.1	0.0	0.6	0.3	0.0	1.0				
Ti	0.5	0.1	0.4	0.5	-0.2	0.1	0.3	0.6	0.4	0.1	-0.1	0.4	0.1	0.4	0.2	1.0			
Tl	0.4	0.5	0.4	0.7	0.7	0.1	0.2	0.2	0.7	-0.3	0.7	0.7	0.4	-0.1	0.4	0.1	1.0		
V	-0.4	0.2	-0.1	-0.5	-0.1	0.3	0.2	-0.1	-0.1	0.7	-0.1	-0.5	0.3	0.5	-0.1	-0.1	-0.3	1.0	
Zn	0.7	0.1	0.4	0.5	0.3	0.5	0.4	0.6	0.4	-0.2	0.1	0.6	0.4	0.0	0.4	0.4	0.3	-0.3	1.0

Table S3. Correlation matrix of elemental concentration in indoor and outdoor samples: insoluble fraction.

	Ce	*Co*	*Cs*	*Cu*	*Fe*	*Li*	*Mn*	*Mo*	*Ni*	*Pb*	*Rb*	*Sb*	*Sn*	*Sr*	*Ti*	*U*	*V*
Ce	1.0																
Co	0.3	1.0															
Cs	0.4	0.5	1.0														
Cu	0.4	0.4	0.7	1.0													
Fe	0.4	0.3	0.8	0.9	1.0												
Li	0.1	0.3	0.6	0.2	0.3	1.0											
Mn	0.3	0.4	0.7	0.8	0.8	0.4	1.0										
Mo	0.1	0.2	0.6	0.8	0.8	0.2	0.7	1.0									
Ni	0.3	0.3	0.5	0.6	0.6	0.1	0.4	0.5	1.0								
Pb	0.5	0.6	0.7	0.8	0.7	0.2	0.6	0.6	0.5	1.0							
Rb	0.4	0.3	0.9	0.7	0.8	0.7	0.9	0.6	0.4	0.6	1.0						
Sb	0.2	0.3	0.4	0.8	0.7	0.1	0.5	0.8	0.5	0.6	0.1	1.0					
Sn	0.3	0.3	0.7	0.9	0.8	0.1	0.7	0.8	0.6	0.8	0.6	0.8	1.0				
Sr	0.7	0.3	0.6	0.5	0.5	0.5	0.7	0.3	0.3	0.6	0.7	0.0	0.3	1.0			
Ti	0.4	0.5	0.6	0.5	0.7	0.5	0.6	0.3	0.2	0.5	0.6	0.3	0.4	0.4	1.0		
U	0.6	0.6	0.9	0.8	0.7	0.4	0.8	0.6	0.5	0.8	0.7	0.6	0.7	0.8	0.6	1.0	
V	0.2	0.2	0.7	0.3	0.4	0.8	0.5	0.4	0.2	0.3	0.8	0.1	0.2	0.6	0.5	0.5	1.0

6.2 (B2) Comparison between PM_{10} oxidative potential of indoor and outdoor environments – The INDOMAP project

In preparation – preliminary results

Maria Agostina Frezzini et al.

Abstract

The health effects associated with human exposure to airborne particulate matter (PM) have been linked to oxidative properties of PM, as the ability of particles to promote the production of reactive species, predicted by the oxidative potential assays (OP). This study, carried out within the INDOMAP project, was aimed to investigate indoor and outdoor OP of PM on long term dataset to understand the redox characteristics of indoor/outdoor PM and the degree of the potential exposure of occupants to them. PM_{10} samples were simultaneously collected indoor and outdoor of different domestic environments for more than one year. This work reports the preliminary results of OP of PM_{10} samples, which was quantified with the ascorbic acid (OP^{AA}), the dithiothreitol (OP^{DTT}), and the dichlorofluorescin (OP^{DCFH}) assays to investigate the contribution of outdoor air and indoor activities to indoor air quality. The most important indoor contributions to OP^{DCFH} and OP^{DTT} were biomass domestic heating systems and cigarette smoke, while OP^{AA} indoor was influenced by domestic activity, such as cleaning habits. OP measurements of outdoor samples appeared generally higher than indoor one with a not pronounced variability between sites, but however dependent on the proximity to busy roads. The discussion of preliminary data provides general information on the differences between indoor and outdoor OP values at the selected sites. However, the discussed results will have to be confirmed with the chemical analysis, which are currently in progress, and will allow to make correlations between obtained values and the contribution of the different emission sources to OP of PM.

1. Introduction

Air pollution is widely recognized as a key topic in public health protection actions (Shaddick et al., 2020; WHO, 2018). Within this context, exposure to particulate matter (PM) is one of the major global health concern (Burnett et al., 2018). PM is a mixture of solid and liquid particles suspended in the atmosphere, with an aerodynamic diameter ranging between 0.01 and 100 μm, from variable sources and with different physical and chemical composition (Ramli et al., 2020; Ali et al., 2019). Nowadays, it is well known that exposure to PM may adversely affect human health by amplifying symptoms of allergies and asthma in persons with already compromised (impaired) health (Pénard-Morand et al., 2010). Therewith, long-term exposure may lead to development of several chronic pathologies like cardiovascular and respiratory disease (Brook et al., 2010), lung cancer (Zhang et al., 2020; IARC, 2010), chronic bronchitis (Pu et al., 2021), as well as neurodevelopmental disorders (Costa et al., 2020). The evaluation of exposure to PM and associated health risks is crucial for planning mitigation strategies and policies. However, while the outdoor air quality (OAQ) can be easily monitored and, thus, subjected to regulation, investigation of indoor air quality (IAQ) is more challenging. Indeed, indoor environments can have much more fluctuating PM levels than the outdoors (Lowther et al., 2019; Adgate et al., 2002). The enclosed nature of indoor spaces favorites PM accumulation

through occupants' activities, such as cooking, smoking, biomass combustion, use of electronic machines and use of consumer products (Zhang et al., 2018; Perrino et al., 2016; Secrest et al., 2016; Huang et al., 2015). Nevertheless, indoor environments can also protect people from exposure to outdoor pollution by avoiding PM penetration (Zhan et al., 2018). Therefore, IAQ and OAQ are strictly connected and the contextualization of IAQ monitoring, as well as the discrimination of the levels and sources of indoor and outdoor PM, is relevant to accurately assess exposures and health risk (Zhang et al., 2021; Lee et al., 2015). It is estimated that humans normally spend the 80% of their daily life indoor (Morawska et al., 2013). Residential indoor locations are considered micro-environments with the highest contribution to the daily exposure to PM (Canha et al., 2018; Zhang et al., 2017). As a consequence of the increasing time spent by people indoors, PM indoor exposure assessment and knowledge of source emission impacts is fundamental for evaluating exposure-response relationships and the health impacts of anthropogenic indoor air pollution (Gonzalez-Martín et al., 2021; Niu et al., 2021). It is largely described that health-endpoints of exposure to PM are related to the formation of reactive species (Reactive Oxygen Species, ROS, Reactive Nitrogen Species, RNS, Reactive Carbon Species, RCS) or free radicals, as the primary source of oxidative stress (Niu et al., 2021; Øvrevik et al., 2019; Li et al., 2015). Acellular assays have been widely used to measure the oxidative potential (OP) of particles, in order to provide a proxy of the oxidative properties of PM (Bates et al., 2019), as they are recognized as valid exposure metrics to investigate the effect of PM on living organisms (Borm et al., 2007). OP of particles is frequently measured by the ascorbic acid assay (OP^{AA}), that provides a measure of the particle-induced depletion of chemical proxies for the cellular ascorbic acid antioxidant, and by the dithiothreitol assays (OP^{DTT}), that is based on the PM-catalyzed electron transfer from a chemical surrogate of cellular reducing agents (i.e. adenine dinucleotide, NADH, and nicotinamide adenine dinucleotide phosphate, NADPH) to O_2 (Pietrogrande et al., 2021; Crobeddu et al., 2020; Bates et al., 2019; Fang et al., 2016). In addition, the dichlorofluorescin assay (OP^{DCFH}) is often applied for determining OP of PM samples, although the assay was originally used to monitoring ROS formation in biological cells (Huang et al., 2016; Halliwell and Whiteman, 2004). DCFH measures particle-bound ROS, that are inherently adherent to the particles, releasing a fluorescent intensity that is converted into equivalent H_2O_2 to express the final ROS concentration (Huang et al., 2016). Each OP assay reflects different oxidative properties of PM, and appears to have different relationships with health outcomes, therefore there are no appropriate criteria for choosing the most representative assay and the synergic application is frequently suggested (Rao et al., 2020; Gao et al., 2020; Bates et al., 2020).

Given the long time spent in home environments, is crucial to assess OP of indoor particles in relation to both the indoor and the outdoor environmental conditions, in order to investigate the health impact of particles present in indoor sources (Khurshid et al., 2019). However, to date, only a few studies have focused on examining the differences and the relationships between indoor and outdoor OP of PM, and very limited studies had examined the influence of domestic activities in determining indoor OP. This study was conducted within the INDOMAP project and involved different domestic environments for 12 months. During the monitoring campaigns in Rome (Italy), indoor and outdoor samplings were carried out in parallel by co-located small and quite samplers, that allowed long-lasting samplings (1-2 two months) at the flow rate of 0.5 L min^{-1} (Massimi

et al., 2020a). Therefore, the aim of the study was to examine OP (OP^{AA}, OP^{DTT} and OP^{DCFH}) of PM_{10} collected indoor as a function of OP of outdoor particles, and to investigate how OP indoor is affected by domestic activities, for evaluating the exposure of the occupants to particles. The main goal of this study is to investigate the differences between indoor-outdoor OP of particles according to various driving factors and the influence of both indoor and outdoor sources in determining indoor OP in order to provide information about the variables affecting the degree of the potential exposure of occupants.

2. Materials and Methods

2.1. Study locations and indoor conditions

The study was conducted within the city of Rome, Central Italy, a density populated city in the middle of Mediterranean Sea with an area of 1290 km^2 and 2.8000.000 inhabitants (Perrino et al., 2019). The monitoring sites, which were distributed within the city, were accurately chosen based on two criteria: their exposure to traffic and urbanization intensity, and the variety of the main activities and habits of the occupants. The geographical coordinates of the 15 selected sites (A, B, C, D, E, G, L, M, N, P, S, T, U, W, X) are reported in Table 1 with the specific characteristics of the sampling sites, obtained administrating an identical questionnaire designed to collect descriptive information including indoor activities (i.e. cooking frequency, house cleaning practices, smoking status), and housing situation (i.e. number of occupants, type of heating).

2.2. Sampling procedure

For the INDOMAP project PM_{10} samplings were performed by using the Smart Samplers (High spatial resolution sampler, HSRS, Fai Instruments, Fonte Nuova, Roma, Italy), operating at 0.5 L min^{-1}, characterized by small size, very low acoustic emissions and inexpensive electricity consumption. The samplers were previously evaluated by Catrambone et al. (2019) in terms of efficiency and repeatability, and already and largely employed during PM monitoring campaigns (Massimi et al., 2020, 2019, 2017).

Each sampling site was equipped with two identical indoor PM samplers, equipped with PTFE (PTFE membrane filters with ring, 37 mm, 2.0 µm pore size, Whatman, Maidstone, United Kingdom) and quartz (QM-A quartz filters, 37 mm, Whatman, Maidstone, United Kingdom) filters, and two identical outdoor samplers, equipped with PTFE and quartz filters too. For this work, only the PTFE were considered. Indoor and outdoor samplers worked in parallel, and PM samples were continuously collected for 2-month periods for more than two years, from May 2019 to April 2021. After the collection, PM_{10} filters were put in petri dish, sealed with parafilm, and stored in a freezer at -20°C under controlled temperature and humidity until the analysis.

2.3. Analytical procedure

The collected PM_{10} PTFE filters were subjected to a complete chemical characterization that was previously optimized and detailed and that will not be completely discussed in this study (Canepari et al., 2014; Perrino et al., 2014; Massimi et al., 2017; 2020a). After the removal of the supporting polymethylpentene ring from each sampled filter, PM membranes were water-extracted in 10 mL of deionized water (produced by Arioso UP 900 Integrate Water Purification System, USA) by rotating agitator (RA, 60 rpm; Rotator, Glas-Col, USA)

and filtered using cellulose nitrate filters (NC filter; pore size 0.45 µm, Merck Millipore Ltd., Billerica, MA, USA). The redox properties of PM were evaluated on the water-soluble fraction of samples that was split in proper aliquots for the considered OP analytical procedures.

2.4. Indoor and outdoor oxidative potential measurements

In this study, three methods were performed to determine the OP of PM_{10} samples: the OP^{AA}, the OP^{DTT} and the OP^{DCFH} assays by following previously optimized methods with slight modifications (Venkatachari et al., 2005, 2007; Cho et al., 2005; Fuller et al., 2014; Fang et al., 2016). The overall experimental procedures are extensively described elsewhere (Simonetti et al., 2018; Frezzini et al., 2019; Massimi et al., 2020b) and briefly summarized in the block diagram in the Figure 1. Additional details on the followed OP procedures, equations adopted for calculating OP and used chemical reagents are reported in supplementary material S1. After the analysis, indoor OP measurements were compared to outdoor OP data.

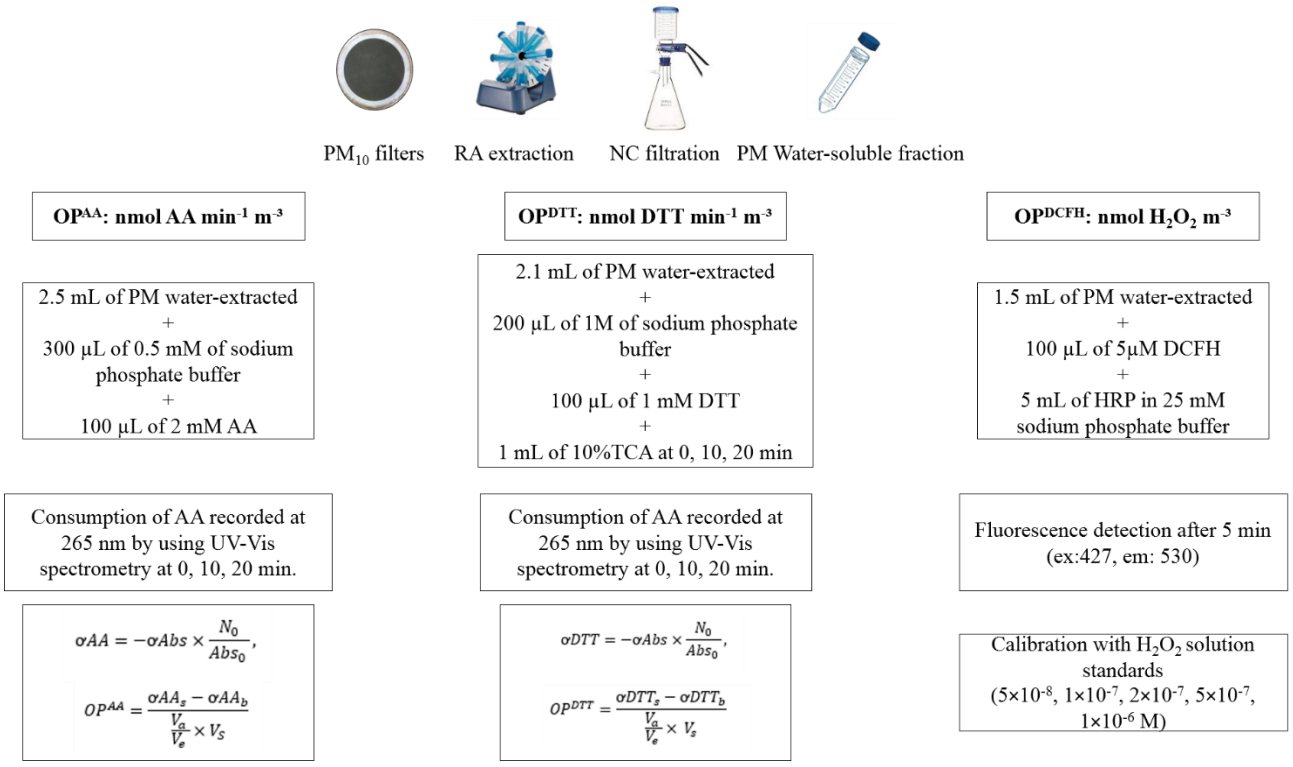

Figure 1. Schematic diagram of the PM_{10} samples preparation and oxidative potential experimental procedures for the OP^{AA}, OP^{DTT} and OP^{DCFH} assays performed on the water-soluble fraction of PM_{10} sample.

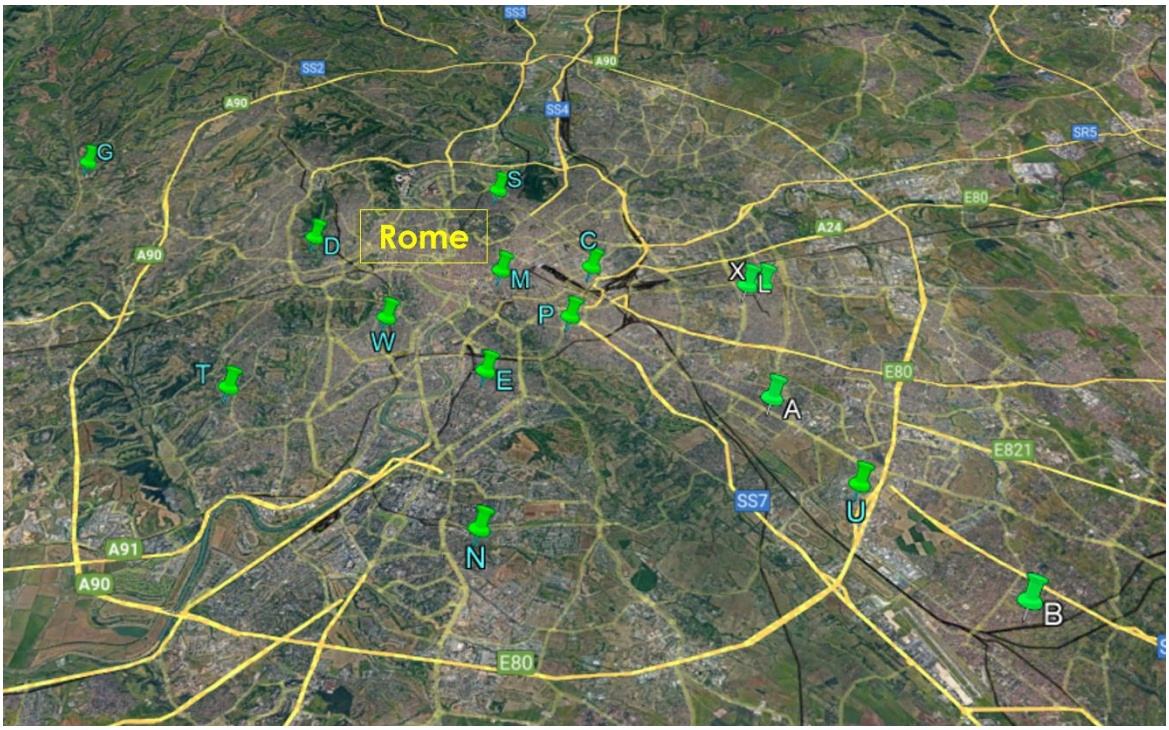

Figure 2. Map of the sampling sites (Google Earth).

Sites	Geographical coordinates	Number of inhabitants	Floor	Distance from the roads (m)	Use of candles/ incense	Air conditioner	Type of stove for cooking	Vacuum cleaner with HEPA filter	Smokers	Biomass domestic heating systems
A	41°51'15.39"N 12°33'47.53"E	3	3	300	No	Yes	Gas	No	/	No
B	41°48'17.35"N 12°36'55.31"E	2	2	300	No	Yes	Gas	No	2	Yes
C	41°53'42.86"N 12°30'56.14"E	2	T	200	Yes	Yes	Induction	Yes	2	No
D	41°54'19.46"N 12°25'52.47"E	3	T	600	No	Yes	Gas	No	/	No
E	41°51'45.31"N 12°29'10.16"E	2	3	200	No	Yes	Gas	No	/	No
G	41°56'3.63"N 12°21'6.79"E	3	2	600	No	No	Gas	No	/	Yes
L	41°53'18.71"N 12°33'39.31"E	2	2	20	No	No	Gas	No	2	No
M	41°53'39.08"N 12°29'19.45"E	3	1	100	No	No	Gas	No	1 (mainly outside)	No
N	41°49'18.01"N 12°29'13.72"E	2	3	100	No	Yes	Gas	No	/	No
P	41°52'44.30"N 12°30'33.34"E	3	4	20	No	Yes	Gas	No	/	No
S	41°55'23.50"N 12°29'10.77"E	2	1	30	No	No	Gas	No	/	No
T	41°51'27.42"N	3	4	200	No	No	Gas	No	/	No

	12°25'1.25"E									
U	41°49'55.12"N 12°34'55.11"E	1	3	400	No	No	Gas	No	/	No
W	41°52'42.90"N 12°27'24.58"E	3	2	200	No	Yes	Gas	No	/	No
X	41°53'19.34"N 12°33'55.77"E	2	2	10	No	Yes	Gas	Yes	2 (mainly outside)	No

Table 1. Geographical coordinates of the 15 selected sites (A, B, C, D, E, G, L, M, N, P, S, T, U, W, X) and specific characteristics of the sampling sites.

3. Results and Discussion

Figure 3 shows the comparison between indoor and outdoor (I and O, respectively) OP measurements of the three assays expressed as average value of all the monitoring periods for each sampling site. Indoor OP values are generally lower than outdoor ones, except in some cases where there are known indoor PM emission sources. In detail, the indoor sources that seem to contribute more to OP^{DCFH} and OP^{DTT} are cigarette smoke, and biomass heating. This is particularly evident in site B, in which biomass domestic heating system is present, and in C, and L sites, where the occupants smoke inside. In fact, OP^{DCFH} and OP^{DTT} are known to be sensitive to fine particles generated from combustion processes (Rao et al., 2020; Simonetti et al., 2018; Conte et al., 2017). G site differed from what was found, despite the presence of biomass heating system which, however, is rarely used.

With regards to OP^{AA}, A is the only site in which indoor value is higher than outdoor one. This is probably due to the use of the vacuum cleaner and, in addition, without HEPA filter. Several studies reported significant particles emission and resuspension caused by the vacuum motor operation, by the direct contact of vacuum cleaner components with flooring and, also, by the action of walking during vacuuming (Vicente et al., 2020; Corsi et al., 2013; Szymczak et al., 2007). Indeed, OP^{AA} is affected by the presence of particles from vacuum cleaner, that are mainly in the coarse fraction and rich in Cu and Fe (Manigrasso et al., 2019; Hassan, 2012), according with findings from previous studies (Massimi et al., 2020b; Rao et al., 2020; Bates et al., 2019; Simonetti et al., 2018).

Outdoor OP values don't show significant variability among the sites, especially in the case of OP^{DTT}. However, OP^{AA} recorded values reflect the proximities of the sites to the roads and, therefore, the influence of vehicular traffic emission to which the assay responds (Massimi et al., 2020b). In detail, C, E, M, P and X are the sites closer to the roads, in which the highest values of OP^{AA} are recorded.

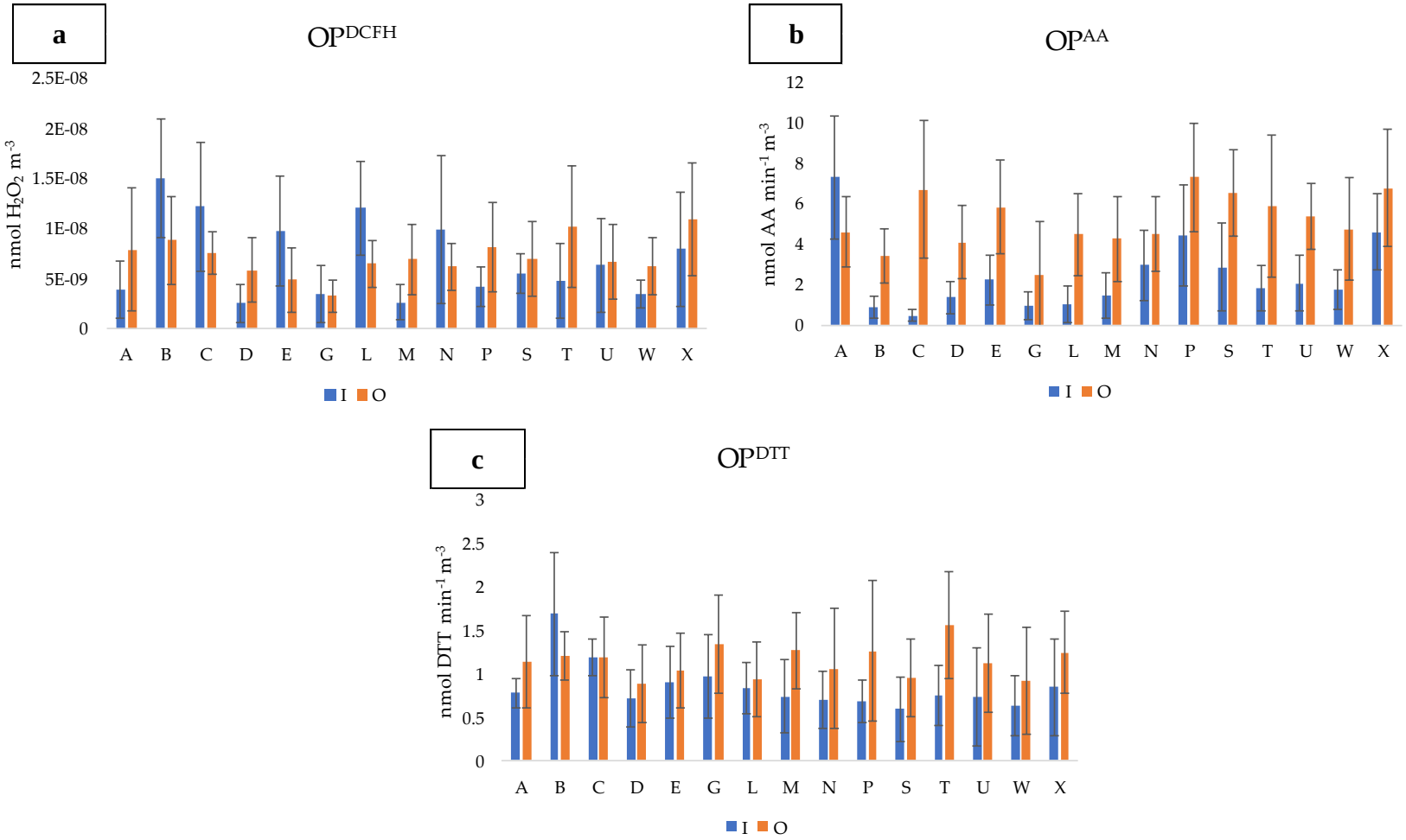

Figure 3. Mean and standard deviation of the oxidative potential values (OP^{DCFH}, panel a; OP^{AA}, panel b; OP^{DTT}, panel c) determined during the monitoring periods at the 15 sampling sites.

4. Conclusions

The presented obtained results arose from a long duration sampling and permitted to explore the differences between OP indoor and outdoor, and to identify the most important indoor contributions to OP. In detail, the predominant emission sources on OP^{DCFH} and OP^{DTT} were biomass domestic heating systems and cigarette smoke, while OP^{AA} indoor was influenced by domestic activity, such as the use of vacuum cleaning. These results will have to be confirmed with the chemical analysis, which are currently in progress, and will allow to highlight correlations between OP values and the intensity and contribution of the different PM sources that are identified and traced with the chemical parameters.

Redox properties of indoor PM deserves further investigation in the future since the exposure to atmospheric particles occurs mainly indoors.

References

Adgate, J. L., Ramachandran, G., Pratt, G. C., Waller, L. A., & Sexton, K. (2002). Spatial and temporal variability in outdoor, indoor, and personal PM2. 5 exposure. Atmospheric Environment, 36(20), 3255-3265. https://doi.org/10.1016/S1352-2310(02)00326-6

Ali, M. U., Liu, G., Yousaf, B., Ullah, H., Abbas, Q., Munir, M. A. M. (2019). A systematic review on global pollution status of particulate matter-associated potential toxic elements and health perspectives in urban environment. Environmental geochemistry and health, 41(3), 1131-1162. https://doi.org/10.1007/s10653-018-0203-z

Bates, J. T., Fang, T., Verma, V., Zeng, L., Weber, R. J., Tolbert, P. E., Abrams, J. Y., Sarnat, S. E., Klein, M., Mulholland, J. A., Russell, A. G., 2019. Review of acellular assays of ambient particulate matter oxidative potential: Methods and relationships with composition, sources, and health effects. Environmental Science & Technology, 53(8), 4003-4019.

Borm, P. J., Kelly, F., Künzli, N., Schins, R. P., Donaldson, K. (2007). Oxidant generation by particulate matter: from biologically effective dose to a promising, novel metric. Occupational and environmental medicine, 64(2), 73-74. http://dx.doi.org/10.1136/oem.2006.029090

Brook, R. D., Rajagopalan, S., Pope III, C. A., Brook, J. R., Bhatnagar, A., Diez-Roux, A. V., et al., Kaufman, J. D. (2010). Particulate matter air pollution and cardiovascular disease: an update to the scientific statement from the American Heart Association. Circulation, 121(21), 2331-2378. https://doi.org/10.1161/CIR.0b013e3181dbece1

Burnett, R., Chen, H., Szyszkowicz, M., Fann, N., Hubbell, B., Pope, C. A., et al., Spadaro, J. V. (2018). Global estimates of mortality associated with long-term exposure to outdoor fine particulate matter. Proceedings of the National Academy of Sciences, 115(38), 9592-9597. https://doi/10.1073/pnas.1803222115

Canepari, S., Astolfi, M. L., Farao, C., Maretto, M., Frasca, D., Marcoccia, M., Perrino, C., 2014. Seasonal variations in the chemical composition of particulate matter: a case study in the Po Valley. Part II:

concentration and solubility of micro-and trace-elements. Environmental Science and Pollution Research, 21(6), 4010-4022.

Canha, N., Lage, J., Galinha, C., Coentro, S., Alves, C., Almeida, S. M. (2018). Impact of biomass home heating, cooking styles, and bread toasting on the indoor air quality at Portuguese dwellings: a case study. Atmosphere, 9(6), 214. https://doi.org/10.3390/atmos9060214

Conte, E., Canepari, S., Frasca, D., Simonetti, G. (2017). Oxidative potential of selected PM components. In Multidisciplinary Digital Publishing Institute Proceedings (Vol. 1, No. 5, p. 108).

Corsi, R. L., Siegel, J. A., Chiang, C. (2008). Particle resuspension during the use of vacuum cleaners on residential carpet. Journal of Occupational and Environmental Hygiene, 5(4), 232-238.

Costa, L. G., Cole, T. B., Dao, K., Chang, Y. C., Coburn, J., & Garrick, J. M. (2020). Effects of air pollution on the nervous system and its possible role in neurodevelopmental and neurodegenerative disorders. Pharmacology & therapeutics, 210, 107523. https://doi.org/10.1016/j.pharmthera.2020.107523

Crobeddu, B., Baudrimont, I., Deweirdt, J., Sciare, J., Badel, A., Camproux, A. C., Bui, L. C., Baeza-Squiban, A. (2020). Lung Antioxidant Depletion: A Predictive Indicator of Cellular Stress Induced by Ambient Fine Particles. Environmental science & technology, 54(4), 2360-2369. https://dx.doi.org/10.1021/acs.est.9b05990

Fang, T., Verma, V., Bates, J. T., Abrams, J., Klein, M., Strickland, M. J., Sarnat, S. E., Chang, H. H., Mullholland, J. A., Tolbert, P. E., Russel, A. G., Weber, R. J. (2016). Oxidative potential of ambient water-soluble PM 2.5 in the southeastern United States: contrasts in sources and health associations between ascorbic acid (AA) and dithiothreitol (DTT) assays. Atmospheric Chemistry and Physics, 16(6), 3865-3879. https://doi.org/10.5194/acp-16-3865-2016

Fuller, S. J., Wragg, F. P. H., Nutter, J., Kalberer, M., 2014. Comparison of on-line and off-line methods to quantify reactive oxygen species (ROS) in atmospheric aerosols. Atmospheric Environment, 92, 97-103. https://doi.org/10.1016/j.atmosenv.2014.04.006

Frezzini, M. A., Castellani, F., De Francesco, N., Ristorini, M., Canepari, S., 2019. Application of DPPH Assay for Assessment of Particulate Matter Reducing Properties. Atmosphere, 10(12), 816. https://doi.org/10.3390/atmos10120816

Gao, D., Ripley, S., Weichenthal, S., Pollitt, K. J. G. (2020). Ambient particulate matter oxidative potential: Chemical determinants, associated health effects, and strategies for risk management. Free Radical Biology and Medicine. https://doi.org/10.1016/j.freeradbiomed.2020.04.028

González-Martín, J., Kraakman, N., Pérez, C., Lebrero, R., Muñoz, R. (2020). A state-of-the-art review on indoor air pollution and strategies for indoor air pollution control. Chemosphere, 128376. https://doi.org/10.1016/j.chemosphere.2020.128376

Halliwell, B., Whiteman, M. (2004). Measuring reactive species and oxidative damage in vivo and in cell culture: how should you do it and what do the results mean?. British journal of pharmacology, 142(2), 231-255. https://doi.org/10.1038/sj.bjp.0705776

Hassan, S. K. M. (2012). Metal concentrations and distribution in the household, stairs and entryway dust of some Egyptian homes. Atmospheric Environment, 54, 207-215.

Huang, W., Baumgartner, J., Zhang, Y., Wang, Y., Schauer, J. J. (2015). Source apportionment of air pollution exposures of rural Chinese women cooking with biomass fuels. Atmospheric Environment, 104, 79-87. https://doi.org/10.1016/j.atmosenv.2014.12.066

Huang, W., Zhang, Y., Zhang, Y., Fang, D., & Schauer, J. J. (2016). Optimization of the measurement of particle-bound reactive oxygen species with 2′, 7′-dichlorofluorescin (DCFH). Water, Air, & Soil Pollution, 227(5), 164. https://doi.org/10.1007/s11270-016-2860-9

Khurshid, S. S., Emmerich, S., Persily, A. (2019). Oxidative potential of particles at a research house: Influencing factors and comparison with outdoor particles. Building and Environment, 163, 106275. https://doi.org/10.1016/j.buildenv.2019.106275

Lee, S., Kim, M. J., Kim, J. T., Yoo, C. K. (2015). In search for modeling predictive control of indoor air quality and ventilation energy demand in subway station. Energy and buildings, 98, 56-65. https://doi.org/10.1016/j.enbuild.2014.10.082

Li, R., Kou, X., Geng, H., Xie, J., Yang, Z., Zhang, Y., Cai, Z., Dong, C. (2015). Effect of ambient PM2. 5 on lung mitochondrial damage and fusion/fission gene expression in rats. Chemical research in toxicology, 28(3), 408-418. https://doi.org/10.1021/tx5003723

Lowther, S. D., Jones, K. C., Wang, X., Whyatt, J. D., Wild, O., Booker, D. (2019). Particulate matter measurement indoors: A review of metrics, sensors, needs, and applications. Environmental science & technology, 53(20), 11644-11656. https://doi.org/10.1021/acs.est.9b03425

Manigrasso, M., Protano, C., Astolfi, M. L., Massimi, L., Avino, P., Vitali, M., Canepari, S. (2019). Evidences of copper nanoparticle exposure in indoor environments: Long-term assessment, high-resolution field emission scanning electron microscopy evaluation, in silico respiratory dosimetry study and possible health implications. Science of the Total Environment, 653, 1192-1203.

Massimi, L., Ristorini, M., Eusebio, M., Florendo, D., Adeyemo, A., Brugnoli, D., Canepari, S., 2017. Monitoring and evaluation of Terni (Central Italy) air quality through spatially resolved analyses. Atmosphere, 8(10), 200. https://doi.org/10.3390/atmos8100200

Massimi, L., Simonetti, G., Buiarelli, F., Di Filippo, P., Pomata, D., Riccardi, C., Ristorini, M., Astolfi, M.L., Canepari, S., 2020a. Spatial distribution of levoglucosan and alternative biomass burning tracers in

atmospheric aerosols, in an urban and industrial hot-spot of Central Italy. Atmospheric Research, 104904. https://doi.org/10.1016/j.atmosres.2020.104904

Massimi, L., Ristorini, M., Simonetti, G., Frezzini, M. A., Astolfi, M. L., Canepari, S., 2020b. Spatial Mapping and Size Distribution of Oxidative Potential of Particulate Matter Released by Spatially Disaggregated Sources. Environmental Pollution, 115271. https://doi.org/10.1016/j.envpol.2020.115271

Morawska, L., Afshari, A., Bae, G. N., Buonanno, G., Chao, C. Y. H., Hänninen, O., Hofmann, W., Isaxon, C., Jayaratne, E. R., Pasanen, P., Salthammer, T., Waring, M., Wierzbicka, A. (2013). Indoor aerosols: from personal exposure to risk assessment. Indoor air, 23(6), 462-487. https://doi.org/10.1111/ina.12044

Niu, X., Jones, T., BéruBé, K., Chuang, H. C., Sun, J., Ho, K. F. (2021). The oxidative capacity of indoor source combustion derived particulate matter and resulting respiratory toxicity. Science of The Total Environment, 767, 144391. https://doi.org/10.1016/j.scitotenv.2020.144391

Øvrevik, J. Oxidative potential versus biological effects: A review on the relevance of cell-free/abiotic assays as predictors of toxicity from airborne particulate matter. Int. J. Mol. Sci. 2019, 20, 4772, https://doi.org/10.3390/ijms20194772.

Pénard-Morand, C., Raherison, C., Charpin, D., Kopferschmitt, C., Lavaud, F., Caillaud, D., Annesi-Maesano, I. (2010). Long-term exposure to close-proximity air pollution and asthma and allergies in urban children. European Respiratory Journal, 36(1), 33-40.

Perrino, C.; Tofful, L.; Dalla Torre, S.; Sargolini, T.; Canepari, S. Biomass burning contribution to PM10 concentration in Rome (Italy): Seasonal, daily and two-hourly variations. Chemosphere 2019, 222, 839-848. https://doi.org/10.1016/j.chemosphere.2019.02.019

Perrino, C., Catrambone, M., Dalla Torre, S., Rantica, E., Sargolini, T., Canepari, S., 2014. Seasonal variations in the chemical composition of particulate matter: a case study in the Po Valley. Part I: macro-components and mass closure. Environmental Science and Pollution Research, 21(6), 3999-4009.

Perrino, C., Tofful, L., Canepari, S., 2016. Chemical characterization of indoor and outdoor fine particulate matter in an occupied apartment in Rome, Italy. Indoor Air, 26(4), 558-570. https://doi.org/10.1111/ina.12235

Pietrogrande, M. C., Bacco, D., Trentini, A., & Russo, M. (2021). Effect of filter extraction solvents on the measurement of the oxidative potential of airborne PM 2.5. Environmental Science and Pollution Research, 1-13. https://doi.org/10.1007/s11356-021-12604-7

Pu, X., Wang, L., Chen, L., Pan, J., Tang, L., Wen, J., Qiu, H. (2021). Differential effects of size-specific particulate matter on lower respiratory infections in children: A multi-city time-series analysis in Sichuan, China. Environmental Research, 193, 110581. https://doi.org/10.1016/j.envres.2020.110581

Ramli, N. A., Yusof, N. F. F. M., Shith, S., Suroto, A. (2020). Chemical and biological compositions associated with ambient respirable particulate matter: a review. Water, Air, & Soil Pollution, 231(3), 1-14. https://doi.org/10.1007/s11270-020-04490-5

Rao, L., Zhang, L., Wang, X., Xie, T., Zhou, S., Lu, S., Xinchun, L., Lu, H., Xiao, K., Wang, W., Wang, Q. (2020). Oxidative Potential Induced by Ambient Particulate Matters with Acellular Assays: A Review. Processes, 8(11), 1410. https://doi.org/10.3390/pr8111410

Secrest, M. H., Schauer, J. J., Carter, E. M., Lai, A. M., Wang, Y., Shan, M., Yang, X., Zhang, Y., Baumgartner, J. (2016). The oxidative potential of PM2. 5 exposures from indoor and outdoor sources in rural China. Science of the Total Environment, 571, 1477-1489. http://dx.doi.org/10.1016/j.scitotenv.2016.06.231

Simonetti, G., Conte, E., Perrino, C., Canepari, S., 2018. Oxidative potential of size-segregated PM in an urban and an industrial area of Italy. Atmospheric Environment, 187, 292-300. https://doi.org/10.1016/j.atmosenv.2018.05.051

Shaddick, G., Thomas, M. L., Mudu, P., Ruggeri, G., Gumy, S. (2020). Half the world's population are exposed to increasing air pollution. NPJ Climate and Atmospheric Science, 3(1), 1-5.

Szymczak, W., Menzel, N., & Keck, L. (2007). Emission of ultrafine copper particles by universal motors controlled by phase angle modulation. Journal of aerosol science, 38(5), 520-531.

Venkatachari, P., Hopke, P. K., Grover, B. D., Eatough, D. J., 2005. Measurement of particle-bound reactive oxygen species in rubidoux aerosols. Journal of Atmospheric Chemistry, 50, 49–58. http://dx.doi.org/10.1007/s10874-005-5013-3

Venkatachari, P., Hopke, P. K., Brune, W. H., Ren, X., Lesher, R., Mao, J., Mitchell, M., 2007. Characterization of wintertime reactive oxygen species concentrations in Flushing, New York. Aerosol Science and Technology, 41, 97–111. https://doi.org/10.1080/02786820601116004

Vicente, E. D., Vicente, A. M., Evtyugina, M., Calvo, A. I., Oduber, F., Alegre, C. B., Castro, A., Fraile, R., Nunes, T., Lucarelli, F., Calzolai, G., Nava, S., Alves, C. A. (2020). Impact of vacuum cleaning on indoor air quality. Building and Environment, 180, 107059.

WHO, 2018. Air Pollution. WHO Global Ambient Air Quality Database (update 2018). Available at: http://www.who.int/airpollution/data/cities/en/ (last accessed 06 June 2018).

Zhan, Y., Johnson, K., Norris, C., Shafer, M. M., Bergin, M. H., Zhang, Y., Zhang, J., Schauer, J. J. (2018). The influence of air cleaners on indoor particulate matter components and oxidative potential in residential households in Beijing. Science of the Total Environment, 626, 507-518. https://doi.org/10.1016/j.scitotenv.2018.01.024

Zhang, L., Xu, H., Fang, B., Wang, H., Yang, Z., Yang, W., Hao, Y., Wang, X., Wang, Q., Wang, M. (2020). Source Identification and Health Risk Assessment of Polycyclic Aromatic Hydrocarbon-Enriched PM2. 5 in Tangshan, China. Environmental toxicology and chemistry, 39(2), 458-467. https://doi.org/10.1002/etc.4618

Zhang, L., Yang, Z., Liu, J., Zeng, H., Fang, B., Xu, H., & Wang, Q. (2021). Indoor/outdoor relationships, signatures, sources, and carcinogenic risk assessment of polycyclic aromatic hydrocarbons-enriched PM 2.5 in an emerging port of northern China. Environmental Geochemistry and Health, 1-15. https://doi.org/10.1007/s10653-021-00819-z

Zhang, N., Han, B., He, F., Xu, J., Zhao, R., Zhang, Y., & Bai, Z. (2017). Chemical characteristic of PM2. 5 emission and inhalational carcinogenic risk of domestic Chinese cooking. Environmental pollution, 227, 24-30. https://doi.org/10.1016/j.envpol.2017.04.033

Zhang, Y., West, J. J., Mathur, R., Xing, J., Hogrefe, C., Roselle, S. J., Bash, J. O., Pleim, J. E., Gan, C., Wong, D. C. (2018). Long-term trends in the ambient PM 2.5-and O 3-related mortality burdens in the United States under emission reductions from 1990 to 2010. Atmospheric chemistry and physics, 18(20), 15003-15016. https://doi.org/10.5194/acp-18-15003-2018

7. (C) Evaluation of PM redox properties and new reports towards standardized OP measurements

Several acellular methods, defined as oxidative potential (OP) assays, have been developed to assess the particulate matter (PM) oxidative capacity and they are considered as predictors of the ability of dust of generating oxidative stress in living organisms. OP is frequently proposed as a more biologically appropriate metric for addressing air quality and human exposure than PM mass concentration. Multiple acellular tests, based on the offline analyses of PM field filters, are available for quantifying particles' OP. Among these, the most generally performed are the 2',7'-dichlorofluorescein (OP^{DCFH}), the ascorbic acid (OP^{AA}) and the dithiothreitol (OP^{DTT}) assays. All the acellular tests are easy to reproduce in laboratories, they require fewer resources than cellular ones, and give quicker readouts of OP measurements. However, there are still fundamental unresolved and debated issues regarding the influence of assay's design and the tests' operative condition on OP obtained results. An important point is related to the stability of the species: short-life oxidant species can react and redox equilibria among PM native species could occur during both the sample storage and the extraction phase.

In this regard, it is possible that, within the conditions that influence OP results, there is also the reaction and/or competition between oxidant and reducing species naturally occurring in PM. Some studies proved the presence of species with likely reducing characteristics (Menetrez et al, 2009; Nemmar et al, 2013). Since the heterogeneous PM composition, is very difficult to identify the exact chemical constituents and, thus, the nature of reducing species is still unknown. However, along with oxidizing species, experimental OP values suggest the possible presence of reducing species in PM and drives the need to deepen knowledge on redox properties of PM. While the use of acellular methods for the assessment of the OP values has been receiving great scientific attention in recent years, there is still a literature gap about acellular assays for identifying reducing species in particulate matter. One of the antioxidant capacity assays is based on the use of the stable free radical DPPH (2,2-Diphenyl-1-picrylhydrazyl; Figure 6). The DPPH assay is a commonly used spectrophotometric method to estimate antioxidant activity of several matrices, such as food and plants (Kedare and Singh, 2011; Hara et al., 2018) by measuring the decrease of absorbance over time. The assay is known to be sensitive towards some classes of reducing species such as phenolic and polyphenolic compounds (Sahu et al., 2013). 2,2-Diphenyl-1-picrylhydrazyl is a stable free radical by virtue of the delocalization of the spare electron over the molecule (Chedea and Pop, 2019), and it accepts electrons or hydrogen radicals from donor compounds (Sridhar and Charles, 2018). DPPH shows a strong absorption band at 517 nm due to its odd electron and solution appears a deep violet color. The resulting decolorization turning yellow is proportional to the number of electrons taken up (Kedare and Singh, 2011; Figure 5). This assay estimates the overall antioxidant capacity of the samples and offers the advantages of being simple and rapid and easily applicable to intensive PM monitoring campaigns.

In this PhD research, the DPPH radical scavenging assay was thus adapted and preliminarily applied to PM with the aim of verifying its possible use as an acellular method for estimating the presence of reducing species, thus for expressing PM reducing potential (RP^{DPPH}).

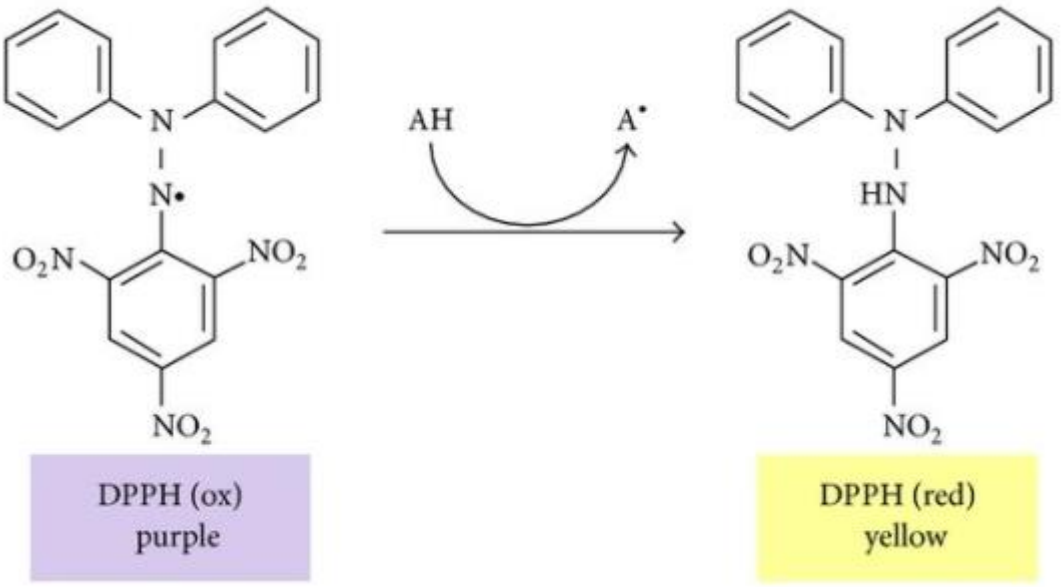

Figure 6. The reaction of DPPH free radical with antioxidant where AH is donor molecule and A is free radical produced (Teixeira et al., 2013).

In order to deepen the critical issues surrounding particles OP this research work was aimed at investigating the stability of PM redox components by analyzing the variability in OP assays (OP^{DCFH}, OP^{AA}, OP^{DTT}) responses depending on the operative conditions by which tests are performed. In detail, the influence of extraction method, filter-storage, as well as time delay between PM sampling and analysis, on OP measurements, was explored. According to Dick et al. (2000) sonication and vortexing during extraction may induce physical changes and alter the biological properties of PM. Therefore, other researchers suggested alternative methods to sonication for filters extraction (Khurshid et al., 2014; Miljevic et al., 2014).

The delay between filter sampling and OP analyses seems to play a crucial role in misestimating particles OP representing additional potential factors altering OP measurements. These include the possible decomposition and/or chemical transformation of the highly reactive components, prior to analysis (Fuller et al., 2014; Campbell et al., 2019) and the aging of the particles on membrane filter surfaces can cause an underestimation of collected reactive species (Hedayat et al., 2015).

Another additional critical issue is related to the choice of membrane filters used for PM sampling. For example, sampling artifacts have been widely related to the use of different membrane filters, including loss of labile species such as ammonium nitrate and organics, adsorption of vapor phase organics, and reactions between particles and incoming gases. (Turpin et al. 1994; Cheng and Tsai 1997; Eatough et al. 2003; Tsapakis and Stephanou 2003; Daher et al., 2011).

Furthermore, the contribution of water-insoluble PM components to aerosol OP has never been clarified so far. The assessment of assess their role in particle oxidative activity still need explanations.

The effects of operative conditions on responses of OP^{DCFH}, OP^{AA} and OP^{DTT} were thus examined. The efficiency and repeatability of three different PM extraction methods (rotating agitator, ultrasonic bath and vortex), the influence of storage conditions and duration of PM collected filters and, finally, the impact of the type of the filter used for PM sampling on OP results were explored. Two monitoring campaigns were carried out by placing co-located PM_{10} samplers working in parallel, thus obtaining multiple equal samples per day, to compare different procedures simultaneously applied on identical samples. In total, over 250 PM_{10} field filters were analyzed to compare the results obtained from the different operative procedures simultaneously applied on equivalent samples. Lastly, to thoroughly assess the particles' role in the PM redox activity, the contribution of water-insoluble PM components to OP was investigated, as well as the PM reducing properties through the 2,2-diphenyl-1-picrylhydrazyl assay (RP^{DPPH}).

With the aim of investigating exposure to PM in real-word conditions, a non-invasive, simple, and efficient method was applied to PM_{10} field filters for the detachment of intact particles. The procedure involves the use of an electrical toothbrush which allows obtaining a PM water-suspension used to perform OP assays and to evaluate the real contribution of water-insoluble particles to PM redox properties. Preliminary results are shown in this topic session.

The following reported works provided new insights on the driving forces of OP measurements, thus giving a very valuable contribution to the standardization of experimental procedures.

7.1 (C1) Application of DPPH Assay for Assessment of Particulate Matter Reducing Properties

Atmosphere (2019), 10 (12), 816, doi: 10.3390/atmos10120816

Maria Agostina Frezzini [1,*], Federica Castellani [1], Nayma De Francesco [1], Martina Ristorini [2,3] and Silvia Canepari [1]

[1] Department of Chemistry, Sapienza University of Rome, Piazzale Aldo Moro, 5, 00185 Rome, Italy; federica.castellani@uniroma1.it (F.C.); defrancesco.nayma@gmail.com (N.D.F.); silvia.canepari@uniroma1.it (S.C.)

[2] Research Institute on Terrestrial Ecosystems, National Research Council, Via G. Marconi, 2, 05010 Porano, Italy; m.ristorini@studenti.unimol.it

[3] Department of Biosciences and Territory, University of Molise, Via Hertz, 86090 Pesche, Italy

* Corresponding author

Keywords: oxidative potential; PM redox properties; 2,2-diphenyl-1-picrylhydrazyl antioxidant assay; air quality monitoring

Abstract

Different acellular assays were developed to measure particulate matter's (PM) oxidative potential (OP), a metric used to predict the ability of PM in generating oxidative stress in living organisms. However, there are still fundamental open issues regarding the complex redox equilibria among the involved species which could include reducing compounds. The aim of this study was the pilot application of the 2,2-diphenyl-1-picrylhydrazyl (DPPH) assay to PM in order to evaluate the presence of reducing species. The assay, commonly applied to biological matrices, was adapted to PM and showed good analytical performances. It allowed the analysis of conventional 24 h airborne PM samples with suitable sensitivity and good repeatability of the measurements. The assay was applied to seven samples representing possible PM contributes (certified urban dust NIST1648a; brake dust; Saharan dust; coke dust; calcitic soil dust; incinerator dust; and diesel particulate matter certified material NIST1650b) and to $PM_{2.5}$ field filters. The same samples were also analyzed for elements. Preliminary results indicated that the assay gave a linear response and that detectable amounts of reducing species were present in PM samples. The combined application of DPPH and conventional OP assays could then permit, in the future, to gain more knowledge about the reaction and/or competition between oxidative and reducing processes.

1. Introduction

Particulate matter (PM) pollution is a serious global problem, especially in urban and industrialized areas [1], threatening both human and environmental health [2]. A growing number of scientific studies have demonstrated links between exposure to ambient PM and adverse health outcomes in human, especially related to cardio-pulmonary diseases [3] and neurological disorders [4]. Over the last few decades, oxidative stress

has been identified as one of the key mechanisms by which PM exerts its negative impacts on cellular systems and, thus, on living organisms [5,6]. Oxidative stress is due to the imbalance between the generation of reactive oxygen species (ROS) alongside reactive nitrogen species (RNS) and the antioxidant defenses [3]. Particulate matter's capacity to elicit damaging oxidative reactions and inflammations is defined as oxidative potential (OP) [7]. Measurements of particles' OP are considered a promising and integrative method for assessing health impacts induced by PM [8]. In fact, it is increasingly recognized that this PM property is more closely associated with adverse health impacts than ordinarily used PM mass concentrations [9]. In this context, many acellular assays were developed to measure oxidative potential in order to gain a proxy of this PM capability [10]. There is still no agreement regarding the most representative assay to determine oxidative potential [11], but most commonly used acellular tests include the ascorbic acid (AA) [12] and dithiothreitol (DTT) [13] assays which consist of mimicking the consumption of a physiological and a surrogate antioxidant, respectively, and 2′,7′-dichlorofluorescin (DCFH) by which particle-bound ROS are determined [14]. Oxidative potential acellular assays present several advantages such as ease of application, a clear and wide description in the literature that make them replicable, and applicability to a high number of samples during monitoring campaigns by generating large data sets with the aim of studying different redox components for detailed investigation [11,15,16]. However, several studies showed that each assay is sensitive to different pathways of ROS/RNS formation [17], and results are also responsive to different ROS/RNS generated by PM components and sources, meaning that each OP assay is seemingly linked to different health endpoints [15]. Therefore, the combined application of different acellular methods on the same samples is strongly suggested. Although some recent studies were focused on the in vivo evaluation of PM's negative impacts on living organisms [18–20], knowledge about the relationships between OP and PM's toxicological effects still presents some important gaps [6,20,21].

Other still unresolved issues are related to the assay's design and the influence of the operative conditions by which OP tests are performed. In fact, over recent years, many researchers underlined how test conditions could influence collected data. For example, recent studies analyzed the effect derived by the choices of extraction solvent (methanol and/or water) and sampling filter type (quartz or Teflon filter) on different OP assays [17,22]. Other researchers studied the impact of sonication-derived free radicals on OP results and suggested alternative extraction methods such as vortexing, magnetic stirrer or orbital shaking to avoid ultrasound-induced radicals [23,24]. The influence of filter-storage conditions also merits further investigation. Moreover, OP assays are commonly performed on PM water-soluble fractions, and another still debated issue concerns the lack of an appropriate standard protocol for measuring the water-insoluble oxidative potential [15]. An additional important point is related to the stability of the species: short-life oxidant species can react and redox equilibria, and among PM native species, this could occur during the sample storage and extraction phase. In this regard, it is possible that, within the conditions that influence OP results, there is also the reaction and/or competition between oxidant and reducing species naturally occurring in PM. In fact, PM is a heterogeneous and complex mixture of particles [25] that varies in composition and it is very difficult to identify the exact chemical constituents [26]. Some studies proved the presence of species with likely

antioxidant and reducing characteristics such as phenols from wood burning [27], phenolic compounds from different sources [28], pollen [29], airborne bioaerosols that are biological in origin [30], and biological and vegetable components [31].

This research was aimed at clarifying the latter aspect by considering the application of an acellular procedure to evaluate the presence of reducing species in PM samples. The 2,2-diphenyl-1-picrylhydrazyl (DPPH) assay is a rapid, simple, and widely used method to evaluate the antioxidant potential of a compound or an extract [32], and it is commonly used for vegetable juice [33], olive oils, and wines [34]. The assay is known to be sensitive towards some classes of reducing species such as phenolic and polyphenolic compounds [35]. 2,2-Diphenyl-1-picrylhydrazyl is a stable free radical by virtue of the delocalization of the spare electron over the molecule [36], and it accepts electrons or hydrogen radicals from donor compounds [37].

The assay is based on the quantitative measurement of the scavenging capacity of antioxidants towards DPPH free radicals [32] by the decrease in absorbance [38]. This test provides information on the antioxidants' capacity to donate hydrogen atoms or electrons [37,39]. To date, no DPPH standard experimental procedures exist; various researchers have used widely different protocols [40,41] based on their treated samples which differ in DPPH concentration, reaction time, and reaction solvent. To our knowledge, this assay has never been applied to PM before.

The aim of this work was to evaluate the applicability of the DPPH assay to PM for measuring reducing potential (RP) due to the presence of antioxidant species which could, in the future, integrate the information about redox properties of PM obtained by OP assays. In this work, the DPPH assay was applied to seven types of widespread components of PM produced by specific emission sources and characterized by very different chemical compositions [19,20] (i.e., urban dust certified for its elemental content, UD; brake dust, BD; Saharan dust, SD; coke dust C; calcitic soil dust, CSD; incinerator dust, ID; and certified diesel particulate matter, D). Moreover, the DPPH assay was applied to $PM_{2.5}$ field samples collected during a short monitoring campaign.

2. Materials and Methods

2.1 Reagents and DPPH Assay

The DPPH solution was prepared according to the procedure described by Chen et al. [42] with slight modifications. The stock solution, prepared daily, was used at a 0.1 mM final concentration: 2 mg of DPPH reagent (Sigma–Aldrich, USA) were weighed (Analytical Balance Gibertini Elettronica E505, sensitivity 0.01 mg) and suspended in 50 mL of ethanol (EtOH) 96%. The mixture was vigorously shaken for 30 min under magnetic stirrer agitation (ARE Heating Magnetic Stirrer; Velp Scientifica, Usmate, Italy) and kept at room temperature in the dark. Experimental data were acquired on a spectrophotometer (Varian Cary 50 Bio UV-Vis; Varian Inc., Palo Alto, CA, USA), set at 517 nm under dim light, by measuring the sample absorbance decrease against the control (blank solution). The DPPH radical scavenging effect results in decolorization and is calculated in terms of percentage reduction of DPPH according to the following equation [43]:

$$\%\ \text{DPPH Reduction} = \frac{(A_0 - A_S)}{A_0} \times 100$$

where A_0 represents the absorbance of the control and A_S is the absorbance of the samples.

The % DPPH reduction values were normalized per sampled air volume (m^3; %DPPHv) or per PM mass amount (mg; %DPPHm).

2.2 Collection and Chemical Characterization of Samples

Certified urban dust (urban particulate matter, NIST168a, Sigma–Aldrich, USA) was used as urban dust. Certified diesel particulate matter (diesel particulate matter, NIST1650b, Sigma–Aldrich, USA) was used as diesel dust. Besides the certified materials UD and D, some of the other major PM sources were considered. Brake dust, collected from the brake linings of three different cars, represents the part of road dust containing the highest concentration of heavy metals and other pollutants [44]. In the Mediterranean area, Saharan dust represents the major contribution to PM after events of long-range transport from North Africa [45]. Saharan dust was collected in Algeria, in the north of the Sahara Desert. Coke dust contains very high concentrations of organic toxic species [46] and was taken from the ground near a coal park. Calcitic soil dust, one of the major natural compounds of PM [20], was collected in rural areas around the city of Rome. Incinerator dust was sampled by a fine-mesh filter placed in a waste-to-energy plant chimney in Northern Italy. Incinerator dust is known to contain various atmospheric compounds, including organic ones [47], such as polycyclic aromatic hydrocarbons (PAHs) [48] and steroids from plant or animal materials not entirely combusted [49]. All types of PM were sieved at 50 µm and stored at −18 °C until use. More specific details about sample collection are reported by Marcoccia et al. [19] and Simonetti et al. [50]. Although the use of these types of PM is not completely representative of real atmospheric dust, it allows to compare different experimental procedures on a homogeneous sample by performing different replicates.

The dimensional distribution of UD, BD, and C was estimated by Simonetti et al. [50] using optical microscopy (Zeiss Imager M1m; Carl Zeiss Inc., Thornwood, NJ, USA). Images were then converted into black/white and automatically enumerated by NIH ImageJ software v.1.46r (National Institute of Health, Bethesda, MD, USA). Although the system did not allow to measure particles smaller than approximately 1 µm, 50% of particles had diameters lower than 10 µm in all the considered samples. This estimation was not possible for the other considered types of PM because of the low contrast of the images.

The 24 h $PM_{2.5}$ field samples were collected from 29 March to 17 April 2019 by a sequential sampler working at 2.3 m^3/h (SWAM5a Dual Channel Monitor, FAI Instruments, Fonte Nuova, Rome, Italy) on PTFE membrane filters (46.2 mm diameter, 2 µm pore size; Whatman, Maidstone, UK) near Ferrara, Italy (Cassana, coordinates: 44°51′4″ N; 11°32′56″ E). Although it was not a long monitoring sampling, it was enough for applying the experimental procedure for demonstration purposes. The $PM_{2.5}$ concentration was automatically measured by beta attenuation. At the same site, the mixing properties of the lower atmosphere were determined by an automated monitor of the natural radioactivity due to the radon progeny (PBL Mixing Monitor, FAI Instruments, Fonte Nuova, Rome, Italy).

The $PM_{2.5}$ filters were extracted by following the procedure detailed by Massimi et al. [51]. Briefly, after removal of the supporting polymethylpentene rings from each sampled filter, PTFE membrane filters were extracted in 10 mL of deionized water (produced by Arioso UP 900 Integrate Water Purification System, USA) by 30 min of rotating agitation (60 rpm; Rotator; Glas-Col, USA). After the extraction, the solutions were

filtered through a nitrocellulose filter (NC; pore size 0.45 μm; Merck Millipore Ltd., Billerica, MA, USA). The extracted solutions were split in their respective aliquots for the analyses. Then, both the NC filter and sampled PTFE filter were acid-digested in a microwave oven (Ethos Touch Control with Q20 rotor, Milestone, Italy) using 2 mL of HNO_3 (67%, Promochem, Wesel, Germany) and 1 mL of H_2O_2 (30% Suprapur, Merck Millipore Ltd., Billerica, MA, USA). Details about the digestion program are reported by Massimi et al. [51]. The PM filters were chemically analyzed by adapting an analytical procedure for the determination of micro and trace element on PM samples, optimized and validated by Canepari et al. [52,53] using inductively coupled plasma mass spectrometry (ICP-MS, Bruker 820-MS, Billerica, MA, USA). The concentrations (ng/m³) of elements (Al, As, Bi, Cd, Ce, Co, Cr, Cs, Cu, Fe, La, Li, Mg, Mn, Mo, Na, Ni, P, Pb, Rb, Sb, Sn, Sr, Ti, Tl, V, Zn, Zr) were determined in both water-soluble and mineralized residue fractions.

2.3 Oxidative and Reducing Potential Assays on Selected Types of PM

The DPPH assay was applied to the seven selected samples by following 4 different protocols to evaluate which experimental procedure better suited which samples. Four DPPH assay experimental procedures with different extraction solutions were compared in terms of limits of detection (LODs), repeatability, and efficiency. First, ethanol and water were compared as extraction solvents ($DPPH_{EtOH}$ and DPP_{H2O}, respectively). Although in the literature, ethanol is commonly used as an extraction solvent to perform the DPPH assay [42,43], water extraction was included in this study as it could permit the integration of this acellular method to the whole chemical characterization procedure on a single PM sample. Regarding water extraction, the effect of the addition of ethanol to the reaction mixture was evaluated ($DPPH_{H2O/EtOH}$), as it could increase the solubility of species involved in the DPPH reaction. Finally, the DPPH assay was directly applied to the suspension of samples without any extraction step in order to verify the possible contribution of insoluble species ($DPPH_{TOT}$).

2.3.1 DPPH Assay on EtOH Extracted Samples

First, the extraction method involved EtOH, according to Mishra et al. [54]. Five milligrams of samples, exactly weighed on analytical balance, were extracted in 5 mL of EtOH 96% by 30 min of rotating agitation (60 rpm). Extracted solutions were filtered through a PTFE syringe filter (PTFE; pore size 0.45 μm; Fulltech Instruments, Rome, Italy), and then 3 mL were mixed with 1.5 mL of DPPH 0.1 mM solution. The mixture was shaken for 30 min by rotating agitation, and then analyzed by UV-Vis spectrophotometry set at 517 nm ($DPPH_{EtOH}$).

2.3.2 DPPH Assay on H_2O Extracted Samples

Five milligrams of each sample were exactly weighed and extracted in 5 mL of deionized water by rotating agitation for 30 min. The extraction solutions were filtered through a nitrocellulose filter (NC filters), and then 2 mL were mixed with 1 mL of DPPH 0.1 mM solution. The mixture was stirred for 30 min by rotating agitation and then analyzed by UV-Vis ($DPPH_{H2O}$).

2.3.3 DPPH Assay on H_2O Extracted Samples with EtOH Addition

Five milligrams of selected types of PM were exactly weighed, suspended in 5 mL of deionized water, and extracted by rotating agitation for 30 min. After the extraction, the solutions were filtered through a nitrocellulose filter (NC filters). According to Scalzo [55], 1.5 mL of extracted samples were mixed with 2 mL of EtOH 96% and 0.5 mL of DPPH 0.1 mM stock solution for 30 min by rotating agitation and then analyzed by UV-Vis as already described ($DPPH_{H2O/EtOH}$). This procedure was also applied to different amount of the two considered certified materials, UD and D (range 2–10 mg), in order to verify the linearity of response.

2.3.4 DPPH Assay on whole Dusts Samples

The RP^{DPPH} on whole samples was directly performed on 4 mg of each type of PM, without any previous extraction step using 1.5 mL of deionized water, 2 mL of EtOH 96%, and 0.5 DPPH 0.1 mM stock solution. The mixture was shaken for 30 min by rotating agitation and filtered through PTFE syringe filter (PTFE filters) prior to UV-Vis analyses ($DPPH_{TOT}$).

Ten blank measurements were performed for each experimental procedure. Limits of detection (LODs) were estimated as three times the standard deviation. Furthermore, for each experimental procedure; three replicates of each type of PM were performed.

2.4. Oxidative and Reducing Potential Assays on $PM_{2.5}$ Filters

Since OPs are commonly evaluated in literature on water-soluble fraction [56,57], in this study, OPs and RP were performed only on water-soluble fraction of $PM_{2.5}$ filters. Ascorbic acid (AA), dithiothreitol (DTT) and 2′,7′-dichlorofluorescin (DCFH) assays were applied to proper aliquots of the extracted solution (Section 2.2.). The followed OPs procedures are detailed by Simonetti et al. [50,58]. Briefly, DTT and AA assays measure the depletion rate of chemical proxies for cellular reductants and antioxidants, respectively [16], by recording the decrease in absorbance by UV-Vis spectroscopy at 412 nm and 265 nm, respectively.

The chemical OP^{AA} protocol is very similar to the OP^{DTT} experimental procedure [15]. During the OP^{DTT} protocol, three aliquots of water-extracted samples (0.7 mL) were incubated with 0.1 mL of DTT 1 mM and 0.2 mL of potassium phosphate buffer (1 M) at 37 °C for times varying from 0 to 20 min. Then, 1 mL of trichloroacetic acid (TCA) was added to the mixture to quench DTT reactions. An aliquot (1 mL) was removed from the solution and mixed with 2 mL of tris-buffer (0.08 M, containing EDTA 4 mM) and with 5,5-dithiobis (2-nitrobenzoic acid; DTNB; 50 µL) to form 2-nitro-5-mercaptobenzoic acid (TNB) by reacting with the residual DTT which was then measured using a spectrometer.

For the AA assay, three aliquots of water-soluble sample fraction (2.5 mL) were mixed with 0.3 mL of potassium phosphate buffer (0.5 mM at pH 7.4) and 0.2 mL of ascorbic acid 2 mM, and the mixture was kept at 37 °C. The absorbance decrease was measured for 20 min by UV-Vis spectroscopy. Absorbance of the blank solution was measured and subtracted from the sample absorbance readings.

The OP^{DTT} and OP^{AA} were expressed as DTT or AA consumption rate per sampled PM volume or per mg of PM (nmol min^{-1} m^{-3}; nmol min^{-1} mg^{-1}) [58].

The DCFH, the most common probe used to quantify particle-bound ROS, is a nonfluorescent reagent that becomes fluorescent (DCF) when oxidized in presence of ROS. 125 µL of DCFH solution (5 µM) and 5 mL

of Horseradish Peroxidase (HRP) dissolved in a sodium phosphate buffer (25 mM at pH 7.4) were added to 1.5 mL of the sample soluble fraction prior to analysis to catalyze reactions [16]. The DCFH-HRP reagent was added to each sample and then analyzed through the emitted radiation at 530 nm by a fluorescence detector (Jasco FP-920; excitation wavelength: 427 nm). The OP^{DCFH} was expressed in nmol H_2O_2 per sampled volume or mass (nmol H_2O_2 m^3; nmol H_2O_2 mg^{-1}) by converting fluorescent intensity to H_2O_2 concentration using least squares regression with a H_2O_2 calibration curve to obtain the final particle-bound ROS measurement [16]. The calibration curve was obtained daily by using a standard H_2O_2 solutions at different concentrations (5×10^{-6}, 1×10^{-7}, 2×10^{-7}, 5×10^{-7}, and 1×10^{-6} M) [49].

One aliquot (1.5 mL) of the extracted solution was also used for the DPPH assay: 2 mL of EtOH 96% and 0.5 mL of DPPH 0.1 mM stock solution were added, and the mixture was shaken for 30 min by rotating agitation. Then, the absorbance of the solutions was measured at 517 nm by UV-Vis spectrophotometry and compared to blank measurements. The DPPH reduction percentage was calculated as already described.

3. Results and Discussion

3.1 DPPH Assay Application on Selected Types of PM

First, four DPPH assay experimental procedures with different extraction solutions were compared in terms of limits of detection (LODs), repeatability, and efficiency.

The LODs were in the range 2–7% of consumed DPPH; the lowest value (2%) was obtained for $DPPH_{EtOH}$ and the highest for $DPPH_{H2O}$ (7%). Our findings about ethanol extraction performances ($DPPH_{EtOH}$) agreed with previous studies reporting that DPPH assay method seems to work well on ethanol-extracted samples, without any interference with the reaction [43]. The $DPPH_{H2O}$ showed the highest LOD, and the worst repeatability can be explained considering that the dissolution of DPPH should be done in organic solvents (i.e. methanol or ethanol) [59] limiting the application of this reagent to pure aqueous systems. The simultaneous use of H_2O and EtOH as reaction media allowed better control of the reaction conditions by increasing DPPH solubility: LOD values for $DPPH_{H2O/EtOH}$ and $DPPH_{TOT}$ were 4%. These results agree with previous studies reporting that antioxidants commonly require polar solvents to be extracted, while DPPH reaction occurs quickly when organic solvents are used as extraction solvents [60]. Ethanol is an organic and polar solvent and resulted to be appropriate for performing DPPH assay [60].

With the aim to evaluate DPPH assay sensitivity and its ability to differently react towards various PM components, seven types of PM, substantially differing for their chemical composition, were used for this experimental stage. Figure 1 reports DPPH reduction (%DPPHm) for each experimental procedure and for the selected samples. All the experimental procedures gave different results among selected types of PM, underlining the expected role of chemical composition on the obtained values, which is reported in Table S1 (Supplementary Materials).

The DPPH assay values were higher when performed on whole dust samples ($DPPH_{TOT}$), compared to the other experimental procedures, especially for UD, BD, and D, confirming the significant contribution of water insoluble species to PM reducing properties [50,61]. Overall, the $DPPH_{EtOH}$ and $DPPH_{H2O}$ performances were

comparable, although $DPPH_{H2O}$ gave higher values than $DPPH_{EtOH}$ for UD; otherwise, $DPPH_{EtOH}$ exhibited higher values than $DPPH_{H2O}$ for D. This is probably due to the different solubility of organic species in water and ethanol. In fact, according to Simonetti et al. [50], UD contains relevant water-soluble organic carbon species (WSOC) that could contribute to the $DPPH_{H2O}$ results. Diesel exhaust particles (D) represent one of the major components of PM in urban areas [26] and are composed of a solid carbon spheres with a high surface area on which a variety of water insoluble organic compounds are adsorbed [62,63].

In general, apart from ID and C, the considered types of PM contain detectable amount of species that can react with DPPH. It is well known that DPPH reacts with species that can donate a hydrogen atom or an electron to free radicals [32]. Although this method had never been applied on PM, these results permit to hypothesize that DPPH acts like free radicals commonly found or formed in PM (especially ROS or other radicals) by simulating their reaction with reducing species. This kind of reaction can also occur during the OP assay's application thus consuming ROS or other radicals and leading to an underestimation of PM's oxidative potential. In fact, the reaction between oxidizing and reducing species could reasonably occur during the filter storage and/or the extraction phase; in these cases, the native particle-bound ROS could be consumed before DCFH assay application. Furthermore, it is worth noting that ascorbic acid is often used as target reducing species for the DPPH calibration curve [43]. Considering that ascorbic acid reacts with ROS/RNS (both during the application of OP^{AA} and in biological fluids [64]), it is reasonable to hypothesize that other reducing species could similarly react with ROS/RNS during OP assays application or in biological systems. The reactive species generated in presence of AA or DTT could be consumed by the mentioned competitive reaction thus lowering their measured formation rate. A more extensive application of DPPH assay could help to gain information about this important issue.

In most literature studies, OP assays are applied to a water-soluble fraction of PM samples collected on membrane filters [16,50,61,65]. Therefore, with a view to add the RP^{DPPH} assay to the detailed PM chemical characterization during monitoring campaigns, water extraction with added EtOH after extraction ($DPPH_{H2O/EtOH}$) could better operate alongside OPs and other chemical analyses.

The existence of a linear relationship between the dust amount and DPPH reduction (%) was tested for two samples, UD and D, by applying a regression model to data that showed a good fit ($R^2 > 0.97$ for both the samples weighted in the range 2–10 mg; Figure S3, Supplementary Materials).

Taking into account these considerations, the $DPPH_{H2O/EtOH}$ experimental procedure was used to perform a DPPH assay on $PM_{2.5}$ field filters. However, it is worth noting that the contribution to RP results, due to the water insoluble species, merits further investigation.

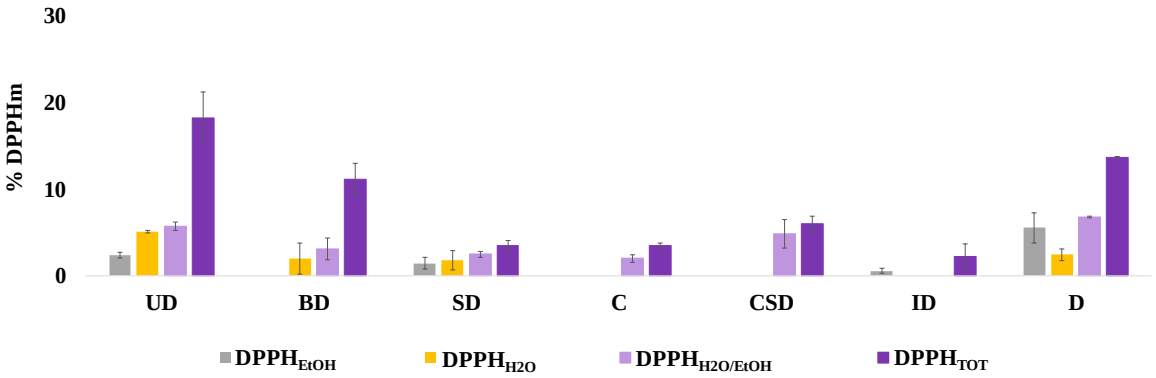

Figure 1. Reducing potential (%DPPHm) of the seven selected types of PM with the four experimental procedures obtained through a 2,2-diphenyl-1-picrylhydrazyl (DPPH) assay performed on EtOH-extracted samples ($DPPH_{EtOH}$), H_2O-extracted samples ($DPPH_{H2O}$), H_2O-extracted samples with added EtOH ($DPPH_{H2O/EtOH}$), and whole dust samples ($DPPH_{TOT}$). The mean ± SD of three replicates are reported. Values below limits of detection (LODs) are not reported. UD: certified urban dust (NIST168a); BD: brake dust; SD: Saharan dust; C: coke; CSD: calcitic soil dust; ID: incinerator dust; D: certified Diesel particulate matter (NIST1650b).

3.2 Oxidative and Reducing Potential Assays on $PM_{2.5}$ Field Filters

A short monitoring campaign was carried out in order to prove the applicability of combined RP^{DPPH} and OP (AA, DTT and DCFH) assays on a single PM sample.

The studied period was characterized by a low wind intensity, nighttime temperature included in the range 7–18 °C and daytime temperature in the range 10–23 °C (data from ARPAE Emilia-Romagna, regional agency for prevention, environment and energy). Meteorological data registered during the monitoring period are reported in the Supplementary Materials (Figure S1). The natural radioactivity, which can be considered a reliable proxy of the lower atmosphere mixing properties [66], indicated, in general, a good dilution of the atmosphere (Figure 2a). During night, an increase i the stability was observed in the first five days of the campaign (29 March to 2 April); then, nighttime stability was also observed until 9–10 April. In the following days, a good mixing was again registered from 13 April, followed by a progressive increase of nighttime stability. In agreement with the great relevance of the low atmosphere dilution properties on air pollutants' concentrations and in the absence of relevant occasional contributes, $PM_{2.5}$ concentrations followed the stability trend (Figure 2b). The $PM_{2.5}$ mass concentration varied in the range 3.8–17 μg/m^3, values that can be considered typical in the studied area during the spring season [67].

Elemental concentrations (mean and min–max range) in the soluble and residual fractions are reported in Table 1. On the whole, the concentrations during the studied period were similar or lower with respect to that previously obtained in the same area during the warm season, and much lower than the typical winter concentrations which are strongly affected by prolonged periods of intense atmospheric stability [67,68].

The RP^{DPPH} and OP assays were performed on water-soluble fractions of collected $PM_{2.5}$ field samples; the results are reported in Figure 3 and Figure S2 (Supplementary Materials), respectively.

Although sampled PM masses were low (about 0.5 mg), the obtained values were above the LOD (0.07% of consumed DPPH per m^3) in every sample, except for one. This indicates that the assay was sufficiently sensitive to be applied to most PM samples. At this early stage of knowledge, the variability of the results among samples can be evaluated by comparison with $PM_{2.5}$ mass concentration and with OP results. In Table 2, the correlation matrix of these parameters is reported. The DPPH assay showed moderate correlation with $PM_{2.5}$ mass concentration ($r > 0.84$).

As can be observed from the correlation matrices, among all the considered parameters (elements in soluble and insoluble fractions of PM filters, RP, OPs; Tables S2 and S3, Supplementary Materials), $PM_{2.5}$ concentration was, in turn, moderately correlated with most of the elements. This evidence indicates a low variability in the sampled PM chemical composition that was mainly modulated by the mixing properties of the low atmosphere, rather than by the strength of local emission sources. In this context, PM chemical composition remained almost constant, while sampled PM mass concentration varied. This consideration was further confirmed by the moderate positive correlation between OP^{DTT} and $PM_{2.5}$ ($r > 0.7$).

It was also true that the short PM sampling period (thus, the DPPH preliminary application to a small sample set and the very low variability in terms of PM chemical composition), did not permit to identify species or sources responsible for DPPH results. However, obtained results confirmed the linearity of the DPPH assay; %DPPHv values correlated with sampled PM mass concentration by assuming a nearly constant PM chemical composition. At this stage of knowledge, the relevance of information that could be obtained by applying a DPPH assay to PM for evaluating its reducing properties still requires an evaluation. In fact, further studies should be addressed both to the identification of species and sources that drive DPPH results and to deepening the environmental significance of the proposed assay. However, with this preliminary study, the applicability of the DPPH assay as a new experimental approach for estimating the presence of PM reducing species was proved.

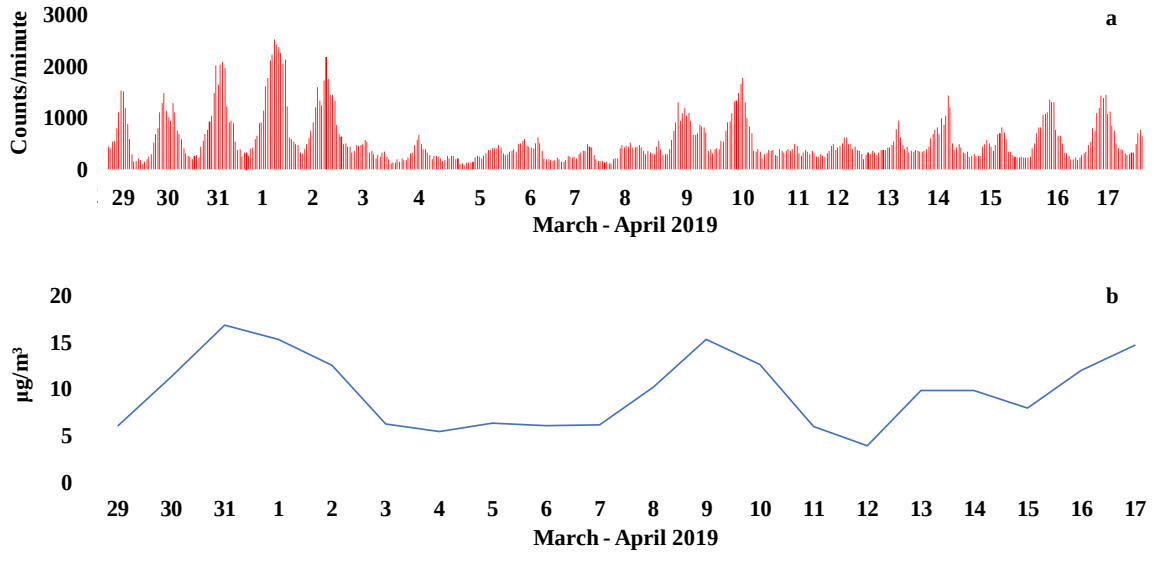

Figure 2. (**a**) Time patterns of natural radioactivity, expressed in counts per min, and (**b**) $PM_{2.5}$ mass concentration (μg/m³) from 29th to 17th March-April at Cassana (FE), Italy.

Table 1. Elemental composition of water-soluble and residual fractions of $PM_{2.5}$ filters collected in Cassana (FE), Italy, from 27 March to 15 April 2019. * The mean was calculated by replacing values below LOD with LOD/2.

Soluble Fraction	**LOD** (ng/m³)	**Mean** (ng/m³)	**Min–Max** (ng/m³)	**Residual Fraction**	**LOD** (ng/m³)	**Mean** (ng/m³)	**Min–Max** (ng/m³)
Al	2.5	2.2 *	2.5–7.1	Al	11	13 *	11–91
As	0.29	0.24 *	0.29–0.48	-	-	-	-
Bi	0.011	0.017 *	0.011–0.049	Bi	0.004	0.036 *	0.004–0.078
Cd	0.022	0.068 *	0.022–0.19	Cd	0.051	0.046 *	0.051–0.22
Ce	0.004	0.005 *	0.004–0.012	Ce	0.047	0.025 *	0.047–0.051
Co	0.005	0.011 *	0.005–0.024	-	-	-	-
Cr	0.054	0.063 *	0.054–0.13	Cr	4.1	2.4	1.6–3.5
Cs	0.002	0.006	0.002–0.016	Cs	0.006	0.003 *	0.006–0.013
Cu	0.057	0.69	0.22–1.5	Cu	0.87	0.69 *	0.87–1.8
Fe	9.2	8.1 *	9.2–36	Fe	21	18 *	21–44
La	0.005	0.004 *	0.005–0.018	La	0.029	0.015 *	0.029–0.034
Li	0.015	0.013 *	0.015–0.026	Li	0.011	0.013 *	0.011–0.019
Mg	6.1	6.2 *	6.1–26	Mg	13	7.1 *	13–16
Mn	0.12	0.66	0.19–1.4	Mn	0.35	0.66 *	0.35–1.1
Mo	0.004	0.11	0.031–0.26	Mo	0.029	0.096	0.029–0.24
Na	7.9	28	11–75	-	-	-	-
Ni	0.58	0.33 *	0.58–0.73	Ni	0.82	0.51 *	0.82–1.8
Pb	0.21	0.92	0.21–2.4	Pb	0.17	1.1	0.44–3.1
Rb	0.11	0.17 *	0.11–0.36	-			
Sb	0.004	0.25	0.038–0.63	Sb	0.17	0.24 *	0.17–0.39
Sn	0.006	0.071	0.026–0.19	Sn	0.11	0.39	0.17–0.71
Sr	0.22	0.22 *	0.22–0.78	-	-	-	-
Ti	0.046	0.075 *	0.075–0.18	Ti	0.79	0.42 *	0.79–0.81
Tl	0.0005	0.002	0.0004–0.011	Tl	0.002	0.003 *	0.002–0.006
V	0.015	0.33	0.031–1.8	V	0.079	0.097 *	0.079–0.38
Zn	2.7	9.6	4.1–40	Zn	15	5.3	1.5–12
Zr	0.006	0.012	0.006–0.032	Zr	0.028	0.071	0.027–0.32

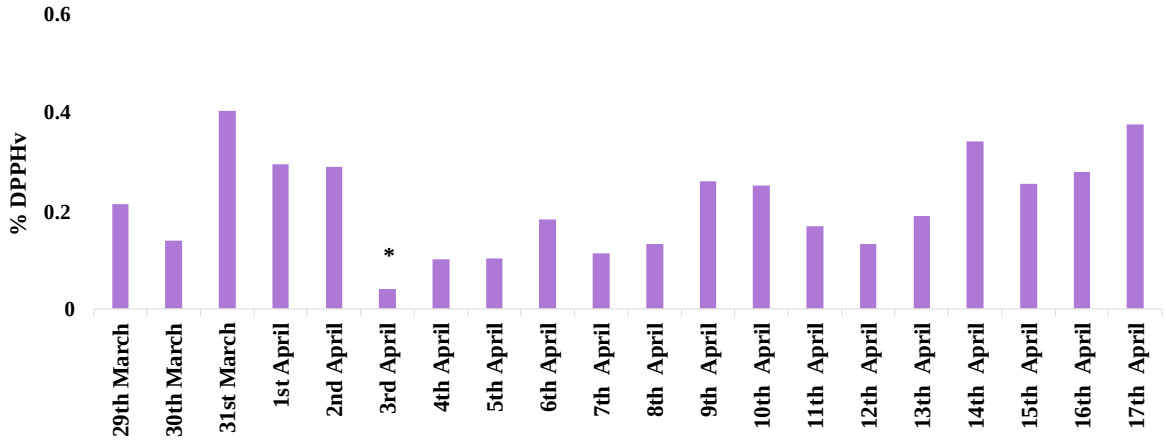

Figure 3. Reducing potential (%DPPHv) obtained through DPPH assay on 24 h $PM_{2.5}$ filters collected in Cassana (FE), Italy, from 29th to 17th March-April 2019. * The value was set at LOD/2.

Table 2. Correlation matrix among PM mass concentration (PM), 2,2-diphenyl-1-picrylhydrazyl assay results (RP), and oxidative potential assays values (ascorbic acid, AA; dithiothreitol, DTT; 2′,7′-dichlorofluorescin, DCFH).

Parameters	PM	RP	AA	DTT	DCFH
PM	-				
RP	0.77	-			
AA	0.19	0.056	-		
DTT	0.63	0.47	0.14	-	
DCFH	0.33	0.52	−0.23	0.34	-

4. Conclusions

In this study, the DPPH radical scavenging assay was adapted and preliminarily applied to PM with the aim of verifying its possible use as an acellular method for estimating the presence of reducing species. The results showed that the assay was sufficiently sensitive to be applied to 24 h PM samples collected by samplers working at 2.3 m^3/h with a good repeatability and linearity.

The described preliminary application of the DPPH assay revealed the presence of reducing species in several components of atmospheric PM derived from various emission sources and, thus, with very different chemical composition; the highest values were measured in urban dust, brake dust, and diesel dust. These outcomes seem to be mainly due to the reactions involving DPPH and organic fraction, but further studies are required to identify the species responsible for DPPH scavenging.

The RP^{DPPH} test is a cost-effective, rapid, and simple acellular method thus offering the same advantages of the OP assays. In the future, the combined application of all these tests to wider sample sets will permit to

better understand redox equilibria among PM native species that might occur during sample storage, extraction phase, and/or application of oxidative potential assays. Furthermore, it is worth considering that reducing species could reasonably react with oxidizing ones, also when PM gets in contact with biological systems, thus exerting a possible opposition to oxidative stress.

The availability of a suitable assay for routinely estimate the amount of reducing species in PM samples could constitute a new and potentially useful tool for acquiring new insight in the field of its redox behavior and health effect.

Author contributions: M.A.F. and S.C. designed the research; M.A.F. elaborated the data and wrote the manuscript; M.A.F. and N.D.F. optimized the procedure and performed the DPPH assay, oxidative potential, and chemical analyses; F.C. and M.R. contributed to the analytical phase; S.C. coordinated the group and supervised the manuscript.

Supplementary Materials

Table S1: Chemical composition of the total fraction (water-soluble and insoluble) of brake dust (BD), coke (C), Saharan dust (SD) and calcitic soil dust (CSD). Mean ± standard deviation of three replicates is reported.

			BD	C	SD	CSD
Technique	**UoM**		Mean ± SD	Mean ± SD	Mean ± SD	Mean ± SD
ICP-MS/XRF	g/Kg	**Al**	15 ± 0.42	13 ± 2	69 ± 2	11 ± 0.21
ICP-MS	mg/Kg	**As**	19 ± 1	1.1 ± 0.062	1.4 ± 0.12	96 ± 11
ICP-MS	mg/Kg	**B**	32 ± 0.073	3.5 ± 0.94	13 ± 0.82	1.6 ± 0.4
ICP-MS	mg/Kg	**Cd**	1.1 ± 0.051	0.07 ± 0.04	0.91 ± 0.071	0.11 ± 0.003
ICP-MS	mg/Kg	**Ce**	26 ± 0.12	0.32 ± 0.11	1.2 ± 0.11	10 ± 1.3
ICP-MS	mg/Kg	**Co**	15 ± 0.54	1.1 ± 0.044	0.73 ± 0.037	1.8 ± 0.11
ICP-MS	mg/Kg	**Cr**	3107 ± 74	10 ± 0.2	52 ± 1	40 ± 2
ICP-MS	mg/Kg	**Cs**	3.2 ± 0.036	0.052 ± 0.011	0.025 ± 0.003	2.8 ± 0.32
ICP-MS	mg/Kg	**Cu**	5051 ± 9	56 ± 12	13 ± 4	14 ± 1
ICP-MS	g/Kg	**Fe**	204 ± 5	17 ± 4	41 ± 0.31	4 ± 0.11
ICP-MS	mg/Kg	**La**	13 ± 0.22	0.31 ± 0.23	27 ± 0.11	5.2 ± 1.1
ICP-MS	mg/Kg	**Mn**	1212 ± 4	46 ± 1	29 ±0.51	121 ± 5
ICP-MS	mg/Kg	**Mo**	175 ± 1	77 ± 0.18	0.16 ± 0.021	0.72 ± 0.095
ICP-MS	mg/Kg	**Ni**	112 ± 3	357 ± 1	7 ± 1	11 ± 1.1
ICP-MS	mg/Kg	**Pb**	683 ± 4	18 ± 0.14	2.5 ± 0.22	12 ± 2.5
ICP-MS	mg/Kg	**Rb**	23 ± 1	1.1 ± 0.11	7 ± 0.6	11 ± 2.4
ICP-MS	mg/Kg	**Sb**	306 ± 1	4 ± 0.011	2.4 ± 0.011	0.41 ± 0.12
ICP-MS	mg/Kg	**Se**	9.3 ± 0.43	9 ± 0.21	1.5 ± 0.13	11 ± 2.1
ICP-MS	mg/Kg	**Sn**	1420 ± 3	15 ± 0.32	0.022 ± 0.011	2.8 ± 0.51
ICP-MS	mg/Kg	**Sr**	257 ± 9	10 ± 7	352 ± 10	525 ± 46
ICP-MS	mg/Kg	**Ti**	527 ± 9	907 ± 21	4542 ± 111	255 ± 6.2
ICP-MS	mg/Kg	**Tl**	0.34 ± 0.12	0.032 ± 0.011	0.034 ± 0.012	0.15 ± 0.039
ICP-MS	mg/Kg	**V**	9 ± 0.47	556 ± 1	6.1 ± 0.41	11 ± 1.1
ICP-MS	mg/Kg	**Zn**	5317 ± 20	260 ± 17	50 ± 20	110 ± 24
ICP-MS	mg/Kg	**Zr**	90 ± 1	12 ± 0.14	9.4± 0.21	14 ± 1.5
ECOC	g/Kg	**EC**	17 ± 1	310 ± 15	< 0.001	< 0.001
TOC	g/Kg	**WSOC**	5.7 ± 0.12	9.5 ± 0.21	0.53 ± 0.02	0.3 ± 0.1
ECOC/TOC	g/Kg	**WIOC**	30 ± 3	146 ± 5	0.10 ± 0.02	41 ± 3

Table S2: Correlation matrix among elemental concentrations, PM mass concentration (PM), 2,2-diphenyl-1-picrylhydrazyl assay (RP) and oxidative potential assays (ascorbic acid, AA; dithiothreitol, DTT; 2′,7′-dichlorofluorescin, DCFH) of extracted fraction of $PM_{2.5}$ filters collected in Cassana (FE), Italy.

	Al	As	Bi	Cd	Ce	Co	Cr	Cs	Cu	Fe	La	Li	Mg	Mn	Mo	Na	Ni	Pb	Rb	Sb	Sn	Sr	Ti	V	Zn	Zr	PM	RP	AA	DTT	DCFH
Al	-																														
As	0.59	-																													
Bi	0.59	0.77	-																												
Cd	0.25	0.29	0.37	-																											
Ce	0.56	0.49	0.47	0.64	-																										
Co	0.67	0.62	0.49	0.33	0.64	-																									
Cr	0.50	0.77	0.81	0.55	0.51	0.45	-																								
Cs	0.64	0.52	0.41	0.47	0.56	0.41	0.46	-																							
Cu	0.62	0.78	0.84	0.67	0.59	0.57	0.91	0.54	-																						
Fe	0.70	0.61	0.72	0.33	0.70	0.78	0.63	0.49	0.68	-																					
La	0.10	-0.04	-0.013	0.63	0.67	0.21	0.13	0.19	0.25	0.25	-																				
Li	0.62	0.65	0.74	0.69	0.64	0.51	0.87	0.66	0.93	0.65	0.28	-																			
Mg	0.77	0.45	0.52	0.32	0.73	0.79	0.48	0.46	0.56	0.89	0.39	0.58	-																		
Mn	0.63	0.75	0.79	0.67	0.56	0.52	0.91	0.61	0.94	0.61	0.15	0.96	0.55	-																	
Mo	0.46	0.64	0.78	0.58	0.66	0.52	0.85	0.41	0.85	0.71	0.35	0.86	0.64	0.84	-																
Na	0.44	0.16	0.16	0.34	0.64	0.64	0.21	0.18	0.32	0.59	0.63	0.34	0.83	0.28	0.44	-															
Ni	0.007	0.20	0.048	-0.066	0.038	0.51	0.076	-0.13	-0.002	0.26	0.10	-0.15	0.27	-0.070	0.058	0.33	-														
Pb	0.58	0.59	0.63	0.51	0.53	0.56	0.62	0.65	0.67	0.68	0.05	0.65	0.48	0.64	0.43	0.17	0.052	-													
Rb	0.64	0.36	0.35	0.40	0.36	0.47	0.48	0.58	0.53	0.49	0.09	0.61	0.52	0.61	0.38	0.26	-0.006	0.43	-												
Sb	0.49	0.72	0.72	0.67	0.44	0.51	0.86	0.55	0.91	0.56	0.10	0.83	0.38	0.87	0.64	0.13	0.04	0.78	0.55	-											
Sn	0.61	0.76	0.75	0.61	0.41	0.56	0.84	0.65	0.89	0.61	0.04	0.82	0.45	0.87	0.63	0.15	0.12	0.81	0.57	0.97	-										
Sr	0.77	0.54	0.60	0.26	0.74	0.81	0.52	0.50	0.58	0.96	0.28	0.59	0.96	0.54	0.66	0.71	0.26	0.59	0.47	0.41	0.49	-									
Ti	0.54	0.52	0.58	0.41	0.56	0.79	0.48	0.42	0.58	0.82	0.14	0.48	0.69	0.47	0.44	0.44	0.34	0.78	0.41	0.65	0.66	0.75	-								
V	0.004	-0.11	-0.37	-0.21	-0.17	0.31	-0.31	-0.16	-0.31	-0.19	0.01	-0.34	-0.022	-0.29	-0.35	0.16	0.65	-0.19	-0.017	-0.19	-0.14	-0.078	-0.044	-							
Zn	0.72	0.52	0.65	0.34	0.69	0.73	0.59	0.55	0.64	0.97	0.26	0.68	0.91	0.61	0.69	0.61	0.19	0.68	0.52	0.51	0.58	0.96	0.76	-0.21	-						
Zr	0.45	0.59	0.73	0.64	0.51	0.53	0.66	0.42	0.79	0.55	0.09	0.69	0.37	0.71	0.56	0.13	-0.002	0.72	0.36	0.85	0.81	0.44	0.72	-0.24	0.49	-					
PM	0.59	0.77	0.79	0.42	0.59	0.49	0.79	0.64	0.76	0.61	-0.05	0.78	0.43	0.81	0.71	0.043	-0.15	0.68	0.44	0.73	0.73	0.54	0.52	-0.35	0.56	0.71	-				
RP	0.31	0.43	0.63	0.59	0.46	0.26	0.65	0.35	0.62	0.38	0.06	0.59	0.21	0.62	0.56	-0.058	-0.16	0.56	0.25	0.68	0.64	0.28	0.50	-0.38	0.33	0.82	0.77	-			
AA	0.22	0.31	0.40	0.31	0.25	0.16	0.43	0.061	0.59	0.36	0.32	0.56	0.33	0.48	0.61	0.35	-0.16	0.15	0.078	0.33	0.32	0.31	0.067	-0.32	0.38	0.22	0.19	0.052	-		
DTT	0.69	0.66	0.60	0.31	0.43	0.66	0.65	0.57	0.65	0.71	-0.01	0.59	0.67	0.67	0.56	0.31	0.23	0.64	0.67	0.67	0.73	0.71	0.73	-0.008	0.71	0.53	0.63	0.47	0.14	-	
DCFH	0.18	0.31	0.43	0.18	0.14	0.23	0.23	0.21	0.26	0.39	-0.20	0.11	0.11	0.15	0.003	-0.16	0.14	0.66	0.19	0.45	0.46	0.23	0.65	-0.24	0.31	0.62	0.33	0.51	-0.23	0.34	-

Table S3: Correlation matrix among elemental concentrations, PM mass concentration (PM), 2,2-diphenyl-1-picrylhydrazyl assay (RP) and oxidative potential assays (ascorbic acid, AA; dithiothreitol, DTT; 2′,7′-dichlorofluorescin, DCFH) of residual fraction of $PM_{2.5}$ filters collected in Cassana (FE), Italy.

	Al	Bi	Cd	Ce	Cr	Cs	Cu	Fe	La	Li	Mg	Mn	Mo	Ni	Pb	Sb	Sn	Sr	Ti	Tl	V	Zn	Zr	PM	RP	AA	DTT	DCFH
Al	-																											
Bi	-0.11	-																										
Cd	0.56	-0.11	-																									
Ce	0.065	0.17	-0.12	-																								
Cr	0.57	0.081	0.61	-0.07	-																							
Cs	0.012	0.17	0.18	-0.14	0.17	-																						
Cu	-0.013	0.89	-0.091	0.00	0.16	0.14	-																					
Fe	0.25	0.68	0.23	-0.10	0.53	0.21	0.77	-																				
La	-0.21	-0.013	-0.19	0.87	-0.24	-0.079	-0.18	-0.22	-																			
Li	0.037	0.39	0.28	-0.21	0.19	0.75	0.44	0.56	-0.19	-																		
Mg	0.69	-0.008	0.69	-0.13	0.71	0.31	0.059	0.45	-0.35	0.29	-																	
Mn	0.0004	0.76	0.18	-0.15	0.22	0.42	0.74	0.74	-0.24	0.62	0.15	-																
Mo	-0.19	0.57	-0.069	0.12	0.013	0.21	0.55	0.37	0.088	0.34	-0.002	0.44	-															
Ni	0.14	-0.04	0.29	-0.37	0.56	0.13	0.21	0.54	-0.24	0.27	0.44	0.11	0.27	-														
Pb	-0.075	0.38	0.058	-0.11	-0.32	0.22	0.21	0.14	-0.04	0.45	-0.22	0.53	0.16	-0.32	-													
Sb	0.19	0.36	0.47	-0.28	0.19	-0.013	0.42	0.55	-0.33	0.43	0.33	0.57	0.48	0.33	0.34	-												
Sn	-0.017	0.85	-0.18	0.06	-0.015	0.18	0.81	0.63	-0.14	0.41	0.039	0.72	0.56	0.032	0.45	0.38	-											
Sr	0.32	-0.13	0.53	0.06	0.66	0.31	-0.16	0.11	-0.02	0.16	0.61	-0.017	-0.008	0.32	-0.23	0.052	-0.34	-										
Ti	0.19	0.42	-0.12	-0.04	0.069	0.078	0.57	0.66	-0.17	0.51	0.22	0.34	0.24	0.35	0.15	0.32	0.63	-0.29	-									
Tl	0.22	0.12	0.61	-0.10	0.32	0.62	0.17	0.21	-0.07	0.61	0.35	0.37	-0.061	0.072	0.26	0.18	-0.075	0.47	-0.14	-								
V	0.13	-0.35	0.61	-0.30	0.59	0.077	-0.27	0.11	-0.21	0.22	0.34	-0.085	-0.18	0.53	-0.23	0.21	-0.45	0.55	-0.16	0.31	-							
Zn	0.44	-0.13	0.48	-0.02	0.46	0.41	-0.17	0.041	-0.21	0.14	0.73	0.093	-0.025	0.062	-0.11	0.11	-0.15	0.79	-0.25	0.37	0.22	-						
Zr	-0.056	0.49	-0.17	0.13	-0.018	-0.24	0.31	0.28	-0.05	-0.025	0.036	0.13	0.28	-0.11	0.14	0.17	0.59	-0.34	0.32	-0.35	-0.34	-0.25	-					
PM	0.024	0.63	-0.25	0.00	-0.25	0.026	0.54	0.19	-0.29	0.17	-0.074	0.43	0.18	-0.53	0.53	0.18	0.64	-0.25	0.24	0.020	-0.58	0.029	0.43	-				
RP	0.30	0.47	0.13	-0.04	0.030	-0.11	0.41	0.31	-0.39	0.15	0.32	0.38	0.23	-0.24	0.45	0.39	0.59	0.015	0.36	-0.027	-0.33	0.31	0.46	0.77	-			
AA	-0.21	0.55	-0.42	0.40	-0.27	-0.29	0.47	0.28	0.42	-0.25	-0.34	0.22	0.25	-0.071	0.093	-0.092	0.51	-0.49	0.26	-0.33	-0.64	-0.52	0.39	0.19	0.052	-		
DTT	-0.13	0.38	-0.003	-0.13	-0.25	-0.18	0.41	0.061	-0.28	0.011	-0.18	0.29	0.041	-0.37	0.31	0.17	0.31	-0.29	0.033	0.13	-0.18	-0.23	0.21	0.63	0.46	0.14	-	
DCFH	0.19	0.12	0.24	0.07	0.012	0.13	0.092	0.12	-0.072	0.27	0.16	0.38	0.14	-0.27	0.46	0.29	0.061	0.26	0.035	0.21	-0.011	0.38	-0.27	0.33	0.51	-0.23	0.34	-

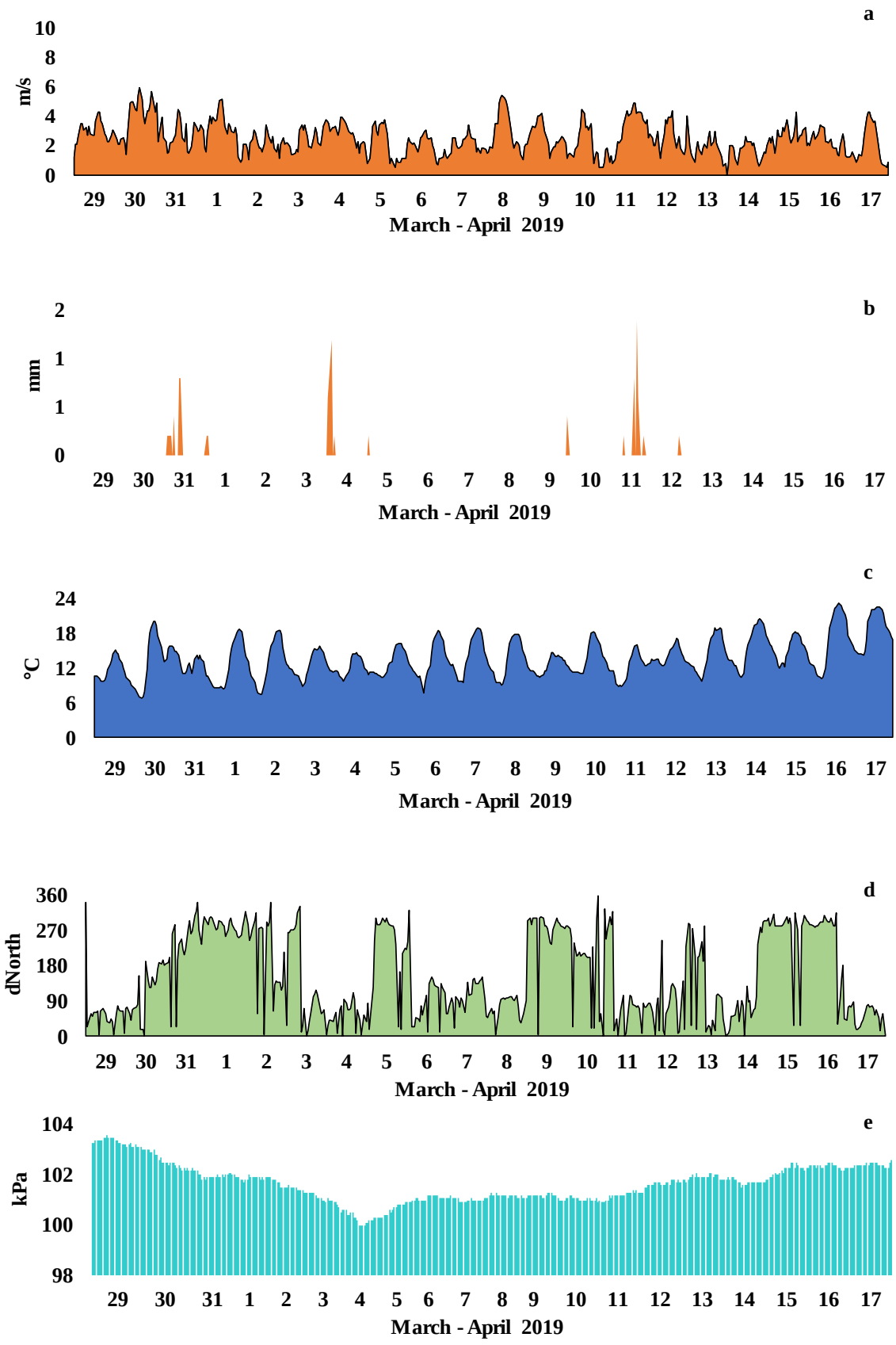

Figure S6: Meteorological data collected from 29th to 17th March-April 2019at Cassana (FE), Italy: wind speed (a), rainfall (b), temperature (c), wind direction (d) and pressure (e).

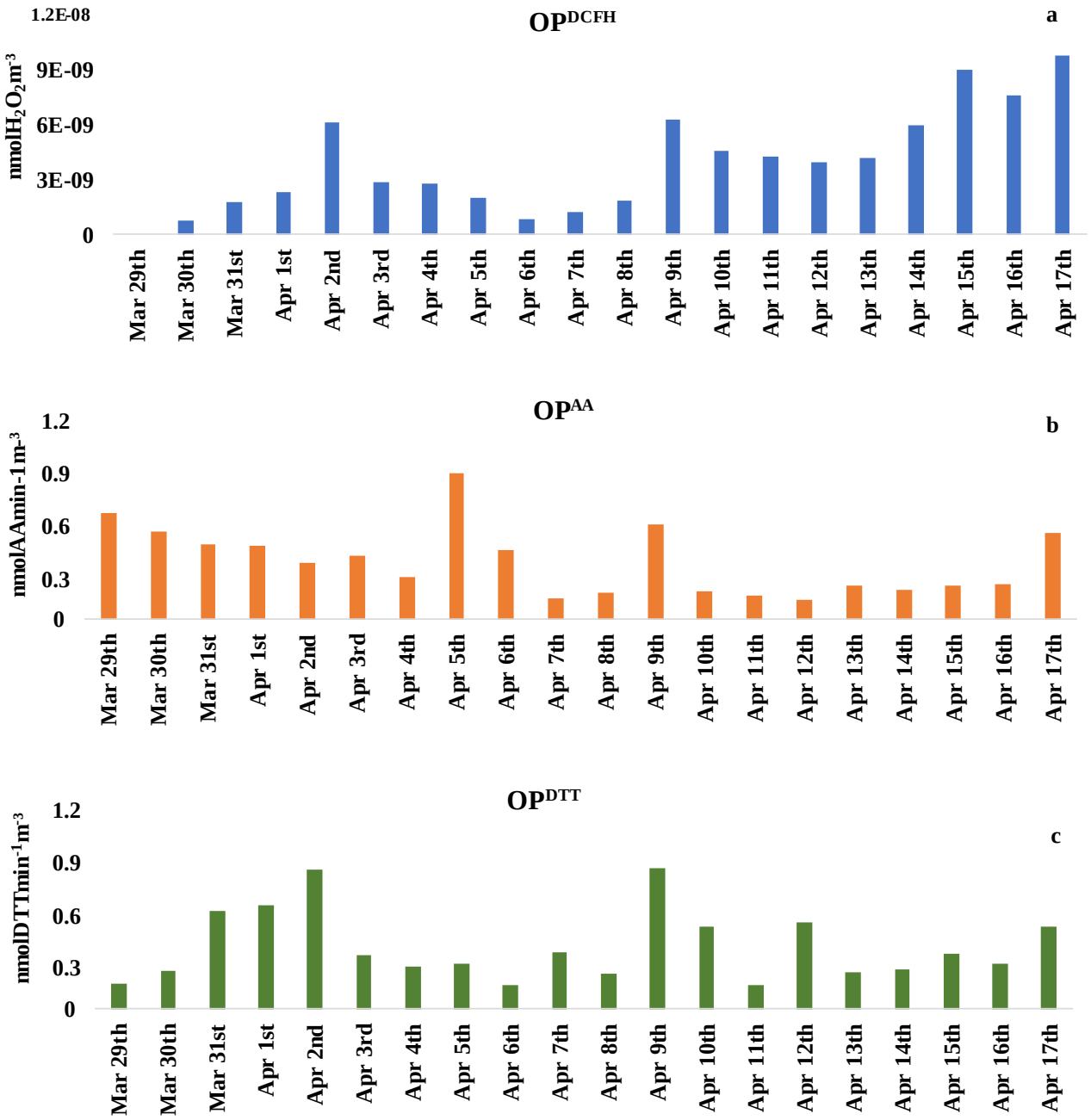

Figure S7: Oxidative potential obtained through 2′,7′-dichlorofluorescin (OP^{DCFH}), ascorbic acid (OP^{AA}) and dithiothreitol (OP^{DTT}) assays on $PM_{2.5}$ filters collected at Cassana (FE), Italy, from 29th to 17th March-April 2019. Values below limits of detection (LODs) are not reported.

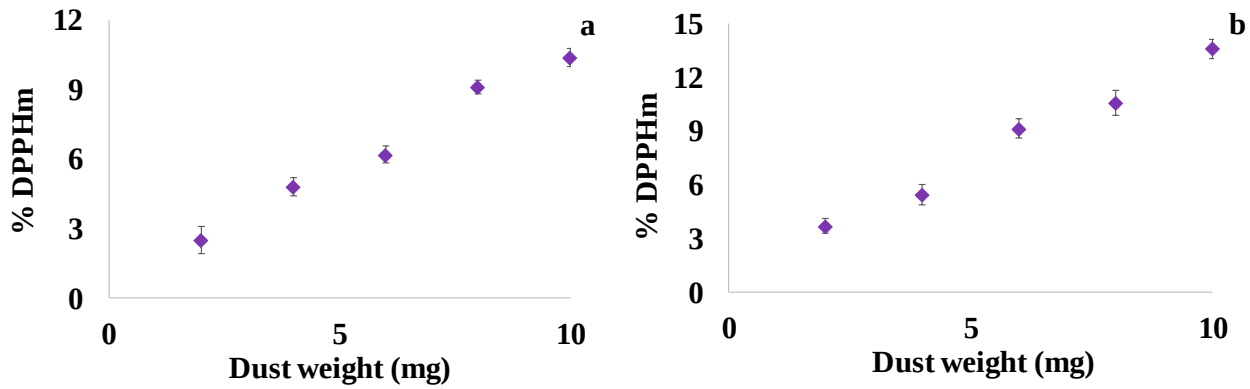

Figure S8: Reducing potential **(**%DPPHm) linearity of response of (a) UD (urban particulate matter certified material, NIST168a) and (b) D (diesel particulate matter certified material, NIST1650b).

References

1. Xu, X.; Yu, X.; Mo, L.; Xu, Y.; Bao, L.; Lun, X. Atmospheric particulate matter accumulation on trees: A comparison of boles, branches and leaves. *J. Clean. Prod.* **2019**, *226*, 349–356, doi:10.1016/j.jclepro.2019.04.072.
2. Lelieveld, J.; Evans, J.S.; Fnais, M.; Giannadaki, D.; Pozzer, A. The contribution of outdoor air pollution sources to premature mortality on a global scale. *Nature* **2015**, *525*, 367.
3. Crobeddu, B.; Aragao-Santiago; L., Bui; L. C., Boland, S.; Squiban, A.B. Oxidative potential of particulate matter 2.5 as predictive indicator of cellular stress. *Environ. Pollut.* **2017**, *230*, 125–133, doi:10.1016/j.envpol.2017.06.051.
4. Kioumourtzoglou, M.A.; Schwartz, J.D.; Weisskopf, M.G.; Melly, S.J.; Wang, Y.; Dominici, F.; Zanobetti, A. Long-term PM2.5 exposure and neurological hospital admissions in the northeastern United States. *Environ. Health Perspect.* **2015**, *124*, 23–29, doi:10.1289/ehp.1408973.
5. Li, S.; Tan, H.Y.; Wang, N.; Zhang, Z.J.; Lao, L.; Wong, C.W.; Feng, Y. The role of oxidative stress and antioxidants in liver diseases. *Int. J. Mol. Sci.* **2015**, *16*, 26087–26124, doi:10.3390/ijms161125942.
6. Øvrevik, J. Oxidative potential versus biological effects: A review on the relevance of cell-free/abiotic assays as predictors of toxicity from airborne particulate matter. *Int. J. Mol. Sci.* **2019**, *20*, 4772, doi:10.3390/ijms20194772.
7. Calas, A.; Uzu, G.; Kelly, F.J.; Houdier, S.; Martins, J.M.; Thomas, F.; Jacob, V. Comparison between five acellular oxidative potential measurement assays performed with detailed chemistry on PM10 samples from the city of Chamonix (France). *Atmos. Chem. Phys.* **2018**, *18*, 7863–7875, doi:10.5194/acp-18-7863-2018.
8. Perrone, M.G.; Zhou, J.; Malandrino, M.; Sangiorgi, G.; Rizzi, C.; Ferrero, L.; Bolzacchini, E. PM chemical composition and oxidative potential of the soluble fraction of particles at two sites in the urban area of Milan, Northern Italy. *Atmos. Environ.* **2016**, *128*, 104–113, doi:10.1016/j.atmosenv.2015.12.040.
9. Yang, A.; Janssen, N.A.; Brunekreef, B.; Cassee, F.R.; Hoek, G.; Gehring, U. Children's respiratory health and oxidative potential of PM2.5: The PIAMA birth cohort study. *Occup. Env. Med.* **2016**, *73*, 154–160, doi:10.1136/oemed-2015-103175.
10. Pietrogrande, M.C.; Russo, M.; Zagatti, E. Review of PM Oxidative Potential Measured with Acellular Assays in Urban and Rural Sites across Italy. *Atmosphere* **2019**, *10*, 626, doi:10.3390/atmos10100626.
11. Ayres, J.G.; Borm, P.; Cassee, F.R.; Castranova, V.; Donaldson, K.; Ghio, A.; Marano, F. Evaluating the toxicity of airborne particulate matter and nanoparticles by measuring oxidative stress potential—A workshop report and consensus statement. *Inhal. Toxicol.* **2008**, *20*, 75–99, doi:10.1080/08958370701665517.
12. Stoeger, T.; Takenaka, S.; Frankenberger, B.; Ritter, B.; Karg, E.; Maier, K.; Schmid, O. Deducing in vivo toxicity of combustion-derived nanoparticles from a cell-free oxidative potency assay and metabolic activation of organic compounds. *Environ. Health Perspect.* **2008**, *117*, 54–60, doi:10.1289/ehp.11370.

13. Cho, A.K.; Sioutas, C.; Miguel, A.H.; Kumagai, Y.; Schmitz, D.A.; Singh, M.; Froines, J.R. Redox activity of airborne particulate matter at different sites in the Los Angeles Basin. *Environ. Res.* **2005**, *99*, 40–47, doi:10.1016/j.envres.2005.01.003.
14. Hung, H.F.; Wang, C.S. Experimental determination of reactive oxygen species in Taipei aerosols. *J. Aerosol Sci.* **2001**, *32*, 1201–1211, doi:10.1016/S0021-8502(01)00051-9.
15. Fang, T.; Verma, V.; Bates, J.T.; Abrams, J.; Klein, M.; Strickland, M.J.; Russell, A.G. Oxidative potential of ambient water-soluble PM2.5 in the southeastern United States: Contrasts in sources and health associations between ascorbic acid (AA) and dithiothreitol (DTT) assays. *Atmos. Chem. Phys.* **2016**, *16*, 3865–3879, doi:10.5194/acp-16-3865-2016.
16. Bates, J.T.; Fang, T.; Verma, V.; Zeng, L.; Weber, R.J.; Tolbert, P.E.; Russell, A.G. Review of acellular assays of ambient particulate matter oxidative potential: Methods and relationships with composition, sources, and health effects. *Environ. Sci. Technol.* **2019**, *53*, 4003–4019, doi:10.1021/acs.est.8b03430.
17. Yang, A.; Jedynska, A.; Hellack, B.; Kooter, I.; Hoek, G.; Brunekreef, B.; Janssen, N.A. Measurement of the oxidative potential of PM2.5 and its constituents: The effect of extraction solvent and filter type. *Atmos. Environ.* **2014**, *83*, 35–42, doi:10.1016/j.atmosenv.2013.10.049.
18. Tayo, L.L.; Lin, Y.H.; Lin, S.L.; Gou, Y.Y.; Hsu10, Y.C.; Hou, W.C.; Chao, H.R. Fine particulate matter-induced toxic effects in an animal model of caenorhabditis elegans. *Aerosol Air Qual. Res.* **2019**, *19*, 1068–1078, doi:10.4209/aaqr.2019.03.0127.
19. Marcoccia, M.; Ronci, L.; De Matthaeis, E.; Setini, A.; Perrino, C.; Canepari, S. In-vivo assesment of the genotoxic and oxidative stress effects of particulate matter on Echinogammarus veneris. *Chemosphere* **2017**, *173*, 124–134, doi:10.1016/j.chemosphere.2017.01.019.
20. Piacentini, D.; Falasca, G.; Canepari, S.; Massimi, L. Potential of PM-selected components to induce oxidative stress and root system alteration in a plant model organism. *Environ. Int.* **2019**, *132*, 105094, doi:10.1016/j.envint.2019.105094.
21. Costabile, F.; Gualtieri, M.; Canepari, S.; Tranfo, G.; Consales, C.; Grollino, M.G.; Simonetti, G. Evidence of association between aerosol properties and in-vitro cellular oxidative response to PM1, oxidative potential of PM2.5, a biomarker of RNA oxidation, and its dependency on combustion sources. *Atmos. Environ.* **2019**, *213*, 444–455, doi:10.1016/j.atmosenv.2019.06.023.
22. Pietrogrande, M.C.; Bertoli, I.; Manarini, F.; Russo, M. Ascorbate assay as a measure of oxidative potential for ambient particles: Evidence for the importance of cell-free surrogate lung fluid composition. *Atmos. Environ.* **2019**, *211*, 103–112, doi:10.1016/j.atmosenv.2019.05.012.
23. Khurshid, S.S.; Siegel, J.A.; Kinney, K.A. Indoor particulate reactive oxygen species concentrations. *Environ. Res.* **2014**, *132*, 46–53, doi:10.1016/j.envres.2014.03.026.
24. Miljevic, B.; Hedayat, F.; Stevanovic, S.; Fairfull-Smith, K.E.; Bottle, S.E.; Ristovski, Z.D. To sonicate or not to sonicate PM filters: Reactive oxygen species generation upon ultrasonic irradiation. *Aerosol Sci. Technol.* **2014**, *48*, 1276–1284, doi:10.1080/02786826.2014.981330.

25. Wei, J.; Yu, H.; Wang, Y.; Verma, V. Complexation of iron and copper in ambient particulate matter and its effect on the oxidative potential measured in a surrogate lung fluid. *Environ. Sci. Technol.* **2018**, *53*, 1661–1671, doi:10.1021/acs.est.8b05731.
26. Oh, S.M.; Kim, H.R.; Park, Y.J.; Lee, S.Y.; Chung, K.H. Organic extracts of urban air pollution particulate matter (PM2.5)-induced genotoxicity and oxidative stress in human lung bronchial epithelial cells (BEAS-2B cells). *Mutat. Res. Genet. Toxicol. Environ. Mutagenesis* **2011**, *723*, 142–151, doi:10.1016/j.mrgentox.2011.04.003.
27. Hawthorne, S.B.; Miller, D.J.; Langenfeld, J.J.; Krieger, M.S. PM-10 high-volume collection and quantitation of semi-and nonvolatile phenols, methoxylated phenols, alkanes, and polycyclic aromatic hydrocarbons from winter urban air and their relationship to wood smoke emissions. *Environ. Sci. Technol.* **1992**, *26*, 2251–2262, doi:10.1021/es00035a026.
28. Simoneit, B.R.; Bi, X.; Oros, D.R.; Medeiros, P.M.; Sheng, G.; Fu, J. Phenols and hydroxy-PAHs (arylphenols) as tracers for coal smoke particulate matter: Source tests and ambient aerosol assessments. *Environ. Sci. Technol.* **2007**, *41*, 7294–7302.
29. Buiarelli, F.; Sonego, E.; Uccelletti, D.; Bruni, E.; Di Filippo, P.; Pomata, D.; Simonetti, G. Determination of the main bioaerosol components using chemical markers by liquid chromatography–tandem mass spectrometry. *Microchem. J.* **2019**, 103974, doi:10.1016/j.microc.2019.103974.
30. Menetrez, M.Y.; Foarde, K.K.; Esch, R.K.; Schwartz, T.D.; Dean, T.R.; Hays, M.D.; Moore, S.A. An evaluation of indoor and outdoor biological particulate matter. *Atmos. Environ.* **2009**, *43*, 5476–5483.
31. Nemmar, A.; Holme, J.A.; Rosas, I.; Schwarze, P.E.; Alfaro-Moreno, E. Recent advances in particulate matter and nanoparticle toxicology: A review of the in vivo and in vitro studies. *Biomed Res. Int.* **2013**, *2013*, 279371, doi:10.1155/2013/279371.
32. Kedare, S.B.; Singh, R.P. Genesis and development of DPPH method of antioxidant assay. *J. Food Sci. Technol.* **2011**, *48*, 412–422, doi:10.1007/s13197-011-0251-1.
33. Sendra, J.M.; Sentandreu, E.; Navarro, J.L. Reduction kinetics of the free stable radical 2, 2-diphenyl-1-picrylhydrazyl (DPPH•) for determination of the antiradical activity of citrus juices. *Eur. Food Res. Technol.* **2006**, *223*, 615, doi:10.1007/s00217-005-0243-3.
34. Sánchez-Moreno, C. Methods used to evaluate the free radical scavenging activity in foods and biological systems. *Food Sci. Technol. Int.* **2002**, *8*, 121–137, doi:10.1106/108201302026770.
35. Sahu, R.K.; Kar, M.; Routray, R. DPPH free radical scavenging activity of some leafy vegetables used by tribals of odisha, India. *J. Med. Plants* **2013**, *1*, 21–27.
36. Chedea, V.S.; Pop, R.M. Total polyphenols content and antioxidant DPPH assays on biological samples. In *Polyphenols in Plants*; Academic Press: Cambridge, MA, USA, 2019; pp. 169–183, doi:10.1016/B978-0-12-813768-0.00011-6.
37. Sridhar, K.; Charles, A.L. In vitro antioxidant activity of Kyoho grape extracts in DPPH and ABTS assays: Estimation methods for EC50 using advanced statistical programs. *Food Chem.* **2019**, *275*, 41–49, doi:10.1016/j.foodchem.2018.09.040.

38. Hasan, S.R., Hossain, M.M.; Akter, R.; Jamila, M.; Mazumder, M.E.H.; Rahman, S. DPPH free radical scavenging activity of some Bangladeshi medicinal plants. *J. Med. Plants Res.* **2009**, *3*, 875–879, doi:10.2116/analsci.18P014.
39. Sirivibulkovit, K.; Nouanthavong, S.; Sameenoi, Y. Paper-based DPPH assay for antioxidant activity analysis. *Anal. Sci.* **2018**, *34*, 795–800.
40. Santos-Sánchez, N.F.; Salas-Coronado, R.; Villanueva-Cañongo, C.; Hernández-Carlos, B. Antioxidant compounds and their antioxidant mechanism. In *Antioxidants*; IntechOpen: 2019, doi:10.5772/intechopen.85270.
41. Sharma, O.P.; Bhat, T.K. DPPH antioxidant assay revisited. *Food Chem.* **2009**, *113*, 1202–1205, doi:10.1016/j.foodchem.2008.08.008.
42. Chen, Y.X.; Liu, X.Y.; Xiao, Z., Huang; Y. F.; Liu, B. Antioxidant activities of polysaccharides obtained from Chlorella pyrenoidosa via different ethanol concentrations. *Int. J. Biol. Macromol.* **2016**, *91*, 505–509, doi:10.1016/j.ijbiomac.2016.05.086.
43. Molyneux, P. The use of the stable free radical diphenylpicrylhydrazyl (DPPH) for estimating antioxidant activity. *Songklanakarin J. Sci. Technol* **2004**, *26*, 211–219.
44. Thorpe, A.; Harrison, R.M. Sources and properties of non-exhaust particulate matter from road traffic: A review. *Sci. Total Environ.* **2008**, *400*, 270–282.
45. Pant, P.; Harrison, R.M. Estimation of the contribution of road traffic emissions to particulate matter concentrations from field measurements: A review. *Atmos. Environ.* **2013**, *77*, 78–97.
46. Taioli, E.; Sram, R.J.; Garte, S.; Kalina, I.; Popov, T.A.; Farmer, P.B. Effects of polycyclic aromatic hydrocarbons (PAHs) in environmental pollution on exogenous and oxidative DNA damage (EXPAH project): Description of the population under study. *Mutat. Res. Fundam. Mol. Mech. Mutagenesis* **2007**, *620*, 1–6, doi:10.1016/j.mrfmmm.2007.02.016.
47. Besombes, J.L.; Maître, A.; Patissier, O.; Marchand, N.; Chevron, N.; Stoklov, M.; Masclet, P. Particulate PAHs observed in the surrounding of a municipal incinerator. *Atmos. Environ.* **2001**, *35*, 6093–6104, doi:10.1016/S1352-2310(01)00399-5.
48. Brines, M.; Dall'Osto, M.; Amato, F.; Minguillón, M.C.; Karanasiou, A.; Grimalt, J.O.; van Drooge, B.L. Source apportionment of urban PM 1 in Barcelona during SAPUSS using organic and inorganic components. *Environ. Sci. Pollut. Res.* **2019**, *26*, 32114–32127, doi:10.1007/s11356-019-06199-3.
49. Dugenest, S.; Casabianca, H.; Grenier-Loustalot, M.F. Municipal solid waste incineration bottom ash: Physicochemical characterization of organic matter. *Analusis* **1999**, *27*, 75–80, doi:10.1051/analusis:1999110.
50. Simonetti, G.; Conte, E.; Massimi, L.; Frasca, D.; Perrino, C.; Canepari, S. Oxidative potential of particulate matter components generated by specific emission sources. *J. Aerosol Sci.* **2018**, *126*, 99–109, doi:10.1016/j.jaerosci.2018.08.011.

51. Massimi, L.; Ristorini, M.; Eusebio, M.; Florendo, D.; Adeyemo, A.; Brugnoli, D.; Canepari, S. Monitoring and evaluation of Terni (Central Italy) air quality through spatially resolved analyses. *Atmosphere* **2017**, *8*, 200, doi:10.3390/atmos8100200.
52. Canepari, S.; Cardarelli, E.; Giuliano, A.; Pietrodangelo, A. Determination of metals, metalloids and non-volatile ions in airborne particulate matter by a new twostep sequential leaching procedure part a: Experimental design and optimization. *Talanta* **2006**, *69*, 581–587, doi:10.1016/j.talanta.2005.10.023.
53. Canepari, S.; Cardarelli, E.; Pietrodangelo, A.; Strincone, M. Determination of metals, metalloids and non-volatile ions in airborne particulate matter by a new two-step sequential leaching procedure: Part B: Validation on equivalent real samples. *Talanta* **2006**, *69*, 588–595, doi:10.1016/j.talanta.2005.10.024.
54. Mishra, S.K.; Singh, P.N.; Dubey, S.D. Evaluation of antioxidant activities in ethanolic extract of Capparis Zeylanica Linn. Root. *Rev. Latinoam. Química* **2013**, *41*, 7–20.
55. Scalzo, R.L. Organic acids influence on DPPH scavenging by ascorbic acid. *Food Chem.* **2008**, *107*, 40–43, doi:10.1016/j.foodchem.2007.07.070.
56. Shao, L.; Hu, Y.; Shen, R.; Schäfer, K.; Wang, J.; Wang, J.; Suppan, P. Seasonal variation of particle-induced oxidative potential of airborne particulate matter in Beijing. *Sci. Total Environ.* **2017**, *579*, 1152–1160, doi:10.1016/j.scitotenv.2016.11.094.
57. Chirizzi, D.; Cesari, D.; Guascito, M.R.; Dinoi, A.; Giotta, L.; Donateo, A.; Contini, D. Influence of Saharan dust outbreaks and carbon content on oxidative potential of water-soluble fractions of PM2. 5 and PM10. *Atmos. Environ.* **2017**, *163*, 1–8, doi:10.1016/j.atmosenv.2017.05.021.
58. Simonetti, G.; Conte, E.; Perrino, C.; Canepari, S. Oxidative potential of size-segregated PM in an urban and an industrial area of Italy. *Atmos. Environ.* **2018**, *187*, 292–300, doi:10.1016/j.atmosenv.2018.05.051.
59. Noipa, T.; Srijaranai, S.; Tuntulani, T.; Ngeontae, W. New approach for evaluation of the antioxidant capacity based on scavenging DPPH free radical in micelle systems. *Food Res. Int.* **2011**, *44*, 798–806, doi:10.1016/j.foodres.2011.01.034.
60. Pyrzynska, K.; Pękal, A. Application of free radical diphenylpicrylhydrazyl (DPPH) to estimate the antioxidant capacity of food samples. *Anal. Methods* **2013**, *5*, 4288–4295, doi:10.1039/c3ay40367j.
61. Fang, T.; Zeng, L.; Gao, D.; Verma, V.; Stefaniak, A.B.; Weber, R.J. Ambient size distributions and lung deposition of aerosol dithiothreitol-measured oxidative potential: Contrast between soluble and insoluble particles. *Environ. Sci. Technol.* **2017**, *51*, 6802–6811.
62. Baulig, A.; Garlatti, M.; Bonvallot, V.; Marchand, A.; Barouki, R.; Marano, F.; Baeza-Squiban, A. Involvement of reactive oxygen species in the metabolic pathways triggered by diesel exhaust particles in human airway epithelial cells. *Am. J. Physiol. Lung Cell. Mol. Physiol.* **2003**, *285*, L671–L679, doi:10.1152/ajplung.00419.2002.
63. Boland, S.; Baeza-Squiban, A.; Bonvallot, V.; Houcine, O.; Pain, C.; Meyer, M.; Marano, F. Similar cellular effects induced by diesel exhaust particles from a representative diesel vehicle recovered from filters and standard reference material 1650. *Toxicol. Vitr.* **2001**, *15*, 379–385, doi:10.1016/S0887-233300040-6.

64. Campbell, S.J.; Utinger, B.; Lienhard, D.M.; Paulson, S.E.; Shen, J.; Griffiths, P.T.; Kalberer, M. Development of a physiologically relevant online chemical assay to quantify aerosol oxidative potential. *Anal. Chem.* **2019**, *91*, 13088–13095, doi:10.1021/acs.analchem.9b03282.
65. Fushimi, A.; Saitoh, K.; Hayashi, K.; Ono, K.; Fujitani, Y.; Villalobos, A.M.; Schauer, J.J. Chemical characterization and oxidative potential of particles emitted from open burning of cereal straws and rice husk under flaming and smoldering conditions. Atmos. Environ. **2017**, 163, 118–127, doi:10.1016/j.atmosenv.2017.05.037.
66. Perrino, C.; Pietrodangelo, A.; Febo, A. An atmospheric stability index based on radon progeny measurements for the evaluation of primary urban pollution. Atmos. Environ. **2001**, 35, 5235–5244, doi:10.1016/S1352-2310(01)00349-1.
67. Perrino, C.; Catrambone, M.; Dalla Torre, S.; Rantica, E.; Sargolini, T.; Canepari, S. Seasonal variations in the chemical composition of particulate matter: A case study in the Po Valley. Part I: Macro-components and mass closure. Environ. Sci. Pollut. Res. **2014**, 21, 3999–4009, doi:10.1007/s11356-013-2067-1.
68. Canepari, S.; Astolfi, M.L.; Farao, C.; Maretto, M.; Frasca, D.; Marcoccia, M.; Perrino, C. Seasonal variations in the chemical composition of particulate matter: A case study in the Po Valley. Part II: Concentration and solubility of micro-and trace-elements. *Environ. Sci. Pollut. Res.* **2014**, *21*, 4010–4022, doi:10.1007/s11356-013-2298-1.

7.2 (C2) Effects of Operating Conditions on PM Oxidative Potential Assays

Atmospheric Environment (2022), 268, 118802, doi: 10.1016/j.atmosenv.2021.118802

Maria Agostina Frezzini[1,*], Nayma De Francesco[2], Lorenzo Massimi[1], Silvia Canepari[1]

[1] Department of Environmental Biology, Sapienza University of Rome, P.le Aldo Moro, 5, Rome 00185, Italy;

[2] Department of Chemistry, Sapienza University of Rome, P. le Aldo Moro, 5, Rome 00185, Italy;

*Corresponding author

Keywords: ascorbic acid (OP^{AA}) assay, dithiothreitol (OP^{DTT}) assay, 2',7'-dichlorofluorescein (OP^{DCFH}) assay, extraction method, PM filters' conservation.

Abstract

Oxidative potential (OP) has been suggested as a biologically relevant exposure metric for estimating particulate matter (PM) capacity to induce oxidative stress in living organisms. However, standardized experimental procedures are not yet available. This study explores how a variety of operating conditions influences responses of several different assays for measuring OP: the 2',7'-dichlorofluorescein (OP^{DCFH}), the ascorbic acid (OP^{AA}) and the dithiothreitol (OP^{DTT}) assays. A recently optimized method for the evaluation of PM reducing properties, based on the 2,2-diphenyl-1-picrylhydrazyl assay (RP^{DPPH}), was also included in the study. Two monitoring campaigns were carried out in Central Italy by using co-located PM_{10} samplers working in parallel, for comparing results obtained from different operating procedures simultaneously applied on equivalent samples.

Extraction efficiency and repeatability of three different water-extraction methods (rotating agitator, ultrasonic bath, and vortex), and the influence of storage duration and conditions on OP results were examined. OP^{DCFH} values were found to be significantly higher when ultrasonic bath (US) was used for extraction, probably due to the formation of free radicals induced by US; for all the OP assays, the highest repeatability was obtained by extracting samples with rotating agitator (RA). Sample storage was confirmed to be a very critical issue as all the assays, except OP^{DTT}, showed a marked dependence on storage time and conditions. The influence of membrane filters used to collect PM was also assessed. No significant differences were observed between samples collected on quartz and polytetrafluoroethylene (PTFE) membrane filters, except for OP^{AA}, that gave significantly higher results for samples collected on PTFE membranes. Lastly, the contribution of water-insoluble PM components to OP was examined and warrants further investigations.

1. Introduction

Airborne particulate matter (PM) pollution is one of the most significant threats for human health (Shiraiwa et al., 2017; Dong et al., 2019). It is now broadly confirmed that PM critically impacts human well-being through exposure to particles that can lead to a wide range of adverse health implications including respiratory and

cardiovascular disease, cancer, diabetes, as well as neurodegenerative disease (Uttara et al., 2009; Andersen et al., 2010; Øvrevik et al., 2019).

An actual common thesis claims that one of the biological key mechanisms involved in developing damaging health effects is the PM ability to induce cellular generation of reactive oxygen species (ROS), at the expense of antioxidant defenses, resulting in oxidative stress responses and in several chronic and acute systemic inflammations (Yang et al., 2014; Øvrevik et al., 2019; Cervellati et al., 2020). Oxidative potential (OP) of PM is considered one of the most relevant predictive factors for the assessment of PM toxicity (Delfino et al., 2011; Gupta et al., 2019), since it is intrinsically influenced by different physiochemical properties governing PM ability to cause oxidation of target molecules, including size, surface area as well as chemical composition (Andrade et al., 2020). Therefore, OP is frequently proposed as a more biologically appropriate metric for addressing human exposure than bulk PM mass concentration (Yang et al., 2016; Bates et al., 2019; Nishita-Hara et al., 2019).

Multiple acellular tests, based on the offline analyses of PM field filters, are available for quantifying particles oxidative potential (Bates et al., 2019), among which the most widely used are the ascorbic acid (OP^{AA}) and dithiothreitol (OP^{DTT}) assays, that evaluate the potential of PM components to deplete a physiological antioxidant and a cellular reductant surrogate, respectively (Cho et al., 2005; Stoeger et al., 2009; Campbell et al., 2019). In fact, ascorbic acid (AA) is the prevalent natural occurring antioxidant in the lung (Godri et al., 2010, 2011; Campbell et al., 2019), while dithiothreitol (DTT) acts as a chemical surrogate of cellular reducing agents, such as nicotinamide adenine dinucleotide (NADH) and nicotinamide adenine dinucleotide phosphate (NADPH) (Kumagai et al., 1997, 2002). The consumption of these antioxidants occurs when PM components catalytically transfer one electron from AA or DTT molecules to molecular oxygen, generating superoxide anion mimicking the crucial initial step of *in vivo* producing ROS (Kumagai et al. 2002; Gupta et al., 2019). Therefore, OP^{AA} and OP^{DTT} have considerable physiological relevance in the assessment of particle toxicity.

2',7'-dichlorofluorescein (OP^{DCFH}) assay is commonly used in biological field as an indicator of oxidative stress for quantifying cellular ROS generation, through a fluorescent-based probe (Venkatachari et al., 2005, 2007; Fuller et al., 2014). However, the test has been adapted to be performed on PM samples for determining total particle-bound ROS and, in the literature, it is conventionally included in OP assays (Hung and Wang, 2001; Simonetti et al., 2017; Zhou et al., 2018; Zhang et al., 2021).

Since there are still doubts and uncertainties regarding the most representative assay to quantify the OP of PM, the synergic application of different acellular methods on the same PM sample is often considered advantageous in providing insightful assessment of particles OP (Ayres et al., 2008; Frezzini et al., 2019; Lin and Yu, 2020; Manigrasso et al., 2020).

All the acellular assays are easy to reproduce in laboratories, they require fewer resources than cellular ones, and give quicker readouts of OP measurements (Yu et al., 2020; Bates et al., 2019; Gupta et al., 2019). In recent years, OP appeared to be the central paradigm in the assessment of PM toxicity, however, there are still several criticisms regarding the effectiveness of this metric to quantify the effects of ambient particles on human health. In fact, OP measurements are strongly influenced by synergic actions of multiple operating

conditions altogether. Among these, the PM filters extraction methods seem to alter OP quantification. In fact, although sonication is the most common approach, some studies underlined the impact of ultrasounds on OP measurements as a result of both the increase of free radicals in the systems, and the degradation of some compounds (Mutzel et al. 2013; Khurshid et al., 2014; Miljevic et al., 2014). This evidence has provided motivation for conducting further investigations to identify an extraction method not affecting OP results. Alternative extraction methods to sonication, such as rotating agitator and vortex, were used in some studies (Perrone et al., 2016; Frezzini et al., 2019), but, to the best of authors knowledge, a systematic comparison among the different extraction techniques has never been undertaken so far.

Another potential factor altering OP measurements is the time delay between filter sampling and OP analyses, that seems to play a crucial role in underestimating particles OP, due to the possible decomposition and/or chemical transformation of the highly reactive components, prior to analysis (Fuller et al., 2014; Campbell et al., 2019). Indeed, it has already been suggested that the aging of the particles on membrane filter surfaces can cause an underestimation of collected reactive species (Hedayat et al., 2015). This is further supported by the previously estimated presence of reducing species in PM (Frezzini et al., 2019) that could reasonably react with oxidizing ones over time, leading to an underestimated OP. Therefore, the assessment of the influence of sample storage conditions and duration on the quantification of PM oxidative potential is essential. In addition, in the literature, most of the OP assays have been applied to polytetrafluoroethylene (PTFE) filters (Yang et al., 2014). However, other types of filters have also been used, , such as quartz filters. Indeed, there is still a lack of information regarding the effect of the type of filter used for the OP measurement.

Lastly, another additional challenge in optimizing OP acellular measurements is assessing the contribution of insoluble species to PM redox activity. OP assays are usually performed on water-soluble fraction of PM samples, that is considered more bioaccessible than the water-insoluble fraction (Shao et al., 2017; Gao et al., 2020). However, a growing scientific evidence underlined the considerable toxicological potential of insoluble particles, showing that it also plays an important role in generating oxidative damage, such as the disruption of the cell membrane (Knaapen et al., 2002; Daher et al., 2011; Zou et al., 2016; Conte et al., 2017; Gao et al., 2017; Piacentini et al., 2019). For example, Akhtar et al. (2010) found that redox-active substances could be strongly bound to solid particles, not completely extracted by water. Furthermore, Yi et al. (2014) demonstrated the capacity of PM insoluble fraction to induce oxidative stress and damage in human lung epithelial cells. Overall, an increasing number of recent findings suggest that the integration of the contribution of water-insoluble species in the OP assessment would be closer to a realistic PM exposure, elucidating actual PM induced health risks.

In general, the use of so many different analytical procedures, coupled with the lack of standardized operating conditions, adds variation in experimental design among laboratories that may contribute to differences between OP results, making a challenge to representatively compare inter-laboratory data (Guo et al., 2019; Lin and Yu, 2019). Therefore, this study is aimed to investigate variability in OP (OP^{DCFH}, OP^{AA}, OP^{DTT}) responses depending on the operating conditions under which the tests are performed. In particular, the influence of extraction method, filter-storage and time delay between PM sampling and analysis, on OP

measurements, were assessed. Furthermore, the influence of the type of filter used on OP results was evaluated. Redox equilibria among PM native species were deepened, due to the use of an assay for estimating the amount of reducing species in PM, defined reducing potential method (RP^{DPPH}; 2,2-diphenyl-1-picrylhydrazyl assay, DPPH) (Frezzini et al., 2019). Then, the contribution of water-insoluble PM components to aerosol OP was examined, in order to assess their role in particle oxidative activity. To the best of authors knowledge, no study has been published so far on the effects of so many operating conditions altogether on OP measurements.
The goal of this study is to gain more information about the driving forces of OP measurements, thus giving a contribution to the standardization of experimental procedures.

2. Materials and Methods

2.1. Sampling sites and methods

A summer and a winter monitoring campaign were carried out to collect PM_{10} field filters to be used for the experimental procedures as reported in Figure 1 that shows the block diagram of the conducted experimental tests. For the summer monitoring period, six PM_{10} sequential samplers working in parallel at the flow rate of 2.3 m^3/h (SWAM5a Dual Channel Monitor, FAI Instruments, Fonte Nuova, Rome, Italy) were employed for 15 days, from July 18th to August 01st , 2019 at the C.N.R. Institute of Atmospheric Pollution Research, located in Montelibretti (geographical coordinates: 42°06′20.55″N; 12°38′24.53″E), a peri-urban area near Rome (Central Italy)

For the winter period, two single-line and one double-line samplers, working in parallel at 2.3 m^3/h, were used (Giano and Gemini, respectively; Dadolab Srl, Cinisello B., MI, Italy) for 42 days, from February 2nd to March 19th, 2020, at the Experimental Botanic Garden of the Sapienza University of Rome, an urban area of Rome (Central Italy; geographical coordinates: 41°54’8.63’’N; 12°31’3.45’’E). All the samplers were equipped with a sampling head for PM_{10} certified UNI EN 12341 (2014). Polytetrafluoroethylene membranes (PTFE, 47 mm diameter, pore size 2µm, Cobetter Filtration Equipment Co., Ltd, Hangzhou, China) were used for the samplings and 24-h PM_{10} field filters were daily collected for both the monitoring campaigns. Quartz PM_{10} filters were parallelly sampled (QM-A quartz filters, 37 mm, Whatman) for 10 days during the winter monitoring campaign. In total, over 250 PM_{10} field filters were collected and analyzed.

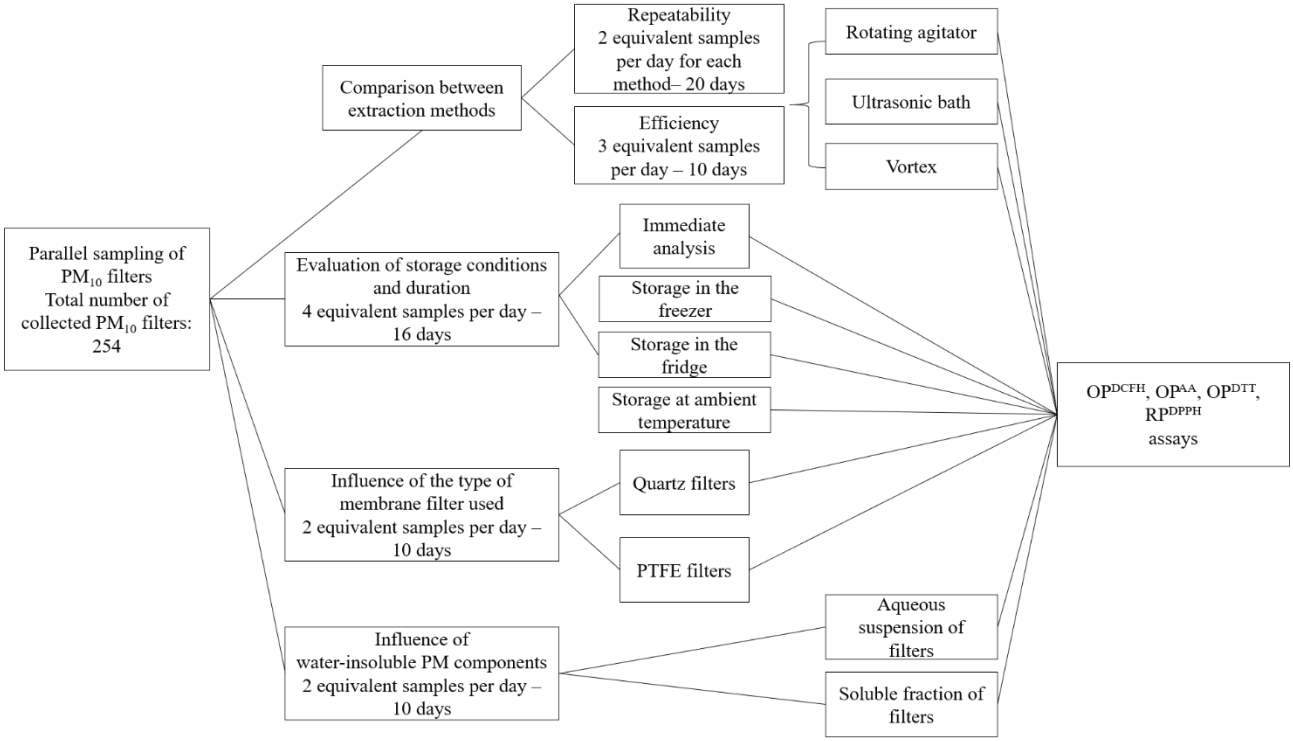

Figure 9. Block diagram summarizing the conducted experimental test of the study.

2.2. Experimental design

PM_{10} collected on PTFE membrane filters was treated by following a previously optimized and detailed procedure (Massimi et al., 2017; 2020a). Briefly, after the removal of the supporting polymethylpentene ring from each sampled filter, apart from some exceptions specified in the text, PTFE membranes were immersed in 10 mL of deionized water (produced by Arioso UP 900 Integrate Water Purification System, USA) and then treated by subsequent different experimental approaches as described below and filtered through a nitrocellulose filter (NC filter; pore size 0.45 µm, Merck Millipore Ltd., Billerica, MA, USA) before analysis.

2.3. Oxidative and Reducing potential measurements

The DCFH, the AA and the DTT assays were used to assess the OP of PM_{10} samples, while the DPPH assay was used for the measurement of the reducing potential.

2.3.1. DCFH assay

DCFH is a non-fluorescent reagent becoming fluorescent dichlorofluorescin (DCF) upon reaction with ROS (Venkatachari et al., 2005) and it is used in combination with horseradish peroxidase (HRP; Sigma–Aldrich, USA), a redox enzyme mainly reacting with hydrogen peroxide and organic hydroperoxides, to catalyze the reactions (Bates et al., 2019; Fuller et al., 2014). DCFH solution was prepared from 2', 7'-dichlorofluorescin diacetate (DCFH-DA; Sigma–Aldrich, USA) according to the procedure provided by Simonetti et al. (2018). Briefly, 125 µL of DCFH reagent (5 µM) and 5 mL of HRP (0.5 units mL^{-1}) dissolved in a sodium phosphate buffer (pH 7.4; 25 mM) were added to 1.5 mL of the extracted solution of PM samples. The reaction mixture was placed in the thermostatically controlled water bath at 37 ºC. After 5 minutes, the concentration of DCF was measured by using fluorescent spectroscopy (Jasco FP-920; excitation at 427 nm, emission at 530 nm).

Standard H_2O_2 solutions (5×10^{-8}, 1×10^{-7}, 2×10^{-7}, 5×10^{-7} and 1×10^{-6} M) were daily used to plot a calibration curve to convert the obtained fluorescence intensity into H_2O_2 equivalents, which are used as indicators of the reactive species reactivity, thus obtaining OP^{DCFH} values (nmol H_2O_2 m^{-3}).

2.3.2. AA assay

For the measurement of AA depletion, the method reported by Fang et al. (2016) was followed with slight modifications. 300 µL of phosphate buffer (0.5 mM) and 100 µL of AA reagent (2 mM; Sigma–Aldrich, USA) were added to 2.5 mL of sample solution. Then, absorbance of the reaction mixture was recorded at 265 nm wavelength, at different reaction times (0, 10 and 20 minutes) by using UV-Vis absorption spectrometry (Varian Cary 50 Bio UV-Vis; Varian Inc., Palo Alto, CA, USA). Blanks were always measured in parallel. OP^{AA} was calculated as the AA consumption rate per sampled volume (nmol AA min^{-1} m^{-3}) according to the equation reported in supplementary material S1.

2.3.3. DTT assay

For the OP^{DTT} protocol, three aliquots of sample solution (0.7 mL) were incubated at 37 °C with 0.1 mL of DTT (1 mM; Sigma–Aldrich, USA) and 0.2 mL of potassium phosphate buffer (1 M) for different reaction times (0, 10 and 20 minutes). Then, 1 mL of trichloroacetic acid (10%TCA; Sigma–Aldrich, USA) was added to the mixture to quench DTT reactions. An aliquot (1 mL) was taken from the solution and mixed with 2 mL of tris-buffer (0.08 M, containing EDTA 4 mM) and with 50 µL of 5,5-dithiobis-2-nitrobenzoic acid (DTNB; Sigma–Aldrich, USA) to form 2-nitro-5-mercaptobenzoic acid (TNB) by reacting with the residual DTT, then measured at 412 nm by using UV-Vis spectrometer. Furthermore, blanks were measured in parallel to samples. OP^{DTT} was expressed as DTT consumption rate per sampled PM volume (nmol DTT min^{-1} m^{-3}), according to the equation reported in supplementary material S1.

2.3.4. DPPH assay

The assay is based on the quantitative measurement of the scavenging capacity of antioxidants towards DPPH free radical by the decrease in absorbance. DPPH assay was previously applied to PM samples with the aim to evaluate the presence of reducing species, thus integrating information about PM redox properties (Frezzini et al., 2019).

Operating in the dark, 2 mL of EtOH 96% and 0.5 mL of DPPH 0.1 mM ethanolic stock solution (Sigma–Aldrich, USA) were added to one aliquot (1.5 mL) of the water-extracted sample solution and the mixture was shaken for 30 min by rotating agitation. The absorbance of the solutions was recorded by UV-Vis spectrophotometry set at 517 nm, by measuring the sample absorbance decrease against the control (blank solution). The DPPH radical scavenging effect resulted in solution decolorization and was calculated in terms of percentage consumption of DPPH per sampled PM volume (RP^{DPPH}; %DPPH Cons m^{-3}), according to the equation reported in supplementary material S1.

2.4. Comparison between extraction methods

The repeatability of OP and RP measurements obtained using the selected extraction techniques was evaluated carrying out binary comparison between twin filters collected in both the monitoring campaigns. Therefore, for each extraction method, 20 pairs of equivalent samples were considered. The PM_{10} duplicate filters (filter A and filter B), immersed in 10 mL of deionized water were subjected to different extraction methods for 30 minutes: the rotating agitation (RA; Rotator, 60 rpm; Rotator, Glas-Col, USA), the sonication (US; Ultrasonic bath; Proclean 10.0 ultrasonic cleaner, Ulsonix, Germany) or the vortexing (V; Vortex Genie 2, 2000 rpm; Scientific Industries, Bohemia, New York). Then, the obtained solutions were filtered through a nitrocellulose filter (NC filter). The water-extracted solutions were thus split in their respective aliquots for the subsequent analyses. Then, OP assays (OP^{DCFH}, OP^{AA} and OP^{DTT}) were performed on the soluble fraction of samples. To evaluate the repeatability of analytical results of OPs performed on PM samples extracted by the different procedures, for each OP assay, the mean relative percentage differences (Δ%) are calculated as averages of the relative errors of each pair of PM_{10} twin filters (δ_i%), as follows:

$$\delta_i\% = \left[\frac{\left|\left(OP^X_{A,i} - OP^X_{B,i}\right)\right|}{\left[\left(OP^X_{A,i} + OP^X_{B,i}\right) \div 2\right]}\right] \cdot 100$$

where OP_A and OP_B are the OP values obtained for the filter A and B, respectively, X can indicate DCFH, AA, DTT or DPPH and i is the considered pair of PM_{10} filters.

The repeatability of each extraction method, and for each assay, was also assessed by calculating the linear regression between the duplicate filters (A vs B):

$$OP_A = mOP_B + q$$

where $m = 1$ and $q = 0$ indicate a perfect equivalence between A and B.

RA, US, and V were also compared in terms of extraction efficiency, that was quantitatively assessed by comparing OP values of daily equivalent samples subjected to different extraction methods. In this case, 3 equivalent samples were collected during 10 days of the winter monitoring campaign. The paired sample *t*-test was used to observe the significance of the differences of results obtained by each extraction method. A *p*-value less than 0.05 was considered statistically significant.

2.5. Sample storage conditions and duration

The effects of both sample storage conditions and time delay between filters sampling and analyses were observed by using four lines (A, B, C and D) of PM_{10} filters sampled in parallel for 15 days during the winter monitoring campaign.

PM_{10} equivalent filters were treated by following a different experimental design for each line:

- line A: each sampled filter was taken from the unloader and immediately analyzed;
- line B: each PM_{10} field filter was taken immediately after its collection, put in petri dish sealed with parafilm, and stored in a freezer at -20°C for 15 days under controlled temperature and humidity before being analyzed;

- line C: each sampled filter remained for 15 days inside the sampler's unloader under constant and controlled temperature due to a Peltier conditioning system, before being subjected to the subsequent analytical procedures;
- line D: each PM_{10} field filter was left into the sampler's unloader for 15 days under constant and controlled temperature due to a Peltier conditioning system and then, put in petri dish sealed with parafilm and stored in a fridge at 4°C for 15 additional days under controlled temperature and humidity, prior to the OP procedures.

In this experimental stage, all the collected PM_{10} filters were extracted by rotating agitator, filtered (NC filters), and then analyzed. The paired sample *t*-test was used to observe significant differences between PM filters from the four sampling lines for each OP assay.

2.6. Influence of membrane filter used

The comparison between OP and RP results obtained from quartz and PTFE filter (Q and P, respectively) was performed by sampling a pair of equivalent PM_{10} filters during 10 days of the winter monitoring campaign. Two sampling lines were thus equipped with quartz and PTFE filters. Then, OP and RP assays were applied to the water-soluble fraction of both Q and P filters as described in 2.3. section. The paired sample *t*-test was used to observe whether the filter type used significantly influenced the OP and RP results.

2.7. Water-insoluble PM components redox activity

The contribution of the water-insoluble components to PM redox potential was evaluated by sampling a pair of equivalent PM_{10} filters for 10 days during the winter monitoring campaign, on the same days as PM_{10} filters were collected for Q and P comparison. The two equivalent samples were used for performing OP and RP directly on the aqueous suspension of the field filters to determine total redox properties (i.e. soluble plus insoluble; OP^T; RP^T). The obtained OP^T and RP^T were compared to OP and RP of water-soluble fraction (OP^{WS}; RP^{WS}) measured on P membranes (section 2.6.). In order to measure OP^T and RP^T, each PM_{10} filters was cut into four equal parts (8 equivalent pieces in total) and used as described above:

- a quarter of each filter was extracted in 1.5 mL of deionized water. Then the DCFH assay was directly applied on the water-extracted solution by following the procedure detailed in 2.3.1. section;
- three quarters of each filter were extracted in 2.5 mL of deionized water, and then used for the three reaction times of AA procedure described in 2.3.2. section;
- three quarters of each filter were extracted in 0.7 mL of deionized water. The obtained suspensions were used for the three reaction times of DTT procedure described in 2.3.3. section;
- a quarter of each filter was extracted in 1.5 mL of deionized water. The DPPH procedure was applied on the obtained suspension as described in 2.3.4. section.

The paired sample *t*-test was used to observe significant differences between OP^T and OP^{WS} for each OP method.

3. Results and Discussion

3.1. Influence of extraction methods on PM redox measurements

The influence of the considered extraction methods (RA, US, and V) on OP and RP results was investigated by assessing the repeatability on 20 twin pairs of PM filters (A and B), extracted by the three selected techniques. The regression parameters obtained between the duplicate filters were reported in Table 1, along with the mean relative percentage difference (Δ%) of each pair of filters for each extraction method and the range of OP and RP values.

Data showed that RA extraction allows obtaining the best repeatability of results. In the case of OP assays, the Δ% were always lower than 20%, the R^2 always greater than 0.90, the *m* very close to 1 (range 0.95 – 0.97) and the *q* were well below the minimum of OP values (less than 10% of those values). The lowest repeatability was obtained by using V that leads to high Δ% (> 30%) and to unsatisfactory linear regression parameters ($0.30 < R^2 < 0.70$). RP^{DPPH} showed regression parameters less acceptable than the OP assays, with all the studied extraction methods, with R^2 ranging from 0.62 to 0.75, probably due to the lower variability range. However, Δ% values were still acceptable in the case of RA extraction (Δ% = 16%).

The regression parameters showed the good linearity of RA for all the three OP assays, as opposed to US and V that do not guarantee a good analytical repeatability of OP measurements. The OP^{DCFH}, OP^{AA}, OP^{DTT} and RP^{DPPH} values obtained for each considered twin pair of PM_{10} filters are reported in supplementary material S2 (Table S2).

Figure 2 reports the OP and RP values related to the evaluation of the extraction efficiency of the three considered methods and the *p*-values of the sample paired *t*-test. Differences between results obtained from samples extracted by different methods were not significant for all the OP and RP assays, except for OP^{DCFH} (panel a), that showed significantly higher values when PM filters were extracted with US ($p < 0.05$ for US vs RA, and US vs V). This is in accordance with previous studies that underlined the role of sonication in producing free radicals, due to thermal reactions and degradation (Hung and Wang, 2001; Kurshid et al., 2014). In fact, as already known, ultrasonic waves can generate cavitation bubbles in the extraction solution, and their collapse leads to high temperature and pressure conditions. Consequently, the molecules inside the cavitation bubbles can undergo pyrolysis, that results in free radicals' generation (Mutzel et al., 2013; Miljevic et al., 2014; Massimi et al., 2020b). The formation of these species may originate positive artifacts altering the obtained OP values, thus overestimating radicals' content in PM samples (Mutzel et al., 2013; Miljevic et al., 2014). Therefore, the highest OP^{DCFH} values found in samples extracted by US are not indicative of higher extraction efficiency of US, but of the generation of radical species.

Although RA and V gave similar OP values, thus appearing to be efficient extraction methods for OP analysis, RA emerged as the most suitable method for the extraction of PM filters and subsequent OP analysis, since it showed high repeatability and avoided the generation of free radicals upon ultrasonic irradiation.

Table 1. Linear regression values, variability range (minimum–maximum) and mean relative percentage differences (Δ%) of the 20 pairs of A and B twin filters.

	OP^{DCFH}				
	R^2	m	q (nmol H_2O_2 m^{-3})	Range (nmol H_2O_2 m^{-3})	Δ%
RA	0.98	0.96	$-4.1\cdot10^{-10}$	$2.8\cdot10^{-9}$ - $6.5\cdot10^{-8}$	19
US	0.67	0.95	$1.1\cdot10^{-9}$	$1.8\cdot10^{-9}$ - $1.5\cdot10^{-8}$	26
V	0.54	0.56	$3.2\cdot10^{-9}$	$2.1\cdot10^{-9}$ - $2.8\cdot10^{-8}$	34
	OP^{AA}				
	R^2	m	q (nmol AA min^{-1} m^{-3})	Range (nmol AA min^{-1} m^{-3})	Δ%
RA	0.95	0.95	0.0097	0.91 - 15	20
US	0.77	0.88	0.51	0.18 - 7.5	98
V	0.71	0.81	0.42	0.39 - 3.4	44
	OP^{DTT}				
	R^2	m	q (nmol DTT min^{-1} m^{-3})	Range (nmol DTT min^{-1} m^{-3})	Δ%
RA	0.91	0.97	-0.019	0.46 - 2.7	16
US	0.62	0.86	0.22	0.16 - 1.8	23
V	0.31	0.81	0.26	0.38 - 3.1	97
	RP^{DPPH}				
	R^2	m	q (%Cons DPPHm^{-3})	Range (%Cons DPPHm^{-3})	Δ%
RA	0.75	0.81	0.23	0.14 - 1.7	16
US	0.69	0.61	0.13	0.031 - 1.2	50
V	0.62	0.69	0.075	0.11 - 0.67	31

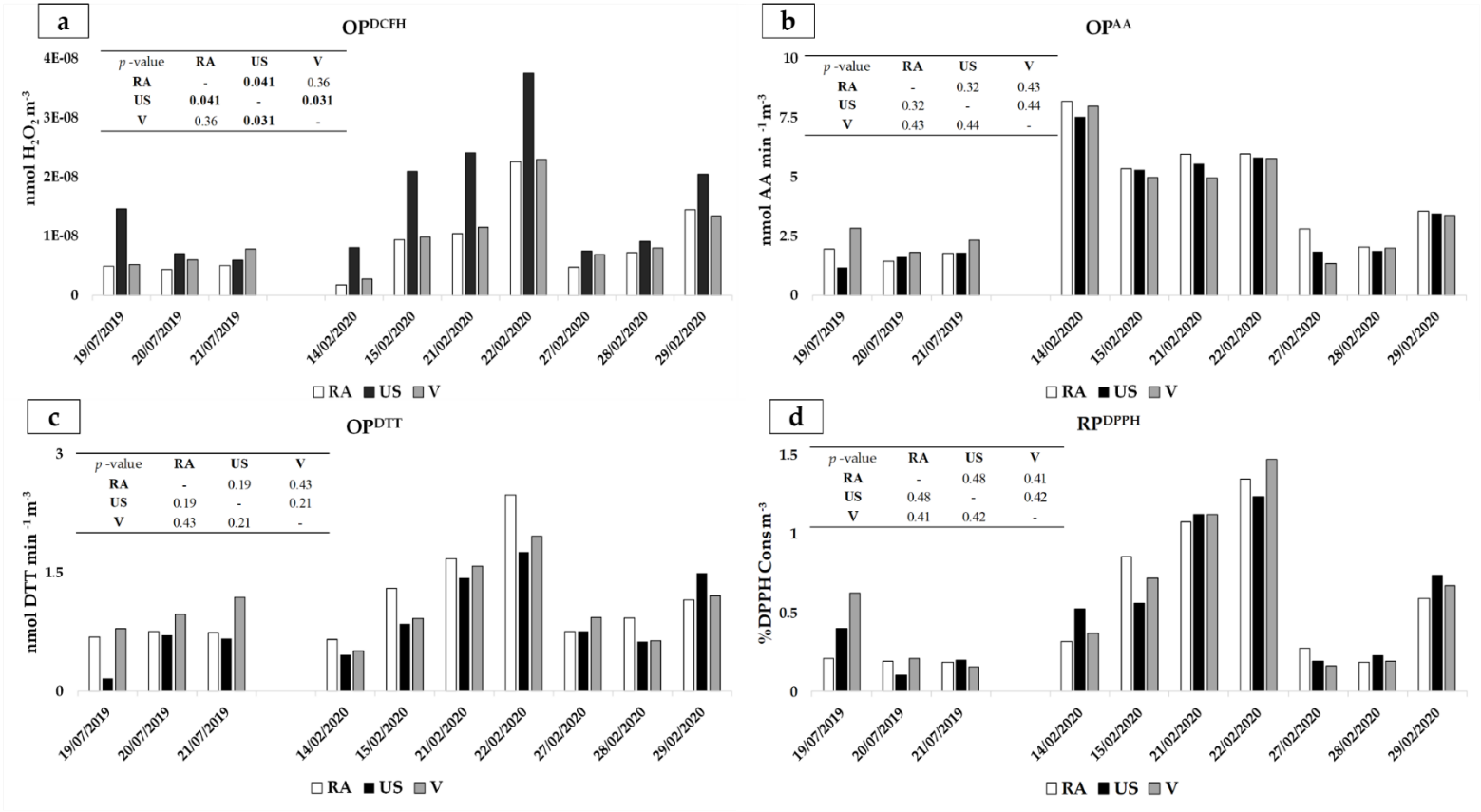

Figure 2. Comparison of OP^{DCFH} (panel a), OP^{AA} (panel b), OP^{DTT} (panel c) and RP^{DPPH} (panel d) between equivalent filters extracted by using the three different techniques: rotating agitator (RA), ultrasonic bath (US) and vortex (V) and the *p* values of the sample paired *t*-test between the three extraction methods. The *p*-value in bold indicate significant differences ($p < 0.05$).

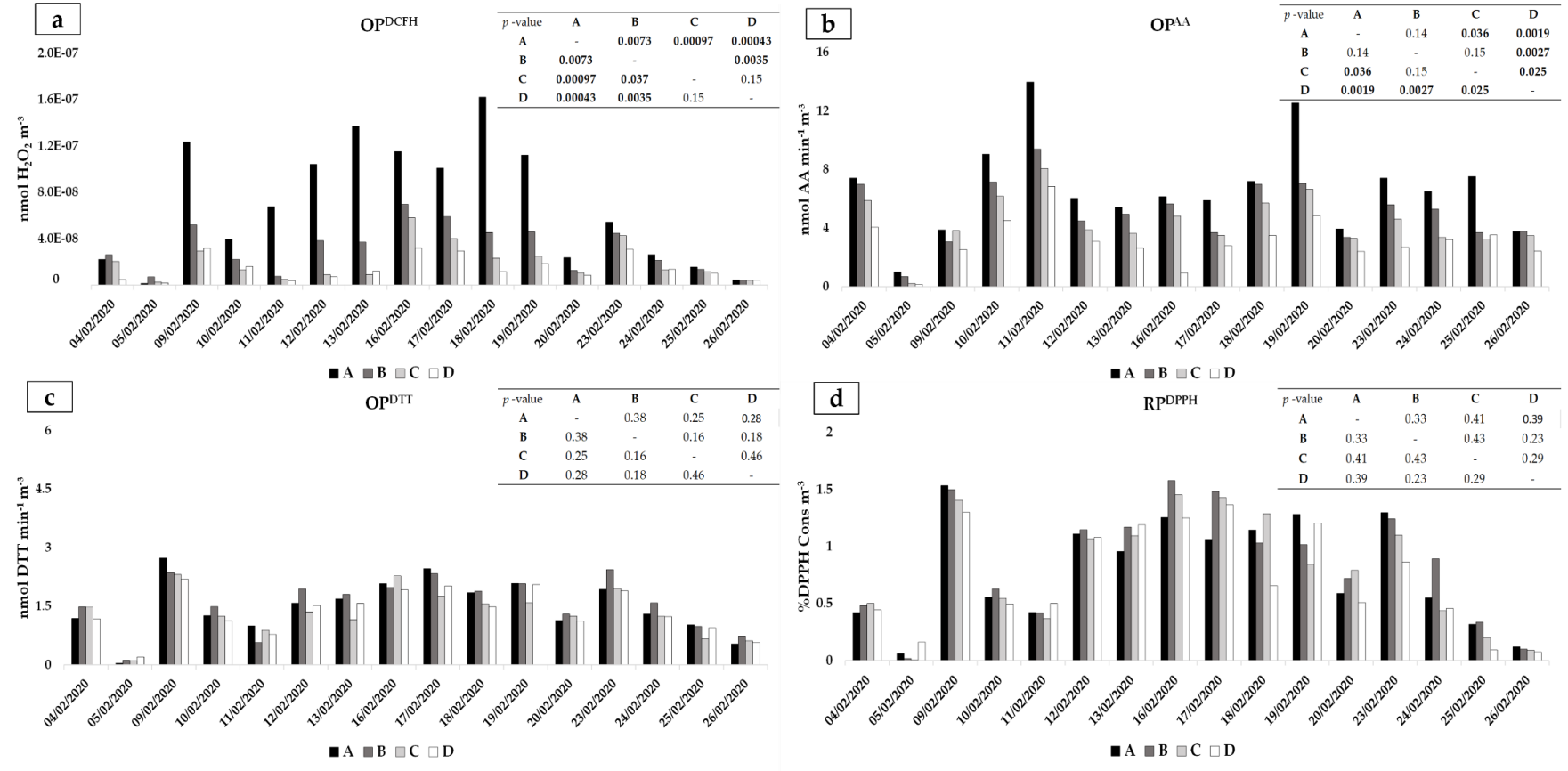

Figure 3. Comparison of OP^{DCFH} (panel a), OP^{AA} (panel b), OP^{DTT} (panel c) and RP^{DPPH} (panel d) between filters subjected to different sample storage condition and duration: A, filters were immediately analyzed after sampling; B, filters were stored in a freezer at -20°C for 15 days before being analyzed; C, filters remained in the samplers' unloader for 15 days before being analyzed; D, filters remained in the samplers' unloader for 15 days and then, stored in a fridge at 4°C for 15 additional days before being analyzed. The *p*-values of the sample paired *t*-test between the four conditions are reported. The *p*-value in bold indicate significant differences ($p < 0.05$).

3.2. Influence of sample storage conditions and duration on PM redox measurements

According to the results from 3.1 section, all the PM_{10} filters used for the evaluation of storage conditions and duration were water-extracted by RA. Results of OP^{DCFH}, OP^{AA}, OP^{DTT} and RP^{DPPH} and the *p*-values of the sample paired *t*-test are reported in Figure 3.

OP^{DCFH} (panel a) values highlighted that DCFH measurements were simultaneously influenced by both sample storage conditions and duration. In fact, OP^{DCFH} was generally higher in samples from line A, whose filters were immediately analyzed after their collection. Line B, whose filters were rapidly placed in the freezer after their collection and analyzed after 15 days, showed OP^{DCFH} values mostly lower than those from line A. Samples from line C were left inside the sampler's unloader for 15 days prior to their analyses and exhibited DCFH values lower than those from lines A and B. Differences between line B and C showed that, within the same sample storage duration, the conditions of filters storage can greatly influence DCFH measurements. Lastly, the lowest DCFH values were obtained from line D filters, that were left into the sampler's unloader for 15 days and then stored in the fridge for 15 additional days, prior to measurements. The paired sample *t*-test showed a significant effect of different storage conditions and duration (A vs C, A vs D, A vs B, B vs D; $p < 0.01$) for DCFH assay. These results agree with previous studies that underlined the short lifetime of sampled particle-bound ROS, generally ranging from only a few minutes to one or more days (Venkatachari et al., 2005; Bates et al., 2019). Although online techniques to quantify the short-lived and labile fraction of particle-bound ROS with DCFH are strongly suggested (Wragg et al., 2016), ROS are still mainly quantified by offline assays in extracts of aerosol particles collected on filters (Fuller et al., 2014; Daellenbach et al., 2020). Therefore, OP^{DCFH} results from this study confirm that the application of this assay to sampled PM filters may be particularly critical, as only the long-lived fraction of ROS remains over time. Therefore, OP^{DCFH} measurements should be performed as rapidly as possible after sampling and, anyway, after an appropriate standardization of storage conditions and durations.

The OP^{AA} showed a clear trend (panel b) with values in the order A > B > C > D with significant differences between B vs D and A vs D ($p < 0.01$) and between A vs C and C vs D ($p < 0.05$). It is well known that the OP^{AA} assay is particularly sensitive toward transition metals (i.e. Cu, Fe, Mn, Sb) generated by non-exhaust traffic emissions, such as brake abrasion and re-suspended dust (Simonetti et al., 2018; Perrone et al., 2019; Lin and Yu, 2020). Consequently, these results may be then interpreted by considering that PM collected on filters might undergo chemical alteration during sampling or storage, such as change in the oxidation state of metals, or alteration of the solubility of redox-active metals (Majestic et al., 2007; Fang et al., 2017; Puthussery et al., 2018). Therefore, collected species responsible for OP^{AA} seem to be subjected to changes over time determining a decrease in their oxidizing capability.

Results from DTT assay (panel c) revealed no significant differences between sample storage conditions and duration, remaining almost constant over time, probably because of the high stability of species responsible for OP^{DTT} (Bates et al., 2019). To give an example, OP^{DTT} has large organic species dependence, among which quinones, that can be directly emitted from traffic or formed from secondary oxidation, are considered remarkably persistent for a considerable time (Valavanidis et al., 2005; Wang et al., 2018).

The DPPH radical scavenging activity of sampled PM (panel d) did not seem to change in relation to filters storage time and conditions. Although not much is yet known about the chemical species responsible for the PM reducing activity, the results from this experimental stage highlighted the stability of this assay for the prediction of the chemical species involved in PM reducing properties.

The results obtained from this experimental stage are closely related to the key research topic focused on testing OP as an air quality metric and to study its biological relevance, that is still under research and investigation. Some studies already reported important findings that, for example, identified short lifetime oxidant species in a fraction of organic aerosols (Brown et al., 2020; Zhang et al., 2021). In this experimental work, the speciation of redox species to identify stable and unstable compounds is not available and is out of the scope of the study.

Overall, at least for the OP^{DCFH} and OP^{AA} assays, these results showed a very significant role of samples storage conditions and durations, which have been poorly investigated in the literature. It is worth noting that the decrease of the values seems not to be constant for each sample and that, for this reason, the variability among samples may be dependent on storage conditions and duration. Consequently, although the OP measured on filters stored for a long time still represents the most adopted procedure (Bates et al., 2019) it could not be truly representative of the real potential of ambient particles to generate reactive species. In support of this evidence and based on current literature, the OP^{DTT} is the assay most relevant to health, due to its greatest associations to health endpoints (Bates et al., 2015, 2019; Fang et al., 2016; Abrams et al., 2017). Otherwise, OP^{AA} still presents a limited utility in epidemiological studies due to the lack of direct associations with adverse health endpoints (Atkinson et al., 2016; Fang et al., 2016).

Given the ROS decay behavior, recent studies presented online measurement technologies to measure OP of PM and could constitute a valid alternative to avoid the loss of reactive species before analyses reducing the time delay before sampling and analysis and possible degradation of compounds on filters. These studies confirmed that OP online measurements, through direct PM sampling into the liquid phase and measurement within a few minutes, are useful and necessary for reliable ROS quantification (King and Weber, 2013; Fuller et al., 2014; Wragg et al., 2016; Eiguren-Fernandez et al., 2017; Puthussery et al., 2018; Zhou et al., 2018; Brown et al., 2019; Campbell et al., 2019). Some of these systems have also given excellent results in terms of collection efficiency of particles (Orsini et al., 2003; Brown et al., 2019). However, although OP online measurements represents an exciting challenge in atmospheric pollution research, offline assays are still mostly performed, as mentioned above (Bates et al., 2019).

3.3. Influence of the type of filter used on PM redox measurements

The comparison between results obtained measuring OP on Q or P filters that were sampled in parallel is reported in supplementary material S3 (Figure 1.S3). OP^{DCFH}, OP^{DTT} and RP^{DPPH} did not appear to be significantly influenced by the choice of the membrane filter. Conversely, a significant effect of the type of filter used was observed for the AA assay ($p < 0.01$). In fact, OP^{AA} on PTFE was found to be generally higher than OP^{AA} on quartz. These results partially reflect those reported by Yang et al. (2014): the attenuation of the OP^{AA} of Q filters might suggest lower extraction efficiency of the OP reactive species from the quartz filters

compared to PTFE filters. On the other hand, OP^{DCFH}, OP^{DTT} and RP^{DPPH} values were less affected by the type of filter used, indicating that reactive components for these assays were efficiently extracted from the quartz as well as from the PTFE filters.

3.4. Influence of water-insoluble PM components redox activity on PM redox measurements

The active role of PM insoluble fraction in determining OP and RP values was assessed by performing OP and RP assays directly on the aqueous suspension of filters, after the extraction with RA and without any preliminary filtration step. Consequently, the effect of both water-soluble and water-insoluble components of PM on its redox potential were simultaneously observed, by adding reagents of each assay directly in contact with the sampled filter (Khurshid et al., 2019). The comparison of OP and RP results between the total and the water-soluble fraction of PM filters (T and WS, respectively) is reported in supplementary material S3 (Figure 2.S3).

Regarding the OP^{DCFH} and OP^{DTT} assays, the *p* value between the total (soluble plus insoluble) and the water-soluble fraction is 0.41 and 0.06, respectively, indicating that the contribution of the water-insoluble PM components redox activity on OP^{DCFH} and OP^{DTT} measurements is not quite significant, at least as far as this set of samples, also considering that the size of the dataset is rather limited. Results showed that OP^{T} is comparable (or even lower than) to OP^{WS}, contrary to what emerged from studies that demonstrated a very relevant contribution of the PM insoluble fraction to OP (Verma et al., 2012; Conte et al., 2017; Piacentini et al., 2019). A possible explanation to these results is that most of the particles of the sampled PM were fixed too deeply in the filter to fully interact with the reagents of the assays. This also represents a possible contribution to the uncertainty of the results. Nevertheless, different studies have claimed that the PM water-soluble fraction shows a higher correlation with OP metrics compared to the insoluble one (Szigeti et al., 2015). Conversely, OP^{AA} results highlighted significant differences between values obtained for T and WS fraction ($p < 0.01$). It is well known that OP^{AA} is particularly sensitive to elements tracing non-exhaust traffic emissions, that mainly constitute the insoluble fraction of PM (Conte et al., 2017; Massimi et al., 2020b). It is therefore possible that a part of these elements significantly influence OP^{T}. RP^{DPPH} shows a similar pattern to that of OP^{AA}, with OP^{T} values significantly higher than OP^{WS} ($p < 0.01$). These findings confirm previously obtained results that have shown higher RP^{DPPH} values for the insoluble fraction of PM, attributable to the contribution of non-exhaust vehicular traffic to RP (Frezzini et al., 2019).

The results of this experimental step does not allow to clarify the real contribution of PM water-insoluble fraction to PM redox potential. Undoubtedly, also the choice of extraction solvent definitely influences the extraction of PM species (Yang et al., 2014). Previous works investigated the contribution of PM insoluble species extracted through different extraction media, such as organic solvents (Calas et al., 2017; Gao et al., 2017; Pietrogrande et al., 2021). In this work the selected extraction media was the water in order to attempt the evaluation of OP due to the water-insoluble fraction of particles. Therefore, results from WS vs T comparison were due to the limitation of the detection method and not to the concrete lack of contribution of

the insoluble fraction to the OP. Furthermore, the operatively difficult of performing OP assays directly on particles that are embedded in the membrane support is not negligible.

To conclude, knowledge of the insoluble chemical species responsible for the possible contribution to redox potential of particles, as well as the mechanisms involved in PM redox activities, would be useful to elucidate the relative health risks for specific health endpoints and, thus, need to be deepened.

4. Conclusions

In this work, the effects of different operating conditions on redox measurements of PM_{10} field filters was assessed. This study highlights the influence of multiple operating conditions on measured oxidative and reducing potential from which necessarily derives the need of standard protocols for obtaining reliable and comparable data, in order to improve the ability of OP to predict health outcomes.

The extraction methods (rotating agitator, ultrasonic bath, and vortex) were compared in terms of repeatability and efficiency and were shown to influence the repeatability of OP^{DCFH}, OP^{AA} and OP^{DTT} and RP^{DPPH} whose best values were obtained by rotating agitator that has proved to be the most suitable PM_{10} extraction method for obtaining repeatable OP data. Results of the extraction efficiency confirmed that sonication of PM_{10} filters leads to the generation of ultrasound-induced radical species that particularly affect OP^{DCFH} values. These positive artifacts should be considered in interpreting results of redox measurements.

The most relevant findings are related to the effects of storage conditions and duration of PM_{10} filters. Although the filters conservation had not influence on OP^{DTT} and RP^{DPPH} values, storage conditions and duration were shown to be extremely significant for OP^{DCFH} and OP^{AA}, leading to outstanding concerns of the reliability of these offline assays for the prediction of the ROS generation pathways in real-word conditions. This aspect should therefore be carefully deepened in order to fully understand which oxidative species are short living, and which ones are long living, thus ensuring more robust evaluation systems in determining OP of PM.

The type of filter used was found to be relevant for the measurement of OP^{AA} values that appeared to be significantly higher when PTFE filters were used.

Ultimately, the role of the PM water-insoluble particles in determining PM redox potential was assessed. Although the redox activity of the insoluble fraction of PM provided a significant contribution to the OP^{AA} and RP^{DPPH} values, its study still merits further investigations.

This study highlights the influence of multiple operative conditions on redox measurements from which necessarily derives the need of standard protocols for obtaining reliable and comparable data, in order to improve the assurance of OP to predict health outcomes.

Author contribution

M.A. Frezzini: Conceptualization, Investigation, Methodology, Data curation, Writing-Original draft preparation N. De Francesco: Investigation, Methodology L. Massimi: Reviewing and Editing S. Canepari: Conceptualization, Supervision, Reviewing and Editing.

Supplementary Material

Supplementary Material S1. Equations adopted for OPs and RP measurements.

AA assay:

$$\sigma AA = -\sigma Abs \times \frac{N_0}{Abs_0}, \qquad OP^{AA} = \frac{\sigma AA_s - \sigma AA_b}{\frac{V_a}{V_e} \times V_S}$$

where σAbs is the slope of the absorbance of operative blanks vs. time (min^{-1}), Abs_0 is the initial absorbance calculated from the intercept of the linear regression of absorbance vs. time, N_0 is the number of AA moles added in the reaction mixture (200 nmol), σAA_s and σAA_b are the rate of AA consumption for the sample and for the blank, respectively (nmol min^{-1}), V_e and V_a are the extraction volume and sample volume added to the reaction mixture, respectively, and V_s is the PM sampled volume (m^3).

DTT assay:

$$\sigma DTT = -\sigma Abs \times \frac{N_0}{Abs_0}, \qquad OP^{DTT} = \frac{\sigma DTT_s - \sigma DTT_b}{\frac{V_a}{V_e} \times V_s}$$

where σAbs is the slope of the absorbance of operative blanks vs. time (min^{-1}), Abs_0 is the initial absorbance calculated from the intercept of the linear regression of absorbance vs. time, N_0 is the number of DTT moles added in the reaction mixture (100 nmol), σDTT_s and σDTT_b are the rate of DTT consumption for the sample and for the blank, respectively (nmol min^{-1}), V_e and V_a are the extraction volume and sample volume added to the reaction mixture, respectively, and V_s is the PM sampled volume (m^3).

DPPH assay:

$$RP^{DPPH} = \frac{\frac{(A_0 \times A_S)}{A_0} \times 100}{V_S}$$

where A_0 represents the absorbance of the control and A_S is the absorbance of the samples; V_S is the PM sampled volume (m^3).

Table S2. OP^{DCFH}, OP^{AA}, OP^{DTT} and RP^{DPPH} values of the 20 twin pairs of PM_{10} filters used for evaluating the repeatability of analytical results obtained by using the three different techniques: rotating agitator (RA), ultrasonic bath (US) and vortex (V).

OP^{DCFH} (nmol H_2O_2 m^{-3})								
RA			**US**			**V**		
A	**B**	**SD**	**A**	**B**	**SD**	**A**	**B**	**SD**
$7.9 \cdot 10^{-9}$	$7.1 \cdot 10^{-9}$	$6.1 \cdot 10^{-10}$	$4.5 \cdot 10^{-9}$	$4.1 \cdot 10^{-9}$	$2.3 \cdot 10^{-10}$	$2.3 \cdot 10^{-9}$	$2.7 \cdot 10^{-9}$	$2.5 \cdot 10^{-10}$
$4.3 \cdot 10^{-9}$	$4.1 \cdot 10^{-9}$	$1.6 \cdot 10^{-10}$	$4.7 \cdot 10^{-9}$	$5.1 \cdot 10^{-9}$	$3.1 \cdot 10^{-10}$	$2.7 \cdot 10^{-9}$	$2.8 \cdot 10^{-9}$	$5.4 \cdot 10^{-11}$
$4.2 \cdot 10^{-9}$	$3.6 \cdot 10^{-9}$	$4.6 \cdot 10^{-10}$	$6.1 \cdot 10^{-9}$	$5.8 \cdot 10^{-9}$	$1.9 \cdot 10^{-10}$	$7.7 \cdot 10^{-9}$	$3.1 \cdot 10^{-9}$	$3.2 \cdot 10^{-9}$
$3.9 \cdot 10^{-9}$	$2.4 \cdot 10^{-9}$	$1.1 \cdot 10^{-9}$	$1.4 \cdot 10^{-8}$	$1.5 \cdot 10^{-8}$	$2.1 \cdot 10^{-10}$	$5.4 \cdot 10^{-9}$	$5.1 \cdot 10^{-9}$	$2.7 \cdot 10^{-10}$

$2.6\cdot10^{-9}$	$2.9\cdot10^{-9}$	$2.5\cdot10^{-10}$	$3.7\cdot10^{-9}$	$4.4\cdot10^{-9}$	$5.2\cdot10^{-10}$	$7.2\cdot10^{-9}$	$4.9\cdot10^{-9}$	$1.6\cdot10^{-9}$
$3.1\cdot10^{-9}$	$4.1\cdot10^{-9}$	$7.4\cdot10^{-10}$	$5.4\cdot10^{-9}$	$6.4\cdot10^{-9}$	$7.1\cdot10^{-10}$	$8.3\cdot10^{-9}$	$7.4\cdot10^{-9}$	$6.1\cdot10^{-10}$
$1.1\cdot10^{-8}$	$7.8\cdot10^{-9}$	$1.9\cdot10^{-9}$	$6.2\cdot10^{-9}$	$4.4\cdot10^{-9}$	$1.3\cdot10^{-9}$	$6.4\cdot10^{-9}$	$2.1\cdot10^{-9}$	$3.1\cdot10^{-9}$
$1.7\cdot10^{-8}$	$1.3\cdot10^{-8}$	$2.6\cdot10^{-9}$	$5.7\cdot10^{-9}$	$6.4\cdot10^{-9}$	$5.1\cdot10^{-10}$	$4.3\cdot10^{-8}$	$1.4\cdot10^{-8}$	$2.1\cdot10^{-8}$
$8.9\cdot10^{-9}$	$7.6\cdot10^{-9}$	$8.7\cdot10^{-10}$	$2.2\cdot10^{-9}$	$4.1\cdot10^{-9}$	$1.3\cdot10^{-9}$	$2.3\cdot10^{-8}$	$1.4\cdot10^{-8}$	$6.9\cdot10^{-9}$
$1.6\cdot10^{-8}$	$1.3\cdot10^{-8}$	$1.9\cdot10^{-9}$	$6.1\cdot10^{-9}$	$7.8\cdot10^{-9}$	$1.2\cdot10^{-9}$	$6.9\cdot10^{-9}$	$8.1\cdot10^{-9}$	$7.8\cdot10^{-10}$
$1.5\cdot10^{-8}$	$1.1\cdot10^{-8}$	$2.9\cdot10^{-9}$	$7.6\cdot10^{-9}$	$7.4\cdot10^{-9}$	$1.6\cdot10^{-10}$	$5.2\cdot10^{-9}$	$6.3\cdot10^{-9}$	$7.7\cdot10^{-10}$
$5.1\cdot10^{-9}$	$4.7\cdot10^{-9}$	$2.7\cdot10^{-10}$	$9.1\cdot10^{-9}$	$1.1\cdot10^{-8}$	$9.7\cdot10^{-10}$	$9.3\cdot10^{-9}$	$7.9\cdot10^{-9}$	$1.1\cdot10^{-9}$
$4.4\cdot10^{-9}$	$4.3\cdot10^{-9}$	$1.4\cdot10^{-10}$	$2.1\cdot10^{-9}$	$1.5\cdot10^{-9}$	$4.3\cdot10^{-10}$	$2.3\cdot10^{-8}$	$1.4\cdot10^{-8}$	$6.9\cdot10^{-9}$
$3.9\cdot10^{-9}$	$6.1\cdot10^{-9}$	$1.5\cdot10^{-9}$	$5.2\cdot10^{-9}$	$1.4\cdot10^{-8}$	$5.9\cdot10^{-9}$	$6.9\cdot10^{-9}$	$8.1\cdot10^{-9}$	$7.8\cdot10^{-10}$
$4.8\cdot10^{-9}$	$6.5\cdot10^{-9}$	$1.2\cdot10^{-9}$	$8.3\cdot10^{-9}$	$1.2\cdot10^{-8}$	$2.9\cdot10^{-9}$	$1.8\cdot10^{-9}$	$2.3\cdot10^{-9}$	$3.3\cdot10^{-10}$
$7.9\cdot10^{-9}$	$9.4\cdot10^{-9}$	$1.1\cdot10^{-9}$	$1.7\cdot10^{-9}$	$2.8\cdot10^{-9}$	$7.5\cdot10^{-10}$	$8.4\cdot10^{-9}$	$6.5\cdot10^{-9}$	$1.3\cdot10^{-9}$
$4.8\cdot10^{-8}$	$4.5\cdot10^{-8}$	$2.4\cdot10^{-9}$	$1.2\cdot10^{-9}$	$2.4\cdot10^{-9}$	$8.7\cdot10^{-10}$	$3.3\cdot10^{-8}$	$2.4\cdot10^{-8}$	$6.9\cdot10^{-9}$
$6.5\cdot10^{-8}$	$6.5\cdot10^{-8}$	$3.5\cdot10^{-10}$	$7.2\cdot10^{-9}$	$6.9\cdot10^{-9}$	$1.9\cdot10^{-10}$	$2.1\cdot10^{-8}$	$1.8\cdot10^{-8}$	$1.6\cdot10^{-9}$
$2.3\cdot10^{-8}$	$2.1\cdot10^{-8}$	$1.9\cdot10^{-9}$	$8.2\cdot10^{-9}$	$7.4\cdot10^{-9}$	$5.5\cdot10^{-10}$	$1.1\cdot10^{-8}$	$1.4\cdot10^{-8}$	$2.1\cdot10^{-9}$
$1.8\cdot10^{-8}$	$1.5\cdot10^{-8}$	$1.8\cdot10^{-9}$	$2.2\cdot10^{-9}$	$3.4\cdot10^{-9}$	$8.7\cdot10^{-10}$	$2.8\cdot10^{-8}$	$3.8\cdot10^{-8}$	$7.4\cdot10^{-9}$

OP^{AA} (nmol AA min^{-1} m^{-3})

RA			US			V		
A	**B**	**SD**	**A**	**B**	**SD**	**A**	**B**	**SD**
4.5	4.2	0.2	2.1	0.82	0.8	1.1	1.7	0.4
4.3	4.3	0.1	1.9	1.5	0.3	2.2	2.3	0.1
5.3	2.8	1.8	3.3	2.1	0.9	1.6	1.9	0.3
2.6	3.1	0.3	0.21	0.15	0.11	4.2	1.4	1.9
2.9	1.8	0.8	1.6	1.6	0.1	2.2	1.4	0.5
4.2	2.5	1.2	1.7	1.9	0.1	2.7	2.1	0.4
1.5	1.4	0.1	1.3	0.95	0.2	2.5	1.8	0.4
0.69	1.1	0.3	3.2	1.7	1.1	1.2	0.89	0.2
1.5	1.7	0.2	1.3	2.9	1.2	0.81	1.1	0.2
1.1	1.7	0.5	0.98	0.85	0.11	0.58	0.89	0.2
1.4	1.5	0.1	0.84	2.9	1.4	1.1	2.3	0.8
1.9	1.9	0.1	0.88	3.5	1.8	0.25	0.52	0.2
1.4	1.4	0.1	6.9	8.1	0.7	3.5	3.2	0.2
1.8	1.7	0.1	5.3	5.4	0.1	0.34	1.9	1.2
2.8	2.1	0.5	5.4	5.7	0.2	1.2	1.1	0.1
2.1	3.5	1.1	5.3	6.4	0.8	3.3	2.9	0.2
11	11	1.0	4.6	3.9	0.4	0.98	0.85	0.11
15	15	1.0	3.6	4.5	0.6	0.19	0.85	0.5
9.2	9.5	0.3	7.1	6.1	0.7	1.2	1.5	0.3

8.5	8.1	0.3	7.1	6.3	0.5	6.9	7.8	0.6

OP^{DTT} (nmol DTT min^{-1} m^{-3})

RA			US			V		
A	**B**	**SD**	**A**	**B**	**SD**	**A**	**B**	**SD**
0.79	0.56	0.17	0.75	0.87	0.081	0.51	0.46	0.033
0.51	0.41	0.071	0.91	0.89	0.011	0.32	0.48	0.12
0.66	0.48	0.13	0.91	1.2	0.20	0.52	0.33	0.14
0.68	0.68	0.00013	0.085	0.24	0.11	0.87	0.71	0.12
0.48	0.54	0.037	0.81	0.61	0.13	1.3	0.67	0.4
0.69	0.74	0.034	0.64	0.69	0.039	1.7	0.71	0.7
0.89	0.73	0.12	0.85	0.86	0.0071	1.5	1.9	0.3
1.1	0.65	0.3	0.45	0.42	0.021	1.2	1.9	0.5
1.1	0.85	0.1	0.21	0.24	0.021	0.81	1.1	0.2
1.2	1.1	0.1	0.99	0.85	0.11	0.58	0.89	0.22
0.94	0.71	0.16	0.72	0.79	0.056	1.1	2.3	0.8
0.63	0.74	0.083	0.63	1.5	0.6	0.25	0.52	0.19
0.67	0.84	0.12	0.46	0.46	0.0041	1.2	1.2	0.035
0.71	0.77	0.039	0.51	1.2	0.5	0.93	0.64	0.21
0.75	0.76	0.0041	1.4	1.5	0.1	1.2	1.2	0.021
1.1	1.2	0.043	1.5	1.9	0.3	1.3	1.9	0.5
2.1	1.9	0.1	0.75	0.79	0.024	0.99	0.85	0.11
2.6	2.7	0.1	1.8	1.4	0.3	0.87	0.75	0.085
1.1	1.4	0.2	1.1	1.2	0.01	1.2	1.6	0.2
1.8	1.7	0.03	0.92	0.99	0.049	1.5	1.1	0.3

RP^{DPPH} (%DPPH Cons m^{-3})

RA			US			V		
A	**B**	**SD**	**A**	**B**	**SD**	**A**	**B**	**SD**
0.73	0.46	0.19	0.46	0.59	0.11	0.51	0.38	0.088
0.38	0.49	0.081	0.41	0.47	0.046	0.46	0.41	0.037
0.71	0.41	0.21	0.59	0.47	0.083	0.76	0.35	0.29
0.59	0.61	0.0077	0.049	0.029	0.014	0.18	0.071	0.075
0.49	0.71	0.15	0.011	0.21	0.11	0.25	0.21	0.029
0.86	0.51	0.26	0.29	0.11	0.13	0.24	0.071	0.12
0.22	0.46	0.17	0.22	0.17	0.036	0.65	0.68	0.020
0.39	0.65	0.18	0.23	0.74	0.36	0.16	0.19	0.019
0.21	0.37	0.12	0.44	0.64	0.14	0.16	0.25	0.061
0.31	0.46	0.11	0.16	0.25	0.061	0.24	0.32	0.057
0.018	0.26	0.17	1.10	1.16	0.049	0.17	0.13	0.028

0.15	0.28	0.091	1.2	1.3	0.051	0.58	0.65	0.049
0.19	0.19	0.00	0.049	0.019	0.022	0.12	0.25	0.092
0.19	0.17	0.019	0.24	0.32	0.057	0.18	0.31	0.085
0.27	0.18	0.069	0.35	0.32	0.022	0.32	0.38	0.042
0.21	0.59	0.27	0.91	0.81	0.072	0.22	0.24	0.014
1.3	1.2	0.055	0.21	0.59	0.27	0.11	0.13	0.014
2.1	1.5	0.44	0.86	0.51	0.26	0.098	0.11	0.0014
0.65	0.89	0.17	0.22	0.46	0.17	0.46	0.45	0.0032
0.84	0.79	0.032	0.65	0.54	0.078	0.18	0.13	0.036

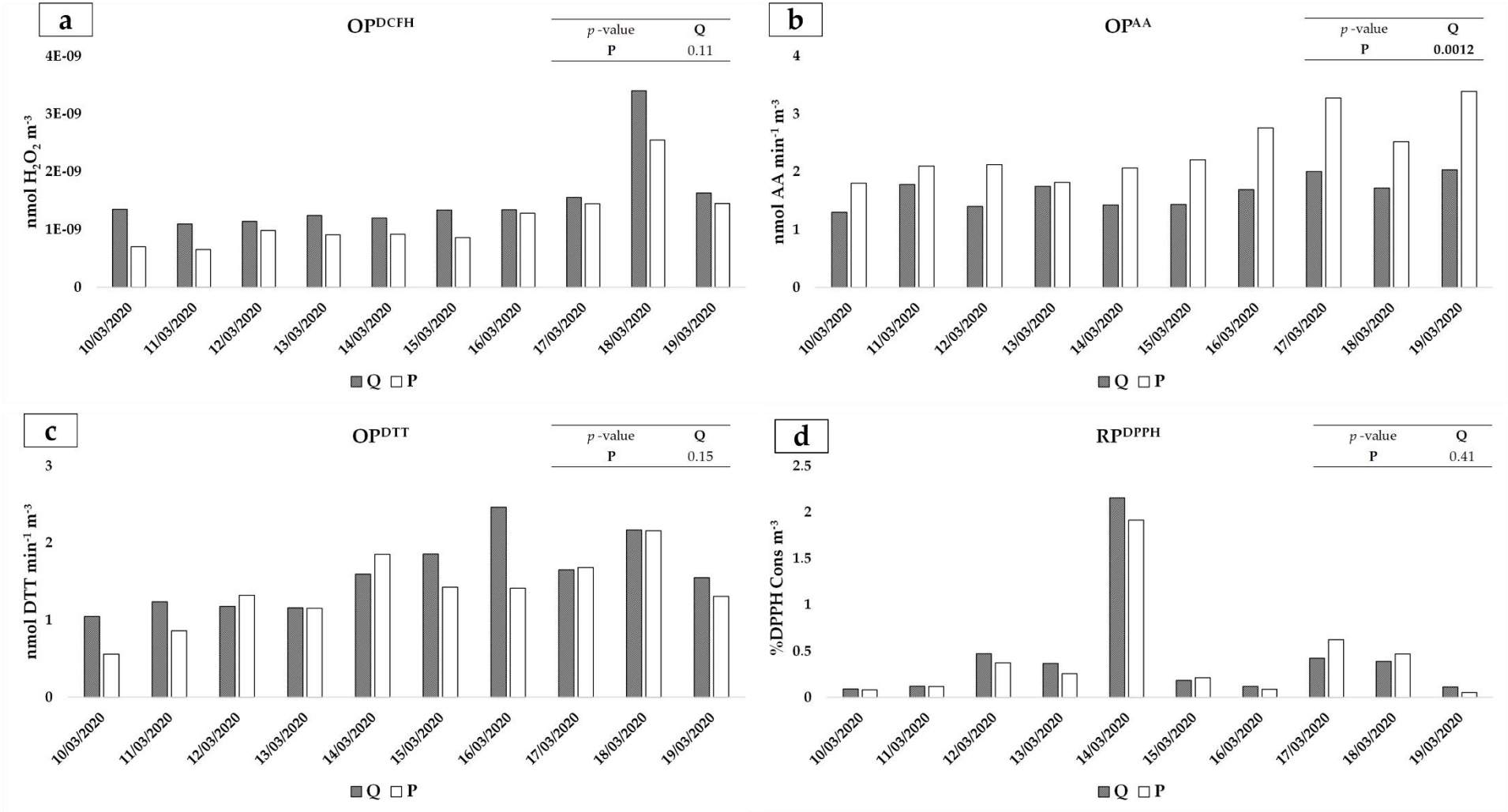

Figure 1.S3 Comparison of OP^{DCFH} (panel a), OP^{AA} (panel b), OP^{DTT} (panel c) and RP^{DPPH} (panel d) between the water-soluble fraction of PM extracted from quartz (Q) and PTFE (P) filters and the *p*-values of the sample paired *t*-test between the filters used. The *p*-value in bold indicate significant differences ($p < 0.05$).

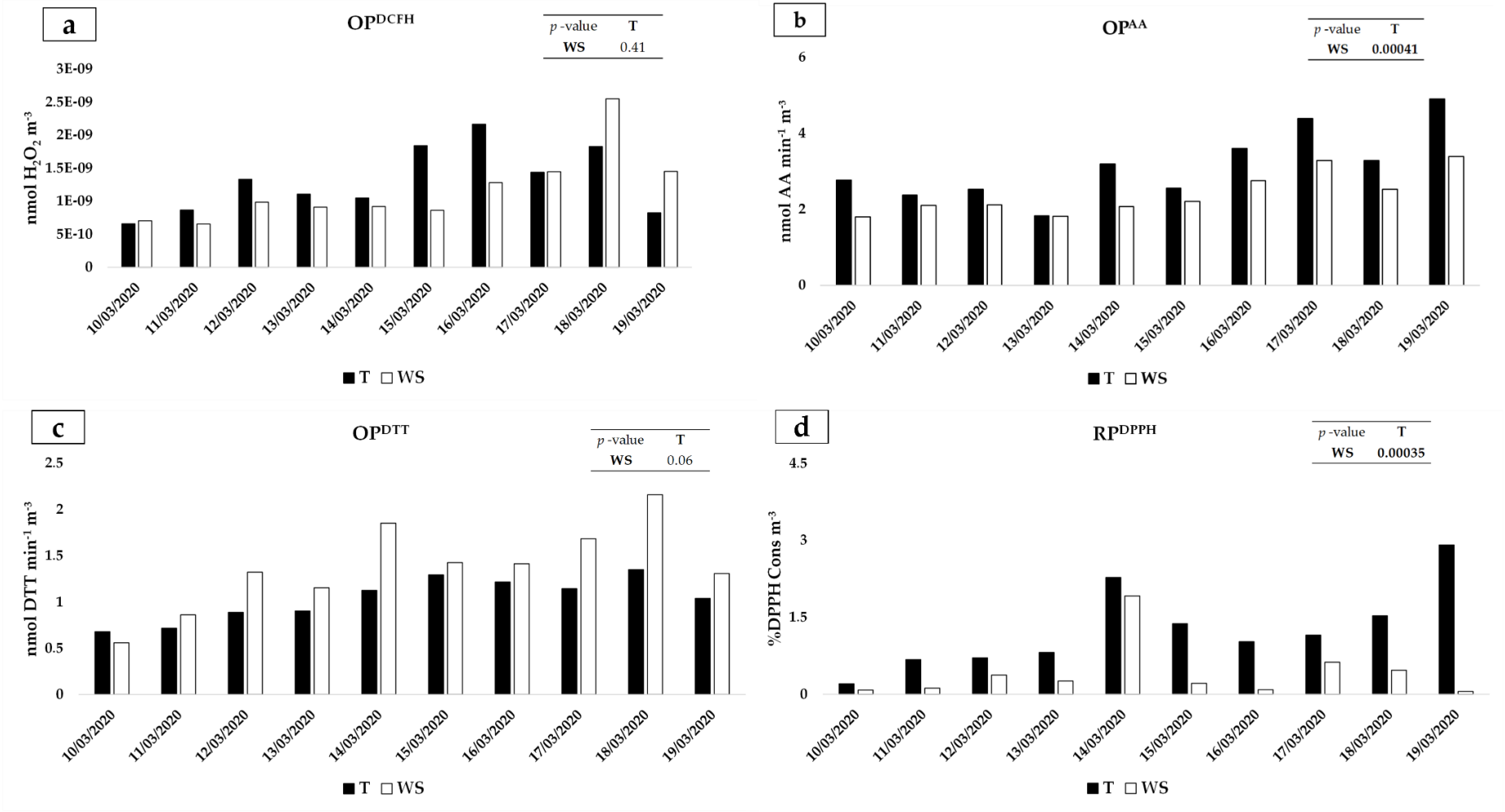

Figure 2.S3 Comparison of OP^{DCFH} (panel a), OP^{AA} (panel b), OP^{DTT} (panel c) and RP^{DPPH} (panel d) between the total (T) and the water-soluble (WS) fraction of PM filters and the *p*-values of the sample paired *t*-test between the two fractions. The *p*-value in bold indicate significant differences ($p < 0.05$

References

Abrams, J. Y., Weber, R. J., Klein, M., Samat, S. E., Chang, H. H., Strickland, M. J., Verma, V., Fang, T., Bates, J.T., Mullholland, J.A., Russell, A.G., Tolbert, P. E., 2017. Associations between ambient fine particulate oxidative potential and cardiorespiratory emergency department visits. Environmental health perspectives, 125(10), 107008. https://doi.org/10.1289/EHP1545

Akhtar, U. S., McWhinney, R. D., Rastogi, N., Abbatt, J. P., Evans, G. J., Scott, J. A., 2010. Cytotoxic and proinflammatory effects of ambient and source-related particulate matter (PM) in relation to the production of reactive oxygen species (ROS) and cytokine adsorption by particles. Inhalation toxicology, 22(sup2), 37-47. https://doi.org/10.3109/08958378.2010.518377

Andersen, Z. J., Olsen, T. S., Andersen, K. K., Loft, S., Ketzel, M., Raaschou-Nielsen, O., 2010. Association between short-term exposure to ultrafine particles and hospital admissions for stroke in Copenhagen, Denmark. European heart journal, 31(16), 2034-2040.

Andrade, C., Molina, C., Sánchez, L. F., Manzano, C. A., Toro, R., 2020. Exploring the oxidative potential and respiratory deposition of size-segregated particulate matter at an urban site. Journal of South American Earth Sciences, 102957.

Atkinson, R. W., Samoli, E., Analitis, A., Fuller, G. W., Green, D. C., Anderson, H. R., Purdie, E., Dunster, C., Aitlhadj, L., Kelly, F.J., Mudway, I. S., 2016. Short-term associations between particle oxidative potential and daily mortality and hospital admissions in London. International journal of hygiene and environmental health, 219(6), 566-572. https://doi.org/10.1016/j.ijheh.2016.06.004

Ayres, J. G., Borm, P., Cassee, F. R., Castranova, V., Donaldson, K., Ghio, A., Harrison, R.M., Hider, R., Kelly, F., Kooter, I.M., Marano, F., Maynard, R.L., Mudway, I., Nel, A., Sioutas, C., Smith, S., Baeza-Squiban, A., Cho, A., Duggan, S., Froines, J., 2008. Evaluating the toxicity of airborne particulate matter and nanoparticles by measuring oxidative stress potential - a workshop report and consensus statement. Inhalation Toxicology, 20(1), 75-99.

Bates, J. T., Weber, R. J., Abrams, J., Verma, V., Fang, T., Klein, M., Strickland, M.J., Sarnat, S.E., Chang, H.H., Mulholland, M.K., Tolbert, P.E., Russell, A. G., 2015. Reactive oxygen species generation linked to sources of atmospheric particulate matter and cardiorespiratory effects. Environmental science & technology, 49(22), 13605-13612. https://doi.org/10.1021/acs.est.5b02967

Bates, J. T., Fang, T., Verma, V., Zeng, L., Weber, R. J., Tolbert, P. E., Abrams, J. Y., Sarnat, S. E., Klein, M., Mulholland, J. A., Russell, A. G., 2019. Review of acellular assays of ambient particulate matter oxidative potential: Methods and relationships with composition, sources, and health effects. Environmental Science & Technology, 53(8), 4003-4019.

Brown, R. A., Stevanovic, S., Bottle, S., Ristovski, Z. D. (2019). An instrument for the rapid quantification of PM-bound ROS: the Particle Into Nitroxide Quencher (PINQ). Atmospheric Measurement Techniques, 12(4), 2387-2401.

Brown, R. A., Stevanovic, S., Bottle, S., Wang, H., Hu, Z., Wu, C., Wang, B., Ristovski, Z. (2020). Relationship between Atmospheric PM-Bound Reactive Oxygen Species, Their Half-Lives, and Regulated Pollutants: Investigation and Preliminary Model. Environmental science & technology, 54(8), 4995-5002.

Calas, A., Uzu, G., Martins, J. M., Voisin, D., Spadini, L., Lacroix, T., Jaffrezo, J. L. (2017). The importance of simulated lung fluid (SLF) extractions for a more relevant evaluation of the oxidative potential of particulate matter. Scientific reports, 7(1), 1-12.

Campbell, S. J., Utinger, B., Lienhard, D. M., Paulson, S. E., Shen, J., Griffiths, P. T., Stell, A.C., Kalberer, M., 2019. Development of a physiologically relevant online chemical assay to quantify aerosol oxidative potential. Analytical chemistry, 91(20), 13088-13095. https://doi.org/10.1021/acs.analchem.9b03282

Cervellati, F., Benedusi, M., Manarini, F., Woodby, B., Russo, M., Valacchi, G., Pietrogrande, M. C., 2020. Proinflammatory properties and oxidative effects of atmospheric particle components in human keratinocytes. Chemosphere, 240, 124746. https://doi.org/10.1016/j.chemosphere.2019.124746

Cho, A. K., Sioutas, C., Miguel, A. H., Kumagai, Y., Schmitz, D. A., Singh, M., Fernandez, F.A., Froines, J. R., 2005. Redox activity of airborne particulate matter at different sites in the Los Angeles Basin. Environmental research, 99(1), 40-47.

Conte, E., Canepari, S., Frasca, D., Simonetti, G., 2017. Oxidative potential of selected PM components. In Multidisciplinary Digital Publishing Institute Proceedings, 1(5), 108. https://doi.org/10.3390/ecas2017-04131

Daellenbach, K. R., Uzu, G., Jiang, J., Cassagnes, L. E., Leni, Z., Vlachou, A., Stefenelli, G., Canonaco, F., Weber, S., Segers, A., Kuenen, J.J.P., Schaap, M., Favez, O., Albinet, A., Aksoyoglu, S., Dommen, J., Baltensperger, U., Geiser, M., El Haddad, I., Jaffrezo, J., Prévôt, A. S., 2020. Sources of particulate-matter air pollution and its oxidative potential in Europe. Nature, 587(7834), 414-419. https://doi.org/10.1038/s41586-020-2902-8

Daher, N., Ning, Z., Cho, A. K., Shafer, M., Schauer, J. J., Sioutas, C., 2011. Comparison of the chemical and oxidative characteristics of particulate matter (PM) collected by different methods: filters, impactors, and biosamplers. Aerosol Science and Technology, 45(11), 1294-1304. https://doi.org/10.1080/02786826.2011.590554

Delfino, R. J., Staimer, N., Vaziri, N. D., 2011. Air pollution and circulating biomarkers of oxidative stress. Air Quality, Atmosphere & Health, 4(1), 37-52. https://doi.org/10.1007/s11869-010-0095-2

Dong, Y. M., Liao, L. Y., Li, L., Yi, F., Meng, H., He, Y. F., Guo, M. M., 2019. Skin inflammation induced by ambient particulate matter in China. Science of The Total Environment, 682, 364-373. https://doi.org/10.1016/j.scitotenv.2019.05.155

Eiguren-Fernandez, A., Kreisberg, N., & Hering, S. (2017). An online monitor of the oxidative capacity of aerosols (o-MOCA). Atmospheric measurement techniques, 10(2), 633-644.

Fang, T., Verma, V., Bates, J. T., Abrams, J., Klein, M., Strickland, M. J., Sarnat, S.E., Chang, H.H., Mulholland, J.A., Tolbert, P.E., Russell, A. G., Weber, R.J., 2016. Oxidative potential of ambient water-soluble PM2. 5 in the southeastern United States: contrasts in sources and health associations between ascorbic acid (AA) and dithiothreitol (DTT) assays. Atmospheric Chemistry and Physics 16(6), 3865-3879. https://doi.org/10.5194/acp-16-3865-2016

Fang, T., Guo, H., Zeng, L., Verma, V., Nenes, A., Weber, R. J., 2017. Highly acidic ambient particles, soluble metals, and oxidative potential: a link between sulfate and aerosol toxicity. Environmental science & technology, *51*(5), 2611-2620. https://doi.org/10.1021/acs.est.6b06151

Frezzini, M. A., Castellani, F., De Francesco, N., Ristorini, M., Canepari, S., 2019. Application of DPPH Assay for Assessment of Particulate Matter Reducing Properties. Atmosphere, 10(12), 816. https://doi.org/10.3390/atmos10120816

Fuller, S. J., Wragg, F. P. H., Nutter, J., Kalberer, M., 2014. Comparison of on-line and off-line methods to quantify reactive oxygen species (ROS) in atmospheric aerosols. Atmospheric Environment, 92, 97-103. https://doi.org/10.1016/j.atmosenv.2014.04.006

Gao, D., Fang, T., Verma, V., Zeng, L., Weber, R. J., 2017. A method for measuring total aerosol oxidative potential (OP) with the dithiothreitol (DTT) assay and comparisons between an urban and roadside site of water-soluble and total OP. Atmospheric Measurement Techniques, 10(8), 2821. https://doi.org/10.5194/amt-10-2821-2017

Gao, D., Mulholland, J. A., Russell, A. G., Weber, R. J., 2020. Characterization of water-insoluble oxidative potential of PM2. 5 using the dithiothreitol assay. Atmospheric Environment, 224, *117327*. https://doi.org/10.1016/j.atmosenv.2020.117327

Godri, K. J., Harrison, R. M., Evans, T., Baker, T., Dunster, C., Mudway, I. S., Kelly, F. J., 2011. Increased oxidative burden associated with traffic component of ambient particulate matter at roadside and urban background schools sites in London. PloS one, 6(7). https://doi.org/10.1371/journal.pone.0021961

Godri, K. J., Green, D. C., Fuller, G. W., Dall'Osto, M., Beddows, D. C., Kelly, F. J., Harrison, R.M., Mudway, I. S., 2010. Particulate oxidative burden associated with firework activity. Environmental science & technology, 44(21), 8295-8301. https://doi.org/10.1021/es1016284

Guo, H. B., Li, M., Lyu, Y., Cheng, T. T., Xv, J. J., Li, X., 2019. Size-resolved particle oxidative potential in the office, laboratory, and home: Evidence for the importance of water-soluble transition metals. Environmental Pollution, 246, 704-709. https://doi.org/10.1016/j.envpol.2018.12.094

Gupta, T., Singh, S. P., Rajput, P., Agarwal, A. K., 2019. Measurement, Analysis and Remediation of Environmental Pollutants. Springer.

Hedayat, F., Stevanovic, S., Miljevic, B., Bottle, S., Ristovski, Z. D., 2015. evaluating the molecular assays for measuring the oxidative potential of particulate matter. Chemical Industry and Chemical Engineering Quarterly, 21(1-2), 201-210. https://doi.org/10.2298/CICEQ140228031H

Hung, H. F., Wang, C. S., 2001. Experimental determination of reactive oxygen species in Taipei aerosols. Journal of Aerosol Science, 32(10), 1201-1211. https://doi.org/10.1016/S0021-8502(01)00051-9

Khurshid, S. S., Siegel, J. A., Kinney, K. A., 2014. Indoor particulate reactive oxygen species concentrations. Environmental research, 132, 46-53. https://doi.org/10.1016/j.envres.2014.03.026

Khurshid, S. S., Emmerich, S., Persily, A., 2019. Oxidative potential of particles at a research house: Influencing factors and comparison with outdoor particles. Building and Environment, 163, 106275. https://doi.org/10.1016/j.buildenv.2019.106275

King, L. E., Weber, R. J., 2013. Development and testing of an online method to measure ambient fine particulate reactive oxygen species (ROS) based on the 2', 7'-dichlorofluorescin (DCFH) assay. Atmospheric Measurement Techniques, 6(7), 1647-1658. https://doi.org/10.5194/amt-6-1647-2013

Knaapen, A. M., Shi, T., Borm, P. J., Schins, R. P., 2002. Soluble metals as well as the insoluble particle fraction are involved in cellular DNA damage induced by particulate matter. In Oxygen/Nitrogen Radicals: Cell Injury and Disease (pp. 317-326). Springer, Boston, MA.

Kumagai, Y., Arimoto, T., Shinyashiki, M., Shimojo, N., Nakai, Y., Yoshikawa, T., Sagai, M., 1997. Generation of reactive oxygen species during interaction of diesel exhaust particle components with NADPH-cytochrome P450 reductase and involvement of the bioactivation in the DNA damage. Free Radical Biology and Medicine, 22(3), 479-487. https://doi.org/10.1016/S0891-5849(96)00341-3

Kumagai, Y., Koide, S., Taguchi, K., Endo, A., Nakai, Y., Yoshikawa, T., Shimojo, N., 2002. Oxidation of proximal protein sulfhydryls by phenanthraquinone, a component of diesel exhaust particles. Chemical research in toxicology, 15(4), 483-489. https://doi.org/10.1021/tx0100993

Lin, M., Yu, J. Z., 2019. Dithiothreitol (DTT) concentration effect and its implications on the applicability of DTT assay to evaluate the oxidative potential of atmospheric aerosol samples. Environmental Pollution, 251, 938-944. https://doi.org/10.1016/j.envpol.2019.05.074

Lin, M., Yu, J. Z., 2020. Assessment of interactions between transition metals and atmospheric organics: Ascorbic Acid Depletion and Hydroxyl Radical Formation in Organic-metal Mixtures. Environmental Science & Technology. https://dx.doi.org/10.1021/acs.est.9b07478

Majestic, B. J., Schauer, J. J., Shafer, M. M., 2007. Development of a manganese speciation method for atmospheric aerosols in biologically and environmentally relevant fluids. Aerosol Science and Technology, 41(10), 925-933. https://doi.org/10.1080/02786820701564657

Manigrasso, M., Simonetti, G., Astolfi, M. L., Perrino, C., Canepari, S., Protano, C., Antonucci, A., Avino, P., Vitali, M., 2020. Oxidative Potential Associated with Urban Aerosol Deposited into the Respiratory System and Relevant Elemental and Ionic Fraction Contributions. Atmosphere, 11(1), 6.

Massimi, L., Ristorini, M., Eusebio, M., Florendo, D., Adeyemo, A., Brugnoli, D., Canepari, S., 2017. Monitoring and evaluation of Terni (Central Italy) air quality through spatially resolved analyses. Atmosphere, 8(10), 200.

Massimi, L., Simonetti, G., Buiarelli, F., Di Filippo, P., Pomata, D., Riccardi, C., Ristorini, M., Astolfi, M.L., Canepari, S., 2020a. Spatial distribution of levoglucosan and alternative biomass burning tracers in atmospheric aerosols, in an urban and industrial hot-spot of Central Italy. Atmospheric Research, 104904. https://doi.org/10.1016/j.atmosres.2020.104904

Massimi, L., Ristorini, M., Simonetti, G., Frezzini, M. A., Astolfi, M. L., Canepari, S., 2020b. Spatial Mapping and Size Distribution of Oxidative Potential of Particulate Matter Released by Spatially Disaggregated Sources. Environmental Pollution, 115271. https://doi.org/10.1016/j.envpol.2020.115271

Miljevic, B., Hedayat, F., Stevanovic, S., Fairfull-Smith, K. E., Bottle, S. E., Ristovski, Z. D., 2014. To sonicate or not to sonicate PM filters: reactive oxygen species generation upon ultrasonic irradiation. Aerosol science and technology, 48(12), 1276-1284. ttps://doi.org/10.1080/02786826.2014.981330

Mutzel, A., Rodigast, M., Iinuma, Y., Böge, O., Herrmann, H., 2013. An improved method for the quantification of SOA bound peroxides. Atmospheric environment, 67, 365-369. https://doi.org/10.1016/j.atmosenv.2012.11.012

Nishita-Hara, C., Hirabayashi, M., Hara, K., Yamazaki, A., Hayashi, M., 2019. Dithiothreitol-measured oxidative potential of size-segregated particulate matter in Fukuoka, Japan: Effects of Asian dust events. GeoHealth, 3(6), 160-173. https://doi.org/10.1029/2019GH000189

Orsini, D. A., Ma, Y., Sullivan, A., Sierau, B., Baumann, K., Weber, R. J. (2003). Refinements to the particle-into-liquid sampler (PILS) for ground and airborne measurements of water soluble aerosol composition. Atmospheric Environment, 37(9-10), 1243-1259. https://doi.org/10.1016/S1352-2310(02)01015-4

Øvrevik, J., 2019. Oxidative potential versus biological effects: A review on the relevance of cell-free/abiotic assays as predictors of toxicity from airborne particulate matter. Int. J. Mol. Sci. 2019, 20, 4772, https://doi.org/10.3390/ijms20194772.

Perrone, M. G., Zhou, J., Malandrino, M., Sangiorgi, G., Rizzi, C., Ferrero, L., Dommen, J., Bolzacchini, E., 2016. PM chemical composition and oxidative potential of the soluble fraction of particles at two sites in the urban area of Milan, Northern Italy. Atmospheric environment, 128, 104-113. https://doi.org/10.1016/j.atmosenv.2015.12.040

Perrone, M. R., Bertoli, I., Romano, S., Russo, M., Rispoli, G., Pietrogrande, M. C., 2019. PM2. 5 and PM10 oxidative potential at a Central Mediterranean Site: Contrasts between dithiothreitol-and ascorbic acid-measured values in relation with particle size and chemical composition. Atmospheric Environment, 210, 143-155. https://doi.org/10.1016/j.atmosenv.2019.04.047

Piacentini, D., Falasca, G., Canepari, S., Massimi, L., 2019. Potential of PM-selected components to induce oxidative stress and root system alteration in a plant model organism. Environment international, 132, 105094. https://doi.org/10.1016/j.envint.2019.105094

Puthussery, J. V., Zhang, C., Verma, V., 2018. Development and field testing of an online instrument for measuring the real-time oxidative potential of ambient particulate matter based on dithiothreitol assay. Atmospheric Measurement Techniques, 11(10), 5767. https://doi.org/10.5194/amt-11-5767-2018

Shao, L., Hu, Y., Shen, R., Schäfer, K., Wang, J., Wang, J., Schnelle-Kreis, J., Zimmermann, R., BéruBé, K., Suppan, P., 2017. Seasonal variation of particle-induced oxidative potential of airborne particulate matter in Beijing. Science of The Total Environment, 579, 1152-1160. https://doi.org/10.1016/j.scitotenv.2016.11.094

Shiraiwa, M., Ueda, K., Pozzer, A., Lammel, G., Kampf, C. J., Fushimi, A., et al. Sato, K., 2017. Aerosol health effects from molecular to global scales. Environmental science & technology, 51(23), 13545-13567. https://doi.org/10.1021/acs.est.7b04417

Simonetti, G., Conte, E., Perrino, C., Canepari, S., 2018a. Oxidative potential of size-segregated PM in an urban and an industrial area of Italy. Atmospheric Environment, 187, 292-300. https://doi.org/10.1016/j.atmosenv.2018.05.051

Stoeger, T., Takenaka, S., Frankenberger, B., Ritter, B., Karg, E., Maier, K., Shulz, H., Schmid, O., 2009. Deducing in vivo toxicity of combustion-derived nanoparticles from a cell-free oxidative potency assay and metabolic activation of organic compounds. Environmental Health Perspectives, 117(1), 54-60. https://doi.org/10.1289/ehp.11370

Szigeti, T., Óvári, M., Dunster, C., Kelly, F. J., Lucarelli, F., Záray, G., 2015. Changes in chemical composition and oxidative potential of urban PM2. 5 between 2010 and 2013 in Hungary. Science of the Total Environment, 518, 534-544. https://doi.org/10.1016/j.scitotenv.2015.03.025

UNI, E., 2014. 12341: 2014. Air Quality–Determination of the PM10 fraction of suspended particulate matter. Reference method and field test procedure to demonstrate reference equivalence of measurements methods.

Uttara, B., Singh, A. V., Zamboni, P., Mahajan, R. T., 2009. Oxidative stress and neurodegenerative diseases: a review of upstream and downstream antioxidant therapeutic options. Current neuropharmacology, 7(1), 65-74.

Valavanidis, A., Fiotakis, K., Bakeas, E., Vlahogianni, T., 2005. Electron paramagnetic resonance study of the generation of reactive oxygen species catalysed by transition metals and quinoid redox cycling by inhalable ambient particulate matter. Redox Report, 10(1), 37-51. https://doi.org/10.1179/135100005X21606

Venkatachari, P., Hopke, P. K., Grover, B. D., Eatough, D. J., 2005. Measurement of particle-bound reactive oxygen species in rubidoux aerosols. Journal of Atmospheric Chemistry, 50, 49–58. http://dx.doi.org/10.1007/s10874-005-5013-3

Venkatachari, P., Hopke, P. K., Brune, W. H., Ren, X., Lesher, R., Mao, J., Mitchell, M., 2007. Characterization of wintertime reactive oxygen species concentrations in Flushing, New York. Aerosol Science and Technology, 41, 97–111. https://doi.org/10.1080/02786820601116004

Verma, V., Rico-Martinez, R., Kotra, N., King, L., Liu, J., Snell, T. W., Weber, R. J., 2012. Contribution of water-soluble and insoluble components and their hydrophobic/hydrophilic subfractions to the reactive oxygen species-generating potential of fine ambient aerosols. Environmental science & technology, 46(20), 11384-11392. https://doi.org/10.1021/es302484r

Wang, S., Ye, J., Soong, R., Wu, B., Yu, L., Simpson, A. J., Chan, A. W. (2018). Relationship between chemical composition and oxidative potential of secondary organic aerosol from polycyclic aromatic hydrocarbons. Atmospheric Chemistry and Physics, 18(6), 3987-4003.

Wragg, F., Fuller, S. J., Freshwater, R., Green, D. C., Kelly, F. J., Kalberer, M., 2016. An automated online instrument to quantify aerosol-bound reactive oxygen species (ROS) for ambient measurement and health-relevant aerosol studies. https://doi.org/10.5194/amt-9-4891-2016

Yang, A., Jedynska, A., Hellack, B., Kooter, I., Hoek, G., Brunekreef, B., Kuhlbusch, T.A.J., Cassee, F.R., Janssen, N. A., 2014. Measurement of the oxidative potential of PM2. 5 and its constituents: The effect of extraction solvent and filter type. Atmospheric environment, 83, 35-42. http://dx.doi.org/10.1016/j.atmosenv.2013.10.049

Yang, A., Janssen, N. A., Brunekreef, B., Cassee, F. R., Hoek, G., Gehring, U., 2016. Children's respiratory health and oxidative potential of PM2. 5: the PIAMA birth cohort study. Occup Environ Med, 73(3), 154-160.

Yi, S., Zhang, F., Qu, F., Ding, W., 2014. Water-insoluble fraction of airborne particulate matter (PM10) induces oxidative stress in human lung epithelial A549 cells. Environmental toxicology, 29(2), 226-233. https://doi.org/10.1002/tox.21750

Yu, H., Puthussery, J. V., Verma, V., 2020. A semi-automated multi-endpoint reactive oxygen species activity analyzer (SAMERA) for measuring the oxidative potential of ambient PM2. 5 aqueous extracts. Aerosol Science and Technology, 54(3), 304-320. https://doi.org/10.1080/02786826.2019.1693492

Zhang, Z. H., Hartner, E., Utinger, B., Gfeller, B., Paul, A., Sklorz, M., Czech, H., Yang, B.X., Su, X.Y., Jakobi, G., Orasche, J., Schnelle-Kreis, J., Jeong, S., Gröger, T., Pardo, M., Hohaus, T., Adam, T., Kiendler-Scharr, A., Rudich, Y., Zimmermann, R., Kalberer, M. (2021). Are reactive oxygen species (ROS) a suitable metric to predict toxicity of carbonaceous aerosol particles?. Atmospheric Chemistry and Physics Discussions, 1-29. https://doi.org/10.5194/acp-2021-666

Zhou, J., Bruns, E. A., Zotter, P., Stefenelli, G., Prévôt, A. S., Baltensperger, U., El-Haddad, I., Dommen, J., 2018. Development, characterization and first deployment of an improved online reactive oxygen species analyzer. Atmospheric Measurement Techniques, 11(1), 65-80. https://doi.org/10.5194/amt-11-65-2018

Zou, Y., Jin, C., Su, Y., Li, J., Zhu, B., 2016. Water soluble and insoluble components of urban PM2. 5 and their cytotoxic effects on epithelial cells (A549) in vitro. Environmental pollution, 212, 627-635. https://doi.org/10.1016/j.envpol.2016.03.022

7.3 (C3) A New Method for the Assessment of the Oxidative Potential of Both Water-soluble and Insoluble PM

Atmosphere (2022), 13(2), 349, doi: 10.3390/atmos13020349

Maria Agostina Frezzini[1], Gianluca Di Iulio[1], Caterina Tiraboschi[1], Silvia Canepari[1], Lorenzo Massimi[1]*

[1]Department of Environmental Biology, Sapienza University of Rome, P.le Aldo Moro 5, 00185, Rome, Italy

*Corresponding author

Keywords: toothbrush detachment; PM water suspension; total oxidative potential (TOP); ascorbic acid (OP^{AA}) assay, dithiothreitol (OP^{DTT}) assay, 2',7'-dichlorofluorescein (OP^{DCFH}) assay; elemental tracers

Abstract: Water-soluble and insoluble fractions of airborne particulate matter (PM) exhibit different toxicological potentials and peculiar mechanisms of action in biological systems. However, most of the research on the oxidative potential (OP) of PM is focused exclusively on its water-soluble fraction, since experimental criticisms were encountered for detaching the whole PM (soluble and insoluble species) from field filters. However, to estimate the actual potential effects of PM on human health, it is essential to assess the OP of both its water-soluble and insoluble fractions. In this study, to estimate the total OP (TOP), an efficient method for the detachment of intact PM_{10} from field filters by using an electrical toothbrush was applied to 20 PM_{10} filters in order to obtain PM_{10} water suspensions to be used for the DCFH, AA and DTT oxidative potential assays (OP^{DCFH}, OP^{AA} and OP^{DTT}). The contribution of the insoluble PM_{10} to the TOP was evaluated by comparing the TOP values to those obtained by applying the three OP assays to the water-soluble fraction of 20 equivalent PM_{10} filters. The OP of the insoluble fraction (IOP) was calculated as the difference between the TOP and the WSOP. Moreover, each PM_{10} sample was analyzed for the water-soluble and insoluble fraction of 10 elements (Al, Cr, Cs, Cu, Fe, Li, Ni, Rb, Sb, Sn) identified as primary elemental tracers of the main emission sources in the study area. A principal component analysis (PCA) was performed on the data obtained to identify the predominant sources for the determination of TOP, WSOP and IOP. Results showed that water-soluble PM_{10} released by traffic, steel plant, and biomass burning is mainly responsible for the generation of the TOP as well as of the WSOP. This evidence gave strength to the reliability of the results from OP assays performed only on the water-soluble fraction of PM. Lastly, the IOP^{DCFH} and IOP^{DTT} were found to be principally determined by insoluble PM_{10} from mineral dust.

1. Introduction

Air pollution is widely recognized as a key topic in public health protection actions [1,2]. Exposure to particulate matter (PM) is one of the major global health concerns [3,4], since it may adversely affect human health leading to the development of several chronic and acute pathologies like cardiovascular and respiratory diseases, lung cancer, bronchitis, diabetes, and neurodevelopmental disorders [5–8]. A growing number of

epidemiologic studies reported associations of PM pollution with health effects also at low levels, often below current air quality standards [9,10]. Therefore, the evaluation of exposure to PM and associated health risks is crucial for planning targeted mitigation strategies and policies to protect human health.

The main cytotoxicity mechanism involved in developing damaging health effects, and promoting chronic diseases, is the PM ability to induce oxidative stress, due to the interaction between cell and particles and production of excess reactive species, such as reactive oxygen species (ROS), reactive nitrogen species (RNS) and reactive carbon species (RCS), which can upset the balance of intracellular oxidants and antioxidants [11–13]. PM can trigger oxidative responses by different pathways, such as the introduction of particle-bound ROS into the respiratory system, or the introduction of redox-active species inducing the catalytic generation of reactive species and, thus, the depletion of antioxidants [14–16].

Acellular assays have been widely used to measure the oxidative potential (OP) of particles in order to provide a proxy of the oxidative properties of PM [17] as they are recognized as valid exposure metrics to investigate the effect of PM on living organisms [18]. OP is frequently measured by the ascorbic acid assay (OP^{AA}), which provides a measure of the particle-induced depletion of chemical proxies for the cellular ascorbic acid antioxidant, and by the dithiothreitol assay (OP^{DTT}) that is based on the PM-catalyzed electron transfer from a chemical surrogate of cellular reducing agents (i.e. adenine dinucleotide, NADH, and nicotinamide adenine dinucleotide phosphate, NADPH) to O_2 [17,19–21]. In addition, the dichlorofluorescin assay (OP^{DCFH}) is often applied to determine OP of PM samples, although the assay was originally used to monitoring ROS formation in cellular environment [22,23]. When applied in acellular assays, DCFH responds to the ROS already present in particles and not to the ROS formed by redox processes (as AA and DTT assays). Indeed, it measures particle-bound ROS, which are inherently adherent to the particles, releasing a fluorescent intensity that is converted into equivalent H_2O_2 to express the final ROS concentration [22]. Therefore, the DCFH assay is conventionally included in OP assays in several works in this research field [17,24–26]. Each OP assay is sensitive to different oxidative properties of PM and appears to have different relationships with health outcomes [16,17,27]. Therefore, there are no appropriate criteria for choosing the most representative assay and the synergic application is frequently suggested [28–30].

Water-soluble and insoluble fractions of PM exhibit different mechanisms of action in biological systems [30–32], and while it has been shown that insoluble species can contribute significantly to the toxicological potential of PM [27,30,33], most of the literature OP data refers only to the PM water-soluble fraction, which is considered as more bioavailable [34,35]. Insoluble species have shown an intrinsically high redox activity and the capability of exerting a wide spectrum of negative health endpoints, such as the generation of oxidative stress markers in human cells, the disruption of the cell membrane, and the induction of cellular DNA damage [11,36–39]. Therefore, different studies suggested that insoluble components of PM may play an important role in generating oxidative damage and highlight the need to investigate the OP of insoluble particles [27,28,40,41]. However, the application of the OP assays on insoluble PM is very difficult and thus it is still not clear how much insoluble PM may give a contribution to the OP.

In a recent work, the contribution of insoluble components to the OP was evaluated directly on the aqueous suspension of PM_{10} field filters, without any preliminary filtration step, by adding reagents of each assay directly in contact with the sampled filter immersed in the extraction solution [15,42]. However, an uncertainty associated to the measurements was observed and was probably due to the operative limits of performing OP assays directly on particles too embedded in the membrane filters. On the other hand, Wang et al. (2013) and Daher et al. (2011) evaluated the redox activity of PM by collecting particles directly into a liquid medium through a BioSampler, and by performing OP assays to the unfiltered aqueous suspension [40,43]. However, the OP of PM is still mainly quantified by offline assays in extracts of aerosol particles collected on filters [25,44]. In other studies, the contribution of PM insoluble species to the OP was evaluated using ultrasounds or organic solvents for the extraction of the insoluble fraction of PM [30,33,45]. However, ultrasounds have been shown to induce the formation of ROS in the solution, while organic solvents may themselves alter the OP of PM oxidative potential, introducing a bias in the toxicological assessment. Moreover, it has been demonstrated that different extraction procedures generate high differences in the measured OP of PM [19], thus leading to misinterpretation of the results obtained. These studies have considered separately the contribution of the water-soluble and/or insoluble fraction to the OP. However, with the aim of investigating the possible toxicological effects related to PM exposure under real-world conditions, it would be useful to apply OP assays directly on a PM water-suspension for the assessment of the overall OP of PM (water-soluble and insoluble species).

To this aim, a non-invasive, simple, and efficient method, recently validated by Massimi et al. [46] for the recovery of the elements in $PM_{10,}$ was used for the detachment and suspension in water of intact PM_{10} from field filters by using an electrical toothbrush [47,48]. The retrieved PM_{10} water suspension was used for the assessment of the overall OP^{DCFH}, OP^{AA} and OP^{DTT} of intact PM_{10} samples (water-soluble and insoluble fraction) and for the evaluation of the real contribution of insoluble particles to PM redox properties.

2. Materials and Methods

2.1. Sampling site and procedure

PM_{10} filters were collected in the city of Terni, in Central Italy, in the Region of Umbria (42° 34'N; 12°39' E) at the sampling site Prisciano (PR) of Environmental Protection Agency of Umbria Region (ARPA Umbria). The sampling site was selected for its proximity of a steel plant (geographical coordinates: 42°34′20.30″ N; 12°40′44.23″ E) and for the high documented concentration of several toxic elements present mainly in the insoluble fraction of PM_{10} [49,50].

Two single-line samplers (Giano sampler, Dadolab Srl, Cinisello B., MI, Italy), equipped with sampling heads for PM_{10} certified UNI EN 12341 (2014) [51] and polytetrafluoroethylene membrane filters (PTFE; 47 mm diameter, pore size 2µm, Cobetter Filtration Equipment Co., Ltd, Hangzhou, China), worked in parallel at 2.3 m^3/h to collect 24-h PM_{10} filters for 20 days, from 5th to 24th of May 2021. In total, 20 couple of twin PM_{10} field filters were collected and analyzed.

2.2. Analytical procedure

PM_{10} filters collected from one of the two sample lines were processed by following a previously optimized and detailed chemical fractionation procedure, involving the water-extraction of PM_{10} filters and the acid digestion of the residue, followed by elemental analysis of both the water-soluble and insoluble fractions [49,50,52,53]. After the removal of the supporting polymethyl pentene ring from each sampled filter, PM_{10} filters were immersed in 10 mL of deionized water (produced by Arioso UP 900 Integrate Water Purification System, Seoul, Korea) and then extracted by rotating agitation (Rotator, Glas-Col, Hangzhou Yooning Instrunents, Hangzhou, Zhejiang, China) for 30 min at 60 rpm. The obtained solution was then filtered through a nitrocellulose filter (NC filter; pore size 0.45 µm, Merck Millipore Ltd., Billerica, MA, USA) to obtain the PM_{10} water-soluble fraction. Subsequently, the PM_{10} filters containing the residue and the nitrocellulose filter used for the filtration were acid-digested in a microwave oven (Ethos Touch Control with Q20 rotor, Milestone, Sorisole, Bergamo, Italy) using 2 mL of HNO_3 (67%, Promochem, Wesel, Germany) and 1 mL of H_2O_2 (30% Suprapur, Merck Millipore Ltd., Billerica, MA, USA). The digested solutions were diluted to 50 mL with deionized water and filtered by nitrocellulose syringe filters (diameter 25 mm, pore size 0.45 µm, GVS Filter Technology, Morecambe, England, UK) to obtain the PM_{10} insoluble fraction. Water-soluble and insoluble fractions of PM_{10} samples were analyzed for the determination of 10 elements (Al, Cr, Cs, Cu, Fe, Li, Ni, Rb, Sb, Sn) in the two fractions using quadrupole inductively coupled plasma mass spectrometry (ICP-MS, Bruker 820-MS, Billerica, MA, USA). Further information about the instrumental conditions and performance of the method is reported in Astolfi et al. [54]. The analyzed elements were selected as they were already identified as primary elemental tracers of the predominant emission sources in the Terni basin [49,50]. The minimum detection limit (MDL), concentrations, the mean and standard deviation of PM_{10} mass, and of the elements analyzed in the water-soluble and insoluble fraction of PM_{10} collected at PR are reported in Table 1. PM_{10} mass concentration data were obtained from ARPA Umbria reports available online (www.arpa.umbria.it, accessed on 7 February 2022). Average solubility percentages (%) of the elements in the 20 PM_{10} samples are shown in Figure 1.

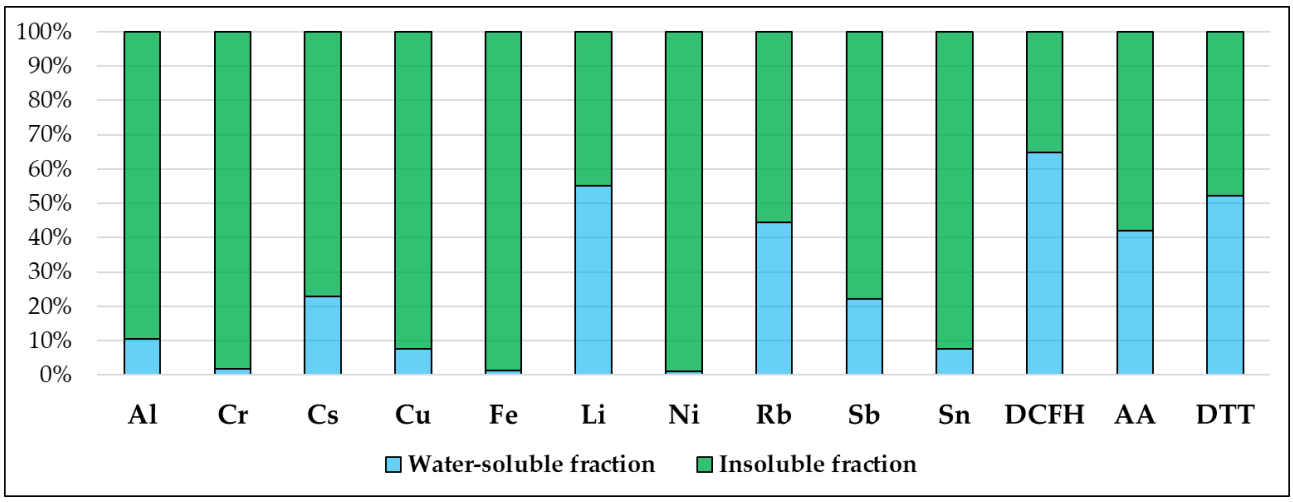

Figure 1. Average solubility percentages (%) of the elements in the 20 PM_{10} samples collected at PR and average contribution percentages (%) of the two solubility fractions to the TOP^{DCFH}, TOP^{AA}, and TOP^{DTT}.

Equivalent PM_{10} filters from the second sample line were instead subjected to PM_{10} toothbrush detachment and suspension in water, as thoroughly described in Massimi et al. [46]. This method has been already applied only by Süring et al. [47,48], who used this procedure to quantify allergen-loaded particles in PM_{10} by flow cytometry. Briefly, each filter was put in a polystyrene Petri dish of 50 mm diameter and overlaid with 10 mL of deionized water. Subsequently, the filter was held with PTFE tweezers and brushed for 2 min using an electrical toothbrush with a sensitive brush head (Braun, Germany, Oral-B Vitality Sensitive). The obtained total PM_{10} water suspension was then used in this study for the application of the three OP assays. The performance of this method for the recovery of the elements in PM_{10} was evaluated by Massimi et al. [46] after applying the chemical fractionation procedure described above to the obtained PM_{10} water suspensions and to equivalent PM_{10} samples not subjected to the toothbrush detachment, revealing an efficiency of approximatively 70% for the recovery of the elements. Moreover, this method is described in Süring et al. [47,48].

2.3. Oxidative potential measurements

The OP^{DCFH}, OP^{AA}, and OP^{DTT} assays were used to assess the OP of the 20 pairs of PM_{10} equivalent samples. To obtain the water-soluble OP (WSOP) and total OP (TOP, water-soluble and insoluble PM_{10}), the three OP assays were simultaneously applied to the water-soluble fraction of PM_{10} filters obtained by following the chemical fractionation procedure described in Section 2.2, and to the PM_{10} aqueous suspension retrieved by applying the toothbrush detachment to the equivalent PM_{10} filters. Furthermore, the OP of the insoluble fraction (IOP) was calculated as the difference between the TOP and the WSOP. The average contribution percentages (%) of the two solubility fractions to the TOP^{DCFH}, TOP^{AA}, and TOP^{DTT} are shown in Figure 1. The OP analytical measurements performed in this study followed the validated and frequently used procedures [26,42,50] largely described below.

Table 1. Minimum detection limit (MDL), concentrations, mean and standard deviation of PM_{10} mass, and of the elements analyzed in the water-soluble and insoluble fraction of the 20 PM_{10} samples collected at PR. PM_{10} mass concentration was not detected (N.D.) on 17, 18, and 24 May 2021.

	Water-Soluble Fraction (ws)											Insoluble Fraction (i)									
	PM_{10}	**Al**	**Cr**	**Cs**	**Cu**	**Fe**	**Li**	**Ni**	**Rb**	**Sb**	**Sn**	**Al**	**Cr**	**Cs**	**Cu**	**Fe**	**Li**	**Ni**	**Rb**	**Sb**	**Sn**
UoM	$\mu g\ m^{-3}$	$ng\ m^{-3}$	$ng\ m^{-3}$	$ng\ m^{-3}$	$ng\ m^{-3}$	$ng\ m^{-3}$	$ng\ m^{-3}$	$ng\ m^{-3}$	$ng\ m^{-3}$	$ng\ m^{-3}$	$ng\ m^{-3}$	$ng\ m^{-3}$	$ng\ m^{-3}$	$ng\ m^{-3}$	$ng\ m^{-3}$	$ng\ m^{-3}$	$ng\ m^{-3}$	$ng\ m^{-3}$	$ng\ m^{-3}$	$ng\ m^{-3}$	$ng\ m^{-3}$
MDL	5	1.7	0.063	0.00076	0.033	3.3	0.045	0.031	0.018	0.051	0.46	4.7	1.9	0.00054	0.44	22	0.018	0.71	0.039	0.074	0.11
05/05/2021	26	21	2.5	0.017	0.73	7.6	0.27	0.4	0.34	0.059	0.065	178	97	0.058	10	661	0.22	31	0.39	0.39	1.1
06/05/2021	37	23	1.6	0.027	0.71	6.9	0.90	0.38	0.45	0.048	0.048	447	135	0.15	20	1157	1.3	59	0.97	0.55	2
07/05/2021	36	25	4	0.025	1.7	9	0.45	0.8	0.43	0.14	0.076	371	246	0.14	23	1618	0.041	74	0.95	1	2.5
08/05/2021	20	29	1.8	0.011	1.3	10	0.22	0.53	0.2	0.14	0.36	117	52	0.035	7	441	0.12	23	0.23	0.32	1.5
09/05/2021	24	30	2.6	0.01	1.1	12	0.12	0.69	0.36	0.14	0.16	143	69	0.039	13	402	0.13	37	0.45	0.24	0.99
10/05/2021	21	10	1.1	0.012	0.93	10	0.15	0.41	0.41	0.2	0.13	148	52	0.051	6.7	306	0.15	9	0.59	0.3	0.68
11/05/2021	21	63	4.1	0.028	1.5	16	0.68	0.6	0.7	0.23	0.22	355	109	0.11	10	879	0.4	24	0.71	0.68	1.5
12/05/2021	25	20	2.2	0.029	1.4	8.2	0.46	0.47	0.41	0.051	0.041	224	114	0.072	17	944	0.3	52	0.43	0.5	1.7
13/05/2021	29	11	2.2	0.022	1.3	7.1	0.66	0.68	0.37	0.05	0.05	158	44	0.034	9	384	0.34	21	0.26	0.22	0.68
14/05/2021	20	28	2.3	0.029	1.3	8.6	0.17	1.1	0.38	0.11	0.24	124	202	0.033	23	1101	0.11	184	0.16	0.46	2.2
15/05/2021	18	7.2	1.2	0.009	0.42	5.5	0.05	0.33	0.16	0.10	0.043	51	39	0.011	4.1	227	0.041	15	0.11	0.19	0.52
16/05/2021	13	25	2	0.012	0.79	9	0.15	0.45	0.33	0.084	0.04	277	508	0.058	31	2791	0.23	151	0.45	0.88	2.8
17/05/2021	N.D.	28	1.5	0.035	0.19	8.3	0.57	0.15	0.55	0.043	0.031	472	153	0.13	14	945	0.8	40	0.71	0.51	2.2
18/05/2021	N.D.	24	2.7	0.019	0.88	7.8	0.28	0.31	0.25	0.062	0.072	121	63	0.038	6.8	409	0.22	13	0.23	0.25	0.8
19/05/2021	20	15	1.1	0.0067	0.35	3.4	0.17	0.13	0.14	0.048	0.15	57	16	0.013	1.8	138	0.078	3.9	0.15	0.11	0.34
20/05/2021	10	58	1.2	0.015	0.72	8.6	0.40	0.35	0.3	0.052	0.044	333	101	0.069	10	604	0.56	34	0.54	0.36	0.92
21/05/2021	33	56	3.2	0.038	1.8	15	1.15	0.92	0.6	0.15	0.11	228	102	0.081	16	796	0.36	64	0.46	0.42	1.3
22/05/2021	31	14	2	0.012	0.91	12	0.11	0.35	0.31	0.45	0.083	182	88	0.046	5.5	344	0.17	10	0.39	0.51	0.71
23/05/2021	17	26	5.2	0.01	1.1	13	0.30	0.49	0.37	0.24	0.084	377	181	0.084	12	1185	0.39	36	0.62	0.65	1.3
24/05/2021	N.D.	9	2.1	0.012	0.9	8.3	0.15	0.51	0.24	0.1	0.074	127	95	0.034	5.3	335	0.13	7.1	0.34	0.24	0.56
Mean	24	26	2.3	0.019	1	9	0.37	0.5	0.36	0.12	0.11	225	123	0.064	12	783	0.3	44	0.46	0.44	1.3
Std. Dev.	7.7	16	1.1	0.01	0.43	3.1	0.29	0.24	0.14	0.1	0.085	127	107	0.04	7.5	613	0.29	47	0.25	0.24	0.72

2.3.1. OP^{AA}

For both the PM_{10} equivalent samples, the OP^{AA} followed the method reported by Fang et al. [21]. Phosphate buffer measuring 300 µL (0.5 mM) and 100 µL of AA reagent (2 mM; Sigma–Aldrich, St. Louis, Missouri, USA) was added to 2.5 mL of sample solution. Then, the absorbance of the reaction mixture was recorded at 265 nm wavelength at different reaction times (0, 10, and 20 min) using UV-Vis absorption spectrometry (Varian Cary 50 Bio UV-Vis; Varian Inc., Palo Alto, CA, USA). Blanks were always measured in parallel. OP^{AA} was calculated as the AA depletion rate per sampled volume (nmol AA min^{-1} m^{-3}) according to Equation (1).

$$\sigma AA = -\sigma Abs \times \frac{N_0}{Abs_0}, \qquad OP^{AA} = \frac{\sigma AA_s - \sigma AA_b}{\frac{V_a}{V_e} \times V_S} \tag{1}$$

where σAbs is the slope of the absorbance of operative blanks vs. time (min^{-1}), Abs_0 is the initial absorbance calculated from the intercept of the linear regression of absorbance vs. time, N_0 is the number of AA moles added into the reaction mixture (200 nmol), σAA_s and σAA_b are the rates of AA consumption for the sample and for the blank, respectively (nmol min^{-1}), V_e and V_a are the extraction volume and sample volume added to the reaction mixture, respectively, and V_s is the PM sampled volume (m^3).

2.3.2. OP^{DTT}

To perform OP^{DTT}, the solution of PM_{10} equivalent samples was split into three aliquots of 0.7 mL each (2.1 mL in total), then incubated at 37 °C with 0.1 mL of DTT (1 mM; Sigma–Aldrich, USA) and 0.2 mL of potassium phosphate buffer (1 M). Then, 1 mL of trichloroacetic acid (10% TCA; Sigma–Aldrich, USA) was added to the mixture at different reaction times (0, 10, and 20 min) to stop the DTT reaction. An aliquot of the reaction mixture (1 mL) was taken and mixed with 2 mL of tris-buffer (0.08 M, containing EDTA 4 mM) and with 50 µL of 5,5-dithiobis-2-nitrobenzoic acid (DTNB; Sigma–Aldrich, USA) to form 2-nitro-5-mercaptobenzoic acid (TNB) for a colorimetric reaction with the residual DTT. The obtained solution was then measured at 412 nm using the UV-Vis spectrometer. Furthermore, blanks were measured in parallel to samples. OP^{DTT} was expressed as DTT consumption rate per sampled PM volume (nmol DTT min^{-1} m^{-3}), according to Equation (2).

$$\sigma DTT = -\sigma Abs \times \frac{N_0}{Abs_0}, \qquad OP^{DTT} = \frac{\sigma DTT_s - \sigma DTT_b}{\frac{V_a}{V_e} \times V_s} \tag{2}$$

where σAbs is the slope of the absorbance of operative blanks vs. time (min^{-1}), Abs_0 is the initial absorbance calculated from the intercept of the linear regression of absorbance vs. time, N_0 is the number of DTT moles added in the reaction mixture (100 nmol), σDTT_s and σDTT_b are the rates of DTT consumption for the sample and for the blank, respectively (nmol min^{-1}), V_e and V_a are the extraction volume and sample volume added to the reaction mixture, respectively, and V_s is the PM sampled volume (m^3).

2.3.3. OP^{DCFH}

DCFH solution was prepared by dissolving 4.873 mg of the 2', 7'-dichlorofluorescein diacetate (DCFH-DA; Sigma–Aldrich, USA) in 5mL of ethanol (EtOH, 96%) in the dark. Then, 20 mL NaOH 0.01M were added to favor the de-acetalization reaction. The obtained solution was kept in the dark at room temperature for at least 30 minutes before use. 125 µL of DCFH reagent (5 µM) and 5 mL of HRP (0.5 units mL^{-1}) dissolved in a sodium phosphate buffer (pH 7.4; 25 mM) were added to 1.5 mL of the solution of PM_{10} equivalent samples. The reaction mixture was placed in the thermostatically controlled water bath at 37 ºC for 5 minutes. The DCFH becomes fluorescent dichlorofluorescein (DCF) upon reaction with ROS. Hence, the concentration of DCF was measured by using fluorescent spectroscopy (Jasco FP-920; excitation at 427 nm, emission at 530 nm). Standard H_2O_2 solutions (5×10^{-8}, 1×10^{-7}, 2×10^{-7}, 5×10^{-7} and 1×10^{-6} M) were used to obtain a calibration curve to convert the fluorescence intensity into H_2O_2 equivalents, which are used as indicators of the reactive species reactivity, thus obtaining OP^{DCFH} values (nmol H_2O_2 m^{-3}).

2.4. Data analysis

The paired sample *t*-test was used to observe the significance of the differences between WSOP and TOP results obtained by each OP method applied to the 20 couples of equivalent PM_{10} samples in order to evaluate the significance of the contribution of insoluble particles to the generation of the TOP. A *p*-value less than 0.05 was considered statistically significant.

A principal component analysis (PCA) was carried out on the matrix of the data (580 data points) composed of 20 PM_{10} samples and 29 variables: OP^{DCFH}, OP^{AA} and OP^{DTT} for the water-soluble OP ($WSOP^{AA}$, $WSOP^{DTT}$ and $WSOP^{DCFH}$), insoluble OP (IOP^{AA}, IOP^{DTT} and IOP^{DCFH}) and total OP (TOP^{AA}, TOP^{DTT} and TOP^{DCFH}), and 10 elements in the water-soluble (Al_ws, Cr_ws, Cs_ws, Cu_ws, Fe_ws, Li_ws, Ni_ws, Rb_ws, Sb_ws, Sn_ws) and insoluble fraction (Al_i, Cr_i, Cs_i, Cu_i, Fe_i, Li_i, Ni_i, Rb_i, Sb_i, Sn_i) of the PM_{10} samples. The matrix of the data was transformed by column mean centering and row and column autoscaling to correct variations in the different scaling of the variables before performing the PCA [55,56]. The principal component analysis was performed using the statistical software CAT (Chemometric Agile Tool) based on the R-project for statistical computing, Ver. 3.0, 32-bit.

3. Results and Discussion

3.1. WSOP vs TOP

The contribution of the PM_{10} insoluble fraction to the TOP was assessed comparing the results obtained by the OP^{DCFH}, OP^{AA}, and OP^{DTT} assays performed on the water-soluble fraction of PM_{10} (WSOP) to the results achieved by applying the three assays to the aqueous suspension of intact PM_{10} (water-soluble and insoluble PM_{10}; TOP). WSOP, TOP, and IOP (insoluble OP obtained from the difference between TOP and WSOP) obtained results are shown in Figure 2 and reported in Table 2 along with the percentage of the contribution of IOP to TOP.

Table 2. WSOP, TOP, and IOP values for the OP^{DCFH}, OP^{AA}, and OP^{DTT} assays applied to the 20 PM_{10} samples collected at PR.

	DCFH				AA				DTT			
	WSOP	**TOP**	**IOP**	**IOP/TOP**	**WSOP**	**TOP**	**IOP**	**IOP/TOP**	**WSOP**	**TOP**	**IOP**	**IOP/TOP**
UoM	nmol H_2O_2 m^{-3}			%	nmol AA min^{-1} m^{-3}			%	nmol DTT min^{-1} m^{-3}			%
MDL	$1.1 \cdot 10^{-10}$				0.0096				0.0058			
05/05/2021	$1.1 \cdot 10^{-8}$	$2.2 \cdot 10^{-8}$	$1.1 \cdot 10^{-8}$	49	0.37	0.42	0.051	12	0.32	0.49	0.17	35
06/05/2021	$6.8 \cdot 10^{-9}$	$1.9 \cdot 10^{-8}$	$1.2 \cdot 10^{-8}$	63	0.25	1.2	0.99	80	0.077	0.79	0.71	90
07/05/2021	$1.1 \cdot 10^{-8}$	$2.2 \cdot 10^{-8}$	$1.1 \cdot 10^{-8}$	51	1.6	2.1	0.36	18	0.43	0.82	0.39	48
08/05/2021	$1.8 \cdot 10^{-8}$	$1.9 \cdot 10^{-8}$	$4.7 \cdot 10^{-10}$	2	0.16	0.94	0.78	83	0.63	0.97	0.34	35
09/05/2021	$1.7 \cdot 10^{-8}$	$2.1 \cdot 10^{-8}$	$3.9 \cdot 10^{-9}$	18	0.67	1.4	0.69	51	0.75	0.89	0.14	15
10/05/2021	$1.1 \cdot 10^{-8}$	$1.2 \cdot 10^{-8}$	$8.7 \cdot 10^{-10}$	8	0.69	1.9	1.2	64	0.86	0.86	0.0015	0.17
11/05/2021	$3.4 \cdot 10^{-8}$	$4.1 \cdot 10^{-8}$	$6.6 \cdot 10^{-9}$	16	0.28	1.6	1.3	82	0.61	1.4	0.83	58
12/05/2021	$8.2 \cdot 10^{-9}$	$2.1 \cdot 10^{-8}$	$1.2 \cdot 10^{-8}$	59	1.5	1.7	0.25	15	0.19	0.22	0.02	9
13/05/2021	$6.9 \cdot 10^{-9}$	$1.2 \cdot 10^{-8}$	$5.2 \cdot 10^{-9}$	43	0.69	1.5	0.84	55	0.52	0.71	0.19	27
14/05/2021	$1.9 \cdot 10^{-8}$	$1.9 \cdot 10^{-8}$	$4.4 \cdot 10^{-10}$	2	0.46	1.5	1.1	69	0.46	0.84	0.38	45
15/05/2021	$1.5 \cdot 10^{-9}$	$2.4 \cdot 10^{-8}$	$2.3 \cdot 10^{-8}$	94	0.62	1.5	0.89	59	0.51	1.1	0.49	49
16/05/2021	$9.3 \cdot 10^{-9}$	$9.9 \cdot 10^{-9}$	$6.3 \cdot 10^{-10}$	6	0.04	0.89	0.86	96	0.26	0.59	0.33	56
17/05/2021	$7.4 \cdot 10^{-9}$	$1.9 \cdot 10^{-8}$	$1.2 \cdot 10^{-8}$	62	0.47	0.91	0.44	48	0.11	1.1	0.96	90
18/05/2021	$1.5 \cdot 10^{-8}$	$3.1 \cdot 10^{-8}$	$1.5 \cdot 10^{-8}$	50	1.1	1.2	0.18	15	0.39	0.78	0.39	50
19/05/2021	$1.4 \cdot 10^{-8}$	$1.8 \cdot 10^{-8}$	$4.3 \cdot 10^{-9}$	23	0.33	0.92	0.59	64	0.0011	0.72	0.72	99
20/05/2021	$1.9 \cdot 10^{-8}$	$1.9 \cdot 10^{-8}$	$1.1 \cdot 10^{-9}$	5	0.14	0.58	0.44	76	0.079	0.11	0.021	21
21/05/2021	$2.2 \cdot 10^{-8}$	$3.3 \cdot 10^{-8}$	$1.6 \cdot 10^{-8}$	42	0.96	1.6	0.65	41	1.19	1.2	0.022	1.8
22/05/2021	$1.9 \cdot 10^{-8}$	$2.9 \cdot 10^{-8}$	$9.8 \cdot 10^{-9}$	33	0.42	0.62	0.21	33	0.056	0.81	0.75	93
23/05/2021	$1.8 \cdot 10^{-8}$	$1.8 \cdot 10^{-8}$	$8.1 \cdot 10^{-10}$	4	0.59	3.9	3.3	85	0.41	0.51	0.11	22
24/05/2021	$1.5 \cdot 10^{-8}$	$2.4 \cdot 10^{-8}$	$8.9 \cdot 10^{-9}$	37	0.59	1.9	1.3	69	0.04	0.31	0.27	86
Mean	$1.4 \cdot 10^{-8}$	$2.2 \cdot 10^{-8}$	$7.6 \cdot 10^{-9}$	35	0.59	1.4	0.82	58	0.39	0.76	0.36	48
Std. Dev.	$7.1 \cdot 10^{-9}$	$7.7 \cdot 10^{-9}$	$6.2 \cdot 10^{-9}$	81	0.42	0.74	0.69	93	0.31	0.32	0.3	91

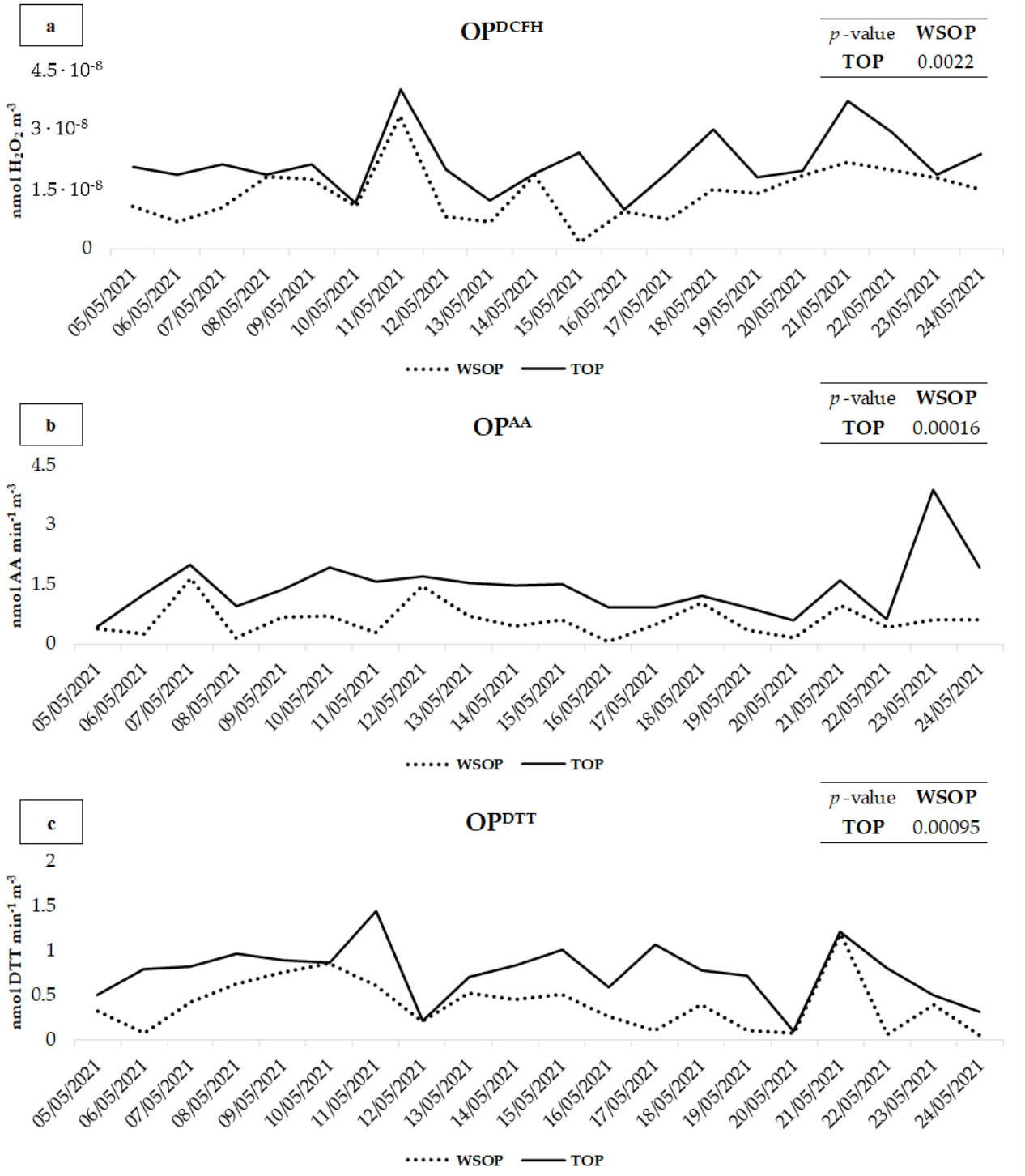

Figure 2. Comparison of OP^{AA} (**a**), OP^{DTT} (**b**), and OP^{DCFH} (**c**) values between the TOP and WSOP of PM_{10} samples collected at PR.

TOP values were found to be significantly higher with respect to those of the WSOP for all the three OP assays. In detail, for the OP^{DCFH}, OP^{AA}, and OP^{DTT} assays, the *p*-value between the TOP and the WSOP is 0.00016,

0.00096, and 0.0022, respectively, confirming a significant contribution of the PM insoluble fraction to the redox properties of the 20 PM_{10} samples.

OP^{AA} (Figure 2b) showed higher values for both the WSOP and the TOP on 7, 10, 11, 21, and 23 May, when the highest concentrations of water-soluble Cu were recorded (Table 1), to which the OP^{AA} is well-known to be selectively responsive [21,57,58].

On 23 May, TOP^{AA} was significantly higher than $WSOP^{AA}$ (3.9 and 0.59, respectively). This was probably due to the higher contribution of crustal dust to PM_{10}. In fact, on that day, much higher concentrations of all the elements released in the insoluble fraction of PM_{10} by resuspension of coarse mineral dust [59–61], such as Al, Cs, Fe, Li e Rb (Table 1), were recorded. It is well-known that OP^{AA} predominantly responds to coarse particles [26,62], and it is assumed that a relevant contribution to the TOP was due to a higher contribution of soil dust on this day.

OP^{DCFH} and OP^{DTT} showed higher TOP with respect to WSOP on 21 and 17 May, respectively, when the highest concentrations of crustal dust elements were recorded, which therefore confirms a significant contribution of soil dust to the TOP. Both the assays exhibited the highest WSOP and TOP on 11 and 21 May, when higher concentrations of Fe, Cr, and Ni from the steel plant [49,63], and Cu, Sb, and Sn from traffic [64–66] were released in water-soluble PM_{10}. Although the insoluble fraction of these elements (especially Fe, to which the DTT was highly sensitive) [67] presented significantly higher concentrations, the OP assays appeared to be predominantly responsive to their water-soluble fraction, which therefore plays a crucial role in the generation of the TOP.

The discussed findings partially agree with the findings of Frezzini et al. [42], which revealed that the insoluble fraction of PM provided a significant contribution to the TOP^{AA} and left open questions regarding the TOP^{DCFH} and TOP^{DTT}, for which the insoluble fraction did not seem to contribute significantly to the TOP, probably due to issues related to the experimental procedure. In detail, the OP^{AA} values were significantly influenced by the PM insoluble fraction, probably due to the higher sensitivity of this assay to the coarser insoluble particles [26,50]. These particles may have moved from the PTFE filters immersed in the aqueous solution during the extraction procedure and reacted with the solutions used for the OP^{AA} assay. Conversely, the insoluble fraction did not determine a significantly higher OP^{DCFH} and OP^{DTT}. This might be explained by the higher sensitivity of these two assays through the fine PM particles [67,68], which are almost predominantly soluble in water [61] and, accordingly, contributed more to WSOP rather than to TOP. Another possible explanation is that particles were probably fixed too deeply in the immersed PTFE filter to fully react with the reagents of the OP^{DCFH} and OP^{DTT} assays to generate significantly higher TOP with respect to WSOP.

The application of the TOP assays directly to the aqueous suspension of intact particles detached from PM_{10} filters overcame the operative limits of performing OP assays directly on solutions containing the immersed PM filter. In fact, the described method allowed the authors to detach and carry in suspension a high fraction of the particles sampled on the filter, approximatively 70% in reference to the recovery of the elements [46].

These results revealed the non-negligible contribution of the insoluble particles to the TOP^{DCFH} and TOP^{DTT}, in agreement with previous findings that demonstrated the relevance of the PM insoluble fraction to the total OP of PM [27,28,45].

3.2. Principal Component Analysis

To identify tracers of emission sources that can determine the above-discussed OP results, explorative PCA was performed on the WSOP, TOP, and IOP values for OP^{AA}, OP^{DTT}, and OP^{DCFH}, and the element concentrations in the water-soluble and insoluble fraction of the 20 PM_{10} samples. Five significant components accounting for 78.4% were obtained from the PCA. The variance explained by each component is of 29.7%, 17.6%, 13.3%, 9.1% and 8.5%, respectively.

The biplot of PC1/PC2 is reported in Supplementary Materials (Figure S1), along with the scores and loadings obtained from the PCA (Table S1). The first component (PC1), which represents 29.7% of the total variance, separates out the samples (scores) in which the highest element concentrations (loadings) were recorded, and largely explains the data variability due to daily variations in atmospheric conditions. However, PC1 only distinguishes samples in which the highest concentrations of all the considered variables were found, as distinct from those characterized by the lowest concentrations. On the contrary, PC2, and PC3, which represent, respectively, 17.6% and 13.3% of the total variance, separate the variables depending on their concentration variability among the sampling days. PC2/PC3 are graphically summarized in the biplot of Figure 3.

PC2 and PC3 account for 31.1% of the total variance. In the biplot, the variables are grouped in 4 main clusters, each one containing tracers of a specific emission source. The cluster on the lower-left part of the biplot includes the insoluble elements typically released by the steel plant and by non-exhaust traffic, such as brake abrasion (Cu_i, Cr_i, Fe_i, Ni_i, Sb_i, and Sn_i) [64–66,69,70]. The cluster on the upper-left part of the biplot contains the same elemental tracers of the group described above in their water-soluble fraction (Cu_ws, Cr_ws, Fe_ws, Ni_ws, Sb_ws, and Sn_ws). The group on the upper-right part of the biplot contains the water-soluble elements mainly released by biomass burning emission sources (Cs_ws, Li_ws, and Rb_ws) [66,71–73]. Lastly, the cluster on the lower-right part of the biplot includes insoluble elements considered as tracers of mineral dust (Al_i, Cs_i, Li_i, and Rb_i) [50,74,75].

Results show that all the three OP assays for the WSOP and TOP are included in the group of traffic and steel plant water-soluble tracers and in the same direction of biomass burning elemental tracers along PC2. On the other hand, WSOP and TOP assays do not seem to respond to the insoluble fraction of the elements released by traffic and the steel plant. This constitutes a first indication that the total OP is dominated by the water-soluble species present in the solution (Figure 1). Although it is known that $WSOP^{AA}$ and $WSOP^{DTT}$ respond predominantly to transition metals, such as Cu and Fe [62,67,76], the TOP, when using both the assays, was found to be sensitive mainly to the water-soluble fraction of these elements, even if Cu and Fe, as well as the other non-exhaust traffic and steel plant elemental tracers, were almost exclusively in their insoluble fraction (Figure 1). Moreover, the predominant dependence of OP^{DCFH} and OP^{DTT} on traffic, steel plant, and biomass

burning water-soluble particles and the higher sensitivity of OP^{AA} to non-exhaust traffic is confirmed [50,77–79]. The response of the OP^{DCFH} and OP^{DTT} assays to biomass burning tracers confirms previous findings [21,50,80,81] and highlights the central role of the water-soluble species in determining PM redox properties, even when TOP is considered.

This represents a key finding, since it gives strength to the reliability of the OP results, even if performed only on the water-soluble fraction of PM_{10}. Overall, the application of the OP assays to the intact particles detached from PM_{10} filters (water-soluble and insoluble fraction) reveals that water-soluble PM_{10} released by traffic, steel plant, and biomass burning was primarily responsible for the generation of the TOP.

Finally, it is worth noting that IOP^{DTT} and IOP^{DCFH} are clustered with the insoluble Al, Cs, Li, and Rb, tracers of mineral dust, thus showing that considering only the insoluble fraction of PM_{10}, OP^{DTT}, and OP^{DCFH} are mainly responsive to soil particles [26,50,82,83]. The results obtained in this study are compared and tabulated with the findings of existing works in the literature in Supplementary Materials (Table S2).

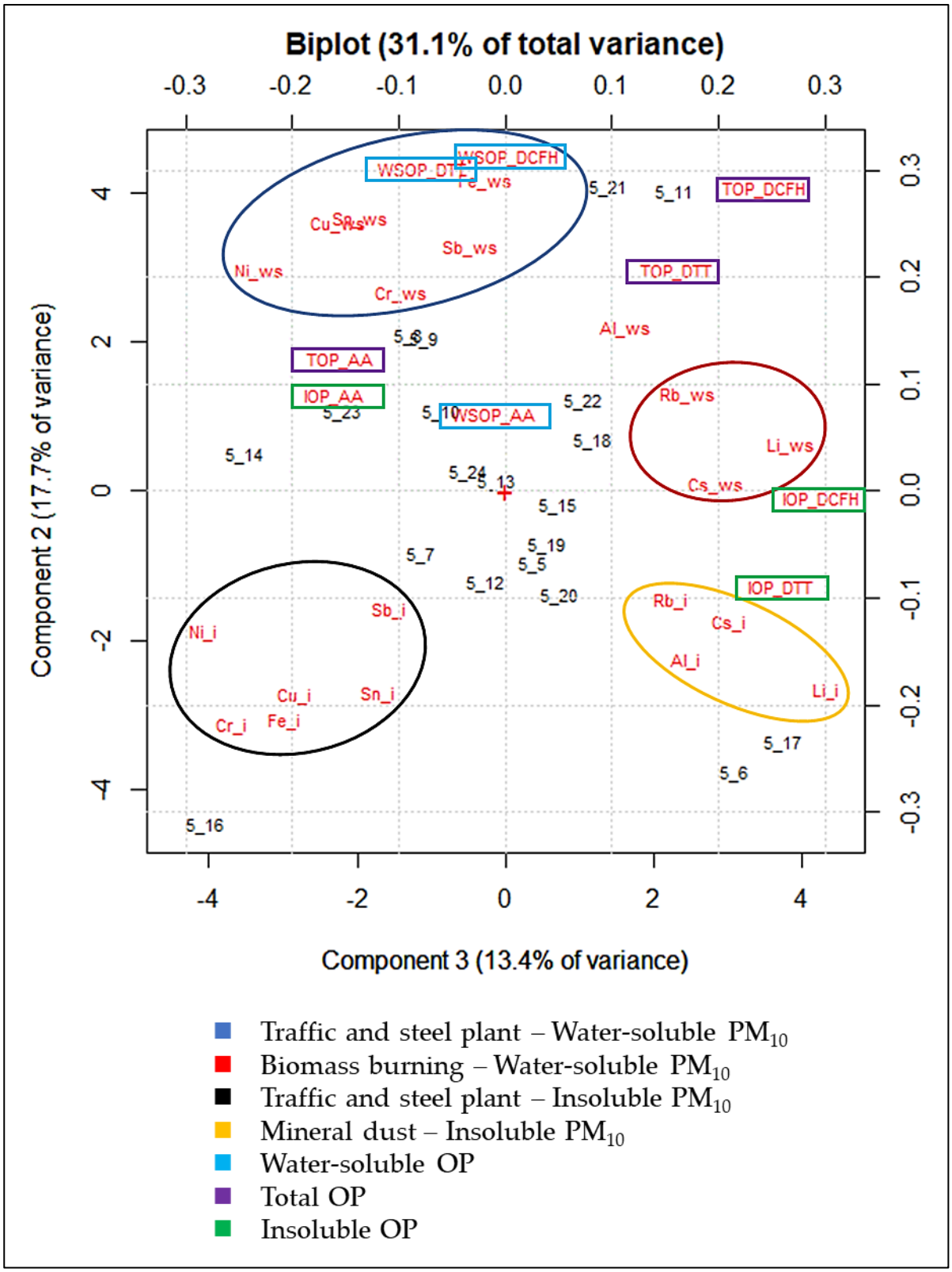

Figure 3. Biplot of PC2/PC3 from the PCA performed on the WSOP, TOP, and IOP values for OP^{AA}, OP^{DTT}, and OP^{DCFH}, and element concentrations in the water-soluble (_ws) and insoluble (_i) fraction of the 20 PM_{10} samples.

4. Conclusions

It is well known that the different PM components are responsible for several effects that can trigger harmful oxidative reactions and inflammation on living organisms, contributing to genotoxicity and cytotoxic mechanisms responsible for cell damage. However, most of the studies conducted so far have exclusively evaluated the toxicity of the water-soluble fraction of PM, which is considered more bioavailable and is more easily extractable. Since it has been shown that insoluble species can contribute significantly to the toxicological potential of PM, the evaluation of the OP of both PM fractions (water-soluble and insoluble) is essential for the assessment of the total health risk induced by PM.

The application of an innovative method for the detachment and suspension in water of intact PM_{10} (water-soluble and insoluble species) from the sampled filters allowed us to evaluate the total OP of PM_{10} collected at a highly polluted industrial site, and to identify specifically the contribution to the OP of every single fraction (water-soluble and insoluble). By performing explorative PCA, it was possible to evaluate the response of the OP^{DCFH}, OP^{AA}, and OP^{DTT} assays to the various elemental fractions, and to identify the different emission sources responsible for the WSOP, TOP, and IOP.

The results confirmed the different sensitivity of the three OP assays to the various PM_{10} components. In particular, the dependence of OP^{DCFH} and OP^{DTT} on traffic, steel plant, and biomass burning water-soluble particles, and the sensitivity of OP^{AA} to non-exhaust traffic, was reinforced.

Moreover, the application of the OP assays to the intact particles detached from PM_{10} filters (water-soluble and insoluble fraction) reveals that water-soluble PM_{10} released by traffic, steel plant, and biomass burning is primarily responsible for the generation of the TOP. This represents a key finding since it gives strength to the reliability of the OP results, even if performed only on the water-soluble fraction of PM_{10}. In addition, the insoluble fraction of PM_{10} was found to be able to contribute to the IOP^{DCFH} and IOP^{DTT}, which seem to respond to mineral particles.

Further studies will have to be carried out to verify these results and to confirm the representativeness of the WSOP and TOP assays by comparison with biological endpoints.

Author contributions: Conceptualization: L.M. and S.C.; Writing – Original Draft Preparation: M.A.F; Formal Analysis: M.A.F., G.D.I., C.T., and L.M.; Data Curation: M.A.F. and L.M.; Writing – Review & Editing: L.M.; Supervision: L.M. and S.C..

Supplementary Material

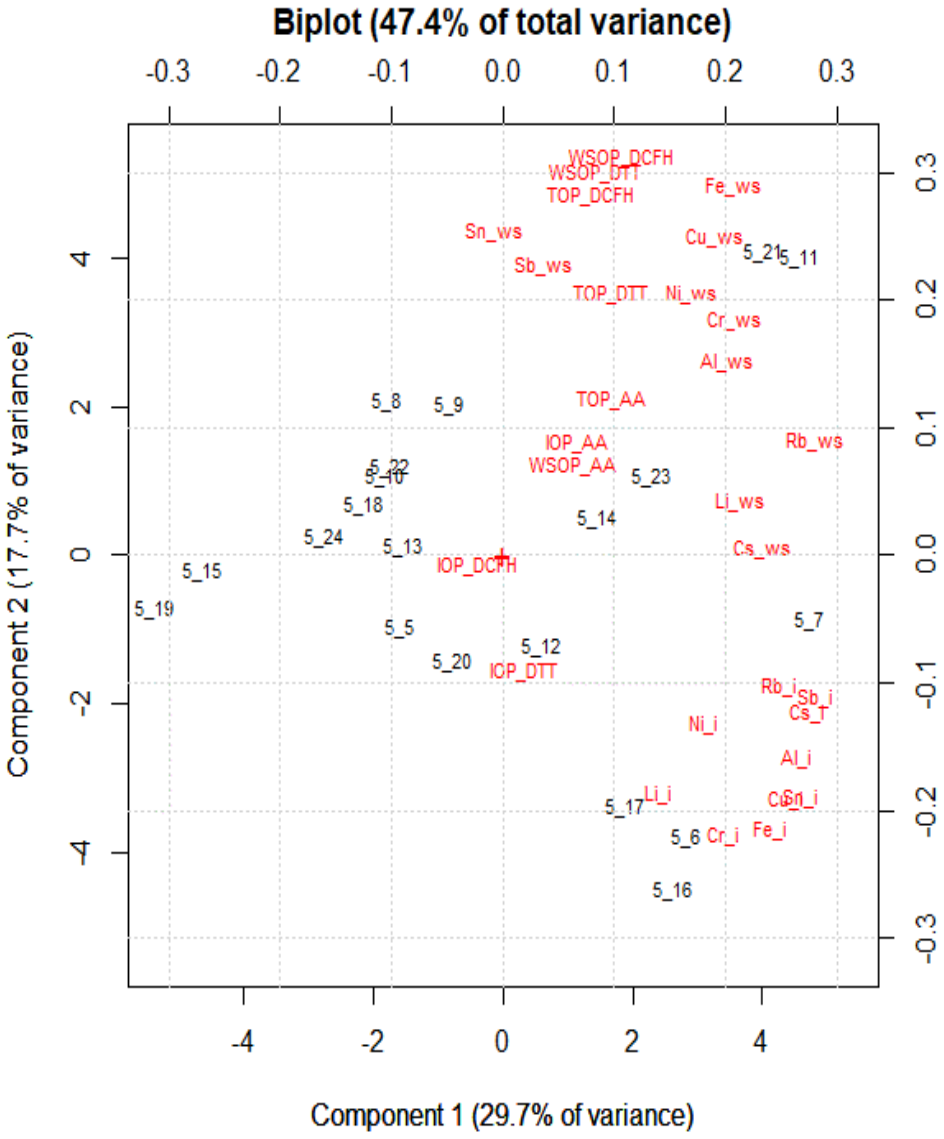

Figure S1. Biplot of PC1/PC2 from the PCA performed on the WSOP, TOP and IOP values for OP^{AA}, OP^{DTT} and OP^{DCFH}, and element concentrations in the water-soluble (_ws) and insoluble (_i) fraction of the 20 PM_{10} samples.

Table S1. Scores and loadings of the five significant components obtained by performing the PCA on the matrix of the data (580 data points) composed of 20 PM_{10} samples and 29 variables.

Scores					
Sampling days	**PC1**	**PC2**	**PC3**	**PC4**	**PC5**
05/05/2021	-1.58623	-0.97751	0.366896	-0.58442	0.525427
06/05/2021	2.825923	-3.78792	3.093845	0.545744	-0.39122
07/05/2021	4.723902	-0.86232	-1.14036	-2.10932	-1.13162
08/05/2021	-1.8033	2.084004	-1.30369	1.441808	1.868484
09/05/2021	-0.83201	2.034397	-1.10832	-0.01011	0.298175
10/05/2021	-1.80823	1.050559	-0.8631	0.088544	-1.31561
11/05/2021	4.579853	4.018884	2.279596	2.541445	0.896487
12/05/2021	0.582918	-1.23078	-0.27615	-2.92858	-0.90267
13/05/2021	-1.53575	0.115022	-0.13071	-1.83719	-0.55313
14/05/2021	1.459193	0.496354	-3.52565	-0.42523	2.837427
15/05/2021	-4.62859	-0.20388	0.716007	-1.35113	-0.341
16/05/2021	2.620193	-4.48785	-4.05242	1.277222	1.632599
17/05/2021	1.889916	-3.38443	3.736475	0.667041	0.574365
18/05/2021	-2.15952	0.67568	1.173823	-1.38265	0.085947
19/05/2021	-5.36124	-0.71588	0.568159	1.140972	0.694384
20/05/2021	-0.78153	-1.41344	0.723884	1.187126	0.323789
21/05/2021	4.018949	4.075919	1.394198	-2.57333	1.033031
22/05/2021	-1.73454	1.199607	1.05762	2.003	0.199001
23/05/2021	2.296258	1.06587	-2.21067	2.274585	-4.77111
24/05/2021	-2.76617	0.247707	-0.49945	0.03448	-1.56275

Loadings					
Variables	**PC1**	**PC2**	**PC3**	**PC4**	**PC5**
Al_ws	0.202118	0.152137	0.112682	0.119205	0.189423
Cr_ws	0.209275	0.185106	-0.09756	0.025169	-0.26846
Cs_ws	0.233754	0.005509	0.198207	-0.25518	0.158213
Cu_ws	0.191098	0.250126	-0.15696	-0.22041	0.000476
Fe_ws	0.207767	0.289439	-0.01825	0.151439	-0.04107
Li_ws	0.213234	0.043432	0.268443	-0.16677	0.013301
Ni_ws	0.170286	0.204958	-0.23076	-0.22054	0.124316
Rb_ws	0.281455	0.09039	0.171594	-0.02445	0.019824
Sb_ws	0.037206	0.226891	-0.03177	0.263081	-0.11452
Sn_ws	-0.007	0.254486	-0.13573	0.191646	0.278418
Al_i	0.263753	-0.15869	0.168546	0.152362	-0.15281
Cr_i	0.198209	-0.21885	-0.25667	0.080872	0.074766
Cs_i	0.273661	-0.12257	0.211103	0.03386	-0.12215
Cu_i	0.25519	-0.19079	-0.19718	-0.09994	0.133902
Fe_i	0.240169	-0.21497	-0.20856	0.043342	0.052501
Li_i	0.13994	-0.18706	0.30071	0.113352	-0.05304

Ni_i	0.180699	-0.1324	-0.28278	-0.06543	0.272648
Rb_i	0.248643	-0.10284	0.15529	0.088082	-0.21192
Sb_i	0.281863	-0.1117	-0.10927	0.076375	-0.05547
Sn_i	0.268744	-0.18949	-0.11911	5.76E-05	0.156959
WSOP_DCFH	0.106592	0.31247	0.003721	0.282605	0.122929
WSOP_AA	0.080588	0.282404	0.244534	-0.01092	0.080655
WSOP_DTT	-0.02158	-0.00766	0.29737	-0.332	-0.04064
TOP_DCFH	0.064564	0.070874	-0.00942	-0.47377	-0.23155
TOP_AA	0.098635	0.122204	-0.15466	-0.02628	-0.48675
TOP_DTT	0.066954	0.088444	-0.16027	0.25711	-0.38284
IOP_DCFH	0.083487	0.300087	-0.07867	-0.19464	0.064812
IOP_AA	0.09791	0.205504	0.161367	0.05422	0.221876
IOP_DTT	0.019403	-0.0906	0.259459	0.264108	0.174796

References

1. World Health Organization. *WHO Global Air Quality Guidelines: Particulate Matter (PM2. 5 and PM10), Ozone, Nitrogen Dioxide, Sulfur Dioxide and Carbon Monoxide: Executive Summary*; WHO: Geneva, Switzerland, 2021.
2. Shaddick, G.; Thomas, M.L.; Mudu, P.; Ruggeri, G.; Gumy, S. Half the world's population are exposed to increasing air pollution. *NPJ Clim. Atmos. Sci.* **2020**, *3*, 1–5. https://doi.org/10.1038/s41612-020-0124-2.
3. IARC. IARC Working Group on the Evaluation of Carcinogenic Risks to Humans. Outdoor Air Pollution. *IARC Monogr. Eval. Carcinog. Risks Hum.* **2016**, *109*, 9.
4. Burnett, R.; Chen, H.; Szyszkowicz, M.; Fann, N.; Hubbell, B.; Pope, C.A., 3rd; Apte, J.S.; Brauer, M.; Cohen, A.; Weichenthal, S.; et al. Global estimates of mortality associated with long-term exposure to outdoor fine particulate matter. *Proc. Natl. Acad. Sci. USA* **2018**, *115*, 9592–9597. https://doi.org/10.1073/pnas.1803222115.
5. Janghorbani, M.; Momeni, F.; Mansourian, M. Systematic review and metaanalysis of air pollution exposure and risk of diabetes. *Eur. J. Epidemiol.* **2014**, *29*, 231–242. https://doi.org/10.1007/s10654-014-9907-2.
6. Losacco, C.; Perillo, A. Particulate matter air pollution and respiratory impact on humans and animals. *Environ. Sci. Pollut. Res.* **2018**, *25*, 33901–33910. https://doi.org/10.1007/s11356-018-3344-9.
7. Costa, L.G.; Cole, T.B.; Dao, K.; Chang, Y.-C.; Coburn, J.; Garrick, J.M. Effects of air pollution on the nervous system and its possible role in neurodevelopmental and neurodegenerative disorders. *Pharmacol. Ther.* **2020**, *210*, 107523. https://doi.org/10.1016/j.pharmthera.2020.107523.
8. Zhang, L.; Xu, H.; Fang, B.; Wang, H.; Yang, Z.; Yang, W.; Hao, Y.; Wang, X.; Wang, Q.; Wang, M. Source Identification and Health Risk Assessment of Polycyclic Aromatic Hydrocarbon-Enriched PM 2.5 in Tangshan, China. *Environ. Toxicol. Chem.* **2020**, *39*, 458–467. https://doi.org/10.1002/etc.4618.

9. Liu, S.; Jørgensen, J.T.; Ljungman, P.; Pershagen, G.; Bellander, T.; Leander, K.; Magnusson, P.K.; Rizzuto, D.; Hvidtfeldt, U.A.; Raaschou-Nielsen, O.; et al. Long-term exposure to low-level air pollution and incidence of asthma: The ELAPSE project. *Eur. Respir. J.* **2021**, *57*, 2003099. https://doi.org/10.1183/13993003.030992020.
10. Chen, J.; Hoek, G. Long-term exposure to PM and all-cause and cause-specific mortality: A systematic review and meta-analysis. *Environ. Int.* **2020**, *143*, 105974. https://doi.org/10.1016/j.envint.2020.105974.
11. Liu, L.; Zhou, Q.; Yang, X.; Li, G.; Zhang, J.; Zhou, X.; Jiang, W. Cytotoxicity of the soluble and insoluble fractions of atmospheric fine particulate matter. *J. Environ. Sci.* **2020**, *91*, 105–116. https://doi.org/10.1016/j.jes.2020.01.012.
12. Øvrevik, J. Oxidative potential versus biological effects: A review on the relevance of cell-free/abiotic assays as predictors of toxicity from airborne particulate matter. *Int. J. Mol. Sci.* **2019**, *20*, 4772.
13. Di Meo, S.; Reed, T.T.; Venditti, P.; Victor, V.M. Role of ROS and RNS Sources in Physiological and Pathological Conditions. *Oxid. Med. Cell. Longev.* **2016**, *2016*, 1245049. https://doi.org/10.1155/2016/1245049.
14. Nozza, E.; Valentini, S.; Melzi, G.; Vecchi, R.; Corsini, E. Advances on the immunotoxicity of outdoor particulate matter: A focus on physical and chemical properties and respiratory defence mechanisms. *Sci. Total Environ.* **2021**, *780*, 146391. https://doi.org/10.1016/j.scitotenv.2021.146391.
15. Gao, D.; Mulholland, J.A.; Russell, A.G.; Weber, R.J. Characterization of water-insoluble oxidative potential of PM2.5 using the dithiothreitol assay. *Atmos. Environ.* **2020**, *224*, 117327. https://doi.org/10.1016/j.atmosenv.2020.117327.
16. Molina, C.; Toro, A.; Manzano, C.A.R.; Canepari, S.; Massimi, L.; Leiva-Guzmán, M. Airborne aerosols and human health: Leapfrogging from mass concentration to oxidative potential. *Atmosphere* **2020**, *11*, 917.
17. Bates, J.T.; Fang, T.; Verma, V.; Zeng, L.; Weber, R.J.; Tolbert, P.E.; Abrams, J.Y.; Sarnat, S.E.; Klein, M.; Mulholland, J.A.; et al. Review of Acellular Assays of Ambient Particulate Matter Oxidative Potential: Methods and Relationships with Composition, Sources, and Health Effects. *Environ. Sci. Technol.* **2019**, *53*, 4003–4019. https://doi.org/10.1021/acs.est.8b03430.
18. Borm, P.J.A.; Kelly, F.; Künzli, N.; Schins, R.P.F.; Donaldson, K. Oxidant generation by particulate matter: From biologically effective dose to a promising, novel metric. *Occup. Environ. Med.* **2007**, *64*, 73–74. https://doi.org/10.1136/oem.2006.029090.
19. Pietrogrande, M.C.; Bacco, D.; Trentini, A.; Russo, M. Effect of filter extraction solvents on the measurement of the oxidative potential of airborne PM2.5. *Environ. Sci. Pollut. Res.* **2021**, *28*, 1–13. https://doi.org/10.1007/s11356-021-12604-7.
20. Crobeddu, B.; Baudrimont, I.; Deweirdt, J.; Sciare, J.; Badel, A.; Camproux, A.-C.; Bui, L.C.; Baeza-Squiban, A. Lung Antioxidant Depletion: A Predictive Indicator of Cellular Stress Induced by Ambient Fine Particles. *Environ. Sci. Technol.* **2020**, *54*, 2360–2369. https://doi.org/10.1021/acs.est.9b05990.

21. Fang, T.; Verma, V.; Bates, J.T.; Abrams, J.; Klein, M.; Strickland, M.J.; Sarnat, S.E.; Chang, H.H.; Mulholland, J.A.; Tolbert, P.E.; et al. Oxidative potential of ambient water-soluble PM2.5 in the southeastern United States: Contrasts in sources and health associations between ascorbic acid (AA) and dithiothreitol (DTT) assays. *Atmos. Chem. Phys.* **2016**, *16*, 3865–3879. https://doi.org/10.5194/acp-16-3865-2016.
22. Huang, W.; Baumgartner, J.; Zhang, Y.; Wang, Y.; Schauer, J.J. Source apportionment of air pollution exposures of rural Chinese women cooking with biomass fuels. *Atmos. Environ.* **2015**, *104*, 79–87. https://doi.org/10.1016/j.atmosenv.2014.12.066.
23. Halliwell, B.; Whiteman, M. Measuring reactive species and oxidative damagein vivoand in cell culture: How should you do it and what do the results mean? *J. Cereb. Blood Flow Metab.* **2004**, *142*, 231–255. https://doi.org/10.1038/sj.bjp.0705776.
24. Zhang, Z.-H.; Hartner, E.; Utinger, B.; Gfeller, B.; Paul, A.; Sklorz, M.; Czech, H.; Yang, B.X.; Su, X.Y.; Jakobi, G.; et al. Are reactive oxygen species (ROS) a suitable metric to predict toxicity of carbonaceous aerosol particles? *Atmos. Chem. Phys.* **2021**, *22*, 1793–1809. https://doi.org/10.5194/acp-22-1793-2022.
25. Daellenbach, K.R.; Uzu, G.; Jiang, J.; Cassagnes, L.-E.; Leni, Z.; Vlachou, A.; Stefenelli, G.; Canonaco, F.; Weber, S.; Segers, A.; et al. Sources of particulate-matter air pollution and its oxidative potential in Europe. *Nature* **2020**, *587*, 414–419. https://doi.org/10.1038/s41586-020-2902-8.
26. Simonetti, G.; Conte, E.; Perrino, C.; Canepari, S. Oxidative potential of size-segregated PM in an urban and an industrial area of Italy. *Atmos. Environ.* **2018**, *187*, 292–300. https://doi.org/10.1016/j.atmosenv.2018.05.051.
27. Piacentini, D.; Falasca, G.; Canepari, S.; Massimi, L. Potential of PM-selected components to induce oxidative stress and root system alteration in a plant model organism. *Environ. Int.* **2019**, *132*, 105094. https://doi.org/10.1016/j.envint.2019.105094.
28. Conte, E.; Canepari, S.; Frasca, D.; Simonetti, G. Oxidative potential of selected PM components. *Multidiscip. Digit. Publ. Inst. Proceeding* **2017**, *1*, 108.
29. Rao, L.; Zhang, L.; Wang, X.; Xie, T.; Zhou, S.; Lu, S.; Liu, X.; Lu, H.; Xiao, K.; Wang, W.; et al. Oxidative Potential Induced by Ambient Particulate Matters with Acellular assays: A Review. *Processes* **2020**, *8*, 1410. https://doi.org/10.3390/pr8111410.
30. Gao, D.; Fang, T.; Verma, V.; Zeng, L.; Weber, R.J. A method for measuring total aerosol oxidative potential (OP) with the dithiothreitol (DTT) assay and comparisons between an urban and roadside site of water-soluble and total OP. *Atmos. Meas. Tech.* **2017**, *10*, 2821–2835. https://doi.org/10.5194/amt-10-2821-2017.
31. Verma, V.; Fang, T.; Xu, L.; Peltier, R.E.; Russell, A.G.; Ng, N.L.; Weber, R.J. Organic Aerosols Associated with the Generation of Reactive Oxygen Species (ROS) by Water-Soluble PM2.5. *Environ. Sci. Technol.* **2015**, *49*, 4646–4656. https://doi.org/10.1021/es505577w.

32. Yi, S.; Zhang, F.; Qu, F.; Ding, W. Water-insoluble fraction of airborne particulate matter (PM10) induces oxidative stress in human lung epithelial A549 cells. *Environ. Toxicol.* **2012**, *29*, 226–233. https://doi.org/10.1002/tox.21750.
33. Fang, T.; Zeng, L.; Gao, D.; Verma, V.; Stefaniak, A.B.; Weber, R.J. Ambient Size Distributions and Lung Deposition of Aerosol Dithiothreitol-Measured Oxidative Potential: Contrast between Soluble and Insoluble Particles. *Environ. Sci. Technol.* **2017**, *51*, 6802–6811. https://doi.org/10.1021/acs.est.7b01536.
34. Gao, D.; Ripley, S.; Weichenthal, S.; Pollitt, K.J.G. Ambient particulate matter oxidative potential: Chemical determinants, associated health effects, and strategies for risk management. *Free Radic. Biol. Med.* **2020**, *151*, 7–25. https://doi.org/10.1016/j.freeradbiomed.2020.04.028.
35. Mukhtar, A.; Limbeck, A. Recent developments in assessment of bio-accessible trace metal fractions in airborne particulate matter: A review. *Anal. Chim. Acta* **2013**, *774*, 11–25. https://doi.org/10.1016/j.aca.2013.02.008.
36. Yan, Z.; Wang, J.; Li, J.; Jiang, N.; Zhang, R.; Yang, W.; Yao, W.; Wu, W. Oxidative stress and endocytosis are involved in upregulation of interleukin-8 expression in airway cells exposed to PM2.5. *Environ. Toxicol.* **2016**, *31*, 1869–1878. https://doi.org/10.1002/tox.22188.
37. Zou, Y.; Jin, C.; Su, Y.; Li, J.; Zhu, B. Water soluble and insoluble components of urban PM2.5 and their cytotoxic effects on epithelial cells (A549) in vitro. *Environ. Pollut.* **2016**, *212*, 627–635. https://doi.org/10.1016/j.envpol.2016.03.022.
38. Knaapen, A.M.; Shi, T.; Borm, P.J.; Schins, R.P. Soluble metals as well as the insoluble particle fraction are involved in cellular DNA damage induced by particulate matter. In *Oxygen/Nitrogen Radicals: Cell Injury and Disease*; Springer: Boston, MA, USA, 2002; pp. 317–326.
39. Soukup, J.M.; Becker, S. Human Alveolar Macrophage Responses to Air Pollution Particulates Are Associated with Insoluble Components of Coarse Material, Including Particulate Endotoxin. *Toxicol. Appl. Pharmacol.* **2001**, *171*, 20–26. https://doi.org/10.1006/taap.2000.9096.
40. Daher, N.; Ning, Z.; Cho, A.K.; Shafer, M.; Schauer, J.J.; Sioutas, C. Comparison of the Chemical and Oxidative Characteristics of Particulate Matter (PM) Collected by Different Methods: Filters, Impactors, and BioSamplers. *Aerosol Sci. Technol.* **2011**, *45*, 1294–1304. https://doi.org/10.1080/02786826.2011.590554.
41. McWhinney, R.D.; Badali, K.; Liggio, J.; Li, S.-M.; Abbatt, J.P.D. Filterable Redox Cycling Activity: A Comparison between Diesel Exhaust Particles and Secondary Organic Aerosol Constituents. *Environ. Sci. Technol.* **2013**, *47*, 3362–3369. https://doi.org/10.1021/es304676x.
42. Frezzini, M.A.; De Francesco, N.; Massimi, L.; Canepari, S. Effects of operating conditions on PM oxidative potential assays. *Atmos. Environ.* **2022**, *268*, 118802. https://doi.org/10.1016/j.atmosenv.2021.118802.
43. Wang, D.; Pakbin, P.; Shafer, M.M.; Antkiewicz, D.; Schauer, J.J.; Sioutas, C. Macrophage reactive oxygen species activity of water-soluble and water-insoluble fractions of ambient coarse, PM2.5 and

ultrafine particulate matter (PM) in Los Angeles. *Atmos. Environ.* **2013**, *77*, 301–310. https://doi.org/10.1016/j.atmosenv.2013.05.031.

44. Fuller, S.; Wragg, F.; Nutter, J.; Kalberer, M. Comparison of on-line and off-line methods to quantify reactive oxygen species (ROS) in atmospheric aerosols. *Atmos. Environ.* **2014**, *92*, 97–103. https://doi.org/10.1016/j.atmosenv.2014.04.006.
45. Verma, V.; Rico-Martinez, R.; Kotra, N.; King, L.; Liu, J.; Snell, T.W.; Weber, R.J. Contribution of Water-Soluble and Insoluble Components and Their Hydrophobic/Hydrophilic Subfractions to the Reactive Oxygen Species-Generating Potential of Fine Ambient Aerosols. *Environ. Sci. Technol.* **2012**, *46*, 11384–11392. https://doi.org/10.1021/es302484r.
46. Massimi, L.; Astolfi, M.L.; Canepari, S. Simple and Efficient Method to Detach Intact PM10 from Field Filters: Elements Recovery Assessment. **2022**. Under Review.
47. Süring, K.; Bach, S.; Höflich, C.; Straff, W. Flow Cytometric Analysis of Particle-bound Bet v 1 Allergen in PM10. *J. Vis. Exp.* **2016**, 117, e54721. https://doi.org/10.3791/54721.
48. Süring, K.; Bach, S.; Bossmann, K.; Wolter, E.; Neumann, A.; Straff, W.; Höflich, C. PM10 contains particle-bound allergens: Dust analysis by Flow Cytometry. *Environ. Technol. Innov.* **2016**, *5*, 60–66. https://doi.org/10.1016/j.eti.2016.01.004.
49. Massimi, L.; Simonetti, G.; Buiarelli, F.; Di Filippo, P.; Pomata, D.; Riccardi, C.; Ristorini, M.; Astolfi, M.L.; Canepari, S. Spatial distribution of levoglucosan and alternative biomass burning tracers in atmospheric aerosols, in an urban and industrial hotspot of Central Italy. *Atmos. Res.* **2020**, *239*, 104904. https://doi.org/10.1016/j.atmosres.2020.104904.
50. Massimi, L.; Ristorini, M.; Simonetti, G.; Frezzini, M.A.; Astolfi, M.L.; Canepari, S. Spatial mapping and size distribution of oxidative potential of particulate matter released by spatially disaggregated sources. *Environ. Pollut.* **2020**, *266*, 115271. https://doi.org/10.1016/j.envpol.2020.115271.
51. ASRO. SR EN 12341: 2014. Air Quality–Determination of the PM10 Fraction of Suspended Particulate Matter. Reference Method and Field Test Procedure to Demonstrate Reference Equivalence of Measurements Methods. 2014. Available online: https://magazin.asro.ro/en/standard/8734 (accessed on 7 February 2022).
52. Canepari, S.; Cardarelli, E.; Pietrodangelo, A.; Strincone, M. Determination of metals, metalloids and non-volatile ions in airborne particulate matter by a new two-step sequential leaching procedure Part A: Experimental design and optimization. *Taanta* **2006**, *69*, 581–587.
53. Canepari, S.; Cardarelli, E.; Pietrodangelo, A.; Strincone, M. Determination of metals, metalloids and non-volatile ions in air-borne particulate matter by a new two-step sequential leaching procedure: Part B: Validation on equivalent real samples. *Talanta* **2006**, *69*, 588–595.
54. Astolfi, M.L.; Protano, C.; Marconi, E.; Massimi, L.; Brunori, M.; Piamonti, D.; Migliara, G.; Vitali, M.; Canepari, S. A new rapid treatment of human hair for elemental determination by inductively coupled mass spectrometry. *Anal. Methods* **2020**, *12*, 1906–1918. https://doi.org/10.1039/c9ay01871a.

55. Conti, M.E.; Iacobucci, M.; Cucina, D.; Mecozzi, M. Multivariate statistical methods applied to biomonitoring studies. *Int. J. Environ. Pollut.* **2007**, *29*, 333. https://doi.org/10.1504/ijep.2007.012809.
56. Massimi, L.; Ristorini, M.; Eusebio, M.; Florendo, D.; Adeyemo, A.; Brugnoli, D.; Canepari, S. Monitoring and Evaluation of Terni (Central Italy) Air Quality through Spatially Resolved Analyses. *Atmosphere* **2017**, *8*, 200. https://doi.org/10.3390/atmos8100200.
57. Calas, A.; Uzu, G.; Kelly, F.J.; Houdier, S.; Martins, J.M.F.; Thomas, F.; Molton, F.; Charron, A.; Dunster, C.; Oliete, A.; et al. Comparison between five acellular oxidative potential measurement assays performed with detailed chemistry on PM10 samples from the city of Chamonix (France). *Atmos. Chem. Phys.* **2018**, *18*, 7863–7875. https://doi.org/10.5194/acp-18-7863-2018.
58. Janssen, N.A.; Yang, A.; Strak, M.; Steenhof, M.; Hellack, B.; Gerlofs-Nijland, M.E.; Kuhlbusch, T.; Kelly, F.; Harrison, R.; Brunekreef, B.; et al. Oxidative potential of particulate matter collected at sites with different source characteristics. *Sci. Total Environ.* **2014**, *472*, 572–581. https://doi.org/10.1016/j.scitotenv.2013.11.099.
59. Massimi, L.; Pietrodangelo, A.; Frezzini, M.A.; Ristorini, M.; De Francesco, N.; Sargolini, T.; Amoroso, A.; Di Giosa, A.; Canepari, S.; Perrino, C. Effects of COVID-19 lockdown on PM10 composition and sources in the Rome Area (Italy) by elements' chemical fractionation-based source apportionment. *Atmos. Res.* **2021**, *266*, 105970. https://doi.org/10.1016/j.atmosres.2021.105970.
60. Lokorai, K.; Ali-Khodja, H.; Khardi, S.; Bencharif-Madani, F.; Naidja, L.; Bouziane, M. Influence of mineral dust on the concentration and composition of PM10 in the city of Constantine. *Aeolian Res.* **2021**, *50*, 100677. https://doi.org/10.1016/j.aeolia.2021.100677.
61. Canepari, S.; Astolfi, M.; Catrambone, M.; Frasca, D.; Marcoccia, M.; Marcovecchio, F.; Massimi, L.; Rantica, E.; Perrino, C. A combined chemical/size fractionation approach to study winter/summer variations, ageing and source strength of atmospheric particles. *Environ. Pollut.* **2019**, *253*, 19–28. https://doi.org/10.1016/j.envpol.2019.06.116.
62. Perrone, M.R.; Bertoli, I.; Romano, S.; Russo, M.; Rispoli, G.; Pietrogrande, M.C. PM2.5 and PM10 oxidative potential at a Central Mediterranean Site: Contrasts between dithiothreitol- and ascorbic acid-measured values in relation with particle size and chemical composition. *Atmos. Environ.* **2019**, *210*, 143–155. https://doi.org/10.1016/j.atmosenv.2019.04.047.
63. Owoade, K.O.; Hopke, P.; Olise, F.S.; Ogundele, L.T.; Fawole, O.; Olaniyi, B.H.; Jegede, O.O.; Ayoola, M.A.; Bashiru, M.I. Chemical compositions and source identification of particulate matter (PM 2.5 and PM 2.5–10) from a scrap iron and steel smelting industry along the Ife–Ibadan highway, Nigeria. *Atmos. Pollut. Res.* **2015**, *6*, 107–119. https://doi.org/10.5094/apr.2015.013.
64. Harrison, R.M.; Allan, J.; Carruthers, D.; Heal, M.R.; Lewis, A.C.; Marner, B.; Murrells, T.; Williams, A. Non-exhaust vehicle emissions of particulate matter and VOC from road traffic: A review. *Atmos. Environ.* **2021**, *262*, 118592. https://doi.org/10.1016/j.atmosenv.2021.118592.

65. Hicks, W.; Beevers, S.; Tremper, A.H.; Stewart, G.; Priestman, M.; Kelly, F.J.; Lanoiselle, M.; Lowry, D.; Green, D.C. Quanti-fication of non-exhaust particulate matter traffic emissions and the impact of COVID-19 lockdown at London Marylebone Road. *Atmosphere* **2021**, *12*, 190.
66. Massimi, L.; Ristorini, M.; Astolfi, M.L.; Perrino, C.; Canepari, S. High resolution spatial mapping of element concentrations in PM10: A powerful tool for localization of emission sources. *Atmos. Res.* **2020**, *244*, 105060. https://doi.org/10.1016/j.atmosres.2020.105060.
67. Charrier, J.G.; Anastasio, C. On dithiothreitol (DTT) as a measure of oxidative potential for ambient particles: Evidence for the importance of soluble transition metals. *Atmos. Chem. Phys.* **2012**, *12*, 9321–9333. https://doi.org/10.5194/acp-12-9321-2012.
68. King, L.E.; Weber, R.J. Development and testing of an online method to measure ambient fine particulate reactive oxygen species (ROS) based on the 2',7'-dichlorofluorescin (DCFH) assay. *Atmos. Meas. Tech.* **2013**, *6*, 1647–1658. https://doi.org/10.5194/amt-6-1647-2013.
69. Charron, A.; Polo-Rehn, L.; Besombes, J.-L.; Golly, B.; Buisson, C.; Chanut, H.; Marchand, N.; Guillaud, G.; Jaffrezo, J.-L. Identification and quantification of particulate tracers of exhaust and non-exhaust vehicle emissions. *Atmos. Chem. Phys.* **2019**, *19*, 5187–5207. https://doi.org/10.5194/acp-19-5187-2019.
70. Thorpe, A.; Harrison, R.M. Sources and properties of non-exhaust particulate matter from road traffic: A review. *Sci. Total Environ.* **2008**, *400*, 270–282. https://doi.org/10.1016/j.scitotenv.2008.06.007.
71. Li, W.; Ge, P.; Chen, M.; Tang, J.; Cao, M.; Cui, Y.; Hu, K.; Nie, D. Tracers from Biomass Burning Emissions and Identification of Biomass Burning. *Atmosphere* **2021**, *12*, 1401. https://doi.org/10.3390/atmos12111401.
72. Pietrogrande, M.C.; Bertoli, I.; Clauser, G.; Dalpiaz, C.; Dell'Anna, R.; Lazzeri, P.; Lenzi, W.; Russo, M. Chemical composition and oxidative potential of atmospheric particles heavily impacted by residential wood burning in the alpine region of northern Italy. *Atmos. Environ.* **2021**, *253*, 118360. https://doi.org/10.1016/j.atmosenv.2021.118360.
73. Karbowska, B. Presence of thallium in the environment: Sources of contaminations, distribution and monitoring methods. *Environ. Monit. Assess.* **2016**, *188*, 1–19. https://doi.org/10.1007/s10661-016-5647-y.
74. Pant, P.; Harrison, R.M. Estimation of the contribution of road traffic emissions to particulate matter concentrations from field measurements: A review. *Atmos. Environ.* **2013**, *77*, 78–97. https://doi.org/10.1016/j.atmosenv.2013.04.028.
75. Canepari, S.; Perrino, C.; Olivieri, F.; Astolfi, M.L. Characterisation of the traffic sources of PM through size-segregated sampling, sequential leaching and ICP analysis. *Atmos. Environ.* **2008**, *42*, 8161–8175. https://doi.org/10.1016/j.atmosenv.2008.07.052.
76. Guo, H.-B.; Li, M.; Lyu, Y.; Cheng, T.-T.; Xv, J.; Li, X. Size-resolved particle oxidative potential in the office, laboratory, and home: Evidence for the importance of water-soluble transition metals. *Environ. Pollut.* **2019**, *246*, 704–709. https://doi.org/10.1016/j.envpol.2018.12.094.

77. Fusaro, L.; Salvatori, E.; Winkler, A.; Frezzini, M.A.; De Santis, E.; Sagnotti, L.; Canepari, S.; Manes, F. Urban trees for bio-monitoring atmospheric particulate matter: An integrated approach combining plant functional traits, magnetic and chemical properties. *Ecol. Indic.* **2021**, *126*, 107707.
78. Calas, A.; Uzu, G.; Besombes, J.-L.; Martins, J.M.; Redaelli, M.; Weber, S.; Charron, A.; Albinet, A.; Chevrier, F.; Brulfert, G.; et al. Seasonal Variations and Chemical Predictors of Oxidative Potential (OP) of Particulate Matter (PM), for Seven Urban French Sites. *Atmosphere* **2019**, *10*, 698. https://doi.org/10.3390/atmos10110698.
79. Pietrogrande, M.C.; Russo, M.; Zagatti, E. Review of PM Oxidative Potential Measured with Acellular Assays in Urban and Rural Sites across Italy. *Atmosphere* **2019**, *10*, 626. https://doi.org/10.3390/atmos10100626.
80. Hakimzadeh, M.; Soleimanian, E.; Mousavi, A.; Borgini, A.; De Marco, C.; Ruprecht, A.A.; Sioutas, C. The impact of biomass burning on the oxidative potential of PM2.5 in the metropolitan area of Milan. *Atmos. Environ.* **2020**, *224*, 117328. https://doi.org/10.1016/j.atmosenv.2020.117328.
81. Hedayat, F.; Stevanovic, S.; Miljevic, B.; Bottle, S.; Ristovski, Z. Review-evaluating the molecular assays for measuring the oxidative potential of particulate matter. *Chem. Ind. Chem. Eng. Q.* **2015**, *21*, 201–210. https://doi.org/10.2298/ciceq140228031h.
82. Altuwayjiri, A.; Pirhadi, M.; Kalafy, M.; Alharbi, B.; Sioutas, C. Impact of different sources on the oxidative potential of ambient particulate matter PM10 in Riyadh, Saudi Arabia: A focus on dust emissions. *Sci. Total Environ.* **2022**, *806*, 150590. https://doi.org/10.1016/j.scitotenv.2021.150590.
83. Almeida, S.M.; Pio, C.A.; Freitas, M.C.; Reis, M.A.; Trancoso, M.A. Source apportionment of fine and coarse particulate matter in a sub-urban area at the Western European Coast. *Atmos. Environ.* **2005**, *39*, 3127–3138. https://doi.org/10.1016/j.atmosenv.2005.01.048.

8. (D) Health effects of atmospheric PM

Nowadays, it is well known that the wide spectrum of adverse health effects exerting by PM is also reflected at cellular level in the activation of many different toxicity mechanisms. The variety of these mechanisms suggest that each emission source may be responsible for specific cellular injuries. To validate this hypothesis, during the PhD research, a collaboration with the Department of Pharmacological and Biomolecular Sciences, University of Milan (Italy), was undertaken and was aimed at assessing the potential genotoxic effects of 5 different sources of PM on human bronchial epithelial cell line BEAS-2B. The characterization of the genotoxic damage revealed that all the PM sources used in this study are particularly active in inducing DNA damage. The study suggested that the cell line model represents a valuable tool for screening the biological activity of PM originated from different emission sources. In the same context, during the PhD years, and specifically in 2019, the **RHAPS project** (Redox-Activity And Health-Effects Of Atmospheric Primary And Secondary Aerosol) was launched with the aim to identify specific properties (or combinations of them) of PM_1 (particles with aerodynamic diameter less than 1 micrometer) from various sources that are responsible for toxicological effects, that can be used as new metrics for health-related outdoor pollution studies. RHAPS aims at providing a new assessment of the sources and nature of PM components responsible for adverse health effects in real-world conditions. In this dissertation, the overall methodology of the RHAPS project is presented, and the phenomenology and the preliminary data observed are introduced.

8.1 (D1) Toxicological Profile of PM from Different Sources in Bronchial Epithelial Cell Line BEAS-2B

Particle and Fibre Toxicology - Submitted to the Journal

Gloria Melzi[1] , Emma Nozza[1] , Maria Agostina Frezzini[2] , Silvia Canepari[2] , Roberta Vecchi[3] , Llorenc Cremonesi[3], Marco Potenza[3], Marina Marinovich[1] , Emanuela Corsini[1]

[1] Department of Pharmacological and Biomolecular Sciences, Università degli Studi di Milano, Via Balzaretti 9, 20133, Milan, Italy

[2] Department of Environmental Biology, Sapienza University of Rome, Via C. De Lollis 21, 00185, Rome, Italy

[3] Department of Physics, Università degli Studi di Milano, Via Celoria 16, 20133, Milan, Italy

Abstract

The toxicity of particulate matter (PM) is strictly associated with its physical-chemical characteristics, as size or chemical composition. These properties are dependent on the particles origin, however the study of the toxicological profile of PM from single sources has rarely been highlighted. Hence, the focus of this research was to investigate the biological effects of PM from five relevant sources of atmospheric PM: diesel exhaust particles, coke dust, pellet ashes, incinerator ashes, and brake dust.

Cytotoxicity, genotoxicity, oxidative, and inflammatory response were assessed in a bronchial cell line (BEAS-2B). BEAS-2B were exposed to different concentrations (25, 50, 100, and 150 μg/mL medium) of particles suspended in water. The exposure lasted 24 hours for all the assays performed, except for reactive oxygen species that were evaluated after 30 minutes, 1 hour, and 4 hours of treatment.

The results showed a different action of the five types of PM. All the sources tested showed a genotoxic action on BEAS-2B, even in absence of oxidative stress induction. Pellet ashes seemed to be the only one able to induce oxidative stress by boosting the formation of reactive oxygen species, while brake dust resulted to be the most cytotoxic. In conclusion, the study elucidated the differential response of bronchial cells to PM samples generated by different sources. The comparison could be starting point for a regulatory intervention since it highlighted the toxic potential of each type of PM tested.

1. Introduction

Air pollution represents a recognized threat for human health, and among its components, particulate matter (PM) is considered one of the most important pollutants (WHO, 2016). PM is constituted by a mixture of solid and liquid particles suspended in the atmosphere. PM can originate from different sources, and consequently has different composition, shape and size (Wilson et al., 2002). Typical PM components are inorganic ions (e.g. ammonium, sulfate and nitrate), elemental and organic carbon (EC and OC, respectively), mineral dust and sea salt particles, heavy metals and polycyclic aromatic hydrocarbons (PAHs) (Hand et al., 2012; Putaud

et al., 2010); their relevance in PM samples depends on the emission sources and varies with particle size distribution (Seinfeld and Pandis, 1998).

The respiratory tract is the first apparatus facing PM adverse effects. Here, larger particles (> 2.5 μm) affect the upper respiratory tract, including oral cavity, trachea, and bronchi; while smaller particles can diffuse to bronchioles and alveoli causing multiple adverse reactions (Liu et al., 2016). PM inhalation can induce remodeling and loss of defensive barriers, e.g. cilia and mucociliary epithelium, or cellular damages (Nozza et al., 2021). Initially, PM deposition induces oxidative stress and production of pro-inflammatory mediators (Arias-Pérez et al., 2020; Corsini et al., 2019, 2013; Marabini et al., 2017; Møller et al., 2020). Later, the onset of DNA damages and their possible misrepair can lead to mutations (Peixoto et al., 2017).

PM sources can be divided in natural and anthropogenic, with the former accounting for about one order of magnitude more than the other at the global scale (Tomasi et al., 2017), but the latter generating the majority of smaller particles (e.g. with aerodynamic diameter less than 2.5 μm) thus promoting a stronger impact on human body. Many studies have been published focusing on the impact of different PM sources on human health (see e.g. Karlsson et al., 2006; Loxham et al., 2019), as well as on the environment (e.g. Mukherjee and Agrawal, 2017; and references therein). In urban areas, PM from vehicular traffic comprising both exhaust and non-exhaust emissions (Pant and Harrison, 2013) - results highly hazardous (Nozza et al., 2021); during wintertime, PM emitted by residential heating using wood and pellet burning is increasing worldwide and its biological effects have been also assessed (Corsini et al., 2019, 2017, and therein cited literature). PM emissions from refinery and incinerator plants must be also taken into account for their potential effects on human health (Frezzini et al., 2019; Marcoccia et al., 2017). Indeed, all these sources release in the environment high quantities of pollutants comprising PAHs, heavy metals, and other toxic elements.

The purpose of this study was to compare the effects of PM obtained from different relevant sources investigating cytotoxicity, oxidative stress, inflammation, and genotoxicity. As experimental model, BEAS-2B cells were used. Cells were exposed to five types of PM characterized by very different chemical composition: diesel exhaust particles (DEP), coke (C), pellet ashes (PA), incinerator ashes (IA), and brake dusts (BD). Results may highlight diverse biological activities reflecting the different origin of the PM, and show the ability of the model to detect subtle differences in both genotoxicity and inflammatory potential.

2. Materials and Methods

Cell culture

BEAS-2B cells were purchased from Sigma Aldrich (Darmstadt, Germany, cod. 95102433) and were grown on CELL-BIND® 75 cm^2 flasks (Corning, New York, USA) at 37 °C, 5% CO_2 in LHC-9 medium (Gibco, Life Technologies, Monza, Italy) with 1% of penicillin/streptomycin solution (Sigma Aldrich). Before experiments, supports were coated with a solution of 0.01% collagen (Sigma Aldrich) in Phosphate Buffered Saline (PBS – Fisher Molecular Biology, Rome, Italy) for 2 hours at room temperature. This solution was removed, supports were washed with PBS and then used for cell seeding.

Particulate Matter samples

As reference PM, NIES certified reference material no. 8 vehicle exhaust particulates DEP was used (Environment Agency NIES, Ibaraki, Japan). Specific details about collection and chemical characterization of coke (C), pellet ashes (PA), incinerator ashes (IA), and brake dust (BD) are largely reported by Marcoccia et al. (2017), Simonetti et al. (2018) and Frezzini et al. (2019). Briefly, C was taken near a refinery plant, PA was produced by pellet burning and collected inside the hood of a domestic stove, IA was sampled by a fine-mesh filter placed in a chimney of a waste-to-energy plant for non-hazardous waste, while BD derived from brake pads linings. All dusts were homogenized and sieved at 50 μm (Giuliani, Torino, Italy) before use.

Treatments

For all the experiments, PM were weighted, suspended in sterile water at 25 mg/mL and stored at 4 °C until use. BEAS-2B were seeded and allowed to grow for 48 hours before treatments. Cells were exposed to 25-50-100-150 μg/mL PM in LHC-9 for 24 hours, where not differently stated.

Size distribution and chemical composition of PM samples

We assessed the particle size distribution in each sample on a particle-by-particle basis with Single Particle Extinction and Scattering (SPES), a light scattering technique described in (Potenza et al., 2015). Solid dust samples were suspended in deionized, sterile water in a beaker at a concentration of ~10 $mg \cdot L^{-1}$, then sonicated and stirred for 60 s. About five minutes elapsed before measurements to allow for deposition of any large particles (~100 μm and larger); we then withdrew the samples into the instrument with a peristaltic pump at 2 ml/min. As revealed by light scattering data, almost all the particles have a compact shape, with the notable exception of DEP samples that included large aggregates. The diameter distributions were estimated by first inferring the refractive index from the SPES data according to the procedure discussed in (Potenza et al., 2015). This analysis gives an estimate of the size of each particle. Effective refractive indexes of non-spherical particles were lower than their corresponding bulk value and even more so for aggregates, as expected (Cremonesi et al., 2020; Kemppinen et al., 2015).

Sample	mode [μm]	std dev [μm]	min [μm]	max [μm]
DEP	0.4; 6.0 (bimodal)	2.4	0.2	10.6
Coke (C)	0.3	0.4	0.2	2.4
Pellet ash (PA)	0.4	0.3	0.3	2.4
Incinerator ash (IA)	0.4	0.6	0.3	3.1
Brake dust (BD)	0.6	0.6	0.2	4.4

Table 1. Overview of the main parameters of the diameter distributions, sampled with a base 10 logarithmic binning.

As shown in ***Table 1***, C, PA, and IA have modal diameters of 0.3-0.4 μm which are comparable to DEP smaller one while BD is slightly larger (0.6 μm).

Among the toxic components present in PM samples, elemental carbon content is relevant in DEP, coke (C), pellet ashes (PA), and brake dusts (BD), accounting for more than 30% of the total carbon detected in the samples (Simonetti et al., 2018). It is noteworthy that C, PA, and IA are rich in PAHs and other noxious organics species (Frezzini et al., 2019; Marcoccia et al., 2017). Regarding minor and trace elements, the highest concentration were detected in DEP, PA, and BD (Ficociello et al., 2020; Piacentini et al., 2019).

Treatments

For all the experiments, PM were weighted, suspended in sterile water at 25 mg/mL and stored at 4 °C until use. BEAS-2B were seeded and allowed to grow for 48 hours before treatments. Cells were exposed to 25-50-100-150 μg/mL PM in LHC-9 for 24 hours, where not differently stated.

Cytotoxicity

Cell viability was assessed using the MTT reduction test (Gerlier and Thomasset, 1986). Briefly, cells seeded in 96-well plates were exposed in triplicate to increasing concentrations of PM for 24 h. After treatment, cells were washed with PBS and incubated at 37 °C, 5% CO_2 for 3 hours in LHC-9 containing 0.5 mg/mL MTT (Sigma Aldrich). Cells were washed with PBS, and formazane solubilized with 100μL/well of DMSO (Sigma Aldrich, Darmstadt, Germany). Absorbance was read at 595 nm in a microplate reader (Molecular Devices, Emax precision microplate reader, San José, CA, USA). Results are expressed as percentage versus control untreated cells (100%).

Evaluation of apoptosis

Cells were seeded in 60 mm Petri dishes and exposed to increasing concentrations of PM for 24 h. After treatments, cells and supernatants were collected and centrifuged for 5 minutes at 2500 rpm. Apoptosis was evaluated using a commercially available kit following supplier's instruction (Alexa Fluor® 488 Annexin V/Dead Cell Apoptosis Kit, Invitrogen, ThermoFisher Scientific, Waltham, USA). Briefly, cells were incubated with Annexin V conjugate with Alexa Fluor® 488 and propidium iodide (PI) for 15 minutes in Annexin Binding Buffer at room temperature (RT). After incubation, samples were suspended in PBS and read on flow cytometry (Novocyte 3000, ACEA Bioscience, Inc., San Diego, USA). 10 000 cells were analyzed by NovoExpress Software (ACEA Bioscience, Inc., San Diego, USA).

Quantification of intracellular ROS (DCFH-DA method)

Cells were seeded in 96-well black plates with clear and flat bottom (Brand, Wertheim, Germany), each treatment was done in triplicate. Cells were treated with increasing concentrations of PM for 30 minutes, 1 hour or 4 hours. After treatments, culture medium was removed and replaced with fresh medium containing 25 μM 2′,7′-dichlorodihydrofluorescein diacetate (Sigma Aldrich) for 30 minutes at 37 °C. Cells were washed with PBS and fluorescence read at 495 nm with Enspire (PerkinElmer, Waltham, USA). Protein quantification

was performed using Lowry method (Lowry et al., 1951) and used to normalize the results. Results are expressed as FU/µg (fluorescence units on micrograms of proteins).

Assessment of genotoxicity: evaluation of H2AX phosphorylation and micronuclei detection

The presence of double strand breaks and micronuclei was performed using immunofluorescence techniques. Cells were seeded on pre-coated 12 mm diameter glass slides in a 24-wells plate. After treatment, cells were fixed in cold methanol at −20 °C for 10 minutes and cells permeabilized with 0.5% Triton-X100 in PBS for 10 minutes. 5% Bovine Serum Albumin (Sigma Aldrich) in PBS was used to block unspecific binding sites. Cells were then incubated overnight at 4 °C with the primary antibody (histone H2AX.XS 139ph antibody, 1:500 – Active Motif, Waterloo, Belgium), allowing the recognition of the phosphorylation of serine-139 of the H2AX histone. Slides were washed with PBS and immediately incubated with the secondary antibody, conjugated with Alexa Fluor® 488 (AlexaFluor® 488 Goat anti-Rabbit IgG H+L, 1:400 – Immunological Sciences, Rome, Italy), for 1 hour at RT. Cells were washed with PBS, and finally slides were mounted with 10 µL of Vectashield® Mounting Medium (containing DAPI – Vector Laboratories, Burlingame, USA). Slides were allowed to dry in order to be read with 100X oil objective with fluorescence microscopy (Axiovert 200M) using DAPI and FITC filters. 100 cells/samples were analyzed to obtain data for the γ-H2AX analysis, while the same samples were used for the evaluation of micronuclei's presence (1000 cells/sample, following the criteria described by (Fenech, 2000)).

Interleukin-8 (IL-8) secretion

Cells were seeded in 60 mm Petri dishes and grown to confluence, subsequently they were treated for 24 hours. At the end of the treatment, supernatants were collected and stored at -20 °C until evaluation. The secretion of the pro-inflammatory cytokine IL-8 was assessed by a commercially available kit following supplier's instructions (Human Interleukin-8 Development Kit, 900-K18, PeproTech, Cranbury, USA; sensitivity range 8-1000 pg/mL). Data are expressed as pg/mL for each sample.

Statistical analysis

Each experiment (*n*) was repeated at least three times. Data are reported as mean ± standard error of the mean. Statistical analysis was performed using software GraphPad Prism 8.0.2 (GraphPad Software, San Diego, USA). One-Way ANOVA test was chosen for the analysis of all results, in association with Dunnett's Multiple Comparison post hoc test. Results were considered significant at $p<0.05$.

3. Results

Cell death

Cells were exposed to increasing PM concentrations (25-50-100-150 µg/mL) for 24 h to assess cell viability using the MTT assay. Results are shown in the ***Table 2***. To a different extent, a concentration-dependent

reduction in cell viability was observed for all PM types, which, however, reached statistically significance at 150 µg/mL for PA and IA, and at all the tested concentrations for BD.

Sample	-	25 µg/mL	50 µg/mL	100 µg/mL	150 µg/mL
Control	100.0 ± 0.0				
DEP		98.3 ± 12.4	76.0 ± 10.9	79.7 ± 6.2	74.3 ± 10.2
Coke (C)		83.0 ± 10.7	84.0 ± 6.4	90.7 ± 4.8	88.3 ± 5.8
Pellet ash (PA)		85.3 ± 2.8	84.7 ± 1.2	82.7 ± 6.1	73.0 ± 10.6 *
Incinerator ash (IA)		76.3 ± 7.6	87.3 ± 7.8	84.7 ± 5.2	65.0 ± 12.0 *
Brake dust (BD)		76.0 ± 3.2 *	69.0 ± 8.7 **	76.0 ± 5.5 *	58.7 ± 9.1 **

Table 2. Evaluation of cell viability through MTT test. BEAS-2B cells were treated with 25, 50, 100, or 150 µg/mL of DEP, C, PA, IA, or BD for 24 hours. In the table are reported the results obtained with MTT assay. Data are expressed as percentage of viable cells normalized on the control samples (100%). Results are expressed as mean ± SEM, *n*=3. Statistical analysis was performed using One-Way ANOVA with Dunnett's post hoc analysis. *p<0.05, **p<0.01 vs. C-. Results are expressed as mean of percentages ± SEM, *n*=3.

To characterize the nature of the cell death observed, the Annexin V test was used. This method allows the classification of a cell population into three different groups: alive, apoptotic, and necrotic cells. Evaluation of the percentage of necrotic cells (***Figure 1***) confirmed the MTT cell viability data, highlighting a statistical significance, compared to control group, at the concentrations of 100 and 150 µg/mL for PA, 50, 100 and 150 µg/mL for IA, as well as at all the concentrations of BD. No differences in apoptotic cells were observed among groups and data are not shown.

ROS production

Figure 2 shows the time-course of ROS formation following exposure to increasing concentrations of PM samples at the different time points of treatments evaluated, i.e. 30 minutes (A) and 1 hour (B). PM obtained from different sources show different effects also for this parameter, with the formation of ROS being evident and statistically significant compared to controls only after PA treatment at the concentration of 100 and 150 µg/mL at 30 minutes, 1 hour, and, only at the highest concentration, at 4 hours (data not shown).

Histone H2AX phosphorylation

The identification of double strand breaks (DSBs), is possible through the study of the phosphorylation of serine-139 on H2AX histone. This is a marker of the DNA repair mechanism, dedicated to the early recognition of DSB sites and evaluable via immunofluorescence.

The amount of DNA damage, defined by the number of fluorescent *foci* per cell, is shown in ***Figure 3***. Treatments with all concentrations of the different PM types induced DSB, as shown by the increase of the number of cells with more than 10 *foci* at 24 hours in a statistically significant manner (the decrease of cells with less than 5 *foci* was also present but the data are not shown). For the intermediate class (6-10 *foci*) relevant variations were not observed.

Micronuclei formation

In ***Figure 4*** data are expressed as percentage of micronuclei number over the control. The increase of micronuclei in PM-treated samples compared to controls results to be statistically significant at all PM concentrations, except for 25 and 50 µg/mL DEP, 50 µg/mL IA, and 25, 50, and 100 µg/mL BD. In particular, the genomic insult is strongly induced by PA and IA, which at its highest concentration peaks at 4.0±1.1% of micronuclei.

Secretion of the pro-inflammatory cytokine IL-8

The effect of different PM samples on IL-8 release is shown in ***Figure 5***. DEP induced the release of IL-8 at the highest concentrations, while among the other PM types, only IA and BD caused a statistically significant secretion of IL-8.

Treatment	µg/mL	Mean ± SEM
C-		100.0 ± 0.0
DEP	25	98.3 ± 12.4
	50	76.0 ± 10.9
	100	79.7 ± 6.2
	150	74.3 ± 10.2
C	25	83.0 ± 10.7
	50	84.0 ± 6.4
	100	90.7 ± 4.8
	150	88.3 ± 5.8
PA	25	85.3 ± 2.8
	50	84.7 ± 1.2
	100	82.7 ± 6.1
	150	73.0* ± 10.6
IA	25	76.3 ± 7.6
	50	87.3 ± 7.8
	100	84.7 ± 5.2
	150	65.0* ± 12
BD	25	76.0* ± 3.2
	50	69.0** ± 8.7
	100	76.0* ± 5.5
	150	58.7** ± 9.1

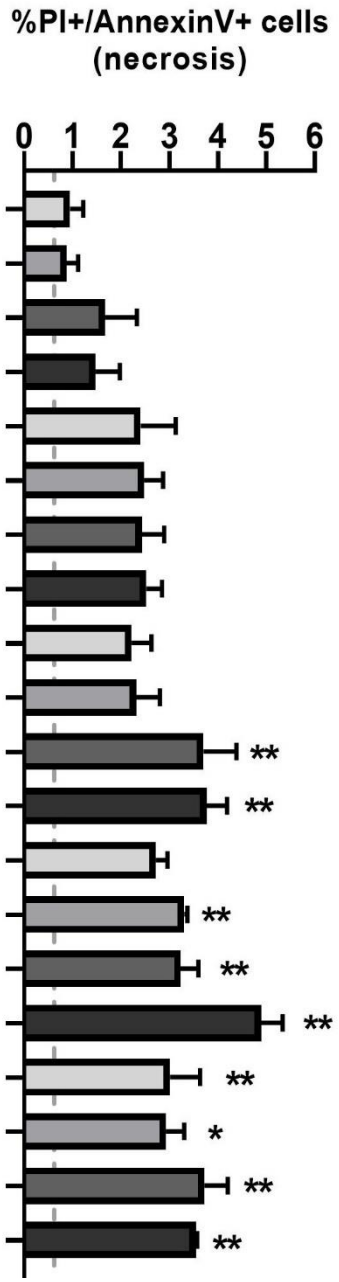

Figure 1. Evaluation of cell viability through MTT test (table) and Annexin V test in flow cytometry (graph). BEAS-2B cells were treated with 25, 50, 100 or 150 µg/mL of DEP, C, PA, IA, or BD for 24 hours. In the table are reported the results obtain with MTT assay. Data are expressed as percentage of viable cells normalized on the control samples (100%). In the graph is shown the percentage of necrotic cells population, evaluated via Annexin V test in flow cytometry (positive to both PI and Annexin V staining). Results are expressed as mean ± SEM, *n*=3. Dashed line represents the control sample data. Statistical analysis was performed using One-Way ANOVA with Dunnett's post hoc analysis. *p<0.05, **p<0.01 vs. C-. Results are expressed as mean of percentages ± SEM, *n*=3.

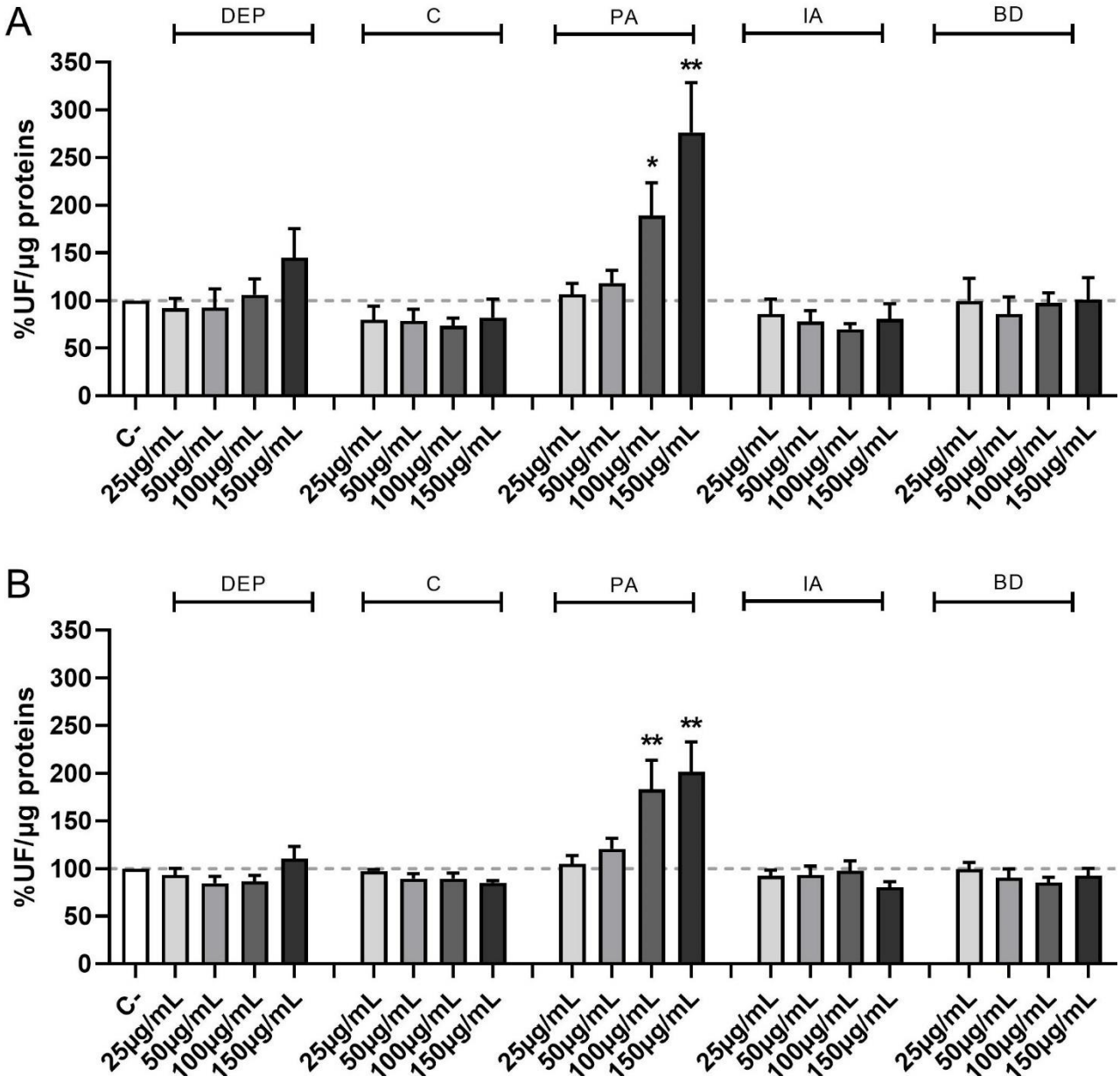

Figure 2. Time course of ROS production following PM exposure. Cells were treated with 25, 50, 100, or 150 µg/mL of DEP, C, PA, IA, or BD for 30 minutes (A) and 1 hour (B). Results are expressed as mean of

fluorescence ± SEM, in percentage compared to C- (fixed at 100%, dashed line), *n*=3. Statistical analysis was performed using One-Way ANOVA with Dunnett's post hoc analysis. *p<0.05, **p<0.01 vs. C-.

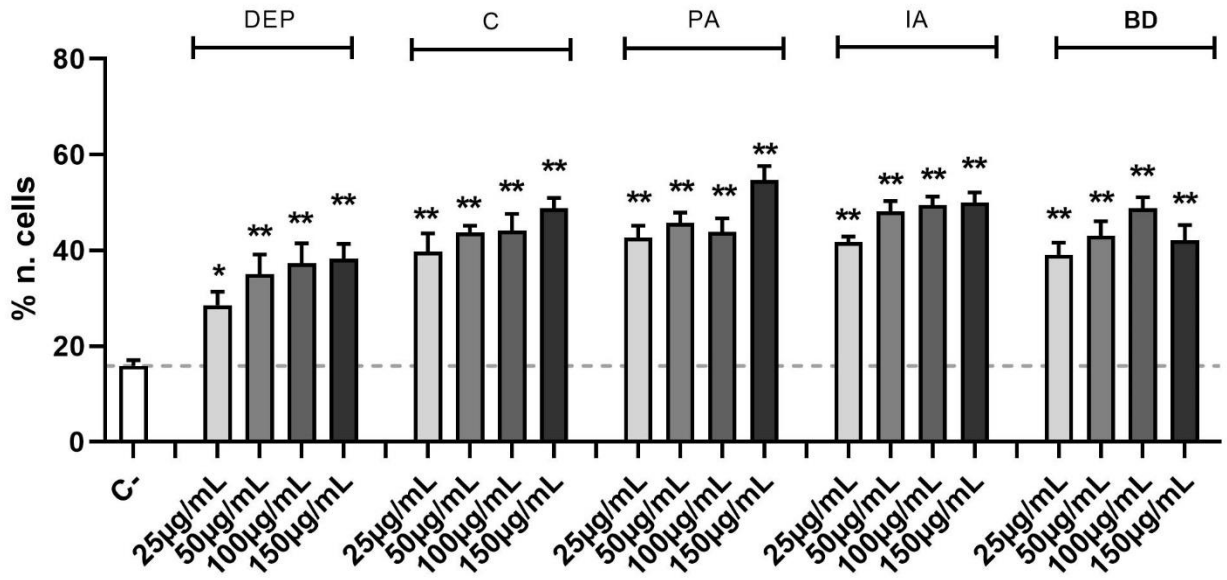

Figure 3. Quantification of DSBs through H2AX evaluation via immunofluorescence. Cells were treated with 25, 50, 100 or 150 µg/mL of DEP, C, PA, IA, or BD for 24 hours. Each graph represents the classification of damage in the 3 populations based on the number of foci: 0-5 foci, absence of damage, 6-10 foci, medium damage, >10 foci, high damage (shown in the graph). Dashed line represents control result. Results are expressed as mean of percentages ± SEM, *n*=3. Statistical analysis was performed using One-Way ANOVA with Dunnett's post hoc analysis. *p<0.05, **p<0.01 vs. C-.

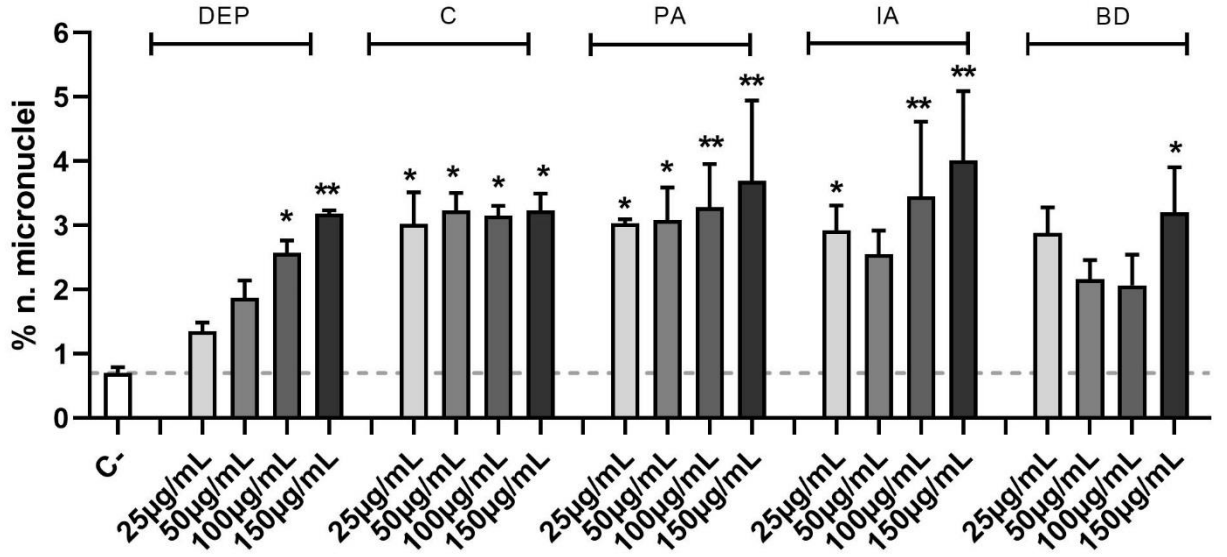

Figure 4. Micronuclei evaluation via immunofluorescence. Cells were treated with 25, 50, 100 or 150 µg/mL of DEP, C, PA, IA, or BD for 24 hours. Control sample is also reported as dashed line. Results are expressed

as mean of percentages ± SEM, *n*=3. Statistical analysis was performed using One-Way ANOVA with Dunnett's post hoc analysis. *p<0.05, **p<0.01 vs. C-.

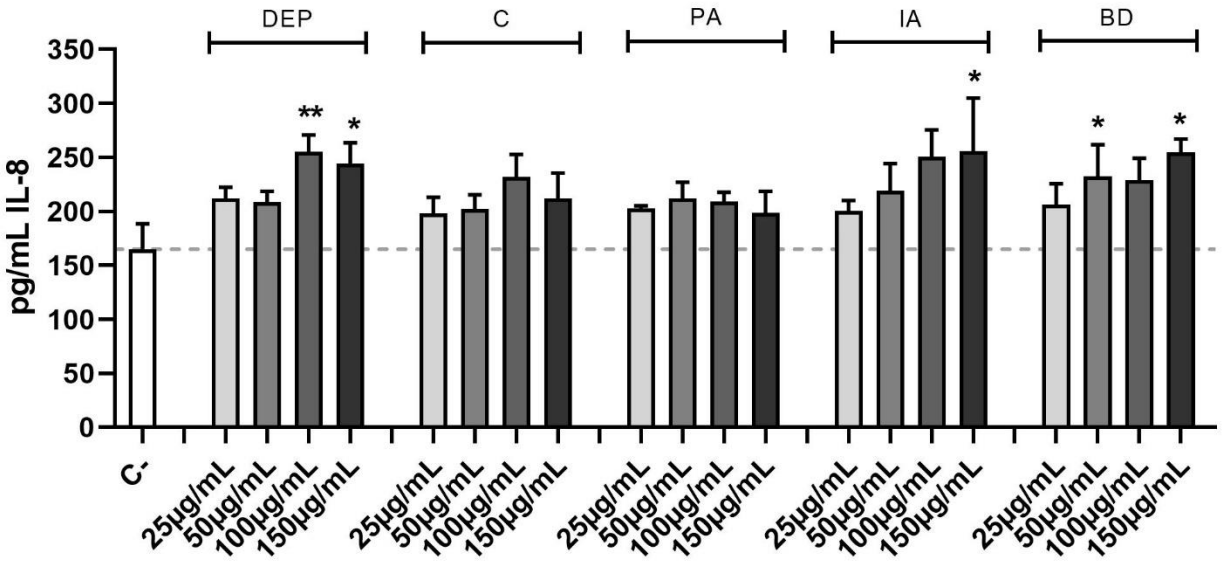

Figure 5. Secretion of IL-8. Cells were treated with 25, 50, 100, or 150 µg/mL of D, C, PA, IA, or BD for 24 hours. Dashed line represents the control sample. Results are expressed as mean of pg/mL ± SEM, *n*=4. Statistical analysis was performed using One-Way ANOVA with Dunnett's post hoc analysis. *p<0.05, **p<0.01 vs. C-.

4. Discussion

The purpose of this study was to investigate the effects of different PM types on cell viability, oxidative stress, DNA damage, and release of a pro-inflammatory mediator in the human bronchial cell line BEAS-2B.

Five different types of PM from various emission sources were tested in parallel. Several studies have attributed toxicological endpoints to BD by demonstrating that brake wear particles, rich in metals as Fe and Cu, can damage cells determining pro-inflammatory cell response, thus triggering oxidative stress reactions (Ficociello et al., 2020; Figliuzzi et al., 2020; Gasser et al., 2009). DEP has been for years one of the main topics of investigations on traffic-derived particulate toxicity (Weitekamp et al., 2020). Toxicity of DEP is mainly related to its small size that permits to penetrate the tissues, coupled with the capability of diesel-combustion derived particles to absorb toxic compounds on their surface, such as complex mixture of organic compounds (Donaldson et al., 2005; Reis et al., 2018; Yan et al., 2021). *In vivo* and *in vitro* experiments showed significant evidence about activation of inflammatory cascades and redox-sensitive signaling pathways (Selley et al., 2020 and references therein). Biomass combustion-derived particles, such as PA used in this work, have emerged as capable of stimulating adverse effects in biological systems, causing DNA damage, as well as altering the cell cycle (Corsini et al., 2013; Marchetti et al., 2019). This is due to the presence of several toxic compounds, such as PAHs and trace elements that are linked to various genotoxic

and carcinogenic effects (Palmer, 2011; Yang et al., 2017). Moreover, this PM is reported to be the more soluble in water (about 40% solubility) among the other analyzed in this study. C is the most hydrophobic instead (Simonetti et al., 2018). Biomass burning-related PM is mainly composed of organic fraction, and it contains high concentrations of organic species which have been considered responsible for genotoxic and oxidative stress effects (Simonetti et al., 2018). Lastly, IA from a waste-to-energy plant for non-hazardous waste is known to contain a variety of organic compounds, including PAHs, as well as non-negligible concentrations of heavy metals, such as Cd, Cu, Pb and Zn (Dugenest et al., 1999; Frezzini et al., 2019). IARC reported some of the compounds present in biomass burning PM emissions to be carcinogenic and mutagenic (IARC, 2012); consequently, IA can exert adverse biological effects (Fortoul et al., 2015; Marchetti et al., 2021; Valavanidis et al., 2008).

At high concentrations a decrease in cell viability was observed, and among the different death pathways, our results indicate necrosis as the most represented and no indication of apoptosis was observed, confirming the previous data reported in literature (Dornhof et al., 2017; León-Mejía et al., 2016; Pan et al., 2013). The cell death observed, in particular caused by BD and the highest concentration of PA and IA, is likely due to the high concentration of heavy metals. Literature data indicate Mn and Cd as heavily cytotoxic for human lung epithelium (Han et al., 2007; Honda et al., 2015). The previous chemical characterization of the PM tested (Ficociello et al., 2020) indicates Mn as one of the main components of PA, while Cd is present in BD at a concentration higher than 2 g/kg.

The chemical characterization of PM from different sources is useful, not only for the quantification of heavy metals, but also for the identification of other toxicants, like PAHs and redox cycling quinones (da Silva Junior et al., 2021; Jung et al., 2012). Indeed, in literature was reported their ROS-generating abilities by undergoing redox recycling and reducing oxygen to produce superoxide radicals (Chung et al., 2006; Verma et al., 2015). In the previous chemical characterization of the PM tested in the current study, the oxidative potential was also assessed using several acellular methods, such as dithiothreitol, ascorbic acid, and 2',7'-dichlorofluorescin assays (Piacentini et al., 2019). The highest oxidative potential was observed for PA and the lowest for C and IA, the results obtained in the present study confirm this capability. However, Piacentini et al. (2019) also found D and BD to have oxidative potential, which was not confirmed in our work. This could be explained by the different time elapsed between sample collection and oxidative potential analysis, that occurred much later for the samples analyzed in this study, suggesting that the same components, whose stability and bioavailability change in time, can show a reduced oxidative potential.

The ability of PM to induce DNA damage, as breaks and genomic aberrations, is well known (Abbas et al., 2019). Two of the most commonly evaluated biomarkers of DNA damage are the phosphorylation of H2AX on serine 139 and the formation of micronuclei (Oh et al., 2011; Sánchez-Pérez et al., 2009). These lesions may be induced by ROS damaging DNA strands, and ultimately generating adducts and breaks (Cooke et al., 2003; Gualtieri et al., 2011). Although the production of ROS is elicited only with PA treatment, all the PM samples tested have been found able to induce genotoxic insult on BEAS-2B, suggesting a direct effect on the

DNA strand not directly linked to ROS production. The amount of damage recognized by γ-H2AX increases in a dose-dependent manner in all PM samples tested. The PM mutagenic potential has been demonstrated and confirmed through the evaluation of micronuclei, with C, PA, and IA being the most effective (De Coster et al., 2008; Vimercati et al., 2020).

Inflammation is another well-described effect associated with PM exposure, mainly derived by the presence of metals, PAHs, and microorganisms (Nozza et al., 2021). In the current study, the PM samples tested showed a different pro-inflammatory potential, with DEP, IA, and BD being the most effective in inducing IL-8 secretion. Studies demonstrated that IL-8 secretion could be induced by PAHs (Corsini et al., 2013; Selley et al., 2020), typically present at high level in DEP and IA, which can explain the secretion. While for BD, which does not contain high levels of PAHs, the presence of Cu could be responsible for the relevant induction of IL-8 secretion observed (Kennedy et al., 1998).

5. Conclusion

The present study showed how PM originated by different sources is characterized by a diverse biological activity. All the investigated samples have significant genotoxic and mutagenic effect on BEAS-2B cell line, which does not appear to be correlated with oxidative stress, but rather with the different chemical composition. In terms of environmental hazardousness, due to the mixture of atmospheric particulate matter emitted from a variety of sources, every source has a noxious effect but with a different genotoxic and pro-inflammatory profile in relation to both particle size and chemical composition. However, it is interesting to note that all samples showed a unimodal size distribution (apart DEP, where large aggregates were also observed) with modes in the submicron range and BD was the sample with a slightly higher mode (at about 0.6 μm).

BD resulted to be the most cytotoxic, as suggested by the presence of high concentration of heavy metals, in particular Fe and Cd. Transition metals, such as Fe, Cd, Ni, and Cu, mainly contained in PA, may undergo Fenton reaction and initiate signaling pathways leading to ROS production as shown in this study (Bates et al., 2019; Crobeddu et al., 2017; Ghio et al., 2012). IA appears to be the most dangerous for bronchial cells: it is active in the generation of genotoxic damage, cytotoxicity, and inflammation induction. This is due to its chemical composition where PAHs and heavy metals were abundant.

Overall, this study indicates that the model represents a valuable tool for screening the biological activity of PM originated from different sources, able to detect subtle differences.

References

Abbas, I., Badran, G., Verdin, A., Ledoux, F., Roumie, M., Lo Guidice, J.M., Courcot, D., Garçon, G., 2019. In vitro evaluation of organic extractable matter from ambient PM2.5 using human bronchial epithelial BEAS-2B cells: Cytotoxicity, oxidative stress, pro-inflammatory response, genotoxicity, and cell cycle deregulation. Environ. Res. 171, 510–522. https://doi.org/10.1016/j.envres.2019.01.052

Arias-Pérez, R.D., Taborda, N.A., Gómez, D.M., Narvaez, J.F., Porras, J., Hernandez, J.C., 2020. Inflammatory effects of particulate matter air pollution. Environ. Sci. Pollut. Res. https://doi.org/10.1007/s11356-020-10574-w

Bates, J.T., Fang, T., Verma, V., Zeng, L., Weber, R.J., Tolbert, P.E., Abrams, J.Y., Sarnat, S.E., Klein, M., Mulholland, J.A., Russell, A.G., 2019. Review of Acellular Assays of Ambient Particulate Matter Oxidative Potential: Methods and Relationships with Composition, Sources, and Health Effects. Environ. Sci. Technol. https://doi.org/10.1021/acs.est.8b03430

Chung, M.Y., Lazaro, R.A., Lim, D., Jackson, J., Lyon, J., Rendulic, D., Hasson, A.S., 2006. Aerosol-borne quinones and reactive oxygen species generation by particulate matter extracts. Environ. Sci. Technol. https://doi.org/10.1021/es0515957

Cooke, M.S., Evans, M.D., Dizdaroglu, M., Lunec, J., 2003. Oxidative DNA damage: mechanisms, mutation, and disease. FASEB J. 17, 1195–1214. https://doi.org/10.1096/fj.02-0752rev

Corsini, E., Budello, S., Marabini, L., Galbiati, V., Piazzalunga, A., Barbieri, P., Cozzutto, S., Marinovich, M., Pitea, D., Galli, C.L., 2013. Comparison of wood smoke PM2.5 obtained from the combustion of FIR and beech pellets on inflammation and DNA damage in A549 and THP-1 human cell lines. Arch. Toxicol. https://doi.org/10.1007/s00204-013-1071-z

Corsini, E., Marinovich, M., Vecchi, R., 2019. Ultrafine particles from residential biomass combustion: A review on experimental data and toxicological response. Int. J. Mol. Sci. 20. https://doi.org/10.3390/ijms20204992

Corsini, E., Vecchi, R., Marabini, L., Fermo, P., Becagli, S., Bernardoni, V., Caruso, D., Corbella, L., Dell'Acqua, M., Galli, C.L., Lonati, G., Ozgen, S., Papale, A., Signorini, S., Tardivo, R., Valli, G., Marinovich, M., 2017. The chemical composition of ultrafine particles and associated biological effects at an alpine town impacted by wood burning. Sci. Total Environ. 587–588, 223–231. https://doi.org/10.1016/j.scitotenv.2017.02.125

Crobeddu, B., Aragao-Santiago, L., Bui, L.C., Boland, S., Baeza Squiban, A., 2017. Oxidative potential of particulate matter 2.5 as predictive indicator of cellular stress. Environ. Pollut. https://doi.org/10.1016/j.envpol.2017.06.051

da Silva Junior, F.C., Felipe, M.B.M.C., Castro, D.E.F. de, Araújo, S.C. da S., Sisenando, H.C.N., Batistuzzo de Medeiros, S.R., 2021. A look beyond the priority: A systematic review of the genotoxic, mutagenic, and carcinogenic endpoints of non-priority PAHs. Environ. Pollut. https://doi.org/10.1016/j.envpol.2021.116838

De Coster, S., Koppen, G., Bracke, M., Schroijen, C., Den Hond, E., Nelen, V., Van De Mieroop, E., Bruckers, L., Bilau, M., Baeyens, W., Schoeters, G., Van Larebeke, N., 2008. Pollutant effects on genotoxic parameters

and tumor-associated protein levels in adults: A cross sectional study. Environ. Heal. A Glob. Access Sci. Source 7, 1–19. https://doi.org/10.1186/1476-069X-7-26

Donaldson, K., Tran, L., Jimenez, L.A., Duffin, R., Newby, D.E., Mills, N., MacNee, W., Stone, V., 2005. Combustion-derived nanoparticles: A review of their toxicology following inhalation exposure. Part. Fibre Toxicol. 2, 1–14. https://doi.org/10.1186/1743-8977-2-10

Dornhof, R., Maschowski, C., Osipova, A., Gieré, R., Seidl, M., Merfort, I., Humar, M., 2017. Stress fibers, autophagy and necrosis by persistent exposure to PM2.5 from biomass combustion. PLoS One 12, 1–20. https://doi.org/10.1371/journal.pone.0180291

Dugenest, S., Casabianca, H., Grenier-Loustalot, M.F., 1999. Municipal solid waste incineration bottom ash: Physicochemical characterization of organic matter. Analusis. https://doi.org/10.1051/analusis:1999110

Fenech, M., 2000. The in vitro micronucleus technique. Mutat. Res. 455, 81–95. https://doi.org/10.1016/s0027-5107(00)00065-8

Ficociello, G., Inverni, A., Massimi, L., Buccini, G., Canepari, S., Uccelletti, D., 2020. Assessment of the effects of atmospheric pollutants using the animal model Caenorhabditis elegans. Environ. Res. 191, 110209. https://doi.org/10.1016/j.envres.2020.110209

Figliuzzi, M., Tironi, M., Longaretti, L., Mancini, A., Teoldi, F., Sangalli, F., Remuzzi, A., 2020. Copper-dependent biological effects of particulate matter produced by brake systems on lung alveolar cells. Arch. Toxicol. https://doi.org/10.1007/s00204-020-02812-4

Fortoul, T.I., Rodriguez-Lara, V., Gonzalez-Villalva, A., Rojas-Lemus, M., Colin-Barenque, L., Bizarro-Nevares, P., García-Peláez, I., Ustarroz-Cano, M., López-Zepeda, S., Cervantes-Yépez, S., López-Valdez, N., Meléndez-García, N., Espinosa-Zurutuza, M., Cano-Gutierrez, G., Cano-Rodríguez, M.C., 2015. Health Effects of Metals in Particulate Matter, in: Current Air Quality Issues. https://doi.org/10.5772/59749

Frezzini, M.A., Castellani, F., Francesco, N. De, Ristorini, M., Canepari, S., 2019. Application of DPPH Assay for Assessment of Particulate Matter Reducing Properties. Atmosphere (Basel). 10, 816. https://doi.org/doi:10.3390/atmos10120816

Gasser, M., Riediker, M., Mueller, L., Perrenoud, A., Blank, F., Gehr, P., Rothen-Rutishauser, B., 2009. Toxic effects of brake wear particles on epithelial lung cells in vitro. Part. Fibre Toxicol. https://doi.org/10.1186/1743-8977-6-30

Gerlier, D., Thomasset, N., 1986. Use of MTT colorimetric assay to measure cell activation. J. Immunol. Methods 94, 57–63. https://doi.org/10.1016/0022-1759(86)90215-2

Ghio, A.J., Carraway, M.S., Madden, M.C., 2012. Composition of air pollution particles and oxidative stress in cells, tissues, and living systems. J. Toxicol. Environ. Heal. - Part B Crit. Rev. https://doi.org/10.1080/10937404.2012.632359

Gualtieri, M., Øvrevik, J., Mollerup, S., Asare, N., Longhin, E., Dahlman, H.J., Camatini, M., Holme, J.A., 2011. Airborne urban particles (Milan winter-PM2.5) cause mitotic arrest and cell death: Effects on DNA, mitochondria, AhR binding and spindle organization. Mutat. Res. - Fundam. Mol. Mech. Mutagen. 713, 18–31. https://doi.org/10.1016/j.mrfmmm.2011.05.011

Han, S.G., Castranova, V., Vallyathan, V., 2007. Comparative cytotoxicity of cadmium and mercury in a human bronchial epithelial cell line (BEAS-2B) and its role in oxidative stress and induction of heat shock protein 70. J. Toxicol. Environ. Heal. - Part A Curr. Issues 70, 852–860. https://doi.org/10.1080/15287390701212695

Hand, J.L., Schichtel, B.A., Pitchford, M., Malm, W.C., Frank, N.H., 2012. Seasonal composition of remote and urban fine particulate matter in the United States 117, 1–22. https://doi.org/10.1029/2011JD017122

Honda, A., Tsuji, K., Matsuda, Y., Hayashi, T., Fukushima, W., Sawahara, T., Kudo, H., Murayama, R., Takano, H., 2015. Effects of air pollution-related heavy metals on the viability and inflammatory responses of human airway epithelial cells. Int. J. Toxicol. 34, 195–203. https://doi.org/10.1177/1091581815575757

IARC, 2012. Arsenic, Metals, Fibres, and Dusts, Iarc Monographs.

Jung, M.H., Kim, H.R., Park, Y.J., Park, D.S., Chung, K.H., Oh, S.M., 2012. Genotoxic effects and oxidative stress induced by organic extracts of particulate matter (PM10) collected from a subway tunnel in Seoul, Korea. Mutat. Res. - Genet. Toxicol. Environ. Mutagen. https://doi.org/10.1016/j.mrgentox.2012.08.002

Karlsson, H.L., Ljungman, A.G., Lindbom, J., Moller, L., 2006. Comparison of genotoxic and inflammatory effects of particles generated by wood combustion, a road simulator and collected from street and subway. Toxicol. Lett. 165, 203–211. https://doi.org/10.1016/j.toxlet.2006.04.003

Kennedy, T.P., Ghio, A.J., Reed, W., Samet, J., Zagorski, J., Quay, J., Carter, J., Dailey, L., Hoidal, J.R., Devlin, R.B., 1998. Copper-dependent inflammation and nuclear factor-κb activation by particulate air pollution. Am. J. Respir. Cell Mol. Biol. https://doi.org/10.1165/ajrcmb.19.3.3042

León-Mejía, G., Silva, L.F.O., Civeira, M.S., Oliveira, M.L.S., Machado, M., Villela, I.V., Hartmann, A., Premoli, S., Corrêa, D.S., Da Silva, J., Henriques, J.A.P., 2016. Cytotoxicity and genotoxicity induced by coal and coal fly ash particles samples in V79 cells. Environ. Sci. Pollut. Res. 23, 24019–24031. https://doi.org/10.1007/s11356-016-7623-z

Liu, S., Cai, S., Chen, Y., Xiao, B., Chen, P., Xiang, X., 2016. The effect of pollutional haze on pulmonary function. J. Thorac. Dis. 8, 41–56. https://doi.org/10.3978/j.issn.2072-1439.2016.01.18

Lowry, O.H., Rosebrough, N.J., Farr, L.A., Randall, R.J., 1951. Protein measurement with the folin phenol reagent. J. Biol. Chem. 193, 365–275.

Loxham, M., Davies, D.E., Holgate, S.T., 2019. The health effects of fine particulate air pollution. Br. Med. J. 367, I6609. https://doi.org/10.1136/bmj.l6609

Marabini, L., Ozgen, S., Turacchi, S., Aminti, S., Arnaboldi, F., Lonati, G., Fermo, P., Corbella, L., Valli, G., Bernardoni, V., Dell'Acqua, M., Vecchi, R., Becagli, S., Caruso, D., Corrado, L.G., Marinovich, M., 2017. Ultrafine particles (UFPs) from domestic wood stoves: genotoxicity in human lung carcinoma A549 cells. Mutat. Res. - Genet. Toxicol. Environ. Mutagen. 820, 39–46. https://doi.org/10.1016/j.mrgentox.2017.06.001

Marchetti, S., Bengalli, R., Floris, P., Colombo, A., Mantecca, P., 2021. Combustion-derived particles from biomass sources differently promote epithelial-to-mesenchymal transition on A549 cells. Arch. Toxicol. https://doi.org/10.1007/s00204-021-02983-8

Marchetti, S., Longhin, E., Bengalli, R., Avino, P., Stabile, L., Buonanno, G., Colombo, A., Camatini, M., Mantecca, P., 2019. In vitro lung toxicity of indoor PM10 from a stove fueled with different biomasses. Sci. Total Environ. https://doi.org/10.1016/j.scitotenv.2018.08.249

Marcoccia, M., Ronci, L., De Matthaeis, E., Setini, A., Perrino, C., Canepari, S., 2017. In-vivo assesment of the genotoxic and oxidative stress effects of particulate matter on Echinogammarus veneris. Chemosphere 173, 124–134. https://doi.org/10.1016/j.chemosphere.2017.01.019

Molina, L.T., 2021. Introductory lecture: Air quality in megacities. Faraday Discuss. https://doi.org/10.1039/d0fd00123f

Møller, P., Scholten, R.H., Roursgaard, M., Krais, A.M., 2020. Inflammation, oxidative stress and genotoxicity responses to biodiesel emissions in cultured mammalian cells and animals. Crit. Rev. Toxicol. https://doi.org/10.1080/10408444.2020.1762541

Mukherjee, A., Agrawal, M., 2017. World air particulate matter: sources, distribution and health effects. Environ. Chem. Lett. 15, 283–309. https://doi.org/10.1007/s10311-017-0611-9

Nozza, E., Valentini, S., Melzi, G., Vecchi, R., Corsini, E., 2021. Advances on the immunotoxicity of outdoor particulate matter: A focus on physical and chemical properties and respiratory defence mechanisms. Sci. Total Environ. 780, 146391. https://doi.org/10.1016/j.scitotenv.2021.146391

Oh, S.M., Kim, H.R., Park, Y.J., Lee, S.Y., Chung, K.H., 2011. Organic extracts of urban air pollution particulate matter (PM2.5)-induced genotoxicity and oxidative stress in human lung bronchial epithelial cells (BEAS-2B cells). Mutat. Res. - Genet. Toxicol. Environ. Mutagen. 723, 142–151. https://doi.org/10.1016/j.mrgentox.2011.04.003

Palmer, K., 2011. IARC Monographs on the Evaluation of Carcinogenic Risks to Humans. Volume 98: Painting, Firefighting and Shiftwork. International Agency for Research on Cancer. Occup. Med. (Chic. Ill). https://doi.org/10.1093/occmed/kqr127

Pan, Y., Li, B., Ran, P., 2013. [Wood smoke condensate had weak proliferation and strong necrotic effects on human airway smooth muscle cells]. Zhonghua jie he he hu xi za zhi 36, 581–586.

Pant, P., Harrison, R.M., 2013. Estimation of the contribution of road traffic emissions to particulate matter concentrations from field measurements: A review. Atmos. Environ. 77, 78–97.

Peixoto, M.S., de Oliveira Galvao, M.F., Batistuzzo de Medeiros, S.R., 2017. Cell death pathways of particulate matter toxicity. Chemosphere 188, 32–48. https://doi.org/10.1016/j.chemosphere.2017.08.076

Piacentini, D., Falasca, G., Canepari, S., Massimi, L., 2019. Potential of PM-selected components to induce oxidative stress and root system alteration in a plant model organism. Environ. Int. 132, 105094. https://doi.org/10.1016/j.envint.2019.105094

Putaud, J., Van Dingenen, R., Alastuey, A., Bauer, H., Birmili, W., Cyrys, J., Flentje, H., Fuzzi, S., Gehrig, R., Hansson, H.C., Harrison, R.M., Herrmann, H., Hitzenberger, R., Hüglin, C., Jones, A.M., Kasper-Giebl, A., Kiss, G., Kousa, A., Kuhlbusch, T.A.J., Löschau, G., Maenhaut, W., Molnar, A., Moreno, T., Pekkanen, J., Perrino, C., Pitz, M., Puxaum, H., Querol, X., Rodriguez, S., Salma, I., Schwarz, J., Smolik, J., Schneider, J., Spindler, G., ten Brink, H., Tursic, J., Viana, M., Wiedensohler, A., Raes, F., 2010. A European aerosol phenomenology - 3 : Physical and chemical characteristics of particulate matter from 60 rural, urban, and kerbside sites across Europe. Atmos. Environ. 44, 1308–1320. https://doi.org/10.1016/j.atmosenv.2009.12.011

Reis, H., Reis, C., Sharip, A., Reis, W., Zhao, Y., Sinclair, R., Beeson, L., 2018. Diesel exhaust exposure, its multi-system effects, and the effect of new technology diesel exhaust. Environ. Int. https://doi.org/10.1016/j.envint.2018.02.042

Sánchez-Pérez, Y., Chirino, Y.I., Osornio-Vargas, Á.R., Morales-Bárcenas, R., Gutiérrez-Ruíz, C., Vázquez-López, I., García-Cuellar, C.M., 2009. DNA damage response of A549 cells treated with particulate matter (PM10) of urban air pollutants. Cancer Lett. 278, 192–200. https://doi.org/10.1016/j.canlet.2009.01.010

Seinfeld, J.H., Pandis, S.N., 1998. Atmospheric Chemistry and Physics: From Air Pollution to Climate Change.

Selley, L., Schuster, L., Marbach, H., Forsthuber, T., Forbes, B., Gant, T.W., Sandström, T., Camiña, N., Athersuch, T.J., Mudway, I., Kumar, A., 2020. Brake dust exposure exacerbates inflammation and transiently compromises phagocytosis in macrophages. Metallomics. https://doi.org/10.1039/c9mt00253g

Simonetti, G., Conte, E., Massimi, L., Frasca, D., Perrino, C., Canepari, S., 2018. Oxidative potential of particulate matter components generated by specific emission sources. J. Aerosol Sci. 126, 99–109. https://doi.org/10.1016/j.jaerosci.2018.08.011

Tomasi, C., Fuzzi, S., Kokhanovsky, A., 2017. Atmospheric Aerosols: Life Cycles and Effects on Air Quality and Climate. Wiley-VCH Verlag GmbH & Co. KGaA, Weinhelm, Germany. https://doi.org/https://doi.org/10.1002/9783527336449

Valavanidis, A., Fiotakis, K., Vlachogianni, T., 2008. Airborne particulate matter and human health: Toxicological assessment and importance of size and composition of particles for oxidative damage and carcinogenic mechanisms. J. Environ. Sci. Heal. - Part C Environ. Carcinog. Ecotoxicol. Rev. https://doi.org/10.1080/10590500802494538

Verma, V., Fang, T., Xu, L., Peltier, R.E., Russell, A.G., Ng, N.L., Weber, R.J., 2015. Organic aerosols associated with the generation of reactive oxygen species (ROS) by water-soluble PM2.5. Environ. Sci. Technol. https://doi.org/10.1021/es505577w

Vimercati, L., Bisceglia, L., Cavone, D., Caputi, A., De Maria, L., Delfino, M.C., Corrado, V., Ferri, G.M., 2020. Environmental monitoring of PAHs exposure, biomarkers and vital status in coke oven workers. Int. J. Environ. Res. Public Health 17, 1–33. https://doi.org/10.3390/ijerph17072199

Weitekamp, C.A., Kerr, L.B., Dishaw, L., Nichols, J., Lein, M., Stewart, M.J., 2020. A systematic review of the health effects associated with the inhalation of particle-filtered and whole diesel exhaust. Inhal. Toxicol. https://doi.org/10.1080/08958378.2020.1725187

WHO, 2016. Ambient air pollution: A global assessment of exposure and burden of disease.

Wilson, W.E., Chow, J.C., Claiborn, C., Fusheng, W., Engelbrecht, J., Watson, J.G., 2002. Monitoring of particulate matter outdoors. Chemosphere 49, 1009–1043. https://doi.org/https://doi.org/10.1016/S0045-6535(02)00270-9

Yan, C., Wu, X., Cao, X., Li, M., Zhou, L., Xiu, G., Zeng, J., 2021. In vitro and in vitro toxicity study of diesel exhaust particles using BEAS-2B cell line and the nematode Caenorhabditis elegans as biological models. Environ. Sci. Pollut. Res. https://doi.org/10.1007/s11356-021-14908-0

Yang, D., Ma, M., Zhou, W., Yang, B., Xiao, C., 2017. Inhibition of miR-32 activity promoted EMT induced by PM2.5 exposure through the modulation of the Smad1-mediated signaling pathways in lung cancer cells. Chemosphere. https://doi.org/10.1016/j.chemosphere.2017.05.152

8.2 RHAPS project: Redox-activity and Health-effects of Atmospheric Primary and Secondary aerosol

The PRIN project **Redox-activity and Health-effects of Atmospheric Primary and Secondary aerosol** (Research Projects of National Interest-RHAPS project) aims to identify specific properties (or combinations of them) of atmospheric particulate matter (PM) from anthropogenic sources that are responsible for toxicological effects, which can be used as new metrics for health-related outdoor pollution studies. The RHAPS project is focused on investigating PM_1 chemical components directly emitted in the atmosphere (defined as "primary" aerosols), as well as chemical species formed *in situ* through atmospheric chemical transformations and dispersed to background areas (defined as "secondary" aerosols). By explicitly accounting for atmospheric transport and reactivity, and using experimental and modelling tools, RHAPS aims at providing a new assessment of the sources and nature of PM_1 components responsible for adverse health effects in real-world conditions.

During the last years, several studies have shown the toxicological potential of secondary organic aerosols (SOA), highlighting the highest intrinsic redox activity and toxicological potential of this group of pollutants (Fushimi et al., 2021; Klyta and Czaplicka, 2020; Gilardoni et al., 2016). Indeed, SOA exhibit relevant oxidative and toxicological potentials and cause oxidative stress in biological cells (Puthussery et al., 2020).

Therefore, in order to predict the oxidative potential of atmospheric particles and to evaluate potential effects of pollution on human health, is crucial to consider that hazard compounds are not emitted from single hotspots and/or point emission sources.

In the framework of RHAPS project, field campaigns and laboratory experiments are focused on the link between the OP by atmospheric secondary organic aerosol (SOA) and PM toxicity. Consequently, modern offline and online instrumentation has been used for studying and tracing aerosol properties and composition, as well as for evaluating source contribution in field condition, at different time resolution.

More specifically, RHAPS has four distinct and specific objectives (Figure 7):

1 - to apportion the sources of ambient PM OP, measured by acellular methods, and toxicity burden (by measured adverse biological effects induced by PM exposures), and assess relevant processes governing their variability in the atmosphere, in the frame of intensive experimental field measurements at urban and rural background sites. A comprehensive characterization of aerosol physical-chemical properties will be carried out by state-of-the-art aerosol measurement techniques at time scales (hourly, sub-hourly) suitable for capturing the effects of major changes in ambient conditions and in emission cycles. The effect of OP and other physical-chemical properties of PM (size-dependent composition, water solubility, particle mass/number/surface, etc.) on toxicological endpoints through *in vitro* studies (oxidative stress, inflammation, DNA damage) will be investigated. To this aim, a relevant number of daily chemically-characterized PM_1 samples will be available in parallel to samples devoted to toxicological assays. Advanced source apportionment models (i.e. Principal Component Analysis, PCA, Positive Matrix Factorization, PMF) based

on multi-time resolution datasets and optical apportionment will be also applied to better single out major PM sources at receptor sites;

2 - to characterize the redox-active capacity of aerosols formed in the atmosphere upon ageing of the emissions (i.e. the secondary organic aerosol, SOA), through focused lab experiments and comparison with field measurements. ChAMBre (Chamber for Aerosol Modelling and Bio-aerosol Research), the unique Italian atmospheric simulation chamber will be used for this task. Pilot SOA generation experiments will be performed to investigate SOA redox activity and toxicological properties;

3 - to assess the dose-response relationship of the toxicological effects in cellular assays, as a function of doses of PM, loadings of OP, and following a critical assessment of the predictive capacity of different PM properties. The huge amount of experimental data on PM properties will be exploited to search alternative or complementary metrics for PM, more closely accounting for the actual PM components responsible for adverse health effects;

4 - to implement air quality models to forecast PM toxicity, by explicitly simulating OP of PM and/or alternative metrics, over the Italian territory. Indeed, current air quality models predict PM mass but not OP/aerosol toxicity, because of the lack of information on OP sources, location, and magnitude.

This project required winter and summer field observations and measurements at two sampling sites of the southern part of the Po Valley: Bologna (BO), as urban site, and San Pietro Capofiume (SPC), as rural site (Belosi et al., 2017). BO site is located in the National Research Council (CNR) Research Area (44°31′29″ N, 11°20′27″ E); SPC site is located at about 30 km north-east of Bologna, in a sparsely populated flat countryside (44°39′15″ N, 11°37′29″ E) (Paglione et al., 2020; Belosi et al., 2017).

The Po Valley, located in northern Italy, is one of the most polluted areas in Europe due to its geomorphological features. It is surrounded by the Alps to the north and northwest and by the Apennines to the south. Frequent and prolonged low-wind periods and stable atmospheric conditions often occur and support the accumulation of locally emitted pollutants, especially during the cold months (Paglione et al., 2020). For these peculiarities, and due to the high density of anthropogenic sources, the Po Valley is frequently object of research in relation to air quality (Farao et al., 2014; Sandrini et al., 2014; Paglione et al., 2020).

The winter monitoring campaign was organized as reported in Table 4.

The summer monitoring campaign was carried out only at BO site as, due to previous experiments on the same area (Paglione et al., 2021, 2020), the atmospheric mixing during the warm season ensures that differences between the two sites are largely reduced.

Field observations included both 24-h (extensive) and high-time resolved data (intensive), collected in parallel during winter and summer 2021. 24-h measurements were carried out during two Extensive Observational Periods (EOPs), each lasting approximatively 60 days: the winter EOP was conducted from January to March 2021, and the summer EOP from the beginning of June to July 2021. Accordingly, two Intensive Observational Periods (IOPs) were carried out, each lasting approximatively 40 days, during which the online equipment was deployed. The winter IOP lasted from 21/01/2021 to the end of February, the summer IOP from beginning of

June 2021 to mid-July 2021. Finally, four super Intensive Observational Periods (SIOPs) were carried out, each lasting four days (from h 8.00 a.m. to h 8.00 a.m.): three winter SIOPs in January /February 2021, and one SIOP in June/July 2021.

Table 4. Observation periods for RHAPS field measurements.

	Winter	**Summer**	**Notes**
Exstensive Observation Period (EOP)	Jan/March 2021	June/July 2021	60+60 days of 24h measurements
Intensive Observation Period (IOP)	21/01-28/02-2021	01/06-16/07-2021	40+40 days of continuous online measurements
Super Intensive Observation Period (SIOP)	26-29 January 2021 2-5 February 2021 16-20 February 2021	29 June-03 July 2021	4+4+4+4 days

For what has been the responsibility of our working group, for the collection of PM_1 samples required for the experimental activities, during the winter monitoring campaign, two single-line samplers were located at BO, and one double-line sampler was placed at SPC (Giano and Gemini; Dadolab Srl, Cinisello B., MI, Italy). During summer samplings, only the double-line sampler was placed at BO site. During both the monitoring periods, PM_1 were collected on PTFE membrane filters (47 mm diameter, 2 μm pore size, PALL Corporation, Port Washington, New York, NY, USA).

For the SIOPs, a Particle Into Liquid Sampler (PILS ADI 2081; Metrohm AG, Herisau, Switzerland) was used for continuous collection of PM as a diluted solution of soluble species in which insoluble particles are suspended (Costabile et al., 2019). Time resolution of sampling was 2 hours. The sampling line was equipped with a PM_1 head and with a denuder line to exclude acid and basic gases from the sampling.

In this context, the activities carried out for RHAPS project during the PhD research concerned the determination of the aerosol redox potential (OP+RP) through multiple measurement techniques. Four assays (OP^{DCFH}, OP^{AA}, OP^{DTT} and RP^{DPPH}) were synergistically applied to 24-h PM_1 field filters collected during the EOPs, since the individual assays respond to different PM properties (as composition and size). OP^{DCFH} was also performed on PILS solutions to measure online oxidative potential of samples. Furthermore, PM_1 samples were chemically characterized for the water-soluble and insoluble fraction of elements (Al, As, Ba, Bi, Ca, Cd, Ce, Co, Cr, Cs, Cu, Fe, Ga, K, La, Li, Mg, Mn, Mo, Na, Nb, Ni, Pb, Rb, Sb, Sn, Sr, Ti, Tl, U, W, Zn, Zr).

By accounting other several factors, such as atmospheric transport and reactivity, and using experimental and modelling tools, this project will provide a new assessment of the sources and nature of PM components responsible for adverse health effects in real-world conditions. Furthermore, pursuing research on the actual PM components and properties, truly determining the biological effective dose in PM, must be considered a top priority for upgrading international air quality standards, as more specific metrics would avoid costly measures targeting sources of PM having negligible or little relative health effects.

In this dissertation preliminary results of RHAPS winter and summer campaigns are reported below.

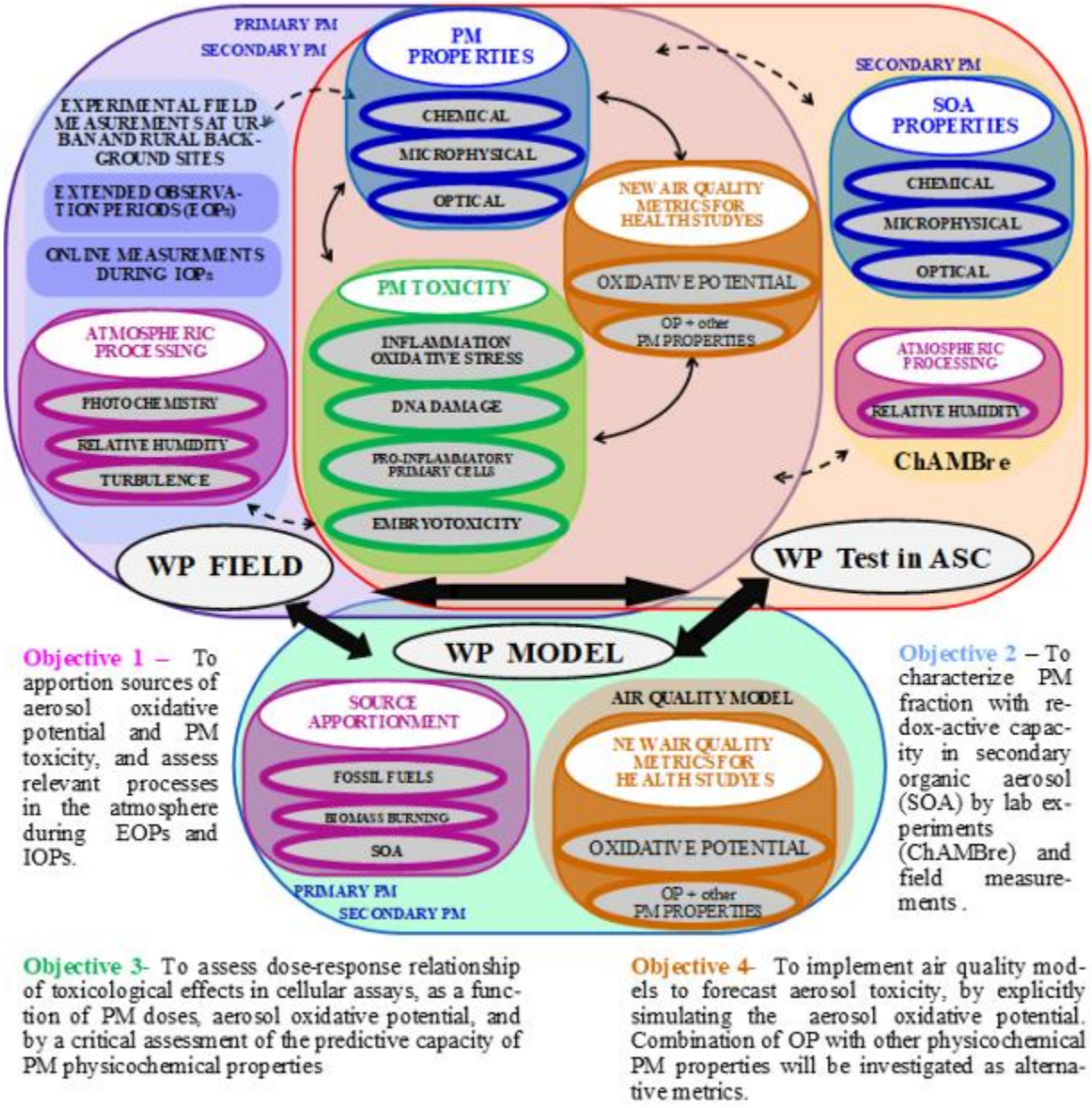

Figure 7. Work packages of RHAPS project including all the activities carried out.

Chemical characterization of PM_1 field filters

Table 5 reports limits of detection (LODs) and descriptive statistics of PM_1 analysed compounds for BO (Table 5a) and SPC site (Table 5b).

The chemical fractionation procedure (Canepari et al., 2006a, Canepari et al., 2006b, Canepari et al., 2010) allows assessing the chemical form (water-soluble, WS; insoluble, I) in which each element is released in PM, which may be typical of peculiar emission source, thus being very efficient for the identification of several sources (Yadav and Rajamani, 2006; Feng et al., 2009; Canepari et al., 2010; Betha et al., 2014).

On the whole, concentration values were comparable between BO and SPC, during the winter period. In fact, it can be observed that there are no significant differences between the values obtained at the two sampling sites, except for Cu, Fe and Sb which are known tracers of non-exhaust emission from vehicular traffic (Massimi et al., 2020b), and are obviously slightly higher at BO site, that represents the urban background. The observed homogeneous composition of PM_1 is compatible on one side with the absence of local emission sources of peculiar relevance, on the other with a uniform spatial distribution of PM, typical of the studied area and due to the frequent development of temperature inversions, which leads to extended periods of high atmospheric stability. These factors determine a horizontal diffusion and a homogeneous mixing of the emission products (Canepari et al., 2014). Furthermore, particles with a.d. < 1 µm exhibit a greater capacity to remain in the lower atmosphere and, thus, to horizontally spread from the point of emission.

OP and RP values at BO and SPC were very similar and comparable, confirming the substantial homogeneity of the air masses in the studied area.

Figures 8, 9 and 10 graphically report the temporal trend of the elements that are selective in tracing different emission sources. Figure 11 reports OP and RP values obtained from the water-soluble fraction of PM_1 samples collected at the two monitoring sites.

Soluble fractions of Cs, Rb, K and Tl (Figure 8), that are typically emitted by domestic biomass heating (Massimi et al., 2020c; Minguillón et al., 2012), show an almost similar trend and temporal variability, with comparable values at both the studied sites. OP^{DTT} values (Figure 11, panel c) are similar at BO and SPC and show a trend in agreement with that of biomass burning tracers. This result appears in line with previous publications, which underlined the responsiveness of OP^{DTT} toward the *fine* fraction of PM released by biomass burning source (Massimi et al., 2020a; Simonetti et al., 2018).

Soluble fractions of Cu, Mn, Mo, and Sn (Figure 9) are mainly released by brake abrasion and resuspension of soil dust, due to non-exhaust vehicular traffic (Massimi et al., 2020b; Pant and Harrison, 2013). Even in this case, element concentrations exhibit a similar temporal trend and no significant differences. OP^{AA} is known to be particularly sensitive toward elements generated by non-exhaust traffic emissions (Simonetti et al., 2018; Perrone et al., 2019; Lin and Yu, 2020) and, indeed, OP^{AA} results (Figure 11, panel b) are in agreement with the trend of Cu, Mn, Mo and Sn. However, values from this assay are very close to the limits of detection due to the fact that OP^{AA} is mainly sensitive to coarse particles (1.8 - 10 µm) (Massimi et al., 2020a; Simonetti et al., 2018).

Lastly, Al, Cs, Fe and Li (Figure 10) in their insoluble fraction are contained in soil and, thus, they are robust tracers of events of mineral dust advection (Massimi et al., 2020b; Canepari et al., 2019). This contribution probably derived from Saharan incursion of dust due to long-range transport contributions, which were checked and confirmed by Dust Regional Atmospheric Model output (DREAM8b v2.0 0.5, Barcelona Supercomputing Center; Nickovic et al., 2001) (Figure 12).

Results from OP^{DCFH} (Figure 11, panel a) are still object of elaboration and interpretation; the same goes for RP^{DPPH} (Figure 11, panel d), which was at its first application in a long and detailed monitoring campaign.

On the whole, during winter period, element concentrations show the same trend and temporal variability between the two selected monitoring sites, confirming the influence of atmospheric stability, which favour the PM permanence time in the atmosphere as well as the PM spatial diffusion (Perrino et al., 2014). In the summer period, when the meteo-climatic conditions favoured the pollutants dilution, a general decrease in element concentrations is detectable at BO site.

Table 5a. Limits of Detection (LOD) and descriptive statistics of PM_1 mass and PM_1 chemical compounds concentrations determined at Bologna (BO) during winter and summer monitoring periods.

	BO									
			Winter (21/01/21 - 17/03/21)				Summer (08/06/21 - 13/07/21)			
	UoM	**LOD**	**Mean**	**Std. Dev.**	**Median**	**Range (min-max)**	**Mean**	**Std. Dev.**	**Median**	**Range (min-max)**
PM_1 mass	µg/m³	-	18	12	16	3.6 - 53	8.5	2.5	7.9	3.6 - 14
As _WS	ng/m³	0.14	0.14	0.10	0.12	0.0010 - 0.39	0.14	0.065	0.13	0.041 - 0.37
Ba _WS	ng/m³	0.20	0.36	0.28	0.31	0.0015 - 1.17	2.0	0.93	1.9	0.59 - 4.8
Bi _WS	ng/m³	0.0037	0.029	0.030	0.020	0.0017 - 0.15	0.0096	0.0085	0.0074	0.00044 - 0.044
Cd _WS	ng/m³	0.041	0.084	0.054	0.077	0.010 - 0.25	0.014	0.0092	0.012	0.00062 - 0.047
Co _WS	ng/m³	0.025	0.041	0.040	0.025	0.0055 - 0.21	0.045	0.034	0.031	0.0070 - 0.15
Cr _WS	ng/m³	0.11	0.12	0.10	0.10	0.00087 - 0.38	0.087	0.030	0.082	0.033 - 0.17
Cs _WS	ng/m³	0.0013	0.0081	0.0052	0.0080	0.00051 - 0.022	0.0017	0.00087	0.0015	0.00040 - 0.0040
Cu _WS	ng/m³	0.057	0.83	0.64	0.65	0.10 - 2.7	0.57	0.34	0.54	0.042 - 1.3
Ga_WS	ng/m³	0.0020	0.0049	0.0033	0.0056	0.00036 - 0.015	0.0022	0.0016	0.0020	0.00029 - 0.0083
K_WS	ng/m³	24	146	90	136	13 - 430	40	30	30	15 - 180
Mn_WS	ng/m³	0.12	0.90	0.82	0.59	0.11 - 3.7	0.53	0.40	0.42	0.069 - 2.2
Mo_WS	ng/m³	0.032	0.48	0.45	0.35	0.031 - 1.7	0.23	0.16	0.18	0.060 - 0.88
Na_WS	ng/m³	23	31	14	28	9 - 79	27	20	21	8.4 - 122
Pb_WS	ng/m³	0.088	0.93	0.82	0.72	0.033 - 3.6	0.20	0.22	0.14	0.0024 - 0.98
Rb_WS	ng/m³	0.031	0.34	0.21	0.32	0.047 - 0.99	0.035	0.038	0.028	0.0059 - 0.21
Sb_WS	ng/m³	0.086	0.36	0.24	0.33	0.027 - 1.2	0.21	0.17	0.19	0.0096 - 0.92
Sn_WS	ng/m³	0.79	0.16	0.14	0.12	0.014 - 0.69	0.13	0.096	0.11	0.018 - 0.43
Tl_WS	ng/m³	0.00092	0.012	0.0076	0.012	0.00087 - 0.028	0.0038	0.0027	0.0031	0.00025 - 0.013
U_WS	ng/m³	0.00045	0.00079	0.00070	0.00058	0.000073 - 0.0045	0.00062	0.00035	0.00056	0.00015 - 0.0015
V_WS	ng/m³	0.011	0.14	0.17	0.070	0.0040 - 0.86	0.23	0.20	0.17	0.023 - 0.90
W_WS	ng/m³	0.014	0.022	0.017	0.020	0.0035 - 0.069	0.010	0.0046	0.0093	0.0037 - 0.023
Zn_WS	ng/m³	0.15	11	7.6	8.5	0.49 - 27	3.8	2.4	3.2	0.29 - 10

Al_I	ng/m³	19	49	46	38	19 - 326	60	91	32	18 - 447
Bi_I	ng/m³	0.0026	0.058	0.040	0.047	0.014 - 0.18	0.034	0.016	0.030	0.0088 - 0.071
Ce_I	ng/m³	0.47	0.45	0.31	0.37	0.16 - 1.6	0.42	0.47	0.27	0.12 - 2.4
Co_I	ng/m³	0.057	0.14	0.074	0.12	0.046 - 0.41	0.15	0.13	0.11	0.065 - 0.65
Cs_I	ng/m³	0.0035	0.0069	0.0048	0.0055	0.0027 - 0.028	0.0077	0.0075	0.0060	0.0033 - 0.039
Fe_I	ng/m³	12	61	42	50	11 - 219	70	61	54	21 - 318
Ga_I	ng/m³	0.0045	0.015	0.014	0.012	0.0042 - 0.094	0.018	0.027	0.010	0.0054 - 0.13
La_I	ng/m³	0.068	0.049	0.031	0.042	0.018 - 0.18	0.047	0.048	0.033	0.014 - 0.25
Li_I	ng/m³	0.017	0.064	0.10	0.046	0.019 - 0.78	0.050	0.067	0.032	0.017 - 0.33
Mn_I	ng/m³	0.28	1.8	0.93	1.6	0.60 - 4.2	1.4	0.73	1.2	0.60 - 4.4
Mo_I	ng/m³	0.027	0.34	0.27	0.26	0.041 - 1.1	0.16	0.12	0.12	0.047 - 0.71
Pb_I	ng/m³	0.26	2.4	1.3	2.0	0.67 - 6.3	0.67	0.31	0.55	0.25 - 1.4
Sn_I	ng/m³	0.091	0.61	0.47	0.49	0.11 - 2.6	0.40	0.35	0.33	0.18 - 2.3
Ti_I	ng/m³	0.43	1.5	2.5	0.94	0.48 - 19	1.4	1.8	0.86	0.43 - 10
W_I	ng/m³	0.021	0.033	0.020	0.029	0.0078 - 0.11	0.013	0.011	0.0095	0.0023 - 0.062
Zr_I	ng/m³	0.024	0.085	0.080	0.074	0.033 - 0.63	0.093	0.048	0.084	0.036 - 0.28
DCFH_WS	nmol H_2O_2 m³	$1.1 \cdot 10^{-10}$	$4.7 \cdot 10^{-9}$	$3.1 \cdot 10^{-9}$	$4.1 \cdot 10^{-9}$	$1.1 \cdot 10^{-10}$ - $1.2 \cdot 10^{-8}$	$1.6 \cdot 10^{-9}$	$1.4 \cdot 10^{-9}$	$1.5 \cdot 10^{-9}$	0 - $4.6 \cdot 10^{-9}$
AA_WS	nmol AA min^{-1} m^{-3}	0.0096	0.37	0.35	0.27	0.018 - 1.9	0.47	0.54	0.23	0 - 2.5
DTT_WS	nmol DTT min^{-1} m^{-3}	0.0058	0.91	0.55	0.83	0.087 - 2.5	0.31	0.17	0.31	0.016 - 0.66
DPPH_WS	% Cons m³	0.0078	0.42	0.42	0.33	0 - 1.8	0.045	0.087	0.046	0 - 0.23

Table 5b. Limits of Detection (LOD) and descriptive statistics of PM_1 mass and PM_1 chemical compounds concentrations determined at San Pietro Capofiume (SPC) during winter monitoring period.

	SPC					
			Winter (21/01/21 - 17/03/21)			
	UoM	**LOD**	**Mean**	**Std. Dev.**	**Median**	**Range (min-max)**
PM_1 mass	µg/m³	-	19	12	18	4.4 - 55
As _WS	ng/m³	0.14	0.16	0.11	0.15	0.0067 - 0.44
Ba _WS	ng/m³	0.20	0.38	0.25	0.31	0.013 - 0.99
Bi _WS	ng/m³	0.0037	0.018	0.014	0.014	0.0024 - 0.076
Cd _WS	ng/m³	0.041	0.12	0.13	0.077	0.0069 - 0.81
Co _WS	ng/m³	0.025	0.039	0.042	0.030	0.0021 - 0.30
Cr _WS	ng/m³	0.11	0.093	0.079	0.079	0.00087 - 0.29
Cs _WS	ng/m³	0.0013	0.0068	0.0042	0.0068	0.00029 - 0.020
Cu _WS	ng/m³	0.057	0.60	0.45	0.49	0.073 - 2.5
Ga_WS	ng/m³	0.0020	0.0043	0.0030	0.0037	0.00058 - 0.018
K_WS	ng/m³	24	153	88	149	9 - 408
Mn_WS	ng/m³	0.12	0.72	0.53	0.56	0.074 - 2.3
Mo_WS	ng/m³	0.032	0.36	0.36	0.25	0.031 - 1.7
Na_WS	ng/m³	23	31	12	29	12 - 87
Pb_WS	ng/m³	0.088	0.70	0.52	0.62	0.070 - 2.2
Rb_WS	ng/m³	0.031	0.35	0.21	0.34	0.026 - 1.1
Sb_WS	ng/m³	0.086	0.31	0.18	0.28	0.025 - 0.63
Sn_WS	ng/m³	0.79	0.13	0.11	0.091	0.014 - 0.57
Tl_WS	ng/m³	0.00092	0.011	0.0062	0.011	0.0010 - 0.024
U_WS	ng/m³	0.00045	0.00074	0.00050	0.00066	0.00015 - 0.0032
V_WS	ng/m³	0.011	0.099	0.12	0.054	0.00022 - 0.50
W_WS	ng/m³	0.014	0.020	0.013	0.017	0.0041 - 0.053
Zn_WS	ng/m³	0.15	8.8	5.2	8.3	0.23 - 21
Al_I	ng/m³	19	59	74	33	11 - 410

Bi_I	ng/m³	0.0026	0.073	0.073	0.047	0.0071 - 0.38
Ce_I	ng/m³	0.47	0.46	0.45	0.27	0.076 - 1.9
Co_I	ng/m³	0.057	0.14	0.075	0.12	0.052 - 0.41
Cs_I	ng/m³	0.0035	0.0075	0.0051	0.0059	0.0024 - 0.027
Fe_I	ng/m³	12	46	33	41	6.8 - 170
Ga_I	ng/m³	0.0045	0.023	0.023	0.014	0.0049 - 0.11
La_I	ng/m³	0.068	0.048	0.047	0.027	0.0073 - 0.19
Li_I	ng/m³	0.017	0.071	0.090	0.046	0.018 - 0.57
Mn_I	ng/m³	0.28	1.8	1.0	1.5	0.47 - 4.5
Mo_I	ng/m³	0.027	0.35	0.34	0.23	0.028 - 1.5
Pb_I	ng/m³	0.26	2.6	1.5	2.2	0.30 - 6.5
Sn_I	ng/m³	0.091	0.64	0.48	0.55	0.07 - 2.4
Ti_I	ng/m³	0.43	1.4	1.8	0.80	0.30 - 8.3
W_I	ng/m³	0.021	0.026	0.016	0.022	0.0067 - 0.084
Zr_I	ng/m³	0.024	0.059	0.055	0.044	0.017 - 0.25
DCFH_WS	nmol H_2O_2 m³	$1.1 \cdot 10^{-10}$	$6.3 \cdot 10^{-9}$	$3.9 \cdot 10^{-9}$	$5.8 \cdot 10^{-9}$	$1.9 \cdot 10^{-10}$ - $1.6 \cdot 10^{-8}$
AA_WS	nmol AA min^{-1} m^{-3}	0.0096	0.55	0.82	0.24	0.010 - 4.6
DTT_WS	nmol DTT min^{-1} m^{-3}	0.0058	0.85	0.47	0.86	0.0058 - 2.0
DPPH_WS	% Cons m³	0.0078	0.41	0.33	0.38	0 - 1.3

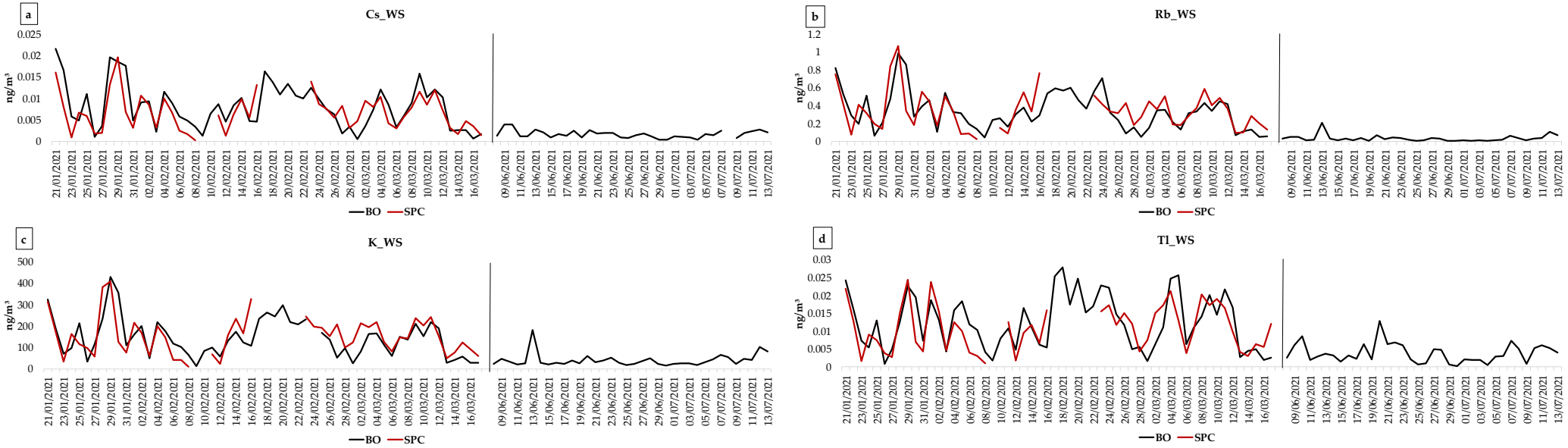

Figure 8. Concentration (ng/m^3) of the water-soluble fraction of Cs (panel a), Rb (panel b), K (panel c) and Tl (panel d) obtained at the two sampling sites (BO and SPC) during winter and summer monitoring period.

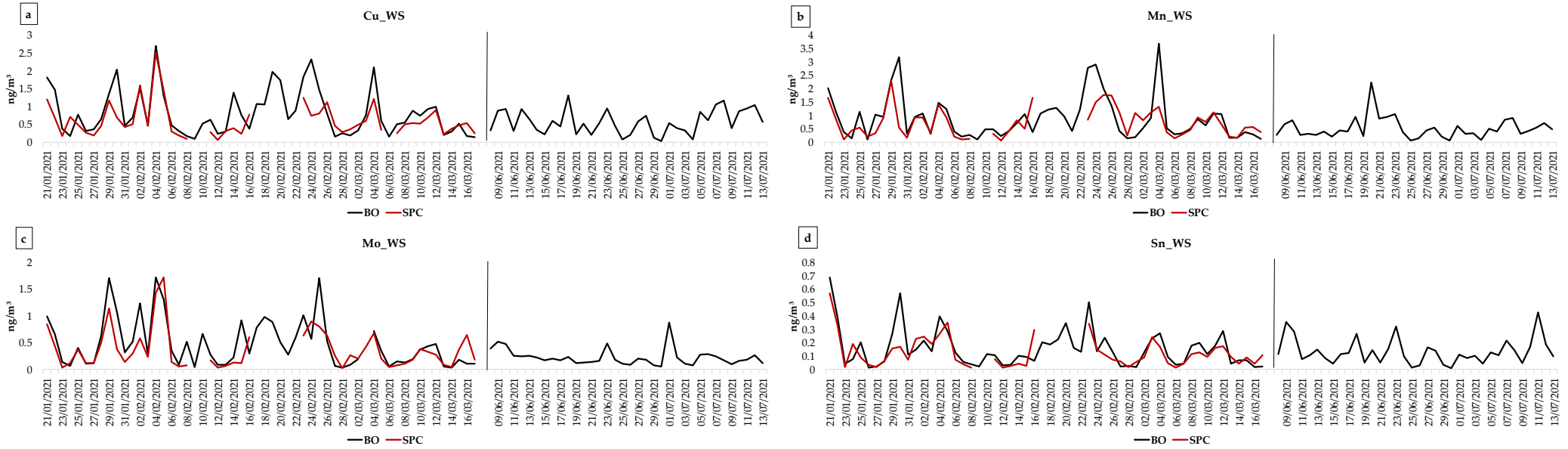

Figure 9. Concentration (ng/m^3) of the water-soluble fraction of Cu (panel a), Mn (panel b), Mo (panel c) and Sn (panel d) obtained at the two sampling sites (BO and SPC) during winter and summer monitoring period.

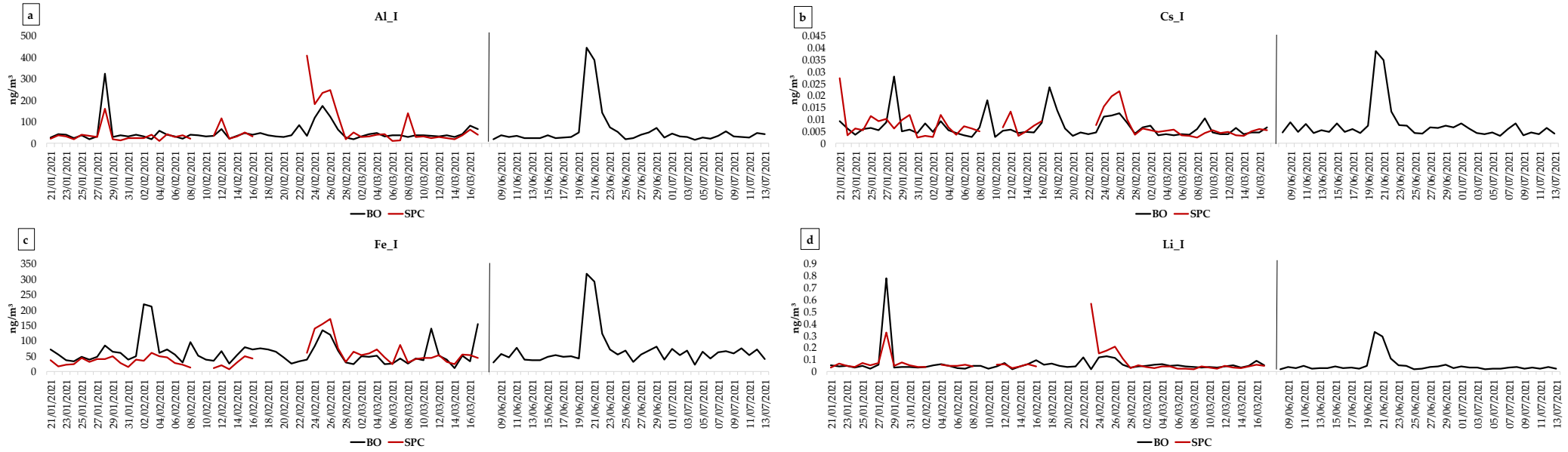

Figure 10. Concentration (ng/m^3) of the insoluble fraction of Al (panel a), Cs (panel b), Fe (panel c) and Li (panel d) obtained at the two sampling sites (BO and SPC) during winter and summer monitoring period.

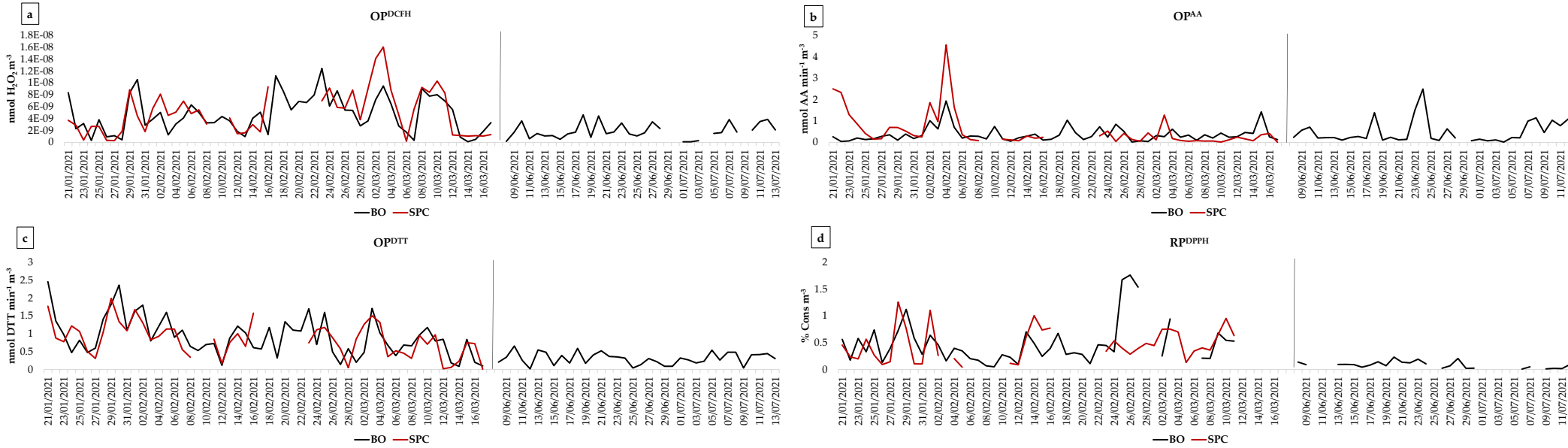

Figure 11. Oxidative (OP^{DCFH}, panel a; OP^{AA}, panel b; and OP^{DTT}, panel c) and reducing (RP^{DPPH}, panel d) potential obtained at the two sampling sites (BO and SPC) during winter and summer monitoring period.

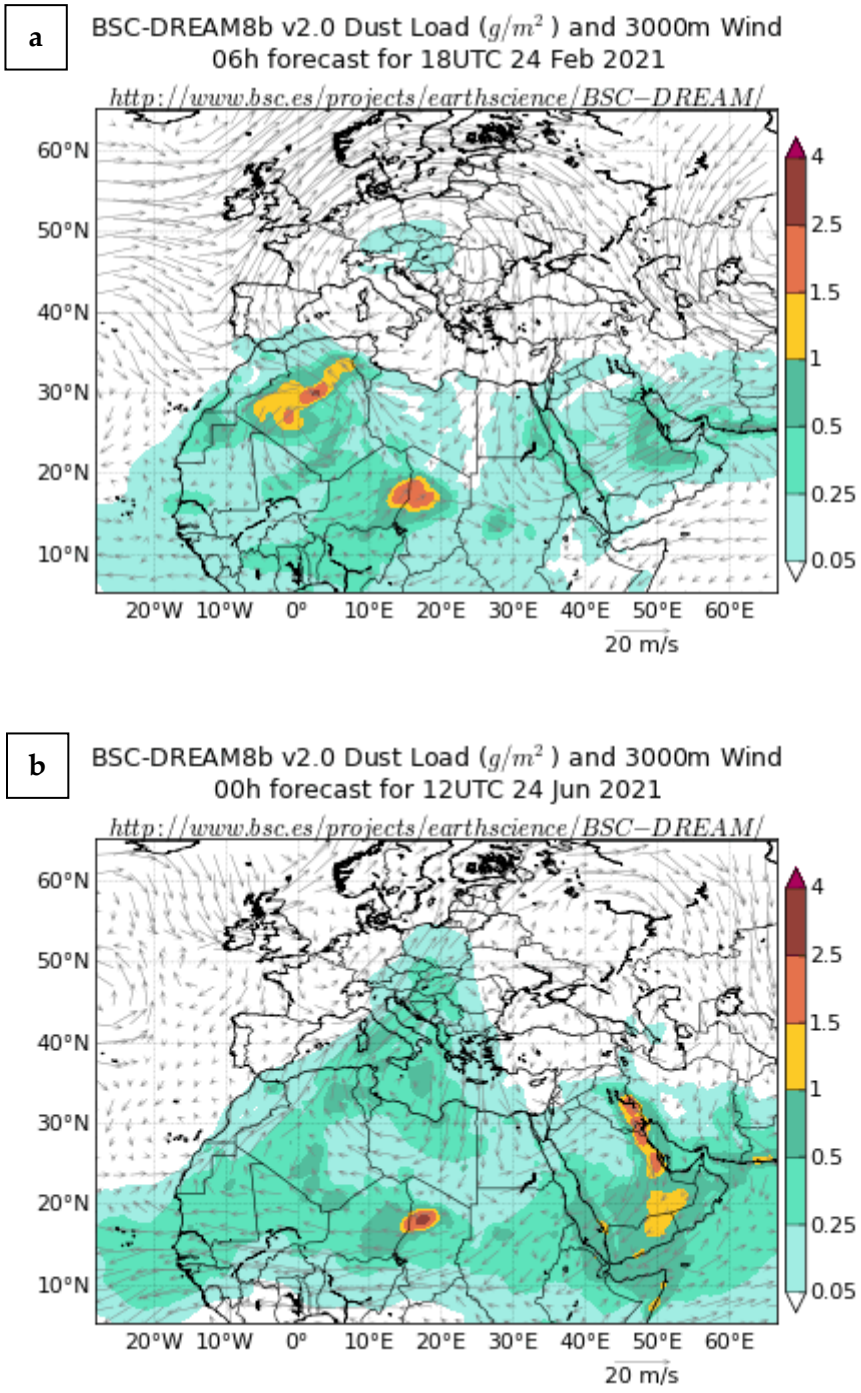

Figure 12. Dust Regional Atmospheric Model output reporting dust incursion during 24 February 2021 (panel a), and 24 June 2021 (panel b).

Principal Component Analysis

Principal component analysis (PCA) was performed on the winter database consisting of the PM_1 water-soluble (_WS) and insoluble fraction (_I) of element concentrations, as well as of the OP and RP data (DCFH, AA, DTT, DPPH), along with other variables derived from analysis carried out by the other research groups (EC, OC, OOA1, OOA2, HOA, BBOA, NH_4^+, NO_3^-, $SO_4^=$, LVG).

The contributions of FF and WB to EC and OC were apportioned through an algorithm based on spectral absorption properties and developed by Massabò et al. (2015).

Hydrocarbon-like organic aerosol (HOA) resulting from the combustion of fossil fuels (e.g., vehicular traffic), biomass burning organic aerosol (BBOA) resulting from biomass combustion, organic aerosols (OOA1 and OOA2) representing secondary formation and/or aging processes in the atmosphere were identified through the High-Resolution Time-of-Flight Aerosol Mass Spectrometer (HR-ToF-AMS) (Paglione et al., 2020). Lastly, NH_4^+, NO_3^-, $SO_4^=$, and levoglucosan (LVG) were obtained by ion chromatography analysis.

The matrix of the data was transformed by column mean centring and row and column autoscaling in order to correct for variations of the data due to the different scaling of the examined variables (Massimi et al., 2020b). Multivariate statistical analyses were performed using the statistical software R (R-project for statistical computing, Ver. 3.0, 32-bit).

Four significant components accounting for 67.3% were obtained. The variance explained by each component is: 37.5%, 16.1%, 8.1% and 5.6%. As reported in Figure 13 first component (PC1) well separates the samples (scores) whereby the highest element concentrations (loadings) were found from the others. Therefore, PC1 is mainly influenced by the dynamics in the atmosphere and, in particular, by the atmospheric stability. However, PC1 does not cluster the elements released by the different emission sources. On the contrary, second, third, and fourth components (PC2, PC3 and PC4, respectively) well separate the elements depending on their concentration variability among the sampling days. The loading plots of PC2/PC3 are reported in Figure 14. Along the PC3 are clustered the species released by vehicular traffic; the insoluble fractions of Ce, Cs, La, Ti, and total concentration of Al, Ca, Fe and Si from mineral dust; species released by biomass burning, as well as those from regional and ammonium nitrate pollution. PC2 well separates the elements at high concentrations in the sampling days where the impact of the identified emission sources was higher. However, PC3 does not separate the four OP and RP assays. For this reason, PC3 and PC4, which explain the 13.9% of the total variance, were represented in the loading plot of Figure 15, since they better cluster chemical species according with emission sources of origin. As reported, the four OP and RP assays are associated to clusters of different tracers confirming the well-known correlations between the assays and the chemical characteristics of the dusts. OP^{AA} is included in a cluster with EC_FF, HOA, OC_FF, Mo_s, Cu_s and Sn_s and confirm the responsiveness of this assay to vehicular traffic (Perrone et al., 2019; Simonetti et al., 2018). OP^{DCFH} is clustered with Al, Si, Fe, and the insoluble fraction of Ce, La and Ti which typically derived from mineral dust incursion (Lokorai et al., 2021). OP^{DTT} is clustered with water-soluble fraction of elements that are well-known

tracers of biomass burning, such as Cs, Li and Rb (Li et al., 2021; Pietrogrande et al., 2021b; Massimi et al., 2020c; Karbowska, 2016).

Positive Matrix Factorization

A receptor modelling approach (RM) based on positive matrix factorization (PMF) was employed to identify sources acting during sample collection. The contribution to PM_1 mass concentration and composition of emission sources during winter monitoring period, was assessed by applying the PMF to the obtained chemical data. The PMF is a factor analysis technique consisting in a weighted least square fit, where non-negativity constraints are imposed in the factor computational process, to reduce rotational freedom of the input data matrix. A detailed description of PMF technique is found in Paatero, (1999) and Hopke, (2000).

The following variables of the winter database were selected to be used for the PMF: PM_1 mass concentration, EC_FF, EC_WB, OC_FF, OC_WB, NH_4^+, NO_3^-, $SO_4^=$, K^+, Al, Si, Ca, Mn, Fe, Cu, Zn, Pb, OP^{DCFH}, OP^{AA}, OP^{DTT}, RP^{DPPH}, LVG.

Figure 16 shows the chemical profiles of the factors (emission sources) identified by PMF at BO and SPC during the winter monitoring period. The presented preliminary data elaboration identified five profiles: wood burning (WB), regional background contribution (REGIONAL), vehicular traffic (TRAFF), secondary aerosol mainly associated with nitrate (NITR), and a component of mineral origin including desert incursion (DUST).

WB factor is mainly described by OC_WB, EC_WB, levoglucosan (Levo) and potassium ion (K^+). Both Levo and K^+ are widely acknowledged as selective tracers of biomasses combustion (Nguyen et al., 2013; Liu et al., 2017; Chowdhury et al., 2007; Sharma et al., 2016). Wood burning is the major PM_1 source during the cold season accounting for about 29 and 35% of the PM_1 mass at BO and SPC, respectively.

Regional background contribution is identified by $SO_4^=$ and NH_4^+ and mainly derived from secondary aerosol formation.

Secondary aerosol, associated with nitrate, is described by NO_3^- and NH_4^+.

Most abundant chemical species describing vehicular traffic factor are typical of both exhaust and non-exhaust emissions, such as organic and elemental carbon (OC_FF and EC_FF, respectively), and Ca, Cu and Mn. The non-exhaust is described by the presence of Ca, that is commonly related to asphalt abrasion, and of Cu and Mn from brake abrasion (Harrison et al., 2021; Lawrence et al., 2013; Thorpe and Harrison, 2008). The exhaust component is represented by OC_FF and EC_FF (Massabò et al., 2015).

The mineral dust profile is described by the abundance of Al, Si and Ca, that are common inorganic tracers of crustal materials (Scotto et al., 2021; Massimi et al., 2021b and references therein). These findings indicated a composition dust rich in silicates, Ca-rich minerals, and metal oxides, that seems to be attributable to dust advection events from African deserts (Pietrodangelo et al., 2013).

Figure 17 shows the relative contribution in percentage of the identified emission sources to the total PM_1 mass concentration and to the single variables measured at BO and SPC, including OP and RP assays. As can be seen in the graph, all the five identified emission sources played a role in impacting PM_1 mass concentration,

even with a different relative contribution. In detail, wood burning (WB), and secondary nitrate (NITR) are the major contributors to PM_1 mass.

As regards to OP and RP assays, Figure 17 shows that all the five identified factors contributed to the considered assays. In detail, the major contribution to DCFH is given by the regional background, that was responsible for approximately 75% of the OP recorded by the considered assay. Vehicular traffic and secondary nitrate were strong contributors to AA, representing approximately 45% and 35%, respectively, as already shown by some previous studies (Weber et al., 2021; Daellenbach et al., 2020; Fang et al., 2016). More than 40% of the DTT is associated with wood burning, according with the findings of previous source apportionment studies (Cesari et al., 2019). DPPH is associated with four emission sources: WB (50%), REGIONAL (20%), TRAFF (10%), DUST (20%). Although this monitoring campaign represented the first field application of the DPPH assay, and results are still to be deepened, the biomass burning seems to have a predominant role in determining the presence of reducing species to whom this assay responds.

Overall, these preliminary findings highlight the importance of the identified emission sources in driving PM-induced toxicity in the Po Valley during winter. The receptor model employed in this study confirmed the importance of anthropogenic sources associated mainly to traffic and to regional scale processes affecting secondary aerosol formation especially during the cold season, in agreement with other authors (Tositti et al., 2013; Marcazzan et al., 2003).

However, further elaborations are required, also including data related to summer monitoring period in order to also consider the seasonality.

Results from this project can be used by policy makers to prioritize the required public health actions and policies to mitigate the adverse health effects of PM by controlling the emissions from sources that are causing most of the PM toxicity in the impacted area of the Po Valley.

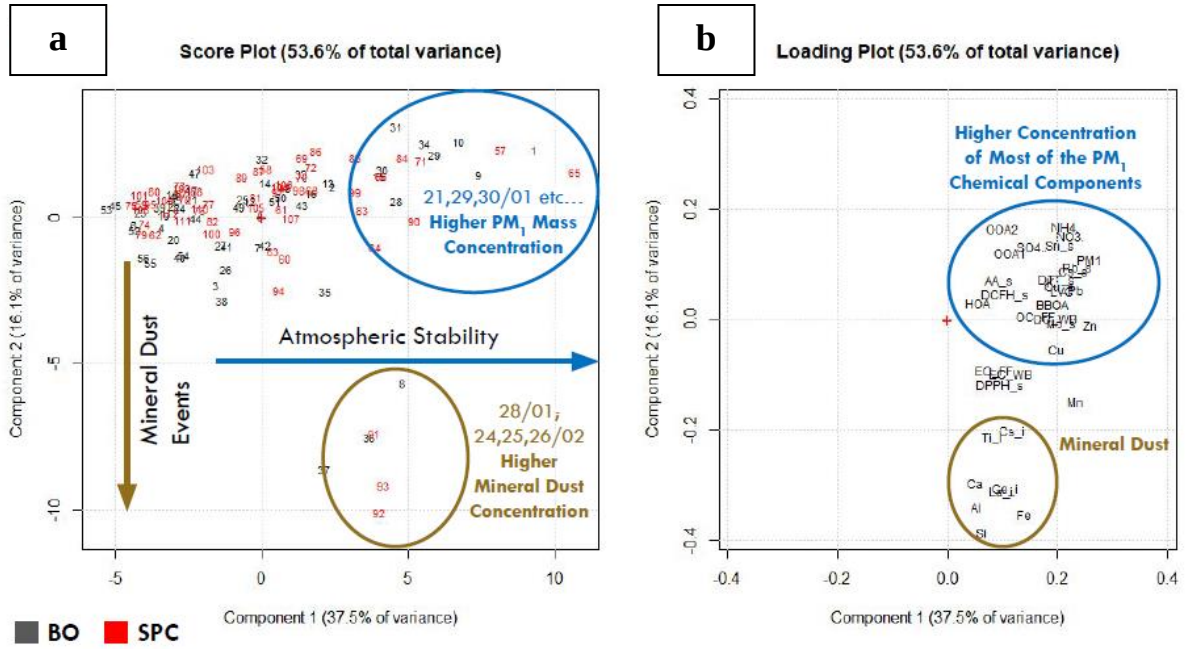

Figure 13. Score (panel a) and loading plot (panel b) of the PCA (PC1/PC2) performed on the selected variables of the winter database, determined at the two monitoring sites, BO and SPC.

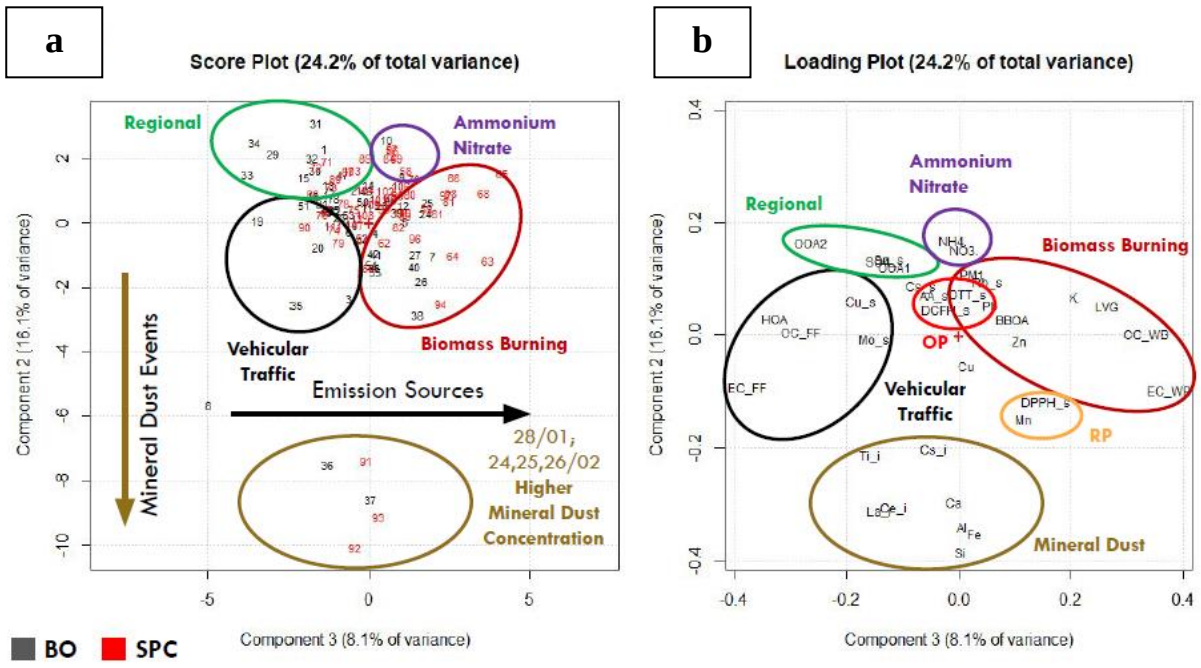

Figure 14. Score (panel a) and loading plot (panel b) of the PCA (PC3/PC2) performed on the selected variables of the winter database, determined at the two monitoring sites, BO and SPC.

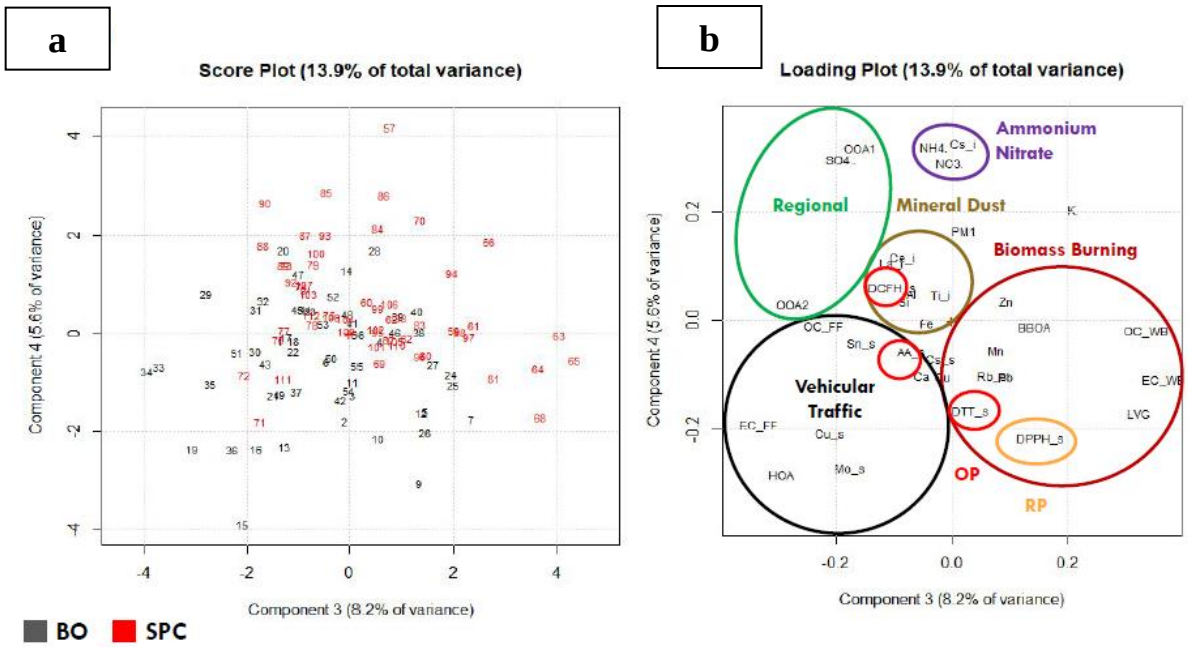

Figure 15. Score (panel a) and loading plot (panel b) of the PCA (PC3/PC4) performed on the selected variables of the winter database, determined at the two monitoring sites, BO and SPC.

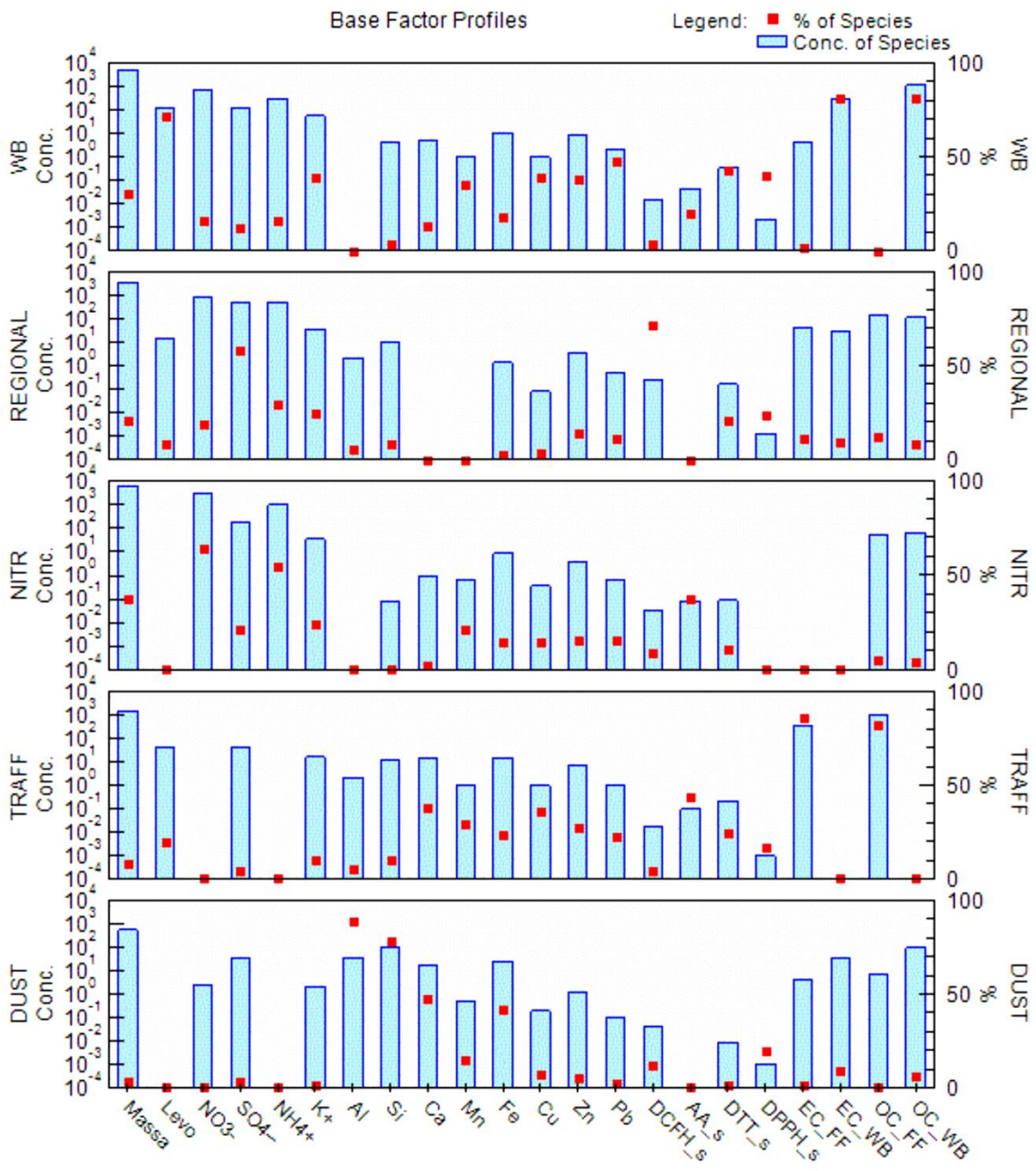

Figure 16. Chemical profiles of the factors identified by PMF at BO and SPC during the winter monitoring period.

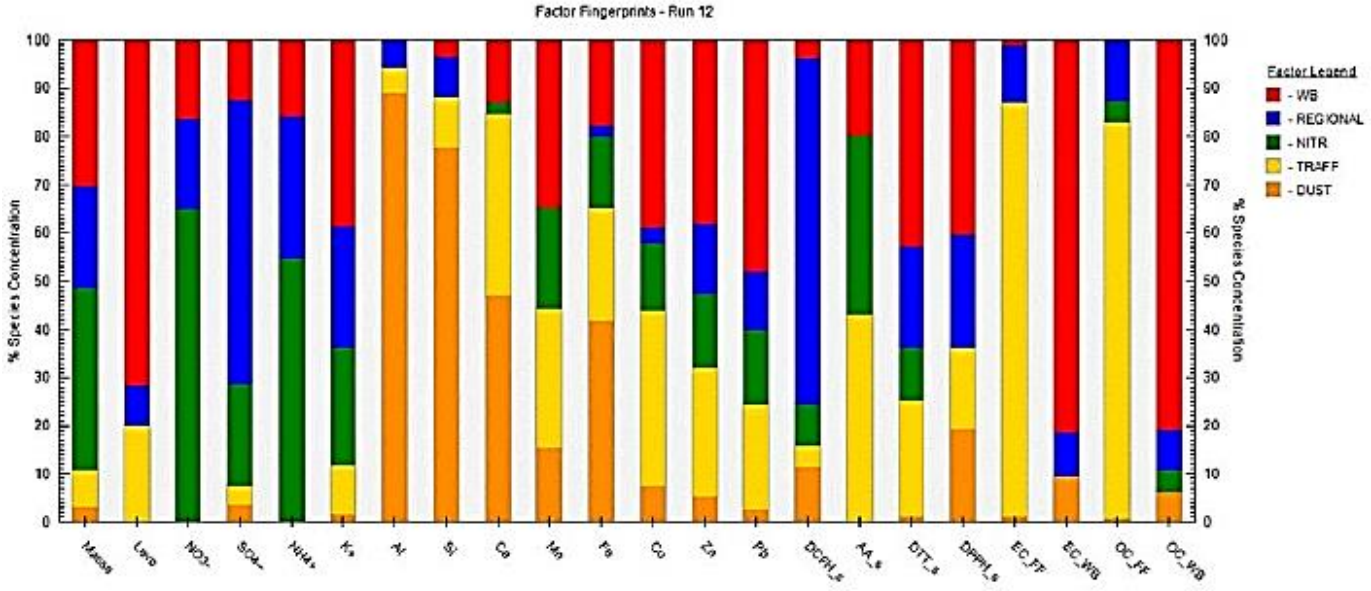

Figure 17. Relative contribution of the main emission sources to the total PM_1 concentration and to the single variables. Values are reported in percentage.

Super Intensive Observation Periods (SIOPs)

During the SIOPs aerosol measurement were carried out for characterizing the aerosol chemical composition with a high time resolution. The SIOPs were planned based on the forecasts of PM_1 concentration peak periods of an air quality model (Developed by University of L'Aquila). Two SIOPs were carried out at BO during the winter monitoring period, and another one during the summer campaign.

A particle-into-liquid sampler (PILS) was used for time-resolved measurement of the oxidative potential (OP) through the DCFH assay (Figure 18). The air flow, passing through a cyclone (cut point 1 μm), was denuded from gaseous species, while aerosol particles were grown in a saturated water vapor chamber to form droplets (See section 1.3.2). These were collected by inertial impact on a collection plate and washed by deionized water. The resulting solution was collected and analyzed for OP^{DCFH} every 2 h, for 4 consecutive days.

At the same time, the Air Liquid Interface System (ALI) was employed for estimating the toxicity of lung cells (human bronchial epithelial cell line BEAS-2B) exposed to ambient PM with selected a.d. cut by a cyclone (Costabile et al., 2017) for 24 hours a day, for 4 days.

Figure 19 shows results of the OP^{DCFH}. Data elaboration and discussion are still in progress, therefore in this dissertation only data obtained during the winter SIOPs are shown.

Figure 18. Fluorescence detector used for OP^{DCFH} measurements.

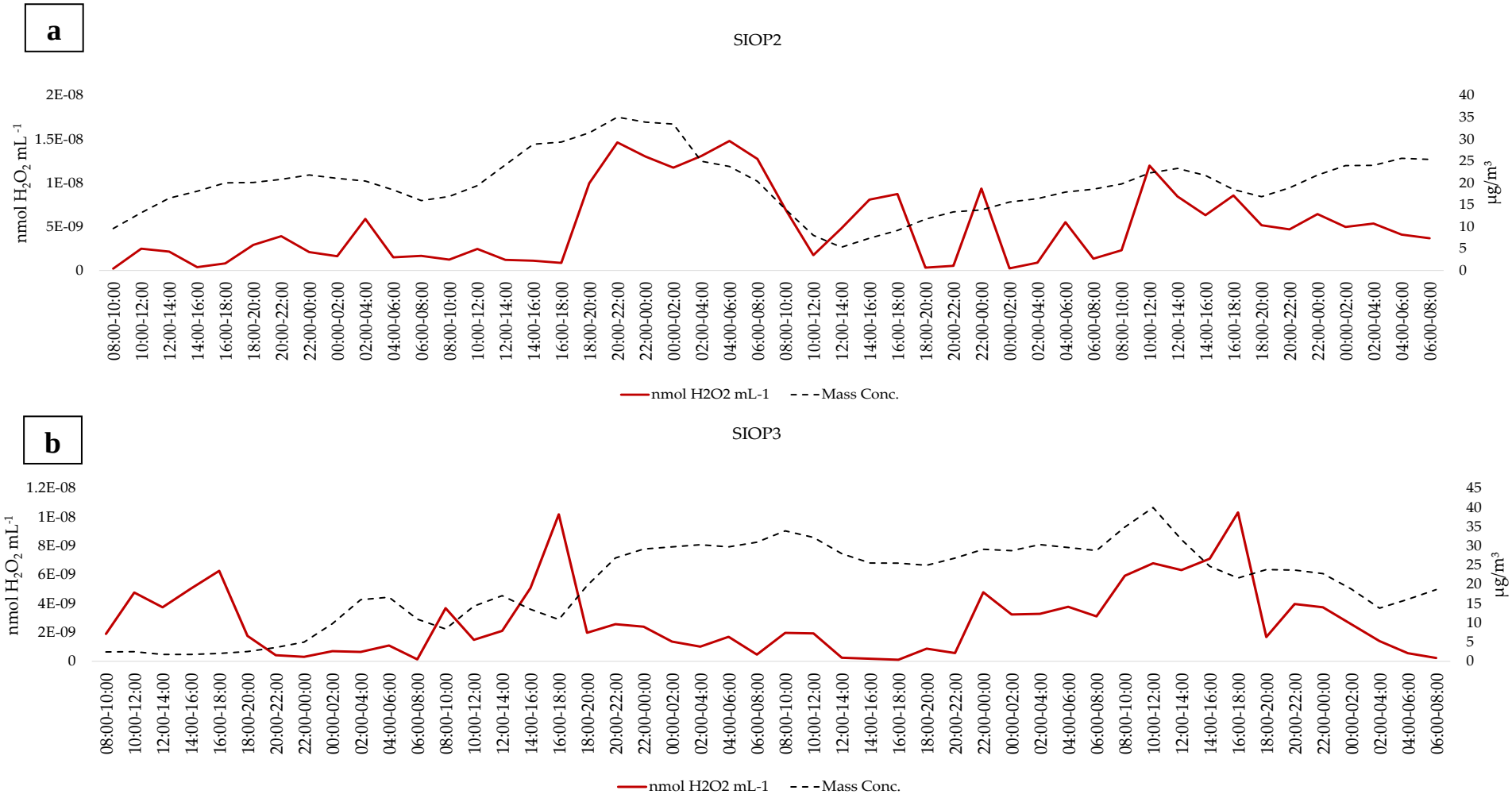

Figure 19. Time series of the OP^{DCFH} during the SIOP2 (panel a; 02-05/02/2021) and SIOP3 (panel b; 16-19/02/2021). For reference, data of PM_1 mass concentration are reported. Limit of detection of OP^{DCFH} is between $6 \cdot 10^{-9}$ and $8 \cdot 10^{-9}$ nmol H_2O_2 m^{-3}.

The obtained data from the two presented SIOPs are contrasting. In fact, during the SIOP2, values of sampling collected during nighttime period were generally higher than those collected during the daytime. On the contrary, during the SIOP3 values from daytime were higher than those from nighttime, with a peak between 16:00 and 18:00 for three days out of four. Overall, data are almost all below the detection limit (assessed between $6 \cdot 10^{-9}$ and $8 \cdot 10^{-9}$ nmol H_2O_2 m^{-3}), therefore are not particularly representative, at least after these preliminary elaboration and interpretation.

As already mentioned, data elaboration are still in progress, and it will be necessary to assess what will emerge from the comparison between OP and toxicological data.

8.2.1 (D2) On the redox-activity and health-effects of atmospheric primary and secondary aerosol: phenomenology

Atmosphere (2022), 13(5), 704, doi: 10.3390/atmos13050704

Francesca Costabile[1*] , Stefano Decesari[2], Roberta Vecchi[3], Franco Lucarelli[4,5], Gabriele Curci[6,7], Dario Massabò[8], Matteo Rinaldi[2], Maurizio Gualtieri[9,$], Emanuela Corsini[10], Elena Menegola[11], Silvia Canepari[12], Lorenzo Massimi[12], Stefania Argentini[1], Maurizio Busetto[2], Gianluca Di Iulio[1], Luca Di Liberto[1], Marco Paglione[2], Igor Petenko[1], Mara Russo[2], Angela Marinoni[2], Gianpietro Casasanta[1], Sara Valentini[3], Vera Bernardoni[3], Federica Crova[3], Gianluigi Valli[3], Alice Corina Forello[4], Fabio Giardi[4], Silvia Nava[4,5], Giulia Pazzi[4], Paolo Prati[8], Virginia Vernocchi[8], Teresa La Torretta[9], Ettore Petralia[9], Milena Stracquadanio[9], Gabriele Zanini[9], Gloria Melzi[10], Emma Nozza [3,10], Martina Iulini[10], Donatella Caruso[10], Lucia Cioffi[10], Gabriele Imperato[10], Flavio Giavarini[10], Maria Battistoni[3,11], Francesca Di Renzo[11], Maria Agostina Frezzini[12], Cinzia Perrino[13], and Maria Cristina Facchini[2]

[1] Institute of Atmospheric Sciences and Climate, National Research Council, 00133 Roma, Italy

[2] Institute of Atmospheric Sciences and Climate, National Research Council, 40129 Bologna, Italy

[3] Dept. of Physics, Università degli Studi di Milano, and INFN-Milan, 20133 Milano, Italy

[4] Dept. of Physics and Astronomy, Università degli Studi di Firenze, 50019 Sesto Fiorentino, Italy

[5] National Institute of Nuclear Physics, INFN-Florence, via Sansone 1, 50019 Sesto Fiorentino, Italy

[6] Dept. of physico chemical science, Università degli Studi dell'Aquila, 67100 L'Aquila, Italy

[7] Center of Excellence in Telesensing of Environment and Model Prediction of Severe events (CETEMPS), Università degli Studi dell'Aquila, 67100 L'Aquila, Italy

[8] Dept. of Physics, Università degli Studi di Genova, and INFN-Genoa, 16146 Genova, Italy

[9] ENEA-SSPT-MET-INAT, 40129 Bologna, Italy

[10] Dept. of Pharmacological and Biomolecular Sciences, Università degli Studi di Milano, 20133 Milano, Italy

[11] Dept. of Environmental Science and Policy, Università degli Studi di Milano, 20133 Milano, Italy

[12] Department of Environmental Biology, University of Rome Sapienza, Roma, 00185, Italy

[13] Institute of Air Pollution, National Research Council, Rome, Italy

[$] Author present address Department of Earth and Environmental Sciences, University of Milano-Bicocca, 20126 Milano, Italy

[*] Corresponding author

Abstract: The RHAPS project was launched in 2019 with the major objective to identify specific properties of the fine atmospheric aerosol from combustion sources that are responsible for toxicological effects and can be used as new metrics for health-related outdoor pollution studies. In this paper, we present the overall

methodology of RHAPS, and introduce the phenomenology and the first data observed. A comprehensive physico-chemical aerosol characterization has been achieved by means of high-time resolution measurements (e.g. number size distributions, refractory chemical components, elemental composition,) and low-time resolution analyses (e.g. oxidative potential, toxicological assays, chemical composition,…). Preliminary results show a high complexity in the relations observed, the link between air quality and toxicological endpoints being not obvious. We explore data from different points of view: source apportionment of PM_1 and the role of source emissions on aerosol toxicity, the oxidative potential as a predictive variable for PM_1 toxicity with focus on the secondary organic aerosol possessing redox-active capacity, exposure-response relationships for PM_1, and air quality models to forecast PM_1 toxicity. We provide a synthesis of results with the outlook to companion papers where data are analyzed in more detail.

Keywords: atmospheric aerosol; chemical composition; secondary aerosol; source apportionment; ultrafine particles; oxidative potential; exposure; toxicology; forecasting; micrometeorology

1. **Introduzione**

Ambient air pollution is the leading environmental risk factor globally. The WHO estimates that exposure to air pollution might be associated with around 7 million deaths, especially from noncommunicable cardiovascular and respiratory diseases [1]. Among air pollutants, $PM_{2.5}$ (particulate matter with an aerodynamic particle diameter less than 2.5 μm) has received special attention. To date, there is evidence of causal relationships between exposure to $PM_{2.5}$ air pollution and all-cause mortality, as well as several diseases, including lung cancer, stroke, respiratory infections, and pulmonary diseases [1,2]. However, our understanding of this relationship is not clear enough.

In 2021, the WHO recommended lowering the $PM_{2.5}$ annual air quality guideline level from 10 to 5 μg m^{-3} to reflect the new evidence about effects occurring at low levels of exposure. Indeed, recent outcomes from seven large prospective cohort studies in Europe focusing on low $PM_{2.5}$ concentrations showed positive associations between long-term exposure to low $PM_{2.5}$ and non-accidental, cardiovascular, non-malignant respiratory, and lung cancer mortality without an indication of a lower threshold (below 1–5 μg m^{-3}) [3]. Among the reasons possibly explaining the occurrence of health effects even at these very low doses, there is the fact that these studies are based on $PM_{2.5}$ mass, a metric that is not ideal for representing the "biologically-active dose" of toxic $PM_{2.5}$. In fact, $PM_{2.5}$ being the same, health impacts can vary significantly depending on the blend of particles and gaseous compounds, as well as additional factors such as mixing, weather, atmospheric chemistry, etc. [4]. Indeed, $PM_{2.5}$ is characterized by a blend of components, complex mixtures of interacting different types from many emission sources, with physicochemical properties significantly varying in time and space that undergo fast atmospheric transformation processes and thus may have very diverse toxicological properties. In 2021, WHO prioritized specific types of PM, i.e., Black Carbon (BC), Elemental Carbon (EC), sand and dust storm particles, and Ultrafine Particles (UFPs) but concluded that the quantitative evidence on independent adverse health effects from these pollutants was still insufficient for new Air quality guideline (AQG) levels [1]. Additionally, a number of studies [5] have highlighted the toxicological potential of

secondary organic aerosols (SOA). This discovery demonstrated that ambient aerosols responsible for potential impacts on human health are not only emitted from pollution hotspots. After emission, new toxic compounds can be formed in the atmosphere, the toxicological properties varying as a function of environmental conditions, such as temperature, solar irradiance [6], and availability of liquid water in the form of fog/cloud droplets or deliquesced aerosols [7]. It is worth noting that seasonal differences in toxicological response were observed, e.g., in the TOBICUP (TOxicity of BIomass Combustion generated Ultrafine Particles) project when summer vs. winter ambient samples of UFPs were assayed. Indeed, for UFP, summer samples induced a more pro-inflammatory response than wintertime ones; in contrast, winter UFP samples generated higher genotoxic effects [8–10]. The CARE field study (Carbonaceous aerosol in the Rome Environment) based in Rome during the winter season involved the deployment of a suite of highly time-resolved physical and chemical aerosol characterization along with in-field toxicological measurements [11,12]. The results show a complex relationship between $PM_{2.5}$ oxidative and pro-inflammatory properties and primary combustion aerosol concentrations and indicate that these are greatly impacted by changes in the size and aging state of the particles in the real atmosphere.

Among the several mechanisms of adverse cellular effects, there are oxygen-free radical-generating activity, DNA oxidative damage, mutagenicity, stimulation of pro-inflammatory factors, and the generation of reactive oxygen species (ROS). These received considerable attention from aerosol scientists, who found in ROS studies an opportunity to link aerosol composition to biological effects [13]. The best candidates for particulate compounds responsible for ROS activity encompass transition metals and specific organic compounds such as quinoid species [13]. Wide ranges of fuels and experimental conditions have been explored in the laboratory to assess the characteristics of combustion aerosols in terms of toxicological endpoints and mechanisms of action (e.g., ROS formation). According to [14] Lakey et al. (2016), the ROS activity of ambient aerosol is a broad function of the logarithm of PM concentrations with a tendency to level off at very high pollution levels. Other authors [15], comparing ROS assays performed on size-segregated PM samples from six cities on three continents, showed that finer aerosol size fractions tend to have a higher ROS activity and that chemical components determining ROS formation include several transition metals and polar organic compounds. Another experiment based in the Po Valley in wintertime showed that fog droplets exhibit a higher intrinsic ROS content with respect to the aerosol particles the fog is formed of [16], indicating that aqueous-phase reactions in deliquesced particles contribute to altering (possibly amplifying) the oxidative potential of PM. The role of PM-induced ROS in lung dysfunction and potentially adverse cardiovascular outcomes set the basis for the development of chemical (a-cellular) assays suitable for low-cost, widespread observations of ROS formation in ambient PM samples. Their use is considerably extending the data availability for proxies of ambient PM toxicity (linked to oxidative potential) in a variety of environments and for diverse source-related PM fractions [17]. The results of such studies suggest that atmospheric processing exerts a great impact on a parameter, the PM oxidative potential (OP), defined by the ability of aerosol particles to oxidize target (bio)molecules and tested as an alternative air quality metric in a few pilot studies [18], although it remains an object of intense research and discussion.

This is the context in which the RHAPS (Redox-Activity And Health-Effects Of Atmospheric Primary And Secondary Aerosol) project was launched in 2019. The major objective of RHAPS is to identify specific properties (or combinations of them) of PM_1 (particles with an aerodynamic diameter less than 1 μm) from combustion sources that are responsible for toxicological effects and can be used as new metrics for health-related outdoor pollution studies (Figure 1). Field campaigns and laboratory experiments in an atmospheric simulation chamber (see Supplementary Material) were carried out with a focus on finding a link between the OP carried by SOA and PM_1 toxicity.

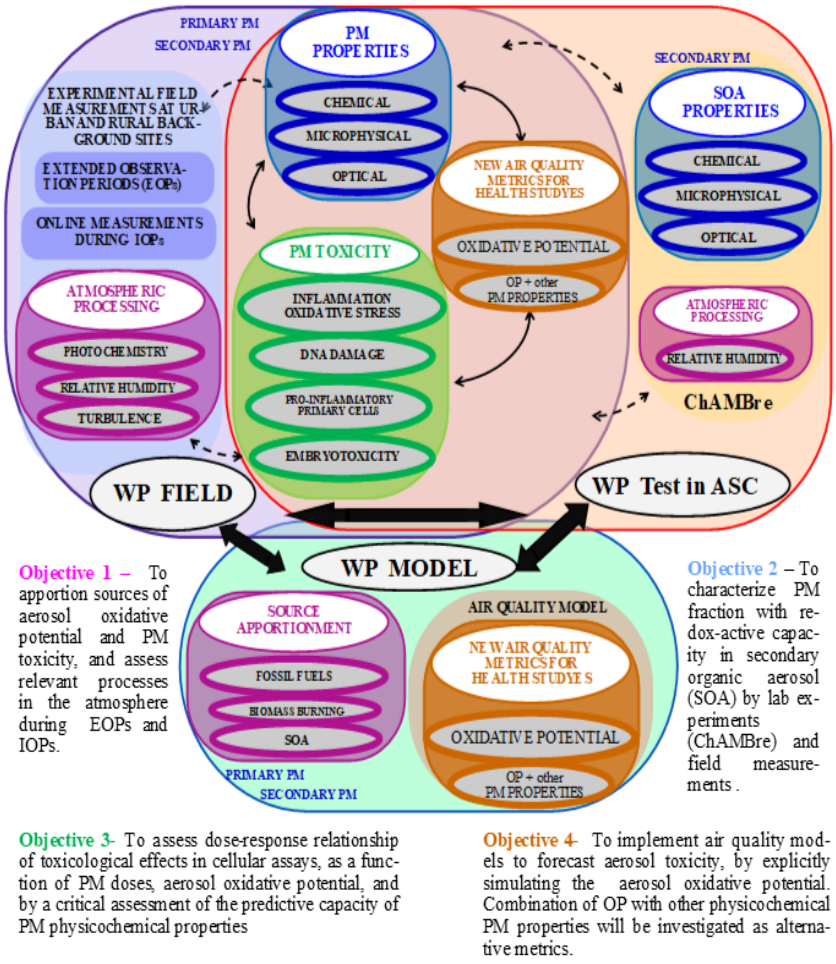

Figure 1. Sketch of the RHAPS project, showing work packages (WP) and objectives.

In this paper, we present the overall methodology of the RHAPS project and introduce the phenomenology and the first data observed, which will be discussed in detail in a series of companion papers.

2. Materials and Methods

2.1. Measurement Sites and Observational Periods

Field observations were carried out in the Po Valley (Italy) using a tandem urban–rural sites combination: BO, urban background, 44°31′29″ N, 11°20′27″ E) and San Pietro Capo Fiume (SPC, rural, 44°39′15″ N, 11°37′29″

E). There are two reasons to focus on the Po basin during RHAPS: (1) it is one of the major air pollution hotspots in Europe, and (2) it provides opportunities to investigate the processes regulating aerosol formation and redox activity in a polluted regional background atmosphere. In the rural Po Valley, aerosols are mainly emitted from residential wood burning and also formed in situ by secondary reactions involving ammonia (from agricultural emissions) and the photochemical products of NOx and VOCs (nitric acid and SOA, respectively).

Considering that PM_1-to-$PM_{2.5}$ average ratios in the investigated area were estimated at 60–80%, with lower values in summer vs. winter [19,20], it is interesting to note that the contribution of secondary sources in the regional background to $PM_{2.5}$ concentrations in the Po Valley varies between 50% (in the largest city, Milan [21]) to more than 70% in district cities and rural background sites [22,23]. The effect of the oxidative potential of SOA on the toxicological properties of the Po Valley aerosol is still poorly characterized. We demonstrated, however, that the concentration of the markers of oxidative stress in PM_1 in the rural Po Valley can be of the same order of magnitude as the concentrations reported for US megacities (Los Angeles) [16]. In the same area, fog water, which is enriched in SOA and depleted of transition metals with respect to the aerosol, showed the highest intrinsic redox activity. It is noteworthy that in summer, field measurements were run only at the background urban site, as the atmospheric mixing during the warm season is such that differences between the two sites are largely reduced.

Given the complexity of observing the phenomena, we elaborated a field measurement strategy combining different periods, combining intensive and super-intensive observational periods (Table 1).

Table 1. Intensive and Super-Intensive Observational Periods (IOPs, SIOPs) during RHAPS.

ID	Winter	Summer
IOPs	21 January 2021–18 March 2021	8 June 2021–14 July 2021
SIOPs	26 January 2021–3 January 2021 2 February 2021–6 February 2021 16 February 2021–20 February 2021	29 June 2021–2 July 2021

During Intensive Observational Periods (IOPs), both daily measurements (from 8.00 a.m. to 8.00 a.m. local time, ca. 60 samples in winter and 35 in summer) and online and high-time resolution instrumentations were operated in parallel. In winter, IOP was conducted from 21 January to 18 March 2021, and in summer from 8 June to 14 July 2021.

A total of four Super-Intensive Observational Periods (SIOPs) were carried out during the project, each SIOP lasting four days (from h 8.00 a.m. to h 8.00 a.m. local time); three SIOPs were carried out in winter (January/February 2021), and one SIOP in summer (June/July 2021). The periods for the SIOPs were planned according to a proper strategy. First, to catch the accumulation of aerosols in the atmosphere, we aimed to have each SIOP lasting four consecutive "stable weather" days, starting from a "clean" day, i.e., good weather possibly following bad weather conditions. Second, to be consistent with emission source paths, we always

started the SIOP on Tuesdays and ended on Saturdays. Finally, we aimed at having SIOPs days representative of four source-specific aerosol types: biomass burning (BB), urban aerosol (i.e., traffic emissions), secondary aerosols, and clean conditions. To proxy these aerosols, we selected a subset of variables, as described in Table 2. The latter were selected according to our experience and knowledge of the measurement sites and the analysis of available experimental data obtained during the first part of the IOPs (i.e., PM_1 chemical components, particle number size distribution, and BC). Every week, we ran a proper air quality model to forecast weather conditions and these variables for the next week, and accordingly, we started (or not) the SIOP.

Table 2. Exemplary of variables used to identify source-specific aerosol types.

Variables	Urban	BB	SOA/SIA	Clean
BC-to-PM1	↑		↓	
BC-to-OA	↑	↓	↓	
AAE (467-660)	↓	↑		
Nitrate mass concentration			↑	↓
Sulfate mass concentration			↑	↓
Primary OC mass concentration	↑	↑		
Secondary OC mass concentration			↑	
Median particle diameter	↓	↓	↑	
PM1 mass concentration			↑	↓
BC mass concentration	↓	↑		↓
Number concentration	↑			↓
Secondary formaldehyde			↑	
Weather conditions	stable	stable	Stable, foggy	Strong winds, low pressure, no rain

2.2. Aerosol and Meteorological Field Measurements

2.2.1. PM_1 Mass and Chemical Composition—Daily Samples Characterization

At both sites, many parallel sampling lines were deployed to collect samples devoted to a comprehensive aerosol chemical characterization in terms of mass concentration, elements, ions, and carbonaceous components (PAHs included), for OP assessment and toxicological assays (see Table 3 for a summary). PM_1 daily samples were collected on PTFE filters (Pall R2PJ047, Pall Life Sciences, Ann Arbor, MI, USA) and on pre-fired 47 mm diameter quartz fiber filters (Pallflex Tissuquartz 2500 QAO-UP, Pall Life Sciences, Ann Arbor MI, USA) according to the specific analysis foreseen for that sample, as reported in Table 3. A total of 813 daily samples were collected in winter and 234 in summer.

Table 3. Summary of sampling lines and filters used.

WINTER CAMPAIGN (21 January 2021–18 March 2021)					
Urban Background Site (BO)					
Sampler	**Flowrate**	**Inlet**	**Sampling Time**	**Filters**	**Target**
Dual channel (Dadolab Gemini)	1.15 m^3/h	Modified PM1	24 h from 8:00 to 08:00 LT	Quartz-fibre PTFE	Ions (by IC), levoglucosan (HPAEC-PAD) Elements (PIXE)

Dual channel (Dadolab Gemini)	1.15 m^3/h	Modified PM1	24 h from 8:00 to 08:00 LT	2 PTFE	Toxicological assays and embryotoxicity
Single channel (Dadolab Giano)	1.15 m^3/h	Modified PM1	24 h from 8:00 to 08:00 LT	PTFE	Water soluble oxidative potential
Single channel (Dadolab Giano)	1.15 m^3/h	Modified PM1	24 h from 8:00 to 08:00 LT	PTFE	Trace metals (ICP-MS)
Single channel (TCR-Tecora Skypost)	1.15 m^3/h	Modified PM1	24 h from 8:00 to 08:00 LT	Quartz fiber	Oxidative potential—OP tot
STRAS	0.5 m^3/h	Modified PM1	1 h	Polycarbonate	1 h resolved elements (PIXE)
Single channel (TCR-Tecora Skypost)	2.3 m^3/h	PM1	48 h from 8:00 to 08:00 LT	Pre-fired quartz fibre	^{14}C
HV sampler (TCR-Tecora)	30 m^3/h	PM1	24 h from 8:00 to 08:00 LT	Quartz fibre	Extra analyses
Rural background site (SPC)					
Dual channel (Dadolab Gemini)	1.15 m^3/h	Modified PM1	24 h from 8:00 to 08:00 LT	Quartz-fibre PTFE	Ions (by IC), levoglucosan (HPAEC-PAD) Elements (PIXE)
Dual channel (Dadolab Gemini)	1.15 m^3/h	Modified PM1	24 h from 8:00 to 08:00 LT	2 PTFE	Toxicological assays and embryotoxicity
Dual channel (Dadolab Gemini)	1.15 m^3/h	Modified PM1	24 h from 8:00 to 08:00 LT	2 PTFE	Water soluble oxidative potential Trace metals (ICP-MS)
Single channel (TCR-Tecora Skypost)	1.15 m^3/h	Modified PM1	24 h from 8:00 to 08:00 LT	Quartz fiber	Oxidative potential—OP tot
STRAS	0.5 m^3/h	Modified PM1	1 h	Polycarbonate	1 h resolved elements (PIXE)
SUMMER CAMPAIGN (08 June 2021–14 July 2021)					
Urban background site (BO)					
Dual channel (Dadolab Gemini)	2.3 m^3/h	PM1	24 h from 8:00 to 08:00 LT	Quartz-fibre PTFE	Ions (by IC), levoglucosan (HPAEC-PAD) Elements (PIXE)
Dual channel (Dadolab Gemini)	2.3 m^3/h	PM1	24 h from 8:00 to 08:00 LT	2 PTFE	Toxicological assays and embryotoxicity
Dual channel (Dadolab Gemini)	2.3 m^3/h	PM1	24 h from 8:00 to 08:00 LT	2 PTFE	Water soluble oxidative potential Trace metals (ICP-MS)
STRAS	0.5 m^3/h	Modified PM1	2 h	Polycarbonate	2 h resolved elements (PIXE)
Single channel (Dadolab Giano)	2.3 m^3/h	PM1	24 h from 8:00 to 08:00 LT	Quartz fiber	Oxidative potential—OP tot
Single channel (TCR-Tecora Skypost)	2.3 m^3/h	PM1	72 h from 8:00 to 08:00 LT	Pre-fired quartz fiber	^{14}C
HV sampler (TCR-Tecora)	30 m^3/h	PM1	24 h from 8:00 to 08:00 LT	Quartz fiber	Extra analyses

The low-volume samplers—many of them provided 2 parallel sampling lines—were operated at 1.15 m^3/h during the winter campaign in order to avoid filter clogging and high pressure drops. To this aim, the sampling inlets were modified by plugging 8 out of 16 nozzles; on the contrary, the flowrate during the summer campaign was set at 2.3 m^3/h, and no modifications to the standard 16 nozzles PM_1 inlet were done. An identical sampling configuration was adopted at both sites.

Mass concentration was gravimetrically determined on PTFE filters using a Sartorius microbalance with 1 μg sensitivity and equipped with an automatic sample changer.

PTFE filters were analyzed by PIXE analysis at the INFN-LABEC accelerator facility in Florence to obtain the elemental concentration of Z > 10 elements [24] and by ICP-MS (Bruker 820-MS, Billerica, MA, USA) at Sapienza University in Rome to retrieve the soluble and/or insoluble fraction of Al, As, Ba, Bi, Cd, Ce, Co, Cr, Cs, Cu, Fe, Ga, K, La, Li, Mn, Mo, Na, Pb, Rb, Sb, Sn, Ti, Tl, U, V, W, Zn, and Zr by applying a chemical fractionation procedure that increases the selectivity of the elements as source tracers [25]. Instrumental conditions and performance of the method are described in [26,27], respectively.

Punches from quartz fiber filters were analyzed at the University of Genoa with Ion Chromatography analysis for major ions (Cl^-, NO_3^-, SO_4^{2-}, Na^+, NH_4^+, K^+, Mg^{2+}, Ca^{2+}) [28] and for levoglucosan (1,6-Anhydro-beta-glucopyranose) with HPLC-PAD following [29]. Further details are reported in the Supplementary Material.

Elemental and organic carbon fractions (EC and OC) were determined on one punch taken from 24 h quartz fiber filters by thermo-optical analysis with an offline OCEC Carbon Aerosol Analyser (Sunset Laboratory Inc., Tigard, OR, USA) by applying the NIOSH-QUARTZ temperature protocol.

PAHs, i.e., benzo(α)anthracene, chrysene, benzo(β)fluoranthene, and benzo(α)pyrene, were also evaluated in samples collected on quartz filters. The samples were prepared according to previous works [30,31] with some modifications. For the quantitative analysis, benz(α)anthracene-D12 was added as an internal standard (200 ng/sample) to all filters. The quantitative analysis was performed using gas chromatography (Varian 3900 GC) supplied by ion trap mass spectrometry (Varian Saturn 2100T). The chromatographic separation was achieved with the TG-5SILMS column. Further details can be found in the Supplementary Material (Table S1-S3).

2.2.2 Non-Refractory PM1 Chemical Components (AMS)

The mass loading and chemical composition of submicron aerosol particles were obtained online by the High-Resolution Time-of-Flight Aerosol Mass Spectrometer (HR-TOF-AMS, Aerodyne Research) [32] at both locations. The HR-TOF-AMS provides measurements of the non-refractory sulfate, nitrate, ammonium, chloride, and organic mass of the submicron particles (NR-PM_1). The working principle of the HR-TOF-AMS is described in detail in [32–34]. Briefly, during all the campaigns, the HR-TOF-AMS was operating in "V" ion path modes every 2.5 min. The resolving power [35] of the V-ion mode was about 2000–2200 during all the campaigns.

Ionization efficiency (IE) calibrations were performed before and after every campaign and approximately once every two weeks during the campaigns. Filter blank acquisitions during the campaign were performed at least once a day to evaluate the background and correct for the gas-phase contribution. All data were analyzed using the standard ToF-AMS analysis software SQUIRREL v1.57 and PIKA v1.16 (D. Sueper, available at: http://cires.colorado.edu/jimenez-group/ToFAMSResources/ToFSoftware/index.html, accessed on 1 September 2021) within Igor Pro 6.2.1 (WaveMetrics, Lake Oswego, OR, USA). The HR-TOF-AMS collection efficiency (CE) was calculated based on aerosol composition, according to [36] and confirmed against parallel offline measurements. At both sampling stations, the aerosol was dried to about 35–40% by means of a Nafion drier before sampling with the HR-TOF-AMS.

2.2.3. Elemental Composition (STRAS)

High-time resolution samples were collected at both BO and SPC using the STRAS sampler (Size and Time-Resolved Aerosol Sampler), which was recently developed as an upgrade of the previous streaker sampler to collect the fine and coarse aerosol fractions with high-time resolution. In RHAPS, a PM_1 inlet was mounted on STRAS, and the particles were sampled with 1 h resolution during winter (for a total of 2352 time slots) and 2 h resolution during summer (for a total of 401 time slots) on a polycarbonate filter; each filter collects up to 168 samples corresponding to 1 week of hourly samples.

STRAS spots were analyzed by PIXE at the INFN-LABEC for offline high throughput determination of elements with Z > 10 [37].

2.2.4. Particle Number Size Distributions

The Particle Number Size Distribution (PNSD) was measured at the urban background site of BO by combining a Mobility Particle Size Spectrometer (TROPOS SMPS) equipped with a butanol-based condensation particle counter (CPC, model 3772, TSI Inc., Shoreview, MN, USA) and a commercial aerodynamic particle sizer (APS, TSI). Particles from 8 to 800 nm of electrical mobility diameter (d_m) were sized and counted by the SMPS; particles from 0.5 to 20 μm of aerodynamic diameter (d_a) were sized and counted by the APS. SMPS data were corrected for penetration errors through the sampling line (TROPOS-made software), penetration efficiency due to diffusion losses (calculated according to [38]) being higher than 98.92% for particles bigger than 15 nm. The aerosol sampling line was dried down to relative humidity of about 30% by means of a Nafion drier.

PM1 mass concentration with 5 min time resolution was constructed from the PNSD data, according to the procedure described elsewhere [11]. In short, PM1 was calculated from the particle volume size distribution under the hypothesis of spherical particles, and a size-dependent particle density varying from 1.25 to 1.5 g cm^{-3}. The daily PM1 from SMPS was then validated according to the daily PM1 measured through the reference procedure, the goodness of fit being $R^2 = 0.99$ (Supplementary Material, Figure S21 and S22).

2.2.5. Absorption and Scattering Coefficients (Aethalometer, PAX, DBAP, Filters)

Optical characterization of the daily samples collected at both sites on quartz fiber filters was performed by Multi-Wavelength Absorption Analyzer [39,40] to retrieve the absorption coefficients at 5 different wavelengths (λ = 850, 635, 532, 405, and 375 nm). A blank filter was used as reference for both winter and summer samples analysis.

In addition to the determination of Ångström Absorption Exponent (AAE) [41], previous research studies showed that multi-wavelength absorption coefficients were proved to be effective for apportioning contributions from fossil fuels and biomass burning combustion sources in aerosol samples [40,42]. The determined absorption coefficients were apportioned following the methodology presented in [40,43] and as previously employed in several field campaigns at urban and rural sites [44,45]. The methodology differentiates and quantifies the contribution to the total absorption of equivalent black carbon (eBC) emitted by wood-burning (eBC_{WB}) and fossil fuel (eBC_{FF}) as well as brown carbon (BrC) due to incomplete combustion.

During the winter campaign, two photoacoustic extinction meters (PAXs, Droplet Measurement Technologies, Boulder, CO, USA) provided the online determination of PM10 absorption and scattering coefficients at λ = 532 and 405 nm, with 1 min resolution.

At the background urban site in Bologna, a 7-wavelength (370, 470, 520, 590, 660, 880, and 950 nm) aethalometer (model A33, Magee scientific [46]) provided eBC mass concentration and AAE with 1 min time resolution. According to the instrument manufacturer, the eBC mass concentration from AE33 was obtained from measurements at λ = 880 nm with a mass absorption coefficient of 7.77 $m^2 g^{-1}$ [46]. The aerosol sampling line was dried to about 20–30% by means of a Nafion drier.

At the rural site of SPC, a Dual Beam Absorption Photometer (DBAP) was used. DBAP5 is a 5-wavelength (from 420 to 870 nm) filter absorption photometer based on dual-beam technology that measures the absorption properties of the particulate matter. Starting from the measurement of the filter light transmission variation over time due to the particle load, it evaluates the attenuation coefficients; then, by applying the appropriate filter correction equations, it evaluates the absorption coefficient and the Equivalent Black Carbon concentration using the Mass Absorption Coefficients. Dual-beam technology is a technique that simultaneously compares the absorption of the particulate matter with the absorption on the white filter, providing more precise measurement, especially in low concentration sites.

2.2.6. EC and OC—Online Measurements

The EC and OC mass concentration with 2 h time resolution was obtained by a Sunset Field Thermal-Optical Analyzer (Model-4 Semi-Continuous OC-EC Field Analyzer—Sunset Laboratory Inc., Sunset Laboratory Inc. Oregon, USA).

Briefly, this instrument collects PM on a quartz fiber filter and automatically analyses it at the end of each sampling period. The instrument inlet is equipped with a cyclone (cut point 1 μm) and a denuder for organics. In this campaign, a time resolution of 2 h (105 min of sampling followed by 15 min of analysis) was chosen as a compromise to get an adequate time resolution (comparable with that of other instruments used in this project) and a sufficient amount of collected sample mass (to maintain a good accuracy in the EC and OC quantification). The instrument was calibrated by sucrose standards, and the NIOSH protocol was used for thermal analysis.

Elemental and organic carbon (EC and OC) on the daily samples on quartz fiber filters were determined through thermal-optical transmission analysis with a Sunset EC/OC analyzer (Sunlab), using the NIOSH5040 protocol [47] corrected for temperature offsets. NIOSH5040 protocol lasts about 12 min, and the highest reached temperature is 940 °C. The instrument was calibrated with a TOC Standard Solution before starting the analysis.

2.2.7. Micrometeorology

To consider mean and turbulent atmospheric processes during the RHAPS field experiment, the meteorological variables (temperature, relative humidity, pressure, wind speed, solar radiation) were measured with a standard meteorological instrument (Lufft weather station WS700) with 1 min time resolution, while to measure the turbulence affecting the atmospheric processes near the surface, high-frequency measurements of the 3 wind

components u, v, w, and virtual temperature T, were made with an ultrasonic thermometer-anemometer uSonic-3 by Metek (sampling frequency 10 Hz) installed at height z = 3.3 m a.g.l. From these measurements we computed the wind speed and direction as well as the fluctuations u', v', w', and T_v' with respect to the 1 h linearly detrended mean wind components (<u>, <v>, <w>) and virtual temperature <T_v> (u' = u − <u>, v' = v − <v>, w' = w − <w>, T_v' = T_v − <T_v>). We estimated the sensible heat flux $H_0 = \rho c_p w' T_v'$ (ρ is the air density, c_p is the specific heat capacity of air at constant pressure) and turbulent kinetic energy TKE = 1/2 ($u'^2 + v'^2 + w'^2$) and the stability parameter z/L, where L is the Obukhov length. H_0 provides a measure of the thermal mixing capability of the atmosphere. TKE represents the intensity of turbulence produced by fluid shear, friction or buoyancy, or through external forcing. As both H_0 and TKE vary significantly in time and in space, they need to be monitored continuously.

2.3. Toxicological Assessment

2.3.1. Oxidative and Reducing Potential

One sampling line operated with PTFE filters was devoted to oxidative and reducing potential assessment; each filter was extracted in 10 mL of deionized water by rotating agitation at 60 rpm for 30 min. The obtained solution was then filtered through a nitrocellulose filter and split into proper aliquots for the dithiothreitol (DTT), ascorbic acid (AA), and 2′,7′-dichlorofluorescein (DCFH) OP assays (OP^{DTT}, OP^{AA}, OP^{DCFH}) and for the 2,2-diphenyl-1-picrylhydrazyl (DPPH) reducing potential (RP) assay (RP^{DPPH}). The OP and RP analytical measurements followed the methods reported in [48–50].

The reducing potential assay is based on the use of the stable free radical DPPH (2,2-Diphenyl-1-picrylhydrazyl). The DPPH assay is a commonly used spectrophotometric method to estimate the antioxidant activity of several matrices, such as food and plants, by measuring the decrease of absorbance over time [51,52]. The DPPH is a stable free radical by virtue of the delocalization of the spare electron over the molecule [53], and it accepts electrons or hydrogen radicals from donor compounds [54]. DPPH shows a strong absorption band at 517 nm due to its odd electron, and solution appears a deep violet color. The resulting decolorization turning yellow is proportional to the number of electrons taken up [51].

A parallel sampling on quartz fiber filters was devoted to water-soluble and total OP determination by the dithiothreitol (DTT) assay. The adopted procedures are those by [55,56] Cho et al. (2005) and Verma et al. (2009), for the water-soluble OP, and by [57] Gao et al. (2017), for the total OP. For the water-soluble OP determination, filter portions were extracted in deionized water by gentle shaking (30 min), and the extracts were filtered using a PTFE 0.45 μm pore syringe filter to remove insoluble materials and filter debris.

For the determination of the total aerosol OP, the procedure was similar to the one described above, with only one notable difference. The quartz fiber filter aliquots were not removed from the extraction solution after the end of the extraction procedure, and they were kept in the primary vial while performing the DTT assay in order to allow both soluble (in the extract) and insoluble (attached to the filter) aerosol components to react with the DTT. Total OP determinations are still ongoing, and the results will not be discussed in the present work. More details about the experimental procedure are presented in the Supplementary Material.

At the urban background site, high-time resolved (2 h time resolution) OP was measured through the 2′,7′-dichlorofluorescein (DCFH) assay (OP^{DCFH}) employing a particle-into-liquid sampler (PILS), which allows for continuous PM collection of a diluted solution of soluble species with suspended insoluble particles [58]. The sampling line was equipped with a PM_1 inlet and a denuder line to keep acid and basic gasses out of the sample. This technique does not guarantee the complete recovery of small and hydrophobic particles because particle growth is achieved through water condensation [59].

2.3.2. Filter-Based Toxicological Assays

To characterize the toxicological effects of PM_1 water extracted from PTFE filters, different in vitro models representative of human lung tissue and targeted cells were used (e.g., BEAS-2B, THP-1). In order to assure the comparability with OP measurements, the extraction procedure (see Supplementary Material) was exactly the same and was carried out on the same days as toxicological measurements. Cells were exposed to increased dilutions of extracts for different times (30 min, 1, 3, and 24 h). After exposure, as an indicator of unwanted biological effects, cell viability (e.g., MTT reduction assay, PI staining, oxidative stress) and release of inflammatory mediators (e.g., IL-8), genotoxicity and mutagenicity (e.g., alkaline comet assay, micronucleus test) were investigated [8,60]. In parallel, to evaluate embryotoxicity, the effects of extracts were tested in Xenopus laevis embryos. Xenopus laevis embryos were exposed during the whole R-FETAX test period (from midblastula to tadpole, according to [61]) to the soluble extracted fraction diluted 1:10 in maintaining solution (see details in Supplementary Material). At the end of the test, tadpoles were morphologically observed under a dissecting microscope (Leica). The developmental degree (to evaluate old- and young-for-age embryos) was evaluated according to [62] developmental scoring system adapted to Xenopus laevis considering the normal table of X. laevis development [63] (details in Supplementary Material). Tadpole length was measured in order to evaluate small- and large-for-age embryos. Statistical analysis was performed comparing data to controls.

2.3.3. Air Liquid Interface

In parallel with PM sampling and subsequent laboratory extraction and exposure, during the SIOPs (Table 1), environmental exposure of air liquid interface (ALI) cultured cells BEAS-2B according to [12] Gualtieri et al. (2018) were used. The expression of oxidative, inflammatory, and DNA damage-related genes was quantified together with measurements of IL-8 and genotoxicity/mutagenicity (e.g., alkaline comet assay, micronucleus test).

2.4. Forecast Modeling System

In order to support campaign planning, a forecast modeling system was devised in the frame of RHAPS. Due to logistic constraints, the scheduling of each Super-Intensive Observational Period (SIOP) had to be determined one week before its beginning. Thus, the modeling system was designed to provide medium-range forecast with one daily update. Due to limitations of the computational resources (a Linux server with 64 cores at 2.7 GHz and 128 Gb RAM), the modeling domains were designed at moderate horizontal resolution (12 km) in order to warrant a daily forecast extended to 16 days ahead.

The global meteorological initial and boundary conditions were taken from the Global Forecast System (GFS) freely provided by the National Centers for Environmental Prediction (NCEP) of the US National Oceanic and

Atmospheric Administration (NOAA). Each day, the operational forecast, run at 06 UTC at 3 hourly and 1.0° × 1.0° resolution, up to 384 h ahead, was automatically downloaded from the NOMADS archive (https://nomads.ncep.noaa.gov/, accessed on 28 April 2022).

The WRF meteorological model [64] version 3.7.1 was used to dynamically downscale the GFS forecast. We used 2 nested domains, covering, respectively, Europe at 36 km of horizontal resolution and Italy at 12 km, and having 33 vertical eta-levels up to 50 hPa, with 11 levels in the bottom 1 km and the first level about 25 m thick. The main model parameterizations adopted were those used in [65], with RRTMG radiation schemes, WSM6 cloud microphysics, Noah land surface model, and Bougeault and Lecarrere boundary layer closure scheme.

The WRF meteorological simulation was used to drive the chemistry-transport simulation using the CHIMERE model [66] version 2014b. We used 2 nested domains over Europe and Italy, respectively, at a horizontal resolution of 0.5° and 0.15°, with 12 vertical levels up to 500 hPa and the first level about 21 m thick. The emission inventories, boundary conditions, and model parameterization were the same used in [65], with anthropogenic emissions taken from the European Monitoring and Evaluation Programme (EMEP, http://www.emep.int, accessed on 28 April 2022) at 0.5° resolution over Europe and from the National Thematic Center for Atmosphere, Climate, Emissions (CTN-ACE) [67] at 5 km resolution over Italy. Biogenic emissions were calculated online using the MEGAN model. The boundary conditions were taken from global models monthly climatology from LMDz-INCA for gases and GOCART for aerosol species. Chemistry was calculated with the MELCHIOR mechanism with a secondary organic aerosol scheme, and we adopted an aerosol sectional model with 10 geometric size bins for particles with diameters from 40 nm to 40 μm.

3. Results

Here we present data and introduce the phenomenology observed during the RHAPS experiment. In order to aid the interpretation of measurements collected during the campaigns, we report first (Section 3.1) a meteorological overview during the two Intensive Observational Periods with a focus on the SIOPs, then (Section 3.2) aerosol properties characterization (Section 3.3), oxidative potential, and (Section 3.4) toxicological assessment. In the following section (Section 4), we give a synthesis of findings with an outlook to companion papers where data are analyzed in more detail.

3.1. Meterological Overview

3.1.1. Meteorology of IOPs

To better describe the meteorology during the IOPs and SIOPs, it is convenient to organize the present brief meteorological analysis in weekly time slots, showing the Tuesday–Friday average synoptic conditions.

In Figure 2, we show the maps over Europe of the average geopotential height anomaly at 500 hPa with respect to the 1981–2010 mean from NCEP/NCAR Reanalysis during the winter campaign, and in Figure 3, the time series of main meteorological variables recorded in Bologna with the indication of the SIOPs.

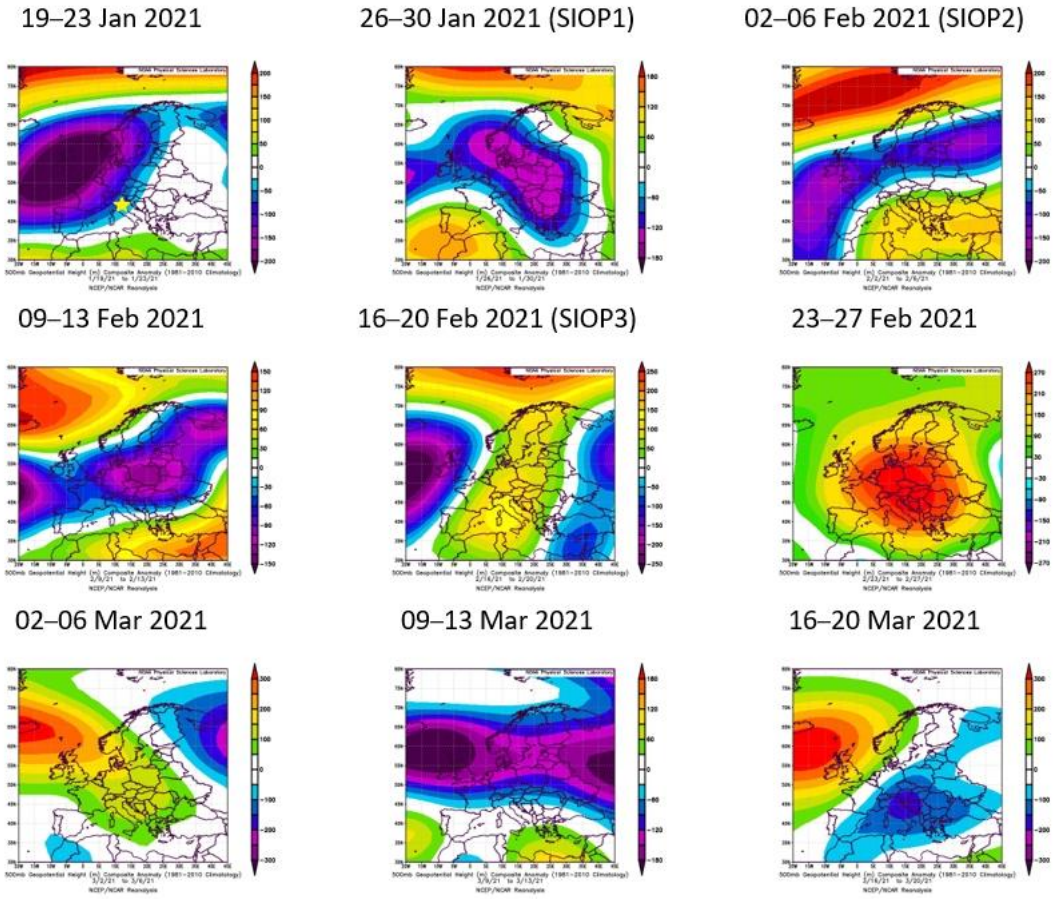

Figure 2. Average geopotential height anomaly at 500 hPa over Europe with respect to the 1981–2010 mean from NCEP/NCAR Reanalysis, during the Tuesday–Friday time slots of the winter Intensive Observational Period (IOP). The yellow star on the first map (**top-left**) denotes the location of the campaign. Cold colors (blue-purple) denote negative anomaly, warm colors (yellow-red) denote positive anomaly. Maps elaborated using the web tool of the NOAA Physical Sciences Laboratory (www.psl.noaa.gov, accessed on 28 April 2022).

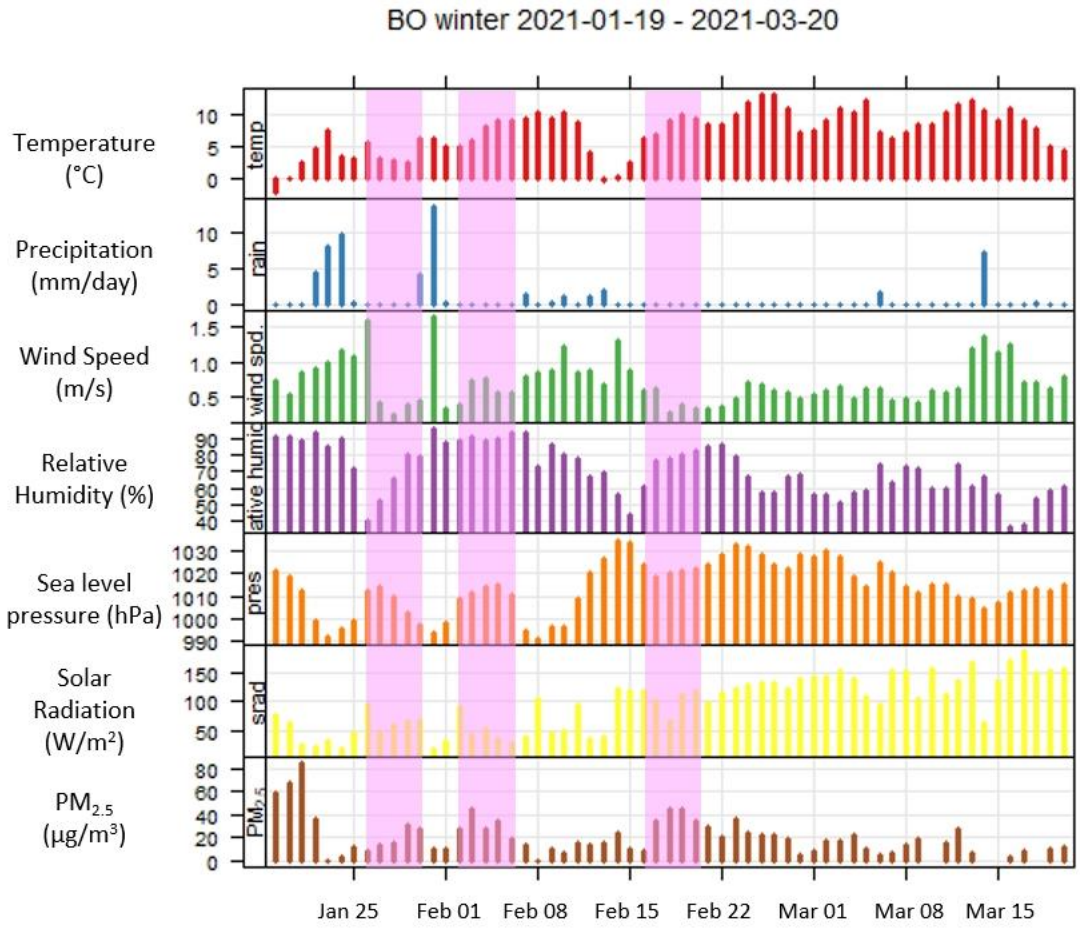

Figure 3. Hourly time series of meteorological variables recorded in Bologna during the winter campaign. Shaded vertical bars denote the three Super-Intensive Observational Periods (SIOP). The first preparatory week (19–23 January) was characterized by a broad depression over western Europe, which induced a south-westerly flow associated with cloudy and humid weather, with moderate wind speed, light rain, and rising temperatures in the Bologna area.

In the supplementary material (Figure S1-S2) we show additional data of the winter campaign.

Starting from the second week (26–30 January), an anticyclonic ridge gradually mounted the western Mediterranean basin, initially determining sunnier and drier conditions. The first SIOP took place during this week. As the anticyclone expanded eastward (02–06 February, SIOP2), the arrival of warm southerly air masses over western Europe favored the formation of low clouds (and fog) with rising temperature and calm winds. A Saharan dust plume was also advected over the low-cloud deck by the end of the week (Figure S3). The $PM_{2.5}$ mass concentrations were generally higher than in the adjacent weeks during the two SIOP periods. In the following week (09–13 February), a cyclonic structure over central Europe pushed the anticyclone to the south, driving a more zonal flow with moderate winds, some light rain, a sharp temperature drop, and a decrease in $PM_{2.5}$ mass concentration.

From the subsequent week (16–20 February, SIOP3), an anticyclone settled over west-central Europe, bringing sunnier weather with increasing temperatures and light winds from the east. These conditions favored the

accumulation of pollutants near the surface because of the reduced ventilation of the Po Valley, resulting in the highest $PM_{2.5}$ mass concentrations of the winter campaign (up to 50 μg m^{-3}). The prevailing anticyclonic circulation persisted in the last week of February and 1 March, but with slightly enhanced ventilation in the Po Valley, which resulted in generally lower $PM_{2.5}$ concentrations with respect to the SIOP3 period. An incursion of Saharan dust also took place in the area, with a peak on 23 February (Figure S4). In the final period (09–20 March), low-pressure systems prevailed in central Europe, yielding a few rain episodes, stronger winds, and reduced $PM_{2.5}$ concentrations over the campaign location.

In Figure 4, we show the maps of geopotential height anomaly, and in Figure 5, the time series in Bologna for the summer campaign (June–July 2021). In the first week (01–05 June), the western Mediterranean was under the influence of the southern offshoots of a high-pressure system over northern Europe, which determined a relatively cold air flow from the north, resulting in mild temperatures and light winds in the campaign area. The following week (08–12 June), the anticyclone was pushed eastward by a reinforcing low-pressure system over south-eastern Europe, which brought clouds, rain, and a modest reduction of $PM_{2.5}$ mass concentration.

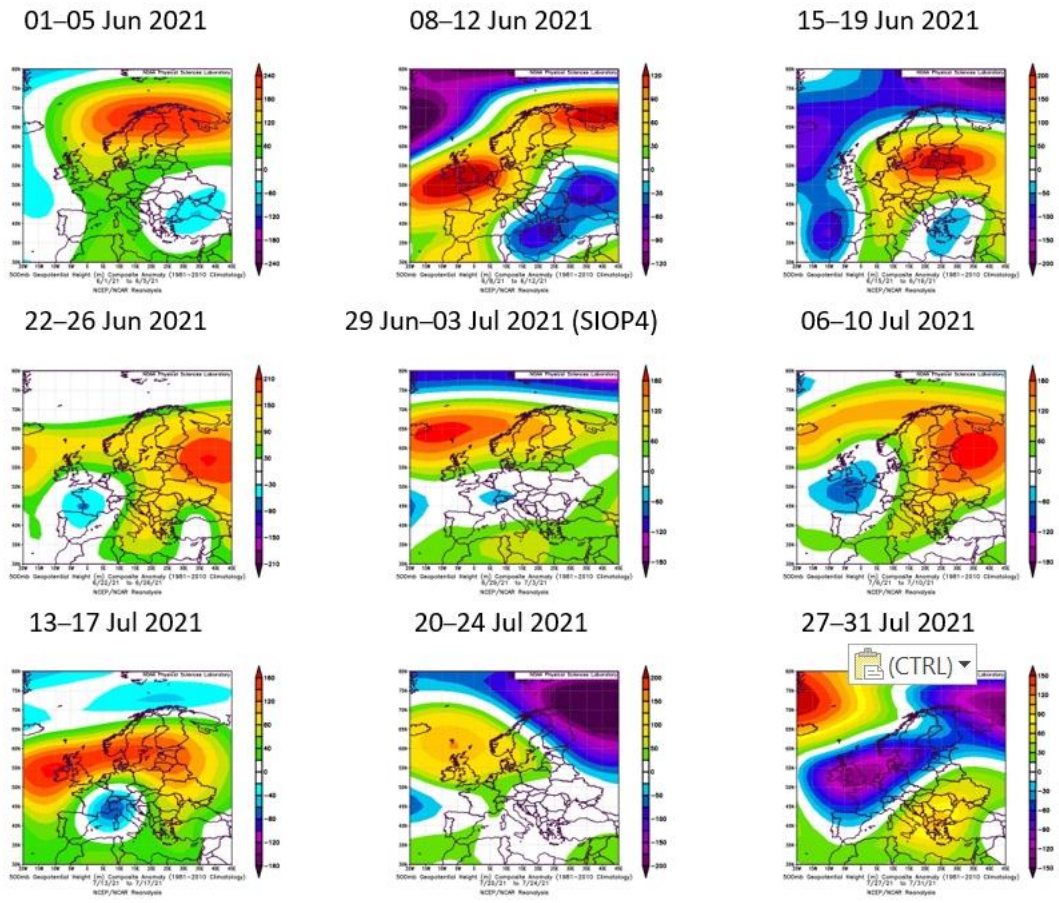

Figure 4. Average geopotential height anomaly at 500 hPa over Europe with respect to the 1981–2010 mean from NCEP/NCAR Reanalysis, during the Tuesday–Friday time slots of the summer Intensive Observational Period (IOP). The yellow star on the first map (**top-left**) denotes the location of the campaign. Cold colors (blue-purple) denote negative anomaly, warm colors (yellow-red) denote positive

anomaly. Maps elaborated using the web tool of the NOAA Physical Sciences Laboratory (www.psl.noaa.gov, accessed on 28 April 2022).

Afterward (15–26 June), a new anticyclone over central Europe took control of circulation over the Mediterranean basin, with south-easterly winds yielding high temperatures and dust advection from northern Africa toward Italy. The peak of the dust event (20–21 June) was well visible from satellite imagery (Figure S5) and was reflected in the highest $PM_{2.5}$ concentrations during the campaign.

In the week that we selected for the SIOP4 (29 June-03 July), the pressure field over southern Europe caused prevailing zonal winds that prevented the arrival of new dusty air masses, but also favored enhanced ventilation of the Po Valley, with a consequent relative reduction of $PM_{2.5}$ concentrations and synoptic-scale pressure until middle July then settled again into a pattern determining a prevailing flow from the south-east, with new dust advection in Italy (not shown). The second half of July was characterized by more variable weather, with a more frequent cloudy sky and few rain episodes, but with favorable conditions for the build-up of $PM_{2.5}$ concentrations.

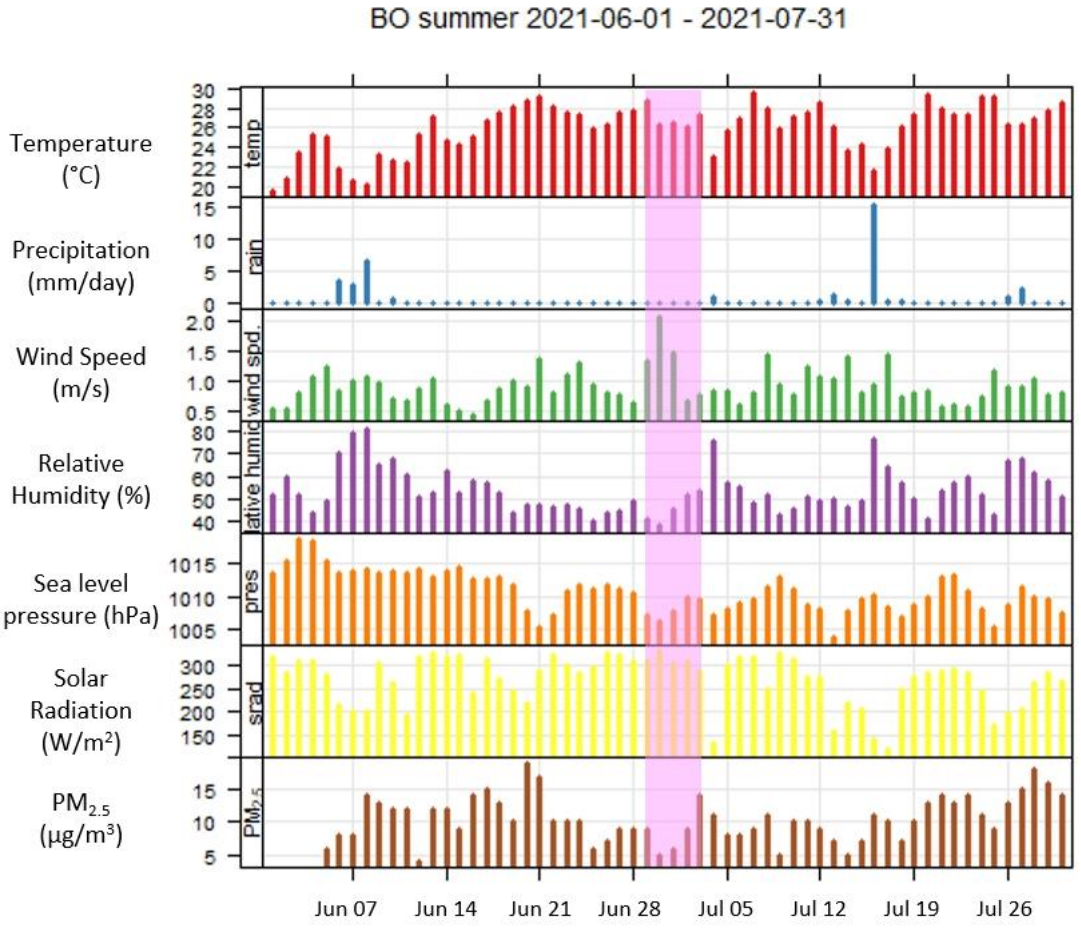

Figure 5. Hourly time series of meteorological variables recorded in Bologna during the summer campaign. Shaded vertical bars denote the three Super-Intensive Observational Periods (SIOP).

The main motivation for the implementation of the operational forecast system was to provide information for the scheduling of the SIOPs, which had to be planned at least one week in advance. In the supplement, we include an assessment of the forecasting skills as a function of lead time (Figure S6).

3.1.2. Micrometeorology during the SIOPs

The time behavior of the temperature (a), wind speed (b), Turbulent Kinetic Energy (TKE) (c), friction velocity (d), H_0 (e), and z/L (f) during the four Super-Intensive Observational Periods, Winter SIOP1, SIOP2, SIOP3, and the summer SIOPS, are shown in Figures 6–9 from 0800 CET of 1 day to 0800 CET of the following day. In the Supplementary (Figures S7-S14) we show variables measured during all the intensive observational periods.

For the sake of clarity, we note that the stability parameter z/L (f), representing the ratio of the sensor height above the ground (z) and the Monin–Obukhov length (L), might be informative of the atmospheric stratification: on land, the Obukhov length is positive (negative) for stable (unstable) stratification and becomes infinite in the limit of neutral stratification.

During SIOP1 (Figure 6), all the variables evidenced a similar behavior with a peak around 1300–1400 CET except for 30 January, which presented between 0000-0800 CET higher values of the temperature and the wind speed, and of all the variables related to mechanical mixing (u* and TKE). The larger values of the wind speed, sensible heat flux, and the variables related to the mechanical mixing were observed on 26 January. On this day, when sensible heat flux was negative, we observed values of TKE and U* larger than those of the other days of SIOP1. The mechanical mixing also had peaks during the afternoon until 0000 CET due to increasing wind speed values.

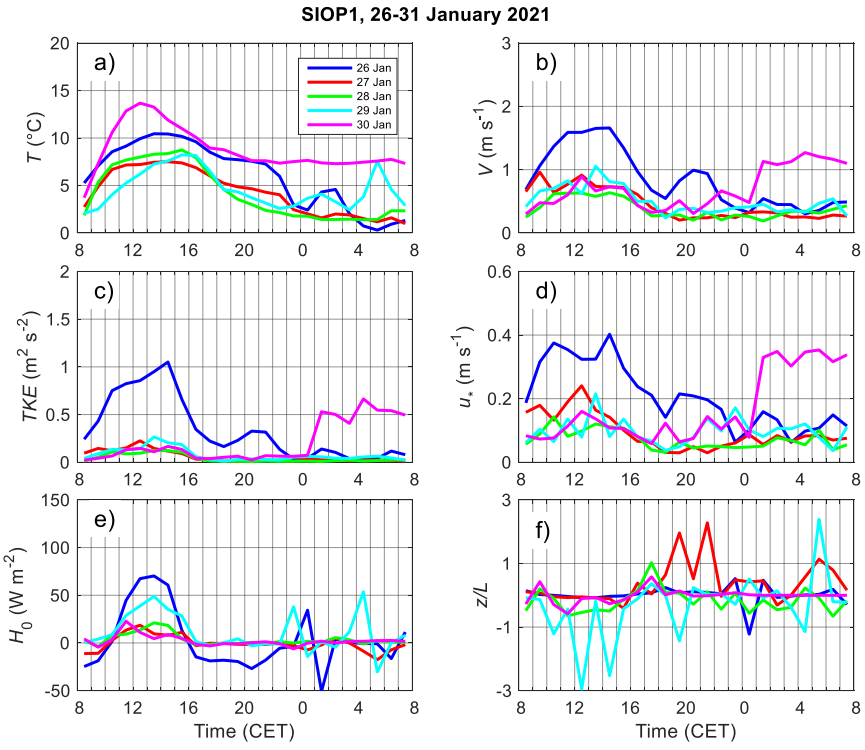

Figure 6. Temperature (**a**), wind speed (**b**), TKE (**c**), friction velocity (**d**), H_0 (**e**), and Z/L (**f**) during the winter SIOP1 from 0800 CET of 1 day to 0800 CET of the following day.

SIOP2 (Figure 7) is characterized by low values of the wind speed, TKE, u*, and temperature without a significant diurnal variation; this behavior is typical of cold and foggy days. The values of the sensible heat flux are below 50 W/m^2 except for 2 February, which evidences a weak diurnal behavior with characteristics similar to those of SIOP1.

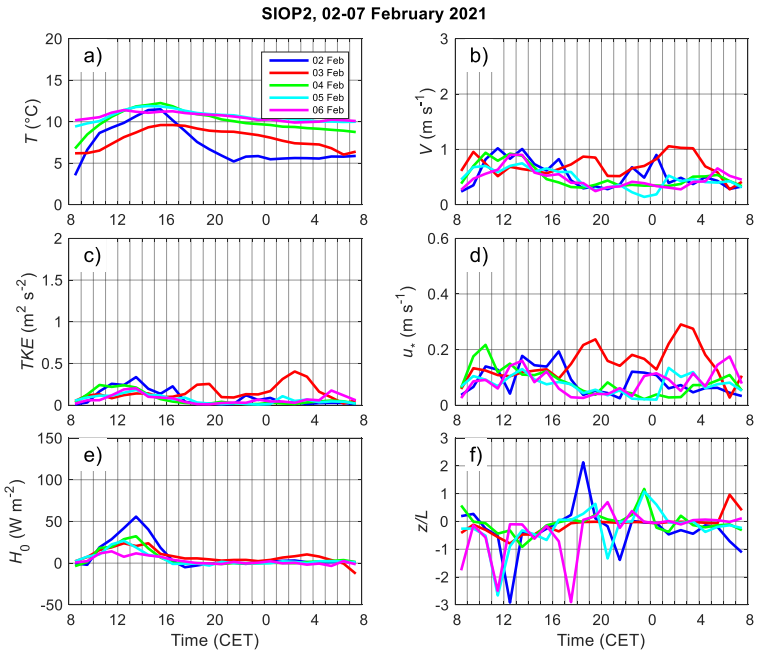

Figure 7. Temperature (**a**), wind speed (**b**), TKE (**c**), friction velocity (**d**), H_0 (**e**), and Z/L (**f**) during the winter SIOP2 from 0800 CET of 1 day to 0800 CET of the following day.

During SIOP3 (Figure 8), all the variables show similar behavior with weak convection between 0800-1600 CET and peaking (all but temperature) between 1200-1400 CET. During SIOP4 (Figure 9), the registered values are those typical of summertime.

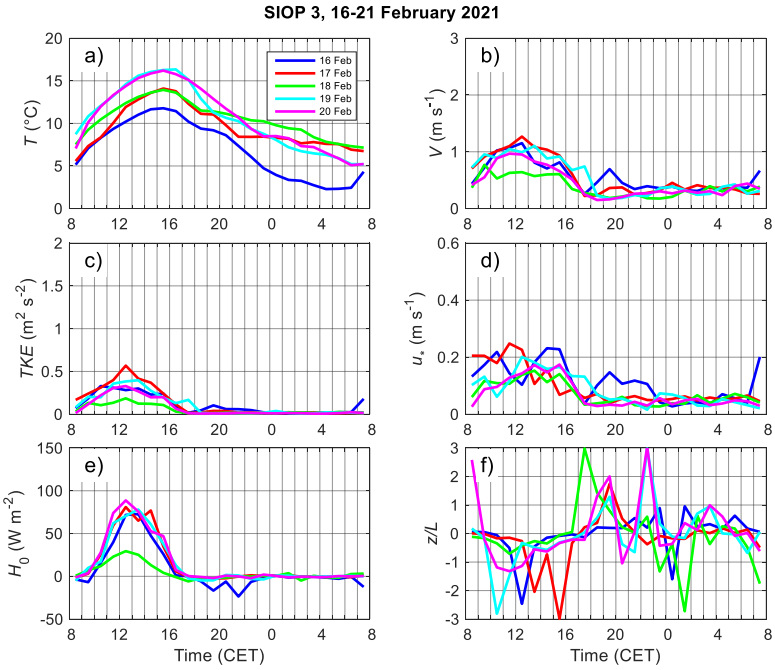

Figure 8. Temperature (**a**), wind speed (**b**), TKE (**c**), friction velocity (**d**), H_0 (**e**), and Z/L (**f**) during the winter SIOP3 from 0800 CET of 1 day to 0800 CET of the following day.

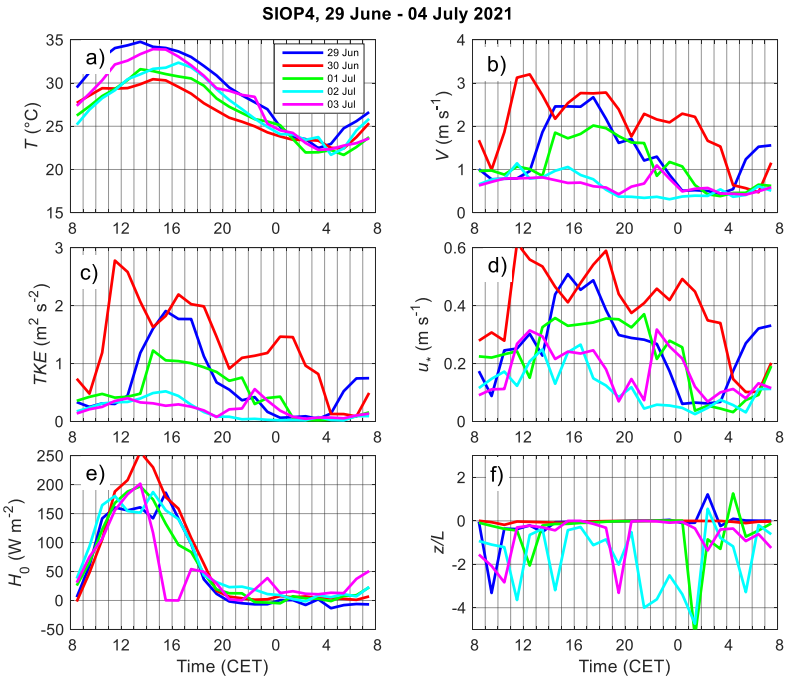

Figure 9. Temperature(**a**), wind speed (**b**), TKE (**c**), friction velocity (**d**), H_0 (**e**), and Z/L (**f**) during the summer SIOP4 from 0800 CET of 1 day to 0800 CET of the following day.

Maximum daily temperatures were between 30° and 35 °C; minimum temperatures were around 22 °C in the early morning. The diurnal behavior of temperature and H_0 was regular during all days. However, the wind

regime in this period was variable and not regular. The first 3 days, 29 and 30 June, and 1 July, were characterized by moderate (for this site) wind speed between 2 and 3 m s^{-1}. On the next days, 2 and 3 July, very weak wind <1 m s^{-1} occurred. The windiest day was 30 June. The values of u* and TKE followed the behavior of wind intensity. The values of the stability parameter z/L indicate the predominance of convective conditions between 0800 and 1600 CET. The occasional presence of unstable stratification also in the evening and nocturnal hours is probably due to the strong heating of the underlying surface covered with asphalt, which conserves higher temperatures during late hours.

3.2. Atmospheric Aerosol Properties

Figure 10 shows the ranges of variability of PM_1 major components as measured at the urban site by the online equipment. We show first the mass concentration of PM_1, as reconstructed by SMPS data and validated on filter-based mass, after the procedure described in [11]. Then, PM_1 components, i.e., organic aerosol, nitrate, ammonium, sulfate, mineral dust tracers (e.g., Si, Ca, Fe, among others), and BC mass concentration are reported. The total number concentration is then represented, together with total surface area concentration and relevant aerosol size representative of the entire aerosol population (calculated as surface-weighted median mobility diameter [68]. Finally, we show the alveolar Lung Deposited Surface Area corresponding to the particle surface area size distribution weighted with the associated lung deposition curve and integrated over the whole particle size, the inhalation fraction according to the ICRP model [43].

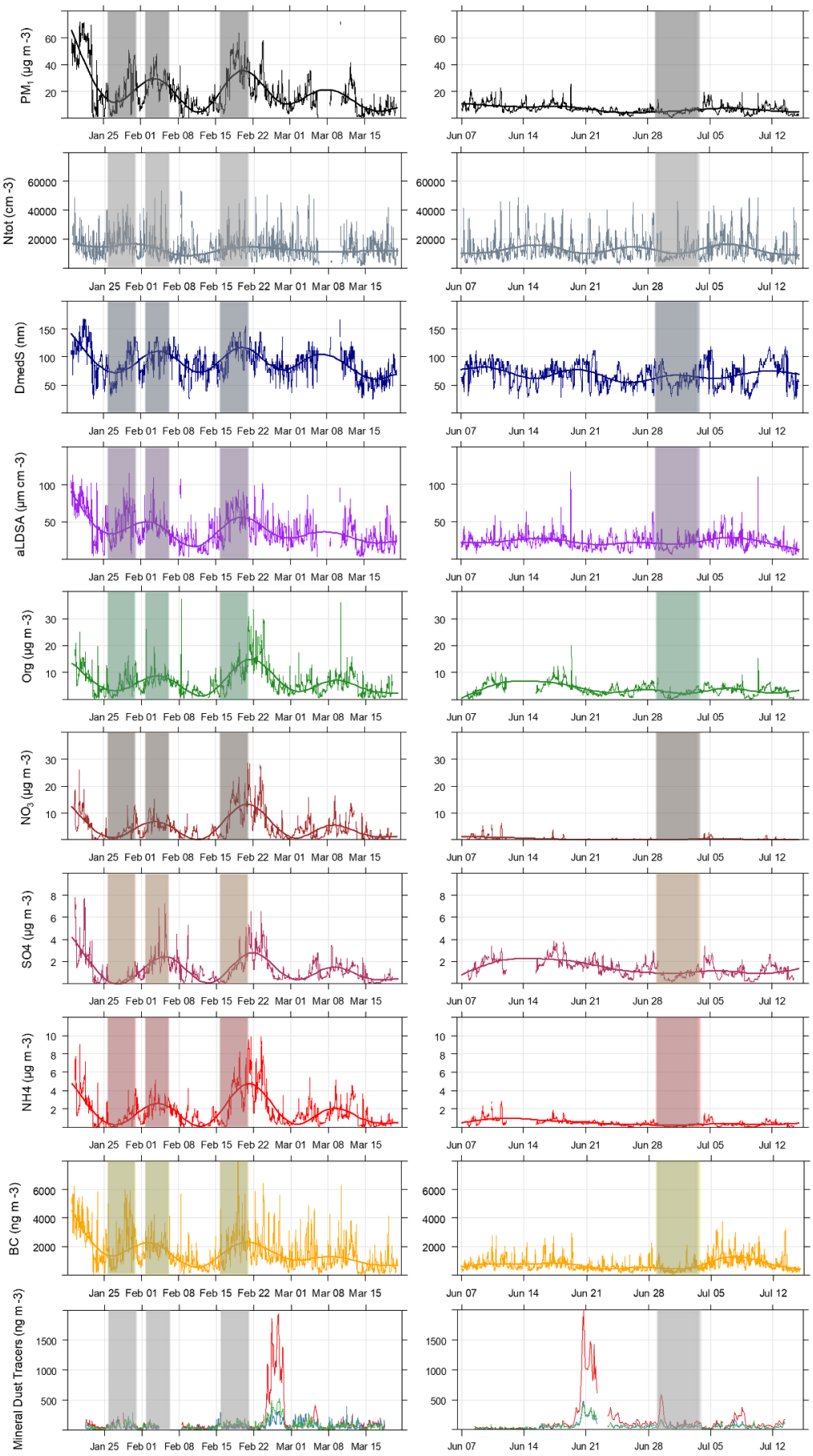
PM1 (µg m-3)
Ntot (cm-3)
DmedS (nm)
aLDSA (µm cm-3)
Org (µg m-3)
NO3 (µg m-3)
SO4 (µg m-3)
NH4 (µg m-3)
BC (ng m-3)
Mineral Dust Tracers (ng m-3)
Jan 25 Feb 01 Feb 08 Feb 15 Feb 22 Mar 01 Mar 08 Mar 15
Jun 07 Jun 14 Jun 21 Jun 28 Jul 05 Jul 12

Figure 10. Time plot of selected aerosol properties during the winter and summer field campaigns. On the left, from top to bottom: mass concentration of PM1 (reconstructed by SMPS data), total number concentration (Ntot), surface-area median particle diameter (Dmed), alveolar Lung Deposited Surface Area (aLDSA), and total surface area concentration (Stot), Organic aerosol, nitrate, ammonium and sulfate, mineral dust tracers (e.g., Si, Ca, Fe, among others) and BC mass concentration. Shadows are intended to indicate the four SIOPs. Statistical data of commonly used aerosol metrics (PM1, BC, LDSA, Particle number and size) are summarized in Table 4.

Table 4. Descriptive Statistics of selected aerosol metrics: PM1 (reconstructed from SMPS) and BC mass concentration, particle number (N_{tot}), alveolar Lung Deposited Surface Area (aLDSA), and particle median diameter (D_{medS}).

Metric	Winter (11 January 2021–31 March 2021)					Summer (27 May 2021–17 July 2021)			
	UoM	Mean	Std.Dev.	Median	Range (min-max)	Mean	Std. Dev.	Median	Range (min-max)
PM1	$\mu g/m^3$	20	15	16	0–76	7	3	6	1–26
N_{tot}	cm^3	13,338	7441	11,928	1256–61,402	12,817	7776	10,586	2018–61,312
D_{medS}	nm	90	26	92	22–167	67	19	66	22–119
a-LDSA	$\mu m^2/cm^3$	39	22	35	2–146	23	9	21	5–117
BC	ng/m^3	1496	1241	1163	6–32,275	677	456	551	33–8463

In the supplementary, we show statistics and data coverage of all the parameters measured at the urban site (Figure S15, Table S4 and S5) and at the rural site of SPC (Figure S16). PAHs concentrations were measured at both sites during winter only, and they are reported in Figure S17 (in pg m^{-3}).

It is worth mentioning that the sampling period—especially during the winter campaign—was characterized by a reduced anthropogenic activity due to COVID-19 pandemic restrictions. During wintertime, there were no relevant differences (i.e., in general, less than 20–25%) in average concentration values when comparing parallel samples collected at BO and SPC. PM1 median mass concentration in winter was 19 ± 1 mg m^{-3} at both sites while, as expected, due to the stronger atmospheric dilution conditions, summertime PM1 concentrations were approximately a factor 2 lower than wintertime ones. During wintertime, a large amount of the PM1 median mass is accounted for by nitrate and organic carbon at both sites, and with comparable shares (18 and 22%, respectively), ammonium explains about 8% of the mass concentration, followed by sulfate (ca. 5%), elemental carbon and mineral dust (ca. 3–5% each), and heavy metal oxides (ca. 1%). In summer, the situation is quite different as the highest PM1 mass share is related to organic carbon (29%), followed by sulfate (15%), mineral dust (12%), ammonium (7%), nitrate and elemental carbon (ca. 3–4% each) and heavy metal oxides (ca. 1%). In both seasons in BO and during the winter campaign at the SPC site, the average unaccounted mass (mainly related to the organic carbon to organic mass conversion factor and to undetected components like water) was in the range of 30–40%. As concerns PAHs concentrations at the urban background site, the most abundant species were benzo(b)fluoranthene and chrysene with average concentrations of 12 pg $m^{-3,}$ followed by benzo(a)pyrene (7 pg m^{-3}) and benz(a)anthracene (3 pg m^{-3}); at the rural site concentration values were slightly lower with 10 and 9 pg m^{-3} for benzo(b)fluoranthene and chrysene, respectively, and 6 pg m^{-3} for benzo(a)pyrene and 2 pg m^{-3} for benz(a)anthracene

As a general feature, we note that particle mass (and surface area) concentrations and diameters were on average larger in winter than in summer. Mean PM1 reconstructed from 5 min SMPS data and BC mass concentration ranged from 20±15 μg m^{-3} to 7±3 μg m^{-3} and from 1.5 ± 1.2 μg m^{-3} to 0.7 ± 0.5 μg m^{-3} in winter and summer, respectively, the mean surface-weighted diameters being 90 ± 26 nm in winter and 67 ± 19 nm in summer. Accordingly, a-LDSA was higher in winter (39 ± 22 $\mu m^2/cm^3$) than in summer (23 ± 9 $\mu m^2/cm^3$). Among PM1 non-refractory components, all variables except sulfates (showing conversely similar values) were larger in winter than in summer. Like sulfates, total particle number concentration was on average similar in winter and summer, mean values being $1.3 \times 10^4 \pm 0.7 \times 10^4$ cm^{-3}. Details on the particle number size distributions are provided in Figure S18 and S19.

These differences reflect different processes, dynamics, and sources governing the atmospheric aerosol in winter as compared to summer and the ability of the related metrics (i.e., number, mass, size of particles) to capture these. For example, in wintertime, higher combustion-related emission sources coupled to lower atmospheric mixing can result in higher particle mass—at least for BC. This is not necessarily the case for the total particle number, which is also significantly influenced by new particle formation (NPF) events. The smaller particle diameters in summer may likely be due to these different NPF rates in winter as compared to summer, coupled with the higher accumulation in the atmosphere (and hence particle aging) in winter. These topics will be analyzed in future publications. Here we note that these general features do reflect into the selected SIOPs. SIOP4 (30 June–3 July 2021), covering the summer period, shows the lowest concentrations of all variables except the particle number. Note an NPF event occurring during SIOP4 (on 2 July), but no NPF occurring during the winter SIOPs. Both SIOP1 (26–30 January 2021) and SIOP3 (16–20 February 2021) cover winter conditions with increasing concentrations and particle diameters (accumulation in the atmosphere). SIOP3 shows higher mass concentrations than SIOP1, which in turn shows higher number concentrations with smaller particle size. SIOP2 (2–6 February 2021) covers a period of stable concentrations with some foggy conditions.

3.3. Oxidative and Reducing Potential

Oxidative and reducing potentials of the 24 h PM_1 samples collected at BO and SPC during the winter and summer monitoring periods are summarized in Table 5.

Table 5. Oxidative and reducing potentials of the 24 h PM_1 samples collected at BO and SPC during the winter and summer monitoring periods.

			OP^{DCFH}	OP^{AA}	OP^{DTT}	OP^{DTT}_{QRTZ}	RP^{DPPH}
		UoM	nmol H_2O_2 m^{-3}	nmol AA min^{-1} m^{-3}	nmol DTT min^{-1} m^{-3}	nmol DTT min^{-1} m^{-3}	% Cons DPPH m^{-3}
		MDL	1.0×10^{-10}	0.01	0.006	0.08	0.008
BO	**Winter**	**Mean**	4.7×10^{-9}	0.37	0.91	0.58	0.42
		SD	3.1×10^{-9}	0.35	0.55	0.25	0.42
		Median	4.1×10^{-9}	0.27	0.83	0.53	0.33
		min-max	1.1×10^{-10}–1.2×10^{-8}	0.018–1.9	0.087–2.5	0.15–1.1	0.25–1.8
		Mean	1.6×10^{-9}	0.47	0.31	0.22	0.045

	Summer	**SD**	1.4×10^{-9}	0.54	0.17	0.10	0.087
		Median	1.5×10^{-9}	0.23	0.31	0.22	0.046
		min-max	7.3×10^{-10}–4.6×10^{-9}	0.022–2.5	0.016–0.66	0.09–0.57	0.15–0.23
SPC	**Winter**	**Mean**	6.3×10^{-9}	0.55	0.85	0.48	0.41
		SD	3.9×10^{-9}	0.82	0.47	0.23	0.33
		Median	5.8×10^{-9}	0.24	0.86	0.43	0.38
		min-max	1.9×10^{-10}–1.6×10^{-8}	0.010–4.6	0.006–2.0	0.22–1.2	0.11–1.3

From Table 5, we can observe that higher values of OP^{DCFH} and OP^{DTT} were measured at both sites in the colder period, characterized by less efficient mixing of air masses and greater accumulation of airborne pollutants. This shows that OP^{DCFH} and OP^{DTT}, as well as PM1 concentration, were mainly modulated by seasonal atmospheric stability. In fact, OP^{DCFH} and OP^{DTT} are known to be predominantly sensitive to finer particles [69–71] that are more influenced by variations in atmospheric conditions and to domestic biomass heating [50,72,73], which is more intense during winter. The same can be pointed out for RP^{DPPH}; indeed, the reducing capacity of PM_1 seems to increase in winter, as well as for OP^{DCFH} and OP^{DTT}. Although not much is yet known about the PM reducing activity, these results highlighted the ability of RP^{DPPH} to predict PM_1 reducing properties.

The need to estimate the reducing potential of PM is related to the stability of the PM species: short-life oxidant species can react, and redox equilibria among PM native species could occur during both the sample storage and the extraction phase. In this regard, it is possible that, within the conditions that could contribute to the estimation of the oxidative potential of PM, there is also the reaction and/or competition between oxidant and reducing species naturally occurring in PM. Some studies proved the presence of species with likely reducing characteristics [74,75]. Although the nature of reducing species is still unknown, some studies proved the presence of species with likely antioxidant and reducing characteristics such as phenols from wood-burning or phenolic compounds from different sources. Furthermore, experimental OP values suggested the possible presence of this kind of species in PM and illustrated the need to deepen knowledge of the redox properties of PM. The estimation of reducing potential is aimed at clarifying the latter aspects by considering the application of an acellular procedure to evaluate the presence of reducing species in PM samples, along with the evaluation of the OP of PM. Therefore, the DPPH radical scavenging assay was adapted and applied to PM in order to verify its possible use as an acellular method for estimating the presence of reducing species, thus expressing PM reducing potential [48]. Preliminary applications of the DPPH assay revealed the presence of reducing species in several components of atmospheric PM derived from various emission sources and, thus, with very different chemical compositions [48]. This assay offers the advantages of being simple, rapid, and easily applicable to intensive PM monitoring campaigns for routinely estimating the amount of reducing species in PM samples. For what was mentioned above, the DPPH assay was applied during the RHAPS project to acquire new insights into the field of PM redox properties and their impacts on health outcomes and endpoints.

All these assays seem to be less affected by inter-site variability. On the contrary, OP^{AA} appears to be less modulated by seasonal variations and more influenced by different contributions of the emission sources at the two sites. The daily contribution of the different emission sources to the oxidative and reducing capacity of PM_1 and the associated toxicological potential will be extensively evaluated in future studies.

3.4. Toxicological Assessment

3.4.1. Effects of PM_1 from Water-Extracted Samples during IOPs

Effects of PM_1 from water-extracted filter samples were investigated in BEAS-2B cells as a surrogate of epithelial lung cells and THP-1 cells as a surrogate of alveolar macrophages. For illustrative purposes, the results of IL-8 release in both cell types are reported in Figure 11.

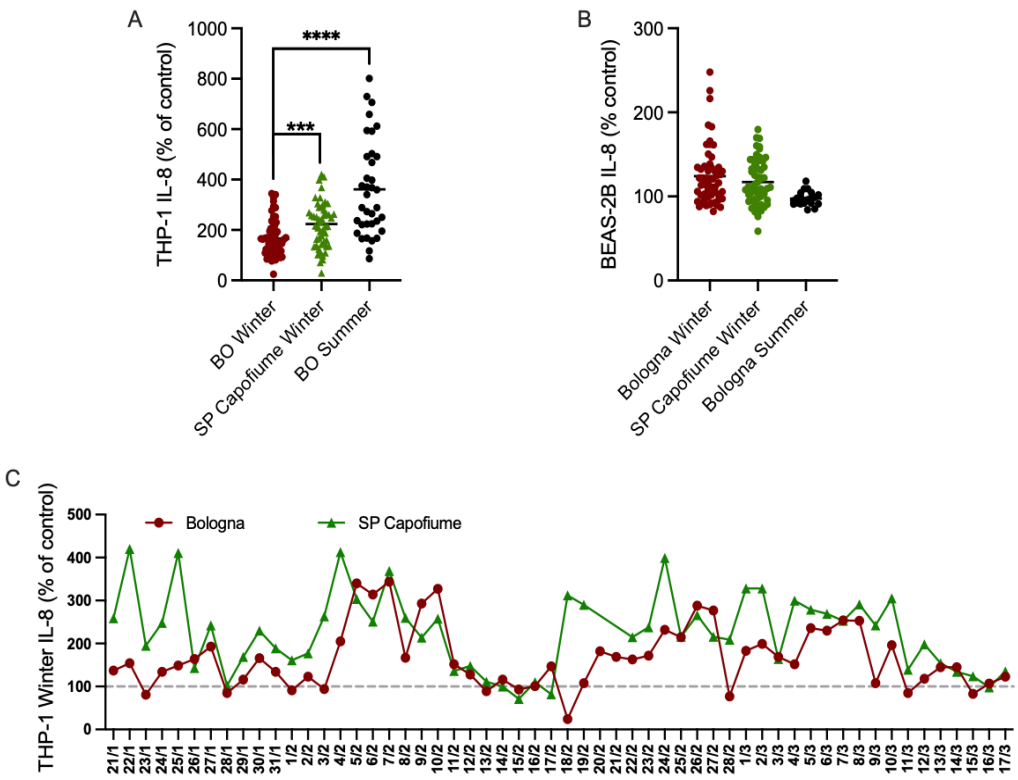

Figure 11. Seasonal and site effects of PM_1 water-extracted filters on IL-8 release. BEAS-2B and THP-1 cells were exposed to 1:10 dilution of the extracts for 24 h. (**A**) Average responses in exposed THP-1 cells. (**B**) Average responses in exposed BEAS-2B cells. (**C**) Daily IL-8 release in THP-1 cells exposed to extracts obtained from winter samples. Asterisks indicate statistically significant differences among groups as evaluated by un-paired two-tailed Student's t-test, with ***p<0.0005 (BO Winter vs SP Capofiume Winter) and ****p<0.0001 (BO Winter vs BO Summer).

Results are expressed as % of control. In THP-1 cells, seasonal and site differences were observed in average responses, with higher releases observed in SPC compared to BO and higher production in summer vs. winter samples obtained in BO. In addition, daily differences in IL-8 release were also observed. Regarding the release

of IL-8 in BEAS-2B cells, no seasonal or site differences in the average responses were found. In the majority of the samples, the release of IL-8 was above control values. These results confirm the ability of the models used to respond to PM_1 water-extracted filters, with a different sensitivity between the two models and in relation to specific components.

Embryotoxicity tests were also performed on the same water extracted samples. Indeed, an embryo represents a complex biological model responding to environmental signals blocking, changing the speed of development, or altering the normal morphogenetical pattern. Preliminary results show that neither lethal nor malformative effects were recorded after the exposure to the water extract fraction (Figure S20).

3.4.2. Effects in Cells Exposed at the Air Liquid Interface during SIOPs

The average responses in exposed cells show a non-significant difference between winter and summer campaigns except for a significant difference in Cxcl-8 gene expression (p = 0.04, ANOVA, Analysis of Variance) and IL-8 release (p = 0.02, ANOVA) that were higher in winter samples (Figure 12). A slight but not significant increase in winter samples is also reported for NQO1 and HMOX genes. However, differences among the different days of exposure are evident for the scatterplot properties, and this distribution of the responses may indicate an altered gene expression in relation to specific aerosol properties.

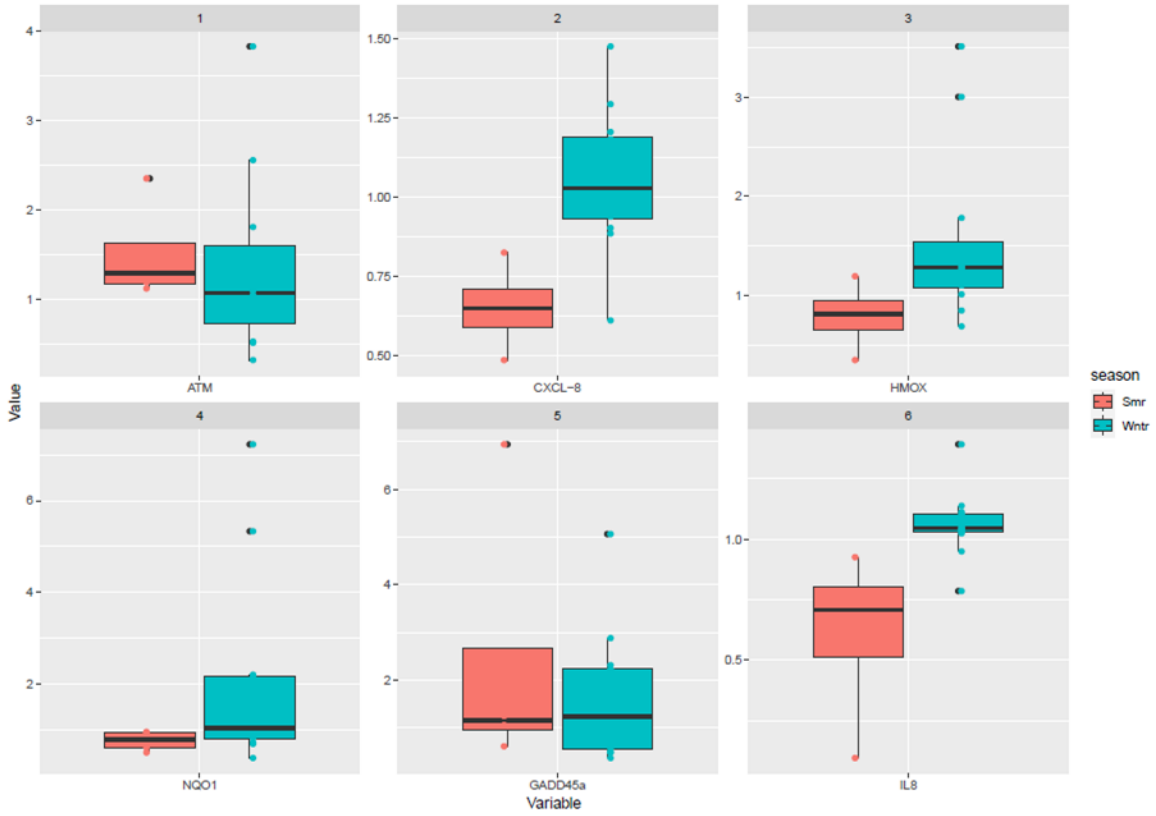

Figure 12. Overview of median (box plot), interquartile range (box plot), 9–95th percentiles (whisker plot) of genes characterized in ALI exposed lung cells. Significant differences were observed for the Cxcl-8 gene (p = 0.04, ANOVA) and for the subsequent release of the IL-8 protein (p = 0.02, ANOVA) with higher expression and release in winter compared to summer exposures.

4. Discussion and Conclusions

Linking air quality and health is still a complex issue. The debate on which particle type is more or less toxic [76] and how to protect human health [3,77] is still unresolved. In the meantime, the last WHO guidelines [1] (WHO 2021) tend to reduce as much as possible the thresholds of safety for human health, suggesting the absence of a safe threshold for $PM_{2.5}$. To target this topic, the RHAPS experiment aims to identify specific properties of PM_1 from combustion sources that are responsible for toxicological effects and can be used as new metrics for health-related outdoor pollution studies. In this paper, we present the overall methodology of the RHAPS project and introduce the phenomenology and the first data observed.

The first results show that at real atmospheric conditions (i.e., PM_1 of about 20 μg m^{-3}):

- high values of PM1 mass concentration do not necessarily translate into high toxicity (i.e., PM1 mass concentration > 50 μg m^{-3}), and conversely, very low values of PM1 (mass concentration < 5 μg m^{-3}) do not necessarily translate into no toxicity;
- high values of BC mass concentration do not necessarily translate into high toxicity (BC mass concentration > 5 μg m^{-3});
- different WSOP assays may give different responses, but in general, high values of WSOP do not necessarily translate into high toxicity.

Notably, these findings were observed during a variety of atmospheric conditions, aerosol properties, and toxicological assessments.

Regarding the atmospheric conditions, in winter (temperature ranging from -5 to 15 °C), we observed sunnier and drier conditions (SIOP1), low-clouds (and fog) with rising temperature and calm winds (SIOP2), Saharan dust plumes with high PM2.5, and accumulation of pollutants near the surface with the highest $PM_{2.5}$ mass concentrations of the winter campaign (up to 50 μg m^{-3}, SIOP3). In summer (temperatures from 0 to 35 °C), we had light winds, clouds, rain, and a modest reduction of $PM_{2.5}$ mass concentration, dust advection with high PM2.5, enhanced ventilation, with a consequent relative reduction of $PM_{2.5}$ concentrations (SIOP4).

Regarding aerosol properties, overall, our data are representative of PM1 concentration from 0 to 60 μg m^{-3}, BC from 0 to 6 μg $m^{-3,}$ and particle number from 0 to 6.0×10^5 cm^{-3}. During wintertime, aerosol particle mass was higher. PM_1 mass concentration was, on average, approx. 20 μg m^{-3} at both the rural and urban sites, and it was mainly accounted for by secondary inorganic ions (i.e., sulfate, nitrate, and ammonium) together with organic carbon. In summer, PM_1 concentrations were approximately a factor 2 lower than wintertime ones, and the major components were sulfates and OC. All PM1 components (BC, OA, nitrates, and ammonium) except sulfates were larger in winter than in summer. Contrarily to most of the PM1 mass components except sulfates, the total particle number concentration was on average similar in winter and summer (on average, 1.3×10^4 cm^{-3}), particle size being smaller in summer (surface-weighted diameter approx. 65 nm in summer, and 90 nm in winter).

Considering WSOP, both OP^{DCFH} and OP^{DTT} were higher at both sites in winter than in summer. Also, the reducing capacity of PM_1 (RP^{DPPH}) seems to increase in winter. Conversely, OP^{AA} is slightly higher (or comparable) in summer than in winter.

These trends (e.g., higher PM1 and BC and/or higher WSOP in winter) do not necessarily reflect the biological responses. Considering the water-extracted samples ("classical approach") during the whole IOPs, we observed IL-8 releases higher in summer than in winter in THP-1 cells, and no seasonal difference in BEAS-2B cells (the majority of the samples having the release of IL-8 above control values). Considering the cells exposed at the Air Liquid Interface directly in the atmosphere ("the original approach" that we developed) during the SIOPs, we observed no significant difference on average between winter and summer for most of the genes analyzed, except for a significant difference in Cxcl-8 gene expression and IL-8 release that were higher in winter. Note that the summer SIOP4 had very low mass concentrations (PM1< 5 mg m-3).

Differences among the different days of exposure are conversely evident.

Therefore, the first findings suggest that high/low PM1 and BC mass concentration and WSOP do not necessarily translate into high/low toxicity but that the complexity of biological responses might go beyond these. These preliminary findings will be discussed in detail in a series of companion papers, with a focus basically on four topics:

1. Source apportionment of PM_1 and the role of source emissions on aerosol toxicity;
2. OP as a predictive variable for PM_1 toxicity with a focus on SOA possessing redox-active capacity;
3. Exposure-response relationships for PM_1;
4. Air quality models to forecast PM1 toxicity.

The hypothesis to test is that the exposure to primary and secondary atmospheric aerosols under conditions representative of the real-life scenario in the atmosphere can differently activate oxidative stress and inflammatory responses. It is worth noting that the real-life scenario is a major focus of the RHAPS project, where exposure is assessed to the real atmospheric concentrations, as pioneeringly proposed during the first CARE experiment [11]. Future papers (manuscripts in preparation) will investigate this by analyzing physicochemical properties and specific metrics (both classical and newly developed) of source-specific primary and secondary aerosol, and exploring connections between all these metrics and the release of biological markers in lung epithelial cells, the focus on oxidative stress-related pathways. Importantly, beyond PM_1 and BC mass concentration, we will include among these metrics the source-apportioned PM_1 oxidative potential and statistical profiles of source-specific aerosol types such as SOA. The assessment of the redox-active capacity of SOA will be derived from the comprehensive RHAPS assessment from in-field and laboratory measurements. Anthropogenic aerosol secondary organic compounds, such as quinones, are considered among the most important players in determining OP [78] and are known to generate from photochemical aging of the emissions of a very broad range of combustion systems [6]. The variability in aerosol properties and in OP will be specifically linked to changes in distinct source contributions with the

novel source apportionment approach of RHAPS by inserting each data value in its original time schedule through advanced receptor modeling [79–82]. The insertion of non-compositional variables (e.g., absorption coefficients or OP) in the same modeling process, the combination with fossil fuel and biomass burning EC and OC components from optical source apportionment as well as the organic aerosol components retrieved from the AMS apportionment will be key for robust source identification and assessment. As the final step, the air quality modeling will be devoted to developing an operational air quality forecast tool for PM toxicity to be deployed on a national scale. Findings will be among the first results of this kind and have the potential to support the development of new metrics for health-related pollution studies and contribute to the cutting-edge research on OP and SOA.

Author Contributions: Conceptualization, F.C. (Francesca Costabile), R.V., S.D., M.C.F.; methodology, F.C. (Francesca Costabile), S.D., R.V., G.C. (Gabriele Curci), S.C., L.M., M.G., M.R. (Matteo Rinaldi), D.M., P.P., S.A., E.C., M.B. (Maurizio Busetto), M.P., F.L., C.P.; modeling, G.C. (GABRIELE CURCI), R.V., F.C. (Federica Crova), A.C.F.; validation, M.R. (Matteo Rinaldi), F.C. (Francesca Costabile), M.P., L.M., S.C., G.V., S.V., R.V., F.C. (Federica Crova), A.C.F., V.B., D.M., S.N., F.G., F.L., M.B. (Maurizio Busetto), L.C., D.C.; **laboratory analyses**, L.M., **M.A.F**., V.V., D.M., F.G., G.P., S.N., G.I., F.G. (Flavio Giavarini), M.R. (Mara Russo); **field measurements**, L.D.L., M.B. (Maurizio Busetto), M.R. (Matteo Rinaldi), M.P., I.P., G.C. (Gianpietro Casasanta), L.D.L., G.V., S.V., F.C. (Federica Crova), A.C.F., L.M., **M.A.F**., A.M., F.G.; toxicological, E.C., M.G., G.M., E.N., M.I., E.M., M.B. (Maria Battistoni), F.D.R., T.L.T., E.P., M.S., G.Z.; **OP assays**, M.R. (Matteo Rinaldi), M.R. (Mara Russo), L.M., **M.A.F**., S.C., G.D.I.; data analyses, F.C. (Francesca Costabile), M.R. (Matteo Rinaldi), M.P., I.P., G.D.I., M.G., S.V., G.V., F.C. (Federica Crova), A.C.F., R.V., G.M., E.C., E.M., M.B. (Maria Battistoni), D.M., S.N.; data curation, F.C. (Francesca Costabile), M.R. (Matteo Rinaldi), M.B. (MAURIZIO BUSETTO), L.D.L.; writing—original draft preparation, F.C. (Francesca Costabile), R.V.; writing—review and editing, F.C. (Francesca Costabile), R.V., S.D., G.C. (Gabriele Curci), L.M., M.G., M.R. (Matteo Rinaldi), S.A., E.C., M.B. (Maurizio Busetto), F.L., M.G.; project administration, S.D., F.C. (Francesca Costabile), R.V.; funding acquisition, M.C.F., S.D., R.V., F.L., G.C. (Gabriele Curci), D.M. All authors have read and agreed to the published version of the manuscript.

References

1. World Health Organization; WHO European Centre for Environment. *WHO Global Air Quality Guidelines: Particulate matter (PM2. 5 and PM10), Ozone, Nitrogen Dioxide, Sulfur Dioxide and Carbon Monoxide*; World Health Organization: Geneva, Switzerland, 2021.
2. Chen, J.; Hoek, G. Long-term exposure to PM and all-cause and cause-specific mortality: A systematic review and meta-analysis. *Environ. Int.* **2020**, *143*, 105974.
3. Stafoggia, M.; Oftedal, B.; Chen, J.; Rodopoulou, S.; Renzi, M.; Atkinson, R.W.; Janssen, N.A. Long-term exposure to low ambient air pollution concentrations and mortality among 28 million people: Results from seven large European cohorts within the ELAPSE project. *Lancet Planet. Health* **2022**, *6*, e9–e18.
4. Li, X.; Jin, L.; Kan, H. Air pollution: A global problem needs local fixes. *Nature* **2019**, *570*, 437–439. https://doi.org/10.1038/d41586-019-01960-7.
5. Künzi, L.; Krapf, M.; Daher, N.; Dommen, J.; Jeannet, N.; Schneider, S.; Geiser, M. Toxicity of aged gasoline exhaust particles to normal and diseased airway epithelia. *Sci. Rep.* **2015**, *5*, 11801.
6. Jimenez, J.L.; Canagaratna, M.R.; Donahue, N.M.; Prevot, A.S.H.; Zhang, Q.; Kroll, J.H.; Worsnop, D.R. Evolution of organic aerosols in the atmosphere. *Science* **2009**, *326*, 1525–1529.

7. Ervens, B.T.B.W.R.; Turpin, B.J.; Weber, R.J. Secondary organic aerosol formation in cloud droplets and aqueous particles (aqSOA): A review of laboratory, field and model studies. *Atmos. Chem. Phys.* **2011**, *11*, 11069–11102.
8. Corsini, E.; Ozgen, S.; Papale, A.; Galbiati, V.; Lonati, G.; Fermo, P.; Marinovich, M. Insights on wood combustion generated proinflammatory ultrafine particles (UFP). *Toxicol. Lett.* **2017**, *266*, 74–84.
9. Corsini, E.; Vecchi, R.; Marabini, L.; Fermo, P.; Becagli, S.; Bernardoni, V.; Marinovich, M. The chemical composition of ultrafine particles and associated biological effects at an alpine town impacted by wood burning. *Sci. Total Environ.* **2017**, *587*, 223–231.
10. Marabini, L.; Ozgen, S.; Turacchi, S.; Aminti, S.; Arnaboldi, F.; Lonati, G.; Marinovich, M. Ultrafine particles (UFPs) from domestic wood stoves: Genotoxicity in human lung carcinoma A549 cells. *Mutat. Res. Genet. Toxicol. Environ. Mutagenesis* **2017**, *820*, 39–46.
11. Costabile, F.; Alas, H.; Aufderheide, M.; Avino, P.; Amato, F.; Argentini, S.; Gobbi, G.P. First results of the "Carbonaceous aerosol in Rome and Environs (CARE)" experiment: Beyond current standards for PM10. *Atmosphere* **2017**, *8*, 249.
12. Gualtieri, M.; Grollino, M.G.; Consales, C.; Costabile, F.; Manigrasso, M.; Avino, P.; Zanini, G. Is it the time to study air pollution effects under environmental conditions? A case study to support the shift of in vitro toxicology from the bench to the field. *Chemosphere* **2018**, *207*, 552–564.
13. Kelly, F.J.; Fussell, J.C. Size, source and chemical composition as determinants of toxicity attributable to ambient particulate matter. *Atmos. Environ.* **2012**, *60*, 504–526.
14. Lakey, P.S.; Berkemeier, T.; Tong, H.; Arangio, A.M.; Lucas, K.; Pöschl, U.; Shiraiwa, M. Chemical exposure-response relationship between air pollutants and reactive oxygen species in the human respiratory tract. *Sci. Rep.* **2016**, *6*, 32916.
15. Saffari, A.; Daher, N.; Shafer, M.M.; Schauer, J.J.; Sioutas, C. Global perspective on the oxidative potential of airborne particulate matter: A synthesis of research findings. *Environ. Sci. Technol.* **2014**, *48*, 7576–7583.
16. Decesari, S.; Sowlat, M.H.; Hasheminassab, S.; Sandrini, S.; Gilardoni, S.; Facchini, M.C.; Sioutas, C. Enhanced toxicity of aerosol in fog conditions in the Po Valley, Italy. *Atmos. Chem. Phys.* **2017**, *17*, 7721–7731.
17. Verma, V.; Fang, T.; Xu, L.; Peltier, R.E.; Russell, A.G.; Ng, N.L.; Weber, R.J. Organic aerosols associated with the generation of reactive oxygen species (ROS) by water-soluble PM2. 5. *Environ. Sci. Technol.* **2015**, *49*, 4646–4656.
18. Janssen, N.A.; Yang, A.; Strak, M.; Steenhof, M.; Hellack, B.; Gerlofs-Nijland, M.E.; Cassee, F. Oxidative potential of particulate matter collected at sites with different source characteristics. *Sci. Total Environ.* **2014**, *472*, 572–581.
19. Sarti, E.; Pasti, L.; Rossi, M.; Ascanelli, M.; PAgnoni, A.; Trombini, M.; Remelli, M. The composition of PM1 and PM2.5 samples, metals and their water soluble fractions in the Bologna area (Italy). *Atmos. Pollut. Res.* **2015**, *6*, 708–718.

20. Vecchi, R.; Marcazzan, G.; Valli, G.; Ceriani, M.; Antoniazzi, C. The role of atmospheric dispersion in the seasonal variation of PM1 and PM2.5 concentration and composition in the urban area of Milan (Italy). *Atmos. Environ.* **2004**, *38*, 4437–4446.
21. Amato, F.; Alastuey, A.; Karanasiou, A.; Lucarelli, F.; Nava, S.; Calzolai, G.; Querol, X. AIRUSE-LIFE+: A harmonized PM speciation and source apportionment in five southern European cities. *Atmos. Chem. Phys.* **2016**, *16*, 3289–3309.
22. Ricciardelli, I.; Bacco, D.; Rinaldi, M.; Bonafè, G.; Scotto, F.; Trentini, A.; Poluzzi, V. A three-year investigation of daily PM2.5 main chemical components in four sites: The routine measurement program of the Supersito Project (Po Valley, Italy). *Atmos. Environ.* **2017**, *152*, 418–430.
23. Gilardoni, S.; Massoli, P.; Paglione, M.; Giulianelli, L.; Carbone, C.; Rinaldi, M.; Facchini, M.C. Direct observation of aqueous secondary organic aerosol from biomass-burning emissions. *Proc. Natl. Acad. Sci. USA* **2016**, *113*, 10013–10018.
24. Lucarelli, F.; Calzolai, G.; Chiari, M.; Giardi, F.; Czelusniak, C.; Nava, S. Hourly elemental composition and source identification by Positive Matrix Factorization (PMF) of fine and coarse particulate matter in the high polluted industrial area of Taranto (Italy). *Atmosphere* **2020**, *11*, 419.
25. Massimi, L.; Ristorini, M.; Astolfi, M.L.; Perrino, C.; Canepari, S. High resolution spatial mapping of element concentrations in PM10: A powerful tool for localization of emission sources. *Atmos. Res.* **2020**, *244*, 105060.
26. Astolfi, M.L.; Protano, C.; Marconi, E.; Massimi, L.; Brunori, M.; Piamonti, D.; Canepari, S. A new rapid treatment of human hair for elemental determination by inductively coupled mass spectrometry. *Anal. Methods* **2020**, *12*, 1906–1918.
27. Canepari, S.; Pietrodangelo, A.; Perrino, C.; Astolfi, M.L.; Marzo, M.L. Enhancement of source traceability of atmospheric PM by elemental chemical fractionation. *Atmos. Environ.* **2009**, *43*, 4754–4765.
28. Piazzalunga, A.; Bernardoni, V.; Fermo, P.; Vecchi, R. Optimisation of analytical procedures for the quantification of ionic and carbonaceous fractions in the atmospheric aerosol and applications to ambient samples. *Anal. Bioanal. Chem.* **2013**, *405*, 1123–1132.
29. Piazzalunga, A.; Fermo, P.; Bernardoni, V.; Vecchi, R.; Valli, G.; De Gregorio, M.A. A simplified method for levoglucosan quantification in wintertime atmospheric particulate matter by high performance anion-exchange chromatography coupled with pulsed amperometric detection. *Int. J. Environ. Anal. Chem.* **2010**, *90*, 934–947.
30. Terzopoulou, E.; Voutsa, D.; Kaklamanos, G. A multi-residue method for determination of 70 organic micropollutants in surface waters by solid-phase extraction followed by gas chromatography coupled to tandem mass spectrometry. *Environ. Sci. Pollut. Res.* **2015**, *22*, 1095–1112.
31. Gosetti, F.; Chiuminatto, U.; Mazzucco, E.; Robotti, E.; Calabrese, G.; Gennaro, M.C.; Marengo, E. Simultaneous determination of thirteen polycyclic aromatic hydrocarbons and twelve aldehydes in cooked

food by an automated on-line solid phase extraction ultra high performance liquid chromatography tandem mass spectrometry. *J. Chromatogr. A* **2011**, *1218*, 6308–6318.

32. Canagaratna, M.R.; Jayne, J.T.; Jimenez, J.L.; Allan, J.D.; Alfarra, M.R.; Zhang, Q.; Worsnop, D.R. Chemical and microphysical characterization of ambient aerosols with the aerodyne aerosol mass spectrometer. *Mass Spectrom. Rev.* **2007**, *26*, 185–222.
33. Jayne, J.T.; Leard, D.C.; Zhang, X.; Davidovits, P.; Smith, K.A.; Kolb, C.E.; Worsnop, D.R. Development of an aerosol mass spectrometer for size and composition analysis of submicron particles. *Aerosol Sci. Technol.* **2000**, *33*, 49–70.
34. Jimenez, J.L.; Jayne, J.T.; Shi, Q.; Kolb, C.E.; Worsnop, D.R.; Yourshaw, I.; Davidovits, P. Ambient aerosol sampling using the aerodyne aerosol mass spectrometer. *J. Geophys. Res. Atmos.* **2003**, *108*, 8425.
35. DeCarlo, P.F.; Kimmel, J.R.; Trimborn, A.; Northway, M.J.; Jayne, J.T.; Aiken, A.C.; Jimenez, J.L. Field-deployable, high-resolution, time-of-flight aerosol mass spectrometer. *Anal. Chem.* **2006**, *78*, 8281–8289.
36. Middlebrook, A.M.; Bahreini, R.; Jimenez, J.L.; Canagaratna, M.R. Evaluation of composition-dependent collection efficiencies for the aerodyne aerosol mass spectrometer using field data. *Aerosol Sci. Technol.* **2012**, *46*, 258–271.
37. Calzolai, G.; Lucarelli, F.; Chiari, M.; Nava, S.; Giannoni, M.; Carrarese, L.; Prati, P.; Vecchi, R. Improvements in PIXE analysis of hourly particulate matter samples. *Nucl. Instrum. Methods Phys. Res. B* **2015**, *363*, 99–104.
38. Hinds, W.C. *Aerosol Technology: Properties, Behavior and Measurement of Airborne Particles*, 2nd ed.; John Wiley & Sons: New York, NY, USA, 1999.
39. Massabò, D.; Bernardoni, V.; Bove, M.C.; Brunengo, A.; Cuccia, E.; Piazzalunga, A.; Vecchi, R. A multi-wavelength optical set-up for the characterization of carbonaceous particulate matter. *J. Aerosol Sci.* **2013**, *60*, 34–46.
40. Massabò, D.; Caponi, L.; Bernardoni, V.; Bove, M.C.; Brotto, P.; Calzolai, G.; Prati, P. Multi-wavelength optical determination of black and brown carbon in atmospheric aerosols. *Atmos. Environ.* **2015**, *108*, 1–12.
41. Moosmüller, H.; Chakrabarty, R.K.; Ehlers, K.M.; Arnott, W.P. Absorption Ångström coefficient, brown carbon, and aerosols: Basic concepts, bulk matter, and spherical particles. *Atmos. Chem. Phys.* **2011**, *11*, 1217–1225.
42. Sandradewi, J.; Prévôt, A.S.; Szidat, S.; Perron, N.; Alfarra, M.R.; Lanz, V.A.; Baltensperger, U.R.S. Using aerosol light absorption measurements for the quantitative determination of wood burning and traffic emission contributions to particulate matter. *Environ. Sci. Technol.* **2008**, *42*, 3316–3323.
43. Bernardoni, V.; Pileci, R.E.; Caponi, L.; Massabò, D. The Multi-Wavelength Absorption Analyzer (MWAA) Model as a Tool for Source and Component Apportionment Based on Aerosol Absorption Properties: Application to Samples Collected in Different Environments. *Atmosphere* **2017**, *8*, 218.
44. Massabò, D.; Altomari, A.; Vernocchi, V.; Prati, P. Two-wavelength thermal–optical determination of light-absorbing carbon in atmospheric aerosols. *Atmos. Meas. Tech.* **2019**, *12*, 3173–3182.

45. Massabò, D.; Prati, P.; Canepa, E.; Bastianini, M.; Van Eijk, A.M.; Missamou, T.; Piazzola, J. Characterization of carbonaceous aerosols over the Northern Adriatic Sea in the JERICO-NEXT project framework. *Atmos. Environ.* **2020**, *228*, 117449.
46. Drinovec, L.; Močnik, G.; Zotter, P.; Prévôt, A.S.H.; Ruckstuhl, C.; Coz, E.; Hansen, A.D.A. The "dual-spot" Aethalometer: An improved measurement of aerosol black carbon with real-time loading compensation. *Atmos. Meas. Tech.* **2015**, *8*, 1965–1979.
47. National Institute for Occupational Safety and Health. NIOSH: Method 5040 Issue 3: Elemental Carbon (Diesel Exhaust). In *NIOSH Manual of Analytical Methods*; National Institute of Occupational Safety and Health: Cincinnati, OH, USA, 1999.
48. Frezzini, M.A.; Castellani, F.; De Francesco, N.; Ristorini, M.; Canepari, S. Application of DPPH assay for assessment of particulate matter reducing properties. *Atmosphere* **2019**, *10*, 816.
49. Frezzini, M.A.; De Francesco, N.; Massimi, L.; Canepari, S. Effects of operating conditions on PM oxidative potential assays. *Atmos. Environ.* **2021**, *268*, 118802.
50. Massimi, L.; Ristorini, M.; Simonetti, G.; Frezzini, M.A.; Astolfi, M.L.; Canepari, S. Spatial Mapping and Size Distribution of Oxidative Potential of Particulate Matter Released by Spatially Disaggregated Sources. *Environ. Pollut.* **2020**, *266*, 115271.
51. Kedare, S.B.; Singh, R.P. Genesis and development of DPPH method of antioxidant assay. *J. Food Sci. Technol.* **2011**, *48*, 412–422.
52. Hara, K.; Someya, T.; Sano, K.; Sagane, Y.; Watanabe, T.; Wijesekara, R.G.S. Antioxidant activities of traditional plants in Sri Lanka by DPPH free radical-scavenging assay. *Data Brief* **2018**, *17*, 870–875.
53. Chedea, V.S.; Pop, R.M. Total polyphenols content and antioxidant DPPH assays on biological samples. In *Polyphenols in Plants*; Academic Press: Cambridge, MA, USA, 2019; pp. 169–183.
54. Sridhar, K.; Charles, A.L. In vitro antioxidant activity of Kyoho grape extracts in DPPH and ABTS assays: Estimation methods for EC50 using advanced statistical programs. *Food Chem.* **2019**, *275*, 41–49.
55. Cho, A.K.; Sioutas, C.; Miguel, A.H.; Kumagai, Y.; Schmitz, D.A.; Singh, M.; Froines, J.R. Redox activity of airborne particulate matter at different sites in the Los Angeles Basin. *Environ. Res.* **2005**, *99*, 40–47.
56. Verma, V.; Ning, Z.; Cho, A.K.; Schauer, J.J.; Shafer, M.M.; Sioutas, C. Redox activity of urban quasi-ultrafine particles from primary and secondary sources. *Atmos. Environ.* **2009**, *43*, 6360–6368.
57. Gao, D.; Fang, T.; Verma, V.; Zeng, L.; Weber, R.J. A method for measuring total aerosol oxidative potential (OP) with the dithiothreitol (DTT) assay and comparisons between an urban and roadside site of water-soluble and total OP. *Atmos. Meas. Tech.* **2017**, *10*, 2821–2835.
58. Simonetti, G.; Frasca, D.; Marcoccia, M.; Farao, C.; Canepari, S. Multi-elemental analysis of particulate matter samples collected by a particle-into-liquid sampler. *Atmos. Pollut. Res.* **2018**, *9*, 747–754.
59. Costabile, F.; Gualtieri, M.; Canepari, S.; Tranfo, G.; Consales, C.; Grollino, M.G.; Simonetti, G. Evidence of association between aerosol properties and in-vitro cellular oxidative response to PM1,

oxidative potential of PM2. 5, a biomarker of RNA oxidation, and its dependency on combustion sources. *Atmos. Environ.* **2019**, *213*, 444–455.

60. Corsini, E.; Budello, S.; Marabini, L.; Galbiati, V.; Piazzalunga, A.; Barbieri, P.; Galli, C.L. Comparison of wood smoke PM2.5 obtained from the combustion of FIR and beech pellets on inflammation and DNA damage in A549 and THP-1 human cell lines. *Arch. Toxicol.* **2013**, *87*, 2187–2199.
61. Battistoni, M.; Bacchetta, R.; Di Renzo, F.; Metruccio, F.; Moretto, A.; Menegola, E. Modified Xenopus laevis approach (R-FETAX) as an alternative test for the evaluation of foetal valproate spectrum disorder. *Reprod. Toxicol.* **2022**, *107*, 140–149.
62. Brown, N.A.; Fabro, S. Quantitation of rat embryonic development in vitro: A morphological scoring system. *Teratology* **1981**, *24*, 65–78.
63. Nieuwkoop, P.D.; Faber, J.; Gerhart, J.; Kirschner, M. *Normal Table of Xenopus laevis (Daudin): A Systematical and Chronological Survey of the Development From the Fertilized Egg till the End of Metamorphosis*; Garland Science: New York, NY, USA, 2020.
64. Skamarock, W.C.; Klemp, J.B.; Dudhia, J.; Gill, D.O.; Barker, D.M.; Wang, W.; Powers, J.G. *A Description of the Advanced Research WRF Version 2*. National Center for Atmospheric Research: Boulder, CO, USA, 2005.
65. Falasca, S.; Curci, G. High-resolution air quality modeling: Sensitivity tests to horizontal resolution and urban canopy with WRF-CHIMERE. *Atmos. Environ.* **2018**, *187*, 241–254.
66. Menut, L.; Bessagnet, B.; Khvorostyanov, D.; Beekmann, M.; Blond, N.; Colette, A.; Coll, I.; Curci, G.; Foret, G.; Hodzic, A.; et al. CHIMERE 2013: A model for regional atmospheric composition modelling. Geoscientific Model Development. **2013**, *6*, 981–1028. https://doi.org/10.5194/gmd-6-981-2013.
67. Deserti, M.; Bande, S.; Angelino, E.; Pession, G.; Dalan, F.; Minguzzi, M.; Stortini, M.; Bonafè, G.; De Maria, R.; Fossati, G.; et al. *Rapporto Tecnico sulla Applicazione di modellistica al Bacino Padano Adriatico*; APAT: Rome, Italy, 2008.
68. Costabile, F.; Gilardoni, S.; Barnaba, F.; Di Ianni, A.; Di Liberto, L.; Dionisi, D.; Gobbi, G.P. Characteristics of brown carbon in the urban Po Valley atmosphere. *Atmos. Chem. Phys.* **2017**, *17*, 313–326.
69. Molina, C.; Toro, A.R.; Manzano, C.A.; Canepari, S.; Massimi, L.; Leiva-Guzmán, M. Airborne aerosols and human health: Leapfrogging from mass concentration to oxidative potential. *Atmosphere* **2020**, *11*, 917.
70. Manigrasso, M.; Simonetti, G.; Astolfi, M.L.; Perrino, C.; Canepari, S.; Protano, C.; Vitali, M. Oxidative potential associated with urban aerosol deposited into the respiratory system and relevant elemental and ionic fraction contributions. *Atmosphere* **2019**, *11*, 6.
71. Simonetti, G.; Conte, E.; Perrino, C.; Canepari, S. Oxidative potential of size-segregated PM in an urban and an industrial area of Italy. *Atmos. Environ.* **2018**, *187*, 292–300.

72. Bates, J.T.; Fang, T.; Verma, V.; Zeng, L.; Weber, R.J.; Tolbert, P.E.; Russell, A.G. Review of acellular assays of ambient particulate matter oxidative potential: Methods and relationships with composition, source and health effects. *Environ. Sci. Technol.* **2019**, *53*, 4003–4019.
73. Verma, V.; Sioutas, C.; Weber, R.J. Oxidative properties of ambient particulate matter-an assessment of the relative contributions from various aerosol components and their emission sources. In *Multiphase Environmental Chemistry in the Atmosphere*; American Chemical Society: Washington, DC, USA, 2018; pp. 389–416.
74. Nemmar, A.; Holme, J.A.; Rosas, I.; Schwarze, P.E.; Alfaro-Moreno, E. Recent advances in particulate matter and nanoparticle toxicology: A review of the in vivo and in vitro studies. *BioMed Res. Int.* **2013**, *2013*, 279371.
75. Menetrez, M.Y.; Foarde, K.K.; Esch, R.K.; Schwartz, T.D.; Dean, T.R.; Hays, M.D.; Cho, S.H.; Betancourt, D.A.; Moore, S.A. An evaluation of indoor and outdoor biological particulate matter. *Atmos. Environ.* **2009**, *43*, 5476–5483.
76. Thurston, G.; Chen, L.; Campen, M. Particle toxicity's role in air pollution. *Science* **2022**, *375*, 506.
77. Al-Kindi, S.G.; Brook, R.D.; Biswal, S.; Rajagopalan, S. Environmental determinants of cardiovascular disease: Lessons learned from air pollution. *Nat. Rev. Cardiol.* **2020**, *17*, 656–672.
78. Chung, M.Y.; Lazaro, R.A.; Lim, D.; Jackson, J.; Lyon, J.; Rendulic, D.; Hasson, A.S. Aerosol-borne quinones and reactive oxygen species generation by particulate matter extracts. *Environ. Sci. Technol.* **2006**, *40*, 4880–4886.
79. Forello, A.C.; Bernardoni, V.; Calzolai, G.; Lucarelli, F.; Massabò, D.; Nava, S.; Vecchi, R. Exploiting multi-wavelength aerosol absorption coefficients in a multi-time resolution source apportionment study to retrieve source-dependent absorption parameters. *Atmos. Chem. Phys.* **2019**, *19*, 11235–11252.
80. Forello, A.C.; Amato, F.; Bernardoni, V.; Calzolai, G.; Canepari, S.; Costabile, F.; Vecchi, R. Gaining knowledge on source contribution to aerosol optical absorption properties and organics by receptor modelling. *Atmos. Environ.* **2020**, *243*, 117873.
81. Ogulei, D.; Hopke, P.K.; Zhou, L.; Paatero, P.; Park, S.S.; Ondov, J.M. Receptor modeling for multiple time resolved species: The Baltimore supersite. *Atmos. Environ.* **2005**, *39*, 3751–3762.
82. Zhou, L.; Hopke, P.K.; Paatero, P.; Ondov, J.M.; Pancras, J.P.; Pekney, N.J.; Davidson, C.I. Advanced factor analysis for multiple time resolution aerosol composition data. *Atmos. Environ.* **2004**, *38*, 4909–4920.

Supplementary Materials

Available at https://www.mdpi.com/article/10.3390/atmos13050704/s1

9. General conclusions and perspectives

The presented PhD research investigated the contribution of emission sources to atmospheric particulate matter concentration (PM) and to its redox properties. In the second part of the study, human health and environmental impact of airborne PM were deepened.

PM field samples were collected in different selected study areas (i.e. Terni, Amersfoort, Rome), and in indoor environments for the application of multidisciplinary approaches based on traditional and innovative methods for PM sampling and analysis for localization and impact assessment of PM released by specific emission sources on environment and human health. PM samples were chemically characterized by applying advanced and robust analytical procedures for the determination of inorganic ions, water-soluble and insoluble elements, water-soluble organic carbon (WSOC), levoglucosan (LVG) and oxidative potential (OP^{DCFH}, OP^{AA}, OP^{DTT}). PM water-soluble and insoluble fraction were separately analyzed through a well-established fractionation procedure to increase the selectivity of elements as source tracers and to estimate the environmental mobility and bio-accessibility of toxic elements. Through the spatial mapping of chemical tracers of PM emissions, the main PM sources acting in the study area were identified and the diffusion of the PM particles was estimated, overcoming the limits connected to the study of PM diffusion through the use of mathematical models. Furthermore, the spatial mapping of OP^{DCFH}, OP^{AA}, OP^{DTT} permitted the individuation of spatial relationships between the OP of PM and its chemical composition and sources, and proved to be a powerful tool, transferable to other monitoring campaigns, for the identification and localization of the emission sources mainly responsible for ROS generation. This last issue is of particular importance as OP is considered one of the most relevant predictive factors in assessment of PM toxicity since it is intrinsically influenced by different physiochemical PM properties. Therefore, OP is frequently proposed as a more biologically appropriate metric for addressing air quality and human exposure than PM mass concentration, appearing to be the central paradigm in the assessment of PM toxicity.

The second part of the research was focused on the study of operative criticisms affecting the relevance of OP as effective realistic metric to quantify the effects of ambient particles on human health. The understanding of redox properties of PM has begun with the optimization of a method to evaluate the presence of species with reducing/antioxidant behavior in PM. The DPPH radical scavenging assay was adapted and preliminarily applied to PM with the aim of verifying its possible use as an acellular method for estimating the presence of reducing species, thus for expressing PM reducing potential (RP^{DPPH}). The preliminary application of the DPPH assay revealed the presence of reducing species in several components of atmospheric PM derived from various emission sources and, thus, with very different chemical composition. The results showed that the assay was sufficiently sensitive to be applied to 24 h PM samples with a good repeatability and linearity. The combined application of DPPH and OP assays to wider sample sets will permit to better understand redox equilibria among PM native species and could constitute a new and potentially useful tool for acquiring new insight in the field of its redox behavior and health effects. In order to deepen the critical issues revolving around particles OP, the stability of PM redox components was assessed by analyzing the variability in OP assays (OP^{DCFH}, OP^{AA}, OP^{DTT}) responses depending on the operative conditions by which tests are performed.

To these aims, two monitoring campaigns were carried out by placing co-located PM_{10} samplers working in parallel, thus obtaining multiple equal samples per day, to compare different procedures simultaneously applied on identical samples. The influence of PM extraction method on OP obtained results was studied by comparing three different techniques: ultrasonic bath (US), vortex (V) and rotating agitator (RA). Results show the good linearity of RA for all the three OP assays that can be considered suitable to extract PM filters in terms of repeatability and to avoid ROS generation that would occur if US and V are used. In fact, the formation of radical species may originate positive artifacts thus altering the obtained OP results of sampled PM.

According to the results from the experimental step regarding the influence of sample storage and duration, it is reasonable to expect that substantial changes may occur over time. In fact, OP^{DCFH} and OP^{AA} measurements are significantly affected by both sample storage condition and duration: collected species responsible for OP seem to be subjected to changes over time determining a decrease in their oxidizing capability. Therefore, OP measured on stored filters for a long time could not be truly representative of the real potential of ambient particles to generate reactive species.

Comparison between quartz and PTFE filters underlines that even the supporting membrane used for PM sampling can influence OP measurements, especially OP^{AA} results.

Results from PM water-insoluble components redox activity are still to be clarified. Values from OP^{AA} and RP^{DPPH} show a significant contribution from insoluble fraction, while results from OP^{DCFH} and OP^{DTT} suggested that sampled reactive species are embedded too deeply in the filter to fully interact with the reagents. In fact, it should be considered that the application of tests directly on the filter is particularly complex due to lack of homogeneity of samples. This important aspect merited further investigations in order to assess the role of insoluble particles in particle oxidative activity, as well as to investigate exposure to PM in real-word conditions. Therefore, a non-invasive, simple, and efficient method was applied to PM field filters for the detachment of intact particles. The procedure involved the use of an electrical toothbrush which allows obtaining a PM water-suspension used to perform OP assays directly on particles, and to evaluate the real contribution of water-insoluble particles to PM redox properties. These experimental steps provided new insights on the driving forces of OP measurements, thus giving a very valuable contribution to the standardization of experimental procedures, allowing to interpret OP results more knowingly.

Another aspect of the study regarded the application of innovative biomonitoring techniques to field campaigns, and their reliability for the assessment of atmospheric element concentrations. PM deposited on the biomass of riparian species (*Arundo donax* (L.)), lichen transplants (*Evernia prunastri* (L.) Ach.), and holm oak (*Quercus ilex* (L)) was chemically characterized, and results were compared to those obtained from field filters collected through traditional monitoring system. The obtained results from the study of *A. donax* as PM biosampler proved the reliability of this biological approach for the evaluation of the atmospheric concentrations of PM elemental components and known source tracers of the steel plant and the vehicular traffic. Lichen transplants *E. prunastri* have demonstrated to be suitable biomonitors of Persistent Organic Pollutants (POPs), due to their ability to reflect the air concentration and spatial variability of these compounds, allowing to obtain a high spatial monitoring network. Lastly, chemical species detected on *Q. ilex* identified

non-exhaust traffic emission (i.e. brake abrasion) as the main sources of the magnetic and metallic fraction of PM bioaccumulated on leaves in the proximity of roads, and the recorded alteration of plant morpho-functional traits was linked to OP^{AA} measured on leaf-deposited PM. The innovative multidisciplinary biomonitoring study demonstrated the potential of plants as cost-effective passive air samplers for diffused monitoring and characterization of PM pollutants in distinct urban environments. This approach will permit to overcome the limits associated to the high cost of a monitoring network based on traditional PM samplers and should be promoted to detect emission sources and distribution patterns of PM when it is impossible to apply a high-density sampling instrument.

The research was also focused on the relationships between different PM-selected components and the *in vitro* generation of genotoxic and mutagenic effect on BEAS-2B cell line, which appeared to be correlated with PM chemical composition. Results highlighted that each emission source has a different genotoxic and pro-inflammatory profile, and that the cellular model, coupled with an accurate PM chemical characterization, represents a valuable tool for screening the biological activity of PM obtained from different sources.

Lastly, the complex and detailed PM chemical characterization during RHAPS project (Redox-activity and Health-effects of Atmospheric Primary and Secondary aerosol, Research Projects of National Interest) allowed to identify primary and secondary sources of PM oxidative potential from field observations. A preliminary apportion of the sources through the PCA and the PMF permitted to estimate the contribution of five main emission sources to the PM mass concentration, chemical composition and oxidative potential.

Future research will be focused on improving the understanding of different aerosol physical-chemical properties (of both primary and secondary PM) that can act and interact to influence PM toxicity in real-world conditions by applying the approaches developed and presented in this study. Furthermore, a quantitative relationship between OP results from acellular assays and ROS concentrations from cell-based assays yet to be elucidated. Therefore, the link between oxidative potential of PM and oxidative stress in toxicological assays certainly represents an area for future investigation. Analysis of PM collected in different areas, coupled with toxicological studies would be useful to further asses the oxidative stress hypothesis of particulate matter, determining the utility of OP in health studies, and improving understanding on the relationship between particulate matter and health outcomes.

10. Communications at congresses and conferences

As presenting author:

• Frezzini M.A., De Francesco N., Canepari S. "*Optimization and application of the DPPH assay for evaluating reducing properties of particulate matter*", 2019, VIII edition of Convegno Giovani Ricercatori, Chemistry Department, Sapienza University or Rome – poster presentation.

• Frezzini M.A., Fusaro L., Salvatori E., Manes F., Canepari S. "*Effects of PM deposition on vegetation in urban environment: chemical characterization and oxidative potential assays on Quercus ilex L. leaves*" ISBN: 978-88-942135-2-2, 2019, International one-day workshop "PM oxidative potential: response of acellular assays to predict PM-induced oxidative stress activity" – poster presentation.

• Frezzini M.A., Castellani F., Ristorini M., Canepari S. "*Evaluation of antioxidant properties of particulate matter by DPPH assay*", 2019,): European Aerosol Conference 2019 – EAC 2019 – poster presentation.

• Frezzini M.A., Castellani F., De Francesco N., Ristorini M., Canepari S. "*Applicazione del saggio del DPPH per la valutazione delle proprietà riducenti del particolato atmosferico*" , 2020, IX edition of Convegno Nazionale sul Particolato Atmosferico – PM2020 – oral presentation.

• Frezzini M.A., Castellani F., De Francesco N., Ristorini M., Canepari S. "*Application of DPPH Assay for Assessment of Particulate Matter Reducing Properties*", 2020, European Aerosol Conference 2020 – EAC 2020 – poster presentation.

As co-author:

• Ristorini M., Massimi L., Simonetti G., Frezzini M.A., Canepari S., Conti M.E., Mele G. "*Air quality biomonitoring in an urban and industrial hot-spot of Central Italy*", 2019, CEMEPE 2019 and SECOTOX – 7th international Conference on Environmental Management, Engineering, Planning and Economic – oral presentation.

• Ristorini M., Massimi L., Frezzini M.A., Canepari S. "*Air quality biomonitoring in an urban and industrial hot-spot of Central Italy*", 2019, VIII edition of Convegno Giovani Ricercatori, Chemistry Department, Sapienza University or Rome – poster presentation.

• Simonetti G., Massimi L., Castellani F., Frezzini M.A., Di Filippo P., Buiarelli F., Canepari S. "*Oxidative potential of particles collected in different workplaces*" ISBN: 978-88-942135-2-2, 2019, International one-day workshop "PM oxidative potential: response of acellular assays to predict PM-induced oxidative stress activity" – poster presentation.

• Fusaro L., Winkler A., Salvatori E., Macrì P., Frezzini M.A., Canepari S., Manes F. "*An integrated approach to assess the effects of particulate matter on functional traits of Quercus ilex L. in an urban area*", 2020, ICP Vegetation, 33rd Task Force Meeting – oral presentation.

• S. Canepari, L. Tofful, M.A. Frezzini, F. Marcovecchio, L. Massimi, M. Ristorini, M. Giusto, S. Pareti, E. Rantica, T. Sargolini, A. Pelliccioni, C. Perrino "*PM in ambienti di studio universitari: stagionalità, composizione chimica, sorgenti, infiltrazione dall'esterno*" , 2020, IX edition of Convegno Nazionale sul Particolato Atmosferico – PM2020 – oral presentation.

• M.L. Astolfi, G. Vitiello, M. Ristorini, M.A. Frezzini, L. Massimi, E. Marconi, M. Papi, M. Marcolini, G. Mele, S. Canepari, M. Conti "*Le api e i prodotti dell'alveare come bioindicatori della qualità dell'aria*" , 2020, IX edition of Convegno Nazionale sul Particolato Atmosferico – PM2020 – oral presentation.

• M. Ristorini, M.A. Frezzini, S. Canepari, L. Massimi "*Valutazione dell'efficienza dell'utilizzo di foglie di A. donax L. per il biomonitoraggio delle concentrazioni atmosferiche di componenti elementari di* PM_{10}" , 2020, IX edition of Convegno Nazionale sul Particolato Atmosferico – PM2020 – oral presentation.

• F. Castellani, L. Massimi, M.A. Frezzini, S. Canepari, M. Ristorini, M.E. Conti, G. Mele, M. Galletti, A. Pileri, A. Antonucci "*Mappatura di inquinanti organici aerodispersi mediante lichene Evernia prunastri in un'area a elevato impatto antropico (Italia centrale)*" , 2020, IX edition of Convegno Nazionale sul Particolato Atmosferico – PM2020 – oral presentation.

• C. Perrino, M.A. Frezzini, F. Marcovecchio, E. Rantica, S. Canepari "*Traccianti chimici del fumo da tabacco in ambienti indoor*" , 2020, IX edition of Convegno Nazionale sul Particolato Atmosferico – PM2020 – poster presentation.

• Melzi G., Nozza E., Frezzini M.A., Canepari S., Corsini E., Vecchi R., Marinovich M. "*In vitro characterization of genotoxic damage induced by various PM sources on the bronchial epithelial cell line BEAS-2B*", 2021, 56th Congress of the European Societies of Toxicology (EUROTOX 2021) – poster presentation.

11. Appendix

11.1 (E) Efficiency Evaluation of Food Waste Materials for the Removal of Pollutants from Wastewater

During the PhD, a parallel line of research was focused on the evaluation of the potential of food waste materials as low-cost adsorbents for the removal of toxic elements, especially volatile organic compounds (VOCs) from wastewater. Release of wastewater particularly rich pollutants from industrial activities is a critical environmental problem. In the last few years, environmental remediation was focused on the use of low-cost adsorbents for the removal of toxic compounds from wastewater. In fact, adsorption is recognized as an effective and economic method for the removal of metals and metalloids because it offers high efficiency and flexibility in operation. Among lo- cost materials, food waste adsorbents compete favorably in terms of cost, efficiency, and ease of operation.

In this research, eight food waste materials (banana peel, potato peel, apple peel, lemon peel, coffee waste, decaf coffee waste, grape waste, and carob peel) were evaluated as potential low-cost biosorbents, comparing their efficiency for the removal of 24 VOCs from synthetic multi-component standard solutions, maintaining homogeneous experimental conditions, which allowed comparing the adsorption capacity of the individual adsorbents. Furthermore, the performances of the food waste materials as biosorbents in a real polluted matrix were investigated by exposing each food waste sorbent to an urban solid waste leachate. Lastly, the adsorption capacity was assessed through the characterization of Langmuir and Freundlich adsorption isotherms as predictive models to better investigate adsorption process and to study the distribution of molecules subjected to adsorption.

Food waste materials, that are available in large amount and at very low costs, appeared to be promising biosorbents for VOCs in aqueous solutions. However, this is a field of ongoing research and constitutes an interesting issue that still need further investigation.

11.1.1 (E1) Food Waste Materials Appear Efficient and Low-Cost Adsorbents for the Removal of Organic and Inorganic Pollutants from Wastewater

Res. & Dev. in Material Science (2018), 5(2), 1-3, doi: 10.0.121.55/RDMS.2018.05.000608

Maria Agostina Frezzini [a], Antonella Giuliano [a], Joshua Treacy [b], Silvia Canepari [a], Lorenzo Massimi [a,*]

[a] Sapienza University of Rome, Department of Chemistry, Piazzale Aldo Moro, 5, 00185 Rome, Italy;

[b] DIT, Dublin Institute of Technology, School of Chemistry & Pharmaceutical Sciences, Kevin Street, Dublin 2, Dublin, Ireland.

* Corresponding author

1. Opinion

Excessive release of organic and inorganic pollutants, due to urbanization and industrialization is a critical environmental problem worldwide [1]. In fact, discharge of wastewater from industrial activities releases effluents particularly rich in toxic and carcinogenic pollutants. In the last few years, environmental remediation was focused on the use of low-cost adsorbents for the removal of metals and metalloids from wastewater.

There are several physic-chemical methods to remove elements from wastewater (chemical precipitation, solvent extraction, reverse osmosis, adsorption, ion exchange and chemical reduction) [1–2]. Adsorption is recognized as an effective and economic method because it offers high efficiency and flexibility in operation [3]. The adsorption phenomenon, in which the transfer of matter is provided from a gas, liquid or dissolved solid phase (adsorbate) to a solid biological adsorbent surface (biosorbent) in contact with it, can be called: "biosorption".

Different biomaterials with high specific surface areas like activated carbons, resins and zeolites have been widely used for heavy metal wastewater treatment. However, to minimize the cost, alternative approaches have been developed using low-cost materials such as agricultural waste by-products [4]. These include the use of modified clay [5-6], soil [7], seed powder [8], sugar cane bagasse [9], coffee and tea waste [10–11], neem bark [12] maize tassels [13], modified coconut fiber [14], coconut husk [15], rice husk [16], oil palm shell [17], fly ash, lime, agricultural ash and saw dust [18–19].

Among these low-cost materials, food waste adsorbents compete favorably in terms of cost, efficiency and ease of operation [20]. Moreover, with the aim of sustainable development, recycling food waste, which amounts to US $680 billion in industrialized countries and US $310 billion in developing countries [21], is beneficial. Food waste adsorbents do not require modification reaction like other materials used in adsorption processes [22]; technical applicability and cost advantages are two key factors for the selection of food waste as low-cost adsorbents for treating wastewater.

In recent studies, the adsorption capacity of several food waste materials (banana peel [22], apple peel [23], eggplant peel [24], potato peel [25], orange peel [26], lemon peel [27-28], watermelon peel [29-30], tomato

peel [31], coffee waste [10-11-32-33] decaf coffee waste, carob peel and grape waste [34-35]) has been assessed by performing adsorption experiments in heterogeneous operating conditions.

Fig. 1. Food waste materials' processing [36].

In a latest study [37], the efficiency of such food waste materials for the removal of metals and metalloids from complex multi-element solutions was evaluated in homogeneous experimental conditions, which allowed to compare the adsorption capacities of the individual adsorbents. The pH selected for the adsorption experiments were pH 2.0 and pH 5.5. The removal efficiency of the food waste adsorbents was also verified on a real polluted matrix; coffee waste and decaf coffee waste resulted the most efficient food waste adsorbents for the removal of Cu, watermelon peel for Pb and grape waste for Ni and Zn. This data confirmed the results obtained by the adsorption experiments performed in synthetic multi-element solutions. Banana peel, watermelon peel and grape waste resulted the most efficient and the least selective adsorbents for the removal of most of the metals and metalloids. Furthermore, the adsorbent surfaces of the food waste materials were analysed by FTIR spectroscopy and showed different types and amounts of functional groups, which demonstrated to act as adsorption active sites for various elements [37].

Considering the high efficiency of the examined low-cost adsorbents for the removal of inorganic pollutants, preliminary studies were conducted in our lab for assessing the potential of the investigated food waste materials to adsorb volatile organic compounds from a real polluted matrix of leachate. Some recent studies have shown the efficiency of low-cost materials for the removal of industrial organic dyes [38-33-39], polycyclic aromatic hydrocarbons [40] and phenolic compounds [41]. However, the food waste adsorbents' efficiency for the removal of volatile organic compounds was not investigated.

Our preliminary studies showed good adsorption capacities of the examined food waste materials for aliphatic and aromatic hydrocarbons. Therefore, it is worth to carry out further studies about volatile organic compounds' removal by food waste adsorbents.

References

1. Fu, F., & Wang, Q. (2011). Removal of heavy metal ions from wastewaters: a review. *Journal of environmental management*, *92*(3), 407-418.

2. Owlad, M., Aroua, M. K., Daud, W. A. W., & Baroutian, S. (2009). Removal of hexavalent chromium-contaminated water and wastewater: a review. *Water, Air, and Soil Pollution*, *200*(1-4), 59-77.

3. Kamar, F. H., Craciun, M. E., & Nechifor, A. C. (2014). Heavy metals: sources, health effects, environmental effects, removal methods and natura l adsorbent material as low-cost adsorbent: short review. Int JScientifi c Engineer Technol Res, 3, 2974-2979.

4. Hegazi, H. A. (2013). Removal of heavy metals from wastewater using agricultural and industrial wastes as adsorbents. *HBRC Journal*, *9*(3), 276-282.

5. Singh, S. P., Ma, L. Q., & Harris, W. G. (2001). Heavy metal interactions with phosphatic clay. *Journal of Environmental Quality*, *30*(6), 1961-1968.

6. Stathi, P., Litina, K., Gournis, D., Giannopoulos, T. S., & Deligiannakis, Y. (2007). Physicochemical study of novel organoclays as heavy metal ion adsorbents for environmental remediation. *Journal of colloid and interface science*, *316*(2), 298-309.

7. Covelo, E. F., Vega, F. A., & Andrade, M. L. (2006). Heavy metal adsorption and desorption by a Eutric Regosol and a District Regosol. In *Geophysical Research Abstracts* (Vol. 8, p. 04553).

8. Mataka, L. M., Henry, E. M. T., Masamba, W. R. L., & Sajidu, S. M. (2006). Lead remediation of contaminated water using Moringa Stenopetala and Moringa oleifera seed powder. *International Journal of Environmental Science & Technology*, *3*(2), 131-139.

9. Mohan, D., & Singh, K. P. (2002). Single-and multi-component adsorption of cadmium and zinc using activated carbon derived from bagasse—an agricultural waste. *Water research*, *36*(9), 2304-2318.

10. Tan, W. T. (1985). Copper (II) adsorption by waste tea leaves and coffee powder. Pertanika 1985, 8, 223–230.

11. Agwaramgbo, L., Lathan, N., Edwards, S., & Nunez, S. (2013). Assessing lead removal from contaminated water using solid biomaterials: Charcoal, coffee, tea, fishbone, and caffeine. *Journal of Environmental Protection*, *4*(07), 741.

12. Ayub, S.; Ali, S.I.; Khan, N.A. Efficiency evaluation of neem (Azadirachta indica) bark in treatment of industrial wastewater. Environ. Pollut. Control J. 2001, 4, 34–38.

13. Zvinowanda, C.M.; Okonkwo, J.O.; Shabalala, P.N.; Agyei, N.M. A novel adsorbent for heavy metal remediation in aqueous environments. Int. J. Environ. Sci. Technol. 2009, 6, 425–434.

14. Igwe, J.C.; Abia, A.A.; Ibeh, C.A. Adsorption kinetics and intraparticulate diffusivities of Hg, As and Pb ions on unmodified and thiolated coconut fiber. Int. J. Environ. Sci. Technol. 2008, 5, 83–92.

15. Tan, W.T.; Ooi, S.T.; Lee, C.K. Removal of chromium (VI) from solution by coconut husk and palm pressed fibres. Environ. Technol. 1993, 14, 277–282.

16. Srinivasan, K.; Balasubramanian, N.; Ramakrishna, T.V. Studies on chromium removal by rice husk carbon. Indian J. Environ. Health 1988, 30, 376–387.

17. Khan, N.A.; Shaaban, M.G.; Hassan, M.A. Removal of heavy metal using an inexpensive adsorbent. Proceedings of UM Research Seminar, University of Malaya, Kuala Lumpur, Malaysia, 11–12 March 1988; pp. 1–5.

18. Ajmal, M.; Rao, R.A.K.; Siddiqui, B.A. Studies on removal and recovery of Cr (VI) from electroplating wastes. Water Res. 1996, 30, 1478–1482.
19. Aliabadi, M., Morshedzadeh, K., & Soheyli, H. (2006). Removal of hexavalent chromium from aqueous solution by lignocellulosic solid wastes. *International Journal of Environmental Science & Technology*, *3*(3), 321-325.
20. Mohammed, M. A., Shitu, A., Tadda, M. A., & Ngabura, M. (2014). Utilization of various Agricultural waste materials in the treatment of Industrial wastewater containing Heavy metals: A Review. *International Research Journal of Environmental Science*, *3*(3), 62-71.
21. Gustafsson, J., Cederberg, C., Sonesson, U., & Emanuelsson, A. (2013). The methodology of the FAO study: Global Food Losses and Food Waste-extent, causes and prevention" -FAO, 2011.
22. Castro, R. S., Caetano, L., Ferreira, G., Padilha, P. M., Saeki, M. J., Zara, L. F., ... & Castro, G. R. (2011). Banana peel applied to the solid phase extraction of copper and lead from river water: preconcentration of metal ions with a fruit waste. *Industrial & Engineering Chemistry Research*, *50*(6), 3446-3451.
23. Mallampati, R., & Valiyaveettil, S. (2013). Apple Peels: A Versatile Biomass for Water Purification?. *ACS applied materials & interfaces*, *5*(10), 4443-4449.
24. Ibrahim, T. H., Babar, Z. B., & Khamis, M. I. (2015). Removal of Lead (II) Ions from Aqueous Solution Using Eggplant Peels Activated Charcoal. *Separation Science and Technology*, *50*(1), 91-98.
25. Aman, T., Kazi, A. A., Sabri, M. U., & Bano, Q. (2008). Potato peels as solid waste for the removal of heavy metal copper (II) from waste water/industrial effluent. Colloids and Surfaces B: Biointerfaces, 63(1), 116-121.
26. Ugbe, F. A., Pam, A. A., & Ikudayisi, A. V. (2014). Thermodynamic properties of chromium (III) ion adsorption by sweet orange (Citrus sinensis) peels. *American Journal of Analytical Chemistry*, *5*(10), 666.
27. Razafsha, A., & Ziarati, P. (2016). Removal of Heavy Metals from Oryza sativa Rice by Sour Lemon Peel as Bio-sorbent. *Biomedical and Pharmacology Journal*, *9*(2), 543-553.
28. Arslanoglu, H., Altundogan, H. S., & Tumen, F. (2009). Heavy metals binding properties of esterified lemon. *Journal of hazardous materials*, *164*(2-3), 1406-1413.
29. Lakshmipathy, R., & Sarada, N. C. (2013). Application of watermelon rind as sorbent for removal of nickel and cobalt from aqueous solution. *International Journal of Mineral Processing*, *122*, 63-65.
30. Lakshmipathy, R., Vinod, A. V., & Sarada, N. C. (2013). Watermelon rind as biosorbent for removal of Cd2+ from aqueous solution: FTIR, EDX, and Kinetic studies. *J Indian Chem Soc*, *90*, 1147-1154.
31. Mallampati, R., & Valiyaveettil, S. (2012). Application of tomato peel as an efficient adsorbent for water purification—alternative biotechnology?. *RSC Advances*, *2*(26), 9914-9920.
32. Kyzas, G. Z. (2012). Commercial coffee wastes as materials for adsorption of heavy metals from aqueous solutions. *Materials*, *5*(10), 1826-1840.

33. Kyzas, G. Z., Bikiaris, D. N., Kostoglou, M., & Lazaridis, N. K. (2013, January). Copper removal from aqueous systems with coffee wastes as low-cost materials. In *E3S Web of Conferences* (Vol. 1). EDP Sciences.

34. Polat, S., Putun, E., Kilic, M., & Putun, A. E. (2013). Biosorption of Cu (II) from aqueous solution by grape waste: Equilibrium, Kinetics and Thermodynamics. *Journal of Selcuk University Natural and Applied Science*, 108-119.

35. Dwyer, K., Hosseinian, F., & Rod, M. (2014). The market potential of grape waste alternatives. *Journal of Food Research*, *3*(2), 91.

36. Climate Change. North American Initiative on Food Waste Reduction and Recovery: http://www.cec.org/our-work/projects/north-american-initiative-food-waste-reduction-and-recovery.

37. Massimi, L., Giuliano, A., Astolfi, M. L., Congedo, R., Masotti, A., & Canepari, S. (2018). Efficiency Evaluation of Food Waste Materials for the Removal of Metals and Metalloids from Complex Multi-Element Solutions. *Materials*, *11*(3), 334.

38. Ali, I., Asim, M., & Khan, T. A. (2012). Low cost adsorbents for the removal of organic pollutants from wastewater. *Journal of environmental management*, *113*, 170-183.

39. Crini, G. (2006). Non-conventional low-cost adsorbents for dye removal: a review. *Bioresource technology*, *97*(9), 1061-1085.

40. Crisafully, R., Milhome, M. A. L., Cavalcante, R. M., Silveira, E. R., De Keukeleire, D., & Nascimento, R. F. (2008). Removal of some polycyclic aromatic hydrocarbons from petrochemical wastewater using low-cost adsorbents of natural origin. *Bioresource technology*, *99*(10), 4515-4519.

41. Ahmaruzzaman, M. (2008). Adsorption of phenolic compounds on low-cost adsorbents: a review. *Advances in colloid and interface science*, *143*(1-2), 48-67.

11.1.2 (E2) Food Waste Materials as Low-cost Adsorbents for the Removal of Volatile Organic Compounds from Wastewater

Materials (2019), 12, 4242, doi: 10.3390/ma12244242

Maria Agostina Frezzini, Lorenzo Massimi, Maria Luisa Astolfi, Silvia Canepari, Antonella Giuliano *

Department of Chemistry, Sapienza University of Rome, Piazzale Aldo Moro, 5, 00185 Rome, Italy.

* Corresponding author

Keywords: volatile organic compounds; adsorption; environmental remediation; food waste materials; wastewater treatment

Abstract

The aim of this work was to study the potential of food waste materials (banana peel, potato peel, apple peel, lemon peel, coffee waste, decaf coffee waste, grape waste, and carob peel) as low-cost adsorbents for the removal of aliphatic and aromatic volatile organic compounds (VOCs) from wastewater. The ability of examined food waste materials to adsorb VOCs from synthetic multi-component standard solutions was evaluated and the examined food waste materials showed high removal efficiency. Performances of coffee waste, grape waste, and lemon peel were detailed by using Trichloroethylene and p-Xylene in mono-component standard solutions. The adsorption capacity of the three selected food wastes was determined by using linear Langmuir and Freundlich isotherm models. Two errors functions, average percentage error (APE) and the chi-square test ($\chi 2$), were used for isotherm optimization prediction. Freundlich isotherm well described the adsorption of VOCs on the considered materials. According to the obtained results, a multilayer, physical, and cooperative adsorption process was hypothesized, particularly evident when the VOCs' concentrations are high. This was confirmed by the high adsorption efficiency percentages (E% > 80%) of VOCs from a real polluted matrix (urban solid waste leachate), containing high concentrations of total organic content.

1. Introduction

Volatile organic compounds (VOCs), aliphatic and aromatic, are a wide class of organic pollutants extensively released in the environment from a variety of anthropogenic sources such as fuel storage and transport, industrial operations [1], manufacture and storage of paints, and combustion processes [2]. Most of the VOCs can cause direct and indirect harmful effects to humans as well as the environment. Moreover, they represent one of the main causes of chronic contamination, especially in industrialized countries, since their chemical and physical properties enable them to persist in the environment. Chlorinated volatile organic compounds (Cl-VOCs) and aromatic hydrocarbons (BTEXs; benzene, toluene, and xylenes) are ubiquitous contaminants frequently detected in the environment. Therefore, human exposure to Cl-VOCs and BTEX is very common; they enter the body through multiple routes, such as inhalation, ingestion, and dermal absorption [3–5]. The

toxicity of these compounds is increased by the fact that VOCs are strongly lipophilic with a capacity to concentrate in fat deposits by determining a long-term exposure [6-7]. Since the beginning of the 20th century, Cl-VOCs were extensively used as solvents for processes such as dry cleaning, production of pesticides, paints, and refrigerants [8,9]. Among them, Trichloroethylene is one of the most prevalent and persistent contaminants detected in polluted environments [10] and has been classified as group 2A by IARC (International Agency for Research on Cancer), as probably carcinogenic to humans [11]. In fact, exposure to Trichloroethylene seems to cause harmful effects on central nervous system and on the immune and endocrine systems in adults [12], and may also contribute to certain types of cancers in adults and children [9].

BTEXs, which have been found mainly in sites contaminated by petrol, gasoline, and petrochemical products [13,14], are well known carcinogens [12,15] that can adversely affect various human organs [16] by causing, for example, irritation of the eyes and reduction of bone marrow function [17]. Hence, it appears indispensable to eliminate these hazardous and mutagenic chemicals from the environment [19].

Several methods for wastewater decontamination from organic pollutants are reported [19–22]. Among these, the adsorption process has been efficaciously used for the removal of organic as well as inorganic compounds from wastewater because of its safety and ease in operation [23–26]. One of the most used materials to adsorb organic pollutants is activated carbon [25,27–29]; however, it has some disadvantages, such as the high cost and the environmental problems related to the regeneration and disposal of its waste [30,31]. During the past years, several studies have been focused on the evaluation of low-cost and environmentally friendly technologies for the removal of pollutants from wastewater. Most of these studies regarded low-cost materials, mainly biosorbents, which were found to be able to reduce availability and concentration of some organic compounds (mainly industrial organic dyes, polycyclic aromatic hydrocarbons, and phenolic compounds) [19,21,30–34].

Among the biosorbents, food waste materials appeared to be efficient for the removal of inorganic pollutants from wastewaters [35–41]. In a recent paper [42], food waste adsorbents were tested on a real polluted matrix and they showed high removal efficiency of various heavy metals. Biosorption by food waste materials has several benefits such as low production costs [43], free availability, and possible reuse of the biosorbents [44]. Moreover, it is essential to use waste as raw material for new products and new applications [45] as a renewable source of biomass [35]. The use of such residual materials might become a viable alternative for wastewater treatment with associated environmental and economic benefits [46].

Since the high danger of volatile organic compounds for humans and the environment along with the scarce amount of studies regarding the biosorption of VOCs by food waste materials, the evaluation of the performances of these materials as VOCs adsorbents constitutes an interesting issue that still should be investigated.

In this study, eight food waste materials (banana peel, potato peel, apple peel, lemon peel, coffee waste, decaf coffee waste, grape waste, and carob peel) were evaluated as potential low-cost biosorbents for the removal of VOCs from wastewater. With this aim, their adsorption efficiency and capacity of aliphatic/aromatic VOCs

from multi-component and mono-component synthetic solutions and from a real polluted matrix were explored.

2. Materials and Methods

2.1. Preparation of the Biosorbents

Food waste powders (n = 8) were employed as low-cost adsorbents: banana peel, potato peel, apple peel, lemon peel, coffee waste, decaf coffee waste, grape waste and carob peel (Figure A1, Appendix A). Preparation of the biosorbents followed the procedure detailed in a recent study [42]. Briefly, food waste materials were sun-dried for a week, grinded with a mortar and sieved to retain particles sized between 0.25 and 0.125 mm. The obtained powders were washed three times with deionized water (produced by an integrate water purification system; Arioso UP 900; Industrial Scientific Corporation, Pittsburg, PA, USA), dried at 55 °C for 48 h in a vacutherm oven (Heraeus VT 6025; Kendro Laboratory Products, Hanau, Germany), and then weighed on an analytical balance (Gibertini Europe 60; Gibertini Elettronica Srl, Milano, Italy).

2.2. Adsorption Experiments

First, removal efficiency of organic pollutants was explored by exposing each biosorbent to a synthetic multi-standard solution containing both aliphatic and aromatic VOCs (Trans-1,2-Dichloroethene, Dichloromethane, 1,1-Dichloroethene, 1,1-Dichloroethane, Chloroform, Carbon tetrachloride, Trichloroethylene, 1,2-Dichloropropane, 1,1,2-Trichloroethane, Tetrachloroethylene, Dibromochloromethane, 1,1,2-Tetrachloroethane, Bromoform, Methyl tert-butyl ether, Benzene, Toluene, Chlorobenzene, Ethylbenzene, m,p-Xylene, o-Xylene, 1,3-Dichlorobenzene, 1,4-Dichlorobenzene, 1,2-Dichlorobenzene). In these preliminary trials, 100 mg of each adsorbent was exposed to 10 mL multi-standard solutions at 20 µg/L by using 20 mL glass vials, hermetically sealed. Multi-standard solutions were obtained by diluting 2 mg/L multi-component solution, prepared by mixing proper aliquots of aliphatic and aromatic standard stock solutions (SPEX CertiPrep, Metuchen, New Jersey, USA) in methanol.

The adsorption kinetic was assessed by keeping both the mass of each waste material (100 mg) and the VOCs concentration (20 µg/L) constant, while increasing exposure time from 1 h to 24 h (1, 2, 3, 4, 5, 6, and 24 h).

All the samples were analysed to determine the equilibrium concentration (C_e), which is the amount of adsorbate remaining in solution after adsorption processes. Multi-component standard solutions without biosorbent were always treated together with each sample set, to trace and control possible VOCs' concentration variability due to loss by evaporation during treatment; VOCs' concentration of these solutions was used as initial concentration (C_0).

The performances of the food waste materials as biosorbents in a real polluted matrix were tested by exposing 100 mg of each food waste sorbent to 10 mL of an urban solid waste leachate. The same procedure described for the synthetic multi-standard solutions was applied to perform the exposure experiments and to determine C_0 and C_e. The total organic content (TOC) of this solution was measured by a TOC analyzer (TOC-VCSH; Shimadzu Corporation, Kyoto, Japan).

The pH of both multi-standard solutions and real polluted matrix, with and without biosorbents, was measured using a pH meter (Criston MicropH 2002, Crisonb Instruments, Barcelona, Spain).

According to results obtained from the just described preliminary trials, two selected target VOCs were chosen for deepening the study of adsorption behavior in synthetic mono-component solutions. Trichloroethylene and p-Xylene were representatives of aliphatic and aromatic classes, respectively. In these trials, adsorption capacity was calculated for three selected food wastes by varying VOCs' concentration in the range 25–2000 µg/L and by keeping constant at 100 mg the adsorbent amount. Coffee waste, grape waste, and lemon peel were chosen for this experimental procedure as biosorbents, with reference to a recent paper in which all the considered food waste materials were characterized in detail by scanning electronic microscopy (SEM), Fourier transform infrared spectroscopy (FTIR), and principal component analysis (PCA) [40]. Specific surface areas were estimated by analyzing 1 g of each adsorbent by krypton gas physisorption (Porosimeter 3Flex 3500; Micromeritrics, GA, USA). Obtained values were included in the range 0.1–0.5 m^2/g. These values were close to the detection limit of the technique and the high uncertainties (about 0.05 m^2/g) did not allow a reliable comparison among materials.

Aromatic and aliphatic VOCs considered in this work were identified by comparison with the analytes registered in NIST Mass Spectral Library (1.6 NIST MS Software Version 2.3) of static headspace gas chromatography coupled to mass spectrometry (SHS-GC-MS) (probability of more than 70%) and quantified.

2.3. GC Analysis

Static headspace gas chromatography coupled to mass spectrometry (SHS-GC-MS; QHSS-40 Headspace sampler, QUMA Elektronik & Analitik GmbH, Wuppertal, Germany; Varian 431-GC and Varian 210-MS, Varian, California, CA, USA) was used for all the VOCs' analyses. After having chosen the exposure time, the glass vials containing the solutions (with or without the biosorbent) were maintained under stirring for 23 min at the constant temperature of 80 °C, then 1 µL of the vapor phase was injected in a capillary column (VF-624 30 m × 0.25 mm × 1 µm; stationary phase composition: equivalent of a 6% cyanopropyl-phenyl/94% dimethylpolysiloxane) with a Hamilton syringe (Hamilton Company, Bonaduz, Switzerland). Helium was used as carrier gas at the flow rate of 1 mL/min. The temperature was kept at 35 °C for 2 min, then it was increased to 50 °C at the rate of 6 °C per minute and, lastly, to 180 °C at the rate of 12 °C per minute. The total duration of the chromatographic run was 16 min.

Chromatograms were registered in selective ion monitoring mode (SIM) by selecting specific mass to charge ratios (m/z) for each analyte. The conditions employed to mass spectrometry and selected fragments and retention times of the considered VOCs and are summarized in Table A1 and Table A2 (Appendix A), respectively.

Final volume of each analysed sample was 10 mL and all the experiments were performed in triplicate. External standard solutions were used for quantification.

2.4. Calculation of Adsorption Efficiency and Adsorption Capacity

Adsorption efficiency (*E%*) was calculated by the following equation:

$$E\%= \left[\frac{(C_0 - C_e)}{C_0}\right] \cdot 100\%, \quad (1)$$

where C_0 (µg/L) is the inlet VOCs' concentration and C_e (µg/L) is the equilibrium concentration after the adsorption process.

Regarding real polluted matrix, for identified species, the adsorption efficiency was roughly estimated by comparing the peak areas in the presence (A_e) and in the absence (A_0) of the biosorbent ($E\%= \left[\frac{(A_0 - A_e)}{A_0}\right] \cdot 100\%$) after adsorption processes.

Adsorption capacity Q_e (µg/g) was determined by following the procedure described in Wang et al. [47], using a mass equilibrium equation:

$$Q_e= \frac{[(C_0 - C_e) \cdot V]}{m}, \quad (2)$$

where V is the volume of solution (L) inside the vial and m is the amount (g) of food waste powder.

2.5. Adsorption Isotherms

The characterization of adsorption isotherms is considered one of the most appropriate methods for the assessment of the adsorbent capacity [47]. Adsorption isotherms play an important role in the predictive modelling procedures to understand what is going on during adsorption process and indicate how molecules, subjected to adsorption, distribute themselves between liquid and solid phases at equilibrium [48,49]. Linear regression analysis was used to obtain adjustable isotherm parameters. Table 1 summarizes the linear forms of Langmuir and Freundlich isotherm models used for this adsorption study. Although Langmuir isotherm model could be linearized into four different types, the reported Langmuir equation, defined Type I, is the most popular linear form used in available literature [50].

Table 1. Linear forms of Langmuir (Type I) and Freundlich isotherm models.

Isotherm Models	**Linear**
Langmuir	$\frac{C_e}{Q_e} = \frac{1}{(K_L \cdot q_m)} + \frac{C_e}{q_m}$
Freundlich	$\ln Q_e = \ln K_F + \left(\frac{1}{n} \cdot \ln C_e\right)$

For Langmuir isotherms, C_e (mg/L) is the equilibrium concentration after adsorption process, Q_e (mg/g) is the adsorption capacity, q_m (mg/g) and K_L (in L/mg) are sorption equilibrium constants. The constant K_L is related to the free energy of adsorption and indicates affinity between the VOCs and the adsorbents [51].

In Freundlich isotherm, K_F (mg/L) and n (dimensionless) are both constants indicative of sorption capacity and sorption intensity, respectively [52,53]. In particular, n indicates the favorability of the adsorption process [52]; a close to unit n value represents good adsorption capacity, meaning VOCs' adsorption is favorable [52]. The evaluation of the correlation coefficients (R^2) is useful to predict which model best matches with the experimental data. In addition, the average percentage error (*APE*) and chi-square test (χ^2) values were

calculated in order to verify the validity of the isotherm models. APE and χ^2, defined ad distribution functions, indicate the fit between the experimental and the predicted values of the adsorption capacity [54] and were used for isotherm optimization prediction [49]: if data from the model are similar to the obtained experimental data, the function values will be small number. APE and χ^2 were calculated as follows:

$$APE\ (\%) = \left[\frac{\sum_{i=1}^{N}\left|\frac{\left(Q_{e,exp} - Q_{e,pre}\right)}{Q_{e,exp}}\right|}{N}\right] \cdot 100, \qquad (3)$$

$$\chi^2 = \sum_{i=1}^{N} \frac{\left(Q_{e,exp} - Q_{e,pre}\right)^2}{Q_{e,pre}},$$

where $Q_{e,exp}$, $Q_{e,pre}$ are experimental and predicted adsorption capacity, respectively; N is the number of observations in the experimental data.

3. Results and Discussion

3.1. Adsorption Efficiency from Multi-Component Solutions

Preliminary tests on synthetic multi-component solutions were performed in order to verify the general behavior of the considered food waste materials as VOCs' biosorbents. First, the rate of the adsorption process was evaluated by exposing the materials to a synthetic mixture of aromatic and aliphatic VOCs for increasing times (1, 2, 3, 4, 5, 6, and 24 h). As shown in Figure A2 (Appendix A), preliminary tests confirmed that 1 h contact time was enough to reach a steady-state VOC concentration, regarding both the liquid/solid and the liquid/gas interfaces. Consequently, all the successive samples were analysed after one hour from preparation. Adsorption efficiency of each examined food waste material (100 mg) from a mixture of aliphatic and aromatic VOCs at 20 µg/L is reported in Table 2. Data show that all the considered biosorbents exhibited some adsorption properties towards organic species; the efficiency of adsorption was very low for some compounds and for some investigated adsorbents, with some exceptions. Coffee and decaf coffee waste appeared to be the most efficient for the removal of most of the organic compounds. For example, among the aromatic compounds, p-Xylene, o-Xylene, 1,2-Dichlorobenzene, 1,3-Dichlorobenzene, and 1,4-Dichlorobenzene were adsorbed in high percentages (*E%* > 50%); within the aliphatic compounds, Trichloroethylene, Tetrachloroethylene, and 1,1,2-Tetrachloroethane showed more than 40% of adsorption efficiency in presence of coffee and decaf coffee waste. Moreover, coffee waste was able to adsorb more than 90% of the Trans-1,2-Dichloroethene in multi-component solution. Apple peel seemed to be efficient for 1,1,2-Tetrachloroethane (*E%* > 50%) and for 1,2-Dichlorobenzene, 1,3-Dichlorobenzene and 1,4-Dichlorobenzene (*E%* > 30%). Lastly, it is worth noting that also grape waste adsorption efficiency is considerable for 1,2-Dichlorobenzene, 1,3-Dichlorobenzene and 1,4-Dichlorobenzene (*E%* > 40%) and 1,1,2-Tetrachloroethane (*E%* > 50%).

In general, looking at Table 2, aromatic compounds seem to be more retained than the aliphatic; moreover, coffee waste, decaf coffee waste, grape waste, and banana peel showed fairly good adsorption efficiency for both aliphatic and aromatic compounds.

Considering the efficiency of the examined low-cost adsorbents for the removal of VOCs from synthetic solutions, other experimental tests were conducted to confirm the potential of the investigated food waste materials to adsorb organic compounds from a real polluted matrix. The chosen real polluted matrix had a very high total organic content (TOC = 7500 mg/L), and a spontaneous pH of 6.5. In Table A3 (Appendix A), pH values both of multi-standard synthetic solutions and real polluted matrix are reported, with and without each adsorbent.

The real polluted matrix (a leachate of urban solid waste) contained a wide variety of VOCs; only some of them were identified by comparison with NIST library (>70% probability). The estimated adsorption efficiencies for these compounds are reported in Table 3. These data indicate that most of organic compounds is strongly retained by these adsorbents. In general, all the materials exhibited very good adsorption properties towards most of the VOCs and the results confirmed that coffee, decaf coffee, and grape waste were the most efficient biosorbents. Estimated efficiencies were much larger than those calculated in synthetic solutions. For example, coffee waste adsorption efficiency (*E%*) of Trichloroethylene was 43 ± 2 and 99 ± 12; lemon peel showed a Chlorobenzene *E%* of 10 ± 1 and 86 ± 12 and grape waste showed a m, p-Xylene *E%* of 34 ± 3 and 96 ± 5 in synthetic and real polluted matrix, respectively. This behavior may be due to the different VOCs' concentration range in real polluted sample compared to the synthetic one, and seems to indicate a cooperative mechanism of adsorption, meaning an increase in the amount of pollutants adsorbed when initial VOCs' concentration was increased. Coffee waste, decaf coffee waste, and grape waste were confirmed to be the most efficient biosorbents for the removal of both aliphatic and aromatic VOCs.

3.2. Adsorption Capacity from Synthetic Mono-Component Solutions

Adsorption processes were further investigated by studying the adsorption isotherms of selected biosorbents and VOCs. Two selected target VOCs were chosen for deepening the study of adsorption behavior in synthetic mono-component solutions. Trichloroethylene and p-Xylene were chosen as representative of aliphatic and aromatic classes, respectively. In these trials, VOCs' concentration was varied in the range of 25–2000 µg/L, keeping constant at 100 mg the adsorbent amount. Adsorption capacity was calculated for three selected food waste biosorbents (coffee waste, grape waste, and lemon peel) according to the results obtained from a previous study, in which all the considered food waste materials were analysed by scanning electronic microscopy (SEM) and Fourier transform infrared spectroscopy (FTIR) [42]. In this study, FTIR spectra were elaborated by principal component analysis (PCA) to group the food waste materials in different clusters, according to functional groups present on the adsorbents' surfaces. First cluster included orange and lemon peel, and was characterized by OH of alcohols, phenols and carboxylic acids; CH, COC, CN, PO of polysaccharides and C=C of lipids and lignin moieties; lemon peel was chosen as representative of this cluster.

Second cluster included coffee and decaf coffee waste, apple, and banana peel, and was characterized by the highest amount of CH bonds of methyl and methylene groups of lipids; coffee waste was chosen as

representative of this cluster. Third cluster included grape waste and carob peel and was characterized by the lowest amount of the identified functional groups; grape waste was chosen as representative of this cluster. Adsorption capacity of coffee waste, grape waste and lemon peel towards Trichloroethylene and p-Xylene is graphically represented in Figure 1. Plots a, b, and c show the adsorption curves of coffee waste, grape waste, and lemon peel for Trichloroethylene. As expected, the adsorption capacity of the three low-cost sorbents increases with increasing the pollutant exposure concentration. Trichloroethylene was adsorbed with the highest values of Q_e (µg/g) in presence of coffee waste, while grape waste and lemon peel were found to be less efficient. Adsorption capacity curves show a quite complex trend and seem to indicate that the adsorbent saturation was reached at the tested conditions. Figure 1 (plots d, e, f), shows the adsorption curves of coffee waste, grape waste, and lemon peel for p-Xylene. The trend of adsorption curves of p-Xylene with all the three biosorbents was in general quite similar to that seen for Trichloroethylene: an increase of adsorption capacity is observed with the increase of pollutant's concentration. p-Xylene adsorption capacity appeared to be higher than that of Trichloroethylene for all the examined food waste materials. For example, coffee waste adsorption capacity can be recalled: the highest Q_e value reached with Trichloroethylene and p-Xylene was 30 µg/g and 80 µg/g, respectively.

Table 2. Adsorption efficiency (*E%*; 100 mg of each biosorbent) of aliphatic and aromatic VOCs from multi-component synthetic solution (20 µg/L). Mean ± SD of three replicates is reported.

Adsorption Efficiency (*E%*) ± SD								
Aliphatic VOCs	**Banana Peel**	**Potato Peel**	**Apple Peel**	**Lemon Peel**	**Coffee Waste**	**Decaf C. Waste**	**Grape Waste**	**Carob Peel**
Trans-1,2-Dichloroethene	2.7 ± 0.4	0.6 ± 0.2	0.7 ± 0.4	1.6 ± 0.8	93 ± 18	7.6 ± 1.4	4.7 ± 1.6	2.3 ± 1.6
Dichloromethane	3.9 ± 0.2	5.7 ± 4.3	8.2 ± 3.2	7.1 ± 1.8	9.8 ± 0.7	13 ± 1	6.2 ± 1.9	3.7 ± 1.1
1,1-Dichloroethene	1.8 ± 0.3	1.1 ± 0.7	3.3 ± 0.8	3.1 ± 1.8	3.9 ± 0.5	12 ± 5	6.7 ± 1.2	1.7 ± 1.3
1,1-Dichloroethane	1.3 ± 0.8	5.6 ± 1.9	2.6 ± 0.2	13 ± 6	12 ± 2	16 ± 1	6.7 ± 1.7	3.1 ± 1.3
Chloroform	5.9 ± 5.4	7.2 ± 2.4	1.5 ± 0.5	5.1 ± 2.6	6.2 ± 2.3	13 ± 1	6.3 ± 1.1	7.7 ± 3.1
Carbon tetrachloride	39 ± 2	4.3 ± 1.9	11 ± 2	6.3 ± 0.3	17 ± 2	16 ± 5	37 ± 12	4.3 ± 1.7
Trichloroethylene	35 ± 1	16 ± 13	36 ± 1	44 ± 1	43 ± 2	51 ± 1	34 ± 2	36 ± 1
1,2-Dichloropropane	1.1 ± 0.2	0.9 ± 0.5	8.3 ± 6.4	4.7 ± 2.1	1.1 ± 0.2	16 ± 1	5.5 ± 3.2	3.8 ± 3.4
1,1,2-Trichloroethane	7.5 ± 6.5	5.4 ± 4.3	13 ± 5	14 ± 4	18 ± 4	25 ± 9	11 ± 1	2.5 ± 0.9
Tetrachloroethylene	17 ± 12	12 ± 4	11 ± 4	1.8 ± 0.9	35 ± 9	47 ± 10	42 ± 7	11 ± 2
Dibromochloromethane	43 ± 5	1.1 ± 0.8	2.5 ± 1.8	1.4 ± 0.8	13 ± 1	27 ± 3	11 ± 2	0.8 ± 0.3
1,1,2-Tetrachloroethane	39 ± 1	23 ± 2	57 ± 7	38 ± 1	73 ± 13	77 ± 1	51 ± 1	8.5 ± 1.8
Bromoform	57 ± 2	1.6 ± 0.9	17 ± 4	1.3 ± 0.6	19 ± 2	25 ± 2	25 ± 2	2.3 ± 0.7
Aromatic VOCs								
Methyl tert-butyl ether	1.8 ± 0.2	9.5 ± 1.9	1.8 ± 0.8	3.1 ± 2.3	10 ± 5	1.5 ± 1.4	1.5 ± 1.1	1.5 ± 1.1
Benzene	1.8 ± 0.8	2.8 ± 0.3	1.8 ± 0.2	1.3 ± 1.2	17 ± 1	19 ± 1	7.1 ± 0.5	5.9 ± 0.3
Toluene	12 ± 1	1.5 ± 1.1	8.5 ± 0.5	3.9 ± 0.3	31 ± 2	33 ± 2	19 ± 2	1.3 ± 0.8
Chlorobenzene	17 ± 1	5.5 ± 0.5	15 ± 1	10 ± 1	37 ± 1	42 ± 1	30 ± 1	2.5 ± 2.1
Ethylbenzene	7.1 ± 1.4	4.8 ± 1.8	9.5 ± 5.5	1.5 ± 0.7	28 ± 1	37 ± 3	24 ± 17	1.6 ± 0.4
m, p-Xylene	35 ± 1	12 ± 1	21 ± 1	15 ± 1	54 ± 1	56 ± 1	34 ± 3	3.3 ± 1.8
o-Xylene	28 ± 1	14 ± 3	24 ± 1	18 ± 4	57 ± 1	58 ± 1	33 ± 5	13 ± 2
1,3-Dichlorobenzene	35 ± 2	12 ± 1	34 ± 1	19 ± 2	67 ± 1	73 ± 2	48 ± 4	12 ± 1

1,4-Dichlorobenzene	43 ± 2	14 ± 1	36 ± 2	20 ± 1	68 ± 1	71 ± 1	47 ± 1	24 ± 1
1,2-Dichlorobenzene	36 ± 1	10 ± 2	37 ± 1	20 ± 2	67 ± 1	73 ± 2	47 ± 2	13 ± 2

These results agree with those obtained from the adsorption experiments in multi-component standard solutions. Coffee waste was found to be the most efficient biosorbent for the removal of both Trichloroethylene and p-Xylene. The most plausible explanation comes from the chemical-physical properties of Trichloroethylene, p-Xylene, and coffee waste composition. FTIR spectra of coffee waste showed peaks of asymmetric and symmetric stretching of hydrophobic C-H bonds of methyl and methylene groups, attributed to the presence of lipids that are available in coffee samples in large amount [42,55]. Considering that Trichloroethylene and p-Xylene are both well-known lipophilic compound [56,57], a significant adsorption on lipid-rich coffee waste was expected. Moreover, according to the SEM micrographs, coffee waste has very porous surface [42] that allows it to adsorb a higher amount of pollutants from wastewater. Finally, lemon peel turned out to be the least efficient adsorbent for Trichloroethylene and p-Xylene with the highest Q_e recorded value of 10 µg/g and 20 µg/g, respectively, probably because of its less porous surface and the presence of polar functional groups [42].

Table 3. Adsorption efficiency (E%; 100 mg of each biosorbent) of VOCs from real polluted matrix of urban solid waste leachate. Mean ± SD of three replicates is reported.

Adsorption Efficiency (*E%*) ± SD								
Aliphatic VOCs	**Banana Peel**	**Potato Peel**	**Apple Peel**	**Lemon Peel**	**Coffee Waste**	**Decaf Waste**	**C. Grape Waste**	**Carob Peel**
1,1-Dichloroethene	20 ± 5	38 ± 9	60 ± 10	79 ± 18	91 ± 16	89 ± 5	87 ± 6	71 ± 11
Dichloromethane	85 ± 11	85 ± 15	90 ± 18	96 ± 15	97 ± 9	97 ± 5	97 ± 10	93 ± 7
Chloroform	24 ± 9	13 ± 6	54 ± 12	83 ± 14	92 ± 10	93 ± 5	90 ± 9	69 ± 16
Trichloroethylene	44 ± 8	39 ± 6	56 ± 13	98 ± 16	99 ± 12	96 ± 6	97 ± 10	86 ± 9
Dibromochloromethane	8.6 ± 2.3	3.2 ± 1.4	47 ± 14	84 ± 10	95 ± 11	93 ± 2	89 ± 8	67 ± 6
Aromatic VOCs								
Toluene	31 ± 9	14 ± 7	59 ± 10	79 ± 18	93 ± 9	91 ± 9	89 ± 15	62 ± 8
Chlorobenzene	45 ± 8	15 ± 6	67 ± 18	86 ± 12	97 ± 9	93 ± 5	93 ± 7	71 ± 7
m, p-Xylene	64 ± 9	27 ± 11	78 ± 10	91 ± 14	99 ± 10	98 ± 2	96 ± 5	77 ± 10
o-Xylene	72 ± 11	26 ± 13	78 ± 12	92 ± 17	93 ± 9	95 ± 8	97 ± 9	78 ± 9
1,3-Dichlorobenzene	77 ± 13	37 ± 15	93 ± 18	98 ± 10	98 ± 7	98 ± 2	97 ± 11	87 ± 7

3.3 Adsorption Isotherms

Sorption equilibrium data for the two VOCs and the three food waste materials were fitted to the Langmuir and Freundlich isotherm models. Although many adsorption models were developed and applied in the literature [58,59], the Langmuir and Freundlich adsorption models are frequently used to describe adsorption mechanism. Although nonlinear isotherm forms are recommended in the field of batch adsorption research to avoid errors resulting from simple linear regression [49,60], in this study, linearized isotherm models were adopted due to the mathematical simplicity [51] and to immediately obtain semi-quantitative isotherm constants. Equilibrium data did not fit Langmuir model for both the studied VOCs and for the considered

biosorbents. Since Langmuir isotherm cannot be applied in this work, the corresponding data are not reported. Linearized Freundlich adsorption isotherms for Trichloroethylene and p-Xylene are reported in Figure 2.

The constants obtained by applying the Freundlich isotherm model are summarized in Table 4. The high correlation coefficients ($R^2 \geq 0.9$) obtained by plotting $\log Q_e$ versus $\log C_e$ for both Trichloroethylene and p-Xylene indicate that these adsorption processes are well represented by the Freundlich model. Lemon peel showed a lower correlation, but it's still significant.

Moreover, the values of n and K_F of the Freundlich model indicate good adsorption intensity and capacity, respectively: n was close to unity for all the examined food waste adsorbents and for both Trichloroethylene and p-Xylene, indicating that VOCs adsorption is favorable [52]. Furthermore, the low values of APE and χ^2 in association with higher R^2 generate a satisfactory fit of Freundlich model to the experimental data, even if they are little higher for lemon peel. To explain these contrasting results, the adsorption processes simulated by the two models are to be considered. Langmuir model represents only monolayer adsorption processes [46] on the outer surface of the adsorbent, without considering any further adsorption [61]. Instead, Freundlich isotherm represents heterogeneous surfaces and sorbent systems [47,62] in aqueous systems [30], in which multilayer adsorption processes are included. According to the increase of the adsorption capacity with increasing of the VOCs' concentration, a multilayer adsorption process can be hypothesized. This is also confirmed by the n values reported in Table 4. In fact, when $n < 1$, the presence of an isotherm called "solvent-affinity isotherm" is suggested [62]; this kind of isotherm represents an increase of the adsorption energy with increasing concentration of pollutants on the adsorbents' surface. Thus, it can be assumed that aliphatic and aromatic VOCs are initially weakly detained by food waste materials through an adsorption on the active sites of the sorbents. At high concentrations, the active sites are completely occupied by the compounds and the adsorption of other pollutants is supported by Van der Waals forces with the molecules already adsorbed, making a physical adsorption within adsorbent layers. The result is an effective adsorption process within the adsorbent layers, caused by strong intermolecular attractions.

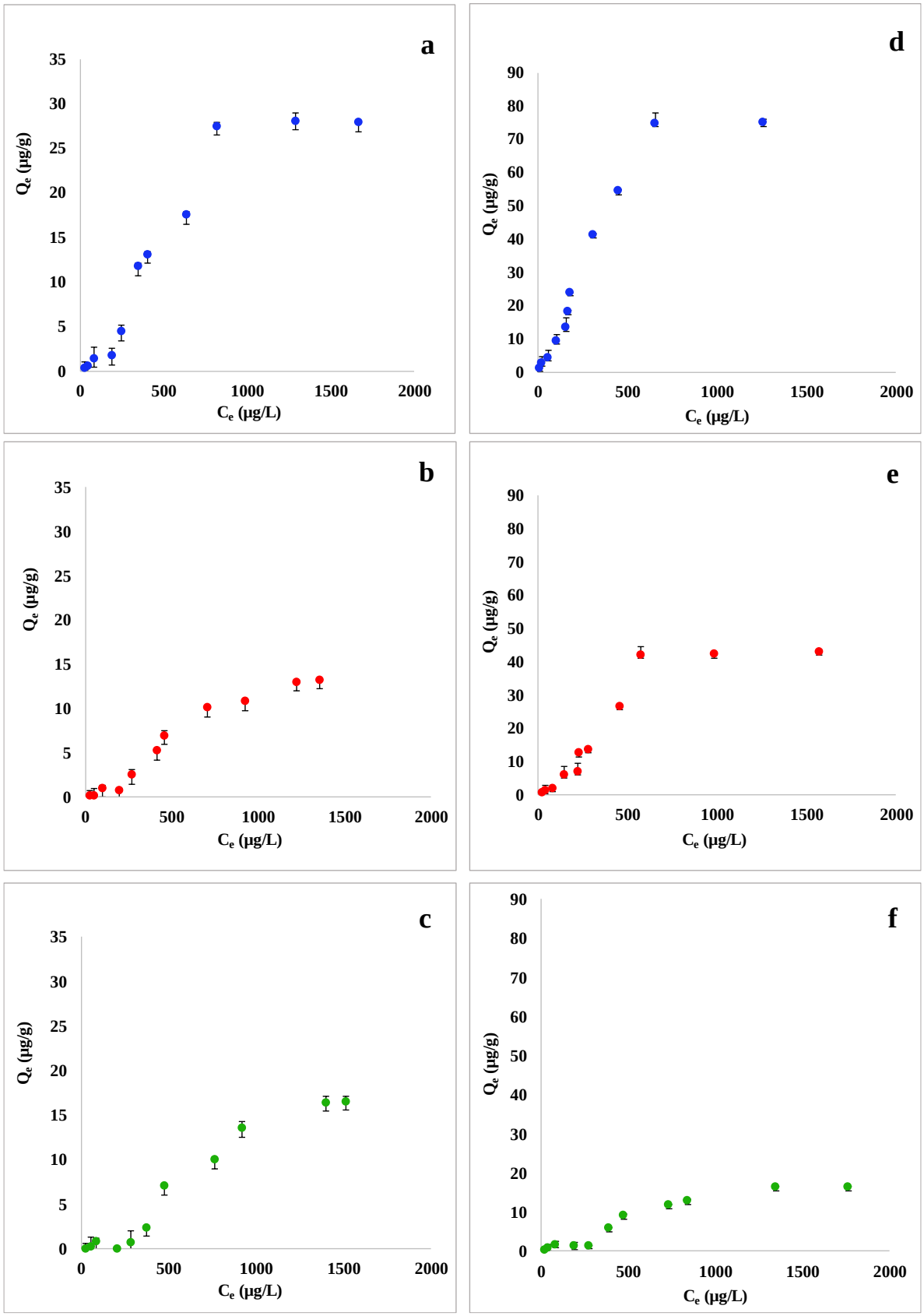

Figure 1. Comparison of adsorption capacity (Q_e, µg/g) isotherms of (**a**) coffee waste, (**b**) grape waste, and (**c**) lemon peel with Trichloroethylene (from 25 to 2000 µg/L; 100 mg of each biosorbent) and (**d**)

coffee waste, (**e**) grape waste, and (**f**) lemon peel with p-Xylene (from 25 to 2000 µg/L; 100 mg of each biosorbent). Mean ± SD of three replicates is reported.

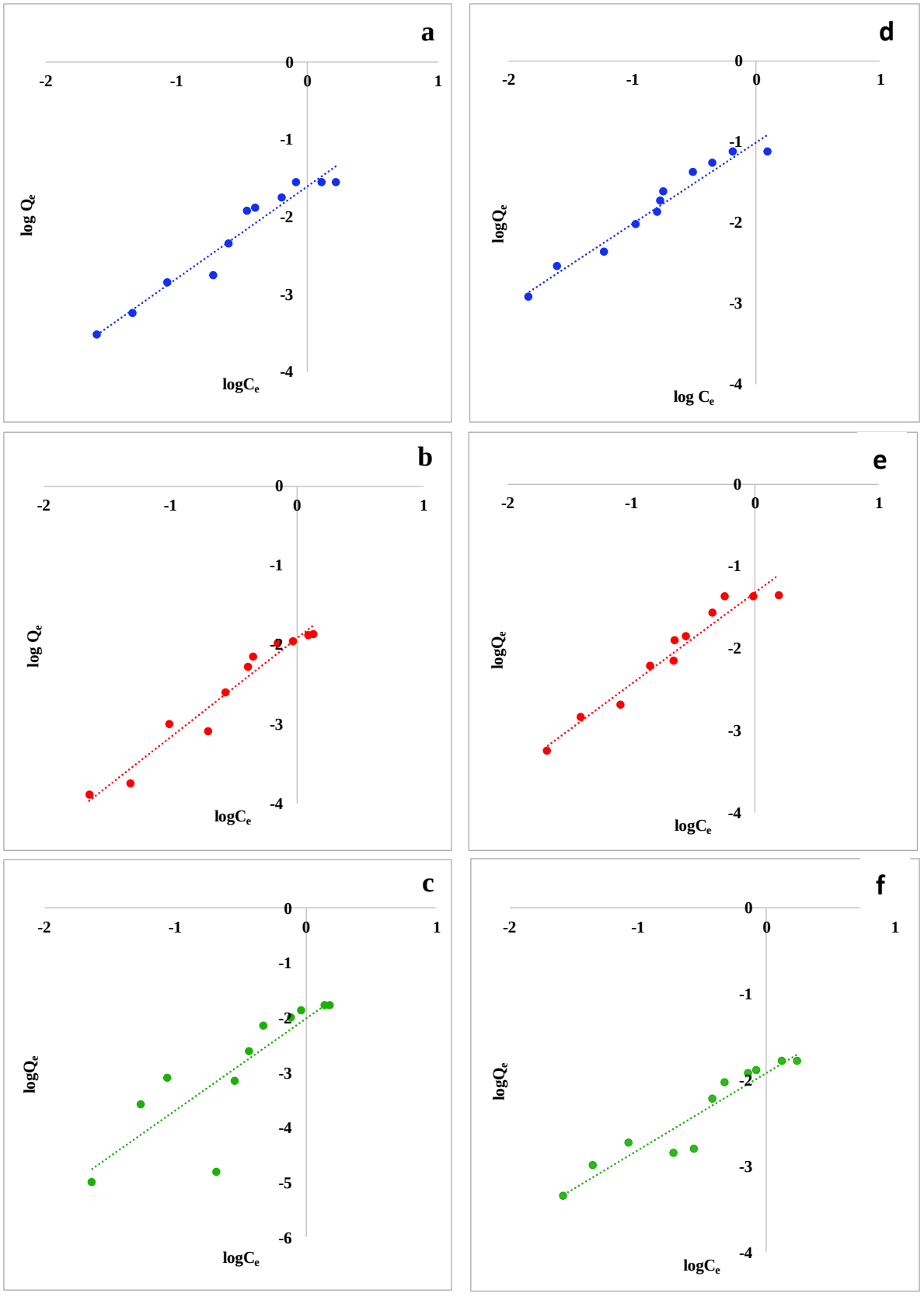

Figure 2. Freundlich isotherms for Trichloroethylene with (**a**) coffee waste, (**b**) grape waste, and (**c**) lemon peel; Freundlich isotherms for p-Xylene with (**d**) coffee waste, (**e**) grape waste, and (**f**) lemon peel.

Table 4. Parameters of Freundlich isotherm for Trichloroethylene and p-Xylene.

	K_F (mg/L)	n	R^2	APE (%)	χ^2
Trichloroethylene					
Coffee waste	0.026	0.83	0.99	2.9	3.1×10^{-5}
Grape waste	0.012	0.79	0.99	5	1.8×10^{-5}
Lemon peel	0.009	0.61	0.97	22	1.3×10^{-5}
p-Xylene					
Coffee waste	0.11	0.98	0.99	0.91	1.2×10^{-5}
Grape waste	0.051	0.89	0.98	0.86	3.4×10^{-6}
Lemon peel	0.012	1.1	0.97	8	1.1×10^{-3}

4. Conclusions

Food waste materials, that are available in large amount and at very low costs, appeared to be promising biosorbents for both aliphatic and aromatic VOCs in aqueous solutions. In general, the aromatic VOCs were better adsorbed than the aliphatic by most of the considered materials. This is confirmed by the high percentages of adsorption efficiency (*E%*).

Adsorption capacities (Q_e) of three chosen food waste materials (coffee waste, grape waste, and lemon peel) with Trichloroethylene (chosen as representative of aromatic VOCs) and p-Xylene (chosen as representative of aliphatic Cl-VOCs) were investigated; coffee waste resulted the most efficient sorbent for the removal of both considered VOCs. This is probably due to the presence of lipids in coffee samples on which Trichloroethylene and p-Xylene compounds are efficiently adsorbed, due to their lipophilic nature.

Adsorption equilibrium isotherms showed that coffee waste is the most efficient material for both p-Xylene and Trichloroethylene adsorption. In all the examined systems, the sorption processes followed much more closely the Freundlich than the Langmuir isotherm model. This indicates a physical adsorption mechanism thanks to London-Van der Waals forces between solute and sorbent, through a cooperative adsorption mechanism, in which the already adsorbed molecules on the sorbent's surface facilitate the adsorption of other molecules. This kind of physical adsorption may be particularly beneficial in field applications, because it gives the adsorbents an opportunity to have great adsorption performance at high pollutant concentrations.

Evaluation of food waste performances as biosorbents in field still needs further deepening, such as the effects of pH on removal capacity, the assessment of the effects of sorbents' particle size, the investigation of repetitive adsorption desorption cycles for material reusability investigation, or even the comparison between other food waste materials' adsorption capacity. Taking into account all the considerations, the results of this preliminary study suggest further investigations about the possible applicative use of these low-cost adsorbents for VOCs' removal from wastewater.

In this context, the efficient adsorption capacity of food waste materials at high VOCs' concentration was preliminarily confirmed by the excellent adsorption efficiencies obtained in a real polluted matrix.

Appendix A

Figure A1. Food waste powders: (**a**) lemon peel, (**b**) grape waste, (**c**) coffee waste, (**d**) carob peel, (**e**) potato peel, (**f**) banana peel, (**g**) apple peel, (**h**) decaf coffee waste.

Table A1. Conditions employed to mass spectrometry (Varian 210-MS ion trap mass spectrometer with electron ionization).

Acquisition Method	Ion Trap Temperature (°C)	Transfer Line Temperature (°C)	Vacuum Manifold Temperature (°C)
SIM (Single Ion Monitoring)	150 °C	180 °C	80 °C

Table A2. GC-MS parameters for VOCs analyses.

VOCs	Retention Time (min)	Fragments (m/z)	Acquisition Range (m/z)
Aliphatic VOCs			
Trans-1,2-Dichloroethene	4.50–4.90	61–96–98	55–100
Dichloromethane	3.90–4.50	49–84–86	49–90
1,1-Dichloroethene	3.20–3.90	61–96–98	60–100
1,1-Dichloroethane	4.90–5.50	63–65–27	60–90
Chloroform	5.50–6.55	83–85–47	45–90
Carbon tetrachloride	6.70–6.90	117–121	75–125
Trichloroethylene	7.40–7.95	130–95–97	55–135
1,2-Dichloropropane	7.95–8.25	63–62–27	60–80
1,1,2-Trichloroethane	9.70–9.86	97–83–61	44–170
Tetrachloroethylene	9.86–10.10	166–164–129	160–175
Dibromochloromethane	10.10–10.75	129–127	80–132
1,1,2-Tetrachloroethane	11.78–11.87	81–82.8–83.8	80–85
Bromoform	11.73–12.02	173–171	75–180
Aromatic VOCs			
Methyl tert-butyl ether	1.11–2.10	44.8–45.8	40–48
Benzene	6.9–7.08	78–77	45–80
Toluene	9.15–9.45	91–92	60–100
Chlorobenzene	10.75–11.00	112–77–114	48–120
Ethylbenzene	11.00–11.13	91–106	85–110
m-Xylene	11.30–11.73	91–106	70–120
p-Xylene	11.30–11.73	91–106	70–120
o-Xylene	11.13–11.30	91–106	70–120
1,3-Dichlorobenzene	12.75–13.71	146–148–111	70–150
1,4-Dichlorobenzene	13.71–13.85	146–148–111	70–150
1,2-Dichlorobenzene	13.85–15.00	146–148–111	70–150

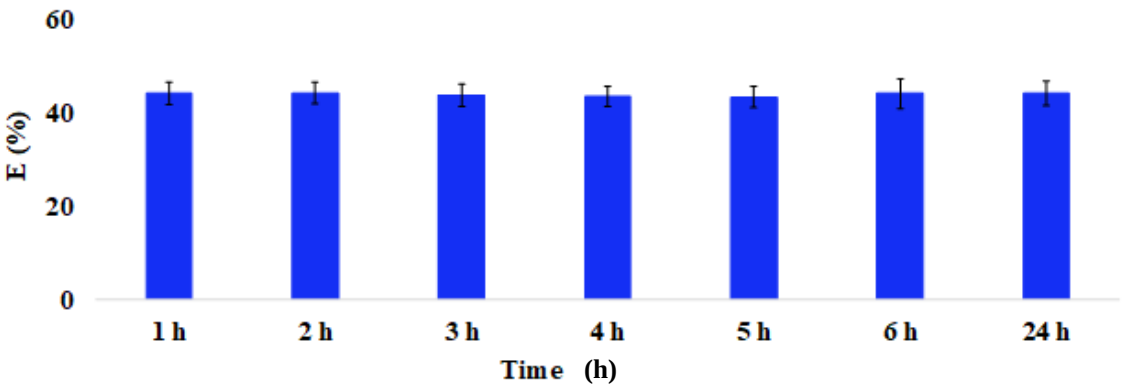

Figure A2. Adsorption efficiency (E%; 100 mg of coffee waste) of Trichloroethylene after 1, 2, 3, 4, 5, 6 and 24 h from preparation. Mean ± SD of three replicates is reported. The adsorption kinetic was

assessed by keeping both the mass of each waste material (100 mg) and the VOCs' concentration (20 µg/L) constant, while increasing exposure time from 1 h to 24 h (1, 2, 3, 4, 5, 6, and 24 h).

Table A3. pH of real polluted matrix and synthetic multi-component standard solution with and without the eight food waste materials.

Food Waste Materials	Real Polluted Matrix	Synthetic Multi-Component Standard Solution
Without adsorbents	6.5	7
Banana peel	5.5	5.8
Potato peel	6.4	7.5
Apple peel	5.9	4.7
Lemon peel	4.7	4.7
Coffee waste	6.2	5.9
Grape waste	6.1	7.1
Carob peel	5.9	5.3
Decaf Coffee waste	6.5	6.2

Author Contributions: Conceptualization, M.A.F., S.C., and A.G.; Data curation, M.A.F. and L.M.; Formal analysis, M.A.F. and A.G.; Methodology, M.A.F. and A.G.; Supervision, M.L.A. and S.C.; Writing—original draft, M.A.F.; Writing, review & editing, M.A.F., L.M. and S.C.

References

1. Atkinson, R. Atmospheric chemistry of VOCs and NOx. *Atmos. Environ.* **2000**, *34*, 2063–2101.
2. Evuti, A.M. A synopsis on biogenic and anthropogenic volatile organic compounds emissions: Hazards and control. *Int. J. Eng.* **2013**, *2*, 145.
3. Kim, J.; Lee, S.S.; Khim, J. Peat moss-derived biochars as effective sorbents for VOCs' removal in groundwater. *Environ. Geochem. Health* **2010**, *41*, 1637–1646.
4. Masih, A.; Lall, A.S.; Taneja, A.; Singhvi, R. Inhalation exposure and related health risks of BTEX in ambient air at different microenvironments of a terai zone in north India. *Atmos. Environ.* **2016**, *147*, 55–66, doi:10.1016/j.atmosenv.2016.09.067.
5. Yang, J.; Wang, K.; Zhao, Q.; Huang, L.; Yuan, C.S.; Chen, W.H.; Yang, W.B. Underestimated public health risks caused by overestimated VOC removal in wastewater treatment processes. *Environ. Sci. Process. Impacts* **2014**, *16*, 271–279.
6. Croute, F.; Poinsot, J.; Gaubin, Y.; Beau, B.; Simon, V.; Murat, J.C.; Soleilhavoup, J.P. Volatile organic compounds cytotoxicity and expression of HSP72, HSP90 and GRP78 stress proteins in cultured human cells. *Biochim. et Biophys. Acta (BBA)-Mol. Cell Res.* **2002**, *1591*, 147–155.

7. Jia, C.; Yu, X.; Masiak, W. Blood/air distribution of volatile organic compounds (VOCs) in a nationally representative sample. *Sci. Total Environ.* **2012**, *419*, 225–232, doi:10.1016/j.scitotenv.2011.12.055.
8. Doherty, R.E. A history of the production and use of carbon tetrachloride, tetrachloroethylene, trichloroethylene and 1, 1, 1-trichloroethane in the United States: Part 1–historical background; carbon tetrachloride and tetrachloroethylene. *Environ. Forensics* **2000**, *1*, 69–81, doi:10.1006/enfo.2000.0010.
9. Huang, B.; Lei, C.; Wei, C.; Zeng, G. Chlorinated volatile organic compounds (Cl-VOCs) in environment—sources, potential human health impacts, and current remediation technologies. *Environ. Int.* **2014**, *71*, 118–138, doi:10.1016/j.envint.2014.06.013.
10. Beamer, P.I.; Luik, C.E.; Abrell, L.; Campos, S.; Martínez, M.E.; Sáez, A.E. Concentration of trichloroethylene in breast milk and household water from Nogales, Arizona. *Environ. Sci. Technol.* **2012**, *46*, 9055–9061.
11. IARC. Summaries & evaluations. *Trichloroethylene* **1995**, *6*, 75.
12. U.S. EPA. Toxicity and exposure assessment for children's health. Trichloroethylene—TEACH chemical summary. Available online: http://www.epa.gov/teach/chem_summ/TCE_summary.pdf
13. Farhadian, M.; Vachelard, C.; Duchez, D.; Larroche, C. In situ bioremediation of monoaromatic pollutants in groundwater: A review. *Bioresour. Technol.* **2008**, *99*, 5296–5308, doi:10.1016/j.biortech.2007.10.025.
14. Kao, C.M.; Huang, W.Y.; Chang, L.J.; Chen, T.Y.; Chien, H.Y.; Hou, F. Application of monitored natural attenuation to remediate a petroleum-hydrocarbon spill site. *Water Sci. Technol.* **2006**, *53*, 321–328, doi:10.2166/wst.2006.066.
15. ACGIH, T. BEIs based on the documentation of the threshold limit values for chemical substances and physical agents and biological exposure indices 2009 Cincinnati. In *Oh Am. Conf. Gov. Ind. Hyg.* 2006.
16. Tunsaringkarn, T.; Siriwong, W.; Rungsiyothin, A.; Nopparatbundit, S. Occupational exposure of gasoline station workers to BTEX compounds in Bangkok, Thailand. *Int. J. Occup. Environ. Med.* **2012**, *3*, 117–125.
17. Costa, A.S.; Romão, L.P.C.; Araújo, B.R.; Lucas, S.C.O.; Maciel, S.T.A.; Wisniewski Jr, A.; Alexandre, M.D.R. Environmental strategies to remove volatile aromatic fractions (BTEX) from petroleum industry wastewater using biomass. *Bioresour. Technol.* **2012**, *105*, 31–39, doi:10.1016/j.biortech.2011.11.096.
18. Anjum, H.; Johari, K.; Gnanasundaram, N.; Ganesapillai, M.; Arunagiri, A.; Regupathi, I.; Thanabalan, M. A review on adsorptive removal of oil pollutants (BTEX) from wastewater using carbon nanotubes. *J. Mol. Liq.* **2018**, *277*, 1005–1025, doi:10.1016/j.molliq.2018.10.105.
19. Ali, I.; Asim, M.; Khan, T.A. Low cost adsorbents for the removal of organic pollutants from wastewater. *J. Environ. Manag.* **2012**, *113*, 170–183, doi:10.1016/j.jenvman.2012.08.028.
20. Coin, R.J.; Niksa, M.J.; Elyanow, D.I. Wastewater treatment enhanced by electrochemistry. *Environ. Prog. Sustain. Energy* **1996**, *15*, 122–127, doi:10.1016/j.biortech.2017.12.078.
21. Crisafully, R.; Milhome, M.A.L.; Cavalcante, R.M.; Silveira, E.R.; De Keukeleire, D.; Nascimento, R.F. Removal of some polycyclic aromatic hydrocarbons from petrochemical wastewater using low-cost

adsorbents of natural origin. *Bioresour. Technol.* **2008**, *99*, 4515–4519, doi:10.1016/j.biortech.2007.08.041.

22. Zinkus, G.A.; Byers, W.D.; Doerr, W.W. Identify appropriate water reclamat'technologies. *Chem. Eng. Prog.* **1998**, 19.
23. Fierro, V.; Torné-Fernández, V.; Montané, D.; Celzard, A. Adsorption of phenol onto activated carbons having different textural and surface properties. *Microporous Mesoporous Mater.* **2008**, *111*, 276–284, doi:10.1016/j.micromeso.2007.08.002.
24. Mohammed, M.A.; Shitu, A.; Tadda, M.A.; Ngabura, M. Utilization of various Agricultural waste materials in the treatment of Industrial wastewater containing Heavy metals: A Review. *Int. Res. J. Environ. Sci.* **2014**, *3*, 62–71.
25. Park, K.H.; Balathanigaimani, M.S.; Shim, W.G.; Lee, J.W.; Moon, H. Adsorption characteristics of phenol on novel corn grain-based activated carbons. *Microporous Mesoporous Mater.* **2010**, *127*, 1–8, doi:10.1016/j.micromeso.2009.06.032.
26. Yu, L.; Wang, L.; Xu, W.; Chen, L.; Fu, M.; Wu, J.; Ye, D. Adsorption of VOCs on reduced graphene oxide. *J. Environ. Sci.* **2018**, *67*, 171–178, doi:10.1016/j.jes.2017.08.022.
27. Bansal, R.C.; Goyal, M. *Activated Carbon Adsorption*; CRC press: Boca Raton, FL, USA, 2015.
28. Derbyshire, F.; Jagtoyen, M.; Andrews, R.; Rao, A.; Martin-Gullon, I.; Grulke, E.A. Carbon Materials in Environmental Applications. In *Chemistry and physics of carbon*; Marcel Dekker Inc.: New York, NY, USA, 2001; pp. 1–66.
29. Zhang, X.; Gao, B.; Creamer, A.E.; Cao, C.; Li, Y. Adsorption of VOCs onto engineered carbon materials: A review. *J. Hazard. Mater.* **2017**, *338*, 102–123, doi:10.1016/j.jhazmat.2017.05.013.
30. Ahmaruzzaman, M. Adsorption of phenolic compounds on low-cost adsorbents: A review. *Adv. Colloid Interface Sci.* **2008**, *143*, 48–67, doi:10.1016/j.cis.2008.07.002.
31. Baek, M.H.; Ijagbemi, C.O.; Se-Jin, O.; Kim, D.S. Removal of Malachite Green from aqueous solution using degreased coffee bean. *J. Hazard. Mater.* **2010**, *176*, 820–828, doi:10.1016/j.jhazmat.2009.11.110.
32. Crini, G. Non-conventional low-cost adsorbents for dye removal: A review. *Bioresour. Technol.* **2006**, *97*, 1061–1085, doi:10.1016/j.biortech.2005.05.001.
33. García-Sabido, D.; López-Mesas, M.; Carrillo-Navarrete, F. Chicken feather fibres waste as a low-cost biosorbent of acid Blue 80 dye. *Desalin. Water Treat.* **2016**, *57*, 3732–3740, doi:10.1080/19443994.2014.986531.
34. Tan, X.; Liu, Y.; Zeng, G.; Wang, X.; Hu, X.; Gu, Y.; Yang, Z. Application of biochar for the removal of pollutants from aqueous solutions. *Chemosphere* **2015**, *125*, 70–85, doi:10.1016/j.chemosphere.2014.12.058.
35. Acharya, J.; Kumar, U.; Rafi, P.M. Removal of heavy metal ions from wastewater by chemically modified agricultural waste material as potential adsorbent-a review. *Int. J. Curr. Eng. Technol.* **2018**, *8*, 526–530.

36. Agwaramgbo, L.; Lathan, N.; Edwards, S.; Nunez, S. Assessing lead removal from contaminated water using solid biomaterials: Charcoal, coffee, tea, fishbone, and caffeine. *J. Environ. Prot.* **2013**, *4*, 741, doi:10.4236/jep.2013.47085.
37. Aman, T.; Kazi, A.A.; Sabri, M.U.; Bano, Q. Potato peels as solid waste for the removal of heavy metal copper (II) from waste water/industrial effluent. *Colloids Surf. B Biointerfaces* **2008**, *63*, 116–121, doi:10.1016/j.colsurfb.2007.11.013.
38. Fu, F.; Wang, Q. Removal of heavy metal ions from wastewaters: A review. *J. Environ. Manag.* **2011**, *92*, 407–418, doi:10.1016/j.huajenvman.2010.11.011.
39. Lakshmipathy, R.; Sarada, N.C. Application of watermelon rind as sorbent for removal of nickel and cobalt from aqueous solution. *Int. J. Miner. Process.* **2013**, *122*, 63–65, doi:10.1016/j.minpro.2013.03.002.
40. Mallampati, R.; Valiyaveettil, S. Application of tomato peel as an efficient adsorbent for water purification—alternative biotechnology? *Rsc. Adv.* **2012**, *2*, 9914–9920.
41. Frezzini, M.A.; Giuliano, A.; Treacy, J.; Canepari, S.; Massimi, L. Food Waste Materials Appear Efficient and Low-cost Adsorbents for the Removal of Organic and Inorganic Pollutants from Wastewater. *Interface Sci.* **2018**, *316*, 298–309, doi:10.31031/RDMS.2018.05.000608.
42. Massimi, L.; Giuliano, A.; Astolfi, M.L.; Congedo, R.; Masotti, A.; Canepari, S. Efficiency evaluation of food waste materials for the removal of metals and metalloids from complex multi-element solutions. *Materials* **2018**, *11*, 334, doi:10.3390/ma11030334.
43. Vieira, R.H.; Volesky, B. Biosorption: A solution to pollution? *Int. Microbiol.* **2000**, *3*, 17–24.
44. Kargi, F.; Cikla, S. Biosorption of zinc (II) ions onto powdered waste sludge (PWS): Kinetics and isotherms. *Enzym. Microb. Technol.* **2006**, *38*, 705–710, doi:10.1016/j.enzmictec.2005.11.005.
45. Mirabella, N.; Castellani, V.; Sala, S. Current options for the valorization of food manufacturing waste: A review. *J. Clean. Prod.* **2014**, *65*, 28–41, doi:10.1016/j.jclepro.2013.10.051.
46. Scheufele, F.B.; Módenes, A.N.; Borba, C.E.; Ribeiro, C.; Espinoza-Quiñones, F.R.; Bergamasco, R.; Pereira, N.C. Monolayer–multilayer adsorption phenomenological model: Kinetics, equilibrium and thermodynamics. *Chem. Eng. J.* **2016**, *284*, 1328–1341, doi:10.1016/j.cej.2015.09.085.
47. Wang, X.S.; Qin, Y. Equilibrium sorption isotherms for of Cu2+ on rice bran. *Process Biochem.* **2005**, *40*, 677–680, doi:10.1016/j.procbio.2004.01.043.
48. Aly, Z.; Graulet, A.; Scales, N.; Hanley, T. Removal of aluminium from aqueous solutions using PAN-based adsorbents: Characterisation, kinetics, equilibrium and thermodynamic studies. *Environ. Sci. Pollut. Res.* **2014**, *21*, 3972–3986.
49. Hamzaoui, M.; Bestani, B.; Benderdouche, N. The use of linear and nonlinear methods for adsorption isotherm optimization of basic green 4-dye onto sawdust-based activated carbon. *J. Mater. Env. Sci.* **2018**, *9*, 1110–1118, doi:10.26872/jmes.2018.9.4.122.
50. Ho, Y.S. Isotherms for the sorption of lead onto peat: Comparison of linear and non-linear methods. *Pol. J. Environ. Stud.* **2006**, *15*, 81–86.

51. Chen, X. Modeling of experimental adsorption isotherm data. *Information* **2015**, *6*, 14–22, doi:10.3390/info6010014.
52. Aly, Z.; Luca, V. Uranium extraction from aqueous solution using dried and pyrolyzed tea and coffee wastes. *J. Radioanal. Nucl. Chem.* **2013**, *295*, 889–900.
53. Iqbal, M.; Saeed, A.; Zafar, S.I. FTIR spectrophotometry, kinetics and adsorption isotherms modeling, ion exchange, and EDX analysis for understanding the mechanism of Cd2+ and Pb2+ removal by mango peel waste. *J. Hazard. Mater.* **2009**, *164*, 161–171, doi:10.1016/j.jhazmat.2008.07.141.
54. Guechi, E.K.; Hamdaoui, O. Sorption of malachite green from aqueous solution by potato peel: Kinetics and equilibrium modeling using non-linear analysis method. *Arab. J. Chem.* **2016**, *9*, S416–S424, doi:10.1016/j.arabjc.2011.05.011.
55. Pujol, D.; Liu, C.; Gominho, J.; Olivella, M.À.; Fiol, N.; Villaescusa, I.; Pereira, H. The chemical composition of exhausted coffee waste. *Ind. Crop. Prod.* **2013**, *50*, 423–429, doi:10.1016/j.indcrop.2013.07.056.
56. Kaneko, T.; Wang, P.Y.; Sato, A. Relationship between blood/air partition coefficients of lipophilic organic solvents and blood triglyceride levels. *Toxicology* **2000**, *143*, 203–208, doi:10.1016/S0300-483X(99)00170-5.
57. Sikkema, J.; Weber, F.J.; Heipieper, H.J.; Bont, J.A.D. Cellular toxicity of lipophilic compounds: Mechanisms, implications, and adaptations. *Biocatalysis* **1994**, *10*, 113–122, doi:10.3109/10242429409065221.
58. Largitte, L.; Pasquier, R. A review of the kinetics adsorption models and their application to the adsorption of lead by an activated carbon. *Chem. Eng. Res. Des.* **2016**, *109*, 495–504, doi:10.1016/j.cherd.2016.02.006.
59. Tan, K.L.; Hameed, B.H. Insight into the adsorption kinetics models for the removal of contaminants from aqueous solutions. *J. Taiwan Inst. Chem. Eng.* **2017**, *74*, 25–48, doi:10.1016/j.jtice.2017.01.024.
60. El-Khaiary, M.I.; Malash, G.F. Common data analysis errors in batch adsorption studies. *Hydrometallurgy* **2011**, *105*, 314–320, doi:10.1016/j.hydromet.2010.11.005.
61. Dada, A.O.; Olalekan, A.P.; Olatunya, A.M.; Dada, O. Langmuir, Freundlich, Temkin and Dubinin–Radushkevich isotherms studies of equilibrium sorption of Zn2+ unto phosphoric acid modified rice husk. *Iosr J. Appl. Chem.* **2012**, *3*, 38–45.
62. Febrianto, J.; Kosasih, A.N.; Sunarso, J.; Ju, Y.H.; Indraswati, N.; Ismadji, S. Equilibrium and kinetic studies in adsorption of heavy metals using biosorbent: A summary of recent studies. *J. Hazard. Mater.* **2009**, *162*, 616–645, doi:10.1016/j.jhazmat.2008.06.042.

11.2 (F) Analytical chemistry for the characterization of environmental matrices

During the last years, innumerable natural and anthropogenic emission sources of toxic compounds have determined air pollution. Among the available air pollution monitoring techniques, biomonitoring has recently become one of the most widely used technique, due to its ease of operation, low-cost, efficiency and specificity (Astolfi et al., 2021; Ristorini et al., 2020). In fact, the use of conventional monitoring instruments in the field is sometimes difficult due to high equipment costs, the need to supply power to the device, and the requirement for human and instrumental resources (Girotti et al., 2020). Several living organisms, which are typical of the environment under study, can act as both a biosensor and a bioaccumulator, and they have shown the capacity of accumulating toxic elements, allowing the monitoring of this kind of pollutants concentrations in the environment for integrated measurements. This is the case for *Apis mellifera* (L.) and beehive products that has been widely investigated in biomonitoring studies (Smith et al., 2019; Zhou et al., 2018; Losfeld et al., 2014). Bees and beehive products can provide additional information on toxic elements pollution, since they can be deposited on the hairy bodies of the bees and then brought into the hive with pollen, or they may be ingested with the nectar of flowers, water, or honeydew (Girotti et al., 2020). Measurements of element concentrations in this kind of samples are relevant for the healthiness assessment of the honey in terms of the presence of essential metals and for ensuring the human health safety by assessing the admissible levels of toxic elements (Astolfi et al., 2020).

Extra virgin olive oil (EVOO) represents an important component of the Mediterranean diet. This vegetable oil has health benefits such as antioxidant properties and is highly regarded for its nutritional value and excellent sensory properties. However, it may contain relatively high quantities of trace elements, including toxic metals. Therefore, monitoring and controlling the presence of inorganic elements in EVOO samples is important for preserving this food's organoleptic quality and nutritional value. Various factors can contribute to trace elements in EVOO, such as soil composition, environmental pollution, or contaminations during oil extraction and conservation. However, trace element analysis and suitable statistical treatment can have an important role in the geographical characterization of different EVOOs, for oil quality control and oil adulteration detection. Considering these aspects, the present study aims to evaluate the most significant relationships between element levels in EVOO and different categorizations, mostly related to the geographical origin using chemometric tools coupled with the inductively coupled plasma mass spectrometry (ICP-MS) method. For this purpose, 45 elements from 237 EVOO samples from 15 Italian regions were analyzed. Also, the antioxidant activity of oils' hydrophilic fraction was estimated.

The presented works have shown that passive sampling methods are essential tools for implementing monitoring strategies.

11.2.1 (F1) An Analytical Method for the Biomonitoring of Mercury in Bees and Beehive Products by Cold Vapor Atomic Fluorescence Spectrometry

Molecules (2021), 26 (16), 4878, doi: 10.3390/molecules26164878

Maria Luisa Astolfi[1], Marcelo Enrique Conti[2], Martina Ristorini[3], Maria Agostina Frezzini[4], Marco Papi[5], Lorenzo Massimi[4], Silvia Canepari[4]

[1] Department of Chemistry, Sapienza University of Rome, 00185 Rome, Italy

[2]Department of Management, Sapienza University of Rome, 00161 Rome, Italy

[3] Department of Bioscience and Territory, University of Molise, 86090 Pesche (IS), Italy

[4] Department of Environmental Biology, Sapienza University of Rome, 00185 Rome, Italy

[5] Association of Beekeepers of Rome and Province, via Albidona 20, 00118 Rome, Italy

*Corresponding author

Keywords: bees; beehive products; biomonitoring; cold vapor atomic fluorescence spectrometry; sample preparation; toxic metal

Abstract

Bees and their products are useful bioindicators of anthropogenic activities and could overcome air quality networks' deficiencies. Among the environmental contaminants, mercury (Hg) is a toxic metal that can be accumulated in living organisms. The first aim of this study was to develop a simple analytical method to determine Hg in small mass samples of bees and beehive products by cold vapor atomic fluorescence spectrometry. The proposed method was optimized for about 0.02 g bee, pollen, propolis and royal jelly, 0.05 g beeswax and honey, or 0.1 g honeydew with 0.5 mL HCl, 0.2 mL HNO3 and 0.1 mL H2O2 in a water bath (95 °C, 30 min); samples were made up to a final volume of 5 mL deionized water. The method limits sample manipulation and the reagent mixture volume used. Detection limits were lower than 3 μg kg^{-1} for a sample mass of 0.02 g, and recoveries and precision were within 20% of the expected value and less than 10%, respectively, for many matrices. The second aim of the present study was to evaluate the proposed method's performances on real samples collected in six areas of the Lazio region in Italy.

1. Introduction

Mercury (Hg) is an ubiquitous and toxic metal that continues to be a public health concern [1–3]. It is released into the environment from both natural and anthropogenic sources [4]. Mercury is present in the atmosphere as an elementary form (Hg0) and it is accumulated through the terrestrial and aquatic food webs as an organic form (methylmercury) [5,6]. Although Hg is associated with several adverse human health effects [7], it is still widely used in the chloralkali industry, for gold mining, and the production of dental amalgam, batteries, pesticides, fungicides, disinfectants, and antiseptics [8]. Because of the mentioned toxic properties, Hg monitoring in food and environmental samples is essential in order to perform reliable risk assessments and

take appropriate actions to protect human health and the environment [9]. According to the current air quality directives in Europe, industrial activities must reduce Hg emissions by implementing control programs and integrated pollution prevention and, at the same time, by improving air quality assessment and monitoring programs [10–13]. Mercury in the atmosphere is mainly assessed by making punctual measurements with manual or automated air quality monitoring stations [14] and applying standardized methodologies, based on current legislation [10]. However, due to the high costs, the monitoring networks for Hg pollution assessment are still characterized by low temporal (generally on an annual basis) and spatial coverage [15]. For the above reasons, there is a growing interest in alternative air monitoring techniques, such as plant, insects, lichens, and mosses that can provide reliable time-integrated estimates of air pollution in a given area at low cost [16–22]. In particular, bees and their products, such as honey, propolis, and pollen, have been proposed as bioindicators of environmental Hg contamination [23– 25]. The assessment of Hg levels in bee products is important not only for their use as possible bioindicators for environmental contamination purposes but also for the potential human exposure due to their dietary, pharmaceutical and cosmetic use [26–30].

Mercury has been studied in honey samples by several authors [24,25,31–42], whereas limited literature data are available regarding the Hg determination in beeswax [42], pollen [24,25,39,41,43,44], propolis [24,45–47], and bees [24,25,31,39,47–49]. Microwave-assisted digestion is the most commonly used technique for preparing bee samples and hive products [32,35,42–44]. However, the microwave-assisted digestion method requires certain sample masses and reagent volumes, often leading to high final dilution factors and a consequent increase in the method detection limits [25,50]. In contrast, some authors miniaturized digestion of honey, pollen and/or bees by heating them in a heat block (80–100 °C) and using very small reagent volumes [25,33]. Throughout the literature, many studies quantify Hg concentrations in bees and beehive product matrices with atomic absorption spectroscopy [38] and inductively coupled plasma–mass or optical emission spectrometry (ICP-MS or ICP-OES, respectively) [25,32,40–43,49], often coupled to cold vapor generation (CV) for matrix separation [24,33–35,37,44,45], electrothermal atomic absorption spectrophotometry [47], and direct Hg analysis using automated commercial instruments, such as the Advanced Mercury Analyser (AMA) [36,39,46], or Direct Mercury Analyser (DMA) [37,48]. CV atomic fluorescence spectrometry (AFS) is a good alternative for total Hg determination, and it has been commonly employed for the analysis of several biological and environmental matrices [51], food [52], and human bodily fluids and tissues [53–55]. Despite this, CV-AFS has rarely been applied for the determination of Hg in honey [35], and, to the best of our knowledge, this technique has not been applied in bees and other beehive products.

This study aimed to miniaturize the sample digestion of bees and beehive products to achieve accurate and reproducible results with low detection limits for the Hg determination by CV-AFS. The proposed analytical method was applied to commercial honeydew and royal jelly samples and bees, honey, beeswax, pollen, and propolis samples collected from six central Italy areas characterized by different exposure to environmental pollution.

2. Results and Discussion

2.1 Comparison with previous methods

The analytical characteristics comparison of the method proposed in the present study with others already developed for Hg determination in bee and beehive products samples is shown in Table S1. In this study, the sample digestion was miniaturized by reducing all volumes and masses to allow sample preparation in one disposable test tube. This prevented sample loss due to the transfer in different tubes and minimized possible contamination. In addition, the use of smaller volumes of reagents allows for lower final dilution factor (5x), and lower method DL and decreases the consumable and chemical waste generated, meeting the ever-increasing demand to comply with green chemistry requirements. The dilution factor, together with the sample mass, the reagent purity, and the chosen instrument, can affect the Hg DL in bees and beehive products, where this metal is generally present in low concentrations. To decrease the method DL, the sample mass could be increased, but sometimes this is not possible (such as for bees or specific pollen). Furthermore, if the analytical method requires sample digestion, the increase in sample mass must necessarily be accompanied by an appropriate volume of reagents to ensure complete sample digestion. Even for methods that do not require sample pre-treatment, such as AMA or DMA (Table S1), the sample mass cannot be randomly increased to ensure complete drying, ashing, and atomization of the sample. In addition, amounts larger than 100 mg of sample can produce a build-up of combustion gases, resulting in a rapid increase of pressure in the furnace [37]. In the literature (see Table S1), some studies use a large final dilution of bees and beehive products samples (25–50x) [24,33,35,36,40,41,44,47,49] to reduce the acidity of the final digest, sometimes compromising the Hg determination. For this purpose, in this study, various sample aliquots (0.05 - 1 g for honey and honeydew, 0.02 - 0.2 g for bees, beeswax, pollen, propolis, royal jelly) were digested at the maximum temperature of 95 °C, considering two different times (30 or 60 min) and using the smallest amount of reagent mixture (0.5 mL HCl, 0.2 mL HNO_3 and 0.1 mL H_2O_2) to employ the smallest dilution factor final (5x). The choice of acid and oxidizing agent (HNO_3 and H_2O_2, respectively) is widely agreed by most of the literature for the selected matrices [24,25,33,35,36,38,41,42,44,47-49], while HCl was selected according to the manufacturer's recommendations.

The proposed sample preparation also appears the fastest procedure (digestion time, 30 min for 120 samples or more) compared to the other sample treatments reported by literature [25,33,40-42,44,47] (Table S1), resulting suitable for routine analysis with high sample throughput and biomonitoring. However, it should be noted that possible volatile Hg species, such as organometallic compounds or metal nanoparticles, could be lost during digestion due to their volatilization.

The analytical characteristics of the proposed method are detailed in the following sections.

2.2 Linearity and Selectivity

The linearity and selectivity of the proposed method were evaluated by preparing calibration curves in aqueous [3% (v/v) HCl and HNO_3] standards and using the standard addition method at Hg concentrations of 0.00, 0.02, 0.04, 0.1, 0.2, 0.4, 0.8, 1.0, and 1.5 μg L^{-1}. Digested samples of each matrix (20 mg) were diluted to reach the same acid ratio as the aqueous standard solutions and used to create calibration curves with the standard addition method. The linearity ranges from 0.02 to 1.5 μg L^{-1} were checked through the linear

regression coefficient (R^2) and verified by the Mandel fitting test. Calibration curve points with percent relative deviation ≥10% from calculated concentrations were tested and removed using the instrument software. The parameters of the calibration curves after the outliers' removal are presented in Table 1. Data of the calibration curves using aqueous standards were obtained by nine independent replicates. The dynamic range was compared with that of other previously published methods (Table S1). In particular, CV-AFS allows the determination of Hg in a wide range of concentrations, showing a dynamic range greater than that possible with other techniques such as CV-AAS, ICP-OES and DMA. The matrix effect was evaluated by comparing the slopes of the calibration curves obtained from aqueous standards and the standard addition method (Table 1). Most of the results showed good data dispersion; however some standard deviation values were of the same order of magnitude as the intercept data, generating a large statistical uncertainty on these data. The t-test at a 95% confidence level was used to evaluate possible significant differences between the angular coefficients of the calibration curves, in accordance with previous studies [25,37,56]. There were no apparent matrix effects between the aqueous and standard addition calibration curves. Thus, these results agree with those obtained for bees, honey and pollen by other authors [25,37].

Table 1. Comparison of calibration curve parameters for Hg determination by cold vapor atomic fluorescence spectrometry (CV-AFS).

Calibration standards	Parameter[a]				
	a	**s(a)**	**b**	**s(b)**	**R^2**
Aqueous standards	9.68E+01	9.68E+01	1.86E+04	1.16E+03	0.999
Bee-addition standards	1.32E+02	3.14E+01	1.64E+04	2.30E+03	0.999
Beeswax-addition standards	7.65E+01	1.05E+01	1.71E+04	2.22E+03	0.999
Honey-addition standards	1.07E+02	1.34E+02	1.61E+04	2.05E+03	0.999
Honeydew-addition standards	1.38E+02	8.58E+01	1.65E+04	1.78E+03	0.999
Pollen-addition standards	1.30E+02	3.73E+01	1.62E+04	2.07E+03	0.998
Propolis-addition standards	3.85E+02	2.50E+02	1.76E+04	1.40E+03	0.999
Royal jelly-addition standards	7.65E+01	1.05E+01	1.80E+04	9.19E+02	0.998

[a] a, intercept; s(a), standard deviation of intercept; b, slope; s(b), standard deviation of slope; R^2, correlation coefficient.

2.3 Detection and Quantification Limits

The DL was calculated based on the calibration curve using a software prepared by Regional Agency for Environmental Protection [57]. Therefore, the DL can be expressed as DL = 3.3 σ/b; where the coefficient 3.3 is called expansion factor and is obtained assuming a 95% confidence level, σ is the standard deviation of the response of the curve, and b is the calibration curve slope. The reached DL of 0.01 µg L^{-1} for aqueous calibration confirmed the excellent sensitivity of the proposed method. The QL was set at the lowest standard curve points of calibration that is 0.02 µg L^{-1}. The DL and QL varied depending on the mass of the analyzed matrix and dilution required before analysis (in this study, 5x). In particular, for a mass of 0.02, 0.05, 0.1, 0.2, and 1 g, the DL was 3, 1, 0.5, 0.3, and 0.05 µg kg^{-1}, and the QL was 5, 2, 1, 0.5, 0.1 µg kg^{-1}, respectively. As shown in Table S1, the obtained DLs are comparable to previously reported AMA or DMA analysis [36,37,39] and ICP-MS analysis [25] and lower than CV-AAS or CV-ICP-OES analysis [24,33].

2.4 Accuracy and Precision

Due to the lack of certified reference material of bees and beehive products, the accuracy and precision (as repeatability and intermediate precision) of the proposed method were evaluated by recovery tests in agreement with other authors [25,36,37] and as indicated by Commission Decision no. 657/2002 [58]. Samples of each matrix (0.05–1 g for honey and honeydew, 0.02–0.2 g for bees, beeswax, pollen, propolis, royal jelly) were spiked with Hg at low (0.02 µg L^{-1}), intermediate (0.2 µg L^{-1}) and high (1 µg L^{-1}) concentration and then digested. The method performance at levels near the QL was evaluated considering the smallest mass of each matrix and the shortest digestion time (30 min). The same solutions were again analyzed on two separate days to assess intermediate precision. The recovery and precision (such as repeatability) data were shown in Tables 2, S1, and S2. Intermediate precision data (not shown) were very similar to repeatability values.

Table 2. Recovery and precision data for Hg in bees and beehive products (n = 3) by water bath digestion (95 °C, 30 min).

		Low level spike (0.02 µg L^{-1})		**Intermediate level spike (0.2 µg L^{-1})**		**High level spike (1 µg L^{-1})**	
Matrix	**Mass (g)**	**R%**	**CV%**	**R%**	**CV%**	**R%**	**CV%**
Honey	0.05	86	5.4	116	9.3	96	7.8
Honeydew	0.1	89	0.4	113	10	91	8.4
Pollen	0.02	92	9.6	90	3.7	95	3.6
Propolis	0.02	104	9.8	98	8.6	91	2.5
Beeswax	0.05	92	10	111	8.5	99	2.0
Royal Jelly	0.02	117	9.3	108	4.4	110	0.9
Bees	0.02	95	8.9	97	4.5	91	10

In summary, the digestion time and mass for each matrix suitable for obtaining recoveries and precision within 20% of the expected value and less than 10%, respectively, were tabulated (Table 3). In this study, the major sources of uncertainty were the recovery of the procedure, instrumental calibration, and repeatability of the

measurements. In contrast, samples' weight was the lowest contribution to the Hg uncertainty, in agreement with a previous study [59].

Table 3. Summary of mass and digestion time that can be used in bees and beehive products.

Matrix	Mass[a] (g)	Digestion time[a] (min)
Bees	0.02-0.2	30 or 60
Beeswax	0.02	60
	0.05-0.1	30 or 60
	0.2	60
Honey	0.05	30 or 60
	0.1	60
Honeydew	0.05	60
	0.1	30 or 60
	0.2	60
Pollen	0.02-0.2	30 or 60
Propolis	0.02	30 or 60
Royal Jelly	0.02-0.2	30 or 60

[a] The method performance at levels near the QL (0.02 µg L^{-1}) was evaluated considering the smallest mass of each matrix and the shortest digestion time (30 min).

2.5 Hg concentrations in real samples

Bees and beehive products (honey, beeswax, pollen, and propolis) from various geographical areas in central Italy (Figure 1) and commercial samples of both honeydew and royal jelly were analyzed to demonstrate the applicability of the proposed method for routine analysis and biomonitoring.

Mercury pollution is an important environmental and public health issue. Elemental Hg can be emitted into the atmosphere by both anthropogenic (mainly artisanal gold mining, fossil fuel combustion, and cement production) and natural (such as a geothermal activity) sources [39]. Subsequently, Hg is transported to land and surface waters through wet and dry deposition, where it can undergo a bioconversion into more volatile or soluble forms such as methylmercury and return into the atmosphere or bioaccumulate in food chains [39]. Also, bees are continuously exposed to contaminants, including Hg. Every day during foraging activities, bees gather nectar, plant resins, and water in the border of 7 km^2 around their beehive and may come into contact with chemicals [47,49]. Therefore, the bee was proposed as a multi-sample contaminant collector because of its high mobility, contact with possible chemicals through inhalation, digestion, and hairs covering its body [40,47,49]. Contaminants adhered to the hairs, such as particles of soil and dust, can be carried into the beehive, thus affecting the composition of the beehive products [42,49]. In addition, Hg captured by the leaves of plants or absorbed from the soil through the plant root system can influence the nectar and pollen composition, which

are brought back into the beehive [42,44]. Furthermore, propolis, produced with plant resin and mixed with salivary secretions and wax, due to its sticky nature of gum, might be used as a bioindicator of atmospheric pollution [46,47].

These considerations form the basis with which bees and their products have been proposed as reliable bioindicators of the environment, including the atmosphere and pollution [40,42,43,46-49,60].

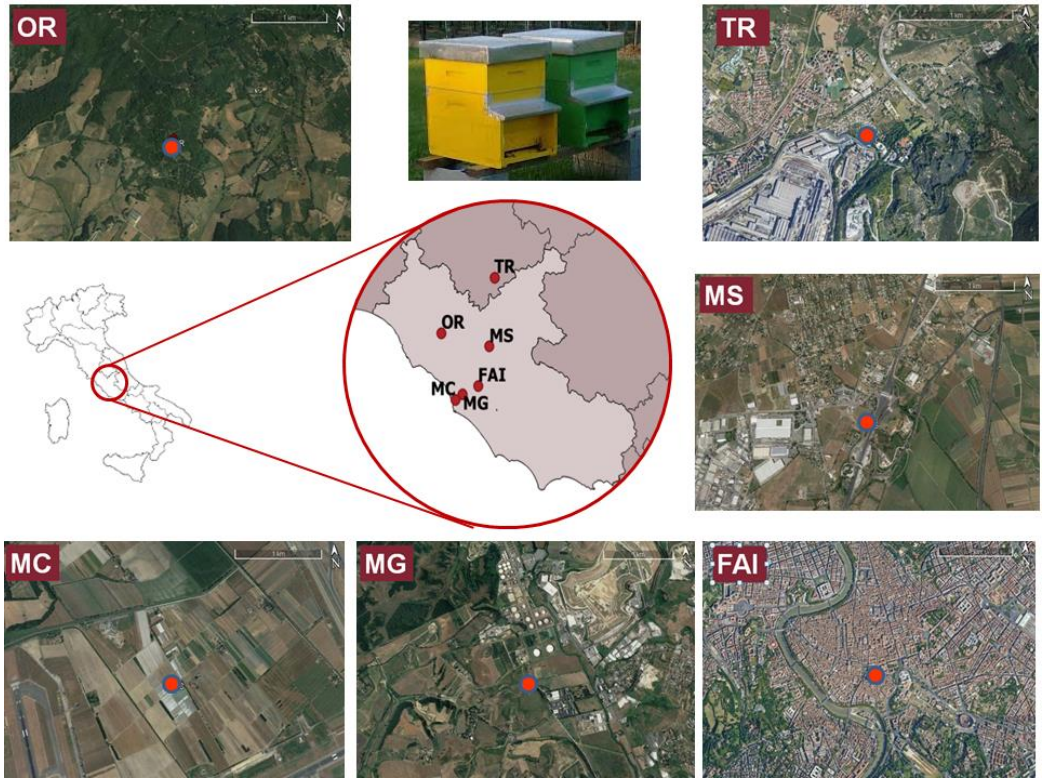

Figure 1. Geographic location of sampled apiaries (central Italy).

The Hg levels in all royal jelly samples were lower than DL, while in honeydew samples were 0.83 ± 0.34 µg kg^{-1}. As shown in Table 4, the Hg concentrations were above the DL for many matrices showing that the proposed method can be used to determine the Hg level in bees and beehive products. Although variation in Hg level across different areas for each matrix indicates the possibility of using the proposed method for biomonitoring, alternative and parallel measurements of the contamination of the environmental compartment of interest are necessary.

For honey, the mean Hg concentrations in this study (0.91–3.37 µg kg^{-1}) are in agreement with the mean contents found in Croatia (0.47–0.52 µg kg^{-1}) by Bilandžić et al. [36] and China (0.34–4.00 µg kg^{-1}) by Ru et al. [35]. In another Italian study, Hg levels were lower than the quantification limit of 2 µg kg^{-1} [32]. The mean Hg levels in pollen (3.2–12.8 µg kg^{-1}) were similar to the concentrations reported in Poland (3.6–6.6 µg kg^{-1}) by Roman [43] and in Brazil (0.4–6.8 µg kg^{-1}) by Morgano et al. [44]. Accordingly to our mean data in propolis (4.6–14.8 µg kg^{-1}), studies from Croatia by Cvek et al. [45] and Spain by Bonvehí and Bermejo [46] reported

Hg concentrations as median of 12 µg kg^{-1} and mean of 8.0 ± 2.5 µg kg^{-1}, respectively. For bees, there are few available data in the literature because of the limited amount of this matrix and consequently high DL values [24,25,40,47,48]. A study by Toth et al. [39] reported Hg concentrations of 39.892 ± 0.035 µg kg^{-1} and 8.224 ± 0.028 µg kg^{-1} in bees from two locations in eastern Slovakia. These results are in accordance with our data ranging from 0.53 to 31 µg kg^{-1}. For beeswax, only one study by Bommuraj et al. [42] reports a concentration value of Hg equal to 62 µg kg^{-1}, while our data fall in the range <1–12.7 µg kg^{-1}. Unfortunately, it was not possible to make a comparison with the literature for honeydew and royal jelly.

In this study, the Hg levels show a typical distribution bind to the anthropogenic development of the areas. Furthermore, in agreement with the observations of other authors on the biological barrier capacity of bees for contamination of honey by Cd and Tl [40], bees seem to work as biofilters also for Hg. In fact, the Hg levels were generally lower in the rural site (OR) and honey samples and higher in the sites with greater anthropogenic impact and bee samples. In particular, bees showed approximately ten times higher mean concentrations in the FAI (16.2 ± 2.7 µg kg^{-1}), MG (16.2 ± 5.6 µg kg^{-1}), and MS (17.8 ± 8.5 µg kg^{-1}) areas than in the OR site (1.76 ± 0.85 µg kg^{-1}). The lowest Hg level was detected in honey samples from OR (0.91 ± 0.23 µg kg^{-1}). The principal anthropogenic sources of Hg pollution are industrial and urban discharges and combustion [35,38].

Table 4. Comparison of mercury occurrence (µg kg^{-1}) in six sampled apiaries (central Italy).

Matrix	Statistics	OR	FAI	MC	MG	MS	TR
Honey	N	14	6	10	10	10	4
	Mean	**0.91^{a,b,c,d,e}**	**2.26^{a}**	**2.68^{b}**	**2.66^{c}**	**2.43^{d}**	**3.37^{e}**
	SD	0.23	0.69	0.75	0.36	0.60	0.60
	Median	0.78	1.92	2.97	2.53	2.07	3.37
	Minimum	0.66	1.80	1.35	2.30	1.95	2.95
	Maximum	1.25	3.06	3.17	3.23	3.20	3.80
Pollen	N	14	NS	12	10	4	4
	Mean	**3.2^{a,b}**	-	7.6	7.5	**12.8^{a}**	**10.4^{b}**
	SD	1.4	-	2.0	1.9	8.0	2.5
	Median	3.0	-	7.2	7.0	12.8	10.4
	Minimum	<3	-	5.1	5.9	7.2	8.7
	Maximum	5.6	-	10.2	10.6	18.5	12.2
Propolis	N	10	NS	NS	4	6	NS
	Mean	**4.6^{a}**	-	-	**7.54^{b}**	**14.8^{a,b}**	-
	SD	1.2	-	-	0.65	2.1	-
	Median	4.8	-	-	7.54	15.7	-
	Minimum	<3	-	-	7.08	12.4	-
	Maximum	5.7	-	-	8.00	16.4	-
Beeswax	N	14	8	14	12	12	4
	Mean	**2.8^{a}**	5.9	6.4	4.8	4.9	**11.5^{a}**

	SD	1.6	2.8	3.0	1.7	3.1	1.8
	Median	2.8	5.2	4.5	4.2	3.9	11.5
	Minimum	<1	3.5	3.3	3.5	3.0	10.2
	Maximum	5.7	9.5	10.6	8.1	11.2	12.7
Bees	N	14	6	14	14	10	4
	Mean	**1.76^{a,b,c}**	**16.2^{a}**	11.0	**16.2^{b}**	**17.1^{c}**	14.5
	SD	0.85	2.7	5.8	5.6	8.5	5.2
	Median	2.09	15.1	10.4	14.5	17.0	14.5
	Minimum	0.53	14.4	1.6	8.3	9.1	10.9
	Maximum	2.65	19.3	20.3	25.3	31.0	18.2

N, samples number; SD, standard deviation; NS, not sampled.

^{a,b,c,d,e} The data in bold with the same superscript letters within rows are significantly different ($p < 0.01$; ANOVA test).

Our results agree with numerous other studies [60,61]. In Toth et al. [39], a statistically significant relationship was described between the locality and Hg content in bees and bee pollen. Moreover, in the study by Dżugan et al. [40], the sampling area and its related emission sources influenced toxic metals concentration in both bee bodies and honey. However, the Hg content in bees may also depend on other factors such as method of rearing bee colonies (including supplemental feeding), age of worker bees, physiological and health status of bee specimens and bee colonies [62]. Due to its physical feature (sticky) and its chemical composition (mainly polyphenols, amino acids, terpenes, and steroids), propolis can absorb Hg and other metals [47,63], thus it can be also used as a bioindicator of air pollution [63,64].

Especially for honey, the assessment of Hg levels is important not only for environmental protection but also for food quality and consumer health [38]. Currently, the Hg presence in honey must not follow specific regulations. However, the Codex Alimentarius states that honey shall be free from metals in amounts that may result in a hazard to human health [65]. A provisional tolerable weekly intake (PTWI) of 0.3 mg (0.042 mg/day) for a 70-kg person (0.004 mg/kg body weight/week) was designed for Hg [66]. Considering the highest Hg concentration of the whole campaign (3.80 μg kg^{-1}), a 20-g daily honey consumption represents a weekly intake of circa 0.2% of the PTWI for Hg. This Hg intake is well below the recommended dose, and the consumption of honey is not considered dangerous for human health.

3. Materials and Methods

3.1 Study areas and sample collection

Samples of royal jelly (n = 2) and honeydew (n = 2) of different brands were purchased in duplicate from the Italian market; while samples of bees, beeswax, honey, pollen, and propolis were collected from six different apiaries, across central Italy from April 2018 to June 2019 (Figure 1). Two beehives were selected at each apiary, and the beekeepers sampled their bee colonies and beehive products into polyethylene screw-cap

containers once every two months in the late morning. The six study locations were chosen to represent sites with different human activities and environmental impacts. Terni (TR) was selected as an industrial area affected by steel mill industry. Rome [city center on the roof of the Apicultural Italian Federation (FAI), Anagnina (MS), Malagrotta (MG), and Maccarese (MC)] was chosen as an urban area influenced by different emission sources, such as traffic pollution in FAI and MS; biomass burning in FAI; various industrial plants, such as refinery, gasifier, hospital waste incinerator, landfill of municipal waste and quarries for the extraction of building materials in MG; and intense air and ship traffic in MC (located next to Fiumicino airport). Lasty, Oriolo Romano (OR) in Viterbo province was selected as a rural area.

After sampling, the samples were transported to the laboratory. For each beehive, bees (n = 20) were dried in a freeze drier (at least 48 h for constant weight) and then were ground in a ceramic mortar coated with parafilm. Beeswax samples were separated from honey, washed in deionized water until all of the residual honey was removed, and dried using a freeze dryer (at least 24 hours for constant weight). All the obtained samples were thoroughly mixed to have a homogeneous sample and were stored at −18 °C until analysis.

3.2 Materials and reagents

Certified Hg standard solution of 1002 ± 7 mg L^{-1} in 10% HNO_3 was obtained from SCP Science (Baie D'Urfé, Canada) and was used for further dilutions in order to prepare eight calibration standard solutions in the range from 0.02 to 1.5 µg L^{-1}. HNO_3 (67%, suprapure), HCl (30%, suprapure), NaOH (98%, anhydrous pellets, RPE for analysis, ACS–ISO) were purchased from Carlo Erba Reagents (Milan, Italy) and H_2O_2 (30%, suprapure) and $NaBH_4$ were obtained from Merck KgaA (Darmstadt, Germany). Deionized H_2O (resistivity, ≤18.2 MΩ cm) from an Arioso Power I RO-UP Scholar UV system (Human Corporation, Songpa-Ku, Seoul, Korea) was used throughout the study.

Graduated tubes (2.5, 5, and 10 mL in polypropylene) were purchased from Artiglass S.R.L. (Due Carrare, PD, Italy), and syringe filters (0.45-µm pore size and cellulose nitrate membrane) were obtained from GVS Filter Technology (Indianapolis, USA).

3.3 Sample preparation and Analysis

Preliminary experiments were conducted to optimize the sample digestion using a water bath (WB12, Argo Lab, Modena, Italy) at 95 °C and ~1 bar. A freeze dryer (Heto Power Dry LL1500) from Thermo Electron Corporation (Waltham, Massachusetts, USA) was employed with a vacuum of 10^{-3} mbar and a condensing plate temperature of -40 °C for drying beeswax and bee samples. An aliquot of the samples (0.05 – 1 g for honey and honeydew, 0.02 – 0.2 g for bees, beeswax, pollen, propolis, royal jelly) was treated with 0.5 mL HCl, 0.2 mL HNO_3, and 0.1 mL H_2O_2 into open graduated tubes for 30 or 60 minutes under a fume hood. Digestion blanks (n = 10) were carried out in the same way. All solutions of the digested samples were colorless and without suspended solid particles except for the honey, honeydew, and propolis solutions obtained from digestion of the largest mass. Thus, digested samples were diluted to a final volume of 5 mL with deionized water, filtered, and then analyzed by an AFS 8220 (Beijing Titan Instrumental Co., Ltd., Beijing, China) with Ar (99.999% purity, SOL Spa, Monza, Italy) as a carrier gas. HCl (5%, v/v) was used as a carrier liquid, and

2% (w/v) $NaBH_4$ in 0.5% (w/v) NaOH was used as a reducing agent. The instrumental optimized parameters were previously described [59]. Duplicate analyses were performed for each sample. Blanks and control standards (at 0.4 μg L^{-1}) were run every 20 determinations to evaluate instrument drift.

3.4 Quality assurance

The analytical performance parameters of selectivity, linearity, detection and quantification limit (DL and QL, respectively), precision, and accuracy were evaluated. The validation process was performed using spiked real sample assays. Method blanks, in-house quality control samples, and spiked and non-spiked real samples (three replicates each) were prepared along with every digested sample batch. Hg standard solution at 2, 20 or 100 μg L^{-1} was made for spikes; 0.05 mL of the spike solution was added to appropriate tubes 30 min before reagents and digestion. At the instrument, the concentration was 0.02, 0.2 or 1 μg L^{-1}. For the recovery determination, the non-spiked real sample concentration was subtracted from that measured in the spiked real sample.

An eight-point calibration curve, consisting of Hg concentrations between 0.02 and 1.5 μg L^{-1}, was prepared using aqueous standards and the standard addition method for each matrix. The DL was defined as the Hg concentration corresponding to three times the digestion blanks' standard deviation (n = 10).

3.5 Statistical analysis

Statistical analysis was performed using the SPSS 25.0 program (IBM Corp., Armonk, NY, USA). All data were normally distributed as confirmed by the Kolmogorov–Smirnov test. One-way ANOVA, followed by Bonferroni post hoc test, was used to determine the significant differences among the Hg concentrations for each matrix in different geographical areas. The probability level of $p < 0.05$ was considered statistically significant. For statistical analysis, in samples where the Hg concentration was below DL, the used values were one half of DL.

4. Conclusions

Coupling water bath digestion with CV-AFS analysis proved a good analytical tool for evaluating Hg contamination in bees and beehive products (beeswax, honey, honeydew, pollen, propolis and royal jelly). Due to the possibility of preparing the sample using a single same autosampler tube, the optimized digestion procedure allows to prevent sample loss, minimize manipulation, and reduce both reagent volumes and final dilution. The proposed method is suitable for small masses (down to 0.02 g) of all selected matrices and can be used for biomonitoring and food quality control. In particular, the results from the application in the field of the proposed method show a higher Hg concentration in bees than the other matrices considered and in areas with a higher anthropogenic impact than the background site. In the future, considering alternative and parallel measurements of the contamination of the environmental compartment of interest, it will be interesting to evaluate whether indeed bees and hive products can be used to assess environmental spatial changes in Hg levels. However, the determination of Hg concentrations in beehive products is also important for potential human dietary exposure. The Hg concentrations in the analyzed samples of honey, honeydew, and royal jelly

are not a cause for concern for consumer health effects. Furthermore, the data in this study can be used as a reference for comparing Hg concentrations to other countries in the world.

Author Contributions: Conceptualization, M.L.A.; methodology, M.L.A.; validation, M.L.A.; formal analysis, M.L.A. and L.M.; investigation, M.L.A., M.R. and M.A.F.; resources, M.L.A., M.E.C., M.P. and S.C.; data curation, M.L.A.; writing—original draft preparation, M.L.A.; writing—review and editing, M.L.A., M.E.C and S.C.; visualization, M.L.A.; supervision, M.L.A.; funding acquisition, M.E.C. All authors have read and agreed to the published version of the manuscript.

References

83. Langford, N.J.; Ferner, R.E. Toxicity of mercury. *J. Hum. Hypertens.* **1999**, 13, 651–656.
84. Clarkson, T.W.; Magos, L. The toxicology of mercury and its chemical compounds. *Crit. Rev. Toxicol.* **2006**, 36, 609–662. doi: 10.1080/10408440600845619.
85. Selin, N.E. Global biogeochemical cycling of mercury: a review. *Annu. Rev. Environ. Resour.* **2009**, 34, 43–63. doi: 10.1146/annurev.environ.051308.084314.
86. United Nations Environment Programme (UNEP). Global Mercury Assessment 2013: sources, emissions, releases and environmental transport. UNEP Chemicals Branch, Geneva, Switzerland. https://wedocs.unep.org/handle/20.500.11822/7984. Accessed 02/05/2021.
87. Agency for Toxic Substances and Disease Registry (ATSDR). **1999**. Toxicological profile for Mercury. Atlanta, GA: U.S. Department of Health and Human Services, Public Health Service. http://www.atsdr.cdc.gov/toxprofiles/tp46.pdf
88. Berglund, M.; Lind, B.; Björnberg, K.A.; Palm, B.; Einarsson, O.; Vahter, M. Inter-individual variations of human mercury exposure biomarkers: a cross-sectional assessment. *Environ. Health* **2005**, 4(20), 1–11. doi: 10.1186/1476-069X-4-20.
89. World Health Organization (WHO). Mercury and Health. Fact sheet. https://www.who.int/news-room/fact-sheets/detail/mercury-and-health. Accessed 02/05/2021.
90. European Food Safety Authority (EFSA). Mercury as undesirable substance in animal feed. Scientific opinion of the Panel on Contaminants in the Food Chain. *The EFSA Journal* **2008**, 654, 1–74.
91. European Food Safety Authority (EFSA). Scientific Opinion on the risk for public health related to the presence of mercury and methylmercury in food. *The EFSA Journal* **2012**, 10(12), 2985.
92. European Parliament. Directive 2004/107/EC of the European Parliament and of the Council of 15 December 2004 relating to arsenic, cadmium, mercury, nickel and polycyclic aromatic hydrocarbons in ambient air. *Off. J. Eur. Communities* **2004**, 23, 3–16.
93. European Parliament. Directive 2008/50/EC of the European Parliament and of the Council of 21 May 2008 on ambient air quality and cleaner air for Europe. *Off. J. Eur. Union* **2008**, 152, 1–44.

94. European Parliament. Directive 2010/75/EU of the European Parliament and of the Council of 24 November 2010 on industrial emissions (integrated pollution prevention and control). *Off. J. Eur. Union* **2010**, 334, 17–119.
95. European Parliament. Regulation (EU) 2017/852 of the European Parliament and of the Council of 17 May 2017 on mercury, and repealing Regulation (EC) No 1102/2008. *Off. J. Eur. Union* **2017**, 137, 1–21.
96. Pirrone, N.; Aas, W.; Cinnirella, S.; Ebinghaus, R.; Hedgecock, I.M.; Pacyna, J.; Sprovieri, F.; Sunderland, E.M. Toward the next generation of air quality monitoring: Mercury. *Atmos. Environ.* **2013**, 80, 599–611. doi: 10.1016/j.atmosenv.2013.06.053.
97. Sprovieri, F.; Pirrone, N.; Ebinghaus, R.; Kock, H.; Dommergue, A. A review of worldwide atmospheric mercury measurements. *Atmos. Chem. Phys. Discuss.* **2010**, 10, 8245–8265. doi: 10.5194/acp-10-8245-2010.
98. Conti, M.E.; Cecchetti, G. Biological monitoring: lichens as bioindicators of air pollution assessment—a review. *Environ. Pollut.* **2001**, 114(3), 471-492. doi: 10.1016/s0269-7491(00)00224-4.
99. Wolterbeek, H.T. Biomonitoring of trace element air pollution: Principles, possibilities and perspectives. *Environ. Pollut.* **2002**, 120, 11–21. doi: 10.1016/S0269-7491(02)00124-0.
100. Bargagli, R. Moss and lichen biomonitoring of atmospheric mercury: A review. *Sci. Total Environ.* **2016**, 572, 216–231. doi: 10.1016/j.scitotenv.2016.07.202.
101. Fortuna, L.; Candotto Carniel, F.; Capozzi, F.; and Tretiach, M. Congruence evaluation of mercury pollution patterns around a waste incinerator over a 16-year-long period using different biomonitors. *Atmosphere* **2019**, 10, 183. doi: 10.3390/atmos10040183.
102. Massimi, L.; Conti, M.E.; Mele, G.; Ristorini, M.; Astolfi, M.L.; Canepari, S. Lichen transplants as indicators of atmospheric element concentrations: a high spatial resolution comparison with PM 10 samples in a polluted area (Central Italy). *Ecol. Indic.* **2019**, 101, 759–769. doi: 10.1016/j.ecolind.2018.12.051.
103. Vitali, M.; Antonucci, A.; Owczarek, M.; Guidotti, M.; Astolfi, M.L.; Manigrasso, M.; Avino, P.; Bhattacharya, B.; Protano, C. Air quality assessment in different environmental scenarios by the determination of typical heavy metals and Persistent Organic Pollutants in native lichen Xanthoria parietina. *Environ. Pollut.* **2019**, 254, 113013. doi: 10.1016/j.envpol.2019.113013.
104. Ristorini, M.; Astolfi, M.L.; Frezzini, M.A.; Canepari, S.; Massimi, L. Evaluation of the efficiency of Arundo donax L. Leaves as biomonitors for atmospheric element concentrations in an urban and industrial area of central Italy. *Atmosphere* **2020**, 11(3), 226. doi: 10.3390/atmos11030226.
105. Bargańska, Z.; Ślebioda, M.; Namieśnik, J. Honey bees and their products: Bioindicators of environmental contamination. *Crit. Rev. Env. Sci. Tec.* **2016**, 46(3), 235–248. doi: 10.1080/10643389.2015.1078220.
106. Maragou, N.C.; Pavlidis, G.; Karasali, H.; Hatjina, F. Cold vapor atomic absorption and microwave digestion for the determination of mercury in honey, pollen, propolis and bees of greek origin. *Global NEST J.* **2016**, 18(4), 690–696.

107. Grainger, M.N.C.; Hewitt, N.; French, A.D. Optimised approach for small mass sample preparation and elemental analysis of bees and bee products by inductively coupled plasma mass spectrometry. *Talanta* **2020**, 214, 120858. doi: 10.1016/j.talanta.2020.120858.
108. Burdock G.A. Review of the Biological Properties and Toxicity of Bee Propolis. *Food Chem. Toxicol.* **1998**, 36, 347–363. doi: 10.1016/s0278-6915(97)00145-2.
109. Kalogeropoulos, N.; Konteles, S.J.; Troullidou, E.; Mourtzinos, I.; Karathanos, V.T. Chemical composition, antioxidant activity and antimicrobial properties of propolis extracts from Greece and Cyprus. *Food Chem.* **2009**, 116(2), 452–461. doi.org/10.1016/j.foodchem.2009.02.060.
110. Tsiapara, A.V.; Jaakkola, M.; Chinou, I.; Graikou, K.; Tolonen, T.; Virtanen, V.; Moutsatsou, P. Bioactivity of Greek honey extracts on breast cancer (MCF-7), prostate cancer (PC-3) and endometrial cancer (Ishikawa) cells: Profile analysis of extracts. *Food Chem.* **2009**, 116(3), 702–708. doi: 10.1016/j.foodchem.2009.03.024.
111. Melliou, E.; Chinou, I. Chemical constituents of selected unifloral Greek bee-honeys with antimicrobial activity. *Food Chem.* **2011**, 129(2), 284–290. doi: 10.1016/j.foodchem.2011.04.047.
112. Burlando, B.; Cornara, L. Honey in dermatology and skin care: a review. *J. Cosmet. Dermatol-US* **2013**, 12(4), 306–313. doi: 10.1111/jocd.12058.
113. Toporcák, J.; Legáth, J.; Kul'ková, J. Levels of mercury in samples of bees and honey from areas with and without industrial contamination. *Vet. Med.* **1992**, 37(7), 405–412.
114. Pisani, A.; Protano, G.; Riccobono, F. Minor and trace elements in different honey types produced in Siena County (Italy*). Food Chem.* **2008**, 107(4), 1553–1560. doi: 10.1016/j.foodchem.2007.09.029.
115. Dos Santos Depoi, F.; Bentlin, F.R.S.; Pozebon, D. Methodology for Hg determination in honey using cloud point extraction and cold vapour-inductively coupled plasma optical emission spectrometry. *Anal. Methods* **2010**, 2, 180–185. doi: 10.1039/b9ay00189a.
116. Domínguez, M.A; Grünhut, M.; Pistonesi, M.F.; Di Nezio, M.S.; Centurión, M.E. Automatic flow-batch system for cold vapor atomic absorption spectroscopy determination of mercury in honey from argentina using online sample treatment. J. Agr. *Food Chem.* **2012**, 60, 4812–4817. doi: 10.1021/jf300637b.
117. Ru, Q.-M.; Feng, Q.; He, J.-Z. Risk assessment of heavy metals in honey consumed in Zhejiang province, southeastern China. *Food Chem. Toxicol.* **2013**, 53, 256–262. doi: 10.1016/j.fct.2012.12.015.
118. Bilandžić, N.; Gačić, M.; Đokić, M.; Sedak, M.; Šipušić, Đ. I.; Končurat, A.; Gajger, I.T. (2014). Major and trace elements levels in multifloral and unifloral honeys in Croatia. *J. Food Compos. Anal.* **2014**, 33, 132–138. doi: 10.1016/j.jfca.2013.12.002.
119. Vieira, H.P.; Nascentes, C.C.; Windmöller, C.C. Development and comparison of two analytical methods to quantify the mercury content in honey. *J. Food Compos. Anal.* **2014**, 34, 1–6. doi: 10.1016/j.jfca.2014.02.001.
120. Meli, M.A.; Desideri, D.; Roselli, C.; Benedetti, C.; Feduzi, L. Essential and toxic elements in honeys from a region of central Italy. *J. Toxicol. Env. Heal.* **2015**, A 78(10), 617–627. doi: 10.1080/15287394.2014.1004006.

121. Toth, T.; Kopernicka, M.; Sabo, R.; Kopernicka, T. The evaluation of mercury in honey bees and their products from eastern Slovakia. *Scientific Papers: Animal Science and Biotechnologies* **2016,** 49, 257–260.
122. Dżugan, M.; Wesołowska, M.; Zaguła, G.; Kaczmarski, M.; Czernicka, M.; Puchalski, C. Honeybees (Apis mellifera) as a biological barrier for contamination of honey by environmental toxic metals. *Environ. Monit. Assess.* **2018**, 190, 101. doi: 10.1007/s10661-018-6474-0.
123. Jovetić, M.S.; Redžepović, A.S.; Nedić, N.M.; Vojt, D.; Đurđić, S.Z.; Brčeski, I.D.; Milojković-Opsenica, D.M. Urban honey - the aspects of its safety. *Arh. Hig. Rada Toksikol.* **2018**, 69(3), 264–274. doi: 10.2478/aiht-2018-69-3126.
124. Bommuraj, V.; Chen, Y.; Klein, H.; Sperling, R.; Barel, S.; Shimshoni J.A. Pesticide and trace element residues in honey and beeswax combs from Israel in association with human risk assessment and honey adulteration. *Food Chem.* **2019**, 299, 125123. doi: 10.1016/j.foodchem.2019.125123.
125. Roman, A. Concentration of chosen trace elements of toxic properties in bee pollen loads. *Pol. J. Environ. Stud.* **2009,** 18(2), 265–272.
126. Morgano, M.A.; Martins, M.C.T.; Rabonato, L.C.; Milani, R.F.; Yotsuyanagi, K.; Rodriguez-Amaya, D.B. Inorganic contaminants in bee pollen from southeastern Brazil. *J. Agr. Food Chem.* **2010**, 58, 6876–6883. doi: 10.1021/jf100433p.
127. Cvek, J.; Medić-Šarić, M.; Vitali, D.; Vedrina-Dragojević, I.; Šmit, Z.; Tomić, S. The content of essential and toxic elements in Croatian propolis samples and their tinctures. *J. Apicult. Res.* **2008**, 47(1), 35–45. doi: 10.1080/00218839.2008.11101421.
128. Bonvehí, J.S.; Bermejo, F.J.O. Element content of propolis collected from different areas of South Spain. *Environ. Monit. Assess.* **2013**, 185, 6035–6047. doi: 10.1016/j.foodchem.2019.125123.
129. Matin, G.; Kargar, N.; Buyukisik, H.B. Bio-monitoring of cadmium, lead, arsenic and mercury in industrial districts of Izmir, Turkey by using honey bees, propolis and pine tree leaves. *Ecol. Eng.* **2016**, 90, 331–335. doi: 10.1016/j.ecoleng.2016.01.035.
130. Perugini, M.; Manera, M.; Grotta, L.; Abete, M.C.; Tarasco, R.; Amorena, M. Heavy metal (Hg, Cr, Cd, and Pb) contamination in urban areas and wildlife reserves: honeybees as bioindicators. *Biol. Trace Elem. Res.* **2011**, 140(2), 170–176. doi: 10.1007/s12011-010-8688-z.
131. Zaric, N.M.; Deljanin, I.; Ilijević, K.; Stanisavljević, L.; Ristić, M.; Gržetić, I. Assessment of spatial and temporal variations in trace element concentrations using honeybees (Apis mellifera) as bioindicators. *PeerJ* **2018**, 6:e5197. doi: 10.7717/peerj.5197.
132. Astolfi, M.L.; Conti, M.E.; Marconi, E.; Massimi, L.; Canepari, S. Effectiveness of different sample treatments for the elemental characterization of bees and beehive products. *Molecules* **2020**, 25, 4263. doi:10.3390/molecules25184263.
133. Melaku, S.; Gelaude, I.; Vanhaecke, F.; Moens, L.; Dams, R. Comparison of pyrolysis and microwave acid digestion techniques for the determination of mercury in biological and environmental materials. *Microchim. Acta* **2003**, 142, 7–12. doi.org/10.1007/s00604-002-0948-y

134. Astolfi, M.L.; Marconi, E.; Protano, C.; Canepari, S. Comparative elemental analysis of dairy milk and plant-based milk alternatives. *Food Control* **2020**, 116, 107327. doi.org/10.1016/j.foodcont.2020.107327.
135. Schlathauer, M.; Reitsam, V.; Schierl, R.; Leopold, K. A new method for quasi-reagent-free biomonitoring of mercury in human urine. *Anal Chim Acta* **2017**, 965, 63–71. doi: 10.1016/j.aca.2017.02.036.
136. Astolfi, M.L.; Protano, C.; Schiavi, E.; Marconi, E.; Capobianco, D.; Massimi, L.; Ristorini, M.; Baldassarre, M.E.; Laforgia, N.; Vitali, M.; Canepari, S; Mastromarino, P. A prophylactic multi-strain probiotic treatment to reduce the absorption of toxic elements: In-vitro study and biomonitoring of breast milk and infant stools. *Env. Int.* **2019**, 130, 104818. doi:10.1016/j.envint.2019.05.012.
137. Astolfi, M.L.; Pietris, G.; Mazzei, C.; Marconi, E.; Canepari, S. Element levels and predictors of exposure in the hair of Ethiopian children. *Int. J. Environ. Res. Public Health* **2020**, 17, 8652. doi:10.3390/ijerph17228652.
138. Oliveira, S.S.; Alves, C.N.; Morte, E.S.B.; Júnior, A.D.F.S.; Araujo, R.G.O.; Santos, D.C.M.B. Determination of essential and potentially toxic elements and their estimation of bioaccessibility in honeys. *Microchem. J.* **2019**, 151, 104221. doi: 10.1016/j.microc.2019.104221.
139. Tenaglia, H.; Venturini, E.; Raffaelli, R. Linee guida per la validazione dei metodi analitici e per il calcolo dell'incertezza di misura- Accreditamento e certificazione. Bologna: Agenzia Regionale Prevenzione e Ambiente dell'Emilia Romagna; 2003. (I Manuali ARPA).
140. Commission Decision 2002/657/EC of 12 August 2002 implementing Council Directive 96/23/EC concerning the performance of analytical methods and the interpretation of results.
141. Astolfi, M.L.; Protano, C.; Marconi, E.; Piamonti, D.; Massimi, L.; Brunori, M.; Vitali, M.; Canepari, S. Simple and rapid method for the determination of mercury in human hair by cold vapour generation atomic fluorescence spectrometry. *Microchem. J.* **2019**, 150, 104186. doi:10.1016/j.microc.2019.104186.
142. Herrero-Latorre, C.; Barciela-García, J.; García-Martín, S.; Peña-Crecente, R.M. The use of honeybees and honey as environmental bioindicators for metals and radionuclides: A review. *Environ. Rev.* **2017**, 25, 463–480. doi: 10.1139/er-2017-0029.
143. AL-Alam, J.; Chbani, A.; Faljoun, Z.; Millet, M. The use of vegetation, bees, and snails as important tools for the biomonitoring of atmospheric pollution—a review. *Environ. Sci. Pollut. Res.* **2019**, 26, 9391–9408. doi:10.1007/s11356-019-04388-8.
144. Zhelyazkova, I. Honeybees—bioindicators for environmental quality. *Bulg. J. Agric. Sci.* **2012**, 18, 435–442.
145. Finger, D.; Filho, I.K.; Torres, Y.R.; Quináia, S.P. Propolis as an indicator of environmental contamination by metals. Bull. Environ. *Contam. Toxicol.* **2014**, 92, 259–64. doi: 10.1007/s00128-014-1199-4.
146. Conti, M.E.; Botrè, F. Honeybees and their products as potential bioindicators of heavy metals contamination. *Environ. Monit. Assess.* **2001,** 69(3), 267-282. doi: 10.1023/A:1010719107006.

147. Codex Alimentarius. Standard for honey (CXS 12–1981). http://www.fao.org/fao-who-codexalimentarius/sh-proxy/en/?lnk=1&url=https%253A%252F%252Fworkspace.fao.org%252Fsites%252Fcodex%252FStandards%252FCXS%2B12-1981%252FCXS_012e.pdf. Accessed 02/05/2021.
148. FAO/WHO. Evaluation of certain food additives and contaminants. Seventy-second Report of the Joint FAO/WHO Expert Committee on Food Additives, Rome, February 16–25, 2010. *WHO Technical Report Series* **2010**, No. 959. Geneva, Switzerland

Supplementary Materials

Table S1 - Summary of the analytical characteristics of the proposed method and comparison with some previous methods published during the last decade (2010-2020).

Reference	Sample matrix	Sample preparation	Total sample digestion time	Technique	LOD	LOQ	Accuracy (R%)	Precision (CV%)	Dynamic range (Log)
This study	Bees, honey, beeswax, honeydew, pollen, propolis, and royal jelly	0.02 g bee, pollen, propolis and royal jelly, 0.05 g beeswax and honey, or 0.1 g honeydew + 0.5 mL HCl, 0.2 mL HNO_3 and 0.1 mL H_2O_2 were digested in a water bath (95 °C, 30 min) → volume completed to 5 mL deionized water.	About 30 min for 120 samples or more.	CV-AFS	0.5 µg kg^{-1} (for a sample mass of 0.1 g)–3 µg kg^{-1} (for a sample mass of 0.02 g)	1 µg kg^{-1} (for a sample mass of 0.1 g)–5 µg kg^{-1} (for a sample mass of 0.02 g)	86 (honey, 0.05 g)–117% (royal jelly, 0.02 g)	<10%	1.9
[1]	Bees, honey, and pollen	20–200 mg bee, 20–100 mg pollen or 50–200 mg honey + 0.2 mL HNO_3 followed by 0.1 mL H_2O_2 in a digestion block (80 °C, 2 h total); samples were made up to a final volume of 6 mL.	2h	ICP-MS	14, and 4 µg kg^{-1} for a honey sample mass of 0.05 and 0.2 g, respectively	-	96 (B)–129% (As) for trace elements and 91 (Pr)–112% (La) for rare earth elements	<15%	-
[2]	Bees, honey, pollen, and propolis	For the bee samples drying at 100 °C for 48 h preceded microwave digestion. 1g honey, and pollen, 0.25 g propolis, or 0.1 g bees dried weight (at 100 °C for 48 h) + 5 mL HNO_3 and 2.5 mL H_2O_2 were digested in the microwave oven (30 min) → volume completed to 25 mL	About 30 min	CV-AAS	50 µg kg^{-1} for honey, 60 µg kg^{-1} for pollen, 300 µg kg^{-1} for propolis and 800 µg kg^{-1} dw for bees	-	64 (propolis)–129% (honey)	<13%	0.6
[3]	Honey	0.1–2 g + 0.5 mL HNO_3 and 0.5 mL H_2O_2 → the mixture allowed to stand for 12 h → heated to 100 °C in a metal block for 3 h → volume brought to 25 mL by adding 0.5 mol L^{-1} HCl.	15 h	Cloud point extraction (CPE), CV-ICP-OES or ICP-OES	2 µg kg^{-1} (CPE CV-ICP OES)–300 µg kg^{-1} (ICP-OES)	-	R% close to 100% when up to 2.0 g of honey were subjected to sonication or up to 1.0 g of	-	0.5 (ICP-OES)-1.5 (CPE CV-ICP OES)

							honey was decomposed with acid.		
[4]	Honey	0.5 g + 3 mL HNO_3 and 4 mL H_2O_2 were digested in the microwave oven (1400 W, 30 min) → volume completed to 50 mL high-purity water	30 min	CV-AFS	0.15 µg kg^{-1}	-	99%	1%	-
[5]	Honey	0.5 g sample + 4 mL HNO_3 and 2 mL H_2O_2 were digested in the microwave oven (1400 W, 30 min) → volume completed to 50 mL double deionised water	30 min	AMA	0.1 µg kg^{-1}	-	99%	-	3.7
[6]	Honey	For CV-AAS analysis: dilution in an acidic solution without heating. In the case of DMA, sample preparation was not necessary.	-	DMA or CV-AAS	1 or 30 µg kg^{-1} using DMA or CV-AAS, respectively	2.5 or 60 µg kg^{-1} using DMA or CV-AAS, respectively	CV-AAS: 98.7–102.4%; DMA: 95.6–99.1%	CV-AAS: 3.5–5.7%; DMA: 2.7–3.4%	1.3 or 1.5 for DMA or CV-AAS, respectively
[7]	Honey	1 g sample + 12 mL HNO_3 and 3 mL H_2O_2 were digested in the microwave oven	-	GF-AAS with a flow injection analysis system	-	-	91–113%	<10%	-
[8]	Bees, honey, and pollen	No sample pretreatment	-	AMA	0.5 µg kg^{-1}	-	-	-	-
[9]	Bees	bee were dried in a moisture analyzer to constant weight at 105 °C and ground → were digested in the microwave oven (45 min) → volume completed to 50 mL	45 min	ICP-OES	1 mg kg^{-1}	-	-	-	-
[10]	Honey, and pollen	0.5 g honey, and 0.3 g pollen + 7 mL HNO_3 and 2 mL H_2O_2 were digested in the microwave oven (from 180 to 240 °C, 40 min) → volume completed to 50 mL with deionized water.	40 min	ICP-MS	-	-	-	-	-
[11]	Beeswax, and honey	0.25 g beeswax + 5 mL HNO_3 and 1 mL H_2O_2 or 2 g honey + 5 mL HNO_3 were pre-digested at room temperature for 30 min,	50 min	High-Resolution ICP-OES	0.1 or 0.3 µg kg^{-1} for honey	0.4 or 9 µg kg^{-1} for honey or	-	-	-

		then digested using microwave oven (20 min)			or beeswax, respectively	beeswax, respectively			
[12]	Pollen	0.65-0.70 g + 10 mL HNO_3 and 3 mL H_2O_2 were digested in the microwave oven →volume completed to 25 mL with a 5% HCl (v/v).	120 min	Hydride Generator coupled with ICP-OES	0.4 µg L^{-1}	2 µg L^{-1}	79–123%	6.4%	-
[13]	Propolis	~0.1 g; no sample pre-treatment	-	AMA-254	-	2 µg kg^{-1}	98%	<5.1%	2
[14]	Honey, and propolis	2 g of lyophilized samples + 5 mL HNO3 were heated at 50 °C for 2 h and then at 110 °C for 18 h; in the next step 5 mL H_2O_2 was added to the digested sample and was heated for 6 h → volume completed to 25 mL.	26 h	GF-AAS	-	-	-	-	-
[15]	Bees	0.7 g of lyophilized sample + 7 ml HNO_3 and 1.5 mL H_2O_2 were digested	-	DMA	-	10 µg kg^{-1}	-	-	-
[16]	Bees	~0.5 g of drieed sample + 7 ml HNO_3 and 2 mL H_2O_2 were digested in the microwave oven → volume completed to 25 mL with deionized water.	30 min	ICP-MS	10 µg kg^{-1}	-	94–108%	-	-

Table S2. Recovery and precision data for Hg in bees and beehive products (n = 3) by water bath digestion (95 °C, 30 min or 60 min).

		Intermediate level spike (0.2 µg L^{-1})				**High level spike (1 µg L^{-1})**			
		30 min		60 min		30 min		60 min	
Matrix	**mass (g)**	**R%**	**CV%**	**R%**	**CV%**	**R%**	**CV%**	**R%**	**CV%**
Honey	0.05	116	9.3	119	8.1	96	7.8	91	0.6
	0.1	104	14	115	4.8	96	3.0	92	4.0
	0.2	79	9.4	116	19	82	3.7	54	28
	1	48	52	71	9.7	82	8.9	18	2.8
Honeydew	0.05	121	6.5	113	4.1	101	3.5	94	4.9
	0.1	113	10	113	2.5	91	8.4	90	9.0
	0.2	107	21	114	2.8	82	1.5	92	2.6
	1	134	9.2	91	11	81	2.6	16	1.6
Pollen	0.02	90	3.7	110	5.9	95	3.6	84	1.4
	0.05	99	6.2	110	6.4	93	5.5	92	3.9
	0.1	116	5.7	113	4.6	91	5.7	91	5.5
	0.2	92	2.3	108	8.0	91	0.9	100	7.3
Propolis	0.02	98	8.6	109	9.3	91	2.5	80	3.9
	0.05	131	4.0	153	21	80	4.3	80	1.0
	0.1	161	15	145	19	55	26	74	37
	0.2	228	9.2	144	56	131	45	99	41
Beeswax	0.02	97	11	116	1.1	99	5.7	95	3.6
	0.05	111	8.5	112	0.7	99	2.0	93	6.1
	0.1	101	0.8	117	1.3	102	9.2	82	4.2
	0.2	110	13	108	0.5	76	39	89	5.0
Royal Jelly	0.02	108	4.4	111	5.8	110	0.9	95	2.0
	0.05	110	2.4	96	2.7	110	0.8	86	3.0
	0.1	100	2.8	87	6.0	101	3.2	89	7.7
	0.2	102	6.7	88	0.8	105	2.2	88	4.4
Bees	0.02	97	4.5	92	9.9	91	10	86	1.1
	0.05	99	4.1	105	8.9	97	9.8	80	0.1
	0.1	82	8.7	100	9.0	93	5.1	85	3.5
	0.2	108	7.8	99	0.7	98	7.0	89	3.6

References

1. Grainger, M.N.C.; Hewitt, N.; French, A.D. Optimised approach for small mass sample preparation and elemental analysis of bees and bee products by inductively coupled plasma mass spectrometry. *Talanta* **2020**, 214, 120858. doi: 10.1016/j.talanta.2020.120858.
2. Maragou, N.C.; Pavlidis, G.; Karasali, H.; Hatjina, F. Cold vapor atomic absorption and microwave digestion for the determination of mercury in honey, pollen, propolis and bees of greek origin. Global NEST J. 2016, 18(4), 690–696.
3. Dos Santos Depoi, F.; Bentlin, F.R.S.; Pozebon, D. Methodology for Hg determination in honey using cloud point extraction and cold vapour-inductively coupled plasma optical emission spectrometry. Anal. Methods 2010, 2, 180–185. doi: 10.1039/b9ay00189a.
4. Ru, Q.-M.; Feng, Q.; He, J.-Z. Risk assessment of heavy metals in honey consumed in Zhejiang province, southeastern China. Food Chem. Toxicol. 2013, 53, 256–262. doi: 10.1016/j.fct.2012.12.015.
5. Bilandžić, N.; Gačić, M.; Đokić, M.; Sedak, M.; Šipušić, Đ. I.; Končurat, A.; Gajger, I.T. (2014). Major and trace elements levels in multifloral and unifloral honeys in Croatia. J. Food Compos. Anal. 2014, 33, 132–138. doi: 10.1016/j.jfca.2013.12.002.
6. Vieira, H.P.; Nascentes, C.C.; Windmöller, C.C. Development and comparison of two analytical methods to quantify the mercury content in honey. J. Food Compos. Anal. 2014, 34, 1–6. doi: 10.1016/j.jfca.2014.02.001.
7. Meli, M.A.; Desideri, D.; Roselli, C.; Benedetti, C.; Feduzi, L. Essential and toxic elements in honeys from a region of central Italy. J. Toxicol. Env. Heal. 2015, A 78(10), 617–627. doi: 10.1080/15287394.2014.1004006.
8. Toth, T.; Kopernicka, M.; Sabo, R.; Kopernicka, T. The evaluation of mercury in honey bees and their products from eastern Slovakia. Scientific Papers: Animal Science and Biotechnologies 2016, 49, 257–260.
9. Dżugan, M.; Wesołowska, M.; Zaguła, G.; Kaczmarski, M.; Czernicka, M.; Puchalski, C. Honeybees (Apis mellifera) as a bio-logical barrier for contamination of honey by environmental toxic metals. Environ. Monit. Assess. 2018, 190, 101. doi: 10.1007/s10661-018-6474-0.
10. Jovetić, M.S.; Redžepović, A.S.; Nedić, N.M.; Vojt, D.; Đurđić, S.Z.; Brčeski, I.D.; Milojković-Opsenica, D.M. Urban honey - the aspects of its safety. Arh. Hig. Rada Toksikol. 2018, 69(3), 264–274. doi: 10.2478/aiht-2018-69-3126.
11. Bommuraj, V.; Chen, Y.; Klein, H.; Sperling, R.; Barel, S.; Shimshoni J.A. Pesticide and trace element residues in honey and beeswax combs from Israel in association with human risk assessment and honey adulteration. Food Chem. 2019, 299, 125123. doi: 10.1016/j.foodchem.2019.125123.

12. Morgano, M.A.; Martins, M.C.T.; Rabonato, L.C.; Milani, R.F.; Yotsuyanagi, K.; Rodriguez-Amaya, D.B. Inorganic contaminants in bee pollen from southeastern Brazil. J. Agr. Food Chem. 2010, 58, 6876–6883. doi: 10.1021/jf100433p.
13. Bonvehí, J.S.; Bermejo, F.J.O. Element content of propolis collected from different areas of South Spain. Environ. Monit. Assess. 2013, 185, 6035–6047. doi: 10.1016/j.foodchem.2019.125123.
14. Matin, G.; Kargar, N.; Buyukisik, H.B. Bio-monitoring of cadmium, lead, arsenic and mercury in industrial districts of Izmir, Turkey by using honey bees, propolis and pine tree leaves. Ecol. Eng. 2016, 90, 331–335. doi: 10.1016/j.ecoleng.2016.01.035.
15. Perugini, M.; Manera, M.; Grotta, L.; Abete, M.C.; Tarasco, R.; Amorena, M. Heavy metal (Hg, Cr, Cd, and Pb) contamination in urban areas and wildlife reserves: honeybees as bioindicators. *Biol. Trace Elem. Res.* **2011**, 140(2), 170–176. doi: 10.1007/s12011-010-8688-z.
16. Zaric, N.M.; Deljanin, I.; Ilijević, K.; Stanisavljević, L.; Ristić, M.; Gržetić, I. Assessment of spatial and temporal variations in trace element concentrations using honeybees (Apis mellifera) as bioindicators. *PeerJ* **2018**, 6:e5197. doi: 10.7717/peerj.5197.

11.2.2 (F2) Multi-element characterization and antioxidant activity of Italian extravirgin olive oils

Frontiers in Chemistry (2021), 9:769620, doi: : 10.3389/fchem.2021.769620

Maria Luisa Astolfi[1*], Federico Marini[1], Maria Agostina Frezzini[2], Lorenzo Massimi[2], Anna Laura Capriotti[1], Carmela Maria Montone[1], Silvia Canepari[2]

[1]Department of Chemistry, Sapienza University of Rome, Rome, Italy

[2]Department of Environmental Biology, Sapienza University of Rome, Rome, Italy

[*]Corresponding author

Keywords: authenticity, chemometrics, inductively coupled plasma mass spectrometry, olive oil, statistical analysis, trace elements, traceability

Abstract

Food product safety and quality are closely related to the elemental composition of food. This study combined multi-element analysis and chemometric tools to characterize 237 extra-virgin olive oil (EVOO) samples from 15 regions of Italy, and to verify the possibility of discriminating them according to different quality factors, such as varietal or geographical origin or whether organically or traditionally produced. Some elements have antioxidant properties, while others are toxic to humans or can promote oxidative degradation of EVOO samples. In particular, the antioxidant activity of oils' hydrophilic fraction was estimated and the concentrations of 45 elements were determined by inductively coupled plasma mass spectrometry (ICP-MS). At first, univariate and multivariate analysis of variance were used to compare the element concentrations, and statistically significant differences were found among samples from different regions. Successively, discriminant classification approaches were used to build a model for extra-virgin olive oil authentication, considering, in turn, various possible categorizations. The results have indicated that chemometric methods coupled with ICP-MS have the potential to discriminate and characterize the different types of EVOO, and to provide "typical" elemental fingerprints of the various categories of samples.

1. Introduction

The elemental composition of foods is of toxicological and nutritional interest and can be considered an important quality parameter (Astolfi et al., 2021a, 2020a, 2020b). In particular, the concentrations of trace elements in extra virgin olive oil (EVOO) are also one of the criteria for the assessment of the quality regarding storable period and freshness (Choe and Min, 2006). In fact, some elements, such as Ca, Co, Cu, Fe, Mg, Mn, Ni, and Sn, can promote the oxidative degradation of this important component of the Mediterranean diet appreciated among consumers for its nutritional properties and specific flavor (Choe and Min, 2006). Other elements (such as As, Cd, Cr, Cu, Hg and Pb) present in EVOO are of great concern because they are toxic and potentially carcinogenic to humans even at low concentration (Tchounwou et al., 2012). The International

Olive Council has established, as a quality criterion, a maximum residue level (MRL) for the content of As, Cu, Pb (0.1 mg kg^{-1}) and Fe (3 mg kg^{-1}) in olive oils and olive–pomace oils (International Olive Council, 2019) and the maximum levels of Cu and Fe in other vegetable oils have been also legislated (Codex Stan 33-1981), varying from 0.1 up to 5.0 mg kg^{-1}. Recently, elements determination in EVOO samples has gained importance for oil geographical traceability and authentication (Zaroualet al., 2021; Aceto et al., 2019; Bajoub et al., 2018; Beltran et al., 2015; Benincasa et al., 2007; Cabrera Vique et al., 2012; Camin et al., 2010; Cordella et al., 2002; Damak et al., 2019; Dugo et al., 2004). In particular, elements are useful in the characterization of protected designations of origin (PDOs) or protected geographical indications (PGIs) (European Union (EU), 2012), and they can also contribute to determine EVOO geographical provenance of non PDO oils (Aceto et al., 2019; Beltran et al., 2015). In fact, the presence of metals in EVOO varies according to their origin and can be due to natural contamination from the soil, environment, fertilizers, genotype of the plant or to the production process and contact with storage materials (Bakircioglu et al., 2013; Chatzistathis et al., 2009; Kabata-Pendias, 2010; Lepri et al., 2011; Yaşar et al., 2012; Zeiner et al., 2015). A suitable statistical treatment of trace element data could allow a geographical characterization of different EVOO samples. Principal component analysis (PCA) and hierarchical cluster analysis (HCA) (Gumus et al., 2017; Luka and Akun, 2019; Russo et al., 2020; Savio et al., 2014;), linear discriminant analysis (LDA) (Damak et al., 2019; Beltran et al., 2015; Cabrera-Vique et al., 2012; Benincasa et al., 2007), classification trees (CTs) (Gumus et al., 2017) and neural networks (ANNs) (Gonzalez-Fernandez et al., 2019; Farmaki et al., 2012) have been used most.

Several beneficial implications of EVOO are derived from its antioxidant content (Dugo et al., 2020; Hannachi et al., 2020). Intake of antioxidant compounds from oil, such as phenols, phenolic acids and flavonoids (Capriotti et al., 2014), is usually related to health well-being. As well known, natural antioxidants play a key role in contrasting reactive species activity in living organisms, thus preventing oxidative stress-related diseases, such as cardiovascular and neurodegenerative illness and many other chronic disorders (Šarolić et al., 2014; Cioffi et al., 2010; Pérez-Jiménez et al., 2008). Moreover, antioxidants prevent lipid oxidations that cause quality degradation and unpleasant taste formation in edible oils (Christodouleas et al., 2015). Therefore, estimating of antioxidant capacity is crucial for evaluating oil's healthy and organoleptic properties. One of the most widely used *in vitro* procedure to routinely and globally estimate oil antioxidant power is the 2,2-Diphenyl-1-picrylhydrazyl spectrophotometric assay (DPPH) that has the possibility of easily being applied to a high number of samples allowing a great level of reliability (Frezzini et al., 2019; Kedare and Singh, 2011). The assay is based on the quantitative measurement of the decrease of absorbance due to the scavenging capacity of antioxidants present in the sample towards DPPH· free radicals (Christodouleas et al., 2015).

All the described aspects making trace element determination, as well as the antioxidant activity of EVOO samples, very important for both economic and health context (Zaroualet al., 2021; Bajoub et al., 2018). In particular, the European Union is the first producer, consumer and exporter of olive oil in the world (Eurostat, 2019; IOC, 2018a,b). Italy follows Spain, the first world producer with an average 20% of the total European olive oil production. About two thirds of total Italian production is represented by EVOO (Carbone et al., 2018). Therefore, the use of a rapid and accurate analytical method for trace elements analysis in EVOO has a

great importance in quality control and food analysis (Shah and Soylak, 2021; Llorent-Martínez et al., 2011). Unfortunately, the determination of trace elements in EVOO samples is particularly difficult to perform, as some of them are present at very low concentrations and due to high complexity of the matrix (Shah and Soylak, 2021; Trindade et al., 2015). Sample preparation of EVOO samples is a critical step and the determination of trace elements in EVOO requires very sensitive instrumental techniques such as inductively coupled plasma - mass spectrometry (ICP-MS) (Astolfi et al., 2021b).

The main purpose of this study is to evaluate the most significant relationships between element levels in EVOO and different categorizations, mostly related to the geographical origin using chemometric tools coupled with the ICP-MS method. For this purpose, 45 elements from a total of 237 EVOO samples from 15 Italian regions were analyzed. Also the antioxidant activity of oils' hydrophilic fraction (HF) was estimated by the DPPH assay. The corresponding data set constituted the basis for building and validating classification models for the discrimination of the samples according to specific categorizations, which reflect possible quality attributes of the oils (and for which there could be a statistically significant number of individuals available). In particular, discriminant classification models were built using partial least squares discriminant analysis (PLS-DA) to account for the possibility of dealing with correlated variables and low samples to variable ratios; moreover, to evaluate model stability and, at the same time, their reliability in an unbiased way, also in cases where the available number of samples per category was not too large, a repeated double cross-validation strategy (rDCV) was adopted.

2. Materials and Methods

2.1 Sample collection

EVOO samples (N = 237) were collected between 2017 and 2018 from 15 production regions of Italy and different cultivars. In particular, a total of 64 EVOO samples were with protected designations of origin (PDOs) and 21 with protected geographical indications (PGIs) (European Union (EU), 2012). Table 1 summarizes the number of EVOO samples according to their geographical provenances in terms of the regions. All samples (~100 mg) were kept in screw-capped glass vials in the dark at room temperature until analysis.

2.2 Chemicals

All the solutions were prepared with deionized water (18.3 MΩ cm resistivity) obtained from an Arioso (Human Corporation, Seoul, Korea) Power I RO-UP Scholar UV deionizer system. HNO_3 at 67% (suprapure; Carlo Erba Reagents, Milan, Italy), H_2O_2 at 30% (suprapure; Merck KgaA, Darmstadt, Germany) and Ar, He and H_2 gases at 99.9995% (SOL Spa, Monza, Italy) were used.

For ICP-MS analysis, all calibration standard solutions were prepared from a 1000 mg L^{-1} multi-element standard solution (VWR International, Milan, Italy) by dilution with 10 % (v/v) HNO_3 and H_2O_2 (2:1 v/v). Single standard solutions of In, Rh, Sc, Th (at 0.010 mg L^{-1} from 1000 ± 5 mg L^{-1}; Merck KGaA, Darmstadt, Germany), and Y (at 0.005 from 1000 ± 2 mg L^{-1}; Panreac Química, Barcelona, Spain) were used as internal standards. A multi-elemental solution containing Ba, Be, Ce, Co, In, Pb, Mg, Tl, and Th (at 0.005 mg L^{-1} from

10.00 ± 0.05 mg L^{-1}; Spectro Pure, Ricca Chemical Company, Arlington, TX, USA) was used to check the instrument performance.

For the estimation of the antioxidant activity of EVOO samples, DPPH was purchased from Sigma Aldrich Co. (St. Louis, MO, USA).

2.3 Sample preparation and analysis

2.3.1 Analysis of elements

Duplicate samples (~0.5 g) of each EVOO variety were accurately weighed in 10-mL disposable graduated tubes (Artiglass, Due Carrare, PD, Italy). Then, 5 mL reagent mixture of 10 % (v/v) HNO_3 and H_2O_2 (2:1 v/v) was added to each tube and heated in a water bath (WB12, Argo Lab, Modena, Italy) at 95 °C for 40 min (Astolfi et al., 2021b). The lower aqueous phase was transferred into a clean tube and subjected to the ICP-MS (820-MS; Bruker, Bremen, Germany) analysis without further dilutions. The elements were monitored in standard and collision-reaction interface (CRI) modes to check and reduce possible polyatomic interference, and the following isotopes were used: ^{7}Li, ^{9}Be, ^{11}B, ^{23}Na, ^{24}Mg, ^{27}Al, ^{28}Si, ^{31}P, ^{39}K, ^{44}Ca, ^{49}Ti, ^{51}V, ^{52}Cr, ^{55}Mn, ^{57}Fe, ^{59}Co, ^{60}Ni, ^{65}Cu, ^{66}Zn, ^{71}Ga, ^{75}As, ^{78}Se, ^{85}Rb, ^{88}Sr, ^{90}Zr, ^{93}Nb, ^{98}Mo, ^{107}Ag, ^{112}Cd, ^{118}Sn, ^{121}Sb, ^{125}Te, ^{133}Cs, ^{137}Ba, ^{139}La, ^{140}Ce, ^{141}Pr, ^{146}Nd, ^{159}Tb, ^{163}Dy, ^{182}W, ^{205}Tl, ^{208}Pb, ^{209}Bi, and ^{238}U. CRI was used with He (30 mL min^{-1}) and H_2 (70 mL min^{-1}) as cell gases. The ICP-MS operating conditions and parameters were as follows: radiofrequency power 1400 W; plasma Ar flow rate 18 L min^{-1}; auxiliary Ar flow rate 1.8 L min^{-1}; nebulizer gas flow rate 0.9 L min^{-1}; peak hopping scanning mode; steady-state analysis mode; dwell time between 50 ms and 100 ms, pump rate 3 rpm; 5 scans/replicate; and 3 replicates/sample. For the quantitative analysis of EVOO samples, calibration curves were built on seven different concentrations between 0.00025-0.05 mg L^{-1} and 0.0125 and 5 mg L^{-1} for all trace and major elements, respectively.

2.3.2 Estimation of antioxidant activity

DPPH assay was performed according to the procedure described by Šarolić et al. (2014) with slight modifications. In detail, ~0.5 g of each EVOO sample were mixed with 1 mL of 80:20 (v/v) CH_3OH:H_2O, and the mixture was blended in an ultrasonic bath (Proclean 10.0 ultrasonic cleaner; Ulsonix, Germany) for 15 min at 30 °C. When the two phases appeared, the hydrophilic phase was collected, and the extraction was repeated another two times. Then, the hydrophilic extracts were combined to get a homogeneous sample. To perform DPPH assay, 50 µL of HF sample were added to 2 mL of methanolic DPPH (0.04 mM), then the mixture was shaken for 30 min by rotating agitation (60 rpm; Rotator; Glas-Col, USA) at room temperature in the dark, and analyzed by UV-Vis spectrophotometry (Varian Cary 50 Bio UV-Vis; Varian Inc., Palo Alto, CA, USA) set at 517 nm, by measuring the sample absorbance decrease against the control (blank solution). Solutions were prepared daily and used fresh, and three replicates of each type of oil were performed. The DPPH radical scavenging activity was calculated in terms of percentage reduction of DPPH according to the following equation:

$$\text{DPPH}\ [\%] = \frac{(A_0 - A_S)}{A_0} \times 100$$

where A_0 represents the absorbance of the blank solution and A_S is the absorbance of the sample.

2.4 Quality assurance

The method accuracy for element determination was checked by recovery assays in the EVOO samples adding element at the low (0.005 and 0.02 mg L^{-1}) and high (0.2 and 1 mg L^{-1}) spike concentrations for all trace and major elements (B, Ca, K, Mg, Na, P, Si, and Sr) and always in the linear calibration range. In addition, accuracy was tested by a certified reference material (Conostan S-21; Lot number: 21550100) obtained from SCP Science (Baie D'Urfé, Canada). The recoveries fell within 20% of the expected value and reproducibility lower than 20% (Astolfi et al., 2021b). The method detection and quantification limits (MDL and MQL, respectively) were in the range 0.004-510 µg kg^{-1} and 2.5-5000 µg kg^{-1}, respectively. Only the Ca, Cr, Mg, Mn, Ni, P, Rb, Ti, and Zn levels in the EVOO samples were 100% greater than the MDL. The possible instrumental drift for the ICP-MS analysis was checked and corrected using an internal standard solution of In, Rh, Sc, Th, and Y (Astolfi et al., 2021b, 2020c). Blank samples and control standards were tested every 20 samples in each run, and re-calibration was performed every 100 samples.

2.5 Statistical Analysis

The data were statistically evaluated according to the procedures of the software SPSS Statistics 25 (IBM Corp., Armonk, NY, USA) for univariate analysis. Analytical replicates were averaged prior to the successive elaboration. Non parametric tests (Kruskal–Wallis and pairwise post-hoc) were applied because of the unequal numbers of samples per group and the not normal distribution (Soliani, 2003). The element concentrations measured below MDL were substituted by its half value (MDL/2) for the statistical elaboration (Farmaki et al., 2012). A p-value lower than 0.05 was considered statistically significant.

Partial least squares discriminant analysis (PLS-DA; Ståhle and Wold, 1987; Barker and Rayens, 2003) implemented through in-house written functions running under Matlab environment (R2015b, v.8.6, The Mathworks Inc., Natick, MA) was used to build multivariate classification models. PLS-DA is a regression-based classification model which operates by coding class belonging by means of a dummy binary response matrix (or vector, when the problems involve only pairs of classes, as in the present study). In particular, if discrimination is sought between two categories, class belonging of the training samples is described by the vector y, having 1 in correspondence of all the individuals from the first class and 0 in all the remaining positions (i.e., those corresponding to the second group). A PLS model (Wold et al., 1983) is then built between the experimental data X and the dummy vector y, and the predicted value of the response ($\hat{\boldsymbol{y}}$) constitutes the basis for the classification of the samples: since the predicted responses are real-valued, an optimal threshold y_{thres} has to be calculated so that, if the predicted response is greater than y_{thres}, the sample is predicted as class 1, otherwise as class 2. In the present study, the threshold was calculated by applying LDA on the predicted responses calculated on the training samples (Perez et al., 2009).

The reliability of the classification models was evaluated by means of a repeated double-cross-validation (rDCV) procedure (Filzmoser et al., 2009). Double-cross-validation (DCV) is a validation strategy which involves two nested loops of cross-validation: an inner loop for model selection (i.e., for choosing the optimal number of latent variables) and an outer loop which mimics an external (i.e., not involved in any model building and/or optimization stage) test set, to be used for estimating the prediction and generalization ability. In order to avoid that the performances of the model depend on a particular sample splitting scheme, the procedure is repeated a sufficient number of times, changing the distribution of the individuals across the different cancelation groups, hence the name "repeated" DCV. Repeating the double-cross-validation procedure allows also having multiple predictions for the same samples which translates to the possibility of estimating confidence intervals for all the classification figures of merit and model parameters.

3. Results and Discussion

3.1 Levels of Elements

Table 2 shows the concentration of the elements in EVOO from all over Italy. The content of Tl was below the respective MDL (0.06 μg kg^{-1}) in all the samples. Si, Te and Nb were found above the MDL (270, 0.03 and 0.04 μg kg^{-1}, respectively) only in one, three and seven percent of all samples. Only the Ca, Cr, Mg, Mn, Ni, P, Ti and Zn levels in the EVOO samples were 100% greater than the MDL. The maximum concentrations for As (4.0 μg kg^{-1}), Cu (41.6 μg kg^{-1}), Fe (582 μg kg^{-1}), and Pb (22.1 μg kg^{-1}) were lower than the MRLs established by the IOC for olive and pomace-olive oils, which are 100 μg kg^{-1} for As, Cu, and Pb and 3000 μg kg^{-1} for Fe (International Olive Council, 2009). Calcium showed the highest concentration ranging from 1230 to 35700 μg kg^{-1}, whereas from 10- to 50-fold lower levels were found for Fe, Mg, Na, P and Zn (median = 77, 91, 110, 272 and 111 μg kg^{-1}, respectively).

Concentrations of elements obtained in this study were compared to levels measured in EVOO from several other Mediterranean countries (Tables S1-S4). Levels of many elements showed wide variability even within the same country. The Ag, Ba, P and Sn data were not considered because these elements are not completely extracted with the method used. As regards the content of B, Be, Dy, Nd, Pr, Si, Tb and Te, we could not find other data for EVOO in the literature. Our results were similar to those reported by another study on Italian EVOO (Benincasa et al., 2007); on the contrary, they differed significantly from other data concerning most of the elements investigated in the EVOOs of Spain (Beltran et al., 2015; Llorent-Martínez et al., 2014), Croatia (Pošćić et al., 2019), Tunisia (Damak et al., 2019) and Turkey (Gumus et al., 2017). The concentrations of Ca (1230-35700 μg kg^{-1}), Cr (0.4-839 μg kg^{-1}), Mg (21-723 μg kg^{-1}), and Ni (2.1-49.7 μg kg^{-1}) found in this study were in the similar range to that found in other Italian EVOO (Ca = 1850-26900 μg kg^{-1}; Cr = 116-437 μg kg^{-1}; Mg = 56-1030 μg kg^{-1}; and Ni = nd-46.9 μg kg^{-1}) as reported by Benincasa et al. (2007), but from 10 to 100 times higher than the levels reported in Croatian (Pošćić et al., 2019) and Turkish EVOO (Gumus et al., 2017). Fe concentrations (<12-582 μg kg^{-1}) varied from 100 times lower to 100 times higher than the level of Fe quantified in EVOO from Turkey (1-14670 μg kg^{-1}) by Gumus et al. (2017) and Croatia (0.19–2.57 μg kg^{-1}) by Pošćić et al. (2019) or Spain (0.5-1.2 μg kg^{-1}) by Beltran et al. (2015), respectively. This variability

in the concentrations of the elements present in EVOO samples may depend on various factors related to the geochemistry of the provenance soil but also to physiological aspects typical of the species from which a particular EVOO derives (Giaccio and Vicentini, 2008).

Grouping the data according to geographic origin as north (Emilia Romagna, Liguria, Lombardy, Trentino Alto Adige, and Veneto), center (Abruzzo, Lazio, Marche, Tuscany and Umbria) and south (Apulia, Calabria, Campania, Sardinia and Sicily) of Italy, it is possible to identify elements that differ significantly from one group to another (Table 3). In particular, the EVOO samples from northern Italy had significantly higher levels of Cs, Fe, Na, P, and Pr than those from central Italy and Fe, Pr, and U than those from southern Italy. Both Fe and Pr appear to provide a good tool for tracing the EVOO production chain in accord with other authors (Aceto et al., 2019; Damak et al., 2019). Iron is common in silicates and carbonates present in soil (Pohl, 2011); however some authors reported that Fe may be present in edible oils as a result of storage and processing contaminations (Mendil et al., 2009; Zeiner et al., 2010). Praseodymium and the other lanthanides do not have a defined role in the metabolism of plants; therefore their distribution remains almost unchanged in the passage from the soil to the fruits (Aceto et al., 2019). For this reason these elements can be used as fingerprints to discriminate the geographic origin of the EVOO samples (Aceto et al., 2019; Farmaki et al., 2012). In addition, the analysis of some elements in EVOO, such as Cs and Rb, which can be easily mobilized in the soil, can be linked to a geogenic source rather than an anthropogenic origin (such as extraction process or cultivation practices) and can be help in the geographical traceability of EVOO samples (Kelly, Heaton, & Hoogewerff, 2005).

By comparing the concentrations of the elements in the EVOO samples from each region (Tables S5-S7), the number of elements that differ significantly increases. Table 4 shows a summary of all the elements that differ significantly according to the region. Emilia Romagna was not considered for the comparison because there was only one EVOO sample to consider. EVOOs from Lombardy did not have levels of elements that are significantly different from those of oils from all other regions. Considering the other oils of northern Italy, the EVOOs from Trentino and Liguria differed significantly from the EVOOs from Marche only for the content of Na, which in the EVOOs from Marche (median = 38 μg kg^{-1}) was about 4 times lower; while the EVOOs from Veneto had a higher content of Fe (median = 218 μg kg^{-1}) than the oils from Abruzzo (median = 15 μg kg^{-1}) and a higher content of Fe and Na (median = 218 and 174 μg kg^{-1}, respectively) compared to the Marche. The EVOO samples from Lazio differed significantly for a large number of elements (Ba, Ca, Cd, Ce, Cs, Dy, Ga, La, Mg, Na, Nd, Pr, Pb, Rb, Sb, Sr, Tb, Ti, U) compared to Tuscany, Abruzzo, Campania and Marche. In all cases, levels of Cd (median = 0.14 μg kg^{-1}), La (median = 0.20 μg kg^{-1}) and Rb (median = 0.48 μg kg^{-1}) were higher than those of oils from other regions mentioned above.

3.2 Antioxidant activity

Following the extraction and storage of EVOO, it is inevitable that an oxidation process occurs, which leads to a deterioration of the oil (Bendini et al., 2007). Some factors such as temperature, light, oxygen and other chemical elements, unsaturated fatty acid composition, the presence of antioxidants can affect the oxidation process differently (Frankel 1985). Phenolic compounds have antioxidant capacities in EVOO since they can

eliminate peroxyl and alkoxy radicals and chelate transition metal ions present in traces (Visioli et al., 1998). Several elements are known for their antioxidant properties (Thiruvengadam et al., 2020; Perna et al., 2012). Indeed, in the present study (Table S8), significant correlations were observed between the antioxidant activity and elements. A positive and significant moderate correlation ($r = 0.500–0.768$, $p = 0.05$) was observed between Al, Ca, Fe, V, and Zr in EVOOs from Abruzzo, Ba in EVOOs from Apulia, B, Mn, Se, and V in EVOOs from Sardinia and the DPPH% data. Conversely, a low and positive correlation ($r<0.4$) was recorded between Ba and Ni and the antioxidant activity of all samples. Other elements (Ag, Cr, Cu, Li, Sb, Si, and Tl) might not affect the antioxidant properties as non-significant correlations were observed between them.

Tables S5-S7 show the antioxidant activity measured by the DPPH assay (DPPH%) in the EVOO samples from each region. EVOOs from central and southern Italy showed higher antioxidant activity than oils from northern Italy. In particular, Table 4 shows that EVOOs from Sicily had a significantly lower DPPH% (median=18.2%) than oils from Abruzzo (median=47%), Apulia (median=37.6%) and Tuscany (median=36.2%); while the EVOOs from Liguria had significantly lower DPPH% (median=15.7%) compared to Tuscany. The highest data of DPPH% (67.3%) was found in the oils of Campania. Cioffi et al. (2010) demonstrated that oils from Campania have antioxidant properties, which are very likely due to the presence of high contents of phenolic compounds.

3.3 Classification of EVOOs according to geographical origin

At first, the possibility of discriminating the different EVOOs according to their geographical origin was considered. In particular, due to the unavailability of the information about the origin of all the samples and to the unbalancedness in the distribution of samples per class, when considering the oils of known origin, several two-class models (i.e., comparing two regions at a time) were built and validated. Here it must be further stressed that all the regions for which the available number of certified individuals was too low to be considered representative have not been included in the comparison.

In all cases, PLS-DA analysis was carried out on the matrix made up of the concentrations of the elements presenting at least 70% of the values above the limit of detection (so to avoid possible artifacts related to data imputation) and including also TEAC and DPPH. Models were built after autoscaling and validated by means of a repeated double-cross-validation procedure with 50 runs, 10 cancelation groups in the outer loop (the one mimicking the external test set) and 5 in the inner loop (the one used for model selection, i.e., definition of the optimal number of latent variables). The results obtained are summarized in Table 5, where the accuracy, the mean correct classification rate and the sensitivities for the two compared classes are reported. Since two-class discriminant models were calculated, due to symmetry the sensitivity of a class (true positive rate) is the specificity (true negative rate) of the other category; this is why sensitivities only have been reported. Moreover, since the number of samples per class was, in some cases, highly unbalanced (Table 1), we have decided to report both classification accuracy (percentage of correctly classified samples irrespectively of the category over the total number of samples) and the mean correct classification rate, which is the average of the specificities of the two classes.

As anticipated in the materials and methods section, the use of repeated double cross-validation allows obtaining not only a point estimate of the figures of merit on the validation (outer loop) samples, but also their confidence intervals, so to be able to evaluate the consistency of the results.

By looking at the Table 5, it is evident how the different models result in different reliability, with some presenting rather low classification performances. On the other hand, there are some models which result in an overall accuracy higher than 75%, with a comparable mean correct classification rate (suggesting that the classification performances are not affected by the numerosity of the samples; Table 1). Additionally, the standard deviation of the figures of merit for these models are relatively low (corresponding roughly to one more sample being correctly or wrongly classified with respect to the reported averages), confirming the consistency of the obtained classification. Based on these considerations, only the best models will be discussed in detail in the remainder of this section, namely, Lazio vs Abruzzo, Lazio vs Sicily, Abruzzo vs Calabria and Abruzzo vs Sicily.

The first model to be examined is the one discriminating Lazio samples from the oils from Abruzzo, for which an overall 76.2±3.9% classification accuracy on the outer loop samples was registered. By looking at the individual sensitivities together with their confidence intervals (73.1±3.9% for Lazio and 81.0±7.7% for Abruzzo), it can be stated that the two categories are predicted comparably well. These results can also be graphically appreciated in Figure 1, where the mean scores of the outer loop samples along the only canonical variate of the model together with their 95% confidence intervals are displayed. It is evident from the Figure 1 how almost all the Abruzzo samples have positive scores, while the large majority of Lazio samples are characterized by negative coordinates on the component, indicating a good separation between the categories.

Figure 1 – PLS-DA model for the discrimination between Lazio and Abruzzo samples: mean scores of the rDCV outer loop samples along the only canonical variate of the model together with their 95% confidence intervals. Legend: red bars – Lazio; blue bars – Abruzzo.

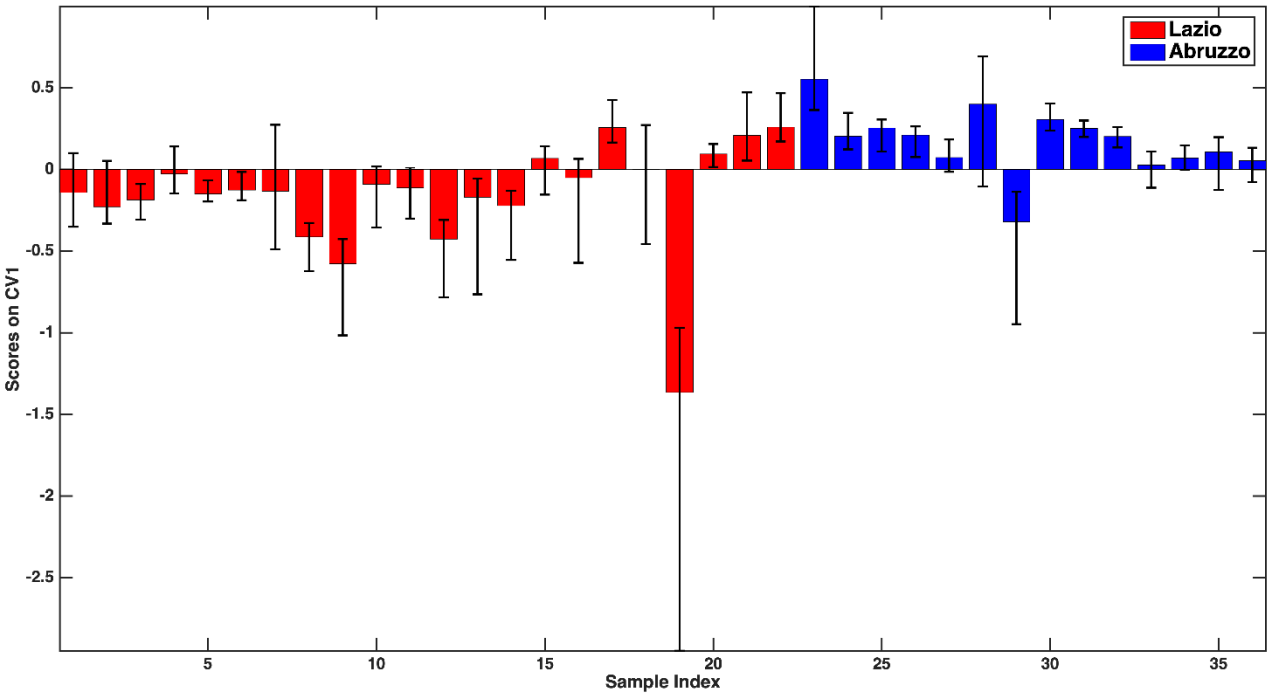

For the sake of interpretation, another advantage of the rDCV procedure is that confidence intervals can also be calculated for model parameters, so to be able to identify which are the variables that contribute significantly to the discrimination (e.g., by inspecting the values of the associated regression coefficients or of the VIP scores). Moreover, investigating the sign of the regression coefficients also allows postulating whether the associated predictor is more or less concentrated in a category with respect to the other. In particular, the variables found to significantly contribute to the discriminant model were V, Fe, Zn, Rb, antioxidant capacity (all higher in Lazio samples), and Ni and antioxidant activity in the DPPH assay (higher in the oils from Abruzzo).

As far as the Lazio vs Sicily model is concerned, a slightly higher accuracy was obtained (79.4±3.1%), the individual sensitivities being 81.9±4.9% for Lazio and 76.1±2.8% for Sicily. Analogously to what described above, the discrimination between the two classes can also be visually appreciated in Figure 2, where the mean scores of the outer loop samples along the only canonical variate of the model together with their 95% confidence intervals are displayed.

Figure 2 – PLS-DA model for the discrimination between Lazio and Sicily samples: mean scores of the rDCV outer loop samples along the only canonical variate of the model together with their 95% confidence intervals. Legend: red bars – Lazio; blue bars – Sicily.

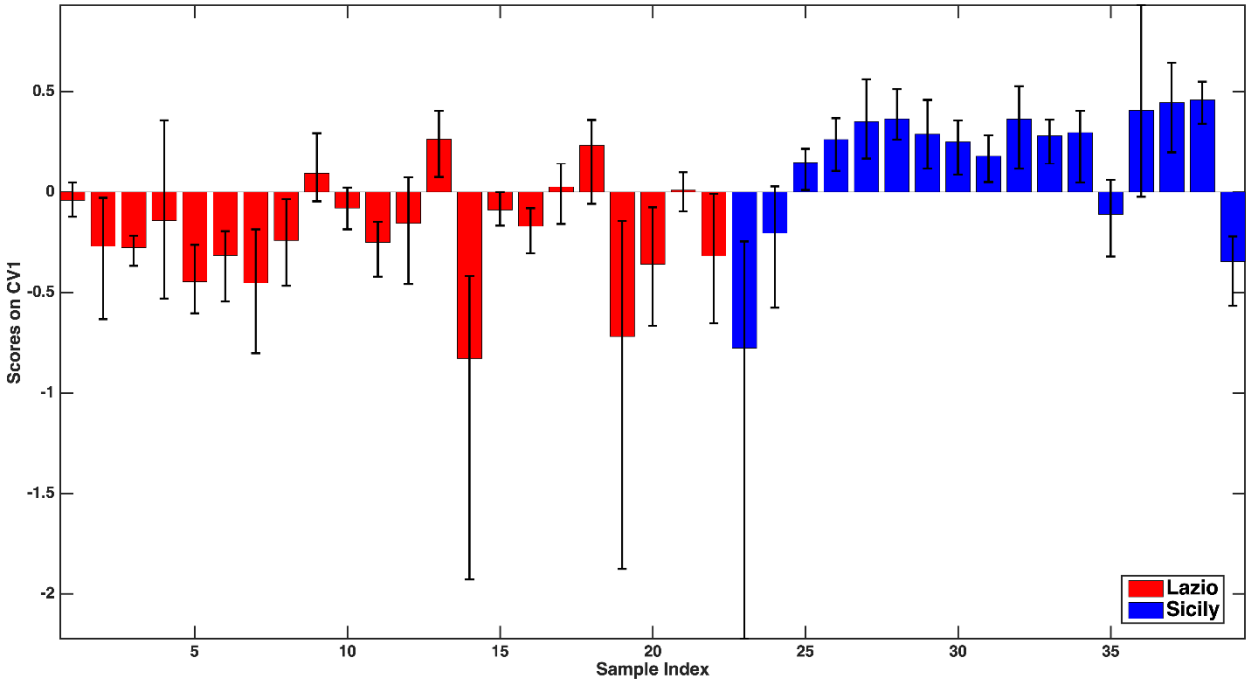

In this case, based on the values of the PLS-DA regression coefficients, all the variables found to significantly contribute to the discriminant model (Na, Mg, P, Ti, Rb, antioxidant activity in the DPPH assay) should be, on average, higher in the oils from Lazio. When considering the model discriminating Abruzzo oils from the Calabrian ones, an overall 81.4±6.1% accuracy on the outer loop samples was obtained, the mean correct classification rate (81.0±7.1%), as well the individual sensitivities for the two categories (82.9±4.35% for Abruzzo and 79.1±12.2% for Calabria), being almost equal. In particular, the higher standard deviation of the sensitivity for Calabria is due to the very limited number of samples in that class. When looking at the significant predictors, only five variables (P, V, Fe, Zn and antioxidant activity) were identified, and the coefficients indicate that they all should be, on average, higher for the Abruzzo samples.

Lastly, the Abruzzo vs Sicily model resulted in an accuracy of 75.0±4.3%, the sensitivities being 81.2±7.6% for Abruzzo and 69.7±5.9% for Sicily. Inspection of the model parameters led to identify as significant the contribution of Na, Ni and antioxidant activity (in the DPPH assay with higher data in the oils from Abruzzo) and of V and Fe, more concentrated in the samples from Sicily.

3.4 Classification of EVOOs according to cultivar and to whether organically produced

In a second stage of the study, the possibility of discriminating oil samples according to their cultivar was explored. In this case, given the available information about the samples and the fact that only a relatively small fraction of the analyzed oils was monovarietal, the investigation was restricted to the comparison of Coratina (21 samples) and Frantoio (12 samples) (Table 1). The PLS-DA classification approach was validated through a repeated double-cross-validation strategy as described in the previous section and resulted in an overall accuracy of 68.9±6.2%, and 80.7±8.8% and 61.9±7.6% sensitivities for Frantoio and Coratina, respectively, corresponding to a mean correct classification rate of 71.3±6.2%. Investigation of the model

parameters suggested that 5 variables only, namely P, Ti, Zn (higher in Coratina), Fe and Ni (more concentrated in Frantoio) significantly contributed to the discriminant model.

Lastly, the possibility of discriminating whether the oil was organically produced or not was also attempted, but the classification model resulted in a very poor accuracy (close to 50%) suggesting that, at least for the investigated samples, organic cultivation has little impact on the elemental composition with respect to non-organic production.

Table 1. Number of samples of extra virgin olive oil for each considered category.

	Region	All samples	Oil production			Cultivar (number of samples)
			Organically	Non-organically	Not reported	
Northern Italy	**Trentino Alto Adige 1**	7	2	4	1	Blend (3); Casaliva (1); Coratina (2)
	Liguria2	6	0	4	2	Lavagnina (1); Taggiasca (4)
	Lombardy3	3	0	2	1	Blend (1); Casaliva (1); Leccino (1)
	Veneto4	3	1	2	0	Blend (2); Grignano (1)
	Emilia Romagna14	1	0	1	0	Careggiolo (1)
Central Italy	**Abruzzo12**	14	3	11	0	Blend (8); Dritta (3); Intosso (3)
	Lazio5	24	6	8	10	Blend (5); Canino (3); Frantoio (1); Itrana (2); Leccino (2); Rosciola (1)
	Marche	7	2	5	0	Ascolana (2); Blend (1); Leccino (1); Orbetana (1); Raggiola (2)
	Toscany6	79	33	42	4	Blend (38); Arancino (1); Coratina (1); Frantoio (10); Leccino (4); Moraiolo (7); Nocellara (1); Olivastra Seggianese (1); Pendolino (1); Raggiolo (1)
	Umbria7	8	0	8	0	Blend (8)
Southern Italy	**Apulia9**	33	6	18	9	Blend (3); Coratina (18); Frantoio (1); Leccino (1); Ogliarola (2); Olivastra (1); Peranzana (4); Pichioline (2)
	Calabria8	12	5	6	1	Blend (3); Carolea (2); Nocellara (1); Ottobratica (4)
	Campania 13	7	0	7	0	Blend (2); Cammarotana (1); Ortice (1); Ravece (1); Salella (1)
	Sardinia10	12	1	11	0	Bosana (3); Blend (6); Semidana (1)
	Sicily 11	21	4	14	3	Blend (4); Biancolilla (2); Cerasuola (1); Leccio del

Corno (1); Nocellara (9); Tonda Iblea (3)

Table 2. Method detection limits (MDL; µg kg^{-1}) and element levels [median, minimum (min) and maximum (max); µg kg^{-1}] in extra-virgin olive oils (EVOO; n = 237) from all over Italy.

Element	MDL	Italian EVOO samples			
		%n >MDL	median	min	max
Ag	0.06	27	<0.06	<0.06	0.86
Al	9	85	34	<9	1300
As	0.3	28	<0.3	<0.3	4.0
B	20	16	<20	<20	770
Ba	0.7	49	<0.7	<0.7	175
Be	0.004	43	<0.004	<0.004	0.431
Bi	0.1	23	<0.1	<0.1	1.0
Ca	510	100	4090	1230	35700
Cd	0.07	67	0.09	<0.07	0.97
Ce	0.1	65	0.2	0.1	3.5
Co	0.05	70	0.12	<0.05	2.16
Cr	0.3	100	5	0.4	839
Cs	0.007	55	0.008	<0.007	0.101
Cu	0.6	99	3.2	<0.6	41.6
Dy	0.005	19	<0.005	<0.005	0.055
Fe	12	99	77	<12	582
Ga	0.06	15	<0.06	<0.06	0.69
K	40	24	<40	<40	939
La	0.05	70	0.10	<0.05	0.79
Li	0.06	32	<0.06	<0.06	6.07
Mg	10	100	91	21	723
Mn	0.5	100	2.4	1.1	43.5
Mo	0.3	20	<0.3	<0.3	2.0
Na	25	98	110	<25	585
Nb	0.04	7	<0.04	<0.04	0.11
Nd	0.03	52	0.03	<0.03	13.8
Ni	0.5	100	5.6	2.1	49.7
P	60	100	272	127	650
Pb	0.3	99	0.9	<0.3	22.1
Pr	0.008	40	<0.008	<0.008	1.65
Rb	0.06	99	0.24	<0.06	1.77
Sb	0.02	16	<0.02	<0.02	0.37
Se	0.6	48	<0.6	<0.6	7.8
Si	270	1	<270	<270	3340
Sn	0.06	63	0.08	<0.06	1.94
Sr	1	65	3	1	58
Tb	0.006	19	<0.006	<0.006	1.28
Te	0.03	3	<0.03	<0.03	0.06
Ti	0.4	100	1.9	0.8	10.7
Tl	0.06	0	<0.06	<0.06	<0.06
U	0.005	30	<0.005	<0.005	0.050
V	0.08	98	0.53	<0.08	1.40
W	0.3	38	<0.3	<0.3	5.1
Zn	20	100	111	54	749
Zr	0.1	57	<0.1	<0.1	2.3

Table 3. Element levels [median, minimum (min) and maximum (max); µg kg^{-1}] in extra-virgin olive oils from north (n = 20), central (n = 132) and south (n = 85) Italy.

Element	North Italy[a]				Central Italy[b]				South Italy[c]			
	%n >MDL	median	min	max	%n >MDL	median	min	max	%n >MDL	median	min	max
Ag	25	<0.06	<0.06	0.26	30	<0.06	<0.06	0.86	25	<0.06	<0.06	0.22
Al	75	32	<9	615	86	34	<9	1291	86	34	<9	1298
As	25	<0.3	<0.3	2.8	28	<0.3	<0.3	4.0	28	<0.3	<0.3	2.2
B	20	<20	<20	85	15	<20	<20	734	16	<20	<20	770
Ba	50	0.6	0.4	99.5	49	2.9	<0.7	175	48	<0.7	<0.7	147
Be	40	<0.004	<0.004	0.431	37	<0.004	<0.004	0.272	49	0.004	<0.004	0.061
Bi	40	<0.1	<0.1	0.2	23	<0.1	<0.1	0.4	19	<0.1	<0.1	1.0
Ca	100	4590	1480	9170	100	3648	1229	35709	99	4278	1432	24122
Cd	70	0.12	<0.07	0.33	66	0.09	<0.07	0.97	67	0.09	<0.07	0.61
Ce	70	0.2	<0.1	0.7	69	0.2	0.1	3.5	60	0.2	0.1	1.0
Co	90	0.11	<0.05	0.59	68	0.13	<0.05	1.23	69	0.08	<0.05	2.16
Cr	100	3.7	0.5	839	99	5.0	0.4	123	100	4.1	0.5	533
Cs	80	**0.013**[a]	<0.007	0.080	52	**0.007a**	<0.007	0.084	55	0.008	<0.007	0.101
Cu	100	4.6	<0.6	20.7	99	3.0	<0.6	40.9	100	3.3	<0.6	41.6
Dy	20	<0.005	<0.005	0.010	20	<0.005	<0.005	0.026	17	<0.005	<0.005	0.055
Fe	100	**158**[a,b]	<12	495	99	**70**[a]	<12	403	100	**86**[b]	14	582
Ga	35	<0.06	<0.06	0.33	11	<0.06	<0.06	0.69	16	<0.06	<0.06	0.59
K	40	<40	<40	293	20	<40	<40	673	26	<40	<40	939
La	80	0.13	<0.05	0.41	70	0.08	<0.05	0.79	67	0.11	<0.05	0.71
Li	40	<0.06	<0.06	1.67	29	<0.06	<0.06	6.07	35	<0.06	<0.06	4.42
Mg	100	97	37	262	100	90	21	723	99	96	28	613
Mn	100	2.7	1.5	7.1	99	2.3	1.1	18.6	100	2.6	1.4	43.5
Mo	30	<0.3	<0.3	1.3	19	<0.3	<0.3	1.7	20	<0.3	<0.3	2.0
Na	100	**131**[a]	87	331	99	**102**[a]	<25	585	100	114	<25	513
Nb	15	<0.04	<0.04	0.05	5	<0.04	<0.04	0.06	8	<0.04	<0.04	0.11
Nd	80	0.06	<0.03	1.39	47	<0.03	<0.03	6.43	53	0.03	<0.03	13.8
Ni	100	5.2	2.5	29.5	100	6.0	2.1	40.6	100	5.4	2.4	49.7
P	100	**309**[a]	220	650	99	**269**[a]	127	522	100	272	189	548
Pb	100	1.2	<0.3	4.3	100	0.8	<0.3	22.1	100	1.1	<0.3	8.7
Pr	70	**0.012**[a,b]	<0.008	0.359	38	**<0.008**[a]	<0.008	1.58	35	**<0.008**[b]	<0.008	1.65
Rb	95	0.29	<0.06	1.10	100	0.24	0.06	1.77	100	0.26	<0.06	1.36
Sb	10	<0.02	<0.02	0.04	17	<0.02	<0.02	0.37	16	<0.02	<0.02	0.14
Se	55	0.6	<0.6	6.8	49	<0.6	<0.6	6.9	44	0.6	<0.6	7.8
Si	0	<270	<270	<270	1	<270	<270	3344	1	<270	<270	442
Sn	80	0.10	<0.06	0.45	59	0.06	<0.06	0.60	65	0.09	<0.06	1.94
Sr	80	3	1	7	64	3	1	34	63	3	1	58
Tb	25	<0.006	<0.006	0.112	20	<0.006	<0.006	1.13	16	<0.006	<0.006	1.28
Te	5	<0.03	<0.03	0.05	1	<0.03	<0.03	0.05	6	<0.03	<0.03	0.06
Ti	100	2.2	1.2	8.1	99	1.8	0.8	5.6	100	2.1	1.1	10.7
Tl	0	<0.06	<0.06	<0.06	1	<0.06	<0.06	0.08	0	<0.06	<0.06	0.03
U	55	**0.006**[a]	<0.005	0.044	31	<0.005	<0.005	0.044	24	**<0.005**[a]	<0.005	0.050
V	100	0.50	<0.08	1.04	99	0.52	<0.08	1.21	100	0.55	<0.08	1.40
W	40	<0.3	<0.3	2.0	37	<0.3	<0.3	2.3	39	<0.3	<0.3	5.1
Zn	100	145	55	283	99	98	54	749	99	143	57	672
Zr	55	0.1	0.1	0.6	53	0.1	0.1	1.8	63	0.1	0.1	2.3

Table 4. Summary of **s**ignificant differences within medians of the 45 selected elements and antioxidant activity (DPPH%) among all samples from Italian regions by Kruskall–Wallis and pairwise post-hoc tests. A p-value lower than 0.05 was considered statistically significant.

	Trentino	**Liguria**	**Veneto**	**Lazio**	**Toscany**	**Umbria**	**Calabria**	**Apulia**	**Sardinia**	**Sicily**
Toscany		DPPH%		Cd,Cs,Dy,Ga,La,Na,Nd,Pr,Rb,Sb,Tb,Ti,U	-					
Umbria				Dy,U		-				
Apulia					Ti,Zr			-		
Sardinia				La,Tb,U				Al	-	
Sicily				U	Be,DPPH%			DPPH%	Be	-
Abruzzo		DPPH%	Fe	Ba,Ca,Cd,Ce,Dy,La,Mg,Nd,Rb,Sr,Tb	Ni	Fe,Se	Fe	Ce,La,Ni,Zn,Zr		As,Ba,Ca,Ce,Fe,La, Ni,Zn,DPPH%
Campania				Ba,Cd,La,Mg,Na,Rb,U			Na	La	Na	Ba,La
Marche	Na	Na	Fe,Na	Ba,Cd,Ce,Cs,La,Na,Nd,Mg,Pb,Pr,Rb,Ti,U		Fe	Cd,Fe,Na	Na,Rb,Ti	Na	Ba,Be,Rb

Table 5. PLS-DA discrimination between pairs of geographical origin. Figures of merit estimated on the outer loop of the rDCV procedure (expressed as mean ± standard deviation).

Class1	Class2	% Accuracy	Mean % correct classification rate	% Sensitivity (Class1)	% Sensitivity (Class2)
Lazio	Abruzzo	76.2±3.9	77.1±4.2	73.1±3.9	81.0±7.7
Lazio	Sicily	79.4±3.1	79.0±2.9	81.9±4.9	76.1±2.8
Lazio	Puglia	68.8±5.2	68.9±5.2	64.6±6.2	73.2±7.6
Lazio	Tuscany	75.2±1.8	69.2±2.3	57.8±4.2	80.6±2.1
Lazio	Calabria	61.7±5.1	54.4±5.5	71.9±5.9	36.9±8.5
Abruzzo	Calabria	81.4±6.1	81.0±7.1	82.9±4.3	79.1±12.2
Abruzzo	Sicily	75.0±4.3	75.5±4.4	81.2±7.6	69.7±5.9
Abruzzo	Tuscany	58.2±3.4	54.6±5.6	49.3±11.6	59.9±4.0
Abruzzo	Puglia	54.3±6.6	54.2±6.8	53.6±9.6	54.8±7.5
Sicily	Tuscany	69.5±2.7	65.8±4.1	59.9±7.6	71.8±2.8
Sicily	Puglia	70.7±4.3	70.2±4.2	65.4±4.9	74.9±6.5
Tuscany	Puglia	64.6±3.1	55.1±4.9	72.5±2.9	37.7±9.3

4. Conclusion

This study showed that the As, Cu, Fe, and Pb levels in the analyzed samples were far below the MRLs, which certifies the high quality of Italian EVOO.

The element concentrations allow to distinguish well some geographical origins of the EVOO samples and also, although slightly less well, the two cultivars Coratina and Frantoio. On the other hand, given the high heterogeneity of the data set, it is not possible to distinguish organic oils from non-organic ones. This is probably due to the fact that within the two classes the variability related to geographical origin and cultivar is added.

This study can be used to create datasets for element levels in EVOOs for each production region to support geographic origin authentication. In the future, other information will have to be considered together with the elemental profile of EVOO such as climatic factors, bioavailable fraction of the total content of elements to further corroborate the use of the elements as a marker of provenance.

Author contributions

MLA: conceptualization, investigation, methodology, validation, formal analysis, visualization, data curation, writing—original draft preparation, writing—reviewing and editing and supervision. FM: methodology, validation, formal analysis, writing—original draft preparation and writing—reviewing and editing. MAF: investigation. LM: formal analysis. ALC: resources. CMM: resources. SC: resources and supervision.

References

Aceto, M., Calà, E., Musso, D., Regalli, N., and Oddone, M. (2019). A preliminary study on the authentication and traceability of extra virgin olive oil made from Taggiasca olives by means of trace and ultra-trace elements distribution. *Food Chem.* 298, 125047. doi: 10.1016/j.foodchem.2019.125047.

Astolfi, M.L., Marotta, D., Cammalleri, V., Marconi, E., Antonucci, A., Avino, P., Canepari, S., Vitali, M., and Protano, C. (2021a). Determination of 40 elements in powered infant formulas and related risk assessment. *Int. J. Env. Res. Pub. He.* 18, 5073. doi: 10.3390/ijerph18105073.

Astolfi, M.L., Marconi, E., Vitiello, G., and Massimi, L. (2021b). An optimized approach for sample preparation and elemental analysis of extra-virgin olive oil by inductively coupled plasma mass spectrometry. *Food Chem.* 360, 130027. doi: 10.1016/j.foodchem.2021.130027.

Astolfi, M.L., Conti, M.E., Marconi, E., Massimi, L., and Canepari, S. (2020a). Effectiveness of different sample treatments for elemental characterization of bees and beehive products. *Molecules* 25, 4263. doi:10.3390/molecules25184263.

Astolfi**,** M.L., Marconi, E., Protano, C., and Canepari, S. (2020b). Comparative elemental analysis of dairy milk and plant-based milk alternatives. *Food Control* 116, 107327. doi: 10.1016/j.foodcont.2020.107327.

Astolfi, M.L., Protano, C., Marconi, E., Massimi, L., Brunori, M., Piamonti, D., Migliara, G., Vitali, M., and Canepari S. (2020c). A new treatment of human hair for elemental determination by inductively coupled mass spectrometry, *Anal. Methods* 12, 1906–1918. doi: 10.1039/c9ay01871a.

Ballus, C. A., Meinhart, A. D., de Souza Campos, F. A., and Godoy, H. T. (2015). Total phenolics of virgin olive oils highly correlate with the hydrogen atom transfer mechanism of antioxidant capacity. *J. Am. Oil Chem. Soc.* 92, 843–851. doi: 10.1007/s11746-015-2629-0.

Bajoub, A., Bendini, A., Fernández-Gutiérrez, A., and Carrasco-Pancorbo, A. (2018). Olive oil authentication: A comparative analysis of regulatory frameworks with especial emphasis on quality and authenticity indices, and recent analytical techniques developed for their assessment. A review. *Crit. Rev. Food Sci. Nutr.* 58, 832–857. doi: 10.1080/10408398.2016.1225666.

Bakircioglu, D., Bakircioglu Kurtulus, Y., and Yurtsever, S. (2013). Comparison of extraction induced by emulsion breaking, ultrasonic extraction and wet digestion procedures for determination of metals in edible oil samples in Turkey using ICP-OES. *Food Chem.* 138, 770–775. doi: 10.1016/j.foodchem.2012.10.089.

Barker, M., and Rayens, W. (2003). Partial least squares for discrimination. *J. Chemometr.* 17, 166–173. doi: 10.1002/cem.785.

Beltrán, M., Sánchez-Astudillo, M., Aparicio, R., and García-González, D. L. (2015). Geographical traceability of virgin olive oils from south-western Spain by their multi-elemental composition. *Food Chem.* 169, 350–357. doi: 10.1016/j.foodchem.2014.07.104.

Bendini, A., Cerretani, L., Carrasco-Pancorbo, A., Gómez-Caravaca, A. M., Segura-Carretero, A., Fernández-Gutiérrez, A., and Lercker, G. (2007). Phenolic molecules in virgin olive oils: a survey of their sensory properties, health effects, antioxidant activity and analytical methods. An overview of the last decade. *Molecules* 12(8), 1679–719. doi: 10.3390/12081679.

Benincasa, C., Lewis, J., Perri, E., Sindona, G., and Tagarelli, A. (2007). Determination of trace element in Italian virgin olive oils and their characterization according to geographical origin by statistical analysis. *Anal. Chim. Acta* 585, 366–370. doi: 10.1016/j.aca.2006.12.040.

Cabrera-Vique, C., Bouzas, P.R., Oliveras-López, M.J. (2012). Determination of trace elements in extra virgin olive oils: A pilot study on the geographical characterisation, Food Chem. 134(1), 434–439. doi: 10.1016/j.foodchem.2012.02.088.

Camin, F., Larcher, R., Perini, M., Bontempo, L., Bertoldi, D., Gagliano, G., Nicolini, G., and Versini, G. (2010). Characterisation of authentic Italian extra-virgin olive oils by stable isotope ratios of C, O and H and mineral composition. *Food Chem.* 118, 901–909. doi: 10.1016/j.foodchem.2008.04.059.

Capriotti, A. L., Cavaliere, C., Crescenzi, C., Foglia, P., Nescatelli, R., Samperi, R., and Laganà, A. (2014). Comparison of extraction methods for the identification and quantification of polyphenols in virgin olive oil by ultra-HPLC-QToF mass spectrometry. *Food Chem.*158, 392–400. doi: 10.1016/j.foodchem.2014.02.130

Carbone, A., Cacchiarelli, L., and Sabbatini, V. (2018). Exploring quality and its value in the Italian olive oil market: a panel data analysis. *Agric. Econ.* 6, 6. doi: 10.1186/s40100-018-0102-8.

Chatzistathis, T., Therios, I., and Alifragis, D. (2009). Differential uptake, distribution within tissues, and use efficiency of manganese, iron, and zinc by olive cultivars Kothreiki and Koroneiki. *HortScience* 44, 1994–1999. doi: 10.21273/HORTSCI.44.7.1994.

Choe, E., and Min, D. B. (2006). Mechanisms and factors for edible oil oxidation. *Compr. Rev. Food Sci. Food Saf.* 5, 169–186. doi: 10.1111/j.1541-4337.2006.00009.x.

Cioffi, G., Pesca, M. S., De Caprariis, P., Braca, A., Severino, L., and De Tommasi, N. (2010). Phenolic compounds in olive oil and olive pomace from Cilento (Campania, Italy) and their antioxidant activity. *Food Chem.* 121(1), 105–111. doi: 10.1016/j.foodchem.2009.12.013.

Codex Stan 33-1981. Standard for Olive Oils and Olive Pomace Oils. Adopted in 1981. Revision: 1989, 2003, 2015. Amendment: 2009, 2013. URL: http://www.fao.org/input/download/standards/88/CXS_033e_2015.pdf. (accessed on April 2021).

Cordella, C., Moussa, I., Martel, A. C., Sbirrazzuoli, N., and Lizzani-Cuvelier, L. (2002). Recent developments in food characterization and adulteration detection: Technique-oriented perspectives. *J. Agric. Food Chem.* 50, 1751–1764. doi: 10.1021/jf011096z.

Christodouleas, D. C., Fotakis, C., Nikokavoura, A., Papadopoulos, K., and Calokerinos, A. C. (2015). Modified DPPH and ABTS assays to assess the antioxidant profile of untreated oils. *Food Anal. Methods* 8(5), 1294–1302. doi: 10.1007/s12161-014-0005-6.

Damak, F., Asano, M., Baba, K., Suda, A., Araoka, D., Wali, A., Isoda. H., Nakajima, M., Ksibi, M., and Tamura, K. (2019). Interregional traceability of Tunisian olive oils to the provenance soil by multielemental fingerprinting and chemometrics. *Food Chem.* 283, 656–664. doi: 10.1016/j.foodchem.2019.01.082.

Dugo, G., La Pera, L., Giuffrida, D., Salvo, F., and Lo Turco, V. (2004). Influence of the olive variety and the zone of provenience on selenium content determined by cathodic stripping potentiometry (CSP) in virgin olive oil. *Food Chem.* 88, 135–140. doi: 10.1016/j.foodchem.2003.12.036.

Dugo, L., Russo, M., Cacciola, F., Mandolfino, F., Salafia, F., Vilmercati, A., Fanali, C., Casale, M., De Gara, L., Dugo, P., Mondello, L., and Rigano, F. (2020). Determination of the phenol and tocopherol content in italian high-quality extra-virgin olive oils by using LC-MS and multivariate data analysis. *Food Anal. Methods* 1–15. doi: 10.1007/s12161-020-01721-7.

European Union (EU) (2012). The Commission Regulation No. 1151/2012 of 21 November 2012 on quality schemes for agricultural products and foodstuffs OJ L 343/1, 14.12.2012. Available online: https://eur-lex.europa.eu/legal-content/EN/TXT/PDF/?uri=CELEX:32012R1151&from=EN (accessed on August 2021)

Eurostat (2019). Olive trees - Area by age and density classes (area in ha). Available online: http://appsso.eurostat.ec.europa.eu/nui/show.do?dataset=orch_olives3&lang=en (accessed on August 2021).

Farmaki, E. G., Thomaidis, N. S., Minioti, K. S., Ioannou, E., Georgiou, C. A., and Efstathiou, C. E. (2012). Geographical characterization of Greek olive oils using rare earth elements content and supervised chemometric techniques. *Anal. Lett.* 45, 920–932. doi: 10.1080/00032719.2012.655656.

Frankel, E. N. (1985). Chemistry of autoxidation: mechanism, products and flavor significance. In: Flavor Chemistry of Fats and Oils. Min, D. B.; Smouse, T. H., Eds.; AOCS Press: Champaign, IL (USA), 1–37.

Frezzini, M. A., Castellani, F., De Francesco, N., Ristorini, M., and Canepari, S. (2019). Application of DPPH assay for assessment of particulate matter reducing properties. Atmosphere, 10(12), 816. doi: 10.3390/atmos10120816.

Giaccio, M., and Vicentini, A. (2008). Determination of the geographical origin of wines by means of the mineral content and the stable isotope ratios: A review. *J. Comm. Sci. Technol. Qual.* 47(I–IV), 267–284.

Gonzalez-Fernandez, I., Iglesias-Otero, M. A., Esteki, M., Moldes, O. A., Mejuto, J. C., and Simal-Gandara, J. (2019). A critical review on the use of artificial neural networks in olive oil production, characterization and authentication. *Crit. Rev.Food Sci. Nutr.* 59 (12), 1913–1926. doi: 10.1080/10408398.2018.1433628.

Gumus, Z.P., Celenk, V. U., Tekin, S., Yurdakul, O., and Ertas, H. (2017). Determination of trace elements and stable carbon isotope ratios in virgin olive oils from Western Turkey to authenticate geographical origin with a chemometric approach. *Eur. Food Res. Technol.* 243, 1719–1727. doi: 10.1007/s00217-017-2876-4.

Hannachi, H., and Elfalleh, W. (2020). Enrichment of olive oil with polyphenols from oleaster leaves using central composite design for the experimental measurements. Anal. Lett. 1–18. doi: 10.1080/00032719.2020.1774599.

International Olive Council (IOC) (2018a). IOC data for the 2017/18 crop year show a year-on-year increase in the production of olive oil. Available online: http://www.internationaloliveoil.org/news/view/698-year-2018-news/1049-ioc-data-for-the-2017-18-crop-year-show-a-year-on-year-increase-in-the-production-of-olive-oil. (accessed on August 2021).

International Olive Council (IOC) (2018b). World Olive Oil Figures. Available online: http://www.internationaloliveoil.org/estaticos/view/131-world-olive-oilfigures. (accessed on August 2021).

International Olive Council (IOC) (2019). Trade standard applying to olive oils and olive-pomace oils. COI/T.15/NC No. 3/Rev. 15. Available online: https://www.internationaloliveoil.org/wp-content/uploads/2020/07/Trade-standard-T15-NC3-Rev15-EN.pdf. (accessed on April 2021).

Kabata-Pendias, A. (2010). Trace elements in soils and plants (4th ed.). Boca Raton, CRC Press. doi: 10.1201/b10158.

Kelly, S., Heaton, K., and Hoogewerff, J. (2005). Tracing the geographical origin of food: The application of multi-element and multi-isotope analysis. *Trends Food Sci. Techol.* 16, 555–567. doi: 10.1016/j.tifs.2005.08.008.

Kedare, S. B., and Singh, R. P. (2011). Genesis and development of DPPH method of antioxidant assay. *J. Food Sci. Technol.* 48(4), 412–422. doi: 10.1007/s13197-011-0251-1.

Lepri, F.G., Chaves, E.S., Vieira, M.A., Ribeiro, A.S., Curtiu, A.J., De Oliveira, L.C.C., and De Campos, R.C. (2011). Determination of trace elements in vegetable oils and bio-diesel by atomic spectrometric techniques – a review. *Appl. Spectrosc. Rev.* 46, 175–206. doi: 10.1080/05704928.2010.529628.

Llorent-Martínez, E. J., Ortega-Barrales, P., Fernández-de Córdova, M. L., and Ruiz-Medina, A. (2011). Analysis of the legislated metals in different categories of olive and olive-pomace oils. *Food Control* 22, 221–225. doi: 10.1016/j.foodcont.2010.07.002.

Luka, M.F., and Akun, E. (2019). Investigation of trace metals in different varieties of olive oils from northern Cyprus and their variation in accumulation using ICP-MS and multivariate techniques. *Environ. Earth Sci.* 78, 578. doi: 10.1007/s12665-019-8581-9.

Mendil, D., Uluözlü, O. D., Tüzen, M., and Soylak, M. (2009). Investigation of the levels of some element in edible oil samples produced in Turkey by atomic absorption spectrometry. *J. Hazard. Mater.* 105, 724–728. doi: 10.1016/j.jhazmat.2008.10.046.

Pérez, N., Ferré, J., and Boqué, R. (2009). Calculation of the reliability of classification in discriminant partial least-squares binary classification. *Chemometr. Intell. Lab.* 95, 122–128. doi: 10.1016/j.chemolab.2008.09.005.

Pérez-Jiménez, J., Arranz, S., Tabernero, M., Díaz-Rubio, M. E., Serrano, J., Goñi, I., and Saura-Calixto, F. (2008). Updated methodology to determine antioxidant capacity in plant foods, oils and beverages: Extraction, measurement and expression of results. *Food Res. Int.* 41(3), 274–285. doi: 10.1016/j.foodres.2007.12.004.

Perna, A. M., Simonetti, A., Intaglietta, I., Sofo, A., and Gambacorta, E. (2012). Metal content of southern Italy honey of different botanical origins and its correlation with polyphenol content and antioxidant activity. *Int. J. Food Sci. Technol.* 47, 1909–1917. doi: 10.1111/j.1365-2621.2012.03050.x.

Pohl, W. L. (2011). Economic geology: Principles and practice. Wiley-Blackwell, ISBN: 978-1-444-33663-4. doi:10.1002/9781444394870.

Pošćić, F., Turk, M. F., Bačić, N., Mikac, N., Bertoldi, D., Camin, F., Špika, M. J., Žanetić, M., Rengel, Z., and Perica, S. (2019). Removal of pomace residues is critical in quantification of element concentrations in extra virgin olive oil. *J. Food Compos. Anal.* 77, 39–46. doi: 10.1016/j.jfca.2019.01.002.

Russo, G., Beritognolo, I., Bufacchi, M., Stanzione, V., Pisanelli, A., Ciolfi, M., Lauteri, M., and Brush, S. B. (2020). Advances in biocultural geography of olive tree (Olea europaea L.) landscapes by merging biological and historical assays. *Sci. Rep.* 10, 7673. doi: 10.1038/s41598-020-64063-8

Šarolić, M., Gugić, M., Tuberoso, C. I. G., Jerković, I., Šuste, M., Marijanović, Z., and Kuś, P. M. (2014). Volatile profile, phytochemicals and antioxidant activity of virgin olive oils from Croatian autochthonous varieties Mašnjača and Krvavica in comparison with Italian variety Leccino. *Molecules* 19(1), 881–895. doi: 10.3390/molecules19010881.

Shah, N. S., and Soylak, M. (2021): Advanced methodologies for trace elements in edible oil samples: a review. *Crit. Rev. Anal. Chem.* Mar 15, 1–20. doi: 10.1080/10408347.2021.1895710.

Ståhle, L., and Wold, S. (1987). Partial least squares analysis with cross-validation for the two-class problem: a Monte Carlo study. *J. Chemom.* 1, 185–196. doi: 10.1002/cem.1180010306.

Tchounwou, P.B., Yedjou, C.G., Patlolla, A.K., and Sutton, D.J. (2012). Heavy metals toxicity and the environment. Exp. Suppl. 101, 133–164. doi: 10.1007%2F978-3-7643-8340-4_6.

Thiruvengadam, M., Ghimire, B. K., Kim, S. H., Yu, C. Y., Oh, D. H., Chelliah, R., Kwon, C., Kim, Y. J., and Chung, I. M. (2020). Assessment of mineral and phenolic profiles and their association with the antioxidant, cytotoxic effect, and antimicrobial potential of Lycium chinense Miller. *Plants (Basel, Switzerland)* 9(8), 1023. doi: 10.3390/plants9081023.

Visioli, F., Bellomo, G., and Galli, C. (1998). Free radical-scavenging properties of olive oil polyphenols. *Biochem. Biophys. Res. Commun.* 247(1), 60–64. doi: 10.1006/bbrc.1998.8735.

Wold, S., Martens, H., and Wold, H. (1983). The multivariate calibration problem in chemistry solved by the PLS method. In Matrix Pencils. Lecture Notes in Mathematics, 1st ed.; Kågström, B., Ruhe, A., Eds.; Springer, Berlin/Heidelberg, Germany, 973, 286–293. doi: 10.1007/BFb0062108.

Yaşar, S. B., Baran, E. K., and Alkan, M. (2012). Metal determinations in olive oil, Olive oil - Constituents, quality, health properties and bioconversions, Dr. Dimitrios Boskou (Ed.), ISBN: 978-953-307-921-9, InTech. Available online: http://www.intechopen.com/books/olive-oil-constituents-quality-healthproperties-and-bioconversions/metal-determinations-in-olive-oil. (accessed on July 2021).

Zaroual, H., Chénè, C., El Hadrami, E. M., and Karoui, R. (2021). Application of new emerging techniques in combination with classical methods for the determination of the quality and authenticity of olive oil: a review. *Crit. Rev. Food Sci. Nutr.* 1, 1–24. doi: 10.1080/10408398.2021.1876624.

Zeiner, M., Steffan, I., and Cindric, I. J. (2005). Determination of trace elements in olive oil by ICP-AES and ETA-AAS: A pilot study on the geographical characterization. *Microchem. J.* 81, 171–176. doi: 10.1016/j.microc.2004.12.002.

Zeiner, M., Juranovic-Cindric, I., and Skevin, D. (2010). Characterization of extra virgin olive oils derived from the Croatian cultivar Oblica. *Eur. J. Lipid Sci. Technol.* 112, 1248–1252. doi: 10.1002/ejlt.201000006.

Supplementary Materials

Available at: https://www.frontiersin.org/articles/10.3389/fchem.2021.769620/full#supplementary-material

12. References

Abbas, Z., Steenari, B. M., Lindqvist, O. (2001). A study of Cr (VI) in ashes from fluidized bed combustion of municipal solid waste: leaching, secondary reactions and the applicability of some speciation methods. Waste Management, 21(8), 725-739.

Abrams, J. Y., Weber, R. J., Klein, M., Samat, S. E., Chang, H. H., Strickland, M. J., et al., Tolbert, P. E. (2017). Associations between Ambient Fine Particulate Oxidative Potential and Cardiorespiratory Emergency Department Visits. Environmental Health Perspectives, 125(10).

Akhtar, U. S., McWhinney, R. D., Rastogi, N., Abbatt, J. P., Evans, G. J., Scott, J. A. (2010). Cytotoxic and proinflammatory effects of ambient and source-related particulate matter (PM) in relation to the production of reactive oxygen species (ROS) and cytokine adsorption by particles. Inhalation toxicology, 22(sup2), 37-47.

Ali, M. U., Liu, G., Yousaf, B., Ullah, H., Abbas, Q., Munir, M. A. M. (2019). A systematic review on global pollution status of particulate matter-associated potential toxic elements and health perspectives in urban environment. Environmental geochemistry and health, 41(3), 1131-1162.

Agay-Shay, K., Friger, M., Linn, S., Peled, A., Amitai, Y., Peretz, C. (2013). Air pollution and congenital heart defects. Environmental research, 124, 28-34.

Almeida, S. M., Pio, C. A., Freitas, M. C., Reis, M. A., Trancoso, M. A. (2006). Source apportionment of atmospheric urban aerosol based on weekdays/weekend variability: evaluation of road re-suspended dust contribution. Atmospheric Environment, 40(11), 2058-2067.

Andrade, C., Molina, C., Sánchez, L. F., Manzano, C. A., Toro, R., 2020. Exploring the oxidative potential and respiratory deposition of size-segregated particulate matter at an urban site. Journal of South American Earth Sciences, 102957.

Araujo, J. A., Nel, A. E. (2009). Particulate matter and atherosclerosis: role of particle size, composition and oxidative stress. Particle and fibre toxicology, 6(1), 1-19.

Astolfi, M. L., Conti, M. E., Marconi, E., Massimi, L., Canepari, S. (2020). Effectiveness of different sample treatments for the elemental characterization of bees and beehive products. Molecules, 25(18), 4263.

Ayres, J. G., Borm, P., Cassee, F. R., Castranova, V., Donaldson, K., Ghio, A., Harrison, R.M., Hider, R., Kelly, F., Kooter, I.M., Marano, F., Maynard, R.L., Mudway, I., Nel, A., Sioutas, C., Smith, S., Baeza-Squiban, A., Cho, A., Duggan, S., Froines, J., 2008. Evaluating the toxicity of airborne particulate matter and nanoparticles by measuring oxidative stress potential - a workshop report and consensus statement. Inhalation Toxicology, 20(1), 75-99.

Barry, R. G., Chorley, R. J. (1992). Atmosphere, weather and climate. 6th ed. Routledge, London.

Barnaba, F., Bolignano, A., Di Liberto, L., Morelli, M., Lucarelli, F., Nava, S., et al., Gobbi, G. P. (2017). Desert dust contribution to PM10 loads in Italy: Methods and recommendations addressing the relevant European Commission Guidelines in support to the Air Quality Directive 2008/50. Atmospheric environment, 161, 288-305.

Barone, T. L., Lall, A. A., Zhu, Y., Yu, R. C., Friedlander, S. K. (2006). Inertial deposition of nanoparticle chain aggregates: theory and comparison with impactor data for ultrafine atmospheric aerosols. Journal of Nanoparticle Research, 8(5), 669-680.

Bates, J. T., Fang, T., Verma, V., Zeng, L., Weber, R. J., Tolbert, P. E., Abrams, J. Y., Sarnat, S. E., Klein, M., Mulholland, J. A., Russell, A. G., 2019. Review of acellular assays of ambient particulate matter oxidative potential: Methods and relationships with composition, sources, and health effects. Environmental Science & Technology, 53(8), 4003-4019.

Bekö, G., Carslaw, N., Fauser, P., Kauneliene, V., Nehr, S., Phillips, G., Saraga, D., Schoemaecker, D., Wierzbicka, A., Querol, X. (2020). The past, present and future of indoor air chemistry. Indoor air, 373-376.

Belosi, F., Rinaldi, M., Decesari, S., Tarozzi, L., Nicosia, A., Santachiara, G. (2017). Ground level ice nuclei particle measurements including Saharan dust events at a Po Valley rural site (San Pietro Capofiume, Italy). Atmospheric Research, 186, 116-126.

Berglund, G. I., Carlsson, G. H., Smith, A. T., Szöke, H., Henriksen, A., Hajdu, J. (2002). The catalytic pathway of horseradish peroxidase at high resolution. Nature, 417(6887), 463-468.

Bernardoni, V., Elser, M., Valli, G., Valentini, S., Bigi, A., Fermo, P., Piazzalunga, A., Vecchi, R. (2017). Size-segregated aerosol in a hot-spot pollution urban area: Chemical composition and three-way source apportionment. Environmental Pollution, 231, 601-611.

Betha, R., Behera, S. N., Balasubramanian, R. (2014). 2013 Southeast Asian smoke haze: fractionation of particulate-bound elements and associated health risk. Environmental Science and Technology, 48(8), 4327-4335.

Buettner, G. R., Jurkiewicz, B. A. (1996). Catalytic metals, ascorbate and free radicals: combinations to avoid. Radiation research, 145(5), 532-541.

Buiarelli, F., Sonego, E., Uccelletti, D., Bruni, E., Di Filippo, P., Pomata, D., et al. Simonetti, G. (2019). Determination of the main bioaerosol components using chemical markers by liquid chromatography–tandem mass spectrometry. Microchemical Journal, 149, 103974.

Bussotti, F., Pollastrini, M. (2015). Evaluation of leaf features in forest trees: Methods, techniques, obtainable information and limits. Ecological indicators, 52, 219-230.

Calas, A., Uzu, G., Martins, J. M., Voisin, D., Spadini, L., Lacroix, T., Jaffrezo, J. L. (2017). The importance of simulated lung fluid (SLF) extractions for a more relevant evaluation of the oxidative potential of particulate matter. Scientific reports, 7(1), 1-12.

Campbell, S. J., Utinger, B., Lienhard, D. M., Paulson, S. E., Shen, J., Griffiths, P. T., et al., Kalberer, M. (2019). Development of a physiologically relevant online chemical assay to quantify aerosol oxidative potential. Analytical chemistry, 91(20), 13088-13095.

Canepari, S., Perrino, C., Olivieri, F., Astolfi, M.L. (2008). Characterisation of the traffic sources of PM through size-segregated sampling, sequential leaching and ICP analysis. Atmospheric Environment, 42, 8161-8175.

Canepari, S., Astolfi, M. L., Farao, C., Maretto, M., Frasca, D., Marcoccia, M., Perrino, C. (2014). Seasonal variations in the chemical composition of particulate matter: a case study in the Po Valley. Part II: concentration and solubility of micro-and trace-elements. Environmental Science and Pollution Research, 21(6), 4010-4022.

Canepari, S., Pietrodangelo, A., Perrino, C., Astolfi, M. L., Marzo, M. L. (2009). Enhancement of source traceability of atmospheric PM by elemental chemical fractionation. Atmospheric Environment, 43(31), 4754-4765.

Canepari, S., Cardarelli, E., Giuliano, A., Pietrodangelo, A. (2006a). Determination of metals, metalloids and non-volatile ions in airborne particulate matter by a new twostep sequential leaching procedure part A: Experimental design and optimization. Talanta, 69, 581–587. https://doi.org/10.1016/j.talanta.2005.10.023

Canepari, S., Cardarelli, E., Pietrodangelo, A., Strincone, M. (2006b). Determination of metals, metalloids and non-volatile ions in airborne particulate matter by a new two-step sequential leaching procedure: Part B: Validation on equivalent real samples. Talanta, 69(3), 588-595.

Cassee, F. R., Héroux, M. E., Gerlofs-Nijland, M. E., Kelly, F. J. (2013). Particulate matter beyond mass: recent health evidence on the role of fractions, chemical constituents and sources of emission. Inhalation Toxicology, 2514, 802-812.

Castellani, F., Massimi, L., Vitali, M., Canepari, S., Guidotti, M., Conti, M. E., Protano, C. (2020). High spatial resolution analysis of polybrominated diphenyl ethers (PBDEs) using transplanted lichen Evernia prunastri: A case study in central Italy. Science of the Total Environment, 742, 140590.

Catrambone, M., Canepari, S., Cerasa, M., Sargolini, T., Perrino, C. (2019). Performance evaluation of a very-low-volume sampler for atmospheric particulate matter. Aerosol and Air Quality Research, 19(10), 2160-2172.

Cesari, D., Merico, E., Grasso, F. M., Decesari, S., Belosi, F., Manarini, F., De Nuntiis, P., Rinaldi, M., Volpi, F., Gambaro, A., Morabito, E., Contini, D. (2019). Source apportionment of PM2. 5 and of its oxidative potential in an industrial suburban site in south Italy. Atmosphere, 10(12), 758.

Charrier, J.G., Anastasio, C., 2012. On dithiothreitol (DTT) as a measure of oxidative potential for ambient particles: evidence for the importance of soluble transition metals. Atmos. Chem. Phys. 12, 9321–9333.

Chedea, V. S., Pop, R. M. (2019). Total polyphenols content and antioxidant DPPH assays on biological samples. In Polyphenols in Plants (pp. 169-183). Academic Press.

Chen, X., Guo, M., Feng, J., Liang, S., Han, D., Cheng, J. (2019). Characterization and risk assessment of heavy metals in road dust from a developing city with good air quality and from Shanghai, China. Environmental Science and Pollution Research, 26(11), 11387-11398.

Cheng, Y.-H., Tsai, C.-J. (1997). Evaporation Loss of Ammonium Nitrate Particles During Filter Sampling. J. Aerosol Sci., 28:1553–1567.

Chiam, Z., Song, X. P., Lai, H. R., Tan, H. T. W. (2019). Particulate matter mitigation via plants: Understanding complex relationships with leaf traits. Science of the total environment, 688, 398-408.

Chirizzi, D., Cesari, D., Guascito, M. R., Dinoi, A., Giotta, L., Donateo, A., Contini, D. (2017). Influence of Saharan dust outbreaks and carbon content on oxidative potential of water-soluble fractions of PM2. 5 and PM10. Atmospheric Environment, 163, 1-8.

Cho, A. K., Sioutas, C., Miguel, A. H., Kumagai, Y., Schmitz, D. A., Singh, M., Fernandez, F.A., Froines, J. R., 2005. Redox activity of airborne particulate matter at different sites in the Los Angeles Basin. Environmental research, 99(1), 40-47.

Chowdhury Z, Zheng M, Schauer JJ, Sheesley RJ, Salmon LG, Cass GR, Russell AG (2007) Speciation of ambient fine organic carbon particles and source apportionment of PM2.5 in Indian cities. J Geophys Res 112:D15303

Chubarova, N. E., Androsova, E. E., Kirsanov, A. A., Vogel, B., Vogel, H., Popovicheva, O. B., Rivin, G. S. (2019). Aerosol and its radiative effects during the Aeroradcity 2018 Moscow experiment. Geography, Environment, Sustainability, 12(4), 114-131.

Cohen, A. J., Brauer, M., Burnett, R., Anderson, H. R., Frostad, J., Estep, K., Balakrishnan, K., Brunekreef, B., Dandona, L., Dandona, R., Feigin, V., Freedman, G., Hubbell, B., Jobling, A., Kan, H., Knibbs, L., Liu, Y., Martin, R., Morawska, L., Pope, C.A., Shin, H., Straif, K., Shaddick, G., Thomas, M., van Dingenen, R., van Donkelaar, A., Vos, T., DPhil, C.J.L.M., Forouzanfar, M. H. (2017). Estimates and 25-year trends of the global burden of disease attributable to ambient air pollution: an analysis of data from the Global Burden of Diseases Study 2015. The Lancet, 389(10082), 1907-1918.

Conte, E., Canepari, S., Frasca, D., Simonetti, G. (2017). Oxidative potential of selected PM components. In Multidisciplinary Digital Publishing Institute Proceedings (Vol. 1, No. 5, p. 108).

Conti, M. E., Cecchetti, G. (2001). Biological monitoring: lichens as bioindicators of air pollution assessment—a review. Environmental pollution, 114(3), 471-492.

Contini, D., Costabile, F. (2020). Does air pollution influence COVID-19 outbreaks?.

Costabile, F., Alas, H., Aufderheide, M., Avino, P., Amato, F., Argentini, S., et al., Petralia, E. (2017). First results of the “Carbonaceous aerosol in Rome and Environs (CARE)” experiment: Beyond current standards for PM10. Atmosphere, 8(12), 249.

Crobeddu, B., Aragao-Santiago, L., Bui, L. C., Boland, S., Squiban, A. B. (2017). Oxidative potential of particulate matter 2.5 as predictive indicator of cellular stress. Environmental Pollution, 230, 125-133.

Cross, C. E., van der Vliet, A., O'Neill, C. A., Louie, S., Halliwell, B. (1994). Oxidants, antioxidants, and respiratory tract lining fluids. Environmental health perspectives, 102(suppl 10), 185-191.

Daellenbach, K. R., Uzu, G., Jiang, J., Cassagnes, L. E., Leni, Z., Vlachou, A., Stefenelli, G., Canonaco, F., Weber, S., Segers, A., Kuenen, J.J.P., Schaap, M., Favez, O., Albinet, A., Aksoyoglu, S., Dommen, J., Baltensperger, U., Geiser, M., El Haddad, I., Jaffrezo, J., Prévôt, A. S. (2020). Sources of particulate-matter air pollution and its oxidative potential in Europe. Nature, 587(7834), 414-419.

Daher, N., Ning, Z., Cho, A. K., Shafer, M., Schauer, J. J., Sioutas, C. (2011). Comparison of the chemical and oxidative characteristics of particulate matter (PM) collected by different methods: filters, impactors, and biosamplers. Aerosol Science and Technology, 45(11), 1294-1304.

Das, R., Khezri, B., Srivastava, B., Datta, S., Sikdar, P. K., Webster, R. D., Wang, X. (2015). Trace element composition of PM2. 5 and PM10 from Kolkata–a heavily polluted Indian metropolis. Atmospheric Pollution Research, 6(5), 742-750.

De Marco, A., Screpanti, A., Mircea, M., Piersanti, A., Proietti, C., Fornasier, M. F. (2017). High resolution estimates of the corrosion risk for cultural heritage in Italy. Environmental Pollution, 226, 260-267.

Delfino, R. J., Staimer, N., Vaziri, N. D., 2011. Air pollution and circulating biomarkers of oxidative stress. Air Quality, Atmosphere & Health, 4(1), 37-52.

Delfino, R. J., Staimer, N., Tjoa, T., Gillen, D. L., Schauer, J. J., Shafer, M. M. (2013). Airway inflammation and oxidative potential of air pollutant particles in a pediatric asthma panel. Journal of exposure science & environmental epidemiology, 23(5), 466-473.

DELLA REPUBBLICA, I. P. Attuazione della direttiva 2008/50/CE relativa alla qualità dell'aria ambiente e per un'aria più pulita in Europa (GU 15 settembre 2010, n. 216, suppl.

Dellinger, B., Pryor, W. A., Cueto, R., Squadrito, G. L., Hegde, V., Deutsch, W. A. (2001). Role of free radicals in the toxicity of airborne fine particulate matter. Chemical research in toxicology, 14(10), 1371-1377.

Dey, S. K., Sugur, K., Venkatareddy, V. G., Rajeev, P., Gupta, T., Thimmulappa, R. K. (2021). Lipid peroxidation index of particulate matter: Novel metric for quantifying intrinsic oxidative potential and predicting toxic responses. Redox Biology, 102189.

Di Vaio, P., Cocozziello, B., Corvino, A., Fiorino, F., Frecentese, F., Magli, E., et al., Perissutti, E. (2016). Level, potential sources of polycyclic aromatic hydrocarbons (PAHs) in particulate matter (PM10) in Naples. Atmospheric environment, 129, 186-196.

Dick, C. A. J., Stone, V., Brown, D. M., Watt, M., Cherrie, J. W., Howarth, S., Seaton, A., Donaldson, K. (2000). Toxic and Inflammatory Effects of Filters Frequently Used for the Collection of Airborne Particulate Matter. Atmos. Environ., 34:2587–2592.

Duarte, R. M., Gomes, J. F., Querol, X., Cattaneo, A., Bergmans, B., Saraga, D.,Maggos, T., Di Gilio, A., Rovelli, S., Villanueva, F. (2021). Advanced instrumental approaches for chemical characterization of indoor particulate matter. Applied Spectroscopy Reviews, 1-41.

Dubey, B., Pal, A. K., Singh, G. (2012). Trace metal composition of airborne particulate matter in the coal mining and non–mining areas of Dhanbad Region, Jharkhand, India. Atmospheric Pollution Research, 3(2), 238-246.

Duffin, R., Tran, L., Brown, D., Stone, V., Donaldson, K. (2007). Proinflammogenic effects of low-toxicity and metal nanoparticles in vivo and in vitro: highlighting the role of particle surface area and surface reactivity. Inhalation toxicology, 19(10), 849-856.

Dzubay, T. G. (1977). X-ray fluorescence analysis of environmental samples. Ann Arbor Science Publishers.

Eatough, D. J., Long, R. W., Modey, W. K., Eatough, N. L. (2003). Semi-Volatile Secondary Organic Aerosol in Urban Atmospheres: Meeting a Measurement Challenge. Atmos. Environ., 37:1277–1292.

EPA, (1997). Reference Method for the Determination of Particulate Matter as PM10 in the Atmosphere. Federal Registrer, 62, No 138, Appendix M to part 50.

Fang, G. C., Zheng, Y. C. (2014). Diurnal ambient air particles, metallic elements dry deposition, concentrations study during year of 2012–2013 at a traffic site. Atmospheric Environment, 88, 39-46.

Fang, T., Verma, V., Bates, J. T., Abrams, J., Klein, M., Strickland, M. J., Sarnat, S.E., Chang, H.H., Mulholland, J.A., Tolbert, P.E., Russell, A. G., Weber, R.J., (2016). Oxidative potential of ambient water-soluble PM2. 5 in the southeastern United States: contrasts in sources and health associations between ascorbic acid (AA) and dithiothreitol (DTT) assays. Atmospheric Chemistry and Physics 16(6), 3865-3879.

Fang, T., Verma, V., Guo, H., King, L. E., Edgerton, E. S., Weber, R. J. (2015). A semi-automated system for quantifying the oxidative potential of ambient particles in aqueous extracts using the dithiothreitol (DTT) assay: results from the Southeastern Center for Air Pollution and Epidemiology (SCAPE). Atmospheric Measurement Techniques, 8(1), 471-482.

Fang, W., Yang, Y., Xu, Z. (2013). PM10 and PM2. 5 and health risk assessment for heavy metals in a typical factory for cathode ray tube television recycling. Environmental science & technology, 47(21), 12469-12476.

Farao, C., Canepari, S., Perrino, C., Harrison, R. M. (2014). Sources of PM in an industrial area: comparison between receptor model results and semiempirical calculations of source contributions. Aerosol and Air Quality Research, 14(6), 1558-1572.

Feng, X. D., Dang, Z., Huang, W. L., Yang, C. (2009). Chemical speciation of fine particle bound trace metals. International Journal of Environmental Science & Technology, 6(3), 337-346.

Feng, S., Gao, D., Liao, F., Zhou, F., Wang, X. (2016). The health effects of ambient PM2. 5 and potential mechanisms. Ecotoxicology and environmental safety, 128, 67-74.

Fuller, S. J., Wragg, F. P. H., Nutter, J., Kalberer, M., 2014. Comparison of on-line and off-line methods to quantify reactive oxygen species (ROS) in atmospheric aerosols. Atmospheric Environment, 92, 97-103.

Fushimi, A., Nakajima, D., Furuyama, A., Suzuki, G., Ito, T., Sato, K., Fujitani, Y., Kondo, Y., Yoshino, A., Ramasamy, S., Schauer, J.J., Fu, P., Takahashi, Y., Saitoh, K., Saito, S., Takami, A. (2021). Source contributions to multiple toxic potentials of atmospheric organic aerosols. Science of The Total Environment, 773, 145614.

Gao, Y., Lee, S. C., Huang, Y., Chow, J. C., Watson, J. G. (2016). Chemical characterization and source apportionment of size-resolved particles in Hong Kong sub-urban area. Atmospheric Research, 170, 112-122.

Gil, H., Buitrago, C. P., Calderón, J. A. (2017). Atmospheric corrosion of copper and silver influenced by particulate matter. Journal of Solid State Electrochemistry, 21(4), 1111-1119.

Gilardoni, S., Massoli, P., Paglione, M., Giulianelli, L., Carbone, C., Rinaldi, M., Decesari, S., Sandrini, S., Costabile, F., Gobbi, G.P., Pietrogrande, M.C., Visentin, M., Scotto, F., Fuzzi, S., Facchini, M. C. (2016). Direct observation of aqueous secondary organic aerosol from biomass-burning emissions. Proceedings of the National Academy of Sciences, 113(36), 10013-10018.

Giordano, S., Spagnuolo, V., Capozzi, F. (2021). Biomonitoring of Air Pollution. Atmosphere 2021, 12, 433.

Girotti, S., Ghini, S., Ferri, E., Bolelli, L., Colombo, R., Serra, G., Porrini, C., Sangiorgi, S. (2020). Bioindicators and biomonitoring: honeybees and hive products as pollution impact assessment tools for the Mediterranean area. Euro-Mediterranean Journal for Environmental Integration, 5(3), 1-16.

Gratani, L., Crescente, M. F., Varone, L. (2008). Long-term monitoring of metal pollution by urban trees. Atmospheric Environment, 42(35), 8273-8277.

Grantz, D. A., Garner, J. H. B., Johnson, D. W. (2003). Ecological effects of particulate matter. Environment international, 29(2-3), 213-239.

Gupta, T., Singh, S. P., Rajput, P., Agarwal, A. K., 2019. Measurement, Analysis and Remediation of Environmental Pollutants. Springer.

Hamanaka, R. B., Mutlu, G. M. (2018). Particulate matter air pollution: effects on the cardiovascular system. Frontiers in endocrinology, 9, 680.

Hara, K., Someya, T., Sano, K., Sagane, Y., Watanabe, T., Wijesekara, R. G. S. (2018). Antioxidant activities of traditional plants in Sri Lanka by DPPH free radical-scavenging assay. Data in brief, 17, 870-875.

Harrison, R. M., Allan, J., Carruthers, D., Heal, M. R., Lewis, A. C., Marner, B., Murrells, T.,Williams, A. (2021). Non-exhaust vehicle emissions of particulate matter and VOC from road traffic: A review. Atmospheric Environment, 262, 118592.

He, C., Morawska, L., Hitchins, J., Gilbert, D. (2004). Contribution from indoor sources to particle number and mass concentrations in residential houses. Atmospheric environment, 38(21), 3405-3415.

Hedayat, F., Stevanovic, S., Miljevic, B., Bottle, S., Ristovski, Z. D., (2015). Evaluating the molecular assays for measuring the oxidative potential of particulate matter. Chemical Industry and Chemical Engineering Quarterly, 21(1-2), 201-210.

Henninger, S. M. (2013). When Air Quality Becomes Deleterious—A Case Study for Kigali, Rwanda. Journal of Environmental Protection, 04(08):1–7.

Hering, S. V., Flagan, R. C., Friedlander, S. K. (1978). Design and evaluation of new low-pressure impactor. I. Environmental Science & Technology, 12(6), 667-673.

Hinds, W. C. (1999). Aerosol Technology: Properties, Behavior, and Measurement of Airborne Particles (2 edition). New York: Wiley-Interscience.

Hoffmann, M., Kleine-Weber, H., Schroeder, S., Krüger, N., Herrler, T., Erichsen, S., et al., Pöhlmann, S. (2020). SARS-CoV-2 cell entry depends on ACE2 and TMPRSS2 and is blocked by a clinically proven protease inhibitor. cell, 181(2), 271-280.

Hopke, P. K. (2000). A guide to positive matrix factorization, in workshop on UNMIX and PMF as applied to PM2. 5. Edited by Willis, RD, RTP, NC. EPA 600/A-00/048.

Huffman, J. A., Treutlein, B., Pöschl, U. (2010). Fluorescent biological aerosol particle concentrations and size distributions measured with an Ultraviolet Aerodynamic Particle Sizer (UV-APS) in Central Europe. Atmospheric Chemistry and Physics, 10(7), 3215-3233.

Hung, H. F., Wang, C. S., 2001. Experimental determination of reactive oxygen species in Taipei aerosols. Journal of Aerosol Science, 32(10), 1201-1211.

Janghorbani, M., Momeni, F., Mansourian, M. (2014). Systematic review and metaanalysis of air pollution exposure and risk of diabetes. European journal of epidemiology, 29(4), 231-242.

Janssen, N. A. H., Gerlofs-Nijland, M. E., Lanki, T., Salonen, R. O., Cassee, F., Hoek, G., et al., Krzyzanowski, M. (2012). Health effects of black carbon, The WHO European Centre for Environment and Health, Bonn, Germany. World Health Organisation Regional Office for Europe, Copenhagen, Denmark.

Jaoui, M., Kamens, R. M. (2001). Mass balance of gaseous and particulate products analysis from α-pinene/NO x/air in the presence of natural sunlight. Journal of Geophysical Research: Atmospheres, 106(D12), 12541-12558.

John W (2001) Size Distribution Characteristics of Aerosols in: Baron, P. A., Willeke, K. Aerosol Measurement – Wiley InterScience New York. EC (1997). Working Group on Particles. Position Paper on Ambient Air Pollution by Particulate Matter. http://europa.eu.int/comm.

Kedare, S. B., Singh, R. P. (2011). Genesis and development of DPPH method of antioxidant assay. Journal of food science and technology, 48(4), 412-422.

Kelly, F. J., Dunster, C., Mudway, I. (2003). Air pollution and the elderly: oxidant/antioxidant issues worth consideration. European Respiratory Journal, 21(40 suppl), 70s-75s.

Kelly, F. J., Fussell, J. C. (2012). Size, source and chemical composition as determinants of toxicity attributable to ambient particulate matter. Atmospheric environment, 60, 504-526.

Kim, K. H., Kabir, E., Kabir, S. (2015). A review on the human health impact of airborne particulate matter. Environment international, 74, 136-143.

King, L. E., Weber, R. J., (2013). Development and testing of an online method to measure ambient fine particulate reactive oxygen species (ROS) based on the 2', 7'-dichlorofluorescin (DCFH) assay. Atmospheric Measurement Techniques, 6(7), 1647-1658.

Kleinman, M. T., Sioutas, C., Froines, J. R., Fanning, E., Hamade, A., Mendez, L., Meacher, D., Oldham, M. (2007). Inhalation of concentrated ambient particulate matter near a heavily trafficked road stimulates antigen-induced airway responses in mice. Inhalation Toxicology, 19(sup1), 117-126.

Klyta, J., Czaplicka, M. (2020). Determination of secondary organic aerosol in particulate matter–Short review. Microchemical Journal, 157, 104997.

Kousehlar, M., Widom, E. (2020). Identifying the sources of air pollution in an urban-industrial setting by lichen biomonitoring-A multi-tracer approach. Applied Geochemistry, 121, 104695.

Kramer, A. J., Rattanavaraha, W., Zhang, Z., Gold, A., Surratt, J. D., Lin, Y. H. (2016). Assessing the oxidative potential of isoprene-derived epoxides and secondary organic aerosol. Atmospheric Environment, 130, 211-218.

Kumagai, Y., Arimoto, T., Shinyashiki, M., Shimojo, N., Nakai, Y., Yoshikawa, T., Sagai, M., 1997. Generation of reactive oxygen species during interaction of diesel exhaust particle components with NADPH-

cytochrome P450 reductase and involvement of the bioactivation in the DNA damage. Free Radical Biology and Medicine, 22(3), 479-487.

Kumagai, Y., Koide, S., Taguchi, K., Endo, A., Nakai, Y., Yoshikawa, T., Shimojo, N., 2002. Oxidation of proximal protein sulfhydryls by phenanthraquinone, a component of diesel exhaust particles. Chemical research in toxicology, 15(4), 483-489.

Lai, H. K., Kendall, M., Ferrier, H., Lindup, I., Alm, S., Hänninen, O., Jantunen, M., Mathys, P., Colvile, R., Ashmore, M.R., Cullinan, P., Nieuwenhuijsen, M. J. (2004). Personal exposures and microenvironment concentrations of PM2. 5, VOC, NO2 and CO in Oxford, UK. Atmospheric Environment, 38(37), 6399-6410.

Laskin, A., Laskin, J., Nizkorodov, S. A. (2015). Chemistry of atmospheric brown carbon. Chemical reviews, 115(10), 4335-4382.

Lawrence, S., Sokhi, R., Ravindra, K., Mao, H., Prain, H. D., Bull, I. D. (2013). Source apportionment of traffic emissions of particulate matter using tunnel measurements. Atmospheric environment, 77, 548-557.

Lee, B. K. (2010). Sources, distribution and toxicity of polyaromatic hydrocarbons (PAHs) in particulate matter. In Air pollution. IntechOpen.

Li, Q., Wyatt, A., Kamens, R. M. (2009). Oxidant generation and toxicity enhancement of aged-diesel exhaust. Atmospheric Environment, 43(5), 1037-1042.

Lin, M., Yu, J. Z. (2019). Dithiothreitol (DTT) concentration effect and its implications on the applicability of DTT assay to evaluate the oxidative potential of atmospheric aerosol samples. Environmental Pollution, 251, 938-944.

Lin, M., Yu, J. Z., (2020). Assessment of interactions between transition metals and atmospheric organics: Ascorbic Acid Depletion and Hydroxyl Radical Formation in Organic-metal Mixtures. Environmental Science & Technology.

Lin, P., Yu, J. Z. (2011). Generation of reactive oxygen species mediated by humic-like substances in atmospheric aerosols. Environmental science & technology, 45(24), 10362-10368.

Lionetto, M. G., Guascito, M. R., Caricato, R., Giordano, M. E., De Bartolomeo, A. R., Romano, M. P., et al., Contini, D. (2019). Correlation of oxidative potential with ecotoxicological and cytotoxicological potential of PM10 at an urban background site in Italy. Atmosphere, 10(12), 733.

Liu, X., Zhai, Y., Zhu, Y., Liu, Y., Chen, H., Li, P., Peng, C., Xu, B:, Li, C., Zeng, G. (2015). Mass concentration and health risk assessment of heavy metals in size-segregated airborne particulate matter in Changsha. Science of the Total Environment, 517, 215-221.

Liu, B., Wu, J., Zhang, J., Wang, L., Yang, J., Liang, D., Dai, Q., Bi, X., Feng, Y., Zhang, Q. (2017). Characterization and source apportionment of PM2. 5 based on error estimation from EPA PMF 5.0 model at a medium city in China. Environmental Pollution, 222, 10-22.

Lohmann, R., Ockenden, W. A., Shears, J., Jones, K. C. (2001). Atmospheric distribution of polychlorinated dibenzo-p-dioxins, dibenzofurans (PCDD/Fs), and non-ortho biphenyls (PCBs) along a north− south Atlantic transect. Environmental science & technology, 35(20), 4046-4053.

Lokorai, K., Ali-Khodja, H., Khardi, S., Bencharif-Madani, F., Naidja, L., Bouziane, M. (2021). Influence of mineral dust on the concentration and composition of PM10 in the city of Constantine. Aeolian Research, 50, 100677.

Losacco, C., Perillo, A. (2018). Particulate matter air pollution and respiratory impact on humans and animals. Environmental Science and Pollution Research, 25(34), 33901-33910.

Losfeld, G., Saunier, J. B., Grison, C. (2014). Minor and trace-elements in apiary products from a historical mining district (Les Malines, France). Food chemistry, 146, 455-459.

Luo, Z., Zhang, L., Li, G., Du, W., Chen, Y., Cheng, H., Tao, S., Shen, G. (2021). Evaluating co-emissions into indoor and outdoor air of EC, OC, and BC from in-home biomass burning. Atmospheric Research, 248, 105247.

Maas, S., Scheifler, R., Benslama, M., Crini, N., Lucot, E., Brahmia, Z., et al., Giraudoux, P. (2010). Spatial distribution of heavy metal concentrations in urban, suburban and agricultural soils in a Mediterranean city of Algeria. Environmental pollution, 158(6), 2294-2301.

Mahoney J.R., Graf, E. (1986). Role of Alpha-Tocopherol, Ascorbic Acid, Citric Acidand EDTA as Oxidants in Model Systems. Journal of Food Science, 51(5), 1293-1296.

Mamane, Y., Perrino, C., Yossef, O., Catrambone, M. (2008). Source characterization of fine and coarse particles at the East Mediterranean coast. Atmospheric Environment, 42(24), 6114-6130.

Manigrasso, M., Simonetti, G., Astolfi, M. L., Perrino, C., Canepari, S., Protano, C., Antonucci, A., Avino, P., Vitali, M., 2020. Oxidative Potential Associated with Urban Aerosol Deposited into the Respiratory System and Relevant Elemental and Ionic Fraction Contributions. Atmosphere, 11(1), 6.

Marcazzan, G. M., Ceriani, M., Valli, G., Vecchi, R. (2003). Source apportionment of PM10 and PM2. 5 in Milan (Italy) using receptor modelling. Science of the Total Environment, 317(1-3), 137-147.

Marcovecchio, F., Perrino, C. (2021). Contribution of Primary Biological Aerosol Particles to airborne particulate matter in indoor and outdoor environments. Chemosphere, 264, 128510.

Massabò, D., Caponi, L., Bernardoni, V., Bove, M. C., Brotto, P., Calzolai, G., Cassola, F., Chiari, M., Fedi, M.E., Fermo, P., Giannoni, M., Lucarelli, F., Nava, S., Piazzalunga, A., Valli, G., Vecchi, R., Prati, P. (2015).

Multi-wavelength optical determination of black and brown carbon in atmospheric aerosols. Atmospheric Environment, 108, 1-12.

Massimi, L., Ristorini, M., Eusebio, M., Florendo, D., Adeyemo, A., Brugnoli, D., Canepari, S. (2017). Monitoring and evaluation of Terni (Central Italy) air quality through spatially resolved analyses. Atmosphere, 8(10), 200.

Massimi, L., Castellani, F., Protano, C., Conti, M. E., Antonucci, A., Frezzini, M. A., et al., Canepari, S. (2021a). Lichen transplants for high spatial resolution biomonitoring of Persistent Organic Pollutants (POPs) in a multi-source polluted area of Central Italy. Ecological Indicators, 120, 106921.

Massimi, L., Pietrodangelo, A., Frezzini, M. A., Ristorini, M., De Francesco, N., Sargolini, T., Amoroso, A., Di Giosa, A., Canepari, S., Perrino, C. (2021b). Effects of COVID-19 lockdown on PM10 composition and sources in the Rome Area (Italy) by elements' chemical fractionation-based source apportionment. Atmospheric Research, 105970.

Massimi, L., Ristorini, M., Simonetti, G., Frezzini, M. A., Astolfi, M. L., Canepari, S. (2020a). Spatial mapping and size distribution of oxidative potential of particulate matter released by spatially disaggregated sources. Environmental Pollution, 266, 115271.

Massimi, L., Ristorini, M., Astolfi, M. L., Perrino, C., Canepari, S. (2020b). High resolution spatial mapping of element concentrations in PM10: A powerful tool for localization of emission sources. Atmospheric Research, 244, 105060.

Massimi, L., Simonetti, G., Buiarelli, F., Di Filippo, P., Pomata, D., Riccardi, C., Ristorini, M., Astolfi, M.A., Canepari, S. (2020c). Spatial distribution of levoglucosan and alternative biomass burning tracers in atmospheric aerosols, in an urban and industrial hot-spot of Central Italy. Atmospheric Research, 239, 104904.

McWhinney, R. D., Badali, K., Liggio, J., Li, S. M., Abbatt, J. P. (2013). Filterable redox cycling activity: a comparison between diesel exhaust particles and secondary organic aerosol constituents. Environmental science & technology, 47(7), 3362-3369.

Menetrez, M. Y., Foarde, K. K., Esch, R. K., Schwartz, T. D., Dean, T. R., Hays, M. D., et al., Moore, S. A. (2009). An evaluation of indoor and outdoor biological particulate matter. Atmospheric environment, 43(34), 5476-5483.

Minguillón, M. C., Querol, X., Baltensperger, U., Prévôt, A. S. H. (2012). Fine and coarse PM composition and sources in rural and urban sites in Switzerland: local or regional pollution?. Science of the Total Environment, 427, 191-202.

Miri, M., Aval, H. E., Ehrampoush, M. H., Mohammadi, A., Toolabi, A., Nikonahad, A., et al., Abdollahnejad, A. (2017). Human health impact assessment of exposure to particulate matter: an AirQ software modeling. Environmental Science and Pollution Research, 24(19), 16513-16519.

Morakinyo, O. M., Mokgobu, M. I., Mukhola, M. S., Hunter, R. P. (2016). Health outcomes of exposure to biological and chemical components of inhalable and respirable particulate matter. International journal of environmental research and public health, 13(6), 592.

Moreno, E., Sagnotti, L., Dinarès-Turell, J., Winkler, A., Cascella, A. (2003). Biomonitoring of traffic air pollution in Rome using magnetic properties of tree leaves. Atmospheric Environment, 37(21), 2967-2977.

Moreno-Ríos, A. L., Tejeda-Benítez, L. P., Bustillo-Lecompte, C. F. (2022). Sources, characteristics, toxicity, and control of ultrafine particles: An overview. Geoscience Frontiers, 13(1), 101147.

Mudway, I. S., Stenfors, N., Duggan, S. T., Roxborough, H., Zielinski, H., Marklund, S. L., et al., Kelly, F. J. (2004). An in vitro and in vivo investigation of the effects of diesel exhaust on human airway lining fluid antioxidants. Archives of Biochemistry and Biophysics, 423(1), 200-212.

Muhammad, S., Wuyts, K., Samson, R. (2020). Immobilized atmospheric particulate matter on leaves of 96 urban plant species. Environmental Science and Pollution Research, 27(29), 36920-36938.

Nemmar, A., Holme, J. A., Rosas, I., Schwarze, P. E., Alfaro-Moreno, E. (2013). Recent advances in particulate matter and nanoparticle toxicology: a review of the in vivo and in vitro studies. BioMed research international, 2013.

Nguyen, Q. T., Skov, H., Sørensen, L. L., Jensen, B. J., Grube, A. G., Massling, A., Glasius, M., and Nøjgaard, J. K. (2013). Source apportionment of particles at Station Nord, North East Greenland during 2008–2010 using COPREM and PMF analysis. Atmospheric Chemistry and Physics, 13(1), 35-49.

Nickovic, S., Papadopoulos, A., Kakaliagou, O., Kallos, G. (2001) Model for prediciton of desert dust cycle in the atmosphere. J. Geophys. Res., 106, 18113-18129.

Nishita-Hara, C., Hirabayashi, M., Hara, K., Yamazaki, A., Hayashi, M., 2019. Dithiothreitol-measured oxidative potential of size-segregated particulate matter in Fukuoka, Japan: Effects of Asian dust events. GeoHealth, 3(6), 160-173.

Nowak, D.J., Crane, D.E., Stevens, J.C. (2006). Air pollution removal by urban trees and shrubs in the United 723 States. Urban Forestry & Urban Greening 4, 115–123.

Nozza, E., Valentini, S., Melzi, G., Vecchi, R., Corsini, E. (2021). Advances on the immunotoxicity of outdoor particulate matter: A focus on physical and chemical properties and respiratory defence mechanisms. Science of The Total Environment, 146391.

Oakes, M., Rastogi, N., Majestic, B. J., Shafer, M., Schauer, J. J., Edgerton, E. S., Weber, R. J. (2010). Characterization of soluble iron in urban aerosols using near-real time data. Journal of Geophysical Research: Atmospheres, 115(D15).

O'brien, P. J. (1991). Molecular mechanisms of quinone cytotoxicity. Chemico-biological interactions, 80(1), 1-41.

Orsini, D. A., Ma, Y., Sullivan, A., Sierau, B., Baumann, K., Weber, R. J. (2003). Refinements to the particle-into-liquid sampler (PILS) for ground and airborne measurements of water soluble aerosol composition. Atmospheric Environment, 37(9-10), 1243-1259.

Øvrevik, J. (2019). Oxidative potential versus biological effects: a review on the relevance of cell-free/abiotic assays as predictors of toxicity from airborne particulate matter. International journal of molecular sciences, 20(19), 4772.

Paatero, P. and Tapper, U. (1994), Positive matrix factorization: A non-negative factor model with optimal utilization of error estimates of data values. Environmetrics, 5: 111-126.

Paatero, P. (1999). The multilinear engine—a table-driven, least squares program for solving multilinear problems, including the n-way parallel factor analysis model. Journal of Computational and Graphical Statistics, 8(4), 854-888.

Paglione, M., Gilardoni, S., Rinaldi, M., Decesari, S., Zanca, N., Sandrini, S., Giulianelli, L., Bacco, D., Ferrari, S., Poluzzi, V., Scotto, F., Trentini, A., Poulain, L., Herrmann, H., Wiedensohler, A., Canonaco, F., Prevot, A.S.H., Massoli, P., Carbone, C., Facchini, M.C., Fuzzi, S. (2020). The impact of biomass burning and aqueous-phase processing on air quality: a multi-year source apportionment study in the Po Valley, Italy. Atmospheric Chemistry and Physics, 20(3), 1233-1254.

Paglione, M., Decesari, S., Rinaldi, M., Tarozzi, L., Manarini, F., Gilardoni, S., et al., Nenes, A. (2021). Historical Changes in Seasonal Aerosol Acidity in the Po Valley (Italy) as Inferred from Fog Water and Aerosol Measurements. Environmental science & technology.

Pant, P., Harrison, R. M. (2013). Estimation of the contribution of road traffic emissions to particulate matter concentrations from field measurements: A review. Atmospheric environment, 77, 78-97.

Park, J., Park, E. H., Schauer, J. J., Yi, S. M., Heo, J. (2018). Reactive oxygen species (ROS) activity of ambient fine particles (PM2. 5) measured in Seoul, Korea. Environment international, 117, 276-283.

Park, S. S., Son, S. C. (2017). Relationship between carbonaceous components and aerosol light absorption during winter at an urban site of Gwangju, Korea. Atmospheric Research, 185, 73-83.

Perrino, C., Catrambone, M., Canepari, S. (2020). Chemical composition of PM10 in 16 urban, industrial and background sites in Italy. Atmosphere, 11(5), 479.

Perrino, C., Marcovecchio, F. (2016). A new method for assessing the contribution of primary biological atmospheric particles to the mass concentration of the atmospheric aerosol. Environment international, 87, 108-115.

Perrino, C., Canepari, S., Pappalardo, S., Marconi, E. (2010). Time-resolved measurements of water-soluble ions and elements in atmospheric particulate matter for the characterization of local and long-range transport events. Chemosphere, 80(11), 1291-1300.

Perrone, M. R., Bertoli, I., Romano, S., Russo, M., Rispoli, G., Pietrogrande, M. C. (2019). PM2. 5 and PM10 oxidative potential at a Central Mediterranean Site: Contrasts between dithiothreitol-and ascorbic acid-measured values in relation with particle size and chemical composition. Atmospheric Environment, 210, 143-155.

Pietrodangelo, A., Salzano, R., Rantica, E., Perrino, C. (2013). Characterisation of the local topsoil contribution to airborne particulate matter in the area of Rome (Italy). Source profiles. Atmospheric Environment, 69, 1-14.

Pietrogrande, M. C., Perrone, M. R., Manarini, F., Romano, S., Udisti, R., Becagli, S. (2018a). PM10 oxidative potential at a Central Mediterranean Site: Association with chemical composition and meteorological parameters. Atmospheric Environment, 188, 97-111.

Pietrogrande, M. C., Dalpiaz, C., Dell'Anna, R., Lazzeri, P., Manarini, F., Visentin, M., Tonidandel, G. (2018b). Chemical composition and oxidative potential of atmospheric coarse particles at an industrial and urban background site in the alpine region of northern Italy. Atmospheric Environment, 191, 340-350.

Pietrogrande, M. C., Bacco, D., Trentini, A., Russo, M. (2021). Effect of filter extraction solvents on the measurement of the oxidative potential of airborne PM 2.5. Environmental Science and Pollution Research, 1-13.

Pio, C., Alves, C., Nunes, T., Cerqueira, M., Lucarelli, F., Nava, S., Calzolai, G., Gianelle, V., Colombi, C., Amato, F., Karanasiou, A., Querol, X. (2020). Source apportionment of PM2. 5 and PM10 by Ionic and Mass Balance (IMB) in a traffic-influenced urban atmosphere, in Portugal. Atmospheric environment, 223, 117217.

Przybysz, A., Popek, R., Stankiewicz-Kosyl, M., Zhu, C. Y., Małecka-Przybysz, M., Maulidyawati, T., et al., Wińska-Krysiak, M. (2021). Where trees cannot grow–Particulate matter accumulation by urban meadows. Science of The Total Environment, 147310.

Popek, R., Gawrońska, H., Wrochna, M., Gawroński, S. W., Sæbø, A. (2013). Particulate matter on foliage of 13 woody species: deposition on surfaces and phytostabilisation in waxes–a 3-year study. International Journal of Phytoremediation, 15(3), 245-256.

Querol, X., Viana, M., Alastuey, A., Amato, F., Moreno, T., Castillo, S., Pey, J., de la Rosa, J., Sanchez de la Campa, A., Artinano, B., Salvador, P., Garcia Dos Santos, S., Fernandez-Patier, R., Moreno-Grau, S., Negral, L., Minguillon, M.C., Gil, J.I., Inza, A., Ortega, L.A., Santamaria, J.M., Reff, A., Eberly, S. I., Bhave, P. V. (2007). Receptor modeling of ambient particulate matter data using positive matrix factorization: review of existing methods. Journal of the Air & Waste Management Association, 57(2), 146-154.

Rai, P. K. (2016). Impacts of particulate matter pollution on plants: Implications for environmental biomonitoring. Ecotoxicology and environmental safety, 129, 120-136.

Ramli, N. A., Yusof, N. F. F. M., Shith, S., Suroto, A. (2020). Chemical and biological compositions associated with ambient respirable particulate matter: a review. Water, Air, & Soil Pollution, 231(3), 1-14.

Rao, L., Zhang, L., Wang, X., Xie, T., Zhou, S., Lu, S., et al., Wang, Q. (2020). Oxidative Potential Induced by Ambient Particulate Matters with Acellular Assays: A Review. Processes, 8(11), 1410.

Rattanavaraha, W., Rosen, E., Zhang, H., Li, Q., Pantong, K., Kamens, R. M. (2011). The reactive oxidant potential of different types of aged atmospheric particles: An outdoor chamber study. Atmospheric Environment, 45(23), 3848-3855.

Reff, A., Eberly, S. I., Bhave, P. V. (2007). Receptor modeling of ambient particulate matter data using positive matrix factorization: review of existing methods. Journal of the Air & Waste Management Association, 57(2), 146-154.

Ristorini, M., Astolfi, M. L., Frezzini, M. A., Canepari, S., Massimi, L. (2020). Evaluation of the efficiency of Arundo donax L. leaves as biomonitors for atmospheric element concentrations in an urban and industrial area of central Italy. Atmosphere, 11(3), 226.

Rosianu, A. M., Leru, P. M., Stefan, S., Iorga, G., Marmureanu, L. (2021). SIX-YEAR MONITORING OF ATMOSPHERIC POLLEN AND MAJOR AIR POLLUTANT CONCENTRATIONS IN RELATION WITH METEOROLOGICAL FACTORS IN BUCHAREST, ROMANIA. ROMANIAN REPORTS IN PHYSICS, 73(4).

Saarnio, K., Teinilä, K., Saarikoski, S., Carbone, S., Gilardoni, S., Timonen, H., Aurela, M., Hillamo, R. (2013). Online determination of levoglucosan in ambient aerosols with particle-into-liquid sampler–high-performance anion-exchange chromatography–mass spectrometry (PILS–HPAEC–MS). Atmospheric Measurement Techniques, 6(10), 2839-2849.

Sæbø, A., Popek, R., Nawrot, B., Hanslin, H. M., Gawronska, H., Gawronski, S. W. (2012). Plant species differences in particulate matter accumulation on leaf surfaces. Science of the Total Environment, 427, 347-354.

Sahu, R. K., Kar, M., Routray, R. (2013). DPPH free radical scavenging activity of some leafy vegetables used by tribals of Odisha, India. J. Med. Plants, 1(4), 21-27.

Sager, T. M., Kommineni, C., Castranova, V. (2008). Pulmonary response to intratracheal instillation of ultrafine versus fine titanium dioxide: role of particle surface area. Particle and fibre toxicology, 5(1), 1-15.

Samara, C. (2017). On the redox activity of urban aerosol particles: Implications for size distribution and relationships with organic aerosol components. Atmosphere, 8(10), 205.

Sandrini, S., Fuzzi, S., Piazzalunga, A., Prati, P., Bonasoni, P., Cavalli, F., Bove, M.C., Calvello, M., Cappelletti, D., Colombi, C., Contini, D., de Gennaro, G., Di Gilio, A., Fermo, P., Ferrero, L., Gianelle, V., Giugliano, M., Ielpo, P., Lonati, G., Marinoni, A., Massabò, D., Molteni, U., Moroni, B., Pavese, G., Perrino, C., Perrone, M.G., Perrone, M.R., Putaus, J., Sargolini, T., Vecchi, R., Gilardoni, S. (2014). Spatial and seasonal variability of carbonaceous aerosol across Italy. Atmospheric Environment, 99, 587-598.

Schifano, P., Lallo, A., Asta, F., De Sario, M., Davoli, M., Michelozzi, P. (2013). Effect of ambient temperature and air pollutants on the risk of preterm birth, Rome 2001–2010. Environment international, 61, 77-87.

Scotto, F., Bacco, D., Lasagni, S., Trentini, A., Poluzzi, V., Vecchi, R. (2021). A multi-year source apportionment of PM2. 5 at multiple sites in the southern Po Valley (Italy). Atmospheric Pollution Research, 12(11), 101192.

See, S. W., Wang, Y. H., Balasubramanian, R. (2007). Contrasting reactive oxygen species and transition metal concentrations in combustion aerosols. Environmental Research, 103(3), 317-324.

Setti, L., Passarini, F., De Gennaro, G., Barbieri, P., Perrone, M. G., Borelli, M., et al., Miani, A. (2020). SARS-Cov-2RNA found on particulate matter of Bergamo in Northern Italy: first evidence. Environmental research, 188, 109754.

Sharma, R. K., Agrawal, M. (2005). Biological effects of heavy metals: an overview. Journal of environmental Biology, 26(2), 301-313.

Sharma, S. K., Mandal, T. K., Jain, S., Sharma, A., Saxena, M. (2016). Source apportionment of PM 2.5 in Delhi, India using PMF model. Bulletin of environmental contamination and toxicology, 97(2), 286-293.

Simoneit, B. R., Bi, X., Oros, D. R., Medeiros, P. M., Sheng, G., Fu, J. (2007). Phenols and hydroxy-PAHs (arylphenols) as tracers for coal smoke particulate matter: source tests and ambient aerosol assessments. Environmental science & technology, 41(21), 7294-7302.

Simonetti, G., Frasca, D., Marcoccia, M., Farao, C., Canepari, S. (2018a). Multi-elemental analysis of particulate matter samples collected by a particle-into-liquid sampler. Atmospheric Pollution Research, 9(4), 747-754.

Simonetti, G., Conte, E., Perrino, C., Canepari, S. (2018b). Oxidative potential of size-segregated PM in an urban and an industrial area of Italy. Atmospheric Environment, 187, 292-300.

Slezakova, K. and Morais, S. (2012). Indoor air pollutants: Relevant aspects and health impacts. Environmental Health - Emerging Issues and Practice.

Smith, K. E., Weis, D., Amini, M., Shiel, A. E., Lai, V. W. M., Gordon, K. (2019). Honey as a biomonitor for a changing world. Nature Sustainability, 2(3), 223-232.

Solgi, E., Keramaty, M., Solgi, M. (2020). Biomonitoring of airborne Cu, Pb, and Zn in an urban area employing a broad leaved and a conifer tree species. Journal of Geochemical Exploration, 208, 106400.

Sportisse, B. (2009). Fundamentals in air pollution: from processes to modelling. Springer Science & Business Media.

Sridhar, K., Charles, A. L. (2019). In vitro antioxidant activity of Kyoho grape extracts in DPPH and ABTS assays: Estimation methods for EC50 using advanced statistical programs. Food Chemistry, 275, 41-49.

Steenhof, M., Gosens, I., Strak, M., Godri, K. J., Hoek, G., Cassee, F. R., et al., Pieters, R. H. (2011). In vitro toxicity of particulate matter (PM) collected at different sites in the Netherlands is associated with PM composition, size fraction and oxidative potential-the RAPTES project. Particle and fibre toxicology, 8(1), 1-15.

Stevens, C.J., Bell, J.N.B., Brimblecombe, P., Clark, C.M., Dise, N.B., Fowler, D., Lovett, G.M., Wolseley, P.A., 2020. The impact of air pollution on terrestrial managed and natural vegetation. Philos. Trans. Royal Society A 378 (2183), 20190317.

Taghvaee, S., Sowlat, M. H., Diapouli, E., Manousakas, M. I., Vasilatou, V., Eleftheriadis, K., Sioutas, C. (2019). Source apportionment of the oxidative potential of fine ambient particulate matter (PM2. 5) in Athens, Greece. Science of The Total Environment, 653, 1407-1416.

TASK, I. (1966). Deposition and retention models for internal dosimetry of the human respiratory tract. Health Physics, 12, 173-207.

Teixeira, J., Gaspar, A., Garrido, E. M., Garrido, J., Borges, F. (2013). Hydroxycinnamic acid antioxidants: an electrochemical overview. BioMed research international, 2013.

Thakur, M., Pathania, D. (2020). Environmental fate of organic pollutants and effect on human health. In Abatement of Environmental Pollutants (pp. 245-262). Elsevier.

Thompson, J. E. (2018). Airborne particulate matter: human exposure and health effects. Journal of occupational and environmental medicine, 60(5), 392-423.

Thorpe, A., Harrison, R. M. (2008). Sources and properties of non-exhaust particulate matter from road traffic: a review. Science of the total environment, 400(1-3), 270-282.

Timonen, H., Aurela, M., Carbone, S., Saarnio, K., Saarikoski, S., Mäkelä, T., Kulmala, M., Kerminen, V.M., Worsnop, D.R., Hillamo, R. (2010). High time-resolution chemical characterization of the water-soluble fraction of ambient aerosols with PILS-TOC-IC and AMS. Atmospheric Measurement Techniques, 3(4), 1063-1074.

Tofful, L., Canepari, S., Sargolini, T., Perrino, C. (2021). Indoor air quality in a domestic environment: Combined contribution of indoor and outdoor PM sources. Building and Environment, 108050.

Tositti, L., Brattich, E., Masiol, M., Baldacci, D., Ceccato, D., Parmeggiani, S., Stracquadanio, M., Zappoli, S. (2014). Source apportionment of particulate matter in a large city of southeastern Po Valley (Bologna, Italy). Environmental Science and Pollution Research, 21(2), 872-890.

Tsapakis, M., and Stephanou, E. G. (2003). Collection of Gas and Particle Semi-Volatile Organic Compounds: Use of an Oxidant Denuder to Minimize Polycyclic Aromatic Hydrocarbons Degradation During High-Volume Air Sampling. Atmos. Environ., 37:4935–4944.

Tung, N. T., Cheng, P. C., Chi, K. H., Hsiao, T. C., Jones, T., BéruBé, K., et al., Chuang, H. C. (2021). Particulate matter and SARS-CoV-2: a possible model of COVID-19 transmission. Science of The Total Environment, 750, 141532.

Turpin, B. J., Huntzicker, J. J., Hering, S.V. (1994). Investigation of Organic Aerosol Sampling Artifacts in the Los Angeles Basin. Atmos. Environ., 28:3061–3071.

Ueno, D., Watanabe, M., Subramanian, A., Tanaka, H., Fillmann, G., Lam, P. K., et al., Tanabe, S. (2005). Global pollution monitoring of polychlorinated dibenzo-p-dioxins (PCDDs), furans (PCDFs) and coplanar polychlorinated biphenyls (coplanar PCBs) using skipjack tuna as bioindicator. Environmental Pollution, 136(2), 303-313.

UNI, E., 2014. 12341: 2014. Air Quality–Determination of the PM10 fraction of suspended particulate matter. Reference method and field test procedure to demonstrate reference equivalence of measurements methods.

UNION, P. (2008). Directive 2008/50/EC of the European Parliament and of the Council of 21 May 2008 on ambient air quality and cleaner air for Europe. Official Journal of the European Union.

Upadhyay, S., Ganguly, K., Stoeger, T. (2014). Inhaled ambient particulate matter and lung health burden. EMJ Respir, 2, 88-95.

Vallero, D.A. (2008) in Fundamentals of Air Pollution (Fourth Edition). Chapter 11 - Sampling and analysis. Pages 263-333

van den Hooven, E. H., Pierik, F. H., de Kluizenaar, Y., Willemsen, S. P., Hofman, A., van Ratingen, S. W., et al., Jaddoe, V. W. (2012). Air pollution exposure during pregnancy, ultrasound measures of fetal growth, and adverse birth outcomes: a prospective cohort study. Environmental health perspectives, 120(1), 150-156.

Vankadari, N., Wilce, J. A. (2020). Emerging COVID-19 coronavirus: glycan shield and structure prediction of spike glycoprotein and its interaction with human CD26. Emerging microbes & infections, 9(1), 601-604.

Venkatachari, P., Hopke, P. K., Grover, B. D., Eatough, D. J., 2005. Measurement of particle-bound reactive oxygen species in rubidoux aerosols. Journal of Atmospheric Chemistry, 50, 49–58.

Venkatachari, P., Hopke, P. K., Brune, W. H., Ren, X., Lesher, R., Mao, J., Mitchell, M., 2007. Characterization of wintertime reactive oxygen species concentrations in Flushing, New York. Aerosol Science and Technology, 41, 97–111.

Verma, V., Fang, T., Guo, H., King, L., Bates, J. T., Peltier, R. E., Edgerton, E., Russell, A.G., Weber, R. J. (2014). Reactive oxygen species associated with water-soluble PM 2.5 in the southeastern United States: spatiotemporal trends and source apportionment. Atmospheric Chemistry and Physics, 14(23), 12915-12930.

Verma, V., Rico-Martinez, R., Kotra, N., King, L., Liu, J., Snell, T. W., Weber, R. J. (2012). Contribution of water-soluble and insoluble components and their hydrophobic/hydrophilic subfractions to the reactive oxygen species-generating potential of fine ambient aerosols. Environmental science & technology, 46(20), 11384-11392.

Verma, V., Ning, Z., Cho, A. K., Schauer, J. J., Shafer, M. M., Sioutas, C. (2009). Redox activity of urban quasi-ultrafine particles from primary and secondary sources. Atmospheric Environment, 43(40), 6360-6368.

Viana, M., Pey, J., Querol, X., Alastuey, A., De Leeuw, F., Lükewille, A. (2014). Natural sources of atmospheric aerosols influencing air quality across Europe. Science of the total environment, 472, 825-833.

Visentin, M., Pagnoni, A., Sarti, E., Pietrogrande, M. C. (2016). Urban PM2. 5 oxidative potential: Importance of chemical species and comparison of two spectrophotometric cell-free assays. Environmental Pollution, 219, 72-79.

Wang, Y., Arellanes, C., Curtis, D. B., Paulson, S. E. (2010). Probing the source of hydrogen peroxide associated with coarse mode aerosol particles in Southern California. Environmental science & technology, 44(11), 4070-4075.

Wang, Y., Zhuang, G., Xu, C., An, Z. (2007). The air pollution caused by the burning of fireworks during the lantern festival in Beijing. Atmospheric Environment, 41(2), 417-431.

Weber, S., Uzu, G., Favez, O., Borlaza, L. J. S., Calas, A., Salameh, D., et al., Jaffrezo, J. L. (2021). Source apportionment of atmospheric PM 10 oxidative potential: synthesis of 15 year-round urban datasets in France. Atmospheric Chemistry and Physics, 21(14), 11353-11378.Weber, R. J., Orsini, D., Daun, Y., Lee, Y. N., Klotz, P. J., Brechtel, F. (2001). A particle-into-liquid collector for rapid measurement of aerosol bulk chemical composition. Aerosol Science & Technology, 35(3), 718-727.

Westerdahl, D., Fruin, S., Sax, T., Fine, P. M., Sioutas, C. (2005). Mobile platform measurements of ultrafine particles and associated pollutant concentrations on freeways and residential streets in Los Angeles. Atmospheric Environment, 39(20), 3597-3610.

Wiseman, C. L. (2015). Analytical methods for assessing metal bioaccessibility in airborne particulate matter: a scoping review. Analytica chimica acta, 877, 9-18.

Wragg, F., Fuller, S. J., Freshwater, R., Green, D. C., Kelly, F. J., Kalberer, M., (2016). An automated online instrument to quantify aerosol-bound reactive oxygen species (ROS) for ambient measurement and health-relevant aerosol studies.

Wrapp, D., Wang, N., Corbett, K. S., Goldsmith, J. A., Hsieh, C. L., Abiona, O., et al., McLellan, J. S. (2020). Cryo-EM structure of the 2019-nCoV spike in the prefusion conformation. Science, 367(6483), 1260-1263.

Xia, T., Kovochich, M., Nel, A. (2006). The role of reactive oxygen species and oxidative stress in mediating particulate matter injury. Clin Occup Environ Med, 5(4), 817-836.

Yadav, S., Rajamani, V. (2006). Air quality and trace metal chemistry of different size fractions of aerosols in N–NW India—implications for source diversity. Atmospheric Environment, 40(4), 698-712.

Yamamoto, S. S., Phalkey, R., Malik, A. A. (2014). A systematic review of air pollution as a risk factor for cardiovascular disease in South Asia: Limited evidence from India and Pakistan. International journal of hygiene and environmental health, 217(2-3), 133-144.

Yang, A., Janssen, N. A. H., Brunekreef, B., Cassee, F. R., Hoek, G., Gehring, U. (2016). Children's respiratory health and oxidative potential of PM2.5: the PIAMA birth cohort study. Occupational and Environmental Medicine, 73(3), 154-160.

Yang, A., Janssen, N. A., Brunekreef, B., Cassee, F. R., Hoek, G., Gehring, U., 2016. Children's respiratory health and oxidative potential of PM2. 5: the PIAMA birth cohort study. Occup Environ Med, 73(3), 154-160.

Yatkin, S., Bayram, A. (2008). Determination of major natural and anthropogenic source profiles for particulate matter and trace elements in Izmir, Turkey. Chemosphere, 71(4), 685-696.

Zhang LW, Chen X, Xue XD et al (2014) Long-term exposure to high particulate matter pollution and cardiovascular mortality: a 12-year cohort study in four cities in northern China. Environ Int 62:41–47.

Zhang, Z. H., Hartner, E., Utinger, B., Gfeller, B., Paul, A., Sklorz, M., Czech, H., Yang, B.X., Su, X.Y., Jakobi, G., Orasche, J., Schnelle-Kreis, J., Jeong, S., Gröger, T., Pardo, M., Hohaus, T., Adam, T., Kiendler-Scharr, A., Rudich, Y., Zimmermann, R., Kalberer, M. (2021). Are reactive oxygen species (ROS) a suitable metric to predict toxicity of carbonaceous aerosol particles?. Atmospheric Chemistry and Physics Discussions, 1-29.

Zhang, L., Ou, C., Magana-Arachchi, D., Vithanage, M., Vanka, K. S., Palanisami, T., Masakorala, K., Wijesekara, H., Yan, Y., Bolan, N., Kirkham, M. B. (2021). Indoor Particulate Matter in Urban Households: Sources, Pathways, Characteristics, Health Effects, and Exposure Mitigation. International Journal of Environmental Research and Public Health, 18(21), 11055.

Zhou, J., Bruns, E. A., Zotter, P., Stefenelli, G., Prévôt, A. S., Baltensperger, U., El-Haddad, I., Dommen, J., 2018. Development, characterization and first deployment of an improved online reactive oxygen species analyzer. Atmospheric Measurement Techniques, 11(1), 65-80.

Zhou, X., Taylor, M. P., Davies, P. J., Prasad, S. (2018). Identifying sources of environmental contamination in European honey bees (Apis mellifera) using trace elements and lead isotopic compositions. Environmental science & technology, 52(3), 991-1001.

Zwack, L. M., Paciorek, C. J., Spengler, J. D., Levy, J. I. (2011). Modeling spatial patterns of traffic-related air pollutants in complex urban terrain. Environmental Health Perspectives, 119(6), 852-859.